Digital Object Identifier: 10.1109/ULTSYM.2008.2014

Abstract Book

Temple of Heaven

Forbidden City

Summer Palace

2008 IEEE International Ultrasonics Symposium (IUS)

(Including Short Courses)

Beijing International Convention Center (BICC)
Beijing, China, November 2-5, 2008

Sponsored by the IEEE Ultrasonics, Ferroelectrics, and Frequency Control Society (UFFC-S)

In Cooperation with the Acoustical Society of China and the Institute of Acoustics, Chinese Academy of Sciences

The Great Wall

ISSN: 1051-0117 ISBN: 978-1-4244-2428-3 (For Softbound); 978-1-4244-2480-1 (For DVD) IEEE Catalog No.: CFP08ULT-PRT (For Softbound); CFP08ULT-DVD (For DVD)

Table of Contents

Front and Back Matters:

Oral Sessions, Monday, November 3, 2008:

Poster Sessions, Monday, November 3, 2008; 3:00 p.m. – 4:30 p.m.:

Oral Sessions, Tuesday, November 4, 2008:

Poster Sessions, Tuesday, November 4, 2008; 3:00 p.m. – 4:30 p.m.:

Oral Sessions, Wednesday, November 5, 2008:

Poster Sessions, Wednesday, November 5, 2008; 3:00 p.m. – 4:30 p.m.:

Welcome From the General Chair

***Jian-yu Lu*, Ph.D.**

Welcome to Beijing!

The 2008 IEEE International Ultrasonics Symposium (IUS) will be held in the Beijing International Convention Center (BICC), Beijing, China, from ***November 2-5, 2008***. This will be the first time the IUS goes to Beijing, the capital of China. Beijing is a city of a long history and a great culture. It has served as the capital of China for long periods of times. Therefore, Beijing will be a great tourist attraction for the conference attendees and their guests besides the technical program. As we know, the 2008 Summer Olympics and Paralympics will be held in Beijing in August and September 2008, respectively. Beijing is preparing for this event by building and improving a lot of infrastructure and cleaning up the environment, and is welcoming hundreds of thousands of visitors. Thus, Beijing will become more beautiful after the Olympics. The 2008 IEEE IUS will take advantage of the improved transportation and vastly increased hotel capacity of Beijing after the Olympics. The BICC is located within the Olympic Complex and thus will be convenient for the conference attendees to visit the complex.

The 2008 IEEE IUS will also bring together more closely the ultrasonics communities around the world with the communities of China and East Asia to further the research and development of ultrasonics theories and applications. The 2008 IEEE IUS is expected to be another success in the history of this annual conference that started in the early 1960s and has grown to have more than 1000 attendees in recent years.

Look forward to seeing you in Beijing.

***Jian-yu Lu*, Ph.D.**
General Chair
2008 IEEE International Ultrasonics Symposium

Message from the Technical Program Committee Chair

***Keith A. Wear*, Ph.D.**

Welcome to the IEEE International Ultrasonics Symposium at the Beijing International Convention Center in Beijing, China, November 2-5, 2008.

The first day will feature short courses on topics of current interest in ultrasonics. The next three days will include parallel oral and poster sessions covering: 1) Medical Ultrasonics, 2) Sensors, NDE & Industrial Applications, 3) Physical Acoustics, 4) Microacoustics - SAW, FBAR, MEMS, and 5) Transducers & Transducer Materials. Awards will be given to the top student presentations.

In addition to the technical program, the social and guest programs will allow attendees to explore the rich history and culture of Beijing. There are many interesting sites in Beijing, including Tiananmen Square, the Forbidden City, the Great Wall of China, the Summer Palace, the Temple of Heaven, and the Ming Tomb.

On behalf of the Technical Program Committee, I would like to thank you for joining us for this symposium.

***Keith A. Wear*, Ph.D.**
Technical Chair
2008 IEEE International Ultrasonics Symposium

Symposium Organizing Committee

General Co-Chair
Overall Management:
***Jian-yu Lu*, Ph.D. (General Chair)**
Department of Bioengineering
The University of Toledo
Toledo, Ohio 43606, U.S.A.
jilu@eng.utoledo.edu

General Co-Chair
China Relationship:
***Hailan Zhang*, Ph.D.**
Institute of Acoustics
Chinese Academy of Sciences
Beijing 100080, China
zhanghl@mail.ioa.ac.cn

Technical Chair:
***Keith A. Wear*, Ph.D.**
Food & Drug Administration
Silver Spring, MD 20993, USA
keith.wear@fda.hhs.gov

Finance:
***Jan Brown*, Ph.D.**
JB Consulting
West Whately, MA 01039, U.S.A.
Jan.brown@ieee.org

Short Course:
***Roman Gr. Maev*, Ph.D.**
University of Windsor
Ontario N9B 3P4, Canada
maev@uwindsor.ca

Exhibits:
***Mark Schafer*, Ph.D.**
Sonic Tech. Inc.
Ambler PA 19002, U.S.A.
marks@sonictech.com

Publicity:
Overall:
***Sorah Rhee*, Ph.D.**
Boston Scientific
Fremont, CA 94538, U.S.A.
sorah.rhee@ieee.org

Publicity:
Asia and Pacific:
***Ji Wang*, Ph.D.**
Ningbo University
Zhejiang 315211, China
wangji@nbu.edu.cn

Proceedings:
***Kendall R. Waters*, Ph.D.**
SVMI
Fremont, CA 94539, U.S.A.
kendall.waters@ieee.org

Corporate Sponsors

The Following Companies Have Donated Money to the 2008 IEEE International Ultrasonics Symposium:

Thank You: Shanghai Apex Electronics Technology Co. Ltd.

http://www.apex-ultrasound.com

Exhibitors / Schedule

Exhibition Schedule:

Monday, November 3, 2008: 8:00 a.m. - 5:00 p.m.
Tuesday, November 4, 2008: 8:00 a.m. - 5:00 p.m.
Wednesday, November 5, 2008: 8:00 a.m. - 12:00 noon.

List of Exhibitors at the 2008 IEEE International Ultrasonics Symposium as of October 10, 2008 (a total of 20):

- **Beijing Zhongxun Sifang Science & Techonolgy CO. LTD:** *http://www.bjzxsf.net*
- **Bossa Nova Technologies:** *http://www.leepipe.com and http://www.bossanovatech.com/*
- **DASEL** *http://www.daselsistemas.com and http://ultrascope.info/index.asp*
- **Electronics Innovation Ltd:** *http://www.eandiltd.com/*
- **Ferroperm Piezoceramics A/S:** *http://www.ferroperm.net*
- **IEEE:** *http://www.ieee.org*
- **Imasonic:** *http://www.imasonic.com and http://www.imasonic.fr/*
- **Lecoeur Electronique:** *http://www.lecoeur-electronique.com/*
- **Onda Corporation:** *http://www.ondacorp.com/index1.html*
- **Polytec GmbH:** *http://www.polytec.com/*
- **Precision Acoustics Ltd.:** *http://www.acoustics.co.uk*
- **Prosonic:** *http://www.prosonic.co.kr/*
- **Shanghai Apex Electronics Technology Co. Ltd:** *http://www.apex-ultrasound.com*
- **Sonora Medical Systems:** *http://www.4sonora.com/*
- **Sound Technology Inc.:** *http://www.sti-ultrasound.com*
- **Tegal Corporation:** *http://www.tegal.com/*
- **Terason Ultrasound, Division of Teratech:** *http://www.terason.com/index.asp*
- **Texas Instruments Semiconductor Technologies (Shanghai) Co. Ltd:** *http://www.ti.com.cn*
- **The Piezo Institute:** *http://www.piezoinstitute.com*
- **TRS Technologies, Inc.:** *http://www.trstechnologies.com*

Notes:

- Some of companies that have signed up for the exhibition after July 15, 2008, the deadline for inclusion of their names in this book, may not be listed here.
- A list of all exhibition companies at the Ultrasonics Symposia from 1996-2007 can be viewed via the "Exhibits" link at the conference website at: http://ewh.ieee.org/conf/ius_2008.

Plenary Session

Plenary Session:

8:00 a.m. – 10:00 a.m., Monday, November 3, 2008
Convention Hall 1, Beijing International Convention Center (BICC), Beijing, China

Welcome:

Conference organizers and others
UFFC-S President

Awards and Recognitions:

IEEE Award:
IEEE Fellow Award 2008

IEEE UFFC Society Awards:
Achievement Award 2008
Distinguished Service Award 2008
Outstanding Paper Award 2007
2008-2009 Distinguished Lecturer Award

Ultrasonics Award:
Rayleigh Award 2008

Note: The order of presentations above is to be determined.

Plenary Speaker:

Title of Presentation:

Acoustics of Traditional Chinese Theatrical Buildings

Author:

Jiqing Wang, Professor, Institute of Acoustics, Tongji University, Shanghai, China 200092, E-mail: wongtsu@126.com

Abstract:

The traditional Chinese theatrical building is a unique form in the architectural world. The Chinese opera matured as early as the Song and Yuan Dynasties, 11th–14th Centuries, and Chinese theatrical buildings developed accordingly. As the Chinese opera plays on the principle of imaginary actions, no realistic stage settings are required. But since ancient times, Chinese audiences have placed great demands on vocal performances; therefore, the acoustic effect of a theatre is a major concern to the audience as well as the performers.

Pavilion stages, that are small in area, open on three sides, and thrusting into the audience area, are commonly found in traditional Chinese theatres, both in the courtyard type and the auditorium type. Numerous theatres of the kind built in the Qing Dynasty, 17th–19th Centuries still exist, and in fact at the present day, some are still functioning in good condition. A study on the sound effects of the traditional Chinese theatres has been conducted with the knowledge of modern architectural acoustics.

As the courtyard theatre was a popular type of traditional Chinese theater at that time, its acoustic phenomenon is quite different from that of an enclosed space due to the absence of a roof. Therefore, the classic room acoustics, such as Sabine reverberation formula, is no longer applicable. It is well known that the parameter of reverberation time T60 shows the decay rate only, however it cannot properly characterize the prominent change in the fine structure of the echogram, particularly in case of a large reduction of reflections from the ceiling during the decay process. The sense of so-called 2.5D reverberation time in a courtyard space would differ from that of the equivalent 3D reverberation time in an enclosed space. Based upon the characteristic analysis of the sound field in an open-top space, a preliminary study on the acoustics of the courtyard theatre, both objectively and subjectively, will be introduced.

Additional Materials Related to the Talk:

To get additional information of the talk, please check the link "Plenary Speaker" at the conference website: http://ewh.ieee.org/conf/ius_2008.

Biography of the Author:

Jiqing Wang is a Professor of Acoustics, Institute of Acoustics, School of Science (1981-present), and was also once the Director of Graduate Program on Architectural Science, School of Architecture and Urban Planning (1985-2002), Tongji University, Shanghai, China. He is a Fellow of Acoustical Society of China and a Fellow of Acoustical Society of America. He has served as the Chairman of the National Building Science Committee (1996-2000), President of the Acoustical Society of Shanghai (1987-1991), executive member of the Acoustical Society of China (1988-1998), technical member of the Acoustic Standardization Committee of China since 1980, and editor-in-chief for the Chinese journal of Technical Acoustics (1990-2004). He was the author and co-author of five books on architectural acoustics in Chinese, and published over 130 papers. He has also delivered several plenary, keynotes, invited and professional lectures worldwide.

Conference Venue / Business Center / Coat Handling

Conference Venue:

Beijing International Convention Center (BICC)
No. 8, East Beichen Road
Andingmen Wai
North Sihuan Road
Chaoyang District
Beijing 100101, China
Tel. 011-86-10-84985588 or 011-86-10-84980248
Fax: 011-86-10-84970107 or 011-86-10-84980256
Web: http://www.bcghotel.com/english/index.asp

Notes:

- There will be no coat hanging services at BICC.
- The Business Center of BICC for printing, copying, and faxing opens from 8:00 a.m. – 5:00 p.m., Monday through Friday. In addition to BICC, the business centers in both nearby Continental Grand Hotel and Crowne Plaza Hotel also open during the business hours above.
- BICC is about 400 m to the southeast of the National Olympic Stadium that will host the opening ceremony of the 2008 Beijing Olympics. A photo of the National Olympic Stadium taken from the third floor of BICC on May 29, 2008 is shown below.

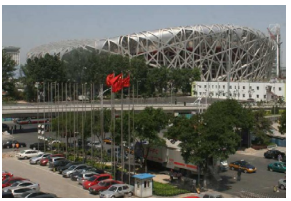

Conference Registration

Introduction:

The deadline for early conference registration with discount registration fees is ***Tuesday, September 12, 2008*** (midnight, Pacific Standard Time). After September 12, 2008, attendees with credit cards (Visa, Master, or American Express) can continue to register

at higher fees until the conference ends on November 5, 2008. However, registrations via fax or mail will not be accepted after ***Friday, October 17, 2008*** (5:00 p.m., Eastern Standard Time), and these attendees are requested to register on-site with cash. A full conference registration will include Monday lunch (November 3, 2008), Monday evening buffet dinner (November 3, 2008), and Tuesday evening banquet with traditional Chinese shows (November 4, 2008). Each full conference registrant will also get a bag to hold the advance program and abstract books, and will receive a gift from the 2008 IEEE International Ultrasonics Symposium (IUS). Please pay attention to the "Notes" below for additional information on the conference registration. Complete registration information can be found at the conference website: http://ewh.ieee.org/conf/ius_2008.

Please register for a correct registration type. Different badges will be issued for corresponding registration types. Badges and tickets are required for various conference events and for technical sessions.

List of Registration Fees:

Registration Type	By September 12, 2008	After September 12, 2008
(1) IEEE Member:	***$600***	***$700***
(2) Non-IEEE Member:	***$750***	***$850***
(3) Student (Show Student ID at Conference):	***$150***	***$150***
(4) Retiree:	***$150***	***$150***
(5) Life IEEE Member (Show Life Member Card at Conference): **	***$0***	***$0***
(6) One-Day Registration (without DVD Proceedings): *	***$350***	***$350***
A Registrant above May Add: **(1) Additional DVD Proceedings: ***** **(2) Short Courses:** **(3) Guests:**	 ***$75*** ***$150*** ***$50*** **(Student /Retiree)** ***$75***	 ***$75*** ***$150*** ***$50*** **(Student /Retiree)** ***$75***

Notes:

- "*" ***One-Day Registration*** includes event tickets for the day of registration only.
- "**" ***Life Member*** is defined by IEEE as at least 65-year old and the age plus years of IEEE membership should be equal or greater than 100. Life members should show their IEEE Life Member card or evidence of Life Membership when getting registration materials.
- "***" A ***Full Registration*** (IEEE Member, Non-IEEE Member, Student, Retiree, or Life IEEE Member) will include one DVD conference proceedings. If you need additional DVD proceedings, you may order them when you register. A printed

version of the Proceedings will only be available by ordering directly from IEEE after the Symposium.

- A ***Full Registration*** will also include Monday lunch (November 3, 2008), Monday evening buffet dinner (November 3, 2008), and Tuesday evening banquet with traditional Chinese shows (November 4, 2008).
- ***Guest Registration*** includes three guest breakfasts in addition to the three meals above. Guests are NOT allowed to attend any technical sessions except for the Monday morning plenary session.
- For those who register for ***Short Courses Only***, they will NOT get a badge or any conference materials such as books and meal/show tickets, and will NOT be allowed to register for guests or to attend any technical sessions. They can only register on-site on either Saturday, November 1, or Sunday, November 2, 2008.
- As indicated in the table above, ***students*** are required to show their valid identifications (IDs) to the registration desks to qualify for the student rates and get any registration materialS.

Online Registration Link:

Important: Because all registration materials will be prearranged sequentially according to your ***Registration Number*** (i.e., the PIN number such as "IEEEIUS-398" in your automatic reply email when you register), to speed up the process for picking up the registration materials, please bring this number with you to the conference.

Online Conference Registration of the 2008 IEEE IUS:
https://www.yesevents.com/ius/account.asp
Questions on Registration: Phone: (800)937-8728;
Fax: (410)559-2217; Email: *2008IEEEIUS@yesevents.com*

Onsite Registration Date and Time:

Date	Beijing Time
Saturday, Nov. 1, 2008:	***6:00 p.m. - 9:00 p.m.***
Sunday, Nov. 2, 2008:	***7:00 a.m. - 7:00 p.m.***
Monday, Nov. 3, 2008:	***7:00 a.m. - 6:00 p.m.***
Tuesday, Nov. 4, 2008:	***7:00 a.m. - 5:30 p.m.***
Wednesday, Nov. 5, 2008:	***7:00 a.m. - 1:00 p.m.***

On-site Registration Procedure (at the 2nd floor of BICC):

- The on-site registration window is from Saturday, November 1, to Wednesday, November 5, 2008, Beijing Time. During this window, the online registration system (see the "Online Registration Link" above) will allow "***Pay Cash On-Site***" option, in addition to paying with credit cards.
- During the on-site registration hours shown in the table below, all attendees should register through computers that have dedicated internet connections at the registration desks or computers of their own via the "Online Registration Link"

above to enter their personal data and order items such as short courses and additional DVD proceedings. The registration desks will only collect cash and/or distribute registration materials such as badges and tickets according to your registration items. Please make sure that your personal information entered is accurate because it will be used to send DVD proceedings to you.

- After personal data have been entered online, registration fees can be paid in Chinese Yuans (RMB) at the then prevailing exchange rates to the registration desks, or paid by a Visa, MasterCard, or American Express via on-line kiosks (computers) at the registration desks through the "Online Registration Link" above.
- Students are required to show their valid identifications (IDs) to the registration desks to qualify for the student rates and get registration materials.
- Life IEEE Members are required to show their Life IEEE Member Cards or evidence of Life Members to the registration desks to get registration materials.
- **Short Courses Only** registrants can only register on-site on either Saturday, November 1, or Sunday, November 2, 2008. These attendees will NOT receive a badge or any conference materials such as books and meal/show tickets, and will NOT be allowed to register for guests or to attend any technical sessions.
- Please check the "Notes" above for additional registration information.

PDF Registration Form (via Fax or Mail):

Please check "Conference Registration" link at the conference website for details of registering via fax or regular mail at: http://ewh.ieee.org/conf/ius_2008.

Registration Cancellation and Refund Policy:

Please check "Conference Registration" link at the conference website for details of the cancellation policy at: http://ewh.ieee.org/conf/ius_2008.

Visa Application

Obtaining Visa Application Document (Formal Letter of Invitation):

Nationals from many countries including those from the United States of America need a visa to enter the People's Republic of China. A formal Letter of Invitation recognized by the Chinese Government is required when applying for visa. The deadline for requesting the Letter of Invitation is ***September 30, 2008***, after which a timely deliver of the letter is not guaranteed.

The Letter of Invitation is handled by the China International Conference Center for Science and Technology (CICCST). The CICCST Contact Information is as follows: Phone/Fax: 011-86-10-82116226; Email: *bjsjcenter@sina.com*.

Please check the "Visa Application" link at the conference website for the procedures to get the Letter of Invitation and for advices on applying for visa at: http://ewh.ieee.org/conf/ius_2008.

Conference Hotels

Introduction:

The 2008 IEEE International Ultrasonics Symposium has contracted with the China International Conference Center for Science and Technology (CICCST) to secure discount rates for a group of 7 hotels. The deadline to book the hotel rooms is ***September 15, 2008***, after which the rate will not be guaranteed. The number of rooms in each hotel is limited and will be booked on the "first come first serve" principle.

Please check the "Conference Hotels" link at the conference website for the procedures of booking a hotel room at: http://ewh.ieee.org/conf/ius_2008. The CICCST Contact Information is as follows: Phone/Fax: 011-86-10-82116226; Email: *bjsjcenter@sina.com*.

Table of Hotels:

Hotel Names (and Walking Time)	Prices	Deadlines
Continental Grand Hotel (4-star) (Connected to BICC):	Standard: *RMB 828 ** Suite: *RMB 1,188*	*September 15, 2008*
Crowne Plaza Hotel Park View Wuzhou (5-star) (5 minutes):	Standard: *RMB 1,500* Luxury: *RMB 1,700*	*September 15, 2008*
Grand Skylight Catic Plaza Hotel (4-star) (8 minutes):	Standard: *RMB 1,050* Suite: *RMB 1,250*	*September 15, 2008*
Beijing Ao You Hotel (3-star) (10 minutes):	Single: *RMB 350* Standard: *RMB 500* Suite: *RMB 800*	*September 15, 2008*
Ya Yun Cun Hotel (3-Star) (12 minutes):	Standard: *RMB 380* Suite: *RMB 480*	*September 15, 2008*
Celebrity International Grand Hotel (5-Star) (18 minutes):	Standard: *RMB 950* Suite: *RMB 1,100*	*September 15, 2008*
Beijing Tibet Hotel (3-Star) (18 minutes):	Standard: *RMB 650* New Part: *RMB 750*	*September 15, 2008*

- "*" "RMB" means Chinese Yuan (CNY). The currency exchange rates will be determined at the time of transactions. To get a rough idea of the exchange rates of Chinese Yuan, one could check at http://www.x-rates.com/d/CNY/table.html.
- The prices in the table include ***one breakfast*** and ***all taxes***. Special services such as laundry, room services, and mini-bars are the responsibilities of attendees.
- Please notice that the tap water in China is not drinkable. Please drink water only from boiled thermal bottles, designated drinking buckets, or bottle water.

Location of Hotels on Maps:

The maps that show the location of the hotels can be downloaded via the "Conference Hotels" link at the conference website: http://ewh.ieee.org/conf/ius_2008.

Notes for Taxi Drivers:

The English-Chinese translation of the hotel address for each of the 7 hotels above can be downloaded via the "Taxi / Bus Help" link at the conference website: http://ewh.ieee.org/conf/ius_2008.

Nearby Shopping and Food

Shopping and Food:

Beijing has more than 100 shopping centers. One of them is the North Star Shopping Center that is located near BICC. There are also many native Chinese restaurants in walking distances from BICC.

Please follow the "Nearby Shopping / Food" link at the conference website to obtain maps to locate the Shopping Center and food streets at: http://ewh.ieee.org/conf/ius_2008.

Local Transportation

Transportation from Airport to Conference Hotels:

It is relatively inexpensive to travel by taxi in Beijing. In May 2008, it costs about RMB 70 (about $10.30 USD) from the Airport to the Beijing International Convention Center (BICC) (about 24 km). By the time of our conference, subway will be an option to go from the Airport to BICC via two transfers. The cost of subway in May 2008 was RMB 2 (about $0.30 USD) for one-way trip.

There may be shuttle buses to various hotels from the airport. Please check the "Taxi / Bus Help" link at the conference website for more information: http://ewh.ieee.org/conf/ius_2008.

Going to the Center of Beijing:

Although taxi in Beijing is a convenient way for transportation, to avoid traffic jams, it is advised to take subways to the center of Beijing. A subway stop will be built for the Beijing Olympics and it will be in a short walking distance from BICC. For details, please check the "Beijing City / Subway Maps" link at the conference website: http://ewh.ieee.org/conf/ius_2008.

Beijing City and Subway Maps:

Electronic version of Beijing city maps can be downloaded through the link, "Beijing City / Subway Maps", at the conference website: http://ewh.ieee.org/conf/ius_2008. At the following websites, one can get subway maps too: http://www.chinahighlights.com/beijing/map/beijing-subway-map.htm and http://www.beijing-visitor.com/map-of-beijing-subway.htm

Cheaper Air Tickets

Airport Code:

Beijing has only one commercial airport. The airport code is PEK.

Tips to Get Cheaper Air Tickets:

Some tips to get cheaper air tickets are given in the link, "Cheaper Air Tickets", at the conference website: http://ewh.ieee.org/conf/ius_2008.

Beijing Weather

Weather and Coats:

In early November, Beijing is dry (average of 0.45 in precipitation) and shows a continental weather pattern. It will be relatively warm (average around 58° F or 14° C) during the day and cold (average around 38° F or 3° C) after sunset. Thus, a warm jacket may be needed at night if you go outside.

Please follow the "Beijing Weather" link at the conference website for more information: http://ewh.ieee.org/conf/ius_2008.

Monday Lunch

Lunch at Monday Noon:

A lunch from 12:00 noon - 2:00 p.m. on Monday, November 3, 2008, will be provided by the 2008 IEEE International Ultrasonics Symposium for all registered conference attendees (including all guests and exhibitors, but not for those who only register for short courses). The lunch will provide an additional networking opportunity for all conference attendees while they enjoy the Chinese food. The lunch will be held in Convention Hall #1 of the Beijing International Convention Center (BICC). Cash bars will be provided for drinks.

Note: A lunch ticket will be issued and is required for the lunch. Thus, it is advised to keep the ticket with your badge (insert it in the back of the badge) to avoid misplacing or losing it.

Monday Evening Buffet / Social

Monday Evening Buffet Dinner:

A Chinese buffet dinner for social networking will be provided by the 2008 IEEE International Ultrasonics Symposium from 6:30 p.m. - 10:00 p.m. on Monday, November 3, 2008, for all registered conference attendees (including all guests and exhibitors, but not for those who only register for short courses). The dinner will be held in Convention Hall #1 of the Beijing International Convention Center (BICC). Two free tickets for drinks will be provided for each registrant. Cash bars will be available for additional drinks.

Note: In addition to the drink tickets, a dinner ticket will be issued and required for the dinner. Thus, it is advised to keep the tickets with your badge (insert them in the back of the badge) to avoid misplacing or losing them.

Tuesday Evening Banquet / Shows

Tuesday Banquet Dinner and Traditional Chinese Shows:

A banquet dinner with Chinese food and traditional Chinese shows will be provided by the 2008 IEEE International Ultrasonics Symposium from 6:30 p.m. - 10:00 p.m. on Tuesday, November 4, 2008, to entertain all registered conference attendees (including all guests and exhibitors, but not for those who only register for short courses). The shows will expose conference attendees with traditional Chinese culture. The banquet will be held in the elegant theater-style Convention Hall #1 of the Beijing International Convention Center (BICC). Cash bars will be available for drinks.

Note: A banquet/shows ticket will be issued and required for this event. Thus, it is advised to keep the ticket with your badge (insert it in the back of the badge) to avoid misplacing or losing it.

Photos of some traditional Chinese shows can be viewed through the link "Tuesday Dinner/Shows" on the conference website at: http://ewh.ieee.org/conf/ius_2008.

Beijing Local Guest Tours

Beijing Local Tours Organized by CICCST:

The China International Conference Center for Science and Technology (CICCST) has organized three Beijing local tours from November 3-5, 2008 (one for each day), for guests of attendees during the 2008 IEEE International Ultrasonics Symposium (IUS). CICCST will be fully responsible for these tours and thus both the 2008 IEEE IUS and IEEE are not liable to any accidents or any parts of the tours. Individual tours may be cancelled if there are not enough participants for the tours.

Please follow the "Three Local Guest Tours" link at the conference website for the procedures of booking the tours at: http://ewh.ieee.org/conf/ius_2008.

The CICCST Contact Information is as follows: Phone/Fax: 011-86-10-82116226; Email: *bjsjcenter@sina.com*.

Post-Conference China Tours

Post-Conference China Tours:

There are many commercial companies who provide China tours. Conference attendees could use the key words such as "China Tours" in Google to find a large list of companies who provide such tours.

The China International Conference Center for Science and Technology (CICCST) has organized some China tours for the conference attendees of the 2008 IEEE International Ultrasonics Symposium (IUS). CICCST will be fully responsible for these tours and thus both the 2008 IEEE IUS and IEEE are not liable to any accidents or any parts of the tours. Individual tours may be cancelled if there are not enough participants for the tours.

Please follow the "China Tours" link at the conference website for the procedures of booking the tours at: http://ewh.ieee.org/conf/ius_2008.

The CICCST Contact Information is as follows: Phone/Fax: 011-86-10-82116226; Email: *bjsjcenter@sina.com*.

Other Beijing / China Tours

Other Tours:

There are many commercial companies who provide both Beijing tours and China tours. Conference attendees could use the key words such as "Beijing Tours" or "China Tours" in Google to find a large list of companies who provide such tours.

Some information on other Beijing Tours and China Tours can be found via the links, "Other Beijing Tours" and "China Tours", respectively, from the conference website at: http://ewh.ieee.org/conf/ius_2008.

Guest Breakfasts

Three Guest Breakfasts:

The 2008 IEEE International Ultrasonics Symposium will provide three guest breakfasts (Monday-Wednesday, November 3-5, 2008) for all registered conference guests (admitted with Guest badges). The breakfasts will provide an additional networking opportunity among the guests. Please check the message boards near the conference registration desks to find the room and time of the breakfasts before you go. (Tentatively, the breakfasts are scheduled in the Conference Room 311A on the 3rd floor of BICC.)

Exhibitor Breakfast

Wines and Breakfast for Exhibitors:

In the afternoon of Sunday, November 2, 2008, during the exhibition setup on the 2nd floor foyer of the Beijing International Convention Center (BICC), exhibitors (with exhibitor badges) will be provided a couple of wines by the Organizing Committee for them to enjoy.

In addition, on Wednesday, November 5, from 7:00 a.m. - 8:00 a.m. in the Conference Room 311C (on the third floor of BICC), exhibitors (with exhibitor badges) will be provided a breakfast. The breakfast would be a good opportunity for exhibitors to provide feedbacks to the Organizing Committee to help future IEEE IUS to provide better services for exhibitors.

Please check with the registration desk for any changes of the schedule and rooms before you go to the breakfast. An exhibit badge is required to join the breakfast.

Student Breakfast / Meet with President

Networking Opportunity for Students:

All students (with valid student IDs) attending the 2008 IEEE International Ultrasonics Symposium are invited to attend a complimentary breakfast on ***Tuesday, November 4, 2008, from 7:30 a.m. - 9:00 a.m., in Conference Rooms 311B and 311C*** (3rd floor) (tentatively) of the Beijing International Convention Center (BICC). You can locate the room through the Condensed Program or the Floor Plan at the conference website. The final date, time, and room assignments might change and thus please check with the conference registration desk at BICC to confirm before you go. The breakfast will be a good opportunity for students to directly ask questions to the IEEE UFFC society president, UFFC Society officials, and members of the IEEE UFFC Administrative Committee, as well as for students to network with each other.

Coffee Breaks

Coffee Breaks:

There will be coffee breaks for both short courses on Sunday (November 2, 2008) and for the conference from Monday (November 3, 2008) to Wednesday (November 5, 2008). The schedule and locations of the coffee breaks can be found from either the "Condensed Program" link at the conference website: http://ewh.ieee.org/conf/ius_2008, or sheets near the end of this booklet.

Conference at a Glance Boards

Boards for "Conference at a Glance":

The 2008 IEEE International Ultrasonics Symposium will place two 5 m x 3.5 m boards on the 1st and 2nd floors, respectively, of the Beijing International Convention Center (BICC). These boards will provide attendees information on technical program, floor plan, and poster locations in a single place. To locate the poster board of a particular poster, please use the poster label such as ***P1A024-01***, where "***024***" after ***P1A*** represents the location of the poster.

For detailed description of poster labels, please check the "Poster Presentation Guide" at the conference website for detail: http://ewh.ieee.org/conf/ius_2008.

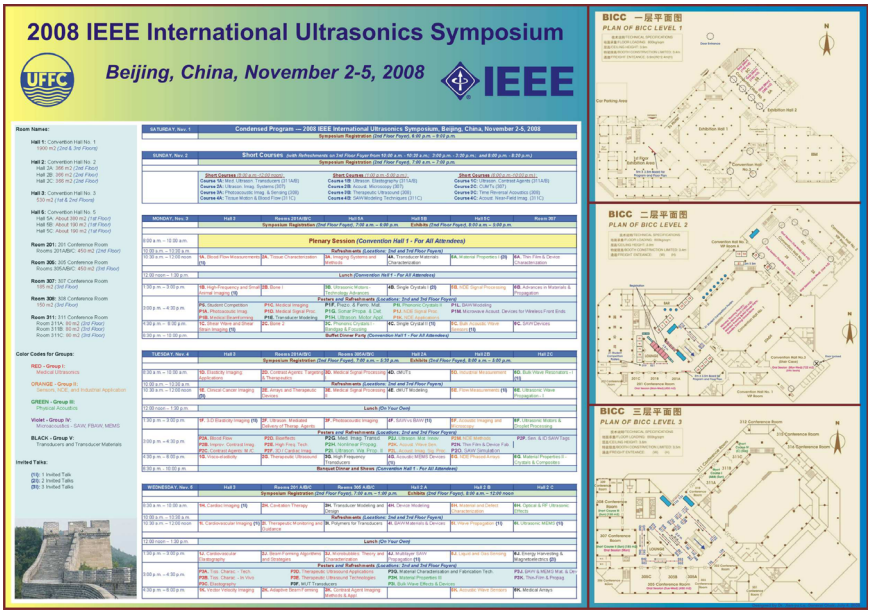

Speaker Ready Room

Speaker Ready Room and Schedule:

The schedule of the ***Speaker Ready*** room (***Conference Room 310***) is as follows:

Saturday, Nov. 1: 2:00 p.m. - 5:00 p.m. (for short courses).
Sunday, Nov. 2: 7:30 a.m. - 12:00 noon; 1:00 p.m. - 5:00 p.m.
Monday-Wednesday (Nov. 3-5): 7:30 a.m. - 5:00 p.m.

Please follow closely the instructions on the "Oral Presentation Guide" at the conference website to prepare your presentation and avoid any technical difficulties of your presentations at: http://ewh.ieee.org/conf/ius_2008.

Oral Presentation Guide

Important Information for Oral Presenters:

The Oral Presentation Guide on the conference website provides detailed instructions, tips to avoid technical difficulties, and good practices for your presentations. It is accessible via the link, "Oral Presentation Guide", at the conference website: http://ewh.ieee.org/conf/ius_2008. It is the responsibility of authors to follow the guide closely.

Poster Presentation Guide

Important Guide for Poster Presenters:

The Poster Presentation Guide on the conference website provides information needed to prepare your presentations. It also gives a detailed description of poster labels and their use in finding the locations of poster boards. The layout of the poster boards is shown on the floor plan near the end of this booklet. Please check the link, "Poster Presentation Guide", at the conference website for details: http://ewh.ieee.org/conf/ius_2008.

Session Chairs / Session Summary Form

Duties of Session Chairs:

Duties of session chairs of both oral and poster sessions can be viewed on the conference website via the link "Session Chairs". Session Summary Form is also available from the web at: http://ewh.ieee.org/conf/ius_2008. Session Chairs should fill out the form after each session since any presentations that are not properly presented during the conference will not be included in the conference proceedings. In addition, a list of all session chairs is also on the web.

Message Boards

Message Boards for Attendees:

There will be message boards for attendees near the registration area. Please check the "BICC Floor Plan / Location" link at the conference website or the floor plan at the end of this booklet for details: http://ewh.ieee.org/conf/ius_2008.

Wired and Wireless Internet Access

Internet Access:

Wireless internet will be available to attendees during the conference in the 2nd and 3rd floor foyers of the Beijing International Convention Center (BICC). Tables and chairs will be available on the 2nd floor foyer of BICC for attendees to place their laptops. There will also be a designated internet café that allows attendees to connect Ethernet cables to their computers or use internet-ready conference computers in Conference Room 303 at the third floor of BICC. Since only a few computers are available in the internet café, there may be lines if many people need to use them.

Policy on Photography / Recording

Photography or Recording:

To respect the privacy of presenters and minimize interruptions to the conference, photography and sound recording are not allowed in any technical sessions (both oral and poster) except the plenary session.

Meeting Planner

Individual Meeting Planner:

To individualize the program of the conference, one could use the Meeting Planner that is accessible via the "Meeting Planner" link at the conference website: http://ewh.ieee.org/conf/ius_2008.

Program and Abstract Books

Extra Copies of Program and Abstract Books:

Except for guest registration and registration for Short Course Only, each attendee will receive a print copy of this Program book and an Abstract book. If attendees need additional copies of these books, they could purchase them from the registration desks near the end of the conference in the morning of Wednesday, November 5, 2008. This will ensure that newly registered attendees can get the books first. (To reduce costs, the total number of books printed is limited.)

Electronic Copies of Books:

Electronic copies of both the Program and Abstract books are on the conference website through the links, "Full Program" and "Abstract Book", respectively, at: http://ewh.ieee.org/conf/ius_2008. The electronic copies contain full colors while the printed books do not.

Conference Proceedings

Context-Sensitive Multimedia DVD Proceedings:

This will be the first year that the IEEE International Ultrasonics Symposium produces context-sensitive multimedia DVD proceedings, based on the experiences of our context-sensitive multimedia IEEE Transactions on Ultrasonics, Ferroelectrics, and Frequency Control (TUFFC). To prepare and submit proceedings papers, please follow the link, "Paper Submission" from the conference website at: http://ewh.ieee.org/conf/ius_2008.

Print Copy of the Proceedings:

The 2008 IEEE International Ultrasonics Symposium will not provide a print version of the conference proceedings. Attendees who need such proceedings can order them directly from IEEE after the DVD proceedings are produced.

Proceedings Paper Submission Deadline:

The submission deadline of proceedings papers is ***Midnight, Sunday, November 2, 2008*****, Beijing Time,** which is earlier than that of previous years. Please notice that the deadline is firm to ensure a timely publication of the proceedings.

Important Note:

Because the conference proceedings are a record of the conference papers that are actually presented, to have your paper included (published) in the proceedings, you must present AND defend the paper during the conference by yourself or by someone who is knowledgeable of the presentation subject and is designated by you.

Technical Program Committee

Technical Program Committee (Total 136 Members):

The Technical Program Committee (TPC) of the 2008 IEEE International Ultrasonics Symposium is as follows:

Group 1: Medical Ultrasonics:

Vice Chair of TPC:
Stanislav Emelianov, Ph.D.
University of Texas at Austin
Austin, Texas, U.S.A.

Members:

1. **Olivier Basset:** *CREATIS, Université Lyon I, France*
2. **Geneviève Berger:** *National Centre for Scientific Research (CNRS), France*

3. **Ayache Bouakaz:** *INSERM, Université Tours, France*
4. **Charles Cain:** *University of Michigan, USA*
5. **Richard Chiao:** *Siemens Medical Solutions, USA*
6. **Jan D'hooge:** *Catholic University Leuven, Belgium*
7. **Paul Dayton:** *UNC Chapel Hill and NC State University, USA*
8. **Emad Ebbini:** *University of Minnesota, USA*
9. **David Evans:** *University of Leicester, UK*
10. **Kathy Ferrara:** *University of California Davis, USA*
11. **Stuart Foster:** *University of Toronto, Canada*
12. **James Greenleaf:** *Mayo Clinic College of Medicine, USA*
13. **Anne Hall:** *General Electric Medical Systems, USA*
14. **Christopher Hall:** *Philips Research North America, USA*
15. **Peter Hoskins:** *The University of Edinburgh, UK*
16. **John Hossack:** *University of Virginia, USA*
17. **Kullervo Hynynen:** *University of Toronto, Canada*
18. **Michael F. Insana:** *University of Illinois, Urbana-Champaign, USA*
19. **Jorgen Jensen:** *Technical University of Denmark, Denmark*
20. **Nico de Jong:** *Erasmus Medical Centre and University of Twente, The Netherlands*
21. **Hiroshi Kanai:** *Tohoku University, Japan*
22. **Jeff Ketterling:** *Riverside Research Institute, USA*
23. **Michael Kolios:** *Ryerson University, Canada*
24. **Chris de Korte:** *Radboud University Nijmegen Medical Centre, The Netherlands*
25. **Nobuki Kudo:** *Hokkaido University, Japan*
26. **Pai-Chi Li:** *National Taiwan University, Taipei, Taiwan*
27. **Jian-yu Lu:** *University of Toledo, USA*
28. **Leonardo Masotti:** *Università degli Studi di Firenze, Italy*
29. **Tom Matula:** *University of Washington, USA*
30. **James G. Miller:** *Washington University in Saint Louis, USA*
31. **Kathy Nightingale:** *Duke University, USA*
32. **William O'Brien:** *University of Illinois, Urbana-Champaign, USA*
33. **Georg Schmitz:** *Ruhr-Universität Bochum, Germany*
34. **Ralf Seip:** *Philips Research North America, USA*
35. **Mickael Tanter:** *Laboratoire Ondes et Acoustique, ESPCI, France*
36. **Tom Thomas:** *Boston Scientific, Inc., USA*
37. **Kai Thomenius:** *General Electric's Corporate R&D, USA*
38. **Hans Torp:** *Norwegian University of Science and Technology, Norway*
39. **Piero Tortoli:** *Università degli Studi di Firenze, Italy*
40. **Ton van der Steen:** *Erasmus Medical Center, The Netherlands*
41. **Keith Wear:** *US Food and Drug Administration, USA*

Group 2: Sensors, NDE, and Industrial Application:

Vice Chair of TPC:
Jafar Saniie, Ph.D.
Illinois Institute of Technology
Chicago, Illinois, U.S.A.

Members:

1. **Robert C. Addison:** *Rockwell Science Center, USA*
2. **Walter Arnold:** *Fraunhofer Institute for Nondestructive Testing, Germany*
3. **Nihat Bilgutay:** *Drexel University, USA*

4. **Ramazan Demirli:** *Canfield Scientific, USA*
5. **Eric S. Furgason:** *Purdue University, USA*
6. **David Greve:** *Carnegie Mellon University, USA*
7. **Edward Haeggstrom:** *University of Helsinki, Finland*
8. **Jacqueline Hines:** *Applied Sensor Research and Development Corporation, USA*
9. **Fabien J. Josse:** *Marquette University, USA*
10. **Lawrence W. Kessler:** *Sonoscan Inc., USA*
11. **Pierre T. Khuri-Yakub:** *Stanford University, USA*
12. **Mario Kupnik:** *Stanford University, USA*
13. **Jun-ishi Kushibike:** *Tohoku University, Japan*
14. **Roman Maev:** *University of Windsor, Canada*
15. **Kentaro Nakamura:** *Tokyo Institute of Technology*
16. **Massimo Pappalardo:** *University di Roma TRE, Italy*
17. **Tony Sinclair:** *University of Toronto, Canada*
18. **Bernhard Tittman:** *Pennsylvania State University, USA*
19. **Jiromaru Tsujino:** *Kanagawa University, Japan*
20. **John F. Vetelino:** *University of Maine, USA*
21. **Paul Wilcox:** *University of Bristol, UK*
22. **Donald E. Yuhas:** *Industrial Measurement Systems, Inc., USA*

Group 3: Physical Acoustics:

Vice Chair of TPC:

Yook-Kong Yong, Ph.D.
Rutgers University
Piscataway, New Jersey, U.S.A.

Members:

1. **Robert Aigner:** *TriQuint Semiconductor, USA*
2. **Art Ballato:** *U.S. Army, USA*
3. **Jan Brown:** *JB Consulting, USA*
4. **Weiqiu Chen:** *Zhejiang University, China*
5. **David Hecht:** *DLH Consulting, USA*
6. **Fred Hickernell:** *Retired from Motorola, USA*
7. **Yonkee Kim:** *U.S. Army, USA*
8. **Amit Lal:** *Cornell University, USA*
9. **C.S. Lam:** *Epson Electronics America, Inc., USA*
10. **John Larson:** *Avago Technologies, USA*
11. **Moises Levy:** *Department of Physics, Naples, Florida, USA*
12. **George Mansfeld:** *Russian Academy of Sciences, Russia*
13. **Vitold Poghar:** *Scientific and Technological Center of Unique Instrumentation of Russian Academy of Science, Russia*
14. **Valeri Proklov:** *Institute of Radio Engineering & Electricity, Russia*
15. **Edgar Schmidhammer:** *EPCOS, Germany*
16. **Susan Schneider:** *Marquette University, USA*
17. **Bikash Sinha:** *Schlumberger-Doll Research, USA*
18. **Ji Wang:** *Ningbo University, China*
19. **Qing-Ming Wang:** *University of Pittsburgh, USA*

Group 4: Microacoustics - SAW, FBAW, MEMS:

Vice Chair of TPC:
Peter Smith, Ph.D.
McMaster University
Hamilton, Ontario, Canada

Members:

1. **Sylvain Ballandras:** *LPMO, France*
2. **Kushal Bhattacharjee:** *RF Micro Devices, USA*
3. **Sergey Biryukov:** *Leibniz Institute for Solid State and Materials Research Dresden (IFW), Germany*
4. **Jidong Dai:** *RF Monolithics, USA*
5. **Yasuo Ebata:** *Fujitsu Media Device Ltd., Japan*
6. **Gernot Fattinger:** *Sawtek, USA*
7. **Ken-ya Hashimoto:** *Chiba University, Japan*
8. **Daniel Hauden:** *CNRS_LPMO, France*
9. **Mitsutaka Hikita:** *Kogakuin University, Japan*
10. **Chunyun Jian:** *Nortel Networks, Canada*
11. **Jyrki Kaitila:** *Infineon, Germany*
12. **Jan Kuypers:** *University of California, USA*
13. **Ken Lakin:** *TFR Technologies, USA*
14. **Don Malocha:** *University of Central Florida, USA*
15. **David Morgan:** *Impulse Consulting, UK*
16. **Hiroyuki Odagawa:** *Tohoku University, Japan*
17. **Mauricio Pereira da Cunha:** *University of Maine, USA*
18. **Viktor Plessky:** *GVR Trade SA, Switzerland*
19. **Bob Potter:** *Vectron International, USA*
20. **Leonard Reindl:** *Albert-Ludwigs-University Freiburg, Germany*
21. **Arne Ronnekleiv:** *Norwegian Institute of Technology, Norway*
22. **Richard Ruby:** *Avago Tech, USA*
23. **Clemens Ruppel:** *EPCOS AG - SAW RD SAM, Germany*
24. **Takahiro Sato:** *Samsung, Japan*
25. **Marc Solal:** *Sawtek, USA*
26. **Robert Weigel:** *Friedrich-Alexander University, Germany*

Group 5: Transducers and Transducer Materials:

Vice Chair of TPC:
Scott Smith, Ph.D.
GE Global Research
Niskayuna, New York, U.S.A.

Members:

1. **Sandy Cochran:** *University of Dundee, UK*
2. **Christopher Daft:** *Siemens Medical Solutions, USA*
3. **Levent Degertekin:** *Georgia Institute of Technology, USA*
4. **Charles Emery:** *Mirabilis Medica, USA*
5. **John Fraser:** *Philips Medical Systems, USA*
6. **Jean-Francois Gelly:** *GE Healthcare, France*

7. **Reinhard Lerch:** *Friedrich-Alexander-Universität Erlangen-Nuremberg, Germany*
8. **Geoff Lockwood:** *Queen's University, Canada*
9. **Clyde Oakley:** *W. L. Gore, USA*
10. **Omer Oralkan:** *Stanford University, USA*
11. **Paul Reynolds:** *Weidlinger Associates, USA*
12. **Yongrae Roh:** *Kyungpook National University, Korea*
13. **Ahmad Safari:** *Rutgers University, USA*
14. **Mark Schafer:** *Sonic Tech Inc., USA*
15. **Thomas Shrout:** *Pennsylvania State University, USA*
16. **Kirk Shung:** *University of Southern California, USA*
17. **Stephen Smith:** *Duke University, USA*
18. **Wallace Smith:** *Office of Naval Research, USA*
19. **Yasuhito Takeuchi:** *Kagoshima University, Japan*
20. **Vasandara Varadan:** *University of Arkansas, USA*
21. **Jian Yuan:** *Boston Scientific, USA*
22. **Qiming Zhang:** *Pennsylvania State University, USA*
23. **Qifa Zhou:** *University of Southern California, USA*

Invited Speakers

Invited Talks (21 in Total):

Please click on the links to jump to the abstracts on web:

Group 1: Medical Ultrasonics:

- Talk #1.1 (1I-3): ***Jan D'hooge (Presenter)***, *Piet Claus, Jens-Uwe Voigt, and Frank Rademakers*, **"Functional imaging of the heart,"** Department of Cardiovascular diseases, Catholic University of Leuven, Leuven, Belgium. (Abstract ID: 1185)
- Talk #1.2 (1C-5): ***Mathias Fink (Presenter)***, *Mickael Tanter, **Jeremy Bercoff, and **Jacques Souquet*, **"Supersonic Shear Wave Elasticity Imaging,"** *ESPCI, Laboratoire Ondes et Acoustique, Paris, France. **Supersonic Imagine, Aix en Provence, France. (Abstract ID: 908)
- Talk #1.3 (1B-3): ***F. Stuart Foster***, **"Micro-ultrasound Takes Off (In the Biological Sciences),"** Imaging Research, Sunnybrook Health Sciences Centre and University of Toronto, Toronto, Ontario, Canada. (Abstract ID: 590)
- Talk #1.4 (1H-3): ***Hiroshi Kanai (Presenter)***, **Junya Ohkohchi, and **Hideyuki Hasegawa*, **"Ultrasonic Imaging of 3-Dimensional Propagation of Electric Excitation and Vibrations in Human Heart,"** *Department of Electronic Engineering, Tohoku University, Sendai, Miyagi, Japan. **Graduate School of Biomedical Engineering, Tohoku University, Sendai, Miyagi, Japan. (Abstract ID: 36)
- Talk #1.5 (1F-5): ***Richard Prager (Presenter)***, *Andrew Gee, Graham Treece, Joel Lindop, and Nick Kingsbury*, **"Deconvolution and elastography based on 3D ultrasound,"** Department of Engineering, University of Cambridge, United Kingdom. (Abstract ID: 111)
- Talk #1.6 (1A-1): ***Hairong Zheng (Presenter)*** *and **Robin Shandas*, **"Ultrasound Particle Velocimetry: an Emerging Technique in Cardiology,"**

*Shenzhen Institute of Advanced Technology, Chinese Academy of Sciences, Shenzhen, Guangdong, China. **University of Colorado at Boulder, Boulder, CO, USA. (Abstract ID: 1178)

Group 2: Sensors, NDE, and Industrial Application:

- Talk #2.1 (5E-1): ***Saul Jacobson***, **"New Developments in Ultrasonic Gas Analysis and Flowmetering,"** 403 Huon Road, TAS 7004, Australia. (Abstract ID: 1017)
- Talk #2.2 (5I-1): ***Claire Prada (Presenter)*** *and Mathias Fink*, **"Invariants of the time reversal operator and ultrasonic applications,"** Laboratoire Ondes et Acoustique, CNRS, Université Paris 7, ESPCI, Paris, France. (Abstract ID: 1187)
- Talk #2.3 (5C-1): ***Michael Thompson (Presenter)*** *and **Scott Ballantyne*, **"Ultra High Frequency Acoustic Wave Detection of HIV Antibody,"** *Chemistry, University of Toronto, Toronto, Ontario, Canada. **Maple Biosciences, Toronto, Ontario, Canada. (Abstract ID: 130)

Group 3: Physical Acoustics:

- Talk #3.1 (6I-1): ***Eun Kim***, **"Piezoelectric MEMS for Audio Signal Transduction, Microfluidic Management, Resonant Mass Sensing, and Movable Surface Micromachined Structures,"** Electrical Engineering - Electrophysics, University of Southern California, Los Angeles, CA, USA. (Abstract ID: 647)
- Talk #3.2 (5A-4): *Bikash Sinha and ***Vivian Pistre (Presenter)***, **"Applications of Sonic Waves in the Estimation of Petrophysical, Geophysical and Geomechanical Properties of Subsurface Rocks,"** *Mathematics and Modeling, Schlumberger-Doll Research, Cambridge, MA, USA. **Well Placement and Safety, Schlumberger Beijing Geoscience Centre, Beijing, China. (Abstract ID: 304)
- Talk #3.3 (5A-3): ***Yue-Sheng Wang***, **"Interfacial Waves and Stability at the Frictional Sliding Interface between Two Solids,"** Institute of Engineering Mechanics, Beijing jiaotong University, Beijing, China. (Abstract ID: 1177)
- Talk #3.4 (6D-1): ***Yook-Kong Yong (Presenter)***, *Mihir Patel, and **Masako Tanaka*, **"Theory, and Experimental Verifications of the Resonator Q and Equivalent Electrical Parameters due to Viscoelastic, Conductivity and Mounting Supports Losses,"** *Civil and Environmental Engineering, Rutgers University, Piscataway, New Jersey, USA. **Epson Toyocom, Japan. (Abstract ID: 258)

Group 4: Microacoustics – SAW, FBAR, MEMS:

- Talk #4.1 (4F-1): ***Robert Aigner***, **"SAW and BAW Technologies for RF Filter Applications: A Review of the Relative Strengths and Weaknesses,"** TriQuint Semiconductor, Apopka, Florida, USA. (Abstract ID: 405)
- Talk #4.2 (4J-1): ***Ken-ya Hashimoto (Presenter)***, *Yiliu Wang, *Tatsuya Omori, *Masatsune Yamaguchi, **Michio Kadota, **Hajime Kando, and **Teruhisa Shibahara*, **"Piezoelectric Boundary Wave Devices: Their Underlying Physics and Applications,"** *Dept. EEE, Chiba University, Chiba, Chiba, Japan. **Murata MFG, Co. Ltd., Yasu, Shiga, Japan. (Abstract ID: 21)

- Talk #4.3 (4G-1): ***C.S. Lam***, **"A Review of the Recent Development of MEMS and Crystal Oscillators and Their Impacts on the Frequency Control Products Industry,"** Integrated Device Technology, Inc., Andover, MA, USA. (Abstract ID: 407)

Group 5: Transducers and Transducer Materials:

- Talk #5.1 (4B-1): *Sung-Min Lee, Dong-Ho Kim, and* ***Ho-Yong Lee (Presenter)***, **"PMN-PZT Single Crystals and Composites for Transducer Applications,"** Ceracomp Co., Ltd., Sunmoon University, Asan, Chungnam, South Korea. (Abstract ID: 326)
- Talk #5.2 (4B-4): *Dan Zhou and* ***Haosu Luo (Presenter)***, **"Vibration Mode and Relevant Ultrasonic Applications of Ferroelectric Single Crystals Pb(Mg1/3Nb2/3)O3-PbTiO3,"** Shanghai Institute of Ceramics, CAS, Shanghai, China. (Abstract ID: 877)
- Talk #5.3 (4C-1): ***Wei Ren (Presenter)**, *Peng Lin, *Zheng Wang, *Xiaoqing Wu, *Peng Shi, *Xi Yao, **Qifa Zhou, **Dawei Wu, **Benpeng Zhu, and **K. Kirk Shung*, **"Piezoelectric Thin and Thick Films for Transducer Applications,"** *Electronic Materials Research Laboratory, Xi'an Jiaotong University, Xi'an, Shanxi, China. **NIH Transducer Resource Center and Department of Biomedical Engineering, University of Southern California, Los Angeles, CA 90089, USA. (Abstract ID: 723)
- Talk #5.4 (6J-3): ***Stewart Sherrit***, **"The Physical Acoustics of Energy Harvesting,"** Advanced Technologies Group, Instrument Mechanical Engineering Section, Jet Propulsion Laboratory, Pasadena, CA, USA. (Abstract ID: 90)
- Talk #5.5 (6J-4): ***Orest G. Symko (Presenter)*** *and Myra Flitcroft*, **"Ultrasonic Thermoacoustic Energy Conversion,"** Department of Physics, University of Utah, Salt Lake City, Utah, USA. (Abstract ID: 1181)

Invited Clinical Session Speakers

Invited Clinical Session Speakers:

The 2008 IEEE International Ultrasonics Symposium has included a special clinical session to show how medical ultrasound technologies are used in clinical practices. This special session consists of the following half-hour invited presentations. Please click on the links below to jump directly to the abstracts. (Note: This session is organized by Dr. Stuart Foster, University of Toronto, Canada.)

- Talk #1 (1E-1): ***Peter Burns***, **"Making Microbubbles Work for Ultrasound: Technical and Broader Challenges,"** Dept Medical Biophysics, University of Toronto, Toronto, ON, Canada. (Abstract ID: 957)
- Talk #2 (1E-3): ***Yuxin Jiang***, **"The Clinical Application of Ultrasound Contrast Imaging,"** Department of Diagnostic Ultrasound, Pekin Union Medical College Hospital, Beijing, China. (Abstract ID: 836)
- Talk #3 (1E-2): ***Stephanie Wilson***, **"The Role of Contrast Enhanced Ultrasound (CEUS) in Oncology,"** Department of Diagnostic Imaging, Foothills Medical Centre, Calgary AB, Canada. (Abstract ID: 1189)

Talk #1:

Title: Making Microbubbles Work for Ultrasound: Technical and Broader Challenges

Peter Burns, Dept Medical Biophysics, University of Toronto, Toronto, ON, Canada.

Abstract:

Background, Motivation and Objective: Although it has been 10 years since microbubble contrast agents were first approved for clinical use, adoption has been slow, in spite of considerable technical advances and many successful clinical studies.

Statement of Contribution/Methods: Methods for contrast specific imaging exploit the nonlinear response of bubbles at or near resonant excitation. Simple filtering for higher harmonics has given way to broadband methods using phase and/or amplitude modulation of a sequence of pulses. With suitable detection methods, linear, nonlinear, moving and stationary targets can all be segmented from the echo and shown in real time. The tendency of bubbles to disrupt at low peak negative pressures also offers a potential role for coded excitation on transmit. Deliberate disruption of bubbles with a few high MI pulses can clear the image plane and allow measurement of its replenishment by contrast offering a unique way to quantify microvascular flow and perfusion volume.

Results: At least 3 million clinical contrast studies have been performed: safety and tolerability have proven excellent. Clinical applications have focused on areas in which ultrasound already plays an important diagnostic role. In cardiology, contrast can aid visualisation of the endocardium, especially important in wall motion studies, and has been shown to improve the accuracy of stress echo. It can also image and measure myocardial perfusion in real time, at rest and with stress, with spatial resolution superior to the current nuclear medicine standard, SPECT. In radiology, perfusion can be imaged in many organs, but work has concentrated on the liver, where contrast can help characterise focal lesions with an accuracy comparable to contrast CT and MRI. It also aids in lesion detection, in real time guidance of interventions such as RF ablation and in monitoring response to tumor therapy, especially using the new antiangiogenic agents.

Discussion and Conclusions: In spite of demonstrated efficacy and safety, widespread adoption into the clinic has been slow. Two reasons are proposed. First, although bubbles are approved for perfusion imaging in more than 60 countries, the US, which has approved no radiology indications, is not among them. Second, while contrast ultrasound is often less expensive than competing modalities, physician reimbursement may be less too, dampening enthusiasm among practitioners. We conclude that future clinical studies should focus on applications unique to microbubbles, exploiting, for example, their confinement to the blood pool and the ability to image them in real time. Approval of a perfusion indication by the US FDA is crucial. Widely available, robust contrast specific imaging modes are needed. The intriguing capacity of bubbles to potentiate therapies, including drug delivery, should be pursued. For diagnosis, translation of microbubble contrast applications to clinical practice may come more quickly in cost driven rather than profit-driven healthcare systems.

Dr. Peter Burns is Professor and Chairman of Medical Biophysics and Professor of Radiology at the University of Toronto and Senior Scientist at Sunnybrook Health

Sciences Centre, Toronto. He received his degree in Mathematical Physics in 1973 and, following a postgraduate fellowship in History and Philosophy of Science, a PhD in Radiodiagnosis in 1983. He subsequently held faculty positions in Radiology at Yale University and Thomas Jefferson University in Philadelphia. He moved to Toronto in 1991. He was part early efforts to detect flow in small blood vessels with Doppler, including the first ultrasonic detection of tumor blood flow. He subsequently worked on Doppler methods for flow detection and hemodynamic measurement in the abdomen and pelvis. In 1988 he began research with microbubbles as ultrasound contrast agents, focusing on the development of nonlinear methods such as harmonic, pulse inversion and amplitude modulation imaging as well as their clinical applications in perfusion imaging of the heart, abdomen and tumors. He has published more than 130 papers, 4 books and holds several patents in diagnostic ultrasound. He received the World Federation of Ultrasound in Medicine and Biology Pioneer Award (1988); the Ian Donald Gold Medal for Technical Achievement (2002); Innovation and Excellence Trophy of the Société Canadienne de Radiologie (2002), was the Euroson Lecturer of the European Society for Ultrasound in Medicine (2005); the Donald McVicar and Brown Lecturer of British Medical Ultrasound Society (2006) and is the IEEE Ultrasonics, Ferroelectrics, and Frequency Control Society Distinguished Lecturer for 2008.

Talk #2:

Title: The Clinical Application of Ultrasound Contrast Imaging

Yuxin Jiang, Department of Diagnostic Ultrasound, Pekin Union Medical College Hospital, Beijing, China.

Abstract:

Background, Motivation and Objective: Contrast-enhanced ultrasound imaging is the area of greatest interest in ultrasound medicine currently. The recent improvements of contrast agent and the contrast specific scanning techniques have given new possibilities for the further research and clinical application. We are having researches in the basic theory study and further clinical applications in China, so that ultrasound contrast imaging can be better recognized and widely applied in the clinical practice.

Statement of Contribution/Methods: The introduction of second-generation microbubble contrast agents, such as SonoVue and self-made perfluorocarbon ultrasound contrast agent, and the advent of specialized imaging techniques enabled real-time contrast-enhanced imaging. In our study, Sonovue and the gray scale harmonic imaging technique were adopted to evaluate the characteristic contrast enhanced pattern of liver, kidney, gynecology, breast and thyroid lesions, etc.

Results: Our clinical research shows that contrast enhanced ultrasounographic imaging can improve the diagnostic potential of sonographic examinations in different clinical applications, including the better observation of small vessels, the real-time assessment of the blood perfusion pattern in an organ or area of interest, with a significantly higher detection rate and diagnostic accuracy especially for the tumor of liver, kidney and gynecology. Otherwise, contrast enhanced ultrasound imaging holds the potential for a better visualization and diagnosis of peripheral vascular and some deep-located vessels, such as carotid, brain arteries and renal arteries, etc. The area of great promise and growth also lies in the clinical research of breast and thyroid.

Discussion and Conclusions: With the fast development and the intrinsic advantages of contrast enhanced ultrasound imaging, it is gaining more and more popularity. Ultrasound doctors should pay efforts to do further research in this state of art technique, which may open a new prospect for the ultrasound medicine.

Dr. Yuxin Jiang is a director of the Department of Diagnostic Ultrasound, Peking Union Medical College Hospital, Beijing, China; Professor of the Chinese Academy of Medical Sciences & Peking Union Medical College in Beijing, China; President of the Society of Ultrasound in Medicine of Chinese Medical Association. Dr. Jiang has lead a team from China to present at ASUM ASM 2006 on topics relating to ultrasound guided therapy, e.g., use of contrast in ultrasound, and various interventional techniques. Dr. Jiang will discuss topics relating to ultrasound guided therapy, e.g., HIFU and Radio Frequency, use of contrast agents in ultrasound, and various interventional techniques now used in China.

Talk #3:

Title: The Role of Contrast Enhanced Ultrasound (CEUS) in Oncology

Stephanie Wilson, Department of Diagnostic Imaging, Foothills Medical Centre, Calgary AB, Canada.

Abstract:

Background, Motivation and Objective: The oncology patient is susceptible to the development of tumor masses in many locations and their detection and diagnosis is usually within the realm of diagnostic imaging. While ultrasound may show tumors, additional imaging with CT and or MR scan is generally required for their confident diagnosis. We address the tremendous contribution of contrast enhanced ultrasound (CEUS) in the imaging of this population.

Statement of Contribution/Methods: Contrast agents for ultrasound are comprised of tiny bubbles of gas in a supporting shell. Their intravenous injection results in tissue perfusion, analogous to that seen on contrast enhanced CT and MR, and also incredible vessel visualization more similar to that seen with angiography. These attributes allow for improved detection and characterization of tumors in many parts of the body.

Results: Characterization of tumors of the liver is the most accepted indication for CEUS where it is complimentary to CT and MR scan. Liver lesion detection and also the difficult question of diagnosis of hepatocellular carcinoma are further accepted strategies for the use of CEUS as the detection of small nodules in the cirrhotic liver on screening sonography is enhanced by the performance of CEUS at the time of nodule detection. Detection of liver masses is also improved by CEUS as the addition of contrast agent increases the conspicuity of liver masses on sonography such that more and smaller masses may be detected than at baseline.

CEUS is also valuable when added to intraoperative liver ultrasound, contributing to management decisions for the patient undergoing surgery. Further, CEUS is a critical component of radiofrequency ablation (RFA) techniques especially when performed at the time of the procedure where it may reduce the requirement for repeat procedures performed for incomplete ablation. CEUS is suitable for monitoring patients with prior RFA or transarterial chemoembolization (TACE).

CEUS contributes to the characterization of renal masses, especially cystic RCC, where vascularity in septae and nodules is shown with a sensitivity surpassing both CT and MR scan. Further, in other locations such as the pancreas, spleen, ovary, prostate and breast, CEUS may show the presence of vascularity in real-time with the resolution of standard gray-scale ultrasound.

Discussion and Conclusions: CEUS changes totally the role of ultrasound in the evaluation of the patient with cancer. CEUS may be performed on any organ with a suitable acoustic window where the addition of vascular information may contribute to diagnosis. Its performance is independent of renal function making it a perfect first choice for the characterization of all masses in the oncology patient. To confirm that a mass is a malignant tumor or to confirm that it is not, CEUS is an easily performed and readily available technique. For these reasons, CEUS deserves a fundamental role in the future of oncological diagnosis.

Dr. Stephanie R. Wilson was born and educated in Western Canada but has made Toronto her home for the duration of her professional life. In 2007, she relocated to her home province where she is now Professor of Radiology at the University of Calgary and a member of the department of Diagnostic Imaging at Foothills Medical Centre, Calgary, CANADA. Dr Wilson has invested her research, academic and practice pursuits on imaging of the gastrointestinal tract, pancreas and liver. Since 1992, Dr Wilson has collaborated with Dr. Peter Burns from University of Toronto/Medical Imaging Research on the investigation of microbubble contrast agents for the evaluation of their use in Medical Imaging. Their major accomplishments to date include their investigation of the diagnosis and characterization of tumors of the liver. Burns and Wilson shared a grant from the Canadian Institute for Health Research (CHIR) for these investigations.

Apart from her research pursuits, Dr. Wilson has been the recipient of annual prestigious University of Toronto Faculty of Medicine teaching awards including the Colin R. Woolf Award for Excellence in Continuing Education Teaching in 1992, and the Wightman-Berris Academy Award for Individual Teaching Excellence in 2005. She has authored over 100 peer reviewed publications and many book chapters and is an editor of the highly successful two volume reference on ultrasound, entitled Diagnostic Ultrasound, often referred to as the "Bible of Ultrasound", now in its third edition. Dr Wilson served as the first woman president of the Canadian Association of Radiologists and was also the recipient of their Gold Medal for her contribution to radiology.

Short Courses

Short Courses (a Total of 12):

8:00 A.M. - 12:00 Noon, Sunday, November 2, 2008:

- **Short Course 1A (Conference Room 311A/B): Medical Ultrasound Transducers**, ***Douglas G. Wildes*** and ***L. Scott Smith***, GE Global Research Center, Niskayuna, NY, USA.
- **Short Course 2A (Conference Room 307): Ultrasound Imaging Systems: from Principles to Implementation**, ***Kai E. Thomenius***, GE Global Research Center, Niskayuna, NY, USA.

- **Short Course 3A (Conference Room 308): Photoacoustic Imaging and Sensing**, ***Stanislav Emelianov***, Biomedical Engineering Department, University of Texas at Austin, USA.
- **Short Course 4A (Conference Room 311C): Estimation and Imaging of Tissue Motion and Blood Velocity**, ***Hans Torp*** and ***Lasse Lovstakken***, Department of circulation and medical imaging, Norwegian University of Science and Technology, Trondheim, Norway.

1:00 P.M. - 5:00 P.M, Sunday, November 2, 2008:

- **Short Course 1B (Conference Room 311A/B): Ultrasound Elastography: Quantitative Approaches**, ***Jeffrey Bamber*** and ****Paul Barbone***, *Institute of Cancer Research and Royal Marsden Hospital, UK. **Boston University, USA.
- **Short Course 2B (Conference Room 307): Acoustic Microscopy - Fundamentals and Applications**, ****Roman Gr. Maev***, *****Naohiro Hozumi***, ******Kazuto Kobayashi***, and *******Yoshifumi Saijo***, *Centre for Imaging Research and Advanced Materials Characterization, University of Windsor, Ontario, Canada. **Department of Electrical & Electronic Engineering, Aichi Institute of Technology, Toyota, Japan. ***Honda Electronics Co. Ltd., Aichi, Japan. ****Tohoku University, Sendai, Japan.
- **Short Course 3B (Conference Room 308): Therapeutic Ultrasound**, ***Lawrence A. Crum***, Applied Physics Laboratory, University of Washington, Seattle, WA, USA.
- **Short Course 4B (Conference Room 311C): SAW Modeling Techniques**, ***Victor P. Plessky***, GVR Trade SA, Bevaix, Switzerland.

6:00 P.M. - 10:00 P.M, Sunday, November 2, 2008:

- **Short Course 1C (Conference Room 311A/B): Ultrasound Contrast Agents: Theory and Experiment**, ****Nico de Jong*** and *****Michel Versluis***, *Erasmus MC, The Netherlands. **University of Twente, The Netherlands.
- **Short Course 2C (Conference Room 307): CMUTs: Theory, Technology, and Applications**, ***B.T. Khuri-Yakub***, ***Ömer Oralkan***, and ***Mario Kupnik***, E.L. Ginzton Laboratory, Stanford University, USA.
- **Short Course 3C (Conference Room 308): Time Reversal Acoustics**, ***Mathias Fink***, École Supérieure de Physique et de Chimi de la Ville de Paris, France.
- **Short Course 4C (Conference Room 311C): Acoustical Near-Field Imaging**, ***Walter Arnold***, Fraunhofer Institute for Non-Destructive Testing, Saarbrücken, Germany.

Short Course 1A (8:00 A.M. - 12:00 Noon, Sunday, November 2, 2008):

Course Title: Medical Ultrasound Transducers

Douglas G. Wildes and ***L. Scott Smith***, GE Global Research Center, Niskayuna, NY, USA.

Course Description: This course will provide an introduction to the design, fabrication, and testing of medical ultrasound transducers. Starting from an overview of the basic types of phased-array transducers (linear, convex, sector), we will discuss how the design

for a probe is derived from its target application and how equivalent-circuit, finite-element, and acoustic field models can be used to optimize the design and accurately predict performance. A discussion of the structure of an ultrasound probe will lead to a survey of the different types of materials used in probes and their critical properties. Typical fabrication processes will be introduced and common problems in probe manufacturing will be summarized. Methods for evaluating completed transducers will be discussed. The course will highlight recent developments in probe technology, including single crystal piezoelectrics, cMUT transducers, catheters, multi-row and 2D arrays, and electronics in probes, and will discuss performance advantages and fabrication difficulties which may be associated with each.

Douglas G. Wildes is a physicist with GE Global Research. He earned an A.B. in physics and mathematics from Dartmouth College and a Ph.D. in low-temperature physics from Cornell University, then joined GE in 1985. Since 1991, Dr. Wildes' research has focused on aperture design, fabrication processes, and high-density interconnect technology for multi-row and 4D imaging transducers for medical ultrasound. Dr. Wildes has 23 issued patents and 19 external publications. He is a member of the American Physical Society and a Senior Member of the IEEE.

L. Scott Smith is a physicist with GE Global Research. He earned B.S. and Ph.D. degrees in physics from the University of Rochester and the University of Pennsylvania respectively. Joining GE in 1976, he developed phased array probes for medical ultrasound. More recently, he examined novel probe materials and led projects on pediatric endoscopes and adaptive acoustics. Dr. Smith has 43 issued patents and over 35 refereed publications. He is a member of the American Physical Society and a Senior Member of the IEEE where he serves as Vice Chair for Transducers on the Ultrasonics Symposium's Technical Program Committee.

Short Course 2A (8:00 A.M. - 12:00 Noon, Sunday, November 2, 2008):

Course Title: Ultrasound Imaging Systems: from Principles to Implementation

Kai E. Thomenius, GE Global Research Center, Niskayuna, NY, USA.

Course Description: The design of medical ultrasound imagers is undergoing important changes brought about by advances in semiconductors and signal/image procession technologies coupled with changes in medical practice and the utilization of medical imaging in general. Unique aspects of data acquisition and processing in the ultrasound scanner enable opportunities not available to other imaging modalities. The goal of this course is to review the system design of ultrasound scanners from a linear systems point of view including transduction, beam formation, and image formation functions. We will discuss analytical methods used in developing the design of a scanner in use today. The key points to be covered deal with methods of analysis of array data, the interaction of transmit and receive beams with clinically relevant targets, and how this interaction is used in the generation of clinically useful images. The means by which these analytical methods contribute to a system design and the trade-offs involved are reviewed. The last several years have seen steady migration of functionality into software; this has enabled significant miniaturization of scanners. The impact of this on system design and the size of ultrasound scanners of the future will be discussed.

Kai E. Thomenius is a Chief Technologist in the Imaging Technologies Organization at General Electric's Global Research facility in Niskayuna, NY, USA. His focus is on

Ultrasound and Biomedical Engineering. Previously, he has held senior R&D roles at ATL Ultrasound Inc., Interspec Inc., Elscint Inc., as well as several other ultrasound companies. In addition, he is currently an Adjunct Professor in the Electrical, Computer, and Systems Engineering Department at Rensselaer Polytechnic Institute where he teaches a course in general imaging. Dr. Thomenius' academic background is in electrical engineering with a minor in physiology; all of his degrees are from Rutgers University. His long-term interests have been in ultrasound beam formation and miniaturization of ultrasound scanners, propagation of acoustic waves in inhomogeneous media, and determination of physiological information from the echoes that arise from such beams. Dr. Thomenius is a Fellow of the American Institute of Ultrasound in Medicine.

Short Course 3A (8:00 A.M. - 12:00 Noon, Sunday, November 2, 2008):

Course Title: Photoacoustic Imaging and Sensing

Stanislav Emelianov, Biomedical Engineering Department, University of Texas at Austin, USA.

Course Description: This course is designed to provide both a broad overview and a comprehensive understanding of photoacoustic (also known as optoacoustic and, more generally, thermoacoustic) imaging, sensing and spectroscopy. With a brief historical introduction, we will begin the course by examining the foundations of photoacoustics, including derivations and a discussion of governing equations. We will also review relevant optical properties of the tissues and related topics of laser-tissue interaction. The experimental aspects of photoacoustic imagining and sensing will then be discussed with emphasis on system hardware and signal/image processing algorithms. Techniques to increase contrast and to differentiate various tissues in photoacoustic imaging will be presented. The course will conclude with an overview of several experimental systems capable of photoacoustic imaging, and discussion of current and potential biomedical and clinical applications of photoacoustics.

Stanislav Emelianov received B.S. and M.S. degrees in Physics and Acoustics in 1986 and 1989, respectively, from the Moscow State University, and a Ph.D. degree in Physics in 1993 from the Moscow State University and the Institute of Mathematical Problems of Biology of the Russian Academy of Science. In 1989, he joined the Institute of Mathematical Problems of Biology, where he was engaged in both mathematical modeling of soft tissue biomechanics and experimental studies of noninvasive visualization of the mechanical properties of tissue. Following his graduate work, he moved to the University of Michigan, Ann Arbor, as a post-Doctoral Fellow in the Bioengineering Program and in the Electrical Engineering and Computer Science Department. From 1996 to 2002, Dr. Emelianov was a Research Scientist at the Biomedical Ultrasonics Laboratory of the Biomedical Engineering Department at the University of Michigan. During his tenure at Michigan, Dr. Emelianov was involved primarily in the theoretical and practical aspects of elasticity imaging using ultrasound and MRI. Dr. Emelianov is currently teaching and conducting research in the Department of Biomedical Engineering at the University of Texas at Austin. His research interests are in medical imaging and therapeutics, including ultrasound, photoacoustic, elasticity and multi-modality imaging, photothermal therapy, cellular/molecular imaging and therapy, functional imaging, etc.

Short Course 4A (8:00 A.M. - 12:00 Noon, Sunday, November 2, 2008):

Course Title: Estimation and Imaging of Tissue Motion and Blood Velocity

Hans Torp and ***Lasse Lovstakken***, Department of circulation and medical imaging, Norwegian University of Science and Technology, Trondheim, Norway.

Course Description: This course provides a basic understanding of the physical principles and signal processing methods for estimation of blood and tissue motion. The course begins with an overview of currently used techniques for velocity estimation using pulsed- and continuous-wave Doppler, and color flow imaging. Statistical models for the received signal, as well as commonly used velocity estimators will be developed. Simulation methods for ultrasound signals from moving blood and tissue will be discussed and examples in Matlab will be shown. The suppression of clutter from slowly moving targets is central to all processing schemes and will be given special attention. Also, current methods of tissue velocity and strain rate imaging will be given special elaboration. More advanced topics will also be covered. An overview of current adaptive filter schemes for attenuating clutter will be given, and 2-D / 3-D vector velocity estimation techniques will also be presented. The principles and practical limitations of these methods will be discussed, and potential applications in blood velocity imaging and myocardial velocity- and strain imaging will be shown.

Hans Torp received the MS degree in mathematics in 1978, and the Dr. Techn. Degree in electrical engineering in 1992; both from the University of Trondheim, Norway. Since 1980 he has been working with ultrasound technology applied to blood flow measurements and imaging at the University of Trondheim, in cooperation with GE-Vingmed Ultrasound. He is currently professor of medical technology at the Norwegian Univesity of Science and Technology, and has since 1987 given courses on ultrasound imaging and blood flow measurements for students in electrical engineering and biophysics. His research interests include statistical signal- and image processing with application in medical ultrasound imaging.

Lasse Lovstakken received the Masters degree in Engineering Cybernetics in 2002 and a PhD in Medical Technology in 2007, both at the Norwegian University of Science and Technology, in Trondheim, Norway. He is currently working as a post doctoral research fellow at the Department of Circulation and Medical Imaging at the Norwegian University of science and Technology. His research interests include signal and image processing with applications in ultrasound imaging, with a special focus on imaging of blood and tissue movement.

Short Course 1B (1:00 P.M. - 5:00 P.M., Sunday, November 2, 2008):

Course Title: Ultrasound Elastography: Quantitative Approaches

Jeffrey Bamber and ****Paul Barbone***, *Institute of Cancer Research and Royal Marsden Hospital, UK. **Boston University, USA.

Course Description: There is evidence that ancient cultures extending back thousands of years used palpation to assess the mechanical properties of tissues, and thus detect and characterise disease or injury. Simple palpation continues to be of value in modern medicine, both practiced by doctors and as a technique for self-examination, but palpation is limited to a few accessible tissues and organs, and the interpretation of the information sensed by the fingers is highly subjective. Ultrasound elastography aims to

display images that are related to a broad range of parameters that describe the spatial and temporal variations in tissue viscoelasticity. It does so by processing time-varying echo data to extract the spatial and/or temporal variation of a stress-induced tissue displacement or strain. In recent years the method early form has emerged as a real-time imaging modality available as an option on several commercial ultrasound systems, and is starting to prove clinically valuable, for example in breast cancer diagnosis. Nevertheless, in its present form it remains a strongly subjective technique and continues, as with palpation, to require considerable interpretive skills to be learnt. There are good reasons to believe that a more quantitative and objective analysis will lead to clinically more valuable measures of tissue composition, function or state, with images that are easier to interpret. This short course will outline some of the limitations and pitfalls of current elastographic methods, and will then introduce the opportunities for, potential value of and challenges for making elastography more quantitative. It will then review work on modeling tissues and their mechanical behavior, the fundamentals of ultrasound elastographic experimental techniques required for quantitative imaging, the use of static, vibrational and impulsive loads, the inverse methods for measurement and image reconstruction, methods for stress measurement, and shear wave propagation methods. This will lead to a discussion of the likely consequences for medical applications and future instrumentation. Examples of results will be presented for a range of medical application areas and for various mechanical characteristics such as shear modulus, nonlinearity, anisotropy, friction at mechanical discontinuities, as well as properties that determine viscoelastic and poroelastic behavior.

Jeffrey Bamber is head of the Ultrasound and Optics Physics Team, and is Senior Tutor for the Research Degrees Program at The Institute of Cancer Research Sutton, U.K. He has an honorary position as a Medical Physicist within the Royal Marsden Hospital, Sutton. He received a BSc in Physics from the University of Kent at Canterbury in 1972, an MSc in Biophysics and Bioengineering from the University of London in 1974, and a PhD in Biophysics in 1980, also from the University London. He continued as a research scientist following his PhD at the Institute of Cancer Research, becoming a team leader in 1986. His research interests have included: acoustic characteristics of tissues, ultrasound image speckle and texture, speckle reduction, ultrasound aberration, psychophysics of perception of information in ultrasound images and movies, ultrasonic methods in breast cancer, measurement of tumor volume and blood flow, ultrasound tissue motion tracking, tissue elasticity imaging, temperature imaging, high frequency ultrasonic imaging and tissue characterization, ultrasound and optical methods in skin cancer, microbubble contrast agents, ultrasound guidance of focused ultrasound therapy and radiotherapy, ultrasound in radiation dosimetry, microbubbles as gene therapy vectors, and molecular imaging. Prizes for work to which he has contributed include 5 best paper awards in peer reviewed journals and 2 book publishing awards for excellence. He is a past vice-president of the International Society for Skin Imaging, a past president of the International Association for Breast Ultrasound, and currently serves on the Council of the British Medical Ultrasound Society.

Paul E. Barbone is Associate Professor of Mechanical Engineering at Boston University. He received Bachelors of Engineering Science and Mechanics from Georgia Institute of Technology in 1986, a Masters of Mechanical Engineering in 1987 from Stanford University, and a PhD in Mechanical Engineering from Stanford University in 1992. He did postdoctoral research at the University of Cambridge (1992-1993) in the Department of Applied Mathematics and Theoretical Physics, served as lecturer at School for Advanced Studies in Industrial and Applied Mathematics, Valenzano, Italy (1992), and was Haddow Fellow and visiting Researcher at the Institute of Cancer Research, Sutton,

UK (2000-2001). His research approach is mathematical and theoretical analysis. He works mainly on forward and inverse problems in acoustics and solid mechanics, and sidelines in the analysis of computational formulations. Over the past several years, his research focus has been inverse problems in "Biomechanical Imaging:" imaging the mechanical properties of tissues in situ and in vivo. His research work has been recognized through prizes from US National Science Foundation, US Office of Naval Research, Acoustical Society of America, and the J. William Fulbright Foundation.

Short Course 2B (1:00 P.M. - 5:00 P.M., Sunday, November 2, 2008):

Course Title: Acoustic Microscopy - Fundamentals and Applications

Roman Gr. Maev, ****Naohiro Hozumi***, *****Kazuto Kobayashi***, and ******Yoshifumi Saijo***, *Centre for Imaging Research and Advanced Materials Characterization, University of Windsor, Ontario, Canada. **Department of Electrical & Electronic Engineering, Aichi Institute of Technology, Toyota, Japan. ***Honda Electronics Co. Ltd., Aichi, Japan. ****Tohoku University, Sendai, Japan.

Course Description: The goal of this course is to introduce the fundamentals and major principles of scanning acoustic microscopy. This course aims to describe advanced acoustic microscopy methods for investigating the microstructure and physical mechanical properties of materials of different nature, from crystalline to biomaterials. The materials discussed during this course cover most aspects of physical principles and applications of high-resolution acoustic microscopy and reflects the modern research status in this field. Included are different topics in physical acoustics, ultrasound, solid state physics, materials characterization and nondestructive evaluation. Special attention will be paid to the principle and application of several types of scanning acoustic microscopes for medical and biological use. Progress in digital measurement and pulse technology has remarkably upgraded the performance of these types of microscopes and this will be described within the course. The sound speed microscope which conventionally used tone-burst and analog phase detector was improved in accuracy, stability and operation ability. It can be used for characterization of tissue sliced and mounted on a slide glass. It can visualize not only acoustic impedance but bulk modulus, attenuation constant and density. The acoustic impedance microscope can visualize the acoustic impedance of a cross section in touch with a plastic substrate by transmitting an acoustic beam from the rear side of the substrate. This type of microscopy has an advantage that the measurement can be performed in vivo, introducing no contamination into the target system. With a wide frequency range up to 400 MHz, both types of microscopes can observe with a special resolution as fine as cell structure. Discussed will be the principle of the sound speed and acoustic microscopes driven by a wide band pulse and several examples of observation of cerebella tissue and cultured cells will be shown. In addition, there will be a presentation of recent results in acoustic microscopy technology development achieved by Honda Electronics (Japan) and Tessonics (Canada). The detail of the hardware and software of those microscopes that are commercially available will be described. The prototype microscopes have been improved a lot after being commercialized. The hardware, software and biomedical applications of these microscopes will be described with a large number of examples as additional illustrations. This course will conclude with an overview of the future perspectives of the general principles of microscopic observation using various ultrasound waves as well as the most promising future applications.

Roman Gr. Maev received his Ph.D. from the Physical Institute of the Russian Academy of Sciences in 1973 and his D.Sc. in acoustic microscopy from the Russian Academy of Sciences, Moscow, in 2002. From 1994 to 1997, he held a post as Director of the Acoustic Microscopy Center of the Russian Academy of Sciences, then established a Centre for Imaging Research and Advanced Material Characterization at the University of Windsor, Canada. He is currently a Full Faculty Professor at the Physics Department of the same University and since 2001 the Chairholder of the NSERC/DaimlerChrysler/Industrial Research Chair in Applied Solid State Physics and Material Characterization. Professor Maev's research interests focus on the fundamentals of condensed matter, physical acoustics, ultrasonic imaging, and acoustic microscopy. He has published numerous books, more than 300 scientific papers, and holds twenty patents.

Naohiro Hozumi was born in Kyoto, Japan on April 2, 1957. He received his B.S., M.S. and Ph.D. degrees in 1981, 1983 and 1990 from Waseda University. He was engaged in Central Research Institute of Electric Power Industry (CRIEPI) from 1983 to 1999. He was an associate professor of Toyohashi University of Technology from 1999 to 2006. Since 2006, he has been a professor of Aichi Institute of Technology. He has been engaged in the research in insulating materials and diagnosis for high voltage equipment, acoustic measurement for biological and medical applications, etc. He was awarded in 1990 and 1999 from IEE of Japan for his outstanding research papers. He is a member of IEEE, IEE of Japan and the Acoustic Society of Japan.

Kazuto Kobayashi was born in Aichi, Japan on June 8, 1952. He received B.S. degree in electrical engineering from Shibaura Institute of Technology, Tokyo, Japan in 1976. He is currently a director of Department of Research and Development at Honda Electronics Co. Ltd. in Toyohashi, Japan. His research activities and interests include medical ultrasound imaging, signal processing and high frequency ultrasound transducers.

Yoshifumi Saijo was born in Yokohama, Japan on July 21, 1962. He received the M.D. and the Ph.D. degrees in 1988 and 1993 from Tohoku University. He is currently a Professor of the Department of Biomedical Imaging at the Graduate School of Biomedical Engineering of Tohoku University. He is concurrent with Institute for International Advanced interdisciplinary Research of Tohoku University and the Department of Cardiovascular Surgery of Tohoku University Hospital. His main research interests are assessment of biomechanics of cells and tissues by high frequency ultrasound and clinical ultrasonic evaluation of cardiovascular system with intravascular ultrasound and transesophageal echocardiography. He was awarded in 1997 for his outstanding research paper in Ultrasound in Medicine and Biology, the official journal of the World Federation of Ultrasound in Medicine and Biology. He is a member of The Japan Society of Ultrasonics in Medicine, Japanese Society of Echocardiography and Japan Circulation Society.

Short Course 3B (1:00 P.M. - 5:00 P.M., Sunday, November 2, 2008):

Course Title: Therapeutic Ultrasound

Lawrence A. Crum, Applied Physics Laboratory, University of Washington, Seattle, WA, USA.

Course Description: The use of ultrasound in medicine is now quite commonplace, especially with the recent introduction of small, portable and relatively inexpensive,

hand-held diagnostic imaging devices. Moreover, ultrasound has expanded beyond the imaging realm, with methods and applications extending to novel therapeutic and surgical uses. These applications broadly include: Tissue ablation, acoustocautery, body contouring, site-specific and ultrasound mediated drug activity, extracorporeal lithotripsy, and the enhancement of natural physiological functions such as wound healing and tissue regeneration. A particularly attractive aspect of this technology is that diagnostic and therapeutic systems can be combined to produce totally non-invasive, image-guided therapy. This general lecture will review a number of these exciting new applications of ultrasound and address some of the basic scientific questions and future challenges in developing these methods and technologies for general use in our society. We shall particularly emphasize the use of High Intensity Focused Ultrasound (HIFU) in the treatment of benign and malignant tumors as well as the introduction of acoustic hemostasis, especially in organs which are difficult to treat using conventional medical and surgical techniques.

Lawrence A. Crum is currently Principal Physicist in the Applied Physics Laboratory and Research Professor of Bioengineering and Electrical Engineering at the University of Washington. He has held previous positions at Harvard University, the U. S. Naval Academy and the University of Mississippi, where he was F. A. P. Barnard Distinguished Professor of Physics and Director of the National Center for Physical Acoustics. He has published over 300 articles in professional journals, holds an honorary doctorate from the Universite Libre de Bruxelles, and was recently awarded the Helmholtz-Rayleigh Silver Medal of the Acoustical Society of America. He is Past President of the Acoustical Society of America, the World Council on Ultrasonics, and of the Board of the International Commission for Acoustics.

Short Course 4B (1:00 P.M. - 5:00 P.M., Sunday, November 2, 2008):

Course Title: SAW Modelling Techniques

Victor P. Plessky, GVR Trade SA, Bevaix, Switzerland.

Course Description: This course provides introduction to the design techniques of SAW devices. The course includes and will discuss: a) SAW excitation on piezoelectrics by linear charges, elementary theory of the Interdigital Transducer (IDT) with non-reflecting electrodes, design of typical IDTs on quartz and LiNb, delay lines characteristics and matching issues. b) Single Phase Unidirectional Transducer (SPUDT)- design and applications. c) Propagation of SAW in periodic structures, coupling of modes (COM) model, and simulation with COM model of IDTs and reflectors. d) Modeling of SAW devices based on Green's function software. e) CRF/DMS filter design – examples of device simulation; optimization software f) Synchronous resonators, extraction of COM parameters, and ladder filters design. g) Design of SAW-tags. During the lecture, the attendee will see demonstrations of design processes for typical filter specifications. The COM model will be presented in details sufficient for practical use. The course will conclude with a review of unsolved problems and challenges in the SAW devices design area.

Victor P. Plessky was born near Gomel, Belarus. He now lives and works in Switzerland. Before leaving the USSR in 1991, he worked as a head of laboratory in IRE of Academy of Sciences in Moscow region in Russia. He received his Ph.D. degree from the Moscow Institute of Physics and Technology in 1978, and received his Doctor of Science degree in physics and mathematics from the Institute of Radio-engineering and

Electronics (IRE RAS, 1987). He received the Full Professor title from the Russian Government in1995. For the last 16 years he has worked in Switzerland, first as a Principal Scientist at the company Micronas SA. He now is an owner and CEO of the consulting company GVR Trade SA. His main spheres of interest are theory of microacoustics, surface acoustic waves (SAW) theory and devices, devices for signal filtering and frequency control, SAW sensors and SAW-tags. A few of his works in periodic structures have received wide recognition. Dr. V. Plessky worked as Visiting Professor in HUT (Finland), Freiburg University (Germany), Uppsala University (Sweden), EPFL (Switzerland). He has authored or co-authored over 200 papers and many patents. For many years he serves ad TPC member of the IEEE Ultrasonics Symposium.

Short Course 1C (6:00 P.M. - 10:00 P.M., Sunday, November 2, 2008):

Course Title: Ultrasound Contrast Agents: Theory and Experiment

Nico de Jong and ****Michel Versluis***, *Erasmus MC, The Netherlands. **University of Twente, The Netherlands.

Course Description: The course consists of 6 topics: a) An overview will be presented of the (clinical and pre-clinical available) contrast agents, including the properties and characteristics of the gas inside the bubble and the shell surrounding it. b) Models of the behavior of small bubbles in an ultrasound field will be discussed. Simple models based on a one dimensional mass-spring system and more complicated models including gas and shell properties. c) Experimental acoustic methods for UCA will be presented for characterizing the bubbles in suspension, including harmonic and sub-harmonic scattering, absorption and attenuation. Also the influence of ambient pressure, temperature and gas concentration will be discussed. d) Experimental optical and acoustical methods for characterizing individual bubbles. e) Imaging methods for contrast agents, e.g. fundamentals, harmonic, subharmonic and superharmonic and multi-pulse methods like the pulse inversion, power modulation etc. and new methods including chirp excitation and radical modulation. f) Molecular imaging and ultrasound mediated drug delivery: Interaction between mammalian cells and ultrasound in the presence of (targeted) bubbles will be discussed.

Nico de Jong graduated from Delft University of Technology, The Netherlands, in 1978. He got his M.Sc. in the field of pattern recognition. Since 1980, he has been a staff member of the Thoraxcenter of the Erasmus University Medical Center, Rotterdam, The Netherlands. At the Dept. of Biomedical Engineering, he developed linear and phased array ultrasonic probes for medical diagnosis, especially compound and transesophageal transducers. In 1986 his interest in ultrasound applications shifted toward the theoretical and practical background of ultrasound contrast agents. In 1993 he received his Ph.D. for "Acoustic properties of ultrasound contrast agents." His current interests are 3D (matrix) transducers, bubble behavior and fast framing camera systems. Since 1996 he organizes, together with the cardiologist Dr. Folkert ten Cate, the annual European Symposium on Ultrasound Contrast Imaging, held in Rotterdam and attended by approximately 175 scientists from all over the world. Since 2003 Nico de Jong is part-time professor at the University of Twente.

Michel Versluis graduated in Physics in 1988 at the University of Nijmegen, the Netherlands, with a special interest in Molecular Physics and Astrophysics. Later, he specialized in the application of intense tunable UV lasers for flame diagnostics resulting

in a successful defense of his PhD thesis in 1992. Michel Versluis is now a lecturer at the University of Twente, the Netherlands, in the Physics of Fluids group working on the experimental study of bubbles and jets in multiphase flows and granular flows. He also works on the use of microbubbles as a tool for medical diagnosis and therapy. Dr. Verluis teaches various courses in Fluid Mechanics, one of them focusing on the physics of bubbles.

Short Course 2C (6:00 P.M. - 10:00 P.M., Sunday, November 2, 2008):

Course Title: CMUTs: Theory, Technology, and Applications

B.T. Khuri-Yakub, ***Ömer Oralkan***, and ***Mario Kupnik***, E.L. Ginzton Laboratory, Stanford University, USA.

Course Description: This course provides basic knowledge and understanding of capacitive micromachined ultrasonic transducers (CMUTs) and their applications. After a short background discussion of previous implementations of capacitive ultrasonic transducers, we will provide all the information necessary for the successful design of a CMUT: The simple parallel plate capacitor transducer and its electrical equivalent circuit model will be explained in detail, including the derivation of all essential design equations, and the theoretical device performance limits. An approximate analytical model, that better represents the realizable membrane of a CMUT, will be presented next. By discussing a possible beyond pull-in point operation regime (collapse mode), the motivation for a more sophisticated finite element model is given, and the key techniques of finite element analysis based CMUT designs are explained and demonstrated using brief examples. After explaining these techniques, we compare the two main domains in which a CMUT can operate, i.e. as an airborne device and in immersion. Only for immersed operation the periodic structure of a CMUT array needs to be considered to minimize parasitic cross-talk effects. Two acoustic cross-talk modeling techniques will be discussed for that purpose. Then, the two main CMUT fabrication techniques, i.e. sacrificial release and direct wafer bonding, are explained and compared to each other. Next, we discuss device characterization which will cover optical displacement, electrical input impedance, then acoustical measurements of output pressure, receive sensitivity, impulse response and dynamic range. Then, non-conventional CMUT designs are addressed, such as piston CMUTs, CMUTs with various cell-shapes, and CMUTS with non-uniform cavities. Besides an overview of several CMUT applications, we conclude the course by giving two detailed design examples, one for an airborne device for chemical/biological sensing applications and one for medical imaging applications. A comprehensive copy of the presentation will be made available to the course participants.

Butrus (Pierre) T. Khuri-Yakub is a Professor of Electrical Engineering at Stanford University. He received the BS degree in 1970 from the American University of Beirut, the MS degree in 1972 from Dartmouth College, and the Ph.D. degree in 1975 from Stanford University, all in electrical engineering. He was a Research Associate (1965-19780 then Senior Research Associate (1978-1982) at the E. L. Ginzton Laboratory of Stanford University and was promoted to the rank of Professor of Electrical Engineering in 1982. His current research interests include medical ultrasound imaging and therapy, micromachined ultrasonic transducers, smart bio-fluidic channels, microphones, ultrasonic fluid ejectors, and ultrasonic nondestructive evaluation, imaging and microscopy. He has authored over 400 publications and has been principal inventor or co-inventor of 76 US and International issued patents. He was awarded the Medal of the City of Bordeaux in 1983 for his contributions to Nondestructive Evaluation, the

Distinguished Advisor Award of the School of Engineering at Stanford University in 1987, the Distinguished Lecturer Award of the IEEE UFFC society in 1999, a Stanford University Outstanding Inventor Award in 2004, and a Distinguished Alumnus Award of the School of Engineering of the American University of Beirut in 2005.

Ömer Oralkan received his B.S. degree from Bilkent University, Ankara, Turkey, in 1995, his M.S. degree from Clemson University, Clemson, SC, in 1997, and his Ph.D. degree from Stanford University, Stanford, CA, in 2004, all in electrical engineering. He joined the research staff at the E. L. Ginzton Laboratory of Stanford University in 2004 as an Engineering Research Associate. He was promoted to the rank of Senior Research Engineer in 2007. His past and present research interests include analog and digital circuit design, semiconductor device physics and fabrication, micromachined sensors and actuators, and medical imaging. His current research focuses on the design and implementation of integrated systems for catheter-based medical imaging applications, photoacoustic imaging, and chemical and biological sensor arrays. Dr. Oralkan has authored and co-authored over 80 publications and received the 2002 Outstanding Paper Award of the IEEE Ultrasonics, Ferroelectrics, and Frequency Control Society. He is a member of the IEEE, SPIE, and AIUM.

Mario Kupnik is a research associate of electrical engineering at Stanford University. He received his Diplom Ingenieur degree in electronics engineering from Graz University of Technology, Austria in 2000. After working as an Analog Design Engineer for Infineon Technologies AG, he received his Ph. D. in physical measurement techniques at the University of Leoben, Austria in 2004, and then completed a two-year PostDoc at the Khuri-Yakub Ultrasonics Group, Stanford University in February 2007. Mario Kupnik has more than five years teaching experience in the field of electrical engineering, two of these years at the graduate level. His present research interests include the design, modeling, fabrication, and application of micromachined sensors and actuators, with a main focus on capacitive micromachined ultrasonic transducers mainly for air-coupled applications. Examples are transit-time gas flowmeters for hot and pulsating gases, ultrasonic nondestructive evaluation using noncontact ultrasound, nonlinear acoustics, and bio/chemical gas sensing applications (electronic nose). He holds several patents relating to analog front-end circuits for contactless smart card systems, ultrasonic transit-time gas flowmeters, and CMUT fabrication techniques. He serves as a technical program committee member of the IEEE Ultrasonics Symposium.

Short Course 3C (6:00 P.M. - 10:00 P.M., Sunday, November 2, 2008):

Course Title: Time Reversal Acoustics

Mathias Fink, École Supérieure de Physique et de Chimi de la Ville de Paris, France.

Course Description An acoustic Time Reversal Mirror (TRM) refocuses an incident acoustic field to the position of the original source regardless of the complexity of the medium between this "probe" source and the TRM. TRM's have now been implemented in a variety of physical scenarios from MHz ultrasonics with order centimeter aperture size to hundreds/thousands of Hz in ocean acoustics with order hundred meter aperture size. Common to this broad range of scales is a remarkable robustness exemplified by observations at all scales that the more complex the medium between the probe source and the TRM, the sharper the focus. The potential for applications in many areas of acoustics is quite high. The objective of this course is to provide the acoustical physics overview and description of the experimental implementation of time reversal and phase

conjugate processes as related to ultrasonics and imaging, nondestructive testing, medical ultrasonics, propagation in random media, room acoustics, waveguides, and ocean acoustics.

Mathias Fink is a Professor of Physics at the École Supérieure de Physique et de Chimi de la Ville de Paris (ESPCI) and at Paris 7 University (Denis Diderot), France. In 1990 he founded the laboratory Ondes et Acoustique at ESPCI. In 2002, he was elected at the French Academy of Engineering and in 2003 at the French Academy of Science. His area of research is concerned with the propagation of waves in complex media and the development of numerous instruments based on this basic research. The domain of applicability of these instruments is vast: medical imaging and therapy, non-destructive testing, underwater acoustics, seismology, telecommunications and instrumentation. He has a long history of collaboration with industry. He works with companies in a wide variety of sectors including medical, aeronautics, underwater acoustics, nuclear, metallurgy, and instrumentation. He pioneered many innovative approaches based on time-reversal mirrors and on the development of a new imaging concept: transient elastography. He has over 40 patents, 300 publications, edited 2 books and supervised 48 PHD students.

Short Course 4C (6:00 P.M. - 10:00 P.M., Sunday, November 2, 2008):

Course Title: Acoustical Near-Field Imaging

Walter Arnold, Fraunhofer Institute for Non-Destructive Testing, Saarbrücken, Germany.

Course Description: Acoustical imaging modes can be classified into near-field, focusing techniques, and holographic techniques. This four hour course discusses, in particular, near-field imaging modes. Examples are ultrasonic force microscopy, atomic force acoustic microscopy, and impedance imaging such as Fokker-bond tests. Their resolution in terms of the antenna size (i.e. probe size) and wavelength employed both at the surface and in the depth of the component to be imaged, are discussed. Besides the underlying contrast mechanism, the course also covers the signal analysis and capture techniques. Finally a comparison is made to classical acoustical imaging based on focusing probes, holographic imaging, and phased arrays principles. The examples are underlined by applications in non-destructive testing.

Walter Arnold has authored and co-authored about 300 publications (200 in Non-Destructive Testing, others in Solid State and Applied Physics and Materials Science), holds 10 patents and has edited two books besides organizing several conferences both on a national and international level. He has guided 140 master theses and 27 PhD theses. Dr. Arnold was the head of the research department at Fraunhofer-Institute for Non-Destructive Testing (IZFP) in Saarbrücken, Germany until his retirement at the end of 2007. Parallel to his position at the IZFP, Dr. Arnold was and still is professor of Materials Science at the Saarland University, Dept. Materials. He is an Honorary Fellow Indian Institute of Non-Destructive Testing, Fellow Institute of Physics, London.

Student Competition Finalists

Student Paper Competition Finalists (a Total of 21):

This is the 8th year of the student paper competition (started from the 2001 IEEE International Ultrasonics Symposium in Atlanta, Georgia, USA). 21 Student Paper Competition finalists have been selected during the 2nd Technical Program Committee meeting of the 2008 IEEE International Ultrasonics Symposium, which was held from June 14-15, 2008 in Chicago, Illinois, USA. The finalists should check the award selection criteria at the link: Student Paper Competition for the requirements of their presentations.

Final Winners of the Student Paper Competition:

Seven final winners of the student paper competition will be selected from the 21 finalists above. The criteria of the awards are in the link "Student Paper Competition" at the conference website: http://ewh.ieee.org/conf/ius_2008.

Group 1: Medical Ultrasonics (9 finalists):

- **Finalist #1.1 (PS001-01) (3F-2):** ***Bo Wang (Presenter)***, *Andrei Karpiouk, and Stanislav Emelianov*, **"Design of Catheter for Combined Intravascular Photoacoustic and Ultrasound Imaging,"** Biomedical Engineering, University of Texas at Austin, Austin, TX, USA. (Abstract ID: 309)
- **Finalist #1.2 (PS002-02) (2F-6):** ***Linsey C. Phillips (Presenter)***, **Alexander L. Klibanov, **Doug K. Bowles, *Brian. R. Wamhoff, and *John A. Hossack*, **"Intra-Vascular Ultrasound (IVUS) Delivery of DNA Via Microbubble Carriers to an Injured Artery In vivo,"** *University of Virginia, Charlottesville, VA, USA, **University of Missouri, Columbia, MO, USA. (Abstract ID: 1094)
- **Finalist #1.3 (PS003-03) (3E-5):** ***Egon J.W. Merks (Presenter)***, *Nicolaas Bom, Nico de Jong, and Antonius F.W. van der Steen*, **"Quantitative Bladder Volume Assessment on the Basis of Nonlinear Wave Propagation,"** Biomedical Engineering, Erasmus MC, Rotterdam, Netherlands. (Abstract ID: 291)
- **Finalist #1.4 (PS004-04) (2D-3):** ***Hong Chen (Presenter)***, *Andrew A. Brayman, Michael R. Bailey, and Thomas J. Matula*, **"Microbubble dynamics in microvessels: Observations of microvessel dilation, invagination and rupture,"** Center for Industrial and Medical Ultrasound, Applied Physics Laboratory, University of Washington, Seattle, WA, USA. (Abstract ID: 609)
- **Finalist #1.5 (PS005-05) (2H-4):** ****Adam Maxwell (Presenter)***, **Charles Cain, **Hitinder Gurm, ***J. Brian Fowlkes, and *Zhen Xu*, **"Non-invasive thrombolysis induced by histotripsy pulsed cavitation ultrasound therapy,"** *1Department of Biomedical Engineering, University of Michigan, Ann Arbor, Michigan, USA, **Department of Internal Medicine, University of Michigan, Ann Arbor, Michigan, USA, ***Department of Radiology, University of Michigan, Ann Arbor, Michigan, USA. (Abstract ID: 68)
- **Finalist #1.6 (PS006-06) (2I-5):** ****Jerome GATEAU (Presenter)***, ***Laurent MARSAC, *Mathieu PERNOT, *Jean-Francois AUBRY, *Mickael TANTER, *Mathias FINK*, **"Reaching the optimal focusing and steering capabilities of transcranial HIFU arrays based on time reversal of acoustically induced**

cavitation bubble signature," *Laboratoire ondes et Acoustique, INSERM, CNRS UMR 7587, ESPCI, PARIS, France, **SUPERSONIC IMAGINE, Aix-en-Provence, France. (Abstract ID: 248)

- **Finalist #1.7 (PS007-07) (2K-5):** ***Shun-Li Wang (Presenter)*** *and Pai-Chi Li*, **"High Frame Rate Adaptive Imaging Using Coherence Factor Weighting and the MVDR Method,"** National Taiwan Univ., Taipei, Taiwan. (Abstract ID: 1083)
- **Finalist #1.8 (PS008-08) (1K-5):** ***Torbjørn Hergum (Presenter)***, *Thomas Renhult Skaug, **Knut Matre, and Hans Torp*, **"Estimation of Valvular Regurgitation Area by 3D HPRF Doppler,"** *Department of circulation and medical imaging, Norwegian University of Science and Technology, Trondheim, Norway, **Institute of Medicine, University of Bergen, Bergen, Norway. (Abstract ID: 1040)
- **Finalist #1.9 (PS009-09) (2E-6):** ***John Ballard (Presenter)*** *and Emad Ebbini*, **"Image-Guided Refocusing of Dual-Mode Ultrasound Arrays(DMUAs),"** University of Minnesota, USA. (Abstract ID: 384)

Group 2: Sensors, NDE, and Industrial Application (3 finalists):

- **Finalist #2.1 (PS010-10) (5C-2):** ***Donald McCann (Presenter)***, *Mitchell Wark, Paul Millard, David Neivandt, and John Vetelino*, **"The Detection of Chemical and Biological Analytes Using a Monolithic Spiral Coil Acoustic Transduction Sensor,"** University of Maine, Orono, ME, USA. (Abstract ID: 131)
- **Finalist #2.2 (PS011-11) (5G-5):** ***Sean Mc Sweeney (Presenter)*** *and **WMD Wright*, **"Improving the Bandwidth of Air Coupled Capacitive Ultrasonic Transducers Using Selective Networks,"** *Electrical and Electronic Engineering Dept, University College Cork, National University of Ireland, Mallow, Cork, Ireland, **Electrical and Electronic Engineering, University College Cork, National University of Ireland, Cork, Cork, Ireland. (Abstract ID: 589)
- **Finalist #2.3 (PS012-12):** ***Montserrat Parrilla (Presenter)***, *Jose Brizuela, Jorge Camacho, Alberto Ibañez, Patricia Nevado, and Carlos Fritsch*, **"Dynamic focusing thorough arbitrary geometric interfaces,"** Instituto de Automática Industrial (CSIC), La Poveda (Arganda), Madrid, Spain. (Abstract ID: 154)

Group 3: Physical Acoustics (3 finalists):

- **Finalist #3.1 (PS013-13) (6E-5):** ***Satyanarayan Bhuyan (Presenter)*** *and Junhui Hu*, **"Wireless Drive of a Piezoelectric Plate by Dipole Antenna,"** Nanyang Technological University, Singapore. (Abstract ID: 72)
- **Finalist #3.2 (PS014-14) (6H-5):** ***Pierre-Adrien Mante (Presenter)***, *Arnaud Devos, and Jean-François Robillard*, **"Towards thin film complete characterization using picosecond ultrasonics,"** IEMN-CNRS, France. (Abstract ID: 593)
- **Finalist #3.3 (PS015-15) (6H-6):** ***Taisuke Yoshida (Presenter)***, *Mami Matsukawa, and **Takahiko Yanagitani*, **"Simultaneous observation of induced longitudinal and shear acoustic phonons by Brillouin Scattering,"** *Faculty of Engineering, Doshisha University, Kyotanabe, Japan, **Department of Applied Physics, Nagoya Institute of Technology, Nagoya, Japan. (Abstract ID: 1015)

Group 4: Microacoustics - SAW, FBAW, MEMS (3 finalists):

- **Finalist #4.1 (PS016-16):** ***Gunilla Wingqvist (Presenter)***, *Lilia Arapan, Ventsislav Yantchev, and Ilia Katardjiev*, **"Temperature Compensation of Thin AlN Film Resonators utilizing the Lowest order Symmetric Lamb mode,"** Solid State Electronics, Uppsala University, Uppsala, Sweden. (Abstract ID: 620)
- **Finalist #4.2 (PS017-17) (4J-2):** ***Yiliu Wang (Presenter)***, *Ken-ya Hashimoto, Tatsuya Omori, and Masatsune Yamaguchi*, **"A Full-Wave Analysis of Surface Acoustic Waves Propagating on a SiO2 Overlay/Metal Grating/Rotated YXLiNbO3 Substrate Structure,"** Graduate School of Engineering, Chiba University, Chiba, Chiba, Japan. (Abstract ID: 217)
- **Finalist #4.3 (PS018-18) (4I-5):** ***Evgeny Milyutin (Presenter)***, *and Paul Muralt*, **"Shear mode BAW resonator based on c-axis oriented AlN thin film,"** Ecole Polytechnique Federale de Lausanne, Switzerland. (Abstract ID: 522)

Group 5: Transducers and Transducer Materials (3 finalists):

- **Finalist #5.1 (PS019-19) (4D-3):** ***Hanne Martinussen (Presenter)***, *Astrid Aksnes, and Helge E. Engan*, **"Investigation of charge diffusion in Capacitive Micromachined Ultrasonic Transducers (CMUTs) using optical interferometry,"** Electronics and Telecommunications, Norwegian University of Science and Technology, Trondheim, Norway. (Abstract ID: 274)
- **Finalist #5.2 (PS020-20) (3G-4):** ***Dawei Wu (Presenter)***, **Qifa Zhou, **Changgeng Liu, **Frank Djuth, and *K Kirk Shung*, **"High-frequency (>100MHz) Piezoelectric PZT Film Micromachined Ultrasonic Arrays,"** *NIH Transducer Resource Center and Department of Biomedical Engineering, University of Southern California, USA, **Geospace Research, Inc, USA. (Abstract ID: 858)
- **Finalist #5.3 (PS021-21):** ***Andrew Logan (Presenter)*** *and John Yeow*, **"1-D CMUT Imaging Arrays Fabricated Using a Novel Wafer Bonding Process,"** Systems Design Engineering, University of Waterloo, Waterloo, Ontario, Canada. (Abstract ID: 418)

Student Travel Support

List of Student Travel Support Awardees:

The list of the student travel support awardees is accessible through the link, "Student Travel Support", at the conference website: http://ewh.ieee.org/conf/ius_2008. To actually receive the award money, all criteria listed in the link above should be met. When all the conditions above are met, the money will be available for the students to pick up on the registration desks in the Beijing International Convention Center during the conference.

IEEE UFFC Society (UFFC-S) Officials

UFFC Society Officials:

Title	Name	Affiliation
President:	**Susan Trolier-McKinstry**	*The Pennsylvania State University*
President-Elect:	**R. Michael Garvey**	*Symmetricom, Beverly, MA*
VP, Ferroelectrics:	**Thomas R. Shrout**	*The Pennsylvania State University*
VP, Frequency Control:	**Samuel Stein**	*Timing Solutions Corp., Boulder, CO*
VP, Ultrasonics:	**Jacqueline H. Hines**	*Applied Sensor R&D Corp., Annapolis, MD*
VP, Publications:	**Donald Yuhas**	*Industrial Measurement Systems Inc., IL*
Secretary-Treasurer:	**Daniel S. Stevens**	*Vectron International - Hudson, NH*

UFFC-S Elected Administrative Committee (AdCom) Members

Elected AdCom Members:

Term	Name	Affiliation
2008 - 2010	**Rich Ruby**	*Avago Technologies, San Jose, CA, USA*
2008 - 2010	**Wilko Wilkening**	*Siemens Medical Solutions, Mountain View, CA*
2008 - 2010	**Yoonkee Kim**	*U.S. Army Communications-Electronics RD&E Center, Ft. Monmouth, NJ, USA*
2008 - 2010	**David Cann**	*Oregon State University, Corvallis, OR, USA*
2007 - 2009	**Roman Maev**	*Windsor Institute for Diagnostic Research, Canada*
2007 - 2009	**Dragan Damjanovic**	*Swiss Federal Institute of Technology, Lausanne*
2007 - 2009	**Mike Driscoll**	*Northrup Grumman Corp., Baltimore, MD*
2007 - 2009	**Ken-ya Hashimoto**	*Chiba University, Japan*
2006 - 2008	**Manfred Weihnacht**	*IFW Dresden (retired), Dresden, Germany*
2006 - 2008	**Sorah Rhee**	*Boston Scientific, Fremont, CA*
2006 - 2008	**Amit Lal**	*Cornell University/DARPA, Arlington, VA*

2006 - 2008	**Tadashi Takenaka**	*Tokyo University of Science, Japan*

Newly Elected AdCom Members

Newly Elected AdCom Members:

The following 4 people have been elected as members of the Administrative Committee (AdCom) of the IEEE Ultrasonics, Ferroelectrics, and Frequency Control society (UFFC-S) for the term from January 1, 2009 to December 31, 2011:

Ultrasonics:

Jian-yu Lu
Department of Bioengineering
The University of Toledo
Toledo, Ohio 43606, USA
Email: jilu@eng.utoledo.edu

Frequency Control:

Gregory L. Weaver
Space Department
Applied Physics Laboratory
The Johns Hopkins University
Laurel, Maryland, USA
Email: gregory.weaver@jhuapl.edu

Ferroelectrics:

Glen Fox
1850 Ramtron Dr.
Ramtron International Corporation
Colorado Springs, CO 80921, USA
Email: glen_fox_pa@msn.com

Regions 8-10 Representative:

Andrew J. Bell
Institute for Materials Research
University of Leeds
United Kingdom, LS2 9JT
Email: A.J.Bell@leeds.ac.uk

UFFC-S Standing Committee Chairs and Vice Chairs

Committee Chairs and Vice Chairs:

Chair	Name	Affiliation
Ultrasonics	**Jacqueline H. Hines**	*Applied Sensor R&D Corp., Arnold, MD*
Ultrasonics Vice-Chair*	**Mauricio Pereira da Cunha**	*University of Maine, Orono, ME*
Ferroelectrics	**Thomas R. Shrout**	*The Pennsylvania State University, PA*
Ferroelectrics Vice-Chair*	**Bruce A. Tuttle**	*Sandia National Laboratories, NM*
Frequency Control	**Samuel Stein**	*Symmetricom, Boulder, CO*
Publications	**Donald Yuhas**	*Industrial Measurement Systems Inc. IL*

Awards	**Helmut Ermert**	*Ruhr-Universität Bochum, Germany*
Awards Vice-Chair*	**Bernhard R.Tittmann**	*The Pennsylvania State University, PA*
Fellows*	**Fred S. Hickernell**	*Motorola (retired), Phoenix, AZ*
Finance	**Herman van de Vaart**	*Honeywell (Retired), Plymouth, MA*
Finance Vice-Chair*	**Jan Brown**	*JB Consulting, West Whatley, MA*
Membership Services	**Rajesh K. Panda**	*Philips Medical Systems, Andover, MA*
Chapters Vice-Chair*	**Elizabeth H. Schenk**	*STERIS Corporation, Mentor, OH*
Nominations	**Peter Smith**	*McMaster University*
Nominations Vice-Chair*	**Ray Filler**	*US Army CERDEC, Fort Monmouth, NJ*
Newsletter Editor*	**Jan Brown**	*JB Consulting, West Whatley, MA*
Web Edior-In-Chief*	**Kendall Waters**	*SVMI, Fremont, CA*
Standards	**Don Malocha**	*University of Central Florida, Orlando, FL*
Standards Vice-Chair*	**Robert W. Schwartz**	*University of Missouri - Rolla, MO*
Transactions EIC*	**Marjorie P. Yuhas**	*Industrial Measurement Systems Inc. IL*
Sr. Past President	**Gerald V. Blessing**	*NIST (retired), Gaithersburg, MD*
Jr. Past President	**Art Ballato**	*US Army CERDEC, Fort Monmouth, NJ*
Sr. Student Member*	**Yinbo Li**	*University of Virginia*
Jr. Student Member*	**Christian Hansen**	*Ruhr-Universität Bochum, Germany*
Jr. Student Member*	**Daniel Tinberg**	*Pennsylvania State University*

IEEE and IEEE UFFC-S Enrollment

Get Free UFFC-S Membership by Joining IEEE on Site:

The 2008 IEEE International Ultrasonics Symposium has a discount conference registration fee for IEEE members. If you are not an IEEE member and wish to receive a member discount when registering on-site, you should join IEEE through the IEEE booth

near the registration desks. As a bonus, we will be able to provide you a free UFFC membership for one year (notice that the UFFC membership can only be offered to IEEE members and it normally requires a small amount of fee on top of the IEEE membership fee). The UFFC membership will allows you to have an on-line access to the IEEE Transactions on Ultrasonics, Ferroelectrics, and Frequency Control (TUFFC) and to receive all UFFC Newsletters for one year. Special IEEE/UFFC-S forms should be filled out in the IEEE booth. Students are not eligible for this offer.

Free UFFC-S Membership for Some IEEE Members:

If you are already an IEEE member in good standing but would like to join the UFFC society the first time when registering the conference during the on-site registration, you will also be eligible to receive a one-year free UFFC membership by filling out the IEEE/UFFC-S forms in the IEEE booth.

UFFC CD Archive

Ordering UFFC CD Archive:

If you are an IEEE member and would like to order an IEEE UFFC digital archive CD set or its updates, please click the "Order CD Archive" link at the conference website at: http://ewh.ieee.org/conf/ius_2008.

Conference Management / Acknowledgments

The 2008 IEEE International Ultrasonics Symposium (IUS) acknowledges the support from the following organizations:

Conference Management in China:

China International Conference Center for Science and Technology (CICCST – http://www.ciccst.org.cn/) has been contracted by the 2008 IEEE IUS to perform various local arrangements such as on-site registration, negotiations of venue, audio/visual, logistics, hotels, visa, exhibits, local tours, post-conference China tours, and arrangements for poster boards, meals, book printing, and entertainments, etc. CICCST is a division under the China Association of Science and Technology (CAST – http://english.cast.org.cn/).

Other Companies:

Mira Digital Publishing, St. Louis, Missouri, USA. – For technical programs (abstract submission, review, conference program, meeting planner, the 2nd Technical Program Committee (TPC) meeting support, and conference books) and the production of the context-sensitive multimedia DVD conference proceedings – http://www.miracd.com/.

YesEvents, Baltimore, Maryland, USA. – For online conference registration with real-time reporting and administration system that also supports the on-site registration – http://www.yesevents.com/.

Doubletree Hotel Chicago O'Hare Airport-Rosemont, USA. – For 2nd TPC meeting of the 2008 IEEE IUS in Chicago, Illinois, USA. – http://doubletree1.hilton.com/en_US/dt/index.do

Industrial Measurement System, Inc., Aurora, Illinois, USA, headed by Dr. Don Yuhas, Vice President for Publication of the UFFC Society. – For sending blast emails for publicity such as announcing deadlines of the conference – http://www.imsysinc.com/.

Cooperation:

The Acoustical Society of China (http://www.i-ince.org/membership/china.htm), and the ***Institute of Acoustics*** (http://www.ioa.ac.cn/english/default.asp), Chinese Academy of Sciences.

Future Ultrasonics Symposia

2009 IEEE International Ultrasonics Symposium:

Location: Rome, Italy.
General Chair: Massimo Pappalardo, *Università degli Studi de Roma Tre, Italia.*

2010 IEEE International Ultrasonics Symposium:

Location: San Diego, California, USA.
General Chair: Bob Potter, *Vectron International - Hudson, NH*

Technical Sessions

Abstracts:

The abstracts are arranged as follows:

- Oral Sessions, Monday, November 3, 2008
- Poster Sessions, Monday, November 3, 2008
- Oral Sessions, Tuesday, November 4, 2008
- Poster Sessions, Tuesday, November 4, 2008
- Oral Sessions, Wednesday, November 5, 2008
- Poster Sessions, Wednesday, November 5, 2008

Author Index:

An author index will follow the abstracts.

1A. Blood Flow Measurements

Hall 3

Monday, November 3, 2008, 10:30 am - 12:00 pm

Chair: **Jorgen Arendt Jensen;**
Technical University of Denmark, Denmark.

1A-1

10:30 AM **Ultrasound particle velocimetry: an emerging technique in cardiology**

Hairong Zheng[1], Robin Shandas[2]; *[1]Shenzhen institute of advanced technology,Chinese Academy of Sciences, shenzhen, guangdong, China, [2]University of Colorado at Boulder, Boulder, CO, USA.*

Background, Motivation and Objective

Development and progression of vascular atherosclerosis and aneurysms are modulated by local hemodynamics such as wall shear stress and blood flow recirculation. However, current non-invasive imaging techniques either cannot resolve the multi-component nature of such flows or are too cumbersome for routine clinical use. We have recently developed a novel contrast-based echo particle image velocimetry technique (Echo PIV) to quantify complex blood flow vectors non-invasively. The method is angle independent, possesses excellent spatial and temporal resolution, and is simpler to use than MRI velocimetry. Here we examine the utility of this method to characterize hemodynamics around carotid plaques and abdominal aortic aneurysms using in vitro phantoms.

Statement of Contribution/Methods

A custom-designed Echo PIV system, including a 7.5 MHz 128-element linear array transducer, custom-designed firing sequences, and a velocimetry algorithm for analyzing the backscattered radio-frequency (RF) data, was used along with commercially available ultrasound contrast microbubbles to obtain velocity vectors through models of carotid stenosis and abdominal aortic aneurysms. Both steady and pulsatile flows were used.

Results

Echo PIV was able to resolve and quantify the complex hemodynamics around carotid plaques and abdominal aortic aneurysms, including proximal flow velocity vectors and distal vortex recirculation patterns. The method was also capable of producing time-resolved multi-component velocity, shear stress and vorticity maps. Good agreement between peak velocities found by Echo PIV and those measured by conventional ultrasound Doppler was also found.

Discussion and Conclusions

The Echo PIV method provides an easy, direct and accurate means of quantitatively yet non-invasively characterizing complex vascular hemodynamics with comparable spatial resolution and superior temporal resolution to MRI velocimetry.

1A-2

11:00 AM **A Bi-directional, Real-time Blood Flowmeter using an Implantable CMUT Array**

Mengli Wang[1], Jingkuang Chen[1], Xiaoyang Cheng[1], Tongsheng Zhang[2], Xueyuan Liu[3]; *[1]University of new mexico, Electrical Engineering, USA, [2]University of new mexico, Department of Neurology, USA, [3]The Eastman Kodak Company, USA.*

Background, Motivation and Objective

Blood flow rate provides important information for detection of early-stage strokes, irregularity of cerebral circulation, as well as many other cardiovascular and brain disorders. Currently the non-invasive blood flowmeters, including laser Doppler and piezoelectric ultrasound flowmeters deliver restricted flow rate resolution for blood flow deep inside the tissue. Previously, we reported the development of a needle-shaped CMUT array for invasive blood flow measurement. Based on this implantable CMUT array, this paper describes the development of a blood flowmeter with a board-level signal processing circuit that enables real-time monitoring of the blood flow rate and the flow direction.

Statement of Contribution/Methods

This implantable blood flowmeter uses a CMUT array integrated on a needle- shaped silicon substrate working as both for ultrasound transmission and reception. The transmitter was driven by a train of tone bursts of 40 volts with a fundamental frequency of 6MHz and PRF of 10KHz which gated 20 cycles of the oscillator signals. The ultrasound transmitted from the CMUT was directed into the vessel where they were reflected by the blood cells and the vessel walls. The acoustic signals returning to the CMUT receiver were fed into a 40dB preamplifier. By mixing this amplified signal with the original ultrasound signal through a demodulator, the Doppler shift signal was identified. The echo ultrasound was then sampled by a pulse delayed in time domain from the transmitted burst corresponding to detecting the signal at a specific distance. A phase quadrature sensitive demodulation technique was used for the detection of the flow direction.

Results

A roller pump was used to circulate a blood mimicking fluid through a rubber tube with an inner diameter of 4.8mm in the experiment. The bidirectional blood flow velocity was shown in figure (b) in which the positive velocity means forward flow with respect to the transducer array orientation while the negative velocity means a reverse flow. Both the rate and direction of blood flow were displayed in real time about 5-10 ms per signal segment. The resolution of the flowmeter was 2mm/second per 10Hz of Doppler frequency shift.

Discussion and Conclusions

Real-time blood flow measurement using an implantable CMUT array has been demonstrated. Higher flow rate resolution is achievable if ultrasound transducers of higher frequencies are used.

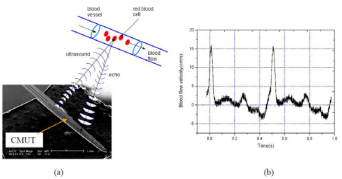

Figure: (a) Schematic of Doppler blood flow measurement using an implantable CMUT array. (b) Blood flow rate and flow direction measured in real time.

1A-3

11:15 AM **Duplex scanning using sparse data sequences**

Sara Klingenberg Møllenbach, Jørgen Arendt Jensen; *Technical University of Denmark, Dept. of Electrical Engineering, Lyngby, Denmark.*

Background, Motivation and Objective

The velocity distribution in vessels can be displayed using duplex scanning where B-mode acquisitions are interspaced with the velocity data. This gives an image for orientation, but lowers the maximum detectable velocity by a factor of two. Other pulse sequences either omits the B-mode image or leaves gaps in the velocity data, which makes it difficult to output audio data.

Statement of Contribution/Methods

The near full velocity range can be maintained and B-mode images shown by using a sparse data sequence with velocity and B-mode samples intermixed. The B-mode samples are placed in a (sparse) periodical pattern, which makes reconstruction of the missing samples possible. The periodic pattern has the length T samples, where M are for B-mode and A for velocity estimation. The missing samples can now be reconstructed using a filter bank. One filter bank reconstructs one missing sample, so the number of filter banks corresponds to M. The number of sub filters in every filter bank is the same as A. Every sub filter contains fractional delay (FD) filter and an interpolation function. Many different sequences can be selected to adapt the B-mode frame rate needed. The drawback of the method is that the maximum velocity detectable is scaled by the factor A/T.

The approach has been investigated using in vivo RF data from the Hepatic vein and Aorta from a 33 year old healthy male. A B-K Medical 3535 ultrasound scanner has been used in Duplex mode with a B-K 8556, 3.2 MHz linear array probe. The sampling frequency, the fprf and the resolution is 15MHz, 3.5 kHz, and 12 bit sample. The resulting data contains 8000 RF lines with 128 samples at a depth of 45mm for the vein and 50mm for Aorta.

Results

Sparse sequences are constructed from the full data sequences to have both a reference sequence and sparse data sequences. After reconstruction the reference and the reconstructed spectrum are almost identical when characterized by the Signal to Noise Ratio (SNR). This is investigated and optimized by altering the number of filter coefficients, the implementation of the fractional delay filter, and the sparse sequence. The hepatic vein data are processed with 9 filter coefficients, a FD filter implemented with a Knab window and sequence length T of 7 RF lines. By removing 1 line the SNR is calculated to be 74.49 dB, by removing 3 lines the SNR is 71.67dB. If instead 4 (over half) RF lines are removed the SNR is 68.96 dB, making it possible to have two sequences at the same time. The investigation of Aorta show, that because the spectrum is wider, it puts some restrains on the selection of the sequence. The shortest sequence for getting a good spectrum consist of 6 lines, with one missing line (12.5%, SNR = 56.33 dB).

Discussion and Conclusions

Using sparse sequences both B-mode and velocity data can be acquired with only a modest degradation in maximum velocity. The reconstruction gives errors below the normal noise level in velocity data, and the full audio signal is precisely reconstructed from the data.

1A-4

11:30 AM **Systematic Validation of the Echo Particle Image Velocimetry Technique using a Patient Specific Carotid Bifurcation Model**

Fuxing Zhang[1], Craig Lanning[2], Luciano Mazzaro[1], Bryan Rech[1], Jiusheng Chen[1], S. James Chen[3], Robin Shandas[1,2]; *[1]University of Colorado at Boulder, Dept. of Mechanical Engineering, Boulder, CO, USA, [2]The Children's Hospital, Dept. of Pediatric Cardiology, Aurora, CO, USA, [3]Univ. of Colorado Health Science Center, Division of Cardiology, Aurora, CO, USA.*

Background, Motivation and Objective

Full field opaque flow measurement technique has significant applications in evaluating details of cardiovascular hemodyamics non-invasively. Echo Particle Image Velocimetry (Echo PIV) is a simple-to-use method that has shown promising results in the measurement of blood flow characteristics. However, no systematic validation of Echo PIV in a realistic vascular anatomy against reference-standard methods has been done.

Statement of Contribution/Methods

A patient-specific carotid bifurcation model was created using biplane angiography data from an adult human male. The model reproduced vascular geometry accurately, while allowing for both Optical PIV and Echo PIV to be performed on the same flow field. A pulsatile pump and a compliance chamber were used to produce physiologically realistic flow conditions, with a peak velocity around 70 cm/s, heart rate of 75 beats/min, mean Reynolds number of 1484, and a Womersley number of 16.1. Echo PIV spatial resolution was 0.9 (mm) x 0.7 (mm) in lateral and axial directions, and its temporal resolution was 1.4 msec in this study (Best temporal resolution can be up to 0.7 msec).

Results

Centerline and near wall velocity profiles obtained from Optical PIV and Echo PIV were compared at common branch (CCA), carotid sinus (CS) and internal branch (ICA). Results show that the Echo PIV measurements agreed well with Optical PIV results at each position (mean error = 7.7% +/- 3.5%). Radial velocity profiles from both techniques within the CCA over one cycle are shown below. Shear rates from Echo PIV agreed well with those obtained from Optical PIV at all locations as well (mean error = 9.2% +/- 5.7%). Echo PIV was capable of quantitatively recording the complex flow fields observed within the sinus region with both high temporal and high spatial resolution, including recirculation, flow separation, and transient vortices.

Discussion and Conclusions

Echo PIV provided full-field instantaneous velocity measurements within a physiologically realistic carotid bifurcation vascular anatomy with very good agreement to Optical PIV (discrepancy < 10%) over a wide variety of flow conditions.

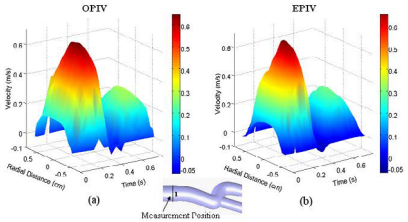

1A-5

11:45 AM **Monitoring X-ray Contrast Agent Injections with Doppler Ultrasound**

Lars Hoff[1], Knut Brabrand[2], Nicolay Berard-Andersen[3], Gjermund Fjeld Olsen[3], Svein Medhus[4]; *[1]Vestfold University College, Horten, Norway, [2]Rikshospitalet University Hospital, Oslo, Norway, [3]Neorad AS, Oslo, Norway, [4]ITec Consulting AS, Baerum, Norway.*

Background, Motivation and Objective

During CT examinations, approximately 100 ml of x-ray contrast agent is regularly injected intravenously at flow rates up to several ml per second. In some rare cases, some or all the contrast agent may leak out of the vein and into the surrounding tissue, causing an extravasation with potential harm to the patient. In other cases, equipment failure may prevent the contrast agent from being injected. This may cause an unsatisfactory CT examination, while exposing the patient to x-ray radiation, and the procedure must be repeated. Hence, there is a need for a system to reliably monitor contrast agents injections. We have developed a dedicated CW Doppler ultrasound unit for this purpose.

Statement of Contribution/Methods

X-ray contrast agents consist of water soluble molecules forming a homogeneous liquid without ultrasound scatterers. Intravenous injection of the agent generates turbulence and creates a heterogeneous mixture of blood and contrast agent. This increases ultrasound scattering, and the flow velocity is higher than in the spontaneous venous blood. Hence, an ultrasound Doppler should be able to detect increases in both acoustic backscatter and flow velocity

We have designed a system using a 4 MHz transducer with three transmit elements formed as rods, 13 mm long and 3 mm wide. The elements are placed in a line perpendicular to the blood vessel and firing at 45° angle to the blood velocity. Three identical receive elements are mounted parallel to the transmit elements. The elements are molded into a flexible silicon probe, which is attached to the patient's arm with elastic tape. CW excitation is chosen, in order to be independent of depth. This creates an “acoustic net” across the patient's arm, detecting anything that moves.

Dedicated analog electronics for the three channel Doppler unit was developed using standard electronic components. Quadrature demodulation gives a baseband signal in the audible range, and allows separation into positive and negative velocities. The resulting six audio channels are digitized at 25 kS/s, analyzed real-time in a laptop PC, and presented as spectrograms and total power.

Results

The system has been tested on 143 patients in various CT centers. Preliminary data analysis shows that the system is able to monitor contrast injections. A correct injection normally shows a strong increase in received power and a spread out velocity spectrum. Four cases of extravasations and equipment failure were detected as either delayed or missing increase in power.

Discussion and Conclusions

A dedicated ultrasound Doppler system can be used to monitor x-ray contrast injections, and the system can detect errors caused by equipment failure or extravasation.

2A. Tissue Characterization

Room 201 A/B/C

Monday, November 3, 2008, 10:30 am - 12:00 pm

Chair: **Shin-ichiro Umemura;**
Tohoku University, Sendai, Japan.

2A-1

10:30 AM **Signed Echo Imaging of Carotid Arteries**

Shin-ichiro Umemura[1], Takashi Azuma[2]; [1]*Tohoku University, Biomedical Engineering, Sendai, Miyagi, Japan,* [2]*Hitachi Central Reserach Laboratory, Kokubunji, Tokyo, Japan.*

Background, Motivation and Objective

The phase of an echo reflected at an impedance change interface carries the sign of the change, but the detection of the phase of each echo is difficult in medical ultrasonic imaging because of the interference with adjacent echoes. We proposed a novel method for detecting the sign of echoes[1,2].

[1] S. Umemura and T. Azuma, Proc. 2006 IEEE Ultrasonic Symp., pp.1580-83 (2006).

[2] S. Umemura and T. Azuma, Proc. 2007 IEEE Ultrasonic Symp., pp.1760-63 (2007).

Statement of Contribution/Methods

Two times of transmission/reception at central frequencies of Nf and (N+1)f, where N is a natural number, are performed. Then, phase-sensitive detection between the (N+1)-th power of the echo signal at Nf and N-th power of the echo signal at (N+1)f gives the signed echo signal, because the odd-th power of the echo signal carries the sign of the original echo signal while the even-th power always has the same positive sign.The proposed signed echo imaging was applied to human carotid arteries. Transmission/reception at 10 MHz was performed immediately after those at 5 MHz at each beam position with a commercially available wide-band probe. The RF echo signals were captured and the phase sensitive detection between the signal at 10 MHz and the square of the signal at 5 MHz was performed in a computer.

Results

The signed echo images obtained with a healthy volunteer (Fig. 1) and a volunteer with plaques (Fig. 2) are shown, where blue and red colors show the negative and positive signs, respectively. The intimae and medina of the far-side arterial wall of a healthy volunteer are typically stained in blue. In contrast, the suspected plaques are partly stained in reddish color.

Discussion and Conclusions

The proposed signed echo imaging may have a potential to characterize plaques on carotid arterial walls.

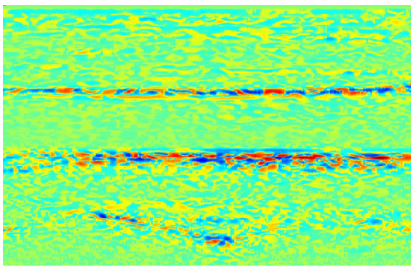

Fig.1 Carotid artery of a healthy volunteer.

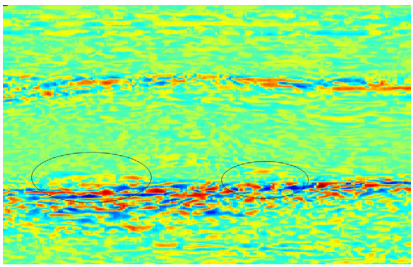

Fig.2 Carotid artery of a volunteer with plaques.

2A-2

10:45 AM **Viscoelasticity of lung tissue with surface wave method**

Xiaoming Zhang, Randall Kinnick, James Greenleaf; *Mayo Clinic, Physiology and Biomedical Engineering, Rochester, MN, USA.*

Background, Motivation and Objective

Considerable interest in the elastic properties of soft tissue has increased in medicine due to their clinical relevance for monitoring the progression of various diseases as well as a biomarker for cancer. Most newly developed imaging modalities use the shear wave to estimate the elasticity of tissue. These include shear wave elasticity imaging, supersonic shear wave imaging, acoustic radiation force impulse imaging, and vibro-acoustography. We have developed a novel surface wave method for non-invasively estimating the elasticity of tissue [X. Zhang et al., J. Acoust. Soc. Am., vol. 122, 2522-2525, 2007]. In this method, a localized ultrasound radiation force is remotely and non-invasively applied inside the tissue. The surface wave speed is used to estimate the elasticity of tissue.

Statement of Contribution/Methods

In this paper, we have extended this method for measuring viscoelastic material properties of animal lungs. The lung of a 14 Kg porcine is casted in a tissue mimicking gelatin phantom. The lung can be pressurized through a connecting tube to its trachea. A small force less than one Newton is generated by a mechanical shaker on the lung. The surface wave propagation on the lung is measured by laser. This method is independent of the excitation probe. It measures the speed and decay of the surface wave propagation on the lung.

Results

The shear elasticity μ1 and shear viscosity μ2 are, respectively, μ1 =3.69 kPa and =8.61 PaS for 0 mm Hg pressure (relative to the ambient air pressure). The shear elasticity and shear viscosity are, respectively, μ1 =5.66 kPa and μ2 =8.93 PaS for 5 mm Hg pressure. The shear elasticity and shear viscosity are, respectively, μ1 =7.99 kPa and μ2 =10.37 PaS for 10 mm Hg pressure.

Discussion and Conclusions

A noninvasive surface wave method can be used for measuring the viscoelasticity of lung. Although the ultrasound can't get through the lung, the surface wave can be generated by the radiation force of ultrasound and measured by ultrasound on the surface of lung. This new method may be used for diagnosing the lung's disease as well as evaluating the lung's function.

2A-3

11:00 AM **Texture analysis of ultrasound liver images with contrast agent to characterize the fibrosis stage**

Olivier Basset[1], Francois Duboeuf[1], Bertrand Delhay[1], Elisabeth Brusseau[1], Christian Cachard[1], Jean-Pierre Tasu[2]; *[1]Universite de Lyon, Creatis, France, [2]CHU Poitiers, France.*

Background, Motivation and Objective

Because ultrasound imaging is a simple, reliable and non-invasive modality, it is particularly indicated for assessing the liver fibrosis stage. An ultrasound evaluation of the liver fibrosis stage of chronic liver disease can be performed by assessing various ultrasound factors such as the liver size, the bluntness of the liver edge, the coarseness of the liver parenchyma, nodularity of the liver surface, the size of the lymph nodes around the hepatic artery, the irregularity and narrowness of the inferior vena cava, ... However, the conventional definition of the fibrosis stage of the liver based on evaluation of these ultrasound factors is imperfect and lacks accuracy and reliability. The present work proposes to identify the liver fibrosis stage from a characterisation of the perfusion from ultrasound images. A liver disease leads to changes in the organ perfusion that can be emphasised on ultrasound images by injecting contrast agent. In the evolution of the disease, 5 stages are usually defined and a visual evaluation of these stages is often difficult.

Statement of Contribution/Methods

In the present study, we propose to characterize the evolution of the perfusion when the contrast agent is injected from image texture analysis and ultrasound tissue characterization techniques. Texture analysis consists in extracting parameters characterizing the arrangements of the more or less regular patterns that constitute the image. Different texture analysis techniques are implemented: statistical methods (co-occurrences matrices), model-based methods, to provide a set of parameters that is a signature of the tissue pathological state.

Results

To validate this approach, a set of 21 sequences of images livers at different pathological stages is used. The sequences represent at the beginning the liver without contrast agent and about 20 s later the contrast agent is fully distributed in the tissue. A window of homogeneous tissue is extracted each second for processing.

74 textural features were extracted from 8 different texture analysis methods and were calculated on each image. The features presenting an intercorrelation coefficient larger than 0.95 were eliminated and 30 features remain for the statistical analysis. 8 features were calculated to represent the evolution of each textural parameter during contrast agent diffusion.

The results show that the texture analysis of images corresponding to the fully distributed contrast agent is more relevant to identify the stage of fibrosis than the features characterizing the evolution of the texture. In particular, a classification of the samples in two classes (the 2 highest pathological grades versus the 3 lowest) exhibits a sensitivity of 63 % and a specificity of 91 %. The statistical significance was set to $p<0.05$.

Discussion and Conclusions

These results show the potentiality of combining contrast agent and texture analysis on ultrasound images. A study on a larger number of samples will be conducted.

2A-4

11:15 AM **Computer aided detection of prostate cancer based on GDA and predictive deconvolution**

Simona Maggio[1], **Luca De Marchi[1],** Martino Alessandrini[2], Nicolo Speciale[1]; *[1]University of Bologna, DEIS, Bologna, Italy, [2]University of Bologna, ARCES, Italy.*

Background, Motivation and Objective

Early diagnosis and treatment of prostate cancer is essential to decrease the mortality rate for this malignancy. Current screening programs, based on prostate-specific antigen testing and digital rectal examination are a matter of controversy, because they can detect only advanced-stage tumors. Up to 40% of prostate cancers are isoechoic on ultrasound and therefore "invisible" to Trans-rectal Ultrasound (TRUS) images. For this reason, different features should be computed from the acquired RF signal to extract information for tissue classification. Moreover, deconvolution could be employed to reduce the transducer influence on the procedure. This work presents a multi-feature computer-aided detection (CAD) system for prostate cancer based on multifeature nonlinear classification.

Statement of Contribution/Methods

Textural, spectral, and fractal features, envelope parameters and morphologic characteristics of US images can be used to highlight changing in RF signal distribution and acoustic information. Such amount of features results in high computational cost and in redundant information for classification purposes. We implemented an Hybrid Feature Selection technique, based on min-Redundancy Max-Relevance algorithm and misclassification error, to prune feature set and select from 10 to 40 parameters. Analysis about supervised and unsupervised feature extraction techniques leads to choose a Generalized Discriminant Analysis (GDA) algorithm with Gaussian kernel to map data in a space where linear classification is able to accurately separate different regions. Final classification is performed through a Fisher Linear Discriminant. Different blind deconvolution algorithms based on adaptive filtering were tested as pre-processing procedures, to eliminate the effect of the transducer point spread function which produces an unphysical blurring of the back scattered echo.

Results

The propose CAD system was trained on 1,000 random samples, constituted by Region of Interests (ROIs) coming from 37 TRUS images (classified through biopsy in 22 malignant and 15 benignant cases). The obtained classification model was tested on 37 different prostate frames (about 110,000 ROIs). The model is characterized by sensitivity ranging from 0.82 to 0.89, specificity ranging from 0.90 to 0.96, accuracy ranging from 0.90 to 0.95 and area under ROC curve from 0.95 to 0.96, by varying the number of features, from 10 to 40.

Discussion and Conclusions

CAD systems working on TRUS images perform more objective prostate cancer diagnosis and simplify biopsy guidance. Our approach to prostate cancer detection is based on RF echo signal analysis, nonlinear mapping of data and Fisher linear classification and includes deconvolution as a preprocessing step. This approach provides a system performing highly accurate detection inside the prostate zone and it can be considered a suitable tool for both diagnosis and mini invasive therapies.

2A-5

11:30 AM Improving the quality of QUS imaging using full angular spatial compounding

Roberto Lavarello, Michael Oelze; *University of Illinois at Urbana-Champaign, Electrical and Computer Engineering, USA.*

Background, Motivation and Objective

Quantitative ultrasound (QUS) techniques make use of information from backscattered echoes normally discarded in conventional B-mode imaging. Using scattering models and spectral fit methods, properties of tissue microstructure can be estimated. The variance of QUS estimates is usually reduced by processing data obtained from a large region of interest (ROI), which severely limits the spatial resolution of the technique. In this work, the use of full angular (i.e., 360°) spatial compounding is proposed as a means of improving the variance and spatial resolution of QUS.

Statement of Contribution/Methods

Simulations were performed using f/4 transducers with 10 MHz center frequency and 50% -6-dB bandwidth. The synthetic phantoms consisted of two concentric circular cylindrical regions. The inner and outer cylinders had radii of 7 mm and 12.5 mm, respectively. Both cylinders had a scatterer concentration of 9 scatterers per resolution cell. The average scatterer diameters (ASDs) for the outer and inner cylinders were set to 60 μm and 30 μm, respectively. A total of four different random scatterer populations were generated and analyzed. ASD estimates were obtained using data obtained at up to 256 angles of view. For an initial assessment of the improvement in variance when using compounding, ROIs of size 16λ by 16λ were used. This ROI size lies above current thresholds for QUS ROI selection as found in the literature. Next, ASD estimates were obtained using ROIs of size 8λ by 8λ, which lie below current thresholds for QUS ROI selection. The standard deviation of the ASD estimates was used as quality metric for the results.

Results

Consistent results were obtained among all synthetic phantoms analyzed under the same conditions. When using ROIs of size 16λ by 16λ and 64 angles of view, the average of the estimated ASD standard deviations were 1.96 μm and 2.98 μm in the outer and inner cylinders, respectively. The use of multiple views reduced the ASD standard deviation by average factors of 3.94 and 4.67 in the outer and inner cylinders, respectively when compared to the single view case. When using ROIs of size 8λ by 8λ and 64 views, the average estimated ASD standard deviations were 2.75 μm and 3.77 μm in the outer and inner cylinders, respectively. The precision for the outer and inner cylinders improved by average factors of 5.28 and 5.36, respectively when compared to the single view case. Using more than 64 views did not result in significant further improvement of the precision of the estimates for both ROI sizes.

Discussion and Conclusions

The use of full angular compounding was found to significantly improve the trade off between spatial resolution in QUS imaging and precision of QUS estimates. These results suggest that QUS imaging can achieve optimal performance on a platform capable of producing views of an object from 360°, e.g., a tomographic breast scanner.

2A-6

11:45 AM Using resolution enhancement compression to reduce variance of scatterer size estimates from ultrasonic backscattered signals

Jose R. Sanchez, Darren Pocci, Michael L. Oelze; *University of Illinois at Urbana-Champaign, Electrical and Computer Engineering, Urbana, Illinois, USA.*

Background, Motivation and Objective

Quantitative ultrasound (QUS) imaging techniques based on ultrasonic backscatter have been used successfully to diagnose and monitor disease. The contrast resolution of QUS images depend on the variance of QUS estimates. The variance of QUS estimates decreases with increasing bandwidth of the imaging system. Therefore, increasing the bandwidth of the imaging system through a novel coded excitation scheme is hypothesized to improve the contrast resolution of QUS imaging. The variance of QUS estimates is also decreased with increasing echo signal-to-noise ratio (eSNR) achieved through coded excitation resulting in further improvements in QUS imaging.

Statement of Contribution/Methods

Resolution enhancement compression (REC), a coded excitation and pulse compression technique, was used to enhance the -6-dB bandwidth of an ultrasonic imaging system. The objective of this study was to combine REC with QUS (REC-QUS), and evaluate and compare improvements in scatterer size estimates obtained using the REC technique to conventional pulsing (CP) methods. Simulations and experimental measurements were

conducted with a weakly focused (f/4) single-element transducer (center frequency of 10 MHz and a -6-dB bandwidth of 80%). Using REC, the -6-dB bandwidth was enhanced to 152%. In simulations, a software phantom was generated with a lesion and background region containing scatterers with diameters 10 μm smaller than the scatterers in lesion. In experimental measurements, a tissue mimicking phantom that contained glass spheres with scatterer diameters that range from 45 to 53 -μm was evaluated. Estimates of average scatterer diameter in the simulations and experiments were obtained by comparing the normalized backscattered power spectra to theory. Improvements in REC-QUS over conventional QUS were quantified through estimate bias and variance.

Results

In simulations, scatterer diameter estimates from the lesion resulted in a bias and variance of 6.15 and 147.1 for CP and 2.49 and 2.8 for REC. Conversely, for the background the bias and variance were 22.4 and 84.4 for CP and 11.4 and 13.8 for REC. The smaller variance in estimates associated with the REC method leads to improved detection and differentiation of the lesion from the background when compared to CP. In experimental measurements, the mean and variance of estimates were 66.5 and 145.6 for CP and 51.7 and 17.2 for REC. Similarly, estimates of variance decreased by 88% by using REC-QUS over conventional QUS.

Discussion and Conclusions

By using REC, the broadening of bandwidth and gain in eSNR yielded improved QUS estimates in terms of decreased bias and variance. These results suggest that REC-QUS has the potential to improve the diagnostic capabilities of QUS imaging techniques for clinical applications.

3A. Imaging Systems and Methods

Hall 5A

Monday, November 3, 2008, 10:30 am - 12:00 pm

Chair: **Jeff Ketterling;**
Riverside Research Institute, NY, USA.

3A-1

10:30 AM **3-D Laparoscopic Imaging**

Michael Zipparo[1], **Clyde Oakley[1],** Rich Denny[1], Said Azim[1], Michael Berman[2], V Balannik[2], A Zilberman[2], R Nechushtai[3], S Soferman[2], D Kopelman[4]; *[1]W. L. Gore and Associates, Inc., Englewood, CO, USA, [2]Biomedicom, Jerusalem, Israel, [3]The Hebrew University, Life Science Institute, Jerusalem, Israel, [4]emek Medical Center, Department of Surgery B, Afula, Israel.*

Background, Motivation and Objective

Laparoscopic ultrasound enables surgeons to visualize the internal structure of organs, providing an important adjunct to optical guidance. Because the imaging array is placed in direct contact with the organ of interest without intervening tissue that can attenuate and distort the sound field, a higher operating frequency can be used to facilitate higher resolution images. Development of 3-D imaging capability can enable easier visualization of organ morphology, an important consideration for physicians adopting a new modality who may not have a high degree of training and experience in interpreting 2-D images.

Statement of Contribution/Methods

A 7 MHz, 128 element linear array laparoscope probe with two-way articulation and 135 degree rotation capability was modified to facilitate acquisition of multiple image planes. The rotation feature naturally enables volumetric reconstruction when in contact with an organ much better than probes with four-way articulation. A brushless DC motor was used to drive the rotation, and a 6 degree of freedom position sensor was used to register the image plane locations and correct for any backlash in the mechanism. Acquisition was performed at 3 seconds per volume.

Results

The mechanically driven conventional linear array allows better resolution images with less complexity than would be possible using an electronic 2-D array. The 3-D volume reconstruction was demonstrated during a live animal model laparoscopic procedure. Multiplanar reconstruction of the gall bladder shows the display of three orthogonal image planes simultaneously with a volume rendering. A GUI interface allows selection of any image plane. A transparency adjustment feature is shown to optimize the rendering for tissue border demarcation. Simulated tumors are detected, and a blood vessel tracking feature co-displays the cursor location of blood vessels traced on one plane to the location on each orthogonal image plane as well as the 3-D volume rendering.

Discussion and Conclusions

Future development of systems will allow the superposition or co-display of ultrasound images with images generated from different modalities such as CT and MRI. The guidance of tools incorporating their own position sensors will be possible, e.g. RF ablation instruments. Increased frame rate might be made possible through the development of an integrated motor rotation system and image processing hardware and software upgrades.

3A-2

10:45 AM An Inertial-Optical Tracking System for Portable, Quantitative, 3D Ultrasound

Abraham Goldsmith[1], Dr. Peder C. Pedersen[1], Dr. Thomas L. Szabo[2]; *[1]Worcester Polytechnic Institute, Deptartment of Electrical and Computer Engineering, Worcester, MA, USA, [2]Boston University, Department of Biomedical Engineering, Boston, MA, USA.*

Background, Motivation and Objective

Freehand 3D scanning provides an unrestricted scanning area at the cost of accuracy. 2D array and mechanical scanning produce limited volumes but are more accurate. The goal of this work is to implement an accurate, freehand 3D imaging system using integrated tracking sensors.

Statement of Contribution/Methods

Our contribution is the development of a 5 DOF calibrated tracking system that can be attached to or contained completely within the ultrasound transducer. This tracking system allows an accurate 3D volume to be reconstructed from a sequence of non-parallel and unevenly spaced image frames acquired by freehand scanning. We use an optical tracking sensor combined with a multi-lens optical system to track the transducer position on the skin surface. Angular velocity and linear acceleration are measured using a 3-axis MEMS gyroscope and accelerometer. A navigation computer is implemented in an FPGA which integrates the angular rate signals to compute angle, measures linear acceleration to recover initial pose, and performs coordinate transformations to track the probe relative to its starting position. Stradwin 3D ultrasound software combines the position and pose information from the tracking system with image frames from a Terason t3000 ultrasound transducer to provide real-time 3D volume reconstruction.

The system was designed to fit into an existing transducer housing with little modification. The optical system was implemented with and without an image conduit coupling the skin surface image to the sensor. Utilizing an image conduit allows the electronics to be moved away from the scanning end of the transducer, where space is at a premium.

Results

Reconstruction performance was evaluated by scanning a cylindrical inclusion in a CIRS model 044 ultrasound phantom. Scan patterns were chosen to provide performance data for individual degrees of freedom, including X and Y position, yaw, and pitch. 3D images were reconstructed with and without the position and orientation information. The 3D images of the inclusion were manually segmented and their volumes compared to the known inclusion volume. For straight line scan paths, the measured volume had an average error of 1.63% using the position information compared to 3.95% without. Scan paths that varied in the X and Y linear dimensions had an average volume error of 2.94% using the position information compared to 14.1% without. Scan paths that included yaw angle variation had an average volume error of 5.86% using the position information compared to 17.06% without.

Discussion and Conclusions

This work demonstrates the feasibility of using sensors inside the ultrasound probe to reconstruct accurate 3D images. Accurate freehand scanning makes ultrasound a more useful diagnostic tool by making it easier to capture useful data and enabling enhanced visualization. This work has additional relevance for mobile ultrasound, where low cost, size, and portability are valuable.

3A-3

11:00 AM A Novel Flexible, Conformable Ultrasonic Transducer System

Rahul Singh[1], Shyam Natarjan[2], David Bennet[2], Michael Lee[2], Priyamvada Tewari[2], Warren Grundfest[3], Hua Lee[1], Elliott Brown[1], Martin Culjat[2]; *[1]University of California, Santa Barbara, Electrical and Computer Engineering, Santa Barbara, CA, USA, [2]University of California, Los Angeles, Center for Advanced Surgical and Interventional Technology (CASIT), Los Angeles, CA, USA, [3]University of California, Los Angeles, Bioengineering, Los Angeles, CA, USA.*

Background, Motivation and Objective

A novel medical ultrasound system using flexible, conformal transducer arrays has been designed and demonstrated. Current medical ultrasound techniques require scanning with rigid multi-element arrays to obtain images over curved body surfaces. A thin flexible conformal array transducer has the advantage that it can be wrapped around extremities and curved surfaces, providing multiple unique "looks" around internal objects and allowing for high resolution volumetric images in real-time without the need for scanning.

Statement of Contribution/Methods

A flexible, conformal ultrasound transducer and imaging system has been developed, with the concept illustrated in Fig. 1. The transducer array was fabricated on a "flexible substrate" comprised of silicon islands held together with polydimethyl siloxane (PDMS) joints. The active elements of the array were PZT-5H with a backing layer to improve bandwidth and a paraylene cover to match the array to biological tissue. A portable, lightweight transceiver was developed consisting of a digital signal processor, a microcontroller, and a capture interface. The return signals are captured by 14-bit analog-to-digital converters while the transmit signal was generated using 14-bit digital-to-analog converters. The captured data is then reconstructed into image using processing techniques based on a backward propagation algorithm. PZFlex, a finite element time domain piezoelectric simulator, was used to model and simulate the system by generating the acoustical data that was used for input to the image processing algorithms. A soft tissue phantom was built to verify the simulated results experimentally.

Results

The imaging system operates at center frequency of 14 MHz and has a pulse width of 0.25 mm in water. Finite element models of the flexible, conformal transducer and human tissues were implemented in PZFlex, and the resulting simulated waveforms were inputted into the image reconstruction algorithm. A corresponding soft tissue phantom was fabricated and experimental data collected off the phantom was inputted into the algorithm as well.

Discussion and Conclusions

The resulting images, while preliminary, demonstrate the feasibility of the flexible conformable ultrasound array concept. However, further refinements to the transducer architecture, pulsing, and image processing algorithms are needed to improve image quality.

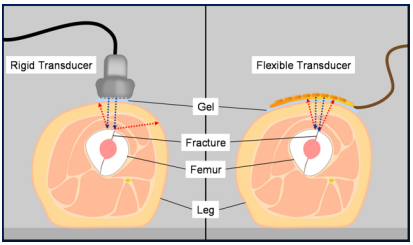

3A-4

11:15 AM **Magnitude, Origins, and Reduction of Abdominal Ultrasonic Clutter**

Muyinatu Lediju[1], Michael Pihl[1], Stephen Hsu[1], Jeremy Dahl[1], Caterina Gallippi[2], Gregg Trahey[1]; *[1]Duke University, Biomedical Engineering, Durham, NC, USA, [2]University of North Carolina, Biomedical Engineering, Chapel Hill, NC, USA.*

Background, Motivation and Objective

Clutter is a noise artifact in ultrasound images that degrades contrast and corrupts diagnostic information. It is most easily observed in anechoic or hypoechoic regions, such as in cysts, blood vessels, and urine in in-vivo bladders. Several sources of clutter include: reverberation; off-axis scattering; returning echoes from previously-transmitted pulses; and random thermal, electronic, and acoustic noise. Harmonic imaging is one method known to reduce clutter in some patients. The objective of this research is to quantify and compare clutter magnitudes in fundamental and harmonic images, identify relative sources of clutter in in-vivo bladder images, and propose an alternative method to reduce clutter in abdominal images.

Statement of Contribution/Methods

Field II simulations were performed to determine magnitudes of clutter noise due to beamforming. Clutter magnitudes were also quantified in fundamental and harmonic images of two phantoms and five in-vivo bladders. Contour plots and graphs of clutter as a function of distance were used to assess clutter magnitudes. In-vivo bladder experiments were performed to distinguish between several sources of clutter. The abdomen above the in-vivo bladder was axially displaced during successive-frame image acquisition, and Finite Impulse Response (FIR) and Blind Source Separation (BSS) motion filters were applied to the resulting data to reduce clutter arising from the abdominal wall.

Results

The minimum clutter signals in the simulated and phantom bladder images were -53 dB and -30 dB, respectively, each relative to their respective echogenic borders. The average magnitude of clutter in in-vivo bladder images from five volunteers was -15 ± 3 dB, relative to the mean signal of the bladder wall outline. The abdominal wall was the main contributor to clutter in bladder images. Random thermal, acoustic, and electronic noise and echoes from previously-transmitted pulses were found to be minimal contributors. FIR and BSS motion filters reduced abdominal clutter by 3-9 dB and 15-24 dB, respectively, in fundamental images and by 0-12 dB and 12-15 dB, respectively, in harmonic images.

Discussion and Conclusions

The simulated and phantom images contain clutter resulting from the isochronous volume of the beamformer point spread function. Sound reverberation in abdominal tissue is believed to cause the majority of clutter in in-vivo bladder images, which is greater than that in simulated and phantom data. Off-axis scattering is most likely the cause of clutter adjacent to the lateral and distal bladder walls. The clutter measured in in-vivo bladder images is postulated to be the minimum amount of clutter present in images of other abdominal organs. This clutter complicates the detection of subtle or low-contrast lesions. One promising method for reducing abdominal clutter is to displace the abdomen during successive-frame image acquisition and motion filter the clutter that moves with the abdominal wall.

3A-5

11:30 AM **Sources of image degradation in fundamental and harmonic ultrasound imaging**

Gianmarco Pinton, Gregg Trahey; *Duke University, Biomedical Engineering, Durham, NC, USA.*

Background, Motivation and Objective

Although harmonic imaging is used extensively, the mechanisms for image quality improvement are still poorly understood. In the simplified case of a homogeneous medium the improvements in harmonic imaging can be linked to reductions in the main lobe width and the height of side lobes. It has been suggested, however, that the primary benefit of harmonic imaging is reduction of clutter noise and less sensitivity to phase aberration. This requires complex simulations or experiments that incorporate the effects of tissue heterogeneities and multiple scattering, which has imposed significant challenges in describing and quantifying the mechanisms of image quality improvement with harmonic imaging.

Statement of Contribution/Methods

We investigate and quantify the losses in image quality for fundamental and harmonic imaging due to three sources of image quality degradation using a novel numerical algorithm that simulates ultrasonic propagation in a medium with heterogeneities in nonlinearity, attenuation, density, and speed of sound. The numerical simulations generate the full pressure waveforms at every point in the simulated field and therefore allow great flexibility in calculating the ultrasound images and PSFs. This numerical implementation models the fine structure of human tissue and the arrangement of the tissue in the human body. The simulation of a 2.1 MHz diagnostic transducer through a measured representation of the human abdominal layer generated the transmit-receive PSFs.

Results

A comparison of the theoretical and simulated power spectrum of the backscatter from a field of randomly distributed scatterers in the Rayleigh regime is presented. Transmit-receive PSFs were calculated for a typical 0.6 fractional bandwidth ultrasonic pulse. These PSFs distinguish between clutter occurring in the isochronous volume, in the region preceding the pulse, and in the region trailing the pulse.

Discussion and Conclusions

There are three distinct conclusions that can be drawn from the presented data. First the primary source of image degradation in the fundamental PSF comes from reverberation in the near-field abdominal structures. Measurements of the reverberation clutter alone indicate that it is 26 dB higher for the fundamental PSF compared to the harmonic PSF and that it is the single largest source of clutter. Second phase aberration is the largest source of clutter in the harmonic PSF. When phase aberration is removed using a uniform velocity and unchanged impedance medium the harmonic PSF exhibits an 11 dB improvement in the isochronous volume, which is significantly larger than the 0.9 dB improvement from reverberation clutter subtraction. Finally clutter in the PSFs occurs primarily from low level contributions distributed over a large area, especially in the fundamental PSF where plots of the radial distribution show no appreciable decrease with increasing distance.

3A-6

11:45 AM **Ultrasound Breast Imaging using Full Angle Spatial Compounding: In-vivo results**

Christian Hansen[1], Markus Hollenhorst[2], Nils Hüttebräuker[1], Wilko Wilkening[3], Lothar Heuser[2], Gernot Schulte-Altedorneburg[2], Helmut Ermert[1]; *[1]Ruhr-University Bochum, Dept. of Electrical Engineering and Information Technology, Group for High Frequency Engineering, Bochum, Germany, [2]Ruhr-University Bochum, Institute of Radiology, Neuroradiology and Nuclear Medicine, Bochum, Germany, [3]Ruhr Center of Excellence for Medical Engineering (KMR), Bochum, Germany.*

Background, Motivation and Objective

For Full Angle Spatial Compounding (FASC) ultrasound data is acquired in one cross-sectional plane from aspect angles all around an object. FASC aims at improving image quality by achieving an isotropic resolution and reducing artifacts, speckle and depth dependency. Though FASC has already been investigated in the 1980s, recent improvements in ultrasound imaging (e.g. harmonic imaging, beam forming and array technology) encourage a re-assessment. Furthermore, it was shown in-vitro that FASC can also improve contrast imaging. To apply FASC to breast imaging, we developed an add-on system to a conventional ultrasound scanner, integrated into an examination couch. Here, we present first in-vivo results obtained from this system on patients with breast lesions.

Statement of Contribution/Methods

Controlled by servo-motors an ultrasound probe is moved fully around a female breast in a water tank. From multiple viewing angles of the same section plane beamformed rf-data was acquired using a Siemens Acuson Antares in phase-inversion mode and the Ultrasound Research Interface. A low frequency curved array (CH4-1, 2.5 MHz) was used to achieve a high penetration depth, a wide field of view and an optimal excitation of contrast agents. All A-lines gathered under all viewing angles were corrected for refraction at the water-tissue-interface and for the different speeds of sound of the two media before being superimposed and interpolated to form a compound image. Compound images of multiple section planes were combined to form 3D data sets.

Results

We scanned both healthy volunteers and volunteering patients to evaluate the image quality of our system. Though the center frequency used was low, the obtained compound images show a high isotropic resolution of 1.03 mm (PSF, in-vitro). Breasts were depicted holistically and structures inside (cooper-ligaments or breast lesions) were clearly visible. The correction of refraction helped to reconstruct the correct geometry and to minimize the loss in resolution. Figure 1 shows the uncorrected (a) and corrected (b) compound image of a patient with a breast carcinoma (arrow).

Discussion and Conclusions

In-vivo results of FASC show high potential for breast imaging. Further clinical studies will determine the sensitivity and specificity in comparison to a mammography or MRI. Those studies will also focus on in-vivo perfusion imaging with contrast agents.

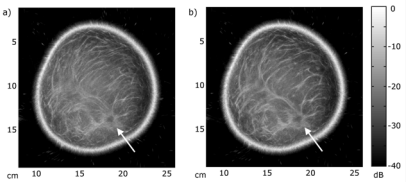

4A. Transducer Materials Characterization

Hall 5B

Monday, November 3, 2008, 10:30 am - 12:00 pm

Chair: **Yongrae Roh;**
Kyungpook National University, South Korea.

4A-1

10:30 AM **A High Power Adapter for the HP4194A Impedance Analyzer**

Daniel Stutts; *Missouri University of Science and Technology, Mechanical Engineering, Rolla, MO, USA.*

Background, Motivation and Objective

The HP4194A impedance analyzer has long been used to the impedance of piezoelectric structures by exciting the device under test (DUT) by a low power test signal over the frequency band of interest. The HP4194A is capable of producing a test voltage of up to 1 V RMS, and is adequate for low-field, linear characterization. However, it is well known that pronounced nonlinear effects due to high-field excitation can be very important in application of common piezoelectric material. Therefore, since the HP4194A is limited to a 1V RMS test signal, it cannot stimulate nonlinear field effects in any sample of reasonable thickness.

Statement of Contribution/Methods

Hence, in order to measure these effects, while at the same time, leveraging the comprehensive functionality of the HP4194A, a high-power adapter (HPA) was designed. The high-power adapter takes the low-voltage test signal from the HP4194A, and amplifies it up to a maximum of 1280 V_{pp} at a maximum power of 1.25kW. The amplified voltage signal is applied to the DUT, and the resulting current measured, scaled, and returned back into the HP4194A inputs for measurement.

Results

The performance of the HPA was experimentally verified on a variety of lead zirconate titanate (PZT) samples, over a range of field strengths, and nonlinear effects, including the jump phenomenon, were observed.

Discussion and Conclusions

The HPA has subsequently been used in the characterization of high-density capacitors, and has proven to be a relatively cost effect means to extend the functionality of the venerable HP4194A. The basic design will be presented, as well as experimental results, and example HP measurement control code used during testing.

4A-2

10:45 AM **Fundamental Performance Characterisation of High Frequency Piezocomposites made with Net-shape Viscous Polymer Processing for Medical Ultrasound Transducers**

Duncan MacLennan[1], Christine Demore[2], **George Corner[3],** Tim Button[4], Jocelyn Elgoyhen[4], Hana Hughes[4], Carl Meggs[4], Sandy Cochran[2]; *[1]University of Strathclyde, DTC Medical Devices, Glasgow, United Kingdom, [2]University of Dundee, Institute for Medical Science and Technology, Dundee, United Kingdom, [3]NHS Tayside, Ninewells Hospital, Dundee, United Kingdom, [4]Applied Functional Materials Ltd, Birmingham, United Kingdom.*

Background, Motivation and Objective

High frequency(HF) ultrasonic transducers are desired for medical examinations requiring high spatial resolution. Piezoelectric ceramic – polymer composites have improved acoustic matching and piezoelectric coupling compared to bulk ceramics but a typical 1-3 piezocomposite is around 30 µm thick when optimized for 50 MHz operation, requiring ceramic pillar structures of 15 µm or less. Fabrication by standard dice-and-fill technology is thus challenging. This may be overcome using micromoulding of ceramic paste produced by viscous polymer processing (VPP). Characterisation is urgently needed to aid use of this material in HF transducers. Traditional characterisation is impossible due to the small structures involved and such measurements are required to account for the wide variation in properties of piezocomposite compared to conventional homogeneous materials.

Statement of Contribution/Methods

This paper reports definitive results from detailed characterisation of multiple HF composites, both before and after inclusion in transducers. Measurement of fundamental properties are based on electrical impedance spectroscopy and data fitting to a theoretical model based on the 1-D piezoelectric wave equation and homogenized piezocomposite model of Smith and Auld [1]. Properties derived from 1-D models have been incorporated into finite element models for verification and compared to monolithic materials, $LiNbO_3$, PVDF, P(VDF-TrFE) and PMN-PT, and composites made from both PZT and $LiNbO_3$ using dice-and-fill.

Results

Results from fitted models and experimental impedance measurements showed a close correspondence. The VPP piezocomposites investigated showed effective piezoelectric properties within the following ranges: c_{33}: 1.76 -6.77 ($x10^{10}$ Nm^{-2}), e_{33}: 2.04-8.50 (C/m), ε_R^S: 70.6 – 460, d_{33}: 7.82-12.70 ($x10^{-11}$m/V), h_{33}: 2.01-2.09 ($x10^9$ V/m) and k_T: 0.45-0.51.

Discussion and Conclusions

Intensive characterisation of VPP composite confirms reports [2] that this method has good potential for fabrication of HF piezocomposites. The performance characteristics show the material compares well with data from commercial materials and alternative material types. The characterisation reported here will assist in improving composite properties. Comparison of parameters such as permittivity indicate that further benefits, such as array fabrication, are viable.

1. Smith WA, Auld BA "Modeling 1-3 Composite Piezoelectrics: Thickness Mode Oscillations". IEEE Trans. Ultrason., Ferroelect., Freq. Contr., vol. 38 pp 40-47, 1991

2.A. Abrar, D.Zhang, B.Su, T.W.Button, K.J.Kirk and S.Cochran "1-3 connectivity piezoelectric ceramic-polymer composite transducers made with viscous polymer processing for HF ultrasound" Ultrasonics, pp. 479 – 48, 2004

4A-3

11:00 AM **Characterisation of an Epoxy Composite Filler Suitable for Microfabrication Processes**

A.L. Bernassau, D. Hutson, C.E.M. Démoré, S. Cochran; *Institute of Medical Science and Technology, United Kingdom.*

Background, Motivation and Objective

High frequency array transducers (>30 MHz) based on fine-scale ceramic-epoxy composites are currently being developed for medical imaging applications. These arrays are feasible because of the net-shape 1-3 piezocomposites being developed by collaborators [1], and the photolithographic patterning of the array electrodes, which have shown good results for fabricating the small electrodes (30 µm pitch). These techniques require the epoxy used to fill the composite to be resistant to chemicals such as acetone and heat up to 100 °C. The epoxy must also have low viscosity for successful filling and minimal shrinkage to prevent composite distortion during curing. We report on the characterization and optimization of the properties of an epoxy for high frequency array fabrication.

Statement of Contribution/Methods

The epoxy chosen for this work is Epofix (Struers, Solihull, UK), which was originally designed for metallography applications. In the work reported here, samples have been cured for two hours at different temperatures: room temperature, 60 °C, 80 °C and 100 °C. Solvent resistance, decomposition of the material, degassing and hardness of the material were then evaluated as a function of the curing temperature using stylus-based surface profiling (Veeco, Cambridge, UK), Raman spectroscopy, mass spectrometry and the nano-indentation technique (Hysitron, Minneapolis, USA), respectively. Also, the acoustic and dielectric properties of the samples were measured.

Results

Raman spectroscopy has shown no decomposition of the material for the four different samples. The samples cured at higher temperature show a better resistance to the chemicals and the epoxy was softer by approximately 10 % when cured at room temperature than when cured at higher temperatures. The hardness of the sample cured at 100 °C was found to be 0.24 GPa. Mass spectrometer analyzes have shown no degassing of the Epofix under vacuum. However, when heated and under vacuum a degassing of the epoxy was observed. Acoustic properties as longitudinal velocity, density, shear waves and dielectric properties vary minimally with curing temperature, and were found to be similar to other epoxies commonly used as piezocomposite fillers.

Discussion and Conclusions

Acoustic and material characterisation has demonstrated that Epofix is suitable as a substrate for photolithography as well as a filler for fine-scale piezocomposite materials for high frequency operation. For optimum properties and performance, the epoxy should be cured at 100 °C.

[1] T.W.Button, et al, IEEE Ultrasonics Symposium, pp.1625 – 1628, 2005

4A-4

11:15 AM **Method for Curvature Measurements with Ultrasound**

Elfgard Kuehnicke[1], Michael Lenz[1], Hans-Georg Trier[2], Jörg Sorber[1], Gerald Gerlach[1]; *[1]TU Dresden, Germany, [2]TIMUG e. V. Bonn, Germany.*

Background, Motivation and Objective

For a number of applications, the distance and the curvature radius of an object interface are the main parameters of interest. Examples are the preparation of eye surgery, the detection of inclusions in solid materials, the detection of bubbles in two phase flows, and the process control of growth processes.

As B-mode measurements are subject to strong system inherent measurement inaccuracies, they reproduce the topographical structure only roughly. This paper therefore studies a novel non-scanning method for curvature measurements.

Statement of Contribution/Methods

For the measurements, an annular array is used. The curvature information is obtained by varying the sending wave front, and at the same time split up the sound field at the ultrasound receiver. The size, shape and electrical focusing of a 6-element ultrasound annular array have been optimised for this purpose by sound field calculations, so that the array allows for the sound to be focused in front of, onto, and behind the interface layer.

As measurement objects for the first practical studies, different spherically curved balls with a curvature radius from 6 to 20 mm were used. The balls were placed at a distance of z=10mm in water.

Depending on the reflector curvature radius and the particular focusing depth, the sound pressure distribution on the ultrasound receiver varies in a characteristic way (Fig. 1).

For the given measurement set up, the sound field on the ultrasound receiver was calculated as a function of the focus depth. This gives calibration curves for the determination of the curvature radius.

Results

The simulations show, that the radius of a convex curvature can be determined with only six transducer elements without scanning with an accuracy of better than 1%. The measurements show, that the performance and accuracy depend on the exact realisation of the array design.

Discussion and Conclusions

Further simulations demonstrate, that the method is also applicable for structures with several interfaces.

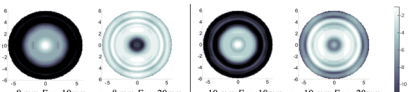

Fig. 1: Ultrasound pressure distribution on the ultrasound receiver as a function of the curvature radius *r* of the reflector. The simulations apply to a measurement distance of *z* = 10 mm in water. The distance *Foc* of the ultrasound focal zone is varied.

4A-5

11:30 AM **Hybrid Ultrasonic Characterization Method for the Full Matrix Electromechanical Coefficients of Ferroelectric Relaxor-based Single Domain 0.93Pb(Zn1/3Nb2/3)O3 ¨C0.07PbTiO3 Single Crystal**

Rui Zhang, Zhu Wang, Wenwu Cao; *Harbin Institute of Technology, China.*

Background, Motivation and Objective

The relaxor based (1-x)Pb(Zn1/3Nb2/3)O3-xPbTiO3 [PZN-xPT] ferroelectric single crystal systems with composition near the Morphotropic Phase Boundary (MPB) exhibit superior electromechanical property at room temperature. these single crystal systems possess extremely attractive application potential in making large

displacement actuators, high sensitivity medical ultrasonic imaging transducers with superior broadband characteristics, and many other electromechanical devices

Statement of Contribution/Methods

For theoretical studies and device designs, obtaining the complete material property data sets is very crucial. In this paper, a complete data set of electromechanical coefficients of ferroelectric relaxor-based PZN-7%PT single crystal with single domain was measured by a hybrid ultrasonic method

Results

It was found that the electromechanical coupling coefficient k33 and the piezoelectric constant d33 for single domain PZN-7%PT are 54% and 200 pC/N, respectively. Both of them are much smaller than those of multi-domain PZN-7%PT poled along [001] direction. However, the shear piezoelectric constant d15 of single domain PZN-7%PT crystal can reach 4600 pC/N, which is much higher than that of multi-domain PZN-7%PT crystal.

Discussion and Conclusions

The full matrix electromechanical coefficients data set reported in this paper will be helpful to understand the physical mechanism of the superior electromechanical properties of these relaxor-based ferroelectric single crystal systems, and also benefits the design of broadband high frequency medical ultrasonic transducers employing PZN-7%PT crystals as the core transduction element

4A-6

11:45 AM **PZT piezoelectric thick film with enhanced electrical properties for high frequency ultrasonic transducer applications**

Benpeng Zhu, Dawei Wu, Qifa Zhou, K.Krik Shung; *NIH Transducer Resource Center, Department of Biomedical Engineering, University of Southern California, USA.*

Background, Motivation and Objective

Very high frequency (>100MHz) transducer is being explored as clinical tools for the examination of the anteriror segment of the eye, skin and intravascular imaging. It is very difficult and time-consuming to lap down and mechanically machine very thin piezoelectric ceramics or crystal in the fabrication of high frequency single element transducers and arrays. Therefore, piezoelectric thick-film technology may be a good low-cost alternative.

Statement of Contribution/Methods

In this paper, piezoelectric Pb(Zr0.52Ti0.48)O3 thick film of approximately 10 μm thickness with enhanced electrical properties has been fabricated on the (111) Pt/Ti/SiO2/Si substrate using a ceramic power/sol-gel solution modified composite method. The PZT composite solution was prepared from PZT powder (Piezo Technologies K-600) and PZT solution (0.4M) in mass ratio 1: 4. A 1-min rapid thermal annealling (RTA) at the desired temperature was performed to crystallize each layer.

Results

X-ray diffraction analysis and scanning electron microscope revealed that the film was in the well-crystallized perovskite phase and cracked free. At 1 KHz, The dielectric constant and the loss were 1925 and 0.015, respectively. The remnant polarization was 42.0μC/cm2 at room temperature. A high frequency single element acoustic transducer with parylene as the matching layer was designed and fabricated from high quality PZT thick films. It showed a bandwidth at -6 dB of 50% at 156 MHz.

Discussion and Conclusions

Using a sol-gel modified composite method, we have successfully fabricated high dielectric constant PZT thick film with a thickness around 10 μm in well-crystallized perovskite phase.The film exhibited good dielectric and ferroelectric properties.The dielectric constant and the polarization of the film are much lager than those of the films reported in the literature. Using this PZT thick film, a high frequency single element transducer (156 MHz) with 50% bandwidth was fabricated. The measured performance was in good agreement with the result modeled by piezoCAD.

5A. Material Properties I

Hall 5C

Monday, November 3, 2008, 10:30 am - 12:00 pm

Chair: **Jan Brown;**
JB Consulting, MA, USA.

5A-1

10:30 AM **Ultrasonic Determination of Elastic Stiffness Tensor Components of Porous Materials: Sample Geometry, Inhomogeneity, and Wavelength Dependencies**

Christoph Kohlhauser, Christian Hellmich, Josef Eberhardsteiner; *Vienna University of Technology, Institute for Mechanics of Materials and Structures, Vienna, Vienna, Austria.*

Background, Motivation and Objective

Ultrasonic longitudinal and transversal bulk waves propagating in a medium generate very small strains and thus enable the direct determination of elastic normal and shear stiffness coefficients of materials, respectively. These diagonal coefficients are obtained from velocity measurements of waves transmitted in symmetry planes of anisotropic materials. Determination of the phase velocity in general planes yields the off-diagonal coefficients of anisotropic stiffness tensors. Application of ultrasound is especially of interest for porous materials, because mechanical testing may be strongly biased by inelastic deformations within the microstructure of such materials.

Statement of Contribution/Methods

The wavelength, dependent on the frequency of the ultrasonic wave, defines the scale of the characteristic loading of the structure built up by the considered material. According to continuum (micro)mechanics, this scale must be considerably larger than the material volume scale (also called representative volume element - RVE) which, in turn, is required to be much larger than the inhomogeneities within this material volume. Hence, waves detect materials at different length scales. The propagation velocity of longitudinal and transversal ultrasonic waves, at frequencies ranging from 0.1 to 20 MHz, was measured in 22 differently shaped isotropic specimens (bar, cube, plate) and in 4 cubes with cylindrical pores of different diameter (i.e. a macroscopic transversely isotropic material with an isotropic matrix) all made of an aluminum alloy.

Results

In an infinite (non-dispersive) medium, the measured (bulk) velocity is independent of the frequency of the wave, and depends exclusively on the mass density and stiffness of the investigated material. However, in finite samples, the ultrasonic wave velocity depends on geometrical parameters, including the frequency-governed wavelength.

In a dimensionless form, the wave velocity divided by the square root of stiffness over mass density is a function of the wavelength and of a characteristic cross-sectional length of the sample, both divided by the sample height. Our measurements show that low values (0.01...0.1) of the cross section-over-height parameter, indicating bar-type samples, are indeed related to bar wave propagation, in particular if the wavelength-over-height parameter exceeds a value of 1.

Discussion and Conclusions

For smaller values of the latter parameter, the lateral deformation of the sample is constrained through the existence of several wave nodes, so that mixed waves with velocities between bar and bulk wave propagate. The principle of separation of scales for bulk wave loading in materials is validated and transition regions are identified.

The results from these transmission-through tests show for given sample geometries and inhomogeneity sizes, which transducer frequencies ensure bulk wave propagation and stiffness determination at specific material length scales.

5A-2

10:45 AM **High Frequency Propagation Measurements in Microstructured Solids**

Andrew Dawson[1], Paul Harris[2], Roger Young[2], Gideon Gouws[1]; [1]*Victoria University of Wellington, New Zealand,* [2]*Industrial Research Limited, New Zealand.*

Background, Motivation and Objective

In NDT highly ordered sample microstructure may extend over large areas. This can influence high frequency propagation and unsuspected guided wave modes can occur. If these are not considered, especially in near surface measurements, the presence of such modes may negatively impact on results. An example of such a material is aluminum which is easily oxidized at its interfaces to exhibit a regular porous character to significant depths. However it is also thought that such microstructure could also be used to significant advantage especially in flaw contact measurements.

Statement of Contribution/Methods

Porous aluminum samples have been prepared by etching to have a highly regular porous microstructure and over a range of pore sizes down to pores of diameter 30 nm with spacing 60 nm. The pores extend fully through the 160um thickness making the IRL samples highly collinear. Commercial samples of similar pore sizes were also obtained which, by SEM analysis, were found to be far less collinear. The 6mm diameter samples are immersed and being hygroscopic the pores are water filled.

Focused immersion Panametrics transducers were used to illuminate the samples at 50 and 100MHz and a Precision Acoustics needle hydrophone used as receiver. The transmitter position and angle were adjusted by micrometers. The measurement without sample provides alignment and a propagation time reference for the transmission velocity calculation.

Results

The velocity and amplitude of the transmitted wave was determined for angles up to 40 degrees. The highly collinear samples demonstrated a near constant velocity of 5.2Km/s, the S0 Lamb velocity for these materials. However the commercial sample velocity at normal, 5.7Km/s, fell notably with angle, ~4.0 Km/s @ 40deg. Significant transmitted amplitude was recorded for both the collinear and commercial samples for angles to 40 deg [Note for solid aluminium the p critical angle is 14deg and the s critical angle 29deg]. Data for the differing pore size and collinear samples, and frequencies will be presented.

Discussion and Conclusions

That the collinear IRL samples transmit significant energy for angles to 40 deg with a constant velocity can be of significant value in transducer design. For example, as a face material in flaw contact measurement the scattered return signal would not undergo refraction at the coupling fluid / transducer interface. Rather the collinear microstructure acts to normalize the wavefront into the transducer and in so doing increase the return signal effective collection area and SNR.

5A-3

11:00 AM **Interfacial Waves and Stability at the Frictional Sliding Interface between Two Solids**

Yue-Sheng Wang;; *Beijing jiaotong University, Institute of Engineering Mechanics, Beijing, China.*

Background, Motivation and Objective

Interfacial waves play an important role in many fields such as geophysics, seismology and non-destructive evaluation, etc., and thus have received considerable attention. Most of the published papers are concerned with the welded interface. However, contact interfaces, smooth or frictional, are also common in practical cases. The slip dynamics and Rayleigh-Stoneley-wave theory involving frictional contact interfaces are attracting more and more scientists working with experimental, numerical and analytical tools.

Statement of Contribution/Methods

In this paper, the theoretical study is presented on the interfacial waves and stability at a frictional interface between two anisotropic elastic or piezoelastic solids that are pressed together by remote pressure and meanwhile sheared by remote shearing traction and electric load. The external loads may or may not lead to steady rigid sliding between two solids. A perturbation field propagating steadily along the interface is examined by ignoring the details of the perturbation source. The local stick¨Cslip motion at the frictionally contact interface caused by the perturbed slip pulse is studied. The Stroh formalism, together with the concept of the surface impedance tensor is

employed. The boundary value problem involving unknown slip/stick zones is cast to a Cauchy singular integral equation with an unknown integral interval.

Results

By solving the singular integral equations analytically, the explicit expressions of interface waves, which could satisfy the boundary conditions and energy balance, are therefore obtained. The explicit solutions are obtained. The existence conditions are given. Particularly, the existence conditions and physical properties of interface waves have been further discussed based on numerical calculations for practical examples.

Discussion and Conclusions

The results show: 1)Slip-stick frictional interface waves might exist in most material combinations. In some specific cases, the waves will involve 1/2 singularity at one end of slip zones while be bounded at the other end, which in the meantime requires enough large frictional coefficient. The wave speed ranges are related to the frictional coefficient. In more general cases, the interface waves will involved singularity weaker than 1/2 at one end of slip zones while be bounded at the other end. 2)Between the anisotropic elastic or piezoelastic media that are steadily frictionally sliding under the applied tractions, there will be no such interface waves that could change the stresses so as to cause the local slip motion at the interface, i.e., self-excited oscillations of instable interface waves will not transformed to the steady slip-stick motion at the interface without separation.

5A-4

11:30 AM **Applications of sonic waves in the estimation of petrophysical, geophysical and geomechanical properties of subsurface rocks**

Bikash Sinha[1], **Vivian Pistre[2];** *[1]Schlumberger-Doll Research, Mathematics and Modeling, Cambridge, MA, USA, [2]Schlumberger Beijing Geoscience Centre, Well Placement and Safety, Beijing, China.*

Background, Motivation and Objective

Sonic waves play an important role in estimating rock properties that are crucial in an efficient and safe production of oil and gas wells. An acoustic source in a fluid-filled borehole can generate both nondispersive headwaves as well as relatively stronger borehole guided modes. Processing of waveforms recorded with adequate spatial sampling yields sonic velocities in the surrounding formation over the receiver aperture. These velocities are then transformed into elastic moduli of the propagating medium. Elastic moduli of the formation provide many useful petrophysical, geophysical and geomechanical attributes of porous rocks that constitute hydrocarbon bearing formations. Petrophysical attributes of hydrocarbon bearing formations include porosity, pore pressure, and fluid mobility. Geophysical attributes of the formation deal with anisotropy characterization of formations on a seismic scale. Geomechanical properties of rock consists of estimating in-situ formation stresses and strengths as a function of radial position away from the borehole surface.

Statement of Contribution/Methods

Compressional velocity through a porous rock has been used to estimate porosity using Wyllie time-average equation whereby an interval transit time is decomposed into transit times in the solid and fluid components of the composite structure. Rock porosity can then be estimated using compressional velocity of the rock matrix and pore fluid in conjunction with measured velocity in the composite structure. There are well established correlations that help identify formation lithology in terms of the compressional to shear velocity ratio or the Poisson's ratio of the material. Plots of compressional to shear velocity ratio against compressional transit time help identify intervals containing limestone, dolomite, salt and quartz.

Results

Recent applications of elastic moduli of rocks in a reasonably uniform lithology are in the estimation of fluid mobility in porous rocks; formation stresses; and fracture characterization. The presence of a fluid-filled borehole in a tectonically stressed formation causes both radial and azimuthal heterogeneities in rock stresses. Formation stresses are estimated using an acoustoelastic model based on nonlinear continuum mechanics. This model predicts crossing dipole dispersions to be an indicator of stress differential in the borehole cross-sectional plane. In-situ rock strength can be estimated using radial variations of shear velocities obtained from the inversion of borehole dispersions. Estimates of rock stresses and strength help maintain wellbore stability during drilling and production.

6A. Thin Film & Device Characterization

Room 307

Monday, November 3, 2008, 10:30 am - 12:00 pm

Chair: **Jidong Dai;**
RF Monolithics, USA.

6A-1

10:30 AM **Analysis of Resonant SAW – Plate BAW Interaction in Periodical Couplers**

Ventsislav Yantchev[1], Victor Plessky[2], Ilia Katardjiev[1]; [1]*Uppsala University, Solid State Electronics, Uppsala, Sweden,* [2]*GVR Trade SA, Bevaix, Switzerland.*

Background, Motivation and Objective

Surface acoustic waves scattering into a semi-infinite solid have been studied since the early 60-ies. When a substrate with finite plate-like dimensions is considered, the scattering into bulk waves is transformed into scattering to bulk plate modes. There have been some attempts to model the phenomenon but the most interesting case of interaction of SAW with BAW resonator, i.e. scattering in quasi-perpendicular direction was not considered. The resonant interaction between Rayleigh SAW and near-onset Lamb Waves, through the coupling effect of an infinite periodical grating defined on the plate surface is theoretically described and its characteristics revealed.

Statement of Contribution/Methods

The analysis proposed is based on the Bloch theorem. The grating boundary conditions are considered presuming a weak surface perturbation. Further, the eigenmodes along with amplitude ratios inside such types of gratings are determined.

Results

The modes' dispersion is found to exhibit a complex stopband structure (Fig. 1). In the vicinity of the resonance condition the interaction of the waves generates new 3-component eigenmodes. Specifically, two independent eigenmodes have been found to co-exist in the structure due to the presence of the periodic grating. One of them is represented by two contra-propagating SAWs coupled to a near-onset Lamb wave while the other one is represented by a near-onset Lamb wave generating two contra-propagating SAWs. The latter judgment has been reached through comparison of the SAW reflection and BAW transmission coefficients, respectively. Initial results on resonant coupling between Blustejn-Gulyaev and shear plate modes are also presented.

Discussion and Conclusions

The proposed work clarifies the behavior of a new kind of resonant structures for future devices.

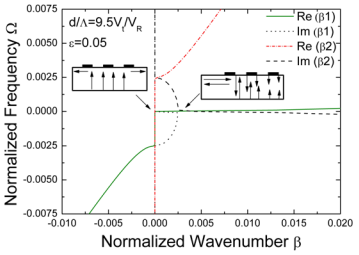

6A-2

10:45 AM **Pure-shear mode BAW resonator consisting of (11-20) textured AlN films**

Takahiko Yanagitani[1], Masato Kiuchi[2]; *[1]Nagoya Institute of Technology, Department of Applied Physics, Nagoya, Japan, [2]National Institute of Advanced Industrial Science and Technology, Osaka, Japan.*

Background, Motivation and Objective

We have previously studied pure-shear mode FBAR or SH-SAW devices using (11-20) textured ZnO films [1]. On the other hand, (11-20) textured AlN films have a number of potential advantages compared to the ZnO films, such as their high acoustic velocity, electrical breakdown strength, and chemical stability. In addition, temperature coefficient of elastic constant c_{44} and intrinsic acoustic attenuation of the AlN is expected to have smaller value than that of ZnO.

This presentation reports the first synthesis of the in-plane oriented (11-20) AlN film on a silica glass substrate. Piezoelectric properties of the film were also investigated using HBAR structure (Cu/AlN/Al/silica glass substrate).

Statement of Contribution/Methods

Ion beam sputtering deposition system with single ion gun was used for AlN film deposition. This ion gun plays two roles, sputtering nitrided Al metal target and bombarding the substrate surface. Nitrogen ion beam with 3 keV was irradiated normal to the target surface and parallel to the substrate surface simultaneously during the deposition.

Results

(10-10) and (11-20) peaks were observed in the XRD pattern (Fig.1). (0002) peak was not observed. FWHM values of the (11-20) ω-scan rocking curve and φ-scan curves in (11-22) pole figure of the film were found to be 4.6° and 23°, respectively. These results show high in-plane and out-of-plane (11-20) preferred orientation.

Discussion and Conclusions

Figure 2 shows the impulse response of the resonator. Shear wave echo train reflected from the bottom substrate surface and the top film surface were clearly observed without any excitation of longitudinal waves. These films are good candidate for pure-shear mode FBAR and SH-SAW sensors.

[1] T. Yanagitani et al., IEEE UFFC 54 (2007) 1680.

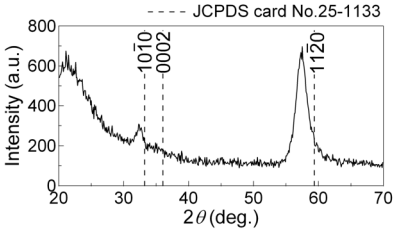

Fig. 1 XRD pattern of the AlN film/silica glass. Peak shifts are probably due to a residual stress in the film.

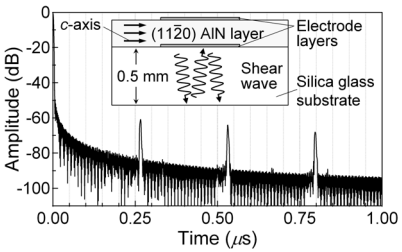

Fig. 2 Impulse response of the shear mode AlN HBAR, inverse Fourier transform of the reflection coefficient S_{11}.

6A-3

11:00 AM **Study of Frequency Dependent Lateral Leakage in RF BAW Device by Laser Probe System**

Nan Wu, Keisuke Kashiwa, Ken-ya Hashimoto, Tatsuya Omori, Masatsune Yamaguchi; *Chiba University, Graduate School of Engineering, Chiba, Chiba, Japan.*

Background, Motivation and Objective

The authors have recently developed a phase-sensitive laser probe system based on the Sagnac interferometer for the diagnosis of RF SAW/BAW devices. High quality 2D images of SAW/BAW field patterns can be captured in several minutes. Currently the system operates at frequencies upto 2.5 GHz.

We also developed integrated software which can process complex image data acquired by the laser probe under user-friendly interface.

Statement of Contribution/Methods

This paper describes the application of the developed hardware and software to the diagnosis of frequency dependent energy leakage occurring in RF BAW devices.

Results

Fig. 1(a) shows a 2D image obtained by the measurement at 1,816 MHz (near the series-resonance). The transversal resonance pattern is clearly observed in the oval region where the resonator is placed. Fig. 1(b) shows the result of the 2D FFT of this image. Several concentric circles are seen. The circles indicate the propagation of waves with different lateral wavenumbers. The brightest center circle corresponds to the thickness vibration of the longitudinal wave.

Figure 2(b) shows the result when the outermost circle was only extracted and the IFFT was applied. It is seen that the wave energy for the mode leaks away under the upper electrode of the resonator.

Discussion and Conclusions

Figures 2(a) and (c) show the results where the same procedure was applied to the measured data at two different frequencies. Compared Figs. 2(a) and (c) with Fig. 2(b), it is clear that the energy leakage is very frequency dependent. That is, the energy leakage is significant only near the series-resonance and weak at 1,812.5 MHz (below the series-resonance) and 1,840 MHz (near the parallel-resonance). At the presentation, the discussion will be made in detail.

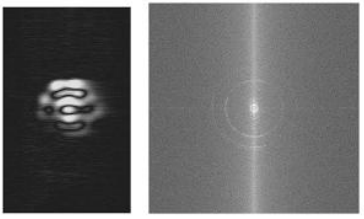

(a) x-y space (b) β_x-β_y space

Fig. 1 Measured field distribution (1,816 MHz)

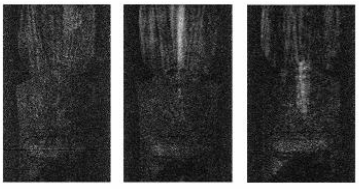

(a) 1,812.5 MHz (b) 1,816 MHz (c) 1,840 MHz

Fig. 2 Results of the IFFT after the extraction

6A-4

11:15 AM **Improvement of liquid-phase SH-SAW sensor device on 36°Y-X LiTaO3 substrate**

Takashi Kogai[1], Hiromi Yatsuda[1], Showko Shiokawa[2]; [1]*Japan Radio Co., Ltd., Japan,* [2]*SAW&SPR-Tech Co.,Ltd., Japan.*

Background, Motivation and Objective

In this paper we describe liquid-phase Shear Horizontal Surface Acoustic Wave (SH-SAW) sensors to detect conductivity and permittivity of the liquids. The conventional sensor device was composed of two-channel SH-SAW delay-lines on 36°Y-X LiTaO3substrates. One delay line has a metallized propagation area and the other has an unmetallized propagation area. However, in the case of the low-permittivity liquids, the SH-SAWs in the delay line with an unmetallized propagation area can be degraded owing to the lack of SH-SAW energy concentration of the surface. Thus the obtained permittivity and conductivity of the liquids were slightly different from the exact values.

Statement of Contribution/Methods

We designed three kinds of SH-SAW delay-lines; with a metallized propagation area, an unmetallized propagation area and a grating-structured propagation area. The center frequency of the devices was 30 MHz and the thickness of the substrate was 0.5 mm. To evaluate SH-SAW energy concentration of the surface in the liquids having different permittivities, dioxane-water mixture liquids with different concentrations were used. Our sensor devices have air-cavities above the IDTs which are composed of epoxy walls that surround the IDT and glass roofs. The air cavities can isolate the IDTs, from the liquids. On the other hand, the propagation area where SH-SAWs can propagate is open to the liquid. So we can directly dip the sensor devices into the liquids and measure the characteristics of the delay-lines.

Results

In the delay-line with unmetallized propagation area, the measured SH-SAW velocity changes in the liquids having different permittivity were compared with calculated results from a perturbation theory and an exact theory. As a result, although the exact theory showed a better agreement with the measured results, some errors for the low permittivity liquids were observed. In addition, in the measured results for low permittivity liquids, unexpected SH-SAW attenuations were observed. On the other hand, in the delay-line with a grating-structured propagation area, the SH-SAW attenuations were nearly unaffected and the SH-SAW velocity changes can be observed by the permittivity. It is cleared that the delay-line with a grating-structured propagation area is effective for low permittivity liquids in replacement of the delay-line with an unmetallized propagation area.

Discussion and Conclusions

In the delay-line with an unmetallized propagation area, SH-SAW can be attenuated due to a lack of SH-SAW energy concentration of the surface and the insufficient thickness of the substrate. On the other hand, the delay-line with a grating-structured propagation area is effective for low permittivity liquids. As a result, three-channel delay-line SH-SAW sensor devices were proposed to detect conductivity and permittivity of the liquids.

6A-5

11:30 AM **Nanoparticle patterning on 128-YX-LN substrates: the effects of surface acceleration and boundary layer streaming**

Ming Tan, James Friend, Leslie Yeo; *Monash University, Machanical Engineering, Clayton, Victoria, Australia.*

Background, Motivation and Objective

Nanoparticle patterning on a vibrating solid surface according to the vibration modes of the solid is the result of extremely high solid surface acceleration and acoustic streaming within/beyond the steady boundary layer. In this work, airborne smoke particles (SP) with an average particle diameter of 10^{-7}m are employed. These aerosols are at least one order of magnitude smaller than the fine-powders used in Reeder's experiments, and yet no special handling of the particles is required, making this method more attractive than the conventional method.

Statement of Contribution/Methods

In the experiments, SAW devices with frequencies ranging from 20 MHz to 130 MHz and airborne SP with an average particle diameter of 0.1 μm were employed. A simple numerical model has been developed to estimate the magnitude of the dominant forces pulling the nanoparticles to their final locations.

Results

Figure 1 shows SP deposited on the surface of the SAW devices. For 20 MHz SAW, SP deposition formed distinct parallel lines on the substrate surface. Standing-SAW was generated on the 20 MHz bidirectional transducers because no absorbing gels were used to prevent wave reflection. Results obtained from scanning LDV measurements [Fig. 1(a)] revealed dark lines (high SP regions) to be nodal lines where the vibration amplitudes were minimal. The surface acoustic wave launched on the 128-YX-LN substrate has an extremely high acceleration magnitude [Fig. 1(b)].

Discussion and Conclusions

Forces that have been included in this study are: 1. van der Waals force, 2. gravitational force, 3. impact force (F_{Imp}), and 4. nonlinear interaction forces (F_{Rad} and F_{drag}^{dc}) [5]. The impact force is at least 2 orders of magnitude higher than the adhesive force for Rp **O** (10^{-7}) m particle diameter. However, as particle size reduces to the sub-nanometer range, the van der Waals force begins to overcome the impact force. Once nanoparticles are lifted from the high displacement amplitude regions, the transverse acoustic radiation pressure [F_{Rad}^{x} ~ **O** (10^{-15}) N] and acoustic streaming drag [$F_{drag}^{dc(x)}$ ~ **O** (10^{-16}) N] transport the dislodged particles to the adjacent low amplitude regions, where the gravitational and adhesion forces overcome the impact force.

Discussion and Conclusions

Forces that have been included in this study are: 1. van der Waals force, 2. gravitational force, 3. impact force (FImp), and 4. nonlinear interaction forces (FRad and Fdragdc) [5]. The impact force is at least 2 orders of magnitude higher than the adhesive force for Rp O (10-7) m particle diameter. However, as particle size reduces to the sub-nanometer range, the van der Waals force begins to overcome the impact force. Once nanoparticles are lifted from the high displacement amplitude regions, the transverse acoustic radiation pressure [FRadx ~ O (10-15) N] and acoustic streaming drag [Fdragdc(x) ~ O (10-16) N] transport the dislodged particles to the adjacent low amplitude regions, where the gravitational and adhesion forces overcome the impact force.

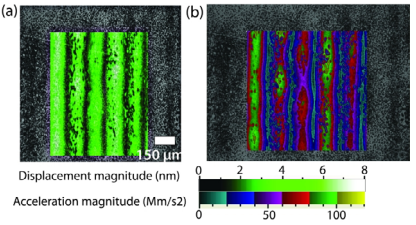

6A-6

11:45 AM **Wafer-Level Packaged SAW Filters with Resistance to Transfer Molding**

Toru Fukano, Yoshihiro Okubo, Junya Nishii, Ikuo Obara; *Kyocera Corporation, R&D Center,Keihanna, Kyoto, Japan.*

Background, Motivation and Objective

In response to the increasing demand for integrating multiple wireless standards into a single front-end module, surface acoustic wave (SAW) filters have become smaller and thinner in recent years. Packaging technology has supported this evolution of SAW filters. Conventional chip-scale packaging (CSP) structures for SAW filters are based on flip-chip bonding of a SAW chip onto a ceramic substrate, where the free space for the SAW displacements is naturally made available between the chip and the substrate. However, the use of ceramic substrate and the need for bonding area in the conventional packaging structures make it more challenging to meet the needs for smaller dimensions. In order to achieve smaller dimensions, particularly lower profile, a variety of wafer-level packaging (WLP) technologies have been applied to the packaging of SAW filters. Last year, the authors reported a class of WLP SAW filters with the size 0.8mm X 0.6mm. The electrical performance of those filters were as good as that of the conventioal CSP counterparts. Our WLP SAW filters have shown good resistence to several environmental tests, but they have not been tested with transfer molding.

Statement of Contribution/Methods

The cavity structure, which we reported last year, was constructed by resin materials. In order to make sure that the cavity has sufficient physical strength, some layers of hard materials were added on top of the ceiling of the cavity. We have fabricated WLP SAW filters with hard layers of various thickness, and performed transfer molding tests to investigate the effect of the layer thickness.

Results

We have observed the cross section of the WLP structure after the molding tests in order to evaluate the degree of the deformation of the cavity. It is shown that, for typical designs, the change of the cross-section of the cavity due to the molding can be made smaller than ten percent of the original size.

Discussion and Conclusions

It has been confirmed that our new WLP structure is well resistant against transfer molding.

1B. High-Frequency and Small Animal Imaging

Hall 3

Monday, November 3, 2008, 1:30 pm - 3:00 pm

Chair: **Yoshifumi Saijo;**
Tohoku University, Sendai, Japan.

1B-1

1:30 PM **Vital Observation and Featuring Techniques of Functional Cell-Surface Proteins Using Acoustic Impedance Microscope**

Sachiko Yoshida[1], Shiho Masaki[1], Seiji Iwasa[1], Kazuto Kobayashi[2], Naohiro Hozumi[3]; *[1]Toyohashi University of Technology, Material Science, Toyohashi, Japan, [2]Honda Electronics Co. Ltd., Toyohashi, Japan, [3]Aichi Institute of Technology, Toyota, Japan.*

Background, Motivation and Objective

Two-dimensional acoustic impedance imaging is useful for observation of vital tissues without chemical denaturalization. In the previous report, the methodology of micro-scale imaging of cross sectional acoustic impedance of vital cerebellar slices was described, and its usability to observe morphological properties was shown. In this report, we would prove the feasibility to feature the acoustic impedance corresponding to particular proteins.

Statement of Contribution/Methods

L-type Calcium channel protein expresses developing neuronal cell surface in cerebellar cortex. Cadmium ions or Calciseptine bind L-type Ca^{2+} channel specifically. Vital cerebellar slices removed from postnatal 14 to 25 day rat were sliced 400 µm thickness and treated with either 100µM Cd^{2+} or 100 nM *p*-cymene Ruthenium-Calciseptine complex, and observed using acoustic microscope HMS-1000 (Honda Electronics Co. Ltd.). *p*-cymene Ruthenium-Calciseptine complex was synthesized using mixture of *p*-cymene Ruthenium and Calciseptine for several days under the anaerobic conditions. Cerebellar slices were mounted on a flat 0.5 mm thick plastic made of polymethylmetacrylate (PMMA), and a reference material, of which acoustic impedance was known, was also placed on the same substrate.

Results

Treatment with Cd^{2+} made the acoustic impedance elevated in particular neuronal layer. As in figure, the impedance of cerebellar slice treated with Cd^{2+} (B) increased more than it without Cd^{2+} (A). This increment was canceled by co-administration of a competitive L-type Ca-channel blocker. Calciseptine, a specific L-type Calcium channel blocking peptide, reacted to *p*-cymene Ruthenium for more than 5 days, and made the impedance of the neuronal layer elevated. The increment of impedance by Cd^{2+} or *p*-cymene Ruthenium-Calciseptine depended on the cerebellar developmental process.

Discussion and Conclusions

We conclude that heavy metal binding to particular proteins was useful for the characterization of an acoustic impedance. Furthermore, we speculated p*p*-cymene Ruthenium complexes to several specific agents might visualize the distribution of particular molecules in vital tissues acoustically.

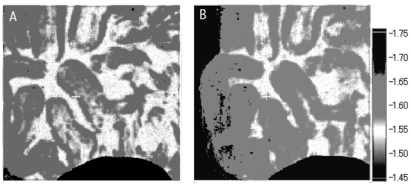

1B-2

1:45 PM **ECG-gated imaging of a mouse heart using a 40-MHz annular array**

Jeffrey A. Ketterling[1], Orlando Aristizabal[2], Daniel H. Turnbull[2]; [1]*Riverside Research Institute, New York, NY, USA,* [2]*New York University School of Medicine, Skirball Institute of Biomolecular Medicine, USA.*

Background, Motivation and Objective

The adult mouse heart can extend up to 4 mm in a short-axis cross section with heart cycles as short as 130 ms. Assessing normal and abnormal heart morphology and dynamics using high-frequency ultrasound would require fine spatio-temporal resolution. ECG-gated imaging with a 40-MHz annular array presents an opportunity to achieve high frame rates and improved depth of field with a relatively small number of transducer elements, without the need to rapidly scan the transducer. Gated imaging is a technique in which M-mode data, referenced to some start trigger, such as an ECG, are acquired at a series of lateral positions and then reassembled into B-mode images. Gated imaging is only effective when imaging objects with periodic motion, such as the heart. We present an ECG-gated, high-frame-rate imaging approach implemented with a 40-MHz annular array. The system was first validated with a moving phantom and then *in vivo* images were acquired of a mouse heart.

Statement of Contribution/Methods

Modifications were made to our 40-MHz, 5-element, annular-array-scan system to permit triggered-M-mode acquisition using an arbitrary trigger source. At a given position, data were acquired at a fixed PRF, starting with the gate trigger. The process was repeated until we acquired transmit-to-receive data for all array element combinations and then the transducer was moved to a new position and the process was repeated. The data were then post-processed to create synthetically focused images. For heart imaging, an anesthetized mouse was positioned in a physiological monitoring stage which provided a TTL trigger that was in phase with the R-wave of the ECG signal.

Results

The system was initially tested using a 40-MHz, single-element transducer and gated images were acquired of a rod attached to a linear actuator moving over a span of 2.5 mm at a rate of 3.2 Hz. The gate trigger was generated by a motion controller and occurred at one end of the rod's motion. High-speed movies of the moving rod were successfully generated at 500 fps. We then digitized *in vivo* data of a murine heart using an ECG-trigger. A software-based respiratory trigger was included to help reduce motion artifacts. The synthetically focused B-mode images showed several cardiac cycles over a 1.2 s duration captured at 100 fps over a depth of 1 cm and a width of 6 mm.

Discussion and Conclusions

Gated imaging with a 40-MHz annular array permitted high-speed imaging of cyclically moving events without the complexity of a linear array and without the need for high-speed mechanical motion. Gated imaging with an annular array permits superior image quality versus single-element transducers without any added complexity for the data acquisition.

1B-3

2:00 PM **Micro-ultrasound Takes Off (In the Biological Sciences)**

F. Stuart Foster; *Sunnybrook Health Sciences Centre and University of Toronto, Imaging Research, Toronto, Ontario, Canada.*

Background, Motivation and Objective

Disease models in the mouse have become a central part of modern biomedical research. The next major project following the sequencing of the mouse genome is the coordinated and systematic knocking out of each of the mouse's ~ 30,000 genes and the discovery of the phenotypes associated with these mutations. In addition, subtle gene variations that predispose individuals to disease will be studied in ever increasing numbers. The National Institutes of Health in the United States and other international organizations are betting 100's of millions of dollars that this will lead to critical discoveries needed along the path to better healthcare. Imaging will play a major role in this enterprise and ultrasound will take its rightful seat at the table. The successful development of high frequency mechanical sector imaging has led to an entirely new community of ultrasound users whose backgrounds are not necessarily in imaging or medicine. They are physiologists, cell and molecular biologists, developmental biologists, and animal scientists.

Statement of Contribution/Methods

This talk will describe the path of instrument and applications development for high frequency "micro-ultrasound" for mice. Basic imaging, Doppler, and contrast imaging modes will be reviewed and the current state of the art in high frequency imaging of the mouse will be discussed.

Results

Examples of functional imaging of inflammation, cardiovascular disease, and tumour microcirculation will be used to illustrate the potential and limitations of the current technology. Potential for molecular imaging will be explored in a melanoma xenograft model in which the expression pattern of VEGFR-2 is studied. In contrast imaging, performance improvements will require optimization of the microbubbles themselves, a better understanding of microbubble interactions at high frequencies in both the bound and unbound state, and improved capabilities for nonlinear excitation.

Discussion and Conclusions

One of the barriers to development of micro-ultrasound imaging has always been the lack of high frequency arrays. This barrier is about to disappear. The latest results on the development of composite materials, high frequency linear arrays, and beamformers will be presented. These devices will dominate the next generation of micro-ultrasound imaging systems. Speculation on the future of micro-ultrasound technology and applications will be discussed.

1B-4

2:30 PM **40 MHz Annular-Array In Utero Imaging of Mouse Embryos with Chirp Coded Excitation**

Orlando Aristizábal[1], Jonathan Mamou[2], Daniel H. Turnbull[1], Jeffrey A. Ketterling[2]; *[1]NYU School of Medicine, Structural Biology, New York, NY, USA, [2]Riverside Research Institute, F.L. Lizzi Center for Biomedical Engineering, New York, NY, USA.*

Background, Motivation and Objective

Ultrasound biomicroscopy (UBM) has the potential of high throughput for in utero phenotyping of mouse embryos. However, the effectiveness of UBM is limited by a shallow transducer depth-of-field (DOF) and increased attenuation from overlying fat and other tissues. In these studies, coded signals were used to excite a 40-MHz annular-array in order to increase DOF, penetration depth and signal-to-noise ratio (SNR) without degrading axial and lateral resolutions.

Statement of Contribution/Methods

A 5-element annular-array transducer was fabricated using a P(VDF-TrFE) membrane and its performance was characterized. The array had a 6-mm total aperture and a 12-mm focal length. The array was excited with a 4 µs linear chirp spanning 15 to 65 MHz and with standard mono-cycle excitation. Mouse embryos were imaged in utero at embryonic day 12 and each image consisted of 151 RF lines with 50 µm interline separation. RF data were first decoded using a mismatched filter. Then, synthetic focusing was performed by applying a delay-and-sum algorithm over 41 focal zones using the 25 transmit-to-receive (TR) signals. Fixed focus images were simulated by directly summing the 25 TR signals. For each excitation mode, 3D stacks consisting of 120 planes separated by 50 µm were digitized and stored for offline 2D and 3D analysis.

Results

The P(VDF-TrFE) based array transducer was 20 % more sensitive over a similar PVDF one. The increased penetration depth from chirp excitation (d) allowed visualization of the whole embryo, which extended 5 mm below the geometric focus (a, yellow arrow). Fine structures in the embryonic head were revealed because of the DOF increase for both mono-cycle (b) and chirp (e) array focusing. The 12 dB increase in SNR of the chirp images allowed the contours of the brain ventricles (e, yellow v's) to be distinguished from the surrounding tissue with greater contrast. Consequently, semi-automatic surface rendering of the brain ventricles for the mono-cycle dataset revealed reconstruction errors (c, white arrows) not present for the chirp dataset.

Discussion and Conclusions

In utero mouse imaging using coded excitation with a 40-MHz annular array permits an increase in penetration depth and SNR, relative to mono-cycle excitation, without sacrificing lateral and axial resolution. The increased SNR enhanced brain ventricle contrast and segmentation accuracy.

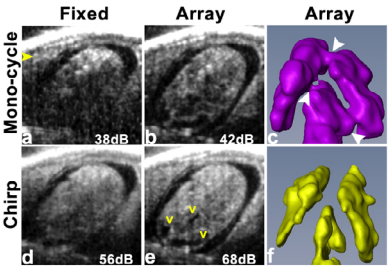

1B-5

2:45 PM **3D Mouse Imaging with High-Frequency Ultrasound (20 MHz) Using Limited-Angle Spatial Compounding**

Joern Opretzka, Michael Vogt, Helmut Ermert; *Ruhr-University Bochum, Dept. of Electrical Engineering and Information Technology, Bochum, Germany.*

Background, Motivation and Objective

For ultrasound imaging of small animals often standard systems for human medicine or special high frequency ultrasound systems are used. The former are limited to frequencies below 15 MHz, therefore their resolution is not sufficient for some applications. High-frequency systems (typically around 40 MHz) offer a very high resolution, but mostly use fixed-focus transducers, which results in a short range and a small depth of field. In this paper, an imaging system with a center frequency of 20 MHz is presented. Spatial compounding is used to improve image quality in terms of an optimized range/resolution combination. By moving the transducer in a plane parallel to the scanned surface, three-dimensional (3D) data sets are recorded.

Statement of Contribution/Methods

We have implemented a 3D ultrasound system with a single-element fixed-focus transducer (20 MHz center frequency, 13 MHz bandwidth) for pulse-echo-measurements. A mechanical set-up allows a transducer movement over an area of 28 mm x 28 mm in a plane perpendicular to the axial direction. Additionally the transducer can be tilted up to +/- 40° in the lateral/axial imaging plane. In this plane, compound images with an axial and lateral resolution (-6 dB) of 76 µm and 170 µm, respectively, are reconstructed by combining pulse echo data sets recorded at different angles. 3D data sets are obtained by recording compound data sets and stepwise movement of the transducer perpendicular to the image plane. The elevational resolution was measured by means of wire phantom measurements. From the 3D data set cross section images and maximum intensity projections are calculated offline by ray casting.

Results

The system was characterized by means of measurements on a wire phantom. The resolution in the elevational direction is 200 µm, if not limited by a larger elevational step size. The maximum dynamic range of echo signals is 60 dB, which allows for an axial field of view of 15 mm. The signal-to-noise ratio is improved by spatial compounding, which is clearly visible in results of speckle phantom measurements. Results of experiments carried out on fresh naked mouse cadavers will be presented. Data were acquired with an angular resolution of 2.5° and an elevational step size of 500 µm. Compared to conventional B-mode images, speckle noise is reduced. Imaging of highly reflecting structures is improved because of the insonation angle diversity. Shadowing artifacts, for example of ribs, are reduced as well.

Discussion and Conclusions

For applications, where real-time capability is not required, the proposed imaging system offers high potential by improved image quality through spatial compounding.

This work is supported by the German Research Foundation (Deutsche Forschungsgemeinschaft, DFG), grant ER 94/31-1.

2B. Bone I

Room 201 A/B/C

Monday, November 3, 2008, 1:30 pm - 3:00 pm

Chair: **Keith Wear;**
US Food and Drug Administration, USA.

2B-1

1:30 PM **Frequency dependence of backscatter from thin, oblique, finite-length cylinders measured with a focused transducer – with applications in cancellous bone**

Keith Wear[1], Gerald Harris[2]; [1]*USA Food and Drug Administration, Center for Devices and Radiological Health, Silver Spring, MD, USA,* [2]*Food and Drug Administration, Center for Devices and Radiological Health, Silver Spring, MD, USA.*

Background, Motivation and Objective

Ultrasound attenuation in calcaneus accurately predicts hip fracture risk. Greater understanding of attenuation mechanisms, including scattering, may help lead to improved ultrasound-based technology for diagnosis of fracture risk. A model for scattering from cancellous bone (Wear, J Acoust Soc Am, 106, 3659-3664, 1999) that assumed infinite-length, perpendicular trabeculae, has been generalized to allow for finite-length, oblique trabeculae.

Statement of Contribution/Methods

The echo from a thin cylinder (e.g. bone trabecula) is computed from the line integral of the transducer directivity along the cylinder axis. Echoes from multiple cylinders are summed incoherently. Backscatter measurements were performed with a broadband transducer (center frequency = 500 kHz) on 1) a single nylon wire as a function of tilt angle (phi) relative to perpendicular, and 2) a cancellous bone phantom containing randomly-positioned nylon wires. Backscatter coefficient (BC) over the diagnostic frequency (f) range (300 – 700 kHz) was fit to a power law, BC = A X f^n. Directivity was measured with a hydrophone.

Results

Theory and experiment agree that that backscatter power from a single nylon wire is reduced by about 50 percent (compared with normal incidence) near phi = 7 degrees (at 500 kHz). The model predicts that the power-law exponent n decreases from 4 for very short cylinders (i.e. point scatterers) to an asymptotic value of 3 for cylinders 6 mm and longer. For the cancellous bone phantom, n was measured to be 2.8 ± 0.25.

Discussion and Conclusions

The new model predicts n = 3 for a collection of sufficiently long randomly-positioned nylon wires and shows good agreement with measurements from a cancellous-bone-mimicking phantom (n = 2.8 ± 0.25) and with previous measurements from cancellous bone in vitro (n = 3.3 ± 0.2).

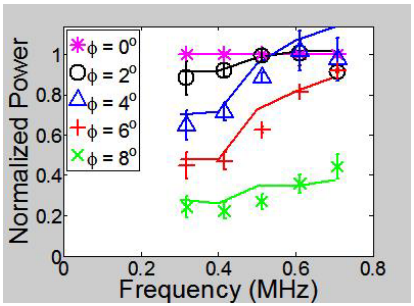

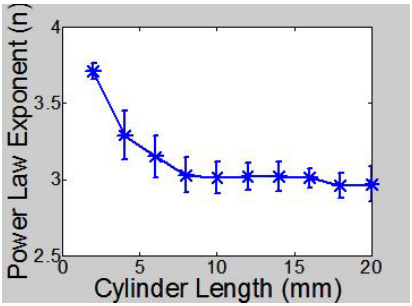

2B-2

1:45 PM **Experimental Assessment of the Relative Impact of Multiple Wave Interference and Phase-sensitive Detection on the Apparent Negative Dispersion in Cancellous Bone**

Adam Bauer, Christian Anderson, Benjamin Johnson, Mark Holland, James Miller; *Washington University, Physics, St. Louis, Missouri, USA.*

Background, Motivation and Objective

Previous work from our laboratory has demonstrated that the apparent negative dispersion observed in studies of cancellous bone can result from the interference of two propagating modes, each of which exhibits a positive dispersion consistent with the Kramers-Kronig relations. We have also demonstrated that this negative dispersion can arise when two temporally overlapping signals are incident upon a finite-aperture, phase- sensitive receiver. The goal of the present study is to quantify the relative effects of interference in the field and phase cancellation at the face of a receiver on measurements of three increasingly more complex phantoms.

Statement of Contribution/Methods

The simplest phantom consisted of a 1 cm thick Lucite plate with a small step discontinuity. A second phantom consisted of a Lucite plate (v= 2750 m/sec) and a Lexan plate (v= 2250 m/sec) bonded seamlessly. A third phantom consisted of a Lucite plate with 182 cylindrical holes of 3 mm diameter drilled in a 5.4 cm by 5.0 cm grid pattern. Computer-controlled, through-transmission, water-immersion scans of the phantoms were performed with the transmitted beam positioned systematically relative to the spatial discontinuities. The transmitting transducer consisted of a single-element, planar, 3.2 cm diameter transducer centered at 500 kHz. The through-transmitted signals were received by a 0.6 mm diameter membrane hydrophone that was raster scanned in 0.05 mm steps over a 2.8 cm by 2.8 cm grid coaxial with the transmitting transducer. Signals received by the pseudo array were processed offline to emulate phase-sensitive and phase-insensitive receivers of increasing aperture size. Apparent phase velocities and apparent attenuation coefficients were determined as functions of frequency for each configuration.

Results

For the stepped- and bonded-plate phantoms, phase cancellation at the receiver played a progressively larger role as the receiver aperture size was increased systematically, whereas for smaller diameter apertures interference in the field played the dominant role. For the Lucite phantom with the water-filled cylindrical holes, effects arising from multiple scattering resulted in time domain signals that continued for a relatively long time compared with those from the other two phantoms. In this case, the relative impact of interference in the field and phase cancellation at the receiving aperture depended upon the portion of the received time domain trace that was gated for the apparent phase velocity and attenuation determinations.

Discussion and Conclusions

Results suggest the potentially confounding role of time- and frequency-domain artifacts on measurements and illustrate the advantages of two-dimensional receiving arrays in determining the speed of sound (SOS) and slope of attenuation (nBUA) for the clinical assessment of osteoporosis. Supported in part by NSF 57238 and NIH HL 40302.

2B-3

2:00 PM **Comparison between microelastic bone properties assessed by scanning acoustic microscopy and nanoindentation**

Fabienne Rupin[1], Amena Saied[1], Davy Dalmas[2], Françoise Peyrin[3], Kay Raum[4], Etienne Barthel[2], **Pascal Laugier[1];** *[1]University Pierre et Marie Curie, France, [2]Saint-Gobain Recherche-CNRS, France, [3]INSERM-CNRS-ESRF, France, [4]Martin Luther University of Halle-Wittenberg, Germany.*

Background, Motivation and Objective

Tissue-level elastic coefficients can be extracted from acoustic impedance measurements using scanning acoustic microscopy (SAM) [K Raum, et al. Phys Med Biol, 51, 733-746, 2006]. As an extension of previous SAM studies reported by our group, this work aimed at validating acoustic microscopy as a modality to map elastic modulus at the tissue-level. Toward this goal a face-to-face comparison was conducted between SAM and nanoindentation estimates of elastic modulus.

Statement of Contribution/Methods

Three embedded transverse sections taken from 3 female human femoral mid-diaphysis were explored by SAM (8µm-spatial resolution). The acoustical tissue elastic modulus Ea of cortical bone was obtained by combining acoustic impedance and bone density derived from degree of mineralization of bone (DMB) provided by Synchrotron µ-CT (10-µm-spatial resolution), assuming a Poisson's ratio of 0.3. Nanoindentation measurements (2-µm-depth indents) were done in 2 line scans (30 indents each at 30-µm-interval) across the radial direction extending from the periosteal to the endosteal of each anatomical quadrant. Ea was compared to nanoindentation estimates of elastic modulus En. Indent images, acoustic impedance and DMB maps were digitally matched using a custom developed image fusion and analysis software for subsequent comparison between site-matched estimates of moduli and DMB.

Results

Comparison between Ea and En performed on homogeneous calibration materials (aluminium, PMMA and polycarbonate) of known Poisson ratio (n) yielded a difference of less than 1%. Results for the bone samples, indicated in the Table, are in general agreement with published results. Differences between Ea and En may likely be due to the fixed assumed value of the Poisson's ratio (v=0.3), since values comprised between 0.15 and 0.45 have been reported in the literature.

Discussion and Conclusions

Despite these differences, a highly significant linear correlation between Ea and En was found (R^2=0.64, p<0.001, RMSE=1.8 GPa) suggesting that SAM can reliably be used as a modality to quantitatively map the local variations of tissue-level Young's modulus.

Tissue type	Z (Mrayl)	Ea (GPa)	En (GPa)	DMB(g.cm-3)
Osteonal	8.5±1.8	31±12	18.4±2.9	0.92±0.09
old osteonal interstitial	9.4±1.2	36±9	20.6±2.5	0.98±0.05
Primary interstitial	10.2±1.1	42±8	21.4±2.0	0.99±0.06
All	9.1±1.7	35±12	19.5±3.0	0.95±0.08

2B-4

2:15 PM **Numerical study of the dependence of the ultrasonic parameters on apparent modulus of human cancellous bone assessed by micro finite element analysis**

Guillaume Haiat[1], Frederic Padilla[2], Myriam Svrcekova[3], Yan Chevalier[3], Dieter Pahr[3], Pascal Laugier[2], Philippe Zysset[3]; *[1]CNRS, B2OA, Paris, 75010, France, [2]CNRS, Laboratoire d'Imagerie Paramétrique, Paris, France, [3]TU Wien, Institut für Leichtbau und Struktur-Biomechanik, Wien, Austria.*

Background, Motivation and Objective

Quantitative ultrasound (QUS) has been shown to be useful to assess bone quality and to predict bone fracture risk. Characteristics of ultrasound transmission through cancellous bone are governed by bone material and structural properties. However, the translation of QUS results into bone strength remains elusive. The aim of this study is to investigate the relationship between broadband ultrasonic attenuation (BUA), speed of sound (SOS), and the apparent elastic modulus of cancellous bone (E), which is a surrogate marker for bone strength. An ancillary objective is to compare the ability of QUS variables and of bone quantity (BV/TV) alone to predict bone strength.

Statement of Contribution/Methods

Bone samples (see Figure) were prepared from human femur specimens and scanned with synchrotron radiation micro-computed tomography. Finite-difference time domain simulations of wave propagation were performed in three orthogonal directions of the 3-D microstructures of trabecular bone. BUA and SOS values were derived for each sample and each direction. In parallel, a voxel-based micro finite element linear analysis was employed to compute the apparent Young's modulus (E) of each sample and each direction of testing.

Results

In the antero-posterior direction, which is perpendicular to the main trabecular alignment, highly significant linear relationships were found between SOS and E (R^2=0.92, RMSE=26.3 MPa), BUA and E (R^2=0.79, RMSE=42.3 MPa) and BV/TV and E (R^2=0.81, RMSE=39.6 MPa). The prediction of E was slightly improved with a multiple linear regression model combining SOS and BUA (R^2=0.95, RMSE=22 MPa). When the direction of propagation is perpendicular to the antero-posterior direction, the predictive value of the QUS parameters is comparable, except when two longitudinal wave modes are obtained (fast and slow waves).

Discussion and Conclusions

Our results suggest that SOS has a significantly better predictive power of E compared to BUA. QUS perform significantly better than BV/TV alone to predict the elastic modulus of cancellous bone. Since apparent modulus of cancellous bone was shown to be closely related to apparent strength, this study demonstrates the potentiality of QUS technique to assess fracture risk when the direction of testing is not parallel to the main trabecular alignment.

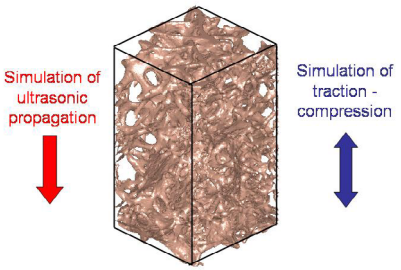

2B-5

2:30 PM **Microstructural simulation of ultrasonic wave propagation through vertebral trabecular bone samples**

Liesbet Goossens[1], Jef Vanderoost[1], Siegfried Jaecques[2], Steven Boonen[3], Jan D'hooge[4], G. Harry van Lenthe[1], Walter Lauriks[5], Georges Van der Perre[1]; *[1]K.U.Leuven, Division of Biomechanics and Engineering Design, Leuven, Belgium, [2]K.U.Leuven, BIOMAT Research Cluster, Leuven, Belgium, [3]K.U.Leuven, Leuven University Centre for Metabolic Bone Diseases, Leuven, Belgium, [4]K.U.Leuven, Division of Cardiovascular Imaging and Dynamics, Leuven, Belgium, [5]K.U.Leuven, Acoustics and Thermal Physics Section, Leuven, Belgium.*

Background, Motivation and Objective

The use of ultrasound as an alternative diagnostic "screening" tool for osteoporosis has extensively been studied. One ultrasound parameter that has shown promise is the speed-of-sound (SOS) as it has been correlated experimentally to bone strength. Unfortunately, to date, a complete mechanical understanding of these findings is still missing. The aim of this study was therefore to look into the direction dependency of SOS, and the possibility to predict the microstructure starting from SOS.

Statement of Contribution/Methods

Fifteen human trabecular bone samples (4x4x4 mm³) from the lumbar spine were acquired; the samples had been scanned using micro-CT (resolution 14 micron) in order to obtain the 3D representation of their trabecular bone architecture. Three-dimensional numerical simulations were subsequently performed on all samples using a finite element (FE) approach (MSC/Nastran) based on the general equations of motion. As such, SOS could be estimated. Additionally, the apparent elastic modulus ES was calculated directly from the FE model. All simulations were performed at a frequency of 1MHz in the three main directions of the bone sample (resulting in 45 simulations): anterior-posterior (AP), medio-lateral (ML) and cranio-caudal (CC).

Results

Figure 1 shows the relationship between ES and SOS. Two groups can be distinguished. The first group contains the measurements in the CC direction. They display high velocity values and a wide range of elastic moduli. The calculations in the transverse directions (AP and ML) are situated in the second group. This group is characterized by low values of the structural elastic moduli and a wide range of velocities.

Discussion and Conclusions

The direction dependency of these results could be understood by a simple model of trabecular bone. For the lumbar spine, this simple model has main trabeculae in the CC direction and smaller struts, arranged randomly connecting the main trabeculae, in the AP and ML direction. The simulated velocity is the velocity of the fastest wave through the bone sample, i.e., the wave that covers the shortest distance through the trabeculae. From these results can be concluded that ultrasonic wave propagation is direction dependent.

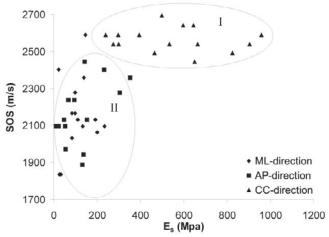

2B-6

2:45 PM **Propagation of ultrasonic longitudinal wave in the cancellous bone covered by the subchondral bone of bovine femur**

Takaaki Koizumi[1], Kazufumi Yamamoto[2], Yoshiki Nagatani[3], Hiroki Soumiya[1], Takashi Saeki[1], Yuichiro Yaoi[1], Mami Matsukawa[1]; *[1]Doshisha University, Kyotanabe, Kyoto, Japan, [2]Hamamatsu University School of Medicine, Hamamatsu, Shizuoka, Japan, [3]Kobe City College of Technology, Kobe, Hyogo, Japan.*

Background, Motivation and Objective

The ultrasonic longitudinal wave in the cancellous bone separates into the fast and slow waves. This phenomenon strongly depends on the bone structure. However, the structure of bone with cancellous part is complicated, showing the distribution of anisotropy and bone volume fraction. Especially, the pore size and number in the bone increases gradually from the hard surface to the inner part, in head and lower end of femur, where cancellous bone is found inside. The understanding of wave propagation mechanism in this complicated structure is important, for the precise in vivo bone evaluation using two waves. In this study, then, the ultrasonic wave propagation in the bone with cancellous part is experimentally investigated.

Statement of Contribution/Methods

Cancellous bone specimens covered by cartilage and subchondral bone were obtained from the distal epiphysis of a 27-months-old bovine bone femur. Specimen dimension was about 10 by 10 mm in size and 11.84 mm in thickness. This thickness was filed down from 11.84 to 2.41 mm. Ultrasonic pulse measurements were performed using a polyvinylidene fluoride (PVDF) focus transmitter (Custom made, Toray) and a self-made flat PVDF receiver. A single sinusoidal signal between 1 and 6 MHz was applied to the transmitter. Ultrasonic wave always entered perpendicular to the hard surface of the bone, which was immersed in water.

Results

We have filed down the sample from the hard surface part and observed waveform changes. At the thickness of 5.91 mm, there was no wave separation. However, at the thickness of 4.21mm, a clear wave separation was observed at 6MHz. At smaller thickness, the separation was confirmed at lower frequencies. The figure shows a typical separated waveform. This result indicates that the changes of averaged pore size affect the separation. From optical microscopic observation, we can find that small pores near the hard surface gradually become larger and finally form cancellous structure in the inner part. As the averaged pore size increases due to the filing down, we can find wave separation at lower frequencies in thin specimens.

Discussion and Conclusions

The wave separation in the bone having both hard subchondral and cancellous parts was investigated. Wave separation was not observed, but appeared gradually when we filed down the hard part.

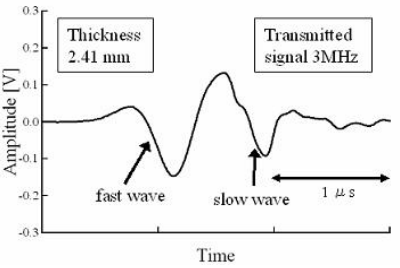

3B. Ultrasonic Motors - Technology Advances

Hall 5A

Monday, November 3, 2008, 1:30 pm - 3:00 pm

Chair: **Ji Wang;**
Ningbo University, Ningbo, China.

3B-1

1:30 PM **Configuration of a screw-shape ultrasonic motor**

Atsuyuki Suzuki[1], Yusuke Nakamura[1], Tetsugi Ueoka[2], Jiromaru Tsujino[2]; [1]*Tokuyama college of technology, Japan,* [2]*Kanagawa university, Japan.*

Background, Motivation and Objective

Ultrasonic motors have superior characteristics, such as high torque, silent motion, no magnetic noise, and free of any magnetic influences. So, it is expected that the ultrasonic motor will be used in many applications. However, the application of the ultrasonic motor is limited to an autofocus mechanism of a camera and so on. The ultrasonic motor which has been put to practical use is a traveling-wave type motor. But, it is difficult to obtain higher torque by the traveling-wave type motor because of its weak structure. To obtain a higher torque motor, we devised a new standing-wave type ultrasonic motor.

Statement of Contribution/Methods

In this study, we made a screw-shape ultrasonic motor using bolt-clamped Langevin type longitudinal vibration transducers (BLTs). The BLT is common vibration source in high-power ultrasonic applications and features high strength and large amplitude. Figure shows a configuration of the devised ultrasonic motor. Three BLTs are installed in shape of a screw to obtain complex vibration. Vibration characteristics and driving characteristics were measured. The ultrasonic motor will be open to utilization in various ways by improving its torque. High-torque applications such as a robot arm and an open door system in case of an earthquake are expected.

Results

Vibration characteristics of the ultrasonic motor were measured using two laser Doppler vibrometers. An elliptical vibration locus was observed at the driving surface of the screw-shape ultrasonic motor. It indicates that complex vibration is obtained using the screw-shape structure. We designed the ultrasonic motor to operate in a longitudinal vibration mode. But, the measured mode was a bending vibration mode. Performance of the motor will be improved by operating in longitudinal vibration mode. Driving characteristics of the ultrasonic motor were measured. The maximum revolution speed was 32 rpm at a frequency of 47.2 kHz.

Discussion and Conclusions

To obtain a higher torque motor, we devised a new ultrasonic motor. We developed a way to obtain complex vibration by installing BLTs in shape of a screw. The maximum revolution speed was 32 rpm, and the validity of the screw-shape structure was confirmed.

Performance of the ultrasonic motor will be improved by matching a resonance frequency of the ultrasonic motor to a resonance frequency of BLTs.

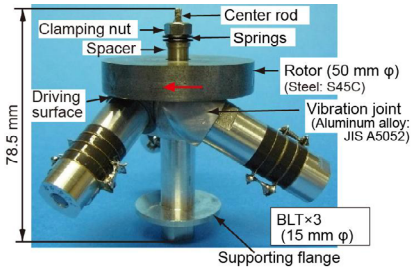

3B-2

1:45 PM **Design and Control of Spherical Two Degree-of-Freedom Traveling Wave type Ultrasonic Motor**

Fu Ping[1], Shen Runjie[2], Shuai Guanju[3], Guo Jifeng[2]; *[1]Minjiang Univercity, China, [2]Zhejiang university, China, [3]Zhejiang Wanma Group Electron Co. Ltd, China.*

Background, Motivation and Objective

Multi degree-of-freedom motions are being widely used in many industrial fields. In robot driving, for example, many junctions of robot need multi degree-of-freedom.

Though there are many kinds of multi degree-of-freedom motors in the world now, they are large and complicated. And precise position is sometimes difficult because adjustment mechanism is bulky.

Multi degree-of-freedom ultrasonic motor still has some characteristics of ultrasonic motor. Now traveling wave type ultrasonic motors become popular and easy to be realized. Its structure is not complex and difficult to be realized. And it can produce large torque compared with other kinds of multi degree-of-freedom ultrasonic motors.

Statement of Contribution/Methods

This paper deals with design and control of spherical two degree-of-freedom traveling wave ultrasonic motors. It consists of three parts: the first one concerns with the driving principle and basic structure of this kind of spherical ultrasonic motor. Secondly some basic problems of motor are to be presented. Then structure of motor and optimal structure of stator and tuning devices are to be explained. Rotor adjustment device and improvement of stator performance are also presented in this paper.

Results

In the third part results of measured values from a photo type USM is compared with the theoretical results. The diameter of prototype motor is 45mm in rotor and 30mm in stator. Maximum output torque is 119mNm and maximum speed is 12r/min. The driving circuit and position control system is based on phase-difference PI strategy. Through experiments its feasibility is verified with high position accuracy.

Discussion and Conclusions

From the above discussion and practical experiments availability of devices is to be verified. Results are used for designing theory and performance improvement of two degree-of-freedom spherical traveling wave ultrasonic motor

3B-3

2:00 PM **The measurement on vibration friction coefficient of ultrasonic motor***

Jin Yi Liew, **Yu Chen,** TieYing Zhou; *Tsinghua University, Department of Physics, Beijing, China.*

Background, Motivation and Objective

An ultrasonic motor of the friction type is driven by the friction force between the stator and the rotor. However the classical Coulomb friction law can not be used to explain the driven mechanism of an ultrasonic motor under the condition of high frequency vibration between the stator and the rotor. In our early study (A study on the friction of a self-correction ultrasonic stepping motor, Ultrasonics, 2002; 39:667) a vibration friction model is offered to explain a phenomenon in an ultrasonic motor experiment, in which the friction coefficient was considered as a function of the vibration amplitude.

Statement of Contribution/Methods

In this paper, we show some experimental results to verify our vibration friction model. The tangential friction force between a stator and a rotor under various vibration amplitudes by changing the input voltages were measured. The friction coefficient is calculated according to its definition, namely the tangential friction force divided by the normal pressure. It was measured that the input voltage was proportional to the vibration amplitude of the stator by using a laser vibrometer.

Results

With the increasing of the input voltage or says the amplitude, it was found that the vibration friction coefficient decreases. The experimental results showed a good agreement with the theoretical calculations.

Discussion and Conclusions

This vibration friction model would be used to explain the driven mechanism of an ultrasonic motor in a further work.

*This work is supported by NSFC(50577035, 10676015) and 863 AA02Z472

3B-4

2:15 PM **Nonlinear flexural vibrations of piezoelectric ceramic tubes in Besocke-style scanners**

Hui Zhang, Shu-yi Zhang; *Institute of Acoustics, Nanjing University, Nanjing, Jiangsu, China.*

Background, Motivation and Objective

The ultrasonic actuators with piezoelectric ceramic tubes have been used in the scanning tunneling microscopes (STM) and atomic force microscopes (AFM) recently. In which, high precision micro-positioning technology is essential, which are required to provide the motion in nanometer scales with high accuracy, speed, and load capacity. Generally, improvements of these performances depend on vibration characteristics of the piezoelectric ceramic tubes.

Statement of Contribution/Methods

In the paper, considering the effects of the nonlinear friction, a nonlinear flexural vibration model of the piezoelectric ceramic tubes in the Besocke-style scanner based on Timoshenko beam theory is presented.

Results

The model is applied to study the nonlinear vibration, and the results show the frequency of the tube is sensitive to the distributions of stick-slip motions of the sapphire ball on rail. For the specific motion distribution there is an instable vibration range where the "ratting modes" are induced. If the normal magnetic force applied on the rail or large vibration amplitude of the ball is available, a stable vibration range with maximal frequency will appear.

Discussion and Conclusions

The model provides an effective method to study the flexural vibration of beam with nonlinear boundary conditions, which is applicable to a wide diversity of electromechanical beam systems.

This work is supported by National Natural Science Foundation of China (No. 10774074) and Natural Science Foundation of Jiangsu Province of China (No. BK2007725).

3B-5

2:30 PM **A High Power Linear Ultrasonic Motor Using Push-Pull Type Longitudinal and Bending Hybrid Langevin Transducer with Single Foot**

Shi Shengjun, Chen Weishan, Liu Junkao, Xie Tao, Liu Yingxiang; *Harbin Institute of Technology, China.*

Background, Motivation and Objective

Langevin type linear ultrasonic motors (LUSM) exhibit higher power and efficiency by adopting PZT d33 mode. However, existing longitudinal-bending hybrid LUSM using Langevin transducer can not output enough power to meet requirements of aerospace mechanism where USM were supposed to make full use of their merits. The analysis indicated that: due to imperfect structure, low power was mainly caused by conflict of two driving trajectories, which also made control complex; the best driving point should be located at antinode of bending modal. To obtain large thrust force, high speed and good controllability, a new structure LUSM was proposed and studied.

Statement of Contribution/Methods

As shown in Fig.a, flange bolt fasten the middle horn, end cap longitudinal and bending PZT together to form the hybrid trasducer. Holes were drilled at the nodal point of the longitudinal modal for the gripper to apply preload. In order to increase the vibration amplitude and velocity, the middle horn were designed as two 1/4 wavelength exponential horns whose tip ends were connected at driving foot. The frequency degeneration were carried out as follows: by using sensitivity analysis in FEM software ANSYS, among structure parameters in Fig.b, high sensitive parameters were selected and adjusted to make the longitudinal and bending resonant frequency as near as possible. Furthermore, FEM harmonic analysis was used to study the relationship between elliptical trajectory shape at driving foot tip and the electrical signal phase differences and magnitude.

Results

A prototype was fabricated to study the frequency and mechanical properties of the proposed LUSM. The measured longitudinal and bending resonant frequencies were 27.510kHz and 27.835kHz respectively. The typical mechanical outputs were maximum velocity of 1280mm/s under the preload of 100N and maximum thrust force 45N under the preload of 350N. The motor can also be driven to move by only exciting bending port while appropriate impedance being connected in series to longitudinal port.

Discussion and Conclusions

Proposed LUSM increase the power density and efficiency compared with the existing ones; Experiment results agree well with FEM results, which shows sensitivity analysis is an effective method in degenerating frequency; There exists coupling effect bewteen longitudinal and bending vibration, so further investigation shold be carried out on decoulpling drive.

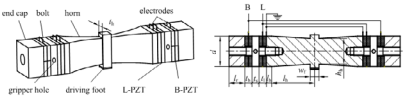

(a) Three dimentional structure (b) Sectional view

3B-6

2:45 PM **A New Type of Tubular Traveling-Wave Ultrasonic Motor**

Rafael Pippi[1], **Cesar Rodrigues[2],** Rafael Tambara[2], Marcelo Dal Alba[2]; *[1]CEFET/SC, DDE, Chapecó, SC, Brazil, [2]UFSM, PPGEE, Santa Maria, RS, Brazil.*

Background, Motivation and Objective

According to their driving method, piezoelectric actuators could be classified as: (1) Quasi-static, or (2) resonant. Resonant actuators are also called ultrasonic motors, and can be further divided into standing-wave and traveling wave motors. Traveling wave ultrasonic motors, focused in this paper, needs two phase-shifted sinusoidal voltage driving sources to generate a traveling deformation wave on its stator surface. Traveling or propagating wave motors can be designed intending linear, rotary, or combined (screw) movements. The objective of this paper is to analyze the conditions for producing traveling-waves in tubular structures, and propose a new class of linear ultrasonic motors.

Statement of Contribution/Methods

In this study, we demonstrate that traveling waves can be produced in a metallic tubular structure, and that they can be used to implement traveling-wave ultrasonic motors. A proof-of-concept prototype was initially built and tested. Although some slider displacements were observed for several frequencies, tests results did not allow us to elucidate which conditions lead to efficient movement production. Thus, investigations were complemented with Finite Element Analysis (FEM), allowing the identification of problems with the prototype. From simulations results, it is possible to identify how to size, and excite the tube for traveling wave production.

Results

The prototype consists of a phosphor bronze tube with two externally fixed PZT rings. It has an external diameter of 17 mm, internal diameter of 14mm, and length of 55mm. Bench tests were carried out with the prototype for frequencies ranging from 20 kHz to 120 kHz. Significant displacements, with speeds as high as 7 cm/s, were observed at 60.48, 58,48, 54.70, and 61.79 kHz. But for the first two, as the direction did not inverted by switching the input phases, the movement could be attributed to standing waves. Reversible velocities up to 3.4 cm/s were measured, for 54.70, and 61.79 kHz, but the repeatability was poor. The FEM simulations were used to complement our observations. Transient analysis was performed to investigate how strain distributes along the tube for each resonance mode. We finally find that when a tube with a length of 55mm and diameter of 30.5mm is submitted to vibrations generated by two PZT-APC841 rings, excited with 35Vrms, 64876Hz, strain magnitudes of $2.6 f$Ým (longitudinal), and $3.5 f$Ým (radial) could be obtained.

Discussion and Conclusions

FEM Transient analysis shows that longitudinal traveling waves could be produced if ceramic rings are placed near the deformation maxima of the tube, and excited in a frequency close to the chosen resonance modes. Longitudinal vibrations found are 3600% higher than those simulated for prototype dimensions, and the radial component is 90% higher.

4B. Single Crystals I

Hall 5B

Monday, November 3, 2008, 1:30 pm - 3:00 pm

Chair: **Sandy Cochran;** *Univ. of Dundee, UK.*

4B-1

1:30 PM **PMN-PZT Single Crystals and Composites for Transducer Applications**

Sung-Min Lee, Dong-Ho Kim, **Ho-Yong Lee;** *Ceracomp Co., Ltd., Korea, Republic of.*

Background, Motivation and Objective

Crystallographically engineered Relaxor-PT single crystals, specifically PMN-PT and PZN-PT, offer very high piezoelectric and electromechanical coupling coefficients (d33>2,000 pC/N; k33>0.9), promising for next generation electromechanical devices such as ultrasonic transducers and actuators. However, these piezoelectric single crystals exhibit relatively low TC, TRT and EC, and thus have very limited usage range. In contrast to the growth of relaxor-PT single crystals, PZT and relaxor-PZTs can not be readily grown in single crystal form because of their incongruent melting behavior. Attempts to grow single crystals of PZT and relaxor-PZTs have been made by numerous researchers, resulting in crystallites too small (2 ~ 3 mm in size) to allow adequate property measurements. If PZT and relaxor-PZTs materials could be grown in single crystal form, PZT and realxor-PZT single crystals have been expected to have remarkable and wide range of dielectric and piezoelectric properties such as high K3T, TC, TRT and EC.

Statement of Contribution/Methods

The solid-state crystal growth (SSCG) technique is to grow a single crystal in a polycrystalline precursor by continuous grain growth of an external seed single crystals without complete melting of major components. In the SSCG process, no melting of PZT is involved and thus the issue of incongruent melting can be avoided. It is also readily amenable to dopant modifications which give us the family of piezoelectrically "soft" and "hard" PZT and relaxor-PZT single crystals, similar to "soft" and "hard" ceramics we have today. In this investigation, undoped and doped MPB PMN-PZT single crystals were fabricated using the SSCG technique and their dielectric/piezoelectric properties characterized.

Results

The undoped and doped (Fe-, Mn-, and In-) PMN-PZT single crystals of high TC (> 180~300oC) and EC (> 3.5~10 kV/cm) were sucessufully fabricated by the SSCG technique and their dielectric/piezoelectric properties characterized. Especially the temperature dependence of the piezoelectric/electromechanical properties, the dc bias effect on TRT (or the application usage temperature range), the high field unipolar strain, and the development of an internal bias were investigated and compared to PMN-PT single crystals. Piezoelectric single crystal-polymer composites were also prepared by using undoped and doped PMN-PZT single crystals and their dielectric/piezoelectric properties characterized.

Discussion and Conclusions

Compared to PMN-PT single crystals, the high TC/EC PMN-PZT single crystals were found to exhibit a much wider usage range with respect to electric field as well as temperature, and thus are better candidates for application in transducers and actuators. Along with high TCs, the ability for dopant engineering using the SSCG technique has been demonstrated to piezoelectrically "harden" crystals (Qm = 500 ~1,000) via the development of an internal bias.

4B-2

2:00 PM **Micromachined High-frequency PMN-PT Single Crystal Ultrasound Transducer for Medical Imaging**

Jiyan Dai, Jue Peng, Sient Ting Lau, Heng Li; *The Hong Kong Polytechnic University, China.*

Background, Motivation and Objective

Piezoelectric single crystal Pb(Mg1/3Nb2/3)O3-xPbTiO3 (PMN-xPT) has been extensively studied in the past several years due to their large piezoelectric properties. The high d33 (2200pC/N) and k33 (93%) values make the PMN-PT single crystal attractive for medical ultrasonic devices, and it has been applied in phased-array probes. On the other hand, high-frequency ultrasonic transducer (HFUT) is becoming a growing research area in recent years, because some new applications requiring frequencies higher than 30 MHz are emerging, such as ophthalmological and dermatological imaging, as well as intravascular imaging with probes mounted on catheter tips.

Statement of Contribution/Methods

Here we present the acoustical design, fabrication of high-frequency (larger than 20 MHz) ultrasound transducers based on PMN-30PT single crystal. We have demonstrated a micromachined 35 MHz ultrasound transducer with a small aperture size (0.7 mm) fabricated by micromachining of <001>-oriented Pb(Mg1/3Nb2/3)O3-30%PbTiO3 (PMN-PT)-on-silicon wafer.

Results

The pulse-echo characteristics of the transducer are measured and the results show that the non-focused single element transducer has a center frequency of 35 MHz and a -6dB bandwidth of 34%. Owing to the excellent electromechanical coupling coefficient (64.4%) of PMN-PT membrane, the transducer exhibits good energy conversion performance with a very low insertion loss down to 8.3 dB at the center frequency.

Discussion and Conclusions

The transducer is promising for intravascular ultrasonic imaging and other applications. With optimization of acoustic matching layers, the bandwidth can be improved further.

4B-3

2:15 PM **Micromachined PMN-PT Single Crystal Composite Transducers -- 15-75 MHz PC-MUT**

Xiaoning Jiang[1], Kevin Snook[1], An Cheng[2], Wesley Hackenberger[1], Xuecang Geng[3]; *[1]TRS Technologies, Inc., USA, [2]Penn State University, USA, [3]Blatek, Inc., USA.*

Background, Motivation and Objective

Single crystal piezoelectric composites are advantageous for broadband and highly sensitive transducers for both medical and NDE ultrasound. The dice-and-fill process is currently used for PMN-PT single crystal composite fabrication, where low dicing speed, crystal damage due to mechanical interaction in dicing, and difficulty of achieving small kerfs (< 10 um) for high frequency ultrasound have been obstacles to the extensive applications of PMN-PT single crystal composite transducers. The recently discovered piezoelectric composite-based micromachined ultrasound transducer (PC-MUT) technique utilizes deep reactive ion etching (RIE) to form high aspect ratio PMN-PT posts without mechanical interaction induced damage, and high frequency 1-3 composites (25-40 MHz) were successfully fabricated with coupling coefficients of ~ 0.75 in 2006. A 35 MHz linear array study using PC-MUT composites was reported by the same group in 2007. In this paper, further investigation on PC-MUT to develop < 15 MHz and > 40 MHz PMN-PT single crystal composites is presented for single element and array transducers, for a broader range of ultrasound imaging applications.

Statement of Contribution/Methods

PMN-PT single crystal/epoxy 1-3 composites with the frequency of 15 - 75 MHz were designed and fabricated using a deep reactive ion etching process. The composite was then characterized and transducers (75 MHz) and arrays (12-element 40 MHz array) were prototyped, followed by electrical characterization of the full transducers and pulse-echo testing.

Results

The kerf width for 75 MHz, 60 MHz and 15 MHz 1-3 composites are < 3 um, < 4um and ~ 20 um, respectively. The etching depth ranged from 40 um for 75 MHz composite to ~ 120 um for 15 MHz composite. The measured effective coupling coefficient is about 0.67-0.75. Pulse-echo experiments showed that the bandwidth of 75 MHz

PC-MUT is about 85% (Figure 1). More results on 35-40 MHz PC-MUT linear arrays will be reported in the full paper.

Discussion and Conclusions

The successful fabrication of PMN-PT single crystal 1-3 composite transducers and arrays with frequency of 15 MHz - 75 MHz suggest that PC-MUT technology is promising for a broad range of ultrasound imaging applications.

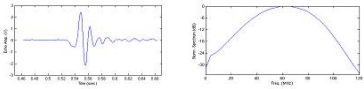

Figure 1. Time domain and spectral magnitude of echo response from a TRS 75 MHz PC-MUT transducer.

4B-4

2:30 PM **Vibration mode and relevant ultrasonic applications of ferroelectric single crystals Pb(Mg1/3Nb2/3)O3-PbTiO3**

Dan Zhou, **Haosu Luo;** *Shanghai Institute of Ceramics, CAS, China.*

Background, Motivation and Objective

Modern medical ultrasonic imaging relies almost exclusively on piezoelectric transducers to convert mechanical waves to electrical signals and vice versa. The vast majority of these devices incorporate a polycrystalline piezoelectric based on the composition Pb(Zr1-x, Tix)O3, generally known as PZT. These materials offer electromechanical properties k33 of 75% and piezoelectric properties d33 of 600 pC/N. Recently, much research work has been reported on the relaxor ferroelectric single crystals (1-x)Pb(Mg1/3Nb2/3)O3-xPbTiO3 (PMN-PT) with superior properties of k33 (~94%), d33 (>2000pC/N), etc. Such excellent performances will lead to large improvement of sensitivity and resolution in medical ultrasonic imaging systems.

Statement of Contribution/Methods

The electromechanicl factors were measured according to IEEE standards by HP4194A impedance analyzer.

The single element PMN-PT transducer was fabricated with the same structure as PZT transducer.

The PMN-PT/Epoxy composites and array transducers were simulated with PiezoCAD.

Results

The PMN-PT crystals were investigated of electromechanical factors k33, kt, k33' and piezoelectric constant d33, with different orientation and cuts for various medical ultrasonic applications. Based on the longitude extension mode (k33), the PMN-PT/Epoxy 1-3 composites were modeled and fabricated. The holistic kt (>90%) of the composites far exceeds that of the PZT ceramics (only ~50%). The relatively low acoustic impedance makes the acoustic matching to human tissue much easier. The results will be favorable for single element ultrasonic transducers, such as Doppler blood flow imaging applications. For medical linear and phase array transducers, the coupling factor k33' is a key indicator. The PMN-PT resonators of this vibration mode were studied systematically with orientations and poling conditions. The optimized cut type of PMN-PT for array applications was obtained with k33' of 92%, which is larger than that 70% of conventional PZT ceramics.

Then, ultrasonic transducer devices utilizing PMN-PT were investigated. The PMN-PT pulse wave 2MHz TCD probe was manufactured with 30% broader bandwidth and 4dB higher sensitivity compared with PZT probe. These enhanced performances were induced by relatively high kt (62%) and d33 of PMN-PT. The single element transducer based on PMN-PT/Epoxy 1-3 composites was simulated with broader bandwidth and higher echo response than PZT transducers. The PMN-PT 3.5MHz linear array transducer was also simulated with the similar effects.

Discussion and Conclusions

The PMN-PT were investigated and optimized for various medical ultrasonic transducer applications. The ultrahigh piezoelectric and electromechanical constants were obtained in PMN-PT. Three types of fabricated or simulated medical transducers utilizing PMN-PT all show improved pulse length, bandwidth and sensitivity. So the next generation of high performance ultrasonic transducers is expected.

5B. NDE Signal Processing

Hall 5C

Monday, November 3, 2008, 1:30 pm - 3:00 pm

Chair: **Ramazan Demirli;**
Canfield Scientific, USA.

5B-1

1:30 PM **Ultrasonic Signal Compression Using Optimal Wavelet Tree Decompositions and Adaptive Thresholding**

Erdal Oruklu, Namitha Jayakumar, Jafar Saniie; *Illinois Institute of Technology, Electrical and Computer Engineering, Chicago, IL, USA.*

Background, Motivation and Objective

We present an adaptive design methodology for ultrasonic signal compression using wavelet transform for data compaction. The critical features which influence the performance of the wavelet based compression are: the selection of wavelet kernels; the number and the sequence of decomposition levels; and the thresholding criterion. The determinations of these critical features are associated with: type of the experimental data used such as overlapping/non-overlapping echoes and reverberant patterns; sampling rate of A-scan, B-scan and C-scan; and center frequency and the bandwidth of the transducer.

Statement of Contribution/Methods

We introduce a systematic design flow consisting of two main stages for ultrasonic signal compression. The first stage of the algorithm is concerned with finding the maximum energy compaction. This is accomplished by applying wavelet transform and search for optimal subband decomposition tree structure for a particular combination of a wavelet kernel and the experimental input data. The algorithm iteratively searches for the optimal wavelet kernel and the decomposition tree structure. In order to satisfy the computation timing constraints, we have examined the wavelet families exhaustively, and narrowed the selection to a limited subset of wavelets. The second stage of the algorithm is concerned with the coefficient reduction using thresholding techniques. Instead of using a global threshold, an adaptive thresholding is applied locally to each subband. The iterative nature of the algorithm ensures that the scales (subbands) that retain most of the total signal energy are preserved while the coefficients in other scales (mostly higher detail scales) are eradicated aggressively.

Results

We studied compression ratio versus peak signal-to-noise ratio (PSNR) for experimental ultrasonic data sets including narrowband, broadband, reverberant, and interfering scattering echoes. Typically, 85% compression ratio can be obtained for 25dB PSNR. Furthermore, the results indicate that narrowband signals can be compressed better than broadband signals due to their superior energy compaction. It is also confirmed that the location of the wavelet scale containing maximum energy depends on the sampling rate and echo bandwidth. It has been observed that Symmlet 6, Coiflet 5, and Daubechies 10 are most robust wavelet kernel choices.

Discussion and Conclusions

An adaptive compression algorithm has been presented for ultrasonic signals, which is data-dependent and optimal within a subset of wavelet transforms. If a particular wavelet kernel matches to the ultrasonic echo signal, more correlation and more compact representation can be achieved. The performance of the compression algorithm has been quantified with experimental data and shown to offer significant resilience to different experimental data sets.

5B-2

1:45 PM **Sparse deconvolution of ultrasonic NDE traces ---- a preliminary study**

Guangming Zhang[1], David Harvey[1], Derek Braden[2]; *[1]Liverpool John Moores University, General Engineering Research Institute, Liverpool, Merseyside, United Kingdom, [2]Delphi Electronics & Safety, Liverpool, United Kingdom.*

Background, Motivation and Objective

Under simplifying assumptions, the recorded ultrasonic trace y in ultrasonic non-destructive evaluation (NDE) is usually modelled as a 1-D convolution between an impulse response h and the reflectivity r of the insonified medium. The convolution smears out the details in the reflectivity and makes interpretation of closely spaced reflectors difficult. The purpose of deconvolution is to estimate r, based on knowledge of h and the observed y. A standard solution is Wiener filtering that takes r to be a stationary Gaussian process. However, in many applications the incident pulse often changes considerably as it passes through the medium due to dispersive attenuation. In general, the exact nature of these changes is poorly known. Thus it is necessary to estimate both the reflectivity and the pulse from the same data, with the additional complication that the pulse is slowly time-varying.

In addition, for media with a layered structure the reflectivity is sparse, i.e., only a limited number of randomly located samples have non-zero values. Some suboptimal methods have been devised by using the sparseness constraint. Bernoulli-Gaussian has commonly been used to model the sparse r, which is then recovered by maximum a posteriori (MAP) estimation. These solutions have mainly been limited to the time-invariant case.

Statement of Contribution/Methods

In this work, we propose a new deconvolution approach to deal with non-stationary sparse ultrasonic signals in accounting for pulse variances. A recently developed sparse dictionary learning method -- the K-SVD algorithm is utilized to learn a time-varying pulse matrix. Each element of the matrix represents an individual pattern of possible local impulse responses. An ultrasonic signal is decomposed into a sparse and redundant representation by a sparse overcomplete representation method -- the sparse Bayesian learning algorithm over the learned pulse matrix. The reflectivity sequence is finally estimated from the resulting sparse signal representation.

Results

The proposed method has been tested by using real ultrasonic NDE data acquired from modern microelectronic packages. Experimental results show that rapidly varying pulses are tracked with high accuracy, thus enabling successful reflectivity estimates.

Discussion and Conclusions

The preliminary results demonstrate the superior performance of the proposed method for real NDE data. Further study on the proposed method is ongoing. We are investigating the effect of different dictionary learning techniques and sparse signal representation algorithms on the performance of the proposed technique. We are also attempting to understand the change in impulse response through dictionary learning and justify the convolution model.

5B-3

2:00 PM **Special probe waveforms for flaw detection at "hot spots"**

David Greve, Irving Oppenheim; *Carnegie Mellon University, Electrical and Computer Engineering, Pittsburgh, PA, USA.*

Background, Motivation and Objective

In some ultrasonic inspection applications it is desirable to probe for flaws or cracks in a specific location known to be vulnerable to failure (a "hot spot"). It is well known that the time-reversed Green's function for wave propagation from location A to B can focus energy onto a particular location B if it is applied to a transmitting transducer at location A. This energy focusing results from constructive reinforcement of multiple reflections at location B.

Statement of Contribution/Methods

In this paper we examine the creation of a special probe waveform that, when applied to an emitting transducer at location A, results in a strong received signal at that transducer at a particular later time only when a scattering center is present at location B. The probing waveform can be calculated directly from the Green's function for propagation from A to B. Such a probe waveform can be used to detect scattering centers at the "hot spot" location B.

Results

We have synthesized a probe waveform for propagation in a two-dimensional plate. We have shown by simulation that scattering centers at location B result in strong reflections at the expected time. Strong reflections are absent when no scattering center is present at B or if a scattering center is at a different location. Finally, we comment on the advantages and difficulties associated with applying this approach to three-dimensional objects.

Discussion and Conclusions

A probe waveform has been synthesized for a two-dimensional plate and has been shown to have the expected behavior. This approach represents a possible approach for rapid detection of flaws at particular locations.

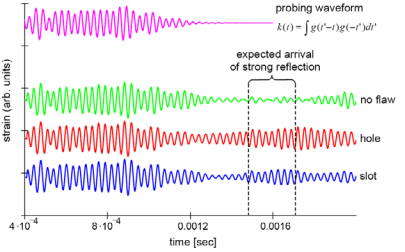

5B-4

2:15 PM **S-Transform Applied To Ultrasonic Nondestructive Testing**

Muhammad A. Malik[1], Jafar Saniie[2]; [1]*University of Hail, Electrical Engineering, Hail, Saudi Arabia,* [2]*Illinois Institute of Technology, USA.*

Background, Motivation and Objective

The joint time-frequency (t-f) display of non-stationary backscattered ultrasonic echoes reveals important information to characterize the target echoes in the non-destructive testing of materials. Generalized t-f distribution (e.g., Wigner-Ville distribution, Chow-Williams Exponential distribution, etc.) applied to ultrasonic backscattered echoes generates artifacts known as cross-terms. These cross-terms mask the t-f information of the target echoes and make the evaluation of the material difficult. An alternative is Gabor Transform (GT), which displays the joint t-f information without generating cross-terms. However, the fixed window of GT limits its t-f resolution. The signal components with period longer than the window width may be misinterpreted and the time resolution of high frequency signal components is limited due to the finite window width.

Statement of Contribution/Methods

In this paper we apply a novel t-f method, S-transform (ST), which uses the t-f representation of Gabor Transform with a frequency dependent window. We have explored the performance of S-transform as applied to Ultrasonic non-destructive testing of materials. S-Transform detects multiple target echoes in both time and frequency without the apriori knowledge of the measurement system's characteristics.

Results

Simulation results depict correct t-f information of multiple Gaussian Echoes under low SNR environment. In addition, experimental results will be provided that demonstrate better and reliable detection and characterization of backscattered target echoes in the presence of microstructure noise.

Discussion and Conclusions

S-Transform (ST), which combines the time-frequency representation of the Gabor Transform and multi-resolution feature of Wavelet Transform, is a unique t-f representation. It adapts the Fourier Transform (FT) in analyzing the localized signal by applying a frequency- dependent time-scaling window. These characteristics make the ST a useful tool to characterize the ultrasonic backscattered target echoes embedded in the microstructure noise for flaw detection in the materials.

5B-5

2:30 PM **Ultrasonic Guided-Waves Characterization with Warped Frequency Transforms**

Luca De Marchi[1], Alessandro Marzani[2], Salvatore Caporale[3], Nicolo Speciale[1]; *[1]University of Bologna, DEIS, Bologna, Italy, [2]University of Bologna, DISTART, Italy, [3]University of Bologna, ARCES, Italy.*

Background, Motivation and Objective

In elongated solids of finite dimension (waveguides) the constructive interference of stress bulk waves due to the structure geometry generates Guided Waves (GWs). For a given excitation frequency one or more stress GWs can propagate along the waveguide each with defined wavelength, phase velocity, energy velocity, attenuation and wavestructure. Due to the interaction between the wave wavelength and the waveguide geometry some or all of these wave features modify, varying the frequency of propagation (dispersive behaviour). This property, along with other specific GWs belongings, allows to employ ultrasonic GWs as a probing tool. Today, GWs based applications for nondestructive evaluation, material characterization, impact and shock induced wave propagation, acoustic focusing and advanced material design are becoming a common practice in the industry. For an efficient design and everyday use of these techniques, GWs dispersive features must be unveiled and managed for the given test structure. To this aim, the main objective of this study is to extract and characterize propagation modes.

Statement of Contribution/Methods

This work proposes a decomposition method capable to extract the dispersive behaviour of GWs that propagates in plate (Lamb Waves) from a recorded time transient-waveform over a wide frequency range. Plate's dispersion waves have characteristic time-frequency representations (TFRs). Unfortunately, any TFR is subjected to the time-frequency uncertainty principle. This limitation prevents the capability of distinguishing multiple, closely spaced Lamb modes with spectrograms or scalograms. To this aim we implemented a new warped frequency transform (WFT) which allows a more flexible tiling of the time-frequency domain. Such tiling can be chosen to match the spectro-temporal structures of the different propagating modes by selecting an appropriate warping map to reshape the frequency axis. In this work we propose design and calculation strategies for non-smooth maps tailored to this specific application. The described transformation is fast and invertible.

Results

An application to propagating GWs in a single layer isotropic aluminun plate is presented to show the potential of the proposed procedure. Time-transient events obtained both artificially, from dedicated FEM simulations, and experimentally, via an hybrid laser-piezoelectric ultrasonic set-up, are considered. The results show that WFT limits interference patterns which appear with others TFRs and produces a sparse representation suitable for characterization purposes.

Discussion and Conclusions

The work presents a new TFR matched to the time-frequency structures of Lamb Waves. The new tool efficiently represents the different GWs with non-linearly frequency modulated atoms. In the proposed decomposition energy peaks extraction is a simpler task and can be performed to obtain reliable mode representation and characterization.

5B-6

2:45 PM **Estimation of Chemical Reaction Kinetics Using Ultrasound**

Johan E. Carlson[1], Veli-Matti Taavitsainen[2]; *[1]Lulea University of Technology, Dept. of Computer Science and Electrical Engineering, Lulea, Sweden, [2]EVTEK University of Applied Sciences, Dept. of Mathematics, Espoo, Finland.*

Background, Motivation and Objective

In ultrasonic measurement systems, what we can directly observe is essentially limited to frequency dependent speed of sound and frequency dependent attenuation. However, in many practical applications, what we really want to know are some implicit properties of the systems under investigation. In some cases, these properties can be derived from the acoustic properties by well-established physical principles (e.g. density, bulk modulus, elastic properties, etc). In other cases, the properties of interest affect the ultrasonic wave propagation in a more complicated way, which may not be possible to derive from first principles. The ultrasound properties are, however, correlated to the physical properties of interest, and as such they carry information that can be exploited.

Chemical reactions are examples of such systems, where the mechanical properties of the chemical compound are changing during the reaction. This, in turn, results in changes in acoustic properties that can be observed. A model for the kinetics of the chemical reaction may be available, but the relation to ultrasound properties is unknown.

Statement of Contribution/Methods

In this paper we present a technique for implicitly finding the kinetic parameters for the setting reaction of calcium sulfate cements, based on measurements of ultrasound attenuation spectra. The spectra are measured throughout the setting reaction, using a 3 MHz transducer in a pulse-echo configuration.

The kinetic behavior of the chemical reaction is modeled as a system of coupled differential equations, and the model parameters of are estimated using a non-linear least-squares approach. In each iteration of the optimization algorithm, the correlation between the model and the observed ultrasound spectra is exploited so that the model best describes variation in the observed data.

Results

We show with experiments on the setting of calcium sulfate cements how the model parameters can be estimated using attenuation spectra, and then used to determine mass fractions of the constituents of the reaction. The figure shows the estimated mass fractions as a function of the reaction time.

Discussion and Conclusions

The results presented here are a demonstration of a potentially powerful technique, i.e. that indirect observations of the behavior of a dynamic system (in this case ultrasound spectra) can be used to estimate the model parameters.

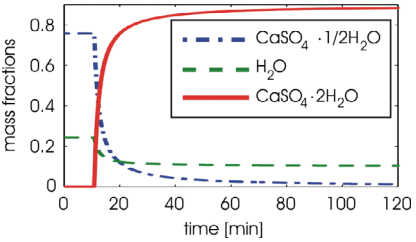

6B. Advances in Materials & Propagation

Room 307

Monday, November 3, 2008, 1:30 pm - 3:00 pm

Chair: **Jan H. Kuypers;**
University of California Berkeley, CA, USA.

6B-1

1:30 PM **Fabrication of SHF range SAW devices on AlN/Diamond-substrate**

Tatsuya Omori, Atsushi Kobayashi, Yuya Takagi, Ken-ya Hashimoto, Masatsune Yamaguchi; *Chiba University, Graduate School of Engineering, Chiba, Japan.*

Background, Motivation and Objective

High performance SAW devices employing diamond substrates overlaid with piezoelectric thin films such as ZnO and/or AlN are believed to play a key role in future communication systems and high speed signal processing in an SHF range. One of the reasons for this is simply because the extremely high SAW velocities of about 10,000 m/s are supported in their structures; such high velocities would enable us to develop SAW devices in an SHF range instead of employing very thin electrodes, which may cause not only difficult problems in production but considerable deterioration in Q-factors. From this point of view, this paper describes the preparation of AlN thin films on diamond substrates for SAW device applications. Both transversal filters and resonators are fabricated to characterise SAW propagation on the AlN/diamond structure and discuss their performance.

Statement of Contribution/Methods

AlN thin films are deposited on diamond substrates by DC-TFTS (Target Facing Type of Sputtering with DC-power source) using an arc-killer. For the prepared thin films, their surface roughness and crystallographic properties are evaluated by AFM and XRD. In particular, the former is most responsible to both the electrode patterning on the film and SAW propagation, whilst the latter to the piezoelectricity obtainable for SAW excitation. Simple SAW transversal filters and one-port resonators having electrodes of the width of 0.5 um are fabricated on the AlN film/diamond substrate structure to discuss their performance.

Results

It was confirmed by the XRD analysis that the c-axis oriented AlN films are deposited on diamond substrates, the FWHM of the rocking curve associated with the c-axis being 4.0 degrees. In the AFM image, densely-packed AlN grains of the order of 0.1 um in size were observed, from which the surface roughness of the films was estimated to be about Ra = 5 nm. From the frequency responses of the SAW transversal filters, the phase velocity of SAWs on a 0.8 um thick AlN film on a diamond substrate was estimated to be about 9,700 m/s, which is in good agreement with theoretical calculation. The minimum insertion loss for the transversal filter was about 10dB at 4.8 GHz. Although the one-port resonator was only fabricated as a trial, the Q-factors and capacitance ratio obtained were already 350 and 110, respectively, at 4.6 GHz. From the resonator result, the coupling factor K2 was estimated to be about 0.9%, which may be the contribution of the good c-axis orientation.

Discussion and Conclusions

It is suggested from the result that both the macroscopic and microscopic qualities of the AlN films deposited on diamond substrates by DC-TFTS could be applicable to practical SAW devices in an SHF range. In particular, one may be able to develop high-Q SAW resonators and high performance filters provided that they are optimally designed. It is concluded that the AlN/diamond substrate structure prepared by DC-TFTS is one of the strongest candidates for high performance SAW devices in an SHF range.

6B-2

1:45 PM **Large Q.f Product for HBAR using smart cut ™ reported LiNbO3 on LiNbO3 substrate**

Mathieu Pijolat[1], Jean Sebastien Moulet[2], Alexandre Reinhardt[1], Emmanuel Defaÿ[1], Chrystel Deguet[1], Dorian Gachon[3], Sylvain Ballandras[3], Marc Aïd[1], Bruno Ghyselen[2]; *[1]CEA-LETI, Grenoble, France, [2]Silicon-on-Insulator Technologies (SOITEC), 38926 Crolles Cedex, France, [3]Femto ST, UMR CNRS-UFC-ENSMM-UTBM 6174, 25044 Besançon Cedex, France.*

Background, Motivation and Objective

High overtone Bulk Acoustic Resonators (HBAR) have been investigated for several years as frequency sources and filters mainly because of their very high quality factors at gigahertz range and above. State of the art is a Q.f product of 1.1.1014 for Aluminium Nitride on Sapphire obtained by Lakin et al. In this paper, we propose a HBAR using a single crystal X-cut LiNbO3 (LNO) thin layer reported by Smart Cut ™ on a LNO substrate. These orientations were chosen for the excitation of pure shear waves, as they are expected to exhibit high coupling strength on LNO (in excess of 40%) and Q factors larger than those of longitudinal waves.

Statement of Contribution/Methods

LNO on LNO HBAR structures have already been studied by Gachon et al. Here, a new approach is proposed using the Smart Cut ™ technology, in order to transfer a thin layer of single crystal piezoelectric material. Resulting composite substrates were developed in the frame of the CEA-SOITEC joined program. In this way, a 3-inch X cut LNO single-crystal layer has been successfully reported onto a carrier wafer comprising a metallic electrode. This technique allows us to obtain thin homogenous films (less than 1 µm thick), suitable for high frequency applications. RF characterisation was performed between 1 and 4 GHz using a 2 port resonator design.

Results

The implemented devices have been tested using a RF probing station and a network analyser, allowing for the determination of HBARs acousto-electric characteristics from experimental admittance curves. We observe clear resonances corresponding to shear in-plane modes. The approach for data extraction consists in fitting the experimental measurements using theoretically computed admittances obtained with a scattering matrix method. Adjusting material parameters and losses allows a perfect matching between simulated and experimental data for both real and imaginary parts of the admittance of the resonator. Q values above 40 000 are extracted at 1.95 GHz which yields Q.f products around 8.1013, close to the state of the art.

Discussion and Conclusions

HBAR with sub-micron LNO layer reported by Smart cut ™ have been experimentally proved. We achieved excellent quality factors and Q.f products. The next step is to prove the feasibility of self resonating layer by decoupling the substrate effect.

6B-3

2:00 PM **High Temperature Stability of Langasite Surface Acoustic Wave Devices**

Mauricio Pereira da Cunha[1], Robert Lad[2], Thomas Moonlight[2], George Bernhardt[2], David Frankel[2], Blake Sturtevant[2]; *[1]University of Maine, Electrical and Computer Engineering, Orono, ME, USA, [2]University of Maine, USA.*

Background, Motivation and Objective

High temperature acoustic wave (AW) devices capable of operating above 600°C and in hostile environments have opened potential applications for monitoring industrial processes, power plants, and aerospace systems. The authors have reported on the development of thin film electrodes to allow surface acoustic wave (SAW) device operation up to 800°C on langasite (LGS) crystals. This success motivated further study of the electrode material and protective ceramic overlayer, and investigations of long term performance, and temperature cycling behavior, reported in this work.

Statement of Contribution/Methods

High temperature electrode stability was investigated by varying the rhodium (Rh) and ZrO2 concentrations in co-deposited Pt/Rh/ZrO2 thin films. X-ray diffraction (XRD) analysis before and after heating to 1000°C was correlated to SAW device high temperature performance. Nitrogen rich and oxygen rich SiAlON compositions were explored as ultra-thin passivating ceramic layer. In addition to long term (4080 hours) testing at 800°C, LGS SAW devices were repeatedly cycled between 20 and 850°C to verify device consistency and repeatability.

Results

It has been found that after a first annealing of Pt/Rh/ZrO2 electrode films to 850°C, the frequency response of the SAW devices becomes very consistent: the figure shows results from six consecutive cycles from 20 to 850°C. In addition, continuous device operation at 800°C over 5½ months (4080 hours) confirmed stable performance of the SAW device. The upper right picture shows part of the SAW device structure after this test period. XRD analyses verified that the presence of ZrO2 is essential to deter recrystallization/de-wetting and grain growth which leads to rapid electrode failure in Pt electrodes above 600°C. The center picture shows the superior Pt/Rh/ZrO2 electrode uniformity when a protective ceramic SiAlON overlayer (left part of the image) is present, as opposed to no SiAlON (right part). Packaging materials and techniques, picture on the left, are also discussed in the paper.

Discussion and Conclusions

In conclusion, the novel electrode and ultra-thin passivation layer enabled excellent stability performance of LGS SAW devices over long term operation and under extreme thermal cycling conditions, establishing this technology as a strong candidate for high temperature sensor and frequency control applications.

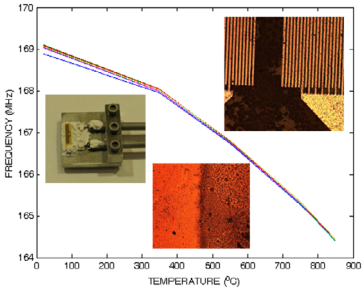

6B-4

2:15 PM **SAW-Relevant Material Properties of Langasite in the Temperature Range from 25 to 750 °C: New Experimental Results**

Ismail Shrena[1], Jochen Bardong[2], Martin Schmitt[3], David Eisele[1], Elena Mayer[1], Leonhard Michael Reindl[1];
[1]University of Freiburg - IMTEK, Department of Microsystems Engineering, Freiburg, Germany, [2]CTR AG, SAW Sensor Systems, Villach, Austria, [3]University of Applied Sciences Coburg, Institute of Sensor and Actuator Technology (ISAT), Coburg, Germany.

Background, Motivation and Objective

Due to increasing demands by industry for wireless sensor applications at high temperatures, materials are needed that can withstand temperatures up to 1000 °C. For this purpose SAW-devices have advantages in comparison to devices based on other technologies, for example semiconductors. Unfortunately traditional SAW materials such as quartz and lithium niobate can be used at temperatures not higher than about 570 °C or 350 °C, respectively, because of phase transition or decomposing effects. The relatively new piezoelectric material langasite ($La_3Ga_5SiO_{14}$) preserves its piezoelectric properties up to its melting point at about 1470 °C and seems to be applicable for SAW devices at high temperatures. The aim of this work is to determine the acoustical parameters of langasite up to the highest possible point of temperature and to investigate different material combinations for the metalization and measurement setup, which withstand these high temperatures.

Statement of Contribution/Methods

The paper presents measurements of transfer functions for delay lines on langasite at frequencies ranging from 150 MHz to 1 GHz, at temperatures from 25 to 750 °C. Two temperature-compensated cuts with Euler angles (0°, 138.5°, 26.6°) and (0°, 30.2°, 26.6°) have been studied. The devices were fabricated using langasite as substrate, with two different platinum (Pt) layer heights (45 nm and 75 nm), on a zirconium (Zr) adhesion layer (4 nm). Several oxides, such as IrO_2 and Ta_2O_5 were tested as alternative adhesion layers. These measurements have been done with a special setup consisting of steel/ceramic coaxial cables, and measurements of the transfer function S_{21} were done in steps of 5 K, using a network analyzer. A special signal processing algorithm utilizing cross-correlation was implemented in MATLAB and used for the analysis of measured data.

Results

The material parameters relevant for SAW devices, such as phase velocity, propagation loss and electromechanical coupling coefficient, have been determined as a function of temperature, and the temperature coefficient of delay

TCD was calculated. The propagation loss shows an anomalous temperature distribution with a peak at about 500 °C.

Discussion and Conclusions

The evaluation of the acoustical properties of langasite up to 750 °C confirms that langasite can be used as substrate material for SAW transponders for wireless sensing at high temperatures.

6B-5

2:30 PM **Thin Films of PZT- based Ternary Perovskite Compounds for MEMS**

Kiyotaka Wasa[1], Isaku Kanno[1], Hidetoshi Kotera[1], Norihiro Yamauchi[2], Tomoaki Matsuhima[2]; *[1]Kyoto University, Japan, [2]Panasonic, Japan.*

Background, Motivation and Objective

The ternary perovskite compounds of bulk ceramics, the combination of binary perovskite compounds Pb(Zr,Ti)O3 (PZT) with relaxor ferroelectric materials such as Pb(Mn1/3 Nb2/3)O3, show high piezoelectric coupling and high mechanical quality factor Qm. So, thin films of the ternary perovskite compounds will be useful for a fabrication of high precision MEMS with lower operating voltage under the optimum chemical composition compared with conventional binary compound PZT MEMS. However, it is not clear whether the bulk piezoelectric properties will be realised in the thin films due to the imperfection of thin film structure. Recently we have established a reliable epitaxial growth process of single crystal thin films using magnetron sputtering to overcome the imperfection of the thin film structure. In this paper we will describe the fabrication of the single crystal thin films of the ternary perovskite xPbMn1/3Nb2/3O3-(1-x)PZT on SRO/Pt coated (001)MgO substrates to and clarify the material composition effects on the piezoelectricity

Statement of Contribution/Methods

In the experiments the growth temperature of the ternary thin films was around 600oC. The resultant films showed (001)single domain/ single crystal perovskite structure. Doping of PMnN to PZT will increase coupling factor and Qm according to the bulk ceramic data. To confirm the doping effects on the thin film piezoelectric properties, thin film cantilever of xPbMn1/3Nb2/3O3- (1-x)PZT at x=0.06 for PZT(45/55) was fabricated on the MgO beam (MgO beam :10mm in length, 0.3mm in thickness, and 2mm in width) for the evaluation of piezoelectric coupling factor

Results

It was found typical deflections of the PMnN-PZT thin film cantilever were 1£gm at 10V. The piezoelectric constant, d31 value, estimated from the displacement of the cantilever was d31 =-102pC/N. The observed d31values were almost the same or slightly higher than non-doped PZT thin films and high enough for the practical use. Measurenents of P-E hysteresis loop showed thin films of xPbMn1/3Nb2/3O3-(1-x)PZT exhibited hgihly square with Pr=60□EC/cm2 and Ec=110kV/cm indicating hard ferroelectric behavior. So, present PMnN-PZT thin films will show both high Qm and high coupling. These expectations have been confirmed by the direct measurements of Qm and kt at FBAR structure; kt=0.6-0.7 and Qm=160-185 at 4-5GHz for the film thickness of 250-300nm.While the Qm of intrinsic PZT thin films was lower than 150 although the kt was almost the same to the values for doped PZT.

Discussion and Conclusions

In conclusion we have clarlified the composition effect on the piezoelectricity for the ternary compound thin films.

6B-6

2:45 PM **Fabrication and Characterization of PMnN-PZT Films with High Piezoelectricity**

Tao Zhang[1], Kiyotaka Wasa[2], Shu-yi Zhang[1], Zhao-jiang Chen[1], Feng-mei Zhou[1], Zhong-ning Zhang[1], Yue-tao Yang[1]; *[1]Lab of Modern Acoustics, Institute of Acoustics, Nanjing University, Nanjing 210093, China, [2]Department of Micro-engineering, Kyoto University, Kyoto 606-8501, Japan.*

Background, Motivation and Objective

The high electromechanical coupling coefficient is an important factor for developing acoustic and electronic devices and also MEMS techniques, so the piezoelectric films with high piezoelectricity are expected to be fabricated.

Statement of Contribution/Methods

A kind of ternary compound films, i.e., 6%PMnN-doped PZT(50/50) (mole percent) films, is epitaxially grown on the Si substrates by a RF magnetron sputtering and quench technique, in which the doping is available for improving the electromechanical coupling factor and the mechanical quality factor simultaneously, which attracts the MEMS applications.

Results

The crystal structures and lattice constants of the ternary compound 6%PMnN-94%PZT(50/50) films, expressed as PMnN-PZT films hereafter, are measured by XRD, which show that the crystal structures exhibit multi-orientations including (001), (101) and (111), however the (111) is the dominating growth orientation. Besides, the doping of Nb and Mn makes the lattice constants larger than those of the PZT(50/50).

The piezoelectricity of the films is measured by the bending beam (cantilever) method. The measurement results show the transverse piezoelectric coefficient is excellent, i.e., e31=10.7 C/m^2, and the films have the high electromechanical coupling factors, in which the k31 is about 54.4%.

The ferroelectricity of the films is studied by Sawyer Tower circuit, and the results show that the saturation polarization intensity (Ps) is about 32 $\mu C/cm^2$, and the residual polarization intensity (Pr) is about 17 $\mu C/cm^2$, and the coercive electric-field intensity $2E_c$ is 144 kV/cm. The results display that the doping of PMnN makes the ferroelectricity stronger.

Discussion and Conclusions

In addition, the dielectric constants, dielectric loss and the Curie temperature of the films are measured by LCR meter. The results show that the additive PMnN makes the dielectric constant and dielectric loss slightly larger, and also makes the Curie temperature lower, which, however, can be ignored by comparing with the advantages of the PMnN-PZT films.

This work is supported by National Natural Science Foundation of China, No. 10774074.

1C. Shear Wave and Shear Strain Imaging

Hall 3

Monday, November 3, 2008, 4:30 pm - 6:00 pm

Chair: **James Greenleaf;**
Mayo Clinic College of Medicine, MN, USA.

1C-1

4:30 PM **Optimal design of ultrasonic beam profiles for acoustic radiation force based elastography**

Jeremy Bercoff[1], Mickael Tanter[2], Mathias Fink[2], Jacques Souquet[1]; [1]*Supersonic Imagine, Aix en Provence, France,* [2]*Laboratoire Ondes et Acoustique, Paris, France.*

Background, Motivation and Objective

Elastography methods relying on acoustic radiation force to induce tissue motion has been widely proposed in recent years. Forsake of simplicity, these methods are usually implemented on classical imaging probes in order to avoid US image quality degradation. This leads to strong compromises affecting three parameters for Acoustic radiation force imaging techniques: the low amplitude of the shear stress due to acoustic output limitations, the limited penetration depth of the induced stress due to imaging probe geometry and low frame rate of such imaging techniques due to probe heating issues. The objective of this work is to propose a robust and efficient way to induce radiation force in tissues while meeting regulatory safety requirements without sacrificing image quality

Statement of Contribution/Methods

A new probe design is proposed for breast application: a 1.5D linear probe with a central row devoted to imaging and two external rows designed to optimizing the efficiency of the radiation force generation: the central frequency is half of the imaging frequency, the width of the elements increased by two and the elevation focus is three times deeper than imaging one. The efficiency of this new probe design has been evaluated on the ShearWaveTM Elastography imaging mode (SWE). A simulation study has been conducted coupling the Field II software to simulate ultrasound beam geometry and the analytical viscoelastic green's function to deduce transient shear stress induced by the beam. Then, simulation results have been compared to in vitro experiments conducted using several designed probes. The elastography imaging mode performance has been estimated for both the 1D and the 1.5D probes and quantified in vitro and in vivo

Results

The push penetration depth is increased by 50 % and 4 times less acoustic energy is needed to induce the same amplitude shear waves. The far elevation focus plays an important role: it minimizes the beam attenuation in the near field and spreads the shear wave source in the elevation direction leading to a less diffracting and then more efficient shear wave propagation in the imaging plane. The low central frequency of the external transducers allows a better compromise between radiation force generation and penetration and significantly reduces probe heating. The combination of those features leads to significant performance increase of the SWE mode: the imaging penetration depth is increased by 50 % (from 40 to 60 mm) and the imaging frame rate by a factor 8 (from 1 to 8 Hz)

Discussion and Conclusions

A new probe design, meeting the requirements for acoustic radiation force based elastography, has been proposed without degrading quality of classical ultrasound modes. This design brings important improvements on the SWE mode. Future studies need to be conducted to assess probe performance and reliability in clinical conditions

1C-2

4:45 PM **Rapid Shear Wave Measurement for SDUV with Broadband Excitation Pulses and Non-Uniform Sampling**

Yi Zheng[1], Aiping Yao[1], Shigao Chen[2], James Greenleaf[2]; *[1]St. Cloud State University, Electrical and Computer Engineering, St. Cloud, MN, USA, [2]Mayo Clinic College of Medicine, Physiology and Biomedical Engineering, Rochester, MN, USA.*

Background, Motivation and Objective

Excitation using broadband pulses for Shearwave Dispersion Ultrasound Vibrometry (SDUV) has been proposed (Chen et al, 2008). The goal of this work is to develop a method that allows non-uniform sampling and simultaneously detects all harmonics of tissue motion induced by the broadband excitation pulses so that the shear wave can be rapidly estimated with minimized bias and distortion.

Statement of Contribution/Methods

Long tonebursts of ultrasound repeated at frequency fe generate shear waves at fe and its harmonics. Resulting tissue motion is detected by pulse echo ultrasound interleaved with the broadband excitation tonebursts. A high PRF for detection pulses is desired to obtain enough harmonics with minimized sampling aliasing. However, interference with the excitation toneburst puts a bottleneck on the upper limit of achievable PRF, if the detection pulses are placed uniformly along time. To solve this problem, we use a high PRF and throw away the samples corrupted by interference every 1/fe seconds. Such non-uniform samples can be accommodated by Kalman filter. The tissue vibration is modeled by a state space equation that includes all harmonics. The state space equation is recursively updated by Kalman filter with measurements to simultaneously estimate the tissue motion at several harmonics.

Experiments were conducted to validate the method. Broadband pulses were transmitted to a tissue region with an excitation fe of 156.25 Hz. The detection transducer has a center frequency of 7.5 MHz. The detecting pulses were sampled at 100 MHz in the fast time. To have uniform samples in the slow time, the excitation pulse width was 0.25 ms and detecting PRF was 2.5 kHz (16 times of 156.25). When the excitation pulse width increased to 0.4 ms and the detection PRF increased to 5 kHz, there were 32 pulses between two broadband pulses and the sample interval become non-uniform between every group of 32 samples.

Results

The method is applied to estimate phase shifts of the shear wave along the distance from 2 mm to 6 mm from the vibration center. The estimates with a long vibration pulse width (0.4 ms) and a high PRF (5 kHz) provide the best results that have linear phase shifts, minimum distortion and bias.

Discussion and Conclusions

Tissue motion can be rapidly measured using interleaved broadband excitation pulses and detecting pulses. Kalman filter can simultaneously estimate all harmonics of the tissue motion induced by the broadband pulses. Non-uniform samples can be processed by the Kalman filter. Long excitation pulses with a high detecting PRF improve the accuracy of the estimates. [This research is supported by NIH grant EB2167.]

1C-3

5:00 PM **Shear Wave Induced Resonance: a new excitation mode for dynamic elastography imaging**

Anis Hadj Henni, Cedric Schmitt, Guy Cloutier; *Research Center, University of Montreal Hospital, Laboratory of Biorheology and Medical Ultrasonics, Montreal, Quebec, Canada.*

Background, Motivation and Objective

In the context of dynamic elastography imaging of soft biological tissues, methods to generate low frequency shear waves are of two types: those using an external vibrating source and those based on ultrasound radiation force to induce shear waves deeply in tissues. These techniques are extensively utilized to vibrate localized pathologies like prostate and breast tumors. Paradoxically, none of them take advantage of the confined geometry of wide variety of pathologies. Using an appropriate incident wave, shear wave induced resonance elastography (SWIRE) consists in forcing the mechanical resonance of a confined mechanical heterogeneity to amplify its motion contrast with respect to surrounding tissues for a better discrimination. Combined to a theoretical model, SWIRE can also serve to characterize viscoelasticity of heterogeneities.

Statement of Contribution/Methods

Applied to vascular elastography, SWIRE of a cylindrical soft inclusion was investigated. By appropriately selecting an incident shear horizontal (SH) wave, resonance of the heterogeneous inclusion was made possible. Experiments were performed on an agar-gelatin phantom to measure eigenfrequencies and eigenmodes of resonance. Besides this, an analytical model was developed to simulate and physically understand the resonance phenomenon.

Results

Figure [1] shows images of the two first eigenmodes. Enhanced displacements within the inclusion and surrounding medium allowed identifying a clear segmentation of the inclusion. The first mode imposes to the whole cylinder an in-phase vibration along its axis while in the second mode, the inclusion is shared in two equivalent parts vibrating in opposite phases.

Discussion and Conclusions

These results show the potential of SWIRE to enhance elastographic image quality and to discriminate heterogeneities. In the absence of ultrasound echogenicity contrast, the amplification of displacements at resonance allows to identify a mechanical heterogeneity directly from the eigenmode images. The spectral displacement response (eigenfrequencies, bandwidth…) of an inclusion to a given SH excitation is related to its viscoelasticity and that of the surrounding medium. Consequently, SWIRE can serve to characterize the viscoelasticity of heterogeneities, and their rheological models, by solving an inverse problem involving measured and simulated spectra.

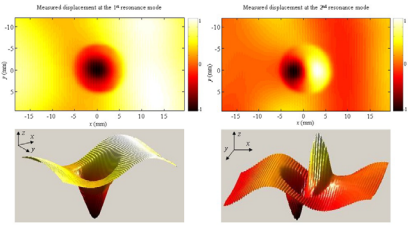

Figure [1] Top: images of experimentally measured displacement fields at the first (100 Hz) and second (150 Hz) eigenfrequencies. Bottom: 3D representation of the first and second measured eigenmodes showing out-of-plane displacement fields.

1C-4

5:15 PM **Simultaneous imaging of artery-wall strain and blood flow realized by high frame rate acquisition of RF echoes**

Hideyuki Hasegawa, Hiroshi Kanai; *Tohoku University, Japan.*

Background, Motivation and Objective

Blood flow measurement is an important practical routine in diagnosis of atherosclerosis. In addition, mechanical properties of arterial walls affected by atherosclerosis (including atherosclerotic plaque) are significantly different from those of normal arteries, and various studies have been recently conducted to measure the artery-wall regional elasticity (strain). It would be useful if the strain and blood flow could be assessed simultaneously because vulnerability of plaque is closely related to its mechanical property and shear stress due to blood flow.

Statement of Contribution/Methods

A high frame rate acquisition of ultrasonic RF echoes, which is required for blood flow measurement, was achieved using parallel beam forming (PBF). A plane wave was transmitted using 96 elements of a 10-MHz linear array probe, and 24 receiving beams were created for each transmit using apertures consisting of 76 of the 96 elements. Plane waves were transmitted three times from different aperture positions, and total 72 receiving beams were created. This procedure realizes a high frame rate (3500 Hz) compared with conventional linear scan (several tens of Hz) with a lateral field of view of 15 mm.

Results

Spatial resolution of the system was evaluated by imaging a fine nylon wire (100 ƒÊm in diameter) embedded in agar. The width at half maximum of the lateral beam profile by PBF (0.8 mm) was same as that by conventional linear scanning (CLS), and the width at -20 dB was similar (1.6 mm) compared with CLS (1.4 mm). The accuracy in strain estimation was evaluated by experiments using a cylindrical phantom. Strain was estimated by our phase-sensitive correlation estimator [Hasegawa and Kanai, IEEE Trans UFFC, 2008 (in press)]. The error of the

measured strain from the theory and the standard deviation were 4.8% and 9.5%, respectively. Furthermore, Figs. (a) and (b) show images of a carotid artery obtained at 0 s and 0.15 s from the time of the R-wave of electrocardiogram. Power of echoes from blood particles are successfully imaged together with wall strain during the period when the blood flow velocity was high (Fig. (b)).

Discussion and Conclusions

Simultaneous imaging of artery-wall strain and blood flow was achieved by high frame rate acquisition of RF echoes using PBF. The proposed method would provide useful information for diagnosis of atherosclerosis, such like plaque vulnerability.

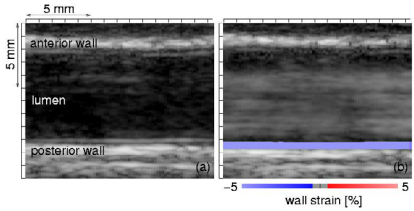

1C-5

5:30 PM **supersonic shear wave elasticity imaging**

Mathias Fink[1], Mickael Tanter[1], Jeremy Bercoff[2], Jacques Souquet[2]; *[1]Laboratoire Ondes et Acoustique, ESPCI, Paris, France, [2]Supersonic Imagine, Aix en Provence, France.*

Background, Motivation and Objective

This lecture presents a review of the applications of Supersonic Shear Imaging (SSI)modality.

Statement of Contribution/Methods

This technique is based on the combination of a dynamic radiation force induced in tissue by a set of ultrasonic beams and an ultrafast imaging sequence (5000 Images/s) capable of catching in real time the propagation of resulting shear waves. A shear source moving at a supersonic speed is remotely induced in tissues by the use of a special transmit beamforming sequence. It radiated quasi-plane shear waves propagating in a Mach cone. The local shear wave velocity is recovered using a time of fligth technique and enables the two dimensionnal (2D) maping of shear elasticity. This imaging modality is implemented on conventional probes driven by dedicated ultrafast echographic platforms. Consequently, it can be performed during a standard echographic exam.

Results

The preliminary clinical results demonstrate the clinical feasibility of this new elastography technique in providing quantitative assesment of relative stiffness of breast tissues. Experimental results will emphasize the potential of this elastography technique for many others potential applications such as liver, cardiovascular, opthalmologic and muscular applications.

Discussion and Conclusions

Beyond elasticity imaging, a complete in vivo assessment of tissue rheology can be performed using this approach. Dispersion effects affecting the propagation of visco-elastic waves in soft tissues are a key to understanding the rheological behavior of human tissues. New signal processing approaches based on the Supersoinic shear imaging modality were also developed and introduce a new concept of shear wave spectroscopy that could potentially become a great tool in tissue characterization and medical diagnosis.

2C. Bone II

Room 201 A/B/C

Monday, November 3, 2008, 4:30 pm - 6:00 pm

Chair: **Pascal Laugier;**
Université Paris VI, Paris, France.

2C-1

4:30 PM **How Ultrasound Bidirectional Axial Transmission Reflects Geometry of Long Bones?**

Thiên-Ly Pham, Maryline Talmant, Pascal Laugier; *Université Pierre et Marie Curie Paris 6, CNRS, Laboratoire d'Imagerie Paramétrique, Paris, France.*

Background, Motivation and Objective

Axial transmission (AT) techniques assess bone properties along the long bones axis over a length of a few cm. This technique has been advocated to be appropriate for cortical thickness assessment. Some techniques measure the speed of waves transmitted axially in one direction (monodirectional AT) whereas other techniques average the speed of waves that are transmitted axially in two opposite directions (bidirectional AT) [Bossy et al. IEEE Trans Ultrason Ferroelec Freq Contr 51(1), 71-79, 2004]. The issue addressed here is the comparison between monodirectional and bidirectional techniques.

Statement of Contribution/Methods

Propagation was simulated using a finite difference method at 1MHz in a set of 46 human radii. Individual 2-D geometry of the samples was reconstructed from X-Ray computed tomography (pixel size=100µm). The material constituting the bone models was considered to be a homogenic transverse isotropic medium with generic elastic properties taken from literature. Bone geometry was characterized by the variation of cortical thickness along the bone axis. Signal processing was focused on the first arriving signal. Additional simulations were performed on plates whose thickness is constant and in the range of cortical thickness of the specimen.

Results

The best fit obtained in plates between the velocity and plate thickness was found to be a quadratic law (R^2=0.88). Results show that both monodirectional velocities - proximal (3980±94m/s) and distal (3967±104m/s) - are poorly quadratically correlated to mean thickness under receivers (proximal: R^2=0.19, distal: R^2=0.39) whereas bidirectional velocity (3971±44m/s) is significantly correlated to mean thickness (R^2=0.68).

Discussion and Conclusions

In addition to eliminating the effect of the overlying soft tissue, bidirectional technique reflects well the thickness whereas monodirectional velocity does not.

2C-2

4:45 PM **Analysis of Reflection and Transmission Coefficients of Ultrasonic Guided Wave in Fracture Long Bones by Hybrid Boundary Element Method**

Kailiang Xu, Dean Ta, Weiqi Wang; *Fudan University, Department of Electronic Engineering, Shanghai, China.*

Background, Motivation and Objective

Using ultrasonic guided wave to assess long bone has gained considerable attention since it has great potential in reflecting material and structural properties of bones. This paper focuses on using the hybrid boundary element method (HBEM) to analyze ultrasonic guided wave propagation characteristics in fracture long bones.

Statement of Contribution/Methods

The hybrid boundary element model combines traditional boundary element equation with guided wave expansion equation. In this method, we consider the scattering of guided waves through surface cracks within cortical bones. In the cases of L(0,1), L(0,2) and L(0,3) incident modes, interaction of modes with crack is investigated by

numerically calculating the reflection and transmission coefficients for different depth-to-width ratio of cracks, and this simulation is done within a frequency ranging from 0.05 to 2.0 MHz.

Results

The numerical results demonstrate that mode conversion phenomena take place when the guided wave propagated through the crack of cortical bone. The results show that the transmission coefficients always provide more crack information than the reflection coefficients. Furthermore, for different cracks, most of the transmission coefficient curves have peaks which are not overlapped. These properties may prove useful in fracture classification and pattern recognition. Secondly, the primary output modes, which include the transmission and reflection modes, are the same as the incidence modes. Thirdly, in some situations, the reflection and transmission coefficients decided by different depth-to-width ratios are superposed in a very wide frequency range. While this finding may indicate difficulty in using the superposed coefficients to detect the crack features, this paper serves to provide insight in properly selecting the incidence and output modes. Lastly, it is observed that the peaks of the reflection and transmission coefficient curves always appear simultaneously and complementarily. This is characterized by the law of conservation of energy, which makes the results much more believable.

Discussion and Conclusions

The present HBEM is capable of optimizing the guided wave modes and the range of frequency for characterization of different cracks in long cortical bones.

2C-3

5:00 PM **A theoretical and experimental study of bone's microstructural effect on the dispersion of ultrasonic guided waves**

Maria Vavva[1], Vasilios Protopappas[2], Leonidas Gergidis[1], Antonios Charalambopoulos[1], Dimitrios Fotiadis[2], Demos Polyzos[3]; *[1]University of ioannina, Material Science and Engineering, Ioannina, Greece, [2]University of Ioannina, Unit of Medical Technology and Intelligent Information Systems, Greece, [3]University of Patras, Mechanical Engineering and Aeronautics, Greece.*

Background, Motivation and Objective

Bone is a composite with complex structure and microstructural features. Previous studies on the ultrasonic evaluation of bone have been largely based on the classical elasticity. However, classical elasticity cannot adequately describe the mechanical behavior of materials with microstructure, in which the stress state has to be defined in a nonlocal manner. Bone's microstructural effects can be modeled in a macroscopic framework by employing enhanced theories as those proposed by Cosserat brothers, Mindlin and Eringen.

In a previous work, we performed ex vivo measurements on an intact tibia using 1 MHz waves and the received guided modes were analyzed using the Lamb theory. The results showed that the Lamb theory was not effective in characterizing the modes that propagate in bone. In this study, we adopt the simplest form of gradient elasticity (Mindlin FormII) to derive for the first time the dispersion curves for a bone-mimicking plate and investigate whether this theory can better interpret ex vivo measurements.

Statement of Contribution/Methods

The free plate problem was analytically solved (plate thickness 4mm, density 1.5 g/cm^3, longitudinal velocity 4107 m/s, shear velocity 1842 m/s). The microstructure was taken into account by using the Mindlin FormII gradient elasticity. Two additional terms are now included in the constitutive equations: a) the gradient coefficient g, introduced in the strain energy to balance the dimensions of strains and strain gradients and b) the micro-inertia term h, in the kinetic energy. These two coefficients represent the characteristic length of bone and their values are set close to the osteons' size. The plate was considered free of stresses and additionally free of double stresses. The frequency characteristic equations were solved numerically using root-finding techniques.

Ex vivo measurements were made on the midshaft of an intact sheep tibia using 1 MHz broadband excitation. Two transducers were placed in contact with the bone along its long axis at a 30 mm separation. Signal analysis was performed in the time-frequency (t-f) domain which has been proved effective in representing mode dispersion by using only one received signal.

Results

The Rayleigh wave was found to be dispersive. For low frequencies (<0.4 MHz), the dispersion curves of the modes predicted by the gradient theory were slightly modified from those of the Lamb modes. Conversely, for frequencies larger than 0.4 MHz the curves were significantly different with the velocity asymptotically approximating that of the Rayleigh wave.

Several modes were identified in the t-f domain of the ex vivo signal by superimposing the curves of the gradient theory.

Discussion and Conclusions

We derived the velocity dispersion curves for a medium whose microstructure was described by an enhanced elasticity theory. Analysis of ex vivo measurements showed that mode detection was better when using the gradient theory rather than the classical elasticity theory.

2C-4

5:15 PM **Anomalous behavior of ultrasonic velocity dispersion in bovine cortical bone**

Guillaume Haiat[1], Magali Sasso[2], Salah Naili[2], Mami Matsukawa[3]; *[1]CNRS, B2OA, Paris, 75010, France, [2]Université Paris-Est, Laboratoire de mécanique Physique, Créteil, France, [3]Doshisha University, Laboratory of Ultrasonic Electronics, Kyoto-fu, Japan.*

Background, Motivation and Objective

Cortical bone quality is determinant in bone fragility and its ultrasonic evaluation has now become possible in clinical practice, for example using axial transmission devices. However, the interaction between a broadband ultrasonic pulse and this complex multiscale medium remains poorly understood. The frequency dependence of phase velocity, which may impact clinical measurements, has been sparsely investigated. Our objective is to evaluate in vitro the physical determinants of velocity dispersion in bovine femoral cortical bone samples.

Statement of Contribution/Methods

The samples are cut along the bone axis and circumference from three 36-month old bovine femurs. Ultrasonic measurements are performed with a substitution method using self-made broadband PVDF transducers. Velocity dispersion is evaluated for each sample between 3.5 and 4.5 MHz in three perpendicular directions after compensating for diffraction effects. Bone Mineral Density (BMD) and the microstructure of each sample are assessed using a dual x-ray absorptiometry device and optical microscopy, respectively.

Results

Precision of dispersion measurement in the axial (radial and tangential, respectively) direction is equal to 1.3 m/s (respectively 0.8 m/s and 1.3 m/s). After compensating for diffraction effects, mostly positive, but also negative values of dispersion are obtained. Analysis of variance (ANOVA) tests reveal no significant effect of the direction of propagation. The anatomical location as well as the type of microstructure significantly affect dispersion values. Dispersion values are correlated with BMD in the radial direction (R^2=0.4, RMSE = 3.3 m/s, $p<10^{-5}$) but no correlation was found in the other directions of propagation.

Discussion and Conclusions

Negative dispersion, which has been refered to as “anomalous”, is mainly obtained in the tangential direction and in samples constituted of mixed microstructure. The Figure gives an example of an optical microscopy obtained for a mixed microstructure (size: 3×4 mm). Negative dispersion may be explained by phase cancellation effects due to the presence of different microstructures within the same sample. Dispersion is related to broadband ultrasonic attenuation values, especially in the radial direction. Results are compared with the nearly local Kramers-Kronig relationships, showing good agreement in the radial direction.

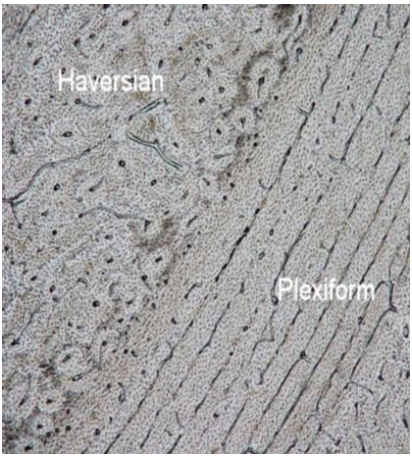

2C-5

5:30 PM **A Minute Bone Bending Angle Measurement Method using Echo-Tracking for Assessment of Bone Strength In Vivo**

Ryoichi Sakai[1], Koichi Miyasaka[1], Eiichi Minagawa[1], Toshiki Ohtsuka[1], Akimitsu Harada[1], Yoshihiro Yoshikawa[1], Juntaro Matsuyama[2], Kenji Tobita[2], Kozo Nakamura[2], Isao Ohnishi[2]; *[1]Aloka Co.,Ltd., Tokyo, Japan, [2]University of Tokyo, Department of Orthopaedic Surgery, Faculty of Medicine, Tokyo, Japan.*

Background, Motivation and Objective

The purpose of this study was to develop a new ultrasound diagnostic system for non-invasive and quantitative assessment of bone fracture healing mechanical properties. In the previous papers [1], [2], we reported that we had developed a new ultrasound method to measure a minute bone deformation using the multi-point echo-tracking (ET) and that it had a great potential for non-invasive and quantitative diagnosis of bone healing. In this paper, we present a newly developed measurement system for assessing deformation of human tibias in vivo with a dedicated probe, a transmitting/receiving system and analysis software using a three-point bending (TPB) test which we previously reported [2]. Furthermore, we report results of a performance evaluation of the developed system.

Statement of Contribution/Methods

First, for a study on in vivo measurement, we developed a TPB diagnostic system that consisted of a leg-holder to provide accurate and reproducible positioning of a lower leg and an automated loading device to apply predetermined force on the tibial surface. Second, in order to measure minute bending angle of the bone induced by the small load, we also developed a dedicated, small and light probe which was constructed of two matrix-array transducers, a transmitting and receiving system for the probe and software to be able to analyze an extremely small bone bending angle from the received radio frequency (RF) signals. Finally, we evaluated the accuracy of the developed system in bending angle measurement using a metallic plate with a known surface roughness. Furthermore, we evaluated the reproducibility of the system in the in vivo measurement by repeatedly measuring the bending angle of the tibias of 5 healthy volunteers every week for one month.

Results

We have developed a system which measures the minute bone bending angle of the tibia generated by a computer controlled loading device. The evaluation of the accuracy of the measured bending angle using the metallic plate for calibration showed that a standard deviation (SD) of the measurement was 0.004 degrees. Then, we performed an in vivo measurement of normal tibia. The results showed that the mean bending angle of the normal adult tibias

under a load of 25N and a supporting span of the tibial length was 0.058 degrees with a SD of 0.01 degrees. In addition, SD of the data for the measurement repeatability was 0.006 degrees.

Discussion and Conclusions

We developed a bending angle measurement system for the human tibia using a TPB test and obtained an excellent accuracy of the system and also confirmed the repeatability was sufficient to quantitatively assess healing of the tibia through the measurement of the tibia of human volunteers.

[1]Proc. IEEE Ultrasonics Symposium, 2006: 13-16

[2]Proc. IEEE Ultrasonics Symposium, 2007: 1116-1119

2C-6

5:45 PM **Osteoblasts growth following insonations with low intensity pulsed ultrasounds of different frequencies**

Show-Huie Chen, Chun-Yi Chiu, Shyh-Hau Wang; *Chung Yuan Christian University, Biomedical Engineering, Chung Li, Tao Yuan, Taiwan.*

Background, Motivation and Objective

The osteoblasts (OBs) are important cells contributing to bone remodeling, in which their growths were found to be modulated by ultrasound insonation. However, it is still lacking thorough discussion on the effect of insonation frequency on the OBs growth. Thus, this study is to extensively explore current issue by insonating OBs with low intensity pulsed ultrasound (LIPUS) of different frequencies.

Statement of Contribution/Methods

An ultrasonic stimulation system, capable of flexibly adjusting frequency, intensity, and duty cycle of the transmission signals, was fabricated. Experiments were performed by arranging a sample of $5x10^4$ cells/ml OBs been stimulated daily with a 20% pulsed ultrasound of 1 kHz repetition frequency, 100 mW/cm^2 (SATA), and frequencies of either 1 or 3 MHz, for 10 minutes within a period of 9 days. The responses of OBs following ultrasound stimulation were evaluated by cell morphology, viability, alkaline phosphatase (ALP) activity, and mineralization determined by the Alizarin red-S histochemical staining.

Results

Results showed that OBs proliferation tended to increase with the frequency of ultrasonic stimulations. The viability of OBs insonated with 1 and 3 MHz ultrasounds tended to increase to 1.1 and 1.2 fold with that of control groups, respectively. Furthermore, those of the ALP activity increase to 1.5 and 1.1 fold associated with insonations with 1 and 3 MHz ultrasounds, respectively. The largest proliferation rate and activity of OBs were found to be at 7-8 days after cells were seeded. Moreover, more mineralized nodules were produced from insonated OBs than that of control group. This study revealed that both proliferation and activation of ALP synthesis of OBs may be enhanced by LIPUS insonation.

Discussion and Conclusions

After LIPUS insonation, the temperature variation in the culture medium was measured to be lower than 0.5¢J, which indicated that the effect of insonation on the OBs growth is primarily corresponding to the non-thermal effect of ultrasound. Results of current study suggest that the ultrasonic bioeffect of OBs maybe frequency dependent, in which lower frequency ultrasound tends to be more effective in promoting the OBs growth.

3C. Phononic Crystals I - Bandgap & Focusing

Hall 5A

Monday, November 3, 2008, 4:30 pm - 6:00 pm

Chair: **Yook-Kong Yong;**
Rutgers University, NJ, USA.

3C-1

4:30 PM **Study of transmission property of the one-dimensional phononic crystal thin plate by the Eigen-Mode-Matching theory**

Zhilin Hou, **Badreddine Assouar;** *LPMIA, Nancy University - CNRS, Vandoeuvre les Nancy cedex, France.*

Background, Motivation and Objective

Elastic wave propagation in periodic composite materials, called phononic crystal (PC), are receiving more and more attentions in the past decades. Because of their existing of the elastic band gaps, PC structure have many potential practical utilities such as the perfect acoustic mirror, acoustic sensor ... Recently, waves in thin PC plate with free surface had been investigated, complete band gaps in one- or two-dimensional thin PC plate are predicted theoretically and verified experimentally. However, we find that, because of the lack of the suitable numerical method, almost all of the theoretical works about the PC plate are concentrated on the band structure calculation. We know that from the transmission (or reflection) spectrum of a system, one can obtain many information if a suitable incident signal is used. The purpose of this work is to extend the Eigen-Mode-Matching Theory (EMMT) into the PC thin plate system, by which the transmission property of the one-dimensional PC thin plate with and without uniform substrate can be investigated.

Statement of Contribution/Methods

The idea of EMMT is original developed for two-dimensional bulk wave. We have proved recently that the conventional PWE method can be modified to calculate the band structure of the PC plate with free surface by constructing an imaginary two dimensional infinite system by stacking the considered PC plates and the vacuum layers along the thickness direction periodically. Then, the EMMT can also be extended to deal with the PC plate transmission analysis accordingly. We find that, in the EMMT, the incident wave can be easily set as the eigen modes in the inputting end (the symmetric or anti-symmetric lamb wave). By this method, the transmission spectra of the PC and the PC plate with substrate (PCS) of the incident symmetric and anti-symmetric lamb mode can be calculated.

Results

As examples, the one-dimensional W/Si PC plate and the PCS plate constructed by W/Si PC coated on the Si substrate are investigated. Because the incident wave is chosen as a single symmetric or anti-symmetric mode, the transmission coefficient (TC) of the systems shows a Fabry-Pérot resonance in the low frequency range. From the TC we have found that the bands of the PC plate can be separated into two parts which can only be excited by the anti-symmetric and symmetric lamb waves separately. However, for the band in PCS system, because of the existing of the substrate layer, the interaction between the lowest two bands occurs, and as a consequence, a low band gap appears.

Discussion and Conclusions

We explain this phenomenon as a diffraction effect across the interface between the PC and the substrate slice. For the transmission spectrum, this kind of interaction makes the energy conversion between the anti-symmetric and symmetric mode, which means that around the frequency of band edge, the symmetric (anti-symmetric) lamb mode component in the output end can be found even if the incident wave is the pure anti-symmetric (symmetric) lamb mode.

3C-2

4:45 PM **Study of complete band gaps in two-dimensional square and triangular steel-water phononic crystals**

Cunfu He, **Huanyu Zhao,** Bin Wu, Ruiju Wei; *Beijing University of Technology, China.*

Background, Motivation and Objective

In this Letter, We investigated theoretically and experimentally propagation of acoustic waves in two-dimensional square and triangular steel-water phononic crystals (PCs) , which are consist of two-dimensional periodical structures of steel cylinders embedded in water.

Statement of Contribution/Methods

The band structure diagrams of phononic crystals were obtained by the plane wave expansion (PWE) method. Transmission spectra of acoustic waves were measured experimentally and compared with simulations of ones by finite-difference time-domain (FDTD) method in PCs.

Results

As a result, a complete acoustic band gap is demonstrated experimentally along the two high-symmetry directions of the Brillouin zone and is good agreement with theoretical calculation in square steel-water PCs.

Moreover, in triangular lattice steel-water PC we have calculated band structure that exists flat bands, which name deaf bands. The measured transmission spectra of acoustic waves show the existence of complete band gaps and deaf bands that are identified by comparing band structure computations. While the experimental results of transmission spectra are coincided with the simulations of FDTD well.

3C-3

5:00 PM **Band gap analysis of two-dimensional phononic crystals based on boundary element method**

Feng-lian Li, Yue-sheng Wang; *Beijing Jiaotong University, Institute of Engineering Mechanics, Beijing, China.*

Background, Motivation and Objective

The phononic crystal is an artificial crystal constructed by scatterers periodically embedded in a homogeneous host material. The primary motive for these investigations has been the search for so-called full phononic band gaps. Thus, phononic crystals have widespread applications in engineering and play a central role in the analysis of vibrationless environments for high-precision mechanical systems.

Several methods have already been developed to compute the elastic band gaps, but each method presents several drawbacks from the computational point of view. Recently, some researchers successfully calculate the band structures of photonic crystals with BEM.

The main objective of this paper is to extend the BEM to the elastic band gap analysis of two-dimensional phononic crystals.

Statement of Contribution/Methods

Consider a system composed of an array of straight, infinite cylinders (scatterers) embedded in an elastic background material (matrix). For time harmonic wave fields, the out-of-plane propagation of waves is considered here.

Due to the periodicity of the structure, we restrict our attentions to a unit cell. The periodic Green's function satisfying the Bloch theorem is adopted as the fundamental solution. Then the boundary integral equation for the matrix and the inclusions are derived.

The boundary conditions are the continuities of the transverse displacement field and the stress field on the interface between the matrix and the inclusions.

We solve the system of equations by discretizing the above derived boundary integral equations. Ewald summation method will be adopted to calculate the Green's function.

Results

We investigate the case with Au cylinders embedded in the epoxy host in square lattice. The filling fraction is 0.44. Figure 1 shows the dispersion relation of the elastic modes propagating along z axis. The results are compared with those computed by the wavelet method. It indicates that two results are in good agreement for the low frequencies.

Discussion and Conclusions

The ability of a boundary element scheme to handle the binary system makes the method an important tool for the study of elastic band gaps. In addition, the application of Ewald sum technique drastically improves the convergent rate of the Green's function series which can be calculated accurately with only a small number of terms.

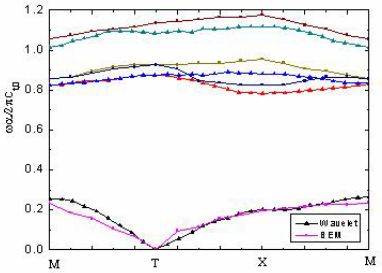

3C-4

5:15 PM **Band structure of evanescent waves in phononic crystals**

Vincent Laude[1], Boujemaa Aoubiza[2], Younes Achaoui[1], Sarah Benchabane[1], Abdelkrim Khelif[1]; *[1]Institut FEMTO-ST, Micro Nano Sciences & Systems dept., Besancon, Franche-Comté, France, [2]Université de Franche-Comté, Laboratoire de Mathématiques de Besançon, Besancon, Franche-Comté, France.*

Background, Motivation and Objective

Phononic crystals are two- or three-dimensional periodic structures that consist of two materials with different elastic constants, giving rise to absolute stop bands under specific geometrical conditions. In addition, their unique dispersion properties can be used to design efficient waveguides or to obtain unusual refraction properties. Band structures are usually employed to describe phononic crystals, as they provide one with all propagative waves in the periodic medium (Bloch waves). The purpose of this communication is to discuss the evanescent wave solutions and their calculation.

Statement of Contribution/Methods

Evanescent waves must be considered in propagation problems whenever scattering, diffusion, or diffraction by a finite object are investigated. In the context of phononic crystals, they appear very naturally within frequency band gaps. Indeed, since no waves can propagate within a band gap, only evanescent waves are left to explain the exponentially-decreasing transmission of acoustic waves. We have extended the classical plane wave expansion (PWE) method so that it includes complex wave vectors in the direction of propagation. To do so, it is necessary to consider a fixed frequency and to solve for the wave vector, in contrast to the traditional way of obtaining band structures by considering any Bloch wave vector within the first Brillouin zone and solving for the frequency of allowed modes.

Results

The new complex PWE method has been used to generate band structures for two-dimensional silicon - void phononic crystals. Both propagative and evanescent solutions are found at once. The decay constants within band gaps are thus found and shown to depend on the polarization of the waves. The complex graphs also allow to identify clearly the different branch systems in the band structure and to connect bands below and above band gaps. Furthermore, the distribution of the acoustic fields of evanescent modes can be computed. Their transformation from below to above a band gap and within will be shown.

Discussion and Conclusions

The proposed extended PWE method yields at once all solutions of the wave equation in a phononic crystal, including propagative and evanescent waves. It is expected to become the basic building block to solve scattering problems in phononic crystals. In addition, it directly gives the eigenfrequency contours that are required to understand refraction (positive or negative) in phononic crystals.

3C-5

5:30 PM **Negative refraction of transverse waves in an elastic phononic crystal**

Anne-Christine Hladky[1], Jérôme Vasseur[1], Bertrand Dubus[1], Bahram Djafari-Rouhani[1], Didace Ekeom[2], Bruno Morvan[3]; *[1]IEMN, Lille, Nord, France, [2]Microsonics, France, [3]LOMC, Le Havre, France.*

Background, Motivation and Objective

Phononic crystals are periodic structures exhibiting absolute band gaps i.e. frequency bands in which the propagation of elastic waves is forbidden in all directions. If the presence of a band gap opens up potentialities for filtering applications, it is also possible to use unusual properties in the pass bands of the dispersion curves. Researches are carried out on phononic crystals presenting a negative refraction that can focus acoustic waves.

Statement of Contribution/Methods

This paper reports a numerical analysis of negative refraction process using a phononic crystal with an elastic solid matrix, whereas, to our knowledge, recent works were devoted to phononic crystals made of solid inclusions in a fluid matrix. The phononic crystal considered in this study is made of a periodic arrangement of holes in aluminum.

Results

Dispersion curves are discussed and conditions for which negative refraction can appear are identified. These conditions are obtained for the transverse waves, whereas the longitudinal waves are evanescent. A calculation is performed with a prism shape phononic crystal and it clearly exhibits a negative refraction angle. Several analyses are provided with a view to characterizing the wave leaving the phononic crystal.

Discussion and Conclusions

Negative refraction is clearly obtained for transverse waves. Improvement of the device are discussed, with a view to finding a satisfying compromise between the impedance matching, to ensure the transmission of the waves between the phononic crystal and the external elastic medium, and the refraction indices of the media that have to be tuned. Finally, experiments are under progress.

3C-6

5:45 PM **General analytical scheme for determining the characteristic caustic points in phonon focusing patterns of cubic crystals**

Litian Wang; *\{O}stfold University College, Mathematics and Physics, Sarpsborg, Norway.*

Background, Motivation and Objective

Slowness surface for the bulk wave propagation in anisotropic media can be divided in to concave/saddle and convex regions by the so called parabolic line. In the phonon imaging, the focusing pattern is determined by the parabolic lines and its characteristic points (cuspidal/ parabolic caustic points) in the symmetry planes are associated with either the inflection points or the parabolic points on the slowness surface.

Statement of Contribution/Methods

By employing the Stroh formalism, the caustic points resulted from both the parabolic points and inflection points are investigated by examining the degeneracies in the Stroh eigenvalues equation. A set of analytical expressions for the location of these parabolic caustic points in cubic crystals is derived.

Results

The general scheme for determining various caustic points is based on the recognition of the connection between the inflection/parabolic points on the slowness surface and the extraordinary degeneracies appeared in the Stroh eigenvalue equation.

Discussion and Conclusions

The geometric and algebraic constraints in such a connection make it possible to resolve all the caustic points in the symmetry planes analytically without solving either the Christoffel equation or the Stroh equation. The scheme can also be applied to crystals with other symmetries and the results can be readily applied to other related fields.

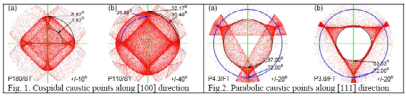

Fig. 1. Cuspidal caustic points along [100] direction

Fig.2. Parabolic caustic points along [111] direction

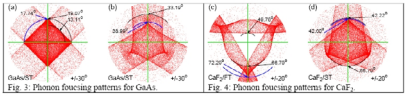

Fig. 3: Phonon focusing patterns for GaAs.

Fig. 4: Phonon focusing patterns for CaF_2

4C. Single Crystal II

Hall 5B

Monday, November 3, 2008, 4:30 pm - 6:00 pm

Chair: **Clyde Oakley;**
W. L. Gore, USA.

4C-1

4:30 PM **Piezoelectric Thin and Thick Films for Transducer Applications**

Wei Ren[1], Peng Lin[1], Zheng Wang[1], Xiaoqing Wu[1], Peng Shi[1], Xi Yao[1], Qifa Zhou[2], Dawei Wu[2], Benpeng Zhu[2], K. Kirk Shung[2]; *[1]Electronic Materials Research Laboratory, Xi&[prime]an Jiaotong University, Xi&[prime]an 710049, China, [2]University of Southern California, Los Angeles, CA 90089, NIH Transducer Resource Center and Department of Biomedical Engineering, USA.*

Background, Motivation and Objective

In recent years, the demands for miniaturized devices integrated with microelectronics have increased significantly, leading to great interests in the design and fabrication of thin/thick film transducers. Lead zirconate titanate (PZT) is an attractive material for transducer applications due to its excellent electromechanical properties. Such devices often require crack-free films with thickness of 1~10 μm. A polymer-assisted deposition and PZT powders/sol-gel solution composite thick films have been developed to prepare PZT thick films.

Statement of Contribution/Methods

$PbZr_{0.52}Ti_{0.48}O_3$ (PZT) thin and thick films with thickness of 1~10 μm have been prepared by a metallo-organic decomposition process modified by a polymer, poly(vinyl acetate) (PVAc). It's found that with an increase of PVAc in PZT solutions, the single-layer thickness of PZT films increases from 0.07 μm to 0.47 μm. When PVAc-related organic compounds are decomposed, nano-sized pores are formed and provide space for the structural and stress relaxation. It prevents the crack formation and increases the uncracking critical thickness of PZT films.

In addition, PZT composite thick films up to 30 μm-thick have been successfully prepared with a spin-coating of PZT powers/sol-gel composite solution. The electric properties of the films were evidently enhanced by infiltration of PZT sol-gel into composite films and optimization of PZT powders to PZT sol-gel mass ratio in composite solution. Transducer and array at a frequency high than 100 MHz have been fabricated using above PZT thick films by MEMS technology.

Results

Dielectric, ferroelectric, and piezoelectric properties of PZT films have been thoroughly investigated. For PVAc modified PZT films, with the increase of the film thickness from 0.95 μm to 9.9 μm, the dielectric constant increases from 1070 to 1600, while the dielectric loss is in a range of 0.03~0.04 at 1 kHz. Remanent polarization increases from 36.1 $\mu C/cm^2$ to 55.3 $\mu C/cm^2$, while coercive field decreases from 57.3 kV/cm to 40.9 kV/cm. The piezoelectric coefficient d_{33} increases from 43.9 pm/V to 200 pm/V.

Discussion and Conclusions

Using PZT thick films, high-frequency transducers and kerfless array at a frequency high than 100 MHz will be presented. Meanwhile, the effect of the residual stresses of PZT films on devices has been investigated.

4C-2

5:00 PM **Elastic, Piezoelectric and Dielectric Properties of PIN-PMN-PT Crystals Grown by Bridgman Method**

Jun Luo[1], Shujun Zhang[2], Thomas Shrout[2], Wesley Hackenberger[1]; *[1]TRS Technologies, Inc, State College, PA, USA, [2]Pennsylvania State University, Material Research Institute, University Park, PA, USA.*

Background, Motivation and Objective

It was demonstrated that single crystals of ternary compositions, $Pb(In_{1/2}Nb_{1/2})O_3$ - $Pb(Mg_{1/3}Nb_{2/3})O_3$ - $PbTiO_3$ (PIN-PMN-PT), exhibit elevated T_{rt} (rhombohedral-to-tetragonal phase transition temperature) and E_C (coercive field) compared to $Pb(Mg_{1/3}Nb_{2/3})O_3$ - $PbTiO_3$ (PMN-PT) crystals. This can potentially improve the temperature and electric stability of crystal transducers. To fully understand PIN-PMN-PT crystals, the relationship between electric field and temperature operating ranges and In concentration was studied. In addition, elastic, piezoelectric and dielectric properties were characterized.

Statement of Contribution/Methods

PIN-PMN-PT single crystals with 26%-59% PIN were successfully grown by Bridgman technique. The diameter of as-grown crystals was up to 40mm. For the compositions with PIN content higher than 36%, the melt became less stable and pyrochlore phase formed during solidification. The dielectric temperature relationship and strain field behavior of the crystals with different PIN content were investigated. Five sets of <001>-cut samples with different modes were prepared and the full set of elastic, piezoelectric and dielectric properties were determined by the resonance method.

Results

T_{rt} of PIN-PMN-PT crystals with 26%-36% PIN were roughly in the range of 115 -135°C, and T_{rt} increased with the increasing In concentration in the rhombohedral side of the morphotropic phase boundary (MPB). E_C of the above crystals were on the order of 4.5-5.6kV/cm. Table 1 compares the crystal properties of a PIN-PMN-PT composition with PMN-29%PT.

Discussion and Conclusions

PIN-PMN-PT crystals exhibit much higher T_{rt} and E_C than PMN-PT crystals (80-95°C and 2-2.5kV/cm, respectively), which suggests a strong impact of the In concentration on these properties. PIN-PMN-PT crystals possess high electromechanical properties similar to those of PMN-PT; meanwhile, PIN-PMN-PT can be operated under much higher temperature and electric driving field, which significantly benefits the transducer design.

Table 1: Measured and Derived Electromechanical Coupling Factors, k_t, Dielectric Permittivity, ε_3 (ε_0), d_3 (pC/N), and g_3 (10^{-3}Vm/N) for the crystals of a PIN-PMN-PT composition and PMN-29%PT

Material	k_{33}	k_{31}	k_{31} (45°)	k_t	d_{33}	d_{31}	g_{33}	g_{31}	ε_{33}^T	ε_{33}^S
PIN-PMN-PT	0.91	0.47	0.83	0.57	1356	-650	34.4	-16.5	4450	729
PMN-PT	0.91	0.44	0.81	0.60	1540	-699	32.2	-14.6	5400	910

4C-3

5:15 PM **Frequency Dependent Properties of High Permittivity PMNT Piezoelectric for Ultrasonic Transducer Applications**

Shujun Zhang[1], Hyeong Jae Lee[2], Xiaoning Jiang[3], Eugene Gerber[2], Thomas Shrout[2]; *[1]Pennsylvania State University, Materials Research Institute, University Park, PA, USA, [2]Pennsylvana State University, USA, [3]TRS Technologies, Inc., USA.*

Background, Motivation and Objective

Pb(Zr,Ti)O3-5H piezoelectric ceramics are widely used in medical ultrasonic applications due to their high electromechanical coupling (k33 < 75%). However, their relatively low clamped dielectric permittivity (< 1500) limits their usefulness in high frequency medical transducer with small aperture and array elements. Thus, high permittivity piezoelectric materials are desired. Relaxor based Pb(Mg1/3Nb2/3)O3-PbTiO3 (PMNT) piezoelectrics with high permittivity and coupling have attracted much attention in medical ultrasonic applications in the form of both polycrystalline and single crystals.

Statement of Contribution/Methods

In this work, the clamp dielectric permittivity and electromechanical coupling of monolithic PMNT and 1-3 composites were investigated as a function of frequency (1.5M-50MHz). The dice and fill technique was used to fabricate composites < 20MHz, while the novel micromachining method1 was used to fabricate composites with frequencies higher than 20MHz. Meanwhile, fine grain size (< 1 micron) PMNT polycrystalline ceramic (dielectric

permittivity ~7000, coupling k33 ~78%) were developed from the point of view for manufacturability and improved the mechanical and dielectric strength.

Results

High frequency PMNT single crystal/epoxy 1-3 composites were prepared and the electromechanical coupling factor of the composites was achieved in the range of 72-85%.

Discussion and Conclusions

The high permittivity PMNT in both polycrystalline and single crystal is promising for high frequency ultrasound transducers for medical and NDE/NDT imaging applications.

4C-4

5:30 PM **Broadband (10^{-2}-$2x10^{10}$ Hz) dielectric response in hard and soft PZT ceramics**

Li Jin, Viktor Porokhonskyy, Dragan Damjanovic; *Swiss Federal Institute of Technology - EPFL, Ceramics Laboratory, Lausanne, Switzerland.*

Background, Motivation and Objective

The most widely used family of piezoelectric materials $Pb(Zr,Ti)O_3$ (PZT) is employed in two main variants: hard (acceptor doped) materials exhibit lower but more stable properties while soft (donor doped) compositions exhibit less stable but higher properties. This difference is attributed mainly to contribution from domain walls displacement which is considered restricted in hard and relatively easy in soft materials. However, hardening and softening mechanisms are still poorly understood. In this paper we present results of a study of dielectric properties of hard and soft PZT ceramics over a broad frequency range with a goal to deepen understanding of softening and hardening mechanisms.

Statement of Contribution/Methods

PZT ceramics with tetragonal and rhombohedral structures were prepared by solid state method. Fe^{3+} and Nb^{5+} were added in place of (Zr,Ti) as acceptors and donors. Dielectric spectra of doped and undoped ceramics were measured in quasi-continuous way by a number of spectroscopy methods: lock-in/charge amplifier technique was used from 10^{-2} to 10^{3} Hz, an LCR-meter from 10^{1} to 10^{6} Hz, high-frequency reflectometry from 10^{5} to $1.8x10^{9}$ Hz and a sleeve resonator method from $5x10^{9}$ to $2x10^{10}$ Hz. In the last technique quasi-continuous data were obtained by measuring a number of modes of different symmetry. The influence of poling state, thermal quenching and micro-structure on dielectric function is analyzed.

Results

The dielectric spectra are dominated by two main features. Nearly constant loss behavior ($1/f$-noise) was observed over at least ten decades in frequency while a sharp dispersion region was located between 10^{8} and $2x10^{10}$ Hz. The intensity of the constant loss behavior is the strongest in rhombohedral soft materials and becomes lower in hard and tetragonal samples. On decreasing frequency and below the GHz dispersion region, hard materials exhibit nearly constant permittivity from 10^{8} to 10^{0} Hz, and a rapid increase below 1 Hz. In soft materials permittivity increases nearly linearly on linear-log scale with decreasing frequency.

Discussion and Conclusions

The dispersion in the GHz range is discussed in terms of electromechanical resonances of grains and domain-walls relaxation. The splitting of the loss peak in poled samples indicates that domain structure plays an important role in this dispersion. Linear dependence of the permittivity on logarithm of frequency in soft materials is consistent with contribution of domain walls moving in a random potential landscape. Constant permittivity in hard ceramics indicates that movement of domain walls is restricted within deep potential wells. Finally, the increase of the permittivity and loss in hard ceramics below 1 Hz could be tentatively associated with a charge hopping mechanism.

4C-5

5:45 PM **Improved Properties for Piezoelectric Crystals in the Lead Indium Niobate-Lead Magnesium Niobate-Lead Titanate Ternary System**

Jian Tian[1], Pengdi Han[1], James Carroll[2], David Payne[2]; *[1]H. C. Materials Corp., USA, [2]University of Illinois at Urbana-Champaign, Materials Sciences and Engineering, USA.*

Background, Motivation and Objective

Binary PMN-PT crystals have superior properties (e.g., d_{33} ~ 2000 pV/m, k_{33} ~ 0.9) compared with PZT ceramics. Recently, ternary $Pb(In_{1/2}Nb_{1/2})O_3$-$Pb(Mg_{1/3}Nb_{2/3})O_3$-$PbTiO_3$ (PIN-PMN-PT) crystals have demonstrated enhanced thermal and electrical stability. To further improve critical material properties and understand composition-property relationship, PIN-PMN-PT crystals of refined compositions were systematically grown and characterized.

Statement of Contribution/Methods

PIN-PMN-PT crystals were grown by a modified Bridgman method. To optimize the properties, compositions were chosen close to the morphotropic phase boundary (MPB) in the rhombohedral region. From each crystal boule, specimens were selected from the base to the top of the crystal, and prepared into plates and bars. Selected dielectric, piezoelectric and elastic properties were measured along the [001] crystallographic direction.

Results

Values of dielectric constant K ranged from 3500 to 6000, piezoelectric strain coefficient d_{33} ~ 1000-2000 pV/m, voltage coefficient g_{33} ~ 30-40 $\times 10^{-3}$ Vm/N, electromechanical coupling factors k_{33} ~ 0.87-0.92 and k_t ~ 0.56, coercive field E_C > 7.0 kV/cm, depoling temperature $T_{R/T}$ increased to 140 °C, Curie temperature T_C up to 200 °C, and elastic compliance s^E_{33} of 40-70 $\times 10^{-12}$ m^2/N.

Discussion and Conclusions

Compared with binary PMN-PT, ternary PIN-PMN-PT crystals show significantly improved coercivity (3×) and thermal stability (~ 50 °C increase in $T_{R/T}$) while exhibiting excellent dielectric and piezoelectric properties. As a result, ternary crystals can be used at reduced, or zero bias field, which will simplify the design and improve the robustness of crystal-based transducers. In addition, increase in depoling temperature will improve transducer reliability while reducing temperature-dependent variations in transducer performance. Such improvements are important for a wide range of applications for piezoelectric crystals.

5C. Bulk Acoustic Wave Sensors

Hall 5C

Monday, November 3, 2008, 4:30 pm - 6:00 pm

Chair: **John Vetelino;**
University of Maine, ME, USA.

5C-1

4:30 PM **Ultra high frequency acoustic wave detection of HIV antibody**

Michael Thompson[1], Scott Ballantyne[2]; [1]*University of Toronto, Chemistry, Toronto, Ontario, Canada,* [2]*Maple Biosciences, Toronto, Ontario, Canada.*

Background, Motivation and Objective

Screening and detection of HIV disease in patients requires assaying of blood or serum samples for antibody. For rapid screening, the detection of only one antibody is required, but for confirmation of the presence of the disease up to 10 are mandatory. Such assays are highly time consuming and costly, and involve significant skilled labour. It is the specific overall objective of this project to develop an electronic signalling approach to the detection of HIV in biological fluids. The technology incorporates a biosensor methodology which will be designed for the clincal laboratory. The basis is ultra high frequency acoustic wave technology

Statement of Contribution/Methods

Our contribution has three distinct but connected goals. First we have developed a flow through system which incorporates a bulk acoustic wave sensor in an analytical configuration. The sensor is a conventional 20 MHz quartz device which is excited not by the usual electrode technique, but by a flat spiral coil. Secondary electric fields drive the device up to the 50th harmonic thus generating high sensitivity.

The second crucial aspect of the project is the attachment of antibody probes to the device surface. These probes which are based on peptide structures bind antibody which is then detected by the sensor. We have designed and developed new linking agents for attaching probes at optimum surface density but also that avoid the vexing non-specific adsorption problem.

The thired part of the work involves the use of the whole configuration to analyse real samples such as human serum

Results

We have demonstrated that the sensor can be operated with facility in a flow-injection apparatus. The faces of the device must be extremely parallel and have optimum surface physical nature as shown by AFM. XPS and other surface techniques have been used widely to demonstrate the presence of peptide probes on the quartz surface. The linkers are based on customized silane chemistry and constitute new molecules for the surface bioanalytical chemist. The binding of antibody in the flow system yields signals in the thousands of Hz. In serum we can acheive ratios of signal over non-specific adsorptive noise at up 5 to 1.

Discussion and Conclusions

The system described above is being developed for commercial application in the clinical lab. Required for the future is the design and implementation of a multiplexed system involving series or parallel flow. Also the prototype instrument requires significant design engineering for non-technical users. The instrument will then be tested in the clinical environment

5C-2

5:00 PM **The Detection of Chemical and Biological Analytes Using a Monolithic Spiral Coil Acoustic Transduction Sensor**

Donald McCann, Mitchell Wark, Paul Millard, David Neivandt, John Vetelino; *University of Maine, Orono, ME, USA.*

Background, Motivation and Objective

The monolithic spiral coil acoustic transduction (MSCAT) sensor platform is a novel bulk acoustic wave (BAW) device which is excited by a gold spiral coil antenna photolithographically deposited on one side of an AT-quartz wafer. The MSCAT platform can operate at very high frequencies by efficiently exciting high harmonic transverse shear modes with the application of a high frequency RF signal to the spiral coil. Since one surface of the MSCAT device is bare, this device can be used as a sensing platform upon which one deposits analyte selective chemical or biological films. The bare surface allows the detection of analyte induced mechanical (mass and viscoelasticity) and electrical (conductivity and dielectric constant) property changes in the film. In order to demonstrate the applicability of a MSCAT device as a sensor, the MSCAT platform is coated with biological and chemical films selective to Escherichia coli (E. coli) O157:H7 (hereafter referred to as E. coli), the E. coli strain most often responsible for serious illnesses in humans, and saxitoxin (STX), the most dangerous neurotoxin associated with shellfish poisoning stemming from red tide, respectively.

Statement of Contribution/Methods

A method for optimizing the number of turns and coil width and spacing of the MSCAT's antenna was developed using the Box-Behnken design method. MSCAT sensing platforms were then coated with biological films selective to E. coli based on antibody-antigen interactions and chemical films selective to STX based on the 18-crown-6 ether. Each MSCAT sensor was the exposed to E. coli and STX and the changes in resonant frequency were monitored.

Results

It was found that the most critical parameter in achieving efficient operation of the MSCAT device was the coil width. The MSCAT sensor operating at its fundamental frequency (5 MHz) was exposed to E. coli and exhibited a frequency shift approximately five times greater than similar tests performed with quartz crystal microbalance (QCM) sensors. In order to determine the lower detection limit and resolution of the MSCAT sensor, the sensor was operated at its 11th harmonic (55 MHz) and exposed to decreasing concentrations of E. coli. The resonant frequency was then monitored to obtain a dose response curve. The MSCAT sensor was able to detect E. coli in concentrations as low as 104 microbes/mL, 2 orders of magnitude lower than the QCM sensor. Similar results relating to the detection limit and resolution were also obtained for STX.

Discussion and Conclusions

A method for optimizing the MSCAT sensors' spiral coil antenna geometry was performed and it was shown that the coil width was the most critical parameter. The MSCAT was found to be significantly more sensitive than the QCM sensor due to the fact that it can detect both electrical and mechanical property changes and operate at high frequencies. Since the MSCAT has been excited up to the 81st harmonic, the MSCAT device may also be used in high frequency resonator applications.

5C-3

5:15 PM **Monolithic Lateral Field Excited Well Structures in Quartz**

Shane Winters[1], George Bernhardt[2], David Frankel[2], John Vetelino[2]; [1]*University of Maine, Orono, Maine, USA,* [2]*University of Maine, USA.*

Background, Motivation and Objective

Recently, wells have been etched on AT-cut quartz wafers and a resonant transverse shear mode (TSM) has been excited by electrodes placed at the bottom of the well and underneath the well on the opposite side of the crystal, creating a QCM array. Although this sensor offers the possibility of performing multiple sensing operations on a single substrate, there are some shortcomings. First, since the bottom of each well or sensing surface is coated with gold, only analyte induced mechanical changes (mass and viscosity) can be sensed. Second the array structure is complicated since electrodes and interconnects are located on the sensing surface of the QCM platform array. Recently, a Lateral Field Excited (LFE) sensor platform has been developed at the University of Maine which can overcome the deficiencies of a QCM. The LFE sensor platform has a bare surface with no electrodes or interconnects, allowing both analyte induced mechanical and electrical film changes to be monitored. The objective of this paper is to report the fabrication and excitation of LFE sensor elements configured in a well structure, which can be the fundamental building block of an LFE sensor array on a single AT-Cut quartz substrate.

Statement of Contribution/Methods

The well structures were etched on an AT-Cut quartz substrate using a wet etch technique. The LFE electrodes were photolithographically deposited underneath the wells on the opposite side of the crystal. The oscillation frequency of the TSM was determined using admittance measurements of the device on a Network Analyzer.

Results

Several wells were etched on an AT-Cut quartz substrate with depths ranging from 1 micron to 80 microns and diameters ranging from 1 to 8 mm. The surface roughness of the bottom of the wells ranged from about 20 to 80 angstroms. The TSM was successfully excited in each of the well structures by electrodes fabricated underneath the well on the opposite side of the crystal The fundamental resonant frequencies of each of the well structures was shown to be inversely proportional to depth.

Discussion and Conclusions

The fabrication and subsequent excitation of a resonant TSM in LFE well structures of various depths and diameters in an AT-Cut quartz substrate has been demonstrated. The fact that each well can have a different depth and hence a different resonant frequency will minimize cross talk between adjacent wells. These results imply that it is possible to create a monolithic LFE sensor array that uses well structures as a fundamental building block.

5C-4

5:30 PM **Novel electrode configurations of lateral field Excited acoustic wave devices on (yxl)-58° $LiNbO_3$**

Wenyan Wang, Chao Zhang, Zhitian Zhang, Yan Liu, Guanping Feng, Gang Jing; *Tsinghua University, Department of Precision Instruments and Mechanology, Beijing, China.*

Background, Motivation and Objective

AT-cut quartz and parallel gap electrode configuration have been used in lateral field excitation (LFE) acoustic wave sensors. However, recent studies on lithium tantalate LFE devices have provided more comprehensive understanding on LFE sensors′ behavior. In the present study, Lithium niobate was used in developing LFE devices and several novel electrode configurations were investigated.

Statement of Contribution/Methods

Theoretical calculations show that for slow shear c mode of the (yxl)-58° $LiNbO_3$ substrate, the LFE coupling coefficient reaches to its maximum of 95.46% when the applied lateral field is parallel to the crystallographic x-axes. Several 5 MHz LFE devices with different electrode configurations were fabricated, including the split-parallel-gap electrode, single-turn Archimedes spiral electrode, two-turn Archimedes spiral electrode and two-turn symmetric spiral electrode, which were shown in Fig.1, a, b, c and d, respectively. The surface in contact with liquids was free of electrode. The reflection coefficients of these devices were measured in air and liquid using a network analyzer HP8752A. A LFE device with the single parallel gap electrode configuration was fabricated and tested for the comparison.

Results

A major resonance peak was observed in all devices in air which corresponds to the lateral field excited shear waves. However, devices with the single parallel gap electrode and the two-turn symmetric spiral electrode offer higher Q value than other devices. When these devices were exposed to water, the center frequency of their resonance peaks shifted to lower level with different magnitude. It is found that the device with the split-parallel-gap electrode shows the maximum frequency change compared to other devices and is about 10 times larger than that of the single-parallel gap electrode. The frequency change of the device with the single-turn Archimedes spiral electrodes is similar to that of the two-turn Archimedes spiral electrode device.

Discussion and Conclusions

LFE devices on (yxl)-58° $LiNbO_3$ substrate with different electrode configurations have been fabricated and tested. The LFE device with the split-parallel-gap electrode is shown to have the largest sensitivity to liquid property changes. Theoretical analysis based on the effective orientation of the electric field is presented.

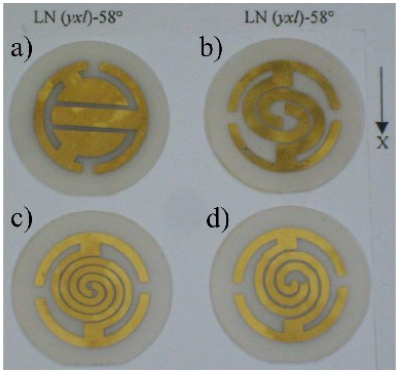

Fig. 1: Four LFE electrode configurations.

5C-5

5:45 PM **More Comprehensive Model of Quartz Crystal Microbalance Response to Viscoelastic Loading**

Raimund Bruenig[1], Manfred Weihnacht[2], Hagen Schmidt[1], Glen Guhr[1]; *[1]IFW-Dresden, Dresden, Germany, [2]InnoXacs, Dippoldiswalde, Germany.*

Background, Motivation and Objective

The use of the quartz crystal microbalance (QCM) is well established to determine physical properties of deposited material on its surface. Common method is to extract these properties from the shift of resonant frequency and motional resistance of the QCM. Several particular frequencies can be taken for the resonant frequency (e. g. admittance maximum, eigenfrequency, phasing zero, etc.) which are all close to the admittance maximum but behave differently when the QCM is loaded. It is therefore necessary to know the specific measured frequency before results (e. g. also from literature) might be compared with each other.

Our studies of monitoring coagulation processes (e. g. with blood, milk) with all its facets of liquid loading, rheologic alterations and the desirable quantitative determination of viscoelastic properties suggested re-examining the method and its issues.

Statement of Contribution/Methods

We present a more general model which reflects the QCM behavior in a wide frequency range that includes the antiresonance and additional modes adjacent to the main shear mode. Using a one-dimensional approach, the electric admittance |Y| of a QCM is calculated as function of frequency depending on parameters like static capacitance, the piezoelectric coupling factor K^2 and the ratio of the acoustic impedance of the QCM to that of a viscoelastic loading.

The electrical admittance of a QCM, especially at frequencies close to the admittance minimum (antiresonance), is usually influenced by further effects like stray capacitance or additional oscillating modes. These parasitic effects have been analyzed experimentally and methods are presented to either suppress or compute their influence on the calculated viscoelasticity.

Results

Explicit mathematical expressions to calculate both the real and imaginary part of the loaded acoustic impedance from the shift of resonant and antiresonant frequency (extrema of |Y|) are derived. Solutions for the shift of other specific frequencies, corresponding to measurement principles implemented in commercial devices, the quality factor or admittance values, are possible too. Additionally, fitting procedures have been applied to extract the complex acoustic load impedance and in turn the viscoelastic properties of the measured fluid.

The extended model has been confirmed experimentally using a set of water-glycerol mixtures as well as polyethylenglycol-solutions as viscoelastic loading and by means of standard methods in parallel.

Discussion and Conclusions

The new wide-frequency model, including the parasitic effects, is useful for measuring liquid properties especially of higher viscosities. To reduce the possible measurement errors the potential influence of the parasitic effects on the measurement signal can be estimated and computed. The additional parameters in the model need to be determined. In the case of the stray capacity it can be done by measuring the admittance at a frequency far away from a resonance.

6C. SAW Devices

Room 307

Monday, November 3, 2008, 4:30 pm - 6:00 pm

Chair: **Victor Plessky;**
GVR Trade SA, Switzerland.

6C-1

4:30 PM **Ring Waveguide Resonator on SAW – Quality Factor vs Electrode Structure Properties**

Sergey Biryukov[1], Hagen Schmidt[1], Manfred Weihnacht[2]; *[1]IFW Dresden, Dresden, Germany, [2]INNOXACS, Dippoldiswalde, Germany.*

Background, Motivation and Objective

Last year a new regular electrode structure for surface acoustic wave (SAW) devices has been proposed [1], [2]. The structure consists of an interdigital transducer in the form of a ring placed on the Z-cut of a hexagonal piezoelectric crystal. Finite thickness electrodes produce the known slowing effect for a SAW in comparison with this SAW on a free surface. The "slow" electrode region and the "fast" surrounding region form an open waveguide structure with the acoustic field concentrated in the electrode region. This structure was named as ring waveguide resonator (RWR) on SAW. Due to its regularity the electrical admittance of RWR does not have sidelobes, which are typical for usual SAW resonators composed of different electrode gratings with gaps. The properties of the new promising structure have to be investigated in details.

Statement of Contribution/Methods

Because of a finite curvature of the waveguide, the propagating SAW mode has unavoidable losses of its energy due to radiation into the surrounding region. In [1], [2] it was shown that corresponding to the radiation losses the resonator quality factor Q could be raised to an acceptable level by increasing of waveguide radius. In the present work the Q-factor dependence on the slowing properties of electrode structure is investigated. The investigation is based on the 2D scalar wave equation in polar coordinates.

Results

For a single crystalline AlN substrate having a SAW velocity of 5770 m/s on free surface and of 5700 m/s to 5400 m/s for the electrode region with an aperture of five wavelengths an estimation of Q-factor gives the following results. For the RWR radius of 50, 100, and 200 wavelengths the Q-factor changed from 30 to 10e4, from 80 to 5e7, and from 300 to 5e15, respectively. So with decreasing of the "slow" region velocity only by 5% the Q-factor of RWR can be increased within many orders.

Discussion and Conclusions

The use of different electrode materials is discussed. It is shown that by changing both the electrode materials and the aspect ratio of electrodes a control of RWR properties over a wide range is possible. The results are appropriate for highly effective RWR design and development.

[1] S. V. Biryukov, G. Martin, and M. Weihnacht. "Ring waveguide resonator on surface acoustic waves," Appl. Phys. Lett., vol. 90, no.17, pp. 173503, 23 April 2007.

[2] S. V. Biryukov, G. Martin, and M. Weihnacht. "Closed regular electrode structure for SAW resonators," in Proc. IEEE Freq. Contr. Symp., 2007, pp. 168-171.

6C-2

4:45 PM **SAW Band Rejection Filters for Mobile Digital Television**

Thomas Bauer[1], Matthias Jungkunz[2], Karl Wagner[1]; *[1]EPCOS AG, SAW RD BT DT, Munich, Germany, [2]EPCOS AG, SAW COM WT AE PD, Munich, Germany.*

Background, Motivation and Objective

The implementation of mobile digital television (DTV) as a feature in cellular telephones is growing in importance. Cellular services and broadcast networks are converging in today's mobile phones. In the system design, interferences between cellular and mobile DTV frequencies must be carefully minimized.

Broadcast services like ISDB-T 1seg and DVB-H, e.g., both located in the UHF band, are influenced by the closely situated cellular transmission bands. To achieve undisturbed mobile DTV reception, respectively high receiver sensitivity, filtering solutions are necessary which provide very low insertion attenuation in the broadcast band, high suppression in the cellular Tx band and appropriate power durability, as the outgoing power of the Tx power amplifier is coupled via the applied antennas to the mobile DTV receiver.

Various regional requirements define the key parameters of such filters in terms of band separation, width of transmission band and width of rejection band.

Statement of Contribution/Methods

Traditional SAW band pass filters provide small-sized and cost-effective solutions, but can not achieve the required transmission band width for multiple broadcasting signal bands in the UHF band. SAW band reject filters, however, allow to realize transmit bands of up to 50% relative bandwidth (e.g., 470-770 MHz) with excellent insertion loss, as well as to reject signals in the Tx bands by more than 40 - 50 dB.

Topologies for band reject filters include ladder networks consisting of series and parallel resonators, whereas unlike in band pass filters, the resonance frequencies of the series resonators are below the resonance frequencies of the parallel resonators. The choice of an optimum filter topology and proper application of inductive matching elements is of vital importance.

Results

Designs for several exemplary cases have been evaluated in measurement. Wide (approx. 50% BW) pass band and narrow (approx. 2% BW) stop band requirements typical for Japanese ISDB-T have been fulfilled using standard LiTaO3 substrate providing a passband insertion attenuation of only 1.6 dB. The device is available in a 1.4 x 1.1 mm² package.

Wider rejection bands (up to 10% BW) typically necessary for European/American DVB-H with high attenuation have been approached applying materials with higher piezoelectric coupling. The larger number of resonators required to realize the wide rejection band leads to a component size of 1.7 x 1.3 mm². An insertion attenuation of 2 dB has been achieved. All designs are capable of handling 24 dBm input power.

Discussion and Conclusions

Applying the methods and technologies presented in this paper allows to fulfill the system requirements regarding RF performance of mobile digital television and results in small-size low-cost components.

6C-3

5:00 PM **Low Loss SAW RF ID Tags for Space Sensor Applications**

Nancy Saldanha, Donald Malocha; *University of Central Florida, Electrical Engineering, Orlando, FL, USA.*

Background, Motivation and Objective

NASA has identified the need for wireless, passive sensors for ground, in-flight, and space exploration. In general, devices must simultaneously sense and tag measurands, such as temperature or pressure, in a multi-sensor environment. SAW sensor devices are ideally suited since they are passive, small, rugged, operate over broad temperatures, and are radiation hard. In a passive, wireless multi-sensor environment, the communication distance of the sensor-tag is related to its insertion loss and the processing gain of the system. To maximize the tag readable distance, the reduction of tag insertion loss is critical. Single frequency CDMA tags for high volume commercial applications must have universal coding schemes and large numbers of codes. The large number of bits for coding

and CDMA operation necessitates reflector banks with >30 dB loss. The relaxation of these parameters allows the design emphasis to be shifted to low-loss reflectors. The use of multiple frequency coded tags reduces adjacent reflector interactions for low insertion loss (<4dB), increased system operation distance, complex coding, and system processing gain. The semi-custom SAW sensor devices provide low loss platforms for multi-sensor integration and diverse embodiments are possible.

Statement of Contribution/Methods

The goal of the current research is to develop a very low loss SAW tag-sensor platform for use in a broad range of sensing applications. The paper will discuss the reflector design aspects with respect to communication, without reference to any particular sensor. The goal is to reduce the coded reflector bank insertion loss to less than 4 dB by investigating long reflector banks which use a multi-tone, anti-interference spectral coding definition that reduces intra-chip reflections and optimizes spectral bandwidth of the device.

Results

The new coding approach is defined and contrasted with the previously defined orthogonal frequency coded (OFC) technique. Auto- and cross- correlation properties of the chips and their relation to reflectivity per strip and reflector length are discussed. Frequency and time-domain inter-symbol interference will be compared and quantified with respect to system performance. Results at 250 MHz of a single frequency CDMA tag will be compared to 4 chip and 8 chip orthogonal frequency coded (OFC), and anti-interference coded SAW tags.

Discussion and Conclusions

The key parameters of insertion loss, cross-correlation and auto-correlation of the two types of frequency coded tags will be analyzed, contrasted and discussed.It is shown that coded reflector banks can be achieved with near zero loss and still maintain good coding properties. Experimental and COM model predicted device results with varying reflector designs and codes are presented.

This work is partially funded from the NASA Graduate Student Research Program (GSRP), Kennedy Space Center.

6C-4

5:15 PM **Two-fingers SPUDT cells**

Guenter Martin[1], Sergey Biryukov[1], Bernd Steiner[2], **Bert Wall[2];** *[1]IFW Dresden, Dresden, Germany, [2]Vectron International, Teltow, Germany.*

Background, Motivation and Objective

The previously best known SPUDT cell types like DART, EWC, Hanma-Hunsinger and FEUDT include at least three fingers. Due to their construction they have a unidirectional effect for pure mode directions. SPUDT cells including two fingers only are hitherto known for so-called NSPUDT directions only which are not any pure mode directions. In this case, usual solid-finger cells are used. The purpose of the proposed paper is to find SPUDT cell types consisting of two fingers only for pure mode directions. Moreover, SPUDT cells composed of two fingers suited to complete imperfect NSPUDT behavior or to compensate that are to be found.

Statement of Contribution/Methods

The new SPUDT cells are called two-finger cells abbreviated by TF cells. They consist of two fingers of different width and polarity. TF cells with different values of coupling factors and reflectivity for pure mode directions on substrates like 128ºYXLiNbO3, YZLiNbO3 and STX quartz were found by means of an optimization procedure. The optimization software uses a MATLAB optimization function and the cell analysis described in [1]. The minimum finger and gap width have been given. Moreover, TF cells are obtained for off-axis propagation directions, for instance, for SST quartz. On this cut, we search for TF cells which complete the distance of transduction and reflection center to wavelength/8 or compensate this distance. The existence of the unidirectional effect of a TF cell type is checked experimentally.

Results

By means of a test layout the forward direction of a TF-cell SPUDT on 128ºYXLiNbO3 was determined experimentally. The values of coupling factor and reflectivity of some TF cell types and the corresponding cell structure parameters are presented. The properties of the new cells are compared with those of conventional SPUDT cells. The reflectivity of TF cells on 128ºYXLiNbO3 turns out to be two up to three times larger than that of DART and Hanma-Hunsinger cells at the same metal layer thickness. The coupling factor is clearly larger than that of DART cells and comparable with that of Hanma-Hunsinger cells. Furthermore, properties of TF cells on

STX and SST quartz are reported. In the latter case, examples for completing and compensating imperfect NSPUDT behavior are given.

Discussion and Conclusions

TF cells obviously offer the greatest advantage on crystal cuts with a large coupling factor. The reason of the large reflectivity for high coupling materials is discussed. Moreover, it is shown that the distance transduction – reflection center of wavelength/8 is not achieved for a given cell structure on materials with a too small coupling factor. The large reflectivity of TF cells on high coupling cuts offers the possibility to design very short SPUDTs.

[1] S. V. Biryukov and M. Weihnacht, J. Appl. Phys. Vol. 96 (2004), p. 3117

6C-5

5:30 PM **SAW ID-tag for industrial application with large data capacity and/or anticollision capability**

Gudrun Bruckner, Rene Fachberger, Jochen Bardong; *CTR AG, Villach, St. Magdalen, Austria.*

Background, Motivation and Objective

Passive operation is a known quality of SAW ID-tags. The absence of batteries is an obvious advantage for industrial applications where furnaces or chemical process chambers are involved, given that the tag itself sustains this harsh environment. For a unique object tagging a sufficient number of codes must be provided along with an adequate reading distance. The aim of this work was to design SAW ID-tags based on reflective delay lines which fulfill these requirements. Furthermore the use of a linear block code and a new decoding method [1] should allow the separation of two randomly chosen tags within one antenna beam (anticollision).

Statement of Contribution/Methods

Different types of delay lines were designed operating in the 2.45 GHz ISM band. To reduce the number of reflectors and to fulfill the anticollision criteria, a pulse position encoding scheme with base 16 has been employed. To increase the temperature stability of the SAW device an Al/Ti sandwich layer was applied on white $LiNbO_3$ substrate material. The SAW devices were packaged in metal housings with glass feed throughs using a polyimide adhesive. A number of packaged ID-tags were mounted to a slot antenna suitable for industrial use and the reading performance was measured in the 2.45 GHz ISM band using a FSCW reader. The probability to identify two randomly chosen tags positioned in one antenna beam was measured to evaluate the anticollision capabilities.

Results

ID-tags with a code volume of 2^{20} to 2^{32} were successfully realized. With the 2^{32} type a reading range of 5m with a 100% and 5.5m with a 95% identification probability was achieved. The packaging technology featured a lifetime of more than 3000h at 300°C and 200h at 350°C. Cycling tests from room temperature to 220°C are ongoing. So far the tags have undergone more than 4000 cycles without degradation.

To attain anticollision capabilities the available number of codes is reduced, as a part of the information on the tag is needed for code reconstruction. For the tested tags the theoretical code volume is reduced from 2^{32} to 2^{16}. Due to a non ideal behavior of the tags under test codes with neighboring peak positions were rejected and thus the available codes were further reduced to 526. Within this limits a successful separation of two tags could be demonstrated for all configurations tested.

Discussion and Conclusions

SAW ID-tags sustaining process temperatures of 350°C with a code capacity of 2^{32} have been produced and tested. A reading distance of several meters was demonstrated rendering the tags ideal for industrial applications. First simultaneous measurements of two tags were performed for a reduced code space of 526.

[1] M.Brandl, S.Schuster, S.Scheiblhofer, A.Stelzer, 'A New Anti-Collision Method for SAW-Tags Using Linear Block Codes,' to be published at the IEEE Frequency Control Symposium, 2008

6C-6

5:45 PM **The OmniSAW device concept**

Abdelkrim Khelif, Abdelkrim Choujaa, Jean-yves Rauch, Valérie Petrini, Hanane Moubchir, Sarah Benchabane, Vincent Laude; *Femto-st institute, Micro Nano sciences&systems, Besançon, France.*

Background, Motivation and Objective

Recently, phononic band gap materials, the so-called phononic crystals, have been made possible through the use of periodic structures by analogy with electrons in semiconductor crystals. These materials allow the propagation of elastic waves to be regulated. In other words, they play the role of perfect mirrors for elastic waves in the band gap frequency window, i.e., forbidding propagation for all polarizations and directions. This area of research has received much attention because of the fundamental interest in localization of elastic energy and the potential applications of phononic bad gaps. The Omnidirectional acoustic mirror for surface acoustic waves (OmniSAW) device is the first illustration of the capabilities of these new materials to confine the elastic energy and control the dispersion of waves through the geometries.

Statement of Contribution/Methods

Here, we report on the theoretical and experimental evidence of the occurrence of omnidirectional elastic band gaps in one-dimensional phononic crystal structures. The structure consists of a periodic layer deposited on a specific substrate that exhibit total reflection of waves for all incident angles and polarizations in a given frequency range. We present the influence of the composition and filling fraction of the layered structures as well as of the substrate nature on the omnidirectional band gap properties.

By adding a defect made of a piezoelectric layer, for instance aluminum nitride, in the finite-sized and otherwise perfect layered structure, selective resonance modes occur within the omnidirectional bang gap under certain conditions. In this case, the elastic energy is localized in the defect layer. The frequencies of the defect modes are sensitive to the nature of the material and to the layer thicknesses.

Results

We present an omnidirectional acoustic mirror extending from 2.5 to 6.5 GHz. Excitation of surface modes is allowed by using interdigital transducers (IDTs) on top of the piezoelectric film. The electrical measurements confirm the existence of a surface acoustic mode around 5 GHz trapped in the piezoelectric film by the omnidirectional band gap mirror, in accordance with theoretical predictions. The phase velocity of the surface mode is around 54000 m/s.

Discussion and Conclusions

Using an omnidirectional acoustic mirror, an OmniSAW devices at an operating frequency of a few GHz have been demonstrated.

Monday Poster Sessions

PS. Student Competition Finalists

2nd and 3rd Floor Foyers

Monday, November 3, 2008, 3:00 pm - 4:30 pm

PS001-01

Design of Catheter for Combined Intravascular Photoacoustic and Ultrasound Imaging

Bo Wang, Andrei Karpiouk, Stanislav Emelianov; *University of Texas at Austin, Biomedical Engineering, Austin, TX, USA.*

Background, Motivation and Objective

Intravascular photoacoustic (IVPA) imaging is a promising imaging tool for detecting and differentiating the atherosclerotic plaques. Previously, we have demonstrated the utility of intravascular photoacoustic imaging using a laboratory system where the excised arterial tissue sample was irradiated with the laser beam from the outside while the intravascular ultrasound (IVUS) imaging catheter, inserted into the lumen, was used to receive the photoacoustic signal. However, for in-vivo IVUS and IVPA imaging, a combined catheter consisting of IVUS transducer and light delivery system is needed. In this paper we report our initial experience towards design and fabrication of a catheter capable of simultaneous IVPA and IVUS imaging.

Statement of Contribution/Methods

The combined IVUS/IVPA imaging catheter was built based on a clinical, 40 MHz, single element IVUS catheter (Boston Scientific, Inc.). A 0.6 mm diameter optical fiber was used for light delivery. The proximal end of the fiber was coupled with a laser system. The distal tip of the optical fiber was polished at a 45 degree angle and placed inside a quartz tube. Both ends of the tube were sealed with epoxy to retain air around the fiber tip. As a result, such fiber assembly, when submersed into water, was irradiating the light sideway. The IVUS catheter was then attached to the optical fiber such that the ultrasound beam from the transducer and the laser beam from the optical fiber were aligned. To test the combined IVUS/IVPA imaging catheter, a model of the atherosclerotic vessel was fabricated. Specifically, within the otherwise homogeneous polyvinyl alcohol background, three 0.4% graphite inclusions of 1 mm diameter were positioned at different depths inside of the approximately 6-mm thick vessel wall to simulate various plaques in the artery. During imaging studies, the catheter was inserted into the lumen, and the phantom was rotated using a stepper motor. At each angular position, both photoacoustic and ultrasound A-lines were collected by a 14-bit GAGE A/D card operating at 200 MHz sampling rate. The IVUS and IVPA images were formed off-line from 256 equally spaced beams.

Results

The IVPA images of the phantom obtained using the combined IVUS/IVPA catheter clearly identifies the inclusions located at specific depths. At the same time, co-registered IVUS images visualized the structure of the phantom. Finally, combined IVUS/IVPA images further outlined the location and extent of the inclusions within the vessel wall.

Discussion and Conclusions

Overall, IVPA and IVUS images of sufficient quality were obtained using the initial prototype of the combined IVUS/IVPA catheter. Using optical fibers of smaller diameter, the size of the combined catheter can be further reduced. Therefore, our studies suggest that optical fibers can be used to deliver enough optical fluence for intravascular photoacoustic imaging of the vessel. Furthermore, other approaches in design of IVUS/IVPA imaging catheter will be discussed.

PS002-02

Intra-Vascular Ultrasound (IVUS) Delivery of DNA Via Microbubble Carriers to an Injured Artery In vivo

Linsey C. Phillips[1], Alexander L. Klibanov[1], Doug K. Bowles[2], Brian. R. Wamhoff[1], John A. Hossack[1]; *[1]University of Virginia, Charlottesville, VA, USA, [2]University of Missouri, Columbia, MO, USA.*

Background, Motivation and Objective

The most common therapy for narrowed, atherosclerotic arteries is balloon angioplasty and is often followed by stent placement. This procedure causes injury to the vessel wall and over time, cells from the artery wall (primarily smooth muscle cells) proliferate in response to injury and re-occlude the vessel (restenosis). A novel therapy to prevent restenosis involves the use of delivering an anti-proliferative gene via microbubbles which are ruptured via catheter-based intravascular ultrasound at the site of vessel injury. Insonation of microbubbles by ultrasound has been shown to increase gene delivery at low frequencies. We hypothesize that plasmid DNA encoding a reporter gene (red fluorescent protein, RFP) can be delivered to a pig carotid artery wall *in vivo* using cationic microbubble carriers and intravascular ultrasound.

Statement of Contribution/Methods

Cationic microbubbles were formed during ultrasonic dispersion of decafluorobutane gas in an aqueous micellar mixture of phosphatidylcholine, PEG stearate, and distearyl trimethylammonium propane. Negatively charged DNA plasmids expressing red fluorescent protein (CMV-RFP) were electrostatically coupled to microbubbles.

A modified IVUS catheter (Boston Scientific) was positioned 1mm away from cells and translated over an area of 2cm2. *In vitro* application of 5 or 11 MHz Guassian pulses at a PNP of 120 kPa, and PRF of 5kHz was applied to cultured smooth muscle cells exposed to CMV-RFP plasmid bearing microbubbles for at total of 6 minutes.

Balloon angioplasty was performed on pig right carotid vessels (n=2) *in vivo*. (The pig is the gold standard for restenosis studies.) Following angioplasty, microbubbles were infused through a port hole in a catheter located 2cm upstream of the IVUS transducer. 5 MHz unipolar pulses (PRF = 5 KHz, PNP =120 kPa) were emitted from the IVUS catheter at the location of vascular injury (2cm in length) for a total of 4 minutes during plasmid conjugated-microbubble infusion. Three days following insonation, arteries were excised and processed for frozen sectioning and nuclei staining. Successful plasmid transfection was measured by fluorescent microscopy and quantified as % of vessel perimeter cells expressing RFP.

Results

Ultrasound mediated gene delivery from microbubbles using IVUS *in vitro* resulted in 11.5 fluorescent cells/cm2 (<1%). (Previously reported ultrasound / bubble mediated gene delivery are typically low ~1-5%.) Cells exposed to plasmid-microbubbles without US resulted in 0% transfection. Injured pig arteries exposed to microbubbles and ultrasound resulted in 23.3± 6.0% transfection whereas contralateral controls resulted in 3.6±2.6% transfection.

Discussion and Conclusions

To the authors' knowledge, this is the first example of *in vivo* cationic gene delivery via IVUS, which has promise for localized intra-vascular gene therapy for preventing restenosis.

PS003-03

Quantitative Bladder Volume Assessment on the Basis of Nonlinear Wave Propagation

Egon J.W. Merks, Nicolaas Bom, Nico de Jong, Antonius F.W. van der Steen; *Biomedical Engineering, ErasmusMC, Rotterdam, Netherlands.*

Background, Motivation and Objective

Catheterization is the gold standard for bladder volume assessment, but it is invasive and introduces the risk of infections and trauma. To reduce the need for a urinary catheter, a new method has recently been introduced that non-invasively and instantaneously measures the volume of liquid filled cavities on the basis of nonlinear wave propagation with a single diverging acoustic beam. The method exploits the relatively higher nonlinear behavior of liquid compared to tissue.

Previously obtained results from using a fast-rotating phased array probe and high end echo system have proven the feasibility of the method. A 15 dB increase of the 2nd harmonic was observed on a 500 ml bladder phantom relative to a tissue-only phantom. In-vivo measurements on a bladder containing 450 ml urine showed an increase of 10 dB at the 2nd harmonic compared to an empty bladder. The objective of this study is to design a simple transducer that generates a single diverging acoustic beam and to obtain a calculation method that quantitatively relates the spectral contents of the received RF-data to the insonified liquid volume.

Statement of Contribution/Methods

Progressive volume pulse-echo measurements were performed on healthy volunteers. The experimental setup included a custom multilayer transducer that is capable of generating sine wave bursts with centre frequency of 2 MHz and peak amplitudes of 500 kPa at the transducer surface, which could induce significant nonlinear wave

propagation. The transducer bandwidth enabled receiving up to the 4th harmonic. To create the diverging acoustic beam, a defocusing lens was applied to the transducer. Volumes between 0 and 600 ml with 100 ml increments were measured. Reference measurements were performed with a commercial bladder volume instrument. Subject-specific acoustic loss and nonlinearity of the region anterior to the bladder influenced the volume estimation. A calculation scheme was applied that subtracted the nonlinear behavior of the anterior bladder region from the nonlinear behavior of the posterior bladder region, leaving only the fraction of nonlinearity (FON) contributed by the liquid region.

Results

Linear regression analysis on the data obtained from the progressive volume measurements resulted in a slope of 4.6 L/FON and an intercept of 118 ml. The 95% confidence interval of the slope was [4.6 ± 0.7]. By correcting for the nonlinear behavior of the anterior bladder region and looking at only the fraction of nonlinearity contributed by the liquid region, the relative standard deviation of the slope was reduced from 19.3% to 8.4% for the individual progressive measurements. Hence, the repeatability of the method increased significantly.

Discussion and Conclusions

A calculation method was developed that quantitatively relates the spectral contents of the received RF-data to the liquid volume present within a single diverging acoustic beam in-vivo.

This work was supported by the Dutch Technology Foundation (STW) under Grant 06652

PS004-04

Microbubble dynamics in microvessels: Observations of microvessel dilation, invagination and rupture

Hong Chen, Andrew A. Brayman, Michael R. Bailey, Thomas J. Matula; *Center for Industrial and Medical Ultrasound, Applied Physics Laboratory, University of Washington, Seattle, WA, USA.*

Background, Motivation and Objective

The fundamental interaction of an acoustically activated microbubble with small blood vessels is poorly understood. Understanding this interaction is important for designing better imaging schemes, and for targeting and drug delivery applications. High speed microscopy provides a tool to study interaction and response mechanisms.

Statement of Contribution/Methods

Following an approved U.W. IACUC protocol, ultrasound contrast agent microbubbles, Evan's blue and fluorescent dyes were perfused into the rat mesentery. These tissue samples were harvested for ex vivo observation. Evan's blue was used to facilitate identification of microvessels and also as an indicator of blood vessel permeability changes. Fluorescence images were taken to examine the integrity of blood vessels. Tissue samples were exposed to short pulses of 1 MHz ultrasound. 14 high-speed microphotographic images were acquired for each experiment with shutter speeds of 50 ns and each image separated by 150 ns.

Results

At low acoustic negative pressure (~1.5 MPa), bubble expansion caused microvessel dilation by approximately 1.2x. During bubble collapse, the vessel invaginated to approximately 0.9x of its original diameter (11 μm). At high negative pressure (near 11 MPa), the vessel dilated by approximately 2.5x, followed by invagination of 0.4x of its original diameter (17 μm). Vessel dilation and invagination were correlated temporally with bubble growth and collapse. At high pressure, the bubble and/or its fragments could be observed outside the original vessel, suggesting that the vessel had ruptured at some point. Vessel damage was also inferred by observation of fluorescent dye extravasation. An example of vessel dilation, invagination, and rupture can be seen in the following figure (pixel intensity values in the region around the blood vessel wall have been enhanced).

Discussion and Conclusions

Our observations confirm some aspects of previous modeling and observational findings. However, direct observation of ultrasound-induced vessel invagination appears novel, and may be an important mechanism related to vessel damage. It remains uncertain if the vessel was damaged during dilation, invagination, or from a violent bubble collapse. It's possible that both dilation and invagination contribute to vascular rupture. Work supported by NIH (5R01EB000350 and P01DK43881).

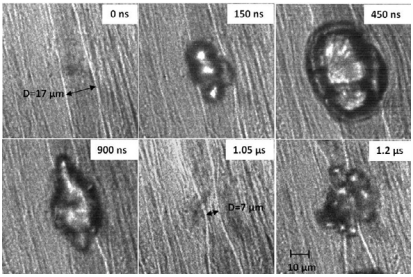

PS005-05

Non-invasive thrombolysis induced by histotripsy pulsed cavitation ultrasound therapy

Adam Maxwell[1], Charles Cain[1], Hitinder Gurm[2], J. Brian Fowlkes[3], Zhen Xu[1]; *[1]University of Michigan, Department of Biomedical Engineering, Ann Arbor, Michigan, USA, [2]University of Michigan, Department of Internal Medicine, Ann Arbor, Michigan, USA, [3]University of Michigan, Department of Radiology, Ann Arbor, Michigan, USA.*

Background, Motivation and Objective

Blood clot formation is an essential response to injury but can be the cause of many cardiovascular diseases. Current treatments to remove blood clots (thrombolysis) include thrombolytic drugs and/or catheter-based techniques, both of which have significant drawbacks including risks of excessive bleeding and infection. Our goal is to develop a non-invasive thrombolysis method based on **Histotripsy**, a technique that mechanically fractionates soft tissue using controlled ultrasound cavitation. This paper investigates the feasibility and efficacy of this new approach to thrombolysis.

Statement of Contribution/Methods

Blood clots were formed *in-vitro* from whole porcine blood by adding $CaCl_2$ solution. Clots were placed in a 6 mm diameter LDPE tube and treated by histotripsy. The treatment targeting and monitoring were guided by ultrasound imaging. The histotripsy treatment consisted of 5 cycle ultrasound pulses delivered at a 1 kHz pulse repetition frequency and peak negative pressures of up to 14 MPa. Clots were treated until completely dissolved. Acoustic backscatter during treatment was collected for cavitation detection. Clots were also treated under flow rates up to 50 cm/sec in a circulatory model. To evaluate possible vascular damage, clots were treated in excised canine aorta and vena cava and histology of the vessels was examined for damage.

Results

Histotripsy can completely fractionate a clot weighing 300 mg (4 mm in diameter and 2 cm in length) in ~0.5 – 5 minutes (mean = 2.7 minutes, n = 32 clots). Histotripsy thrombolysis was initiated at peak negative pressures ≥ 8 MPa, and only after initiation of a cavitating bubble cloud was detected. The thrombolysis rate (clot weight/treatment time) increased with increasing pressure. Histotripsy fragmented the clot into debris no larger than 60 µm in diameter, with over 90% (by volume) of the debris having diameters < 8 µm. The treated vessels were intact upon initial histological evaluation. Histotripsy thrombolysis was effective both in high flow and static environments. The treatment targeting and progress can be clearly seen on an ultrasound image. Moreover, we observed that clot fragments are attracted to the vicinity of the bubble cloud, and can be trapped and further fragmented at the focus.

Discussion and Conclusions

Our results suggest that histotripsy is an effective and efficient non-invasive method for thrombolysis guided by real-time imaging. Most clot debris fragments generated are smaller than red blood cells. Large clot fragments can be trapped near the bubble cloud and further fractionated. This phenomenon is possibly due to a particular fluid flow pattern created by cavitation-induced microstreaming. We plan to use this property to create a Non-invasive Embolization Trap (NET) to prevent embolization caused by escaping clot fragments. These results suggest that histotripsy has the potential to emerge as a safe and effective non–invasive thrombolytic.

PS006-06

Reaching the optimal focusing and steering capabilities of transcranial HIFU arrays based on time reversal of acoustically induced cavitation bubble signature.

Jerome Gateau[1], Laurent Marsac[2], Mathieu Pernot[1], Jean-Francois Aubry[1], Mickael Tanter[1], Mathias Fink[1];
[1]Laboratoire ondes et Acoustique, INSERM, CNRS UMR 7587, ESPCI, Paris, France, [2]Supersonic Imagine, Aix-en-Provence, France.

Background, Motivation and Objective

Brain treatment with High Intensity Focused Ultrasound (HIFU) can be achieved through the skull by multichannel arrays using time-reversal focusing. Such a method requires a reference signal either sent by a real source embedded in brain tissues or computed from a virtual source, using CT based simulations. This non-invasive computational method allows precise focusing, but discretization and modeling errors can result in a reduction of the accessible acoustic pressure at focus in comparison with real experimental time-reversal using an implanted hydrophone. The goal of this study is to demonstrate the feasibility of reaching the optimal focusing based on the initial corrections obtained from CT-scan simulations. The optimal acoustic pressure at focus is recovered by inducing a cavitation bubble through the skull bone and using its ultrasonic emission for time-reversal transcranial focusing. The potential of this technique for improving both transcranial focusing and electronic beamsteering performances is investigated.

Statement of Contribution/Methods

Ex vivo experiments are performed on a half skull immersed in a degassed water tank maintained at 37 C. The ultrasound array is composed of 136 high-power individual transducers (central frequency 1MHz) mounted on a spherical surface with a semi random distribution. The simulation uses a 3D finite differences code and a model of the half skull based on CT data. Cavitation events occur in an agar gel, phantom for in vivo bubble formation. The pressure field at 1MHz is scanned at low amplitude levels with a hydrophone mounted on a 3D gantry.

Results

Ex vivo CT guided simulations allowed us to reach, at the geometrical focus of the array, 83% of the optimal pressure (hydrophone based time reversal). Cavitation bubbles were then created transcranially at this location with computed emission pulses. The 1MHz component of a single bubble acoustic emission was selected, time reversed and reemitted, restoring a mean pressure ratio of 96% (+/- 2%). The new focal peak, i.e the location of the cavitation event, was localized in the -2dB focal area of the initial pulse corresponding to a 0.5 mm uncertainty. When performing electronic steering from a reference signal optimally focusing at the geometrical focal point, 90% of the optimal pressure is still reached up to 8 mm away to the initial position in the focal plane. With six reference signals from cavitation bubble spots equally distributed on a 6 mm radius circle, this area was extended to 12 mm. Such cavitation bubbles were generated using electronic steering.

Discussion and Conclusions

A new non-invasive method to correct skull aberrations has been validated. From CT images based simulations, the focusing was restored through the skull by inducing a cavitation bubble at the targeted location, and the corrected zone was extended by electronic beam steering and discreet bubbles generation This method should greatly benefit transcranial brain therapy.

PS007-07

High Frame Rate Adaptive Imaging Using Coherence Factor Weighting and the MVDR Method

Shun-Li Wang, Pai-Chi Li; *National Taiwan University, Taipei, Taiwan.*

Background, Motivation and Objective

Adaptive imaging has been extensively studied. Although some success has been demonstrated, these approaches generally are not suitable for high frame rate (HFR) imaging where broad transmit beams are required. In this study, we propose an effective adaptive imaging method suitable for HFR imaging based on coherence factor (CF) weighting and the minimum variance distortionless response (MVDR) method.

Statement of Contribution/Methods

The CF is a focusing quality index estimated from receive-channel data. It is the ratio between the energy of the coherent sum to the total incoherent energy. This method is an adaptive weighting technique in which the amplitude of each image pixel is weighted by the corresponding CF such that the unwanted sidelobes are reduced. Direct implementation of the CF weighting in HFR imaging does not provide satisfactory results because broad transmit beams required for HFR imaging affect accuracy of CF calculations. In this study, we solve this problem

by applying the MVDR method to the delayed channel data. Specifically, the MVDR method is used for angle of arrival estimation. The beam sum data are then weighted by the estimated CF.

Results

A synthetic transmit aperture method is used for HFR imaging. Only 8 firings are required to form an image. Both simulations and clinical breast imaging data are used. In the simulations, an anechoic cyst phantom is imaged with a maximum $\pi/2$ near field phase screen. The correlation-based method proposed by Flax/O'Donnell is also implemented for performance benchmarking. The contrast and the contrast-to-noise ratio (CNR) improvements are 7.7 dB and 39.2% with the proposed method, respectively. Only 2.1 dB and 21.4% improvements are achieved using the correlation-based method. Clinical breast data are also acquired using a programmable array system. The following figures show images of a fibroadenoma lesion (left: original image, right: with the proposed method). With the proposed data, the contrast enhancement is 3.3 dB and the CNR enhancement is 13.4%.

Discussion and Conclusions

The proposed method combines CF weighting with the MVDR method. Simulations and clinical breast data are used to demonstrate the image quality improvement. Even for HFR imaging with only 8 firings per image, effective contrast enhancement and better lesion boundary can be achieved. Efficacy of the proposed method is clearly demonstrated.

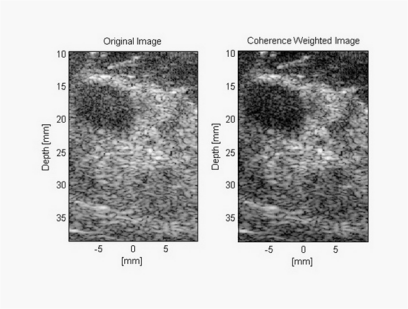

PS008-08

Estimation of Valvular Regurgitation Area by 3D HPRF Doppler

Torbjørn Hergum[1], Thomas Renhult Skaug[1], Knut Matre[2], Hans Torp[1]; *[1]Norwegian University of Science and Technology, Department of circulation and medical imaging, Trondheim, Norway, [2]University of Bergen, Institute of Medicine, Bergen, Norway.*

Background, Motivation and Objective

Determining the severity of leakage through a heart valve is important, but difficult. Two of the parameters which are clinically interesting in this regard are the area and the geometry of the lesion. Current practice for non-invasive measurement of the severity of valvular regurgitation is qualitative, and based upon using color flow- and spectral Doppler techniques.

Statement of Contribution/Methods

In search for quantitative measurements of regurgitant severity we used 3D high pulse repetition frequency (HPRF) color flow imaging to measure the Doppler signal from multiple beams distributed over the laminar vena contracta region near the orifice. A steep clutter filter was used to separate the jet flow Doppler signals from the Doppler signals of the slowly-moving blood of the ambiguous sample volumes.

The power from the closely spaced ultrasound beams are summed to yield the total Doppler power, which is known to be proportional to the amount of blood moving above the clutter-filter cutoff velocity. The cross sectional area of the jet was found by scaling the summed Doppler power from these beams using both a-priori knowledge of the lateral extent of the beams and a reference beam which is completely covered by the orifice.

Both in vitro trials and computer simulation have been used for validation. The in vitro measurements were made using a pulsatile flow phantom holding porcine valves with six different holes, ranging from mild to severe mitral regurgitation. The method can be applied to other high-velocity valvular jets.

Results

The mean value and standard deviation from the in vitro trials are plotted as red in the figure showing true area vs. estimated area. Two computer simulations are also included in the figure, the dashed and dotted lines are simulations respectively with- (blue) and without (black) stochastic variation.

Discussion and Conclusions

Small holes of sizes comparable to a single ultrasound beam are overestimated as expected from simulations, and the estimates of the larger holes fits well with the line of identity (green). According to the stochastic simulations the method should underestimate the area of large orifices, but this is not seen in the in vitro data. Regardless of this the in vitro data enables us to distinguish between the different regurgitation degrees.

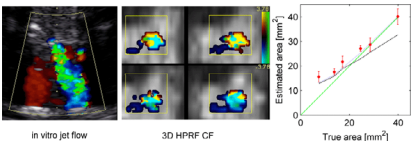

PS009-09

Image-Guided Refocusing of Dual-Mode Ultrasound Arrays(DMUAs)

John Ballard, Emad Ebbini; *University of Minnesota, USA.*

Background, Motivation and Objective

A major advantage of imaging with dual-mode ultrasound arrays (DMUAs) is their inherent registration between imaging and therapeutic modes during image-guided surgery which allows for image-based feedback for refocusing the therapeutic beam. Specifically, this capability is critical in image-guided thoracic surgeries where the target is partially obstructed by the rib cage, thus limiting the access and distorting the geometrically-focused high-intensity focused ultrasound (HIFU) therapeutic beam.

Statement of Contribution/Methods

Images obtained with single-transmit focus (STF) imaging, in which the therapeutic beam is used at diagnostic levels, allow the user to select target and critical locations for optimizing the power deposition. We have developed an optimal refocusing method that takes advantage of the acoustic window of the intercostals spacing in order to minimize the power deposition over the critical regions (ribs) while maintaining or improving the power deposition at the target location (tumor).

Results

The algorithm is verified experimentally with a 64-element 1MHz DMUA, in an attenuating tissue mimicking phantom (~.5 dB/cm/MHz) with embedded Plexiglas ribs. Thermocouples are used to measure sub-therapeutic temperatures across the ribs and at the target location before, during and after 5 seconds of HIFU exposure for both the geometric focusing and the optimized refocusing while normalizing the driving power for both cases. An increase of normalized temperature (per watt of input power) greater than 20% was observed at the target after refocusing. At the same time, a reduction in normalized temperature rise across the ribs was greater than 60%. Statistics showed that the maximum variance between measurements when the experiment was rerun a minimum of 5 times for each case was approximately 5%. In addition, STF images taken with the refocused HIFU beam showed increased echogenicity at the target and reduced echogenicity at the ribs. This can be quantified by the intensity of the grayscale images. These images show a typical improvement of 5 dB at the focus with a reduction of 2dB across the ribs.

Discussion and Conclusions

The results show that STF DMUA imaging provides suitable feedback for refocusing the HIFU beam in the presence of strongly scattering targets. The robustness and repeatability of the algorithm were demonstrated by embedding the ribs within a block tissue-mimicking phantom to approximate realistic conditions and repeating each experiment multiple times. The results also show that grayscale STF images themselves provide useful feedback on the improvement in the quality of the refocusing beam, i.e. the relative echogenicity of the ribs is reduced upon refocusing indicating reduction in incident power. These results are generally consistent with the directly measured temperatures at the target and rib locations.

PS010-10

The Detection of Chemical and Biological Analytes Using a Monolithic Spiral Coil Acoustic Transduction Sensor

Donald McCann, Mitchell Wark, Paul Millard, David Neivandt, John Vetelino; *University of Maine, Orono, ME, USA.*

Background, Motivation and Objective

The monolithic spiral coil acoustic transduction (MSCAT) sensor platform is a novel bulk acoustic wave (BAW) device which is excited by a gold spiral coil antenna photolithographically deposited on one side of an AT-quartz wafer. The MSCAT platform can operate at very high frequencies by efficiently exciting high harmonic transverse shear modes with the application of a high frequency RF signal to the spiral coil. Since one surface of the MSCAT device is bare, this device can be used as a sensing platform upon which one deposits analyte selective chemical or biological films. The bare surface allows the detection of analyte induced mechanical (mass and viscoelasticity) and electrical (conductivity and dielectric constant) property changes in the film. In order to demonstrate the applicability of a MSCAT device as a sensor, the MSCAT platform is coated with biological and chemical films selective to Escherichia coli (E. coli) O157:H7 (hereafter referred to as E. coli), the E. coli strain most often responsible for serious illnesses in humans, and saxitoxin (STX), the most dangerous neurotoxin associated with shellfish poisoning stemming from red tide, respectively.

Statement of Contribution/Methods

A method for optimizing the number of turns and coil width and spacing of the MSCAT's antenna was developed using the Box-Behnken design method. MSCAT sensing platforms were then coated with biological films selective to E. coli based on antibody-antigen interactions and chemical films selective to STX based on the 18-crown-6 ether. Each MSCAT sensor was the exposed to E. coli and STX and the changes in resonant frequency were monitored.

Results

It was found that the most critical parameter in achieving efficient operation of the MSCAT device was the coil width. The MSCAT sensor operating at its fundamental frequency (5 MHz) was exposed to E. coli and exhibited a frequency shift approximately five times greater than similar tests performed with quartz crystal microbalance (QCM) sensors. In order to determine the lower detection limit and resolution of the MSCAT sensor, the sensor was operated at its 11th harmonic (55 MHz) and exposed to decreasing concentrations of E. coli. The resonant frequency was then monitored to obtain a dose response curve. The MSCAT sensor was able to detect E. coli in concentrations as low as 104 microbes/mL, 2 orders of magnitude lower than the QCM sensor. Similar results relating to the detection limit and resolution were also obtained for STX.

Discussion and Conclusions

A method for optimizing the MSCAT sensors' spiral coil antenna geometry was performed and it was shown that the coil width was the most critical parameter. The MSCAT was found to be significantly more sensitive than the QCM sensor due to the fact that it can detect both electrical and mechanical property changes and operate at high frequencies. Since the MSCAT has been excited up to the 81st harmonic, the MSCAT device may also be used in high frequency resonator applications.

PS011-11

Improving the Bandwidth of Air Coupled Capacitive Ultrasonic Transducers Using Selective Networks

Sean Mc Sweeney[1], WMD Wright[2]; [1]*University College Cork, National University of Ireland, Electrical and Electronic Engineering Dept, Mallow, Cork, Ireland,* [2]*University College Cork, National University of Ireland, Electrical and Electronic Engineering, Cork, Cork, Ireland.*

Background, Motivation and Objective

One of the key limitations on using CUT (Capacitive Ultrasonic Transducers) and cMUTs[1] (Capacitive Micromachined Ultrasonic Transducers) in air is their relatively narrow bandwidth which although superior to that of current piezoceramic devices[2] could be improved. Most air coupled capacitive devices could benefit hugely through the use of selective networks[3] for bandwidth expansion, resonance reinforcing, or a combination of both. This work has investigated the application of pole/zero manipulation techniques to modify and enhance the transmission characteristics of capacitive transducers through front end mounted components. The main objective was to positively enhance the performance characteristics of capacitive transducers.

Statement of Contribution/Methods

A modified electrical equivalent circuit for CUTs to include the selective networks used was developed. The work assessed the effects of a tuned amplifier on the passband of the devices studied and then focused on more complicated network designs for enhancement. Simulations of the effects of the networks on the devices using equivalent circuit models were carried out and the response curves to pulsed operation were calculated and compared to experimental measurements from a pair of fixed CUTs with a combined centre frequency of 280kHz and 3dB bandwidth of 160kHz.

Results

Increases in centre frequency of 25% and 3dB bandwidth of 77% using a single tuned amplifier were obtained. Resonance reinforcing, resonance shifting and ripple suppression were also studied through the manipulation of the q factor and pole location of such an amplifier. Performance enhancements were studied for a number of CUT aperture sizes and membrane thicknesses and a comparative study of the theoretical and experimental effect of these variations was conducted. With the appropriately designed network, enhancement of peak resonance with a simultaneous bandwidth expansion was obtained at the expense of other operating parameters such as stopband ripple. Simulations of more complicated circuit designs using equivalent circuit models of capacitive devices[4,5] showed that the maximum level of passband ripple observed for the bandwidth expansion method using a single tuned amplifier was reduced while achieving simultaneously the same 3dB results.

Discussion and Conclusions

The implication for bandwidth expansion of a capacitive transducer through selective network design is significant, allowing increased resolution in imaging systems, ultrasonic ranging and non destructive evaluation. Significant improvements have been observed without additional signal manipulation, through digital means or otherwise, in certain transmission properties of the devices. Future work will expand on the enhancement of capacitive transducers through the use of hybrid resonator circuits and other related methods.

Monday Poster

PS012-12

Dynamic focusing thorough arbitrary geometric interfaces

Montserrat Parrilla, **Jose Brizuela,** Jorge Camacho, Alberto Ibañez, Patricia Nevado, Carlos Fritsch; *Instituto de Automática Industrial (CSIC), La Poveda (Arganda), Madrid, Spain.*

Background, Motivation and Objective

The use of array technology in Non-Destructive-Testing (NDT) applications requires setting the focal laws in emission and in reception for every array element. Frequently wedges are inserted or the inspection of the part is carried out by immersion. In these cases, the presence of interfaces complicates the focal law computing task due to refraction effects. If the number of foci is limited (i.e., single focus in emission and in reception), the Fermat's principle can be applied to accurately compute the focal laws.

However, state-of-the art equipment allows dynamic focusing, which provides increased resolution, signal to noise ratio and contrast. With dynamic focusing, the number of focal laws to be computed increases by two or three orders of magnitude and the computing time by the Fermat's principle increases accordingly.

The main objective of this work is to present new methods which provide the dynamic focusing focal laws with the required accuracy and less computing burden.

Statement of Contribution/Methods

Several methods of focal law computing thorough arbitrary geometry interfaces are analyzed. As a background, the general purpose method based on the Fermat principle is described. Then, a new approach, the Fast Focal Law Computing (FFLC) technique is presented. It is based in solving an equation by an iterative method. It is shown that, for most applications and following the proposed processing method, no iterations are required, being nearly as fast as a closed formula method.

The Fermat and the FFLC methods are compared with regard to accuracy and computing time for dynamic focusing of a diversity of interface shapes. Then, both methods are applied to compute the dynamic focal laws into aluminum parts with artificial flaws, using a 5 MHz transducer. Wedges are applied for planar interfaces and water immersion is used for shaped parts with an irregular geometry.

Results

It is shown that the proposed FFLC algorithm obtains the dynamic focal laws in about 1/20 the computing time required by the conventional Fermat's principle application. This represents getting the equipment ready for inspection in a few seconds, instead of several minutes. Furthermore, focusing errors of the FFLC are very small and comparable to those produced by the standard method. Thus, image quality is not impaired in spite of the low time spent in computing the focal laws.

Discussion and Conclusions

The FFLC is presented and analyzed. It provides a fast method to compute focal laws for dynamic focusing into parts of arbitrary shape. Images obtained with the computed focal laws are of the same quality that those obtained with more costly methods. This is due to the very low timing errors produced by the FFLC technique.

PS013-13

Wireless Drive of a Piezoelectric Plate by Dipole Antenna

Satyanarayan Bhuyan, Junhui Hu; *Nanyang Technological University, Singapore.*

Background, Motivation and Objective

In most applications of piezoelectric devices, electric energy is applied to the devices via lead wires soldered on the electrodes of piezoelectric components. But the lead wires may fall off at large vibration and high input voltage, and this causes the breakdown of piezoelectric devices. Thus, there is a need to introduce a wireless approach to apply electric energy to the piezoelectric devices. Wireless drive of a piezoelectric plate using an electric dipole antenna is explored in this work.

Statement of Contribution/Methods

To transmit relatively large electric energy to a piezoelectric plate, an electric dipole antenna in series with an inductor is used as shown in Fig. 1. The ac electric field, produced by plate-shaped live and ground electrodes of the antenna is transmitted to the piezoelectric plate placed 6 mm away form antenna plane. The separation between antenna electrodes is 5 cm. The electric resonance of dipole antenna with an inductor generates a large voltage across the dipole antenna.

Results

Fig. 2 shows the frequency characteristic of the output power of the piezoelectric plate operating in the thickness mode. At resonance frequency 772 kHz of the plate, a maximum output power of 12mW is achieved when the dipole antenna is in series electric resonance with an inductor because of the large voltage 1436Vrms across the antenna for an input voltage source of 150Vrms. The power transmitted to the load drops as the plate is detuned from resonance. An equivalent circuit of the wirelessly driven piezoelectric plate operating in the thickness mode has been developed. It is known that the circuit has a current source, resulting from the electric field which is different from the conventional piezoelectric plate driven by a voltage applied via lead wires.

Discussion and Conclusions

A piezoelectric plate operating in the thickness mode is wirelessly driven by the electric field generated by a dipole antenna. At resonance a maximum output power of 12mW is achieved with an electrode area of 900 cm 2 , input source voltage of 150Vrms, and 6mm from the antenna plane. An equivalent circuit of the wirelessly driven piezoelectric plate is derived which has a current source, resulting from the external electric field.

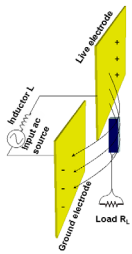

Fig.1. Experimental setup

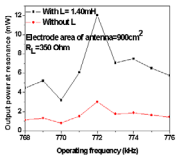

Fig.2. Frequency Characteristics

PS014-14

Towards thin film complete characterization using picosecond ultrasonics

Pierre-Adrien Mante, Arnaud Devos, Jean-François Robillard; *IEMN-CNRS, France.*

Background, Motivation and Objective

Mechanical characterization of thin films is a main issue in the microelectronic industry. The knowledge of these properties is necessary in many fields such as copper line interconnection and bulk acoustic wave resonators. A few techniques are reliable at this scale. Nano indentation or conventional laser-ultrasonic techniques can't be effective in film thinner than 500 nm. Picosecond ultrasonics can also be used for thin film characterization. It is an efficient method to excite and detect vibrations within a thin film. A strong optical pulse warms a material surface, which leads to the creation of an acoustic wave propagating at the sound velocity. The waves propagation is longitudinal and it modifies the optical properties of the material. These modifications can be detected by a second time-shifted optical pulse.

Statement of Contribution/Methods

In this technique we use a metallic very thin film as a transducer and only longitudinal waves can be generated. Due to that the full mechanical properties of thin layer cannot be measured. Here we show that thanks to a nanostructuration of the transducer, in-plane propagating waves are added using the same experimental setup. In the case of an isotropic medium, we have now access to all the acoustic properties.

Results

We realized and studied 2D lattices of metallic nanocubes using e-beam lithography deposited onto the thin film to be charaterized. In a first experiment we will present results obtained on a 600nm-thick silica film.

Discussion and Conclusions

Experiments were performed both on the lattices and out of the array of nanocubes. We respectively obtained the Rayleigh's velocity and the longitudinal velocity of silica. Then we can deduce Poisson's ratio and Young's modulus of silica: E=72GPa and nu=0.16, which is in very good agreement with literature. This first result demonstrates that we are able to extract longitudinal sound velocity, Rayleigh's velocity, Young's modulus and Poisson's ratio in submicronic layers. Further results obtained on other materials isotropic and anisotropic will be also presented.

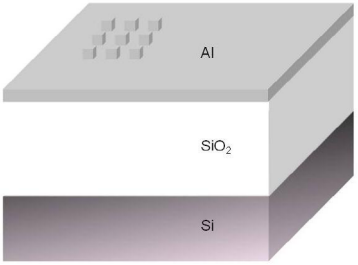

PS015-15

Simultaneous observation of induced longitudinal and shear acoustic phonons by Brillouin Scattering

Taisuke Yoshida[1], Mami Matsukawa[1], Takahiko Yanagitani[2]; *[1]Doshisha University, Faculty of Engineering, Kyotanabe, Japan, [2]Nagoya Institute of Technology, Department of Applied Physics, Nagoya, , Japan.*

Background, Motivation and Objective

Brillouin scattering measurement is a nondestructive method for measuring acoustic wave velocity at minute part of the material. This technique also enables us to measure longitudinal and shear wave velocities simultaneously. However, the measurement accuracy of the velocities is lower than those of other method such as pulse-echo measurement. This is mainly due to the weak Brillouin light scattering from the thermal phonons. In this study, we propose the use of induced longitudinal and shear waves for solving this problem.

Statement of Contribution/Methods

A c-axis tilted ZnO thin film transducer was deposited on side of the silica glass bar with the size of 3x10x35 mm^3. Thus, excited continuous longitudinal and shear waves were propagated in the silica glass sample. Brillouin spectrum from silica glass sample were measured using RIΘA scattering geometry [1]

Results

Figure 1 shows the Brillouin spectrum of longitudinal mode phonons observed without and with longitudinal and shear waves excitation. A pair of peaks observed at 3.6 GHz corresponds to the scattering from longitudinal mode phonons. This frequency is near the thickness extensional third overtone mode resonant of the film transducer. Strongly amplified Stokes peak is observed due to the excited longitudinal wave propagating in one direction. Also for shear mode phonons, amplified Stokes peak at 3 GHz (thickness shear fifth overtone mode resonant frequency) is observed as shown in Fig. 2.

Discussion and Conclusions

This technique is useful for the sample which is easy to deteriorate because this technique realizes larger scattering even the use of lower laser power. Ref. [1]: J. K. Krüger et al., J. Phys. D: Appl. Phys **31** (1998) 1913.

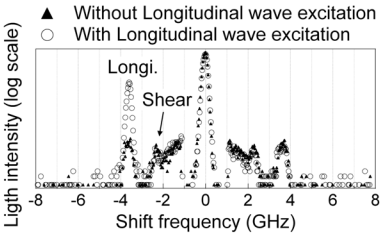

Fig. 1 Brillouin spectra of longitudinal phonons in silica glass sample.

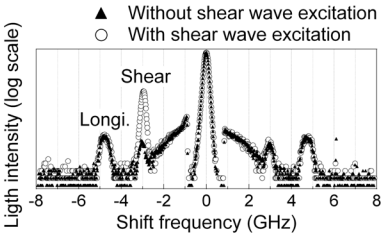

Fig. 2 Brillouin spectra of shear phonons in silica glass sample.

PS016-16

Temperature Compensation of Thin AlN Film Resonators utilizing the Lowest order Symmetric Lamb mode.

Gunilla Wingqvist, Lilia Arapan, Ventsislav Yantchev, Ilia Katardjiev; *Uppsala University, Solid State Electronics, Uppsala, Sweden.*

Background, Motivation and Objective

Micromachined Thin film plate acoustic wave resonators (FPAR) utilizing the lowest order symmetric Lamb wave (S0) propagating in highly textured 2µm thick Aluminum Nitride (AlN) membranes were successfully demonstrated [1]. The proposed devices had a SAW-based design and demonstrated Q factors of up to 3000 at a frequency of 900MHz as well as design flexibility with respect to the required motional resistance. A drawback of the proposed devices was the negative TCF of -20 ppm/K. Thus despite the promising features demonstrated, further device optimization is required.

Statement of Contribution/Methods

In this work composite membrane employing the opposite temperature coefficients of delay of the DC sputtered AlN and the thermally grown SiO2 is used as a platform for the design of temperature compensated FPAR. The theoretical analysis, based on the Adler's algorithm, revealed the possibility to achieve temperature compensation retaining the device electromechanical coupling. Further, the 1D equivalent model analysis suggested the use of Mo electrodes as a higher reflective alternative to the typically used Al in SAW-type reflecting gratings. Thus Mo being a material sustainable to electro-migration and with significantly smaller TCD, enables further device minimization as well.

Results

The zero TCF devices demonstrated in here are synchronous type resonators fabricated on to composite AlN/SiO2 membrane consisting of relative thicknesses of d/λ=0.166 and D/λ~0.07, respectively. λ=12µm is the acoustic wavelength. The number of strips used in the reflectors is as small as 30 due to high reflectivity of the Mo electrodes. Q factors of around 1000 have been measured at a frequency of 850 MHz.

Discussion and Conclusions

The latter is sufficient but slightly lower than the Q=1800 achieved for the synchronous noncompensated FPAR [1]. The observed reduction in Q is due to a slight non-uniformity of the thermally grown SiO2 layer caused by the limited selectivity of the Si/SiO2 Reactive Ion etching used for the membrane micromachning. Solutions of the problem are further suggested. In conclusion temperature compensated FPARs with reduced size and high Q are

designed and micromachined on to low resisitve silicon wafers. Their potential applications include integrated frequency sorces as well as narrow band filters and gas sensors

[1] V. Yantchev and I. Katardjiev, "Micromachined Thin Film Plate Acoustic Resonators Utilizing the Lowest Order Symmetric Lamb Wave Mode", IEEE Trans. UFFC., vol. 54, No.1, pp. 87-95, 2007

Monday Poster

PS017-17

A Full-Wave Analysis of Surface Acoustic Waves Propagating on a SiO2 Overlay/Metal Grating/Rotated YX-LiNbO3 Substrate Structure

Yiliu Wang, Ken-ya Hashimoto, Tatsuya Omori, Masatsune Yamaguchi; *Chiba University, Graduate School of Engineering, Chiba, Japan.*

Background, Motivation and Objective

The authors have recently reported a full wave analysis of piezoelectric boundary acoustic waves (PBAWs) propagating in a SiO2 overlay/Cu grating/rotated YX-LN substrate structure [1]. In the analysis, the finite element method is used for the grating region, while the spectral domain analysis is applied to an isotropic overlay region as well as a piezoelectric substrate region. The paper discusses in detail how the excitation and propagation characteristics of the shear-horizontal (SH) and Rayleigh-type PBAWs are dependent upon the Cu grating thickness, substrate rotation angle and metallization ratio.

The structure consisting of a SiO2 overlay of finite thickness is also directly applicable to the development of high performance SAW filters [2]-[3]. To the best of authors' knowledge, however, it seems that detailed discussions have not yet been made on the propagation characteristics of the SH- and Rayleigh-type SAWs.

Statement of Contribution/Methods

This paper describes a full wave analysis of the SH- and Rayleigh-type SAW propagation in a finite SiO2 overlay/metal grating/rotated YX-LN substrate structure shown in Fig. 1.

Results

It is shown that the structure supports four types of propagation modes. Two modes concentrate their energy near the metal grating, and become the PBAWs when h2 gets infinite. Their electromechanical coupling is relatively strong even when h2 is large.

One of the other two modes concentrates its energy near the top surface of the SiO2 layer. With an increase in h2, its propagation characteristics approach to those for the non-piezoelectric Rayleigh-type SAW on a semi-infinite SiO2 layer, rapidly losing its piezoelectric coupling.

The remaining mode is the basis of a series of guided modes bounded in the SiO2 layer, in which the SiO2 layer behaves as a waveguide because of its low acoustic wave velocities.

Discussion and Conclusions

Detailed discussions are made on the dependence of the propagation characteristics of these four modes on the design parameters such as the layer and grating thickness. It is also discussed how the propagation characteristics are affected by the SiO2 flatness denoted by h3 in Fig. 1.

References

[1] Y.L.Wang, et al, Proc. IEEE Freq. Contr. Symp. (2008) [to be published]

[2] M.Kadota and T.Kimura, Proc. IEEE Ultrason. Symp. (2006) pp. 2305-2309.

[3] H.Nakamura, et al, Jpn. J. Appl. Phys., 47, 5B (2008) [to be published]. (330)

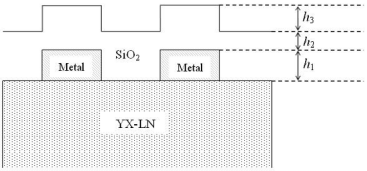

Fig. 1 Controlled shape SiO_2 overlay/metal grating/rotated YX-$LiNbO_3$ structure

PS018-18

Shear mode BAW resonator based on c-axis oriented AlN thin film

Evgeny Milyutin, Paul Muralt; *Ecole Polytechnique Federale de Lausanne, Switzerland.*

Background, Motivation and Objective

Thin film bulk acoustic wave resonators (TFBAR's) also showed potential as gravimetric sensors. In contrast to RF filters working with longitudinal modes, bio-medical applications usually require detection in a liquid, thus must employ shear modes. The principle has recently been successfully demonstrated with TFBAR devices employing tilted c-axis growth of ZnO [1, 2]. In this work, we show that it is also possible to use non-tilted AlN thin films when interdigitated (ID) electrodes (IDE) are used. A true shear BAW thickness mode can be excited. Parasitic Lamb waves are avoided by the use of acoustic reflectors.

Statement of Contribution/Methods

Performance and design of shear modes in AlN(001) films excited by ID electrodes were simulated by finite element modeling using the boundary element method (FEM-BEM). Devices have been fabricated with 1.5 microns thick (001)-textured AlN thin films on top of a Bragg reflector composed of 5 double layers of SiO2/AlN. The Al electrode system was defined by photolithography along with a lift-off process.

Results

The performances of resonators were assessed in air and silicon oil. Typically resonance frequency of the devices was between 1.8-1.9GHz. By using different electrode periodicities, the BAW nature of the resonance was confirmed through the absence of a shift. A quality factor of about 1000 was achieved when operated in air. Under immersion, the Q-factor decreased to 260. Experimental results are in a good agreement with simulations, when we consider acoustic emission through the Bragg grating as the only loss factor.

Discussion and Conclusions

The achieved results and the simplicity of fabrication of proposed device show their potential as gravimetric sensors for immersed applications. The achieve Q-factor is higher than reported in literature for tilted c-axis resonators [3]. Further optimization of design and materials is going on. The integration of an immobilization layer is in development.

1. Link, M., M. Schreiter, J. Weber, R. Gabl, D. Pitzer, R. Primig, W. Wersing, M.B. Assouar, and O. Elmazria, C-axis inclined ZnO films for shear-wave transducers deposited by reactive sputtering using an additional blind. J.Vac.Sci.Techn. A, 2006. 24: p. 218-222.

2. Weber, J., W.M. Albers, J. Tuppurainen, M. Link, R. Gabl, W. Wersing, and M. Schreiter, Shear mode FBAR as highly sensitive liquid biosensors. Sensors and Actuators A, 2006. 128: p. 84-88.

3. G. Wingqvist, J. Bjurstrom, L. Liljeholm, V. Yantchev, I. Katardjiev, Shear mode AlN thin film electro-acoustic resonant sensor operation in viscous media, Sensors and Actuators B 123 (2007), 466-473

PS019-19

Investigation of charge diffusion in Capacitive Micromachined Ultrasonic Transducers (CMUTs) using optical interferometry

Hanne Martinussen, Astrid Aksnes, Helge E. Engan; *Norwegian University of Science and Technology, Electronics and Telecommunications, Trondheim, Norway.*

Background, Motivation and Objective

Capacitive Micromachined Ultrasonic Transducers (CMUTs) have been developed and fabricated at our department. The main goal is to use an improved version of these structures to perform medical imaging to detect unstable plaque in the coronary arteries. Unstable plaques are fatty lipid pools contained in the wall of the coronary arteries by a thin fibrous cap. A rupture of this cap can lead to an infarction. The CMUTs have a radius of 5.7µm and a center frequency of about 30MHz in air. When an RF voltage is applied in addition to a DC bias the membrane will vibrate and generate ultrasound waves. This DC bias is in the order of 30V and leads to a charge diffusion in the CMUTs. This work investigates this process in detail.

Statement of Contribution/Methods

A heterodyne interferometer has been built in order to characterize the CMUTs. The setup can measure absolute phase and amplitudes. By using two acousto-optic modulators in the reference arm of the interferometer we can measure acoustic frequencies in the range 10kHz-1.2GHz. The results from the interferometer are supplemented with measurements from a network analyzer. The network analyzer takes the mean of all currents generated by CMUTs whereas the interferometer inspects individual CMUT elements.

Results

The vibrating membrane in the CMUT is made of silicon nitride, which ideally is an insulator. However, we observe a charge diffusion through this membrane influencing the response of the CMUTs. There are two possible mechanisms. One is that positive charges diffuse from the bottom electrode through the silicon substrate and into the silicon nitride membrane. The other is that negative charges from the top electrode diffuses into the silicon nitride membrane. An experiment investigating the resonance frequency as a function of time indicated that the latter mechanism is dominant. Measurements from both the interferometer and the network analyzer supported this conclusion.

Discussion and Conclusions

The measurements presented here are performed in air. Under loading conditions such as water or tissue the frequency bandwidth of the CMUT increases substantially. The charge diffusion problem may therefore not be a major problem when the CMUT is operated in water.

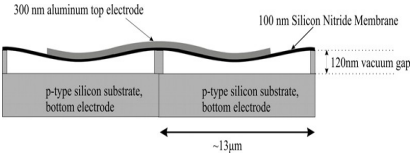

PS020-20

High-frequency (>100MHz) Piezoelectric PZT Film Micromachined Ultrasonic Arrays

Dawei Wu[1], Qifa Zhou[1], Changgeng Liu[2], Frank Djuth[2], K. Kirk Shung[1]; [1]*University of Southern California, NIH Transducer Resource Center and Department of Biomedical Engineering, USA,* [2]*Geospace Research, Inc, USA.*

Background, Motivation and Objective

High frequency (>30 MHz) ultrasonic imaging has been extensively used for imaging of the eye, blood vessel, skin and small animals. Fabrication of the transducers, which is the most critical component of the ultrsound imaging system, becomes especially challenging when very high frequency (>100 MHz) is required. Conventional lapping-and-dicing methods with bulk piezoelectric materials are no longer a viable approach. During recent years, the advance of microelectromechanical system (MEMS) methods has offered significant opportunities for miniaturized devices. This paper presents the latest development of high-frequency (>100MHz) micromachined ultrasonic linear arrays with high-quality PZT thick films.

Statement of Contribution/Methods

Both kerfless and kerfed arrays were fabricated with the PZT thick films which were prepared by spin-coating PZT composite solution. To fabricate the kerfless array, a layer of Cr/Au was patterned onto PZT film surface by using photolithographic techniques. A conductive epoxy, E-solder 3022, was used as a backing material after the silicon substrate was removed. One major problem with the kerfless arrays is their large crosstalk. To decrease the crosstalk, Inductively coupled plasma-Reactive ion etching (ICP-RIE) SF6 based dry etching was selected to etch the PZT thick films into kerfed arrays. The kerfs of the array were next filled with non-conductive epoxy; the front surface of the array elements were coated with Cr/Au electrodes. E-solder was poured in as the backing material after etching away the silicon substrate.

Results

A representative element of the kerfless array was found to have a center frequency of 120 MHz, -6 dB bandwidth of 40% and an insertion loss of around -40 dB. Its bandwidth increased to 60% after a layer of parylene was deposited as a matching layer. The etched PZT film array has a thickness of 15 μm and etched profile angle of 75° as shown below. Charactrization of the array has been carried out. Results show great promise for this technology in fabricating linear arrays at a frequency higher than 50 MHz.

Discussion and Conclusions

High-frequency (>100 MHz) PZT linear kerfless arrays are fabricated and tested. Preliminary results of the etched linear kerf array are promising. The results show that integrating PZT films into MEMS devices can serve as a feasible solution to high-frequency ultrasonic array fabrication.

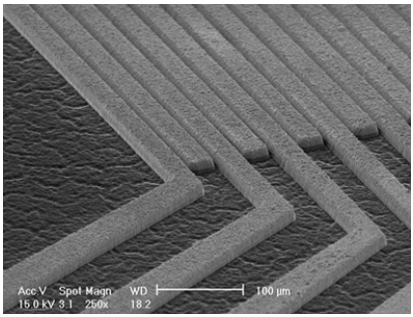

PS021-21

1-D CMUT Imaging Arrays Fabricated Using a Novel Wafer Bonding Process

Andrew Logan, John Yeow; *University of Waterloo, Systems Design Engineering, Waterloo, Ontario, Canada.*

Background, Motivation and Objective

Capacitive micromachined ultrasonic transducers (CMUTs) are a promising alternative to conventional piezoelectric transducers for medical imaging and diagnostics.They have demonstrated image quality on par with commercial piezoelectric transducers, while the use of semiconductor fabrication technologies to manufacture ultrasonic imaging arrays has a number of advantages such as batch fabrication, reduced element lay-out constraints and the potential for on-chip electronic circuit integration.

Statement of Contribution/Methods

Here we report the fabrication and testing of 1-D CMUT arrays using a novel wafer bonding process whereby the membrane and the insulation layer are both silicon nitride. The use of a user-grown insulating membrane layer avoids the need for expensive SOI wafers, reduces parasitic capacitance, and allows more freedom in selecting the membrane thickness while also enjoying the other benefits of wafer bonding fabrication.

Results

A 128x1 element array with a center frequency of 16 MHz in air and 7 MHz in immersion and a 64x1 element array with a center frequency of 40 MHz in air 25 MHz in immersion are discussed. Figure 1 is an SEM image of the 128 element device (left) and 64 element device (right). Figure 2 is the transmission pulse of the 128 element device (left) and the Fourier transform of the transmission (right). The device is biased at 100 V and a voltage spike is applied using a commercial ultrasonic pulser/receiver. Signal is detected using a commercial hydrophone. The device has a -6 dB bandwidth of 105%.

Discussion and Conclusions

The devices discussed here are suitable for phased array imaging without grating lobes. The element dimensions are 100 µm x 5 mm and 30 µm x 2 mm for the 128 and 64 element devices respectively. The devices will be used for biological imaging purposes.

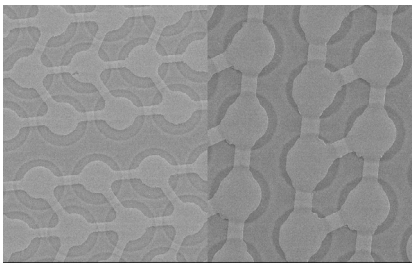

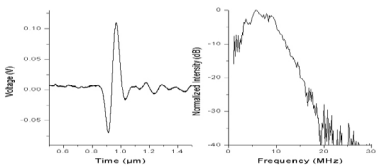

Monday Poster

P1A. Photoacoustic Imaging

2nd and 3rd Floor Foyers

Monday, November 3, 2008, 3:00 pm - 4:30 pm

Chair: **Xueding Wang;**
University of Michigan, MI, USA.

P1A023-01

In Vivo Photoacoustic Micro-imaging of Microvascular Changes in Achilles Tendon of Mice

Po-Hsun Wang[1], Jer-Junn Luh[2], Meng-Lin Li[1]; *[1]National Tsing Hua University, Department of Electrical Engineering, Hsinchu,Taiwan, [2]National Taiwan University, School and Graduate Institute of Physical Therapy, College of Medicine, Taipei, Taiwan.*

Background, Motivation and Objective

Tendon injuries arising from inflammation or overuse are a common clinical problem for athletes, typically in Achilles tendon. Several studies indicate that Achilles tendinitis is accompanied with neovascularization or hypervascularity; thus, assessments of vascularity are important when assessing inflammation changes in tendon injuries. Photoacoustic imaging, taking the advantages of good ultrasonic resolution and high optical absorption contrast, has been shown a promising tool for vascular imaging. For this, photoacoustic microscopy offers a unique opportunity to monitor micro-vascular changes in tendon injuries in a mouse model in vivo, which high frequency color Doppler may have difficulties to detect.

Statement of Contribution/Methods

In this study, a 25-MHz dark-field confocal photoacoustic microscopy (PAM) is used to image microvascular changes in Achilles tendon of mice before and during collagenase-induced tendonitis. A wavelength of 532 nm are used for photoacoustic excitation because blood vessels own strong optical absorption at this wavelength, guaranteeing that photoacoustic signals mainly come from vessels. Coregistration of PAM B-mode images with 25-MHz ultrasound (USM) ones is also performed. The spatial resolution of the used PAM and USM is, respetively, 36 μm and 100 μm in axial, and 150 μm and 140 μm in lateral.

Results

The figure shows the results where (a), (c) and (b), (d) are USM and PAM B-mode images, respectively, the two dashed lines indicate the tendon position, (a) and (b): normal tendons, and (c) and (d): tendons with tendonitis, imaged five days post collagenase injection. PAM and USM images are shown in linear scale and a 45 dB dynamic range, respectively. The cross-section of tendon and the thickness of dermis in (c) are larger than those in (a) due to inflammation and edema. The increase of dermis thickness is also revealed by the PAM images. Proliferation of new blood vessels within the tendon is also observed in (d).

Discussion and Conclusions

We demonstrate the potential of photoacoustic microscopy in exploring the microvascular and morphological changes in mouse Achilles tendon in vivo. Future work includes time-course assessments of microcirculation changes in tendinitis before and after treatment. More cases and histological verifications will be used to obtain statistically significant data.

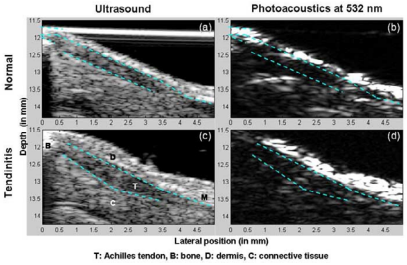

P1A024-02

Experimental Evaluation of a High-Speed Photoacoustic Tomography System

Xueding Wang[1], Larry Mo[2], J. Fowlkes[1], Paul Carson[1]; *[1]University of Michigan, Ann Arbor, Michigan, USA, [2]Zonare Medical Systems, Mountain View, CA, USA.*

Background, Motivation and Objective

A high-speed photoacoustic tomography (PAT) system has been developed using a commercial ultrasound (US) unit (z.one, ZONARE Medical Systems). The advantage of this US unit is that it has a research package that supports simultaneous 64 parallel channel data acquisition, and efficient transfer of multiple channel data frames via an Ethernet link to an external PC. Based on back-projection algorithms for computed tomography, the multi-channel data can be used to reconstruct the optical absorption distribution of the region of interest. The purpose of this study is to evaluate the performance of this system by imaging phantoms and excised tissue specimens.

Statement of Contribution/Methods

Synchronization between the laser firing and US data acquisition was enabled by a frame trigger signal derived from the US probe connector circuit. For each laser pulse, 64 channels of 16-bit in-phase/quadrature (I/Q) data can be acquired from a 128-element L10-5 linear probe, and processed on an external PC using various image reconstruction algorithms. Experiments were conducted on vessel phantoms made from transparent micro-tubing filled with whole canine blood and on ex vivo fresh canine prostate specimens with injected blood clots mimicking tumor lesions. For comparison, the same sample specimens were also imaged in US spatial compounding mode using the same scan geometry as for PAT.

Results

Preliminary results indicate that an object can be imaged successfully on both of the two modes with ultrasonic and optical contrast presented simultaneously. For the PAT image of the micro-flow vessel phantoms, the vessels embedded in a gel phantom are presented clearly with good contrast-to-noise ratio and with spatial resolution better than 1.2 mm. For the study on the canine prostate specimens, the lesion generated 1 cm deep in the prostate can be visualized accurately by PAT based on intrinsic optical contrast.

Discussion and Conclusions

In order to perform the most rigorous reconstruction for quantitative optical absorption imaging, the receive bandwidth of a PAT system should be able to accommodate broadband PAT signals from biological tissues. However, like most commercial US arrays, the L10-5 array used in this study has a -6 dB frequency band of only 4.9 to 9.3 MHz centered at about 7.5 MHz. To make this system ready for clinic use, the bandwidth as well as the receiving sensitivity needs to be improved further.

P1A025-03

A large 2D CMUT array for 3D photoacoustic imaging

Srikant Vaithilingam[1], [1]Te-Jen Ma, [1]Cenk Yildiz, [1]Kwan-Kyu Park, [1]Xuefeng Zhuang, [1]Ira Wygant, [1]Yukio Furukawa, [2]Aya Kamaya, [1]Omer Oralkan, [1]Mario Kupnik, [2]R. Brooke Jeffrey Jr., Butrus T. Khrui-Yakub[1]; *[1]Stanford University, USA, [2]Stanford University Medical Center, USA.*

Background, Motivation and Objective

Many photoacoustic imaging systems rely on mechanically scanned single focus transducers or a 1D array of transducers; neither alternative can provide true 3D images in real-time. Our proposed system is based on large two dimensional capacitive micromachined ultrasonic transducer (CMUT) arrays with integrated electronics and fiber

optics for true 3D photoacoustic imaging. Our research aims to provide technology for a handheld probe to allow freehand real-time 3D photoacoustic imaging.

Statement of Contribution/Methods

We fabricate a 64x64-element CMUT array by using direct wafer bonding and local oxidation of silicon (LOCOS) in combination with trench-isolated through-wafer interconnects to connect to each element independently. This allows flip-chip bonding of the CMUT array to a custom-designed integrated circuit. Thus, each transducer element has its own dedicated low-noise preamplifier. The laser excitation is delivered through optical fibers. For the image reconstruction we utilize synthetic aperture imaging along with coherence weighting.

Results

As proof of concept that a larger 2D array will improve the image quality, we mechanically scanned a 16x16 element CMUT array in the x and y directions to simulate the aperture of a 64x64 element CMUT array. This CMUT array has a center frequency of 2.5 MHz, and is integrated with transmit-receive front-end electronics. A 6-ns wide, 690-nm laser pulse illuminated the phantom with an intensity of 14 mJ/cm^2. The phantom consisted of three transparent fishing wires with a diameter of 150-µm and two black colored fishing wires with a diameter of 180-µm. In the 3D volume rendered images of the phantom (Figure) we overlaid the photoacoustic image (red) on the pulse-echo image (white). Both the photoacoustic and pulse-echo images were reconstructed using synthetic aperture imaging combined with coherence weighting.

Discussion and Conclusions

This experiment demonstrates that by changing from a 16x16 to a 64x64 element array we are able to realize a photoacoustic imaging system with significantly improved image quality in terms of resolution and coverage volume. Our latest CMUT fabrication technology in combination with integrated electronics and fiber optics allows us to realize such a 3D photoacoustic imaging system.

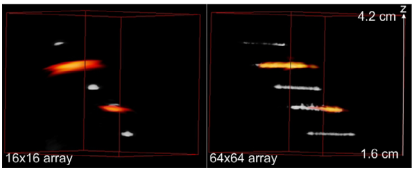

P1A026-04

Simulation Study of Photoacoustic Coded Excitation using Golay Codes

Martin Mienkina[1], Annika Eder[1], Claus-Stefan Friedrich[2], Nils Gerhardt[3], Martin Hofmann[2], Georg Schmitz[1]; *[1]Ruhr-University Bochum, Institute of Medical Engineering, Germany, [2]Ruhr-University Bochum, Institute of Photonics and Terahertz-Technology, Germany, [3]photonIQ Technologies GmbH, Germany.*

Background, Motivation and Objective

Photoacoustics (PA) is a new imaging modality based on the generation of ultrasound due to laser irradiation. Commonly, Q-switched Nd:YAG lasers are used for the generation of PA signals. Alternatively, applying pulsed laser diodes to PA imaging is attractive since they are cheaper and handier. Although laser diodes exhibit low pulse energy, the pulse repetition frequency (PRF) of pulsed laser diodes is significantly higher than the PRF of Nd:YAG lasers thus averaging can be used for increasing the SNR. For averaging the applied PRF is limited by the echo time. To further increase the SNR we propose the usage of coded excitation for pulsed PA imaging. Since Golay Codes do not exhibit range sidelobes, we decided to evaluate their performance for photoacoustic coded excitation (PACE) by a simulation study based on experiments.

Statement of Contribution/Methods

Golay Codes consist of 2 bipolar, complementary code sequences. For PACE the codes must be split into 4 unipolar sequences since no negative light emission is possible. Thus 4 light sequences are sent and 2 of the received ultrasound responses are subtracted before being correlated with the bipolar codes. First experiments are conducted to provide the PA impulse response of the system under investigation. A spherical absorber made of black plastic is irradiated by a pulsed laser diode (pulse: 7 µJ energy, 31 ns duration, 905 nm wavelength), the resulting ultrasound waves are received by a 10 MHz ultrasound transducer (25 mm diameter, 75 mm spherically focused), amplified by 54 dB and sampled by an A/D card (14 bit, 100 MS/s). To be able to flexibly vary the PRF over a broad range the acoustic response to a coded laser excitation is simulated by the superposition of independent experiments according to the coding scheme. The SNRs of coding schemes are compared to averaging as a function of PRF and coding length. For averaging a maximal PRF of 16.6 kHz is applied due to an acquisition

depth of 9 cm. For each coding scheme the acquisition duration is computed, the equivalent number of possible averages is determined, and the SNR of each averaging procedure is calculated.

Results

The SNR gain of the Golay Codes with respect to one impulse response ranges from 5 dB for a 4 bit sequence to 26 dB for a 512 bit sequence. No range sidelobes are detectable and the acoustic response of the optical absorber is equivalent to the signal obtained from averaging. The comparison of the coding schemes with equivalent averaging procedures shows that for coding PRFs lower than 60 kHz Golay coding exhibits a lower SNR than averaging for sequences up to 512 bit. For coding PRFs higher than 100 kHz codes longer than 16 bit show a higher SNR than averaging. For a PRF of 250 kHz and a coding length of 512 bit the coding gain rises to 6.2 dB.

Discussion and Conclusions

Improving SNR by coding is feasible since state-of-the-art laser diode pulsers exhibit PRFs up to 1 MHz. Further improvements can be achieved by employing coding schemes adapted to the dynamic range of the PA imaging system.

P1A027-05

Photoacoustic measurement of optical-transport Green functions in turbid media using progressive optical-source-acoustic focus separations

Roger Zemp; *University of Alberta, Electrical & Computer Engineering, Edmonton, Alberta, Canada.*

Background, Motivation and Objective

We present a novel photoacoustic scheme for measuring radiative transport Green functions in optically-turbid media, including biological tissues. This is a first step towards more sophisticated quantitative imaging techniques for extracting optical absorption and scattering coefficients in tissue.

Statement of Contribution/Methods

We constructed a novel photoacoustic probe, consisting of an optically transparent prism, lenses, optical-index matching fluid, and a 25-MHz focused ultrasound transducer. The acoustic properties of the optical index-matching fluid were characterized, and found to have a speed of sound only 3% less than that of water, an acoustic impedance of 1.2 MRayl, and an acoustic attenuation only 2.5 dB/cm more than water at 25 MHz. 6-ns pulses of 532-nm laser light were focused using a translatable lens assembly. The probe allowed for precise control over the location of the light-spot relative to the ultrasonic focal axis.

Results

1-D images of absorbing phantom-targets were acquired. Additionally, by receive-focusing the ultrasound transducer on a point- or line-target, and moving the optical illumination spot, we effectively measured the optical transport Green's function in turbid media for varied phantom properties.

Discussion and Conclusions

Feasibility for measuring Green's functions of optical transport in turbid media has been established for the first time to our knowledge. This approach may lead to several schemes for quantitative estimation of absorption and scattering parameters of tissue.

Monday Poster

P1B. Medical Beamforming

2nd and 3rd Floor Foyers

Monday, November 3, 2008, 3:00 pm - 4:30 pm

Chair: **John Hossack;**
University of Virginia, USA.

P1B028-01

A New ultrasonic synthetic Aperture Tissue Doppler imaging System

Moo-Ho Bae[1], Han-Woo Lee[2], Sung Bae Park[1], Jeong-Ho Ham[2], Kyoung Bo Lee[1], Mok-Kun Jeong[3], Yung-Gil Kim[2];
[1]Hallym Univ., Department of Electronic Engineering, Korea, Republic of, [2]Medison Co. LTD., Korea, Republic of, [3]Daejin Univ., Korea, Republic of.

Background, Motivation and Objective

Tissue Doppler Imaging (TDI) is a method that can diagnose disease by detecting and imaging of the tissue movement. Particularly, color-coded TDI method can render the movement of the real-time 2D sectional image by colors and overlay to the B-mode image. Recently, clinical importance of this method becomes apparent. On the other hand, synthetic aperture imaging is being developed as a focusing method that can obtain high resolution image and being attempted for a real-time implementation and currently, it is very close to obtain this goal.

Until now, there are several attempts for a color Doppler imaging on a synthetic focusing system which is consists of combination of these two methods. However, most of them required huge computational power.

In this paper, a new, simple, auto-correlation based color-coded TDI method is proposed. This method can be implemented using a velocity detection and compensation method which described in [1]. In that, received signal from each transmission treated as ensemble data of the color Doppler so that there is no issue for a dropping of frame rate compare to conventional color Doppler and TDI which require multiple transmission to the single scanline.

Statement of Contribution/Methods

Miscalculated velocity detection caused by rotation of the low resolution image (LRI) side-lobe is corrected by moving the location of the virtual source in certain order, that is, location of the virtual source is not transmitted in order like 1,2,3,4,... but in 1,3,2,5,4,7,6,... Number increases in +2, -1, and so on (we call it staggering). By calculation the pairs with increasing number and pairs with decreasing number separately, phase rotation of the side-lobe is compensated. This method can be directly applied color-coded TDI.

Results

Field II program is employed for computer simulation, in which beam simulation is done by modeling an expanding vessel, and RF data is generated for each channel. Fig. 1 shows the computer simulation results, comparing images with and without the virtual source position staggering.

Discussion and Conclusions

Fig. 1 (a) shows severe distortion in the velocity estimation while it is cleared in (b), the proposed method.

References

1. Moo-Ho Bae et al, "A New Motion Estimation and Compensation Method for Real-Time Ultrasonic Synthetic Aperture Imaging," Proc. 2007 IEEE Ultrason. Symp., pp. 1511~1513

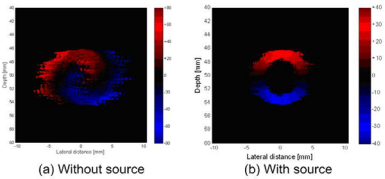

(a) Without source position staggering (b) With source position staggering

Fig. 1 Image Comparison

P1B029-02

A Modified Synthetic Aperture Imaging Approach with Axial Motion Compensation

Billy Y. S. Yiu, Ivan K. H. Tsang, Alfred C. H. Yu; *The University of Hong Kong, Medical Engineering Programme, Pokfulam, Hong Kong, China.*

Background, Motivation and Objective

Synthetic aperture (SA) imaging provides an alternate mean of obtaining ultrasound images. However, since this approach is based on coherent summation of low-resolution images (LRI) acquired from different point sources along an array, its image quality may be degraded if motion is present in between firings. To address such a problem, motion compensation should be applied during SA image formation.

Statement of Contribution/Methods

In this work, we report a modified SA imaging scheme that can compensate for the effects of axial motion on the image quality. The scheme first acquires data by making use of an interleaved firing sequence where a center-point firing is carried out in between each point-source firing. It then estimates the mean axial shift between two LRIs by performing a cross-correlation analysis on the pre-beamform data of successive center-point firings. The estimated value is in turn converted into phase and multiplied onto the LRI of each point-source firing to compensate for possible aberration during SA image formation. To test out our proposed scheme, we conducted a cyst-phantom imaging experiment using a Sonix-RP scanner. During the experiment, pre-beamform data was acquired using our interleaved firing scheme (transmit waveform: one-cycle 9.5 MHz pulse) for 97 virtual point sources laterally spaced apart at 0.3mm and axially located at 10mm behind the probe. This data acquisition procedure was repeated for a range of inter-firing probe displacements (15-90 um) introduced via a motion stage. From the acquired data, motion-compensated SA images were formed using our modified image formation method, and their contrast resolution was compared to those formed without motion compensation.

Results

The proposed imaging scheme reduced the amount of blurring seen in SA images when uniform axial motion is present during data acquisition (see figure). Without motion compensation, the contrast resolution in the distal cysts dropped by as much as 35.6% (relative to the SA image taken without motion) for the range of inter-firing displacements examined. On the contrary, this contrast resolution drop was only 16% when our compensation strategy was applied.

Discussion and Conclusions

Our proposed scheme showed potential in obtaining quality SA images in the presence of motion, albeit this performance gain was achieved at the cost of doubling the number of firings per image frame.

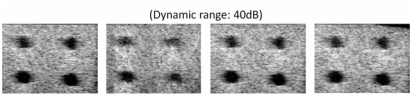

P1B030-03

A New Ultrasonic Synthetic Aperture Tissue Harmonic Imaging System

Moo-Ho Bae[1], Han-Woo Lee[2], Sung Bae Park[1], Ra-Young Yoon[2], Min Hye Jeong[1], Deok Gon Kim[1], Mok-Kun Jeong[3], Yung-Gil Kim[2]; *[1]Hallym Univ., Department of Electronic Engineering, Korea, Republic of, [2]Medison Co. LTD., Korea, Republic of, [3]Daejin Univ., Korea, Republic of.*

Monday Poster

Background, Motivation and Objective

Tissue harmonic imaging (THI) is a method that can obtain B-mode image through nonlinear ultrasound propagation inside of tissue medium. It' s been widely used in the clinical application because of various advantages such as better contrast resolution, less sensitiveness to the phase aberration.

On the other hand, synthetic aperture imaging (SAI) is being developed as a focusing method that can obtain high resolution image.

It is desirable to take an advantage of combining the merits of above two methods, however, there is one problem for employing a usual SAI method. Usually, position of the virtual source is placed on the surface or behind of the array transducer. In this case, physical focal point is not placed in the tissue medium so that beam amplitude at the focal point is severely reduced compare to conventional transmission focal point where is placed in the tissue medium. Roughly, amplitude of the 2nd harmonic is in proportion to the square of the amplitude of the fundamental element.

Statement of Contribution/Methods

Problem stated above can be solved by moving the virtual source of SAI to the front of the transducer [1] so that actual Tx focal point is formed. Preferably, wide Tx aperture increase the beam amplitude at the Tx pocal point. Compare to conventional THI system, it produces much bigger 2nd harmonic amplitude so that improved SNR and lateral resolution can be obtained.

Results

Proposed method is tested on the Medison's modified Accuvix XQ system. RF echo data from the individual channel is acquired by using the 6.5MHz linear array transducer and it is processed off-line. Effectiveness of the method is confirmed by comparing constructed image of the test phantom and tissue medium with two different cases: 2nd harmonic-non-synthetic and 2nd harmonic-synthetic. The processed images of the test phantom and the in vivo carotid image are shown in Fig. 1.

Discussion and Conclusions

As expected, SNR and resolution both are greatly improved. SNR of the image increases by the SAI introduced in THI, and also by the tight Tx focusing with large Tx aperture. Large Tx aperture is not so desirable in conventional THI system because it deteriorates image uniformity, however, there is no problem with the SAI in [1].

References

1. M. H. Bae et al., "A study of synthetic-aperture imaging with virtual source elements in B-mode ultrasound imaging systems," IEEE UFFC, Vol. 47, No. 6, pp. 1510-1519, Nov. 2000.

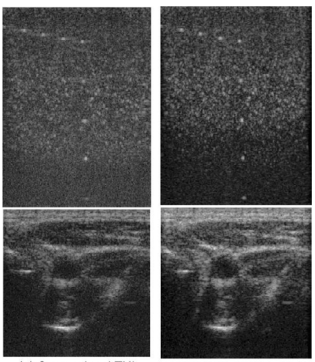

(a) Conventional THI (b) SAI+THI

Fig 1. Image Comparison

P1B031-04

Optimization of Beams with Nonspherical Extended Depths of Focus for Reconfigurable 2D Arrays

Fong Ming Hooi[1], Kai Thomenius[2], Rayette A. Fisher[2], Paul L. Carson[1]; [1]*University of Michigan, Ann Arbor, MI, USA,* [2]*GE Global Research, Niskayuna, NY, USA.*

Background, Motivation and Objective

Array elements in reconfigurable arrays are formed by electronically linking smaller transducer subelements. The flexibility of such reconfigurable 2D arrays allows us to utilize various beamforming techniques with a limited number of channels. To take advantage of these arrays for breast imaging, we are investigating different beamforming techniques to allow for extended range of focus in the transmit beam. By developing such beams, fewer transmit pulses will be needed, leading to a valuable increase in frame rate. Our objective is to develop and optimize these beamforming techniques for balance between range and image quality.

Statement of Contribution/Methods

A hybrid aperture model combining spherical and conical focusing was developed to produce beams with a long, relatively uniform, focal zone. This beamforming technique was tested with Field II simulations using a 7.5MHz 22 mm diameter, aperture of annular rings. Relative ratio of spherical to conical aperture size, overall diameter, ring arrangement, spherical focal depth, and conical angle were varied to optimize the beams according to three image quality measures: depth of range, beam width, and energy distribution ratios. These optimized beams were then compared to traditional spherical beamforming via point spread functions (PSF) and contrast-to-noise ratios (CNR) from simulations with spherical voids of 3 mm diameter at multiple depths up to 4.5 cm.

Results

The optimized beams generated from the hybrid apertures encompassed a larger depth range than their spherical equivalents with depth coverage ~1.2-1.5 cm vs. 0.8-1.0 cm per beam, respectively. Beamwidth calculations from the PSFs showed better performance of the hybrid at the focal depth extremes, while spherical beams showed a slightly tighter beamwidth at the focus.

Initial results from six different scattering phantoms at depths beyond the foci of 0.7, 1.9, 2.8, and 3.7 cm (for 4.5 cm coverage) yielded average CNR values of 2.51, 2.44, 2.62, 2.57 and 2.02, 1.97, 2.34, 2.21 for the hybrid and spherical apertures, respectively. The chosen hybrid apertures performed significantly better over the same extended range than did a spherical focus ($p<0.5$). Both hybrid and spherical apertures were comparable at the focus as differences in CNR were statistically insignificant.

Discussion and Conclusions

Per the simulation results comparing hybrid and spherical focusing, we conclude that the hybrid aperture is a viable method for transmitting beams that cover a larger range without sacrificing image quality. To cover a range of 4.5 cm, the number of transmit beams can be reduced to four compared to the conventional six to eight required with spherical transmit beams.

References: United States Patent 6865140

P1B032-05

Design of a 64-channel Digital High Frequency Linear Array Ultrasound Imaging Beamformer on a Massively Parallel Processor Array Platform

Chang-Hong Hu, Ping Sun, Fan Zheng, Jonathan M. Cannata, K. Kirk Shung; *University of Southern California, Biomedical Engineering, Los Angeles, CA, USA.*

Background, Motivation and Objective

In recent years, digital ultrasound beamformers for high frequency ultrasound were exclusively implemented on DSPs or FPGAs. Because digital beamformers as well as color flow imaging, especially for high frequency ultrasound, require tremendous computing power with high signal band-width to process large amounts of data in parallel, DSPs are limited by the parallel processing capability and throughput while FPGAs are getting more complicated in implementation and more expensive to develop. Therefore, new technologies are being pursued in implementing ultrasound digital beamformers. This paper reports the alternative way of implementing a 64-channel digital beamformer with a 256-element linear array transducer mainly using software on a chip rather than using

the hardware design required for FPGAs. We are currently developing a 30 MHz linear array and system, and only the system design is detailed in this paper.

Statement of Contribution/Methods

In this design, an Ambric¡¯s Massively Parallel Processor Array (MPPA), which includes 336 asynchronous processors and communicates through a configurable structure of channels with a 128-bit high speed (100MHz) Input/Output(I/O) port, is used to implement the 64-channel digital beamformer. Besides the beamformer, the system is composed of 256-channel analog front-end pulser/receiver, 64-channel of Time-Gain Compensation (TGC), 64-channel of high-speed digitizer, a host PC and a PCI Express-based accelerator in the Am2045 chip with a 512 Mbytes external memory. This system is designed to handle a 256 elements linear array or a 64 elements phased array transducer. The system provides 64 channels of excitation pulsers while receiving simultaneously at a 150 MHz sampling rate with 12-bit resolution. The digitized data from all channels of one frame are first stored in the internal memory of MPPA. The coarse delays are integer multiples of the sampling clock rate. They are achieved by dynamically updating the memory addresses which are loaded in the delay coefficients table. Random Memory Access capability of MPPA enables processors to randomly access data while it is still in channels, which eliminate the necessity of moving all data from I/O ports into memory before they can be processed. The fine delays are implemented by FIR filters with an interpolation factor of 4. This technique and architecture allow dynamic receive focusing, aperture growth, spatial filtering, and scan conversion by software only.

Results

The 64-channel beamformer¡¯s functional correctness and its expected execution behavior have been verified by Ambric¡®s integrated simulator prior to realizing it physically. This paper describes the system architecture, analog and digital front-end design, as well as implementation of beamformer using MPPA. Preliminary images obtained with this high speed system on a wire phantom with a high frequency linear array will be given also.

P1B033-06

Sigma-Delta Dynamic Receive Beamforming

Donald Liu[1], Daniel Brueske[1], Todd Willsie[1], Daft Chris[2]; [1]*Siemens Medical Solutions, Ultrasound Group, Issaquah, WA, USA,* [2]*Siemens Medical Solutions, Ultrasound Group, Mountain View, CA, USA.*

Background, Motivation and Objective

Sigma-delta conversion is an analog-to-digital conversion technology that utilizes oversampling and noise shaping to achieve high dynamic range. It is an attractive technology for use with ultrasound beamforming due to its small size, low power, and small time-delay quantization. In addition, sigma-delta conversion offers a trade-off between bandwidth and dynamic range that closely matches the needs of ultrasonic imaging in different modes. However, dynamic receive beamforming commonly used in ultrasonic imaging disrupts the spectral shaping of quantization noise and causes a significant degradation in in-band signal-to-quantization-noise ratio (SQNR). This issue has been the subject of several symposium papers and patents in recent years.

Statement of Contribution/Methods

A new signal processing architecture was developed to address this issue. After mixing to baseband and sigma-delta conversion, element signals are dynamically decimated by a comb filter (a type of FIR filter) under the control of dynamic receive delays. The dynamic receive delays cause signals to be stretched by varying amounts depending on the receive F-number. By treating dynamic decimation as stretching the signal through sample repetition at the sigma-delta sampling rate followed by a uniform decimation, we examined the in-band SQNR as a function of the oversampling ratio, the receive F-number, and the nominal decimation rate based on the new architecture.

Results

For 2nd order single-bit low-pass sigma-delta conversion, the in-band SQNR at various processing stages have been simulated assuming a realistic Gaussian signal with normalized rms amplitude 0.15, and the results are tabulated below. The standard deviation of these SQNR values is about 0.5 dB. For decimation by 8 and 16, third-order comb filters require 22 and 46 taps, respectively.

Discussion and Conclusions

As shown above, direct sample repetition causes a significant degradation of in-band SQNR. With comb filtering, the SQNR degradation due to dynamic receive focusing is much reduced. For a higher oversampling ratio (or a narrower signal bandwidth), a longer comb filter is required to maintain the SQNR. The presented architecture provides a simple and effective solution to the dynamic receive artifacts associated with sigma-delta conversion.

In-band SQNR Under Various Conditions

Oversampling ratio	32			128			
SQNR after sigma-delta conversion	37.7			67.6			(dB)
Rx Fnum	1	2	∞	1	2	∞	
Maximum signal stretch rate	6.3%	1.6%	0	6.3%	1.6%	0	
Direct sample repetition	10.8	16.2	37.7	16.8	22.4	67.6	(dB)
Repetition after comb & deci by 8	35.4	37.5	38.6	45.7	51.9	67.7	(dB)
Repetition after comb & deci by 16	39.7	40.1	40.3	61.6	62.3	67.8	(dB)

P1B034-07

A Simple Method That Can Compensate the Refraction of the Array Transducer Lens

Moo-Ho Bae[1], Han-Woo Lee[2], Sung Bae Park[1], Ra-Young Yoon[2], Jeong-Ho Ham[2], Se Hoon Chang[1], Dae Young Kim[1], Mok-Kun Jeong[3], Yung-Gil Kim[2], *[1]Hallym Univ., Department of Electronic Engineering, Korea, Republic of, [2]Medison Co. LTD., Korea, Republic of, [3]Daejin Univ., Korea, Republic of.*

Background, Motivation and Objective

A fixed acoustic lens is often employed for elevation focusing of the one dimensional array transducer which is widely used in the diagnostic ultrasound scanner. This lens generates refraction in the lateral direction. If this is not properly considered in the beamformer, main-lobe width will be widen and side-lobe level will be heighten, as a result, performance is considerably degraded. However, real time calculation of time delay is quite difficult so that pre-calculated look-up table method is generally used. However, in the design of the low cost portable scanner, such method is still in the burden. In this paper, a practical solution which uses conventional focusing delay calculation algorithm in the free space is derived and precise approximation of the refraction is attempted by adjusting the parameters of input variables of the algorithm.

Statement of Contribution/Methods

Two cases with a linear array transducer and a convex array transducer are examined by using both PZFLEX and ray tracing simulation. With ignorance of the influence of the lens, degradation of beam characteristics and error of the focusing delay is measured and attempts are made to identify the input variable of the focusing delay algorithm in free space for a simple approximation.

Results

For a linear array transducer, center frequency = 6.5MHz, 128 elements, pitch = 0.3mm, lens sound speed=980m/sec and maximum lens thickness = 1.067 mm is considered. If lens is ignored, for example, in the case of f number=1 with focal length z=20mm, focusing delay error of the out most element is 49.3ns and if lens does not exist, one-way CW Full-width-Half-Maximum[FWHM] beam width become 0.18mm, if lens exists but is ignored, FWHM beam width is increased to 0.45mm. To compensate the influence of the lens, axial position of the element is assumed to advance 0.25mm. As a result, focusing delay peak error is reduced to 5ns and RMS error is reduced to0.6n] with f number=1 and focal length z=2~80mm showing beam width approaches to the ideal case.

For a convex array transducer, center frequency = 6.5MHz, 192 elements, view angle = 148.9degree, element surface radius = 10mm, lens surface radius = 10.635mm, lens sound speed=1000m/s is considered. It is assumed that lens surface radius is little larger than actual one and calculation result of the free space focusing delay shows very similar to lens refraction considered actual case. When element surface radius is assumed to 10.29mm, with f number = 1 and focal length z=0~100mm, peak error of the focusing delay reduced to 6.5ns and RMS is reduced to 3.3ns. Beam width also approaches to the ideal case.

Discussion and Conclusions

Influence of the acoustic lens for elevation focusing cannot be ignored even though a sizable computation or a huge look-up table is required for real time operation. In this paper, it is shown that actual focusing delay can be precisely approximated only with simple manipulation of the variables of the free space focusing delay computation algorithm.

P1B035-08

Ultrasound Breast Imaging Technique Using Two Opposing Array Transducers

Mok Kun Jeong[1], Sung Jae Kwon[2], Sung Min Cho[2], Moo Ho Bae[3], Young Gil Kim[4], *[1]Daejin University, Electronics, Pocheon, Kyeonggi, Korea, Republic of, [2]Daejin University, Korea, Republic of, [3]Hallym University, Korea, Republic of, [4]Medison Co. LTD., Korea, Republic of.*

Background, Motivation and Objective

Although mammography is widely being used in the diagnosis of breast cancers, it has a radiation hazard. In order to cope with the low resolution problem of medical ultrasonic imaging, speed of sound and attenuation imaging can be used complementarily with B-mode imaging. We propose a new method for imaging protruding objects such as the human breast with two opposing linear array transducers.

Statement of Contribution/Methods

The objective is to image tissue interposed between two linear array transducers that are facing each other. We obtain two B-mode images from both array transducers and construct a compound image with reduced speckle noise and artifacts such as shadowing and reverberation. An added benefit of the method is that data can be acquired in transmission mode by transmitting with one array and receiving with the other array and vice versa, making it possible to construct images of attenuation and speed of sound with data acquired over a limited angle range.

Results

Experiments were conducted on a 40-mm thick phantom containing 7-mm diameter cylinder whose speed of sound is different from that of the background, and compound images as well as speed of sound images were constructed. The two array transducers connected to a clinical ultrasound scanner (Accuvix, Medison, Seoul, Korea) were separated by a distance of 40 mm, and a phantom was placed between them. Compound images were constructed using RF data acquired from each direction. The images were found to reduce speckle and dependence on insonation angle at all imaging depths compared to those from a single linear transducer array. To construct speed of sound images, the two array transducers were interfaced to a switchboard where any element in one array transducer can be selected for use as a transmitter while any element in the other array transducer can be used as a receiver. The time of flight was measured in transmission mode for every combination of transmit and receive elements, and speed of sound images were constructed from data available over a limited range of transmit and receive angles. We were able to identify the cylinders whose speed of sound was different from that of the background from both compound and speed of sound images.

Discussion and Conclusions

We present a new method of imaging breast by interposing it with two opposing array transducers. By constructing compound, as well as speed of sound, images on a phantom, and attenuation images using the method, the feasibility of in vivo breast imaging with improved diagnostic capability was demonstrated.

P1B036-09

Evaluation of aberration parameters estimated from a low frequency transmission for medical acoustic imaging

Hirofumi Taki[1], Tetsuya Matsuda[1], **Toru Sato[2];** *[1]Kyoto University, Department of Systems Science Biomedical Engineering, Graduate School of Informatics, Kyoto, Kyoto, Japan, [2]Kyoto University, Department of Communications and Computer Engineering, Graduate School of Informatics, Kyoto, Kyoto, Japan.*

Background, Motivation and Objective

One of the major causes to deteriorate the medical acoustic imaging quality is phase aberration occurred from the distortion of the medium. Several algorithms have been proposed for aberration correction; however, it remains technological challenges. For aberration correction, many medical acoustic imagers employ the time delay estimation based on the correlation between waveforms at two observation points. In this study, we evaluate the accuracy of the time delay estimation corresponds to the transmit frequency utilizing the normalized cross correlation.

Statement of Contribution/Methods

We employ a low transmit frequency in order to increase the similarity of the speckle signals received at two array elements for the accurate estimation of the aberration parameters. The aberration parameters estimated from the low transmit frequency is applied to the high transmit frequency event to acquire the acoustic image with high spatial resolution.

Results

To evaluate the accuracy of the time delay estimation, we use a simulated digital tissue map with the skin of 2mm in thick, the subcutaneous fat layer of 2cm in thick, and muscle under the subcutaneous fat layer. Minute fat droplets are distributed over the muscle layer, and account for 5 percent of the layer. In this study we investigate the transmit beam patterns utilizing Spectral Flex, a computer simulation tool based on the pseudo-spectral method. We estimate the time delays for aberration correction from the received signals when transmit frequency is 1, 2 and

4MHz. We set the difference between time delays of adjacent array elements less than one half of the wavelength in order to remove false peaks, the selection among false correlation peaks. Figure shows the 4MHz transmit frequency beam patterns employing the three time delay values mentioned above. The half power width and peak sidelobe level of the three transmit beam patterns employing 1, 2 and 4MHz for aberration correction are 1.83, 3.53, 2.63mm and -9.15, -3.18, -2.75dB, respectively.

Discussion and Conclusions

When the echo data consists of speckle signals from randomly distributed scatters without a beacon signal, the echo data of low transmit frequency can estimate the accurate time delay for aberration correction, and the high transmit frequency imaging using the time delay estimated from low frequency echo data improves the focusing quality under the distortion propagation.

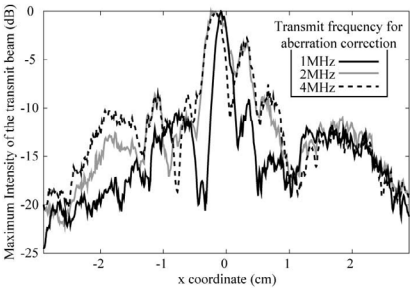

P1B037-10

Abersim: a Simulation Program for 3D Nonlinear Acoustic Wave Propagation for Arbitrary Pulses and Transducer Geometries

Halvard Kaupang[1], **Martijn Frijlink[1],** Trond Varslot[2], Svein-Erik Måsøy[1]; *[1]NTNU Norwegian University of Science and Technology, Department of Circulation and Medical Imaging, Trondheim, Norway, [2]Australian National University, Department of Applied Mathematics, Canberra, Australia.*

Background, Motivation and Objective

Abersim is a toolkit for simulating 3D nonlinear acoustic wave propagation through an attenuating medium. It has a MATLAB interface, which enables the use of MATLAB for visualization, pre- and post processing. The core routines have been implemented in C for efficiency, and to take advantage of MPI parallel computing resources. Abersim may be downloaded from www.ntnu.no/abersim.

Software for simulating nonlinear directional wave propagation using the parabolic approximation is already available. The parabolic approximation refers to an approximation in the diffraction term, leading to the KZK equation. Abersim avoids this approximation. By operator splitting, the forward-propagating part of the diffraction term is solved using a retarded time and the angular spectrum method. Optionally, for axisymmetric cases, the parabolic approximation can be used in combination with an FDTD solution. The attenuation term is solved for power law absorption of the form a*f^b with arbitrary choices of a and b.

Abersim has previously been validated through comparison of 2D simulations to analytic solutions, a numerical solution to the full wave equation and experimental measurements in water [1]. This study compares the 2D and 3D diffraction and absorption of the linear part of Abersim to results obtained from Field II [2].

Statement of Contribution/Methods

Linear simulations with Abersim, where the nonlinear term was not taken into account, were performed and compared to Field II simulations. 3D simulations for both axisymmetric and array transducers calculated the wave propagation for various excitation pulses (f_c = 2 MHz) through different homogeneous media. Diffraction and attenuation were compared by means of pulse shapes, beam profiles and side lobe levels.

Results

Spatial and temporal sampling determined the accuracy and calculation time for both Abersim and Field II. Both simulation tools gave similar results for linearly propagated waves. For example, an axisymmetric source (diameter of 19 mm, f-number of 3.2) excited with a Gaussian enveloped sine pulse (50% fractional bandwidth) in a lossless medium, resulted in axial beam profiles that differed <0.5 dB.

Another example of 3D wave propagation of a 20%-bandwidth pulse from a 64-element array transducer (aperture of 18.6 x 13 mm, elevation and azimuth focus at 60 mm) in an attenuating medium (0.5dB/cm/MHz), resulted in almost identical pulse shapes and beam profiles for Abersim and Field II. The differences in energy levels of the main and side lobes at focus were <0.15 dB.

Discussion and Conclusions

The attenuation and diffraction parts of the 3D nonlinear simulation program Abersim showed to give very similar results to Field II for arbitrary source geometries and various pulses. The available implementation could be a useful tool in nonlinear acoustics.

[1] T. Varslot and G. Taraldsen, IEEE Trans on UFFC, 52(9):1473-1482,2005.

[2] J. A. Jensen and N. B. Svendsen, IEEE Trans on UFFC, 39(2):262-267,1992.

Monday Poster

P1B038-11

Determination of Temporal Bone Isoplanatic Patch Sizes for Transcranial Phase Aberration Correction

Francois Vignon[1], **William Shi[1],** Jeffry Powers[2]; [1]*Philips Research North America, Briarcliff Manor, NY, USA,* [2]*Philips Healthcare, Bothell, WA, USA.*

Background, Motivation and Objective

Phase aberration is a leading cause of transcranial ultrasound image degradation. For realignment of aberrated per-element signals, a delay map corresponding to the aberrator is often computed from signals backscattered from a region of interest (ROI) in the imaged medium. However, such a map is only effective for correcting the aberration in a limited area, called the Isoplanatic Patch (IP), around the ROI. For the purpose of transcranial aberration correction, the IP size through the temporal bone window is investigated.

Statement of Contribution/Methods

A reflective phantom made of 8 wires distributed on a 77° sector of 8 cm radius and a 9th wire placed centrally 1 cm shallower, is imaged at a central frequency of 3.2 MHz using a two-dimensional probe (Philips X7-2) through an aperture of ~1x1 cm^2 on each of 12 *ex vivo* human temporal bone samples. A thin slice of *ex vivo* beef muscle (~0.5 cm) is placed between each skull sample and the probe to mimick extracranial soft tissues. The probe placement is adjusted until obtaining the best possible transtemporal image of the wires (Fig. 1a). A delay map is estimated from signals from the central wire with a correlation-based algorithm, and the aberration is corrected in receive on all imaging beams with that same delay map. The brightness of each wire is compared before and after correction to estimate the angular extent of the IP. In addition, a healthy male volunteer is scanned transtemporally at 2.4 MHz with a one-dimensional probe (Philips S5-1). A delay map is estimated from signals from an ROI in the brain with a correlation based method and used to correct phase aberration in receive. Speckle brightness is compared before and after correction to estimate the size of the IP.

Results

Fig. 1b shows the wires' brightness improvement (mean ± standard deviation) as a function of their angular distance to the central wire in the phantom experiments. The mean IP size is 36°, standard deviation 18°. The in vivo experiment showed that the IP is large in depth (>10cm), but limited angularly (<23°).

Discussion and Conclusions

Phase aberration correction with a single delay map is effective for transcranial ultrasound applications that require focusing in a limited angular field of view (Doppler, zoom). A regular sector (~90°) imaging requires multiple delay maps for different steering directions.

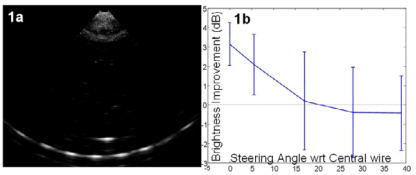

P1C. Medical Imaging

2nd and 3rd Floor Foyers

Monday, November 3, 2008, 3:00 pm - 4:30 pm

Chair: **Olivier Basset;**
CREATIS, Université Lyon I, France.

P1C039-01

Influence of the transducer geometry on the phase of the second harmonic reduction signal

Mirza Pasovic[1], **Olivier Basset[1],** Guillaume Matte[2], Antonius F.W. van der Steen[2], Nico de Jong[2], Christian Cachard[1]; *[1]Université de Lyon, INSA-LYON, Université Lyon 1, CRNS 5220, INSERM U630, CREATIS-LRMN, Villeurbanne, Rhone-Alpe, France, [2]ErasmusMC, Thorax centre, Biomedical Engineering, Rotterdam, Holland, Netherlands.*

Background, Motivation and Objective

Ultrasound contrast harmonic imaging is one of the most used contrast detection method in common system used for diagnostic. Its success comes from the higher non linearity of bubbles compared to tissue. A way further enhance contrast to tissue ratio would be to suppress locally second harmonic due to non linear propagation in tissue. Reducing higher harmonics from surrounding medium is a challenge that has been previously studied by others. Christopher (IEEE-UFFC, 1999) proposed to transmit inverted replica of back propagated signal, Krishnan (IEEE-UFFC-1998, 1997) back propagated only second harmonic and added inverted replica of it to excitation, Shen (IEEE-UFFC, 2007) proposed transmitting third harmonic to reduce the second harmonic. All of the methods are limited by need of broad band transducers and reduction of only one single component of second harmonic band. In our study, a custom made dual frequency phased array transducer (Bouakaz IEEE-UFFC 2003, Bouakaz PMB 2004) is used to transmit 2 different signals: the imaging signal and the Second Harmonic Reduction Signal (SHRS). In this paper we study the optimal phase of SHRS to achieve a maximum second harmonic frequency reduction in a region of interest depending upon the several properties of transducer apertures.

Statement of Contribution/Methods

Our work is concentrated on the phase of the SHRS, and how the dimensions of the probe (width, height, kerf, pitch) and propagating distance influences the phase needed to achieve the reduction of the second harmonic. In simulations, a KZK simulator (Voormolen, 2007) for rectangular transducers allowed defining different probe dimensions. In these simulations, influence of medium properties and excitation pressure were also investigated. Water tank experiments were done using a needle hydrophone, a programmable ultrasound scanning system, which has possibility to set different frequency and phase of the electrical excitation signals on each element and custom made ultrasound probe constructed of interleaved low frequency and high frequency elements.

Results

The relation between the probe geometry and the phase of SHRS has been validated with simulation and experimental measurements. Probe dimension were: width 22 mm, height 13 mm, 50 microns kerf, 250 microns pitch and 88 interleaved elements. Excitation frequency is 1 MHz and SHRS frequency is 2 MHz. The simulation showed that for this probe, phase of SHRS should be 42°, measurements showed an optimal reduction at 45°. A 30dB reduction of second harmonic was achieved.

Discussion and Conclusions

Size and number of active elements, influence value of SHRS phase to obtain an optimal reduction of second harmonic. Nonlinearity of the medium, density and speed of sound had no influence on the phase of SHRS. This work shows that the probe geometry and then the diffraction are of main importance for finding the optimal SHRS phase.

P1C040-02

Motion detection in ultrasound image-sequence using tensor voting

Shuqiang Guo, Honghui Han, Masafumi Inba, Yasutaka Tamura, Hirotaka Yanagida; *Yamagata University, Graduate School of Science and Engineering, Japan.*

Background, Motivation and Objective

In my laboratory,a high-speed ultrasound imaging system have been developed. The system adopts synthetic aperture focusing techniques and short duration coded signals to realize high-speed data acquisition. However, many artifacts appear in the reconstructed image sequence because of the incompleteness of the transmitted code and insufficient number of array elements. We examined the application of the tensor voting for stable motion detection and artifact reduction in synthetic aperture focusing technique.

Statement of Contribution/Methods

The geometry of the array and the imaging space are shown in Fig.1 , The local feature structure in spatio-temporal space is extracted using the tensor voting technique. In this research, the tensor voting in 3-dimensional space of **x,z,t** are carried out to each x-z cross-sectional image. Tensors are calculated from the gradient vectors in the space, and enhanced by the voting. The eigenvalues and the eigenvectors of the obtained tensors are calculated. The velocity component along the z-axis,Vz,is estimated by the equation,Vz=-Elt/Elz,where Elt,Elz are components of the eigenvector along t and z axis,respectively.

Results

A simulation assuming 2MHz, 32 transmitters and 32 receivers was carried out. The velocity of a single point target was estimated with relative error of 10% in 100 m/s velocity range for 0.5 ms transmission intervals. Fig.2 shows the images of the same object using conventional and enhanced image using the values obtained by tensor voting.

Discussion and Conclusions

The future enhanced image was obtained using values obtained by tensor voting in spatio-temporal space. The ability of velocity estimation of the object was confirmed by the simulation. The level of artifacts were reduced in the future enhanced image obtained by tensor voting.

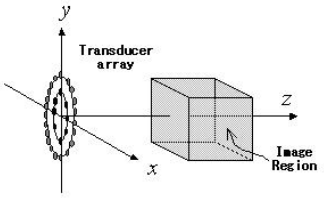

Fig.1 Geometry of the array and the imaging space

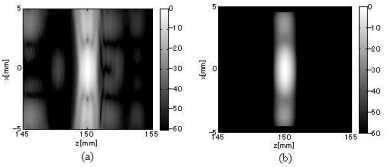

Fig.2 (a): Image obtained by conventional method for point objects
(b): Future enhanced image obtained by tensor voting

P1C041-03

Two approaches for tomographic density imaging using inverse scattering

Roberto Lavarello, Michael Oelze; *University of Illinois at Urbana-Champaign, USA.*

Background, Motivation and Objective

Inverse scattering is one of the most robust acoustic tomography methods, allowing for the reconstruction of quantitative images of acoustic parameters. Most acoustic tomography methods neglect density variations in order to obtain speed of sound and attenuation profiles. However, density may also contain useful information or provide additional sources of image contrast. In this work, two approaches for density imaging using inverse scattering were explored through simulations in order to evaluate the feasibility of density imaging for practical experimental applications.

Statement of Contribution/Methods

The first method for density imaging consisted of inverting the wave equation by solving for a single functional that depended on both speed of sound and density variations. The distorted Born iterative method (DBIM) was used to obtain the functional using single frequency data. Density and speed of sound profiles were separated by

combining DBIM reconstructions at two or more frequencies (MF-DBIM approach). The second method consisted of solving for two functionals simultaneously: one that depended only on compressibility and one that depended only on density variations. A T-matrix approach was used to relate these functionals to the scattered data. For all cases, the analytic solution for scattering by concentric circular cylinders was used to generate the synthetic measurements.

Results

The MF-DBIM approach allowed separation of density and speed of sound profiles at high SNR values and less than an order of magnitude between the largest and smallest frequencies used. However, even with the use of total variation regularization, relative root mean square error (RRMSE) values in excess of 45% in density contrast were obtained at an SNR of 26 dB. When using the T-matrix approach and single frequency data to reconstruct homogeneous cylinders, convergence of density and compressibility reconstructions to their correct values was not guaranteed, but the speed of sound was correctly reconstructed. An expression to predict the reconstructed density for a given speed of sound contrast was derived and validated. The T-matrix approach converged when multiple frequency data and frequency hopping was used, but required to have a ka product smaller than one at the lowest frequency. The T-matrix approach was found to be less sensitive to noise and termination tolerance than the MF-DBIM approach, and resulted in density reconstructions with RRMSE values around 25% with SNR values of 26 dB.

Discussion and Conclusions

In this work, the limiting factors for two density imaging approaches were determined. The MF-DBIM requires a very high SNR to obtain reliable quantitative reconstructions, while the T-matrix approach requires excessively large bandwidths when imaging large targets. These limitations will serve as reference points for further algorithmic improvements required for practical implementation of density imaging on ultrasound tomographic systems.

P1C042-04

Spectroscopic Imaging of Nano-particle Distribution in Biological Tissue Using Optically Assisted Ultrasonic Velocity-Change Detection

Sunsuke Kawakami, Satoshi Ishibashi, Naoki Nakamura, Takashi Mukaiyama, Tetsuya Matsuyama, Kenji Wada, Toshiyuki Matsunaka, Kenji Kono, Hiromichi Horinaka; *Osaka Prefecture Univ., Japan.*

Background, Motivation and Objective

In recent years, there has been extensive research related to the application of nano-particles in medical diagnostics and treatment. This is because they have function as markers of liposomes and dendrimers for transporting drugs or photo-thermal materials. We already succeeded in imaging the distribution of Au nano-particles in highly scattering medium using the optically assisted ultrasonic velocity-change detection method.

For practical application to biological tissue, we intended to obtain the ultrasonic velocity change images of biological tissue phantom under light illumination with various wavelengths.

Statement of Contribution/Methods

A phantom was made of the chicken meat including Au nano-rods inside. The light was guided by the optical fiber around the ultrasonic array transducer to illuminate the phantom. The Nd: YVO4 second harmonics laser (532nm), Ti: sapphire laser (740-840nm) and the laser diode (912nm) were used as light sources. The echo pulse waveforms through the array transducer connected to the equipment were stored in a personal computer. The ultrasonic velocity change images were constructed from the time shift of echo pulse waveforms measured before and after light illumination.

Results

It was difficult to show the nano-particle distribution in the phantom by normal B-mode. In contrast, ultrasonic velocity change images showed the nano-particle distribution and temperature change due to the optical absorption. Fig.1 shows the ultrasonic velocity change images which correspond to illumination at 740nm, 800nm and 912nm, individually. Closed circles show the temperature change which was obtained from ultrasonic velocity change measured by light illumination with various wavelengths. The solid line shows the optical-absorption spectrum of Au nano-rods measured by ordinary spectroscopy. Temperature change by illumination well corresponds with the optical absorption spectrum.

Discussion and Conclusions

We obtained the optical absorption spectrum information of Au nano-rods in the chicken meat by the optically assisted ultrasonic velocity-change detection method. Experimental results show that our method has the potential to apply to the spectroscopic imaging for identification of nano-particles in biological tissue.

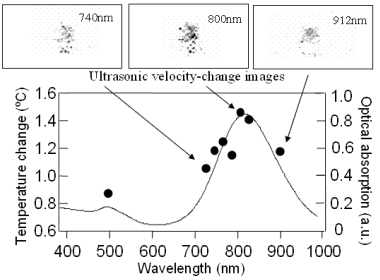

Fig.1Spectrum information of Au nanorod in chicken meat measured by the optically assisted ultrasonic velocity-change imaging method.

P1C043-05

Attenuation Measurements for Ultrasonic Breast Imaging: Comparisons of Three Approaches

Chen-Han Chang, Sheng-Wen Huang, Pai-Chi Li; *National Taiwan University, Taipei, Taiwan.*

Background, Motivation and Objective

Various approaches have been proposed to identify malignant breast tumors using ultrasound. In this study, we implement three different approaches and compare their performance based on phantom imaging. The three approaches are: spectral estimation using periodogram (PER), limited angle tomography (LAT) and minimum side difference (MSD). Note that all three approaches are based on attenuation measurements and can breadily implemented using current B-mode imaging setup.

Statement of Contribution/Methods

First, PER is implemented by estimating the center frequency using the periodogram of A-line data. Averaged PER can also be used to reduce estimation variance. Second, LAT is based on an approach that we previously proposed for reconstructing the attenuation coefficient distribution in the breast using a linear array. An additional metal plate at the bottom of the image needs to be used as a reflector to provide tomography data. Finally, MSD is calculated using gray-level values of areas posterior to the region of interest (ROI), and left and right posterior to the ROI. The imaging setup consists of a 5-MHz 128-channel linear array, a programmable digital array system and a breast phantom. The phantom is custom-built by Dr. Ernest Madsen (Department of Medical Physics, University of Wisconsin-Madison, MI). It contains materials mimicking the following breast tissues: glandular tissue, fat, cysts and tumors.

Results

Results of phantom experiments are shown in Table 1. Both PER and LAT provide reasonable estimation results. As for MSD, for fat cases, the values are from -1.52 to 2.57 dB. For cyst cases, the values are 0.43 and 2.72 dB. For tumor cases, the values are from -8.58 to -5.66 dB.

Discussion and Conclusions

Although both PER and LAT provide reasonable estimation results, PER generally suffers from large variance particularly when ROI is small. This is because in this case there are only a limited number of data samples to be used for spectral estimation. For LAT, on the other hand, a small ROI can actually benefit estimation because the limited angle problem becomes less severe (i.e., the angular extent for the data going through the ROI becomes larger). For MSD, although results generally spread over a wide range, but simple thresholding can still be applied to distinguish different tissue types. This indicates that MSD can be used as an important feature in computer aided diagnosis.

Table 1. Phantom results: comparing PER with LAT (AC: attenuation coefficient).			
ROI type	True AC (dB/cm/MHz)	PER AC (dB/cm/MHz)	LAT (dB/cm/MHz)
Tumor	1.47	1.44	1.73
Cyst	0.16	0.07	0.07
Fat	0.44	0.62	0.31
Glandular tissue	0.55	0.54	0.55

P1C044-06

Comparison of regularization methods for 2D myocardial strain estimation in the mouse

Florence Kremer[1], Hon Fai Choi[1], Stian Langeland[2], Emiliano D'Agostino[3], Piet Claus[1], Jan D'hooge[1]; *[1]Katholieke Universiteit Leuven, Imaging and Cardiovascular Dynamics, Department of Cardiovascular Diseases, Belgium, [2]GE Vingmed, Horten, Norway, [3]Medical Image Computing, Department of Electrical Engineering (ESAT), Katholieke Universiteit Leuven, Belgium.*

Background, Motivation and Objective

Myocardial strain assessment in the mouse using real time imaging at a frame rate of 300Hz based on speckle tracking has been shown feasible. It remains however challenging given the low frame rate to heart rate ratio, leading to significant de-correlation noise between subsequent image frames. In that context, regularization plays an important role. In literature, multiple methods have been proposed. The aim of this study was thus to compare the impact of different geometrical regularizers on the accuracy of the 2D strain estimation in the mouse heart.

Statement of Contribution/Methods

A kinematic model of the murine heart with a short-axis of 2.5mm, a long axis of 8mm and a wall thickness of 1mm, simulating 15° torsion, 60% EF and a heart rate of 570bpm was used. Short axis ultrasound images with realistic properties at the middle of the heart were simulated using a convolution model. This procedure was repeated 5 times to obtain 5 independent data sets.

The motion between subsequent frames was initially estimated on the RF data using a 2D kernel of [0.5 λ, 2.5 λ], with λ the wavelength, 50% overlap, and the sum-of-squared-difference as a similarity measure. From end-diastole until end-systole, the motion between successive image pairs was regularized and subsequently cumulated. As a quality measure, the obtained ES displacements were compared to the ground truth and expressed in terms of SSD for all myocardial points.

Different geometrical regularizers were used, forcing the motion across the wall to behave either linearly, as a quadratic curve, as a plane (with 1°, 2° or 3° length) or with limited spatial curvature. The statistical analysis was performed using ANOVA.

Results

All regularization methods improved the motion assessment ($p < 0.05$). Differences between regularizers are shown in Table 1.

Discussion and Conclusions

In this work, six different regularizers were compared for the evaluation of the displacement in the mouse heart. Linear and planar regularizers did not differ significantly, whereas the quadratic regularizer was clearly worse. Conversely, the curvature method showed a tendency to estimate displacement more robustly, although this did not reach statistical significance.

Table 1: SSD with respect to ground truth

Axial Motion	Nothing	Linear	Quad.	Plan 1°	Plan 2°	Plan 3°	Curv.
Mean	8.812	5.624	6.508†	5.591	5.574	5.448	5.087*
SD	0.585	0.503	0.547	0.507	0.538	0.526	0.735
Lateral Motion	**Nothing**	**Linear**	**Quad.**	**Plan 1°**	**Plan 2°**	**Plan 3°**	**Curv.**
Mean	20.729	13.737	15.543†	13.676	13.574	13.447	11.997*
SD	0.507	1.263	0.879	1.291	1.277	1.307	1.334

†Significantly different from curvature regularization

*Significantly different from quadratic regularization

P1C045-07

Feasibility of non-linear simulation for Field II using an angular spectrum approach

Yigang Du, Jørgen Arendt Jensen; *Technical University of Denmark, Center for Fast Ultrasound Imaging, Lyngby, Denmark.*

Background, Motivation and Objective

The simulation of non-linear fields is most often restricted to single element, circularly symmetric sources, which are not used in clinical scanning. To obtain a general and valuable simulation array transducers of any geometry with any excitation, focusing and apodization should be modeled. Field II is restricted to simulate these for the linear case and the purpose of this paper is to develop a general frame work for extending it to non-linear simulation.

Statement of Contribution/Methods

The extension to the non-linear domain is made by using the angular spectrum approach (ASA), where the field is calculated in a plane close to the transducer surface. This calculation is performed using Field II and, thus, includes modeling array transducers of any geometry with any excitation, focusing and apodization. The propagation in the linear or non-linear medium is then performed using the angular spectrum approach. The first step in deriving this procedure is to find the accuracy of the approach for linear propagation, where the result can be validated using Field II simulations. The ASA calculations are carried out by 3D fast Fourier transform using Matlab, where lambda/2 is chosen as the spatial sampling rate to reduce aliasing errors. Zero-padding is applied to enlarge the source plane to a (4N-1)×(4N-1) matrix to overcome artifacts in terms of the circular convolution. The source plane with N=61 samples along both side, is 0.05mm away from a 5 MHz planar piston transducer, which is simulated by Field II.

Results

To determine the accuracy, different sampling intervals and zero-paddings are compared and the errors are calculated with Field II as a reference. The results are shown in the table below.

Discussion and Conclusions

It can be seen that zero-padding and lambda/2 sampling improve the results and the price of an increase in computation time. The angular spectrum approach in combination with Field II opens for the possibility of simulating the non-linear acoustic propagation for any kind of array transducers.

mean errors	sampling interval	zero-padding 2N-1	4N-1	6N-1	8N-1	10N-1
near field (z=10mm)	lambda/2	25.68%	12.85%	10.39%	9.81%	10.09%
	lambda/4	14.63%	11.95%	9.55%	9.67%	9.50%
far field (z=100mm)	lambda/2	18.07%	5.79%	4.18%	4.07%	1.62%
	lambda/4	17.49%	6.23%	2.87%	3.23%	3.84%

P1C046-08

Comparison of the performance of different tools for fast simulation of ultrasound data

Hang Gao[1], Torbjorn Hergum[2], Hans Torp[2], Jan D'hooge[1]; *[1]Catholic University of Leuven, Cardiovascular Diseases, Leuven, Belgium, [2]Norwegian University of Science and Technology, Circulation and Medical Imaging, Trondheim, Norway.*

Background, Motivation and Objective

Simulation of ultrasound data is often performed for developing new ultrasound data processing techniques. The spatial impulse response method (as implemented in FieldII) has typically been used as the 'gold standard' due to excellent accuracy in the linear domain. When scatterer numbers become significant and when 3D volumetric data sets need to be computed, calculation times can become an issue. In order to solve this problem, two alternative methods have recently been proposed both of which are based on the principle of convolving a set of point scatterers with a point spread function. "FUSK" operates in the frequency domain while "COLE" runs in the spatio-temporal domain. The aim of this study was to compare both methodologies in terms of accuracy and processing speed using FieldII as a reference.

Statement of Contribution/Methods

A phantom (70x20mm) containing 3 cystic regions was generated 10 times at different scatterer densities (10-100-500 mm3) resulting in a total of 30 phantoms. Each phantom was scanned using FieldII, FUSK and COLE using

identical ultrasound system settings. In order to describe the accuracy of the resulting images, the root-mean-squared-error (RMS) was calculated locally (mask 11x11 pixels) using the FieldII images as ground truth. Subsequently, an average RMS was extracted in 5 equally sized layers across the phantom to look for depth-dependency of the result. A two-way ANOVA was used for statistical comparison using 'method' and 'depth' as co-factors. Finally, 10 homogeneous phantoms were generated with scatterer density well above the limit for Rayleigh scattering. The sum-of-squared-residuals (SSR) between the measured histogram of the resulting images and its Rayleigh fit was calculated.

Results

There was no significant difference in average RMS for FUSK and COLE (24.04±6.93 vs. 23.54±7.58 (p = NS)). ANOVA showed a significant depth dependency of the accuracy of both methods but this dependency was not method-dependent (no interaction). SSR for Rayleigh fitting the gray scale histogram was significantly smaller ($p<0.05$) for COLE (1.3±0.2 vs. 1.8±0.5). Average processing times are listed in the table below.

Discussion and Conclusions

Both convolution based simulation tools showed similar accuracy as expressed by regional RMS error but at 100 to 1000 times less computation time than the reference method.

Mean CPU time (s)	Density 10/mm3	Density 100/mm3	Density 500/mm3
COLE	1.0	9.7	47.7
FUSK	9.4	30.2	122.3
FieldII	990	10860	52200

Table: Average calculation time per phantom expressed in seconds of CPU time

Monday Poster

P1C047-09

Estimating Frequency Depentdent Attenuation to Improve Gain Distribution in B-mode Imaging

Sten Roar Snare, Hans Torp; *Norwegian Uiversity of Science and Technology (NTNU), Department of Circulation and Medical Imaging, Trondheim, Norway.*

Background, Motivation and Objective

The last decade, there has been a trend to make smaller ultrasound equipment. For the pocket size scanners, say Acuson P10, there is no space for all the buttons and sliders found on full-size scanners. Automatic setting of gain is of utmost importance. This work presents a method for estimating frequency dependent attenuation as a step in improved setting of time gain compensation (TGC). Most TGC algorithms work with envelope detected data. Thus, they may introduce artifacts and hide useful clinical information. This method attacks the problem from a signal processing view. It is based on linear acoustics and signal processing tehniques applied to radio frequency (RF) data. First, a frequency estimator is applied to the received RF data. The estimated frequency spectrum is then corrected for scattering, diffraction and the probe transfer function. The resulting power spectrum is used for estimation of the frequency dependent attenuation. Previuous work has used the attenuation estimate for tissue characterisation, in order to detect pathology. Here, it is used for improving TGC.

Statement of Contribution/Methods

After derivation of the algorithm, the method is verified by simulation (Field) and phantom experiments. The transducer is a conventional phased linear array transducer (GE Vingmed M3S) using a broadband transmit pulse with center frequency of 2.2MHz. The recordings are done on a CIRS40 (CIRSINC) tissue mimicking phantom. We estimate the frequency downshift with depth using AR spectrum estimators of first and second order. We compensate for the diffraction effect by a modified method earlier used in tissue characterisation. The scattering from tissue is assumed to behave as isotropic Rayleigh scattering. The downshift is estimated by looking at the centroid of the diffraction corrected spectrum estimates. The attenuation estimates is used to improve the gain distribution in the image.

Results

We will present estimates of the frequency dependent attenuation from a CIRS40 phantom together with Field simulations. We show how AR models can be used for this estimation, and illustrate the importance of using diffraction correction. Frequency estimators in B-mode imaging tend to suffer from high variance. A first order AR estimator Hamming windowed over 1.14° and 7.4mm, gives a standard deviation for the estimate in speckle of 5.74e^4 [Hz] or 2.3% of transmit frequency. This is a drawback for tissue characterisation. In gain algorithms, the lateral resolution is of less importance, and lateral averaging can be increased to reduce variance.

Discussion and Conclusions

Based on the experiments, we will conclude on whether estimation of the frequency dependent attenuation is a feasible way to improve automatic gain setting. This method make use of frequency information to improve display of amplitude data. It constitutes an alternative way of applying tissue characterisation methods to improve "Auto focus" features on modern ultrasound scanners.

P1C048-10

Analysis of the Difference-frequency Wave Generated by the Interaction of Two Axisymmetric and Co-focused Ultrasound Beams

Glauber Silva[1], Farid Mitri[2], Mostafa Fatemi[2]; [1]*Instituto de Matemática Pura e Aplicada, Laboratory of Fluid Dynamics, Rio de Janeiro, RJ, Brazil,* [2]*Mayo Clinic College of Medicine, Department of Physiology and Biomedical Engineering, Rochester, MN, USA.*

Background, Motivation and Objective

This study investigates the propagation and interaction of two concentric co-focused ultrasound beams at different frequencies in the presence of an inclusion inside the focal region. Interaction of the two primary ultrasound beams gives rise to an acoustic field at the difference frequency. The difference-frequency wave may have three distinct sources: the acoustic field resulting from vibration of a target located in the beam path, parametric interaction of the primary beams, and the nonlinear interaction between the scattered components of the primary beams. The motivation for this study is to better understand the wave mechanisms in vibro-acoustography.

Statement of Contribution/Methods

We analyze propagation of two axisymmetric ultrasound beams taking into account the parametric and nonlinear interaction of the primary as well as the scattered beams. Our study stems from Aanonsen's wave equation, which accounts for diffraction, absorption, and medium nonlinearity. The beamforming and nonlinear scattering problem are solved by means of the Green's function method. An experiment to measure the difference-frequency pressure scattered by a 0.25 mm-diameter sphere is described. A comparison of different wave components at the difference-frequency is reported for the first time.

Results

We found that the difference-frequency scattered wave is chiefly caused by the nonlinear interaction of the "scattered" primary beams, and its sound level is about 60 dB higher than the difference frequency component that is generated by the parametric interaction of the primary beam and then scattered by the sphere. Furthermore, the scattered field at the difference-frequency depends directly on the nonlinearity of the medium and the product of the pressure amplitude of the primary beams.

Discussion and Conclusions

In conclusion, the nonlinear interaction of the scattered primary beams is dominant for the collinear axisymmetric beam formation with inclusions smaller than the primary beam waist. This research is supported by NIH grants CA 127235, CA 91956, and CNPq (Brazilian Agency) 150745/2007-9.

P1C049-11

Image-based ECG Sampling of IVUS Sequences

Aura Hernàndez-Sabaté, David Rotger, Debora Gil; *Computer Vision Center, Computer Science, Bellaterra, Barcelona, Spain.*

Background, Motivation and Objective

IntraVascular Ultrasound (IVUS) enables 3D visualization and measurements of coronary arteries. A major concern during in vivo acquisitions is that the catheter motion in and out the artery due to heart beat hinders 3D reconstruction and measures. Longitudinal motion artifacts might be overcome by ECG-gating sequences, which return a static sequence synchronized with cardiac phase. ECG-based pullbacks use either specific hardware (not always available) or the ECG signal (requiring delicate computations). The potential of IVUS images processing for phase retrieval still remains unexplored. This paper presents a fast approach to image-based ECG sampling.

Statement of Contribution/Methods

Minimum and maximum lumen areas correspond to the beginning of the QRS complex (end-diastole) and T-wave peak (end-systole) of the ECG signal. Given that lumen area evolution is related to other phenomena induced by cardiac motion, we use tissue density of mass for cardiac phase retrieval. By the ultrasound properties, the image local mean (LM) reflects, for each pixel along the sequence, the conservation of density of mass and, thus, LM extrema contain information about cardiac phase. In order to extract it, LM Fourier development is filtered with

two different bandpass filters: Butterworth and Gaussian-based centered at the cardiac frequency. The extrema of the average of the filtered signals, FLM, reflecting cardiac motion (i.e. with a cardiac amplitude over a given percentile) retrieves phase information. Ridges give a sampling at end diastole while valleys at end systole.

Results

Figure 1 shows the performance of our method in 2 large longitudinal cuts (left) sampled at end diastole rate (right). The validity of our ECG-sampling was determined by computing the difference between FLM extrema and the frames (manually picked) achieving extrema lumen areas. We considered segments between 400 and 500 frames long. The Butterworth signal deviation was 0.47 ± 0.76 seconds (14 ± 23 frames), while Gaussian-based ones achieved 0.13 ± 0.13 seconds (4 ± 4 frames).

Discussion and Conclusions

Exploring LM evolution is a fast way to retrieve cardiac phase from IVUS. Butterworth signals are too regular for long segment gating (16.6 seconds). Results for Gaussian-based signals encourage comparison to samplings obtained from ECG signals.

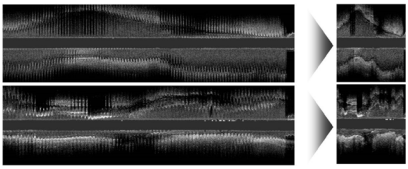

P1C050-12

Optimum design of echogenic needles for ultrasound guided nerve block

Yun Jing[1], Assad Oberai[2], Robert Bocala[2], Paul Bigeleisen[3]; [1]*Rensselaer Polytechnic Institute, Troy, NY, USA,* [2]*Rensselaer Polytechnic Institute, Mechanical Engineering, USA,* [3]*UPMC Presbyterian Hospital, USA.*

Background, Motivation and Objective

When the angle of insonation exceeds 45 degrees it can be difficult to image a smooth needle while performing ultrasound guided nerve block. Recently, an echogenic needle with a screw groove machined into the distal 1 cm of the needle was created, and was experimentally proved that the tip can readily be differentiated from the shaft. The purpose of this paper is to study the reason why the visibility of the tip is improved by making such grooves, and further to find out an optimum design of the echogenic needle.

Statement of Contribution/Methods

Finite element method (FEM)is first used to study the scattering sound field resulted from this type of needle. The simulation results agree well with a “grating equation” and explain the visibility enhancement by making the grooves into the distal of the needle. In addition, the “grating equation” is employed to further study the groove period effect on the scattering field so that the optimization of the needle design is possible. Since we are concerned about increasing backscattering in this specific case, the angle of peak scattering is desired to be as close as possible to the incident angle. Therefore, we search for the ratio of the ultrasound wavelength to the grating wavelength that would minimize the maximum difference between the incident angle and peak scattering angle over a range of incident angles. We then use FEM to determine the optimum groove depth that would provide the strongest backscattering from the needle.

Results

Through the simluation, it is found that for the ultrasound frequency at 13Mhz, the best ratio between the ultrasound wavelength and the period of the groove is 1.21, and the optimum groove depth is 0.03mm.

Discussion and Conclusions

An optimum design of the echogenic needle for ultrasound guided nerve block is proposed in this paper for 13Mhz working frequency. Both FEM and the "grating equation" are used to determine the optimum groove period and depth which can provide intense backscattering from the needle tip to enhance visibility. The same idea can be applied to other frequencies of ultrasound as well.

P1C051-13

Parametric Imaging of Blood Perfusion with Low-Cost Diagnostic Ultrasound Equipment

Hui Zhong, Xiaolin Gu, Mingxi Wan, Xiaowen Hu, Dan Lv, Liang Shen, Xiaomei Zhang; *Xi'an Jiaotong University, The Key Laboratory of Biomedical Information Engineering of Ministry of Education, Xi'an, Shaanxi, China.*

Background, Motivation and Objective

Developments on ultrasound contrast-specific imaging methods make it possible to detect the deep microvessel and evaluate blood perfusion noninvasively. In this study, we attempt to implement parametric imaging to assess blood perfusion of organs quantitatively with a low-cost diagnostic ultrasound equipment.

Statement of Contribution/Methods

We proposed a novel ultrasound contrast imaging method called PISSD method, which combined pulse-inversion (PI) technique with sum-squared-differences (SSD) algorithm. Based on the PISSD method, perfusion parametric imaging was realized. First, pulse inversion harmonic (PIH) imaging method was used to form original contrast images. Then, SSD values were calculated with the same RF signals as the PIH method. A reference was set up, which is defined as the mean SSD value of the whole image before contrast agent appears in the concerned imaging plane. The regions of the PIH images were regarded as tissue if their corresponding SSD values were lower than the reference and we set the PIH values of these regions to zero. At the same time, the regions with higher SSD values than the reference were regarded as UCAs and their PIH values remained. Thus, we obtained the PISSD images. Time-intensity curves (TICs) in each small region of interest (ROI) were gained from a sequence of PISSD images. Perfusion parametric images were acquired based on the parameters estimated from TICs.

Results

The perfusion parametric imaging is implemented based on a modified diagnostic ultrasound equipment with low-cost. Ultrasonic Doppler flow phantom was used to validate the PISSD method for perfusion parametric imaging, and the results suggested that PISSD method can provide 5 to 10 dB higher contrast-to-tissue ratio (CTR) than PIH method. Experiments of kidney of rabbit were performed under optimized conditions where motion artefacts were minimized. The results also showed that the CTR of PISSD images were higher than that of PIH images. Perfusion parametric images were obtained including peak intensity, area under curve, mean transit time and so on.

Discussion and Conclusions

It was indicated that parametric images based on PISSD method can possess more accurate assessment for blood perfusion. The perfusion parametric imaging method proposed by us can be easily realized on low-cost diagnostic ultrasound equipment and has promise to be widely applied clinically.

P1C052-14

Compact Ultrasound Scanner with Simultaneous Parallel Channel Data Acquisition Capabilities

Larry Mo[1], Derek DeBusschere[1], Glen McLaughlin[1], Xueding Wang[2], J. Brian Fowlkes[2], Paul Carson[2], Dave Napolitano[1], Wenli Bai[1], Ken Fowkes[1], Andrew Irish[1]; *[1]ZONARE Medical Systems, Inc., USA, [2]University of Michigan Health System, USA.*

Background, Motivation and Objective

The ″IQscan″ research package for a commercially available compact ultrasound system has been significantly expanded with two major enhancements: 1) a command-and-control system from an external PC that provides support for adjustment of imaging parameter values and for acquisition of raw data for off-line processing; 2) a single-zone research imaging mode that supports the receive data capture from 64 transducer channels simultaneously over multiple image frames.

Statement of Contribution/Methods

In the new 64-channel raw data capture mode, over 300,000 64-channel I/Q range samples (max. 1500 per frame) can be captured to an 88-MByte CINE buffer. IQscan further provides the capabilities to 1) turn transmit pulsing and/or focusing on/off; 2) select the use of left, right or center 64-element receive aperture; 3) control the acquisition frame rate from a few Hz to over 1.5 kHz; 4) select receive channel pre-processing parameter values; and 5) extract the 16-bit CINE I/Q data. Two calibration studies using a 128-element L10-5 linear array are presented. First, channel I/Q data was captured from a pulse-echo scan of a hypo-echoic phantom (0.5 dB/cm-MHz attenuation) with 0.1 mm diameter nylon-fiber targets at various depths. Transmit focusing was turned off and the channel data was processed off-line using a dynamic receive focusing algorithm to form a B-mode image.

Second, a basic calibration study of a photoacoustic tomography (PAT) system (system details in a separate abstract submission by Wang et al.) is reported. Specifically, a Nd:YAG pumped laser with a 10 Hz repetition rate was used to illuminate a single 50 micron (i.d.) tubing filled with fresh blood. The ultrasound array, oriented in a plane orthogonal to the tubing, was operating only in receive mode at a 10 Hz frame rate. Channel data frames acquired using the left and right receive apertures were combined off-line to realize an effective full aperture. The detected channel data was back-projected to obtain an optical absorption coefficient (OAC) image.

Results

For the example of a 4 cm depth setting with the L10-5 probe, the number of 64-channel I/Q frames that can be stored in CINE is about 800. If channel data capture is not selected, then up to 3000 A-mode I/Q lines can be captured at a maximum 2 kHz rate, which should prove useful for blood/tissue motion analysis. In the phantom calibration studies, the pulse-echo image shows line-spread-functions at depths of up to 4 cm. They are found to be in good agreement with a FIELD II simulation based on a virtual 2D model of the phantom. For the PAT study, the total time needed for signal acquisition of a 2D image is 0.2 s, and the OAC image shows FWHM-axial and lateral resolutions of 0.8 and 2.1 mm respectively.

Discussion and Conclusions

IQscan enables acquisition of simultaneous parallel channel data together with reconstructed I/Q image data. This should find applications in a broad range of research including beamforming, motion studies, PAT and elastography.

P1C053-15

A Mobile Medical Device for Point-of-Care Applications

Oh-hyun Kwon, Hak-yeol Sohn, Jeong Cho, Hee-chul Yoon, Sin-hyeok Seo, Wang-young Sohn; Tai-kyong Song,
Electronic Engineering, Sogang University, Seoul, Korea, Republic of.

Background, Motivation and Objective

Portability, wireless communication, medical imaging, and measurements of various bio signals are key features of a medical diagnosis device aimed for point-of-care (POC) services. We have developed a hand-held POC device that can provide ultrasound color-flow images as well as B-modes and some important clinical information such as body temperature, blood pressure, the percentage of oxygen saturation in blood, blood glucose levels, and so forth.

Statement of Contribution/Methods

The whole system consists of one front-end PC-board (100mm by 125mm), one back-end PC board (80mm by 130mm), and an LCD panel (65mm by 85mm). The front-end board includes a 32-channel analog receiver block, 32 10-bit ADCs with serial LVDS outputs, and a single FPGA to implement all the digital circuits for 32-channel transmit/receive beamforming and real-time system control. Through combined use of sparse array and extended aperture techniques, 64-channel beamforming can be achieved effectively. To reduce the board size and improve the impedance matching, a small analog board including HV multiplexers and limiters for all the 32 channels is mounted inside the probe head. The back-end digital board has a FPGA which implements the entire ultrasound signal processing functions. Also built on the digital board is a small Xscale (Intel PXA270) embedded Linux system to support voice recording, memory card, digital camera, WIFI interface and other PDA functions. All the clinical information measured by various biosignal sensors can be sent to the embedded processor through a Zigbee (IEEE 802.15.4 standard) wireless interface. The WIFI card installed in this device makes it possible to transfer and retrieve ultrasound images, patient pictures, and other patient information to and from a remote server system. Each of the major signal processing blocks such as receive beamformer, dynamic filter and decimators, magnitude calculator, log compressor, and digital scan converter, is designed with a hardware-efficient architecture for reducing the circuit size and power consumption level. The device is powered by a Lithium polymer battery to achieve the maximum scanning time of more than an hour.

Results

A prototype of the fore-described POC device has been developed and verified to support most features included in the design requirements. The prototype has been rebuilt with revised PC-boards to improve the performance. We will present the images obtained with the new hand-held POC device and other application results combining ultrasound images and various bio signals.

Discussion and Conclusions

A new medical diagnosis device for POC applications has been developed which can provide ultrasound images, measure various bio signals through a wireless body area network, and support wireless communication for remote

diagnosis. The size and power consumption can further be reduced through SoC fabrication of the major hardware components implemented on the FPGAs in the prototype system.

P1C054-16

Interactive Ultrasound Training System

Christian Banker[1], Peder Pedersen[1], Thomas Szabo[2]; *[1]Worcester Polytechnic Institute, Electrical and Computer Engineering, Worcester, MA, USA, [2]Boston University, Biomedical Engineering, Boston, MA, USA.*

Background, Motivation and Objective

Ultrasound imaging relies heavily on the ability of the sonographer, requiring extensive hands-on training on healthy humans, thus limiting the diagnostic skills taught and number of trainees. The Interactive Ultrasound Training System is an inexpensive, software-based training system, in which the trainee scans a lifelike manikin using a sham transducer. The observed ultrasound image is generated from a pre-stored 3D image volume and is controlled by the sham transducer's position and orientation. Based on the selected 3D volume, the manikin may represent normal anatomy, exhibit a specific trauma or present a given physical condition.

Statement of Contribution/Methods

Training data sets were generated from sets of parallel, overlapping individual 3D scans on a CIRS anthropomorphic phantom and an ATS 539 calibration phantom, using a Terason t3000 ultrasound system with a calibrated 6 degree of freedom (DoF) magnetic tracking sensor attached to the transducer. A given set of 3D image volumes was subsequently stitched together, to form a large, composite volume. Simulation software was developed for visualization of an image plane extracted from the stored 3D image volume, according to the position and orientation of the sham transducer containing a 6 DoF tracking sensor. An Ascension TrakSTAR tracking system is used to provide accurate position and orientation tracking in a small, unobtrusive package. Embedding the tracking transmitter into a manikin and the tracking sensor in a transducer shell has removed the awareness of the tracking system.

Results

The training system provides a very realistic training experience. The simulation software is able to continuously display convincing B-mode scan images, smoothly updated in real time. The software interface also permits users to specify the scan depth and select between different transducer geometries, applying appropriate transformations to the image. Successful methods of data capture have been developed, permitting the acquisition of data volumes composed of multiple transducer sweeps. Calibration procedures have also been developed to properly align ultrasound scans to the sensor's position and orientation information. Data can be acquired from nearly any ultrasound scanner as long as a video feed is available and a position sensor is attached to the transducer for acquisition.

Discussion and Conclusions

The ultrasound training system can provide cost-effective and convenient training of physicians and sonographers. Captured image data of a given pathology can be used repeatedly for training. Future work will focus on implementing learning assessment based on scan pattern and ability to locate image features on a touch screen, and establishing a web-based database of compressed 3D image volumes captured from human patients. The training system is an innovative new approach to training and is a powerful tool for training sonographers in recognizing a wide variety of medical conditions.

P1C055-17

Phase Corrected Scattering Integral and the acoustic field in biomedical tissue with speed of sound and density variations

Rosemary Thompson[1], Whayne Padden[2], Charlie Macaskill[1]; *[1]University of Sydney, Centre for Mathematical Biology, School of Mathematics & Statisics, Sydney, NSW, Australia, [2]University of Sydney, School of Mathematics & Statisics, Sydney, NSW, Australia.*

Background, Motivation and Objective

This study concerns the acoustic field in biomedical tissue in the presence of inhomogeneous regions that are neither very small nor very large compared to the ultrasound wavelength. Such inhomogeneities are commonly associated with objects of clinical interest, such as lesions or plaques. In general both the average sound speed and the average density over the object are different to their background values, and the geometry is irregular. The acoustic field at any point can be expressed as the sum of incident and scattered parts, and different approximations are used to find the scattered part. We seek a treatment of the scattering integral that is practical and specifically suited to biomedical problems.

Statement of Contribution/Methods

Our Phase Corrected Scattering Integral (PCSI) method is developed further and evaluated relative to certain well-established approximation methods. With sound speed only variations the PCSI gives excellent results for the field within and near to biomedical inhomogeneities, in cases where the Born approximation gives very poor results. In the present study we first examine the behaviour of the PCSI approximation in the far field and compare it with a paraxial (Kirchhoff) approximation. We then show how the PCSI approach, developed for sound speed variations, can be extended to allow for both sound speed and density variations.

Results

We present results for objects with scaled wavenumber in the range 1 to 100, with sound speed variations of order 10%, and density variations of this order or more. A simple ray model is used to find the phase correction used in the PCSI method. In the Kirchhoff approximation the total phase shift due to the inhomogeneneity is effectively lumped at one spatial location. Numerical results obtained for a scattering cylinder show that exact and PCSI results are always closely comparable; they agree with Kirchhoff results in the far field. We also demonstrate analytically that the far field PCSI is equivalent to Kirchhoff. With sound speed and density variations, we show that the scattering integral can be recast into a form that allows the PCSI method to effectively calculate the contribution due to each effect separately. Comparison with exact results again shows that PCSI results are remarkably accurate.

Discussion and Conclusions

The PCSI method gives accurate results within, close to and far from weak scattering objects, and so it can be used directly if different sized objects are present. When there are both sound speed and density variations, the scattering integral is usually written as the sum of monopole and dipole terms. Expressing this integral differently allows the PCSI method to be applied, with little increase in computational effort, to cases where both physical quantities vary. We conclude that the PSCI is an effective and accurate method for finding the acoustic field for biomedical problems, where there is weak scattering due to sound speed and/or density variations, and irregular geometry.

P1C056-18

Transcranial Shear-Mode Ultrasound Imaging: Characterization of Point Spread Function and Assessment of Excitation Techniques

Ali Yousefi[1], **Kullervo Hynynen[2];** [1]*University of Toronto, Electrical and Computer Engineering, Canada,* [2]*Sunnybrook Research Institute, Medical Biophysics, Canada.*

Background, Motivation and Objective

Transcranial sonography is hindered by poor acoustic windows and skull induced distortions to the ultrasound beam. Shear pressure waves in the skull bone have a better impedance match with those in water and have been shown to produce a more coherent focus inside the skull. The purpose was to compare longitudinal and shear wave transskull ultrasound imaging.

Statement of Contribution/Methods

Pulse-echo Point Spread Function (PSF) was obtained by imaging a 1.6mm brass sphere behind ex vivo human craniums with a focused F2/1MHz transducer. The skulls were oriented relative to the imaging transducer to produce both shear-mode and conventional longitudinal-mode transcranial propagation. Brightness images from each mode were assessed and compared using reference scans of the target without the skull in place. Skull-induced distortions to the PSF were quantified offline using images of the target.

Shear-mode transmission was achieved by ensuring that the angle of incidence of the wavefront into the skull bone was greater than 45°, beyond Snell's critical angle for longitudinal pressure waves. A linear frequency-modulated (FM) chirp with a 0.25MHz-1.75MHz sweep was used in conjunction with a pulse compression filter for quantifying gain in SNR relative to a short broadband imaging pulse.

Results

A better localization along the propagation axis but worse detail-resolution was achieved in shear-mode as compared to longitudinal-mode (see Table I). Gains in SNR of 23±1 dB and 19±2 dB were achieved in longitudinal-mode and shear-mode respectively when using an FM chirp as compared to a broadband pulse. This improvement in SNR allowed for compensation of frequency-dependent attenuation in the skull, resulting in a greater than 20% improvement in detail resolution.

Discussion and Conclusions

Shear-mode ultrasound can enhance transcranial imaging for use in clinical neurology. The SNR limitations of a broadband imaging pulse in highly attenuating skull bones were overcame with FM coded-excitations.

TABLE I. TRANSCRANIAL POINT SPREAD FUNCTION MEASUREMENTS

	Longitudinal Mode	Shear Mode
PSF 6dB Lateral Beam Width [% Increase]	65 ± 40	110 ± 40
Symmetry Ratio	87 ± 6	84 ± 10
Pulse Echo Transmission Efficiency [%]	6 ± 4	1 ± 0.7
Displacement Error in X-Y plane [mm]	0.95 ± 0.6	2.4 ± 0.8
Displacement Error along Z axis [mm]	1.8 ± 0.7	0.42 ± 0.3

Data from 36 scans across the 3 skull samples. Point target 25mm from inner surface of skull.

Monday Poster

P1C057-19

An Intraoperative Transcranial Ultrasound Monitor (ITUM): Preliminary Results with Human Subjects

Phillip Jason White[1], Steve Whalen[2], Sai Chun Tang[1], Greg T. Clement[1], Alexandra J. Golby[2]; [1]*Harvard Medical School, Brigham and Women's Hospital, Department of Radiology, Boston, MA, USA,* [2]*Harvard Medical School, Brigham and Women's Hospital, Department of Neurosurgery, Boston, MA, USA.*

Background, Motivation and Objective

A prototype ultrasound device to be applied continuously during neurosurgery to monitor for brain shift has been designed, constructed, characterized, and tested with adult healthy volunteers. The intraoperative transcranial ultrasound monitor (ITUM) incorporates four novel design aspects to achieve efficacy: (1) a focused ultrasound transducer with a pressure field profile that selectively monitors specific intracranial regions; (2) a lowered effective ultrasound frequency (f = 0.96 MHz) to overcome attenuation stemming from the skull bone; (3) shear-mode transmission through the skull bone to enhance energy transmission and reduce beam aberration; and (4) low ultrasound duty-cycle for time-extended application. After thorough characterization and testing in benchtop experiments, the device was tested with healthy adult volunteers to validate device performance by comparison with MRI data. Experiments have been performed with 7 subjects, out of which 4 yielded results that demonstrated the anticipated correlation between MRI data and ultrasound signals. The remaining 3 experiments yielded inconclusive results due to mispositioning of the ultrasound device (2 subjects) and excessively noisy MRI data (1 subject).

Statement of Contribution/Methods

For each subject, the ITUM was positioned to transmit through the acoustic window at the temporal bone. To achieve shear-mode transmission through the skull bone, the transducer was positioned to transmit at 31° to normal incidence with respect the skull's outer surface, resulting in a postero-medial path of propagation from the temporal bone, through the insula, and towards the right lateral ventricle. An oblique T1-weighted MRI scan, spatially registered with the ultrasound propagation path, was performed immediately after the ITUM scan.

Results

Analysis was performed by comparing the MRI data along the ultrasound propagation path and the signal generated by the ITUM (Fig. 1). For each of the 4 subjects, 3 echogenic interfaces were observed to be correlated with the MRI data: (A) fat-muscle interface, (B) bone-brain interface, and (C) the CSF-brain interfaces at the insular cortex.

Discussion and Conclusions

These preliminary results establish a basis from which future improvements on the device can be tested, eventually leading to clinical trials with surgery patients. (NIH 1U41RR019703-01A2 and P01-CA67165)

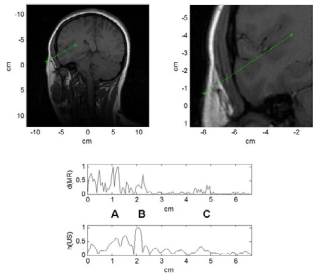

P1C058-20

Transcranial backscatter imaging of foreign bodies

Caleb H. Farny, Sai Chun Tang, **Greg T. Clement;** *Harvard Medical School, Radiology, Boston, MA, USA.*

Background, Motivation and Objective

Undetected embedded foreign objects in the brain pose a dangerous threat in the battlefield, where access to advanced medical imaging facilities may be limited. It is of great interest to develop a portable ultrasound device to detect foreign bodies that have penetrated the skull. We recently developed a portable, battery-powered ultrasound device for the purpose of interrogation of the sinus cavity via the maxilla bone. A similar device may serve as a suitable platform to detect the presence of foreign bodies using transcranial ultrasound imaging.

Statement of Contribution/Methods

Several parameters were studied to understand optimal sonication conditions for detection of a steel sphere positioned inside an ex vivo human skull. Multiple sphere diameters ranging from 0.5 – 3 mm and multiple sonication positions were tested to evaluate the maximum interrogation region. The effect of transducer aperture and center frequency on the imaging volume was also examined. Planar transducers with a 0.5 and 1 MHz center frequency were excited with a broadband pulse and longitudinal and shear mode coupling were investigated to obtain optimal transmission. The interrogation region was evaluated by separately scanning a needle hydrophone, to evaluate transmission characteristics, and a steel sphere, where the received signal was used to evaluate the backscattered signal, inside the skull.

Results

The normalized backscattered pressure from a 1 MHz planar transducer off a 3 mm diam. steel target scanned inside an ex vivo human skull is shown below. The targets were clearly apparent, despite high attenuation and distortion caused by the skull. The lower frequencies were found to provide superior signal-to-noise, due to the lower attenuation. The backscatter cross-section from the 3 mm diameter target resulted in a -6 dB diameter of approximately 11 mm.

Discussion and Conclusions

As expected, distortion from transmission through the skull altered the pressure distribution, but for the immediate goal of detecting the presence of foreign bodies, these effects are not necessarily undesired. Distortion may actually assist in spreading the signal by maximizing the interrogation region inside the skull. The large backscatter cross-section also assists in detecting the target, increasing detectability of small objects embedded behind the skull. [Support by UltraDiagnostics and USAMRMC:NPI-0704-0071]

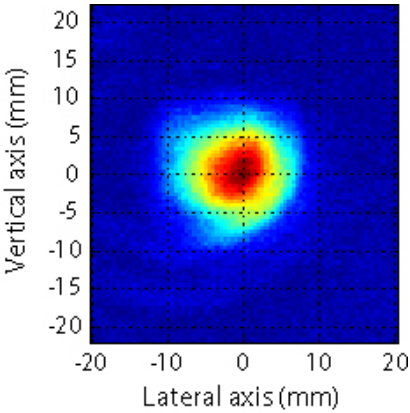
20
15
10
5
0
-5
-10
-15
-20
Vertical axis (mm)
-20
-10
0
10
20
Lateral axis (mm)

P1D. Medical Signal Processing

2nd and 3rd Floor Foyers

Monday, November 3, 2008, 3:00 pm - 4:30 pm

Chair: **Svetoslav Nikolov;**
Technical University of Denmark, Denmark.

P1D059-01

Range Measurement using Ultrasound FMCW Signals

Masanori Kunita, Masamitsu Sudo, Takashi Mochizuki; *Aloka Co., LTD., Research Laboratory, OME-SHI, Tokyo, Japan.*

Background, Motivation and Objective

Low peak power frequency-modulated continuous-wave(FMCW) radar is used in various fields, such as vehicle collision warning systems, airborne radio altimeters, and other applications. The authors proposed an ultrasound FMCW range measurement system based on the same principle as the FMCW radar. In the proposed system, the transmitter and receiver operate at very low voltage. This advantage suggests the possibility of designing a small and simple transmitter/receiver using low power ICs. Although pulsed ultrasound imaging is safe to patients, it is always a good idea to find a method that can use a minimum ultrasound power for diagnosis.

Statement of Contribution/Methods

The sawtooth and isosceles sawtooth functions are selected as the frequency modulation signals for the ultrasound FMCW range measurement system to achieve sufficient range resolution in human body. An ultrasound FMCW signal is transmitted into human tissue and the reflection signal is received after the two-way propagation time in human body. Instantaneous frequency difference between the transmitted and received signals is proportional to the propagation time in the system. Therefore, the range information may be obtained from the frequency spectrum of the baseband signal which is generated by multiplying the transmitted signal by the received signal. The spectrum and range resolution were calculated based on the basband signal analysis. The calculation results suggest that the system has similar range resolution to conventional ultrasound pulse diagnosis systems. We verified the calculated results by the experiments using electrical delay line and an ultrasound phantom.

Results

We measured the baseband frequency spectrum versus electrical delay time with the sawtooth and isosceles sawtooth frequency modulation signals and observed that harmonics peak frequency moved to a higher frequency band as the delay time increased. The relationship between the harmonics peak frequency spectrum and the delay time agreed with the calculated results. Next, we measured the frequency spectrum in the baseband signal using an ultrasound phantom. We confirmed a linear relationship between the harmonics peak frequency and the delay time in a range of 0-170 micro seconds. These experimental data agreed well with calculated results. The 3 dB bandwidth of the baseband peak frequency spectrum was 1 -3kHz with the sawtooth modulation signal and it was equivalent to the range resolution of 0.5- 1.5mm in human body.

Discussion and Conclusions

The measured frequency spectrum and its bandwidth satisfied the range resolution required in a medical diagnostic ultrasound system. We conclude that the proposed system has a possibility of decreasing ultrasound peak power to less than 1/100 of that of conventional pulse ultrasound diagnostic systems.

Monday Poster

P1D060-02

Three-dimensional segmentation of high-frequency ultrasound data echo-signal from dissected lymph nodes

Alain Coron[1], **Jonathan Mamou[2],** Masaki Hata[3], Junji Machi[3], Eugene Yanagihara[3], Pascal Laugier[1], Ernest J. Feleppa[2]; *[1]UPMC Univ Paris 06, UMR 7623, Laboratoire d'Imagerie Paramétrique, Paris, France, [2]Riverside Research Institute, F. L. Lizzi Center for Biomedical Engineering, New York, NY, USA, [3]University of Hawaii and Kuakini Medical Center, Honolulu, HI, USA.*

Background, Motivation and Objective

Quantitative high-frequency ultrasound (QHFU) imaging methods are under investigation to evaluate their ability to detect small nodal metastases in lymph nodes freshly dissected from cancer patients. To apply these methods, a critical preprocessing step is 3D segmentation of the lymph-node ultrasound echo-signal dataset. Segmenting the residual fat layer and the lymph node is critical in order to avoid bias in the QHFU estimates (e.g., scatterer size and acoustic concentration) due to attenuation and to exclude estimates obtained from the fat regions. Segmentation also provides absolute measurements of the lymph-node that are necessary to match 3D ultrasound with 3D histology.

Statement of Contribution/Methods

Following dissection from the patient, lymph nodes are manually defatted and 3D ultrasound data are acquired with a 26-MHz center-frequency transducer (6-mm aperture and 12-mm focal length). A 3-step, 3D, region-based segmentation method is used. First, RF-signal envelopes are downsampled using cubic spline approximation coefficients obtained with Mallat's pyramidal algorithm. Second, the watershed transform of the H-minima transform of the norm of the gradient of the envelope approximation is calculated to obtain an oversegmentation composed of many regions. Third, each region is classified by comparing its mean-pixel value, M, with two prescribed thresholds Tl and Th. If M<Tl, the region is labeled as surrounding saline, if Tl<=M<=Th, the region is labeled as nodal, and if M>Th, the region is labeled as fat.

Results

The figure shows the segmentation of a non-metastatic lymph node from a colon-cancer patient on three orthogonal B-scans (z is depth). The fat and lymph-node regions are enclosed in red and green volumes, respectively, which appear as closed curves on these projections.

Discussion and Conclusions

Results obtained on several lymph nodes visually indicate that most pixels are correctly classified. Nevertheless, the method needs to be improved because occasional pixels are still misclassified. For example, the method could be refined to incorporate region neighborhoods (e.g., to reclassify a fat region surrounded by lymph-node regions as lymph node) and attenuation. Attenuation is problematic for large lymph nodes for which deeper tissues are classified as saline because they are highly attenuated. Work supported in part by NIH Grant CA100183.

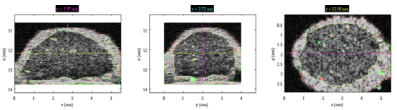

P1D061-03

Spectral analysis of ultrasound rf image data to monitor bubble formation in HIFU treatment

Chang-yu Hsieh, Penny Smith, Guoliang Ye; *University of Oxford, Biomedical Engineering, Department of Engineering Science, Oxford, United Kingdom.*

Background, Motivation and Objective

The high power intensities in HIFU often result in bubble production, either through cavitation or boiling, which are believed to be a primary contributor to tissue necrosis. Some HIFU protocols rely on the evidence of cavitation as a strong indicator of tissue lesions. Cavitation is normally associated with hyperechoic regions ('bright up') in ultrasound B-mode image feedback. However, this bright up area may indicate different physical events, for example tissue heating (known to alter backscatter), necrosis, or bubble formation (cavitation or boiling). Spectral analysis of the r.f. signal underlying the B-mode image provides more information on the physical cause. Usual methods based on the Fourier transform require long time series for good spectral resolution, reducing spatial accuracy. This work is establishing algorithms to analyse the spectral data at high spatial resolution so local changes can be more easily identified.

Statement of Contribution/Methods

The paper discusses an ARMA model, based on the underlying statistics of the signal, to provide good spatial and spectral resolution, establishing methods to determine the best model order from the ultrasound echo A-line data. The technique is used to analyse signals from HIFU in water, where boiling is observed visually, and in ex-vivo beef liver, using a 1MHz HIFU transducer, with the image acquired using a wideband (5-15MHz) linear array probe (from BK transducers) with the Analogic 320 CASA engine, which provides access to the ultrasound r.f. (A-line) data with 40MHz sampling rate.

Results

Results show that resolution can be obtained to the order of about one pixel in the B-mode image. Results from water give increased spectral content at high frequencies in the regions close to the HIFU focus, and also show low frequency components at around 3-5kHz. It is suggested that this is owing to boiling bubbles, and results from transducer vibration causing electrical noise at these frequencies (since they are well below the transducer bandwidth. In tissue there is correlation between areas of strong hyperechoicity and power at high frequencies.

Discussion and Conclusions

The results suggest that good spatial and spectral resolution can be obtained by the design of suitable algorithms. In ultrasound guided HIFU the technique provides a useful addition to B-mode analysis, with no additional time penalty in data acquisition.

P1D062-04

A Correction Scheme for Refraction and Time-of-Flight Artifacts in Limited-Angle Spatial Compound Imaging with High-Frequency Ultrasound

Joern Opretzka, Michael Vogt, Helmut Ermert; *Ruhr-University Bochum, Dept. of Electrical Engineering and Information Technology, Bochum, Germany.*

Background, Motivation and Objective

It has already been shown that skin imaging with high-frequency ultrasound (HFUS) in the 20 MHz range is improved by applying limited-angle spatial compounding. In HFUS systems usually mechanically moved single-element fixed-focus transducers are used and a water path between transducer and tissue is required. The difference in speeds of sound (SOS) of water and skin causes beam refraction at the skin surface and time-of-flight (TOF) mapping errors. In this paper, refraction and TOF artifacts are analyzed, and a ray-tracing correction approach is presented.

Statement of Contribution/Methods

We have implemented a HFUS compound imaging setup. A single-element transducer is mechanically moved along the lateral coordinate and tilted in the lateral/axial imaging plane to obtain data from different angles of insonation. We analyzed the resulting errors from SOS differences in uncorrected compound images based on an analytical model, which assumes different but constant SOS for water and skin. A ray tracing algorithm was applied to the individual images used for compounding to correct refraction at the boundary and TOF artifacts in the skin. For this purpose, the skin surface is segmented by involving a priori knowledge about the boundary's smoothness and shadowing by hairs. While the SOS of water can be obtained experimentally by wire phantom measurements, the SOS of the skin, which is not exactly known, was iteratively changed to optimize the compound image in terms of resolution. Due to refraction and TOF errors, structures inside the skin appear at different positions for different angles of insonation. The resulting position shifts are taken as measures of the image correction quality. By minimizing those shifts the mean SOS of the skin can be determined. The superposition of image frames after the final correction step delivers the compound image with optimized resolution within the scope of the aforementioned assumptions.

Results

The proposed correction scheme was evaluated by measurements on phantoms in-vivo on skin. In phantoms with two compartments (water: 1480 m/s; salt-water: 1600 m/s) and in speckle phantoms the positions of polypropylen fibers were tracked. After correction a compound image was computed with an axial and a lateral resolution (-6 dB) of 81 µm and 161 µm, respectively. The geometry of the phantom was reconstructed correctly. For application on skin measurements on test persons with different types of lesions were carried out. If structures were existent, that were visible from different angles, the correction scheme could be applied.

Discussion and Conclusions

Based on the performed analysis and the proposed correction scheme, the image quality of the implemented HFUS compound system is improved. The obtained results can be applied to HFUS skin and small animals imaging systems with mechanically moved transducers.

This work is supported by the German Research Foundation (Deutsche Forschungsgemeinschaft, DFG), grant ER 94/31-1.

Monday Poster

P1D063-05

Statistical spectral analysis for echo signals from microbubbles and solid spheres

Yan Yan[1], James Hopgood[1], Robin Steel[2], **Vassilis Sboros[2]**; *[1]Institute for Digital Communications, University of Edinburgh, Edinburgh, Scotland, United Kingdom, [2]Medical Physics, University of Edinburgh, Edinburgh, Scotland, United Kingdom.*

Background, Motivation and Objective

The spectral analysis of echo signals from linear and non-linear scatterers is important for understanding ultrasound contrast microbubble (MB) behavior and assisting pulse design. Most pulse designs assume a theoretical MB behavior instead of using experimental data despite it being accepted that theoretical models have not succeeded in describing MB behavior. Fourier transform (FT) based non-parametric spectral analysis methods are widely used but have limitations. This study is the first to incorporate receiver characteristics and to introduce a parametric model for the estimation of temporal and spectral content of experimental echo signals. This study improves spectral analysis performance and helps understand MB behavior.

Statement of Contribution/Methods

A modified scanner (Sonos5500 Philips Medical Systems, MA, USA) is used to acquire echo signals from linear scattering copper spheres. The transmit pulses are 6-cycle sinusoidal signals with fundamentals 1.28 to 3.7MHz. The receiver characteristic is accounted by deconvolving the received signals with the receiver response; the deconvolution filter is designed by analyzing the theoretical and experimental solid sphere echo signals. The filtered echo signal is then modeled as a sum of sinusoids embedded in noise. Bayesian inference is used to obtain the posterior density of the frequencies present, and numerical estimates are obtained using reversible jump Markov chain Monte Carlo techniques.

Results

The performance of our algorithm is compared with a ground truth by analyzing synthetic data. Evaluated over many Monte Carlo runs the average error is just 0.01%. Our method is then applied to real experimental data generated with a transmit pulse with fundamental f0=1.28MHz and peak negative pressure 300kPa. The Bayesian method detects more subharmonics at 0.5f0 and ultraharmonics at 1.5f0 or 2.5f0 than FT does; this is important for the analysis of MB behavior. When the receiver response is not taken into account, frequency estimation errors result; if f0 lies in a region where the receiver attenuates the signal, f0 is not correctly identified: the largest peak occurs at 2.52MHz and is misidentified as the f0 rather than a harmonic. Incorporating the receiver response into the analysis results in correct detection of f0. The frequency content of the received MB signal using the FT results in peaks at 2.60, 2.98, 3.25, 3.52 and 3.75MHz. Some of these peaks are spurious, whereas our method produces three frequencies at 2.52, 3.13 and 3.78MHz. These are the 2nd, 2.5th and 3rd harmonics, consistent with the transmitted pulse.

Discussion and Conclusions

This study presents a robust temporal and spectral estimation algorithm and accounts for the receiver response. The superiority of our method over the FT is demonstrated and the method will help with understanding MB behavior. This may also progress to the automatic classification of echo signals and is intended to be used for adaptive pulse sequence design.

P1D064-06

Pulse wave velocity in the Carotid artery

Gertrud Laura Sørensen, Julie Brinck Jensen, **Jesper Udesen,** Iben Kraglund Holfort, Jørgen Arendt Jensen; *Technical University of Denmark, Denmark.*

Background, Motivation and Objective

Arteriosclerosis is a very common cause of death in the western world. To measure the degree of arteriosclerosis the pulse wave velocity (PWV) can be used, due to the relation between PWV and the stiffening of the arteries. It

is therefore desirable to find methods for estimating the PWV locally. The fact that the PWV is 3-4 m/s in the aorta and even faster in smaller arteries, motivates the use of a method with a fast data acquisition. This paper investigates whether it is possible to find a local measure of the PWV using plane wave ultrasound which uses a pulse repetition frequency (PRF) of 4 kHz. Furthermore the influence of the high PRF is investigated.

Statement of Contribution/Methods

Plane wave ultrasound is not focused in transmit and the transmitted pulse consists of a 13 bit Barker code on each transducer element. The code is used to increase SNR. The image is focused in receive using traditional delay-and-sum receive beamforming. Using the RASMUS experimental ultrasound scanner, data from the Carotid artery of a 36 year old healthy male is obtained. Data is acquired during a period of 2.2 seconds using a 5 MHz linear array transducer. The distension wave form (DWF) of the arterial wall is found by cross-correlating segments of the vessel wall in consecutive ultrasound images. Thereafter the PWV is found from the delay between two DWFs at two different spatial positions along the artery. The delay is obtained by using a sum-of-squared differences estimator.

Results

There has been estimated 4 PWV's from 4 different pairs of DWFs. The corresponding PWVs are: 5.73 m/s, 6.68 m/s 6.39 m/s and 8.52 m/s. Also the PWV was found as a function of PRF for two of the DWFs and the result is given in the figure.

Discussion and Conclusions

The estimated values of the PWV's are realistic as the values of PWV in the Carotid artery given in the literature are 5-10 m/s. When observing the figure the graph seems to stay approximately constant above 1000 Hz, indicating that PWVs estimated with different PRFs above 1000 Hz would give almost the same results. The highest frequency content of the DWFs has been estimated to be around 200 Hz, which explains the appearance of the graph for PRFs below 400 Hz.

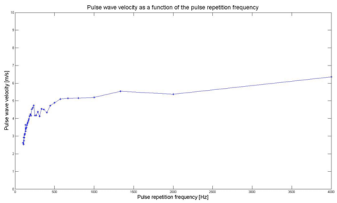

P1D065-07

Semi-Implicit Scheme based Nonlinear Diffusion Method in Ultrasound Speckle Reduction

Bo Wang, Dong C. Liu; *Sichuan University, Computer Science College, Chengdu, Sichuan, China.*

Background, Motivation and Objective

Because of the presence of speckle noise, the image resolution is not so desirable. Recently, a class of anisotropic diffusion based methods has been developed, which can reduce the speckle noise, and at the same time, preserve and enhance the edge/borders. Speckle Reducing Anisotropic Diffusion (SRAD) is an important representative of these methods. It is an explicit scheme based method with very slow processing speed due to the severe restriction in time step size (TSS), and it is sensitive to noise due to its small window size to calculate ratio of mean and variance. Using semi-implicit scheme (e.g., additive operator splitting AOS) methods to discretize SRAD (called ASRAD), we could use large TSS for speed-up. However, artifacts brought by ASRAD degrade the image. In this paper, we aim to solve above problems. Our method could be generalized to solve other explicit scheme based nonlinear diffusion speckle reduction methods.

Statement of Contribution/Methods

Our new nonlinear diffusion method improves the accuracy of ASRAD. In ASRAD, the discrete formulation of divergence operator is not accordingly dependent on four directions, this imbalance of divergence brings artifacts near the edge/borders, and because of the window it used to obtain the ratio of sample variance and mean is only four pixels, ASRAD may not stable numerically. We regulate the divergence operator to assure that the diffusion along four directions of each pixel is balanced by using the average of the centre diffusion and its four directions separately as diffusion coefficients in each direction. In this way, our new diffusion method satisfies the criteria for

discrete nonlinear diffusion scale-space for arbitrarily large TSS. Moreover, our method eliminates the artifact brought by the imbalance of the divergence operator and keeps the speed efficiency of ASRAD unchanged.

Results

Experiments show that using our extended nonlinear diffusion method, the speckle reduction result is better than that of ASRAD.The artifacts near the strong edge produced by ASRAD are eliminated by using our method.

Discussion and Conclusions

As increasing the TSS (i.e., to speed up the processing), the artifacts introduced in our method is not as heavy as in ASRAD. And the computation efficiency of our methods is almost the same as ASRAD.

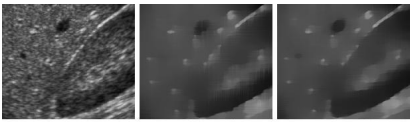

P1D066-08

Independent component analysis based speckle reduction for improved visualization of diseased liver tissue structures

Tadashi Yamaguchi[1], Hiroyuki Hachiya[2]; [1]*Chiba University, Japan,* [2]*Tokyo Inst. of Tech., Japan.*

Background, Motivation and Objective

Most speckle reduction methods use texture or spectral features in a specific region-of-interest (ROI) to eliminate attenuation effects, but finding an optimal ROI size is difficult. In this study, we investigate whether independent component analysis (ICA) can be applied to ultrasound images recorded by a clinical machine to develop a generalized speckle-reduction system. The ICA-algorithm is applied to fibrotic livers.

Statement of Contribution/Methods

Recorded echoes are modeled as the sum of two independent signals: the signal reflected from tissue structures and the speckle signal which is an interference noise. ICA can be used to separate independent information sources from mixed signals, but needs more inputs than sources for successful separation.

We fabricated a homogeneous-liver mimicking phantom generating speckle similar to that of liver using a combination of agar and graphite. Attenuation and speed-of-sound values were that of normal liver. We hypothesized that phantom echoes will simulate liver echoes with a variable mixing rate necessary to apply ICA as additional input. The ICA-algorithm performance was evaluated when incident ultrasound beams were varied.

Results

The ICA-algorithm was applied on liver (a) and on phantom (b) data using identical incident beams. Results yielded only the positive signals (c) and both positive (d) and negative signals (e). Fibers and vessel walls which were buried in speckle and were difficult to visualize in the original liver image were easily visualized in the extracted negative image.

The size of the extracted structures extended in depth and lateral directions but depended on the speckle size at the lower frequency when transmitting or receiving frequencies of the phantom data were varied. Similar results were obtained when focal depths were varied.

Discussion and Conclusions

ICA produced positive and negative signals with resolutions similar to each input although both inputs had only positive amplitudes. When ultrasound beams were varied, interference affected the independency of the two input signals and the ICA-algorithm performance degraded. Nevertheless, ICA was always successful when applied to an ultrasonic image with proper addition inputs.

In future works, we will investigate signal independence from tissues with variables acoustic properties, and also from the same tissue but with different ultrasonic beams.

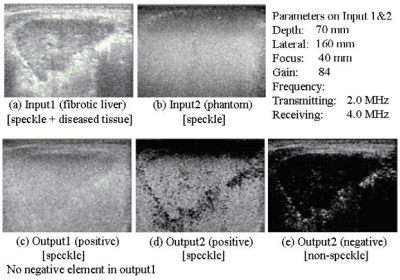

P1D067-09

Separation of Nonlinear Pulse-Echo Signals Based on System Identification by Volterra Filters

Pornchai Phukpattaranont; *Prince of Songkla University, Department of Electrical Engineering, Hat Yai, Songkhla, Thailand.*

Background, Motivation and Objective

Volterra filters have been extensively utilized as a appropriate mathematical model for a wide variety of nonlinear physical phenomena. The success of Volterra filters as the nonlinear models for other physical systems provides the inspiration for applying them with nonlinear ultrasound problems. We present the application of a system identification based on a second-order Volterra filter (SID-SVF) to separate nonlinear signals from a nonlinear pulse-echo ultrasound system (NPS). Its advantages and limitations are also discussed.

Statement of Contribution/Methods

The NPS to be identified is simulated based on the Field II program. Nonlinearity is generated at each scattering particle location with the solution of the Khokhlov-Zaboloskaya-Kuznetsov (KZK) equation. The system consists of a linear array transducer and a synthetic phantom. The 192-element linear array is used to scan the phantom with 64 active elements and a Hanning apodization in transmit and receive. The synthetic phantom is composed of scattering particles located at uniform random positions in a 20 mm × 3 mm × 1 mm volume. The filter coefficients of the SID-SVF are determined by solving a system of linear equations, which is formed in the frequency domain using inputs and their corresponding outputs from the NPS. Gaussian white noise is added to pulse-echo data at various SNR values.

Results

After the system is identified, we transmit a 3-cycle sinusoidal pulse at 2 MHz with a Hanning weighting to both systems for validation. The left panel shows an example comparison of the pulse-echo line from the NPS (dotted) with the linear (thin) and quadratic (thick) outputs from the SID-SVF. The right panel shows their corresponding spectra. It can be seen that the linear and quadratic kernels appropriately predict the linear and the second order nonlinearity covering the whole transducer bandwidth in a very low SNR condition.

Discussion and Conclusions

The SID-SVF provides satisfactory results as a model for separating nonlinear pulse-echo signals. Its main advantage over other methods such as a linear bandpass filtering is that the SID-SVF is capable of separating the second nonlinearity embedded in the noise signal levels. However, the reduction in computational complexity of the method is needed for more practical applications.

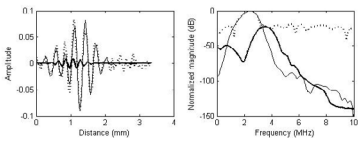

P1D068-10

A new dynamic decimation filter architecture using polyphase MACs for medical ultrasound imaging

Choong Lee, Jeong Cho, Tae-Wan Kim, Jung-Jun Kim, Tai-Kyong Song; *Sogang University, Electronic engineering, Seoul, Korea, Republic of.*

Monday Poster

Background, Motivation and Objective

Medical ultrasound scanners require a decimation filter capable of changing its length and coefficient values dynamically. For hardware implementation, it is important to design such a dynamic decimation filter (DDF) with a fixed number of multipliers in such a way that the number of multiplications per unit time should be minimized. A simple data path structure for feeding the filter must also be taken into account. The purpose of this work is to propose an efficient DDF architecture which is particularly useful when L-fold interpolation is employed prior to dynamic decimation for controlling decimation ratio in finer steps.

Statement of Contribution/Methods

Let us consider the case where a 2-fold upsampler is followed by a programmable M-fold decimator. Without loss of generality, one can assume that the decimation filter length N is proportional to M, that is, N=MK. The proposed architecture is based on a M-phase polyphase structure consisting of M subphase filters, each having length K. Typically, the decimator output is obtained by taking the sum of outputs of the M subphase filters. One can obtain the same output as shown in Fig. 1(a), where each partial sum Pk, the sum of kth multiplier outputs of all the M subphase filters, is calculated individually and then all the K partial sums are added sequentially with a single delay. Since each partial sum is obtained every M clock cycles with an input data block consisting of M consecutive original input samples, it can be calculated using a simple MAC which computes the product of each pair of filter coefficients and input data and adds all the products in accumulative manner. Other partial sums can be obtained similarly for the delayed block data. Consequently, the M-fold decimator can be implemented with K MACs. In addition, the 2-fold upsampler can be omitted by properly separating each polyphase filter into two subdivided filters of length M0 and M1, where M0+M1=M. The final structure for the entire dynamic decimation filter is shown in Fig. 1(b). Fig. 1(c) shows the structure of each MAC.

Results

The proposed M/2-fold DDF is implemented on a commercial FPGA device for the case of K = 8. Experimental results show that it performs dynamic decimation without an error.

Discussion and Conclusions

The proposed DDF architecture is very simple and flexible. The filter characteristics can be controlled by simply changing the number of MACs.

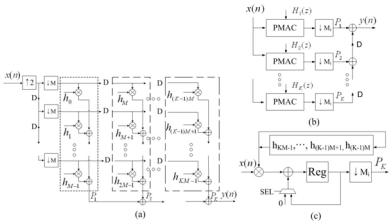

P1E. Transducer Modelling

2nd and 3rd Floor Foyers

Monday, November 3, 2008, 3:00 pm - 4:30 pm

Chair: **Levent Degertekin;**
Georgia Institute of Technology, GA, USA.

P1E069-01

Energy harvesting with piezoelectric cantilever transducer

Jiang-bo Yuan, Tao Xie, Wei-shan Chen, Jun-kao Liu; *Harbin Institute of Technology, Harbin, China.*

Background, Motivation and Objective

The development of wireless monitoring systems has been of great interest because wireless transmission has been proven as a convenient means to transmit signals while minimizing the use of many long wires. However, the wireless transmission systems need sufficient power to function properly. Conventionally, batteries are used as the power sources of the remote sensing systems. However, due to their limited lifetime, replacement of batteries has to be carried out periodically, which is inconvenient. Piezoelectric materials are considered it was ideal sources of such energy because they can convert mechanical strain energy into electrical energy or vice versa. Energy can be reclaimed and stored for later use to recharge a battery or power a device through a process called energy harvesting.

Statement of Contribution/Methods

In this paper, the voltage sensitivity of the rectangular and trapezoidal layer piezoelectric cantilever transducers were modeled by the theory developed for the piezoelectric constitutive equations and thermodynamic equilibrium. The calculated results by modal were found to be in good agreement with the experiment. Power generation from the rectangular and trapezoidal layer piezoelectric cantilevers were investigated by experiments, some practical applications such as wireless transmission will be discussed as energy harvester.

Results

Performance of the prepared prototype was tested by the experiment system. A maximal output power of about 8.6mW can be obtained from the rectangular piezoelectric cantilevers at the operating frequency of 180 Hz across a resistive load of 80k¦, .It was shown that the output voltage of the piezoelectric cantilevers increases with the resistive load. The voltage approaches15V when the resistive load is 80k¦, with around dynamic force 1N. Nevertheless, the electrical power decreases when the load resistance is further increased. And a maximal output power of 24.2mW can be harvested from the trapezoidal piezoelectric cantilevers at 130 Hz across the resistive load of 80k¦, while the voltage of 23.5 V can be generated under the same condition.

Discussion and Conclusions

In this study, a piezoelectric sensor/generator is investigated. The theoretical model was developed to determine the magnitude of power. The results predicted by the theoretical model were validated by the experimental data. An excellent consistency was found between the theoretical and experimental results. Power generation from the rectangular and trapezoidal piezoelectric cantilevers were investigated. The results show the trapezoidal piezoelectric cantilevers generated higher power with the same force and the volume of PZT compared with the rectangular layer piezoelectric cantilevers. The useful power output of the piezoelectric cantilevers can power itself , it also is potential to use as energy harvester here to power a wireless sensor network. Indeed, this power level is already enough for some wireless communication systems.

P1E070-02

Acoustic Waves in LiNbO3/SiO2/Water/Silicon Rubber Structures

Alexander Darinskii[1], **Manfred Weihnacht[2],** Hagen Schmidt[3]; *[1]Institute of Crystallography RAS Moscow, Russian Federation, [2]Innoxacs Dippoldiswalde, Germany, [3]IFW Dresden, Germany.*

Background, Motivation and Objective

The development of ultrasonic methods for the control of small fluid volumes is one of the trends in modern microfluidics. In particular, tests show that a SAW propagating on a solid substrate accelerates the mixing in the adjacent fluid layer. The design of SAW microfluidic devices poses a number of challenges, such as the correct evaluation of the exploitable acoustic wave, the understanding of how the operating characteristics of the IDT and the reflectors depend on different parameters of the structural components of the device.

Statement of Contribution/Methods

The work studies theoretically the generation and propagation of acoustic waves in the following structure: the water layer is sandwiched between the YZ- LiNbO3 substrate coated with a SiO2 layer and silicone rubber. First we find the characteristics of plane waves traveling along even interfaces with no electrodes by solving numerically and analytically the appropriate dispersion equations. Afterwards, via FEM computations, we estimate the COM-parameters of the metallic grating located on the LiNbO3/SiO2 interface. FEM is used to compute the wave fields in the electrode, the SiO2 and water layers as well as partly in the substrate and rubber. The wave fields below and above the computational cell are found with the aid of the eigenfunction expansion method.

Results

The plane wave spectrum is computed and the behavior of the real vl' and imaginary vl" parts of the leaky wave velocity as functions of the water layer thickness hw and the electric boundary conditions is analyzed (the wave leaks into silicone rubber assumed to be semi-infinite). Given the spectrum branch, and independently of its number, vl"(hw) has a minimum. The corresponding hw-value is such that vl'(hw) approximately equals the leaky wave velocity vl0' at hw=0. The dependence of the COM-parameters is investigated on hw, the SiO2 coating thickness, the presence or the absence of corrugation on the SiO2 coating surface that is in contact with the fluid, the electrode thickness and material. It is found that the reflection kp and the transduction an coefficients remain high even when the water layer is several wavelengths thick if the frequency is close to the value f0 =vl0'/2p, where p is the grating period. Corrugation on the SiO2 layer increases significantly kp. It appears that under identical conditions, Al electrodes yield larger values of kp than Cu electrodes. The dielectric permittivity of the fluid does not affect kp and an crucially if the SiO2 layer is not very thin.

Discussion and Conclusions

The obtained results reveal that an IDT can generate efficiently acoustic waves in fluid layers up to several wavelengths thick. With thicker layers the coefficient an becomes small. However, given the branch of the wave spectrum, an and kp are rather large in the same range of hw-values so that the SAW is able to produce the acoustic streaming causing simultaneously both mixing and pumping.

P1E071-03

Optimal design of a wideband multi-mode ring transducer

Yongrae Roh, Zhi Tian, Susung Lee, Wonseok Lee; *Kyungpook National University, School of Mechanical Engineering, Daegu, Daegu, Korea, Republic of.*

Background, Motivation and Objective

For underwater communication applications, a transducer of low-directionality and of wide bandwidth is required. In this paper, a new 33-mode PZT/polymer composite ring transducer is designed by the finite element method. The transducer is expected to provide in-plane omni-directionality, and to have the fractional bandwidth over 100%, which is not achievable with other conventional underwater transducers.

Statement of Contribution/Methods

The ring transducer consists of a piezocomposite ring, a front impedance matching layer, and a backing layer. First, the electromechanical coupling factor of the piezocomposite ring was analyzed in relation to the PZT/polymer¡¯s volume ratio, and the optimal volume ratio was determined to achieve the highest coupling factor while preserving structural robustness over a predetermined level. Although the single PZT/polymer composite construction had pretty broad bandwidth, further substantial improvement of the bandwidth was achieved by controlling the thicknesses of the piezocomposite layer, front matching layer and the backing layer. Thicknesses of the three layers were optimized to induce multi-mode vibration of the ring transducer. Fundamental circular vibration mode was coupled with the second elliptical vibration mode for a particular combination of the layer thicknesses.

The effects of varying the thickness of the three layers were investigated through harmonic analyses with ANSYS¢ç and the results were utilized to analyze the variation trends of the 33-mode ring transducer performance. The analyzed performances were center frequency, fractional frequency and sound pressure level of the transducer. Bandwidth optimization of the 33-mode ring transducer was carried out through statistical analysis of the finite element analysis results and formulating the transducer performance using a second order multiple regression model. The optimal combination of the thicknesses of the three layers was determined by minimizing the target function to achieve the widest -6 dB bandwidth while satisfying such constraints that the center frequency should be 23 kHz and sound pressure level should be over 135 dB re 1upa/v@1m. The minimization was performed by means of the sequential quadratic programming method of Phenichny and Danilin (SQP-PD).

Results

The designed multi-mode ring transducer showed the highest -6 dB bandwidth of 105% at the center frequency of 23 kHz. Validity of the design was checked by constructing an experimental transducer model, and measuring its performance in a water tank. Good agreement was confirmed between measured data and the numerical results.

Discussion and Conclusions

An underwater multi-mode ring transducer of maximum bandwidth was designed, and validity of the design was confirmed through experiments. The design scheme developed in this paper can be applied to optimize the structure of general underwater transducers to have a wider bandwidth at various operation frequencies.

P1E072-04

Optimising the Design of a New Electrostatic Transducer Incorporating Fluidic Amplification

Anthony Mulholland[1], Ewan Campbell[2], Gordon Hayward[2]; [1]*University of Strathclyde, Department of Mathematics, Glasgow, Scotland, United Kingdom,* [2]*University of Strathclyde, Department of Electronic and Electrical Engineering, Glasgow, Scotland, United Kingdom.*

Background, Motivation and Objective

The transmission of ultrasound into air has many potential applications however the available devices are often limited in terms of the amplitude and bandwidth of the transmitted wave. Musical instruments overcome this problem by using the natural resonances of cavities and pipes. Motivated by this, a new electrostatic transducer, whose backplate consists of a series of drilled pipes, has recently been proposed [1]. The device consists of a thin circular membrane positioned over a conducting backplate. This backplate has a patterned arrangement of drilled holes (pipes) that connect to the air cavity between the membrane and backplate. It has been shown experimentally that this design can lead to a 24 dB increase in the amplitude of operation of the device. Although this is a simple extension to a conventional electrostatic transducer the addition of the pipes increases the number of parameters needed in a given design quite considerably. The objective of this paper is therefore to build a simple, theoretical model of this device and use it to determine the design parameters that optimise its output.

Statement of Contribution/Methods

In this paper, we will derive a new model that considers the interaction of the membrane with the air load, the air cavity below, and the series of drilled pipes in the backplate. A one-dimensional (in space) dynamical model is proposed so that the inverse problem, of determining the design parameters for a desired output, is not computationally prohibitive. Energy losses in the vibrating membrane due to viscous damping and attenuation of the acoustic waves in the air conduits are also taken into account. The dynamical equations are solved analytically in each component of the device, these are then connected using the interface conditions of continuity of displacement and pressure, and boundary conditions into the air load at both faces of the device close the system of algebraic equations that arise. The model is then able to produce solutions to the forward problem of predicting the mechanical impedance of the device and the displacement of the membrane as a function of the device's design parameters. By comparing this output to that of a desired output the inverse problem of determining the design parameters can then be tackled.

Results

The model has been implemented and its output compared to experimental results from a manufactured device. There is reasonable agreement considering the simplified nature of the model. Importantly however, the model results indicate how this design could be improved to maximise the device's output.

Discussion and Conclusions

A new design for an electrostatic ultrasound transducer, whose operational characteristics are optimised by use of a mathematical model, is proposed. The design is a simple extension of a well-established design and yet a marked improvement in its output is realised.

[1] E. Campbell, W. Galbraith and G. Hayward. Proc. 2006 IEEE Intl. Ultras. Symp. , pp 1445-1448.

Monday Poster

P1E073-05

Finite Element Analysis of a Piezoelectric Acoustic Levitator

Marco Aurélio Brizzotti Andrade, Flávio Buiochi, Julio Cesar Adamowski; *Universidade de São Paulo, Brazil.*

Background, Motivation and Objective

A basic acoustic levitator consists of a transducer and a reflector. The mathematical models commonly used in the analysis of acoustic levitators require the previous knowledge of the displacement distribution on the transducer face. Therefore, the complete levitator analysis requires at least two steps. First, it is necessary to use a numerical model to determine the displacement amplitudes of the ultrasonic transducer. Then, these displacements are used in another numerical model to determine the acoustic radiation potential that acts on the levitated object. Aiming the modeling of the entire acoustic levitator, including the piezoelectric transducer, this work describes its Finite Element Analysis. The simulation of the acoustic levitator includes the fluid-structure interaction between the transducer and air, and the coupling between the electrical and mechanical properties of the piezoelectric material.

Statement of Contribution/Methods

The acoustic levitator used in this work consists of a 20 kHz bolt-clamped Langevin type PZT transducer and a stainless steel plane reflector. The harmonic analysis of the levitator was done in a finite element package (ANSYS), using axysimmetric elements. The finite element method is used to calculate the electrical impedance, the displacement of the transducer face, and the acoustic pressure and velocity fields produced by the transducer. The pressure and velocity values are used in the Gor'kov expression to calculate the acoustic radiation potential on a small rigid sphere. The numerical electrical impedance was compared to that obtained experimentally by a HP4194A impedance analyzer. The displacement of the transducer face was measured by using a MTI-2100 fiber-optic vibration sensor and it was compared to that obtained by ANSYS.

Results

The levitator was used to levitate small Styrofoam spheres. The positions of the spheres were compared to the positions of minimum acoustic radiation potential, as shown in Figure.

Discussion and Conclusions

The numerical electrical impedance and the displacements obtained by the finite element method showed very good agreement with that obtained experimentally. The positions of minimum acoustic radiation potential also showed good agreement with the equilibrium positions of the Styrofoam spheres.

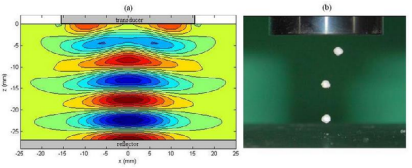

P1E074-06

Testing of a one dimensional model for Field II calibration

David Bæk[1], Jørgen Arendt Jensen[1], Morten Willatzen[2]; *[1]Technical University of Denmark, Center for Fast Ultrasound Imaging, Department of Electrical Engineering, Kgs. Lyngby, , Denmark, [2]University of Southern Denmark, Mads Clausen Institute for Product Innovation, Sønderborg, Denmark.*

Background, Motivation and Objective

Field II is a program for simulating ultrasound transducer fields. It is capable of calculating the emitted and pulse-echoed fields for both pulsed and continuous wave transducers. We examine an adapted one dimensional transducer model originally proposed by Willatzen (2001) to calibrate Field II. This model is modified to calculate

the required impulse responses needed by Field II for a calibrated field pressure and external circuit current calculation. The testing has been performed with Pz27 crystal discs from Ferroperm Piezoceramics, (Kvistgaard, Denmark).

Statement of Contribution/Methods

The transmitted acoustic pressures from two sets of each five disc samples with 10mm diameters were measured in an automatic water bath needle hydrophone setup together with the current flow through the driving circuit. Resonance frequencies at 2.1 MHz and 4 MHz were applied. Two types of circuits were considered, one circuit with a simple resistance load of 47.5 Ω and one with an example of a LR tuning circuit typically found in commercial transducers. The acquisitions and excitations were performed with an Agilent MSO6014A oscilloscope and an Agilent 33220A Function Generator.

The measurements were averaged 128 times to minimize measurement noise and then compared to the calibrated Field II program for 1, 4, and 10 cycle excitations. Two data sets were applied for modeling, one real valued Pz27 data set, manufacturer supplied, with electrical tolerances of +/- 10%, mechanical tolerances of +/-2.5%, and one complex valued dataset found in literature, Alqueró et al. (2004), that implicitly accounts for attenuation.

Results

The measurements were compared to the model by comparing the root mean square (RMS) of the errors relative to the RMS of the measurement averages. Our results show that the model has a relative current error in the range of 6-10% at 4MHz and 8-17% at 2.1MHz with the real data set. This is to be compared with the measurement errors for the currents which were in the range of 3-4%. A similar simulation with the complex data set shows an error in the range of 8-20% at 4MHz and 16-49% at 2.1 MHz. The relative RMS errors on the pressure measurements and modeled pressures show that the measured errors were in the range of 17-19%, which is to be compared with errors within 18-25% for the real valued data set, and 40-55% for the complex valued data set.

The significantly large error with the complex valued data set is due to a slight error, 1.6-2.3%, in the pulse phases, and an overshoot error of 7-15%. Furthermore, pulse tails have turned out to be the most difficult to model, where pulse excitation times are better to be captured. The model also accounts for the tuning circuits.

Discussion and Conclusions

The presented research has shown the very importance of applying correct data sets for this one dimensional model. The real valued data set achieved the smallest errors, within 6-10% for currents and 18-25% for Field calculated pressures, being acceptably close to the measured errors.

P1E075-07

Geometry Effect On Piezo-Composite Transducer With Triangular Pillars

Jianhua Yin[1], Mike Lee[1], Jeremy Brown[2], Stuart Foster[1]; [1]*Sunnybrook Health Science Center, Toronto, Canada,* [2]*Dalhousie University, Canada.*

Background, Motivation and Objective

At frequencies higher than about 20MHz, air-kerf array transducers are difficult to make using conventional dicing saw techniques. High frequency arrays made of piezo-composite materials have the advantages of lower acoustic impedance to better match tissue and the flexibility to facilitate an elevation focus without using an acoustic lens. However developing a high-frequency piezo-composite material for such arrays is still a challenge due to the extremely small pillar dimensions required to avoid the interference from the lateral resonances.

Statement of Contribution/Methods

Recently, success in developing high-frequency transducers made of piezo-composite materials with triangular pillars has been reported. The use of triangular pillar piezo-composite material was shown to suppress the lateral resonances that appear in square pillar composites. To further understand how the geometry of the pillars affects the lateral resonance, the piezo-composite material with triangular pillars of different angles are investigated in this work.

Results

The performance of composite transducers with triangular pillars of 30, 40, 45, 50 and 60 degree angles were simulated using PZFlex (Weidlinger Assc. Inc.). The pitches are 40um, kerfs 15um and thickness 45um for all devices. A backing of 30% PZT loaded epoxy was attached to the composite and no matching layer applied. The simulation results show that there are almost no change in bandwidth(~70%), central frequency (~30MHz) and the amplitude of the pulse among the transducers with pillars of different angles. However, from the electrical impedance of the transducers, large differences in the lateral resonances can be found. The lateral resonance

causes a ripple in the passband of the frequency response and a secondary pulse after the main in pulse response. This secondary pulse produces a ghost in imaging and need to be suppressed. The simulation results show that the composite with 45 degree pillars has the lowest secondary pulse (-22dB below the main pulse). The secondary pulse becomes larger when the angle of the pillars deviates from 45 degree. Composites with 30 and 60 degree pillars have the secondary pulses -15dB and -10dB below the main respectively. A detailed analysis of the lateral resonance versus the geometry will be presented.

Discussion and Conclusions

Experimental composite samples have also been made to compare with the simulation results. Three composite transducers with 30, 45 and 60 degree pillars were made from PZT5H. The PZT plates were diced with a 17um dicing saw blade and filled with PZT loaded epoxy. The electrical impedances and the pulse echoes were measured and the experimental results compared to theoretical predictions. Simulation and experiment both show that the composite with 45 degree pillars has better lateral resonance suppression.

P1E076-08

Modelling of the Electro-Acoustic Behaviour in Integrated Piezoelectric Structures under External Mechanical Stress

Pascal Tran, Guy Feuillard, **Mickael Lematre;** *LUSSI - University of Tours, France, Metropolitan.*

Background, Motivation and Objective

The developpement of piezoelectric integrated structures is mostly based on thin or thick film technology. In this case, the piezoelectric layer is laid down on a substrate and submitted to thermal treatment. In particular, after the sintering process, due to the difference of thermal expansion coefficients between the film and the substrate, a non uniform shrinkage appears that leads to a degradation of the functional properties of the structure through residual stress. Thus, it has become necessary to understand the role of residual and/or external mechanical stress in piezoelectric layers in order to predict the performance of integrated structures, especially for their electro-acoustic behaviour.

Statement of Contribution/Methods

In a first part, a bulk piezoelectric material with an external mechanical stress is considered. For this, Christoffel's equations for a piezoelectric material are modified to take into account a uniform mechanical stress tensor on a given cross-section. In a second part, the KLM model of a piezoelectric material under external mechanical stress is used by introducing into the standard KLM model the previous Christoffel's equations. Thus, it allows to predict the electro-acoustic behaviour of a piezo-electric material submitted to an external mechanical stress.

Results

A numerical study of the influence of an external stress is led on the slowness curves and associated polarizations, on coupling coefficients Kt and on electro-acoustic response of a lithium niobate based material. In order to correspond to the most practical configurations, the stress is applied in the same direction as the direction of propagation of the mode. Hence, it allows to consider different crystallographic cuts where, for each of them, we consider a direction of wave propagation and applied stress that is along the z axis.

Discussion and Conclusions

It can be shown that a lateral mechanical stress could couple pure transverse mode to piezoelectricity because of a slight rotation of the polarisation vector. It can also be noticed that the influence of the stress depend on its applied direction. In particular, the slowness curves and associated polarizations of the quasi-longitudinal and quasi-shear modes are more sensitive in the direction of propagation corresponding to the so-called Y+36° cut as far as the X-Y plane is concerned. In the same manner, the coupling coefficient Kt is more sensitive in the direction corresponding to an azimutal and incident angle both equal to about 60 degrees. This direction also corresponds to the initial (stress free) maximum of Kt. The global behaviour of the Kt coefficient shows that, for lithium niobate, its value increase when the applied stress is positive (traction) and decrease in the other case (compression).

Future work will consist in considering the influence of an external mechanical stress gradient in order to take into account more complex phenomenon.

P1E077-09

Finite Element Simulation of Piezoelectric Devices with Gyration and Temperature Effects

Andrey Nasedkin, Alexander Belokon; *Southern Federal University, Research Institute of Mechanics and Applied Mathematics, Rostov-on-Don, Russian Federation.*

Background, Motivation and Objective

In present work new models and numerical methods for dynamic behaviors of piezoelectric devices with rotation and temperature effects are presented. The special finite element techniques and computer programs are used for analyses of piezoelectric vibratory gyroscopes and transformers.

Statement of Contribution/Methods

For piezoelectric vibratory gyroscopes, working on "energy trapped" effects, we can introduce the small parameter. This parameter is the ratio between rotation frequency and principal resonance frequency. For modelling the work of such piezoelectric gyroscope we use the solution expansion in series with this small parameter. In first phase we solve the eigenvalue problems and the harmonic problem close to resonance frequency. Obtained mechanical displacements are stored in the nodes of finite element mesh for utilization in the next step. In the second phase we solve the problem with axial rotation and relative displacement in the resonance frequency. These Coriolis' forces are considered as nodal body forces.

For analysis of piezoelectric transformers and smart-devices with temperature effects we consider thermopiezoelectric problems. In classical coupled system of thermopiezoelectric equations the damping components are added. The finite element formulation of coupled thermopiezoelectric problems in general case and in the case of partial relatedness is obtained.

Results

Developed methods are applied in the special program modules for finite element package ANSYS. The new piezoelectric finite elements with Coriolis' forces and axial rotation are built. The optimization calculations for discovery new effective piezoelectric vibratory gyroscopes are realized.

For analysis of piezoelectric devices with temperature effects in ANSYS we propose the special techniques. In ANSYS it is possible to solve successfully the static piezoelectric problems with thermal stresses using coupled-field analysis technique. Using additional macros we also solve the problem about dissipative heating of piezoelectric Rosen multilayer transformers under harmonic vibration. In particular, having solved in ANSYS the harmonic piezoelectric problem by standard way one can find the displacement field. Using this field we calculate averaged dissipative function. This dissipative function is further considered as additional thermal source in heat flow problem, which is solved in ANSYS.

Discussion and Conclusions

A new technique expands the possibilities of the analysis for different piezoelectric devices with gyration and temperature effects. We apply this technique for harmonic step-by-step analysis of some piezoelectric vibratory gyroscopes and piezoelectric Rosen multilayer transformers. The calculations have shown the high efficiency of the proposed models for analysis of piezoelectric devices with rotation and temperature effects especially second infinitesimal order relatively to principal electro-mechanical vibrations.

Monday Poster

P1F. Piezoelectric & Ferroelectric Materials

2nd and 3rd Floor Foyers

Monday, November 3, 2008, 3:00 pm - 4:30 pm

Chair: **Levent Degertekin;**
Georgia Institute of Technology, GA, USA.

P1F078-01

The Lead-free Piezoelectric Ceramic Materials will be used for green and environmental protection type Medical Ultrasonic Equipments

Li Li Quanlu; *Shaanxi Normal University, Institute of Applied Acoustics, School of Physics and Information Technology, Xi'an, Shaanxi, China.*

Background, Motivation and Objective

Piezoelectric ceramics have wide-ranging important applications in the many fields. This paper summarizes developing status quo and the problems in applications of the lead-free piezoelectric ceramic materials firstly, and gives out the present main research directions of lead-free piezoelectric ceramics, which are: and (Bi Na) Ba TiO (BNBT), etc basic lead-free piezoelectric ceramics and bismuth (Bi) layer structure piezoelectric ceramics to use for green and environmental protection type medical ultrasonic equipments,etc.

Statement of Contribution/Methods

At present work, the lead-free piezoelectric ceramic materials (Bi1/2Na1/2)0.94Ba0.06TiO3 is prepared by dry ceramic processing involving powder mixing, perpressing of compacts, presintering, grinding to powder, granulation, dry pressing, de-adhesive, sintering, finishing after sintering, metallization, polarizing, ageing, testing and measuring, up until piezoelectrical ceramic elements. After fabrication and metallization, lead-free piezoelectric ceramic crystals cannot possess piezoelectricity and become piezoelectric elements when polarized. As the lead-free piezoelectric ceramic materials (Bi1/2Na1/2)0.94Ba0.06TiO3 crystalline pellets (made by ourselves) have all passed ageing, their properties must be tested and measured by IEEE standard on piezoelectricity.

Results

In present work, some properties of the lead-free piezoelectric ceramics obtain max value 879, d33©„160pC/N, kp©„28.46%, respectively, when MnO2 is 0.3wt%. In the range of Mn-doping, the mechanical quality factor show reverse change trend. When MnO2 ranges from 0wt% to 0.3wt%, the mechanical quality factor decrease evidently, and then increase for MnO2 >0.3wt%, and attained min value 152.26 at MnO2©„0.3wt%. However, dielectric loss show different change trend with Mn-doping. From 0wt% to 0.15wt%, dielectric loss increase, between 0.15wt% and 0.3wt%, dielectric loss decrease, and then again ascended for MnO2 > 0.3wt%. The min value of dielectric loss is 0.026 at MnO2©„0.3wt%. In addition, large electromechanical coupling factor and electrical resistivity could be gained under low polar electric field when right MnO2 were added, which indicate that proper MnO2 effectively decrease coercive electric field.

Discussion and Conclusions

The piezoelectrical ceramic materials and devices also need in company with medical ultrasonic appearances (including ultrasonic power source, electric circuits, etc) to develop forward. Ultrasonic medicine which can unquestionable be attained when new-technology and high-techniques (including materials, devices, and, a complete set of equipment, etc) is joined or applied. In the other respect, the lead-free piezoelectric ceramics have wide-ranging important applications in medical ultrasonics fields (including medical piezoelectric ultrasonic diagnosis transducers and medical piezoelectric ultrasonic therapeutic transducers, etc).etc.

P1F079-02

Stable resonance characteristics in CuO-modified lead-free 0.94(K0.5Na0.5)NbO3-0.06LiNbO3 ceramics sintered at optimal temperature

Yang Ying, **Wan Dandan;** *Precision Driving Laboratory, Nanjing University of Aeronautics and Astronautics, Nanjing, Jiangsu, China.*

Background, Motivation and Objective

In recent years, (K0.5Na0.5)NbO3 lead-free piezoelectric ceramics have been extensively investigated. Although a large d33 could be achieved by doping Li, Ta, and Sb into KNN ceramic, the mechanical quality factor Qm,

a key parameter for frequency devices, is relatively low for KNN ceramics. The smaller Qm value of piezoelectric ceramics cannot satisfy the basic requirements of piezoelectric

ceramic frequency devices. The goal of our study is to exploit KNN-based ceramics with high Qm by conventional ceramic processing.

Statement of Contribution/Methods

Lead-free piezoelectric ceramics with the nominal composition of (1-x)(K0.5Na0.5)NbO3-xLiNbO3[(1-x)KNN-xLN] have been synthesized by conventional solid-state sintering. Effects of the sintering conditions on the phase structure, micro-morphology evolution and piezoelectric properties of the ceramics were investigated. The phase structure and the micro-morphology were analyzed by X-ray diffraction (XRD) and scanning electron microscope (SEM).

Results

The ceramics synthesized at 1020¯C1080¡æ showed a phase transition from orthorhombic to tetragonal symmetry, which is analogous to the morphtropic phase boundary (MPB). Because of this polymorphic phase transition, high piezoelectric coefficient d33 and electromechanical coupling factor kp were obtained in the nominal composition 0.94KNN-0.06LN ceramic sintered at optimum temperature; however, the mechanical quality factor Qm is still relatively low for these KNN-LN ceramics. In order to improve the resonance characteristics , CuO has been doped in 0.94KNN-0.06LN ceramics.

Discussion and Conclusions

Our results show that the doping of CuO is effective in promoting the densification of the KNN ceramics and hardening of piezoelectric properties. CuO-modified lead-free 0.94(K0.5Na0.5)NbO3-0.06LiNbO3 ceramics sintered at optimal temperature show stable resonance characteristics.

P1F080-03

Comparison between Synchronized Switching Damping technique and Velocity-Controlled Switching Piezoelectric Damping

Yuan-Ping Liu[1], Dejan Vasic[1], Francois Costa[1], Wen-Jong Wu[2], Chih-Kung Lee[3]; *[1]Ecole Normale Superieure de Cachan, Cachan, Ile-de-France, France, [2]National Taiwan University, Department of Engineering Science and Ocean Engineering, Taipei, Taiwan, [3]National Taiwan University, Institute of Applied Mechanics, Taipei, Taiwan.*

Background, Motivation and Objective

For vibration suppression, piezoelectric shunt damping is widely used since it is easy to implement without a heavy amplifier. However, the limitation of a passive shunt damping is that it is very sensitive to the environment. The semi-active control was thus proposed to enhance the robustness of a passive shunt damping. Popular semi-active control methods are synchronized switching damping (SSD) techniques. Previous research shows that the passive shunt damping gives a better performance at the resonance frequency, but is characterized by a poor bandwidth, while the SSD techniques gives a poorer performance but has a much wider bandwidth. Ideal damping control is where performance is maximized and where the bandwidth is widest. A velocity-controlled switching piezoelectric damping (VSPD) which was proposed to track the maximum power factor of a piezoelectric layer, was compared to a SSD techniques to see which performed better and had a wider bandwidth. The major objective of this paper was to compare the two different semi-active damping techniques and to find the better of the two.

Statement of Contribution/Methods

As a semi-active control is a nonlinear type of control, it is difficult to analyze the damping. Therefore, a work cycle was proposed to compare these two techniques. A work cycle is a curve on the stress/strain plane which represents the energy state of the piezoelectric material. The area of a work cycle represents the energy dissipated from the damping, i.e. damping performance. From the work cycle, we can compare the performance of these two types of damping. We derived the theoretical shape of the work cycles and used our simulation as well as

experimental work to verify the results. In addition, we also compared the two damping types from a viewpoint of power factor which is one of the main parameters in designing an ideal piezoelectric damping control tool.

Results

A comparison of the two techniques is shown in Figure. Results show the VSPD has having the better performance of the two. In addition, both techniques seem to possess a similar bandwidth as all other semi-active control methods.

Discussion and Conclusions

A work cycle implies a waveform formation and the VSPD shows a very obvious square waveform. Results obtained show that the VSPD possesses better damping than a SSD. More importantly, based on the work cycle, results show that the VSPD offers the better shunt damping.

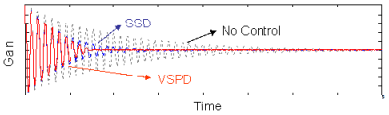

P1F081-04

Structural and electrical properties of Bi0.5(Na1-xKx)Tio3 thick films by a novel water-based gel-tape casting process

Tiantian Xie, Shenglin Jiang, Maoyan Fan; *Huazhong University of Science and Technology, China.*

Background, Motivation and Objective

In recent years, with the growing demands for global environmental protection, lead-free materials have gained much attention on an increasing degree. Sodium-bismuth titanate is one of the most important lead-free piezoelectric materials with perovskite structure discovered by Smolenskii et al in 1960. The NBT composition exhibits a strong ferroelectricity and high Curie temperature Tc=320 ¡æ, it has been considered to be a good candidate to substitute lead-based materials(e.g., PZT), which have been widely used for various applications such as ultrasonic generators, actuators, filters and other electronic devices.

Statement of Contribution/Methods

Lead-free piezoelectric Bi0.5(Na0.82K0.18)Tio3(BNKT) thick films have been prepared by a novel process water-based gel-tape-casting, which is developed by combined gel-casting and tape-casting technologies together. The fabrication process was shown in Fig.1.

Results

The organic additive in this process was about 3.5wt% of powder which was largely lower than conventional tape-casting and screen printing. The thickness of the films was about 100¦Ìm.

Discussion and Conclusions

Its structural, dielectric, and piezoelectric properties were also characterized. The XRD pattern in Fig.2 shows typical peroveskite polycrystalline structure. The SEM figure in Fig3 shows a homogeneous microstructure and the average grain size is about 1¡«3¦Ìm. The Sample sintered at 1140¡æ exhibited the best electrical properties that the dielectric constant, dielectric loss and piezoelectric charge coefficient d33 are 896, 0.05 and 93pC/N, respectively. Compared with other process, gel-tape-casting was a simple, environmental friendly and effective method to fabricate lead-free piezoelectric ceramics.

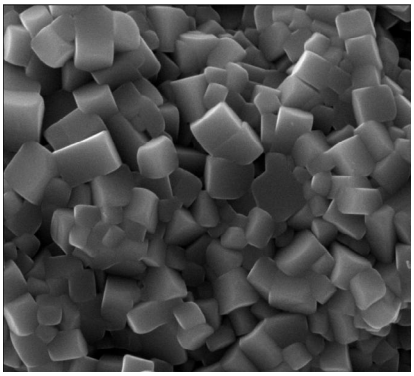

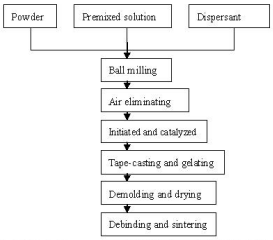

Fig.1 Fabrication process of BNKT piezoelectric thick films by gel-tape-casting

P1F082-05

PIN-PMN-PT Single Crystal High Frequency Ultrasound Transducers for Medical Applications

Q.F. Zhou[1], B.P. Zhu[1], D.W. Wu[1], C.H. Hu[1], J. M. Cannata[1], J. Tian[2], P. D. Han[2], K.K. Shung[1]; *[1]NIH Resource on Medical Ultrasonic Transducer Technology, Department of Biomedical Engineering, University of Southern California, Los Angeles, CA, USA, [2]H. C. Materials Corp., Bolingbrook, Illinois, USA.*

Background, Motivation and Objective

Medical imaging transducers utilize a piezoelectric material as the active element to transform the electric input into a mechanical wave propagating into the imaging target and transform the echo back into electric output signal. PMN-PT single crystal have superior piezoelectric properties (e. g., d33=2000-3000 pC/N, k33=85-95%). Currently, PMN-PT single crystals have been commercialized in advanced commercial ultrasound system. However, for the binary PMN-PT crystal, the coercive field (2.5 kV/cm) is low for high drive applications and the low de-poling temperature (TR/T ~ 75-95 oC) leads to undesirable changes in crystal properties and transducer performance with temperature. Recently, H. C. Materials Corp. has developed ternary PIN-PMN-PT single crystals with higher coercivity and improved thermal stability. In this work, high frequency ultrasound transducers using the ternary PIN-PMN-PT single crystals were fabricated and characterized.

Statement of Contribution/Methods

A (001) PIN-PMN-PT single crystal was used as the active material of the transducer. Previous results show that this new single crystal displays superior electromechanical coupling coefficient, high transition temperature and lower dielectric loss. First, the sample was lapped to 50 ¦Ìm. A matching layer made of Insulcast 501 and Insulcure 9 (American Safety Technologies, Roseland, NJ) and 2-3 ¦Ìm silver particles (Sigma-Aldrich Inc., St. Louis, MO) was cured over the PIN-PMN-PT and lapped to 12 ¦Ìm. A conductive backing material, E-solder 3022 (VonRoll Isola, New Haven, CT), was cured over the opposite side of the PMN-PT and lapped to 3 mm. Active element plugs were diced out at 0.5 mm aperture. An electrical connector was fixed to the conductive backing using a conductive epoxy. Vapor deposited parylene with a thickness of 14 ¦Ìm was used to coat the aperture as second matching layer. A high frequency transducer (38 MHz) of small aperture has been successfully fabricated. A poling study under different mechanical conditions was investigated. The pulse echo and the insertion loss of transducers were measured.

Results

The measured center frequency and -6 dB fractional bandwidth of the PIN-PMN-PT crystal transducer were 38 MHz and 45 %. The two-way insertion loss was approximately 12 dB. The output voltage without external amplifier was 2.0 V.

Discussion and Conclusions

The results showed that the sensitivity of the PIN-PMN-PT transducer exceeds that of the PMN-PT needle transducer which we previously reported.In vivo high frequency pulsed wave Doppler patterns of blood flow and in vitro ultrasonic backscatter microscope (UBM) images of the rabbit eye have been acquired for the demonstration of potential biomedical applications.

Monday Poster

P1G. Sonar Propagation and Detection

2nd and 3rd Floor Foyers

Monday, November 3, 2008, 3:00 pm - 4:30 pm

Chair: **Valery Proklov;**
IRE RAS, Russia.

P1G083-01

Simulation Model of Bottom Reverberation Signals for Horizontal Bistatic Receiving Array

Zhang Minghui, **Sun Hui;** *Harbin Engineering University, China.*

Background, Motivation and Objective

The reverberation is heard as a long, slowly decaying, quivering tonal blast following the ping of an active sonar system, and is one of basic physical phenomena in the underwater acoustics. The reverberation often forms the primary limitation on active sonar system performance,so the bottom reverberation signals model for horizontal bistatic receiving array is established.

Statement of Contribution/Methods

In the present work, the bottom reverberation signals model based on ray acoustics theory is developed using unit scattering model. The radius of space correlation of bottom scattering coefficient is used to set scattering units. The bottom scattering coefficient is formed with LAMBERT Law. Making the assumption with a constant sound speed, the scattering from the sea surface, multi-path effect and the inter-influence of bottom scattering units are ignored. And also, with an isotropy sea floor, the projecting transducer and receiving array units are without directivity, the incident wave spreads in the form of spherical wave, and the signal from each scattering unit attenuates spherically.

Results

Making use of emulated multi-array-elements data after the bottom reverberation signal model is verified correctly in theoretically, the relation between characteristics of bottom space correlation and sea ambient parameters are analyzed. The emulation result shows that the space correlation of bottom reverberation signal for horizontal bistatic receiving array does not change with angle factor of LAMBERT Law and difference of scattering coefficient, instead it increases as correlation radius of bottom scattering coefficient decreases.

Discussion and Conclusions

The results were got when the projecting transducer and receiving array units are in one line. So the space correlation of bottom reverberation signal for horizontal bistatic receiving array when the projecting transducer and receiving array units are in different line will be discussed in the future.

P1G084-02

The Research on Technique of Underwater Noise Source Identification by NAH in Semi-space

Dejiang Shang, Yongwei Liu, Chao Zhang, Lihua Liu; *Harbin Engineering University, College of Underwater Acoustics, Harbin, China.*

Background, Motivation and Objective

The technique of near field acoustic holography (NAH, hereafter) is an efficient way to identify noise sound sources. The sound quanta, such as sound pressure, particle velocity and sound intensity in the sound field, can be reconstructed from the measurement of complex sound pressure in the holography surfaces near the noise sound sources. However, in recent years, most research has been done on sound radiation of vibrating structures in no boundary space (free field). In fact, the vibrating structures usually radiate sound waves in three dimensional semi-space, for example, the sound radiation problems of vibrating structures in the air, ships and underwater submarines, etc. On these conditions, sound pressure measured in the holography surfaces is the summation of incident sound pressure and reflected sound pressure. The radiation properties of the whole sound field can¡¯t be

predicted accurately by the technique of NAH in full-space. This limitation has restricted the engineering application of NAH in full-space to some extent.

Statement of Contribution/Methods

Based on the technique of NAH in full-space, the theoretical model and the technique of NAH in semi-space are founded by the principles of mirror method. The algorithm of Fast Fourier Transforms (FFT) has been introduced into the theoretical model of NAH in semi-space. This technique has considered the water surface as the absolutely soft boundary. Then the measured sound field underwater has been dealt with by the dissymmetry due to water surface, so that the equivalent free sound field can be gotten. This technique can also overcome the disadvantages of the Boundary Element Method (BEM) to resolve the problems of noise sound sources identification in semi-space, such as the use of the semi-space Green function, the calculation of complex transformation matrix, the more consummation of time and the existence of singularity solution, etc.

Results

The theoretical model of NAH in semi-space has been simulated by the software MATLAB. Then, the parameters, such as the location, the size, the shapes of holography surfaces and the distance between measurement points are analyzed by numerical simulation, so as to investigate the error of sound filed reconstruction in semi-space. After that, the whole measurement system has been built up and the correctness of the technique in semi-space has been validated by the experiment. The frequency ranges from 3 to 10 kHz in the experiment. The conditions of single sound source and many sound sources near water surface have been investigated by the technique of NAH in semi-space respectively. The experimental results have sufficiently revealed the advantages of underwater noise sound sources identification by the technique of NAH in semi-space.

Discussion and Conclusions

It is an efficient way to deal with the problems of noise sound sources identification near water surface by the technique of NAH in semi-space.

P1G085-03

The Investigation on Measuring the Coefficient of Sound Absorption at 20-60 kHz in Turbid Seawater

Yongwei Liu, De jiang Shang, Qi Li, Fengyang Chi; *Harbin Engineering University, College of Underwater Acoustics, Harbin, China.*

Background, Motivation and Objective

When naval mine-hunting sonars and side-scan surveying sonars are operated in shallow coastal environments, which are characterized by high levels of suspended fine clay particles relative to open ocean, the effect of sound absorption caused by suspended particles in the water may greatly decrease these sonars¡¯ detection performance. This kind of water is also characterized as turbid seawater. In order to account for this effect in sonars performance predictions, it is necessary to calculate the absorption coefficient in particulate suspensions. However, the sound absorption properties of suspended particulate matter in natural bodies of water are not well characterized.

Statement of Contribution/Methods

The main difference between turbid seawater and clear seawater is that there are fine clay particles suspended in turbid seawater. In the paper, a reverberation time technique has been developed for the laboratory measurement of sound absorption at 20-60 kHz in dilute suspensions, and the measuring system has also been built up. In the test volumes employed, the effect is small. It is therefore measured by taking the difference in reverberation times of a volume of water with and without fine clay particles. This greatly reduces the effect on the measurement of the other sources of absorption. Even so, it is necessary to design the experiment to characterize and minimize acoustic losses which occur at the surfaces of the container, the hydrophones, and their cables, and losses associated with bubbles and turbulence.

Results

The pure water is taken to calibrate the energy loss of the measuring system. After that, the coefficient of sound absorption in the magnesium sulfate solutions of known concentrations has been measured and compared to theoretical predictions, so as to estimate the measurement error of the system. The measured results agree well with that predicted by theory.

In clear seawater, the main cause of sound absorption at 20-60 kHz is the electrolyte magnesium sulfate. In order to characterize absorption by natural marine particles measurements in representative suspensions are required. So the solute in turbid seawater is mainly the magnesium sulfate and fine clay particles. Many turbid seawater samples of different concentrations have been measured. The results demonstrate that at a fixed frequency, the coefficient of

sound absorption in turbid seawater is augmenting approximately with the increased concentrations. If the concentrations of fine clay particles In turbid seawater are below 110mg/L, the fine clay particles don't cause additional sound absorption. However, if the concentrations of fine clay particles in turbid seawater are above 140mg/L, the coefficient of sound absorption in turbid seawater is as twice at least as that in clear seawater.

Discussion and Conclusions

It is concluded that sound absorption measured in this paper is appropriate for estimating the sound absorption in dilute suspensions of fine clay particles.

P1G086-04

A method for detecting of the target echo in reverberation noise

Chen Wenjian, Sun Hui, Zhu Jianjun, Zhu Guangping, Zhang Minghui; *Harbin Engineering University, Harbin, Heilongjiang, China.*

Background, Motivation and Objective

In active sonar detection, reverberation is the dominant background interference. This paper is devoted to detection of target echo corrupted by the reverberation noise they have created.

Statement of Contribution/Methods

Based on the Fractional Fourier Transform theory, a new method for detecting the target echo is proposed in this paper when linear frequency modulation signals are used in sonar, which take advantage of the differences between reverberation and target echo in the time-frequency domain.The detection scheme is synthesized in Fig.1.

Results

An example of reverberation noise generated by a linear chirp is presented in Fig.2(a). The output of the detector is presented in Fig.2(b).

Discussion and Conclusions

From the result of analyzing the imitated and experimental signal, it can be found that the new method has the ability to detect target echo in reverberation.

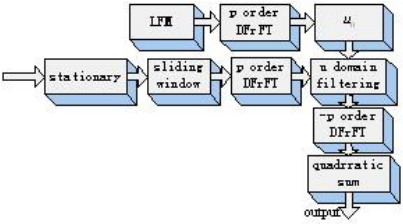

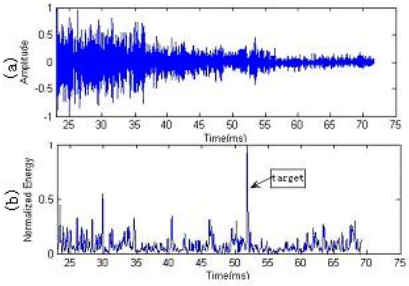

P1H. Ultrasonic Motor Applications

2nd and 3rd Floor Foyers

Monday, November 3, 2008, 3:00 pm - 4:30 pm

Chair: **Takefumi Kanda;**
Okayama University, Japan.

P1H087-01

Study of an Ultrasonic Rotary Motor Used for a Locking System

Jose Fernandez, **Markus Flueckiger,** Yves Perriard; *EPFL, Lausanne, Vaud, Switzerland.*

Background, Motivation and Objective

Ultrasonic motors are used in a wide range of industrial applications notably because of their advantages of compact size, high torque at low speed and fast response. In this study, an ultrasonic motor has been designed to fit into a mechatronic lock cylinder, which represents an important and innovative extension of its application field. Such mechanical-electronical lock cylinder needs some sort of actuation to change the state of the lock. DC motors are currently the most widespread type of actuators used for this purpose. Unfortunately, they use most energy at low speed and they do not hold a defined position when energy is cut. The goal of this study is therefore to research and develop an ultrasonic motor that would largely reduce the complexity of the lock cylinder, making it more reliable and energy efficient.

Statement of Contribution/Methods

A standing wave rotary ultrasonic motor has been initially designed to fit into the lock cylinder. The approach consists in performing a FE modeling of the motor structure. After finding the different vibration modes, it is possible to find out the axial and tangential deformation amplitudes of the resonator allowing the motor rotation when a pre-stressing force is applied to the rotor. Using an optimization methodology based on a sensitivity analysis using in particular the design of experiments method and then a FE optimization, it is possible to maximize the deformation amplitudes in both directions to obtain higher torque and speed of the motor. Along with this process, prototypes are built in order to validate the adopted design methodology and verify if the chosen motor concept is appropriate.

Results

The first FE results have shown that the maximal deformation amplitudes are found using a resonator with a third vibration mode at a resonance frequency of 411kHz. Axial and tangential displacements are about 0.16µm and 0.22µm respectively when a voltage of 100V is applied to the piezoelectric ceramic. Some prototypes have been built and tested. The deformation amplitudes have been measured with an laser interferometer and these results were comparable to the ones obtained by FE simulations. Other comparison results between FE simulations and experimental results are also presented.

Discussion and Conclusions

Results have shown that it is possible to find deformation amplitudes in the micrometer range if the applied voltage is increased for the third vibration mode. Elliptic trajectory of the surface points of the resonator has also been observed. By comparing FE simulations with experimental results obtained by measuring the admittance response and also the deformation amplitudes, it could be noticed that the results are similar and the design methodology could be validated. Further developments are needed to verify if the concept of standing wave type ultrasonic motor is appropriate to fulfill the requirements that will allow the integration of the ultrasonic motor in the lock cylinder.

P1H088-02

Performance simulation of ultrasonic motors for compression cardiac assist

Ming Yang[1], Wangfu Zang[2], Shiyang Li[1]; *[1]Shanghai Jiaotong University, China, [2]Shanghai Ruijin Hospital, China.*

Background, Motivation and Objective

Heart transplantation is an accepted method to treat end-stage heart failure, but the demands for heart donors is much more than the supply. Therefore, some mechanical devices are required to assist or replace the weakened heart. Up to now, many kinds compression cardiac assist devices based on pneumatic and fluid driving approaches have been developed. However, these devices require tubes through the skin to connect air or liquid pumps, which are main causes of infection and restrain the movement of patients. It is therefore necessary to exploit new possible actuators. Ultrasonic motors are potentially attractive actuators for compression cardiac assist due to their small sizes, light weight, simple structures, fast response, large force density, and silent motion. So performance simulation study of ultrasonic motors for compression cardiac assist is carried out to investigate the feasibility.

Statement of Contribution/Methods

Compression Cardiac assist device wraps around the weakened heart and supports the circulation by compressing the weakened heart from its epicardial surface, and accordingly increase heart pumping capacity. To simplify the modeling process, the heart shape is assumed to be a half sphere, where sphere wall of heart is stretched as a result of the difference between the blood pressure inside the heart and the surrounding pressure outside the heart. Therefore Frank-Starling relationship and circulatory system model are used to construct the mathematical model of interaction between the weakened heart and the compression cardiac assist devices.

Results

Considering the geometry of the heart, three commercial available ultrasonic motors are selected and connected in series or in parallel, simulation results suggest that compression cardiac assist device based on these motors has limited effect on improving performance of weakened heart. If nine ultrasonic motors are matrix connected in three rows and three columns, the strain of the compression cardiac assist reaches 18.7% with an assisted pressure of 132mmHg, and the weakened heart is almost recovered to its normal status in terms of blood pressure variation and volume contraction.

Discussion and Conclusions

The current commercial ultrasonic motors cannot drive effectively to get an obvious improvement of a weakened heart. If a single linear ultrasonic motor has a size of 20mm x 25mm x 8mm, simulation result shows that increasing a pulling force to 24N will be desired for the development of future linear ultrasonic motors as actuators of compression cardiac assist devices.

P1H089-03

Genetic Algorithm Optimization for a Surgical Ultrasonic Transducer

Daniel Porto, Aurélien Bourquard, Yves Perriard; *EPFL- STI - LAI, Lausanne, Switzerland.*

Background, Motivation and Objective

Nowadays everyone knows someone who suffers from back pain. In most cases a surgical intervention has to be done and different manual methods are already used to cut the human tissue or to remove the spinal disc. Nevertheless, the surgeons are not always fully satisfied due to the tedious, time consuming and taxing of the existing devices. One interesting solution is the development of an ultrasonic piezoelectric transducer that could have an improved efficiency and facilitate the surgeons work.

Statement of Contribution/Methods

An ultrasonic transducer composed of a piezoelectric stack, eight mechanical transmission parts and three exponential horns for the movement amplification is chosen. Finite Element Analysis (FEA) tools are used to obtain the displacement amplitude of the cutting tip in a frequency domain and the vibrational displacement along the actuator. The transducer has eleven geometric parameters to be optimized, that are diameters or lengths. The materials for that case are chosen but could also be optimized. The genetic algorithm optimization routines are developed with Matlab software to maximize the vibrational amplitude of the transducer at the resonant frequency.

Results

Three genetic algorithms have been developed. The first one is called upgr1 and is based on conditional genetic operators: the diversity of the population decreases at each generation. The second one is called upgr2 and is based on a specific crossover operator definition with a local search method. The third algorithm is called upg12 and is a

combination of both the previous algorithms. The different algorithms have been evaluated and compared with a lot of well known test functions; with and without constraints. The third algorithm showing very good results in most of the test cases, it is used to optimize the piezoelectric transducer.

In less than 5000 evaluations (simulations), at the resonant frequency of 22.5 kHz, the optimizations give an amplitude of the cutting tip of about 4.8 microns and the total length of the transducer is about 340 millimetres.

Discussion and Conclusions

In a previous work, an optimization of a piezoelectric transducer has been done with a pseudo-gradient method based on an analytical developed model. When comparing the vibration amplitude with the two methods (pseudo-gradient and genetic algorithms), the results are almost the same. The advantage of the genetic algorithms resides in the low number of simulations needed to obtain good results. Which makes optimizations of full FEA models truly envisioned.

P1H090-04

Rotation Phase Analysis of Surface Particle Motion of Coiled Waveguide caused by Flexural Ultrasound Wave

Kohei Tomoda, **Masataka Ishiguro,** Masayuki Tanabe, Kan Okubo, Norio Tagawa; *Tokyo Metropolitan University, System Design, Hino, Tokyo, Japan.*

Background, Motivation and Objective

We have developed a traveling wave-type miniature ultrasonic motor using a helical coiled waveguide as a stator [1], and have already applied it to an IVUS probe [2]. In this motor, the elliptical motion of the surface particle due to the flexural ultrasonic waves rotates the rotor, which can be placed adjacently inside or outside the stator, via the frictional force. For high frequencies, rotational directions of both of the inner rotor and the outer rotor are consistent with those of usual traveling wave-type ultrasonic motor. However, for low frequencies, the outer rotor rotates inversely. In [3], we examined the rotational direction of the surface particle motion of a coiled waveguide for low frequencies, and we clarified that the directions at the inner surface and at the outer surface are the same, which is not realized by a straight-line waveguide. In this study, we examine the rotation phase at the both surfaces.

Statement of Contribution/Methods

In this study, using the PZFLEX, which is a standard simulator for ultrasound propagation, and modeling a helical coiled waveguide with a stainless steel wire, we simulate the surface particle motion due to traveling flexural waves at both of the inner and the outer surfaces for low frequencies.

Results

As shown in the figure, at the whole positions of a coiled waveguide, it was confirmed that the rotation phases at the both surfaces are almost the same in addition to the rotational direction. The properties of the symmetric and the anti-symmetric mode of the Lamb wave in a straight-line waveguide are also shown in the figure, in which the arrows in the elliptical loci indicate the phase relation.

Discussion and Conclusions

In a coiled waveguide, the motion phase along the surface normal direction coincides with that of the anti-symmetric mode in a straight-line waveguide, but the rotation direction at the outer surface equals to that of the symmetric mode. These properties indicate that the complicated wave mode exists. It is desirable to investigate the detail and the microscopic mechanism of this mode.

[1] T.Moriya, et al., IEEE Ultrasonics Symp., pp.1546-1549 (2005)

[2] S.Xie, et al., IEEE Ultrasonics Symp., pp.1301-1304 (2006)

[3] S.Xie, et al., IEEE Ultrasonics Symp., pp.2284-2286 (2007)

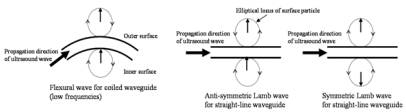

P1H091-05

A tiny ultrasonic motor used in an OCT endoscope*

TieYing Zhou, **Yu Chen,** Ping Xue, Tao Liu; *Tsinghua University, Department of Physics, Beijing, China.*

Monday Poster

Background, Motivation and Objective

To make an ultrasonic motor of small diameter, the bending mode ultrasonic motor (BM-USM) is often used. The tube-type tiny BM-USMs were reported from 2000 to 2003. In 2001, a BM-USM with a piezoelectric cylindrical rod of a diameter 1mm was developed at Tsinghua University and was used in a prototype of an optical coherence tomography (OCT) endoscope.Recently in order to minimize the size of USM and simplify its fabrication, a tiny cube shaped USM was developed.

Statement of Contribution/Methods

The structure and the method of polarization are shown in Figs.1 (a)and (b). The stator is a piezoelectric cube with dimensions 0.8mm¡Á0.8 mm¡Á4mm. The length of the four truncated edge was optimized with the use of an infinite element analysis, which is 0.15mm. Four silver electrodes are uniformly deposited on the side surface of the stator. When electric signals, sin ¡¢cos ¡¢-sin ¡¢-cos , are applied to the four electrodes respectively, the wobble motion of the USM is excited.

Results

A prototype of the motor was fabricated. The no-load rotation speed is 2460 rpm and stall torque is about 3.5 Nm, when the driving voltage was 65Vp-p. The cubical USM have been utilized in a prototype of OCT endoscope. The chicken esophagus in vitro was examined by circular scanning of 4 frames/s and its image is shown in Fig.2. The axial resolution is 25 m and the lateral resolution is 30 m.

Discussion and Conclusions

This cubic ultrasonic motor has shown good performance and has application potential.

*This work is supported by 863 AA02Z472 and NSFC(50577035£¬10676015)

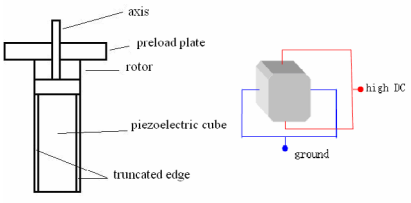

Figure 1 a cube shaped USM

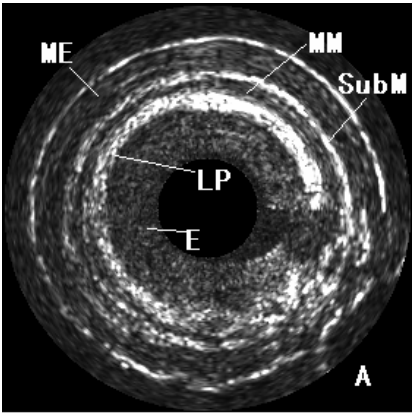

Figure 2. The image of a chicken esophagus

P1I. Phononic Crystals II

2nd and 3rd Floor Foyers

Monday, November 3, 2008, 3:00 pm - 4:30 pm

Chair: **Jan Brown;**
JB Consulting, MA, USA.

P1I092-01

Finite Element Method for Analysis of Band Structures of Phononic Crystals

Jianbao Li[1], Yuesheng Wang[1], Chuanzeng Zhang[2]; [1]*Beijing Jiaotong University, Institute of Engineering Mechanics, Beijing, China,* [2]*University of Siegen, Department of Civil Engineering, Germany.*

Background, Motivation and Objective

Phononic crystal is a periodic structure composed of periodic arrays of two or more material components. An important property of a phononic crystal is the existence of phononic band gaps. Due to this property, phononic crystals are expected to manipulate acoustic waves and thus have many potential applications. Phononic crystals have received extensive attention since the pioneer work of Kushwaha.

Several numerical methods have already been developed and applied to the analysis of phononic crystals, most of them have various disadvantages. Some analyses of plane wave propagation in periodic structures by using FE may be found in some literatures, however it is less used in calculation of the band structures of phononic crystals.

The paper aims to analyze basic behaviors of propagation of acoustic bulk waves in 2D/3D Phononic crystals with the help of MSC.MARC code and user subroutine.

Statement of Contribution/Methods

Consider propagation of a harmonic wave in a phononic crystal. According to Bloch theorem, the following phase relation between the mechanical displacements for nodes lying on the boundary of a unit cell:

$u(x,y)=u(x+a,y+a)\exp[-i(k_x a+k_y a)]$

where k_x,k_y represent wave numbers,and a is lattice constant.

The equation for the FE simulation is:

$([K_R]-\omega^2 [M_R])u=0$

where K_R is the reduced stiffness matrix;and M_R is the reduced mass matrix.

The frequencies and vibration modes of equation can be calculated by using the:subspace iteration or Lanczos iteration.

Results

Figure 1 shows the dispersion relations of a 2D solid-solid phononic crystal composed of Au cylinders embedded in epoxy. For comparison, the results have a good agreement with those obtained by the PWE method. The results indicate that the FE method is precise for the band structure computation of the phononic crystals and can reduce computing time to a certain extent.

Discussion and Conclusions

We have extended the FE method to analyze acoustic wave propagation in 2D/3D phononic crystals. The FE method has features of better convergence and fast evaluation speed.It can provide the accurate results with the help of FE code.The present research can serve as a basis for both numerical and experimental investigations of phononic crystal structures.

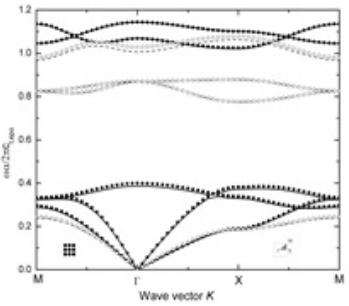

P1I093-02

Influence of heterogeneous external fields on propagation of bulk acoustic waves in crystals

Boris Sorokin[1], Aleksandr Marushyak[2], Kirill Aleksandrov[3]; [1]*Siberian Federal University, Solid State Physics, Krasnoyarsk, Russian Federation,* [2]*Siberian Thermotechical Institution, IT, Krasnoyarsk, Russian Federation,* [3]*L.V. Kirensky Institute of Physics, Siberian Branch of the Russian Academy of Sciences, , Krasnoyarsk, Russian Federation.*

Background, Motivation and Objective

There are acoustoelectronic devices for which it is necessary to take into account the influence of heterogeneity of deformation of working element of device. For example there are piezoelectric sensors of force and acceleration.

Statement of Contribution/Methods

Propagation of bulk acoustic waves of small amplitude in crystals is based on classic Green-Christoffel's equation which solutions are associated with three acoustic waves propagating along any directions and having orthogonal polarization directions.

If the crystal is subjected to the influence of static uniaxial pressure, classic equation will have the previous form but Green-Christoffel's tensor components will be functions of external uniaxial pressure now. In this case effects of so-called geometrical and physical non-linearity of the crystal should be taken into account. First one is defined by finite deformation of the sample, second one is associated with the changing of material constants of crystals by the pressure. It is convenient to write down the Green-Christoffel's equation corresponding to coordinates of the undeformed state. In the case of static and homogeneous bias fields Green-Christoffel's tensor components have not dependence from the time and coordinates.

On the basis of above mentioned ideas the Green-Christoffel's equation describing the propagaion of acoustic waves in non-homogeneous crystalline media has been obtained. Now we have taken into account the coordinate dependence of deformation gradients. It was shown that using the hypothesis of weak heterogeneity of deformation the modified Green-Christoffel's tensor does not change its form but it is necessary to consider material constants and field tensors as continuous functions of coordinates. So this approach allows to examine the heterogeneous case as homogeneous one in the local area of the selected material point of a crystal and it may to bind the moving trihedral of wave normal vectors with any point of crystal media.

Results

The account of heterogeneity of crystal deformation finally results in the appearance of dependence of wave propagation direction and wave phase velocity from the time. This effect is caused by the moving of the wave in different moments of time along areas of crystal being in the different states of deformation determining the continuous change the density and material elastic properties of crystal. This position is confirmed by the numeral calculations of propagation of small amplitude bulk acoustic waves in the [100], [010], [001], [110] directions of $Bi_{12}SiO_{20}$ crystal under the action of uniaxial heterogeneous pressure along [001].

Discussion and Conclusions

The theory results may be apply to any crystals if its elastic and non-linear elasstic constants are known.

P1I094-03

Essential Role of Material Parameters on Two-dimensional Phononic Crystals

Zhou Xiaozhou[1], Wang Yuesheng[1], **Zhang Chuanzeng[2]**; [1]*Beijing Jiao-tong University, China,* [2]*University of Siegen, Germany.*

Background, Motivation and Objective

Since the pioneer work of Kushwaha (Phys. Rev. Lett., 1993, 71: 2022), a great deal of attention has been focused on the so-called phononic crystals ¡ª the artificial periodic elastic structures based on the traditional natural crystals and photonic crystals. A physical character of the phononic crystals is the existence of phononic band gaps (PBGs) in which the sound and elastic waves are all forbidden. Phononic crystals have numerous potential engineering applications, on the most of which the basis depends on the existence of PBGs. So it is essential to find out the way how to tune the available PBGs.

PBGs are dominated by some factors, including structural parameters and material parameters. Compared with a great many researches of structural parameters, there are restricted investigations on material ones, which involve the elastic constants and the mass density. So far, most of investigations have been made based on some given material. There is hardly any discussion of the PBGs dominated fundamentally by material parameters. We hope to realize these details for more effective applications of engineering PBGs.

Statement of Contribution/Methods

To investigate our above suggestions, the discussion of material parameters was made starting off wave equations. We obtain a clear equation expression with dominative parameters, which are the material parameters¡ªthe mass density ratio and the constant of elastic constants. Then we focus on anti-plane elastic wave for the cases of the two-dimensional periodic systems of cylindrical rods in a square (hexagonal) lattice. The calculation of phononic band gaps was achieved by plane-wave expansion method. We obtain the details of the material parameters to tune the PBGs.

Results

Figure 1 shows the normalized gap width of the lowest band gaps as a function of the mass density ratio and of the contrast of elastic constants in square lattice. The dot ¡°A¡± (¡°B¡±) describes the band gaps on a periodic array of nickel (steel) alloy cylinders in an aluminum (epoxy) alloy background.

Discussion and Conclusions

The figure provides a guide for the feasibility of designing PBGs which can be made by an appropriate choice of the materials. The result shows concrete material parameters determining PBGs are the mass density ratio and the contrast of elastic constants. The material ranges for band-gaps are affected by the filling fraction and crystal lattice forms.

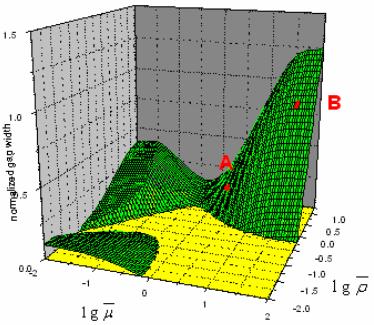

P1I095-04

Study on band structures and localization phenomenon of 2D phononic crystals with 1D quasi-periodicity

Ali Chen, Yuesheng Wang; *Beijing Jiaotong University, Institute of Engineering Mechanics, Beijing, China.*

Background, Motivation and Objective

In 1993, Kushwaha proposed the concept of phononic crystals (PNCs), artificial periodic elastic/acoustic structures that exhibit so-called phononic band gaps. Since then a great deal of work has been devoted to the study of PNCs. Another topic that is now receiving increasing interest is the wave propagating in quasi-periodic PNCs.

In this paper, we will use the localization factor which is defined as the smallest positive Lyapunov exponent to characterize the band structures and localization phenomenon of wave propagating in the 2D PNCs with the quasi periodicity of Fibonacci sequence in one direction (QPNC).

Statement of Contribution/Methods

We use the plane-wave-based TMM to obtain the transfer matrix. And then the localization factor can be calculated.

Results

Figure 1 shows the band structures of the QPNC presented by the localization factors (the black solid line) and the transmission coefficients (the red dashed line). It is seen that the two parameters predict the same band gaps, e.g. the frequency intervals of (0.295, 0.33) and (0.46, 0.83).

Discussion and Conclusions

We use the localization factor to present the band structures of the 2D PNCs with the quasi periodicity in one direction and periodicity in the other direction. The results show that the localization factor is an accepted and effective parameter in characterizing the band structures and localization behaviors of QPNCs.

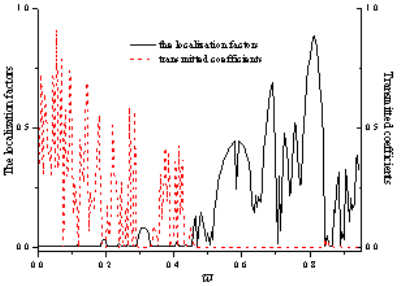

P1I096-05

Research on two-dimensional phononic crystal with magnetorheological material

Bin Wu, **Ruiju Wei,** Cunfu He, Huanyu Zhao; *Beijing University of Technology, Beijing, China.*

Background, Motivation and Objective

In this letter, we used plane wave expansion (PWE) method to compute the band structure of a two-dimensional phononic crystal of epoxy embedded in Magnetorheological elastomers (MRE). Phononic crystals (PCs), also named acoustic band gap (ABG) materials are composites made of periodic distributions of scatters embedded in matrix. The most interesting phenomena of these structures is the existence of complete phononic band gaps, which forbid the propagation of elastic or acoustic waves regardless of mode or wave vector. Potential applications of these structures include acoustic filters, sound and vibration isolators, and acoustic waveguide et al.

Recently, magnetorheological (MR) materials have attracted much attention. As a class of new smart materials, its mechanical and rheological properties can be controlled continuously, rapidly and reversibly by the application of an external magnetic field. This is called magnetorheological effect. Magnetorheological elastomers are such composites where magnetic particles (like carbonyl iron particles) are suspended in a non-magnetic solid or gel-like matrix (like natural and synthetic rubbers). The shear-modulus of MRE varies with applied magnetic field.

With the research on the MRE materials, it will be possible to tune the band structure of PCs intellectually.

Statement of Contribution/Methods

Because of the periodicity of the PCs system, those material parameters in the equation of propagation of elastic waves can be expanded in the 2D Fourier space. By applying Bloch theorem, we can obtain an algebra eigenvalue equation. Accordingly, the band structures for the transverse modes can be obtained by letting K scan the irreducible region of the first Brillouin zone.

Results

Calculated the band structure of the PC composites and obtained large sonic band gaps

Discussion and Conclusions

Discussed the dependence of the band gap on the filling fraction

P1I097-06

Electromechanical coupling coefficient of semiconducting hexagonal crystal measured by Brillouin scattering

Takahiko Yanagitani[1], Taisuke Yoshida[2], Mami Matsukawa[2]; *[1]Nagoya Institute of Technology, Department of Applied Physics, Nagoya, Japan, [2]Doshisha University, Faculty of Engineering, Kyotanabe, Japan.*

Background, Motivation and Objective

Hexagonal thin films such as PZT, ZnO and AlN have been extensively used in thin film resonators and SAW devices. Electromechanical coupling coefficient of the film is one of the most important parameter determining the device performances. In this study, we have tried to measure electromechanical coupling coefficient k_{15} of the a-plane oriented ZnO single crystal and polycrystalline films. The k_{15} value was estimated from acoustic velocities which were measured by Brillouin scattering. This technique has several advantages compared with resonant ultrasound spectroscopy (RUS) and acoustic microscopy, such as, hypersonic frequencies, noncontact, and local measurement (<10 μm). Especially, measurement in hypersonic frequencies is the most important matter for measuring the piezoelectric properties in the semiconducting crystals (ZnO, GaN, SiC et.al.). In the case that acoustic wave frequency is much slower than carrier mobility, piezoelectric polarization should be canceled out by carriers. For example, this phenomenon becomes pronounced in less than 100 Ω·m at 1 GHz.

Statement of Contribution/Methods

For a-plane hexagonal plate, k_{15} value can be determined by velocities of two shear horizontal waves: propagating toward c-axis (V_{paral}) and perpendicular to the c-axis (V_{verti}), using the equation $k_{15}=\{1-(V_{paral}/V_{verti})^2\}^{1/2}$. These two velocities were measured by shift frequencies of Brillouin spectra using RIΘA scattering geometry.

Results

In-plane anisotropy of shear horizontal wave velocity in the ZnO single crystal was plotted in Fig.1. k_{15} value determined from these velocities corresponded to the Smith's constant (k_{15}=0.26). In polycrystalline ZnO films, Brillouin peaks were broadened due to large phonon attenuation and light scattering at grain boundaries. Therefore, the two velocities cannot be determined accuracy.

Discussion and Conclusions

k_{15} value of the semiconducting ZnO single crystal was measured easily by Brillouin scattering technique. We intend to introduce the idea for measuring k_{33} value.

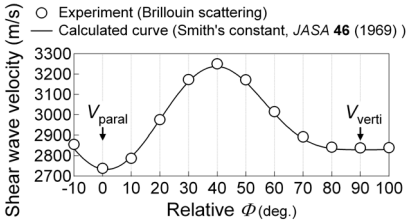

Fig. 1 In-plane anisotropy of shear horizontal wave velocity measured in ZnO single crystal.

P1I098-07

Defects in Single-Crystalline Silicon High Frequency Phononic Crystal Slabs

Saeed Mohammadi[1], Ali A. Eftekhar[1], Abdelkrim Khelif[2], William D. Hunt[1], Ali Adibi[1]; [1]*Georgia Institute of Technology, Atlanta, Georgia, USA,* [2]*Institut Femto-ST, France.*

Background, Motivation and Objective

Phononic crystals (PCs) are special types of inhomogeneous materials with periodic variation in their elastic (or acoustic) properties. PCs, if properly designed, show frequency ranges in which propagation of elastic waves is completely prohibited. Within these frequency ranges, called complete phononic band gaps (CPBGs), elastic energy can be confined and manipulated by the PC structure. PC structures with CPBGs are consequently of great interest as they can be used to add new functionalities and improvements to the conventional acoustic/elastic wave-based devices. Recently, there has been a growing interest in PC structures with two-dimensional (2D) periodicity and a finite thickness in the third dimension, called PC plates (or slabs). PC slabs are interesting as the elastic waves are manipulated by the PC structure in the plane of periodicity while it is confined within the finite thickness of the slab structure in the third dimension, preventing the loss of energy out of the plane of periodicity. We have recently shown theoretically that large CPBGs can be achieved in PCs made by perforating single crystalline silicon slabs (plates).

Statement of Contribution/Methods

In this paper the first experimental evidence for large CPBGs in (Si) PC plates will be presented. The geometry of the structure is chosen using the plane wave expansion (PWE) and finite element (FE)methods to provide a wide CPBG in the PC slab. The structure is then fabricated on a silicon on insulator (SOI) substrate using a 5-mask CMOS-compatible fabrication process. Transducers are embedded besides the structure to excite and detect elastic energy to measure the transmission through the PC slab. A sharp drop in the transmission spectrum is observed matching very well with the theoretically predicted CPBG.

Confirming the existence of CPBGs in the designed PC slab, several waveguides and cavities have been designed and theoretically investigated by introducing defects to the structure.

Results

The fabricated PC structure is composed of a free-standing 15μm thick Si with holes of radius 6.5 μm etched in a honeycomb arrangement through the slab with the spacing of 15μm between the nearest holes. More than 30dB drop in the transmission of waves is observed between 113MHz and 151MHz confirming the existence of CPBG in the PC.

Waveguides and cavities with high degrees of confinement of elastic energy are created by introducing line and point defects in the PC structure that operate within the frequency range of the confirmed CPBG.

Discussion and Conclusions

The achievement of CPBGs in PC slab structures in Si, as well as their support of highly-confining waveguides and cavities within the range of CPBG, adds new powerful functionalities to micro/nano-mechanical devices that can lead to new high-performance, integrated, high-frequency devices with potential applications in wireless communication and sensing systems.

P1I099-08

Properties of a Phononic Crystal with Band-Gaps and Anomalous Ultrasound Refraction

Derek Wright, Richard Cobbold; *University of Toronto, Inst. Biomat. Biomed. Eng., Toronto, Ontario, Canada.*

Background, Motivation and Objective

Phononic crystals are composite acoustic materials, made up of crystal arrangements of scatterers suspended in a host medium. As ultrasound waves pass through such a material, the scattered waves interfere constructively or destructively depending on the crystal design parameters and operating conditions. Some of the effects already experimentally demonstrated using carefully designed phononic crystals are transmission band-gaps, negative wave refraction, ultrasound focusing in 2D and 3D, and tunnelling. To explore some of these effects and assess their importance in ultrasound beam design and manipulation, we have constructed a 2D crystal.

Statement of Contribution/Methods

Our 2D phononic crystal consisted of a square array of stainless steel cylinders with a lattice constant of 3.66 mm, suspended in water. The crystal has a filling fraction of 0.58, and has 11 rows and 37 columns of cylinders. It was designed so that waves normal to its surface are in the direction, since this direction was deemed to provide the most interesting phononic crystal effects. Furthermore, the crystal was expected to exhibit band-gaps, waveguiding, and anomalous refraction of ultrasound waves.

The crystal behaviour was first simulated using the finite-difference time-domain and plane-wave expansion methods and the results were subsequently compared with measurements made by suspending the crystal in a water tank measurement system. The system comprised of a fixed source, the stationary crystal, and a moveable hydrophone driven in four axes (x, y, z, θ) by stepper motors. The source was powered by a pulser, and the hydrophone was raster-scanned on the other side of the crystal. This allowed the capture and reconstruction of the relative pressure field in real and k-space (Fourier space) over a broad range of frequencies.

Results

Our crystal has shown a band-gap from 180kHz to 290kHz in addition to higher-order band-gaps. In addition, the received relative pressure field has shown anomalous refraction that corresponds well with the predicted crystal dispersion curves. By removing certain rows and columns it was found that the crystal behaved as a waveguide within the band-gap regimes.

Discussion and Conclusions

It has been shown that our 2D phononic crystal demonstrates many interesting effects, including band-gaps, waveguiding, and anomalous refraction. These effects have the potential for providing a new degree in flexibility for ultrasound transducer design and beam manipulation.

Monday Poster

P1J. NDE Signal Processing

2nd and 3rd Floor Foyers

Monday, November 3, 2008, 3:00 pm - 4:30 pm

Chair: **Jafar Saniie;**
Illinois Institute of Technology, IL, USA.

P1J100-01

Time of Flight Ultrasonic CT Based on ML-EM for Wooden Pillars

Honghui Fan, Shuqiang Guo, Yasutaka Tamura, Hirotaka Yanagida; *Yamagata University, Graduate School of Science and Engineering, Japan.*

Background, Motivation and Objective

There are some reports for the nondestructive inspection of wooden pillars by using ultrasound. Tomikawa et al. applied the ultrasonic time-of-flight computed-tomography (CT) to wood. Yanagida et.al reported that the ring shaped artifact in the CT image of wood was caused by orthotropic acoustic property of wood. They removed the ring artifact by nonlinear back projection method. Back projection method was used for reconstructed method in their paper. Recently, Maximum Likelihood -Expectation Maximization (ML-EM) method has been used by medical application. In this paper, we confirm the ML-EM method is applied for wooden pillars.

Statement of Contribution/Methods

The ML-EM algorithm iteratively corrects the estimated slowness from using the algorithm shown in Fig 1.

Results

The inspection object is hardwood (Robinia psedoacacia L.), and diameter of the artificial defect is 33mm.The center of defect from center of the wooden pillars is 50mm.

The reconstructed images based on FBP and ML-EM method are shown in Fig.2

In total, 270 TOF data were obtained by experiments. In case of FBP and ML-EM 2, interpolation data was used. TOF data was obtained by interpolation. FBP reconstructed by 2304 data and ML-EM 2 was reconstructed by 630 data. The defect was observed in all image, however, some line artifacts were observed in ML-EM 1. The image of ML-EM 2 was similar to the image of FBP.

Discussion and Conclusions

A defect of 33 mm in diameter was detected by ML-EM method. When the TOF data was fewer than 300, the reconstructed image had some line artifacts. It is highly possible that the same artifact will appear in the image for the field works. To apply ML-EM method for field works, we should obtain more TOF data or use an interpolation in imaging process.

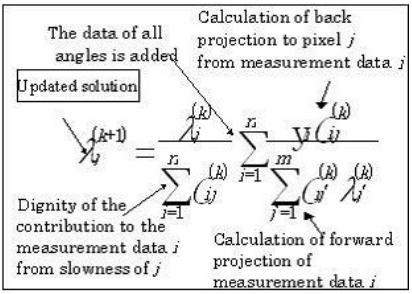

Fig. 1 The basic formula of the image reconstruction by the ML-EM algorithm

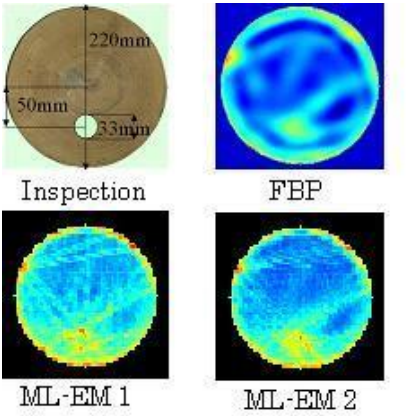

Fig. 2 The reconstruction images

P1J101-02

Analysis of Hilbert-Huang Transform for Ultrasonic Nondestructive Evaluation

Yufeng Lu[1], **Erdal Oruklu[2]**, Jafar Saniie[2]; *[1]Bradley University, Electrical and Computer Engineering, Peoria, IL, USA, [2]Illinois Institute of Technology, Electrical and Computer Engineering, Chicago, IL, USA.*

Background, Motivation and Objective

In the ultrasonic nondestructive evaluation of materials, the backscattered echoes contain important physical information along the propagation path. These echoes often interfere with each other due to closed locations, boundaries, orientations, and sizes of random reflectors and they also may be contaminated by noise. Hence, it becomes problematic to unravel the desired information necessary for material characterization. Therefore, signal processing methods capable of characterizing the nonstationary behavior of ultrasonic signals for NDE applications are highly sought-after.

Statement of Contribution/Methods

The Hilbert-Huang transform (HHT) which is a combination of empirical mode decomposition (proposed by Huang) and Hilbert spectrum analysis that decomposes the signal into narrow-band components, has been used to process the nonstationary signals in structural health monitoring and seismic traces. In this investigation we explore the application of HHT in order to decompose and analyze ultrasonic signals for NDE applications. HHT is represented by a series of intrinsic mode functions which have an equal number of extreme and zero-crossings and reveal the physical oscillation properties of materials. These intrinsic mode functions are extracted from the ultrasonic signal using an iterative sifting process. The process is implemented as follows: first, all the local maxima are interpolated to obtain the maxima envelop. In a similar way, the minima envelop is obtained. Then the new data set is updated by subtracting the average of the two envelopes from the original signal until the intrinsic mode function is isolated from the signal. These intrinsic mode functions and their Hilbert spectrum are able to characterize the local variation and nonstationary behavior of ultrasonic signals for the nondestructive evaluation of materials.

Results

In this study, we demonstrate the application of Hilbert-Huang transform in ultrasonic signal processing. The performance of the algorithm is evaluated in order to characterize the ultrasonic backscattered echoes from materials with different grain sizes and defects. Through simulation and experimental studies, it has been shown that Hilber-Huang transform reveals signal features which can be correlated to the presence of defect and characteristics of grain scattering within the materials. HHT is also compared to conventional time-frequency representations for ultrasonic signal analysis and feature extraction.

Discussion and Conclusions

Numerical and analytical results indicate that the Hilbert-Huang transform is an effective tool for ultrasonic signal analysis accounting for narrow-band, broadband, and dispersive echoes. This algorithm can be utilized in the analysis of ultrasonic signals often encountered in flaw detection, signal classification, and pattern recognition.

Monday Poster

P1J102-03

An Efficient Sparse Signal Decomposition Technique for Ultrasonic Signal Analysis Using Envelope and Instantaneous Phase

Ramazan Demirli[1], Jafar Saniie[2]; [1]*Canfield Scientific, Inc, USA,* [2]*Illinois Institute of Technology, Electrical and Computer Engineering Department, USA.*

Background, Motivation and Objective

Sparse signal decomposition techniques have been widely used in recent years due to their efficiency in ultrasonic signal analysis. These techniques iteratively decompose ultrasonic signal in terms of model echoes (e.g., Gaussian echo, Chirplet echo, etc) that characterize local signal signatures. The decomposed echoes (or the parameters) are then used for subsequent analysis, for example, for feature extraction and system identification. The first critical step in these decomposition techniques is the windowing (i.e., partitioning) of the data for identification of dominant signal features. This step has a great implication on the subsequent step that involves parameter estimation based on the assumed echo model or finding the best matched echo from a predefined dictionary of echoes. Therefore, a robust windowing technique that successively partitions ultrasonic data into dominant echo components is highly desirable for sparse signal decomposition algorithms.

Statement of Contribution/Methods

In this study, we obtain envelope and instantaneous phase via analytical signal representation to guide ultrasonic data partitioning in the time domain. This type of partitioning is also meant to serve the initial guessing operation prior to the parameter estimation. Envelope and instantaneous phase provide important clues for local changes in the ultrasonic signal. The local maxima of the smooth envelope along with the changes in the instantaneous phase provide meaningful boundaries for echo structures. These boundaries are expected to provide an accurate data partition for the subsequent echo estimation.

Results

We present results that demonstrate the proposed echo windowing technique is significantly faster than the Time-Frequency (TF) techniques and provide meaningful echo localization and parameter estimation results. In particular, we demonstrate the efficiency of the algorithm in parameter estimation for ultrasonic experimental data acquired from a steel sample that contains flaw echoes buried in grain scattering noise where the SNR is about 0 dB.

Discussion and Conclusions

The echo windowing techniques utilized for ultrasonic signal analysis are often application specific. For example, TF representations using wavelet transform and chirplet transform have been used to localize echoes in TF plane. Even though these techniques perform well in localization, the windowing technique is inherently dependent on the assumed echo model. Furthermore, obtaining a TF representation of the data is computationally expensive and requires repetitive updates, i.e., calculating the TF of the estimated echo and subtracting its contribution from that of the original data. The proposed echo windowing technique reduces these redundant computations and offers a more efficient and practical solution for real-time ultrasonic signal analysis.

P1J103-04

Improved SVM for detecting signal in reverberation

Zhu Guang-ping, **Sun Hui;** *College of Underwater Acoustic Engineering Harbin Engineering University, Harbin, Heilongjiang, China.*

Background, Motivation and Objective

The detection of a bottom target echo is usually a difficulty task since the seafloor reverberation, due to diffusion of the transmitted signal by the rough seafloor. While the size of the range bearing resolution cell is reduced, the reverberation becomes non-Gaussian distribution, resulting in an increase in the probability of false alarm using matched filter. The non-Gaussian reverberation probability distribution is usually unknown, even if it is known, the optimal detector is too difficulty to be droved.

Statement of Contribution/Methods

We proposed an improved support vector machine (SVM) for detecting the target echo. We applied the C-SVM algorithm for constructing detector. For easily deciding threshold to improve detector, the output of detector is in [-1,1] . If input vector x is target echo, the output value is close to 1, contrarily close to -1. We tried to construct new

kernel functions according to Mercer theory for improving performance of SVM . We found, when kernel function is exp((xy+1)^d) and d=2, the probability of detection is highest.

Results

In the experiment, the performance of this detector in Gaussian and non-Gaussian reverberation were respectively showed in Fig.1and Fig.2, and compared with Gaussian kernel SVM, radial basis function (RBF) network, and matched filter (MF). Of course probability of false alarm is 0.005.

Discussion and Conclusions

The performance of improved SVM detector is most optimal than RBF network and MF, even better than Gaussian kernel SVM in close Gaussian distribution reverberation. In non-Gaussian reverberation, the performances of SVM detectors were also better than RBF and MF, the detection capability of improved kernel SVM is same as conventional Gaussian kernel SVM, but the former is robust.

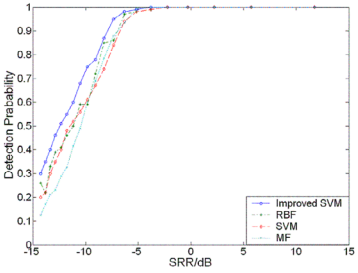

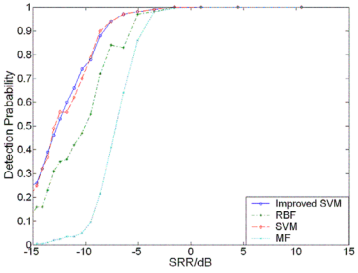

Monday Poster

P1K. NDE Applications

2nd and 3rd Floor Foyers

Monday, November 3, 2008, 3:00 pm - 4:30 pm

Chair: **Larry Kessler;**
Sonoscan, USA.

P1K104-01

Progress of Matching Network for Passive Remote Hybrid Sensor Based on SAW Resonator

Dongxiang Zhou, Jianling Wang, Qiuyun Fu, Wei Luo; *Huazhong University of Science & Technology, Department of Electronic Science & Technology, Wuhan, Hubei, China.*

Background, Motivation and Objective

The passive remote sensors attract many researchers next decade because of their broad applications. The SAW resonator and the matching network with an integrated traditional sensing element make up a hybrid SAW resonator sensor especially suitable for passive wireless applications. The classical design method of matching networks has two disadvantages for such sensors. S. Klett proposed that the well-matched resonator behaving as a series RLC circuit is the necessary condition for interrogation and applied the PI matching network. But there is not great improvement. Here, we present an improved design method for the matching network.

Statement of Contribution/Methods

The previous matching networks have two disadvantages. One is that the strong mismatch occurs if the impedance of sensing element shifts from the well-matched point. The other is that the matching network reduces the Q at the match point. The improved design method in this paper is matching the whole sensor configuration at the series resonant frequency of the SAW resonator simulated by an equivalent series RLC circuit. The series resonant frequency point varies with one reactance component and keeps well-matched. The realized matching network is T-type including three reactance components, and the third is a sensing element. With the varying of the sensing element, the peak frequency of reflection coefficient changes, it is fit for the requirement of sensitivity. Simultaneously, the peak amplitude almost does not change. It is helpful for the low mismatch. The method realizes both high Q factor and low mismatch.

Results

The simulated Q is above 10000 and almost remains unchanged. Compared with the previous values far below 1000, the improvement is obviously. For the range of sensing elements from 1 to 10 pF, the stand wave ratio (SWR) is smaller than 1.02 while in the previous papers it is from 1 to 3. Our results show in the right figure.

Discussion and Conclusions

In this paper, we report the improved design method of matching networks for SAW resonator sensors, including the design theory, design steps, comparisons to previous design methods, and applications in remote hybrid sensor based on SAW resonators. With the improved design method, both low mismatch and high Q factor are obtained simultaneously, and also the enough sensitivity.

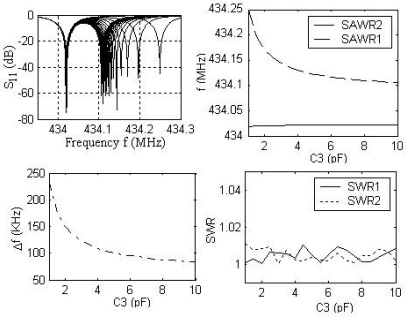

P1K105-02

NDE Using Laser Generated Ultrasound and Integrated Ultrasonic Transducer Receivers

Cheng-Kuei Jen[1], Kuo-Ting Wu[2], Makiko Kobayashi[1], Alain Blouin[1]; *1National Research Council Canada, Industrial Materials Institute, Boucherville, Quebec, Canada, 2McGill University, Electrical and Computer Engineering, Montreal, Quebec, Canada.*

Background, Motivation and Objective

Generation of ultrasound using pulsed lasers have the advantage of non-contact, fast scanning, very broad bandwidth for NDE of parts with complex shapes and at elevated temperatures. Significant R&D and applications have been reported using optical methods to detect the laser generated ultrasound, however, in order to provide sufficient detection sensitivity the cost of the receiver may still be high. Electromagnetic and air coupled ultrasonic transducers have been also used for the detection but the sensitivity and bandwidth remains relatively low. Therefore to develop an alternative approach using integrated ultrasonic receivers with high sensitivity and broad bandwidth which can operate at high temperatures and curved surfaces is the objective of this research.

Statement of Contribution/Methods

Sol-gel fabricated thick (>40μm) piezoelectric film integrated ultrasonic transducers (IUTs) coated directly onto steel, aluminum (Al) and graphite/epoxy (Gr/Ep) composites substrates serve as the receivers without the need of couplant for the laser generated ultrasound. Such IUTs may be fabricated on-site and desired patterns may be made with convenience. These IUTs operated in a thickness vibration mode can use various mode conversion configurations and serve as longitudinal, shear, symmetric, anti-symmetric and shear horizontal plate wave receivers. Since semi-conductor pulsed lasers can be used as versatile even portable ultrasonic signal generators with optical fiber waveguide for long distance application and IUT array as miniature and low power ultrasonic receivers, this configuration is of attraction to various NDE Applications.

Results

One semiconductor pulsed laser operated at 10Hz and 100mJ and another at 1000Hz and 50μJ are used for the generation of ultrasound. Their pulse widths are less than 10ns. Point and line sources of different sizes for laser generation have been used. IUTs using piezoelectric lead-zirconate-titanate or bismuth titanate ceramic powders have been made onto steel and Al blocks with flat and curved surfaces, 2 mm thick steel and Al plates and Gr/Ep composites of 7mm and 2.7 mm thick. Selective longitudinal, shear, symmetrical, anti-symmetrical and shear-horizontal plate waves have been obtained with good signal to noise ratio. Ultrasonic NDE of metals up to 400°C and Gr/Ep composite have been carried out. A crack detection approach using laser generated plate waves at many locations and IUT array located at the edges of a large aluminum plate will be demonstrated.

Discussion and Conclusions

IUTs are miniature in size and light weight. Since they have high sensitivity similar to commercially available broad band UTs and are used only as receivers, battery operation in long life is expected. Both laser generation and IUT can be used for curved surfaces and high temperature operation, possibilities for NDE of large and complex structures in harsh conditions may be possible.

P1K106-03

Laser-Ultrasonic Shear Wave Inspection

Bruno Pouet, Nicolas Lefaudeux, Sebastien Breugnot, Philippe Clemenceau; *Bossa Nova Technologies, USA.*

Background, Motivation and Objective

Historically, ultrasonic inspection was first based on longitudinal waves. Ultrasonic inspection based on shear waves was not as broadly used, mainly because of limitations associated with generation and detection of shear waves. With piezoelectric transducers, shear waves are generally generated and detected through mode conversion (only SV, no SH). Over the past decades, electromagnetic acoustic transducer (EMAT) has emerged a very efficient technique for generating and detecting shear waves (both SV and SH), but EMATs are essentially limited to inspection on conductive material and at frequency below 10MHz. A non-contact and high-frequency technique, and not limited to conductive material, will be highly valuable for NDE.

Statement of Contribution/Methods

Thanks to its remote and high-frequency capability, laser ultrasonic (LU) has great potential for nondestructive inspection. To date, successful industrial application of LU has been limited to inspection based on longitudinal wave and detection of the out-of-plane surface displacement. By altering the laser beam profile, we demonstrate that laser can also be used for non-contact generation of SH-wave. This generation is truly non-destructive as it is achieved in the thermoelastic regime. Complementary to SH-wave laser generation, we also present a LU receiver for simultaneous measurement of the out-of-plane and of the in-plane displacements (multi-component). By taking advantage of recent developments in multi-channel electronic processing, the multi-component interferometer exhibits the same compact optical architecture as a single-component (out-of-plane) interferometer.

Results

Experimental results are presented demonstrating the capability for LU inspection based on laser generation and detection of shear waves propagating normal to the sample surface. Experiments are carried-out on aluminum samples. For characterization of the LU generation, we measured P-wave and S-wave directivity, showing good agreement with the predictions. Characterization of the compact interferometer for simultaneous in-plane and out-of-plane measurements is also carried out.

Discussion and Conclusions

Potential applications to NDE is then discussed.

P1K107-04

Design method for big 2-D ultrasonic arrays with controlled grating lobes levels

Javier Rodrigo Villazón Terrazas, Alberto Ibáñez Rodríguez, Montserrat Parrilla Romero, Patricia Nevado Carvajal; *Instituto de Automatica Industrial IAI-CSIC, Ensayos no Destructivos, Madrid, Spain.*

Background, Motivation and Objective

The 3-D ultrasonic image systems are subject to significant interest in industrial NDE applications. An important topic is the design of 2-D arrays to conform and deflect narrow beams with a short number of elements to maintain system complexity in technologically admissible levels. The problems that this array design presents are: grating lobes formation, the loss of radiated energy and the sensitivity in reception.

The capacitive micromachined ultrasonic transducers (cMUT) fabrication technology, permits a flexible control of the shape and position of the array's elements making possible to test new array designs to manage big array apertures with not too many elements, and to have beam patterns with low grating lobes levels.

Statement of Contribution/Methods

In arrays with inter-element distances bigger than a half of a wavelength, periodicity in the elements layout is the main contribution to growing of grating lobes. Breaking this periodicity or modifying the shape of elements are some of the possible ways for reducing grating lobes and maintaining a narrow main lobe. In our approach, we start with a regular layout of elements formed by sets of elementary radiating cells (which can be implemented as cMUT cells). By introducing small shifts to the position of each cell the shape of elements is modified and the periodicity of the layout is reduced. In order to accomplish this goal we propose to use an optimization technique based on the evolution. The fitness function that we use, describe the behaviour of our ultrasonic 2-D array in a spherical volume of study.

The evolutionary algorithm used is the NSGA-II, which allows us to find a suitable active set of cells located in an appropriate form. Furthermore, the proposed algorithm is flexible with respect to array geometry, fitness function, codification and other genetic parameters that control the population sizes and combination strategies.

Results

A flexible technique for reducing the grating lobes is described. The technique gives a good coverage to implement more than one fitness function, since it is designed for that purpose. The type of codification and initial population influences the obtained results. Also shows that by using properly shaped elements in 2-D arrays and distributing them in aperiodic form, the grating lobes level are reduced (around 10 dB), on the other hand it makes possible to steer the ultrasonic beam in all directions in the scanned volume. The design obtained, can be physically put in practice by the use of cMUT's technology.

Discussion and Conclusions

This technique can be used in other kind of implementation cells for each element, like do diamond elements, circular elements, etc... These cells could have the shape of a rectangular matrix, rhomboid matrix, segmented rings, or spirals arrays.

P1K108-05

A large aperture ultrasonic receiver for through-transmission determination of elastic constants of composite materials

Marcelo H.G. dos Santos, Marco Aurelio Andrade, Flavio Buiochi, **Julio Adamowski;** *University of Sao Paulo, Mechatronics, Sao Paulo, SP, Brazil.*

Background, Motivation and Objective

The determination of elastic constants of anisotropic materials by measurement of the density and ultrasonic velocities has been studied by several researchers in the last four decades. The accuracy of elastic constants is highly dependent on the precision of the velocity measurement. There are several factors which introduce errors when measuring velocities, such as: parallelism of the sample surfaces, temperature gradients, velocity dispersion, acoustic diffraction, mechanical precision of the measurement device, etc. It can be shown that an infinite-plane receiver with uniform sensitivity yields a plane wave-only measurement. In practice this receiver is obtained by using a piezoelectric PVDF thin-film receiver, sufficiently large to intercept the entire propagating wave. This technique avoids the beam diffraction effect that occurs when using limited size ultrasonic transducers. This effect increases as the frequency decreases for the same size of transducer. On the other hand, the velocity dispersion effect, present in composite materials, increases with frequency. This work describes the use of a large aperture PVDF receiver in angle beam through-transmission method of velocity measurement in fiber reinforced composites.

Statement of Contribution/Methods

The large-aperture receiver is a 52-µm thick PVDF membrane with gold electrodes. The PVDF membrane is bonded to a matched backing material, stiff enough to prevent low frequency bending vibration. The effective diameter of the receiver is 80-mm, and it was chosen in order to intercept the entire field produced by the lowest frequency transmitter used in this work. The experiments have been made in a goniometer which has an angular resolution of 0.01 degree in two rotation axes. To analyze the diffraction and dispersion effects, measurements where conducted in a 9.5 mm thick aluminum plate, a 4.5 mm acrylic plate and a 2.12 mm unidirectional carbon-fiber/epoxy plate. It was used a set of 5 pairs of 19 mm diameter ultrasonic transducers (1.0, 2.25, 3.5, 5.0 and 10.0 MHz). Experiments were conducted using a pair of transducers and a 19 mm diameter transducer as emitter and the large diameter receiver. The temperature was kept constant (21.0 ±0.1 degree C).

Results

Analyzing the diffraction effect, it was observed that the longitudinal velocity in the aluminum plate increases more than 1 % when using a pair of 1MHz transducers. That effect disappears when using the large aperture receiver and it is negligible when using a pair of 10 MHz transducers. On the other hand, it was observed that in the acrylic plate the longitudinal velocity increases 0.7%, and increases more than 0.8% in the carbon-fiber/epoxy plate (density = 1576 kg/m3), from 1 to 10 MHz.

Discussion and Conclusions

As a compromise between axial resolution and velocity dispersion, the elastic constants of the unidirectional carbon-fiber/epoxy composite were determined in the frequency of 2.25 MHz, showing good agreement with tensile test results.

P1K109-06

Implicit Calibration of Simulation Models for Ultrasonic Transducers

Johan E. Carlson, Fredrik Hägglund, Jesper Martinsson, Amin Saremi; *Lulea University of Technology, Dept. of Computer Science and Electrical Engineering, Lulea, Sweden.*

Background, Motivation and Objective

There are several software packages available for simulation of ultrasound wave fields (e.g. Field II and DREAM). These packages provide valuable tools for simulation of ultrasound measurement systems. In many cases, however, it is of interest to build a simulation model of a real-world ultrasound transducer. This involves identifying both the electro-acoustic impulse response and the spatial impulse response of the transducer, based on measurements of the sound pressure field. The problem is that both of these impulse responses are unknown, and what we can observe is a combination of the two (provided we have access to a calibrated hydrophone). However, the electro-acoustic impulse response does not depend on the observation point (location of the hydrophone). The spatial impulse response does, but given a number of parameters to the simulation package, this can be calculated. The task is then to use observations to find both the electro-acoustic impulse response and the parameters for the simulation model of the spatial impulse response.

Statement of Contribution/Methods

In this paper we show how the principle of implicit calibration can be used to simultaneously estimate the electro-acoustic impulse response, $h_e(t)$, and the spatial impulse response, $h_{SIR}(t, \mathbf{r}; \boldsymbol{\theta})$, of a transducer, where $\mathbf{r}$ is the location of the observation point and $\boldsymbol{\theta}$ is the vector of simulation model parameters. The principle is based on the use of a calibrated hydrophone to capture the sound field in a number of points in front of the transducer. We then use a numerical least-squares optimization technique to find the parameters of the simulation model. For each iteration of the algorithm, we then estimate the electro-acoustic impulse response by means of linear regression. The combination results in a simultaneous estimate of the two unknown properties, $h_e(t)$ and $\boldsymbol{\theta}$, thus enabling us to accurately predict the sound pressure field in each point.

Results

We first demonstrate the general principle by simulations with the DREAM toolbox, showing how a simulation model of a simple circular transducer can be obtained. The simulations are then verified with measurements using a 5 MHz transducer and a calibrated hydrophone. The results show that the proposed method can be used to derived accurate simulation models for real-world transducers.

Discussion and Conclusions

The results show that the proposed method can be used to accurately adapt simulation models to real-world transducers. We are able to estimate both the electro-acoustic and spatial impulse responses, respectively.

The example in this paper shows how to do this using the DREAM toolbox, but the method is easily adaptable to other toolboxes, such as Field II.

P1K110-07

Thin Finite Plate Modeling and Experimental Studies on Lamb Wave Propagation at Various Boundary Conditions

Yuan Liu[1], Jean-Pierre Nikolovski[2], Nazih Mechbal[3], Moustapha Hafez[2], Michel Vergé[3]; [1]*Sensory Interfaces Laboratory, CEA LIST and LMSP (CNRS 8106), ENSAM, France,* [2]*CEA LIST, Sensory Interfaces Laboratory, Fontenay-aux-Roses, France,* [3]*ENSAM, LMSP (CNRS 8106), Paris, France.*

Background, Motivation and Objective

Lamb waves have often been used for localization of a contact between an index and a plate [E. Dieulesaint et al, French patent FR 8903074, 1989]. In some approaches, the measurement principle may rely on the time delay of an acoustic wave propagating in plate [JP. Nikolovski et al, IEEE Ultrasonics Symposium Proceedings 1997] and in others on the cross correlation of a predefined acoustic signature associated with the position [R.-K Ing et al, Appl.Phsy.Lett., 2005]. In that second situation, the boundary condition will make a strong impact on the definition of acoustic signature. As a consequence, cross correlation techniques may find difficulties when it comes to calibration and repeatability in mass production.

Recently, some efforts have been made to numerically evaluate the effect of various boundary conditions in the propagation of A0 Lamb waves undergoing multi-reflections [G. Ribay et al, J.Acoust.Soc.Am., 2006]. The results remain to predict experimental behaviour that could avoid experimental calibration.

Statement of Contribution/Methods

In this paper, we describe the realization and integration of a test bench used to measure the dependency of thin plate resonance modes on different boundary conditions. Experimental results are compared with computer simulations based on finite element analysis (FEA), which is intended to be used as a predictive method.

Our Lamb wave resonator is made with a 75mm x 75mm thin finite copper plate (thickness = 350 μm) and four piezoceramic transducers (diameter = 7mm, thickness = 0.5mm). The plate is maintained by foams and one duralumin substrate. And the transducers are bonded to the middle of plate edges with a conductive glue circuitworks CW2400; they are used as actuators or receivers for Lamb wave generation, respectively.

The Lamb wave resonator is integrated in the test bench, with a function generator and a data acquisition card. Matlab codes are created for data acquisition and signal processing.

Results

The resonance modes of a thin finite plate propagating A0 Lamb Waves are investigated according to various boundary conditions imposed by a mounting frame. Effects of the boundary conditions are described qualitatively and quantitatively by Finite element analysis, and by experimental verification. Theory of A0 Lamb wave propagation in a plate provides input parameters for the numerical modeling.

Results obtained at different boundary conditions show that the resonances are much more dependent on boundary condition at low frequencies than those at high frequencies.

Discussion and Conclusions

In fact, we could find that lower frequency leads to longer wavelength and larger normal amplitude at free boundary condition. Then there will be stronger disturbance when damping effect comes from the mounting frame. On the other hand, the higher frequency leads to smaller wave velocity and larger longitudinal component which means the wave is less disturbed at the edges. More details will be given in full paper.

P1K111-08

Research on clamping force in resonant ultrsound spectroscopy

Hang Guo, Yi Zhang, Liming Zou; *Xiamen University, Pen-Tung Sah MEMS Research Center, Xiamen, Fujian, China.*

Background, Motivation and Objective

Resonant Ultrasound Spectroscopy (RUS)is a dynamic method to determine the elastic constants of solids. In our previous study, RUS was used for characterize MEMS structures and a new microfabricated PZT/Si transducer for RUS was developed. In the RUS measurement, the sample of solids is required to contact piezoelectric transducers for excitation and detection of its vibrations, and an amount of clamping force is needed to obtain high signal to noise ratio for the useful measured spectrum. However, the clamping force will shift natural frequencies of the sample. Thus, the accuracy of RUS is affected. The main objective of this paper is to study the clamping force effect on RUS accuracy and fesibility of using RUS to characterize the carbon nanotubes (length greater than 100 micrometer)with high accuracy.

Statement of Contribution/Methods

We developed a method to study the clamping force effect in RUS. A static structural analysis for the sample under the clamping force is first made by using finite element method in ANSYS to turn the effect of the clamping force into the pre-strain of the sample, and then the natural frequencies of the pre-strained sample are calculated. Meanwhile, a model on piezoelectric transducers used in RUS is set up from the bending of an equivalent cantilever in order to control the clamping force for RUS measurment.

Results

The results show that clamping force effect on RUS differs from the size of the sample that needs to be tested. For the general centi- or milli- meter scale solid sample, the clamping force should be controled in the milli-Newton scale so that the clamping force shifts the sample's natural frequencies in tens to hundreds of parts per million(ppm), which will affect the RUS accuracy within 5%. For using RUS to characterize the microscale sample, for example, a carbon nanotube with diameter of 50 naometer and length of 100 micrometer, the clamping force should be controlled in the nano-Newton scale to make the inaccuracy less than 5%. The ultra-thin (0.1-1 micrometer thick, 0.5-1mm wide) cantilever piezoelectric transducers fabricated by using MEMS technology can meet this requirement.

P1K112-09

Welding of flat copper braid wires using ultrasonic complex vibration - Direct machining of terminal parts on flat braided wires

Jiromaru Tsujino[1], Tetsugi Ueoka[1], Eiichi Sugimoto[2]; *[1]Kanagawa University, Faculty of Engineering, Yokohama, Kanagawa, Japan, [2]Asahi EMS Co., Ltd, Tokyo, Japan.*

Monday Poster

Background, Motivation and Objective

Braid wires are flexible and vibration-proof, and used widely for connecting various electrical equipments including battery earth wire. Braid wire end is usually connected using a solder or solderless terminal, and connected to the equipment by fixing bolts. Direct machining of terminal part of flat braided wire using a 20 kHz ultrasonic complex vibration is studied. Using conventional linear vibration system, rigid terminals could not obtained.

Statement of Contribution/Methods

Braid wires consist of 256 to 30560 thin wires of 0.03 to 0.26 mm diameter. Thin wires are bundled partially and braided to flat braid wire. Used specimens are flat braided wires of 12 mm and 15 mm wide and 2 mm thick which consist of 4064 and 5088 thin copper wires of 0.03 mm diameter.

Several direct machining methods were tested using (1) resistance welding method which requires large current, (2) 20 kHz longitudinal vibration equipment with static force of over 40,000 N and (3) 20 kHz complex vibration welding equipment with static clamping force 1,000 N.

Results

Resistance welding method could make 0.8-mm-thick terminal part of the braid wire but requires very large current and machining conditions are rather critical.

Second method that induces vertical vibration to the braid wire from one side using a 20 kHz longitudinal vibration under static force of 40,000 N could make 1.0-mm-thick terminal part but the terminal obtained are not sufficiently rigid using over 15 μm (peak-to-zero value) vibration amplitude.

Third method induces parallel vibration to the braid wire under static clamping force 1,000 N using a 20 kHz complex vibration system with a complex vibration converter which has diagonal slits. Using complex vibration of elliptical locus, the terminal part obtained is 0.8 mm thickness and all thin wires were completely joined to a flat plate shape using vibration amplitude of 16 μm.

Discussion and Conclusions

Attached figures show the 20 kHz ultrasonic complex vibration welding system with 15 mm square welding tip and conditions of welded braided wires using (1) resistance welding and (3)complex vibration welding methods. The terminal by (1) resistance welding remains braid structure. The surface and side conditions of terminals by ultrasonic complex welding are flat and thin wires are completely welded. Thicknesses of the terminals were under 0.8 mm and rigid terminals were obtained.

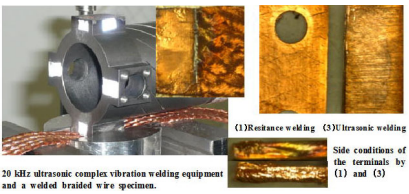

P1L. BAW Modeling

2nd and 3rd Floor Foyers

Monday, November 3, 2008, 3:00 pm - 4:30 pm

Chair: **Alexandre Volatier;**
TriQuint Semiconductor, USA.

P1L113-01

Piezo Thermo Elastic Model for the Design Optimization of Resonant Beams

Gabriele Vigevani, Jan Kuypers, Albert Pisano; *University of California at Berkeley, Mechanical Engineering, Berkeley, CA, USA.*

Background, Motivation and Objective

Resonating beam structures using Microelectromechanical Systems (MEMS) technology have been receiving strong attention to obtain miniature high performance resonators for timing and sensing applications [1][2]. Piezoelectric materials are gaining an increasing interest because of better capacitance ratio (Co/Cm) and impedances suitable for circuits. Increasing the Q-factor is a key to improve phase noise performance for frequency references and to improve the signal-to-noise ratio for sensors. For beams thermo elastic damping (TED) is often the dominant energy loss mechanism that limits the device Q-factor [2]. The effect of TED for a vibrating beam is shown in Fig.1 (a). Within the beam cross section the opposite sign of the axial strain causes a temperature gradient which leads to an irreversible heat flux. The understanding of TED including the effect of piezoelectricity and pyroelectricity are crucial for an optimized design.

Statement of Contribution/Methods

In this study we introduce a thermo piezo elastic damping (TPED) analytical model for piezoelectric beams. Starting from the Euler Bernoulli theory for simple thermo elastic beams developed by Lifshitz and Roukes [2] we consider the piezo thermo elastic constitutive equations and derive a closed-form expression for the Q-factor of a beam.

Results

We applied the theory to beams of aluminum nitride (AlN), a c-axis oriented piezoelectric and pyroelectric material, because of its CMOS compatible properties. The model shows that the piezoelectric and pyroelectric effects, for a fixed-fixed beam, reduce the Q-factor by an amount of 15%. We confirm that by setting the piezoelectric and pyroelectric coefficients to zero, our model coincides with the solution derived by Lifshitz and Roukes.

Discussion and Conclusions

Our results demonstrate the importance of the TPED as energy loss mechanism for miniature resonators. The theory shows that the effect of TPED can be minimized by selecting the optimal geometrical dimensions for resonating beam based structures such as double-ended tuning fork (DETF).

[1] A. Isobe, K. Asai, H. Matsumoto, and N. Shibagaki, IEEE Ultrasonics Symposium 2006, pp. 560-563

[2] Ron Lifshitz and M. L. Roukes, Physical review B, Vol. 61, n. 8, pp. 5600-5609

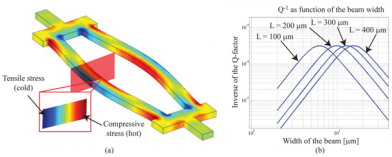

Fig. 1: Temperature gradient generated in a vibrating beam (a). Inverse of the Q-factor as function of the width of a beam for aluminum nitride according to the developed thermo piezo elastic damping theory (b).

P1L114-02

An eigenmode superposition model for lateral acoustic coupling between thin film BAW resonators

Tuomas Pensala, Johanna Meltaus, Markku Ylilammi; *VTT, Micro- and Nanoelectronics, Espoo, Finland.*

Monday Poster

Background, Motivation and Objective

A thin film BAW resonator presents standing plate wave resonances between its lateral edges. If an evanescent plate wave solution exists outside the energy-trapping edge, an exponentially damped tail of the vibration extends there. Should another region (e.g. another resonator or feed electrode) with propagating plate wave solutions lie within the reach of the tail, energy transfer may occur across the gap. A plate wave dispersion based model is developed to predict such transmission. The model can be used to study parasitic coupling between adjacent resonators or devices analogous to the monolithic crystal filter (MCF).

Statement of Contribution/Methods

For different lateral regions of a thin film resonator layer stack (e.g. metallised and non-metallised), we calculate plate wave dispersion curves. Using the dispersion data as input, we formulate a transfer matrix method in one lateral dimension to find the eigenmodes of the system. With effective electromechanical coupling coefficient imported from 1D-simulation in the thickness direction, and given Q-values for all modes, we calculate a coupling coefficient for each eigenmode. Based on these, a modal superposition is formed to extract vibrational and electrical responses of the system at any frequency.

The method is extended to the case of several metallised regions forming N electrical ports, and the response is calculated with respect to each port acting as the driving one in turn. Y-parameter description of an electrical N-port is obtained and signal transmission via laterally propagating acoustic waves between electrically separated resonators can thus be calculated.

The same scheme can be extended to two lateral dimensions in an arbitrary lateral geometry using FEM to solve the eigenmodes of the Helmholtz equation with frequency dependent wave number obtained from dispersion calculation.

Closely placed AlN thin film BAW resonators on dispersion tailored W-SiO2 mirrors were fabricated. Variations in the geometry of the resonators and the gap separating them were included. Two-port S-parameters across two resonators were measured. The same structures were simulated by the developed models and comparison was made to validate the method.

Results

Measured insertion loss (IL) between adjacent square resonators shows a spiky form with many lateral resonances interplaying. The peak level of IL stays mostly below –20dB. Parallel narrow stripe resonators show a smoother passband-like behaviour extending up to -10dB. Strong contribution from the 2nd thickness shear mode is also observed in both device types. Modelled characteristics show a good qualitative match to the measured ones.

Discussion and Conclusions

The model developed coincides with observations in a qualitative fashion well enough to be used as a ‘quick and dirty’ simulation tool in place of FEM. Especially, replacing heavy 3D-FEM for arbitrary lateral geometries is very appealing.

P1L115-03

Modelling of 2-D Lateral Modes in Solidly-Mounted BAW Resonators

Johanna Meltaus[1], Tuomas Pensala[1], Kimmo Kokkonen[2]; *[1]VTT Technical Research Centre of Finland, Espoo, Finland, [2]Helsinki University of Technology, Espoo, Finland.*

Background, Motivation and Objective

Suppressing unwanted lateral modes in bulk-acoustic wave (BAW) resonators is important for obtaining a spurious-free electrical response. Methods include border design [1], used in solidly-mounted resonators (SMRs), and electrode shape tailoring [2]. In SMRs, asymmetric resonator shapes have been shown to reduce spurious content [3].

For modelling lateral modes in SMRs, 3-D FEM is often inconveniently slow, if possible at all. We apply a "semi-3D" FEM model that allows calculating resonance modes in arbitrary 2-D electrode configurations. The model is applied to systematically study the shape and electromechanical coupling of higher-order lateral vibration modes in SMRs with various electrode shapes.

Statement of Contribution/Methods

The "semi-3D" approach used in this work allows simulating vibrational eigenmodes in arbitrary-shaped electrodes. Dispersion characteristics of different regions are calculated using the analytical 1-D model of the resonator stack. The obtained dispersion curve is imported to FEM software and used to solve the Helmholtz equation in two dimensions. The model enables calculation of eigenmode spectra and the coupling strength of modes.

The approach is applied to various resonator shapes. Resonator stacks have W/SiO2 mirror and AlN piezo layer, with type 1 dispersion. Results obtained with the model are compared to vibration characteristics measured with a laser interferometer. Furthermore, correspondence between the lateral eigenmode excitation and the spurious resonance content of measured electrical response is studied.

Results

Simulations of elliptical and rectangular resonators with varying aspect ratio reveal the changing eigenmode shapes as the resonator shape deviates from fully symmetrical (circle or square). A decrease in mode coupling strength is observed for both ellipses and rectangles as compared to the symmetrical case. Elliptical resonators have an "optimal" aspect ratio with minimal coupling of lateral modes, whereas for rectangles, the coupling of the strongest modes remains essentially constant despite the changing aspect ratio. Spurious content of the measured electrical frequency response of elliptical resonators shows a weak minimum around the aspect ratio corresponding to the "optimal" case found with simulations.

Discussion and Conclusions

The "semi-3D" modelling approach used in this work provides a relatively fast method to simulate lateral mode shapes in SMRs with arbitrary electrode configurations. This approach can be applied to, e.g., studying spurious responses arising from lateral waves excited in different structures.

[1] J. Kaitila, M. Ylilammi, J. Ellä, and R. Aigner. Proc. IEEE Ultrasonics Symp., pp. 84-87 (2003).

[2] R. Ruby, J. Larson, C. Feng, and S. Fazzio, Proc. IEEE Int. Microwave Symp., pp. 217-220 (2005).

[3] A. Link, E. Schmidhammer, H. Heinze, M. Mayer, M. Schmiedgen, B. Bader, K. Wagner, and R. Weigel, Proc. IEEE Ultrasonics Symp., pp. 1179-1182 (2005).

P1L116-04

Green's Function Analysis of Lamb Wave Resonators

Jan Kuypers, Yun-Ju Lai, Ting-Ta Yen, Chih-Ming Lin, Albert Pisano; *University of California at Berkeley, Mechanical Engineering, Berkeley, CA, USA.*

Background, Motivation and Objective

There is a great drive in identifying an acoustic RF device technology that is able to cover a wide range of frequencies on a single die within realistic cost and yield margins. The goal is to obtain single-die solutions for RF front-ends, filter banks and TCXO-dies offering multiple reference frequencies. Lamb wave devices using thin piezoelectric aluminum nitride (AlN) plates have been shown to achieve electromechanical coupling coefficients of 2.9% [1] (theory: up to 3.5%) and offer a very high phase velocity of almost 10,000 m/s. This makes Lamb wave devices suitable for RF oscillators and narrowband RF filters. The CMOS compatibility of AlN processing is of importance for a future monolithic integration [2]. However, the analysis and design of oscillators and filters requires a precise simulation tool.

Statement of Contribution/Methods

In this work we compute the effective permittivity for Lamb waves propagating in AlN plates and use this in a Green's function based model that has been used for higher order SAW device modeling [3]. The computation is adapted to incorporate the strong frequency dependence of the phase velocity and coupling. Although these devices utilize the lowest symmetric Lamb mode, S0, the model accounts for all existing modes (A0, A1, S1, …). In order to reduce the computation cost the simulation uses an interpolation scheme of the K-matrix entries in the frequency domain. This technique does not affect the accuracy as it is applied prior to the cascading of matrices and therefore is not exposed to singularities.

Results

The effective permittivity for a 2 µm thick AlN plate with a bottom metallization is shown in Fig. 1(a). The impedance of the Lamb wave resonator (LWR) is computed in Fig. 1(b). As the resonance frequency is determined by the plate dimensions the LWR can be understood as an over-moded resonator. In the given case the large bandwidth of the IDT due to the low electrode count is able to excite these different modes besides the main response (f5).

Discussion and Conclusions

We have developed a higher order Green's function model that is of importance for the analysis and design of Lamb wave devices for oscillators, filters and sensors.

[1] M. Benetti et al., Proc. Ultras. Symp. 2007, pp. 1673-1676

[2] M.-A. Dubois et al., 3rd Int. Symp. Acou. Wave Dev. Fut. Mob. Comm. Sys., 2007, pp. 111-115

[3] J. H. Kuypers et al., Proc. IEEE Ultras. Symp. 2005, pp. 1550-1555

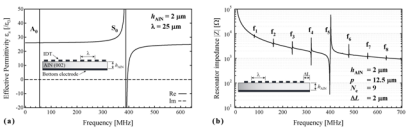

P1L117-05

Effect of size and shape on the performances of BAW resonators: a model and its applications

Claude Muller, Marc-Alexandre Dubois; *CSEM, , Neuchatel, Switzerland.*

Background, Motivation and Objective

BAW devices have been studied and fabricated for a long time now and millions of devices are sold every year. This accomplishment was made possible thanks to tremendous efforts spent on the development of the fabrication technology on one side, and to many theoretical works on the other side. Some of these works are well-known and largely used, as for example the MBVD equivalent circuit and the Mason model. A few groups went further and developed more comprehensive models. Though they allow a deeper understanding of the physics of BAW, these theories are quite complex and require powerful simulation tools. It is the aim of this paper to present a new,

simple theory that gives an original view on the functioning of BAW resonators. Simple relations between the size and shape of a BAW resonator and its performances are established.

Statement of Contribution/Methods

The proposed theory is based on a central parameter A/p, which is the ratio between the area A and the perimeter p of the BAW resonator. For a given technology, the model allows calculating the coupling coefficient k2eff and the quality factors, Qs and Qp, as functions of the size and shape of the resonator. A technology is characterized by various 'intrinsic' parameters such as ideal k2eff, and intrinsic Qs. They are obtained by a fit of the impedance curve of resonators of various sizes with a very complete equivalent circuit.

Results

Fig. 1 shows an example of the theory prediction together with measured data at 2.5 GHz. The model predicts that small resonators (small A/p) have a largely reduced coupling coefficient relative to large resonators which show a coupling close to the ideal coupling. Measurement confirms this. The model was also successfully applied to resonators of different shape. It correctly predicts the variation of coupling and quality factors between triangular, rectangular, pentagonal, elliptical and circular resonators.

Discussion and Conclusions

The proposed theory is complementary to other theoretical works. Its force relies on its ease of use and interpretation. The model is a performing tool to characterize a given technology. It also allows optimizing the design and layout of complex structures such as filters.

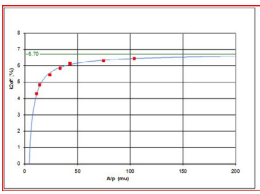

Fig. 1: • Comparison of the coupling coefficient calculated from the theory (blue curve) with the measured data (red dots). The green line represents an upper limit corresponding to a resonator of infinite size.¶

P1L118-06

Nonlinear distributed model for IMD prediction in BAW resonators

Eduard Rocas[1], Carlos Collado[1], Jordi Mateu[2], Alberto Padilla[1], Joan M. O'Callaghan[1]; *[1]UPC, Spain, [2]UPC and CTTC, Spain.*

Background, Motivation and Objective

The BAW filters are presently used in many communication systems. To fully incorporate them into communication systems characterization of their nonlinear response is required.

Although there are many works concerned about the nonlinear behavior of piezoelectric based components, there are only few studying the intermodulation distortion (IMD) in BAW filters. These studies are usually based on phenomenological equivalent circuit models that do not consider the distributed nature of the acoustic wave.

This work extends the well-known distributed KLM model to account for the nonlinear effects and obtains a close-form expression of observables third order IMD in BAW based components. This expression has been verified using a commercial circuit analysis simulator (Advanced Design Systems).

Statement of Contribution/Methods

A. Origin of the nonlinear behavior

Although it is widely accepted the elasticity to be the main contribution to the nonlinear response there are also other sources that may be accounted for, such as the piezoelectric constant and permittivity. These sources may be drawn together in a unique term, C^D to be used in the propagation equation:

$c^D=c^E+e^2\div\varepsilon^S$

Where c^E accounts for the stiffness, e is the piezoelectric constant and ε^S is the permittivity.

B. Nonlinear circuit model

Using the acoustic wave propagation equations:

$dv \div dx = -dF \div (Ac^D dt)$

$dF \div dx = -A\rho dv \div dt$

we may identify the linear distributed inductance $L_d = A\rho$, and nonlinear distributed capacitance as, $C_d = 1 \div (Ac^D)$, being the only term that accounts for the nonlinear effects.

Assuming C_d depends on the voltage and current through the acoustic transmission line we may write:

$C_d(v,i) = C_0 + J_{NL}(v) + K_{NL}(i)$

Monday Poster

Results

Assuming a quadratic nonlinear dependence on both the voltage and current, and considering an standing wave distribution (in resonance) along the acoustic transmission line, we obtain the voltage at the IMD frequency $\omega_{12} = 2\omega_1 - \omega_2$, as:

$V_{12,max} = jQ_L V^2_1 V^*_2 [9\omega_{12} J_q Z^2_0 + \omega_{12} K_q] \div (16\omega_{12} L_d)$

where Q_L is the loaded quality factor and J_q and K_q set the strength of the quadratic nonlinearities.

Discussion and Conclusions

This analysis can be used to predict the IMD occurring in BAW based devices and their impact in the communication systems. By relating the nonlinear response with the material parameters one could find to design highly linear BAW component.

P1L119-07

Nonlinear effects in solidly-mounted ZnO BAW resonators

Arto Nurmela, Hannu Salminen, Tomi Mattila, Markku Ylilammi; *VTT Technical Research Center of Finland, Finland.*

Background, Motivation and Objective

Nonlinear properties of piezoelectric materials become important when thin-film piezoresonators are driven at high power levels. Harmonics generation and intermodulation distortion are examples of undesirable nonlinear effects in, e.g., mobile phone front-end filters based on thin-film bulk-acoustic wave (BAW) resonator technology. Although the nonlinear effects have been studied in 13 MHz silicon BAW MEMS resonators [1, 2], the available literature on nonlinear effects in GHz-range BAWs is scarce [3]. In this work we have studied the nonlinearity of solidly-mounted ZnO thin-film BAW resonators.

Statement of Contribution/Methods

Nonlinear effects were studied by measuring the transmission response of the ZnO BAW resonator [4] at high power levels. The resonator was decoupled from the 50 Ohm termination impedances by 20 pF capacitors in order to allow the excitation of high mechanical vibration levels at the series resonance frequency. (Inset in Fig.1.) The measurements were done with input power levels ranging from +5 dBm to +29 dBm at the resonator input. In order to detect the nonlinear bifurcation point (hysteresis), the transmission response was recorded using both up- and down-frequency sweeps.

Results

At low excitation power (+5 dBm) the measured series and parallel resonance frequencies of the studied device were approximately 941 MHz and 970 MHz, respectively. (Fig.1.) When increasing the excitation power level, the transmission response exhibits a Duffing-behavior with tilting direction towards lower frequencies. The transmission shows a two-valued (bifurcation) response starting at +15 dBm. Fig. 1 shows a pronounced hysteresis response at +26 dBm and +29 dBm input power.

Discussion and Conclusions

Emergence of strong nonlinear effects in solidly-mounted ZnO resonators at high excitation power levels is demonstrated. A bifurcation point (two-valued hysteretic response) is observed starting at +15 dBm. Capacitive decoupling from the terminating impedance was utilized to allow the excitation of high mechanical vibration levels at undamped series resonance.

[1] V. Kaajakari et al., J. Microelectromech. Syst., 13, 715 (2004).

[2] R. Abdolvand, F. Ayazi, 2007 IEEE Ultrasonics Symp., 608 (2007).

[3] R. Aigner et al., 2005 IEEE MTT-S Int., 429 (2005).

[4] J. Molarius et al, 2005 IEEE Ultrasonics Symp., 1816 (2005).

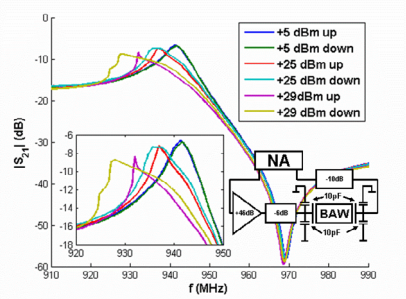

P1L120-08

Thermoelastic FEM-BEM model for Solidly Mounted Resonator

Didace Ekeom[1], Bertrand Dubus[2]; [1]*Microsonics, Saint-Avertin, France,* [2]*IEMN, Lille, France.*

Background, Motivation and Objective

A Solidly Mounted Resonator (SMR) is an ultra-thin piezoelectric layer deposited between two electrodes which operates in longitudinal thickness mode. Minimization of dissipative losses is a major goal in SMR design. For an accurate simulation, thermoelastic damping phenomenon related to the irreversible heat dissipation induced by the coupling between heat transfer and strain rate during the resonator vibration and acoustic radiation into the substrate have to be taken into account.

Statement of Contribution/Methods

In this work a thermal-piezoelectric-elastic finite element-boundary element formulation is developed, in harmonic regime. The piezoelectric layer is modeled by thermal-piezoelectric finite elements, the Bragg mirror by thermo-mechanical finite elements and the substrate by boundary elements. The boundary elements are based on an elastodynamic half-space Green function.

Results

Results are presented for two AlN based SMR operating at about 2 GHz and insulated from the substrate by a four-layer SiN/SiOC and W/SiO2 Bragg mirror. Computations present resonator key performance parameters, such as coupling factor, quality factor, and temperature coefficient frequency. Spurious modes are identified and analysed.

Discussion and Conclusions

Thermoelastic and acoustic radiation effects are shown, their contributions in the resonator Q-factor value are clearly identified.

P1L121-09

A Convolution-Perfectly Matched Layer (C-PML) absorbing boundary condition for elastic wave propagation in piezoelectric solids – Application to surface and Lamb waves propagation

Li YiFeng[1], **Bou Matar Olivier[1],** Galopin Elisabeth[2], Ducloux Olivier[2]; *[1]IEMN, LEMAC, France, [2]IEMN, France.*

Monday Poster

Background, Motivation and Objective

Since its introduction in 1994 by Berenger for Maxwell's equations, the Perfectly Matched Layer (PML) technique has become classical in numerical simulations of wave propagation. The most attractive properties of a PML layer is that, before discretization, no reflection occurs at the interface between the physical domain and the absorbing layer for any frequency and angle of incidence. Moreover, PML layer has proven to be very efficient for acoustic (in fluid) and elastic (in solid) wave equations.

Statement of Contribution/Methods

In this study, we extend the Convolution-Perfectly Matched Layer (C-PML) method we have developped (J. Acoust. Soc. Am. 118(5), pp. 2880-2890, 2005) for first-order and second-order systems, describing elastic waves in velocity and stress formulation, to the equations of elastic waves propagation in piezoelectric solids. An interpretation of the C-PML as an effective anisotropic piezoelectric solids is proposed. This new formulation facilitates implementation in COMSOL Multiphysics software. It will be descibed in frequency (for harmonic linear waves simulation) and time domain for fluid, solid and piezoelectric media. The main advantage of C-PML over classical PLM layer is that it is a more stable and highly effective at absorbing signals of long time-signature scheme.

Results

We illustrate the efficiency of this second-order perfectly matched layer based upon 2-D benchmarks with surface waves and Lamb waves. For surface waves, an integrated Surface Acoustic Wave (SAW) streaming system developped in our lab in order to decrease of the response time of µ-mixing systems, by bringing fresh analyte to the sensing surface has been modeled. In this system a Rayleigh SAW is generated using interdigitated transducers (IDT) laid on a X-cut LiNbO3 substrate, with an interdigit of 50 µm. Such waves are radiated on one half of the studied microchambers consisting in microliter droplets situated between a hydrophobic substrate and a glass cover. The good agreement between simulations and experimental results, open to us the opportunity to optimize the system.

Discussion and Conclusions

In the case of Lamb waves, some instabilities appear in classical PML and C-PML implementation, when inverse modes (phase and group velocities with different signs) take place. It will be demonstrated that this problem can be overcomed in 2D with a modified version of the C-PML, which is a kind of sponge layer (but with nearly perfect impedance matching in the case of 2D lamb wave simulation).

P1M. Microwave Acoustic Devices for Wireless Front Ends

2nd and 3rd Floor Foyers

Monday, November 3, 2008, 3:00 pm - 4:30 pm

Chair: **Robert Weigel;**
University of Erlangen, Germany.

P1M122-01

Novel MMS SAW filter structure with a new type of chirping for High Load Impedance applications

Aleh Loseu, Jagan Rao; *RF Micro Devices, USA.*

Background, Motivation and Objective

Single ended – Balanced (Se-Bal) SAW filters are widely used in RF Front End stages of mobile devices with differential Low Noise Amplifiers (LNA). Typically SAW filters are designed to have standard terminating impedances (for example 50 Ohms Single Ended input and 100, 150 or 200 Ohms balanced output). These devices are matched then to the LNA by 3 element pi-matching networks (2 Capacitors and 1 Inductor) on the PCB or laminate. An alternative will be to design the filter to have such load impedance that it can be matched to the LNA by only a single parallel inductor. Such a custom design can provide smaller module size, simpler module layout, lower cost (components, materials and assembling) and, in some cases, even better performance. However, the Trade Off is loss of flexibility. The load seen by the filter is a strong function of LNA input impedance and layout of the laminate/PCB traces. Any change of the laminate layout will require a redesign of the filter. Filters to be used in this new configuration may need to have non-standard port impedance (for example 300-400 Ohms on the differential output port). Traditional DMS filter structures and known design approaches may not be sufficient to design these filters.

Statement of Contribution/Methods

In this work we propose new multi-mode (MMS) LSAW filter structures with multiple IDTs (3, 4, 5 or even more) connected electrically in series between output ports. This structure has naturally high output impedance which can be matched to high impedance LNA with a single matching inductor. But traditional chirping (chirping the junctions between adjoining transducers) with multiple IDTs in series causes fangs inside the passband of the filter. To eliminate this problem we propose a new chirping configuration in which edges of the inner IDTs in the series chain remain regular and central their areas become chirped (modulated).

Results

We show simulation and measurement results of EGSM SAW filter employing the above mentioned MMS SAW filter structure. The device has four output IDTs connected in series with the novel chirping. Devices fabricated on 42-LiTaO3 having passband insertion loss of better than 2.2 dB over full temperature range (-30 to +85 degree C) along with the necessary transition band steepness, amplitude and phase balance and return loss.

Discussion and Conclusions

New simple and very small size MMS LSAW filter structure has been proposed. New type of chirping for some transducers has been demonstrated and analyzed. Finally, a comparison between traditional and new chirping is provided and efficiency on the new chirping for proposed structure was demonstrated.

P1M123-02

Design of Narrower Bandwidth Ladder-type Filters with Sharp Transition Bands Using Mutually Connected Resonator Elements

Tomoya Komatsu, Yasutomo Tanaka, Ken-ya Hashimoto, Tatsuya Omori, Masatsune Yamaguchi; *Chiba University, Dept. EEE, Chiba, Japan.*

Background, Motivation and Objective

The ladder topology is widely used for developing wideband and low-loss filters using SAW/BAW resonators, in which the filter passband width is inherently limited by the electromechanical coupling factor K^2 of the piezoelectric material employed. On the other hand, the passband width is adjustable for narrow bandwidth applications by designing the parameter C_{0p}/C_{0s}, where C_{0p} and C_{0s} are the static capacitance of resonators Yp and Ys placed at parallel and series arms, respectively. Although the increased C_{0p}/C_{0s} offers the narrowed passband width and increased out-of-band rejection, the transition bands lose the sharpness. For this reason, the capacitance ratio γ is sometimes increased intentionally for narrower passband width applications at the expense of the increased insertion loss.

Statement of Contribution/Methods

This paper proposes a design technique to narrow the passband width of ladder-type filter without sacrificing the insertion loss, the out-of-band rejection and the sharpness in the transition bands. It is shown that the passband width is successfully narrowed by adding resonator element(s) which form new additional attenuation poles in the transition bands.

Results

First, it is shown that two attenuation poles are formed in the passband or transition bands by connecting an additional resonator in series with Yp in one of the parallel arms. It is found that when the resonance and anti-resonance frequencies of the additional resonator are set equal to those of Ys, the two attenuation poles appear symmetrically with respect to the center of the passband. It is also shown that the optimal filter topology can be determined in a simple manner by applying the derived M transformation to the traditional ladder-type filter design.

This method is also realized by connecting an additional resonator in parallel with Ys in one of the series arms and setting its resonance and anti-resonance frequencies equal to those of Yp. As an extension of this idea, one can form more than two attenuation poles by adding more than two resonators in either series or parallel with Yp or Ys, respectively.

Secondly, it is shown that successively applying the Δ-Y transformation to the filter design, we can derive various filter topologies. This is most effective in adjusting the impedance level of each resonator suitable for device implementation.

Discussion and Conclusions

Finally, we demonstrate that a narrower bandwidth, steep transition bands and large out-of-band rejection are simultaneously realized by combining the technique discussed here with controlled C_{0p}/C_{0s}. Namely, a narrowed passband width and enhanced out-of-band rejection are mainly owed to the increased C_{0p}/C_{0s}, while the steep transition bands are achieved by newly formed attenuation poles at frequencies nearby the passband edges.

P1M124-03

Surface Acoustic Wave Duplexer composed of SiO2 film with Convex and Concave on Cu-electrodes/LiNbO3 Structure

Yasuharu Nakai, Takeshi Nakao, Kenji Nishiyama, Michio Kadota; *Murata Mfg. Co., Ltd, Japan.*

Background, Motivation and Objective

Currently, the duplexers composed of surface acoustic wave (SAW) or film bulk acoustic resonators (FBAR) have been actively developed. Authors have already realized 3.0x2.5x1.2 or 2.5x2.0x0.48mm3 size SAW duplexers for Personal Communication Services in US with an excellent temperature coefficient of frequency (TCF)□@by using□@the a shear horizontal (SH) wave on flattened-SiO2-film/Cu-electrodes/36-48YX-LiTaO3 structure for Rx (receiving side) and Rayleigh wave on SiO2-film/Cu-electrodes/120-128YX-LiNbO3 structure for Tx (transmission side).

When the SiO2 film is deposited on interdigital transducers (IDTs)/substrate in order to improve the TCF, the surface of the SiO2 always has periodic convex portions of the same thickness as fingers of the IDT over their fingers. Their large convex portions cause deterioration in the frequency characteristics of their SAW devices. In order to avoid this phenomenon, the faltten-SiO2 surface, that the convex portions were removed, has been applied to the SAW duplexers.

Statement of Contribution/Methods

This time, authors intentionally attempted to make the convex portions on the SiO2 film on the positions of the gap of IDT instead of the finger positions, though authors couldn□ft expect whether the frequency characteristics were improved or deteriorated. Authors calculated and measured the various SAW characteristics.

Results

As the results, the calculated and measured results showed the increase of the reflection coefficient and the improvement of the TCF. In addition to them, the measured results showed that a power durability have been drastically improved without any deterioration in the frequency characteristics by making the convex portions on the SiO2 film over the gap portions of the IDT.

Discussion and Conclusions

The surface on the SiO2 film always has convex portions over the finger positions of the IDT and concave ones over the IDT's gap positions, after the SiO2 is deposited on the IDT/substrate to improve the TCF. By making opposite structure, that is, convex ones over the gap positions and concave ones over the finger positions, authors calculated and measured the various SAW characteristics. As the results, in addition to the increase of the reflection coefficient and the improvement of the TCF, the power durability have been drastically improved (several times) without any deterioration in the frequency characteristics.

P1M125-04

Surface Acoustic Wave filter in high frequency with Narrow Bandwidth and Excellent Temperature Property

Michio Kadota, Takeshi Nakao, Takaki Murata, Kenji Matsuda; *Murata Mfg. Co., Ltd, Japan.*

Background, Motivation and Objective

Radio frequency (RF) filters in high frequency using surface acoustic wave (SAW) such as MediaFLO™ and Time Division Synchronous Code Division Multiple Access in China handy phone system require a narrow bandwidth. So, the SAW substrates for their RF filters are also required to have a very excellent temperature coefficient of frequency (TCF). Rayleigh wave on ST-X quartz substrate and on langasite one, and a shear horizontal (SH) type of Leaky SAW (LSAW) on Ta-electrode/ST-90X quartz one having excellent TCF have too small electro-mechanical coupling factor to realize above-mentioned bandwidth by using a multi-mode SAW resonator filter.

Statement of Contribution/Methods

Rayleigh wave on a ZnO film/Al-electrode/quartz and LSAW on a flattened SiO2/high density metal electrodes/36-48YX-LiTaO3 structures with good TCF have suitable coupling factor to realize them. A large reflection coefficient is required to realize the resonator filter. Though the latter has the large reflection coefficient, the farmer has small one. So, authors also attempted to apply a high density metal electrode instead of Al electrode of the former structure to realize the large reflection coefficient. And authors tried to develop the RF SAW resonator filters by using their structures.

Results

The RF resonator filter for MediaFLO composed of the flattened SiO2/high density metal electrodes/36-48YX-LiTaO3 structure showed a good frequency characteristic and an excellent TCF of 1.01 ppm/deg. But, one composed of the ZnO film/high density metal electrode/quartz was required to improve a little more though its reflection coefficient using the high density metal electrodes such as Au, Pt, Ta was larger than that using the Al-electrode.

Discussion and Conclusions

Authors attempted to develop the resonator filters composed of the ZnO film/high density metal electrode/quartz and the flattened SiO2/high density metal electrodes/36-48YX-LiTaO3 to realize the RF filter required a narrow bandwidth and excellent TCF. As the result, the RF resonator filter for MediaFLO composed of the latter structure showed a good frequency characteristic and an excellent TCF of 1.01 ppm/deg.

P1M126-05

Small-sized SAW Duplexers with Wide Duplex Gap on a SiO2/Al/LiNbO3 Structure by Using Novel Rayleigh-mode Spurious Suppression Technique

Hidekazu Nakanishi, Hiroyuki Nakamura, Yosuke Hamaoka, Yukio Iwasaki, Hiroki Kamiguchi; *Panasonic Electronic Devices Co., Ltd., Japan.*

Background, Motivation and Objective

We have successfully developed the novel Rayleigh-mode spurious suppression technique for SAW duplexers with wide duplex gap on a SiO_2/Al/$LiNbO_3$ structure. The small-sized SAW duplexers with wide duplex gap in UMTS, were realized by employing this technology. The SAW duplexers, which have been widely used in cell band, are required to satisfy the specification on every UMTS band. Especially, Band I and Band IV systems have a wide duplex gap. So, it was difficult to accomplish good performances in the SAW duplexers for Band I and Band IV by the 36°YX-$LiTaO_3$ which cell band SAW duplexer have employed. The substrate, which has higher electro-mechanical coupling coefficient (K2) and smaller temperature coefficient of frequency (TCF) than those of 36°YX-$LiTaO_3$, is needed to realize the miniaturized SAW duplexers for Band I and Band IV with low loss and high attenuation.

Statement of Contribution/Methods

We employed the SiO_2/Al/5°YX-$LiNbO_3$ structure to materialize the substrate satisfying both characteristics. However, there was a big problem of spurious response caused by Rayleigh-mode on this structure. To solve this problem, we focused on the relationship between the spurious response and the shape of SiO_2. The shape of SiO_2 was controlled by deposition technique. Applying this technique to the SAW duplexer for Band I, we could realize the SAW duplexer for Band I with excellent performances. Moreover, we also realized the SAW duplexer for Band IV by applying this technique. Transmitting frequency band of Band IV is lower than that of Band I. So, the optimized thicknesses of Al electrode for Band I and Band IV are different each other. The spurious response is different on every the thickness of Al electrode. Therefore, we focused on the relationship between the shape of SiO_2 and the thickness of Al electrode to suppress the spurious.

Results

We have successfully cleared the optimum shape of SiO_2 with taking account of the difference of the electrode thickness to achieve a good performance in Band IV duplexer. The shape of SiO_2 which can suppress the spurious depended on the thickness of Al electrode. By controlling the shape of SiO_2, the Rayleigh-mode spurious of both Band I and Band IV duplexers can be suppressed. As the result, the SAW duplexers have sufficient wide pass band and small TCF.

Discussion and Conclusions

We have established the SiO_2 shape control technique for the spurious suppression. Our duplexers show the excellent performances for actually use. Insertion loss of transmitting band for Band I and for Band IV are 1.2dB and 1.3 dB. And, the TCF is about -30ppm/ºC. The size of these duplexers is 2.5mm×2.0mm.

P1M127-06

Balanced Front-End SAW Modules with Improved Selectivity at Low Frequency Offsets for Handheld Transceivers

Sergei Doberstein; *ONIIP, Russian Federation.*

Background, Motivation and Objective

The balanced low-loss longitudinally-coupled resonator (LCR) SAW filters are successfully employed in the balanced hybrid SAW modules for high frequency handheld transceivers [1]. However these modules have a high frequency (HF) shoulder with a relative level of 30-45 dB at the low frequency offsets from a center frequency. It is relate with a frequency response form of the LCR SAW filters [2] employed in these modules.

Statement of Contribution/Methods

This paper presents the new balanced front-end SAW modules with the improved selectivity at the low frequency offsets and fractional bandwidth of 1.5-6% for the 440-470 MHz handheld transceivers. The modules contain 2 SAW filters connected across a low noise bipolar transistor amplifier. The balanced LCR SAW filters on 42° YX $LiTaO_3$, 64° YX, 41° YX , 49° YX and 36° YX $LiNbO_3$ [3] were used in these modules to suppress the HF shoulder in the frequency response. For a fractional bandwidth of 1.5% the first filter is realized in a 4-pole two- or three-transducer scheme on 42° YX $LiTaO_3$. The second filter with a wider fractional bandwidth is realized in the 4-pole two- or three-transducer scheme on 64° YX $LiNbO_3$. These two types of the filters have a different distribution of the HF shoulders in the frequency responses. A combination of these two types of the filters with the

different fractional bandwidths provides an efficient suppression of the HF shoulder in the frequency response of the modules. Similarly for the fractional bandwidths of 4% a pair of the filters with the different fractional bandwidths on 64° YX and 41° YX $LiNbO_3$ was used and for the fractional bandwidths of 6% the pair of the filters on 41° YX and 36° YX $LiNbO_3$ was used. The optimization of a SAW filter-amplifier-SAW filter system is provided with a computer simulation using an equivalent circuit model.

Results

The 440-470 MHz samples of the balanced front-end modules have shown an amplitude ripple of 1 dB within a 3-dB bandwidth of 6.6 - 33 MHz, 10 dB gain, improved suppression up to 50 dB at the low offsets of ±14 - ±33 MHz and high suppression of 90 dB at the large offsets of ±22 - ±44 MHz from the center frequency. The modules provided a noise factor of 2 dB with a current consumption of 5 - 7 mA and supply voltage of 3 V in the 13.3x6.5x1.8 mm SMD packages.

Discussion and Conclusions

We have developed the new balanced hybrid SAW modules with improved selectivity at the low frequency offsets from a center frequency then the previous ones [1] and we shall use them in the front-end of 440-470 MHz handheld transceivers for the better suppression of the local oscillator and image frequencies.

1. S. A. Doberstein, Proc. IEEE Ultrason. Symp., 2007, pp. 1665-1668.

2. T. Morita et al., Proc. IEEE Ultrason. Symp., 1992, pp. 95-104.

3. P. G. Ivanov et al., Proc. IEEE Ultrason. Symp., 1996, pp. 61-64.

P1M128-07

Compact Ladder Type SAW Resonator Filter

Anatoly Rusakov, **Jidong Dai;** *RF Monolithics, Dallas, TX, USA.*

Background, Motivation and Objective

One of the few disadvantages of ladder resonator filter in comparison with its longitudinally coupled rival is its relatively big size and layout complexity. Common 2-section SAW ladder filter has at least 5 resonators. In order to keep number of electrodes and aperture of each resonator close to optimal, it is common to use serial or parallel connected resonators in each ladder arm [1], so the number of resonators can be up to 10. To avoid the interaction between resonators, they are placed in separate acoustic tracks and that increased the sizes and makes interconnection between resonators long and complex.

Statement of Contribution/Methods

The nature of constrains on number of electrodes is in the following. Ladder filters on lithium tantalite have the best performances if they consist of resonators with long IDT and short reflectors and these IDT and reflectors have identical period of electrodes. Because reflectors are shorter, their reflection band (where reflection coefficient from reflectors ~1) is slightly wider than IDT's stop band (where transmission coefficient through IDT ~0) and the resonance occurs on the left edge of the stop band of IDT. Outside the stop band of IDT, long IDTs work better because they have less unwanted resonance there and better main resonance. Within the stop band, short IDT has advantages over long one because in the stop band LSAWs in IDT transform to bulk waves under bus bars and that radiation deteriorates performances of the resonator [2].

The present paper introduces method how to place 2 or more resonators in 1 acoustic track with common reflectors and connect them parallel or serial electrically. Outside the reflection band the reflection coefficient of reflectors is small and that acoustic track works as resonator with long IDT, what is optimal there. Within the stop band of IDT, the reflection coefficient of reflectors is strong and the acoustic track works as several separated short resonators, what is optimal there. Ladder filter becomes small and interconnections – short and easy.

Results

The results of simulation are presented along with experimental data. The result is ladder filter with 8 resonators placed in 4 acoustic tracks that allowed reducing size and improving insertion loss and performances.

Discussion and Conclusions

The proposed approach to design ladder filters on lithium tantalite provides improving performances and reducing size. The small size is important not only for relatively low frequency filters but for high frequency RF filters too, because short and easy interconnection between resonators mean better IL when metal thickness is thin.

[1] S. N. Kondratiev and T. Thorvaldsson, 2000 IEEE Ultrasonics Symposium, pp. 109-112.

[2] J. V. Knuuttila, P. T. Tikka, C. S. Hartmann, V. P. Plessky, and M. M. Salomaa, Electron. Lett. 35, 1115 (1999).

P1M129-08

Study on SAW Devices Having Face to Face Aligned Packaged Structure

Takanori Yamazaki, Yuji Terao, Keishin Koh, Koji Hohkawa; *Kanagawa Institute of Technology, Japan.*

Background, Motivation and Objective

A simple method for a high performance packaging on SAW devices is to cover the device surface by capping structure consisting of the same substrate as that of SAW substrate. In general, these devices would be expected to have relatively higher performance on the stability against temperature, aging, and mechanical perturbation, than the device which would use other packaging materials such as polyimide, silicon-nitride, and metal etc. However, these devices might be supposed to be relatively expensive compared to the material used for packaging structure. Further, for most application such as radio communication, multiple SAW devices would be required to be used in equipment. If we could integrate multiple devices on both faced substrates, device size and cost could be reduced simultaneously. In this paper, we will report some experimental results of face to face aligned packaged SAW device such as temperature stable oscillator and wide band pass filters.

Statement of Contribution/Methods

The face to face packaged of SAW devices substrates is not only to could improve device performance such as pass band characteristics and temperature dependent stability by combining different substrates, but also, it could obtain functional devices which uses mode coupling between waves on two surfaces by reducing the gap thickness between two substrates. The fabricating process steps are 1) first, we fabricated SAW devices on the two kinds of substrate with different temperature coefficient; 2) next, we coated adhesive material such as film photo resist etc. and patterned it on one SAW devices substrate; 3) we bonded other SAW devices substrate on the surface of the SAW devices substrate processed by face to face using bonding equipment and carried out heating treatment; 4) Finally, we formed bump process for wiring.

Results

We fabricated test devices using Quartz substrate and estimate basic characteristics of device to verify the possibility of this packaging method. We investigated effect of various parameters such as adhesive material thickness, dimensions of package and bonding conditions.

Discussion and Conclusions

We also discussed difference methods for wafer level packaging process. The experimental results indicated that this package methed is effective to improve temperature characteristics of oscillator.

P1M130-09

Switchable Low Loss SAW Filter Bank with SAW Notches

Jiansheng Liu, Jiuling Liu, Shunzhou Li, Shitang He, Yong Liang; *Institute of Acoustics, Chinese Academy of Sciences, China.*

Background, Motivation and Objective

Switchable SAW filter banks are widely applied in frequency synthesis, frequency hopping radar and communication system. In these applications, SAW filters are normally required to operate over wide bandwidth and to perform low loss and high stop-band rejection to make system work in adequate signal-to-noise ratio. Moreover, very high rejection at some frequency is required for special purpose. The cascade-connected two stages can implement very high stop-band rejection; however, its volume and insertion loss will increase a lot. bank connected in serial with SAW notch filter can implement small volume, low loss and very high rejection at the special frequencies. In this paper, the design and testing of 4 channel switchable SAW filter bank with SAW notches filter will be presented.

Statement of Contribution/Methods

Slanted-finger interdigital transducer (SIDT) including EWC/SPUDT is adopted to decrease the insertion loss of individual SAW filter. SAW filters are fabricated on YZ LiNbO3 substrate with the insertion loss of less than 6.5dB, 1dB bandwidth of more than 9MHz, 40dB bandwidth of less than 15MHz, stop-band rejection of more than 40dB. SAW notch filter are fabricated on Y36¡ã LiTaO3 substrate with the rejection of more than 30dB and the insertion loss of less than 0.5dB.

Switches are added to both input and output of SAW filters and two SAW notch filters are separately connected to the input and output of the bank.

Results

The experimental filter bank results in the insertion loss of less than 8dB (including the insertion loss of switches), the stop-band rejection of more than 40dB, and the rejection more than 60dB at a special frequency. The frequency performance of the filter bank is shown in Fig.1.

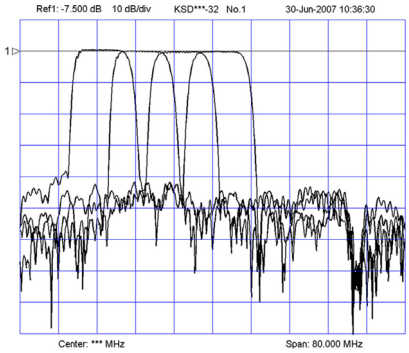

Tuesday Oral Sessions

1D. Elasticity Imaging: Applications

Hall 3

Tuesday, November 4, 2008, 8:30 am - 10:00 am

Chair: **Matthew O'Donnell;**
University of Washington, WA., USA.

1D-1

8:30 AM **Ablation Monitoring with 2D and 3D Elastography**

Hassan Rivaz[1], **Emad Boctor[1],** Gabor Fichtinger[2], Gregory Hager[1], Ioana Flemming[1]; *[1]Johns Hopkins University, USA, [2]Queens University, Canada.*

Background, Motivation and Objective

Hepatocellular carcinoma (HCC) is one of the most common tumors, causing 662,000 deaths worldwide annually. RF ablation therapy of HCC has gained interest recently. Unfortunately, appearance of ablated tumors in B-mode only reveals hyperechoic areas. Accordingly, elastography has been used for monitoring RF ablation by observing that ablated region is harder than surrounding tissue. In this paper, we present in-vivo patient studies of RF ablation monitoring using 2D elastography. We then develop and evaluate a 3D elastography method operating on volumetric data acquired from a 3D probe in ex-vivo studies. The benefits of 3D strain imaging of RF ablation are two-fold: (1) 3D imaging eliminates the need to image the same plane while palpating the tissue, and (2) 3D imaging allows more precise monitoring of temperature deposition which exhibits variations in 3D.

Statement of Contribution/Methods

Our method is based on minimizing a cost function using dynamic programming (DP). The cost function incorporates similarity of echo amplitudes and displacement continuity. A 3D volumetric search in axial, lateral and elevational directions is performed using a hierarchical approach to minimize the cost function. The use of physical priors of tissue motion continuity increases the robustness of the technique. Compared to other optimization techniques, DP is an efficient non-iterative method of global optimization.

Results

We present in-vivo patient studies of monitoring liver ablation with freehand 2D elastography. The thermal lesion was not discernible in the B-mode image but it was clearly visible in the strain image as well as in validation CT. We have collected data from 5 patients and we are planning to perform more experiments.

We also present 3D strain images generated by our proposed method for thermal lesions in ex-vivo experiments and compare the results to the pathology images. The current 3D DP implementation runs in approximately 1min for a typical volume on a 3.8GHz P4 CPU.

Discussion and Conclusions

Good agreement was observed between the size of the thermal lesion in strain images from 2D elastography and CT images in the patient studies. Also, 3D strain images and pathology were in agreement in the ex-vivo studies. Having an elastography system for 3D ablation monitoring with promising ex-vivo results, we are planning to conduct in-vivo patient studies using our active IRB approval.

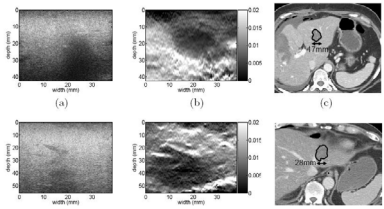

Fig. 1. *In-vivo* images of the thermal lesion produced by RF ablation therapy of HCC. first and second row corresponding to the first and second patients. (a) & (d) B-scan after RF ablation. The shadow in (a) indicates the presence of thermal lesion. It is almost impossible to ascertain the size and position of the thermal lesion from the B-scans. (b) & (e) Strain images after RFA ablation, generated using 2D DP elastography and freehand palpation of the liver tissue. The thermal lesion is visible in dark surrounded by normal tissue in white. (c) & (f) Post-ablation CT scans, with the delineated thermal lesions (The non-unity aspect ratio in the axes of the B-mode and strain images should be considered when comparing them with the CT scans).

1D-2

8:45 AM **Comparison of Ultrasound Strain Images with Multi-modality Imaging Techniques in Liver RF Ablation Assessment: Initial <I>Ex vivo</I> and Clinical Results.**

Anna Fernandez[1], Orpheus Kolokythas[2], Thomas Gauthier[3], Daniel Herzka[1], Hua Xie[1]; [1]*Philips Research North America, Briarcliff Manor, New York, USA,* [2]*University of Washington Medical Center, Seattle, WA, USA,* [3]*Philips Medical Systems, Bothell, WA, USA.*

Background, Motivation and Objective

Ultrasound (US) elastography in liver imaging applications has recently gained interest in the clinical community. Various techniques explore the use of elasticity information for clinical diagnosis of fibrosis and cirrhosis and for assessment of RF or HIFU ablation. Varghese et al. used strain-based elasticity to assess liver RF ablations (RFAs) in in vivo porcine livers by inducing strain through RFA needle push/pulls. Applying the same deformation technique, we conducted compression-based strain imaging for ex vivo and in vivo clinical liver RFA assessment and validated the results against several imaging modalities.

Statement of Contribution/Methods

Phantoms were constructed by embedding bovine livers in a graphite-gelatin mixture. A commercial RF needle (Rita Medical Systems) was inserted and deployed into the phantom. RF data were collected using a linear array on an iE-33 system (Philips) during RF needle pulling before and after a desired 3cm ablation. Strain images were generated offline using a 2D speckle tracking algorithm. For correlation, MRI (Philips) was used to collect T1-weighted images pre- and post-RFA. The phantom was then dissected along the US image plane and photos were taken showing caliper measurements of the ablation. Three additional albeit different phantom experiments were conducted.

Clinical RF data were acquired on two patients with a curved-linear array on an iU-22 system (Philips).The patients had preoperative and postoperative contrast-CT scans that were compared with the US elasticity results.

Results

For one phantom, the CNR of the ex vivo RFA lesion in conventional B-mode and strain images was 0.15 and 12.12, respectively, highlighting the increased sensitivity of strain imaging. The length of the lesion long-axis was 39.6mm, 38.6mm, and 40.2mm as measured by elasticity, MR, and calipers, respectively. With MR as a reference, the elasticity strain image showed 2.5% error and the caliper showed 4.1% error in lesion length. All phantom elasticity results displayed good correlation in lesion size with other modalities and improved CNR compared to B-mode.

The 2 clinical cases showed the potential of US elasticity imaging in an intraoperative setting. Improved lesion contrast was seen in the elasticity images compared to B-mode. In one case, we saw comparable lesion dimension sizes in the elasticity image compared to post-op contrast CT. This suggests that elasticity imaging could provide similar information as shown with contrast-CT without the need for contrast or additional ionizing radiation

Discussion and Conclusions

We demonstrate compression-based elasticity imaging in RFA procedures in ex vivo tissue with MRI comparisons and in vivo clinical cases with CT comparisons. The additional information from elasticity images could enhance the efficacy of RFA treatments during surgery.

1D-3

9:00 AM **Assessment of the elastic properties of heterogeneous tissues using transient elastography: Application to the liver.**

Cécile Bastard[1], Yassine Mofid[1], Jennifer Oudry[1], Jean-Pierre Remenieras[2], Laurent Sandrin[1]; *[1]Echosens, Research and Development Department, Paris, France, [2]Université François Rabelais de Tours, INSERM U930, CNRS FRE 2448, Tours, France.*

Background, Motivation and Objective

The Fibroscan® (Echosens, Paris, France) is a transient elastography based device used to quantify liver fibrosis by following the propagation of a low frequency shear wave and measuring the mean Young's modulus of the liver. This device has been successfully applied to homogeneous tissues such as liver in patients with chronic hepatitis C. Current developments in transient elastography are now headed toward the characterization of heterogeneous tissues. The objective of this study is to characterize focal nodules in human liver and to quantify heterogeneous fibrosis.

Statement of Contribution/Methods

The estimation of the shear wave velocity can be achieved by solving the elastic wave equation taking into account either the 1D, the 2D or the 3D components of the displacement spatial derivatives.

Two methods are investigated: A 1D local inversion is performed on data acquired with a standard Fibroscan® probe composed of a 3.5 MHz transducer mounted on a low frequency vibrator and a 3D local inversion is achieved on data acquired using a new dedicated multi-elements probe connected to an ultra-fast ultrasonic device.

Results

The algorithms are validated on heterogeneous phantoms. The reconstructed 1D shear velocity obtained on a commercial tissue-mimicking phantom (CIRS Inc., USA) containing a hard inclusion located between 23 and 53 mm from its top is in good agreement with the data provided by the manufacturer (1.6 m/s in the background and 2.5 m/s in the inclusion) (Fig. 1). Results are also obtained in the liver *in vivo* on patients with focal nodules.

Discussion and Conclusions

The potential of transient elastography to quantify the elastic properties of heterogeneous tissues is investigated. 1D local inversion and 3D local inversion algorithms are assessed on heterogeneous phantoms and in the liver *in vivo*.

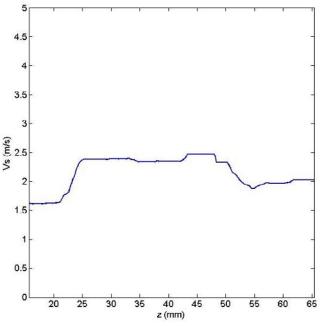

Fig.1: 1D shear velocity reconstructed using a local 3D inversion in a CIRS phantom containing a hard inclusion.

1D-4

9:15 AM **ShearWave™ Elastography: a new ultrasound imaging mode for assessing quantitatively soft tissue elasticity**

Jeremy Bercoff[1], Aline Criton[1], Jacques Souquet[1], Mickael Tanter[2], Thomas Deffieux[2], Jean Luc Gennisson[2], Mathias Fink[2], Valérie Juhan[3], Anne Colavolpe[3], Dominique Amy[4,] Alexandra Athanasiou[5]; *[1]Supersonic Imagine, Aix en Provence, France, [2]Laboratoire Ondes et Acoustique, Paris, France, [3]Hopital La Timone, Marseille, France, [4]Cabinet de Radiologie Amy Fabry, Aix en Provence, France, [5]Institut Curie, Paris, France.*

Background, Motivation and Objective

ShearWave™ Elastography is a new real time ultrasound imaging mode that quantitatively measures local tissue elasticity in kPa. Based on the Supersonic Shear Imaging elastography technique (Laboratoire Ondes et Acoustique, Paris), this new mode may appear as a promising tool to improve breast lesion characterization. This work has three main objectives: Evaluate the technical performance of the new imaging mode (contrast, resolution, penetration), its applicability in clinical routine, and the relevance of the quantitative elasticity measurement for breast cancer diagnosis.

Statement of Contribution/Methods

The ability of the new imaging technique to provide quantitative measurement of soft tissue elasticity was evaluated in vitro on calibrated elastography phantoms. The performance of the imaging technique was evaluated for different elasticity ranges (5 to 150 kPa), different elasticity contrasts (1.2 to 20), and different imaging depths (5 to 60 mm).

The reliability and the potentiality of the new technique for breast imaging were evaluated on 150 clinical cases previously classified.

Reliability of the technique has been evaluated on the 50 first patients using three parameters: A confidence factor estimating the quality of the elasticity measurement algorithm, a reproducibility factor calculated using the variance of consecutives elasticity images acquired under the same operational conditions and a robustness factor which quantifies the repeatability to the probe held by the clinician under different grades of manual compression.

Finally, the relevance of the quantitative elasticity value for breast cancer diagnosis was evaluated using FNA or core biopsy as the reference diagnostic method. A distribution analysis of the elastography values as a function of pathology result (benign vs. malignant) obtained with FNA or core biopsy was performed using the concordance coefficient approach

Results

ShearWave™ Elastography is capable of detecting elasticity contrast ratios of 1.3 with a resolution of 1 mm for a penetration depth of 40 mm using a conventional high frequency linear probe. The technique is reliable and easy to use for breast imaging: Mesurement in kPa of breast tissue elasticity has been successfully achieved in all cases and in a reproductive way. The technique brought new clinical information to the physician that may be used for improving the diagnosis: Malignant lesions had a mean stiffness value of 150 kPa with a standard deviation of 41.6 kPa while benign ones showed a mean elastic value of 62 kPa with a standard deviation of 21 kPa

Discussion and Conclusions

ShearWave™ Elastography is a new ultrasound imaging mode which provides quantitative elasticity measurements. It brings complementary information that could potentially help in breast lesion characterization as an adjunct to B-mode ultrasound.

1D-5

9:30 AM **Ultrasound Displacement Estimation Combining Viterbi Processing and Phase Rotated Correlation Coefficient Filter**

Lingyun Huang[1], Yael Petrank[1], Congxian Jia[2], Sheng-Wen Huang[2], Matthew O'Donnell[1]; *[1]University of Washington, Bioengineering, Seattle, WA, USA, [2]University of Michigan, Biomedical Engineering, Ann Arbor, MI, USA.*

Background, Motivation and Objective

In myocardial strain imaging, peak hopping artifacts are inevitable for most cross-correlation based speckle tracking algorithms if the interframe peak systolic strain is large. To minimize these artifacts, we investigated two motion estimation algorithms. One is Viterbi processing, which identifies the optimal displacement path satisfying material continuity. The other is phase rotation filtering of correlation coefficients, which suppresses peak hopping artifacts if a reasonable estimate of the local strain is assumed. In this paper, these two methods are combined, where Viterbi processing of correlation coefficient data provides the local strain estimate required for phase rotation filtering.

Statement of Contribution/Methods

An in vivo experiment was conducted on a paced rabbit heart to verify the algorithm. Two frames of RF data were acquired using a linear probe (5MHz central frequency, 40 MHz sampling frequency and 0.3mm pitch, Ultrasonix RP, Richmond, BC, Canada) at the beginning of systole. These 2-D RF frames were first transformed to analytical signals, and cross-correlation was performed with kernels extending only one speckle spot in dimension. Viterbi processing was first applied to the cross-correlation coefficient matrix, giving bonuses and penalties to points along possible displacement paths. Subpixel displacements were further estimated using a phase-zero crossing algorithm. Next, normal and shear strain components with respect to axial displacements were estimated using least squares fitting over a 2 mm area. The estimated strains were then used in the phase rotation algorithm to filter correlation coefficient functions. The entire algorithm was performed a 2nd time to refine displacement estimates. For comparison, we also estimate 2-D displacements and strain distributions using non-phase rotated correlation coefficient filters.

Results

As shown in the figure, peak hopping artifacts were dramatically reduced after Viterbi processing and phase-rotated correlation coefficient filtering. Peak hopping areas in displacement and strain estimates were reduced 72.3% and 74.5% respectively.

Discussion and Conclusions

The proposed algorithm significantly reduces peak hopping when large strains are present and improves the image quality of myocardial strain imaging during peak systole.

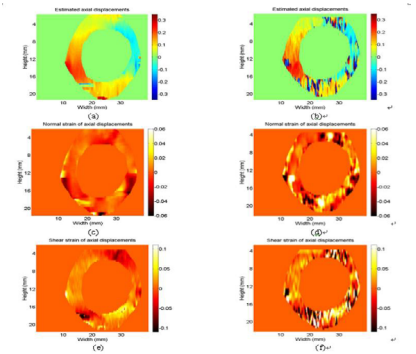

Figure 1. (a) Estimated axial displacement using Viterbi + phase rotated correlation coefficient filter; (b) only non-phase rotated correlation coefficient filter; (c) normal strain with respect to axial displacement using Viterbi + phase rotated correlation coefficient filter; (d) only non-phase rotated correlation coefficients filter; (e) shear strain with respect to axial displacement using Viterbi + phase rotated correlation coefficient filter; (f) only non-phase rotated correlation coefficient filter.

1D-6

9:45 AM **An Algorithm for Strain Reconstruction from Irregularly Sampled, Incomplete Measurements**

Mikhail Danilouchkine, Frits Mastik, **Antonius van der Steen;** *Erasmus Medical Center, Netherlands.*

Background, Motivation and Objective

IVUS palpography was proven to be an indispensable tool for the semi-invasive characterization of atherosclerotic plaques in coronary arteries. The occurrence of the neighboring high and low strain regions serves as an indicator for the rupture-prone location. However, IVUS probe motion hampers accurate determination of the mechanical properties at each location of the luminal surface and frequently results in regions of void strain estimates.

This study proposes a novel algorithm for luminal strain reconstruction from irregularly sampled, incomplete strain measurements.

Statement of Contribution/Methods

Our method is based on the conventional normalized convolution (NC) algorithm. The proposed extension applies the NC algorithm at different levels of the grid pyramid. It starts at the most coarse level with fewer grid points and assigns the value to each grid points in such a way that the difference between the value at irregularly sampled

location and interpolated value is minimal. The results, obtained at a coarse level, are subsequently propagated into a finer level until the finest level is reached.

The luminal strain maps, computed from seven in-vivo IVUS pullbacks, were utilized for validation. A number of strain measurements were artificially removed in a random manner. The strain sparsity ranged from 10% till 90% with 10% increment.

The efficacy of algorithm was assessed via the relative reconstruction error - a ratio of the absolute difference between the true and reconstructed values related to the true strain value expressed as a percentage and averaged over the strain map.

Results

Plot A shows the accuracy of strain reconstruction depending on the strain sparsity. Three images below illustrate the quality of the luminal strain reconstruction (B3) from 30% of available measurements (B2), randomly sampled from the original strain map (B1).

Discussion and Conclusions

The study demonstrates that the detrimental effect of IVUS probe motion on the quality of the luminal strain profile can be reduced via the strain reconstruction algorithm. The reconstructed strain maps from incomplete measurements highly resemblances the original ones. With more than 30% available strain measurement the relative reconstruction error does not exceed 10%.

Acknowledgement: Dutch Foundation for Technical Sciences and Volcano Corp.(Rancho Cordova, USA).

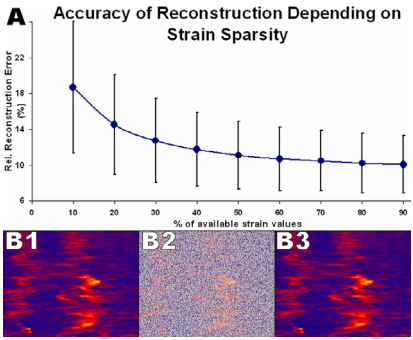

2D. Contrast Agents: Targeting and Therapeutics

Room 201 A/B/C

Tuesday, November 4, 2008, 8:30 am - 10:00 am

Chair: **Tom Matula;**
Applied Physics Laboratory, University of Washington, USA.

2D-1

8:30 AM **Oil-filled polymeric ultrasound contrast agent as local drug delivery system for lipophilic drugs**

Klazina Kooiman[1], Marcel R. Böhmer[2], Marcia Emmer[1], Hendrik J. Vos[1], Ceciel Chlon[2], William T. Shi[3], Christopher S. Hall[3], Suzanne H.P.M. de Winter[2], Karin Schroën[4], Michel Versluis[5], Nico de Jong[1], Annemieke van Wamel[1];
[1]Erasmus MC, Biomedical Engineering, Rotterdam, Netherlands, [2]Philips Research Laboratories Eindhoven, Biomolecular Engineering, Eindhoven, Netherlands, [3]Philips Research North America, Briarcliff Manor, USA, [4]Wageningen University, Food and Bioprocess Engineering Group, Department of Agrotechnology and Food Sciences, Wageningen, Netherlands, [5]University of Twente, Applied Physics, Physics of Fluids, Enschede, Netherlands.

Background, Motivation and Objective

The advantage of using ultrasound contrast agents as drug delivery systems is the local and triggered release of a therapeutic only at the region of interest. In addition, ultrasound imaging will aid the guidance of therapy. This study focuses on the characterization of a novel drug delivery system, based on polymer-shelled microcapsules filled with a mixture of gas and oil, for ultrasound-triggered local release of lipophilic drugs.

Statement of Contribution/Methods

pLA-pFO shelled microcapsules were synthesized using pre-mix membrane emulsification. The resulting capsules contained, apart from a gas phase, hexadecane as drug-carrier reservoir; the absorbing dye Sudan Black was chosen as lipophilic model drug. Sizes were determined using a Coulter Counter Multisizer 3. Efficiency of hexadecane encapsulation was determined using Gas Chromatography/Mass Spectrometry. Morphology was studied with Scanning Electron Microscopy. Attenuation as a function of frequency (0.3-22 MHz) was measured in vitro. Percentile event counts as a function of increasing peak negative pressure (P_) were studied when individual microcapsules were insonified at 1 MHz (signal detected from 3-7 MHz). Microcapsule behavior upon insonification at 1 MHz was studied in more detail with the Brandaris 128 high-speed camera. Ultrasound-triggered drug release (1 MHz) was optically studied using video recording. A GE/VingMed System 5 was used for in vitro imaging at 2.5 MHz.

Results

Microcapsules were synthesized that contained either no oil (Sc), were almost half-filled with oil (Sch), or were almost completely filled with oil (Sh). The spherical microcapsules all had a number weighted mean diameter of 1.25 µm and >99% were below 3.1 µm. Attenuation was highest for Sc. Maximum attenuation for Sc was around 20 MHz, while that for Sch and Sh was around 13 MHz, indicating oil encapsulation lowered the resonance frequency. Sc, Sch, and Sh all showed a threshold in percentile event count, followed by a sharp increase in event counts. At a low MI (P_ of 0.24 MPa), microcapsules typically compressed without cracking. At a high MI (P_ of 0.51 MPa), microcapsules cracked, thereby releasing their content. With increasing P_, a marked enhancement of scatter intensity over a tissue-mimicking phantom was observed for Sc, Sch, and Sh.

Discussion and Conclusions

Microcapsules loaded with different amounts of oil were produced. Using high MI diagnostic ultrasound, the microcapsules could be cracked, thereby releasing the encapsulated drug. Guidance and monitoring of therapy will also be possible because the microcapsules were echogenic and stable at low MI. In conclusion, these novel oil-filled microcapsules have great potential as a local drug delivery system for lipophilic drugs.

Acknowledgments: This project is supported by innovation subsidies collaborative projects by the Dutch Ministry of Economic Affairs under number IS042035.

2D-2

8:45 AM **Ultrasound Activated Paclitaxel Delivery in Mice Using a Combined Therapy and Imaging Probe System**

William Shi[1], Marcel Böhmer[2], Muzaffer Celebi[3], Annemieke van Wamel[4], Chien Ting Chin[1], Ceciel Chlon[2], Alexander Klibanov[3], Christopher Hall[1]; [1]*Philips Research North America, USA,* [2]*Philips Research Europe, Netherlands,* [3]*University of Virginia, USA,* [4]*Erasmus MC, Netherlands.*

Background, Motivation and Objective

Localized therapeutic effects of an experimental therapeutic agent were evaluated using a mouse tumor model (a subcutaneous MC38 tumor on the right hind limb) and a combined ultrasound therapy and imaging probe system (TIPS). TIPS is a dedicated preclinical system including an 8-channel focused therapeutic probe (dia=8cm, F=1), an ultrasound coupling device, and a programmable 2D motion assembly for full treatment coverage. The agent consists of acoustically activatable microcapsules (MCs) with a destruction threshold of 0.5 in MI and median size around 1.5 µm. MCs are partially (50%) filled with an oil containing the anti-cancer drug paclitaxel.

Statement of Contribution/Methods

Thirty two mice were equally but randomly divided in 4 Treatment Groups (TGs): (1) two saline injections on day 0, (2) two MCs injections on day 0, (3) two MCs injections with ultrasound exposure on day 0, and (4) three MCs injections with ultrasound exposure each on day 0, day 1 and day 2. Per injection 50 µl was injected. Each MCs injection contains ~$1x10^8$ MCs. Within 5 min after injection for TG 3 and TG 4, therapeutic ultrasound was turned on and off intermittently (every 10 s) to allow microcapsule destruction and refill of the vascular bed, respectively. The dosage for each 10 s exposure was approximately 500 ultrasound pulses (1.2 MHz, 300 µs, MI=1.5) per mm^2 of the treatment area. An HDI5000 scanner with an imaging probe P7-4 guided the therapeutic ultrasound focus placement inside the tumor. The tumor sizes were measured daily in 2D using a caliper.

Results

No change in tumor echogenic appearance during ultrasound treatment was observed. Relative growths (average and standard deviation) in tumor sizes are partly given in Figure 1.

Discussion and Conclusions

Ultrasound activated paclitaxel delivery substantially retarded the tumor growth for 5 days. The therapy effect of ultrasound (TGs 3 and 4 vs. TGs 1 and 2) is statistically significant (p=0.03) within one day after treatment and then gradually decreases with time. The above results suggest that multiple treatments over a longer period are required for cancer remission. Furthermore TIPS is an effective tool for ultrasound dosage control and imaging guidance in this preclinical study.

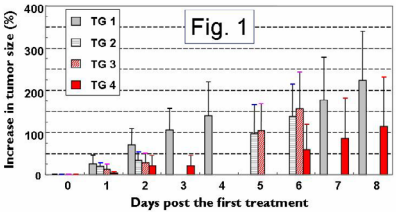

2D-3

9:00 AM **Microbubble dynamics in microvessels: Observations of microvessel dilation, invagination and rupture**

Hong Chen, Andrew A. Brayman, Michael R. Bailey, Thomas J. Matula; *Center for Industrial and Medical Ultrasound, Applied Physics Laboratory, University of Washington, Seattle, WA, USA.*

Background, Motivation and Objective

The fundamental interaction of an acoustically activated microbubble with small blood vessels is poorly understood. Understanding this interaction is important for designing better imaging schemes, and for targeting and drug delivery applications. High speed microscopy provides a tool to study interaction and response mechanisms.

Statement of Contribution/Methods

Following an approved U.W. IACUC protocol, ultrasound contrast agent microbubbles, Evan's blue and fluorescent dyes were perfused into the rat mesentery. These tissue samples were harvested for *ex vivo* observation. Evan's blue was used to facilitate identification of microvessels and also as an indicator of blood vessel permeability changes. Fluorescence images were taken to examine the integrity of blood vessels. Tissue samples were exposed to short pulses of 1 MHz ultrasound. 14 high-speed microphotographic images were acquired for each experiment with shutter speeds of 50 ns and each image separated by 150 ns.

Results

At low acoustic negative pressure (~1.5 MPa), bubble expansion caused microvessel dilation by approximately 1.2x. During bubble collapse, the vessel invaginated to approximately 0.9x of its original diameter (11 µm). At high negative pressure (near 11 MPa), the vessel dilated by approximately 2.5x, followed by invagination of 0.4x of its original diameter (17 µm). Vessel dilation and invagination were correlated temporally with bubble growth and collapse. At high pressure, the bubble and/or its fragments could be observed outside the original vessel, suggesting that the vessel had ruptured at some point. Vessel damage was also inferred by observation of fluorescent dye extravasation. An example of vessel dilation, invagination, and rupture can be seen in the following figure (pixel intensity values in the region around the blood vessel wall have been enhanced).

Tuesday Oral

Discussion and Conclusions

Our observations confirm some aspects of previous modeling and observational findings. However, direct observation of ultrasound-induced vessel invagination appears novel, and may be an important mechanism related to vessel damage. It remains uncertain if the vessel was damaged during dilation, invagination, or from a violent bubble collapse. It's possible that both dilation and invagination contribute to vascular rupture. Work supported by NIH (5R01EB000350 and P01DK43881).

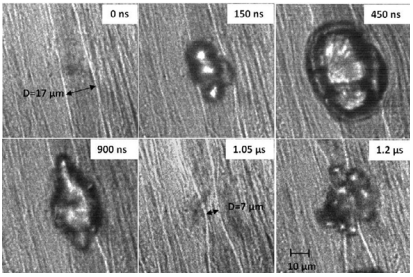

2D-4

9:15 AM **Parameter space for microbubble wall interaction estimated from gel phantom**

Charles Caskey[1], Shengping Qin[1], Paul Dayton[2], Katherine Ferrara[1]; [1]*University of California at Davis, Biomedical Engineering, USA,* [2]*University of North Carolina, Biomedical Engineering, USA.*

Background, Motivation and Objective

The mechanisms for permeability enhancement using contrast ultrasound are not fully understood, although many researchers have demonstrated successful use of contrast agents for drug and gene delivery. Here, we aim to elucidate mechanisms for vascular permeability enhancement by directly observing interaction between microbubble contrast agents and a tissue-like gel phantom during insonation.

Statement of Contribution/Methods

The phantom used in these experiments allows us to flow microbubbles through a small channel (230 µm) and observe microbubble-wall interaction during an acoustic pulse at center frequencies ranging from 500 kHz to 5 MHz. The phantom is made of agarose gel that has similar rigidity to soft tissue in vivo. The injected microbubble concentrations range from sub-clinical dosages to high dosages used in some drug delivery experiments. High-speed images of microbubbles interacting with the vessel wall were acquired during a 10 msec acoustic pulse using a 30 nsec strobe provided by a copper vapor laser. After 20 seconds of insonation using a repetition frequency of 10 Hz, 500-µm polymer beads were used to outline damage to the gel phantom.

Results

During high-amplitude acoustic pulses at 1, 2.25, and 5 MHz with a matched mechanical index (MI) of 1.5, microbubbles dig into the gel phantom vessel wall, creating tunnels with widths of 39.7+/-6.8, 21.8+/-2.3, and 7.4+/-1.5 µm, respectively. Figure 1 shows a microbubble that has moved beyond the phantom vessel boundary as it creates a tunnel in the direction of ultrasound propagation (indicated by arrow). During insonation with 2.25 MHz ultrasound, the area of the vessel wall disruption increases as bubble concentration increases from 1.6 x 10^5 to 2.5 x 10^7 bubbles/mL. Tunnels were observed only for a high microbubble concentration at 2.25 MHz and a peak rarefactional pressure above 0.6 MPa; whereas tunnels were observed at diagnostic and higher concentrations at 1MHz for a peak rarefactional pressure above 1 MPa. Similar effects were not possible using short pulse lengths commonly used in imaging studies.

Discussion and Conclusions

Drug delivery with contrast ultrasound has shown much promise while raising some concerns about the safety of methods employed. Observations of microbubbles and their effects on a gel phantom help identify the mechanisms and associated important parameters for optimizing drug delivery with contrast agents.

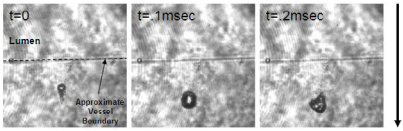

Tuesday Oral

2D-5

9:30 AM **Micro Bubble Adhesion to Target Wall by Frequency Sweep of Ultrasonic Pumping Wave**

Yoshiki Yamakoshi, Hideaki Kawamoto; *Gunma University, Faculty of Engineering, Kiryu-shi, Gunma, Japan.*

Background, Motivation and Objective

Delivery of materials through cell membrane is greatly enhanced by ultrasonic wave in the presence of micro bubbles. Shock wave, sonic jet by bubble destruction as well as micro-streaming play important roles to enhance the cell permeability. However, these mechanisms give influence when the target is in the vicinity of the bubble, bubble density near the target surface must be increased when the permeability enhancement by ultrasonic wave is carried out.

Statement of Contribution/Methods

Aiming at concentrating micro bubbles near the target wall, a novel method is proposed. This method uses an acoustic radiation force directed to the surrounding wall. Ultrasonic pumping wave of frequency f_1 is introduced to the micro bubble flowing liquid, the secondary ultrasonic wave from the oscillating bubbles produces the secondary Bjerknes force between the neighboring bubbles. This force makes bubble aggregation and the aggregated bubbles align at intervals of the wavelength of the secondary ultrasonic wave. Then, if the frequency of the ultrasonic wave decreases to f_2, interval between the aggregated bubbles becomes wider keeping bubble aggregation. This procedure moves the micro bubbles to the target wall. By repeating the frequency sweep from f_1 to f_2, the density of the micro bubbles in the vicinity of the wall increases effectively regardless of the target surface conditions.

Results

Numerical analyses are carried out by solving the equations of motion of n-bubbles system using time differential method. The number of bubbles inside the ROI, reflection coefficient of the wall and the frequency sweep of the ultrasonic pumping wave to the bubble density near the wall are evaluated.

Preliminary experiments are carried out using Levovist bubbles. Frequency of the ultrasonic pumping wave is swept from 4MHz to 3MHz. Polyvinylidene chloride film (thickness is 15 µm) is used as a target. It is observed that the number of trapped bubbles in the proposed method (fig.(b)) is larger than that of the fixed frequency case (fig.(a)).

Discussion and Conclusions

This method uses the secondary Bjerknes force produced between the neighboring bubbles in order to concentrate the micro bubbles to the target wall. Although the frequency sweep sequence has to be optimized, the proposed method might be an useful means in permeability enhancement by ultrasonic wave.

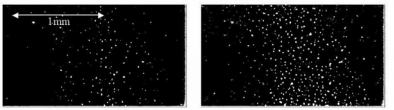

(a) Fixed US frequency f = 3.5 MHz

(b) Frequency sweep (Proposed method) f = 4MHz to 3MHz

2D-6

9:45 AM **Adherence of Platelet and Fibrin Targeted Ultrasound Contrast Bubbles to Human Blood Clots In Vitro**

Savitha Fernandes[1], **Flemming Forsberg[2],** Samuel Gilmore[3], Sergiy Shevchuk[3], Arthur Kerschen[3], Terry Matsunaga[4], Reena Zutshi[3]; *[1]Thomas Jefferson University and Drexel University, USA, [2]Thomas Jefferson University, Radiology, Philadelphia, PA, USA, [3]ImaRx Therapeutics Inc, USA, [4]ImaRx Therapeutics Inc and University of Arizona, USA.*

Background, Motivation and Objective

The purpose of this study was to assess platelet and fibrin targeted ultrasound contrast microbubbles' ability to adhere (with the assistance of radiation force) to fresh platelet and platelet poor clots in vitro under static and dynamic flow conditions.

Statement of Contribution/Methods

Whole blood from healthy volunteers (25 ml) was collected and centrifuged at 1100 rpm for 15 min to separate platelet-rich plasma (PRP), which was separated and centrifuged (3000 rpm, 5 min) to get platelet poor plasma (PPP). Calcium and Thrombin from human plasma were added to form fresh blood clots with upregulated receptors. Clots were placed either in Petri dishes (static experiments) or in a purpose-build flow chamber (dynamic experiments with shear rated varied from 100 to 700 s^{-1}). Platelet targeted (MRX-802-044; ImaRx Therapeutics, Inc., Tucson, AZ), fibrin targeted (MRX-802-0221; ImaRx Therapeutics) or untargeted, control bubbles were added to the clots. Radiation force was employed using a single-element transducer with continuous wave ultrasound (2.5-5 MHz, 100 kHz PRF, 30 s exposure, 8.9-50.2 kPa_{p-p} pressure), to gently push the bubbles onto the clots. Experiments were repeated at least 3 times. Following 3 washes, the number of bubbles attached relative to clot area was determined using a SMZ-10A microscope (200x magnification; Nikon, Melville, NY) and ImagePro Plus software (Media Cybernetics, Silver Spring, MD). Attachment rates between the groups were compared using unpaired t-tests.

Results

The average number of bubbles attached per 1000 μm^2 of clot area using MRX-802-044 was 7.0 ± 4.21 bubbles and 2.72 ± 2.44 bubbles, respectively, in PRP and PPP clots. With fibrin targeted bubbles the corresponding attachments were 11.45 ± 8.52 and 9.25 ± 3.40 bubbles, while typically less than 2 control bubbles adhered per 1000 μm^2 of clot area in either clot type. The differences in adherence rates were statistically significant for MRX-802-0221 compared to MRX-802-044 and to controls in both PRP and PPP clots ($p < 0.05$). Relative to controls more MRX-802-044 bubbles adhered in PRP clots ($p = 0.05$) but not in PPP clots (p = NS) presumably due to the lack of platelets. Dynamic experiments with the flow chamber are ongoing and results will be presented.

Discussion and Conclusions

In conclusion, the in vitro attachment rates of bubbles targeted to human blood clots depend on target availability (i.e., platelet targeted bubbles do better in PRP than in PPP clots). Fibrin targeted bubbles showed the best adherence rates in this study.

This work was supported by NIH HL71433.

3D. Medical Signal Processing I

Room 305 A/B/C

Tuesday, November 4, 2008, 8:30 am - 10:00 am

Chair: **Ton van der Steen;**
Erasmus Medical Center, The Netherlands.

3D-1

8:30 AM **Oriented Demodulation and Frequency Splitting for Directive Filtering Based Compounding**

Paul Liu[1], Dong Liu[2]; [1]*Saset (Chengdu) Inc., Chengdu, Sichuan, China,* [2]*Sichuan University, College of Computer Science, Chengdu, Sichuan, China.*

Background, Motivation and Objective

Compounding reduces speckle by incoherently averaging multiple statistically decorrelated images. Decorrelation occurs from differently angled beams in spatial compounding or from extracting different frequency beams in frequency compounding. Directive filtering based compounding introduced by Dantas and Costa extracts beams of different angles from one frame in 2D spatial frequency domain. To remove artifacts from beams oriented away from the axial axis, we propose varying oriented off-axis demodulation of each filtered RF output. Furthermore, we further split the spectrum at a given orientation to achieve more compounding at the expense of some spatial resolution.

Statement of Contribution/Methods

Spherical wave propagation and backscattering may be viewed as the sum of differently angled uni-directional beams which can be decomposed through directional filters. Therefore, the direction of modulation will be in the direction of the corresponding beams, and we demodulate each filtered output with a Hilbert transform along the corresponding orientation before envelope detection. Furthermore, the spectrum can be split in frequency in addition to orientation using Gabor filters of different frequencies.

Results

The proposed methods were tested with computer simulated data and in-vivo RF data of the neck obtained from the Saset iMago using a linear array 5 MHz probe and compared with previous methods, showing significant reduction of directional undulation artifacts. Spectrum splitting in both orientation and direction gives higher SNR than orientation-only at the expense of slight resolution loss.

Discussion and Conclusions

Undulation artifacts arise due to demodulation along the wrong axis, in this case the assumed axial axis, which we correct by demodulating filter outputs along the corresponding beam direction. Normalization of weak beam directions such as the lateral direction in the compounding process may enhance weak signals such as boundaries oriented axially. Frequency splitting along orientations is a design tradeoff between speckle reduction and resolution depending on tissue location or if images are to be used for clinical diagnosis or for preprocessing for other imaging algorithms.

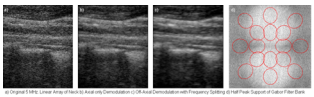

3D-2

8:45 AM **A new frequency compounding technique for super harmonic imaging**

Guillaume Matte[1], Paul van Neer[1], Jerome Borsboom[1], Martin Verweij[2], Nico de Jong[1]; *[1]Erasmus MC, Biomedical Engineering, Rotterdam, Netherlands, [2]T.U. Delft, Deflt, Netherlands.*

Background, Motivation and Objective

Second harmonic imaging is currently the de-facto standard in commercial echographic systems for diagnosis because of its improved resolution and contrast to tissue ratio. An emerging technique called super harmonic imaging is based on a combination of multiple frequency components generated during the propagation of sound in tissue. This combination of third to fifth harmonic has the potential to further enhance resolution and image quality of echographic pictures. In order to fulfil the bandwidth requirements of super harmonic imaging, a special interleaved phased array transducer has been developed [1]. Currently, the achievable bandwidth for phased array elements used in transmission is close to 80%, which involves that generated harmonics will be separated by gaps in the frequency domain. That will introduce specific artefacts visible as ripples in the echo image. We propose a two-pulse technique that reduces the ripple artefacts and recovers the axial resolution.

Statement of Contribution/Methods

This technique consists in firing two lines with a 15% frequency shift for the second firing. Summing the echoes of those two lines will result in filling the gaps in the frequency band of the distorted signal. The optimal choice for the frequency of the second pulse can be derived analytically. Standard detection methods applied to this two-pulse technique will strongly minimize artefacts encountered with envelope detection on super harmonic signals.

Results

Theoretical calculations show an improvement in axial resolution by a factor of 2.7 at the -15dB level compared to second harmonic imaging. For a fair comparison, the super harmonic signal will be compared with the lowest frequency component of its spectrum, which is the third harmonic. A shortening of the pulse is visible in the enclosed figure where axial point spread function simulations of third harmonic and super harmonic pulses are compared. Experimentally, this method shortens the pulse by a factor 2.3 at the -15dB level compared to second harmonic, and 1.9 compared to third harmonic.

Discussion and Conclusions

Super harmonic imaging quality can be further improved by frequency compounding techniques such as the two-pulse method described here.

[1] Bouakaz, A. and N. d. Jong (2003). "Native tissue imaging at superharmonic frequencies." IEEE Trans UFFC 50: 496-506.

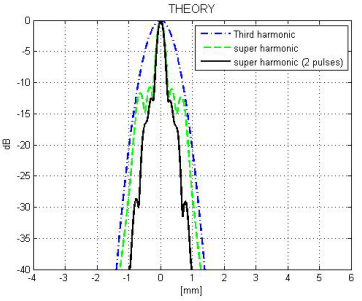

3D-3

9:00 AM **Segmentation of Speckle-Reduced 3D Medical Ultrasound Images**

Peder Pedersen[1], John David Quartararo[1], Thomas Szabo[2], *[1]Worcester Polytechnic Institute, Electrical & Computer Eng., Worcester, MA, USA, [2]Boston University, Biomedical Engineering, Boston, MA, USA.*

Background, Motivation and Objective

Automated, accurate 3D segmentation is critical to achieve the full potential of 3D imaging. Applications include volume assessment of free fluid volumes, cancer treatment efficacy, and quantifications in obstetrics. In this study,

we have targeted numerically modeled cysts, cyst phantoms with varying contrasts, and prostate tissue volumes obtained clinically. Segmentation was performed directly in 3D using the level set method.

Statement of Contribution/Methods

Two categories of preprocessing were evaluated: the Integrated BackScatter (IBS) calculation (applied to RF data) and four different 3D speckle reduction schemes (applied to image data): (i) 3x3x3 median filter, (ii) curvature anisotropic diffusion, (iii) mean-curvature based evolution, and (iv) curvature flow. The segmentation was performed using a 3D level set implementation of the active contour method to evolve a 3D surface. An inverse sigmoid transfer function was applied to the gradient magnitude of the image volumes to generate the feature (speed) image, where high gradients were mapped to low values (speeds). The level set function was manually initialized. Balloon, curvature, and advection forces were applied to the propagating surface and used with the speed image to minimize the energy function of the evolving surface.

Test images were acquired from (i) Fields-II generated 3D cyst images, (ii) 3D scans of tissue-mimicking cyst phantoms with various levels of contrast, and (iii) 3 sets of clinical 3D scans of prostates. To evaluate segmentation accuracy, the ground-truth must be established. For the Fields-II based image volumes, the ground-truth is known. For the cyst phantoms, the dimensions of the physical cysts were known and digitally aligned with the segmented cyst by minimizing the mean square of the Euclidian distance between surface points. The ground-truth for the prostate tumors in the three 3D image volumes was based on hand segmentation by two experienced oncologists.

Results

The mean RMS distances between the hand-segmented surfaces for the same prostate varied from 1.85 mm to 3.07 mm across the 3 image volumes. The level set segmentation yielded a smoother and more realistic looking segmented surface, and using the anisotropic diffusion filter gave a mean RMS distance between hand-segmentation and the level set segmentation of 2.04 mm to 3.19 mm, i.e., on par with the variation between the two MDs. A better segmentation was achieved without the IBS process than with the IBS process. The smallest RMS error was obtained for the Fields-II simulated cysts, in the order of 1.4 mm, while the RMS distance for the 3D tissue-mimicking cyst phantoms spread over a wider range from 1.2 mm to 5.9 mm.

Discussion and Conclusions

Anisotropic diffusion filtering has been found to be a useful speckle reduction tool before 3D segmentation using active contours and the level set method. The work has shown that 3D segmentation techniques hold great promise in furthering the clinical value of 3D imaging.

3D-4

9:15 AM **Ultrasonic Molecular Imaging of Primordial Angiogenic Vessels in the Papilloma Virus Transgenic Mouse with $\alpha_v\beta_3$-Integrin Targeted Nanoparticles Using Renyi Entopy-Based Signal Detection**

Kirk Wallace, Jon Marsh, Lewis Thomas, Robert Neumann, Jeffery Arbeit, Gregory Lanza, Samuel Wickline;
Washington University School of Medicine, Saint Louis, MO, USA.

Background, Motivation and Objective

To detect the binding of molecularly targeted nanoparticles to sparse $\alpha_v\beta_3$ epitopes in primordial angiogenesis, we developed novel, nonlinear entropy-based signal receivers based on information theory, which are sensitive to subtle changes in the shape of an RF signal as contrasted with conventional signal amplitude processing.

We sought to characterize the sensitivity of information-theory-based signal receivers versus conventional signal power analyses for delineation of early neovascularization in the ears of transgenic mice, which is driven by the papilloma virus.

Statement of Contribution/Methods

Eight K14-HPV16 transgenic mice were treated with 0.3 mg/kg i.v. either non-targeted control (n=4) or $\alpha_v\beta_3$-targeted (n=4) nanoparticles and imaged dynamically for one hour using a research ultrasound system (Vevo 660 30MHz probe) modified to acquire digitized RF waveforms. All RF data were processed off-line to reconstruct images using information theoretic and conventional receivers. Image segmentation was performed by thresholding measurements at the 93% level for both data sets. The mean value of pixels segmented was computed at each time post-injection.

Results

The transgenic strain had markedly thickened and stiffened pinnae as compared with normal animals. With conventional image processing techniques, no targeted contrast signal could be detected in angiogenic vessels in

the ears due to the abundance of specular reflections from the skin and cartilage. However, the subtle changes in signal features induced by binding of nanoparticles to neovasculature was clearly distinguished from surrounding echoes, and ultrasound enhancement increased over time. Control mice demonstrated no contrast enhancement, regardless of the image processing method applied.

Discussion and Conclusions

These data demonstrate the ability and complementarity of Renyi Entopy-based receivers in conjunction with targeted nanoparticles to elucidate the presence of $\alpha_v\beta_3$-integrins in primordial neovasculature. The Renyi receiver detected accumulation of targeted nanoparticles 15 min. post-injection: half the time required previously, thus, enhancing the clinical relevance of information-theoretic receivers for detection of angiogenesis.

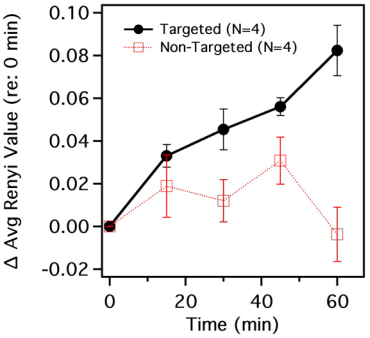

3D-5

9:30 AM **Multi-Frequency Processing for Lumen Enhancement with Wideband Intravascular Ultrasound**

Wenguang Li, Rory Carrill, Jian Yuan, Tat-Jin Teo, Lewis(Tom) Thomas; *Boston Scientific, USA.*

Background, Motivation and Objective

The need to further improve the intravascular ultrasound (IVUS) spatial resolution may drive the transducer center frequency even higher than the current 40 MHz range. Using a higher frequency may face the challenge of much stronger scattering echoes from blood, making image interpretation more difficult. Earlier studies have shown the blood backscatter level increases with ultrasound frequency at a much higher rate than that of tissues. Our method is based on the ratio of the received signal power between the high (60 MHz) and low (20 MHz) frequency ranges from a novel 40MHz wideband IVUS catheter. In this paper we will present our in vitro experiment work and in vivo test on an animal study.

Statement of Contribution/Methods

The in vitro setup consisted of a 4 mm diameter vessel model, a pump and a 40 MHz mechanical IVUS imaging system (iLab, Boston Scientific, Natick, MA, USA). The high-low signal power ratio was measured with two regions of interest, one in blood region and the other in simulated vessel wall. For in vivo testing, an LAD cross-section with thrombus was recorded real-time and the enhanced image sequence was evaluated by an IVUS expert.

Results

The results of high-low frequency ratio for the porcine blood at various flow velocities and for the tissue mimicking wall are summarized in Table 1. The power ratio values of blood regions are consistently higher than those measured from the wall, indicating the potential of applying this ratio to distinguish blood from tissue. Furthermore, our data show the blood power ratio increases as the shear rate decreases at lower flow velocities. The lumen enhancement obtained from the in vivo animal study shows a clear delineation of the thrombus.

Discussion and Conclusions

Most of the previously reported techniques were developed by taking the advantage of the fast and random moving blood speckles in contrast to the slow and consistent motion from the tissue. One common drawback is their inability to detect blood scattering signals effectively at low flow velocities. The multi-frequency approach does not rely on motion differences and is able to even provide a better contrast under the low flow condition. Using this

approach will provide a more robust lumen enhancement that can be combined with the wideband IVUS imaging catheter to obtain better image quality and facilitate image interpretation.

Table 1: Signal power ratio results for porcine blood (37.5°C) and a tissue-mimicking wall

Mean Flow Velocity (cm/s)	Porcine Blood (26% Hematocrit)			Tissue-Mimicking Wall		
	HF Signal Power	LF Signal Power	Power Ratio	HF Signal Power	LF Signal Power	Power Ratio
	(Arb. Units)			(Arb. Units)		
0	70.7	2.6	26.6	11.2	8.2	1.4
5	44.6	1.8	25.0	8.9	8.3	1.1
10	16.9	1.4	12.2	10.2	8.5	1.2
15	18.1	1.7	11.1	19.4	10.7	1.9
20	14.1	1.9	7.4	10.4	6.8	1.6
25	9.3	1.9	5.1	15.1	6.6	2.3
30	11.4	1.8	6.5	9.1	6.0	1.5

3D-6

9:45 AM **Green's Function Method for Modeling Nonlinear Three-dimensional Pulsed Acoustic Fields in Diagnostic Ultrasound Including Tissue-like Attenuation**

Jacob Huijssen[1], Martin D. Verweij[1], Nico De Jong[2]; [1]*Delft University of Technology, Laboratory of Electromagnetic Research, Delft, Netherlands,* [2]*Erasmus Medical Centre Rotterdam, Netherlands.*

Tuesday Oral

Background, Motivation and Objective

In the optimization and development of medical ultrasound transducers and imaging methods, a numerical model that predicts the occurring nonlinear acoustic pressure fields is an invaluable tool. A realistic model should be capable of handling a 3D, large-scale domain of interest, a pulsed excitation and a tissue-like medium exhibiting nonlinearity and a frequency power law-type of attenuation. In the recent years, we have developed the Iterative Nonlinear Contrast Source (INCS) method, a model that is well suited for computing large-scale, nonlinear ultrasound fields of phased array transducers in water. Until now, in this model the attenuation had been neglected. Our objective is to resolve this issue.

Statement of Contribution/Methods

In this contribution, we present an extended INCS method that includes medium attenuation and dispersion of an arbitrary behavior. The INCS method is based on a solution of the Westervelt equation, in which the nonlinear term is treated as a contrast source. The full nonlinear wavefield is then obtained by an iterative solution of the linearized wave problem using a Green's function method. To include medium attenuation, the Green's function of the lossy background medium is obtained by using a complex wavenumber. This requires an adaptation of the numerical evaluation method, which can be done at no extra cost in terms of memory and at a small cost in terms of computation time.

Results

Numerical results for the lossy INCS method are presented for a phased array transducer (64 elements, 19.2 mm aperture, 12 mm elevation width) exciting a focused beam with a source pressure level of 250 kPa and a three-cycle pulse with 1 MHz center frequency, and propagating in liver, which exhibits a frequency power law attenuation with a power $b = 1.14$. Comparison of the linear, lossy field with results from the FieldII program show excellent agreement with a difference of at most 0.1dB. The nonlinear, lossy field is compared with the nonlinear field in a situation where the attenuation is neglected, and in a situation where a square power law attenuation ($b = 2$) has been employed. For these two cases we observe deviations in the axial profile of the second harmonic frequency component up to +5 dB and –2 dB at $z = 60$mm, respectively.

Discussion and Conclusions

From the linear results we conclude that the improved INCS method correctly handles the attenuative medium behavior. From the nonlinear results we conclude that for a tissue-like medium the attenuation results in a significant reduction of the higher harmonics. Moreover, we conclude that a square power law and a frequency power law result in significantly differing nonlinear fields. In order to predict the nonlinear acoustic field of medical transducers as it occurs in a tissue-like medium, it is therefore essential to include a frequency power law attenuation in the model.

4D. cMUTs

Hall 2A

Tuesday, November 4, 2008, 8:30 am - 10:00 am

Chair: **Omer Oralkan;**
Stanford University, CA, USA.

4D-1

8:30 AM **Analysis of Charge Effects in High Frequency CMUTs**

Kjersti Midtbø, Arne Rønnekleiv; *Norwegian University of Science and Technology, Norway.*

Background, Motivation and Objective

At high frequencies it is desired to make the CMUTs relatively large compare to the acoustic wavelength at the centre frequency to avoid too small dimensions on the CMUTs. To make CMUTs that matches to a medium like water impedance wise, it is then desirable to have a stiff material like silicon nitride in the CMUT membrane. But the nitride is prone to charges leaking into the material, which changes the properties of the CMUTs, even without running the CMUT into collapse. As a part of our work with CMUTs at 30 MHz, using elements that are two CMUTs wide, we therefore want to investigate this effect theoretically.

Statement of Contribution/Methods

The measurements show that resonance frequencies of the CMUTs without fluid loading may change by several percent over hours even at constant biasing levels that are far below collapse. We use a CMUT model based on the model described in [1] with only one mode for simplicity. We include charge in the insulating layer due to slow current leakage into the membrane and look at changes in the properties of the CMUT as a transducer.

Results

Theoretically we find that the two factors that in Mason's equivalent circuit are equal, and give the transformer ratio squared, n^2, now become different. The charge penetrating into the membrane reduces the dc-voltage required for collapse, and increases the electromechanical coupling factor K^2 of the CMUT for a given dc-voltage.

To avoid collapse the dc-voltage may have to be reduced. If we reduce the dc-voltage to keep the coupling factor constant, we will see changes in the mechanical resonance frequency, and in the electrical and mechanical Q-factors of the loaded CMUT. If we assume that all the DC charge on the electrode penetrates to the bottom of the membrane, we see an increase in the electrical Q-factor of 8.3 % and a reduction in the mechanical Q-factor of 7.5 %. The mechanical frequency resonance goes down with about 14 %.

Discussion and Conclusions

Using the theoretical model, we have shown that the observed changes in frequency response at constant biasing over time can be explained by leakage of charges in the nitride membrane. Even if we adjust the voltage to keep the coupling coefficient constant, we still have changes in the transducer properties. These changes are however moderate and do not destroy the response of the CMUT.

[1] A. Rønnekleiv, IEEE Trans. on UFFC, vol 52, no. 12, Dec. 2005

4D-2

8:45 AM **Analysis of the Charging Problem in Capacitive Micro-machined Ultrasonic Transducers**

S. Machida, S. Migitaka, T. Kobayashi, H. Tanaka, K. Hashiba, H. Enomoto, Y. Tadaki; *Hitachi, Ltd., Tokyo, Japan.*

Background, Motivation and Objective

Capacitive micro-machined ultrasonic transducers (CMUTs) are one of the candidates for application of MEMS devices. In previous works, there have been various discussions in terms of CMUT characteristics or circuit integration. However, precise discussions on reliability of CMUT are scarce. The charging problem of dielectrics between upper and lower electrodes is of great importance in regards to commercializing reliable CMUT devices,

because charging causes sensitivity change of a CMUT during use. Accordingly, we investigated charging of dielectrics of a CMUT cell operated by DC and AC voltage.

Statement of Contribution/Methods

A CMUT was fabricated by standard two-layer metal processes of 0.25-µm CMOS technology. We applied silicon dioxide as a dielectric material in the gap region between the upper and lower electrodes in stead of the conventionally used silicon nitride. The fabricated device was operated by DC and AC voltage applied to the lower and upper electrodes, respectively. To evaluate the charging effect, the dependence of the capacitance of a CMUT cell on DC voltage was measured. This measurement shows that the charging of dielectrics causes the voltage at the minimum capacitance value (V_{cmin}) to shift. The shift voltage corresponds to the charge quantity accumulated in the dielectrics.

Results

As expected, compared with silicon nitride, silicon dioxide is hard to charge. The V_{cmin} shift, however, rises when the sum of the DC voltage (V_{dc}) and the amplitude of AC voltage (V_{ac}) exceeds the collapse voltage (V_c) of the CMUT cell. Depending on the applied voltage, V_{cmin} asymptotically approaches a certain voltage, and the shift of V_{cmin} finally saturates. Moreover, the shift of V_{cmin} when the CMUT cell is operated by DC and AC voltage is larger than that in the case of DC voltage only.

Discussion and Conclusions

The saturation of the V_{cmin} shift indicates that the shift of V_{cmin} can be estimated from the driving voltage of a CMUT device. It is thus necessary to optimally control the operation voltage in accordance with the estimated shift. This means that the charging is allowable but depends on the allowable sensitivity change of the system using CMUT devices.

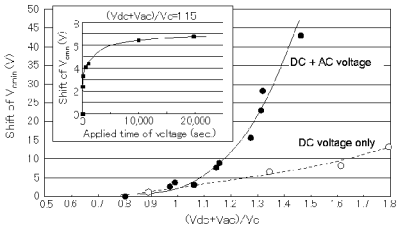

4D-3

9:00 AM **Investigation of charge diffusion in Capacitive Micromachined Ultrasonic Transducers (CMUTs) using optical interferometry**

Hanne Martinussen, Astrid Aksnes, Helge E. Engan; *Norwegian University of Science and Technology, Electronics and Telecommunications, Trondheim, Norway.*

Background, Motivation and Objective

Capacitive Micromachined Ultrasonic Transducers (CMUTs) have been developed and fabricated at our department. The main goal is to use an improved version of these structures to perform medical imaging to detect unstable plaque in the coronary arteries. Unstable plaques are fatty lipid pools contained in the wall of the coronary arteries by a thin fibrous cap. A rupture of this cap can lead to an infarction. The CMUTs have a radius of 5.7µm and a center frequency of about 30MHz in air. When an RF voltage is applied in addition to a DC bias the membrane will vibrate and generate ultrasound waves. This DC bias is in the order of 30V and leads to a charge diffusion in the CMUTs. This work investigates this process in detail.

Statement of Contribution/Methods

A heterodyne interferometer has been built in order to characterize the CMUTs. The setup can measure absolute phase and amplitudes. By using two acousto-optic modulators in the reference arm of the interferometer we can measure acoustic frequencies in the range 10kHz-1.2GHz. The results from the interferometer are supplemented with measurements from a network analyzer. The network analyzer takes the mean of all currents generated by CMUTs whereas the interferometer inspects individual CMUT elements.

Results

The vibrating membrane in the CMUT is made of silicon nitride, which ideally is an insulator. However, we observe a charge diffusion through this membrane influencing the response of the CMUTs. There are two possible mechanisms. One is that positive charges diffuse from the bottom electrode through the silicon substrate and into the silicon nitride membrane. The other is that negative charges from the top electrode diffuses into the silicon nitride membrane. An experiment investigating the resonance frequency as a function of time indicated that the latter mechanism is dominant. Measurements from both the interferometer and the network analyzer supported this conclusion.

Discussion and Conclusions

The measurements presented here are performed in air. Under loading conditions such as water or tissue the frequency bandwidth of the CMUT increases substantially. The charge diffusion problem may therefore not be a major problem when the CMUT is operated in water.

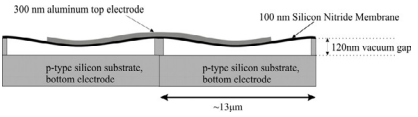

Tuesday Oral

4D-4

9:15 AM **Single chip CMUT arrays with integrated CMOS electronics: Fabrication Process Development and Experimental Results**

Jaime Zahorian, Rasim Guldiken, Gokce Gurun, Muhammad Shakeel Qureshi, Mujdat Balantekin, Paul Hasler, **F. Levent Degertekin;** *Georgia Institute of Technology, USA.*

Background, Motivation and Objective

One of the most important promises of capacitive micromachined ultrasonic transducers (CMUTs) is integration with electronics. This approach maximizes transducer sensitivity by minimizing parasitic capacitances and ultimately improves the signal to noise ratio. Additionally, due to physical size limitations required for catheter based imaging devices, optimization of area occurs when the CMUTs are fabricated directly above the associated electronics. Here, we describe successful fabrication and testing of CMUTs on custom designed CMOS electronics from a commercial IC foundry using low temperature micromachining processes.

Statement of Contribution/Methods

To fabricate CMUTs on CMOS, we modified a low temperature process developed earlier to implement functional interconnects between CMUT array elements and the RX/TX electronics on the same chip while introducing few additional steps. Prefabricated and diced CMOS wafer pieces are first coated with 2µm of insulating silicon oxide via plasma enhanced chemical vapor deposition (PECVD). Etch holes are then defined via a clear field mask and negative photoresist, 2.7µm NR7-1500P, for ease and verification of alignment. The substrate is then processed with a reactive ion etch optimized to yield sloped sidewalls. With this configuration, the same metal layer that forms the bottom electrode of the CMUT, 0.12µm aluminum, establishes reliable electrical contact through the insulation.

Results

Transimpedance amplifier based CMOS electronics were tested before and after CMUT fabrication to investigate post fabrication effects and interconnect quality. The results show that the gain and frequency response of the amplifiers is not altered. Pulse-echo experiments were successfully conducted on CMUTs operating in the 2-6MHz range using the amplifiers, multiplexer and buffers on the same chip (Figure 1). Suitable signal to noise ratio (28dB) is demonstrated with 20V DC bias and 10V pulse in oil bath.

Discussion and Conclusions

Previously high performance CMUTs were fabricated using low temperature, PECVD based processing. Here, CMUT arrays have been successfully fabricated on the same silicon chip containing the front end CMOS electronics using similar processes. This approach enables implementation of small CMUT arrays with optimal use of silicon area without compromising transducer performance.

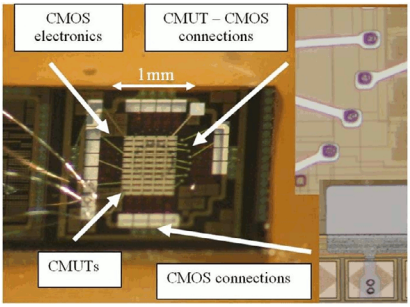

4D-5

9:30 AM **Front-end CMOS electronics for monolithic integration with CMUT arrays: Circuit design and initial experimental results**

Gokce Gurun[1], Muhammad Shakeel Qureshi[1], Mujdat Balantekin[1], Rasim Guldiken[1], Jaime Zahorian[1], Sheng-Yu Peng[1], Arindam Basu[1], Mustafa Karaman[2], Paul Hasler[1], Levent Degertekin[1]; [1]*Georgia Institute of Technology, USA,* [2]*Isik University, Turkey.*

Background, Motivation and Objective

To meet the demands of medical ultrasound imaging using high density arrays with CMUT technology, specialized integrated circuits should be custom designed. Since the parasitic interconnect capacitance is a significant factor degrading the SNR, monolithic integration emerges as a viable option. Hence CMOS-ASICs have been designed to interface with CMUT arrays made on the same silicon substrate by post-CMOS fabrication. Here we describe design strategies for CMUT interfacing for monolithic integration and experimentally demonstrate the advantages of this approach.

Statement of Contribution/Methods

On the same wafer, 27 separate set of IC cells are designed to interface different types of CMUT arrays for IVUS and ICE applications. Circuit topologies include resistive feedback transimpedance amplifiers and charge amplifiers on the receiver side, along with multiplexers and buffers. Gains and bandwidths of receiving amplifiers are optimized separately to fit different array specifications such as number of elements, element size and operation bandwidth. To drive transmit CMUT's a high voltage pulser array is designed in the same 0.35µm 3.3V standard, unmodified CMOS technology by combining existing technological layers in an unconventional way. CMUT arrays are then built on top of the custom made 8" wafer containing these circuits fabricated in a 0.35µm standard CMOS process.

Results

For initial testing, we performed pulse-echo measurements with a CMUT array on an IC consisting of transimpedance amplifiers, multiplexers and buffers to drive 50Ω and 12pF cables. The 32 element electronics cell has 2mm diameter area for intravascular imaging applications. The CMUT test array consists of 5 RX and 6 TX elements fabricated on top of this particular cell (Figure 1). The electronics shows no degradation after CMUT fabrication. With transimpedance gain of 500kΩ and 3MHz bandwidth, an echo signal of 28dB SNR is obtained without any averaging, applying 20V bias and 10Vpp pulse in a 5mm deep oil bath. Characterization of different IC designs in terms of noise, bandwidth and gain is ongoing.

Discussion and Conclusions

Custom ICs including special interconnect structures for post-CMOS CMUT fabrication and high voltage pulsers with unconventional layouts are implemented in 0.35µm standard CMOS process. Initial tests demonstrated successful operation of these monolithic CMUT-on-CMOS arrays.

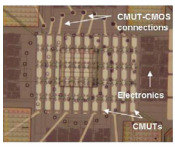

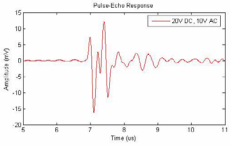

4D-6

9:45 AM **Fabrication and Characterization of Surface Micromachined CMUT with a Bossed Membrane**

Mengli Wang[1], Jingkuang Chen[1], Xiaoyang Cheng[2], Chuan Li[3], Xueyuan Liu[4]; *[1]University of New Mexico, Electrical Engineering, USA, [2]University of New Mexico, USA, [3]Nanyang Technological University, Singapore, [4]The Eastman Kodak Company, USA.*

Background, Motivation and Objective

Capacitive micromachined ultrasonic transducers (CMUT) promise high fractional bandwidth (FBW) at the expense of low gain compared to their PZT counterpart. When the CMUT is immersed in fluid, the dynamic performances including the FBW and the gain are limited by the membrane's higher order vibration modes. Without any additional mask or processing step than that used for planar-membrane CMUT, a CMUT with a boss on the polysilicon membrane has been prototyped and characterized. This bossed CMUT makes use of the second vibration mode for better dynamic response and delivers a broader FBW and a larger gain than its planar-membrane counterpart.

Statement of Contribution/Methods

In order to evaluate the size of the boss on the device characteristics of a CMUT, a finite element analysis (FEA) was carried out using ANSYS. A 2-layer polysilicon surface micromachining process was used to fabricate the bossed CMUT. The boss was formed using a layer of 3 um thick deposited tetraethoxysilane (TEOS) oxide on top of the polysilicon membrane. The same oxide layer was also used to seal the release holes along the peripheral of the polysilicon membrane and therefore no additional mask or processing step was needed. CMUT devices with and without boss while having the same membrane dimension (diameter, thickness, and anchoring configuration) were characterized in water for comparison.

Results

In transmission experiments conducted in water, the FBW of a 46um diameter CMUT was improved from 53% to 103% with the addition of a 15um diameter oxide boss on the center of the membrane which agree with FEM analysis as shown in the figure. The output pressure for the bossed CMUT also increases when driven by the same a.c voltage without d.c bias. From the capacitance-voltage measurement, an increase of electromechanical coupling efficiency of approximately 3%-6% was observed in the bossed CMUT. The boss also changes the recess of radiation pattern from 20º for the planar membrane CMUT to 39º for the bossed CMUT.

Discussion and Conclusions

It was found that a bossed CMUT delivered a larger gain, a broader acoustic bandwidth, and a higher electromechanical coupling efficiency, as well as changed the radiation pattern from its planar-membrane counterpart. This surface-micromachined bossed CMUT does not require any addition fabrication step or mask than its planar-membrane counterpart. The total mask count is seven.

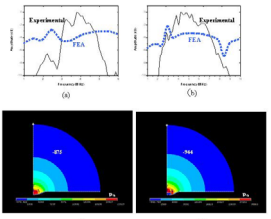

Figure. Experimental results and FEA for the spectrum of ultrasounds transmitted by a 46μm-diameter (a) without boss in water, (b) with an 15μm-diameter boss in water. (c) and (d) are the corresponding pressure contours under the vibration of membrane at frequency 2.5 and 4.0MHz by a uniform force 0.5μN. The dash lines in (a) and (b) are the results from FEA at the location of 11.5×10⁴nm (50×23μm), 50° above the center of membrane (marked by + on the pressure contours in (c) and (d).

5D. Industrial Measurement

Hall 2B

Tuesday, November 4, 2008, 8:30 am - 10:00 am

Chair: **Jir0maru Tsujino;**
Kanagawa University, Yokohama, Japan.

5D-1

8:30 AM **Ultrasonic Velocity Measurement for Analysis of Brick Structure**

Tadashi Kojima[1], Hiroshi Haya[2], Kuniyuki Minegishi[2], Ri Nguyen[3]; *[1]U T Lab., Akishima-shi, Tokyo, Japan, [2]Railway Technical Research Institute, Kiso Dokouzou, Kokubunji-shi, Tokyo, Japan, [3]JRSE Co.,Ltd., Kokubunji-shi, Tokyo, Japan.*

Background, Motivation and Objective

There are brick bridges and tunnels for the railroad constructed more than 100 years ago have been still used. The NDE method for them as maintenance is Impact Test by hand. In order to evaluate the material properties of such brick structures, the ultrasonic velocity measurements were performed and the material properties (Compressive, Tensile strength and Elastic modulus) of the brick structure were analyzed.

Statement of Contribution/Methods

The performed approach to measure the ultrasonic velocity of brick was the crosscorrelation technique between transmitting and receiving pulses of Gaussian, which brought a good result in weak S/N condition. The measurements for real brick structures were performed widely in Kinki, Tokai and Tohoku region along Japanese island and a lot of core samples were obtained at the same time, for which the mechanical tests were performed and the relationships between ultrasonic velocity and material properties of brick were analyzed.

Results

One of the relationships between ultrasonic velocity and material properties (ultrasonic velocity versus compressive strength) is shown in the following figure.

Discussion and Conclusions

The figure is showing a relevant relashonship between ultrasonic velocity and a material property of brick, which means that the ultrasonic velocity measurement could be possible to assume the characteristics of brick structure.

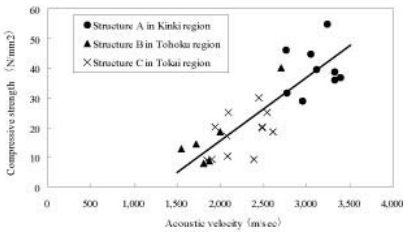

5D-2

8:45 AM **PiQC - A Process integrated Quality Control for Nondestructive Evaluation of Ultrasonic Wire Bonds**

Sebastian Hagenkötter, Michael Brökelmann, Hans J. Hesse; *Hesse & Knipps GmbH, Paderborn, Germany.*

Background, Motivation and Objective

Ultrasonic wire bonding is one of the most frequently used technique in semiconductor production to establish electrical interconnections. Since wire bonded microdevices are used in safety critical systems, a single wire bond

failure might cause a fatal system breakdown. Besides steadily increasing integration level and production speed there are extreme demands concerning the quality control of each single wire bond.

The described process integrated quality control method, called PiQC, copes with this challenging task of a 100% wire bond inspection. Sensor signals are gained and processed during each welding process to calculate quality related values right after a bond's formation.

Statement of Contribution/Methods

For a good bonding process the wire deformation WD and the transducer current I as monitored by state of the art wire bonders have to show well defined time characteristics. But normal wire deformation and current characteristics do not guarantee good bond quality in any cases either.

In the PiQC system besides WD and I also the ultrasonic frequency progression and further signals gained from a newly developed sensor are monitored. The sensor is placed on the transducer mounting, not disturbing nor decelerating bonding but providing a signal very sensitive to the mechanical vibrations at the tip of the bonding tool. All these signals are gained and processed during welding.

For each signal and derived component a quality index is calculated by comparison of the actual signal characteristics with reference characteristics preliminarily learned by the system in an automated procedure. Finally an overall quality index is calculated as a combination of the individual ones.

Because the different types of bond failures affect the available signals in different degree the individual quality indices form a basis for bond failure classification whereas the overall quality index is compared to a threshold for a fast good or failed bond decision.

Results

PiQC has been evaluated in a heavy wire application bonding 300 µm Al wire onto an Al substrate. Reference characteristics were learned from 100 wire loops. Besides normal substrate condition four bond failure types were inserted into the test bonds: bonding on plastic particles from an insufficient housing process, bonding on human sweat contaminated surface, bonding with an inproperly mounted bond tool, bonding one wire onto another.

The overall quality index could be successfully applied to a threshold for an online fast bad bond detection.

The individual quality indices were processed offline with a clustering algorithm. All five bond quality classes were resembled identically in the obtained clusters.

Discussion and Conclusions

The PiQC method has been successfully applied to detect common bond failures without decelerating production. The individual quality indices span a vector space suitable for bond failure classification. Further research will be directed to an online classification.

5D-3

9:00 AM **Evaluating technology of spot weld quality for coated high strength steel sheet based on ultrasonic guide wave**

Zhenhua Chen[1], Yaowu Shi[1], Haiyan Zhao[2]; *[1]Institute of Advanced Materials Processing Technology, School of Materials Science and Engineering, China, [2]Department of Mechanical Engineering, Tsinghua University, China.*

Background, Motivation and Objective

Resistance spot welding is the major production technology and widely adopted in automobile body manufacture. The zinc-coated high strength steel sheet is widely used with increasing demands for higher fuel efficiency and safety requirement in automobiles. However, tiny fluctuation of welding parameters will lead to quality deficient such as stick weld, deficient diameter and spatter in spot welds because of the poor weldability of the high strength steel and the adverse effect of the coated zinc. So the high efficient quality test technology has important meaning for enhancing production efficiency and ensuring safety performance. Ultrasonic testing (UT) is recognized as a promising technology in estimating the quality of the spot welds. Usually, diameter of the weld spot may be estimated through examining the ultrasonic sequence echo, which occurs at the interface between two sheets. The diameter of the transducer should be the same as that of the regular weld spot and the tester must possess special knowledge on the ultrasonic test. Thus, it is difficult to increase the testing efficiency, decrease testing cost and ensure the testing accuracy. When the guided wave propagation characteristic is used, the new technology is more quick, sensitive and economical to exam the sheet structure. In the research, the guided wave is adopted to test the spot weld, and the relationship between the guided wave characteristic amplitude and the spot weld quality can be established.

Statement of Contribution/Methods

The guided wave is difficult to be analyzed because of the complex frequency dispersion phenomenon in the sheet. In the present paper, the wave mode transformation is simplified and the dispersion phenomenon is obviously

decreased by using an ultrasonic oblique incidence method. Moreover, the sound filed, attenuation, sound velocity and the sound components are analyzed in theory and experiment. Thereafter, the guided wave is adopted in the evaluation on spot weld quality of zinc-coated high strength steel.

Results

The interactions between the guided wave and nugget characters such as diameter, indentation, columnar crystals are analyzed and the relationship between the maximum tension load and ultrasonic characteristic amplitude is obtained. According to the relationship, the maximum tension load can be evaluated by the guided wave.

Discussion and Conclusions

The technology proposed in the present work avoids to distinguish the complex wave sequence of the spot weld and has higher sensitivity, especially for stick weld compared with the traditional ultrasonic testing. Besides, the testing cost and requirement of the testing system can be decreased by use of the low frequency transducer. Meanwhile, the inaccessible area can be tested according to the arrangement of the transducers. Thus, the method proposed in this research is an effective nondestructive evaluation method for spot welds of coated high strength steel sheet.

5D-4

9:15 AM **Modeling and Measurement of Piezoelectric Ultrasonic Transducers for Transmitting Guided Waves in Rails**

Philip Loveday; *CSIR, South Africa.*

Background, Motivation and Objective

Guided wave ultrasound is becoming an important method of inspecting structures such as pipelines, aircraft skins and rails. A long range guided wave ultrasound system was developed to detect breaks in welded railway tracks. The system used permanently installed transducers to transmit waves along the rail between transmit and receive stations spaced between 1 and 2 km apart along the length of the rail. The piezoelectric transducers were developed by experimental trial and error and operate satisfactorily, although more effective transmission would enable greater spacing between stations and reduce the system cost. Improvement of the existing transducer, or design of new transducers for other applications, would require a better understanding of the wave propagation in the rail and how these waves are effectively and selectively excited using piezoelectric transducers or transducer arrays. This paper will describe modeling and measurement techniques developed for this purpose.

Statement of Contribution/Methods

The modeling method uses specially formulated semi-analytical finite elements to model the waveguide. These elements include the wave propagation in their formulation and allow a two-dimensional mesh of the waveguide cross-section to be used to compute the propagating and evanescent waves supported by the waveguide, as well as the response of the waveguide to harmonic point forces. This 2-D model is combined with a conventional 3-D finite element model of the piezoelectric transducer. The frequency response of the waveguide is computed, as a superposition of the frequency response of each mode of wave of propagation, and is therefore useful for designing transducers. An IFFT is used to obtain the time-domain response which can be directly compared to measurements. In order to measure the propagation of individual modes we need to extract the modes from measured time-domain responses. A mode extraction algorithm, which uses the modeled dispersion characteristics but no information about the transducer, was developed. The frequency response at a set of measurement locations is described by a superposition (with unknown amplitude coefficients) of the frequency response of the modes that propagate in the frequency range. Experimental time-domain responses are measured and transformed to frequency responses. The amplitude of each mode is estimated using the pseudo-inverse to provide a minimum norm least-squares estimate.

Results

The modeling and measurement techniques were applied to a piezoelectric patch exciting a rail.

Discussion and Conclusions

The computed time-domain response of the rail showed excellent agreement with measurements performed with a laser vibrometer. The mode measurement technique extracted the frequency response of eight modes of propagation from 15 measurement points. The extracted modal responses were used to predict the response at additional measurement points thereby verifying the extraction algorithm.

5D-5

9:30 AM Ultrasonic imaging of solid railway wheels

Montserrat Parrilla, **Patricia Nevado,** Alberto Ibáñez, Jorge Camacho, José Brizuela, Carlos Fritsch; *Instituto de Automática Industrial (CSIC), La Poveda (Arganda), Madrid, Spain.*

Background, Motivation and Objective

Railway wheels undergo severe stresses as the train speed become higher. Small internal cracks may propagate, thus compromising the wheel integrity. The more critical parts of the wheel are the rim, the web and the drills for disc brake fixation. To avoid a catastrophic in-service failure, high-speed and inter-city train wheels are periodically inspected. The inspection must be fast to keep low the train downtime, while accurate crack detection and sizing is essential since passenger safety is involved. This paper addresses such objectives from an integral point of view. The wheels are inspected, without dismantling them, in a single revolution.

Statement of Contribution/Methods

A water-coupled 32-element array of 3.5 MHz was used for the inspection of the web. Every image is composed of a set of individual A-scans obtained at regular steering angles. Each scan-line has its own focus depth. The foci are set at the locus of the more critical part, the brake fixation drill holes. Focal law computing requires knowledge of the water-steel interface geometry, which is measured from indications of the interface and the axle echoes.

Cracks may appear with any direction and may be hidden by wheel features. To get over this problem, a set of 360 images taken at intervals of 1º of a wheel rotation are compounded.

Several cracks were practiced in the brake fixation drill holes, with lengths ranging from 1.5 to 3 mm and diverse orientations. The system detected and sized all the flaws. Also, several holes with depth of 1 to 6 mm. were drilled in both sides of the web as artificial defects. Only the 1 mm. holes were missed with the array disposed for inspecting the wheel in only one turn. All defects are detected in two revolutions inspection with slightly different positions of the array.

Results

An encoder driven approach was followed to get every sectorial image at regular intervals, which greatly simplifies the image compounding process. After this, all the wheel features (web holes, brake disk fixation, etc.) were properly imaged. A wheel inspection takes less than 30 seconds. Cracks of 1.5 mm at the drill holes in radial or tangential directions were correctly detected and sized.

Discussion and Conclusions

Several imaging techniques were combined to get an accurate representation and quantification of cracks on solid railway wheels. The process involves computing the focal laws thorough a water-steel interface for a locus of foci which varies with the beam steering angle. A single image does not guarantee the detection and sizing of flaws, so an image compounding process was performed. This yields a single, fully focused image of the wheel, making visible the presence of cracks with any orientation. Cracks between 1 and 3 mm in length are detected and sized by the system.

5D-6

9:45 AM Smart Screws as Load and Temperature Probes

Kuo-Ting Wu[1], Makiko Kobayashi[2], Cheng-Kuei Jen[2]; *[1]McGill University, Electrical and Computer Engineering, Canada, [2]National Research Council Canada, Industrial Materials Institute, Canada.*

Background, Motivation and Objective

Aerospace structural parts which are held together by screws under tensile stress must be designed and assembled so that these screws are sufficiently loaded to prevent the parts from separating while the structure is in service. A reliable measurement of the axial load or preload in such screws is essential to secure structural safety and a precise control of the fastening force is required. A promising ultrasonic method for load sensing is to use the time-of-flight (TOF) measurement of both longitudinal (L) and shear (S) wave simultaneously travelling along the screw axial direction. All previous works used ultrasonic transducers (UTs) which were bulky and needed ultrasonic couplants and may not be operated at common airframe operation temperatures ranging from -80°C to 100°C. One objective of this research is to develop smart screws equipped with miniature integrated ultrasonic transducers (IUTs) as load sensor which can be used even in-flight. Another objective is to use the screw tip as a high temperature probe.

Statement of Contribution/Methods

Miniature IUTs which are made of piezoelectric ceramic films are directly coated onto the edge, which is in parallel to the axial direction of the screw, of one end of screw tips. They are used to excite and detect both L and S waves simultaneously along the screw axial directions with proper mode conversion angle for S waves and a reflection angle of 45° for L waves without couplant. The mode conversion angle is obtained by the analytic theory. Software based on a finite difference method is used to simulate the mode conversion and both L and S wave propagation along the screw. By creating discontinuities at the screw end opposite to that of the IUT the screw can be also used as a non-invasive high temperature sensor.

Results

Screws made of aluminum (Al) and steel with diameters ranging from 6 mm to 10 mm are used for the experiments. Both L and S waves propagating simultaneously along the screw axis have been obtained. Numerical simulated results agree well with experimental data. The mode conversion process from L to S waves happened in screw tip are demonstrated by numerical simulations. A novel mode conversion design using two edges of the screw to launch two S waves with orthogonal polarizations is given. Discontinuities made by steps of two or three different diameters at the screw end are used for the temperature sensing. Temperatures measured by ultrasound agree also well with those obtained by thermocouple.

Discussion and Conclusions

Miniature IUTs coated onto the one or two edges of one end of screws make the screw smart to monitor the axial load condition. The load monitoring is based on the TOF measurements of both L and S waves. Novel design to generate two S waves having orthogonal polarizations and the usefulness of such acoustic birefringence will be presented. Discontinuities created at the screw tip made such screw act as noninvasive temperature sensor.

6D. Bulk Wave Resonators - I

Hall 2C

Tuesday, November 4, 2008, 8:30 am - 10:00 am

Chair: **John D. Larson III;**
Avago Technology, USA.

6D-1

8:30 AM **Theory, and Experimental Verifications of the Resonator Q and Equivalent Electrical Parameters due to Viscoelastic, Conductivity and Mounting Supports Losses**

Yook-Kong Yong[1], Mihir Patel[1], Masako Tanaka[2]; *[1]Rutgers University, Civil and Environmental Engineering, Piscataway, New Jersey, USA, [2]Epson Toyocom, Japan.*

Background, Motivation and Objective

Current finite element software does not allow for the calculation of a resonator Q without apriori assumptions of the resonator impedance or damping. A novel analytical/numerical method for calculating the resonator Q, and its equivalent electrical parameters due to viscoelastic, conductivity and mounting supports losses is presented. Hence the method presented will be quite useful for designing new resonators, and reducing their time and costs of prototyping. There is also a necessity for better and more realistic modeling of the resonators due to miniaturizations, and the rapid advances in frequency ranges in telecommunication.

Statement of Contribution/Methods

We present new three-dimensional finite elements models of quartz resonators and aluminum nitrite SMR's with viscoelasticity, conductivity, and mounting support losses. For quartz the materials losses attributed to electrical conductivity and acoustic viscosity were obtained from Lee, Liu and Ballato[1], and Lamb and Richter[2], respectively. The losses at the mounting supports were modeled by perfectly matched layers (PML's). The theory for dissipative anisotropic piezoelectric solids given by Lee, Liu and Ballato [1] was formulated in a weak form for finite element applications. PML's were placed at the base of the mounting supports to simulate the energy losses to a semi-infinite base substrate. FE simulations were carried out for free vibrations and forced vibrations of AT-cut quartz resonators, and solidly mounted resonators (SMR's). The FEM models for the SMR's employ periodic boundary conditions[3].

Results

Results for quartz thickness shear AT-cut quartz resonators and SMR's are presented and compared with experimental data. Results for the resonator Q and the equivalent electrical parameters were compared with their measured values. Good comparisons were found. Results for low and high Q AT-cut quartz resonators compared well with their experimental values. FEM models with periodic boundary conditions were employed to calculate the Q of SMR's operating in the range of 1.70 to 1.90 GHz. The Bragg layers of the SMR's consist of three alternating layers of W and SiO2. The resonating element consisted of AlN piezoelectric film with Mo electrodes. Their Q and K_{eff} values showed very good agreement with the measured data. The effect of thermal compensating oxide and Mo electrode resistance on the Q values was studied and compared with the measurement data.

Discussion and Conclusions

Comparisons of the Q and other electrical parameters obtained from the free vibration analysis with their corresponding values from the forced vibration analysis were found to be in excellent agreement. The results were validated by good comparisons with their experimental values. The resulting FE model gives the Q value without prior assumptions of damping factors and impedance. A new method for estimating the Q directly from the frequency spectrum obtained for free vibrations was also presented.

6D-2

9:00 AM **Method for Computing Q vs. Frequency for Piezoelectric Resonators**

David Feld[1], Reed Parker[2], Richard Ruby[2]; [1]*AVAGO Technologies, WSD, San Jose, CA, USA,* [2]*AVAGO Technologies, USA.*

Background, Motivation and Objective

We propose an expression for the unloaded Q of a piezoelectric resonator in terms of its measured S11-parameters. This expression allows us to report the Q not only at the resonant and anti-resonant frequencies, but at a continuum of frequencies. Our work provides a metric by which resonator performance can be compared within a given technology and amongst resonators fabricated in diverse technologies such as FBAR, SAW, & BAW.

Statement of Contribution/Methods

We derive an expression for the Q(freq) of a resonator in terms of its measured S-parameters (S11) in two ways:

(2.1) We fit the S-parameter data to a modified Butterworth Van Dyke (mBVD) model (which fits most resonators). Using a circuit simulator we drive the model from a 1 Watt, 50 ohm power source. At each frequency, we compute Q as being the ratio of the sum of the stored energy in the model's motional capacitor, motional inductor, and plate capacitor to that of the sum of the dissipated power per radian in each of the model's three resistors.

(2.2) We apply the following equation to the measured S-parameter data:

Q(freq)=2*PI*freq*group_delay(S11p)*mag(S11p)/(1-(mag(S11p))^2);where S11p are the resonator S parameters translated by an appropriate source impedance such that at all frequencies S11p is equidistant from the center of the Smith chart. This equation allows us to extract Q vs. frequency directly from the S parameter measurement, e.g. from a network analyzer. The equation gives near identical agreement vs. computation method (above) for resonators with Q's greater than 30.

The Q expression is validated as follows: First we show analytically that the stored energy divided by the dissipated for any series or parallel LRC circuit reduces to the expression. For the more complicated mBVD circuit topology containing both a series and a parallel LRC circuit, we follow the teachings of Bode, and show that for a class of simple circuit topologies including mBVD that the above equation is a good approximation for Q.

Results

To demonstrate our approach, we apply our Q expression to the measured and mBVD modeled S-parameters of an FBAR resonator (fig. 1). The lt. & rt. markers represent the Q at the resonant and anti-resonant frequencies (Fs and Fp).

Discussion and Conclusions

We suggest that the community use our expression as a metric by which Q can be computed and compared to other resonators at all frequencies. Such a standard for Q is long overdue.

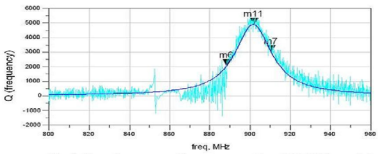

Fig.1 Q vs frequency for measured and MBVD modeled FBAR resonator for a 50 ohm resonator. Left and right markers are at fs and fp respectively.

6D-3

9:15 AM **Constancy on Quality Factor of Dual-T Quartz Crystal Resonator Circuit**

Takehiko Adachi[1], Daisuke Akamatsu[1], Koichi Hirama[2], Yasuhiko Nakagawa[3], Takeshi Yanagisawa[4]; [1]*Yokohama National University, Faculty of Engineering, Yokohama, Kanagawa-ken, Japan,* [2]*Yamanashi University, Faculty of Engineering, Yamanashi-ken, Japan,* [3]*Yamanashi University, Faculty of Engineering, Kofu, Yamanashi-ken, Japan,* [4]*Tokyo Institute of Technology, Kawasaki, Kanagawa-ken, Japan.*

Background, Motivation and Objective

A quartz crystal resonator is widely used in a high precision voltage controlled crystal oscillator (VCXO). Recently, demand for wide tunability of a VCXO has been increasing. Usually the oscillation frequency of VCXO is controlled by varying the capacitance connected in series with the crystal resonator. But this method has the following drawbacks: (1) frequency variation range is limited by the capacitance ration of a crystal resonator

Tuesday Oral

within a few hundred ppm, (2) temperature characteristics of a crystal resonator changes with the variation of the load capacitance, (3) quality factor of a crystal resonator is decreased drastically with the variation of the load capacitance. To overcome these limitations, we proposed a dual-T quartz crystal resonator circuit in 2008 Frequency Control Symposium. And we showed that the frequency tunability of about 1000 ppm can be obtained without deterioration of quality factor.

Statement of Contribution/Methods

In this paper, we have shown detailed characteristics of a dual-T quartz crystal resonator circuit placing emphasis on constancy of its quality factor by theoretical and experimental approaches. The dual-T circuit is composed of two T circuits. Each T circuit is composed of an inductor and a capacitor in a series arm and a crystal resonator in a shunt arm. The inputs of two T circuits are connected to an input terminal via different attenuators. The output terminals of two T circuits are connected to a load resistor. The resonance frequency of a series arm of an inductor and a capacitor is adjusted to almost the same value of the resonance frequency of a crystal resonator. The dual-T circuit shows a single resonant frequency dip characteristics. The resonance frequency of the dual-T circuit can been changed between the resonance frequencies of two crystal resonators by varying the attenuation of two attenuators. We have derived the theoretical equation describing the dependence of the resonance frequency on the attenuations and the circuit parameters. We obtained the range of attenuation ratio showing the linear dependence between resonance frequency and attenuation ratio. We also derived the relation between the quality factor of the dual-T circuit and the quality factors of the component crystal resonators. The quality factor of the dual-T circuit is varied between the quality factors of two crystal resonators.

Results

We have made the measurement and have shown that the frequency change about 2000 ppm can be obtained with constant quality factor comparable to its component crystal resonator. We made an oscillator using this dual-T circuit and also showed about 2000 ppm frequency tunability with constant spectrum profile suggesting constant quality factor.

Discussion and Conclusions

These results showed the effectiveness of our theoretical analysis and practical usefulness of the proposed dual-T quartz crystal resonator circuit.

6D-4

9:30 AM **Unique Properties of HBAR Characteristics**

Georgy Mansfeld, Sergey Alekseev, Natalia Polzikova; *Institute Of Radioengeneering and Electronics RAS, Moscow, Russian Federation.*

Background, Motivation and Objective

The shape of frequency dependences of modulus of electrical impedance of high overtone bulk acoustic wave resonators (HBAR) together with the corresponding numerical data is very informative. These data contain the important information about sound velocities and attenuation coefficients in layers, quality factor of the whole resonator structure Q etc.

Statement of Contribution/Methods

It was shown that at high numbers of harmonics the difference between frequencies of “antiresonance” and “resonance” peaks strongly depends both on electromechanical coupling coefficients and the acoustic wave losses in the structure. The report contains the detailed discussion of the problem based on the derivation and analysis of the rigorous equivalent circuit of the resonators. It supports by numerically simulated and experimentally obtained results. Rigorous expression for square of an effective electromechanical coupling coefficient appropriate for high numbers of harmonics was introduced and discussed.

Results

It was found that in case small values of product is governed mainly by losses so that the absorption coefficient can be found from simple formula . Expressions for calculation of electromechanical coupling coefficient were derived for the case of reasonably high product. To find measured value of together with measured difference between peculiarities on frequency dependence of phase the reflection coefficient of the electromagnetic signal from resonator at the same resonance number are used.

Discussion and Conclusions

The discussion of the experimental setup providing getting of necessary data in a wide frequency band and broad temperature region is presented. The possibility of the use of à simple method of measurement of acoustic losses in thin layers and films composing HBAR is proved.

This work was supported by grants RFBR 07-02-01006-a and 07-02-13581.

6D-5

9:45 AM **Three operation modes of an acoustic wave device with the lateral field excitation structure**

Wenyan Wang, Chao Zhang, Zhitian Zhang, Yan Liu, Guanping Feng, Gang Jing; *Tsinghua University, Department of Precision Instruments and Mechanology, Beijing, China.*

Background, Motivation and Objective

Lateral field excitation (LFE) devices have been developed for applying in frequency control elements for a long time and have recently been found very attractive in liquid sensing applications. The reason for this is that LFE devices offer a number of advantages over thickness field excitation (TFE) devices. Previous works have mostly focused on the LFE itself operation principles and its specific applications. Few researchers have realized that the acoustic wave devices with the LFE structure are of different operation modes. In the present study, three operation modes of LFE devices were presented and investigated.

Statement of Contribution/Methods

Through theoretical calculations using the extended Christoffel-Bechmann method and experiments, three operation modes of the LFE devices, which were referred to as the pure LFE, quasi-LFE and pseudo-LFE modes, were obtained. When the device surface without any electrodes is in contact with a liquid, the liquid acts as an analogy electrode and a serial configuration of two TFE is formed, and the TSMs (Thickness shear modes) can be generated by TFE in addition to LFE, as is named a quasi-LFE mode. If the theoretical resonant impendence caused by the LFE is so high that the resonance can hardly occur in practice, only the TSMs can be generated by the TFE which is caused by the analogy electrode, as is considered a pseudo-LFE mode. When in vacuum or air, the devices have a resonance caused only by the LFE itself and then are considered to work in a pure LFE mode.

Results

Several 5 MHz LFE devices with similar geometry using the AT-cut quartz, (yxl)-16.5° $LiTaO_3$ and (yxl)-58° $LiNbO_3$ crystals were fabricated for verifying the three operation modes. All of the LFE devices were designed to guarantee that their lateral electric field is in the direction of maximum lateral coupling coefficients for slow shear c mode which is 6.15%, 37.91% and 95.46% for the AT-cut quartz, (yxl)-16.5° $LiTaO_3$ and (yxl)-58° $LiNbO_3$, respectively. The impendence at resonance, which was used to explain if the resonance caused by the LFE or TFE would take place, was theoretically derived from the device geometry and material constants and was well in agreement with the measurement results. The experiment results show that the (yxl)-16.5° $LiTaO_3$ and (yxl)-58° $LiNbO_3$ LFE devices in air works under the pure LFE mode and but the quasi-LFE mode in liquid. The results also suggest that the reported AT-cut LFE liquid sensors may well be possible a pseudo-LFE device.

Discussion and Conclusions

The study shows that the three operation mode of LFE devices can be applied to different environments through appropriate selection of the substrate material, its orientation and geometry size, and the geometry of the metal electrodes. It is clear that these results would be a good help in understanding LFE device¡¯s behaviors and designing new LFE devices.

1E. Clinical Cancer Imaging

Hall 3

Tuesday, November 4, 2008, 10:30 am - 12:00 pm

Chair: **Stuart Foster;**
University of Toronto, Canada.

1E-1

10:30 AM **Making microbubbles work for ultrasound: Technical and broader challenges**

Peter Burns; *University of Toronto, Dept Medical Biophysics, Toronto, ON, Canada.*

Background, Motivation and Objective

Although it has been 10 years since microbubble contrast agents were first approved for clinical use, adoption has been slow, in spite of considerable technical advances and many successful clinical studies.

Statement of Contribution/Methods

Methods for contrast specific imaging exploit the nonlinear response of bubbles at or near resonant excitation. Simple filtering for higher harmonics has given way to broadband methods using phase and/or amplitude modulation of a sequence of pulses. With suitable detection methods, linear, nonlinear, moving and stationary targets can all be segmented from the echo and shown in real time. The tendency of bubbles to disrupt at low peak negative pressures also offers a potential role for coded excitation on transmit. Deliberate disruption of bubbles with a few high MI pulses can clear the image plane and allow measurement of its replenishment by contrast offering a unique way to quantify microvascular flow and perfusion volume.

Results

At least 3 million clinical contrast studies have been performed: safety and tolerability have proven excellent. Clinical applications have focused on areas in which ultrasound already plays an important diagnostic role. In cardiology, contrast can aid visualisation of the endocardium, especially important in wall motion studies, and has been shown to improve the accuracy of stress echo. It can also image and measure myocardial perfusion in real time, at rest and with stress, with spatial resolution superior to the current nuclear medicine standard, SPECT. In radiology, perfusion can be imaged in many organs, but work has concentrated on the liver, where contrast can help characterise focal lesions with an accuracy comparable to contrast CT and MRI. It also aids in lesion detection, in real time guidance of interventions such as RF ablation and in monitoring response to tumor therapy, especially using the new antiangiogenic agents.

Discussion and Conclusions

In spite of demonstrated efficacy and safety, widespread adoption into the clinic has been slow. Two reasons are proposed. First, although bubbles are approved for perfusion imaging in more than 60 countries, the US, which has approved no radiology indications, is not among them. Second, while contrast ultrasound is often less expensive than competing modalities, physician reimbursement may be less too, dampening enthusiasm among practitioners.

We conclude that future clinical studies should focus on applications unique to microbubbles, exploiting, for example, their confinement to the blood pool and the ability to image them in real time. Approval of a perfusion indication by the US FDA is crucial. Widely available, robust contrast specific imaging modes are needed. The intriguing capacity of bubbles to potentiate therapies, including drug delivery, should be pursued. For diagnosis, translation of microbubble contrast applications to clinical practice may come more quickly in cost-driven rather than profit-driven healthcare systems.

1E-2

11:00 AM **The Role of Contrast Enhanced Ultrasound (CEUS) in Oncology**

Stephanie Wilson; *University of Calgary, Department of Diagnostic Imaging, Calgary AB, Canada.*

Background, Motivation and Objective

The oncology patient is susceptible to the development of tumor masses in many locations and their detection and diagnosis is usually within the realm of diagnostic imaging. While ultrasound may show tumors, additional imaging with CT and or MR scan is generally required for their confident diagnosis. We address the tremendous contribution of contrast enhanced ultrasound (CEUS) in the imaging of this population.

Statement of Contribution/Methods

Contrast agents for ultrasound are comprised of tiny bubbles of gas in a supporting shell. Their intravenous injection results in tissue perfusion, analogous to that seen on contrast enhanced CT and MR, and also incredible vessel visualization more similar to that seen with angiography. These attributes allow for improved detection and characterization of tumors in many parts of the body.

Results

Characterization of tumors of the liver is the most accepted indication for CEUS where it is complimentary to CT and MR scan. Liver lesion detection and also the difficult question of diagnosis of hepatocellular carcinoma are further accepted strategies for the use of CEUS as the detection of small nodules in the cirrhotic liver on screening sonography is enhanced by the performance of CEUS at the time of nodule detection. Detection of liver masses is also improved by CEUS as the addition of contrast agent increases the conspicuity of liver masses on sonography such that more and smaller masses may be detected than at baseline.

CEUS is also valuable when added to intraoperative liver ultrasound, contributing to management decisions for the patient undergoing surgery. Further, CEUS is a critical component of radiofrequency ablation (RFA) techniques especially when performed at the time of the procedure where it may reduce the requirement for repeat procedures performed for incomplete ablation. CEUS is suitable for monitoring patients with prior RFA or transarterial chemoembolization (TACE).

CEUS contributes to the characterization of renal masses, especially cystic RCC, where vascularity in septae and nodules is shown with a sensitivity surpassing both CT and MR scan. Further, in other locations such as the pancreas, spleen, ovary, prostate and breast, CEUS may show the presence of vascularity in real-time with the resolution of standard gray-scale ultrasound.

Discussion and Conclusions

CEUS changes totally the role of ultrasound in the evaluation of the patient with cancer.

CEUS may be performed on any organ with a suitable acoustic window where the addition of vascular information may contribute to diagnosis. Its performance is independent of renal function making it a perfect first choice for the characterization of all masses in the oncology patient. To confirm that a mass is a malignant tumor or to confirm that it is not, CEUS is an easily performed and readily available technique. For these reasons, CEUS deserves a fundamental role in the future of oncological diagnosis.

1E-3

11:30 AM **the clinical application of ultrasound contrast imaging**

Yuxin Jiang; *Pekin union medical college hospital, Department of diagnostic ultrasound, Beijing, China.*

Background, Motivation and Objective

Contrast-enhanced ultrasound imaging is the area of greatest interest in ultrasound medicine currently. The recent improvements of contrast agent and the contrast specific scanning techniques have given new possibilities for the further research and clinical application. We are having researches in the basic theory study and further clinical applications in China, so that ultrasound contrast imaging can be better recognized and widely applied in the clinical practice.

Statement of Contribution/Methods

The introduction of second-generation microbubble contrast agents, such as SonoVue and self-made perfluorocarbon ultrasound contrast agent, and the advent of specialized imaging techniques enabled real-time contrast-enhanced imaging. In our study, Sonovue and the gray scale harmonic imaging technique were adopted to evaluate the characteristic contrast enhanced pattern of liver, kidney, gynecology, breast and thyroid lesions, etc.

Results

Our clinical research shows that contrast enhanced ultrasounographic imaging can improve the diagnostic potential of sonographic examinations in different clinical applications, including the better observation of small vessels, the real-time assessment of the blood perfusion pattern in an organ or area of interest, with a significantly higher detection rate and diagnostic accuracy especially for the tumor of liver, kidney and gynecology. Otherwise, contrast enhanced ultrasound imaging holds the potential for a better visualization and diagnosis of peripheral vascular and some deep-located vessels, such as carotid, brain arteries and renal arteries, etc. The area of great promise and growth also lies in the clinical research of breast and thyroid.

Discussion and Conclusions

With the fast development and the intrinsic advantages of contrast enhanced ultrasound imaging, it is gainning more and more popularity. Ultrasound doctors should pay efforts to do further research in this state of art technique, which may open a new prospect for the ultrasound medicine.

2E. Arrays and Therapeutic Devices

Room 201 A/B/C

Tuesday, November 4, 2008, 10:30 am - 12:00 pm

Chair: **Shin Umemura;**
Kyoto University, Japan.

2E-1

10:30 AM **Electronically steerable large-scale ultrasound phased-array for noninvasive transcranial therapy**

Junho Song, Kullervo Hynynen; *University of Toronto, Imaging Research, Sunnybrook Health Science Center and Department of Biophysics, Toronto, ON, Canada.*

Background, Motivation and Objective

The objective of the study is to design, fabrication and characterization of a large scale hemispherical ultrasound phased-array with electronic beam focusing and steering ultrasound transducer for transcranial ultrasound therapy. The functionality of the transducer, including its beam steering and focusing capabilities, is evaluated with an ex vivo human skull.

Statement of Contribution/Methods

A focused ultrasound phased-array transducer was constructed with 1372 custom-made PZT-4 cylindrical tube elements. The array had a diameter of 31 cm. The elements had the same dimensions of a 10 mm outer diameter, 6 mm height, and 1.5 mm wall thickness. The gaps between the adjacent elements were constructed to be less than 0.5 mm. A 2000 channel phased-array driving amplifier system developed in-house was used to drive the array. A phase correction was performed to adjust the phase aberration of the ultrasound waveform radiated from each array element. An ex vivo human skull fixed in 10% buffered formaldehyde was used.

Results

The electrical impedance measurement demonstrated that the use of the tube elements provided an electrical impedance of 142.6 Ohms and 0 deg phase at the resonant frequency. The laser vibrometry measurements of the motion of the element demonstrated clear length mode oscillations as expected. The acoustic power conversion efficiency measurement of the single array element was 54 % at 306 kHz and 39 % at 840 kHz, respectively. These measurements showed that the method of using tube elements was well suited for phased array manufacturing since it provided at least an order of magnitude reduction to the electrical impedance when compared with standard plates driven with thickness mode. The ultrasound field measurements showed that the fundamental and third harmonic frequencies of the array were 306 kHz and 840 kHz, respectively. At 306 kHz, an effective beam steering range was found to be approximately 100 mm x 100 mm in the XY plane through an ex-vivo human skull. It was observed the effective range of 100 mm in the Z direction. The focal beam spot size, measured at a 50 % value of its peak pressure-squared value, was as small as 2.3 mm at the geometric center through a skull. At 840 kHz, a smaller focal spot size of 0.7 mm was observed at the geometric focus. The effective range was found to be 30 x 30 x 30 mm^3.

Discussion and Conclusions

This study demonstrated the feasibility of constructing electronically focused and steered ultrasound phased array using cylindrical transducer elements that allow the electrical impedance to be reduced such that effective operation can be achieved without electronic matching circuits. The 1372 element array was shown to be sufficient to produce excellent focusing through the ex vivo human skull and an adequate beam steering range for clinical brain treatments. The lower frequency would be suitable for cavitation enhanced treatments such as focal drug delivery and the higher frequency for thermal and thrombolytic therapies.

2E-2

10:45 AM **Radiation force localization of HIFU therapeutic beams coupled with MR-Elastography treatment monitoring – In vivo application to the rat brain –**

Benoit Larrat, Mathieu Pernot, Jean-François Aubry, Ralph Sinkus, Mickael Tanter, Mathias Fink; *ESPCI, CNRS UMR 7587, université Paris 7, Laboratoire Ondes et Acoustique, Paris, France, France.*

Background, Motivation and Objective

High field magnetic resonance elastography (MRE) has the ability to measure 3D displacement fields with sensitivity down to some hundreds of nanometers. It is also able to assess the mechanical properties of living tissues. Therefore, this technique is of first choice in order to non invasively monitor high intensity focused ultrasound therapy. This latter application is emerging rapidly and need to be coupled to a reliable imaging tool to locate the targeted area and to control the effective necrosis of tissues.

Statement of Contribution/Methods

A complete HIFU+MR monitoring system was designed for "small animal" brain HIFU investigations. All the experiments were performed in a 7T MRI Bruker scanner. An MR-compatible prefocused ultrasonic monoelement operating at 4MHz was used to generate a radiation force induced displacement in tissue samples (turkey breast).

In order to check the position of the focal point, the displacement created by a 5 ms ultrasonic burst was imaged via a dedicated motion sensitized MR sequence. A reference 600µm isotropic resolution elastography acquisition was performed. Then, the ultrasound transducer was turned into HIFU mode by performing two 10s sonication at high power. Finally, MRE was repeated to verify the stiffening of the area of interest.

The MRE experiment consisted in a 200Hz monochromatic mechanical excitation synchronized with an acquisition of the displacement field at one time step during the vibration cycle. This acquisition was repeated for 8 equally-spaced times to cover one full mechanical excitation period. A 3D local inversion algorithm was then applied in order to reconstruct the maps of the complex shear modulus.

For animal tests, rats were anaesthetized with isoflurane (1.5% v/v). They were placed in supine position to ensure a proper coupling for both a low frequency vibrating piezoelectric plate and the ultrasonic transducer. Total duration of the protocol was 2h.

Results

The developed MR sequence allowed the detection of small motion (1 to 20µm) with limited sent energy. In polyvinylalcohol phantom gels, the radiation force induced displacements generated phase wraps in the MR phase image. The proposed HIFU protocol was successfully performed in turkey breast. After the HIFU treatment a significant increase of stiffness was observed at the location of the maximum displacement measured previously. Using the same protocol, in vivo rat experiments were performed for brain HIFU treatment.

Discussion and Conclusions

In this study, the ability of assessing the effect of HIFU therapy with MR-elastography was demonstrated ex vivo and in vivo. A single positioning of the targeted object was needed to sequentially visualize the focal point of the HIFU transducer at non therapeutic levels, burn tissues at that location and measure the mechanical properties before and after the treatment.

2E-3

11:00 AM **Molecular focusing of high-intensity ultrasound: Time-reversal focusing applied to targeted ultrasound contrast agents**

Olivier Couture, Mickael Tanter, Mathias Fink; *LOA, ESPCI, France.*

Background, Motivation and Objective

Microbubbles targeted to disease biomarkers can be used to make high-intensity ultrasound therapy more specific. In general, their presence in a region provides a better coupling between the acoustical, mechanical and thermal energy. However, it would be even more beneficial to focus ultrasound directly on the microbubbles. Using the ability of time-reversal to refocus an amplified ultrasound wave on a source of arbitrary geometry, we present a method to restrict energy deposition on zones of specific biomarkers expression.

Statement of Contribution/Methods

Droplets of avidinated-microbubbles were deposited on biotinylated gelatin to mimic targeting. The gel was then immersed in a water tank equipped with an array made of 80 fully-programmable HIFU transducers working at a 1MHz central frequency. A dedicated disruption imaging sequence was developed to select the echoes from the targeted microbubbles, which were then time-reversed, amplified, elongated and reemitted by the HIFU array. The resulting pressure field at each point was measured using a scanning hydrophone (Onda, USA). Emission signals can either be transmitted in order to build a focused pattern whose shape is corresponding to the contrast agents cloud or decomposed into elementary sets of transmit signals in order to focus point by point. Depending on the size of the focal spot, peak pressure field were typically reaching 5 MPa.

Results

Figure shows the two colored dots of microbubbles on the gelatin surface. When the time-reversed HIFU pulses were emitted, the hydrophone scan showed a pressure-increase corresponding to the original pattern formed by the microbubbles .

Discussion and Conclusions

These experiments demonstrate that it is possible to focus a high-intensity ultrasound beam on a pattern formed by targeted microbubbles using time-reversal. HIFU therapy can thus be guided by the molecular expression related to a disease. This therapy can be modulated, it is independent of the actual presence of the microbubbles during the final stage and it could potentially be used to treat diffuse molecular diseases.

Fig: Optical image of dotted microbubbles on a gel (left) and corresponding pressure distribution of the time-reversed signal from the microbubbles (right).

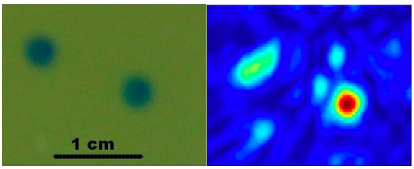

Tuesday Oral

2E-4

11:15 AM **Design and Test of a Monolithic Ultrasound-Image-guided HIFU Device using Annular CMUT Rings**

Mengli Wang[1], Jingkuang Chen[1], Xiaoyang Cheng[1], Jui-Ching Cheng[2], Pai-Chi Li[3]; *[1]University of New Mexico, USA, [2]Chang Gung University, Tao Yuan, Taiwan, [3]National Taiwan University, Taipei, Taiwan.*

Background, Motivation and Objective

High intensity focused ultrasound (HIFU) is a promising modality for minimally invasive and non-invasive therapies. For therapeutic ultrasound, real-time monitoring the biological object being treated is important to the patient's safety and success of operation. While MRI and non-invasive ultrasound imaging have been widely used for this purpose, they either deliver inadequate viewing angle or limited resolution. For many high-precision invasive operations, e.g., peripheral thrombolysis, in-situ imaging capability is badly needed. This paper developed a therapeutic ultrasound chip with built-in ultrasound imaging capability.

Statement of Contribution/Methods

On this chip, high-power capacitive micromachined ultrasonic transducer (CMUT) and imager CMUT are monolithically integrated on a micromachined silicon substrate for minimally invasive treatment. Due to the difference in function, the structure of high-power CMUT uses a thicker membrane and a higher gap than the imager devices to deliver a larger restoring force/pressure during ultrasound transmission. In contrast, the membrane of the imager CMUT was made thin and flexible so it is sensitive to echo ultrasounds. The polysilicon membrane thickness and gap height of the high-power CMUT are 1.3mm and 0.32mm, respectively, while those of the imager CMUT are 1.0mm and 0.17mm, respectively.

Results

Figure (a) shows a SEM photograph of this CMUT chip with dual functions. This chip comprises two concentric high-power (inner) rings and one annular imager CMUT array (outmost) with 48 elements. Different from the imager ring which is divided into multiple small chambers, the high-power CMUT ring is a "swim ring"structure comprising one single camber for a larger effective membrane deformation and thus a higher average acoustic energy. The high-power CMUT ring was able to deliver an output pressure larger than 1.3Mpa under 200V peak-

to-peak a.c. signal. The high-power CMUT ring was used in a preliminary experiment for heating the liver tissue of a pig monitored by a thermocouple. It was found that the tissue heating rate is approximately 0.42°C/minute in the first six minutes of ultrasound bombardment.

Discussion and Conclusions

An ultrasound-image guided HIFU chip built of CMUT arrays was designed and fabricated. The initial heating experiment on a piece of a pig's liver tissue showed the usefulness of the device.

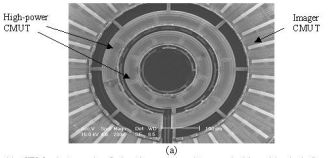

(a)

Fig. (a). SEM photograph of the therapeutic ultrasound chip with dual (imaging & stimulation) function. Two concentric high-power (inner) rings and an annular imager CMUT array (outmost) of 48 elements are integrated on a 100μm-thick silicon substrate for simultaneous stimulation and imaging.

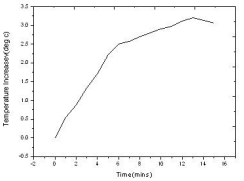

Figure (b): Liver tissue temperature as a function of the ultrasound irradiation time using the high-power CMUT ring as the transmitter.

2E-5

11:30 AM Space-filling, aperiodic array ultrasonic therapy transducers

Balasundar Raju, Christopher Hall; *Philips Research North America, Ultrasound Imaging & Therapy, Briarcliff Manor, NY, USA.*

Background, Motivation and Objective

Ultrasound transducers designed for therapeutic purposes such as tissue ablation or drug delivery require large apertures for adequate spatial localization while providing sufficient power. When periodic arrays are used, the number of elements to avoid grating lobes becomes too large to be economically feasible. Previously, aperiodic arrays had been proposed based on a random arrangement of elements that lead to sparseness and unused surface area. In this work we describe an array that is both space-filling and aperiodic in the placement of the elements that leads to reduced grating lobes while maintaining full surface area coverage to deliver maximum power.

Statement of Contribution/Methods

The mathematical concept of aperiodic tiling was used to develop aperiodic space-filling array transducers. For illustration, a flat 2D array with 255 elements with two shapes was designed based on Penrose tiling to cover an aperture 4 cm x 4 cm with no sparseness while guaranteeing aperiodicity. The areas of the two shapes were 5.94 mm^2 and 3.67 mm^2, the ratio of the two being the golden ratio. Full spatial coverage with two shapes allows for easy impedance matching. The beam patterns (1.2 MHz tone burst of 8 μs duration) from the array were simulated using the FIELD II program in a plane 6 cm from and parallel to the aperture for multiple focal spots. Seventeen focal spots are reported here: One central on-axis and sixteen off-axis spots along a circle of radius 1.5 cm from the axis (i.e. a steering angle of 14^o) all in a plane 6 cm from the aperture. For comparison, beam patterns for the same excitation intensity from other 2D arrays with 256 elements and varying levels of regularity and sparseness were also computed: Periodic array, semi-periodic array along one direction, array with maximally packed circular elements, and random array with circular elements.

Results

The worst relative grating lobe level among all the focal spots were -2.5 dB (periodic and semi-periodic), -4.8 dB (maximally packed circles), -11.4 dB (Penrose), and -14.9 dB (sparse random circles). Both the Penrose and random arrays had beam patterns with commonly accepted grating lobe levels for therapeutic use of -10 dB or lower. However, the main lobe intensity was 71% higher for the Penrose array when the beam was focused on axis due to the full area usage compared to the random array. The Penrose array had smaller side lobes compared to the random array (-16 dB vs. -13.7 dB). The grating lobe levels among the sixteen off-axis focal spots were -12.06 dB ± 0.46 dB, with the best and worst being -12.9 dB and -11.4 dB respectively, indicating that the Penrose array had no directional preference.

Discussion and Conclusions

This work demonstrates that the concept of space-filling aperiodic tiling can be used to generate therapy arrays that are able to provide higher power for the same total transducer area compared to fully random arrays while maintaining acceptable grating lobe levels.

2E-6

11:45 AM **Image-Guided Refocusing of Dual-Mode Ultrasound Arrays(DMUAs)**

John Ballard, Emad Ebbini; *University of Minnesota, USA.*

Background, Motivation and Objective

A major advantage of imaging with dual-mode ultrasound arrays (DMUAs) is their inherent registration between imaging and therapeutic modes during image-guided surgery which allows for image-based feedback for refocusing the therapeutic beam. Specifically, this capability is critical in image-guided thoracic surgeries where the target is partially obstructed by the rib cage, thus limiting the access and distorting the geometrically-focused high-intensity focused ultrasound (HIFU) therapeutic beam.

Statement of Contribution/Methods

Images obtained with single-transmit focus (STF) imaging, in which the therapeutic beam is used at diagnostic levels, allow the user to select target and critical locations for optimizing the power deposition. We have developed an optimal refocusing method that takes advantage of the acoustic window of the intercostals spacing in order to minimize the power deposition over the critical regions (ribs) while maintaining or improving the power deposition at the target location (tumor).

Results

The algorithm is verified experimentally with a 64-element 1MHz DMUA, in an attenuating tissue mimicking phantom (~.5 dB/cm/MHz) with embedded Plexiglas ribs. Thermocouples are used to measure sub-therapeutic temperatures across the ribs and at the target location before, during and after 5 seconds of HIFU exposure for both the geometric focusing and the optimized refocusing while normalizing the driving power for both cases. An increase of normalized temperature (per watt of input power) greater than 20% was observed at the target after refocusing. At the same time, a reduction in normalized temperature rise across the ribs was greater than 60%. Statistics showed that the maximum variance between measurements when the experiment was rerun a minimum of 5 times for each case was approximately 5%. In addition, STF images taken with the refocused HIFU beam showed increased echogenicity at the target and reduced echogenicity at the ribs. This can be quantified by the intensity of the grayscale images. These images show a typical improvement of 5 dB at the focus with a reduction of 2dB across the ribs.

Discussion and Conclusions

The results show that STF DMUA imaging provides suitable feedback for refocusing the HIFU beam in the presence of strongly scattering targets. The robustness and repeatability of the algorithm were demonstrated by embedding the ribs within a block tissue-mimicking phantom to approximate realistic conditions and repeating each experiment multiple times. The results also show that grayscale STF images themselves provide useful feedback on the improvement in the quality of the refocusing beam, i.e. the relative echogenicity of the ribs is reduced upon refocusing indicating reduction in incident power. These results are generally consistent with the directly measured temperatures at the target and rib locations.

3E. Medical Signal Processing II

Room 305 A/B/C

Tuesday, November 4, 2008, 10:30 am - 12:00 pm

Chair: **Pai-Chi Li;**
National Taiwan University, Taipei, Taiwan.

3E-1

10:30 AM **Mirrored Motion-Compensation for Complementary-Coded Medical Ultrasonic Imaging**

Cormac Cannon, John Hannah, Steve McLaughlin; *University of Edinburgh, Institute of Digital Communications, Edinburgh, Lothians, United Kingdom.*

Background, Motivation and Objective

Binary-phase-coded pulses (BPC) exhibit greater resilience to the distorting effects of transducer and medium than comparable FM signals. This improves resolution and SNR at depth but complicates side-lobe reduction.

Complementary BPC pulses eliminate range side-lobes but introduce artifacts caused by tissue-motion in the medium and usually require a reduction in frame-rate. This paper describes techniques to reduce these artifacts while avoiding any reduction in frame rate.

Statement of Contribution/Methods

The principal contribution is a mirrored motion compensation technique for complementary BPC imaging. This avoids any reduction in frame-rate by allowing recursive combination/compensation of data.

Adjacent received reflections correspond to successive codes of the complementary set and are filtered using the appropriate binary code. The motion estimates used to align adjacent filter outputs are derived from their cross-correlation maxima. To reduce the effects of estimate error, two mirrored complementary sums are formed, aligned about their single common filter output. The sum of these is passed through a final filter matched to the transducer and base pulse.

Results

The relative performance of optimised FM signals and complementary BPC signals processed using our techniques are compared under a range of conditions using simulations (Field II) and experimentally.

In the presence of frequency-dependent attenuation, for example, our complementary BPC method provides an SNR gain of 5dB over the equivalent FM signal at a depth of 1cm, increasing to 18dB at a depth of 10cm. This is illustrated in Fig. 1, which shows simulated B-mode images of equally spaced moving point targets. Images (a) and (b) were generated using uncoded and FM signals, respectively. Images (c) and (d) used a 40-bit Golay-encoded signal pair, with (c) and without (d) motion compensation. The motion varied with time over the course of the scan and with depth to simulate the presence of disparate moving regions within the beam.

Discussion and Conclusions

Complementary BPC signals processed by our techniques have been shown to give a valuable improvement in SNR and resolution compared to uncoded and FM-chirp signals. The method would be useful in synthetic-aperture imaging as the same motion estimates could be used for code alignment and compensated aperture synthesis.

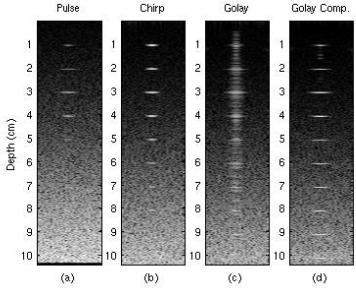

3E-2

10:45 AM **3D Mouse Cardiac Motion Estimation Facilitated using RF Signal Decorrelation**

Christopher D. Garson, Yinbo Li, John A. Hossack; *University of Virginia, Biomedical Engineering, Charlottesville, VA, USA.*

Background, Motivation and Objective

Murine cardiac ultrasound imaging is limited to 2D B-mode or RF data acquisition. The high signal bandwidth and frame rate (>100Hz) required for 3D mouse heart scanning presents a major challenge, making it unlikely that direct capture of finely sampled realtime 3D data will be achieved in the near future. Collecting and registering image sets from intersecting orthogonal 2D scan planes enables the estimation of 3D motion, but only at points along lines of intersection between acquired image frames. We propose the use of RF signal decorrelation to estimate elevational motion directly from the 2D image plane.

Statement of Contribution/Methods

RF data was collected and processed from a 30MHz Vevo 770 scanner. Decorrelation/displacement calibration functions were created by acquiring image sets at precise 0.008 mm elevational increments (using a motion stage) to create a mapping of RF signal decorrelation with respect to independently measured transducer elevational displacement. A mouse heart was scanned along short and long axis imaging planes, producing RF data comprising the entire cardiac cycle. The ECG was acquired simultaneously and used to retrospectively align and assemble frames of data at 8000 frames per second. RF decorrelations were computed along all A-lines. Combining in-plane speckle tracked estimates and out of plane decorrelation based displacement estimates yielded a full 3D displacement data set for the entire cardiac cycle.

Results

The quality of out-of-plane displacements were evaluated by comparing them with lateral displacements in the perpendicular scan plane along intersecting A-lines (i.e. short-axis elevational motion was validated against long-axis lateral motion), illustrated in Fig. 1. Displacements estimated using RF decorrelation were highly correlated with independent (orthogonal) speckle-tracked estimates (R=0.90).

Discussion and Conclusions

Out-of-plane decorrelation provides a promising method for computing 3D displacements from 2D scan-planes of *in vivo* mouse heart RF data. 3D displacement vectors may be used to compute 3D strain that may be useful when analyzing ischemic, normal and "border zone" regions post myocardial infarct.

Figure 1: Out-of-Plane Displacement Detected Using:
1) Short-Axis Decorrelation 2) Orthogonally Acquired Data

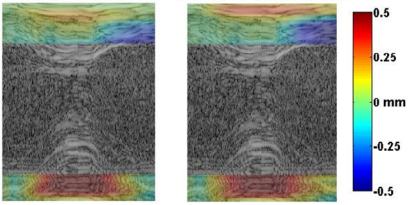

3E-3

11:00 AM **Reducing Peak Hopping Artifacts in Ultrasonic Strain Estimation with the Viterbi Algorithm**

Yael Petrank, Lingyun Huang, Matthew O'Donnell; *University of Washington, Bioengineering, USA.*

Background, Motivation and Objective

Tissue strain can be estimated by correlating kernels in one ultrasonic radio frequency (RF) image to kernels in the next imaging instance. The position of the kernel in the next image yielding the maximum correlation coefficient is used to estimate displacement. At large deformations the magnitude of the correlation coefficient peak can be low and exceeded by secondary peaks. This peak hopping effect can cause significant errors in displacement and strain estimates. The Viterbi algorithm finds the most likely sequence of hidden states in a sequence of observed events. It is suited to motion estimation in elasticity imaging because adjacent tissue elements remain adjacent following deformation. Particularly, tissue elements along an ultrasonic beam in one image lie along a continuous curve in the next imaging instance. The observed “event” is tissue displacement of a pixel. Applying the Viterbi algorithm, we can interpolate the correct displacement of all tissue elements.

Statement of Contribution/Methods

For each beam in an image, a volume of correlation coefficient values between kernels along this beam with kernels in the next image is calculated. A weight volume, equal in size, is developed by giving bonuses and penalties to points lying along possible curves. Continuity of the curve and values of complex correlation coefficient vectors along it, contribute to the accumulated weight. The likeliest curve passes through points with the minimal accumulated weight. The algorithm was tested on a simulated medium, represented by randomly distributed point scatterers with amplitudes obeying a Rayleigh distribution. The pulse had a 5MHz central frequency and the sampling rate was 20MHz. RF data were generated before and after deformation with an average strain of 5%, for a homogenous medium, and for a medium with a stiffer (6 times) inclusion.

Results

The mean of absolute differences between estimated and true strains reduced from 0.214, when displacement estimation was based on the peak correlation coefficient, to 0.0131 when it was based on Viterbi processing, in the homogeneous case, and from 0.428 to 0.0150 in the heterogeneous phantom case.

Discussion and Conclusions

Peak hopping was significantly reduced for large deformation cases using Viterbi processing.

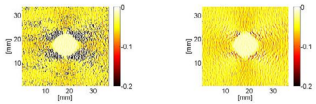

Figure 1: Left: axial strain estimation is by maximal correlation coefficient location. Right: axial strain estimation using Viterbi algorithm

3E-4

11:15 AM **Precision of Needle Tip Localization Using a Receiver in the Needle**

Svetoslav I. Nikolov, Jørgen A. Jensen; *Technical University of Denmark, Department of Electrical Engineering, Kgs. Lyngby, Denmark.*

Tuesday Oral

Background, Motivation and Objective

Many medical procedures require the detection, tracking and guidance of (biopsy) needles. The detection of the position of the needle can be challenging because of specular reflection which deflects the sound in a direction away from the transducer surface. To visualize the tip of small needles often motion is introduced to the discomfort of the patient.

Vilkomerson and co-workers suggested in 1981 the placement of an ultrasound receiver close to the needle tip. The received echoes are detected by add-on hardware. The maximum echo is assumed to originate from a beam directly above the detector, and the time of flight determines the distance to the transducer. The feasibility of the method was demonstrated by the same group in-vivo. The precision of the method has not been previously discussed in literature.

Statement of Contribution/Methods

This paper introduces two methods for estimation of the position of the needle tip and investigates their precision. The first method uses conventional imaging. Instead of detecting the maximum echo, as previously suggested, the center of mass is found both across beams and along the received signals, thus decreasing the sensitivity to noise. The second method is based synthetic aperture (SA) scanning. The position of the tip is found via triangulation which involves solving a system of linear equations. The robustness to noise is ensured through averaging over a number of estimates.

The sensor is a ring, made of piezo-electric film making it possible to receive waves from any direction. An amplifier is placed in the needle handle to amplify the signals, which are sent back to a receive channel in the scanner. The uncertainty of the position (out-of-plane) is indicated by a circle, with a radius proportional to the mean error.

Results

The results were obtained using simulations in Field II. The center frequency is 7 MHz. The transducer array is mechanically focused in elevation plane at 25 mm while the height of the elements is 4.5 mm. The transducer pitch is 202 microns. The sensor is a ring with height of 1 mm and 2 mm diameter. Positions were varied from 10 to 120 mm in depth and from 0 to 20 mm in lateral and elevation direction. The orientation of the needle was varied from 45 to 90 deg. The mean error of position estimation is for the case of conventional and SA imaging is 0.2 and 0.05 mm, respectively.

Discussion and Conclusions

The precision of two methods to determine the position of the needle tip is investigated. Using spherical transmissions yields higher accuracy. Both methods can be extended to 3D if the transmissions originate from transducer elements that are not placed on a line. This is the case of, for example, anorectal probe. Needles equipped with receivers can be used for deploying brachytherapy seeds ensuring high precision of the procedure.

3E-5

11:30 AM **Quantitative Bladder Volume Assessment on the Basis of Nonlinear Wave Propagation**

Egon J.W. Merks, Nicolaas Bom, Nico de Jong, Antonius F.W. van der Steen; *ErasmusMC, Biomedical Engineering, Rotterdam, Netherlands.*

Background, Motivation and Objective

Catheterization is the gold standard for bladder volume assessment, but it is invasive and introduces the risk of infections and trauma. To reduce the need for a urinary catheter, a new method has recently been introduced that non-invasively and instantaneously measures the volume of liquid filled cavities on the basis of nonlinear wave propagation with a single diverging acoustic beam. The method exploits the relatively higher nonlinear behavior of liquid compared to tissue.

Previously obtained results from using a fast-rotating phased array probe and high end echo system have proven the feasibility of the method. A 15 dB increase of the 2nd harmonic was observed on a 500 ml bladder phantom relative to a tissue-only phantom. In-vivo measurements on a bladder containing 450 ml urine showed an increase of 10 dB at the 2nd harmonic compared to an empty bladder. The objective of this study is to design a simple transducer that generates a single diverging acoustic beam and to obtain a calculation method that quantitatively relates the spectral contents of the received RF-data to the insonified liquid volume.

Statement of Contribution/Methods

Progressive volume pulse-echo measurements were performed on healthy volunteers. The experimental setup included a custom multilayer transducer that is capable of generating sine wave bursts with centre frequency of 2 MHz and peak amplitudes of 500 kPa at the transducer surface, which could induce significant nonlinear wave propagation. The transducer bandwidth enabled receiving up to the 4th harmonic. To create the diverging acoustic beam, a defocusing lens was applied to the transducer. Volumes between 0 and 600 ml with 100 ml increments were measured. Reference measurements were performed with a commercial bladder volume instrument. Subject-specific acoustic loss and nonlinearity of the region anterior to the bladder influenced the volume estimation. A calculation scheme was applied that subtracted the nonlinear behavior of the anterior bladder region from the nonlinear behavior of the posterior bladder region, leaving only the fraction of nonlinearity (FON) contributed by the liquid region.

Results

Linear regression analysis on the data obtained from the progressive volume measurements resulted in a slope of 4.6 L/FON and an intercept of 118 ml. The 95% confidence interval of the slope was [4.6 ± 0.7]. By correcting for the nonlinear behavior of the anterior bladder region and looking at only the fraction of nonlinearity contributed by the liquid region, the relative standard deviation of the slope was reduced from 19.3% to 8.4% for the individual progressive measurements. Hence, the repeatability of the method increased significantly.

Discussion and Conclusions

A calculation method was developed that quantitatively relates the spectral contents of the received RF-data to the liquid volume present within a single diverging acoustic beam in-vivo.

This work was supported by the Dutch Technology Foundation (STW) under Grant 06652

3E-6

11:45 AM **2D Filter Design for the Reduction of Beamforming Artifacts in Coarsely-sampled Imaging Apertures**

Yayun Wan, Emad Ebbini; *University of Minnesota, Electrical and Computer Engineering, Minneapolis, Minnesota, USA.*

Background, Motivation and Objective

Beamforming artifacts due to coarse discretization of imaging apertures represent a significant barrier toward the use of array probes in high frequency ultrasound (HFUS) applications. Nyquist sampling of array apertures dictates center-to-center spacing of $\lambda/2$ for elimination of grating lobes in the array pattern. However, this requirement is difficult to achieve using current transducer technologies, even at the lower end of high frequency ultrasonic imaging (in the range 25 - 35 MHz).

Statement of Contribution/Methods

We have previously introduced a *k*-space based 2D post-beamforming filter for restoring image contrast loss due to coarse sampling of the imaging apertures. The 2D regularized imaging operator was obtained and implemented on full frame data in *k*-space using computationally-efficient 2D fast Fourier transform (FFT). The computational efficiency of the 2D filter can be further improved by implementing the filter in the spatial domain provided the filter has finite region of support (ROS). We have developed a weighting algorithm for limiting the ROS to approximately 3% of the full *k*-space implementation.

Results

The algorithm was verified using Field II in imaging a speckle-generating cyst phantom. We simulated two 25 MHz linear arrays with λ/2 and with 2λ element spacing. Images of the cyst phantom are shown in the figure: (a) using the finely sampled array, (b) using the coarsely sampled array, (c) applying the post-beamforming 2D pseudoinverse filter in k-space to the RF data obtained using the coarsely sampled array, and (d) applying the 2D kernel of the filter in spatial-temporal domain. The contrast ratio (CR) was 28.8, 20.4, 28.8 and 28.2 dB for the images in (a), (b), (c) and (d), respectively. In addition, the spatial resolutions were 61.2, 62.2, 71 and 71 ¦Ìm in axial direction and 111.8 120, 128 and 131 ¦Ìm in lateral direction, respectively.

Discussion and Conclusions

The simulation results verify that the 2D spatial filter with finite ROS can ahieve the same level of restoration in CR while maintaing the same level of spatial resolution achieved by the full *k*-space filtering approach. The size of the 2D kernel is only 3% of the size of original filter, which significantl reduces the computational load, allowing for real-time implementation especially with modern hardware platforms optimized for digital filtering.

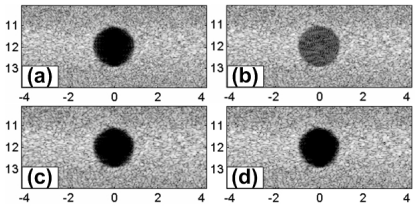

Tuesday Oral

4E. cMUT Modeling

Hall 2A

Tuesday, November 4, 2008, 10:30 am - 12:00 pm

Chair: **Paul Reynolds;**
Weidlinger Associates Inc, USA.

4E-1

10:30 AM **Finite Element Analysis of Stress Stiffening Effects in CMUTs**

Mario Kupnik, Ira O. Wygant, Butrus T. Khuri-Yakub; *Edward L. Ginzton Laboratory, Stanford University, CA, USA.*

Background, Motivation and Objective

Interestingly, for a capacitive micromachined ultrasonic transducer (CMUT), the term "membrane" is the established name for the key component of the device – the moving part of the CMUT cell. However, the term plate seems more appropriate because most demonstrated CMUTs operate in the plate regime in which the bending stiffness (out-of-plane stress) dominates both the static and dynamic behavior. Even CMUTs with vacuum-sealed cavities, biased close to pull-in point, typically have deflection-to-membrane thickness ratios < 10%, which places them in the plate regime. In this work we analyze CMUT designs where stress stiffening affects the devices in terms of static deflection, pull-in, resonance frequency, and sensitivity.

Statement of Contribution/Methods

In the finite element modeling software package ANSYS, stress stiffening (nlgeom command) can be considered in static, modal, and full transient response analyses. In this work, we show how stress stiffening can also be considered in harmonic response analyses, which is useful for predicting frequency response and small-signal sensitivities without running a computationally intensive transient analysis. We perform a prestressed harmonic response analysis in which the nonlinearities are activated during the static analysis. This ensures a correct static operation point calculation, even for CMUT membranes that exceed a deflection-to-thickness ratio of 10%. Then, if one assumes only a small AC excitation, a linear but updated stiffness matrix can be used to calculate the harmonic response. We achieve this by using a prestressed mode superposition harmonic response analysis, which uses the sum of factored mode shapes obtained from a nonlinear prestressed modal analysis. We verified our FEA with static and dynamic displacement measurements for two wafer-bonded devices (single-crystal silicon membranes) with different thicknesses, i.e. only one operates in a more membrane dominated regime.

Results

A direct comparison between the membrane regime design (40-µm-thick membrane, 2000 µm radius, 36 µm gap) and the plate regime design (60-µm-thick membrane, 2000 µm radius, 16 µm gap) revealed that only the FEM that accounts for stress stiffening, shows good agreement with the measurement results for both designs. For the 40-µm-thick membrane, the FEM without stress stiffening overestimates the static deflection by 21%, underestimates the pull-in voltage by 62%, underestimates the peak resonance frequency by 30%, and overestimates the maximum displacement per volt by 53%.

Discussion and Conclusions

Only a model that considers stress stiffening is useful to design CMUTs that operate in a more membrane dominated regime. Ignoring stress stiffening leads to large errors in predicted static deflection, pull-in voltage, resonance frequency, and sensitivity. Stress stiffening can help to realize lightweight membranes, operating at higher frequencies.

4E-2

10:45 AM **Calculation of equivalent parameters in CMUT 1-D theoretical model**

Wenchao Zhou, Ting Yu, Fengqi Yu; *Shenzhen Institute of Advanced Technology, CAS, Shenzhen, 518067, China, Department of Integrated Electronics, Shenzhen, Guangdong, China.*

Background, Motivation and Objective

Theoretical models are very important for designing capacitive micromachined ultrasonic transducers (CMUT). Little research on dynamic behavior of CMUT has been reported so far. In our previous work, a 1-D equivalent theoretical model was proposed to study the dynamic behavior of CMUT using 1-D equivalent parameters obtained from the real 3-D CMUT by FEM simulations. We here propose a theoretical model to calculate these 1-D equivalent parameters in both transmission and reception mode.

Statement of Contribution/Methods

CMUT membranes are typically hexagonal, which can be approximated by circular membranes. The key step to obtain the 1-D equivalent parameters is to acquire the shape function of the CMUT membrane under a DC bias voltage which cannot be solved from the balance equation because of nonlinearity. A simplified model is used here to approximate the membrane shape function. Shape function w(r) can be written as

$$w(r)=\sum \eta_i \varphi_i(r), \qquad (1)$$

where $\varphi_i(r)$ is the ith shape function, η_i is the ith generalized coordinate for the ith shape function. The shape functions $\varphi_i(r)$ are chosen as:

$$\varphi_i(r)=J0(r(\Omega i)^{1/2})/J0((\Omega i)^{1/2})-I0(r(\Omega i)^{1/2})/I0((\Omega i)^{1/2}), \qquad (2)$$

where J0 is the Bessel function of the first kind, I0 is the modified Bessel function of the first kind, and Ωi is the ith non-dimensional natural frequency.

Substitute (1) into the balance equation of the membrane, the shape function can be solved. Having the shape function, the other parameters, such as the equivalent piston area, spring constant, equivalent electrically active area, and piston mass, mechanical damping, can be calculated.

Results

With the calculated 1-D equivalent parameters, we can compute the frequency response of the CMUT in both transmission and reception using the 1-D theoretical model proposed in our previous work. The results obtained using the 1-D parameters and 1-D theoretical model are compared with those of FEM simulations, as shown in Fig.1. The results show that our theoretical model can be used to study a CMUT behavior in a more efficient and comprehensive way without losing accuracy.

Discussion and Conclusions

A theoretical model to obtain 1-D equivalent parameters of a real 3-D CMUT is proposed. The 1-D equivalent parameters are calculated using the approximated shape function. The results are compared with FEM simulations.

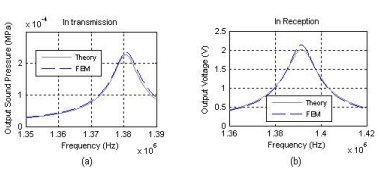

Tuesday Oral

4E-3

11:00 AM **Fast and Accurate CMUT Modeling using Equivalent Circuits with Lumped Parameters**

Arne Rønnekleiv; *Norwegian University of Science and Technology, Norway.*

Background, Motivation and Objective

The analysis of CMUTs is often done by using equivalent circuits, but the available circuits are not well adopted to include off axis steering of an array with several CMUTs per element. Here we show that the theory presented in [1] is well suited to establish equivalent circuits also for this case. The theory combines free acoustic modes of the CMUT membrane with the acoustic impedances and acoustic coupling between these modes due to the liquid. We further want a model with high computational efficiency, which is able to include the viscosity of the fluid.

Statement of Contribution/Methods

We show how the model provides both fast and accurate modeling of a CMUT array. The description assumes an infinite periodic array, and is formulated in k-vector space. The main focus is on the interaction between the CMUTs and the fluid.

The model assumes that different CMUTs only interact through the fluid and that they are mounted on an infinitely stiff backing. Without the loading of the fluid the CMUT membranes have orthogonal vibration modes, which may be used to describe the membrane movement with good accuracy. The interaction with the fluid is obtained through a set of well defined parameters, the self and mutual acoustic impedances of the modes due to the fluid. Making the calculations in the spatial Fourier space rather than real space simplifies our calculations as we only calculate the self/mutual impedance between modes in one period of the structure, one CMUT or one element, for each frequency and k-vector in the excitation of the array. The back side of this is that we have to cover a large range of k-vectors. Interpolating the parameters in frequency and k-vector reduces the calculation burden.

Results

We obtain an equivalent circuit of the Mason type for each mode with parameters that depend on the frequency and k-vector of the excitation. For elements formed by connecting neighbor CMUTs in a periodic pattern of CMUTs, it is shown that an equivalent circuit is obtained by coupling in parallel a set equivalent circuits for given k-vectors, of which normally only one is radiating into the medium. The non radiating equivalents are responsible for resonances that are often referred to as neighbor coupling.

Even for the more complicated case with off axis operation of an array with several CMUTs per element, the required parameters may be calculated in about 0.5 s or less per mode for a 1 to 10 relative frequency range and 0 to 45 degrees steering angle.

Discussion and Conclusions

It is shown how a fairly accurate equivalent circuit based on lumped parameters may be obtained for CMUT arrays, even in the case of off axis radiation with more than one CMUT per element. The model allows fast calculation of CMUT array radiation properties, both versus frequency and steering angle.

1: Arne Rønnekleiv, IEEE Trans. on UFFC, vol. 52, no. 12, Dec. 2005.

4E-4

11:15 AM **Beam Structure for CMUT with Desired Frequency Spectrum**

Hiroki Tanaka, Takashi Azuma, Shuntaro Machida, Kunio Hashiba, Takashi Kobayashi; *Hitachi, Central Research Laboratory, Tokyo, Japan.*

Background, Motivation and Objective

Capacitive micro-machined ultrasonic transducers (CMUTs) have shown many advantages to ultrasound imaging. The acoustical characteristics of a CMUT, such as sensitivity, center frequency, and bandwidth, can be controlled by changing shape or size and thickness of the diaphragm of the CMUT. However, since these parameters change all characteristics simultaneously, to control the desired characteristics, we have to redesign the CMUT, thereby incurring time and cost. According to one-dimensional analysis, the frequency spectrum of a simple plate depends on its stiffness and mass. If stiffness and mass of the diaphragm are controlled independently by thickness only, the desired frequency spectrum for CMUTs with the same shape or size can be obtained. In this study, we show that a CMUT with a beam structure realizes the desired frequency spectrum.

Statement of Contribution/Methods

Equivalent stiffness and mass of a base plate with rectangular beams were calculated by a theoretical approach. The relationship between thickness and width of the base plate and beams, in terms of resonance frequency and

frictional bandwidth (FBW), was investigated. Moreover, a three-dimensional (3-D) model, in which several rectangular beams are placed on the base plate aligned in one direction with constant pitch, was also created with PZFlex™ software. The frequency spectra calculated by the 3-D model are compared with the theoretically estimated spectra.

Results

In the case that beam width (w2) is set to 20% of the width of one element of the base plate (w1) and the relative thicknesses are set as t1/t0 and t2/t0, the theoretical approach shows that a combination of a resonance frequency and a FBW is adjustable over a wide range. However, in the case that w2 is set to 80% of w1, the adjustable range becomes narrower. The center frequency estimated by the theoretical approach shows good agreement with that obtained by the 3-D model (4% difference), and FBW has 30% difference.

Discussion and Conclusions

Specifically,when the beam width is increased, the shape of a CMUT diaphragm with a beam structure becomes close to a simple plate, whose resonance frequency and FBW automatically defined by thickness. Therefore, to effectively change the frequency spectrum by changing the beam thickness, the beam width is made as small as possible (in a range allowed by manufacturability) compared with the base-plate width.

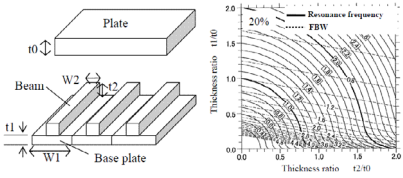

Tuesday Oral

4E-5

11:30 AM **Optimum design of circular CMUT membranes for high quality factor in air**

Kwan Kyu Park, Hyunjoo Jenny Lee, Mario Kupnik, Omer Oralkan, Butrus (Pierre) T. Khuri-Yakub; *Stanford University, Edward L. Ginzton Laboratory, USA.*

Background, Motivation and Objective

In resonant chemical sensor systems, based on the mass loading effect, the equivalent thickness is a key factor to achieve high mass sensitivity. Flexural mode resonators, such as cantilevers or CMUT membranes, benefit from the inherent advantage of having a thin equivalent thickness compared to other resonators (FBARs, SAWs, and QCMs). Further, a high quality factor (Q) of the resonator is desired for low oscillator phase noise. In such a system, the phase noise directly translates into detection limit. For cantilevers, one approach to optimize for high Q is to reduce its size, which is contradictory to the goal of having a sufficient large sensing area for a reliable chemical detection.

Statement of Contribution/Methods

Compared to cantilevers, the CMUT has a vacuum sealed cavity, which eliminates a main loss factor besides the loss on the front side of the membrane (air loss). A CMUT membrane has a larger contact area, which results in higher support loss (clamping loss). In this work we investigate how to minimize the total loss for CMUT resonators to maximize the Q. We fabricated various CMUTs with circular membranes with different thicknesses and radii (4-25 µm). Besides electrical impedance measurements, we performed laser interferometer measurements to determine the Q of these devices at various pressures, including vacuum (50 mtorr). This measurement in vacuum allowed us to identify the amount of loss contribution related to support loss only. Further, all measured results were compared to commonly used analytical models and finite element models.

Results

As an exemplary device, a CMUT membrane with a radius of 9 µm and a thickness of 0.5 µm was chosen. The quality factor in air (Q_{total}) and in vacuum ($Q_{support}$) are 130 and 1000, respectively (Fig. 1a), which translates into a Q_{air} of 150 for this device resonating at 18 MHz.

Discussion and Conclusions

For a given membrane thickness, Q_{air} increases when the radius of the membrane decreases, in contrast to the $Q_{support}$, which will decrease due to the smaller aspect ratio (radius/thickness) of membrane. (Fig. 1b). This observation indicates that a trade-off point exists between these two quality factors. Thus, a thinner membrane has smaller optimal radius for high Q.

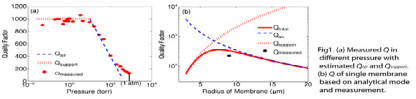

Fig1. (a) Measured Q in different pressure with estimated Q_{air} and $Q_{support}$. (b) Q of single membrane based on analytical mode and measurement.

4E-6

11:45 AM **A Viscoelastic Finite Element Model for Polymer Coatings on CMUTs**

Der-Song Lin, Xuefeng Zhuang, Serena H. Wong, Mario Kupnik, Butrus T. Khuri-Yakub; *Stanford University, Edward L. Ginzton Laboratory, Stanford, CA, USA.*

Tuesday Oral

Background, Motivation and Objective

Providing a reliable passivation of the membranes of a CMUT is essential for immersion imaging applications. Polydimethylsiloxane (PDMS) can be used to encapsulate CMUTs to provide good dielectric insulation, matching acoustic impedance with water and biocompatibility. PDMS encapsulation is widely used in applications such as flexible CMUTs, lens focusing, asymmetric lens beam steering for Doppler flow sensing, and acoustic crosstalk suppression. In this work we study the effect of a PDMS coating on operating characteristics of a CMUT, such as collapse voltage, frequency response in immersion, and output pressure.

Statement of Contribution/Methods

We have developed a finite element model using the commercial software package ANSYS to investigate the effects of PDMS coatings on CMUT membranes. Compared to analytical compound-plate calculations, our model addresses the visco-elastic property of PDMS. Depending on the type of simulation (static vs. harmonic), the Young¡¦s modulus is expressed as a function of frequency. This enables the correct calculation of the static operation point as well as the acoustic behavior without conflict. For verification of our finite element model, three typical CMUT designs (CMUT for high-intensity-focused-ultrasound, and 1D and 2D CMUT arrays for medical imaging) were fabricated and coated with PDMS layers of different thicknesses by mold-casting or spin-coating techniques. We used an impedance analyzer to characterize the collapse voltage. The frequency response and output pressure were measured in oil and water by laser interferometer and hydrophone.

Results

Our FEM results show that both the collapse voltage and peak frequency in immersion are not altered with various thicknesses of PDMS. Further, the FEM predicts the natural frequency of PDMS layer coupled with the membrane vibration causes minor ripples visible in the frequency spectrum. The experimental results demonstrate that 100, and 250 microns of PDMS have no impact on all three types of CMUT membranes in terms of collapse voltage and peak frequency in immersion. The model underestimates (~25%) the fractional bandwidth of the devices.

Discussion and Conclusions

Only a visco-elastic FEM can predict both the DC and AC behavior. In a regular model either the collapse voltage is overestimated dramatically, or the longitudinal wave velocity within PDMS is underestimated, which translates into larger impedance mismatch and faulty echo time. Therefore, it is essential to consider the visco-elastic properties of PDMS during design phase for improved prediction of static operation point and dynamic performance.

5E. Flow Measurements

Hall 2B

Tuesday, November 4, 2008, 10:30 am - 12:00 pm

Chair: **Edward Haeggstorm;**
Institute of Physics, University of Helsinki, Finland, CA, USA.

5E-1

10:30 AM **New Developments in Ultrasonic Gas Analysis and Flowmetering**

Saul Jacobson; *sauljay@gmail.com, Australia.*

Background, Motivation and Objective

Ultrasonic methods have important advantages in the measurement of gas flow, including the ability to measure almost any gas or gas mixture over a wide pressure range and turndown ratio. Ultrasonic gas flowmeters also are capable of measuring bi-directional flow and may be non-intrusive with no pressure loss. In certain cases the sensors may even be clamped on the outside of the pipe. Traditionally the Transit-time method has been used, but more recently interesting developments in Tag Cross-correlation have yielded promising results, particularly for low-pressure clamp-on applications. Ultrasonic flowmeters for gas have been commercially available since the 1980s, and they are widely accepted today for flaregas and stackgas monitoring and for a wide variety of industrial and fuel gas measurements. Highly accurate multi-path meters are approved and commonly used for custody transfer measurement of natural gas. In addition to the many advantages ultrasonic methods have in the measurement of the gas flowrate, ultrasonic propagation characteristics of the gas may also be measured to determine properties of the gas, such as its molecular weight, density or energy content.

Statement of Contribution/Methods

Soundspeed, in conjunction with temperature and pressure measurement were first used in the 1980s to determine the molecular weight and derive the mass flowrate of flaregas. Ultrasonic flowmeters for custody transfer natural gas gained acceptance in the 1990s with the publication of the American Gas Association AGA-9 report, which includes guidelines on the measurement and use of the gas soundspeed. More recently gas soundspeed and other properties such as attenuation have been used for the analysis of binary gases and pseudo-binary gases such as breathing gases, biogas, landfill gas, and process gases. Acoustic impedance has been measured and used to determine the density of high pressure gases.

Results

This paper reviews the methods to analyze binary, ternary and multi-component gases as well as presenting some new results from work conducted by the author and colleagues for biogas, consising primarily of methane and carbon dioxide at 100% RH.

Discussion and Conclusions

A review of the literature finds ultrasonic methods to be an effective means of gas flow measurement and analysis for many applications. The authors experiments found good correlation between ultrasonic methods and gas chromatography for the analysis of “simulated” as well as real biogas.

5E-2

11:00 AM **A New Calibration Method for Ultrasonic Clamp-On Sensors**

Oliver Keitmann-Curdes, Bernhard Funck; *Flexim GmbH, Berlin, Germany.*

Background, Motivation and Objective

Ultrasonic clamp-on flow meters operating with the transit time method use an acoustic calibration factor Ka, which determines the transmission angle in the fluid. Ka can be calculated as the ratio of the sound speed to the angle of transmission in the coupling wedge of the transducers. It can also be found by flow calibrating of the whole clamp-on flow meter at a test rig. The result of a flow calibration, however, depends on parameters as the pipe diameter and the flow profile that are not part of the meter to be calibrated.

The new method allows for direct determination of the acoustic calibration factor Ka. A change Dt of the transit time is produced by moving the transducers over a distance Dx. The acoustic calibration factor Ka then is the ratio of Dx to Dt. With this new method, transducers can be calibrated for a designated flow range and pipe range without the need of calibrated master flow meters and respective pipes and calibration rigs.

Statement of Contribution/Methods

We set up a test rig where a pair of transducers is mounted on a stepper motor axis. An aluminium reflector is mounted at a fixed distance beneath the aligned transducers in a water tank parallel to the stepper motor axis. For the electronics, standard transmitter, amplifier and receiver from Fluxus flowmeters are used for signal generation and reception. Signal processing is performed on a standard PC. The transducers are moved from one position to another and at each position, one pulse is transmitted and recorded. With the transducer positions, pulses, sensor and water temperature for one pair of measurements, the acoustic calibration factor Ka of the sensor can be calculated and thus the sensor can be calibrated.

Results

For the first measurements, different transducers were measured and the results were evaluated statistically. For reproducibility tests with one transducer (dismounted and mounted after each measurement) with 7 measurements, we achieved a medium calibration factor Ka of 4056.65 m/s with a relative standard deviation of 0.04 %. For tests with 18 different transducers of the same type, we achieved a Ka of 4057.81 m/s with a standard deviation of 0.30 %. This higher variation can be seen as a measurement for material parameter changes as the variation for a single transducers is much lower. All measured calibration factors are within the expected range regarding the specific materials used in the transducers.

Discussion and Conclusions

The general possibility of transducer calibration without the use of pipes with calibrated master flow meters could be demonstrated. The reproducibility of the measurements with relative standard deviations far below 1 % promise a stable and reliable calibration method. Especially for low frequency transducers designed for big pipes, the transducers can be easily and inexpensively calibrated in the factory. In the future, our new method will be cross-tested against our in-house calibration rigs with coriolis and IDM flow meters.

5E-3

11:15 AM **Analysis of inhomogeneous stress distribution in surface acoustic wave resonator for wireless blood pressure sensor**

Damien Hermelin[1], Mickael Bruniaux[1], Brahim Belgacem[2], Daniau William[1], Sylvain Ballandras[1]; *[1]Institut FEMTO-ST, Besancon, France, [2]Senseor, Besancon, France.*

Background, Motivation and Objective

Surface Acoustic Wave (SAW) filters and delay lines have been used in telecommunication electronic circuits for many years. The influence of environmental properties (temperature, pressure, etc.) on SAW properties nowaday are well known. Many research groups are exploiting the corresponding effects to develop SAW sensors. The purpose of the presented work is to benefit from the wireless capabilities of such sensors to implement a SAW wireless blood pressure sensor for post surgical follow-up.

Statement of Contribution/Methods

The first part of this work focuses on the design and fabrication of the SAW pressure sensor. The sensor consists of a supported free membrane on a bulk micromachined silicon wafer. The applied pressure modifies the stress in the membrane and hence the resonance frequency of the resonator.

The device is fabricated using standard silicon technologies and clean room facilities. The sensor is composed of an AT quartz plate and a silicon wafer assembled together using a wafer bounding technique. A SAW resonator is built on (AT,X) cut of quartz to benefit from high Q factors together with small thermal drift of the resonance. The resonator is designed to operate in the ISM band at 434MHz.

The second part of this work focuses on the modelling of the sensor. In order to generally analyse the evolution of SAW characteristics on quartz plate under distributed stress, a set of computation tools has been developed to couple a perturbation approach based on finite element analysis (FEA) with a mixed matrix analysis of the resonator electrical response. We then exploit stress sensitivity coefficients together with FEA results to derive the phase velocity associated to each cell of the resonator, as we assume that stress effects within a cell are homogenous. By cascading all the cell contributions, we obtain the admittance of the resonator under inhomogeneous stress. This approach has been developed to predict the influence of non-uniform stress distribution on the resonator's characteristics, i.e. the resonance frequency of course, but also the Q factor, the coupling strength and the impedance changes related to any velocity dispersion within the device.

Results

A pressure sensor prototype has been manufactured and allowed for ex-vivo oscillometric blood pressure measurements. Computation tools developed enable to determine frequency shift of the resonator induced by applied pressure and theoretical and experimental result are compared to demonstrate the accuracy of our analysis.

Discussion and Conclusions

Applying the pressure yields changes in the Q factor and the magnitude of the sensor response. This result is explained using our modelling approach considering the dispersion of the phase velocity induced by the pressure-dependent bending of the plate. Further development of this work will consist in testing in-vivo capabilities of our sensor.

5E-4

11:30 AM **A Novel Nozzle-Diffuser Micropump Actuated by Bubble Formation from Ultrasonic Cavitation**

Ching-Hsiang Cheng, Chen Chao, Yun Zhu, Wallace W. F. Leung; *The Hong Kong Polytechnic University, Research Institute of Innovative Products and Technologies, Hung Hom, Kowloon, Hong Kong, China.*

Background, Motivation and Objective

Low-frequency ultrasound can cause cavitation to generate microbubbles that can be used to actuate a nozzle-diffuser micropump. A similar method of using thermal bubble to actuate the micropump has been reported. Compared with thermal bubbles, cavitational bubbles occur when the local pressure falls below the saturated vapor pressure. This can generate bubble without heating up the pumped fluid. Cavitation can also be induced through the fluidic medium to separate the ultrasonic transducer from the micropump, which can be applied for implantable micropump applications.

Statement of Contribution/Methods

In this paper, we study the nozzle-diffuser micropump that is actuated by the bubble generated from ultrasonic cavitation (Figure 1). The micropump was formed by molding of polydimethylsiloxane (PDMS) elastomer from the patterned SU-8 photoresist on an acrylic substrate. Two pieces of metal tubes were inserted to become inlet and outlet. The molded pump chamber was then bonded to a piece of blank PDMS substrate with the surface activated by oxygen plasma to create a permanent bond. The fabricated micropump is now ready for testing in a ultrasonic cleaner to create bubble inside the pump chamber.

Results

The fabricated micropump has shown a good seal to be filled with water through the inlet and outlet (Figure 2). Vapor bubbles can be formed in the pump chamber when dipping the micropump into the ultrasonic cleaner to induce water cavitation. Different angles of nozzle/diffuser have been designed to optimize the flow rate and back pressure.

Discussion and Conclusions

The surface of the PDMS can be damaged by the cavitation due to its lower stiffness and strength. A coating of parylene is used to increase its surface stiffness as well as provide airtight seal to prevent permeation of fluidic vapor through the PDMS wall.

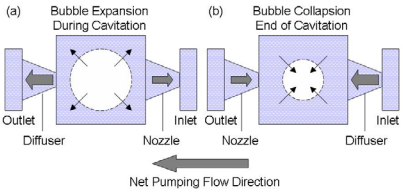

Figure 1: Operation principle of the cavitational micropump, (a) during cavitation, the bubble expands to push the fluid outward that makes the left channel to be diffuser and the right one to be nozzle, which generates a net pumping flow to the left, (b) when ends of cavitation, the bubble collapses to pull the fluid inward, which also gives a net pumping flow to the left.

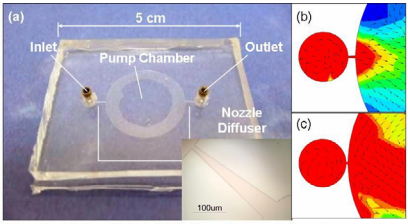

Figure 2: (a) The fabricated PDMS micropump that can be actuated by microbubble generated from ultrasonic cavitation. (b) The simulated result from "Cosmos Floworks" shows flow pattern with 10° nozzle/diffuser angle that is more directional than the (c) 45 ° nozzle/diffuser angle.

6E. Ultrasonic Wave Propagation - I

Hall 2C

Tuesday, November 4, 2008, 10:30 am - 12:00 pm

Chair: **Georg Mansfeld;**
Russian Academy of Sciences, Russia.

6E-1

10:30 AM **Non-axisymmetric ultrasonic guided waves in an embedded waveguide**

Yaacoubi Slah[1], Laguerre Laurent[1], Ducasse Eric[2], Deschamps Marc[2]; [1]*LCPC, RMS, Bouguenais, Nantes, France,* [2]*Imp, Talence, Bordeaux, France.*

Background, Motivation and Objective

In many fields such as civil engineering, mechanical engineering or aeronautics, ultrasonic guided waves are applied in non-destructive evaluation to detect defects in waveguides. They permit to auscultate complex configurations over long distances. A necessary step before detecting defects is to be able to calculate the propagated elasto-dynamical field in healthy waveguides. Hence, the objective of this work is the calculation of this field propagating in a solid cylindrical waveguide embedded in solid medium with the aim of NDE.

Statement of Contribution/Methods

The incident field is generated at the end of the cylinder by a force or velocity source which is Gaussian distributed. For generating non-axisymmetric waves, this source is an off-axis.

First, we decompose this field with respect to the angular position through the combination of vector Hankel transform of order and Fourier series.

Then, each component is decomposed into an infinite sum of rays, i.e. elementary generalized conical waves. These waves undergo multiple reflections with the guiding surface of the waveguide. We use the Generalized Debye Series (GDS) for calculating the global reflection coefficients resulting from these multiple reflections. In a final step, the total field is synthesized by the summation of the incident and reflected rays.

Results

Many outputs of this code can be exploited like velocity field, stress field, energy field in 2D or 3D simulations. Furthermore, time or frequency representations of these fields can be drawn. Special attention is given for the kinetic and potentials energies for many circumferential orders n. (k,f) dispersion diagrams obtained by this code are compared with the results of the DISPERSE Software.

Discussion and Conclusions

Dispersion diagrams (amplitude velocity as a function of wavenumber(k)and frequency f)agrees well with curves dispersion plotted by Disperse software which base on modal decomposition. In addition, by the type of the source excitation(longitudinal,shear or both),some curves branches among all are created. Simulated diagrams traced for some inspection domains (with respect to z-propagation)shows an attenuation due to the leakage in embedding medium. This embedding hasn't the same behaviour with respect to frequency. This behaviour is the same for all waves (axisymetric and non-axisymmetric). In other hand,the non-axisymmetric waves are highlights Energy Bilan. Indeed, for some source positionning, non-axisymmetric waves are generated and have an energy bigger than that of the axisymmetric waves. Therefore, an attention should be paid to non-axisymmetric waves for both source loading and defect detection and characterization.

6E-2

10:45 AM **The acoustoelastic effect of Love waves in elastic-plastic deformed layered rocks**

Jinxia Liu, Zhiwen Cui, **Kexie Wang;** *Jilin University, Changchun, China.*

Background, Motivation and Objective

Love wave, one of most important surface waves, has been widely used in geophysical and geotechnical engineering. In seismic reservoir characterization, effects of stresses and plastically yielded rocks are becoming more recognized. How does the statically deformed state including the elastic and plastic strains induced by applied stresses influence on the phase velocities of Love waves in the layered rocks? We do not know that. In this paper, we attempt to investigate the acoustoelastic effect of Love waves in layered rock with elastic and plastic deformations induced by applied uniaxial stresses on substrates.

Statement of Contribution/Methods

The influence of elastic and plastic strains caused by static deformations on the Love wave propagation in layered rocks is studied based on the acoustoelastic theory for elastic-plastic materials. The material is isotropic in the absence of static deformations in this paper. The dispersion equation of Love waves is obtained by direct boundary conditions.

Results

The acoustoelastic effect of Love waves within a Castlegate layered sandstone deposited on a Berea sandstone is investigated. The results show that there are seven, five and six modes for fh ≤ 6000m/s when the Castlegate layered rock is unstressed state, undergoes statically elastic and elastic-plastic strains, respectively. The phase velocity obviously increases compared with that of unstressed state when the Castlegate layered rock undergoes statically elastic deformation, and decreases compared with that of statically elastic deformation when the layered rock undergoes elastic-plastic strains induced by static deformation. Acoustoelastic effect increases rapidly with the product fh for the layered rock subject to both the elastic and elastic-plastic deformations and approximates a constant value, for thick layer or high frequency limit.

Discussion and Conclusions

The elastic-plastic deformation in the Castlegate layered rock obviously modifies the phase velocity of Love waves and the cutoff point for the high-order modes. However, the change in phase velocity in the elastic-plastic deformed layered rocks is smaller than that in upper-layered rocks only subject to elastic deformations.

6E-3

11:00 AM **Diffraction divergence of SH_0 wave in thin piezoelectric plate of lithium niobate**

Boris Zaitsev, **Andrei Teplykh;** *Institute of Radio Engineering and Electronics of RAS, Saratov Branch, Saratov, Russian Federation.*

Background, Motivation and Objective

Previously anisotropy of an angle between phase and group velocity (PFA) for SH_0 waves in thin $LiNbO_3$ plate and influence of electric boundary conditions on the value of this angle have been studied. The calculations were carried out under condition that the aperture of the wave was infinite. However, the real source of SH_0 waves have always finite sizes. The present paper is devoted to theoretical investigation of the intensity of the acoustic field launched by such source of the finite size and to comparison of theoretical results with experimental data.

Statement of Contribution/Methods

Well known method of calculation of characteristics of acoustic waves in piezoelectric plates assumes that these characteristics and properties of piezoelectric plate itself do not vary in a direction perpendicular to the propagation direction of a wave. However, in real experiments the width of acoustic beam is always limited. In our previous experiment the width of a beam near a source was equal to the effective length of finger overlapping of radiating IDT which was equal 2a=9.8mm. Measurements were carried out in a pulse regime with pulse duration of 5 mks, that allowed to neglect by the reflection of a wave from plate boundaries. We have investigated the diffraction effects caused by finite width of a beam on boundless plate. The SH_0 wave under study has strongly shear-horizontal polarization and wavelength is much greater than plate thickness. This allows to consider only shear-horizontal component of mechanical displacement, which does not depend on depth (coordinates z). In this case we can present the vector function of mechanical displacement as scalar function U(x,y). These assumptions simplify the problem and it looks as problem of diffraction of light on slit in optics, described by Fresnel's formulas. Amplitude U(x, y) is superposition of waves, launched by set of the dot sources located on a linear source $|y|\leq a$ at x=0 having the same frequency ω and known the values of amplitude and a phase of U(0,y). In this work we

Tuesday Oral

assume that U on the source has constant amplitude and phase, namely U(0,y) =1 while |y|≤a and U(0,y) =0 while |y|>a.

Results

Using the described method, we computed profiles of amplitude of SH_0 wave on different distances from source and compared them with experiment. We have found that the given simplified theory correctly explains qualitative behavior of a beam: diffraction divergence and movement of maximum of amplitude in a direction of group velocity, but quantitative agreement between theory and experiment is poor.

Discussion and Conclusions

Bad agreement may be explained by the fact that real IDT consists of several finger pairs and one should consider their contribution to the amplitude of mechanical displacement on source x=0. In this case the specified function U (0,y) will be much more complicated.

Teplykh A.A. thanks Russian science support foundation for financial support.

6E-4

11:15 AM **High frequency wave propagation in structured materials: modelling results**

Roger Young[1], Paul Harris[1], Andrew Dawson[2], Frederic Lecarpentier[1]; *[1]Industrial Research Ltd, New Zealand, [2]Victoria University, New Zealand.*

Background, Motivation and Objective

Image resolution is improved with high probing frequencies, which, however, may be significantly influenced by material microstructure. In this paper we consider ultrasound propagation in an immersed porous aluminium plate which we model as a periodic structure containing water-filled fibre-like pores which are typically a few microns in diameter, and some millimetres in length (across the thickness of the plate).

Statement of Contribution/Methods

A plane wave or point source in the liquid zone (outside the plate) emits a high frequency

(50 MHz) wave packet which is then incident upon the plate along one side. Finite element modelling shows how the incident wave interacts with the plate, and is coupled to the modes which determine the energy propagation within the porous solid.

Results

Both reflected and transmitted waves are generated, and strong transmission persists well beyond the critical angle for aluminium. Within the porous multilayer structure the modelling shows the existence of at least two symmetric modes, fast and slow respectively. For both modes the energy is distributed across the entire composite, that is, fast and slow waves are present in both the solid and the liquid-filled pore space. The energy distribution is strongly dependent on the ratio of pore diameter to pore spacing. The demonstration of our results is assisted by several action sequences which show the various interactions in dynamic form. Some preliminary analytic results support the finite element computations.

Discussion and Conclusions

The modelling component of our investigation has already provided valuable insight and guidance for our experimental program which deals with high frequency ultrasound propagation in structured solids. Further computational and analytic modelling work is planned.

6E-5

11:30 AM **Wireless Drive of a Piezoelectric Plate by Dipole Antenna**

Satyanarayan Bhuyan, Junhui Hu; *Nanyang Technological University, Singapore.*

Background, Motivation and Objective

In most applications of piezoelectric devices, electric energy is applied to the devices via lead wires soldered on the electrodes of piezoelectric components. But the lead wires may fall off at large vibration and high input voltage, and this causes the breakdown of piezoelectric devices. Thus, there is a need to introduce a wireless approach to apply electric energy to the piezoelectric devices. Wireless drive of a piezoelectric plate using an electric dipole antenna is explored in this work.

Statement of Contribution/Methods

To transmit relatively large electric energy to a piezoelectric plate, an electric dipole antenna in series with an inductor is used as shown in Fig. 1. The ac electric field, produced by plate-shaped live and ground electrodes of the antenna is transmitted to the piezoelectric plate placed 6 mm away form antenna plane. The separation between antenna electrodes is 5 cm. The electric resonance of dipole antenna with an inductor generates a large voltage across the dipole antenna.

Results

Fig. 2 shows the frequency characteristic of the output power of the piezoelectric plate operating in the thickness mode. At resonance frequency 772 kHz of the plate, a maximum output power of 12mW is achieved when the dipole antenna is in series electric resonance with an inductor because of the large voltage 1436Vrms across the antenna for an input voltage source of 150Vrms. The power transmitted to the load drops as the plate is detuned from resonance. An equivalent circuit of the wirelessly driven piezoelectric plate operating in the thickness mode has been developed. It is known that the circuit has a current source, resulting from the electric field which is different from the conventional piezoelectric plate driven by a voltage applied via lead wires.

Discussion and Conclusions

A piezoelectric plate operating in the thickness mode is wirelessly driven by the electric field generated by a dipole antenna. At resonance a maximum output power of 12mW is achieved with an electrode area of 900 cm ^{2} , input source voltage of 150Vrms, and 6mm from the antenna plane. An equivalent circuit of the wirelessly driven piezoelectric plate is derived which has a current source, resulting from the external electric field.

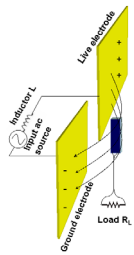

Fig.1. Experimental setup

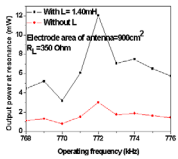

Fig.2. Frequency Characteristics

6E-6

11:45 AM **Thermoacoustic Effect in Thin Metallic Film Contacting with Liquid**

Valeriy Andreev[1], Vladimir Vdovin[2]; [1]*Moscow State University, Physics Department, Moscow, Russian Federation,* [2]*Institute of Radio Engineering and Electronics, Moscow, Russian Federation.*

Background, Motivation and Objective

Microwave radiation in a form of short pulses with 0.1 – 10 ns duration is widely employed for study of radiation - matter interaction. Knowledge of waveform of the pulses is very important for prediction and understanding of physical effects resulted from radiation-matter interaction. We propose to use the thermoacoustic effect for registration of the temporal profiles of short microwave pulses. Under certain conditions the acoustic pulse generated due to thermoacoustic effect can precisely resemble the waveform of the microwave pulse. In particular, a depth of microwave absorption should be much smaller compared to a distance of sound propagation n the course of pulse duration. We demonstrated that a system composed of thin metallic film contacted with liquid can be employed for design of new detector of microwave nanosecond pulses.

Statement of Contribution/Methods

Thermoacoustic effect was studied in thin aluminum films placed in contact with water or ethanol. Aluminum films were deposited onto quartz substrate and their thicknesses were varied in the range 1 - 10 nm. It was shown both theoretically and experimentally that microwave radiation with 5 -30 mm wavelength is absorbed with efficiency up to 60% in the system composed of quartz - aluminum films – water, whereas maximum efficiency is observed in the films of 2 – 2.5 nm thickness. The 8-mm wavelength microwave pulses of 10-ns duration were directed onto layered system quartz – aluminum film – liquid and resulted acoustic pulses were detected with wideband ultrasonic transducer.

Results

At small energies of microwave pulses the detected acoustic signal had a form of unipolar pulse of 18 ns duration. The most effective thermoacoustic generation was observed in the 3.5 nm aluminum film. The efficacy of acoustic generation increased almost 10 times when ethanol was placed in contact with the aluminum film. Generation of acoustic pulses in nonlinear regime was observed when microwave pulse energy exceeded 0.8 mJ and when cone energy concentrator was used. Peak pressure of the acoustic pulse was increased 3-5 times compared to one in linear regime. The pulse profile became asymmetrical: duration of the pulse droop was 5–8 times longer than duration of the pulse front.

Discussion and Conclusions

Theoretical analysis was performed with the use of two-step approach. At the first step the quantity of heat released within the metallic film – liquid due to absorption of microwave energy was calculated. Heat distribution in the system was defined by solving the thermo-conductivity equation. The waveform of acoustic pulse was defined on the base of calculated heat sources. The resulted theoretical profiles are almost identical to microwave ones up to 0.1 ns pulse durations. Duration of the measured acoustic pulses (18 ns) was almost 2 times longer compared to duration of microwave pulse. It was explained by a limited frequency bandwidth of the PVDF transducer (60 MHz).

1F. 3-D Elasticity Imaging

Hall 3

Tuesday, November 4, 2008, 1:30 pm - 3:00 pm

Chair: **Anne Hall;**
General Electric Medical Systems, USA.

1F-1

1:30 PM **Three Dimensional Elastic Modulus Reconstruction for Non-invasive, Quantitative Monitoring of Tissue Scaffold Mechanical Property Changes**

Michael Richards[1], Claire Jeong[2], Scott Hollister[2], Jonathan Rubin[1], Kang Kim[3], [1]*University of Michigan, Department of Radiology, Ann Arbor, MI, USA,* [2]*University of Michigan, Biomedical Engineering, USA,* [3]*University of Pittsburgh, Cardiovascular Institute, USA.*

Tuesday Oral

Background, Motivation and Objective

The field of tissue engineering requires improved methods to monitor tissue growth and function as well as degradation of biomaterial scaffolds following implantation. Invasive methods, such as histology or direct mechanical measurements, are not ideal and non-invasive techniques, such as MRI, CT or US, may only provide morphological information. However, 3D US based Elasticity Imaging (UEI) can provide quantitative mechanical property information to characterize the structure and composition of the tissue and scaffold.

Statement of Contribution/Methods

Porous Poly (1, 8 Octanediol-co-Citrate) scaffolds (D 6 x H 4 mm, porosity=50%) were fabricated. The scaffolds were imbedded in gelatin phantoms and imaged using a 3D scanning system and a commercial linear US probe (Sonix RP, Ultrasonix). 3D RF data was acquired as the phantom was subjected to a quasi-static compression (~5% strain). The elevational increment was 0.4 mm. The scaffolds were imaged before and after a degradation, via agitation in PBS, of ~5% by weight. Independent mechanical measurements were also performed on the scaffolds and gelatin.

An image registration algorithm was developed to measure the 3D displacement field from sets of US images of deforming material. This algorithm minimizes US RF intensities of pre and post deformation images as the pre-deformation image is artificially deformed by the desired displacement. A second algorithm recovers the shear elastic modulus distribution of the material by efficiently solving the 3D inverse problem. This algorithm minimizes the difference in the measured displacement and that predicted by an incompressible, linear elastic model and the desired modulus distribution.

Results

Modulus values of the scaffolds, relative to background, decreased 25% after degradation. US B-mode and UEI images of one scaffold before ((a), (b)) and after ((c), (d)) degradation are shown in figure 1. The modulus values in figure 1(b) and (d) are normalized to the background value.

Discussion and Conclusions

The reconstructed elastic moduli compare well with the direct mechanical measurements. The resulting modulus images can provide an accurate representation of the mechanical property changes of the engineered tissue. UEI, utilizing 3D elastic modulus reconstruction algorithms, may improve the state of the art for non-invasive monitoring of artificial tissue growth in vivo.

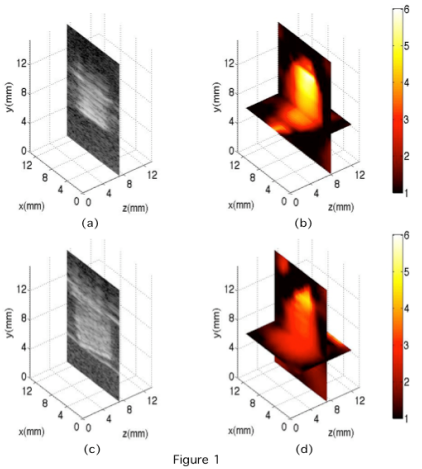

Figure 1

1F-2

1:45 PM **Towards Three-dimensional Acoustic Radiation Force Impulse (ARFI) Imaging of Human Prostates *in vivo***

Liang Zhai[1], Jeremy Dahl[2], Kathy Nightingale[2]; [1]*Duke University, Biomedical Engineering, USA,* [2]*Duke University, USA.*

Background, Motivation and Objective

It has been a challenging task for current imaging modalities to identify cancerous regions within the prostate. Past studies have showed that prostate cancer is stiffer than normal prostate tissues, which provides opportunities for elasticity imaging techniques to detect prostate lesions. Recent studies reported improved prostate cancer detection rates for elastography-guided needle biopsies. Our previous *ex vivo* study demonstrated that ARFI imaging using a VF10-5 linear array was able to visualize the internal anatomy and suspicious lesions in the prostate, which may help improve the diagnostic accuracy of prostate needle biopsy. The objective of this study is to implement ARFI techniques on a 3D wobbler rectal probe that can be used for *in vivo* prostate biopsy guidance.

Statement of Contribution/Methods

A modified Siemens Antares^{TM} scanner and a 3D wobbler rectal probe, EV9F4, are used for this study. The ARFI excitation pulses utilized a focal depth 20 mm, F/#2.0, center frequency 4.7 MHz and 2 X 200 cycles. 4:1 parallel receive was used to reduce the number of push locations. The intensity field was measured in water. Linear extrapolation of derated small values at low power was used to estimate the *in situ* intensity, which was then compared to that of the VF10-5 linear array with settings used for the *ex vivo* studies. ARFI images were acquired with both probes in a homogeneous tissue mimicking phantom to compare the displacements. During 3D ARFI imaging, the internal wobbler motor was programmed using varying delays between data acquisitions. In order to evaluate motion artifacts, a heterogeneous tissue-mimicking phantom was imaged with the delay time ranging from 1 s to 30 s between two adjacent elevational planes. Finally, the system was tested with excised human prostate specimens.

Results

The extrapolated derated (α= 0.7dB/cm/MHz) *in situ* I_{sppa} at focal depth is 3216 w/cm^2, which is about 47% of that used in our *ex vivo* study with the VF10-5 linear array. The corresponding ratio of maximum displacements is 42%. During the motion test, the boundaries of 5 spherical inclusions (E = 31 kPa, D = 3mm) in the heterogeneous phantom (background E = 4 kPa) are clearly visualized with all delay settings. No motion artifacts were observed. With 50 excitation locations (3.6 cm in lateral FOV), the system can perform 3D data acquisition for an average human prostate within 3 minutes with the minimum delay setting (1 s) between adjacent planes. The system

generates an average displacement of 4 µm within the peripheral zone in excised human prostates for structural visualization.

Discussion and Conclusions

With fast 3D data acquisition and sufficient displacements in the peripheral zone of human prostates for structural visualization and lesion detection, the system will be adequate for imaging human prostates *in vivo*.

1F-3

2:00 PM **Full 3D Elasticity Reconstruction Using Supersonic Shear Imaging**

Jeanluc Gennisson[1], Nicolas Felix[2], Thomas Deffieux[1], Jeremy Bercoff[2], Mickael Tanter[1], Mathias Fink[1];
[1]Laboratoire Ondes Et Acoustique, Paris, France, France, [2]Supersonic Imagine, France.

Background, Motivation and Objective

3D information is known to circumvent the operator-dependent aspects of 2D echography diagnosis. Moreover, it was recently shown that the combination of 2D echography and elastography could be a promising tool for in vivo breast cancer diagnosis. In this paper we present a new approach using translated 2D acquisitions with supersonic shear imaging (SSI) technique allowing the 3D volume reconstruction of the investigated medium. The aim of this work is to demonstrate the feasibility of reconstructing both 3D B-mode and elasticity volumes using this translation/rotation approach.

Statement of Contribution/Methods

The SSI technique is based on the combination of a radiation force induced in tissue by an ultrasonic beam and an ultrafast imaging sequence capable of catching in real time the propagation of the resulting shear wave. The local shear wave velocity is recovered using a time of flight algorithm enabling 2D mapping of shear elasticity. Based on a translated 2D plan a new system with a rotary stepper motors was built and used on a calibrated phantom exhibiting harder inclusions for elastography experiments (Madsen et al., UMB, 2006). The ultrasound probe rotates around the phantom and allows for each position (5° step) to recover B-mode images as well as elasticity maps. Then using a regridding algorithm, the full 3D volume of the phantom is reconstructed. In order to compare the geometry obtained with this method, the 3D volume of the phantom was also scanned with a magnetic resonance (MR) device.

Results

Results on calibrated cylindrical phantom are presented for SSI technique. Elasticity maps are reconstructed and values of shear modulus are in good agreement with the ones given by the manufacturer (~25 kPa in hard inclusions, ~12 kPa in parenchyma and ~7 kPa in fat). The geometry of the phantom is well defined and it is shown that the elasticity map and geometry obtained with the SSI technique match very well with the MR magnitude images of the phantom. This study allowed the experimental validation of this new complete 3D US-Elastography approach. Finally the SSI 3D technique is presented on a realistic breast phantom (CIRS, model 059), where advantages of a partial scan of the phantom with elasticity and geometry reconstruction on designated inclusions are reported.

Discussion and Conclusions

The translated SSI technique allows to acquire a full 3D volume in a very short time (<10 min) compared to current 3D system, as for example MR-Elastography (MRE) (~1 h 30 min), for the same volume of acquisition. Moreover, the reconstructed geometry of the investigated medium is well defined and the ultrasound-based resolution of elasticity maps is of the order of one millimeter. Finally, as shown on the breast phantom, using the 2D US based translated approach implemented in a sectorial volume, the full geometry of a 3D inclusion can be imaged and assessed precisely in terms of elasticity in a much reduced time acquisition (<1 min), which is quite important for in vivo acquisition.

1F-4

2:15 PM **3D Strain Imaging Method Dedicated to Large Deformations and Freehand Scanning**

Jean-François Deprez[1], Elisabeth Brusseau[2], Olivier Basset[3]; [1]*Creatis, Lyon, France,* [2]*Creatis - CNRS, Lyon, France,* [3]*Creatis - Université Lyon 1, Lyon, France.*

Background, Motivation and Objective

Ultrasound elastography is now recognized as a promising technique for tissue characterization. Accurately estimating the strain is one of the fundamental challenges in elastography, since the clinician's diagnosis will rely on these estimations.

Yet, most of the techniques used in elastography remain mono- or bi-dimensional and may lead to noisy elastograms if significant lateral or out-of-plane motion occurs.

Moreover, the recent development of 2D (matrix-shaped) transducer arrays to acquire 3D ultrasound data provides new prospects for medical ultrasound applications and in particular for elastography.

Our objective is therefore to develop a 3D technique, to accurately estimate biological soft tissue deformation under load from ultrasound RF volume acquisitions.

Statement of Contribution/Methods

The proposed method is based on a 3D deformation model of the tissues. It locally computes axial strains while considering lateral and elevational motions. Unlike most of other techniques that model the compression-induced local displacement as a 3D shift, our model also locally considers an axial scaling factor in addition to a 3D translation.

Deformation parameters are locally estimated as those maximizing a similarity criterion between an initial region and its deformed version, when the latter is compensated for according to these parameters. Parameter estimation, formulated as a maximization problem under constraints, is processed thanks to a sequential quadratic programming methodology.

Results

The performance of our algorithm was both assessed with simulated and experimental data.

Simulations reproduce the case of a basic homogeneous medium subjected to compressions. A comparison between our 3D method and its 2D counterpart is led, and demonstrates the advantage of considering a 3D approach, especially when significant out-of-plane motion occurs. In 3D, accurate estimations are indeed obtained in a large range of deformations from 0 to 12 %, whereas 2D elastograms become noisy above 4 %.

Ultrasound volumes were then acquired during freehand scanning on a calibrated CIRS phantom dedicated to elastographic studies. The corresponding experimental results enable to perfectly discriminate the hard inclusions embedded in the medium even in configurations inducing large out-of-plane motion. Their boundaries are also clearly identified thanks to the visualisation of a 3D volume.

Discussion and Conclusions

A 3D strain estimation technique has been introduced in this paper. Results on simulated and experimental data demonstrate the ability of our algorithm to provide accurate elastograms. The 3D approach reduces significantly the artefacts on elastograms and remains robust with large deformations and freehand scanning.

1F-5

2:30 PM **Deconvolution and elastography based on 3D ultrasound**

Richard Prager, Andrew Gee, Graham Treece, Joel Lindop, Nick Kingsbury; *University of Cambridge, Department of Engineering, United Kingdom.*

Background, Motivation and Objective

This talk is in two parts and addresses two ways of getting more information out of the RF signal from a 3D mechanically-swept medical ultrasound scanner. The first topic is the use of non-blind deconvolution to improve the clarity of the data, particularly in the direction perpendicular to the individual B-scans. The second topic is strain imaging. We present a robust and efficient approach to the estimation and display of axial strain information.

Statement of Contribution/Methods

For deconvolution, we calculate an estimate of the point-spread function at each depth in the image using Field II. This is used as part of an EM framework in which the ultrasound scatterer field is modelled as the product of (a) a piece-wise smooth and (b) a fine-grain varying function. In the E step, a Wiener filter is used to estimate the scatterer field based on an assumed piece-wise smooth component. In the M step, wavelet denoising is used to estimate the piece-wise smooth component from the scatterer field.

For strain imaging we use a quasi-static approach with efficient phase-based algorithms. Our contributions lie in robust and efficient 3D displacement tracking, point-wise quality-weighted averaging, and a stable display that shows not only strain but also an indication of the quality of the data at each point in the image. This enables clinicians to see where the strain estimate is meaningful and where it is mostly noise.

Results

For deconvolution we will present in-vivo and in-vitro images and simulations with quantitative performance measures. For example, with the blurred 3D data taken as 0dB, we get an improvement of 5.68dB with a Wiener filter alone, 5.90dB with ForWaRD and 7.45dB with our EM algorithm. For strain imaging we will show images based on 2D and 3D data and show how full 3D analysis can be performed in about 20 seconds on a typical computer. We will also present initial results of our clinical study to explore the applications of our system in our local hospital.

Discussion and Conclusions

We have shown that it is possible to use fast phase-based algorithms to provide accurate, stable images. With appropriate point-wise persistence, sufficiently clear and stable images can be presented in real-time to be of clinical interest. Our study of deconvolution with a spatially-varying point-spread function indicates that such algorithms may soon be fast enough to be a cost effective way of improving medical ultrasound images.

2F. Ultrasound Mediated Delivery of Therapeutic Agents

Room 201 A/B/C

Tuesday, November 4, 2008, 1:30 pm - 3:00 pm

Chair: **Larry Crum;**
University of Washington, WA, USA.

2F-1

1:30 PM **An In vivo Investigation of the Use of Pulsed High Intensity Focused Ultrasound for Thrombolysis**

Kullervo Hynynen[1], Cameron Wright[1], David Goertz[2]; *[1]Sunnybrook Health Sciences Centre, Canada, [2]Sunnybrook Health Sciences Centre, Imaging Research, Toronto, Ontario, Canada.*

Background, Motivation and Objective

The majority of sonothrombolysis work to date has used ultrasound to enhance the action of enzymes, or by cavitating contrast agents. In stroke applications, it would be desirable to avoid the serious side effects of tPA, and it may also be useful to not employ contrast agents. It has been previously reported that it is possible to employ pulsed high intensity 0.5 MHz ultrasound in the absence of enzymes, but with a limited exploration of parameters. Such high intensity approaches are viable for use in peripheral blood vessels and, with recent advances in techniques for transcranial therapeutic ultrasound delivery, and may also be possible to employ in the context of stroke therapy. The primary purpose of this work is to investigate the conditions under which high intensity focused ultrasound induces thrombolysis in vivo.

Statement of Contribution/Methods

Experiments were conducted using a rabbit femoral artery clot model initiated by the injection of thrombin. Single element spherically focused air backed transducers were employed, with transmit frequencies of 0.68 MHz (n=23) or 2.0 MHz (n=31). Pulse durations of 10 milliseconds were employed with sonication periods of 60 seconds and pulse repetition frequencies ranging from 1 to 5 Hz. Flow restoration percentage was used as an indicator of success for thrombolysis. Vessels were then excised and inspected for evidence of damage. In some experiments a high frequency (30MHz) ultrasound B-scan and pulsed-wave Doppler system was used to provide information about clot size, the presence or absence of flow, and displacements.

Results

The experiments demonstrated it is feasible to achieve vascular reflow with pulsed HIFU induced thrombolysis at both 0.68 and 2.0 MHz. At 0.68 MHz, there was evidence of the presence of vascular damage for conditions that also produced vascular reflow. At 2 MHz, vascular damage was only observed at the highest transmit levels (410 W acoustic power), while between 47 and 270 W vascular reflow was achieved in the majority of vessels. The results also show that it is possible to measure clot displacements induced by radiation pressure of the therapeutic beam with high spatial resolution and sensitivity.

Discussion and Conclusions

It is feasible to perform in vivo thrombolysis using high intensity focused ultrasound in the absence of tPA and contrast agents without vessel damage at a frequency of 2.0 MHz.

2F-2

1:45 PM **The size of pores on the cell membrane generated in sonoporation**

Yun Zhou, Cheri Deng; *University of Michigan, Biomedical Engineering, Ann Arbor, Michigan, USA.*

Background, Motivation and Objective

Sonoporation generates transient pores on the cell membrane and has been explored as a promising intracellular drug and gene delivery strategy. The pore size in sonoporation determines the size of molecules or agents that can be delivered using the technique, but has not been readily available due to the challenge in measuring the dynamic submicron pores. Post ultrasound assays such as AFM, or SEM, often time consuming and requiring much effort, are sometime used to gauge pore size but are limited to static measurements that may not be accurate. We have previously demonstrated the utility of voltage clamp techniques to monitor sonoporation in real time from the transmembrane current (TMC) change during sonoporation. The TMC of cells under voltage clamp during sonoporation can potentially provide relevant information of the pore size.

Statement of Contribution/Methods

Using single Xenopus oocytes as the model system, whole cell voltage clamp techniques were employed to measure the TMC change during sonoporation (0.2s, 0.3MPa, 1 MHz) of single cell in solution in the presence of Definity microbubbles. By controlling the microbubble concentration, two distinct sets of experiments were designed and conducted to measure the TMC of a single pore and the TMC corresponding to multiple pores, where the number of pores was obtained from analysis of Poisson statistics. An electro-diffusion model was developed to relate the TMC with pore size from the ion flow through the pores on the membrane.

Results

The probability of having single pore was achieved in experiments where the chance of TMC change was reduced to < 0.117, which corresponded to the mean of Poisson distribution at 0.1249. Therefore, the probability of having single pore was calculated to be 93.9% in this set of experiments. The measured maximum TMC amplitudes for a single pore has a mean of 288.6nA and a standard deviation of 225.6nA (n=33). The overall distribution of TMC showed Gaussian characteristics, with 15 of 33 data distributed within 100±100 nA. For experiment involving multiple pores, the mean number of pores was 5.5, estimated from the least square fitting of the measured TMC (n=85) with single pore TMC assuming the number of pores following Poisson distribution. The mean and standard deviation of single pore size was then estimated from an electro-diffusion model from the measured TMC values in this study and were in the order of 1 μm with ~ 50% standard deviation.

Discussion and Conclusions

The distribution of TMC corresponding to a single pore during sonoporation was obtained assuming Poisson statistics. An electro-diffusion model related the pore size and TMC. These results are the first estimation of pore size using real time voltage clamp measurements. The results need to be validated by independent measurements from deterministic experimental conditions involving known bubble number and location, and other direct measurements such as TEM results.

2F-3

2:00 PM **Enhancement of Antiangiogenic Gene Therapy on Hepatocellular Carcinoma by Endostatin and Sonoporation**

Kun-Che Tsai[1], Lih-Hwa Hwang[2], Shu-Jyuan Yang[1], Che-kang Liao[2], Win-Li Lin[1], Ming-Jium Shieh[1], Wen-Shiang Chen[3]; *[1]National Taiwan University, Institute of Biomedical Engineering, Taipei, Taiwan, [2]National Taiwan University, Institute of Microbiology, Taipei, Taiwan, [3]National Taiwan University Hospital, Department of Physical Medicine and Rehabilitation, Taipei, Taiwan.*

Background, Motivation and Objective

Antiangiogenic gene therapy is a promising approach to inhibit neovascularization via angiogenesis, the growth of new blood vessels from preexisting ones. In recent years, hepatocellular carcinoma (HCC) is considered as one of the suitable targets for anti-angiogenic approaches due to its highly neovascularization. On the other hand, ultrasound is believed to be a novel and effective tool to locally deliver gene into target tumors. The purpose of this study is to evaluate the efficacy of employing therapeutic ultrasound (TUS) to deliver genes encoded with an anti-angiogenic factor, endostatin (ED), to suppress the growth of a preclinical HCC model, the inoculated subcutaneous tumor model.

Statement of Contribution/Methods

BALB/c mice were inoculated subcutaneously with HCC, which were then treated with TUS after intramuscular or intratumoral injection of ED+SonoVue, daily or weekly (totally four times each). Tumor growth was evaluated by weight periodically.

Results

The daily intramuscular injection group led to a 40% inhibition in tumor growth, but that through intratumoral injection was 56% (Fig. 1a). Weekly intramuscular and intratumoral injections resulted in a significantly better inhibition of HCC growth up to 74% and 70%, respectively (Fig. 1b).

Discussion and Conclusions

Preliminary in-vivo studies showed that gene product could be found for a week after one ultrasonic transfection. Weekly treatment, either intramuscularly or intratumorally, ensured a sustained ED release and thus a significant better suppression of HCC growth, comparing with treating daily. Daily intratumoral treatment produced 16% more inhibition comparing with treating intramuscularly, which might be related to direct injury of tumor tissue by TUS+SonoVue. Moreover, weekly intramuscular resulted in a slightly increment of HCC suppression (4%), probably due to better transfection in muscular than tumor tissue. These results depict the efficacy of therapeutic ultrasound as a non-viral technology to efficiently deliver genes to tumors by weekly intramuscular treatment approach, and to deliver angiogenic inhibitors to HCC in particular.

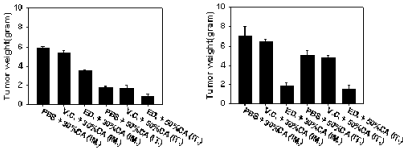

Figure 1. The tumor weight at the end of experiment after treatment with TUS+ED+SonoVue. (a) Daily treatment; (b) Weekly treatment.

2F-4

2:15 PM **Efficacy of Sonophotodynamic therapy (SPDT) mediated to Liposomal Zinc phthalocyanine on a colon carcinoma tumor model**

***A. Sazgarnia*[1]**, *M. H. Bahreyni-Toosi*[1], *M. Bakhshizadeh-Feyz Abadi*[2], *A. R. Khooie*[2], *H. Esmaily*[2]; [1]*Research Center of Medical Physics; Research Institute Avicenna; Mashhad University of Medical Scien, Iran,* [2]*MUMS, Iran.*

Background, Motivation and Objective

Photodynamic therapy (PDT) is one of the non-invasive developing methods for treating superficial and accessible malignancies. Some of photosensitizers are activated by ultrasound irradiation, too. (Principle of sonodynamic-therapy (SDT)). Hence, it is expected that a combined treatment be more effective than photodynamic therapy alone for treating deeper tumors even at a reduced dose of the sensitizer. This study has evaluated the synergistic effects of photodynamic and sonodynamic therapies.

Statement of Contribution/Methods

The colon carcinoma tumors were induced by subcutaneous injection of 5×105 CT26 cells to Balb/c mice. 24 hours after intra-peritoneal injection of zinc phthalocyanine liposomes as a sensitizer, the tumors underwent ultrasound irradiation (1 W/cm2 at 1.0 MHz for 10 minutes) and then light irradiation (300 J/cm2 at 670 nm). Three dimensions of the tumors were measured daily. All of the feasible control groups were considered to ensure the effects of the therapeutic parameteres.

Results

Data has shown, during 10 days after treatments, relative volume of the tumors in the all groups significantly decreased in comparison with the main control group. The best responses were associated with PDT or SDT groups and their efficacies were better than the combined therapy. Longer doubling times of tumors were related to photodynamic, sonodynamic and combination therapies respectively and the shortest was belonged to the control group.

Discussion and Conclusions

Liposomal Zinc phthalocyanine is both photosensitizer and sonosensitizer. PDT and SDT can decrease the growth rate of tumors. Of course, combinational therapy with our protocol does not provide the better effects. This outcome might be related to therapeutic sequence.

2F-5

2:30 PM **Noncavitational Nonporative Ultrasound Elicits Marked In Vivo Augmentation of Tumor Drug Delivery with Targeted Perfluorocarbon Nanoparticles**

Steven Baldwin, Neelesh Soman, Gregory Lanza, **Samuel Wickline;** *Washington University in St. Louis, School of Medicine, St. Louis, MO, USA.*

Background, Motivation and Objective

Augmentation of local drug delivery from targeted nanoparticles (NP) with nondestructive, noncavitational clinical ultrasound (US) offers the potential to enhance therapeutic efficacy in diseases such as cancer while limiting adverse systemic side effects. This lab has demonstrated augmentation of drug delivery from avb3-targeted perfluorocarbon NP and US in cancer cells in vitro (Crowder et al, 2005). This study investigates the utility of conventional, clinical US for augmentation of drug delivery in vivo in a transgenic mouse cancer model (K14-HPV16) that develops squamous cell carcinomas.

Statement of Contribution/Methods

16 mice were injected intravenously with either integrin avb3-targeted or nontargeted NPs complexed with 0.1 mol% fluorescent dye rhodamine. At 30 min post-injection, one ear was treated for 30 min with a commercial US imager (Philips iE33) in Color Doppler mode at MI=1.4 and at 2.3 MHz (other ear served as control). Mice were sacrificed at 2 hrs post-injection and ear sections visualized by fluorescence microscopy. After setting exposure time & color thresholds, area of rhodamine signal was calculated using MicroSuite 5 software (Olympus, PA). The effect of US in enhancing therapeutic benefit of drug bearing NP was examined in mice treated with integrin avb3-targeted NPs loaded with the cytolytic amphipathic peptide melittin, a principal component of bee venom exhibiting antitumor activity (13 mg/kg, 7 doses over 3 weeks). As before, one ear was exposed to US each dose. BRDU stains of proliferating cells were used as an index of antitumor effect.

Results

US-exposed ears exhibited a 5.2 (±1.9 SE) fold rhodamine augmentation as compared to non-exposed ears in the avb3-targeted group ($n=9$, $p<0.05$, Wilcoxon signed-rank test) and a 4.0 (±1.3) fold aug in the nontargeted group ($n=7$, $p<0.01$), indicating a marked effect of material deposition induced by US. In the US therapy trial, ears of transgenic mice exposed to US+NPs show reduced proliferating keratinocytes compared to controls (see Fig) pointing to accelerated reversal of disease progression.

Discussion and Conclusions

Noncavitational US can significantly augment drug-delivery in vivo from molecularly targeted therapeutic NP. This readily available and clinically-benign approach offers possibility for additional measures of tumor targeting with exogenous US energy that improves therapeutic efficacy.

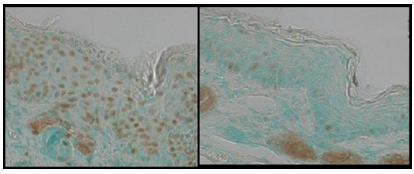

2F-6

2:45 PM **Intra-Vascular Ultrasound (IVUS) Delivery of DNA Via Microbubble Carriers to an Injured Artery *In vivo***

Linsey C. Phillips[1], Alexander L. Klibanov[1], Doug K. Bowles[2], Brian. R. Wamhoff[1], John A. Hossack[1]; [1]*University of Virginia, Charlottesville, VA, USA,* [2]*University of Missouri, Columbia, MO, USA.*

Background, Motivation and Objective

The most common therapy for narrowed, atherosclerotic arteries is balloon angioplasty and is often followed by stent placement. This procedure causes injury to the vessel wall and over time, cells from the artery wall (primarily smooth muscle cells) proliferate in response to injury and re-occlude the vessel (restenosis). A novel therapy to prevent restenosis involves the use of delivering an anti-proliferative gene via microbubbles which are ruptured via catheter-based intravascular ultrasound at the site of vessel injury. Insonation of microbubbles by ultrasound has been shown to increase gene delivery at low frequencies. We hypothesize that plasmid DNA encoding a reporter gene (red fluorescent protein, RFP) can be delivered to a pig carotid artery wall *in vivo* using cationic microbubble carriers and intravascular ultrasound.

Tuesday Oral

Statement of Contribution/Methods

Cationic microbubbles were formed during ultrasonic dispersion of decafluorobutane gas in an aqueous micellar mixture of phosphatidylcholine, PEG stearate, and distearyl trimethylammonium propane. Negatively charged DNA plasmids expressing red fluorescent protein (CMV-RFP) were electrostatically coupled to microbubbles.

A modified IVUS catheter (Boston Scientific) was positioned 1mm away from cells and translated over an area of 2cm2. *In vitro* application of 5 or 11 MHz Guassian pulses at a PNP of 120 kPa, and PRF of 5kHz was applied to cultured smooth muscle cells exposed to CMV-RFP plasmid bearing microbubbles for at total of 6 minutes.

Balloon angioplasty was performed on pig right carotid vessels (n=2) *in vivo*. (The pig is the gold standard for restenosis studies.) Following angioplasty, microbubbles were infused through a port hole in a catheter located 2cm upstream of the IVUS transducer. 5 MHz unipolar pulses (PRF = 5 KHz, PNP =120 kPa) were emitted from the IVUS catheter at the location of vascular injury (2cm in length) for a total of 4 minutes during plasmid conjugated-microbubble infusion. Three days following insonation, arteries were excised and processed for frozen sectioning and nuclei staining. Successful plasmid transfection was measured by fluorescent microscopy and quantified as % of vessel perimeter cells expressing RFP.

Results

Ultrasound mediated gene delivery from microbubbles using IVUS *in vitro* resulted in 11.5 fluorescent cells/cm2 (<1%). (Previously reported ultrasound / bubble mediated gene delivery are typically low ~1-5%.) Cells exposed to plasmid-microbubbles without US resulted in 0% transfection. Injured pig arteries exposed to microbubbles and ultrasound resulted in 23.3± 6.0% transfection whereas contralateral controls resulted in 3.6±2.6% transfection.

Discussion and Conclusions

To the authors' knowledge, this is the first example of *in vivo* cationic gene delivery via IVUS, which has promise for localized intra-vascular gene therapy for preventing restenosis.

3F. Photoacoustic Imaging

Room 305 A/B/C

Tuesday, November 4, 2008, 1:30 pm - 3:00 pm

Chair: **Georg Schmitz;**
Ruhr-Universität Bochum, Germany.

3F-1

1:30 PM **Embracing the era of multicore processors and GPU-computing for realtime ultrasonic and photoacoustic imaging**

Roger Zemp[1], Liang Song[2], Rachel Bitton[3], Kirk Shung[4], Lihong Wang[2]; [1]*University of Alberta, Electrical & Computer Engineering, Edmonton, Alberta, Canada,* [2]*Washington University in St. Louis, Biomedical Engineering, St. Louis, MO, USA,* [3]*Stanford University, USA,* [4]*University of Southern California, USA.*

Background, Motivation and Objective

Moore's law projects that transistor density will double on integrated circuits every 18-24 months and this incessant law of the semiconductor business has driven processors to more and more sophisticated architectures. In the quest for computing speed, realizing higher clock speeds has proved highly problematic, and manufacturers have turned to multi-core computing. Additionally the computer graphics industry has driven the development of very sophisticated computing power in graphical processing units. We report progress in making the most out of this computing power for realtime ultrasound, photoacoustic, and other similar imaging technologies. Presently most commercial ultrasound systems use dedicated hardware to perform realtime beamforming, post-processing, and scan conversion. Emerging applications also use FPGAs or digital-signal-processors. But what about leveraging the multicore CPUs emerging in simple desktop computers? In a few years Moore's law suggest there may be CPUs with hundreds of processor cores on the market, and we show evidence that this may prove spectacular opportunities for realtime imaging systems.

Statement of Contribution/Methods

We demonstrate the ability to perform realtime dynamic-receive ultrasound beamforming using a dual-socket quad-core desktop computer. Scan conversion was offloaded to the GPU using a simple triangular mesh-rendering scheme. High-level multi-threaded software was used for all studies. We studied execution speed as a function of number of processor cores, and image size.

We recently implemented our realtime methods in the context of a high-frequency photoacoustic imaging system that we built based on a 30-MHz ultrasound array transducer and a high-repetition-rate tunable pulsed laser. We have reported this system and its success in realtime imaging of photoacoustic dynamics in vivo.

Results

We here report additional results on the utility of this system for imaging the beating hearts of young athymic nude mice at 50 frames per second. We also pursued additional computational studies investigating the scalability of realtime dynamic-receive beamforming with processor-core count. We found 8 processors to be on average 7.1 times faster than a single processor for realtime beamforming.

Discussion and Conclusions

We conclude that multicore computing technology has vast possibilities for realtime imaging systems. Ultrasound is particularly well-suited for embracing this paradigm since each A-scan line in a B-scan image may be reconstructed in separate parallel threads. We conjecture that the era of multi-core and GPU-computing architectures for realtime imaging systems is just beginning and untapped possibilities remain for the future.

3F-2

1:45 PM **Design of Catheter for Combined Intravascular Photoacoustic and Ultrasound Imaging**

Bo Wang, Andrei Karpiouk, Stanislav Emelianov; *University of Texas at Austin, Biomedical Engineering, Austin, TX, USA.*

Background, Motivation and Objective

Intravascular photoacoustic (IVPA) imaging is a promising imaging tool for detecting and differentiating the atherosclerotic plaques. Previously, we have demonstrated the utility of intravascular photoacoustic imaging using a laboratory system where the excised arterial tissue sample was irradiated with the laser beam from the outside while the intravascular ultrasound (IVUS) imaging catheter, inserted into the lumen, was used to receive the photoacoustic signal. However, for in-vivo IVUS and IVPA imaging, a combined catheter consisting of IVUS transducer and light delivery system is needed. In this paper we report our initial experience towards design and fabrication of a catheter capable of simultaneous IVPA and IVUS imaging.

Statement of Contribution/Methods

The combined IVUS/IVPA imaging catheter was built based on a clinical, 40 MHz, single element IVUS catheter (Boston Scientific, Inc.). A 0.6 mm diameter optical fiber was used for light delivery. The proximal end of the fiber was coupled with a laser system. The distal tip of the optical fiber was polished at a 45 degree angle and placed inside a quartz tube. Both ends of the tube were sealed with epoxy to retain air around the fiber tip. As a result, such fiber assembly, when submersed into water, was irradiating the light sideway. The IVUS catheter was then attached to the optical fiber such that the ultrasound beam from the transducer and the laser beam from the optical fiber were aligned. To test the combined IVUS/IVPA imaging catheter, a model of the atherosclerotic vessel was fabricated. Specifically, within the otherwise homogeneous polyvinyl alcohol background, three 0.4% graphite inclusions of 1 mm diameter were positioned at different depths inside of the approximately 6-mm thick vessel wall to simulate various plaques in the artery. During imaging studies, the catheter was inserted into the lumen, and the phantom was rotated using a stepper motor. At each angular position, both photoacoustic and ultrasound A-lines were collected by a 14-bit GAGE A/D card operating at 200 MHz sampling rate. The IVUS and IVPA images were formed off-line from 256 equally spaced beams.

Results

The IVPA images of the phantom obtained using the combined IVUS/IVPA catheter clearly identifies the inclusions located at specific depths. At the same time, co-registered IVUS images visualized the structure of the phantom. Finally, combined IVUS/IVPA images further outlined the location and extent of the inclusions within the vessel wall.

Discussion and Conclusions

Overall, IVPA and IVUS images of sufficient quality were obtained using the initial prototype of the combined IVUS/IVPA catheter. Using optical fibers of smaller diameter, the size of the combined catheter can be further reduced. Therefore, our studies suggest that optical fibers can be used to deliver enough optical fluence for intravascular photoacoustic imaging of the vessel. Furthermore, other approaches in design of IVUS/IVPA imaging catheter will be discussed.

3F-3

2:00 PM **Development of a hybrid tissue diagnostic system combining high frequency ultrasound and photoacoustic imaging with lifetime fluorescence spectroscopy**

Yang Sun[1], **Douglas Stephens[1],** Jesung Park[1], Yinghua Sun[1], Jonathan Cannata[2], Kirk Shung[2], Laura Marcu[1]; *[1]University of California, Davis, Biomedical Engineering, Davis, CA, USA, [2]University of Southern California, Biomedical Engineering, Los Angeles, CA, USA.*

Background, Motivation and Objective

We report the development and validate a multi-modal tissue diagnostic technology, which combines three complimentary techniques into one system including ultrasound backscatter microscopy (UBM), photoacoustic imaging (PAI), and time-resolved laser-induced fluorescence spectroscopy (TR-LIFS). UBM enables the reconstruction of the tissue microanatomy. PAI maps the optical absorption heterogeneity of the tissue associated with structure information and has the potential to provide functional imaging of tissue. Examination of the UBM and PAI images allows for localization of regions of interest for TR-LIFS evaluation of the tissue composition.

Statement of Contribution/Methods

The hybrid probe consists of a single element ring transducer with concentric fiber optics for multimodal data acquisition. Validation and characterization of the multimodal system and ultrasonic, spectroscopic and photoacoustic data coregistration were conducted in a tissue phantom with fluorescence, ultrasound scattering and optical absorption properties. The TR-LIFS system records the fluorescence decay with the time resolution of approximately 300 ps and a high sensitivity of nM concentration range. The UBM system with the 40 MHz ring transducer can reach the axial and lateral resolution of 30 and 65 µm, respectively. The PAI system with 532 nm excitation light from a YAG laser shows great contrast for the distribution of optical absorbers.

Results

Biological phantom constructed with different types of chicken tissues (muscle, fat, and tendon) was used to demonstrate the complimentary information provided by the three modalities. Fluorescence spectra and lifetimes were compared to differentiate chemical composition of tissues at the regions of interest determined by the coregistered high resolution UBM and PAI image.

Discussion and Conclusions

Current results demonstrates that the fusion of these techniques enables simultaneous detection of compositional, morphological and functional features of biological tissue, suggesting potential applications in diagnosis of human diseases such as tumors and atherosclerotic plaques. This work was supported by NIH R01 HL 067377, USA.

Tuesday Oral

3F-4

2:15 PM **Picosecond Iltrasonics in a Single Biological Cell**

Clement Rossignol, Bertrand Audoin, Mathieu Ducousso; *Laboratoire Mecanique Physique, Universite Bordeaux - CNRS, France.*

Background, Motivation and Objective

The picosecond ultrasonic technique has been developed during last 20 years due to permanent interest in the study of mechanical properties of nano- and micro-layers of metals and semiconductors used in solid state physics and microelectronics. The technique relies on generation, propagation and detection of ultra-short acoustic waves by femtosecond laser pulses. Important advantages of these techniques are the absence of direct contact to the sample and very high frequency range. Until now, the mechanical properties of biological cells have been studied by scanning acoustic microscopy (SAM) and atomic force microscopy (AFM). The AFM technique is used for evaluation of mechanical properties on cellular surface. In spite of demonstration of 8 GHz operation frequency in cryogenic acoustic microscope, the SAM technique has not been widespread for biological and medical tasks due to complicated design demanding liquid helium cooling. The application of contactless and very high frequency picosecond ultrasonic technique should improve significantly the space resolution of acoustic imaging of living cells. In this presentation, the picosecond ultrasonics technique is applied for the non-invasive evaluation of hypersound velocity and attenuation in the cytoplasm of living cells. A first medical application is presented: measurements of the adhesion of obsteoblast cells on prosthesis.

Statement of Contribution/Methods

Reflectometric pump-probe experimental set-up is used to generate and detect acoustic waves in the cells. The radiation of a femtosecond laser is divided in two beams to provide the pump and probe beams. Optical delay line (0-12 ns) is introduced in the probe beam path. Intensity of the reflected probe beam is detected by a photodiode. Such a set-up allows the detection of reflectivity variations at the level of ~10-7. The width at mid height of the space cross-correlation of the pump and probe beams is approximately 1 micron.

Results

Velocity and attenuation of hypersound at from 5 to 17 GHz in cells are measured by a femtosecond laser pump-probe technique. From the velocity, cell compressibility nearby the cell-substrate interface can now be mapped with a lateral resolution better than 1 micron. Also cell adhesion is measured in function of the surface functionalisation.

Discussion and Conclusions

In addition to single cell imaging, the sensitivity of the measurements to cell adhesion suggests promising perspectives for the imaging of the cell grafting on biomaterials. Indeed, mouse osteoblast cells show very different sound velocities with and without peptide deposition on the titanium prosthesis. This is a first step to quantitative measurements of cell adhesion in function of the functionalization of the prosthesis.

3F-5

2:30 PM **Dynamic measurements of the generation and trapping of bubbles by a self-focused femtosecond laser beam**

Kun Yang[1], Yun Zhou[1], Zhenzhen Fan[1], Jingyong Ye[2], **Cheri Deng[1];** *[1]University of Michigan, Biomedical Engineering, Ann Arbor, Michigan, USA, [2]University of Michigan, Center for ultrafast optical sciences, Ann Arbor, Michigan, USA.*

Background, Motivation and Objective

The nonlinear interactions of high peak intensity of femtosecond (fs) laser with biological tissues confines energy absorption to focal volumes, enabling high precision surgical procedures via laser-induced optical breakdown (LIOB) involving bubble generation. Recent observation of generation and trapping of LIOB bubbles by a self-focused laser beam differs from conventional optical tweezer and offers opportunities to explore novel applications. Detail understanding of this process is necessary to study fundamental physics and practical biomedical applications related to LIOB bubbles.

Statement of Contribution/Methods

A custom-built 250 KHz re-generatively amplified Ti:sapphire laser with an output duration of 100 fs and wavelength of 793 nm was used. The laser beam was loosely focused (f-number 15) upward into a body of water. The dynamics of generation and trapping of the LIOB bubbles by the self-focused laser pulses was investigated using time-resolved measurements from spatiotemporally correlated wideband (5 ~ 60 MHz) ultrasound detection of passive and pulse-echo M-mode and B-mode signals as well as fast frame rate (KHz ~ MHz) microscopic framing and streak photography.

Results

This study obtained the first results of the detail spatiotemporal processes of generation and trapping of LIOB bubbles by a self-focused fs laser beam. LIOB occurred at a location, determined by the path length of the laser beam into water and the laser energy. Time resolved measurements revealed a delay of 1-2 ms for the initial generation of one or multiple bubbles (3-10 μm) distributed within 25 μm around the focus, after the initial arrival of the train of consecutive laser pulses (PRF at 250 KHz). These bubbles subsequently often floating away while one bubble that appeared on the path of the laser beam was rapidly (~100 μs) pulled down and trapped to a location 50~100 μm below the original LIOB site by the continuously arriving laser pulses. The trapping of a bubble immediately resulted in the cessation of further bubble generation even when the laser pulses were still on. The duration of the trap was ms ~ s in our experiments, depending on ultimately the medium, bubble size, and the laser energy. The lost or removal of the trapped bubble leaded to immediate resumption of LIOB at the original focus; and the trapping again occurred, exhibiting dynamic-equilibrium in the process. Manipulation of the trapped bubbles including acoustic cavitation and their effects on cells was also investigated.

Discussion and Conclusions

This study presented the first investigation of the detail processes of generation and trapping of LIOB bubbles by a self-focused fs laser, providing valuable knowledge for exploration of new applications of controlled bubble manipulation. A rigorous theory is not currently available and further experiments are needed to allow versatile data collection to accommodate different time scales.

3F-6

2:45 PM **Selective Detection of Cancer using Multi-wavelength Photoacoustic Imaging and Bioconjugated Gold Nanoparticles**

Srivalleesha Mallidi, Timothy Larson, Konstantin Sokolov, Stanislav Emelianov; *University of Texas at Austin, Department of Biomedical Engineering, USA.*

Background, Motivation and Objective

There is a compelling need for a non-invasive imaging tool that can reliably detect, diagnose and characterize cancer at an early stage. Highly proliferative cancer cells overexpress molecular markers such as epidermal growth factor receptor (EGFR). Gold nanoparticles functionalized with anti-EGFR antibodies undergo molecular specific aggregation on the cellular membrane that leads to a red shift in their plasmon resonance frequency. In our previous work with cell-based tissue phantoms, we demonstrated that highly selective detection of cancer is possible with the combination of photoacoustic imaging and molecular specific gold nanoparticles. In this study, we evaluate the efficacy of molecular specific, multi-wavelength photoacoustic imaging technique in detecting subcutaneous tumors ex-vivo.

Statement of Contribution/Methods

The molecular specific photoacoustic imaging was demonstrated ex-vivo using BL6 mice. Subcutaneous implantation of gelatin solution containing (1) dye (ADS740WS) with absorption peak at 740 nm, (2) A431 cells (human epithelial carcinoma) labeled with anti-EGFR gold nanoparticles, (3) A431 cells mixed with polyethylene glycol-thiol (mPEG-SH) coated gold nanoparticles were performed on the mouse. Combined ultrasound and photoacoustic images of the implants were obtained using a 25 MHz, mechanically scanned, single element focused ultrasound transducer and pulsed laser illumination at 532 nm and several wavelengths in the 680 – 900 nm range. To gauge the differences in the optical absorption spectra of the implanted gels, the magnitude of the photoacoustic transients within the regions of interest were analyzed as a function of wavelength.

Results

The contents of the different implants were determined by analyzing the photoacoustic images at multiple wavelengths. Specifically, the photoacoustic transients produced by the gel implant containing dye reached maximum at 740 nm excitation wavelength, in agreement with the absorption peak of the dye. The analysis of the photoacoustic signals obtained from the gel containing cells targeted with gold nanoparticles indicated broadening of the spectra in the NIR region. Indeed, the EGFR-mediated aggregation of gold nanoparticles causes a red-shift in their surface plasmon resonance. The gelatin implant with cells mixed with PEGylated gold nanoparticles (i.e, particles with no molecular specificity) produced photoacoustic transients with maximum at 532 nm, similar to the absorption spectra obtained from isolated gold nanoparticles.

Discussion and Conclusions

In conclusion, the results of our study strongly indicate that highly sensitive detection of asymptomatic pre cancers is possible with multi-wavelength photoacoustic imaging and bioconjugated gold nanoparticles. Further studies are required to evaluate this molecular specific imaging technique in vivo and its potential in combination with phototherapy.

4F. SAW vs BAW

Hall 2A

Tuesday, November 4, 2008, 1:30 pm - 3:00 pm

Chair: **Rich Ruby;**
Avago Technologies, USA.

4F-1

1:30 PM **SAW and BAW Technologies for RF Filter Applications: A Review of the Relative Strengths and Weaknesses**

Robert Aigner; *TriQuint Semiconductor, Apopka, Florida, USA.*

Background, Motivation and Objective

The first part of this paper aims to present facts and figures comparing SAW and BAW technologies with regard to

(a) process complexity / cost , size

(b) function, performance and fundamental limitations

(c) simulation methods and design flow

Based on the criteria above the application space for RF filters in wireless communication will be mapped and selected examples will be discussed in detail.

Statement of Contribution/Methods

The second part of this paper will review how both technologies progressed in recent years and will focus on innovations. Both SAW and BAW keep pushing for better performance and at times compete with each other. Despite that there are surprisingly many areas where SAW and BAW face similar challenges on a path to improved performance and/or lower cost. Commonalities and areas where SAW and BAW learn from each other are:

(a) frequency correction “trimming” methods for yield improvement

(b) materials and processes for acoustic layers

(c) wafer-level-packaging

Results

Results of research and development work at TriQuint in both SAW and BAW will be presented. The emphasis will be on temperature compensated (TC) filters and duplexers. TC SAW shows promise to fulfill demanding duplexer requirements for emerging mobile phone bands. Fully temperature compensated BAW filters enable to fix interference issues in emerging wireless applications.

Discussion and Conclusions

The shockwave FBAR/BAW has generated inside the SAW community a few years ago has passed. It generated a lot of pressure while approaching and a lot of traction while dissipating. Several suppliers now have both technologies in their portfolio while others stick to either the one or the other. SAW is recovering lost market share based on cost advantages and innovations which aim to overcome their main weaknesses. BAW on the other side keeps pushing the performance envelope for filters with extreme specifications. In the history of electronics over the past 50 years there are many cases of a new technology challenging established technologies. Examples range from “Transistor vs. Vacuum tube” and “GaAs vs. Silicon” to “CMOS vs. Bipolar”. Which of those best compares to “BAW vs. SAW” will be speculated about in the discussion.

4F-2

2:00 PM **High Selectivity SAW Duplexer for W-CDMA Band VIII**

Andreas Bergmann, Andreas Waldherr, Hans-Peter Kirschner, Karl Wagner; *EPCOS AG, Surface Acoustic Wave Components, Munich, Germany.*

Background, Motivation and Objective

The special requirements on Band VIII Wideband CDMA (W-CDMA) duplexer are the relatively large bandwidths of 3.9 % for transmitting (TX) and 3.7 % for receiving (RX) filters as well as the low duplex distance of 1.1 %. Moreover, compared to systems at higher frequencies, for 1 GHz systems increased focus is put on miniaturization.

Statement of Contribution/Methods

In order to achieve good RX suppression within the TX band the RX filter comprises one port resonators as well as a DMS track whereas the TX filter is a pure ladder type filter. The center frequencies of these building blocks show different dependency on metallization ratio and layer thickness. The consideration of this relationship within the design process was necessary to achieve a very low relative shift of the right skirt of the TX filter to the left skirt of the RX filter.

Results

Our duplexer is realized in a 3.0x2.5 mm^2 package on LTCC ceramic and offers a suppression of the W-CDMA RX-signal of 50 dB within the TX band. Typical values for attenuation of the W-CDMA signal in the transmission band are 1.7 dB for the TX path and 2.0 dB for the RX path.

Discussion and Conclusions

The comparison between simulation and measurement shows the applicability of the design concept which is the most appropriate one for duplexers with small duplex distance and good RX suppression within the TX band.

4F-3

2:15 PM **Suppression of Transverse Mode Spurious of SAW Resonator on an SiO_2/Al/$LiNbO_3$ Structure for Wideband CDMA Applications**

Hiroyuki Nakamura[1], Hidekazu Nakanishi[1], Tetsuya Tsurunari[1], Ken Matsunami[1], Yukio Iwasaki[1], Ken-ya Hashimoto[2], Masatsune Yamaguchi[2]; *[1]Panasonic Electronic Devices Co., Ltd., Japan, [2]Graduate School of Engineering, Chiba University, Japan.*

Background, Motivation and Objective

The wideband CDMA (W-CDMA) system at 2GHz has a wide duplex gap between transmitting (Tx) and receiving (Rx) bands. When developing a small-sized SAW duplexer for this application, one needs a substrate with a large electromechanical coupling factor (K^2) and good temperature coefficient of frequency (TCF). Although an SiO_2/Al/$LiNbO_3$ structure meets these two requirements, it also supports a certain number of unwanted spurious responses. They are categorized into two types; one is caused by the Rayleigh-mode and the others by the transverse mode. As the authors have previously discussed, the former can be suppressed by controlling the cross-sectional shape of an SiO_2 overlay deposited on resonator electrodes [1]. On the other hand, the latter is commonly suppressed by IDT apodization. However, it degrades Q factor, resulting in increased insertion loss of the duplexer.

Statement of Contribution/Methods

This paper proposes a new technique to suppress the transverse mode responses appearing in the SAW resonators on the SiO_2/Al/$LiNbO_3$ structure. In the technique, the dummy electrodes are only length-weighted in the form of a triangle, which selectively scatter higher-order transverse mode spurious [2]. In addition, the SiO_2 overlay is selectively removed from the dummy electrode region for enhancing the SAW energy confinement in the active electrode region.

Results

This technique was applied to an SAW resonator fabricated on 5°Y-X $LiNbO_3$ substrate. As shown in Fig. 1, the transverse mode spurious responses were successfully suppressed without degrading the Q factor.

Discussion and Conclusions

We applied the proposed technique to the development of a miniature W-CDMA duplexer with the packaged size of 2.5mm×2.0mm. The duplexer exhibited the excellent performance: the insertion losses in the Tx and Rx bands

are 1.2dB and 1.9dB, respectively, the isolations are 53 dB in Rx band and 45 dB in Tx band, and the TCF is about -30 ppm/°C, respectively.

[References]

[1] H.Nakamura, et al, Jpn. J. Appl. Phys., 47, 5B (2008) [to be published]

[2] T.Omori, et al, IEEE Trans. Ultrason., Ferroelec., and Freq. Contr., 54 (2007) pp. 1943-1948.

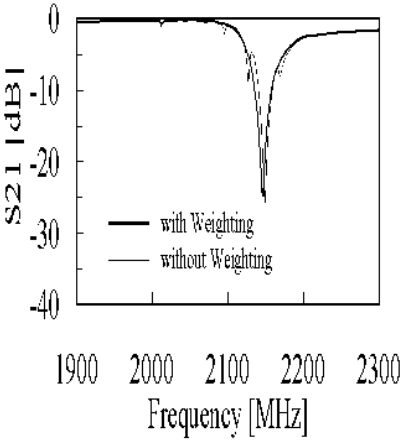

4F-4

2:30 PM **K-Band Ladder Filters Employing Air-Gap type Thin Film Bulk Acoustic Resonators**

Tsuyoshi Yokoyama, Motoaki Hara, Masanori Ueda, Yoshio Satoh; *Fujitsu Limited, Japan.*

Background, Motivation and Objective

A conventional frequency band is very crowded today. Particularly, low microwave band below 6 GHz are used in commercial telecommunications, radars, broadcast services, and wireless LANs. It is important to consider the possibility of devices for high frequency applications over 6 GHz in order to use the frequency band effectively.

A filtering is a key issue in such high frequencies. A thin film bulk acoustic resonator (FBAR) is suitable technology for this purpose. We have been studying FBAR for high frequency application over X-band. A high-performance X-band filter utilizing the FBAR was reported in our previous study. In this study, an air-gap type FBAR for the K-band was developed, and a ladder filter based on the FBAR was fabricated and evaluated.

Statement of Contribution/Methods

The electrode material of the FBAR was discussed to obtain a large electro-mechanical coupling coefficient keff2 in the K-band, and ruthenium (Ru) was selected in this study. As a piezoelectric film of the FBAR, aluminum nitride (AlN) is promising and was adopted. The film thickness of Ru and AlN of the FBAR in the K-band was estimated to be 43nm and 78nm by a finite element method (FEM), respectively.

The FBAR, which composed the filter, is fabricated on the flat silicon substrate and has a dome shape to make an air-gap between the resonator and the substrate. The dome shape is formed by the use of the thin sacrifice layer and the stress of the piezoelectric film and the electrodes.

Results

Figure 1 shows a characteristic of the fabricated FBAR filter. A center frequency, a minimum insertion loss and a fractional bandwidth of the filter were 19.2GHz, -7.5dB and 1.7%, respectively.

In the FBAR, 4.21% of an effective electro-mechanical coupling coefficient keff2, 40 and 68 of a resonance and an anti-resonance Q factors, respectively, were obtained. Both Q factors of the K-band FBAR were smaller than the conventional 2-GHz and the X-band FBAR by the influence of parasitic elements and an increase of the electrode resistance.

Discussion and Conclusions

A ladder type filter for K-band based on the FBAR was developed for the first time in the world. The fabricated K-band FBAR filter operated in the highest frequency band as a filter utilizing an acoustic wave. Performance and some issues of K-band FBAR will be discussed at the Symposium.

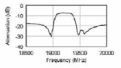

Figure 1. Scattering parameters S_{12} of the K-band filter

4F-5

2:45 PM **BAW PCS-Duplexer Chipset and Duplexer Applications**

Gernot Fattinger[1], Alexandre Volatier[1], Robert Aigner[2], Fabien Dumont[1]; *[1]TriQuint Seminconductor, BAW R&D, Apopka, FL, USA, [2]TriQuint Seminconductor, Acoustic R&D, Apopka, FL, USA.*

Background, Motivation and Objective

In the past years, the PCS duplexer seems to have become essential to any serious competitor in the RF handset filter business. This is especially true in the competition for BAW/FBAR market share, where the PCS application is now a must-have to gain significant volume with any customer.

Statement of Contribution/Methods

In this paper, TriQuint's BAW PCS duplexer chipset will be presented, showing it's performance in various applications, ranging from integration in a PCS power-amplifier module to a standalone, plastic package, 3x3mm duplexer. Design considerations will be reviewed and necessary trade-offs will be discussed.

Results

Representative measurements will be presented to document chip performance as well as the resulting duplexer response. Besides having a low insertion loss and a high rejection and isolation, today's application requirements dictate that special attention has to be paid towards non-linearity (harmonics). This applies to the behavior of the single TX/RX chips as well as the duplexer as a system. Measurements of the corresponding performance parameters will be shown and compared with previous, less optimal designs. Furthermore, power handling requirements are compared to the obtained measurements.

Discussion and Conclusions

To optimize the duplexer performance and reduce the required number of laminate design cycles, electro-magnetic simulations of the whole duplexer application have been performed. A comparison between the simulated and measured performance will be presented, displaying the good agreement between theory and measurement.

Finally, some volume manufacturing issues will be addressed and certain key aspects of a high-yield BAW process will be addressed. In particular, the applied method for frequency trimming is discussed and its necessity and benefits are pointed out.

5F. Acoustic Imaging and Microscopy

Hall 2B

Tuesday, November 4, 2008, 1:30 pm - 3:00 pm

Chair: **David Greve;**
Carnegie Mellon, USA.

5F-1

1:30 PM **Probabilistic Mud Slowness Estimation from Sonic Array Data**

Hugues Djikpesse, **Henri-Pierre Valero;** *Schlumberger-Doll Research, Mathematics & Modeling, Cambridge, MA, USA.*

Background, Motivation and Objective

Until now, the main outputs extracted from waveforms recorded by a high-frequency monopole source in a fluid-filled borehole have been the compressional slowness (inverse of velocity) of the formation and sometimes the shear slowness. However, estimation of near-borehole formation compressional slowness is of significant value for petrophysical and geomechanical applications. Probing the near-borehole (shallow) formation and measuring the radial variation of slowness near-borehole can help to identify damaged or altered zones; this is a highly valuable information for the development of more complex fields requiring additional information beyond the traditional standard slowness log data. Therefore there is increasing interest in the knowledge of the radial formation-slowness profile—from shallow to deep into the formation.

To assist in the provision of this information, it is necessary to provide the compressional and shear slowness profiles as a function of the radial distance into the formation. In 1993, Hornby presented a method for reconstructing a 2D map of near-borehole compressional slowness by inverting the first-arrival time of compressional head waves by using the simultaneous iterative reconstruction technique (SIRT). Even though this approach was of interest, it was difficult to implement this algorithm at wellsite due to the computation load and its high sensitivity to initial velocity model, fluid slowness and standoff (i.e. difference between tool and borehole size) values. Nevertheless, this first tentative proposal yielded encouraging results, albeit the tool used in the study was a prototype.

Discussion and Conclusions

In order to overcome limitations of the proposed method, we propose a simultaneous inversion of the borehole parameters (standoff, fluid slowness) and the radial variation of the compressional and shear slownesses of the formation surrounding the wellbore. We formulate the inverse problem and its resolution using a stochastic, population based particle swarm optimization technique which is suitable to solve highly non-linear problem as the one considered here. The prior information available about the model parameters (including relevant bounds and other constraints) are thereafter specified along with the assessment of the errors associated with the travel time measurements. In contrary to common practice, the uncertainties introduced by the physical assumptions and approximations underlying the resolution of the forward problem, are quantified. They are used with other available prior information in a rich, robust, nonlinear particle swarm tomography (under uncertainty) algorithm to jointly estimate the slowness variation in the borehole and in the surrounding formation. The proposed method is numerically validated using synthetic and real field data.

5F-2

1:45 PM **Development of a Micro-LFB Ultrasonic Device and Its Application to Elastic Inhomogeneity Evaluation of ZnO Crystal**

Jun-ichi Kushibiki, **Yuji Ohashi,** Mototaka Arakawa, Tomoya Tanaka, Sho Yoshida; *Tohoku University, Graduate School of Engineering, Sendai, Miyagi, Japan.*

Background, Motivation and Objective

The line-focus-beam ultrasonic material characterization (LFB-UMC) system is capable of quantitative evaluation for various solid materials, including single crystals, by measuring the phase velocity of leaky surface acoustic waves (LSAWs) propagating on a water-loaded specimen surface. Spatial resolution of this system depends on ultrasonic beam widths along focused direction W and along unfocused direction D formed by the LFB lens. As D for the normal LFB lens is relatively large, it is difficult to detect steep variations of acoustic properties along the unfocused direction on specimen surface. In this paper, to improve the spatial resolution along the unfocused direction, we verify performance of a micro-LFB ultrasonic device in which a ZnO-film transducer is fabricated on a cylindrically convex surface with a large curvature radius R_T.

Statement of Contribution/Methods

We made a micro-LFB lens with the following parameters: lens curvature radius R_L=1.0 mm, aperture half angle θ=60°, transducer curvature radius R_T=13.0 mm, rod length l=12.0 mm, and transducer widths of 1.73 mm along focused direction and 1.50 mm along unfocused direction. We evaluate spatial resolution of the device at 225 MHz by measuring focused acoustic fields using a point-focus-beam lens as a detecting probe. We also verify a capability of anisotropy detection through measurements of angular dependence of LSAW velocities for anisotropic crystal (Ge standard specimen). Furthermore, we demonstrate spatial detectability through measurements of LSAW velocity distributions for a Z-cut ZnO single crystal specimen with large inhomogeneity.

Results

3dB-down width of the acoustic fields along unfocused direction was 0.26 mm for the micro-LFB device, as compared with that of 0.92 mm for normal LFB device. The angular dependence of LSAW velocities for (110)Ge specimen showed velocity variations reflecting crystal symmetry as predicted by theoretical calculations. The measurement results for the Z-cut ZnO crystal clearly showed that the micro-LFB device could detect velocity variations, inhomogeneities, which could not be observed by the normal-LFB device with less spatial resolution.

Discussion and Conclusions

We proposed a micro-LFB lens and demonstrated its performance with higher spatial resolution, also keeping a capability of perfect directionality of the LFB lens. This device will be very useful for characterizing a small size of precious samples.

5F-3

2:00 PM **Measurement Model for Attenuation of Leaky Surface Acoustic Waves by the Line-Focus-Beam Ultrasonic Material Characterization System**

Jun-ichi Kushibiki[1], Mototaka Arakawa[1], **Kenji Otsu[2];** [1]*Tohoku University, Electrical Engineering, Sendai, Japan,* [2]*Tohoku University, Biomedical Engineering, Sendai, Japan.*

Background, Motivation and Objective

The line-focus-beam ultrasonic material characterization (LFB-UMC) system can perform material characterization by accurately measuring the propagation characteristics (viz., phase velocity and attenuation) of leaky surface acoustic waves (LSAWs) excited on the water-loaded specimen surface. Information of the velocity V_{LSAW} is mainly used for material characterization, because of the higher accuracy. In this paper, we studied experimentally an exact model for LSAW attenuation measurement.

Statement of Contribution/Methods

Synthetic silica glass (C-7980, Corning Inc.) and borosilicate glass (C-7740, Corning Inc.) were taken as specimens. LSAW propagation characteristics were measured at 225 MHz.

Results

Table 1 presents the measured and calculated results. The measured attenuations were larger than the calculated ones. The measured normalized attenuation factor is represented as $\alpha_{LSAW} = \alpha_{WL} + \alpha_b + \alpha_s$. The first, second, and third terms are due to the water-loading effect, the acoustic bulk absorption effect, and the structural scattering effect, respectively. α_s can be neglected, because the specimens are homogeneous and optically polished.

Discussion and Conclusions

In the theoretical calculations, water was treated as an ideal fluid and the shear wave component was not considered for the boundary conditions. The main reason of the difference between the measured and calculated attenuations might be caused by the treatment of water loading. In addition, viscosities of longitudinal and shear waves of water were not considered in the calculations, although they could not be neglected in the VHF range. α_b for C-7980 are negligible in the VHF range {$\alpha_l = 1.1 \times 10^{-16} \times f^2$ (1/m), $\alpha_s = 1.9 \times 10^{-16} \times f^2$ (1/m)}, while it must be considered that for C-7740 {$\alpha_l = 2.30 \times 10^{-9} \times f^{1.29}$ (1/m), $\alpha_s = 1.82 \times 10^{-9} \times f^{1.33}$ (1/m)}. Therefore, the difference between the measured and calculated attenuations for C-7740 was larger than that for C-7980. This study suggests that further investigation is needed for completing the exact measurement principle for the LFB-UMC system.

Table. 1 Comparison of measured and calculated LSAW propagation characteristics for C-7980 and C-7740 at 225 MHz.

Specimen	V_{LSAW}	α_{LSAW}		
	(measured) [m/s]	(measured)	(calculated)	Difference
C-7980	3426.19	0.0427	0.0389	0.0037 (9.5%)
C-7740	3127.76	0.0458	0.0412	0.0046 (11.2%)

Tuesday Oral

5F-4

2:15 PM **Scanning acoustic microscopy an application for evaulating varnish layer conditions non-destructively**

Sebastian Brand[1], Peter Czuratis[2], Kay Raum[1]; [1]*University of Halle, Germany,* [2]*SAM TEC GmbH, Germany.*

Background, Motivation and Objective

For preventing corrosion and for surface protection metallic objects are commonly finished with layers of varnish. The integrity of the varnish and potential defect propagation influence the durability of the metal and hence are a measure for the quality of the finishing. Scanning acoustic microscopy provides high axial and lateral resolution, a sufficient penetration depth and is non-destructive. The goal of this work was the development of a method for detection and evaluation of delaminations of varnish layers on metallic surfaces.

Statement of Contribution/Methods

Investigated were samples containing one and two layers of varnish. One group contained priming only whereas the second group contained varnish on top of the undercoat. The surface integrity of the finishing was destroyed by a scratch through all finishing layers. Defect aging was then performed by exposing the samples to a corrosion-friendly atmosphere. Scanning acoustic microscopy combined with signal analysis was performed for investigating the connectivity between the finishing layers and the substrate.

Results

A robust numerical deconvolution technique has been adapted and optimized to enable the separation of strongly overlapping pulses.

Discussion and Conclusions

Echoes originated at the substrate and the finishing layers have been localized and layer thicknesses/distances were estimated. Delaminated spots of the finishing were successfully evaluated using the method developed during this study.

5F-5

2:30 PM **Ultrasonic Phased Array Device for Acoustic Imaging in Air**

Sevan Harput, Ayhan Bozkurt, Feysel Yalcin Yamaner; *Sabanci University, Acoustic Group, Istanbul, Turkey.*

Background, Motivation and Objective

Acoustic imaging technology is widely used for medical purposes, underwater imaging and nondestructive testing applications. With the advances in air coupled transducers, the acoustic imaging in air become popular. However, phased array principles have not been extensively applied for acoustic imaging in air. In this work, we present the design and experimental verification of an ultrasonic phased array device for acoustic imaging in air. The developed device uses phase beamforming technique to electronically sweep the acoustic beam and produce a sector scan for the detection of proximate objects. The intended application of the device is giving mobility aid to visually impaired people. Therefore, compactness and low power consumption are important design criteria. The device is built using 6 transmitter and 4 receiver elements and has an angular resolution of 4.23°.

Statement of Contribution/Methods

An ultrasonic phased array device constructed using commercially available transducers to perform acoustic imaging in air. Each transducer elements have a radius of 1.9 wavelengths and a half-power beamwidth of 43° at 40.8 kHz center frequency. The transmitter array is formed with 2 wavelengths spacing between the elements, but this placement leads to the occurrence of unwanted grating lobes in the array response and decreases the Field of View to 30°. By using a spacing of 2 wavelengths, the FOV of the overall system can not be larger than ±15° with identical receiver and transmitter arrays. For this reason, the receiver array elements are placed with a different spacing. Forming the receiver and transmitter arrays with non-identical element spacing makes the grating lobes to appear at different places. For 3 wavelengths inter-element spacing in receiver array, the first grating lobe of the overall system moves to ±30° and the FOV increases to 60°. This value exceeds the limit imposed by the half-power beamwidth of an individual transducer element and makes the grating lobes to appear outside of the active imaging area.

Results

Developed device scans the imaging area using the phased array technique with an angular resolution of 4.23°. To achieve the same angular resolution without scanning will be more costly. An array would require approximately the same number of transducers but individual elements have to be as wide as the aperture size of the phased array. For this reason, the developed phased array device is more compact than an array of transducers.

5F-6

2:45 PM **Application of chaotic cavities to localizednonlinearity imaging with time reversal**

Bou Matar Olivier, Li YiFeng, Preobrazhensky Vladimir, Pernod Philippe; *IEMN, France.*

Background, Motivation and Objective

Recent results have shown that Nonlinear Elastic Wave Spectroscopy (NEWS) and Time Reversal (TR) techniques can be combined to precisely localize defects, produced by their nonlinear response. NEWS techniques can be used either as a post-treatment of TR used as a tool for ultrasound focusing in order to generate strong localized stress (TR-NEWS), or as a pre-treatment, of TR used as a tool for defect (nonlinear source) identification (NEWS-TR). The TR process can be implemented with a fully programmable multi-elements ultrasonic system. But recently, it has been demonstrated that a single PZT ceramic glued on the sample can also be used as a TR mirror when the sample is multi-reverberant. In this case the quality of the retrofocusing process, and so the microdamage localization, depends on the sample geometry.

Statement of Contribution/Methods

In this study, numerical and experimental results, performed in order to validate and enhance the possibility to localize microdamage with a combination of a time reversal technique, using an emitter with a chaotic shape, and nonlinear elastic wave response, will be presented. The numerical results have been obtained both with a commercial finite element code for linear simulation, and a new high order spectral (using unstructured grids) methods in the case of nonlinear elastic waves propagation. The experimental set-up used is based on the combination of a chaotic cavity glued on the sample for the elastic wave emission (and focalization), and a laser vibrometer in order to image the nonlinear response at the surface of the sample.

Results

Numerical simulations have been used in order to optimize the chaotic cavity shape and material, and the time reversal process. This enable us to find that chirp-coded excitation (instead of single-carrier short pulses) combined with 1-bit time reversal process have to be used in order to transmit more energy per time on the defect, and so increase its nonlinear response, without increasing the peak intensity of the excitation. Images of defects, with a perfectly controlled size (obtained with nanotechnology tools), in a wafer has been obtained by the proposed method.

Discussion and Conclusions

The benefit of using emitters having a more or less chaotic shape is clearly found in breaking the symmetry of the problem, leading to an unambiguous retrofocusing. The obtained results confirm that time reversal techniques with pre- or post-treatment in terms of nonlinear wave phenomena brings about a significant challenge in the future development of new imaging tools of microdamage in samples with complex geometries.

6F. Ultrasonic Motors & Droplet Processing

Hall 2C

Tuesday, November 4, 2008, 1:30 pm - 3:00 pm

Chair: **Takefumi Kanda;**
Okayama University, Japan.

Tuesday Oral

6F-1

1:30 PM **Initial Growth of Ultrasonically Vaporized Perfluorocarbon Microdroplets**

Kevin Haworth, Oliver Kripfgans; *University of Michigan, Radiology, Ann Arbor, MI, USA.*

Background, Motivation and Objective

Acoustic Droplet Vaporization (ADV) is a technique whereby liquid droplets are vaporized into gas bubbles using ultrasound. This process and the resulting bubbles have been proposed for use in occlusion therapy, localized drug delivery, and aberration correction. To increase the efficacy of each of these applications, it is important to understand the nucleation mechanisms and initial bubble growth. High-speed photography can be used to image this process and elucidate the physical processes taking place.

Statement of Contribution/Methods

Forty-five Albumin-stabilized perfluorocarbon droplets (diameters ranging from 4 to 30 microns) were independently vaporized in a 100 micron inner-diameter polyethylene tube using a focused 3.5 MHz single-element transducer (Panametrics, f/#2). Sixteen optical images of each droplet vaporization were obtained with frame rates of up to 13 MHz (12 pixels per micron resolution) using a water immersion microscope and high-speed camera (SIM16, Specialized Imaging, UK).

Results

Nucleation sites appear to be within the droplet based on the deformation of the droplet boundary during the nucleation process. The initial growth of the bubbles oscillates due to the multicycle vaporization pulse and the bubbles are often nonspherical. The maximum bubble diameter observed within the first 2 us was independent of the initial droplet diameter. As a result, smaller droplets produce faster growing bubbles. The radial growth rate ranged from 5 m/s for larger droplets (~15-20 microns) to 25 m/s for smaller droplets (~5-10 microns). Very large droplets (greater than 25 microns) were observed to have cavitation sites within the droplet, but not rupture the albumin shell within the first microsecond of nucleation, as was observed for droplets under 25 microns.

Discussion and Conclusions

The fact that the initial bubble size is independent of initial droplets size indicates that the initial growth process is limited by the rate at which PFC phase-transitions into a gas. Over millisecond or longer time-scales it has previously been observed that larger droplets do form larger bubbles. The variation of initial growth rate of the bubbles (i.e. wall velocity) may be observed via acoustic emissions. This may, in turn, be used to determine, in situ, the size of droplets being vaporized.

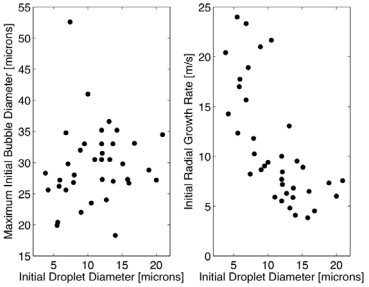

6F-2

1:45 PM **Droplets generation by a torsional bolt-clamped Langevin-type transducer and micropore plate**

Takuya Harada[1], Naoyuki Ishikawa[1], Takefumi Kanda[1], Koichi Suzumori[1], Yoshiaki Yamada[2], Ken-Ichiro Sotowa[3]; *[1]Okayama University, Japan, [2]Okayama Prefecture Industrial Promotion Foundation, Japan, [3]Tokushima University, Japan.*

Background, Motivation and Objective

In the fields of cosmetics, foods production, medical science and so on, droplets which have small and uniform diameters are required. Monodisperse droplets are very important factors which make quality of productions, improve stabilities and facilitate control of properties. The purpose of this study is to realize such droplets by using an ultrasonic vibrating micropore plate. As Langevin type transducer can generate a high power vibration, thick solutions would be also available.

Statement of Contribution/Methods

A torsional bolt-clamped Langevin-type transducer has been used for generating micro droplets in this study. By using the torsional mode, micropore which places same distance from the center would be oscillated equally and multiple micropores can be used. Compared with a longitudinal mode vibrator, the torsional vibrator would generate a lot of droplets. The micropore plate was made of stainless steel and its diameter was 10mm. The diameter of micropore was 16μm and micropore was placed 2mm distance from the center of plate. The plate was attached at the tip of the transducer and was oscillated by the transducer. When the micropore plate did not vibrate, droplets were generated irregularly by surface tension. On the contrary, when the micropore plate vibrated, droplets were generated regularly by ruffling liquid surface.

Results

The micropore plate was oscillated by the transducer torsionally vibration amplitude from 0 to 0.62 $\mu m_{p\text{-}p}$. When the vibrational amplitude is larger, we have succeeded in changing the diameter of droplets and the standard deviation of the diameter. When the vibration amplitude was $0.62\mu m_{p\text{-}p}$ and the resonance frequency was 56kHz, the averaged diameter of droplets was 26.8μm and the standard deviation of the diameter was 1.41 in air. In addition, by using this transducer, W/O (Water-in-Oil) emulsions were also generated. Under the same vibration amplitude and resonance frequency, the averaged diameter of the emulsions was 35.0μm, the standard deviation of diameter was 1.9.

Discussion and Conclusions

From these results about W/O emulsions, the coefficient of variance was estimated to be 5.5. This means that monodisperse droplets have been generated. Therefore we have succeeded in generating uniform micro droplets by using torsional vibrating transducer.

6F-3

2:00 PM **Acoustic trapping of small particles on the surface of a vibrating rod**

Yanyan Liu, Junhui Hu; *Nanyang Technological University, Singapore.*

Background, Motivation and Objective

Ultrasonic particle manipulation has potential applications in many areas, such as pharmaceutical industry, bio-separation etc. In this technology, small particles are trapped, separated, transported and agglomerated by acoustic radiation force. The objective of this work is to explore a new method of acoustic trapping.

Statement of Contribution/Methods

In this work, trapping small particles by a vibrating rod is proposed and developed. A theoretical model is developed to analyze the mechanism of trapping particles by the vibrating rod. Experiments are carried out to verify the model. Based on the model, the effects of particle size, rod radius, and operating frequency are investigated for different fluids. Useful guidelines for optimizing trapping capability are proposed.

Results

Experimental results show that small particles can be trapped on the surface of the vibrating rod in water and trapping capability is optimized when operating at resonance frequency and input voltage of 60 Vrms.

A theoretical calculation has been conducted to investigate the effects of fluid properties, operating frequency, rod radius, and particle radius on the trapping capability and acoustic radiation force. The smallest vibration velocity to trap particles is used to express the trapping capability.

It is found that the smallest vibration velocity is smaller in liquids than that in gas; it's better to choose higher frequency to trap particles in gas while low frequency is more efficient for trapping in liquid. It is also found that in water the acoustic radiation force may change its direction in different frequency, from pushing particles onto the surface of the rod to pushing particles away from the rod.

Discussion and Conclusions

Particle trapping by an ultrasonic vibrating rod has been proposed and investigated. A physical model has been developing which explains the experimental phenomenon qualitatively. And effects of operating frequency, particle size, and rod radius on trapping capability in different mediums are clarified.

6F-4

2:15 PM **FE Analysis and Experimental Characterization of a High Torque Travelling Wave Ultrasonic Motor**

Antonio Iula; *University of Basilicata, Potenza, Italy.*

Background, Motivation and Objective

Ultrasonic motors offer several advantages with respect to electromagnetic ones including high holding torque, very quick start/stop response and high torque density at low speed without gear systems to reduce the speed. The low efficiency and the wear of the contact interface, which causes a short lifetime, are the main drawbacks. Due to the latter characteristics, ultrasonic motors have been exploited mainly in low power and low duty cycle applications.

In aerospace applications, there is also the need for motors able to provide high torque with a very low duty cycle.

The proposed motor is composed of a annular shaped stator and two cone shaped rotors. The rotors are pressed in contact to the inner surface of the stator by means of an opportune pre-stress system. A travelling rotating wave is generated in the stator in order to create an elliptical motion at the interface with the rotor. As the proposed motor is intended for high torque applications, Bolted Langevin Transducers (BLT), designed to excite in the ring radial nonaxialsymmetric modes, have been chosen as vibration generators.

Experimental results carried out on a first prototype, which exploited only two BLTs, have already been published [1]. From a theoretical point of view up to 20 transducer could be symmetrically positioned all around the outer surface of the stator; in this way a significant increment of the output torque is expected.

[1] A. Iula and M. Pappalardo, "A high-power traveling wave ultrasonic motor," IEEE Trans. Ultrason. Ferroelec. Freq. Control, vol. 53, no. 7, pp. 1344 -1351, 2006.

Statement of Contribution/Methods

In the present work, an advanced prototype has been simulated by FEM and experimentally characterized. The main improvement of the new design is the use of three couples of BLTs, opportunely shifted both in space and time as shown in figure. Also, a very lighter version of the rotors was designed and realized, in order reduce inertia and encumbrance and increase controllability, and finally the motor has been clamped to the housing by using two flanges passing through the middle plane of two transducers.

Results

Main characteristics of the motor are summarized as follows: weight 0.67 Kg, working frequency 23.5 kHz, max rotational speed 116 rpm, static torque 0.94 Nm.

Discussion and Conclusions

By increasing the number of driving transducers the output torque and the mechanical power increase at the expense of efficiency.

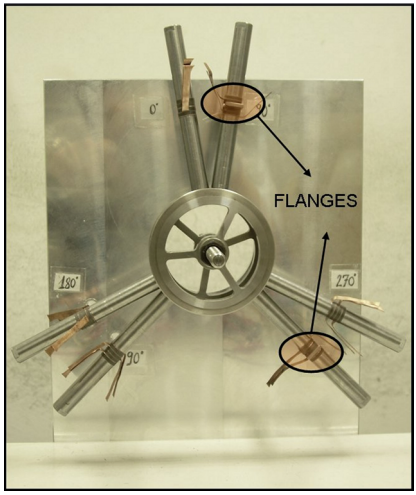

6F-5

2:30 PM **Dielectrophoresis Driven by Acoustic Pulses on Piezoelectric Substrates**

Mikhail S. Berezin, **Vladimir G. Mozhaev**, Anna V. Zyryanova; *Moscow State University, Faculty of Physics, Moscow, Russian Federation.*

Background, Motivation and Objective

Traveling-wave dielectrophoresis (TWD) is a promising method for manipulating micro- and nanoparticles, as well as biological cells. A quasi-wave distribution of electric field instead of true waves is used in the common TWD scheme. Such a distribution is produced near an electrode array with individual phase shifts of alternating voltage at every electrode. An interesting feature of TWD is a backward movement of isolated particles observed under certain conditions both in experiments and in numerical simulations (Masuda, 1987; Gartshtein, 1999). In spite of the attempts to give various interpretations of the backward transport (Schmidlin, 1995), this puzzling property remains incompletely understood. Note that multiple spatial Fourier harmonics of the electrode array field is a complicating factor for solving this problem and interpreting the results. The idea of implementation of TWD driven by true wave like surface acoustic waves propagating on piezoelectric substrates was suggested by us in 2004 (Mozhaev, Zyryanova, IEEE Ultrason. Symp.). The consideration of pure harmonic spatial wave field distribution, natural for the acoustic drive, simplifies the theory and makes it easier to interpret and to explain the particle backward transport. On the other hand, the analytical theory of TWD was previously developed only in the steady-state case without account of important limitations of the dielectrophoretic process both in time and in space. Thus, the aim of the present study is to develop a simple analytical 2D theory of pulsed TWD transport and also to present the results of numerical simulation in the case of pure harmonic in space, but limited in time, wave drive of the acoustic type.

Statement of Contribution/Methods

We are looking for the solution to 2D equation of motion describing the movement of a small particle placed in a fluid near the surface of piezoelectric substrate under the action of electric fields accompanying pulses of surface acoustic waves propagating in the substrate. The introduction of new complex coordinate allows us to reduce two initial equations to single one and integrate it directly. Besides, 4th order Runge-Kutta method is used to find numerical solutions and to produce movies.

Results

The exact analytic solution to the initial value problem of TWD transport is found in the case of inviscid fluid. The analytical solution coincides completely with numerical one in this case. Computational simulations are used to study the peculiarities of TWD transport in the viscous fluid. Both forward and backward transport is predicted by analytical and numerical solutions depending on the initial conditions of the problem.

Discussion and Conclusions

On the basis of analytical solution which is free of numerical errors, pointed out previously as one of the reasons of backward transport, we conclude that the main parameter controlling the direction of particle transport in TWD is the carrier-wave phase with respect to the leading edge of the wave pulses.

6F-6

2:45 PM **Structure design method of bar-structure linear ultrasonic motor**

Zhiyuan Yao, Dong Yang, Xin Wu, Chunsheng Zhao; *Nanjing University of Aeronautics and Astronautics, China.*

Background, Motivation and Objective

By means of the effect of piezoelectric ceramics d33 and Langevin vibrator, larger output force and higher output efficiency are obtained using bar-structure linear motors. In 1999, Kurosawa proposed a piezoelectric vibrator with high speed and large thrust force. This motor achieves output force of 39N, thrust weight ratio of 17, the maximum efficiency of 28%, the maximum speed of 0.55m/sec (driving voltage of 500 Vrms, pre-tightening force of 150N).

Since the non-continuous variable cross-sections will decrease the transmission efficiency of longitudinal wave in the bar-structure. This paper proposes a new design method based on continuous variable cross-section for Langevin vibrators.

Statement of Contribution/Methods

In order to improve the transmission efficiency of longitudinal wave, firstly, using acoustics model, the relationship between the cross-section shape of the bar-structure stator and transmission efficiency of longitudinal wave is discussed.

The longitudinal vibration of Langevin vibrators with continuous variable cross-section is derived as well as its profile function. Meanwhile its acoustic characteristics is also discussed

Results

Depending on the analysis above, an improved linear motor shown in Fig.1 is designed by using the structure with continuous variable cross-section.

Its output characteristics are tested.

Discussion and Conclusions

This paper discusses the effect on transmission efficiency of longitudinal wave of the bar-structure. It shows that the non-continuous variable cross-section causes the energy loss for acoustic wave propagation. The design method based on continuous variable cross-section for Langevin vibrators is proposed, and the profile function of the Langevin vibrator is also given. An improved linear motor is designed. Its maximum speed is up to 235mm/s, the output force is increased to 21.4N and thrust weight ratio of 25 under condition of 200 Vrms by means of testing. The speed-frequency relation, the speed-phase relation, speed-voltage relation of the motor is obtained; the experiment results indicate that the motor has better output performance.

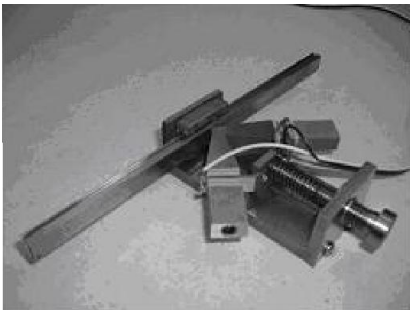

1G. Visco-elasticity

Hall 3

Tuesday, November 4, 2008, 4:30 pm - 6:00 pm

Chair: **Mickael Tanter;**
Laboratoire Ondes et Acoustique, ESPCI, France.

1G-1

4:30 PM **Dynamic Micro-Elastography (DME) applied to viscoelastic characterization of mimicking carotid arteries**

Cedric Schmitt, Anis Hadj Henni, Guy Cloutier; *Laboratory of Biorheology and Medical Ultrasonics, , Montreal, Quebec, Canada.*

Background, Motivation and Objective

Because early signs of atherosclerosis involve hardening of arteries, the development of non-invasive imaging methods to provide in vivo assessments of mechanical properties of vessel walls is clinically relevant. Recently, non invasive elastography was used to assess elasticity moduli of arterial walls by employing a simple mechanical model to solve an inverse problem. Even if the calculated mechanical parameter was very sensitive to wall stiffness, it was defined as a normalized elasticity because in situ measurements of blood pressure were not available. To overcome such a limitation, we propose to use dynamic elastography adapted to vascular applications (shear wave frequency > 500 Hz) to recover the real viscoelasticity of mimicked carotid artery by solving an appropriate 2D inverse problem.

Statement of Contribution/Methods

The experimental setup consisted of a small plate positioned at the surface of the probed phantom, vibrating at frequencies between 500 Hz and 1500 Hz, to generate a plane shear wave orthogonal to its motion. The phantom was made with agar-gelatin in which was embedded a PVA mimicking carotid artery (4.7 mm wall thickness). Displacements in a small region of interest (25 * 30 mm2), centered on the hollow cylinder, were determined with a correlation-based method applied to received RF echoes. These echoes were produced with a 25 MHz high-frequency transducer positioned parallel to the tissue motion. The transducer was translated along the wave propagation direction to acquire and reconstruct 2D RF sequences at a very high frame rate (16 kHz). 2D shear wave displacement maps served as input for the inverse problem formulation. Using a theoretical model simulating the diffraction of a plane shear wave by a hollow cylinder, this problem was solved by minimizing the least square error between experimental and simulated displacement fields according to the material viscoelasticity.

Results

We first investigated the possibility to experimentally generate and measure 500 Hz to 1500 Hz plane shear waves into the mimicking carotid artery. From the reconstructed wave propagation field, we observed particular patterns of wave displacements, i.e. the wave propagated along the wall curvature. It was also observed that the measured wave propagation could well be predicted by the simulation. The inverse problem solution after convergence gave an artery wall elasticity of 7.6 kPa at 500 Hz.

Discussion and Conclusions

This work presents the dynamic vascular micro-elastography method as a promising imaging modality to mechanically characterize a vessel wall. In vitro results were successfully obtained to demonstrate the ability to generate and follow, within a thin mimicking artery wall, plane shear wave propagation of 2 mm to 5 mm wavelength range. To conclude, future investigations about effect of frequency on elasticity dispersion, estimation accuracy and optimization strategy will be pursued to further demonstrate the feasibility of this method.

1G-2

4:45 PM **Investigating the Effects of Viscosity on Focused, Impulsive, Acoustic Radiation Force Induced Shear Wave Morphology**

Michael Wang[1], Mark Palmeri[1], Maritza Hobson[2], Kathryn Nightingale[1]; *[1]Duke University, Biomedical Engineering, Durham, NC, USA, [2]University of Wisconsin-Madison, Department of Medical Physics, Madison, WI, USA.*

Background, Motivation and Objective

As reported by many groups, acoustic radiation force (ARF) can be used to remotely induce shear waves in tissue, and their propagation speed can be used to estimate the shear modulus. We previously reported the LTTP method for shear modulus quantification under elastic assumptions, that is robust when applied to noisy data. The purpose of this study is to evaluate the effects of viscosity on modulus estimates obtained from the LTTP method when applied to viscoelastic (VE) materials.

Statement of Contribution/Methods

In elastic media, the shape of a plane traveling shear wave does not change with propagation; in VE materials, dispersion and frequency dependent attenuation result in decreasing frequency content and amplitude decay with propagation. For focused ARF induced shear waves in VE media, geometric spreading also contributes to morphology changes with propagation. In this study, change in shear wave morphology with propagation distance was investigated. First, the wavespeed was estimated using the LTTP method. Although the initial spatial wavelength is determined by the ARF beamwidth, in our experiments this cannot be evaluated with propagation directly due to variations in the system power supply between sequentially acquired data. Therefore, morphology changes were quantified in the temporal domain, using the temporal front edge width (time between the peak displacement and the half maximum point on the rising edge) at each spatial location. The shear wave width spread (SWWS, ms/mm) with propagation distance was calculated, excluding regions where it had plateaued. Experimentally matched FEM simulations using LS-DYNA were performed in elastic media, and with a 3 parameter (Zener) model of VE for a range of parameters. Experimental data were acquired in an elastic CIRS phantom, a custom, calibrated VE phantom (M.A.H.; Go=4.45 kPa, Ginf=3.21 kPa, tau=1.2 ms), and in vivo in rat and human livers. ARF was generated using a VF7-3 (rats) or CH4-1 (humans) probe on a modified Siemens Antares scanner. Shear wave tracking was performed using Loupas method on 4:1 parallel receive IQ data. Nine repeated excitations were used to monitor a 5mm lateral ROI.

Results

SWWS was negligible in elastic media: simulation (0.007), phantom (0.07). In contrast, SWWS in the VE phantom was appreciable (0.65), with an LTTP estimate of 4.15 kPa for G. The VE simulations indicate SWWS is a function of both tau, and the change between Go and Ginf, and the LTTP estimates are within this range. The mean SWWS was similar in F0 and F3 rat liver groups (0.18, 0.15). In human data, SWWS was challenging to evaluate due to poor SNR. Where quantifiable (n=3), SWWS was consistent with VE behavior (0.12).

Discussion and Conclusions

SWWS is indicative of VE behavior. SWWS is not observed in elastic media, but is observed in VE simulations, phantoms, and in in vivo livers. A Zener VE model provides good agreement with observed experimental behaviors, and the LTTP estimate is within the range of moduli for VE materials.

1G-3

5:00 PM **Skin viscoelasticity with surface wave method**

Xiaoming Zhang[1], Randall Kinnick[1], Mark Pittelkow[2], James Greenleaf[1]; *[1]Mayo Clinic, Physiology and Biomedical Engineering, Rochester, MN, USA, [2]Mayo Clinic, Dermatology, Rochester, MN, USA.*

Background, Motivation and Objective

Characterization of the viscoelastic mechanical properties of the skin is important for improving accurate medical examination and diagnosis of disorders involving cutaneous and subcutaneous tissues; more thoroughly understanding skin biophysical and physiological properties; identifying normal and abnormal skin aging and disease processes; developing and applying improved pharmacologic and other therapeutic interventions; as well as cosmetic applications. Several noninvasive methods have been developed for measurement of mechanical properties of the skin. However, most methods measure a stiffness parameter but not the material properties of skin. For example, the suction method measures the displacement of skin in response to suction. The measurement is dependent on the aperture and fixation of probes and also difficult to interpret.

Statement of Contribution/Methods

We have developed a novel surface wave speed method for noninvasively estimating the elasticity of tissues [X. Zhang et al., J. Acoust. Soc. Am., vol. 122, 2522-2525, 2007]. In this paper, we have extended this method for measuring viscoelastic material properties of human skin. This method is independent of the excitation probe. It measures the speed and decay of the surface wave propagation on the tissue. In this method, a very small force is generated by a mechanical shaker on the skin. The surface vibration of skin is measured using a noncontact method with a laser vibrometer.

Results

With approval by Mayo Clinic Institutional Review Board (IRB), we have conducted human skin testing. The average shear elasticity μ1 and shear viscosity μ2 are, respectively, μ1=14.49 kPa and μ2=12.19 PaS for a young healthy male at the back, calf, forearm, forearm dorsal, palm and thigh.

Discussion and Conclusions

A noninvasive surface wave method has been developed for measuring the viscoelasticity of skin, which can be used to investigate skin material property change due to disease as well as aging. This method is also applicable to other internal organ tissue where the surface wave is generated and measured noninvasively with ultrasound techniques.

1G-4

5:15 PM **Quantification of Liver Stiffness and Viscosity with SDUV: *In Vivo* Animal Study**

Shigao Chen[1], Matthew Urban[1], Yi Zheng[2], Aiping Yao[2], James Greenleaf[1]; [1]*Mayo Clinic, Department of Biomedical Engineering, Rochester, MN, USA,* [2]*St. Cloud State University, Department of Electrical and Computer Engineering, USA.*

Background, Motivation and Objective

Shearwave Dispersion Ultrasound Vibrometry (SDUV) is proposed here as a new technique to quantitatively measure both stiffness and viscosity of soft tissues at any prescribed location (Note: this is not an imaging technique). The goal of this study is to demonstrate the feasibility of SDUV for *in vivo* application in liver, which has major implications for staging of liver fibrosis, a disease with a prevalence of hundreds of millions worldwide.

Statement of Contribution/Methods

SDUV uses a focused ultrasound beam to stimulate (within the studied tissue) cylindrical harmonic shear waves propagating outwards from the beam axis. Shear wave propagation is tracked by a separate ultrasound beam in pulse/echo mode. The phase of shear wave at two locations along its traveling path is used to calculate the shear wave propagation speed. The speed of shear waves at different frequencies is measured and fit with a theoretical Voigt dispersion model to inversely solve for tissue viscosity and elasticity. We have developed and tested a new pulse sequence that makes SDUV compatible with commercial ultrasound scanners. Measurement time for SDUV is about 0.1 second. The following results are obtained with an in-house prototype.

Results

SDUV measurement in a gelatin phantom (shear elasticity μ_1 = 5.4 kPa, shear viscosity μ_2 = 0.38 Pa·s) is confirmed by independent validation (μ_1 = 5.7 kPa, μ_2 = 0.36 Pa·s). *In vivo* measurements in pig liver required temporary breathing suspension and ECG gating. Measurements were made 3.5 cm from the skin surface into the liver. The vibration-generating ultrasound beam had an *in situ* MI of 1.7, and its heating to tissue was estimated to be 0.15 ºC. Results obtained by repeated SDUV measurements in pig liver were $\mu_1 = 2.2 \pm 0.63$ kPa, $\mu_2 = 1.96 \pm 0.34$ Pa·s, which is close to *in vivo* values reported in healthy human subjects by magnetic resonance elastography $\mu_1 = 2.1 \pm 0.26$ kPa, $\mu_2 = 1.7 \pm 0.15$ Pa·s (NMR in Biomedicine, 19:173-179, 2006).

Discussion and Conclusions

SDUV is capable of quantitative measurement of both tissue stiffness and viscosity. *In vivo* application in liver is reliable with breath holding and ECG gating. This research is supported by NIH grant EB002167.

1G-5

5:30 PM **Measuring Viscoelastic Properties with Ultrasonically Generated Microbubbles**

Rei Asami, Ken-ichi Kawabata; *Central Research Laboratory, Hitachi, Ltd., Tokyo, Japan.*

Background, Motivation and Objective

Tissue viscoelasticity is often associated with disease entity and could provide critical information for diagnostics. Microbubble is a potential tool for measuring minuscule changes in viscoelasticity as its acoustic responses are affected by surrounding environmental properties. A promising application with laser-induced optical breakdown method for ophthalmologic uses has already been reported[1]. We aim to expand this application to uses in deeper body region by replacing laser with ultrasound together with submicron size microbubble precursor, phase-change nano droplet (PCND). In this paper, preliminary study on acoustic responses of PCND suspended in gel phantom mimicking varying viscoelasticity, specifically on differences in ultrasound application duration required for bubble induction, oscillation time of generated bubbles and emitted harmonics, is presented.

Statement of Contribution/Methods

PCND is prepared with low boiling-point perfluorocarbon (PFC) mixture and emulsifying agents and emulsified at high pressure (20 MPa). Their final average particle diameter is measured with dynamic laser scattering to be 200 nm.

PCND is suspended in polyacrylamide gel phantom with varying polyacrylamide concentration of 6 to 24 percent to mimic different tissue viscoelasticity. For control, PCND prepared with high-boiling point PFC is used. Gels are then placed in degassed water bath at 37°C and ultrasound is applied at frequency of 3.3 MHz to induce phase-change from liquid droplets to microbubbles. Acoustic response is acquired with hydrophone and analyzed off line.

Results

While peak negative pressure required for phase change induction was kept, oscillation duration of time of generated bubble and harmonics all varied among different viscoelastic properties of surrounding media. In the dilute gel (6%), harmonics emission caused by generated microbubbles lasted for more than 10 μs whereas in the concentrated gel (24%), harmonics emission lasted for less than 2 μs. Higher harmonics up to its 5th was observed even though the duration of those higher harmonics were significantly shorter than those at lower frequency. Ultrasound exposure time required for PCND induction varied less significantly within the range of 30%. Control group did not show any detectable acoustic changes.

Discussion and Conclusions

Viscoelasticity of surrounding media is reflected on acoustic response at all staged of ultrasonic bubble induction from PCND showing great potential of solely ultrasound induced viscoelastic property measurements that is widely applicable to different body regions. We will further investigate the detailed mechanism causing difference at each stage of bubble induction.

Acknowledgement

Part of this work was supported by the New Energy and Industrial Technology Development Organization, Japan.

Reference

[1] Erpelding, T., et al., *Proc. IEEE Ultrasonics Symp.,* 2003,pp 554-557

1G-6

5:45 PM **A Harmonic Motion Imaging-based technique for non-contact mapping and estimating regional viscoelastic properties**

Caroline Maleke, Jonathan Vappou, **Elisa Konofagou;** *Columbia University, Biomedical Engineering, New York, NY, USA.*

Background, Motivation and Objective

Previously, harmonic motion imaging (HMI) technique was shown capable of measuring localized tissue displacement during the application of the acoustic radiation force. In this study, a 1D phased array transducer was used to image the dynamic response in homogeneous phantoms with different stiffnesses throughout the oscillatory force. This method is used to measure the viscoelastic parameter, i.e., storage shear modulus (G') and loss shear modulus (G"), from the measured displacement. Moreover, the results of this technique are compared to mechanical rheometry.

Statement of Contribution/Methods

A 4.68MHz single-element focused ultrasound (FUS) transducer was used to generate an oscillatory force at different modulation frequencies (5, 10, and 50Hz). The resulting dynamic motion was imaged simultaneously using a 1D phased array transducer with a center frequency of 3MHz, sampling frequency of 16MHz, and frame rate of 76Hz. A 1D cross-correlation technique was applied on the acquired RF signals, with a window size equal to 3mm and 83% overlap to estimate and image the resulting incremental axial displacement in 2D.

In order to measure the viscoelastic parameters, we first employed the ratio of G" and G', which can be defined as tan(φ). The phase shift (φ) was measured between the HMI displacement and the applied force. Second, the inverse shear wave propagation method was then used by fitting the propagating shear wave with a sinusoidal damping to estimate G" and G'. Based on the HMI displacements, we were able to obtain the viscosity (G"), elasticity (G') and phase shift (φ). In addition, with these two methods, a rheometer was used to test the same gel samples for comparison purposes. The rotation frequencies applied were between 1 and 10Hz.

Results

From the HMI method, the acrylamide gels were shown virtually purely elastic with the estimated ratio (G''/G') ranging between 0.01 and 0.1. These results were in excellent agreement with those obtained from the rheometer tests on the same acrylamide gels that showed the viscosities to be null, i.e., purely elastic.

Discussion and Conclusions

Since HMI induces an oscillatory force at a localized region inside the medium, the information that we obtain herein could therefore be used to estimate the regional viscoelasticity. Preliminary demonstration in biological tissues will also be shown.

Acknowledgements: This study was supported by the NIH (1R21EB008521)

2G. Therapeutic Ultrasound

Room 201 A/B/C

Tuesday, November 4, 2008, 4:30 pm - 6:00 pm

Chair: **Kullervo Hynynen;**
University of Toronto, Canada.

2G-1

4:30 PM **Optimum Protocols in the Design of 2-D Spherical-Sectioned Phased-Array for 3-D Focused Ultrasound Surgery**

Mingzhu Lu, Mingxi Wan, Xiaodong Wang; *Xi' an Jiaotong University, The Key Laboratory of Biomedical Information Engineering of Ministry of Education, Xi' an, Shanxi , China.*

Background, Motivation and Objective

Phased array offers several advantages over single focused transducer such as simultaneously multi foci, flexible focus patterns, aberration correction and sub-array modalities to steer beam avoiding human-rib-cage obstacles. In order to have the freedom to control the ultrasound in three dimensions, the array element size needs to be small. Theoretically, the element center-to-center spacing should be equal to or smaller than half wavelength, as a result the high intensity gain therapeutic array has a large number of total elements, sometime more than 10,000 elements, and hence a large number of total channel drivers are needed. For practical application purpose, the aims of this study are to decrease the channel numbers of driver to be 128 or less, to take optimal schemes, as well as to maintain flexible high quality multi foci without grating lobes in an elongated focal region.

Statement of Contribution/Methods

Previously, we developed a genetic optimal algorithm which can be used in steering flexible multi foci. Now, in this study we contribute several optimal strategies in design array: Firstly, a basic array is setup; each array element has small projection square size of width 1.5-3.5mm. Secondly, several nearby elements are combined as an element excited by one channel driver; and the elements in a combined element are in electrically parallel connection. So the numbers of channel drivers will decrease. Thirdly, the combined elements are arranged in a periodic manner. Fourthly, multi focus patterns are steered by the genetic algorithm. Finally, the excitation efficient is improved by the weighted matrix approach.

Results

Two styles of combined array elements are used in simulations, one is the four combined element of basic element size 3.5mm with total 612 elements, and another is the nine combined element of basic element size 2.3mm with total 1516 elements. Each array is excited by the 128 channel drivers, and both arrays have same array parameters of 1.3MHz operating frequency, 112 mm aperture diameter and 125 mm radius of curvature. For the four combined element case, the single focus can be steered laterally in a range of 20 mm and axially in a range of 50 mm without grating lobes, while the four foci an be steered along propagation direction in a range of 40 mm. The 3D focus steering volume of the nine combined element is 7 times larger than that of element size 7 mm.

Discussion and Conclusions

The simulation results testify the feasibility of using 128 channel drivers to steering single and multi focus patterns without grating lobes and with elongated focal region. Further study still possible for better combined element arrangement. The practical phased-array focused-ultrasound system will be benefited from this study of optimal schemes.

2G-2

4:45 PM **Thermal Efficiency in Sonotherapy Array Design**

Douglas N. Stephens, Dustin E. Kruse, Chun-Yen Lai, Arif S. Ergun, Stephen Barnes, Katherine W. Ferrara; [1]*UC Davis, Dept. of Biomedical Engineering, USA,* [2]*Siemens Corporate Research, Inc., USA.*

Background, Motivation and Objective

The use of ultrasound for therapeutic applications involving innovative drug delivery methodologies is a promising area of research to enhance the effectiveness of drug delivery to treat a wide range of diseases, including cancer, peripheral vascular disease, and stroke. Rather than use destructive heating, we have used a family of multi-functional arrays which can ultrasonically identify and produce mild heating of specific tissue sites for activated delivery of drug-encapsulated vehicles. Since these triple array probes used are truly multifunctional operating on a commercial imaging system, there is a concern, as with any sonotherapeutic device, for the magnitude of the internal heating and heat dissipation pathways in a device design.

Statement of Contribution/Methods

We have compared three different triple-array probe designs for thermal efficiency and heat transfer characteristics. Each of these multifunctional arrays are comprised of a single center array row of 128 elements operating at 5.3 MHz for imaging, and two 1.5 MHz, 64 element outer arrays operated in parallel for sonotherapy. The laboratory verified KLM model for the low frequency array pair in each probe design has been used to derive estimates of array transmission efficiency, and as well the transducer electrical radiation and dissipation resistances which dictate acoustic output and heat generation respectively. Using the key parameters of each design, we can determine the array heat source function and apply analytical expressions to explain the heat dissipation pathways in the probe itself. Our analytical techniques include the use of equivalent lumped element thermal circuits for the transducer front port path, and application of the PDE heat equation for transient conduction with constant surface heat flux boundary conditions at the transducer backing. The flex circuits themselves act as thermal dissipation fins as the third heat escape pathway.

Results

The multifunctional array probes can be used to deliver up to 5 Watts of acoustic power in mild hyperthermia experiments with small animals. Our analytical expressions have been verified with temperature measurements made in the array backing material and on the array surface. Our early design, the G3, has a triple layer array stack and flex circuit interface connections to support these layers; a later design, the G4, has only a single layer array piezoceramic but has an optimized front port for heat dissipation. These two designs have produced very different thermal dissipation path distributions; the front, back, and flex circuit heat path distributions for the two are 14%, 10% and 76%, and 70%, 16% and 14% for the G3 and G4 designs respectively.

Discussion and Conclusions

These results can be directly related to optimized design features which improve the heat routing in sonotherapy array devices.

2G-3

5:00 PM **Modulating tumor blood flow with pulsed low intensity ultrasound and microbubbles**

David Goertz[1], Raffi Karshafian[1], Kullervo Hynynen[2]; [1]*Sunnybrook Health Sciences Centre, Imaging Research, Toronto, Ontario, Canada,* [2]*Sunnybrook Health Sciences Centre, Canada.*

Background, Motivation and Objective

While it is well established that high intensity focused ultrasound is capable of inducing vascular damage, there has been little work conducted to examine the vascular effects of low intensity therapeutic ultrasound in combination with microbubbles. Reports to date include observations of transient arteriolar constrictions and, with continuous-wave ultrasound, microvascular damage. With the latter, it is possible that thermal and standing wave effects may play significant roles. In this study we examine the feasibility of inducing flow changes in experimental tumors with pulsed low intensity ultrasound and microbubble contrast agents.

Statement of Contribution/Methods

Subcutaneous xenograft melanoma murine tumors (MeWo) were exposed to 1 MHz (740 kPa) pulsed ultrasound following a bolus injection of Definity microbubbles. The treatment burst consisted of a series of fifty 100 microsecond pulses sent at 1 kHz, which was repeated at 10 second intervals for a total duration of one minute. This exposure scheme, designed to avoid standing wave patterns and to minimize thermal effects, was carried out up to three times at 20 minute intervals. The tumors were imaged with 30 MHz ultrasound to assess tumor

morphology and volume. In addition, contrast imaging was performed using a 9 MHz clinical system pre-treatment, during treatment, and at 2 and 24 hour time points post treatment. Contrast enhancement was quantified at the periphery and center of the tumors, which were excised at the end of experiments for hematoxylin and eosin histology.

Results

Contrast imaging performed during therapeutic exposures revealed the rapid destruction of agent within the tumor during a single treatment burst. Transient (<20 minutes) reductions of tumor blood flow were observed following the first treatment burst. With repeated exposures, it was found to be feasible to to induce in flow reductions lasting for at least 24 hours. At the 2 and 24 hour points for example, contrast enhancement in the peripheral region of tumors was reduced by 60-75% relative to baseline values; in the central regions post-treatment enhancement was generally reduced to below detection levels.

Discussion and Conclusions

These results therefore indicate that pulsed (10% duty cycle) low intensity ultrasound in combination with microbubbles is capable of modulating blood flow in experimental tumors. Both transient and sustained flow reductions have implications for ultrasound mediated local drug delivery and potentiation.

2G-4

5:15 PM **A Prototype Design of a Low-Frequency Hemispherical Ultrasound Phased-Array System for Transcranial Blood-Brain Barrier (BBB) Disruption**

Hao-Li Liu, Heng-Wen Chen, Zhen-Hao Kuo, I-Hong Chen, Wen-Cheng Huang; *Chang Gung University, Department of Electrical Engineering, Tao Yuan, Taiwan.*

Background, Motivation and Objective

Focused-ultrasound technology has been demonstrated that not only for successful noninvasive thermal ablation, but also can reversibly disrupt the blood–brain barrier (BBB), which opens a new era in drug delivery to the central nervous system. In ultrasonic energy delivery, ultrasound phased array can steer the ultrasonic energy focus to an arbitrary position by driving each element with a signal of the appropriate phase and bring benefits for treatments. However, current phased array system design emphasized on thermally ablative application but not for BBB disruption application and for brain drug delivery. The purpose of this study was to demonstrate a prototype design of a low-frequency multiple-channel hemispherical focused-ultrasound phased-array system for transcranial disruption of the blood-brain barrier (BBB).

Statement of Contribution/Methods

In this study, we have presented a prototype design of a multiple-channel ultrasound hemispherical phased-array system to perform localized BBB disruption. In our system design, the driving system includes a microcontroller/ field-programmable-gate-array (FPGA)-based control kernel with multiple-channel driving circuits implemented by a high-voltage switching/ LC-resonance/ impedance-matching circuit module. Three hemispherical phased arrays comprising 22, 31, 48, and 80 elements were fabricated and tested. The pressure distributions at the geometric center and at off-center positions were tested experimentally. The focal performance of the different hemispherical arrays was also evaluated theoretically. The ultrasound frequency is tunable from 200 to 400 kHz.

Results

Results showed that the developed phased-array system can successfully drive the hemispherical array with multiple-channel ultrasound signals. The system exhibited a good focusing ability, with it being possible to electrically steer the target position with a wide focus offset, which provides flexibility and performance for locally exposing the brain to ultrasound energy. The results from animal experiments demonstrate the feasibility of disrupting the BBB through the intact animal skull (see Fig. 1).

Discussion and Conclusions

The described system could act as a platform design example or a reference for the development of a transcranial focused-ultrasound phased-array system for the clinical application of brain drug delivery.

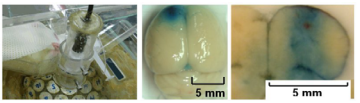

2G-5

5:30 PM **Microbubble dependence and permeability assessment of the ultrasound-induced blood-brain barrier opening in vivo**

Elisa Konofagou, James Choi, Jameel Feshitan, Ann Lee, Mark Borden; *Columbia University, New York, NY, USA.*

Background, Motivation and Objective

Current treatments of neurological and neurodegenerative diseases are limited due to the lack of a truly noninvasive, transient, and regionally selective brain drug delivery method. The brain is particularly difficult to deliver drugs to because of the blood-brain barrier (BBB). Over the past few years, we have been developing methods that combine Focused Ultrasound (FUS) and microbubbles in order to noninvasively, locally and transiently open the BBB so as to treat neurodegenerative diseases. In this paper, the role of the microbubble properties in the BBB opening and its permeability is investigated.

Statement of Contribution/Methods

The left hippocampus of mice was sonicated (frequency: 1.525MHz, pressure: 0.33 MPa, duty cycle: 20%, duration: 1 min) in vivo through the intact skin and skull following intravenous injection of microbubbles. Two different size ranges of lipid-shelled microbubbles (1-2 and 4-5 μm in diameter) were prepared and filtered according to their size based on their buoyancy. The permeability (Ki) of the BBB was quantified using a sequence of MR T1-weighted images (9.4 T, Bruker Medical; Boston, MA) and a previously reported model (Jiang et al., J. Cer. Blood Flow Metab., 25, 583-592, 2005) in order to measure the permeability changes of the BBB as a result of the FUS-induced opening. Gadolinium (Omniscan™; Amersham Health, AS Oslo, Norway; molecular weight: 574 Da) was used as the MR contrast agent, which normally cannot penetrate the BBB.

Results

Bigger microbubbles (4-5 μm in diameter) resulted in a larger gadolinium-enhanced region of BBB opening in the targeted (left) hippocampus compared to the findings using 1-2 μm bubbles. The increased extent of the BBB-opened region is in agreement with previously reported models on the relationship between microbubble resonance and vascular effects (Sassaroli and Hynynen, Phys. Med. Biol., 5293-5305, 2005; Qin and Ferrara, Ultras. Med. Biol.,1140-48, 2007), which have shown that in compliant vessels the natural frequency of 4-μm microbubbles becomes 1.3 MHz, potentially justifying the enhanced effect in the 4-5μm case at the frequency used in this study. Ki maps were obtained across the entire brain and were found highest at the BBB opening site equal to 7 μl/g-min. These values are in agreement with Ki values in BBB disruption reported in tumor models (6.8(±3.5)- 15.1(±8.0) μl/g-min (Ding et al., J. of Brain Res.,195-203, 2006)).

Discussion and Conclusions

This study showed that bigger microbubbles induced larger BBB opening regions at the frequency used. The microbubble is thus as important of a component as the ultrasound beam in accurately predicting the resulting BBB opening. Control over the microbubble size and type sheds important light in the underlying mechanism of the opening. The permeability of the BBB opening was also quantified in vivo. Results will be shown in both non-transgenic (normal) and transgenic (Alzheimer's) mice.

2G-6

5:45 PM **Feasibility of Transient Image-guided Blood-Spinal Cord Barrier Disruption**

Rajiv Chopra, Jeffrey Wachsmuth, **Kullervo Hynynen;** *Sunnybrook Health Sciences Centre, Canada.*

Background, Motivation and Objective

One of the barriers to delivery of therapeutic agents in the spinal cord is the blood-spinal cord barrier (BSCB). Transient disruption of the BSCB using ultrasound could enable the development of novel spinal cord therapies. The objective of this study was to evaluate the feasibility of BSCB disruption in rats.

Statement of Contribution/Methods

A 6mm segment of the upper spine in seven male rats was exposed to ultrasound. A spherically-focused transducer (d=8cm, f=0.8) delivered 10ms bursts of 1MHz ultrasound with a PRF of 1Hz. The free-field peak negative pressure was 1.06MPa. The 300-second exposure consisted of a linear raster scan with 1mm steps after IV injection of Definity microbubbles (0.045ml/kg) in the tail vein. The extent of BSCB disruption was evaluated using contrast enhanced T1-weighted MRI. Behavior and motor function of the rats was observed after the exposures and the spines were harvested for subsequent histology evaluation.

Results

Consistent BSCB disruption was observed as delayed signal enhancement in the spinal cord on the MRI. The relative enhancement was approximately 61% (+/-38), varying across individual animals and exposures. No significant changes in spinal cord appearance were visible on T2-weighted images acquired after each exposure.

Discussion and Conclusions

BSCB opening is feasible in rats using ultrasound. Given the amount of disruption observed by MRI in these experiments, previously published Blood-Brain barrier experiments suggest that large molecule delivery at therapeutic quantities is feasible. The motor behavior of rats appeared normal after each exposure, suggesting repeated opening of the BSCB is safe.

3G. High Frequency Transducers

Room 305 A/B/C

Tuesday, November 4, 2008, 4:30 pm - 6:00 pm

Chair: **Jian Yuan;**
Boston Scientific, USA.

3G-1

4:30 PM **Stiffness controlled SU8-based nanocomposites: application for matching layer for 1 GHz ultrasonic transducer**

Sheng-Xiang Wang[1], Julien Carlier[1], Assane Ndieguene[1], Pierre Campistron[1], Dorothée Callens[1], Bertrand Nongaillard[1], Xing-Zhong Zhao[2]; *[1]Institut d'Electronique de Microélectronique et de Nanotechnologies, France, [2]Wuhan University, China.*

Background, Motivation and Objective

The recent trend toward biological detecting demands higher resolution at the scale of micrometer pushes the operating frequency of acoustic devices up to the gigahertz range. As far as silicon based Lab-on-chip integrating high frequency (~1 GHz) characterization for mechanical properties determination of biological cells concerned, it's necessary to get good matching between silicon and water. Different nanocomposites based on the well-known epoxy-based photoresist SU8 have been achieved and characterized. The aim is to fabricate λ/4 wavelength matching layer with materials enabling adjustable mechanical impedance for the high frequency transducers.

Statement of Contribution/Methods

SU8 2000 resist (Microchem Corperation) and nanosized TiO_2 (~35 nm, Degusay corperation) and $SrTiO_3$ (~ 50 nm, MricroMIT corperation) were ball-milled (Retsch PM100) with an agate jar in order to obtain homogeneous mixture. The microstructure of the mixtures has been characterized (by FIB and SEM) and the properties of the nanocomposite obtained have been measured. The mechanical impedance and the attenuation of this composite material are characterized around 1 GHz thanks to the measurement of S_{11} (reflected to incident electrical waves ratio) parameter and extracting the targeted parameters thanks to signal processing. Insertion loss of the device in water is evaluated and the global gain in transmission is deduced.

Results

Several types of SU8-based nanocomposites have been deposited on the transducers as matching layers. Most of the curves including speed, attenuation and density, depending on the concentration of different nanoparticules in SU8 are presented. Properties of examples of such composites are shown in Table I. Photosensitivity of these composites for lithography application has also been tested.

Discussion and Conclusions

Acoustical characterization of SU8-based nanocomposites at the ultrasonic frequency of 1 GHz was obtained. The results show that by adjusting the concentration of the inorganic particles one can dispose to arbitrary mechanical impedance materials. Application in mechanical matching layer between silicon and water (especially for BioMEMS applications and acoustic microscopy at 1 GHz) allows to gain 5 dB on the transmitted signal.

Table I *acoustic characteristics of nanocomposites at 1GHz*

	SU8	70wt%SU8 /30wt%TiO_2	70wt%SU8/15wt%TiO_2 15wt%$SrTiO_3$	70wt%SU8 30wt%/ $SrTiO_3$
Acoustic impedance (Mrayls)	3.5	6.0	6.5	7.1
Acoustic wave speed v (m/s)	2886	2609	2500	2367
Attenuation α (dB/μm) at (1GHz)	0.33	0.53	0.56	0.66
Density (kg/m³)	1200	2300	2600	3000

3G-2

4:45 PM **60 MHz PC-MUT for Intravascular Ultrasound (IVUS) Imaging**

Jian Yuan[1], Sorah Rhee[1], Xiaoning Jiang[2]; *[1]Boston Scientific Corporation, Fremont, California, USA, [2]TRS Technologies Inc., State College, Pennsylvania, USA.*

Background, Motivation and Objective

High frequency transducers are desired catheter-based intravascular imaging. High frequency intravascular imaging benefits from the use of high sensitivity and broad bandwidths as they allow for an increased depth of field compared to existing devices with high resolution. The 40 MHz PC-MUT developed by the authors in 2006 showed already significant improvement and in this paper, the subsequent development of a 60 MHz PC-MUT as a platform for next generation IVUS catheters will be presented.

Statement of Contribution/Methods

A PMN-PT single crystal 1-3 composite was designed and fabricated using a unique combination of deep reactive ion etching (DRIE) and conventional composite backfilling technique. The 60 MHz composite was characterized and transducer devices were prototyped with suitable backing and matching layers, cable connections and electrical matching network. The incorporation into imaging catheters allowed for imaging of phantoms and a porcine animal model.

Results

Figure 1 shows an etched PMN-PT single crystal array with a kerf width of ~ 4 µm and an etching depth of ~ 40 um. The acoustic performance of the transducer was demonstrated with 56 MHz and a bandwidth of 84% (Figure 2). Imaging results will be presented in comparison to both a 40 MHz PC-MUT transducer as well as well as commercial IVUS catheters.

Discussion and Conclusions

Using the PC-MUT technology, the limitations of traditional dice-and-fill methodology for the fabrication of 1-3 composites have been overcome. The unique combination of DRIE and traditional composite fabrication methodology allowed for the demonstration of a high frequency transducer at 60 MHz. The use of high frequency ultrasound with a broadband transducer device is the key to significantly improve high resolution IVUS imaging.

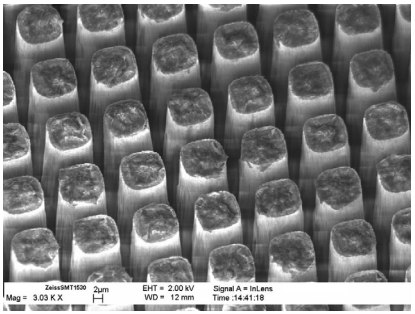

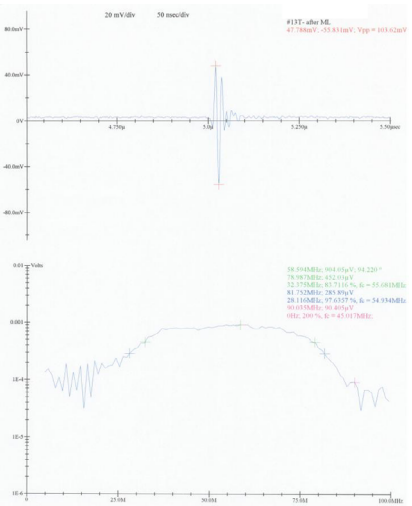

3G-3

5:00 PM **Development of a 30 MHz 1-3 Composite Array for Medical Imaging**

Jonathan Cannata, Jay Williams, Chang-Hong Hu, K. Kirk Shung; *University of Southern California, Biomedical Engineering, Los Angeles, CA, USA.*

Background, Motivation and Objective

High frequency (>30 MHz) ultrasound is currently used for various clinical and research applications. There are several commercial single element transducer based ultrasound scanners available for use in these applications that operate in the 20 MHz to 80 MHz frequency range. However, 1-D array technology is currently being pursued to

improve the quality and functionality of high frequency scanners. Unfortunately at the present time commercial array scanners are not yet available at frequencies above 20 MHz mainly due to limitations in array fabrication technology and the availability of suitable electronics. To meet the demand for a high-quality, high-frequency, ultrasound images we are developing a 30 MHz, 256-element, array and digital beamformer. The array, which is the topic of this presentation, was constructed using 1-3 composite elements spaced at a 50 µm pitch.

Statement of Contribution/Methods

The composite array was developed using a piezoceramic with high dielectric permittivity (L-145N, TFT Corp., Tokyo, Japan). Composite elements were formed using a mechanical dicing saw and the interdigital pair- and phase-bonding techniques. The resultant ceramic posts were approximately 16 µm wide separated by a 4 µm polymer kerf, with two posts and one kerf forming an element in the azimuth direction for a ceramic volume fraction of approximately 64%. Mechanical dicing was used to produce the 14 µm wide inter-element kerfs. A custom designed flexible circuit and mating printed circuit board was used to interconnect the elements with 75-Ohm, 40-AWG coaxial cables (Precision Interconnect, Portland Oregon). Finally, an electroplated single epoxy matching layer was used as the ground plane and to improve the two-way response of the elements.

Results

One flat-aperture 256-element array has been fabricated and two eight-element sub-apertures were tested. All elements were active and produced a pulse-echo response centered at 30 MHz with approximately 60 % -6 dB bandwidth. Element crosstalk was also evaluated. The maximum crosstalk for the nearest and next-nearest neighbor element was -27 dB and -42 dB, respectively.

Discussion and Conclusions

We have developed an effective technique for fabricating high frequency linear arrays. Future arrays will be focused in the elevation direction by conforming the 1-3 composite and flex-circuit to an 8mm radius cylindrically molded epoxy backing substrate. A focused version of this array will be fabricated next followed by a final version with the 256-element cable interconnect and housing for use with our prototype beamformer.

3G-4

5:15 PM **High-frequency (>100MHz) Piezoelectric PZT Film Micromachined Ultrasonic Arrays**

Dawei Wu[1], Qifa Zhou[1], Changgeng Liu[2], Frank Djuth[2], K Kirk Shung[1]; *[1]University of Southern California, NIH Transducer Resource Center and Department of Biomedical Engineering, USA, [2]Geospace Research, Inc, USA.*

Background, Motivation and Objective

High frequency (>30 MHz) ultrasonic imaging has been extensively used for imaging of the eye, blood vessel, skin and small animals. Fabrication of the transducers, which is the most critical component of the ultrsound imaging system, becomes especially challenging when very high frequency (>100 MHz) is required. Conventional lapping-and-dicing methods with bulk piezoelectric materials are no longer a viable approach. During recent years, the advance of microelectromechanical system (MEMS) methods has offered significant opportunities for miniaturized devices. This paper presents the latest development of high-frequency (>100MHz) micromachined ultrasonic linear arrays with high-quality PZT thick films.

Statement of Contribution/Methods

Both kerfless and kerfed arrays were fabricated with the PZT thick films which were prepared by spin-coating PZT composite solution. To fabricate the kerfless array, a layer of Cr/Au was patterned onto PZT film surface by using photolithographic techniques. A conductive epoxy, E-solder 3022, was used as a backing material after the silicon substrate was removed. One major problem with the kerfless arrays is their large crosstalk. To decrease the crosstalk, Inductively coupled plasma-Reactive ion etching (ICP-RIE) SF6 based dry etching was selected to etch the PZT thick films into kerfed arrays. The kerfs of the array were next filled with non-conductive epoxy; the front surface of the array elements were coated with Cr/Au electrodes. E-solder was poured in as the backing material after etching away the silicon substrate.

Results

A representative element of the kerfless array was found to have a center frequency of 120 MHz, -6 dB bandwidth of 40% and an insertion loss of around -40 dB. Its bandwidth increased to 60% after a layer of parylene was deposited as a matching layer. The etched PZT film array has a thickness of 15 µm and etched profile angle of 75° as shown below. Charactrization of the array has been carried out. Results show great promise for this technology in fabricating linear arrays at a frequency higher than 50 MHz.

Discussion and Conclusions

High-frequency (>100 MHz) PZT linear kerfless arrays are fabricated and tested. Preliminary results of the etched linear kerf array are promising. The results show that integrating PZT films into MEMS devices can serve as a feasible solution to high-frequency ultrasonic array fabrication.

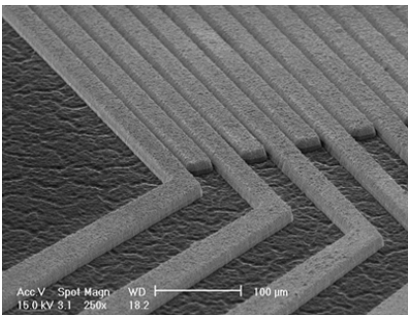

3G-5

5:30 PM **High-Frequency (60MHz - 100MHz) Medical Ultrasound Transducer Arrays Produced by Micromachining Bulk PZT Materials**

Changgeng Liu[1], Dawei Wu[2], Qifa Zhou[2], Frank Djuth[1], Kirk Shung[2]; *[1]Geospace Research, Inc., El Segundo, CA, USA, [2]University of Southern California, Los Angeles, CA, USA.*

Background, Motivation and Objective

High frequency, wideband ultrasound transducer arrays can provide the necessary spatial resolution for use in dermatology, ophthalmology, and other medical applications where high quality subsurface imaging is required. Unlike high frequency single-element transducers, one of the major challenges in developing high-frequency ultrasound arrays is the patterning of small-scale features within the array. For example, traditional dicing methods cannot be used to fabricate array elements that have a pitch of 18 µm and a kerf width of 6 µm, which are nominally used with a 100 MHz linear array. In this research, micromachining techniques are utilized to fabricate high frequency array elements. Instead of using sol-gel PZT thick film, bulk PZT material is employed because of its high electromechanical coupling coefficient.

Statement of Contribution/Methods

A dry etching plasma technique with chlorinated gases was selected to pattern the bulk PZT material. By optimizing the dry etching parameters, such as RF power, gas ratio, and chamber pressure, we obtained vertical profile angles of 83°. An electroplated nickel layer was used as a hard mask for etching the PZT. As designed, a series of 60 MHz to 100 MHz linear arrays were fabricated, and one transducer centered at 67 MHz was packaged and tested.

Results

The 67 MHz linear array transducer has 32 elements with an element width of 24 µm and a kerf width of 12 µm. Element length and thickness are 3 mm and 27 µm, respectively. The transducer was placed inside a metal housing and subsequently evaluated. The electrical impedance of the transducer is about 51 Ω at its center frequency. Values for the -6 dB bandwidth and two-way insertion loss are about 30% and 26 dB, respectively. The crosstalk between adjacent channels is about -25 dB at the center frequency.

Discussion and Conclusions

Simulation results show that the bandwidth will increase to 40% after deposition of a matching layer of parylene material at the front of the transducer. An increase in the backing material impedance from 6 MRayls to 20 MRayls will further increase the bandwidth to 69%. These transducers are currently being refined for use in imaging applications.

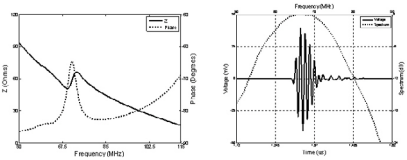

(a) Electrical impedance (b) Pulse echo response

Figure 1: Experimental results for one element of the linear array ultrasound transducer with a center frequency of 67 MHz

3G-6

5:45 PM **High Frequency Transducer with Integrated Electronics**

Susan Trolier-McKinstry; *Pennsylvania State University, Materials Science and Engineering, University Park, PA, USA.*

Background, Motivation and Objective

High frequency ultrasonic transducer arrays (5 - 50 MHz) have been fabricated using thin film piezoelectrics on larger resonating structures. The use of thin films allows much lower driving voltages (< 5V) and so facilitates a custom - designed chip for the drive - receive electronics.

Development of this technology is expected to enable:

- High resolution catheter-based ultrasonic probes.
- Wireless replacements for current ultrasound transducers.

Statement of Contribution/Methods

1D transducer arrays have been made using a xylophone bar transducer, in which the length or width extension mode is excited. This allows spacing the elements at half the acoustic wavelength. Finite element modeling demonstrates that such devices launch a sound wave perpendicular to the substrate surface, and that adequate sound pressure levels can be generated.

Because the drive voltages of these transducers are low, close coupling of the electrical circuitry is possible. Thus, an integrated circuit has been designed to enable significant system miniaturization.

Results

PZT films with thicknesses of 0.5 to 1 micron have been prepared by chemical solution deposition on micromachined resonating structures. As-prepared PZT films have $e_{31,f}$ coefficients of -5 to -12 C/m^2, with the best values obtained from (001) oriented, morphotropic phase boundary compositions. Parylene is used both as a matching layer, and to provide electrical insulation.

Xylophone transducers with different degrees of undercut have been examined. While numerous vibration modes can be detected via impedance spectroscopy of devices measured in air, the flexural modes are largely damped when the transducers are measured in water. Using reference transducers in a pitch-catch mode in a water bath, it has been demonstrated that the thin film 1D array transducers function both on transmit and receive. Work is currently underway to demonstrate the two-way transmit-receive characteristics of the device.

In addition, a CMOS transceiver chip was designed and prototyped in 0.35 µm process technology for a 50 MHz transducer. The CMOS transceiver chip contains a multi-channel data acquisition system which, in conjunction with digital beamforming electronics, enables focusing and beam steering for the ultrasound system in both transmit and receive modes. It also has analog-to-digital converters with an on-chip buffer memory. Testing of the prototype circuitry indicates that all of the components function, though some with reduced frequency ranges.

Discussion and Conclusions

1D and 2D high frequency transducer arrays have been fabricated using piezoelectric thin films on larger resonating structures. Due to the small thickness of the piezoelectric layer, the required driving voltages are small, and the device can be integrated with CMOS electronics. In addition, impedance matching at high frequencies is readily achieved for devices spaced at half the acoustic wavelength.

4G. Acoustic MEMS Devices

Hall 2A

Tuesday, November 4, 2008, 4:30 pm - 6:00 pm

Chair: **Daniel Hauden;**
FEMTO-ST Besancon, France.

4G-1

4:30 PM **A Review of the Recent Development of MEMS and Crystal Oscillators and Their Impacts on the Frequency Control Products Industry**

C.S. Lam; *Integrated Device Technology, Inc., Andover, MA, USA.*

Background, Motivation and Objective

Due to its high Q and temperature-stable properties, quartz crystal based oscillators are important clock sources in consumer, commercial, industrial, and military products The demand for quartz crystal resonators and oscillators continues to rise and the quartz crystal industry has made major progresses in miniaturization, performance enhancement, and cost reduction in the past ten years. The unique fabrication and encapsulation requirements though render quartz crystal resonators and oscillators difficult or close to impossible to be integrated onto the mature silicon based IC platforms. The recent technical breakthroughs of all silicon MEMS (Micro Electro Mechanical Systems) based resonators and oscillators seem to re-ignite the interest in displacing/replacing the quartz crystal technology and to open up again the prospect in clock source integration. Based on a 2006 review paper by the author[1], this paper expands on the subject by reviewing the development of all silicon MEMS oscillators and crystal oscillators in the past few years and commenting on what challenges they face in the highly competitive frequency control products industry. This paper will also touch on the recent development of CMOS oscillators (without moving parts) and piezoelectric-activated silicon MEMS resonators and oscillators.

[1] "An Assessment of the Recent Development of MEMS Oscillators as Compared with Crystal Oscillators," C.S. Lam, Piezoelectricity, Acoustic Waves and Device Applications- Proc. of the 2006 Symposium, Zhejiang University, China, 14~16 December 2006, ed. Ji Wang and Weiqiu Chen, pp. 308-315 (also in http://www.txccorp.com/download/tech_paper/2006-SPAWDA-3.pdf)

4G-2

5:00 PM **Internal Phase Inversion Narrow Bandwidth MEMS Filter**

Jize Yan[1], Ashwin Seshia[1], Kim Le Phan[2], Joost Van Beek[2]; *[1]University of Cambridge, United Kingdom, [2]NXP Semiconductors, Netherlands.*

Background, Motivation and Objective

There is an interest in the development of MEMS-based high-performance, voltage-controlled and highly-selective band-pass filters. We have recently reported electrical and mechanical phase inversion in coupled MEMS resonator arrays as a solution to overcome the effects of capacitive parasitic intrinsic to many microfabrication processes. However, achieving narrow bandwidth (BW) utilising mechanically coupled resonator arrays is challenging at very high frequencies in part due to the practical limitations in coupling very tiny electro-mechanical signals between the resonators. Previous solutions are often restricted by the requirement for high DC voltages that runs counter to the miniaturization and integration trends of RF front ends.

Statement of Contribution/Methods

A novel capacitively coupled twin beam resonator-array internal phase inversion filter is fabricated in a SOI process. Narrow BW (0.0157%) is demonstrated with a very low control-voltage (~ -1V). With differential DC driving, the capacitive-coupling can substantially reduce the BW compared with the mechanical-coupling as no mechanical coupling-spring exists, which normally sets the minimum tunable BW.

Results

A DC-bias is applied on the input port of the MEMS resonator and a small negative control-voltage is applied on the output port as optically shown in Fig 1(a). Then the inverse phase current is induced, which can be coupled with the motional current to construct filter performance as shown in the in Fig. 1(b) (see blue curve), with a

frequency of 4.131MHz, a 3dB-BW of 0.0157% and a 0.15dB ripple measured under -0.98V control-voltage and 14V DC-bias. In contrast, the device is simply a resonator without an applied control-voltage as seen in Fig 1(b) (see black curve). The relation between the control-voltage (output) and the DC-bias (input) is shown in the dotted line in Fig. 1(c). The blue and red curves show the variation in the frequencies of the two resonant peaks. The BW (spacing between blue and red curves) decreases with increasing DC-bias and decreasing control-voltage.

Discussion and Conclusions

Narrow (0.0157%) bandwidth capacitive-coupled resonator-array internal phase inversion MEMS filter is demonstrated under low control-voltage (~ -1V) utilizing a SOI process. The principle can be easily extended to MEMS filters based on other resonator topologies.

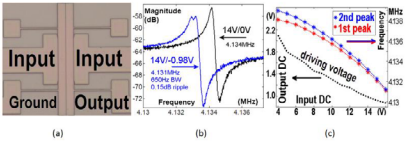

Tuesday Oral

4G-3

5:15 PM **A Layered SAW Device Using Phononic-Crystal Reflective Gratings**

Tsung-Tsong Wu, Wei-Shan Wang, **Jia-Hong Sun;** *National Taiwan University, Institute of Applied Mechanics, Taipei, Taiwan.*

Background, Motivation and Objective

Surface acoustic wave (SAW) devices consisting of inter-digital transducers (IDT) and metal gratings have been widely used as resonators for decades. In order to have good reflection, hundreds of metal strips are usually employed, and it is volume consuming. Phononic crystals (PC) consist of periodic arranged media and perform acoustic band gaps [1]. They can stop surface acoustic wave propagation efficiently with even tens of lattice periods. In other words, PC can be designed as space-sparing wave reflectors. In this paper, a design which combines a two-port SAW devices and phononic crystals acting as gratings is first demonstrated.

Statement of Contribution/Methods

A layered ZnO/Si SAW device is fabricated in this study. By depositing ZnO film on a silicon wafer, the ZnO film provides the piezoelectric medium for IDT to generate and detect SAW on the silicon-based structure. In our previous work, a square lattice PC composed of cylindrical holes on a silicon half space was designed [2, 3]. With a 10 μm lattice constant and filling fraction of 0.283, the PC has a band gap of 194-223 MHz for SAW along the ΓX direction. Considering the dispersion and the electromechanical coupling coefficient of the ZnO/Si layered structure, the frequency of the layered SAW device is designed at 210 MHz. In addition, the finite-difference time-domain (FDTD) method [4] is used to analyze the phenomena of SAW encountering the PC grating. The simulation shows that reflected SAW result in resonant waves, and this helps to optimize the delay line of the two-port SAW device.

Results

Through MEMS process, a two-port SAW device with thirty IDT pairs is realized on the ZnO/Si structure. The IDT was manufactured on the ZnO/Si layered structure and the cylindrical holes were fabricated via inductive coupling plasma on the Si substrate. With the properly designed PC whose band gap contains the frequency of SAW, acoustic waves reflect efficiently from the PC grating of only fifteen lattice periods. The preliminary experiment shows a 7 dB higher insertion loss at the central frequency than the case using traditional grating of three hundred metal strips.

Discussion and Conclusions

In this study, a structure proposed for the first time which combining a SAW device and phononic crystals acting as gratings is designed, realized, and investigated. The experimental results show better frequency response by using phononic crystal as wave reflectors. Moreover, the size of grating is reduced efficiently. This newly proposed structure may provide a new idea for designs of resonators, filters, or other possible applications.

References:

[1] T.-T. Wu, Z.-G. Huang, and S. Lin, Phys. Rev. B, vol. 69, no. 094301, 2004.

[2] T.-T. Wu, Z.-G. Huang, and S. Y. Liu, Zeitschrift für Kristallographie 220, pp. 841, 2005.

[3] T.-T. Wu, L.-C. Wu, and Z.-G. Huang, J. Appl. Phys., vol. 97, no. 094916, 2005.

[4] J.-H. Sun and T.-T. Wu, Phys. Rev. B, vol. 74, no. 174305, 2006.

4G-4

5:30 PM **Fully-Differential Mechanically-coupled PZT-on-Silicon Filters**

Hengky Chandrahalim[1], Sunil Bhave[1], Ronald Polcawich[2], Jeff Pulskamp[2], Daniel Judy[2], Roger Kaul[2], Madan Dubey[2]; [1]*Cornell University, Electrical and Computer Engineering, Ithaca, NY, USA,* [2]*US Army Research Laboratory, Adelphi, MD, USA.*

Background, Motivation and Objective

A growing military interest in developing a mobile radio operating from FM to X-band has created a strong demand for narrow-bandwidth filters. Filter banks composed of high-Q (> 4,000) MEMS resonators are fabricated in silicon, reducing size, weight and power in radios.

Statement of Contribution/Methods

This paper reports on the design of a 2-pole fully-differential filter using mechanically-coupled overtone width-extensional mode (WEM) resonators. Unlike DMR filters, this filter utilizes a spring to couple two WEM resonators (Fig. 1a and b). The small footprint of the coupling spring reduces the filter area compared to electrically-coupled filters [1]. The resonators and filters are fabricated in the 10 µm thick device layer of an SOI wafer to enhance Q and transduced by a 0.5 µm PZT film deposited on the device layer. Overtone modes of WEM resonators are excited by patterning IDT like electrodes on top of the resonators [2].

Results

A 206.3 MHz overtone WEM filter is demonstrated with 653 kHz bandwidth, -25 dB insertion loss (IL, 50 Ω matched) and -62 dB stop-band rejection in air. The PZT transducer has a voltage-tunable piezoelectric response. The filter demonstrated a 20 dB improvement in IL and 0.16% center frequency tuning resulted by applying 20 V tuning voltage. DC voltage improves the piezoelectric coupling coefficient as well as increases the Young's modulus of the PZT film as shown in Fig. 1d.

Discussion and Conclusions

The implementation of fully-differential filter by only using two mechanically-coupled resonators exhibits significant benefits over lattice filters that require large area and cross-over routing. The large shunt capacitance can mask away the PZT motional current, however, the differential configuration cancels the capacitances and enables a 10 dB out-of-band attenuation. In addition, the improvement in coupling coefficient (k_{31}^2) with increased DC bias reduces impedance, thereby improving out-of-band attenuation from 10 to 30 dB. The increase in Young's modulus of the PZT film facilitates a modest frequency tuning capability to the PZT-Silicon composite resonator.

[1] Piazza et al "Channel-Select RF MEMS Filters Based on Self-Coupled AlN Contour-Mode Piezoelectric Resonator," Ultrasonics'07.

[2] Ayazi et al "Enhanced Power Handling and Q in Thin-Film Piezoelectric-on-Substrate Resonators," Ultrasonics'07.

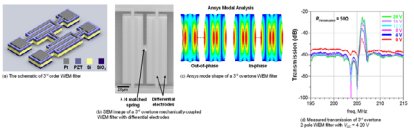

4G-5

5:45 PM **Piezoelectrically transduced Single-Crystal-Silicon Plate Resonators**

Antti Jaakkola[1], Piia Rosenberg[1], Olli Holmgren[2], Kimmo Kokkonen[2], James Dekker[1], Arto Nurmela[1], Tuomas Pensala[1], Tommi Riekkinen[1], Tomi Mattila[1], Ari Alastalo[1]; *[1]VTT technical research center of Finland, Espoo, Finland, [2]Helsinki University of Technology, Department of Engineering Physics, Espoo, Finland.*

Background, Motivation and Objective

Micromechanical resonators are considered as candidates for replacing ceramic and SAW devices used as frequency reference and filter components in modern wireless applications. Often MEMS resonators rely on capacitive transduction. For good electromechanical coupling, sub-100 nm capacitive gap sizes and biasing voltages in excess of 10 V are needed. Especially the latter need is problematic to meet with low cost integrated circuits.

To overcome these problems, we have investigated a resonator transduction mechanism based on a piezoelectric aluminium nitride layer grown on top of the resonator body [1]. In this work we report results on single-crystal-silicon plate resonators [2] with piezoelectric transduction.

Statement of Contribution/Methods

The plate resonators were fabricated on SOI wafers featuring pre-etched cavities. A 300 nm piezoelectric AlN layer was deposited on top of the resonator by reactive sputtering. The top electrode is a sputter deposited 300-nm-thick molybdenum layer, while the highly p-doped Si device layer acts as the bottom electrode. The resonators were released by dry etching, paying special attention for producing anchor structures with very narrow (4 µm) bridges.

Two types of plate resonators are reported here, one with lateral dimensions of 160x160 µm2 designed for operation in square-extensional (SE) mode [2], and another (320x320 µm2) intended to operate in Lamé mode. The resonators are characterized via electrical measurements, and the structures are simulated with a 3D FEM model. Furthermore, the vibration modes of the resonator are characterized with a scanning laser interferometer [3].

Results

The SE resonator has its main resonance at 26 MHz with Q=18000 and with motional resistance Rm=0.24 kOhm. The Lamé resonator main resonance is at 9 MHz featuring Q=17000 and Rm=1.6 kOhm. In addition, both resonators have strong higher-order modes: for example, the Lamé plate has a resonance at 22 MHz with Q=51000 and Rm=1.5 kOhm. The FEM simulations are compared to measured vibration modes.

Discussion and Conclusions

Micromechanical plate resonators with piezoelectric transduction have been designed, manufactured and characterized. The resonance modes of the resonators feature high Q-values and low motional resistances, indicating low losses and good electromechanical coupling

[1] G. Piazza et al. Sensors and Actuators A 111, 71-78, 2004.

[2] V. Kaajakari et al., IEEE Electron Device Letters, Vol. 25, No. 4, pp. 173-175, Apr. 2004.

[3] J. V. Knuuttila et al., Optics Letters, Vol. 25, No. 9, pp. 613-615, May 2000.

5G. NDE Phased Arrays

Hall 2B

Tuesday, November 4, 2008, 4:30 pm - 6:00 pm

Chair: **Robert Addison;**
Rockwell Science Center, USA.

5G-1

4:30 PM **Reduction of Grating Lobes in SAFT Images**

Carlos Julián Martín[1], Oscar Martínez[1], Alberto Octavio[2], Gregorio Godoy[3], Luis Gómez-Ullate[1]; *[1]IAI-CSIC, Department of Systems, Arganda del Rey, Madrid, Spain, [2]IA-CSIC, Department of Signals, Systems and Ultrasonic Technologies, Madrid, Madrid, Spain, [3]University of Jaén, Department of Electronic Engineering, Linares, Jaén, Spain.*

Background, Motivation and Objective

The classical synthetic aperture technique, with only one channel to emit/receive, where the elements of the phased array are sequentially activated, is very popular because it allows decreasing the complexity and the cost of ultrasound imaging systems. Furthermore it has other advantages such as: it is possible to focus the main beam dynamically in emission/reception; the lateral resolution is improved with respect to the original phased array; and also, if the image is composed by fewer lines than elements, it is able to generate images faster than the phase array. However, the contrast achieved with this method is significantly lower than the one obtained with the phase array. This is because the SAFT coarray (sometimes called "effective aperture") resulting from the addition of all the convolutions between the emission and reception sequences, produces an element distribution that doubles the inter-element spacing, thus introducing grating lobes in the beam pattern.

This work presents a new SAFT configuration that uses one element in emission and two elements in reception, which suppresses the grating lobes maintaining the advantages of the classical SAFT. Here, we present this SAFT configuration (that we call Two-elements SAFT or T-SAFT) and its electronic architecture which uses the coarray for generating the images.

Statement of Contribution/Methods

The T-SAFT strategy uses one element in emission and two elements in reception: the one emitting and its adjacent. With this configuration each received signal corresponds with every virtual element of the coarray, where the inter-element distance is now maintained as in the original phased array. The received signals, organized in the coarray structure, with no redundancy, can be processed in one-way using the virtual elements of the coarray. This is because the one way dynamic beamforming of the coarray is equivalent to the two-ways dynamic beamforming of the synthetic aperture. The electronic architecture for dynamic focusing in emission and reception is based on the coarray, what allows a simplification of the beamforming process.

Results

Simulations models and experimental tests have been developed to study the T-SAFT properties. A good agreement between experimentation and simulation confirms the goodness of the proposed method. Also, several apodization models have been used to improve the image quality and experimental. An electronic architecture based on the coarray is also proposed.

Discussion and Conclusions

The proposed T-SAFT configuration, with low hardware requirements, is able to maintain the principal advantages of the classical SAFT avoiding its main disadvantage: grating lobes formation. If two parallel channels are used in reception, the image frame rate is tied to the number of emitting elements in the original array, similar to the classical SAFT mode.

5G-2

4:45 PM **Influence of SAFT Activation Sequence in 2D Arrays Performance**

Carlos Martín[1], Oscar Martínez[1], Alberto Octavio[2], Francisco Montero[2], Luis Gómez-Ullate[1]; *[1]IAI-CSIC, Department of Systems, Arganda del Rey, Madrid, Spain, [2]IA-CSIC, Department of Signals, Systems and Ultrasonic Technologies, Madrid, Madrid, Spain.*

Background, Motivation and Objective

The synthetic aperture technique (SAFT), where only one element of the phase array is activated sequentially to emit and receive, is very popular on 1D phased-array. This technique allows decreasing the number of electronic channels necessary to generate image.

In the last years, the efforts of many researches have been focused on developing 3D real-time scanners based on 2D phased-arrays. In this context, the interest on the synthetic aperture techniques has increased, mainly considering that, under certain conditions, they can accelerate the image composition. In spite of this, there are not many works about the application of the synthetic aperture techniques over 2D array transducers.

The synthetic aperture technique usually use the same element to emit and receive, producing a beampattern with grating lobes. In this work different emit-receive strategies (which we call "activation sequences") are studied and evaluated through the 2D distribution of the elements in the coarray (sometimes also called "effective aperture").

Tuesday Oral

Statement of Contribution/Methods

Several theoretical examples are presented varying the activation sequence in an N*N elements array. Using a fixed sequence of the elements for emission, and varying the sequence of the receiving elements, different coarrays are obtained. From the SAFT coarray, a simple comparative analysis of the different beampatterns is obtained. Using corner elements as origin of the elements' sequence and choosing clockwise or anti-clockwise as evolution directions, eight configurations are studied.

Results

From the eight coarrays obtained, we can point out the following coarray configutions: (1) The classical SAFT, produces the coarray of N*N virtual elements, whose interlement space is double of the original array (grating lobes). (2) One of the sequences produces a single point coarray, producing a spherical wave. (3) Four of the sequences produce linear coarrays in the main directions or in the diagonals. (4) Two of the sequences produce a 2D coarray with reduced inter-element distance (1.4 times of the original array). This solution improves the grating lobes formation with respect to the classical SAFT.

Discussion and Conclusions

In the case of 2D arrays, SAFT techniques produces different beamforming results with only changing the sequence of the emitting-receiving elements. Using the coarray a simple analysis of the beamforming process can be made. We show that some of the sequences improve the results of the classical SAFT.

5G-3

5:00 PM **Estimation of Ultuasonic Location of PD in Power Transformer Based on Modified Multiple Classification Method**

Qing Xie[1], Nan Wang[1], **Yanqing Li[2],** Fangcheng Lv[1], Xin Xiang[1]; *[1]North China Electronic Power University, Department of Electrical Engineering, China, [2]North China Electronic Power University, China.*

Background, Motivation and Objective

Power transformer is one of the most important equipment of electric system, which insulating condition influences the safe operation of power system directly. At present partial discharge (PD) has become one main reason for the insulating deterioration of power transformer, and therefore its detection and assessment have become an important method to inspect the insulating condition of transformer.

The frequency of ultrasonic energy produced by PD is centralized at the period of 50kHz and 300kHz, which peak value frequency is centralized at the period of 70kHz and 200kHz.

In this paper, the signals which emitted by PD sources of power transformer was received by the plane ultrasound phased array sensor. And Modified Multiple Classification Method was applied to estimate the direction of arrival (DOA) of the PD, then we can obtain the location of the PD according to crossover locating method.

Statement of Contribution/Methods

The MUSIC algorithm, presented by Schmidt in 1979, is the most classical super-resolution algorithm. MUSIC algorithm which achieves the evaluation of the DOA of the signal source, is based on the eigenvalue analyzing theory to the array output signal of covariance. The orthogonalality of signals and noise subspace is employed by MUSIC algorithm to form the space angle spectrum function, and search the DOA of the signal by spectrum peak. But to the little signal-to-noise (SNR) close to each other produced by PD sources, MUSIC algorithm is impossible to make a precise location evalution.

Modified Multiple Signal Classification (MMUSIC) algorithm is adopted to execute the DOA estimation of PD sources in the transformer oil tank in this paper. A HermiToeplizt matrix is used to deal with the covariance matrix of the array output signal and to resume the order of covariance matrix of PD sources. As a result, we can estimate the DOA of PD signals more effectively based on MMUSIC than MUSIC.

Results

On the basis of precise evaluation of DOA of single PD signal by two ultrasound phased array sensor, we can obtain the precise location of single PD source by the space crossover of the two DOA.

Discussion and Conclusions

Rader and radio freqency signals commonly used in medical ultrasound were adoptted to simulate the PD signals in this paper (the concrete parameter: 8¡Á8 planar phased array, interval of cell-array d=¦Ë/2= c/f/2=5mm. the center frequency of received ultrasonic 150 KHz, equivalence wave speed as 1500/ms, snapshot few as 1024£¬SNR as 10dB).Then the programme of DOA estimation and crossover location are completed in Matlab.

The simulation result indicates the PD locating method based on ultuasound phased array technique and MMUSIC algorithm is precise and feasible. And it has a good engineering applicable prospect.

5G-4

5:15 PM **Non-Crosstalk Real-Time Ultrasonic Range System with Optimized Chaotic Pulse Position-Width Modulation Excitation**

Zhen-Jing Yao, Qing-Hao Meng, Shao-Ying Lan, Gen-Wang Li; *Tianjin University, Department of Automation, Tianjin, China.*

Background, Motivation and Objective

One problem with the use of multiple ultrasonic ranging sensors (sonar) operating in close proximity is the phenomenon known as crosstalk, where one sonar sensor receives the echo from other transducers. Normally the sonar receiver cannot judge whether the echo is created from its own transmission, so false time-of-flight measurement often occurs. If each sonar transducer is assigned a unique transmission sequence, combining the pulse compression technique in the receivers, the ultrasonic crosstalk can be eliminated. Thus multiple sonar sensors can work simultaneously and the efficiency can be enhanced. This paper mainly addresses how to construct short and unique pulse transmission sequences which ensure both correlation characteristic and energy of echo signals.

Statement of Contribution/Methods

Chaotic pulse position-width modulation (CPPWM) combining with multi-objective optimization strategy is proposed to construct the short and unique pulse transmission sequences which meet the requirements of real-time performance as well as best correlation characteristics and maximal energy of echo signals. Here the best correlation characteristics means that the echo sequences have sharp autocorrelation function and flat cross-correlation, i.e., both the ratio of the amplitude of the maximal side-lobe and the peak in the autocorrelation function, and the ratio of the peak of the cross-correlation function and the peak of the autocorrelation, are minimal. In each CPPWM sequence, the pulse periods are modulated using a chaotic series which is produced by Logistic mapping function. The lower limit and upper limit of the pulse periods as well as the duty ratio are optimized by the Non-dominated Sorting Genetic Algorithm-II (NSGA-II).

Results

Polaroid 600 series instrument grade electrostatic transducers are used in experiments. The nominal frequency of the hardware system is around 50 KHz. Two groups of short pulse transmission sequences are constructed by the CPPWM, and the other two groups by chaotic pulse position modulation (CPPM). Each sequence length is limited to be around 2 ms. Experiments results show that both the echo energy and correlation characteristics of the CPPWM are better than those of CPPM. The distance measurement results by using the optimization solution set demonstrate the accuracy of the proposed method. A real-time multi-sonar system with 16 Polaroid 600 series instrument-grade electrostatic transducers also validates its suitability.

Discussion and Conclusions

The proposed chaotic pulse position-width modulation (CPPWM) combining with the multi-objective optimization can guarantee both the correlation characteristics and energy of the echo signals with short transmission sequence. Thus the efficiency of the non-crosstalk ultrasonic range system can be enhanced. Moreover, the measurement accuracy can also be improved. Future work will analyze the effect of the proposed method on range resolution.

5G-5

5:30 PM **Improving the Bandwidth of Air Coupled Capacitive Ultrasonic Transducers Using Selective Networks**

Sean Mc Sweeney, WMD Wright; *University College Cork, National University of Ireland, Electrical and Electronic Engineering Dept, Mallow, Cork, Ireland.*

Background, Motivation and Objective

One of the key limitations on using CUT (Capacitive Ultrasonic Transducers) and cMUTs[1] (Capacitive Micromachined Ultrasonic Transducers) in air is their relatively narrow bandwidth which although superior to that of current piezoceramic devices[2] could be improved. Most air coupled capacitive devices could benefit hugely through the use of selective networks[3] for bandwidth expansion, resonance reinforcing, or a combination of both. This work has investigated the application of pole/zero manipulation techniques to modify and enhance the transmission characteristics of capacitive transducers through front end mounted components. The main objective was to positively enhance the performance characteristics of capacitive transducers.

Statement of Contribution/Methods

A modified electrical equivalent circuit for CUTs to include the selective networks used was developed. The work assessed the effects of a tuned amplifier on the passband of the devices studied and then focused on more complicated network designs for enhancement. Simulations of the effects of the networks on the devices using equivalent circuit models were carried out and the response curves to pulsed operation were calculated and compared to experimental measurements from a pair of fixed CUTs with a combined centre frequency of 280kHz and 3dB bandwidth of 160kHz.

Results

Increases in centre frequency of 25% and 3dB bandwidth of 77% using a single tuned amplifier were obtained. Resonance reinforcing, resonance shifting and ripple suppression were also studied through the manipulation of the q factor and pole location of such an amplifier. Performance enhancements were studied for a number of CUT aperture sizes and membrane thicknesses and a comparative study of the theoretical and experimental effect of these variations was conducted. With the appropriately designed network, enhancement of peak resonance with a simultaneous bandwidth expansion was obtained at the expense of other operating parameters such as stopband ripple. Simulations of more complicated circuit designs using equivalent circuit models of capacitive devices[4,5] showed that the maximum level of passband ripple observed for the bandwidth expansion method using a single tuned amplifier was reduced while achieving simultaneously the same 3dB results.

Discussion and Conclusions

The implication for bandwidth expansion of a capacitive transducer through selective network design is significant, allowing increased resolution in imaging systems, ultrasonic ranging and non destructive evaluation. Significant improvements have been observed without additional signal manipulation, through digital means or otherwise, in certain transmission properties of the devices. Future work will expand on the enhancement of capacitive transducers through the use of hybrid resonator circuits and other related methods.

5G-6

5:45 PM **Application of a pseudo-3D modeling to Lamb waves generation by surface-bonded piezoelectric transducers.**

Jamal Assaad, Emmanuel Moulin, Najib Abou Layla, Mustapha Baouahi, Sébastien Grondel; *UVHC-IEMN, OAE, Valenciennes, France.*

Background, Motivation and Objective

Built-in ultrasound interrogation systems are seen as a promising solution for structural health-monitoring of civil and aeronautical structures. In this context, integration of small piezoelectric transducers into plates is of particular interest. The generated Lamb waves can be used to monitor large areas of the plate. The objective of this paper is to show that the modeling of a full Lamb-wave emission and reception system (Fig.1) can be done in a relatively simple and flexible way

Statement of Contribution/Methods

First, the emitter behavior and the Lamb wave propagation are predicted using a two-dimensional (2D) hybrid finite element-normal mode expansion model. The receiver electrical response is obtained from a finite element computation with prescribed displacements. Then, a numerical correction is applied to the 2D results to account for the in-plane radiation divergence caused by the finite length of the emitter. In order to describe correctly the radiated field, the stress field in the length direction of the transducer has been supposed to have a parabolic shape. This choice, which is a common way of taking into account apodization of a transducer, allows ensuring stress continuity at the transducer edges. This work is a continuation of the paper published recently about pseudo-3D modeling technique [E. Moulin et al., J. Acoust. Soc. Am., 119, 2575-2578 (2006)].

Results

The displacement field generated at the surface of an aluminum plate by a surface-mounted PZT transducer excited by a 5-cycle, Hanning-windowed sinusoid signal, has been measured for different directions, using a laser interferometer. Then, a PZT receiver of the same kind has been bonded at some distance from the emitter. The electric signal at the receiver electrodes has thus been measured. In each case, the model has provided satisfying predictions of the measured signals

Discussion and Conclusions

The applicability conditions of the model are discussed and differences between the theoretical and experimental results are explained. The advantage of this modular approach is that realistic configuration can be simulated without performing cumbersome 3D modeling and time-consuming computations and physical interpretation is made easier. At last, possible extensions of the model are suggested.

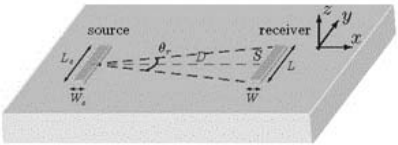

6G. Material Properties II - Crystals & Composites

Hall 2C

Tuesday, November 4, 2008, 4:30 pm - 6:00 pm

Chair: **Bikash Sinha;**
Schlumberger Inc., USA.

6G-1

4:30 PM **Study on Acoustical Physical Constants of ZnO Single Crystal Using the Ultrasonic Microspectroscopy Technology**

Tomoya Tanaka, **Yuji Ohashi,** Mototaka Arakawa, Jun-ichi Kushibiki, Noboru Sakagami; *Tohoku University, Graduate School of Engineering, Sendai, Miyagi, Japan.*

Background, Motivation and Objective

As large-size ZnO single crystal ingots have been recently grown by the hydrothermal synthesis method, such crystal substrates are expected to be used in high-efficient, short wavelength light-emitting-diode (LED) devices as a wide bandgap semiconductor material. We have been developing a method of evaluating ZnO single crystals by the ultrasonic microspectroscopy (UMS) technology. This UMS technology is capable of evaluating materials by measuring the phase velocities of longitudinal and shear waves as well as leaky surface acoustic waves (LSAWs) on a water-loaded specimen surface, with high accuracy. In a previous report, we detected variations in acoustic properties corresponding to those in resistivity of ZnO single crystals, and demonstrated a great potential of the UMS technology. In this paper, we investigate a determination method of acoustical physical constants for ZnO single crystals with high resistivity.

Statement of Contribution/Methods

We prepared three specimens of (100)- (Y-cut), (001)- (Z-cut), and (101)- (28.39°-rotated Y-cut) substrates from three small ZnO single crystals grown by the hydrothermal synthesis method. LSAW velocities at 225 MHz and longitudinal and shear wave velocities at 50-300 MHz were measured for each specimen. Elastic constants and piezoelectric constants were determined from the measured velocities.

Results

The LSAW velocities exhibited 4-m/s difference at maximum as compared with calculated values using the published constants [1]. The results for Z-axis longitudinal velocity and Y-axis Z-polarized shear velocity coupled with piezoelectricity represented velocity dispersion of about 2 m/s at maximum in the measurement frequency range. Acoustical physical constants were determined from measured velocities of five bulk waves and three LSAWs in addition to the dielectric constants and density in [1] (see Table I).

Discussion and Conclusions

Differences of c_{13}^{E} and c_{33}^{E} from the published constants are relatively large among elastic constants, and the absolute values for all piezoelectric constants were smaller than the published ones. Those results must be due to slightly lower resistivity of the ZnO specimen, so the errors in those constants became large. Further investigation will be conducted for determining constants for ZnO single crystals with high resistivity.

Table I. Comparison of determined and published constants of ZnO single crystals.

Constant		Determined	Published [1]	Diff [%]	Constant		Determined	Published [1]	Diff [%]
Elastic constant ($\times 10^{10}$ N/m^2)	c_{11}^{E}	2.093	2.096	-0.14	Piezoelectric constant (C/m^2)	e_{15}	-0.384	-0.480	-19.9
	c_{12}^{E}	1.209	1.205	0.33		e_{31}	-0.166	-0.573	-71.0
	c_{13}^{E}	0.9934	1.046	-5.03		e_{33}	1.126	1.321	-14.8
	c_{33}^{E}	2.161	2.106	2.61					
	c_{44}^{E}	0.4236	0.423	0.14					

[1] R. T. Smith and V. E. Stubblefield, J. Acoust. Soc. Am., Vol. 46, p. 105, July 1969.

6G-2

4:45 PM **ZnO piezoelectric thin film growth and characterization**

Hongming Sun, **Hang Guo;** *Pen-Tung Sah MEMS Research Center, Xiamen University, Xiamen, Fujian, China.*

Background, Motivation and Objective

ZnO piezoelectric thin film has many applications in the micro and nano devices, such as microphone, micro accelerometer and thin film bulk acoustic wave resonator(FBAR). For these applications, high-quality ZnO piezoelectric thin film, which has a tendency to grow with strong preferential orientation and good perfromance on different substrates, is need.

Statement of Contribution/Methods

In this paper, we present the growth and characterization of ZnO piezoelectric thin films. Magnetron RF sputtering technology is used to grow ZnO thin film for piezoelectric applications. We study the influence of annealing process and different substrates, including silicon, aluminum layer and silicon nitride thin film on silicon, on the piezoelectric performance of ZnO thin film by using XRD and SEM to analyze C-axis orientation and crystalline quality of ZnO thin film. Especially, we develop a fabrication process for which the aluminum is still used as the bottom electrode but isolated from the ZnO thin film by a layer of silicon nitride thin film, to meet the requirements of the high quality of the ZnO thin film and compatibility with CMOS technology. The proposed device fabricated by using the developed process is polarized. Then we test the piezoelectric coefficient and intrinsic stress in ZnO thin films under different growth conditions to study the piezoelectric performance of ZnO piezoelectric devices.

Results

The piezoelectric ZnO films with a thickness of 1~1.5 micron prepared by using magnetron RF sputtering technology under different growth conditions are tested with XRD, SEM and electronic instruments. The tested results show that ZnO films grown on silicon nitride thin film have much more prominent C-axis orientation and excellent crystalline than those on aluminum layer. The device proposed is achieved at a specific RF power and O2/Ar gas flow ratio and characterized to have good piezoelectric performance with piezoelectric coefficient d33 of 10.5 pC/N and intrinsic stress of 7500MPa. And the appropriate annealing process can significantly improve the quality of ZnO film crystal. The residual stress in ZnO thin films can be released to about 300 MPa by a annealing process at a temperature of 450¡æ.

Discussion and Conclusions

With the developed process technique for ZnO thin film, many MEMS devices, including bulk micromachined piezoelectric accelerometers, FBARS, and microfluidic devices, are being developed.

6G-3

5:00 PM **Elastic, acoustical and nonlinearity properties of beryllium chalcogenides**

Rajendra Singh, **Rishi Singh,** Manish Singh, Sujeet Chaurasia; *Banaras Hindu Univ. varanasi, India, Physics, Varanasi, Uttar pradesh, India.*

Background, Motivation and Objective

Elastic properties as well as acoustical properties of a solid are very important because they relate to various fundamental solid-state properties such as interatomic potentials, equation of state, phonon related properties, Debye temperature, Gruneisen parameters. Predominant causes for sound attenuation in solids are phonon-phonon interaction, electron-phonon interaction, thermoelastic loss and dislocation damping. At high temperatures, electron mean free path is not comparable to phonon mean free path, thus attenuation due to electron-phonon interaction is not present at higher temperatures. Therefore, phonon-phonon interaction, thermoelastic loss and dislocation damping are the dominant processes that will give rise the appreciable attenuation in high temperature range.

Statement of Contribution/Methods

Elastic, acoustic and nonlinearity properties of beryllium chalcogenides BeS, BeSe and BeTe have been studied over wide temperature range along the three crystallographic directions of propagation viz. [100], [110] and [111] for longitudinal and shear modes of propagation. Second and third order elastic moduli have been obtained using Born model of ionic solids, by taking electrostatic and Born repulsive potentials. Nearest neighbour distance and hardness parameters have been used as input data. Gruneisen parameters, acoustic coupling constants and their ratios have been evaluated for longitudinal and shear waves along different directions of propagation and polarization.

Results

Second and third order moduli are in good agreement with experimental and other theoretical values. Gruneisen parameters, nonlinearity constants and nonlinearity constants ratios and viscous drag coefficients due to screw and edge dislocations are as expected. Temperature variations of acoustic attenuation due to phonon-phonon interaction ((*f*Ñ/f2)p-p) for longitudinal and shear waves have similar trend. Acoustic coupling constant for longitudinal wave increase with temperature and then becomes constant, while for shear wave it remainse almost constant

Discussion and Conclusions

Acoustic attenuation due to thermoelastic loss, ((*f*Ñ/f2)th) as well as dislocation damping have negligible contribution in comparison to attenuation due to phonon-phonon interaction, ((*f*Ñ/f2)p-p), thus confirming that dominant cause of acoustical dissipation in these compounds is phonon-phonon interaction. Anharmonicity of these compounds increases up to room temperature and then becomes approximately constant. Acoustic attenuation due to phonon-phonon interaction and thermoelastic loss follow cube polynomial fit temperature dependence law in temperature range 50K-500K.

6G-4

5:15 PM **Investigations of molecular interactions in polymeric solutions using acoustical characterization techniques**

Rajendra Singh, **Manish Singh,** Rishi Singh, Sujeet Chaurasia; *Banaras Hindu Univ. varanasi, India, Physics, Varanasi, Uttar pradesh, India.*

Background, Motivation and Objective

The electrical conductivity of polymer electrolytes increases many fold as its melting temperature Tm. Hence knowledge of this is of great importance for assessing particular polymer electrolytes for its possible device applications. The melting at Tm results fluctuations/changes in ionic mobility as well as significant change in viscoelastic properties. The former can be studied by measuring associated change in “ionic noise” while the later can be studied by monitoring changes in ultrasonic velocity and attenuation. Molecular processes and interactions can be explored by making ultrasonic absorption and velocity measurements under different physical conditions over a wide frequency range

Statement of Contribution/Methods

The velocity and absorption of ultrasonic waves have been measured in aqueous solutions of poly (ethylene glycol). The velocity of ultrasonic waves was obtained in the frequency range 1MHz-12MHz over a wide range of temperature. The concentration (by weight) ranged from 1% to 10% of poly (ethylene glycol) in water. The shear viscosity was also measured. Measurements were carried out in the temperatures range 35 oC to 65 oC. The density and viscosity have also been measured at different temperatures. The absorption has been measured at 5 MHz using pulse technique.

Results

It was observed that velocity of ultrasonic waves increases as temperature increases at a given concentration, while as concentration increases at a given temperature, velocity was found to increase. The shear viscosity and density measurement shows that it decreases with temperature. At 10 wt % of polymeric solution, it was observed that velocity and absorption show peaks, one at Tm and other at different temperature.

Discussion and Conclusions

Velocity measurements at different temperatures for aqueous polymeric solutions of polymer having molecular weights 2000, 4000 and 8000 shows that there are sudden change in the velocity at T¬m. however, the peak associated with Tm is not unique but splitted into two. It is proposed that the PEG forms complex with water in the salvation shell resulting in the second peak. The approximate values of Tm (taking pronounced peak) is 55 oC, 56 oC and 57 oC for PEG of molecular weights 2000,4000 and 8000 respectively, which is in good agreement with literature values. Hence it is concluded that Tm increases with molecular weight of PEG.

6G-5

5:30 PM **Determination of the Absolute Orientation of LGX Crystals using X-ray Diffraction**

Blake Sturtevant[1], Robert Lad[1], Mauricio Pereira da Cunha[2]; [1]*University of Maine, Physics, Orono, Maine, USA,* [2]*University of Maine, Electrical and Computer Engineering, Orono, Maine, USA.*

Background, Motivation and Objective

Acoustic wave material characterization, device design and fabrication rely heavily on knowledge of the absolute crystal orientation. A simple, non destructive means for evaluating the positive axes of LGX crystals is highly desirable and motivated the present work. In crystals from the point group 32 symmetry, such as quartz, the langasite family (LGX), and gallium phosphate, bulk acoustic waves (BAWs) traveling in the Y-Z plane and making an angle of α with the Y axis do not in general have the same velocity as BAWs traveling at an angle of -α. The absolute orientation of the axes matters.

The polarity of the crystalline X axis can be found by reading the potential across the X faces induced by mechanical compression along the X axis, as prescribed in the IEEE Standard on Piezolectricity. However, the determination of the positive X direction alone leaves two possible orientations for the positive Z direction.

Tuesday Oral

Statement of Contribution/Methods

For crystals lacking a center of symmetry (e.g. quartz), it is found for some crystal planes that I(hkl) ≠ I(hk-l) where 'I' is the intensity of a diffracted X-ray beam off planes with Miller indices (hkl) or (hk-l). The specific X-ray reflections with intensity inequality for quartz, however, do not translate directly to other crystals. This work focuses on the orientation of langatate (LGT) and utilizes the inequality of diffracted intensities to find the absolute orientation of a crystal for cutting and polishing a desired wafer, or for verifying the orientation of a commercially supplied wafer.

The method presented in this work utilizes standard X-ray pole figure measurements obtained using a PANalytical X'Pert Pro MRD X-ray diffractometer and Cu Kα radiation.

Results

Quartz wafers of different orientations were obtained and planes exhibiting the I(hkl) ≠I(hk-l) intensity inequality were measured to reproduce this phenomenon for quartz.

Effort was then put forth to determine planes in LGT which exhibit a large enough intensity inequality to distinguish hkl from hk-l. While many LGT planes were found to have nearly equal diffracted intensities for hkl and hk-l, several X-ray reflections including the (301), (205), (502) were found to have at least a factor of two difference in intensity for hkl compared to hk-l.

These effects were first measured on a Z-cut LGT wafer for identification of the relevant planes. Then the intensities of the (301), (205), and (502) reflections were measured on ±45° Y-rotated wafers, whose absolute orientation had previously been determined by ultrasonic measurements. Selected Miller planes useful for this alignment identification are reported, along with the ratio I(hkl)/ I(hk-l).

Discussion and Conclusions

This work reports on the use of a simple, non-destructive technique to determine the polarity of axes for determination of the absolute orientation of LGX crystals, necessary to obtain the correct wafer orientation for the desired acoustic wave propagation direction.

6G-6

5:45 PM **Viscosity Tensor Components of the Langatate and Langasite**

Sergeev Fedor[1], Georgy Mansfeld[2], Sergey Alekseev[2], Natalia Polzikova[2], Iosif Kotelyanskii[2]; *[1]Moscow Institute of Physics and Technology, Moscow, Russian Federation, [2]Institute of Radioengeneering and Electronics RAS, Moscow, Russian Federation.*

Background, Motivation and Objective

Despite of great interest in very perspective materials for acoustoelectronics "quartz-like" crystals langasite (La3Ga5SiO14) and langatate (La3Ga5.5O14Ta0.5), attenuation of sound waves was measured only in few directions. In present work the full set of components of viscosity tensor was obtained.

Statement of Contribution/Methods

The method of composite acoustic resonator (HBAR) spectroscopy developed in our laboratory was used. Resonators were made by depositing thin-film piezo-transducer on one side of optically polished crystal plates from material under investigation. Each crystal was cut into the set of plates, so acoustic waves in directions of X, Y, Z axes and in YZ plane can propagate perpendicular to the sides of corresponding plate. Parasitic temperature independent losses such as acoustic waves energy scattering on surface roughness and diffraction losses where experimentally studied. They where measured at helium temperature and eliminated from final result.

Results

As a result temperature dependent losses associated with interaction of acoustic waves with thermal phonons was determined in frequency range from 0.6 to 6 GHz. For example we obtained 0.62 dB/us attenuation in Z-cut at 1 GHz which is more than two times lower then that of quartz. Sound attenuation coefficients data for chosen direction and polarizations enabled us to obtain a full set of viscosity tensor components for langatate and langasite. The magnitude of attenuation coefficient in arbitrary direction can be obtained substituting these data into Christoffel equation. Three 3-d surfaces of attenuation coefficients where calculated and plotted.

Discussion and Conclusions

Using method of HBAR spectroscopy the full set of components of viscosity tensor for langasite and langatate -- perspective materials for acoustoelectronics was measured. In frequency range of our experiments the values of sound attenuation coefficient of langatate and langasite was significally lower than that of quarts. Data of viscosity tensor is important for design of piezoelectric devices.

The work was partially supported by RFBR grants 07-02-01006-a and 07-02-13581.

Tuesday Poster Sessions

P2A. Blood Flow

2nd and 3rd Floor Foyers

Tuesday, November 4, 2008, 3:00 pm - 4:30 pm

Chair: **Jorgen Arendt Jensen;**
Technical University of Denmark, Denmark.

P2A023-01

Doppler ultrasound and numerical analysis for the assessment of hemodynamic disturbances in ulcerated carotid arteries

Emily Wong[1], Jaques Milner[1], Meghan Thorne[1], Hristo Nikolov[1], David Steinman[2], Richard Rankin[3], Tamie Poepping[4], David Holdsworth[1]; *[1]Robarts Research Institute, Canada, [2]University of Toronto, Mechanical and Industrial Engineering, Canada, [3]University of Western Ontario, Diagnostic Radiology and Nuclear Medicine, Canada, [4]University of Western Ontario, Physics and Astronomy, Canada.*

Background, Motivation and Objective

Carotid plaque ulcerations, or irregularities in plaque morphology, have been identified as an independent risk factor for stroke. However, it is unknown if this is a consequence of increased thromboembolic activity due to altered hemodynamics resulting from ulcerated geometries. Doppler ultrasound (DUS) in vitro studies provide a quantitative means of comparing geometry-dependent hemodynamics. Furthermore, since DUS is the primary clinical method for evaluating stroke risk patients, detecting differences in DUS parameters produced by ulcerations would be of diagnostic utility. Numerical simulations using computational fluid dynamics (CFD) can supplement experimental DUS studies, providing higher resolution, time-resolved models of 3-D flow fields. CFD is also able to quantify hemodynamic factors that indicate thromboembolic or plaque rupture potential. We conducted an in vitro DUS study of ulcerated carotid geometries to compare the effect of ulceration on hemodynamic patterns and to determine a DUS parameter to discriminate ulcerated plaques. Flow details in these geometries were analyzed using CFD models.

Statement of Contribution/Methods

DUS in vitro flow models were based on an idealized carotid bifurcation geometry of 50% eccentric stenosis. Ulcers of several geometries were each incorporated at the level of the apex on the non-flow divider wall. DUS measurements were acquired using a clinical duplex DUS system, delivering velocity data over a longitudinal central plane; data were analyzed for several spectral indices. The CFD analysis of an elliptical ulcer model was performed with a spatial finite element discretization of over 160,000 quadratic tetrahedral elements to adequately resolve the flow field. Pulsatile flow simulations with boundary conditions and flowrate waveforms matching DUS experimental conditions were iterated for five cardiac cycles.

Results

A quantitative indicator of disturbed flow, called turbulence intensity (TI), was the DUS parameter most sensitive to differences in surface morphology. We demonstrated a significant increase in TI distal to the site of ulceration in a moderately diseased carotid bifurcation by the inclusion of a deep ulcer. Macroscopic flow features and velocity fluctuations in the CFD model were comparable to DUS observations. Oscillatory transitional flow patterns as well as areas of turbulent flow are demonstrated in the post-stenotic region of the ulcer vessel geometry.

Discussion and Conclusions

DUS TI distal to the site of ulceration can indicate differences in carotid plaque surface morphology and may provide useful diagnostic information for the assessment of carotid plaque ulcerations. CFD results indicate that flow post-stenosis is likely transitional, and both disturbed and turbulent flow are present. Comparison of hemodynamic parameters between ulcer models may help to demonstrate the risks of embolism or plaque rupture posed by ulcerated plaques in the carotid bifurcation.

Tuesday Poster

P2A024-02

Ultrasonic Doppler Measurements of Blood Flow Velocity of Rabbit Retinal Vessels with High-Frequency Angled Needle Transducer

Ruimin Chen[1], Dong-Guk Paeng[2], Naoki Matsuoka[3], Hossein Ameri[3], Qifa Zhou[1], Mark Humayun[3], K. Kirk Shung[1]; *[1]University of Southern California, Department of Biomedical Engineering, USA, [2]Cheju National University, Marine Industrial Engineering, Korea, Republic of, [3]University of Southern California, Doheny Eye Institute, USA.*

Background, Motivation and Objective

Retinal vein occlusion (RVO) is the second leading cause of vascular visual loss. Several treatment procedures have been devised to remove obstructions and reestablish blood flow. This study is a quantitative analysis of measuring blood flow velocity from the Doppler spectrum of rabbit retinal vessels using a high-frequency ultrasonic Doppler system with a needle transducer to investigate RVO and to monitor blood flow recovery during/after surgery procedure.

Statement of Contribution/Methods

A directional high-frequency (HF) pulsed-wave (PW) Doppler system with a 45MHz angled lead magnesium niobate-lead titanate (PMN-PT) needle transducer was developed to measure the blood flow velocity of retinal vessels in vivo. Through a 1mm incision in the eye-wall, the needle transducer with a beveled tip of 45° was inserted into the vitreous cavity to access retinal vessels. In order to exclude choroidal blood flow from the retinal flow, an electronic sample and hold time gate was applied to 200 ns from the first echo signals from the tissue. In the first phase of the study, five different rabbit eyes were used to evaluate the repeatability of the measurement. In each eye, 10 repeated measurements were taken from a selected part of a retinal vessel. In the second phase, eight rabbit eyes were used to measure the blood flow velocity. From the vessels at optic nerve area to the branch retinal vessels, five positions from one retinal vessel were selected. The angle between the transducer and retinal vessels at each location was estimated by measuring the same in enucleated rabbit eyes.

Results

The Doppler angle was estimated to be about 70°. The average (± standard deviation) of the peak blood flow velocity of ten Doppler measurements at one position of retinal vessel was 4.08 ± 0.76 cm/s. For 5 different rabbits, the mean was 3.89 ± 0.78 cm/s. From the central to branch retinal vessels, the peak velocity was measured to be slower (10.78 ± 0.44 cm/s to 2.80 ± 0.68 cm/s) and the spectrum was changed from peaky to blunt shape. Since retinal arteries and veins are too close each other, the blood flow velocities from both arteries and veins were measured simultaneously. The Doppler velocity from vein was not pulsating and the velocity was 2.43 ± 0.16 cm/s. Choroidal flow was also measured to be 10.68 ± 0.43 cm/s for comparison.

Discussion and Conclusions

This study is one of the first systematic ultrasonic Doppler measurement of retinal blood flow in vivo. The ultrasonic Doppler measurements of retinal blood flow velocity were repeatable and reliable. This measurement would be useful to investigate RVO and to monitor blood flow velocity of retinal vessels during/after surgery.

Tuesday Poster

P2A025-03

An Improved Method for Estimating the Blood Flow Velocity Vector Using Aperture Domain Data

Angning Yu, Hu Peng; *USTC, Dept. 23, Hefei, Anhui, China.*

Background, Motivation and Objective

Most conventional blood flow estimation methods measure only the axial component of the blood velocity vector. Shun-Li Wang, Meng-Lin Li, Pai-Chi Li proposed in "Estimating the Blood Velocity Vector Using Aperture Domain Data" (ieee trans on uffc, 54(1)) a method in which time shifts resulting from blood motion are calculated for the individual channels using aperture domain data, and a time-shift profile along the array direction as a function of channel index is constructed, and is used to find the axial and lateral components. The problem is the first-order approximation of the time-shift profile used in it causes considerable estimation errors. Therefore, the aim of our study is to develop a new way to process the aperture domain data and improve the accuracy.

Statement of Contribution/Methods

In our method, first, similar to Li's method, a function from the time shifts to the channel positions is constructed. Then, different from Li's method, the function is transformed into an overdetermined system of linear equations in the two variables of the axial and lateral components, and an approximate solution is found using the method of least squares. Since no unnecessary approximation is involved, our method has a higher accuracy than Li's.

The efficacy of the proposed method is verified by computer simulations based on the Field_II program. In the simulations, the transducer array had 64 elements, an aperture size of 1.92 cm, and a center frequency of 5 MHz. The flow velocity ranged from 5 to 35 cm/s and the Doppler angle ranged from 0° to 90°. Scatterers were in a random sample area 0.96 to 4.8 cm from the transducer and ±60° from the axis.

Results

Simulation results show that, when the signal-to-noise ratio is larger than 0 dB,

1, the accuracy when using 8 out of the 64 channels are slightly worse, and the accuracies with 16, 32, and 64 channels are equivalent;

2, the accuracy for the proposed method is independent of the sample area's location, while Li's method works only when the sample area is not near to the transducer and is on the axis;

3, for the proposed method, the estimation error of the compound velocity is smaller than either errors of the axial and lateral components, indicating that the proposed method is more sensitive to the velocity than to the Doppler angle; and

4, (with the sample area on the axis) the mean estimation errors of the velocity, and the axial and lateral components are 3.7%, 1.3, and 8% for the proposed method, and 15%, 3%, and 15% for Li's method.

Discussion and Conclusions

This paper has analyzed Li Pai-Chi's blood velocity vector estimation method, and proposed a new method which improves the estimation accuracy effectively. Also, the proposed method is possible to be extended for 3-D velocity vector measurement.

P2A026-04

Tuesday Poster

In-vivo validation of fast spectral velocity estimation techniques – preliminary results

Kristoffer L. Hansen[1], Fredrik Gran[2], Mads M. Pedersen[1], Jørgen A. Jensen[3], Michael B. Nielsen[1]; *[1]University Hospital of Copenhagen, Denmark, [2]GN Resound, Denmark, [3]Technical University of Denmark, Denmark.*

Background, Motivation and Objective

A common way of displaying blood velocity is to estimate the power spectral density (PSD) as a function of time yielding a spectrogram. The usual method to estimate PSD is by using the averaged periodogram approach, called Welch's method

(WM). WM is dependent on a long observation window (OW)(~ 100 transmissions) to achieve sufficient spectral resolution. Thus, the B-mode will not be updated frequently making it difficult for the medical doctor to navigate. Previously, two adaptive filterbank methods have been suggested to circumvent this problem: the Blood spectral Power Capon method (BPC) and the Blood Amplitude and Phase Estimation method (BAPES). The methods were tested in simulations, controlled experiments in a flow rig and on a single human volunteer. It was indicated that the two adaptive methods displayed sufficient spectral resolution for much shorter OW's than the WM. The purpose of this paper is to

investigate the methods on a larger population and evaluate the spectrograms.

Statement of Contribution/Methods

Ten volunteers were scanned over a. carotis comm. dxt. and 4 different approaches were used to estimate the PSD: WM with a hanning-window (WMhw), WM with a boxcar-window (WMbw), BPC and BAPES. For each approach the window length was varied: 2, 4, 8, 16, 32, 64, 128. Thus, from the same dataset of each volunteer 28 spectrograms were produced. The experimental ultrasound scanner RASMUS and a B-K Medical 7 MHz linear array transducer was used to

acquire the ultrasound (US) data. The artery was scanned with an angle of insonation not exceeding 60°. All 280 spectrograms were then double-blinded randomised and presented for a radiologist for visual evaluation: useful/not useful.

Results

The results of the 280 evaluations are depicted in the figure. The usefulness's of the four methods given in percentage are plotted against OW. It is seen that the four approaches perform almost equally good with OW of 128 and 64 while the WM approaches fail to produce useful spectrograms at OW of 32. BAPES is superior to BPC at OW 16 and all the methods fails at OW shorter than of 16.

Discussion and Conclusions

These preliminary results indicate that BAPES and BPC can be used for estimating PSD with a shorter OW than WM. BAPES and BPC can potentially improve the temporal resolution in the spectrograms and liberate processing time e.g. to increase frame rate of the interleaved B-mode images.

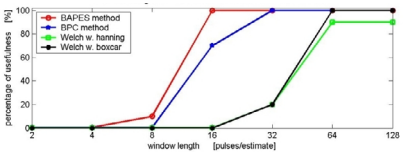

P2A027-05

Transverse Correlation: an Efficient Transverse Flow Estimator - Initial Results

Lasse Henze[1], Iben Kraglund Holfort[1], Jacob Kortbek[2], Jørgen Arendt Jensen[1]; *[1]Center for Fast Ultrasound Imaging DTU Elektro, Denmark, [2]B-K Medical, Denmark.*

Background, Motivation and Objective

Color flow mapping has become an important clinical tool, for diagnosing a wide range of vascular diseases. Only the velocity component along the ultrasonic beam is estimated, so to find the actual blood velocity, the beam to flow angle has to be known. Because of the unpredictable nature of vascular hemodynamics, the flow angle cannot easily be found as the angle is temporally and spatially variant. Additionally the precision of traditional methods is severely lowered for high flow angles, and they breakdown for a pure transverse flow. To overcome these problems we propose a new method, for estimating the transverse velocity component.

Statement of Contribution/Methods

The method measures the transverse velocity component by estimating the transit time of the blood, between two parallel lines, beamformed in receive. A broad emitted beam is used, enabling the parallel lines to be beamformed simultaneously using a single emission. The transit time is estimated by correlating the beamformed lines taken from different emissions. The largest correlation will occur, when the temporal span between the lines being correlated, corresponds to the transit time of the blood. The axial velocity component will cause the lines to be misaligned, so to overcome this, compensation for the axial velocity is applied. Moving the lines up and down respectively performs the compensation. The method has been investigated using simulations performed with Field II. A linear array with 128 elements, a center frequency of 7 MHz and a pitch of 0.208 mm is used. The simulated transducer is a model of a commercially available transducer. No apodization is applied in transmit or receive. The simulated vessel has a radius of 8 mm and its center is placed 28 mm below the transducer, giving an F number of 1.05. The modeled flow is laminar with a parabolic velocity profile and a peak velocity of 0.6 m/s. To evaluate the stability of the method, different signal-to-noise ratios are simulated.

Results

Using 15 emissions per estimate, a standard deviation of 1.64 % and a bias of 1.13 % are obtained for a beam to flow angle of 90 degrees. Using the same setup a standard deviation of 2.21 % and a bias of 1.07 % are obtained for a beam to flow angle of 75 degrees. Using 20 emissions a standard deviation of 3.4 % and a bias of 2.06 % are obtained for a beam to flow angle of 45 degrees. The method performs stable down to a signal-to-noise ratio of 0 dB, where a standard deviation of 5.5 % and a bias of 1.2 % is achieved.

Discussion and Conclusions

A new transverse velocity estimator has been proposed. Realistic flow simulations have been carried out, to test its performance. The estimator is robust and has been able to measure the transverse velocity component, with a low standard deviation without any considerable Bias. The method uses a linear array which enables it easily to be incorporated in an imaging system. The proposed method is less computational expensive compared to pure Speckle Tracking methods.

Tuesday Poster

P2A028-06

A comparison of two-dimensional flow estimation techniques based on computational fluid dynamics: speckle tracking versus vector-Doppler

Abigail Swillens[1], Lasse Lovstakken[2], Hans Torp[2], Patrick Segers[1]; *[1]Ghent University, Institute Biomedical Technology, Belgium, [2]NTNU Trondheim, Institute of Circulation and Medical Imaging, Norway.*

Background, Motivation and Objective

Complex flow in arteries may not be measured using traditional Doppler-based imaging due to beam-to-flow angle-dependencies. Attention has been given to speckle tracking (ST) and vector-Doppler (VD) for 2-D velocity estimation, however limited effort has been done to compare their properties, especially for clinically relevant flow patterns. In this work, this comparison is done by using a novel simulation environment coupling 3-D computational fluid dynamics (CFD) and ultrasound simulations.

Statement of Contribution/Methods

To compare the fundamental properties of the methods, stationary parabolic flow was simulated in a straight tube for varying velocities (20-50 cm/s), flow angles (0-60 deg), out-of-plane angles (0-45 deg), and signal-to-noise ratios (SNR) (0-20dB). Further, realistic velocity fields in a carotid bifurcation were simulated using CFD (Fluent 6.2) in a model based on in vivo MRI data. The Field II software was used to generate ultrasound RF-signals. ST was implemented using the sum-of-absolute-differences method in beam interleaved regions. VD was implemented using a single transmit and two parallel receive beams with a constant angulation of 15 deg. An ensemble of 20 velocity profile estimates was generated for each case and results were analyzed in terms of bias and standard deviation.

Results

Both methods successfully estimated the lateral and axial velocity components of parabolic flow for varying velocities and flow angles with similar bias. However, ST had lower variance for lateral velocities while VD had lower variance for axial velocities. For increasing out-of-plane movement, both methods degraded equally. For decreasing SNR, VD degraded more rapidly than ST in terms of variance. Preliminary results for the carotid bifurcation showed that the performance of both methods degraded for realistic pulsatile flow patterns. However, for disturbed flow regions VD generally performed better than ST, especially in the external carotid branch and at peak systole in the cardiac cycle.

Discussion and Conclusions

By coupling CFD and ultrasound simulations, it was possible to compare two experimental blood velocity estimators in a realistic flow setting with all conditions known. Stationary parabolic flow simulations showed that ST and VD successfully could estimate both axial and lateral velocity components. Further, realistic flow in the carotid bifurcation proved challenging for both methods, and should be further investigated.

P2A029-07

Aiding Vascular Trauma Detection in Human Upper Extremities with Image-Based Models of Blood Flow

Aaron Wang[1], David Liang[2], Charles Taylor[3]; *[1]Stanford University, Bioengineering, USA, [2]Stanford University, EE/Cardiovascular Medicine, USA, [3]Stanford University, ME/Bioengineering, USA.*

Background, Motivation and Objective

Trauma patients need medical attention quickly to stop major bleeding. A portable ultrasound allows for a quick diagnosis of vascular injury, but trained sonographers are usually not available at trauma settings, such as in the battlefield. Luo 2007 quantified ultrasound signatures of bleeding at sites of vessel puncture, which can be used in automated algorithms for diagnosis of suspected bleeding sites. However, trauma patients often have large areas of injury requiring extensive scanning to find the bleeding site. An algorithm that can first assess a vascular tree and identify injured branches would be useful. In this study, we characterized normal arm blood flow with the Power-Law model and evaluated its ability to detect vascular abnormalities by looking for flows that deviate from the model.

Statement of Contribution/Methods

The Power-Law (established for blood flow in the lungs, heart, etc.) was adapted for the arm: blood flow (Q) is proportional to the vessel diameter (d) taken to the power k, $Q \alpha d^k$; where k is defined by the bifurcation pattern of the brachial (b) to ulnar (u) and radial (r) arteries, $d_b^k = d_u^k + d_r^k$. To determine the k value for the arm, ultrasound was performed on 28 healthy arms to measure the arterial diameters and flows, at rest and exercise (30 lb grip, 2.7

Tuesday Poster

watts). Exercise flow patterns were included to simulate the heightened physiologic state that may accompany acute trauma.

Alterations in blood flow split patterns at bifurcations that occur with downstream bleeding may be detectable as a deviation of the patient's measured flow (Q) from the model's predicted flow (Q'). Thus, we defined a bleed detection metric that quantified these "flow split deviations," FSD = $| Q_u/Q_u' - Q_r/Q_r' |$. To evaluate the metric, 3D computational flow simulations of arm trauma were used to estimate the size of punctures detectable. Furthermore, a human case study evaluated whether the metric was able to detect surgically placed arteriovenous fistulas (AVF) in the wrist of dialysis patients.

Results

Blood flows at the brachial bifurcation were adequately described with a k = 2.75 Power-Law, regardless of physiological state. Given the accuracy of flow predictions with the model, simulations with a range of bleed severities estimated that the bleed detection metric could detect a puncture as small as 1/5th the size of a vessel. Also, the metric was able to detect newly placed AVF "abnormalities" in all dialysis patients studied.

Discussion and Conclusions

The simulations and case study suggest that the strategy of identifying flow perturbations at bifurcations may provide a rapid algorithm for localizing active bleeding. Though in vivo animal models of acute bleeding are still needed to determine the metric's true sensitivity, this approach could complement other methods in a comprehensive automatic bleed detection algorithm.

P2B. Improvements in Contrast Imaging

2nd and 3rd Floor Foyers

Tuesday, November 4, 2008, 3:00 pm - 4:30 pm

Chair: **Piero Tortoli;**
Università degli Studi di Firenze, Italy.

P2B030-01

Microbubble Detection by Dual-High-Frequency Ultrasound Excitation

Shin-Yuan Su[1], Che-Chou Shen[2], Chih-Kuang Yeh[1]; *[1]National Tsing Hua University, Department of Biomedical Engineering and Environmental Sciences, Hsinchu, Taiwan, [2]National Taiwan University of Science and Technology, Department of Electrical Engineering, Taipei, Taiwan.*

Tuesday Poster

Background, Motivation and Objective

Ultrasonic contrast agents (UCAs) have been reported to assist in imaging blood perfusion with their nonlinear properties. Nevertheless, for high frequency ultrasound (HFU), a major limitation in microbubble detection is low signal-to-noise ratio (SNR) due to the intense attenuation. Moreover, commercialized UCAs resonate at frequencies below the HFU; thus efficiency of nonlinear oscillations is substantially reduced. In this study, we proposed a novel excitation pulse - dual frequency excitation to induce nonlinear scattering from UCAs efficiently by using HFU.

Statement of Contribution/Methods

The proposed excitation waveform comprises of two sinusoids with slightly different frequencies (i.e., 8.5 and 11.5 MHz), and the resultant low-frequency envelope (i.e., 3 MHz) can reinforce the resonance of UCAs and further improve the SNR. Its envelope with frequency being the difference of the two frequencies, is utilized to stimulate nonlinear oscillation of UCAs for the consonant low-frequency nonlinear generation whereas high imaging resolution is retained because of narrow high-frequency transmit beams. In addition, the envelope component provides the low-frequency driving force for oscillating the UCAs to improve the destruction efficiency, while the destruction sample volume remains small due to the high frequency of the carrier signal.

Results

Hydrophone measurements and phantom experiments of speckle-generating flow phantoms were performed to demonstrate the efficacy the proposed technique. The results show that especially when the envelope frequency is near the UCAs resonance frequency, the envelope of the proposed excitation pulse can induce significant nonlinear scattering from UCAs, the induced nonlinear responses tend to increase with the pulse pressures, and up to 26 dB and 36 dB contrast-to-tissue ratios with second- and fourth-order nonlinear responses, respectively, can be obtained.

Discussion and Conclusions

The experimental results also indicate that dual-frequency excitation consistently results in destruction of UCAs that is superior to using a tone burst at the carrier frequency. The lower envelope frequency generally results in more efficient destruction, especially when the excitation waveform is long enough to guarantee sufficient excitation by the envelope. Potential applications of dual-frequency excitation include a simplified high-frequency microbubble destruction/replenishment imaging system, the localized induction of microbubble cavitation, and the use of sonoporation for drug delivery and gene therapy.

P2B031-02

Transmit phase tuning for wideband harmonic detection of contrast agents

Che-Chou Shen, Yi-Chun Hsieh; *National Taiwan University of Science and Technology, Department of Electrical Engineering, Taipei, Taiwan.*

Background, Motivation and Objective

In ultrasonic harmonic imaging, the contrast-to-tissue ratio (CTR) is generally limited by tissue background signal comprising both the leakage harmonic signal and the tissue harmonic signal, especially in the case of wideband transmit pulse. In this paper, suppression of tissue background signal in harmonic imaging is studied by selecting an optimal phase of the transmit signal to achieve destructive cancellation between the tissue harmonic signal and the leakage harmonic signal.

Statement of Contribution/Methods

For a transmit signal $x(t)=a_f\cos(2\pi f_0 t+\varphi_f)+a_{LH}\cos(2\pi(2f_0)t+\varphi_{LH})$ where φ_f and φ_{LH} are respectively the phases of fundamental signal and leakage signal, the tissue harmonic phase (φ_{TH}) would be twice φ_f and the phase of leakage signal generally increases linearly with φ_f. It is expected that the combined harmonic intensity would be lower when the two components are opposite in phase. Also, it is noted that the φ_{TH} and φ_{LH} increase with φ_f at different rates and thus, the relative phasing between the two harmonic signals can be made by simply tuning φ_f.

Results

With transmit phase tuning, though the tissue suppression is not uniform over the entire second harmonic band because it occurs maximally when the two harmonic signals are equal in magnitude for complete cancellation (Fig. A), the resultant tissue amplitude reduces for a wide range of depths (Fig. B). On the contrary, as compared to tissue, the harmonic amplitude from bubble shows negligible change with phase tuning (Fig. C). The M-images also confirm that the phase tuning can effectively suppress tissue background and highlight the contrast region (Fig. D). The resultant CTR improves for about 4 dB by simply optimizing the transmit phase.

Discussion and Conclusions

The transmit phase tuning is capable of background suppression in contrast harmonic imaging by eliminating tissue harmonics and leakage harmonics simultaneously. It avoids frame rate reduction in multi-pulse methods such as pulse-inversion and can improve CTR without loss of temporal resolution.

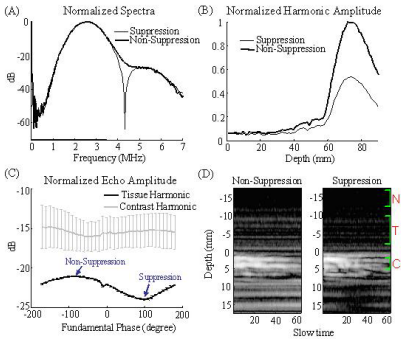

P2B032-03

Radial-Modulation Chirp Imaging for High-Resolution Contrast Detection

Meng-Lin Li[1], Yu-Chen Kuo[2], Chih-Kuang Yeh[2]; *[1]National Tsing Hua University, Department of Electrical Engineering, Hsinchu, Taiwan, [2]National Tsing Hua University, Department of Biomedical Engineering and Environmental Sciences, Hsinchu, Taiwan.*

Background, Motivation and Objective

Most contrast imaging techniques rely on microbubble resonance and detect bubbles at resonance frequencies which, however, are low (~ 2 to 4 MHz) for most commercial contrast agents; the resultant images lack spatial resolution for imaging microbubbles in microvessels. To solve this problem, the concept of radial modulation of bubbles has been introduced to raise the imaging frequency for commercial bubbles. Coded excitation can potentially improve signal-to-noise ratio (SNR) of bubble detection with high frequency ultrasound.

Statement of Contribution/Methods

In this study, we propose a radial-modulated chirp imaging method for high resolution and SNR-improved contrast detection. This method detects bubbles by using a compression filter that selectively compresses the extracted chirp component being modulated by bubbles and suppresses the un-modulated one at tissues. Microbubbles (SonoVue here) are insonated simultaneously with a low frequency pumping signal at the resonance frequency of the bubbles (a 30-cycle 3 MHz tone burst here) and a high frequency chirp imaging signal (a 10 MHz Gaussian chirp). Amplitude of the imaging Chirp will be radial-modulated at the resonance frequency, forming sum-and-difference terms, e.g., a 7 MHz and a 13 MHz Gaussian chirp. Band-pass filtering (BPF) at 7 MHz or 13 MHz is performed. BPF signal differences between tissues and bubbles form the contrast. Then pulse compression is applied to improve axial resolution, SNR and contrast-to-tissue ratio (CTR). Note that different from the reported radial modulation imaging sending two imaging pulses, only one imaging pulse is used here.

Results

The figure shows the results imaging a 1-mm tube containing bubbles, displayed in M-mode on a 30 dB dynamic range. (a) and (b) are original BPF signals without and with the pumping signal, respectively. (c) and (d) are the compressed signals of (a) and (b), respectively. (a) and (c) are normalized by the maximum in (b) and (d), respectively. Signal difference of (b) over (a) is 7 dB while signal difference of (d) over (c) is 14 dB, indicating a 7 dB CTR improvement by the compression filter. The axial resolution is also restored.

Discussion and Conclusions

The results showed that our method have potential in providing high resolution and better SNR contrast detection. The effect of pumping pressure, chirp bandwidth, and harmonics interference will also be discussed.

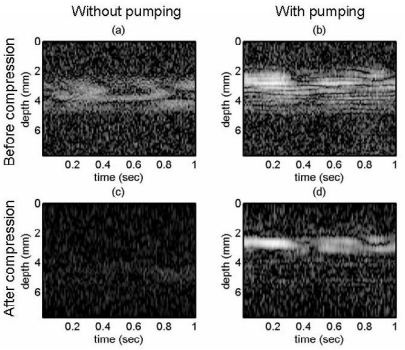

Tuesday Poster

P2B033-04

Contrast Resonance Imaging with Microbubble Resonance Enhancement and Suppression

William Shi[1], Christopher Hall[1], Patrick Rafter[2]; [1]*Philips Research North America, USA,* [2]*Philips Healthcare, USA.*

Background, Motivation and Objective

The objective is to investigate the use of embedded ultrasound imaging pulses for the enhancement and suppression of contrast microbubble resonance to improve contrast imaging sensitivity (without resolution degradation). A set of new multiple-pulse contrast modalities with combinations of Power Modulation (PM), Pulse Inversion (PI) and Contrast Resonance (CR) are evaluated for their imaging sensitivities in comparison to that for the current contrast modality PM&PI.

Statement of Contribution/Methods

A dual-transducer experimental setup was employed to measure scattering from MP1950 (University of Virginia) lipid microbubbles in a test cell. The transmit transducer is a piezocomposite transducer (Imasonic) with a center frequency of 1.6 MHz and a natural focal length of 8 cm. The receive transducer (Panametrics V304) is a broadband receiver with a center frequency of 2.25 MHz and a focal length of 5.1 cm. A sequence of five 2-MHz transmit waveforms (shown below Table 1 as P1, P2, P3, P4 and P5) with a maximal MI of 0.12 were transmitted consecutively at a PRF of 100 Hz: P1=0.5*P2, P2 is a typical imaging pulse, P3=P5-P2, P4=P2+P5, and P5 is a resonance-tuning pulse. Their Scattered Pulses (SPs) are denoted as SP1, SP2, SP3, SP4 and SP5, respectively.

Consequently resultant contrast signals for 5 contrast imaging modes were calculated from the SPs filtered within 1 to 3 MHz. In addition, an interactive numerical tool was employed to simulate encapsulated contrast bubbles with representative lipid shell properties of 4.0 nm shell thickness and 0.8 Pas shear viscosity.

Results

Resonance enhancement and suppression for the embedded imaging pulse P2 in P4 and in P3, respectively, were observed. Formulas for the calculation of resultant SPs and the corresponding CSLs (Contrast Signal Levels) for scattered signals from contrast microbubbles are given in Table 1 for the following 5 contrast imaging: PM&PI, CR, PI&CR, PM&PI&CR and CR&PI. Both experimental (blue) and simulated (red bold in parentheses) rCSLs (relative CSLs to the PM&PI mode) are also provided.

Discussion and Conclusions

New contrast modalities with embedded ultrasound imaging pulses demonstrate great potential for further improving contrast signal strength (up to 8.1 dB) and thus contrast imaging sensitivity over the standard PM or PM&PI.

Table 1

Mode	PM&PI	CR	PI&CR	PM&PI&CR	CR&PI
Resultant SP	SP2 +(2*SP1)	(SP4-SP5) -SP2	(SP4-SP3) -2*SP2	(SP4-SP3) -4*SP1	(SP4-SP5) +(SP3-SP5)
CSL(dB)	16.2 ± 0.9	21.0 ± 0.7	24.0 ± 2.3	24.3 ± 1.7	21.7 ± 1.2
rCSL (dB)	0 (**0**)	4.8 (**6.0**)	7.8 (**6.1**)	8.1 (**11.4**)	5.5 (**7.6**)

** The following are five transmitted pulses:*

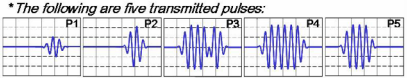

Tuesday Poster

P2B034-05

Singular-Value-Decomposition Investigation of the Sub-harmonic Response of Contrast Agents Excited at 40 MHz

Jonathan Mamou, Sarayu Ramachandran, Jeffrey A. Ketterling; *Riverside Research Institute, F. L. Lizzi Center for Biomedical Engineering, New York, NY, USA.*

Background, Motivation and Objective

Acoustic contrast agents are designed to be used below 10 MHz, but interest is growing in studying the response of agents to high-frequency ultrasound (HFU). In this study, we analyzed the sub-harmonic response of polymer-shelled contrast agents excited at 40 MHz. The echoes from single bubble were analyzed using singular value decomposition (SVD) for their sub-harmonic content at 20 MHz.

Statement of Contribution/Methods

Polycaprolactone-shelled agents (POINT Biomedical, San Carlos, CA) with a mean diameter of 1.1 μm were excited with 40-MHz tone bursts of 10, 15 and 20 cycles. The agents were heavily diluted in filtered water and streamed through a flow-phantom that permitted single-bubble events to be acquired at peak-negative pressures from 0.75 to 5.0 MPa. At each exposure condition, 1000 single-bubble backscatter events were digitized and assembled into a matrix, M; each column contained one event. The SVD of M yielded analyzing vectors and corresponding singular values. Analyzing vectors were ordered by decreasing singular value, and the first analyzing vector whose Fourier transform magnitude peaked at 20 MHz was selected to describe the sub-harmonic events in the complete dataset. A sub-harmonic score (SHS) was computed by summing the absolute value of the sub-harmonic analyzing-vector coefficient of each event multiplied by the magnitude of the Fourier transform of the sub-harmonic analyzing vector at 20 MHz. To test the SVD algorithm, two event libraries were created for each pulse-duration: one with only experimentally-acquired sub-harmonic events and the other without sub-harmonic events. Datasets of 1000 events with prescribed percentages of sub-harmonic events (pSHE) ranging from 0% to 35% were generated by randomly selecting events from both libraries.

Results

Simulation plots of SHS versus pSHE were fit to straight lines. Line fits were excellent (mean-square errors, MSEs<0.0025) for 15 and 20 cycle exposures, but less satisfactory for 10-cycle exposures (MSEs>0.0044). Also, the slope and intercept values of the line fits were nearly the same for each 15-cycle or 20-cycle simulation (SHS=0.50 pSHE + 1.60), but quite different for each 10-cycle simulation (SHS=0.26 pSHE + 1.25). The results suggest that SHS can be inverted to compute pSHE at 15 or 20 cycles, and that the sub-harmonic analyzing vector is a valid descriptor of sub-harmonic events.

Discussion and Conclusions

Our empirical simulations involving experimental data demonstrated the value and ability of our SVD approach to characterize sub-harmonic events. In particular, the sub-harmonic analyzing vector could be interpreted physically to quantify the onset of sub-harmonic events. Experimental results also suggested that half of the sub-harmonic events had positive phase (i.e., a positive coefficient for the sub-harmonic eigenvector) and half had negative phase, which could also be related to the physics of bubble dynamics.

P2B035-06

Ultrasonic contrast detection with third harmonic transmit phasing

Che-Chou Shen, Hong-Wei Wang; *National Taiwan University of Science and Technology, Department of Electrical Engineering, Taipei, Taiwan.*

Background, Motivation and Objective

We have previously developed a novel third harmonic (3f0) transmit phasing method to manipulate tissue harmonic amplitude by transmitting an additional signal at 3f0 frequency together with the original fundamental signal. Since the efficacy of contrast detection relies on harmonic amplitudes of both tissue and bubble, this study focuses on the effects of 3f0 transmit phasing on contrast harmonic generation in order to maximize the contrast-to-tissue ratio (CTR).

Statement of Contribution/Methods

For tissue harmonic suppression, the amplitude and the phase of 3f0 transmit signal have to be carefully selected to produce maximal cancellation between the frequency-sum component (i.e. f0 +f0) and the frequency-difference component (i.e. 3f0 -f0). On the other hand, the extent of bubble oscillation significantly varies with impinging frequency and phase so that the relative magnitudes of the two components could differ from tissue. Consequently, it is expected that the harmonic amplitude from bubble responds differently to 3f0 transmit phasing as compared to its tissue counterpart. Thus, the CTR can be optimally improved with the 3f0 transmit signal that maximizes the difference in harmonic magnitude between bubble and tissue. This hypothesis is tested experimentally.

Results

Results in Fig. A indicate that the contrast harmonic amplitude is obviously less affected in 3f0 transmit phasing. The maximal amplitude reduction for bubble is only 1 dB with a 3f0 phase of 20?while that for tissue is 14 dB with a 3f0 phase of 50? The difference between the two magnitude profiles illustrates that the optimal CTR occurs when the tissue is maximally suppressed. in-vitro B-scan images are also constructed in Fig. B and the CTR is optimally improved for about 9 dB as compared to that without 3f0 transmit phasing.

Discussion and Conclusions

This study confirms that the 3f0 transmit phasing acts differently on bubble and tissue and this distinction can be utilized to optimize the CTR.

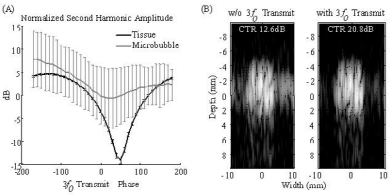

Tuesday Poster

P2B036-07

Image Processing Algorithms for Cumulative Maximum Intensity Subharmonic Ultrasound Imaging: A Comparative Study in the Breast

Jaydev Dave[1], **Flemming Forsberg[2],** Daniel Merton[3], Savitha Fernandes[1], Traci Fox[3], Lauren Leodore[1], Anne Hall[4]; *[1]Thomas Jefferson University and Drexel University, USA, [2]Thomas Jefferson University, Radiology, Philadelphia, PA, USA, [3]Thomas Jefferson University, USA, 4GE Healthcare, USA.*

Background, Motivation and Objective

The purpose of this study was to compare different cumulative maximum intensity (CMI) image processing techniques for depicting vascularity in subharmonic ultrasound images (SHI) of breast lesions. In CMI mode a composite image depicting vascular architecture and blood flow is constructed through maximum intensity projection accumulation of SHI data over consecutive images.

Statement of Contribution/Methods

SHI data (transmitting/receiving at 4.4/2.2 MHz) was obtained from 16 breast lesions using a modified Logiq 9 scanner (GE Healthcare, Milwaukee, WI) as part of a pilot study described elsewhere [Forsberg et al., Radiology, 2007]. CMI data was processed manually and by an automated technique, using 3 different threshold values to reduce motion artifacts. In every case an image of peak contrast flow was chosen based on each of the different techniques. A single image of peak flow was also selected as control. Six blinded and independent readers scored all the randomized images for vessel continuity, detail resolution, presence of artifacts, overall image quality and SNR on a 7 point scale (poor-excellent). Following the initial study, readers also ranked all images within each case on a scale from 1-5 (best-worst). Scores were compared using a double, repeated measures ANOVA with readers and techniques being the independent variables.

Results

The processing techniques were significantly different with regards to vessel continuity, detail resolution and image quality ($p < 0.001$). The single (control) frame was scored significantly worse compared to the manual and automated CMI techniques. For all parameters assessed significant differences were observed between users ($p < 0.001$). One of the users differed markedly from the rest, but repeating the analysis without this user yielded similar results. The rank obtained by each of the techniques (control: 3.85 ± 1.40; manual CMI: 3.45 ± 1.31; automatic CMI 2.70 ± 1.46 to 2.97 ± 1.35; averaged over all users with lower scores being better) was also significantly different ($p < 0.025$). The automated CMI techniques processed data faster and were more reproducible than the manual method.

Discussion and Conclusions

In conclusion, CMI processing techniques (manual and automated) visualize vascularity and produce better image quality than the best single SHI frame. Moreover, the automated techniques save processing time, eliminate user bias and are more reproducible than the manual method.

This work was supported in part by the U.S. Army Medical Research Material Command under DAMD-17-00-1-0464 and by GE Healthcare.

P2B037-08

Molecular Imaging of Thrombus and Ultrasound-Assisted Thrombolysis Using Targeted Ultrasound Contrast Agents

Jia-Ling Ruan, Po-Wen Cheng, Szu-Chia Chen, Yueh-Hsun Chuang, Pai-Chi Li; *National Taiwan University, Taipei, Taiwan.*

Background, Motivation and Objective

Formation of blood clot is a serious cause in many cardiovascular diseases, such as stoke and myocardial infarction. Clinical research has demonstrated capabilities of ultrasound to enhance the thrombolytic effects, with implications to treat the thrombo-occlusive diseases. However, mechanism of ultrasound-facilitated thrombolysis is still unknown but nonetheless acoustic cavitation may play an important role. Ultrasound contrast agents are suitable cavitation nuclei that can reduce the threshold for cavitation induction. Many in vitro models have revealed that the addition of ultrasound contrast agents in ultrasound-augmented thrombolytic experiments may enhance the efficacy of thrombolysis. Furthermore, targeted ultrasound contrast agents that specifically recognize thrombi may help the thrombus detection as well as enhance cavitation effects. Particularly, targeted contrast agents may reduce the distance between microbubbles and the targets. It is our hypothesis that targeted ultrasound contrast agents not only can be used for molecular imaging of thrombus, they may also enhance sonothrombolytic effects.

Statement of Contribution/Methods

We have developed an albumin-based ultrasound contrast agent capable of enhancing both image contrast and cavitation effects. In this study, we further designed the thrombus-targeted ultrasound contrast agents with tirofiban, a glycoprotein IIb/IIIa antagonist that can specifically bind to activated platelets in the thrombus. High frequency (40 MHz) ultrasound imaging were used to confirm the binding ability to thrombi from canine whole blood. In vitro static and flow system for inertial cavitation dose detection were also constructed to study the sonothrombolytic effects with the addition of targeted and nontargeted microbubbles. The influence of microbubble concentration, the flow rate in the flow system, and the thrombus age were also investigated. The efficacy of thrombolysis was measured by the weight loss.

Results

40 % enhancement in image intensity was achieved after the clots were incubated with targeted microbubbles, while in the nontargeted microbubble system, the enhancement was 5 %. On the other hand, thrombolytic efficacy in both static and flow systems were also investigated. Results show that although targeted microbubbles may enhance the ultrasound-aided thrombolytic mechanism, quantitative relations between the cavitation dose and weight loss are difficult to establish.

Discussion and Conclusions

The targeting capabilities of in-house ultrasound contrast agents to thrombus have been demonstrated in vitro. For sonothrombolytic effects, on the other hand, the number of microbubbles may be a much more crucial factor than either their targeting ability or the concentration, since it is directly related to the intensity of acoustic cavitation.

Tuesday Poster

P2B038-09

Monodisperse Microbubble Populations via Microfluidic Chip Flow-Focusing

Yaoyao Cui, Paul Campbell; *University of Dundee, CICaSS Group, Dundee, Scotland, United Kingdom.*

Background, Motivation and Objective

Encapsulated ultrasound contrast agents (UCA) have received considerable recent attention, not only because of their echogenic properties which aid disgnostic imaging, but also for their ability to mediated targeted drug and gene delivery. Ideally, this latter application requires monodisperse populations of microbubbles to optimise abrupt and well controlled response, and thus maximize delivery efficiency. In recent years, several methods of microbubble preparation have been presented which offered some control over the size of bubbles. The intention of this work was to prepare our own microbubbles with quite small and uniform sizes (<5μm), and additionally to study thier distinct bioeffects in vitro.

Statement of Contribution/Methods

Our coated microbubbles are produced by 15mm×15mm×4mm B270 Superwite glass microfludics flow-focusing chips. A 4-way connector with PTFE tubes is connected via thru-holes in top layer of chip, by which could supply shell solution and gas corn separately. A continuous liquid flow rate is controlled by a high precision syringe pump. The shell of our bubbles is based on phospholipid material with slightly changed recipes. Air/ Nitrogen/ perfluorocarbon (PFC) gas has been use for comparison of lasting time of these bubbles. Moreover, preliminary experiments have also been conducted to sonoporate cells with these home-made bubbles and this data set will also be presented.

Results

Mono-disperse micron-sized lipid-coated microbubbles were generated by several geometry sizes of microchannels and precisely controllable flow rate of lipid solution and pressure of gas. Compared with T-junction (~100 μm) flow-focusing method, the average size of produced microbubbles is significant smaller.

Discussion and Conclusions

The benefit of glass flow-focusing chambers over other conventional materials such as polydimethylsiloxane) (PDMS), is twofold. Firstly, glass is obviously capable of withstanding elevated gas pressure, which is beneficial for investigation of microbubble formation. Secondly, the excellent solvent resistance and minimum material adsorption / absorption allow more recipes of bubble shell, which has significant potential for enhanced custom-designing ultrasound contrast agents for drug delivery, targeted imaging and future more therapeutic applications.

P2B039-10

Ultrasound Contrast Imaging Based on a Novel Algorithm Combined Pulse Inversion with Wavelet Transform

Xiaoyan Zhao, Minxi Wan, Hui Zhong, Liang Shen; *School of Life Science and Technology, Xi'an Jiaotong University, The Key Laboratory of Biomedical Information Engineering of Ministry of Education, Xi'an, Shaanxi, China.*

Background, Motivation and Objective

Ultrasound contrast agents (UCA) can be sufficiently detected and imaged with nonlinear methods such as pulse-inversion harmonic technique. Contrast is limited, however, by second harmonic signals scattered from tissues. In this paper, a novel ultrasound contrast imaging method which combines pulse-inversion technique with wavelet transform is proposed to enhance the contrast between bubbles and surrounding tissues.

Statement of Contribution/Methods

Wavelet transform was utilized to analyze the correlation between mother wavelet and received echoes from a pair of inverted transmit pulses respectively. In order to detect bubble signals above surrounding tissues signals, the power spectrum of the selected mother wavelet should be well-matched with the echoes of bubbles. The maximal one of the transformed wavelet correlation coefficients was obtained at an appropriate scale. Wavelet correlation coefficients at this scale were selected to replace the original received echoes. The echoes replaced by wavelet correlation coefficients from the two inverted transform pulses were summed to obtain a beam to differentiate echoes of bubbles and surrounding tissues. In order to obtain better correlation, a new mother wavelet named 'bubble wavelet' is constructed according to the modified Herring equation. Radio frequency (RF) data were acquired from a modified digital diagnostic ultrasound system.

Results

The proposed method was validated by simulations. Experiments were performed on an ultrasonic Doppler flow phantom and results showed that the contrast-to-tissue ratio (CTR) was improved by 6-16 dB depending on types of mother wavelet, scales and depths, compared to that obtained using pulse-inversion-based second-harmonic imaging. Experiments in vivo were also conducted out using kidneys of rabbits and results showed that signals of surrounding tissues can be well suppressed compared to that of bubbles. By using bubble wavelet, the CTR was improved by up to 8 dB relative to Morlet wavelet and Mexican Hat wavelet under the same conditions in both simulation and experiments.

Discussion and Conclusions

It is concluded that the contrast for UCA imaging is improved using this method. There is a high correlation between the bubble wavelet and the echoes from bubbles. Further improvements might be achieved with optimized bubble wavelet which can describe the scattering echoes of the bubbles more accurately.

Tuesday Poster

P2B040-11

Inflow-Time Mapping of Ultrasonic Contrast Agents for Differential Diagnosis of Liver Tumor

Hideki Yoshikawa[1], Takashi Azuma[1], Kenichi Kawabata[1], Kazuaki Sasaki[2], Shin-ichiro Umemura[3]; *[1]HITACHI, Ltd., Central Research Laboratory, Kokubunji, Tokyo, Japan, [2]Tokyo University of Agriculture and Technology, Tokyo, Japan, [3]Tohoku University, Sendai, Japan.*

Background, Motivation and Objective

The artery distribution provides useful information for differential diagnosis of liver tumors. In ultrasonic contrast imaging of liver, the artery vessels are contrasted immediately after the injection of contrast agents, several seconds prior to portal veins. With conventional contrast imaging, it is difficult for an operator to precisely image artery vessels because of the narrow time window.

We aim to establish a new imaging technique, inflow-time mapping (ITM), which visualizes inflow time of contrast agents into vessels to distinguish the artery vessels and the portal veins in liver. Results on an early feasibility study of ITM with rabbits will be presented in this paper.

Statement of Contribution/Methods

Sonazoid® was used as a contrast agent, which was injected into an anesthetized rabbit intravenously. Recording of the ultrasonic images with pulse inversion of the rabbit liver were started for 12 seconds at a rate of 15 frames per second. For each pixel in the obtained images, the time course of grayscale intensity during the recording was measured and the time for reaching a plateau was calculated, which was used as the measure of the inflow time of

contrast agents. Then ITM was generated by coloring each pixel according to the inflow time. Finally, ITM was compared with an original contrast image.

Results

ITM and the original contrast image at 12 seconds after the injection of contrast agent are shown in Figure 1. In ITM, color table is set to give brighter color for longer inflow time, and the artery vessels are clearly distinguishable from the portal veins.

Discussion and Conclusions

The artery and the portal vein can be separately imaged in ITM, which are difficult to distinguish in the original contrast image. This result suggests that ITM would be helpful to easily locate the arterial vasculature, leading to accurate differential diagnosis of liver tumors.

As a further feasibility study, we plan to make ITM of various tumor models and compare the neovascularity between normal, benign and malignant cases.

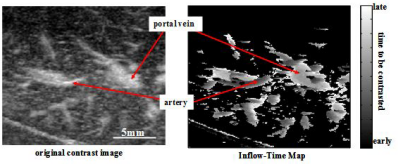

Figure 1. Comparison of Inflow-Time Map with original contrast image

P2C. Contrast Agents: Modeling and Characterization

2nd and 3rd Floor Foyers

Tuesday, November 4, 2008, 3:00 pm - 4:30 pm

Chair: **Jonathan Mamou;**
Riverside Research Institute, New York, USA.

P2C041-01

Monitoring and Modeling of Microbubble Behavior during Ultrasound Mediated Transfection of Cell Monolayers

Karin Hensel[1], Monica Siepmann[1], Abdelouahid Maghnouj[2], Stephan Hahn[2], Georg Schmitz[1]; *[1]Ruhr-University Bochum, Institute of Medical Engineering, Germany, [2]Ruhr-University Bochum, Molecular GI-Oncology, Germany.*

Background, Motivation and Objective

The large scale oscillation of insonified microbubbles (MBs) is considered to be the primary effect for sonoporation and thus enhances cell transfection in gene therapy while destruction of microbubbles is suspected to lead to lower transfection rates. For future in vivo therapy, online acoustic monitoring could be used to determine optimal pulse sequence parameters adaptively. As a first step, we acoustically monitored attenuation caused by MBs during ultrasound mediated transfection of cell monolayers. A model of the interaction of ultrasound, MBs and cells in suspension [1] is adopted for cell layers and transfection efficiency is correlated with the concentration of strongly oscillating microbubbles over time.

Tuesday Poster

Statement of Contribution/Methods

Layers of 293T cells were grown in an Opticell (BioCrystal Ltd., Westerville, OH). Each container was filled with 9.6 ml culture medium containing 100 µg of GFP expressing plasmid DNA and 0.3 ml of SonoVue (Bracco, Milano, Italy). The container was placed in water in the focus of a transducer emitting 5 cycles sine-bursts at 1 MHz repeated 100 times at 10 Hz. The peak negative pressure was varied from 0.1 to 1.2 MPa in seven steps. A second transducer (1 MHz center frequency) detected transmitted signals on the opposite side. The exponential model of ultrasound and MB interaction given in [1] was fit to transmission data. The transducers horizontally scanned the entire cell monolayer at 100 positions using a step size of 6 mm. After experiments, the cells were incubated for 24 hours. Subsequently, the transfection rate was analyzed by flow cytometry.

Results

The recorded transmission signals increased over therapy time in agreement with the adapted model for cell monolayers showing that MB destruction follows an exponential function. Time constants ranged from 1.9 s for 0.1 MPa to 1.0 s for 1.2 MPa. For the initial MB concentration of 1.5x10^7 MB/ml, while employing 0.1 MPa, 90% of the local MB were destructed during the first 4.4 s of therapy; for 1.2 MPa within 2.3 s, respectively. Cell transfection rate also increased with peak negative pressure by a factor of 5 although MBs were destroyed more quickly. Analysing the sound field of the transducer with respect to the destruction threshold of SonoVue reveals that the volume in which microbubbles can oscillate strongly without destruction also increases with the presented peak negative pressures from 210mm^3 to 7082mm^3, resulting in a higher oscillating MB time product.

Discussion and Conclusions

This study shows that the exponential model for cell suspensions can be applied to cell layers and that for optimal transfection efficiency the concentration-time product of actively oscillating microbubbles has to be maximized. The online observation of transmitted and scattered signals from MB provides direct information about cell MB interaction and can be used to adaptively optimize transfection efficiency.

[1] W. Nyborg, Ultrasound MedBiol, 32, pp. 1557-1568, 2006.

P2C042-02

Characterization of Bubble Liposomes by Measurements of Ultrasound Attenuation: Effects of Shell Materials

Katsuji Sakaguchi[1], Nobuki Kudo[1], Ryo Suzuki[2], Kazuo Maruyama[2], Katsuyuki Yamamoto[1]; *[1]Hokkaido University, Graduate school of Information Science and Technology, Sapporo, Hokkaido, Japan, [2]Teikyo University, Department of Biopharmaceutics, School of Pharmaceutical Sciences, Japan.*

Background, Motivation and Objective

"Bubble liposomes" are gas-encapsulated liposomes of several hundred nanometers in diameter. These bubbles are expected to create new applications in the field of gene delivery and drug delivery systems. However, the acoustic characteristics of these bubbles are still unclear due to the small bubble sizes. In this study, the acoustic properties of two types of Bubble liposomes were evaluated by measuring the attenuation of a bubble suspension.

Statement of Contribution/Methods

Wideband pulses of 10 MHz in center frequency were used as probing pulses for the attenuation measurement. The waveforms of probing pulses transmitted through saline or bubble-suspended saline were acquired, and frequency-dependent attenuation (an attenuation curve) was determined as the ratio of frequency spectra of the acquired waveforms. Two types of Bubble liposomes that have different shell chemical compositions, type BL (DSPC: DSPE-PEG(2k) = 94:6) and type BLC (DSPC: cholesterol: DSPE-PEG(2k) = 54:40:6), were used to investigate the effects of shell characteristics on bubble behavior.

Results

In the case of BL, attenuation of probing pulses was constant during repetitive exposure to the pulses in the range of 0.02 to 0.17 MPa. Furthermore, peaks in the attenuation curves at 16-20 MHz, indicating absorption of the acoustic energy by BL, increased with increasing pressure of the probing pulses. At 0.26 MPa, attenuation of the BL suspension decreased every time after exposure to the probing pulses. However, in the case of the BLC suspension, this decrease was observed even at 0.02 MPa, and a peak of the attenuation curve of BLC was observed at around 5 MHz.

Tuesday Poster

Discussion and Conclusions

The function of bubble shell, which is to protect the encapsulated gas from diffusion, was not weakened by repetitive oscillations of BL under the threshold. The difference in threshold pressure for collapse of BL and BLC suggests that the shell material of BLC is brittle compared to that of BL. The peak frequency of the BLC attenuation curve, which is lower than one-third of that of BL, suggests that several destructed bubbles were oscillating as one large bubble. These observation results show that our attenuation measurement method is useful for evaluation of the dynamics and shell characteristics of nano-sized bubbles.

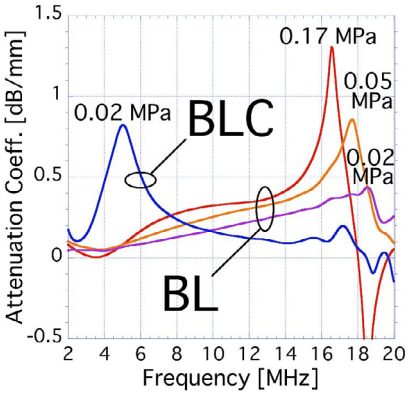

Attenuation Curves of BL and BLC

P2C043-03

Ultrasound Induced Deflation: a method to study the behavior of single bubbles with varying diameter

Francesco Guidi[1], Riccardo Mori[1], Hendrik Vos[2], Nico de Jong[2], Piero Tortoli[1]; [1]*University of Florence, Electronic and Telecommunication, Florence, FI, Italy,* [2]*Erasmus University, Biomedical Engineering, Rotterdam, Netherlands.*

Background, Motivation and Objective

Phospholipids coated microbubbles exposed to ultrasound (US) are known to deflate, with possible impact on the results of diagnostic imaging applications, but the major factors influencing this phenomenon are still not understood. This paper reports on an acousto-optic method allowing to investigate the deflation of single microbubbles exposed to low-pressure US pulses over long time intervals.

Statement of Contribution/Methods

The experimental set-up was based on the acoustic Bubble Behavior Testing (BBT) system, which includes an arbitrary waveform generator, two focussed calibrated transducers, an ultra low-noise amplifier and a large buffer to store the RF echo data over long time intervals. Definity (Bristol-Myers Squibb, USA) microbubbles were held in a 200 µm fiber and exposed to US pulse sequences at rate of 250 pulses per second. The pulse sequences consisted of single tone bursts with acoustic level in the range 50-70 kPa, and frequency cyclically varying from 2 MHz to 4 MHz.

The BBT system was combined with a microscope and a fast camera capturing one bubble image per US pulse. The high sensitivity and resolution of both systems allowed the observation of bubbles with radius down to 1.2 µm, which produced echoes whose amplitude was estimated below 1 Pa. Bubble echoes and images were analyzed to correlate the US excitation and the deflation phenomenon.

Results

The response of about 100 Definity bubbles to different US pulse sequences was observed. Whichever was the initial diameter (≤ 4 µm), all bubbles typically deflated and reached a final stable state in several seconds. Notably, the final radius mainly depended on the US pressure (about 1.4 µm at 65 kPa and 1.7 µm at 50 kPa).

Graphs reporting the echo amplitude as a function of radius show common features for all bubbles. The amplitude tends to decrease together with the bubble radius, showing a knee beyond which the decrease is accelerated. When 2 MHz, 65 kPa pulses were transmitted, the echo levels were 5 Pa at 2.4 µm radius, down to 1 Pa at 1.5 µm, with the knee around 1.8 µm. During deflation, we measured also a considerable reduction of the echo phase lag, covering a 2 radiant variation.

An equivalent behavior was verified for all frequencies (2, 2.5, 3, 3.5, 4 MHz) cyclically used to insonify a same bubble.

Finally, a strong second harmonic response was observed when the bubble was close to resonance and when it approached the final stable radius.

Discussion and Conclusions

The described acousto-optic set-up allows observing and analysing the response of a single bubble with varying diameter, to multiple US frequencies. Different bubbles showing the same behavior suggest that the deflation be independent of the bubble history and mainly related to the driving conditions. The observed second harmonic response is in agreement with the predicted high-amplitude resonant oscillations and the compression-only behavior typical of deflated bubbles.

P2C044-04

Comparison of the acoustic response of attached and unattached BiSphere™ microbubbles

Mairead Butler[1], David Thomas[1], Stephen Pye[2], Carmel Moran[1], W Norman McDicken[1], Vassilis Sboros[1]; [1]*University of Edinburgh, Medical Physics, Edinburgh, United Kingdom,* [2]*NHS Lothian, Medical Physics, , N/A, United Kingdom.*

Background, Motivation and Objective

Two systems which independently allow the investigation of the response of individual unattached and attached microbubbles (MB) have previously been described. Both offered methods of studying the acoustic response of single MBs in well defined acoustic fields. The aim of the work described here was to investigate the response of single attached MBs for a range of acoustic pressures and to compare to the backscatter from unattached single MBs subjected to the same acoustic fields.

Tuesday Poster

Statement of Contribution/Methods

Single attached BiSphereTM (Point Biomedical) MBs were attached to polyester with poly-L-lysine and insonated at 1.6 MHz for acoustic pressures ranging from 300 to 1000 kPa using a Sonos5500 (Philips Medical Systems) research ultrasound scanner. Each MB was aligned to 6 pulse M-mode ultrasound beams, and unprocessed backscattered RF data captured using proprietary hardware and software. The backscatter from these MBs was compared to that of single unattached MBs subjected to the same acoustic parameters. MBs were insonated several times to determine possible differences in rate of decrease of backscatter between attached and unattached MBs.

Results

In total 140 single attached microbubbles have been insonated. At 550 kPa an acoustic signal was detected for 20% of the attached MBs and at 1000 kPa for 63%. At acoustic pressures of 300 kPa no signal was detected. Data for 54 attached MBs were compared to data for 86 unattached MBs. RMS pressure from attached and unattached MBs insonated at 800 kPa was 0.33±0.1 and 0.36±0.1 Pa respectively for the fundamental. The ratio of energy density of the first two backscattered pulses decreased with increasing pressure. However, for unattached MBs the magnitude of the ratio was less than that of attached (at 550 kPa mean ratio attached: 0.85±0.1 unattached: 0.11±0.1. There was no significant difference in the peak amplitude of the backscattered fundamental and harmonic signal for unattached and attached MBs.

Discussion and Conclusions

BiSphereTMMBs comprise an internal polymer shell with an albumin coating, resulting in a stiff shell. TM BiSphereMBs do not oscillate in the same manner as softer shelled MBs, but allow gas leakage which then performs free bubble oscillations. Optically it has been shown that attached lipid MBs have smaller oscillations than unattached MBs. The results here agree with previous acoustic and optical microscopy data which show that a proportion of MBs will scatter and this number increases with acoustic pressure. The lack of difference in scatter from attached and unattached MBs may be due to the free MB oscillation being in the vicinity of the stiff shell, which may provide the same motion damping to a wall. Second pulse exposure shows that the wall becomes important in the survival of the echoes. These high quality measurements can further improve by incorporating MB sizing to increase the specificity of the comparisons between unattached and attached MBs.

P2C045-05

An experimental setup for the determination of the inertial cavitation threshold of ultrasound contrast agents

Michal Mleczko, Georg Schmitz; *Ruhr-Universität Bochum, Institute of Medical Engineering, Bochum, Germany.*

Background, Motivation and Objective

Ultrasound contrast agents consist of microbubbles with diameters in the micron range. Recent developments employ microbubbles for the purpose of targeted drug delivery. If the insonification amplitude is chosen high enough, the microbubble may be destroyed by inertial cavitation. The minimum threshold for inertial cavitation of a microbubble population is thus an important characteristic of an ultrasound contrast agent. Its accurate determination, however, is experimentally challenging since a large number of bubbles needs to be interrogated to give an accurate representation of the entire population. Also, the concentration of bubbles in the test tank must be kept low enough so that individual bubbles cannot interact and cases where this occurs have to be found and discarded. This study proposes a method for the detection of destruction of ultrasound contrast agents by inertial cavitation using a signal processing approach which enables counting the number of bubbles present in the acoustic focus.

Statement of Contribution/Methods

The experimental setup consists of a single-element spherically focused ultrasound transducer with a center frequency of 2.25 MHz (Olympus-NDT A395SU, Waltham, MA) driven by a programmable pulser/receiver (Inoson PCM100, Inoson GmbH, St. Ingbert, Germany), operated in pulse-echo mode. Peak negative pressures of the set-up were determined with a hydrophone. A clinically approved contrast agent (Definity, kindly provided by Bristol-Myers Squibb, New York, NY) was heavily diluted in the measurement tank. The pulser is programmed to transmit 5-cycle bursts with 2.25 MHz center frequency.

Detection is implemented by transmission of two pulses with a time delay of 30 µs between the first destruction and second probing pulse. This time is long enough to ensure bubble destruction is completed and short enough to exclude bubble displacement from the focus Using an expectation maximization algorithm, modulated Gaussian pulses are fitted to the received waveform. By consideration of the time offset between each pulse in the received waveform, the responses to the first and second pulse may be separated and destroyed bubbles are counted.

Results

A destruction curve was recorded at a frequency of 2.25 MHz. Single microbubble destruction events could be reliably detected and separated in the case of multibubble detection, which occurred in 38% of the cases. At a peak negative pressure of 1.1 MPa 20% of the recorded population was destroyed. The maximum size of the 90% confidence interval obtained was 10%.

Discussion and Conclusions

The proposed experimental setup allows for a fully automatic acquisition and evaluation of the cavitation threshold of ultrasound contrast agents. This facilitates gathering the large amounts of data necessary for an accurate determination of the cavitation threshold for an entire frequency band. First results obtained in this study to evaluate the setup are in agreement with values from literature.

P2C046-06

In-vivo Perfusion Quantification by Contrast Ultrasound:Validation of the Use of Linearized Video Data vs. Raw RF Data

Nicolas Rognin, Peter Frinking, Tristan Messager, Marcel Arditi; *Bracco Research SA, Plan-les-Ouates, Geneva, Switzerland.*

Background, Motivation and Objective

In order to be reliable and fairly system- and user-independent, quantification of in-vivo perfusion by contrast ultrasound should ideally be performed on echo-power data estimated from raw echo signals after TGC, because this quantity is directly proportional to the instantaneous contrast agent concentration. The objective of this work was to validate the use of scan-converted and log-compressed video sequences for perfusion quantification, and to assess the accuracy of quantification using linearized video data vs. using raw data. Video sequences have the major advantage of being readily available as DICOM files in most ultrasound systems, compared to raw data which are only accessible to manufacturers and require inconveniently large storage space.

Statement of Contribution/Methods

A rabbit kidney was imaged after administration of a 0.1 ml bolus of SonoVue. Sequences of 60 s realtime rf-data were acquired using a Megas system (Esaote, Genoa, Italy) in CnTI mode, coupled to a "Femmina" digital interface (University of Florence, Italy). The rf-data were demodulated using the Hilbert transform, log-compressed with a dynamic range of 30 to 60 dB, scan-converted and stored as 8-bit color-mapped images. The video sequences were subsequently analyzed to estimate contrast-agent kinetics with a bolus model in regions of interest (ROI), along the following scheme: linearization at the pixel level by inversion of the color-palette luminance, inversion of log-compressions, squaring to estimate echo power, and averaging in ROIs. Perfusion parameters estimated in this way were compared to those derived from direct analysis of rf-data vectors, serving as reference. The relative errors on both peak value and mean transit time were computed for the range of log-compression values considered.

Results

The effects of scan-conversion and 8-bit quantization on the video-processing path were more severe for lower values of log-compression. For example, relative errors in peak echo-power were 0.16%, 0.36% and 13% for log-compression ranges of 50, 40 and 30 dB, respectively. The corresponding errors in mean transit-time estimates were 0.01%, 0.12% and 4%. The outcome of this study is that quantification on linearized video sequences provides results within 1% of those obtained from analyses performed on raw rf-data, for ranges of log-compression above 35 dB.

Discussion and Conclusions

Using video sequences for perfusion quantification, small errors may be introduced when insufficient log-compression is applied before quantization, but they are negligible when log-compression is above 35 dB. This study thus validates the use of off-line quantification software programs, analyzing log-compressed video sequences, provided that the log-compression law of the ultrasound system is known. The results in this case are equivalent to analyzing raw rf-data.

P2C047-07

Applying Real-time Noninvasive Pressure Estimation Obtained from Subharmonic Contrast Microbubble Signals

Lauren Leodore[1], Flemming Forsberg[2]; [1]*Thomas Jefferson University, USA,* [2]*Thomas Jefferson University, Radiology, USA.*

Background, Motivation and Objective

Ambient pressure changes affect the subharmonic signals from ultrasound (US) contrast microbubbles. We have proposed subharmonic aided pressure estimation (SHAPE; U.S. patent 6,302,845) and in this study implemented real-time SHAPE on a commercial US scanner.

Statement of Contribution/Methods

An experimental system for SHAPE was constructed based on two single-element transducers assembled confocally at a 60¡ã angle to each other. A transducer with a bandwidth of 38% and a center frequency of 2.2 MHz (Staveley, East Hartford, CT) was used as the transmitter and a second transducer with a bandwidth of 86% and a center frequency of 3.6 MHz (Etalon Inc., Lebanon, IN) was used as the receiver. Amplified signals were then acquired using a digital oscilloscope (Model 9350AM, Lecroy, Chestnut Ridge, NY) and controlled by a personal computer via LabVIEW (National Instruments, Houston, TX). The relationship between changes in hydrostatic pressure and subharmonic amplitude were analyzed via linear regressions using Stata 9.0 (College Station, TX). Changes in the first, second, and subharmonic amplitudes of six different ultrasound contrast agents were measured in vitro at hydrostatic pressures from 0-186 mmHg, acoustic pressures from 0.35-0.60 MPa and frequencies of 2.5-6.6 MHz at room temperature (25¡ã C). The pressure inside the tank was monitored by a pressure gauge (OMEGA Engineering Inc., Stamford, CT). The optimal parameters for SHAPE (i.e., highest sensitivity) were determined using linear regression analysis and implemented on a Logiq 9 scanner (GE Healthcare, Milwaukee, WI). The real-time implementation of SHAPE was tested in vitro in a flow phantom. In vivo experiments are ongoing and results will be presented.

Tuesday Poster

Results

Over the pressure range studied the 1st and 2nd harmonic amplitudes reduced approximately 2 dB for all US contrast agents. Over the same pressure range, the subharmonic amplitudes decreased by 10-14 dB and excellent linear regressions were achieved with the hydrostatic pressure variations (r2 ¡Ý 0.98, $p < 0.001$). The optimal sensitivity for SHAPE was achieved at a transmit frequency of 2.5 MHz (i.e., receiving at 1.25 MHz) at a 0.35 MPa acoustic pressure using Sonazoid (GE Healthcare, Oslo, Norway) which declined approximately 14.4 dB in vitro. A Logiq 9 scanner was modified to implement SHI on a curve linear transducer 4C with a frequency range from 1.5-4.5 MHz. A pulse inversion technique was used with transmit frequency and power level optimized for sensitivity. The subharmonic signals are displayed in real-time and can also be stored for off-line analysis.

Discussion and Conclusions

Subharmonic contrast signals are a good indicator of hydrostatic pressure. Real-time SHAPE has been implemented on a commercial US scanner and offers the possibility of allowing pressure gradients in the heart to be obtained noninvasively.

This work was supported by in part by AHA grant no 06554414 and NIH HL081892.

P2D. Bioeffects

2nd and 3rd Floor Foyers

Tuesday, November 4, 2008, 3:00 pm - 4:30 pm

Chair: **Chris Hall;**
Philips Research North America, USA.

P2D048-01

Investigation on the Usefulness of the Infrared Image for Measuring the Temperature Developed by Transducer

Satoshi Yamazaki; *Toshiba Medical Systems Corporation, Ultrasound Systems Development Department, Otawara, Tochigi, Japan.*

Background, Motivation and Objective

A standard; IEC/TS62306ED1 defines how to measure temperature rise of Tissue Mimicking Material(TMM) developed by ultrasound transducer. However, it has a difficulty of finding the 3 dimensional position which represents maximum temperature in TMM. It depends on the huge number of measurements with fine pitch's positioning, especially tuning the thickness of the TMM layer between transducer and TMM.

The objective of this feasibility study is to investigate the usefulness of the infrared image for cross sectional surface of TMM from the viewing point of both the measured temperature rise and the depth of maximum temperature.

Statement of Contribution/Methods

First, the comparison was performed between infrared image on the surface of TMM having equivalent consistent to the material of IEC60601-2-37ED2(see Fig. 1 and Fig. 2) and measured temperature from Thermal Test Object(TTO) developed for the measurement on IEC/TS62306ED1 by National Physical Laboratory(UK), as test and reference, respectively. A phased array transducer(Toshiba) was used for 3 minute's radiation and heat conduction to TMM/TTO. The special transmission condition was given only for the comparison. And depth of measured temperature was specified as 5 mm on the infrared image/TMM which was equal to one of thermo couple embedded in TTO.

Next, the depth of maximum temperature was evaluated on the infrared image.

Results

The mean value of measured temperature rise for 3 minute's radiation/heat conduction were 2.2 degree Celsius for infrared image/TMM and 2.1 degree Celsius for TTO, respectively. The standard deviation of them were 0.3 degree Celsius for infrared image/TMM and 0.1 degree Celsius for TTO, respectively.

Although the method of infrared image had a slightly large variation, the mean values were very similar.

The mean depth of maximum temperature was approximately 1 mm with standard deviation of 0.3 mm. It was close to the surface of TMM.

Discussion and Conclusions

The method of infrared image with TMM was useful for measuring the temperature developed by radiation and heat conduction. It was one of the reasonable approach for finding the position of maximum temperature in the TMM since infrared image provided the map of temperature distribution.

On the other hand, it should be considered that the uniformity of initial temperature observed on the surface of TMM affected to the variation of measured temperature.

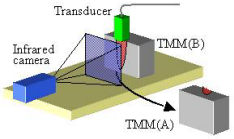

Fig1
Method of infrared image with splitted TMM

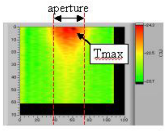

Fig 2
Example of actual infrared image

P2D049-02

Qualitative and quantitative analysis of the molecular delivery through the ultrasound-enhanced blood-brain barrier opening in the murine brain

Shougang Wang, James Choi, Yao-Sheng Tung, Barclay Morrison, Elisa Konofagou; *Columbia University, Department of Biomedical Engineering, USA.*

Background, Motivation and Objective

The presence of blood-brain barrier (BBB), a specialized brain protection system consisting of endothelial cell tight junctions and glial processes, is the major limiting factor to delivering therapeutic agents to the brain [1]. Recent studies have proven that the interaction of focused ultrasound (FUS) and microbubbles can enable the local delivery of large molecules across the BBB, transiently and non-invasively into the murine hippocampus [2]. In this paper, the cellular impact, the size of the opening and the deposition amount were determined through qualitative and quantitative analysis of the molecular delivery to the murine brain parenchyma for the ultimate purpose of ultrasound-facilitated neurodegenerative disease treatment in humans.

Tuesday Poster

Statement of Contribution/Methods

In this study, a 25 ul bolus of lipid-shelled microbubbles (diameter: 4-5 um, concentration: 2*10^8 bubbles/ml) was injected into the tail vein prior to sonication. Pulsed FUS (f=1.525MHz, pressure: 0.57 MPa peak-negative) was applied to the left hippocampus through the intact skin and skull to induce the BBB disruption [2]. Fluorescence-tagged (Texas Red, Invitrogen Corp., Carlsbad, CA USA) dextrans at 3 kDa (Diameter: 2.33+-0.38 nm) and 70 kDa (Diameter: 10.2+-1.4 nm) were then separately injected into the femoral vein at a concentration of 80 ug/g body mass. Upon completion of the in vivo experiments, brain samples were either sliced (n=6) for fluorescence imaging (Olympus IX-81, Melville, NY, USA) or homogenized (n=3) for quantitative analysis using a fluorescence spectrometer (SpectraMAX M2, Molecular Devices, Sunnyvale, CA USA).

Results

In the quantification analysis of 3 kDa dextran, the sonicated (left) hemisphere was infused with 0.74+-0.21 ng, i.e., 0.05% of the systemically administered volume and exhibited a 25% higher molecular volume than the unexposed hemisphere (right control side). Fluorescence imaging at 70 kDa dextran indicated that molecules with diameters of at least 10 nm were capable of traversing the BBB opening and diffusing into the entire hippocampus. The smooth muscle cells engulfing the micro-vessels exhibited higher fluorescence in the case of larger molecules while dextrans at lower molecular weights showed higher diffusivity into the brain parenchyma.

Discussion and Conclusions

In conclusion, significant drug delivery and the net deposition to the sonicated hippocampus (compared to the non-sonicated control) were determined and quantified at the BBB-opened region. As evidenced by fluorescence imaging, the smooth muscle cells, together with endothelial cells, were found to be affected by the ultrasound-microbubble interaction and absorb the larger molecules.

This study was supported by NSF CAREER 0644713, NIH R21 EY018505 and the Kinetic Foundation.

[1] W. M. Pardridge, NeuroRx, vol. 2, pp. 3-14, 2005.

[2] J. J. Choi, M. Pernot, S. A. Small, and E. E. Konofagou, Ultrasound Med. Bio., vol. 33, pp. 95-104, 2007.

P2D050-03

Safety radius for algae eradication at 200 kHz - 2.5 MHz

Michiel Postema[1], Antje Schommartz[2]; [1]*The University of Hull, Department of Engineering, Kingston upon Hull, East Riding of Yorkshire, United Kingdom,* [2]*The University of Hull, Department of Engineering, United Kingdom.*

Background, Motivation and Objective

The benefits of ultrasonics in algae control have been well known [1]. The transmit frequencies used to study this application have been as low as 20 kHz and as high as 1.7 MHz. Eradication equipment has been commercially available. There have been speculations about the physical mechanism behind the algae eradication, specifically about the role of cavitation.

Furthermore, the consequences for swimmers in water subjected to ultrasonic treatment have been unknown. In this study, we investigate the role of eradicator-generated cavitation as a potential danger for swimmers. Furthermore, we give an estimate of swimmer safety radii, based on current regulations.

Statement of Contribution/Methods

To test, whether we could create inertial cavitation conditions under laboratory conditions at voltages similar to in-field equipment, we built three undamped broadband ultrasound transducers with centre transmit frequencies between 200 kHz and 2.5 MHz.

These were inserted into a tank containing oversaturated water and subjected to quasi-continuous 5 V peak-to-peak AC signal at their centre transmit frequencies. The sound fields were measured with a broad-band hydrophone.

Results

In the acoustic focus, the highest sound pressure measured was 68 kPa at 2.2 MHz, i.e., mechanical index MI < 0.05 << 0.3. Clearly, these values are much lower than the cavitation thresholds. Comparing the acoustic output of our transducers to the NATO Undersea Research Centre Human Diver and Marine Mammal Risk Mitigation Rules and Procedures, i.e., 708 Pa between 31.5 kHz and 250 kHz, we find that at very close distance, the threshold for safe diving is surpassed.

Discussion and Conclusions

Taking into account the double-distance sound pressure level and the low attenuation in water, this implies that even at these low voltages, the safe swimming distance is at least several meters away from the sound source. From in-situ measurements of commercial equipment, we estimate the safe radius for swimmers to be 15 m.

Although the worst-case mechanical index close to our transducers is MI << 0.3, some of the acoustic pressures determined are higher than those allowable by the NATO Undersea Research Centre Human Diver and Marine Mammal Risk Mitigation Rules and Procedures.

[1] Zhang, G., Zhang, P., Liu, H., Wang, B.: Ultrasonic damages on cyanobacterial photosynthesis. Ultrasonics Sonochemistry 13(6) (2006), 501–505.

P2D051-04

Ultrasonic Microprobe based in vitro Direct-Mechanical stimulation of Canine Left-Ventricular Tissue

Abhishek Ramkumar[1], Robert F. Gilmour Jr.[2], Abhishek Ramkumar[1]; [1]*Cornell University, Biomedical Engineering, Ithaca, New York, USA,* [2]*Cornell University, Biomedical Sciences, Ithaca, New York, USA.*

Background, Motivation and Objective

Premature ventricular contractions and pacing at physiological rhythms have been demonstrated using focused ultrasound energy suggesting its possible use in pacemakers [1, 2]. Focused ultrasound produces a reversible increase in cell membrane permeability due to acoustic cavitation, with micron size wounds on the cell repaired within minutes by vesicle exocytosis [3]. We present microfabricated silicon ultrasonic horn-driven microprobes used for in vitro direct mechanical stimulation of perfused canine left ventricular (LV) tissue. The result suggests a mechanism of heart tissue excitation by highly local ultrasonic field generation not limited to remotely generated fields and associated low frequency diffraction limits.

Statement of Contribution/Methods

The horn actuator was used for force reduction during cardiac tissue penetration and action potentials (APs) from Pt electrodes on the microprobe were recorded [4]. Here the microprobes embedded in LV tissue were ultrasonically driven by the horn and induced premature ventricular excitations were recorded at a distance of ~1.25 cm by a second set of microprobes. Our hypothesis is that by invasively applying ultrasound energy (~1 W/cm2, 110 KHz, 10 s) cell membranes in the tissue are transiently wounded allowing ions to enter depolarizing the cells to 0 mV, thus leading to premature ventricular APs.

Results

After the ultrasonic stimulation pulse, premature spontaneous APs are initiated after a period of ~ 30 seconds suggesting membrane repair. During this period negative potential spikes are observed at the rate of perfusion, which can be attributed to increase in tissue conductivity due to induced cell membrane permeability. The APs measured due to electrical pacing and ultrasonic stimulation have similar morphology. Electrical behavior of the tissue after stimulation was normal suggesting minimal tissue damage due to ultrasound.

Discussion and Conclusions

The results suggest that invasive ultrasonic stimulation of cardiac tissue provides a means of resetting the electrical activity at the tissue level. This can be used in pacing cardiac tissue as well as a means for defibrillation, serving as a complimentary method to electrical excitation.

References

[1] Dalecki et al., Ultra Med Biol, 17, 4, 1991
[2] Towe et al., TBME, 53, 7, 2006
[3] Schlicher et al., Ultra Med Biol, 32, 6, 2006
[4] Chen et al., TBME, 53, 8, 2006

Tuesday Poster

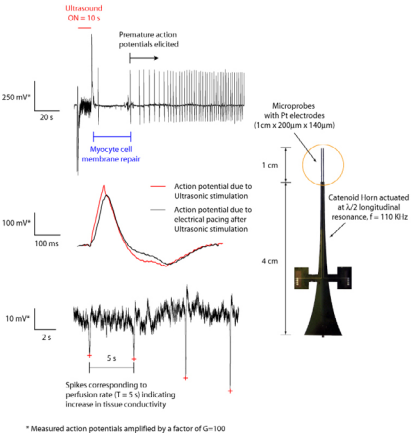

P2D052-05

Investigation on the Parametric Excitation of Shear Waves as a Factor Involved in Ultrasound-Induced Changes in Biological Tissues

Mikhail Mironov[1], Pavel Pyatakov[1], Irina Konopatskaya[1], Gregory Clement[2], **Natalia Vykhodtseva[2];** *[1]Andreev Acoustics Instite, Moscow, Russian Federation, [2]Harvard Medical School, Brigham&Women's Hospital, Radiology, Boston, MA, USA.*

Background, Motivation and Objective

Ultrasound bio-effects have largely concentrated on thermal and cavitation-based mechanisms for affecting tissue. However, the possibility of additional biologically significant mechanical mechanisms has been a matter of considerable interest since the 1950s. This work investigates parametric generation of shear waves as a potential cause of deformation and destruction of biological structures in the micro-scale. Although nonlinear interactions in solids - including the interactions of shear waves - have been widely studied, the parametric interaction suggested here has yet to be taken into consideration.

Statement of Contribution/Methods

Tissue was modeled as an isotropic soft- solid with shear modulus dependent on sound pressure. Specifically, this study investigates the possibility of a parametric excitation of shear waves generated by longitudinal sound waves in a three-wave interaction process (longitudinal + 2 transverse) in solid with low shear modulus. Coupling between longitudinal and shear modes was theoretically predicted. This coupling was expected to be marked by strong fluctuations in the longitudinal wave amplitude, due to energy transfer to and from the shear mode. Experiments were conducted with Agar-based- and polyacrylamide tissue phantoms to determine the existence of amplitude instabilities. Samples were exposed to 0.936MHz pulses (70 - 200ms). Hydrophones were placed on the propagation axis and in the transducer focal plane, 2-3mm above the focus.

Results

Estimations give a sound pressure threshold of 1.7 MPa, above which the shear wave amplitude grows exponentially. This pressure is approximately equivalent to an intensity of 100W/cm2. The characteristic time for the shear wave amplitude growth at 1 MHz is approximately 1 us. The wavelength of the produced shear wave would be ~ 3 um. In preliminary experiments using gel tissue phantoms, a threshold intensity was observed, above which sharp amplitude fluctuations appeared. This threshold varied between of 80 - 160W/cm2. Cavitation was ruled out, based on the absence of the subharmonic emission.

Discussion and Conclusions

Parametric interaction of sound with shear waves may be an additional mechanism responsible for deformation and destruction of biological structures on the micro-scale. Preliminary experiments are consistent with the theory and motivate further exploration.

P2D053-06

High-Intensity Focused-Ultrasound Modifications on the Conduction Properties of Toad's Sciatic Nerve

Yu Wen-li, Zhao Nan, Shao Yuan, Wang Su-pin, **Wan Ming-xi;** *The Key Laboratory of Biomedical Information Engineering of Ministry of Education, Department of Biomedical Engineering, Xi'an Jiaotong University, Xi'an, Shann'xi Province, China.*

Background, Motivation and Objective

Histomorphological method has been used universally in researches on High Intensity Focused Ultrasound (HIFU) modifications on neural tissues, but the dynamic effect is usually unknown. We report on an electrophysiological method to investigate the time-dependent effect of HIFU on the conduction properties of toad's sciatic nerve.

Statement of Contribution/Methods

In vitro toad's sciatic nerve was employed to facilitate delivery and the estimation of modifications of HIFU. A 1.2 MHz single element HIFU transducer (focal dimension of 8.0mm 1.2mm) was used to generate continuous wave. The ultrasound wave with electric power of 180±15W was focused at the nerve. Meanwhile, the Compound Active Potentials (CAPs) was recorded. Once the suppression of the CAPs was observed, HIFU was stopped. And when the recovered CAPs didn't change any more, HIFU was opened again. The approaches above were repeated until CAPs couldn't recover. The peak to peak values of CAPs were calculated. We also tried to apply RP(Recurrence Plots) and its quantified method (Recurrence quantification analysis, RQA) to analyze the dynamic changing process of conduction periodic embeddability induced by HIFU.

Results

The peak to peak values were shown in figure. It was noticed that HIFU could make the CAPs descend significantly and rapidly after a short time of radiation. However, before the nerve was totally damaged, the CAPs had some recoverability once HIFU was stopped. After several times of HIFU treatment, seven times for example in figure, the CAPs couldn't recover any more. The recorded CAPs of 8 nerves indicated similar results. Moreover, it proved that RP could distinguish CAPs with tiny difference. Results of RQA suggested similar suppression and recovery process to the peak to peak values.

Discussion and Conclusions

CAPs analysis of 8 nerves showed that HIFU could achieve conduction block with HIFU treatment time of 60.±39s(mean±SD). This suppression had some reversibility and it couldn't recover after several times of HIFU radiation. In addition, the RP and RQA method was demonstrated to be another effective method for studying HIFU modifications on the conduction properties of toad's sciatic nerve. However, the histological condition of the

nerve was unknown when the conduction block appeared, which may be helpful to investigate the mechanism of HIFU effect on neural condution.

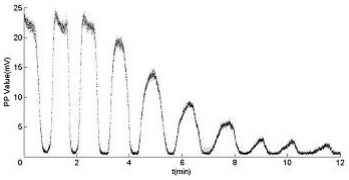

P2D054-07

A dual sensing fibre-optic hydrophone for the simultaneous measurement of acoustic pressure and temperature

Paul Morris[1], Jamie Collin[2], Constantin Coussios[2], Andrew Hurrell[3], Paul Beard[1]; *[1]UCL, Medical Physics and Bioengineering, London, United Kingdom, [2]University of Oxford, Institute of Biomedical Engineering, Dept of Engineering Science, Oxford, United Kingdom, [3]Precision Acoustics Ltd, Dorchester, Dorset, United Kingdom.*

Background, Motivation and Objective

The thermal and acoustic characterisation of medical ultrasound such as HIFU ideally requires the simultaneous measurement of acoustic field parameters and the associated temperature rise at the same spatial position. PVDF hydrophones are commonly used to measure acoustic pressure, and wire thermocouples the temperature, but no single conventional device can record both quantities simultaneously. Furthermore, high intensity fields may cause damage to relatively fragile and expensive PVDF hydrophones and conventional wire thermocouples can be inaccurate due to viscous heating effects. To overcome these limitations, a robust, inexpensive dual sensing fibre optic (FO) hydrophone that can make simultaneous acoustic and thermal measurements without introducing significant self-heating errors has been developed.

Tuesday Poster

Statement of Contribution/Methods

The transduction mechanism of the hydrophone is based on the detection of acoustically and thermally-induced changes in the optical thickness of a 10um thick Fabry Perot polymer film sensing interferometer (FPI) deposited at the tip of a single mode optical fibre (o.d.=125um). The sensor is interrogated using a novel read-out scheme in which the optimum bias point, the point of maximum slope on the FPI transfer function, is continuously tracked. This enables an acoustic waveform to be acquired whilst simultaneously measuring the temperature. The system has been characterised in terms of its acoustic sensitivity, frequency response, directivity, thermal sensitivity and response time. In order to demonstrate its dual measurement capability, a tissue phantom into which the hydrophone was inserted was insonified with the output of a HIFU transducer and the acoustic pressure and temperature variations recorded.

Results

The sensor provides an optically defined element size of 10um, an acoustic bandwidth >50 MHz, a broadband noise-equivalent-pressure of 16 kPa and can measure temperatures up to 70°C with a resolution of 0.1°C and a 10ms response time. The time course of the temperature rise produced in the above phantom was successfully recorded whilst simultaneously capturing acoustic waveforms at discrete times intervals during the heating period. Comparisons with a thin film thermocouple indicate that, unlike conventional wire thermocouples, the thermal measurements are free from significant self-heating artefacts.

Discussion and Conclusions

The characteristics of the FO hydrophone make it suitable for a range of applications in ultrasound metrology. Its wide bandwidth, small element size and high sensitivity lends itself to high frequency diagnostic ultrasound measurements. Its ability to make simultaneous measurements of acoustic pressure and temperature and small physical size suggest it could be used as an implantable probe for characterising therapeutic ultrasound-induced tissue heating, for example to help elucidate the relationship between cavitation and heating in HIFU therapy.

P2D055-08

Simulated and experimental analysis of PVDF membrane hydrophone low-frequency response for accurate measurements of lithotripsy shockwaves

Adam Maxwell[1], Oleg Sapozhnikov[2], Yuri Pishchalnikov[3], Michael Bailey[2]; [1]*University of Michigan, Department of Biomedical Engineering, Ann Arbor, Michigan, USA,* [2]*University of Washington, Applied Physics Laboratory, Seattle, Washington, USA,* [3]*Indiana University School of Medicine, Department of Anatomy and Cell Biology, Indianapolis, Indiana, USA.*

Background, Motivation and Objective

Accurate measurement of pressure waveforms is important for characterization of medical ultrasound equipment. Lithotripsy shockwaves are particularly difficult to measure because of their wide signal bandwidth and large pressures. Even in an ideal environment, it is difficult to calibrate hydrophones over the necessary range of frequencies, which can extend from < 100 kHz to > 40 MHz. In a clinical setting, measurements can experience even greater variability because of uncontrolled conditions. Previously, we found that measurements are very sensitive to effects of water conductivity. Therefore, we are developing techniques to simulate and measure the hydrophone low-frequency response, and to modify the hydrophone to make its sensitivity invariant to the parasitic effects of the conductive medium.

Statement of Contribution/Methods

A broad-focus electromagnetic lithotripter (XX-EM) with a repeatable shock waveform was used to calibrate the PVDF hydrophone. A fiber optic probe hydrophone (FOPH) with known impulse response was used as a measurement standard for secondary calibration (Sapozhnikov et al, IEEE Int. Ultrason. Symp., p.112-115). A low-frequency circuit model for the PVDF membrane electrodes in an infinite conductive medium was developed. The model response was compared with signals recorded by the FOPH and PVDF hydrophone at different levels of water conductivity ranging from 1 – 1300 μS/cm. To correct this distortion, the input impedance of the hydrophone preamplifier was modified to improve the low frequency response and remove waveform distortion.

Results

Measurements with PVDF hydrophones suggested that shockwave parameters, especially peak negative pressure, were very sensitive to water conductivity. Waveforms in water were distorted due to high-pass filtering effects of the water conductivity. Water that was deionized to a low conductivity of 1 μS/cm still caused significant error of the PVDF hydrophone waveform. The model results showed good agreement with the measured waveforms, and provided a correction for the system. When the input impedance was altered appropriately or the hydrophone was submerged in a nonconductive fluid, the PVDF and FOPH waveforms appeared nearly identical.

Discussion and Conclusions

The PVDF hydrophone is capable of measuring lithotripsy shockwaves accurately when the low frequency response is properly taken into account. Measurements and simulation showed that water conductivity has a large impact on pressure measurements, particularly the negative pressure amplitude and duration. By changing the impedance across the membrane electrodes, we were able to make the hydrophone sensitivity independent of frequency in the range of interest, further simplifying measurements. Work supported by NIH DK43881 and NSBRI SMS00402.

P2D056-09

Observation of HIFU shock waveforms and corresponding bioeffects in tissue phantoms and tissue

Vera Khokhlova[1], Michael Canney[1], Olga Bessonova[2], Michael Bailey[1], Lawrence Crum[1]; [1]*University of Washington, USA,* [2]*Moscow State University, Russian Federation.*

Background, Motivation and Objective

Nonlinear propagation effects at HIFU intensity levels may result in formation of shocks and significant increase of heat deposition at the focus due to absorption at the shocks. However, there has been a concern if shocks do form in tissue and therefore if the mechanism of effective shock wave heating is clinically relevant. Tissue absorption and the presence of inhomogeneities may alter nonlinear propagation and prevent formation of shocks; and direct waveform measurements in tissue are technically difficult.

Statement of Contribution/Methods

In this work, a combined measurement and modeling method to determine HIFU waveforms and corresponding bioeffects in the presence of shocks is proposed and tested. Experiments were performed with a 2 MHz transducer of 4.2 cm aperture and 4.5 cm focal length. Low amplitude measurements in water were used to establish boundary

conditions for the KZK-type model. High amplitude focal waveforms then were simulated and measured with a fiber optic probe hydrophone (FOPH) in water, within tissue phantom, or adjacent to excised tissue. Measured and simulated shock amplitudes were used to calculate heat deposition and time to boil. Inception of boiling was detected in transparent phantom using a high-speed camera. In non-transparent samples boiling was detected as an appearance of strong fluctuations in electric power of the transducer due to acoustic wave back scattering from boiling bubbles.

Results

It is shown that at clinically relevant HIFU intensity levels of 6-10 kW/cm2 in situ shock waveforms were present at focus in water, tissue phantoms, as well as after propagation in inhomogeneous ex-vivo liver and porcine body wall samples. Inception of boiling was measured in milliseconds. Time to boil, calculated based on the weak shock theory from the experimental and simulated waveforms was in a good agreement with the measurements.

Discussion and Conclusions

Formations of shocks and ms-scale boiling are relevant to real heterogeneous tissue and clinical HIFU conditions. The presence of boiling leads to echogenicity in B-mode ultrasound images, scattering and redistribution of acoustic energy at the focus. Shock formation effects therefore are necessary to address in developing methods to characterize HIFU acoustic fields. In addition, boiling resulting from enhanced heating due to nonlinear propagation can be mistaken for enhanced heating caused by cavitation.

Work supported by NIH DK43881 and NSBRI SMS00402.

P2D057-10

Role of cytoplasmic calcium and ion channels during insonication of cancer cells with ultrasound contrast agents

Sergei Sokolovski[1], Paul Campbell[2]; [1]*University of Dundee, United Kingdom,* [2]*Dundee University, Dundee, Scotland, United Kingdom.*

Tuesday Poster

Background, Motivation and Objective

Since the discovery that ultrasound(US) can activate ultrasound contrast agents (UCAs) so that they permeabilize the cell membrane (Skyba, Price et al. 1998) has since stimulated the use of UCAs for gene therapy and also drug delivery into cancer cells (Lawrie, Brisken et al. 2000). Briefly, US pulsing activates UCAs which in turn either form microjets or simply create significant shear flow so that the membrane is temporally compromised (Deng, S. et al. 2004; Prentice et al. 2005). Recent studies have shown that, at the earliest stages of the sonication procedure, the UCA activity mechanically affects the cell, causing a rise of cytosolic calcium ([Ca2+]cyt) and in turn membrane hyperpolarisation (Tran, Roger et al. 2005; Juffermans, Kamp et al. 2007; Kumon and Deng 2007; Tran, Le Guennec et al. 2008). Subsequently, the membrane can then reseal only in the presence of the external calcium (Ca2+) (Kumon and Deng 2007; Zhou, S. et al. 2007). These facts and attendant pharmacological studies have hypothesised that sonoporation induced growth of H2O2 production in the cell, which in turn activates Ca2+ entrance to cytoplasm, activating BKCa channels and thus leading to hyperpolarisation .(Juffermans, Dijkmans et al. 2005; Juffermans, Dijkmans et al. 2006; Juffermans, Kamp et al. 2007; Juffermans, Kamp et al. 2008; Tran, Le Guennec et al. 2008).

Statement of Contribution/Methods

However details and consequences of events happened during UCAs sonoporation remain unclear. To verify whether K+ and/or Ca2+ channels on the PM and in/external calcium pools are involved in UCAs-induced mechanical effect, and therefore also with sonoporation of the cells, we established a patch clamp electrophysiological rig together with single cell Ca2+ imaging (Fura2), and have subsequently carried out a battery of preliminary single channels measurements, simultaneously with cytosolic Ca2+ concentration ([Ca2+]cyt) monitoring in various cancer cell lines.

Results

Preliminary results obtained have demonstrated typical mechanical response of the cell on US-induced UCAs by rising of [Ca2+]cyt due to Ca2+ influx through Ca2+ channels on the PM with consequent activation of large conductance K+ channels. At higher pressure and longer duty cycle of US the cells have shown burst of Ca2+ dependent Fura2 fluorescence and drop of PM potential during first 10-25s returning to resting [Ca2+]cyt and PM potential in 5-8 min time.

Discussion and Conclusions

Involvement of cytoplasmic Ca2+and nitric oxide second messenger system in cell response on the sonoporation is discussed in the context of the presently active literature in this exciting area.

P2D058-11

The bioeffects of nanoparticles using ultrasound stimulation in endothelial cell

Po-Hsiang Hsu; *Institute of Biomedical Engineering, National Yang-Ming University, Taipei, Taiwan.*

Background, Motivation and Objective

Although the nanoparticles are broadly applied to biomedical field in recent decades, the uptake mechanism of cells has still not known very well. Endothelial cell is the inner layer of the vascular and directly contact all substance in blood. In this study, we will discuss the bioeffects and cell activities of nanoparticles before and after ultrasound stimulation.

Statement of Contribution/Methods

Human umbilical cord vein endothelial cell (HUVEC) is cultured for ultrasound stimulation. Fluorescent nanoparticles (40 nm, FluoSpheres carboxylate modified-micro spheres) are administrated before experiment. The excitation and emission wavelength of these nanoparticles are 488nm/605nm. The distribution of nanoparticles is observed by confocal microscopy. In our experiment, we will present the relationship between cellular uptakes and intensity of ultrasonic stimulation. We evaluate the effect and distribution in different ultrasound stimulation parameters: time, temperature, and pulse repetition frequency(PRF) on cell.

Results

1. Time

Nanoparticles uptake cureve reached the plateau within 30 min. The total uptake in ultrasound stimulated group is 6 times than non-stimulated.

2. Temperature

The rate of nanoparticles uptake in two groups shows difference in 25¢J, but the variation is small in 0¢J.

3. Pressure

The uptake in 0.6MPa stimulation is greater than 0.2Mpa and non stimulation groups.

4. Pulse repetition rate: PRF

Using 2.25MHz transducer, 0.1K,1K, 10K are used to stimulte the cells. It shows greater uptake in 0.1K, and uptake decreased with increasing PRF.

Discussion and Conclusions

In this study, the ultrasound stimulated parameters: time, temperature, pressure and PRF are very important for nanoparticle uptake in endothelial cell. The metabolic rate of cell is lower at 0¢J, though ultrasound stimulated could easily increase the nanoparticles uptake. The cell morphology in all experiments showed no difference between control and stimulated groups. Ultrasound technique is not only for medical image but also a useful tool to improve cell uptake. New ultrasound techniques combine with nanoparticles uptake based cell therapy will be investigated and the integration in biomedical and clinical applications.

P2E. High Frequency Techniques

2nd and 3rd Floor Foyers

Tuesday, November 4, 2008, 3:00 pm - 4:30 pm

Chair: **Kirk Shung;**
University of Sothern California, CA, USA.

P2E059-01

Comparative Study between Ultrasound Biomicroscopy and Histopathology of Diversion Colitis on Rats

Rodrigo Pacheco[1], Kelly Alves[2], Christiano Espósito[1], Monica Soldan[3], Leonardo Quintella[4], Vera Chagas[5], Alberto Schanaider[1], **Joao Machado[2];** *[1]School of Medicine, Federal University of Rio de Janeiro, Department of Surgery-Center of Experimental Surgery, Rio de Janeiro, RJ, Brazil, [2]COPPE/Federal University of Rio de Janeiro, Biomedical Engineering Program, Rio de Janeiro, RJ, Brazil, [3]Clementino Fraga Filho University Hospital - Federal University of Rio de Janeiro, Division of Gastroenterology, Endoscopy Unit, Rio de Janeiro, RJ, Brazil, [4]Clementino Fraga Filho University Hospital - Federal University of Rio de Janeiro, Division of Pathological Anatomy, Rio de Janeiro, RJ, Brazil, [5]School of Medicine, Federal University of Rio de Janeiro, Department of Pathology, Rio de Janeiro, RJ, Brazil.*

Tuesday Poster

Background, Motivation and Objective

Diversion colitis is a nonspecific inflammatory process observed in excluded colonic segments and the pathogenesis is unknown. Patient evaluation and diagnosis usually require endoscopic and histological analyses with biopsy of the mucosa that eventually leads to some complications such as bleeding and infection. Ultrasound biomicroscopy (UBM) uses high frequencies and has compatible optical microscopic resolution. It is employed for medical and biological purposes including ophthalmic, dermatological and intravascular imaging in humans, mouse embryonic development and tumor biology. Literature reports on UBM visualization of intestinal wall are not found. This experimental study objective is the evaluation of the UBM efficacy as a complementary method to improve the diagnosis and to characterize the course and severity of diversion colitis.

Statement of Contribution/Methods

The present work contributes with the evaluation of diversion colitis by UBM images in vitro. The image instrumentation consisted of an UBM system using a focused 50 MHz PVDF transducer (f-number = 1.5, focal distance = 4.4 mm, -6 dB bandwidth of 31.2 MHz). Nine SPF Wistar rats, Rattus norvegicus (Berkenhout, 1769), were randomly distributed in three groups: I- Control and II and III- Hartmann's colostomy (left terminal colostomy with closure of distal segment). Tissue samples, obtained from each group after necropsy, comprised the distal colon (n=3) for group I and the excluded segment excised 8 weeks in group II (n=3) and 25 weeks in group III (n=3), after colostomy. Each sample, in rectangular fragments of 5x5 mm, was placed on a flat sapphire plate, covered by a PVC membrane (9 μm in thickness) and immersed in saline at 9% and at room temperature. The UBM scanner provided overview images of the sample microstructure. Subsequent to UBM inspection, each sample was fixed in formalin, paraffin-embedded, sectioned, and stained with hematoxilin-eosin for histological analysis.

Results

Mucosa, lamina propria, submucosa and muscular layers were identified in the UBM images and are morphological correlated with the histology of the samples from group I. Regarding the samples from group II, UMB images revealed morphologically preserved muscle layer and enlarged lamina propria and submucosa (due to an edema associated with leukocyte infiltration of the lamina propria and confirmed by histology). For group III, extensive mucosa atrophy was found.

Discussion and Conclusions

Ultrasound biomicroscopy is useful tool and a safety method to evaluate diversion colitis. The morphological results found in ultrasound images for groups I, II and III are similar to those obtained by histological examinations. The results encourage the development of an endoscopic UBM, which could be used to evaluate diversion colitis in vivo.

P2E060-02

Characterising the performance of high resolution ultrasound scanners for small animal work.

Carmel Moran[1], Bill Ellis[2], Sean Smart[3], Stephen Pye[2]; [1]*University of Edinburgh, Medical Physics, Edinburgh, United Kingdom,* [2]*Edinburgh Royal Infirmary, Medical Physics, Edinburgh, United Kingdom,* [3]*Department of Radiation Oncology and Biology, Oxford, United Kingdom.*

Background, Motivation and Objective

Research using small animals continues to play a key role in biological, biomedical and veterinary science. In particular both mouse and rat models have become increasingly popular as research tools due to the fact that 90% of the genomic sequences in these rodents are identical to those found in humans. Foster et al (2002) have recently demonstrated the versatility of employing a high resolution ultrasound scanner to perform small animal micro-imaging in vivo. However, in common with medical imaging systems, the technical performance of high resolution scanners is difficult to quantify.

Statement of Contribution/Methods

We have employed a novel measurement technique previously developed for medical imaging (the Resolution Integral) to study the grey-scale imaging performance of a high resolution scanner with probe centre frequencies of 30-55 MHz. We designed and manufactured a high resolution test object containing 30 wall-less anechoic pipe structures in a block of agar based tissue mimic. The pipe diameters ranged from 50 µm to 1.5 mm. Each probe was scanned over the surface of the test object and a series of images of each pipe was captured. The axial depth range over which each pipe could be visualised (L) was determined, and plotted as a function of α (where α is proportional to the reciprocal of pipe diameter). The Resolution Integral (R) was calculated for each probe by measuring the area under the curve (see figure). Characteristic Resolution and Depth of Field were also determined using the same set of measurements.

Results

Results were obtained using a VisualSonics scanner with probe models 707B, 704 and 708 (centre-frequencies 30, 40 and 55 MHz). The measured values of R were 49, 43 and 44 respectively, and the corresponding Depths of Field / Characteristic Resolutions were 5.5mm / 226 µm, 4.1mm / 190 µm and 3.3mm / 150 µm.

Discussion and Conclusions

We have successfully extended the range of application of Resolution Integral measurement to a high resolution micro-imaging system. This is an important first step in producing a calibration phantom which is easily applied to high frequency scanners.

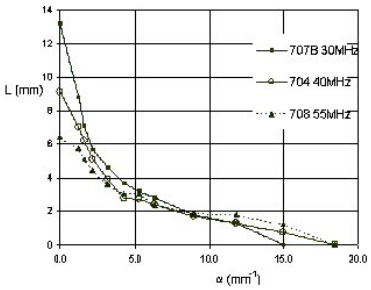

Tuesday Poster

P2E061-03

Development of diagnostic imaging system for regional lymph node micrometastasis with high-frequency ultrasound

Noriko Tomita[1], Sachiko Horie[1], Fuki Oosawa[2], Chen Rui[3], Yukiko Watanabe[1], Kousuke Ohki[2], Hidehiro Morikawa[2], Manabu Fukumoto[3], Shiro Mori[2], Tetsuya Kodama[1]; *[1]Tohoku University, Graduate School of Biomedical Engineering, Sendai, Japan, [2]Tohoku University Hospital, Sendai, Japan, [3]Tohoku University, Institute of Development, Aging and Cancer, Sendai, Japan.*

Background, Motivation and Objective

It is important of diagnosing not only primary tumors but also metastases accurately. Recently, we have created murine lymph node metastasis model and developed a new method to reconstruct the two- and three- dimensional (2D/3D) vessel structures in the model by using nanobubbles (NBs) and high-frequency ultrasound imaging system (central frequency 40MHz). In the present study, we investigated the characteristics of 2D/3D vessel structures in the model. This technique may be useful for early diagnosis of lymph node micrometastasis.

Statement of Contribution/Methods

Murine lymph node metastasis model was established by injecting $1x10^4$ or $5x10^4$murine mammary adenocarcinoma cells expressed luciferase gene constitutively (MRL/N-1-Luc) into the inguinal lymph nodes of MRL/MpJ-*lpr/lpr* mice. Tumor implantation and metastasis were confirmed with *in vivo* bioluminescence imaging system after 3-14 day following inoculation. The 2D/3D images of normal or neoplastic lymph nodes were constructed with a high-frequency ultrasound system (VEVO) with or without NBs injected into the mice tail vein. The shapes of microvessels in lymph node were reconstructed by analyzing the echogenicity of NBs circulating through the blood vessels in the node.

Tuesday Poster

Results

1. Axillary lymph node metastasis from the inguinal lymph nodes were confirmed on day 9 after inoculation into the inguinal lymph nodes.

2. Both of the volumes and the vessel densities of neoplastic lymph nodes were increased with time.

3. The vessel densities in neoplastic lymph nodes (40%) were higher than that in the normal lymph nodes (20%) on day 13 after inoculation.

4. Necrosis formed in lymph node was detected as a low density area on day 13 after inoculation.

Discussion and Conclusions

In this study, lymph node metastasis model were established in MRL/MpJ-*lpr/lpr* mice. With this model, we succeeded in characterizing the 2D/3D vessel structures in the model with a diameter less than 1-cm by using with NBs and high-frequency ultrasound imaging system. This study makes it possible to quantify the vessel density in lymph nodes and to distinguish necrosis area in neoplastic lymph nodes compared to the conventional ultrasonographic images. Our system established in this study may be suited for early diagnosis of lymph node micrometastasis.

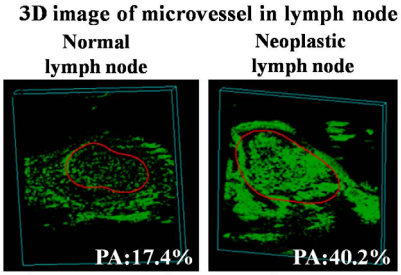

P2E062-04

Improved high-frequency high frame rate duplex ultrasound linear array imaging system

Lequan Zhang[1], Xiaochen Xu[2], Jesse T. Yen[1], Jonathan M. Cannata[1], K. Kirk Shung[1]; *[1]University of Southern California, NIH Transducer Resource Center and Department of Biomedical Engineering, Los Angeles, CA, USA, [2]Texas Instruments Inc., Medical Business Unit, Dallas, TX, USA.*

Background, Motivation and Objective

High-frequency (HF) ultrasound imaging, capable of achieving good spatial resolution at an affordable cost, has been shown to have many biomedical applications including small animal imaging for biological and pharmaceutical research. Cardiovascular and tumor research using mice requires not only B-scan imaging, but also ultrasound Doppler to evaluate blood flow. Due to the especially fast heart rate of a mouse (>400/min), cardiovascular research utilizing mice also requires imaging modalities with high frame rate capability (>100 Frames/sec).

Statement of Contribution/Methods

In this paper, we report recent progress that has been made in the development of a high frame rate duplex HF ultrasound system with both B-scan imaging and Doppler flow measurements, using a 30 MHz 64-element linear array. A 32-channel HF analog beamformer module with dynamic focusing on reception was implemented to improve the image lateral resolution. High-speed timing circuits were used to achieve high imaging frame rate by reducing the acquisition overhead. Therefore, the frame rate of the system relies only on the field of view. The system also included a 64-channel analog front-end pulser/receiver, a HF pulsed-wave (PW) Doppler module, a PC with a 200MS/s 14-bit PCI A/D card and real-time Labview software for data acquisition and image display.

Results

High frame rate B-scan images of mouse hearts have been obtained, as well as the PW Doppler blood flow velocity profiles at the specified location. The system is able to acquire real-time B-mode images at a rate greater than 400 frames per second in a 5 x 12 mm field of view. A wire phantom will be used to evaluate the resolution improvement to the previous 16-Channel beamformer system.

Discussion and Conclusions

In vivo mouse experiment results show a promising future of this system in small animal research. The system will be expanded to support future arrays with more elements.

P2E063-05

A Novel Scan Method Using Angled High Frequency Single Element Needle Transducers

Jin Ho Chang[1], **Dong-Guk Paeng[2],** Rumin Chen[1], Mark S. Humayun[3], K. Kirk Shung[1]; *[1]University of Southern California, Department of Biomedical Engineering, Los Angeles, CA, USA, [2]Cheju National University, Marine Industrial Engineering, Jeju, Korea, Republic of, [3]Doheny Eye Institute, University of Southern California, Los Angeles, CA, USA.*

Background, Motivation and Objective

High frequency ultrasound (HFUS) imaging is suffering from a shallow imaging depth due to high attenuation in spite of its excellent spatial resolution. Since current technology does not allow for linear or sector scanning of a single element transducer in situ in deep tissues, noninvasive HFUS imaging of human tissues is limited to the surface layer of skin and the anterior segment of the eye. This paper proposes a novel scan method with a minimally invasive approach. The proposed method enables us to acquire images of tissues deep inside the body for which the mechanical scanning cannot be used.

Statement of Contribution/Methods

The proposed scan method is to rotate a single element transducer with an angled tip to form a cone-shaped imaging plane, which requires relatively little room to form images. This allows for the use of HFUS to image tissues deep inside the body in a minimally invasive manner. For displaying 3-D information on 2-D space, the cone-shaped surface can be unfolded onto the 2-D space so that polar or sector images can be produced by backend processing used in the conventional systems.

Results

The feasibility of this novel technique was tested by computer simulation of wire phantom images from both sector and rotational scan imaging with an 80-MHz single element transducer with a 45° tip. The -6dB lateral resolutions of these images were similar: at the focal depth of 3 mm, 61 µm in the case of the conventional sector scanning and 62 µm in the case of the rotational scanning. However, point targets away from the center of lateral axis appeared on the image obtained by the rotational scanning with lower brightness than that by the counterpart although the positions of the targets on the both images were equal. This is obvious because the targets were not located on the cone-shaped imaging plane. When the elevational positions of these targets were pulled down in order to place the targets on the cone-shaped imaging plane, however, the targets appeared along the arc of a 3 mm radius on an image with the same brightness as their counterparts.

Longitudinal and cross-sectional images of a small polymide tube were obtained by manually turning a rotational stage while an unfocused 40-MHz PMN-PT needle transducer with 45° angled tip was being held at a fixed position. This mimics the procedure of rotating an angled transducer. These results clearly demonstrate the feasibility of the rotational scanning of deep lying tissues in a minimally invasive manner.

Discussion and Conclusions

Since the rotational scanning takes place very close to the region of interest, it is less susceptible to the penetration depth problem of HFUS. This means that imaging frequency can be further increased to achieve a very high resolution. As a result, the proposed scanning can offer the advantage of allowing high resolution imaging tissues which are not commonly accessible to conventional ultrasound imaging approaches.

P2E064-06

Longitudinal study of adult zebrafish heart regeneration using high frequency echocardiography

Lei Sun[1], Ching-Ling Lien[2], Qiong Wu[2], Jin Ho Chang[3], K. Kirk Shung[3]; *[1]Hong Kong Polytechnic University, Health Technology and Informatics, Hung Hom, Hong Kong SAR, China, [2]Childrens Hospital Los Angeles and University of Southern California, Department of Cardiothoracic Surgery, Los Angeles, CA, USA, [3]University of Southern California, Biomedical Engineering, Los Angeles, CA, USA.*

Tuesday Poster

Background, Motivation and Objective

Understanding heart regeneration in a vertebrate model system is a highly relevant public health concern. Coronary heart disease is among the leading causes of disability and mortality in United States and worldwide. Myocardial infarction (MI) results in irreversible loss of cardiomyocytes by necrosis and apoptosis in the heart. In contrast to mammals, zebrafish hearts have remarkable regenerative abilities. Zebrafish fully regenerate myocardium after 20% ventricular resection and provide a genetically tractable model system to study the mechanisms of heart regeneration.

Statement of Contribution/Methods

In this research, a novel ultrasound bio-microscope (UBM) system was built and utilized to evaluate the morphological and functional changes on adult zebrafish heart regeneration. Over a period of 14 days post amputation (dpa), real-time echocardiographic images as well as ventricular Doppler waveforms were acquired daily at the amputation site. Cardiac scar tissue volume and ventricular Doppler characteristics were calculated and reviewed longitudinally on each individual fish to evaluate the process of zebrafish heart regeneration.

Results

Results consistently showed a decrease of the scar tissue volume and an increase of the myocardium growth over the observed period of time. It is consistent with the previous histological findings. Ventricular Doppler waveform also showed a consistent change during the observed period.

Discussion and Conclusions

Using non-invasive, in vivo, high frequency ultrasonic imaging, we demonstrate the investigation of zebrafish heart regeneration based on longitudinal study. This ultrasound approach, unlike histology-based method or any other invasive method, examines the very same fish on different time points, therefore, eliminates the difference introduced by different fishes. In addition, it also allows functional analysis in addition to morphological study of the heart regeneration process. It is believed that this is the first time of evaluating the functional change of heart regeneration.

P2E065-07

Contrast-Enhanced High-Frequency Ultrasound Imaging of Liver Metastases in Preclinical Models

Rui Chen[1], Noriko Tomita[2], Taisuke Baba[3], Fuki Oosawa[2], Yukiko Watanabe[2], Sachiko Horie[2], Shiro Mori[4], Manabu Fukumoto[3], Tetsuya Kodama[2]; *[1]Graduate School of Biomedical Engineering & Institute of Development,Aging &Cancer, Tohoku University, Sendai, Japan, [2]Graduate School of Biomedical Engineering, Tohoku University, Sendai, Japan, [3]Institute of Development, Aging and Cancer, Tohoku University, Sendai, Japan, [4]Tohoku University Graduate School of Dentistry, Sendai, Japan.*

Background, Motivation and Objective

Colorectal cancer is one of the leading causes of mortality from cancer worldwide. Death from this disease usually is associated with the formation of liver metastases. Preclinical mouse models are essential to the study of liver metastasis, yet their utility has been limited by difficulty in tracking the progression of metastases through time. A multitude of preclinical imaging modalities are under development, yet no single modality should be considered a comprehensive solution for cancer microimaging applications. Recently, ultrasound is an attractive option for preclinical imaging, and then, three-dimensional image of intratumoral vessels has been successful to be constructed using high-frequency contrast-enhanced micro-ultrasound in our previous study. In this study, we attempted to applicate a high-frequency ultrasound system with three-dimensional imaging capabilities and acoustic liposome (nanobubbles) to study the murine liver metastasis.

Statement of Contribution/Methods

SCID mice received and intrasplenic injection of luciferase-expressing C26 cells. One week after inoculation, luciferase activity was measured by in vivo bioluminescence system (IVIS) twice a week. After every time of IVIS imaging, ultrasound imaging was performed by a high-frequency ultrasound system (VEVO) with central frequency 50MHz. During imaging, the mouse was kept under anesthesia and restrained on a heated stage. Ultrasound images were acquired after ultrasound contact gel was applied to the abdomen with and without nanobubbles (mean diameter =714±22) administered from the tail vein. For histologic fonfirmation, the mouse liver was excised after sacrified, formalin-fixed, paraffin-embedded, sectioned and stained with H&E.

Results

1. Murine liver metastases were identified using high-frequency ultrasound. 2. The presence and location of a liver metastasic tumor, which was dectected by ultrasound, was verified by histological sections. 3. Three-dimensional reconstruction could be used to tracking the growth of individual liver metastases. 4. Three-dimensional image of intratumoral vessles by ultrasound and nanobubbles could be benefit for early diagnosis of liver metastases with a minimum detection size.

Discussion and Conclusions

This is the first report to detect and evaluate murine liver metastases with contrast-enhanced high-frequency ultrasound imaging. Compared with traditional histological methods and noninvasive longitudinal imaging modalities, this study may provided a more accurate and sensitive assessment of metastatic progression and tumor vascularization. These results show that three-dimensional high-frequency ultrasound imaging combined with nanobubbles may be useful for early detection, quantitative assessment, and the evaluation of therapeutics in preclinical liver metastasis models.

P2F. 3D / Cardiac Imaging

2nd and 3rd Floor Foyers

Tuesday, November 4, 2008, 3:00 pm - 4:30 pm

Chair: **Hiroshi Kanai;**
Tohoku University, Japan.

P2F066-01

3D Speckle Tracking in Simulated Ultrasound Data of the Left Ventricle

Jonas Crosby[1], Stian Langeland[2], Espen W. Remme[3], Hans Torp[1]; [1]*Norwegian University of Science and Technology, Department of Circulation and Medical Imaging, Trondheim, Norway,* [2]*GE Vingmed Ultrasound AS, Horten, Norway,* [3]*Rikshospitalet University Hospital, Institute for Surgical Research, Oslo, Norway.*

Background, Motivation and Objective

Speckle tracking has become a valuable method for quantitative analysis of the left ventricular motion in 2D ultrasound images, and the new matrix array probes capable of full volume acquisition encourage extension of the methodology into three dimensions. Simulated ultrasound data makes it possible to examine the feasibility of 3D speckle tracking in comparison to the true motion of the underlying model. In this study, we have developed a new 3D speckle tracking method and examined its accuracy when applied on simulated ultrasound data of a left ventricle with myocardial infarction.

Tuesday Poster

Statement of Contribution/Methods

The implemented tracking method follows the speckle pattern motion by SAD block matching and uses correlation coefficients to estimate sub-voxel displacements. The dimensions of the search volumes are reduced by adjusting for the pre-tracked basal motion, and the frame-to-frame displacement vectors are regularized according to the local geometry of the tracking mesh.

The tracking method was applied on simulated full-volume ultrasound data based on a finite element (FE) model of the left ventricle. The initial tracking mesh was set to correspond to the mid wall of the FE model in end diastole and the tracked positions in end systole were compared with the true positions from the model. The tracking was performed both forwards and backwards in time, and the results were weighted linearly through the cardiac cycle.

Results

Figure 1 shows the estimated positions (red markers) versus the reference motion (green markers) in end systole, with lines indicating the initial end-diastolic positions. At end systole, the displacement errors in the speckle tracking method were 22.9 +/- 8.4 % (mean +/- STD) of the total displacements. The angles between real and estimated displacement vectors were 12.9 +/- 20.7 degrees (mean +/- STD).

Discussion and Conclusions

A new 3D speckle tracking method for assessment of left ventricular motion has been developed. The method showedrelaively good agreement with the reference motion when applied on simulated ultrasound data and was able to capture the rotational motion of the left ventricle.

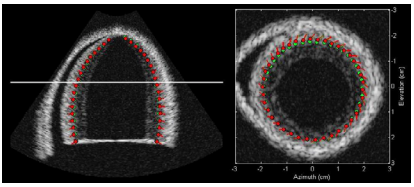

P2F067-02

Cardiac Output Estimation in Non-Standard 3D Echocardiographic Images

Maartje Nillesen[1], Richard Lopata[1], Willem de Boode[2], Inge Gerrits[1], Henkjan Huisman[3], Livia Kapusta[4], Han Thijssen[1], **Chris de Korte[1];** *[1]Radboud University Nijmegen Medical Centre, Clinical Physics Laboratory, Department of Pediatrics, Nijmegen, Netherlands, [2]Radboud University Nijmegen Medical Centre, Department of Neonatology, Nijmegen, Netherlands, [3]Radboud University Nijmegen Medical Centre, Department of Radiology, Nijmegen, Netherlands, [4]Radboud University Nijmegen Medical Centre, Children's Heart Centre, Nijmegen, Netherlands.*

Background, Motivation and Objective

Automated segmentation of the left ventricle (LV) in real-time 3D echocardiographic images can be used for monitoring functional parameters of the LV such as cardiac output (CO). Assumptions about shape and appearance of the heart are often incorporated in the segmentation method. This is advantageous when analyzing echographic images of normal heart geometries in standardized (apical) views. In abnormal heart geometries, for example in children with congenital malformations, this *a priori* knowledge about the shape and anatomy of the LV will result in erroneous segmentation results. Therefore, we developed an automated segmentation method without using *a priori* knowledge.

The aim of this study was to validate the developed segmentation method using CO values obtained by fully automated segmentation of the LV in non-standard images (piglet model) against CO determined invasively with a flow probe fixed around the pulmonary artery.

Statement of Contribution/Methods

Echocardiographic image sequences of five piglets were obtained in radiofrequency (rf) format. ECG-gated full volume images were acquired intra-operatively in a non standard view using a Philips SONOS 7500 live 3D ultrasound system, equipped with an rf-interface and an X4 matrix array transducer (2-4 MHz). Cardiac blood flow was measured simultaneously in the pulmonary artery by an ultrasound flow probe. Three-dimensional adaptive filtering was performed on the demodulated rf-data to optimize the distinction between blood and myocardium. A 3D deformable simplex mesh was then used to segment the endocardial surface. A gradient and a speed force were included as external forces of the model. To balance data fitting and mesh regularity, one fixed set of weighting parameters of internal, gradient and speed forces was used for all datasets.

Results

Taking the CO measurements from the flow probe (650 ± 160 ml; mean ± sd) as a gold standard, excellent correlation (r = 0.99) was observed with the CO estimates obtained from segmentation scheme (590 ± 195 ml). Relative errors varied between 0 and 16%, where the nominal accuracy of the flow probe is 10%. Underestimation of the CO as obtained with the segmentation method might be explained by the relatively low temporal resolution of the full volume datasets.

Discussion and Conclusions

Segmentation results and comparison of CO values indicate that automatic segmentation of 3D full volume images using adaptive filtering and a deformable simplex mesh is feasible. The method can be applied to non-standard heart geometries and without having to impose shape constraints. Underestimation of the CO might be minimized by using higher temporal resolution of the 3D datasets currently available with other equipment.

P2F068-03

Coupled segmentation of endo- and epi-cardial borders in 3D echocardiography

Fredrik Orderud[2], Gabriel Kiss[1], Hans G. Torp[3]; *[1]Norwegian University of Science and Technology, Medical Imaging Laboratory, Trondheim, Norway, [2]Norwegian University of Science and Technology, Computer Science, Trondheim, Norway, [3]Norwegian University of Science and Technology, Circulation and Medical Imaging, Trondheim, Norway.*

Background, Motivation and Objective

The emergence of 3D ultrasound has enabled volumetric imaging of the heart. Several methods for 3D myocardial segmentation have been proposed, most intended for the detection of the epicardium. However, the detection of endo- and epi- cardium allows the estimation of myocardial volume, tracking of (segmental) volume changes and enables wall thickening analysis.

Statement of Contribution/Methods

The purpose of the paper is to present a computationally efficient technique for coupled real-time segmentation of endo- and epi-cardium. For this purpose, we extend a previously developed Kalman-tracking framework using subdivision surfaces.

Apart from the model used for tracking the endocardial wall, a second subdivision surface, depicting the epicardium, is added. To compensate for the lack of ultrasound data near the apex, the epicardial model is regularized with attractors there. Their purpose is to guide the segmentation by incorporating a-priori knowledge regarding the apical shape of the epicadium. For validation purposes, the myocardial volume, which should remain constant, is computed for all recorded frames in each dataset.

Results

Tracking is validated in a 3D echocardiography simulation of an infracted ventricle, as well as in 5 in-vivo recordings (acquired using a Vivid 7 ultrasound scanner, GE Vingmed Ultrasound, Norway). For the simulated data, the proposed method consistently overestimated the myocardial volume on average with 2.67 ml, with a mean computed myocardial volume: 50.46ml +/- 1.89ml. On the patient data the computed mean myocardial volume was: 130.19ml +/- 7.90ml.

Discussion and Conclusions

Accurate tracking results (figure1), both for the phantom and in-vivo data are achieved. Extending Kalman filtering by adding attractors proves useful whenever there is a lack of image data. The results can be further improved by integrating manual placement/editing of the attractors by the human expert, as well as by allowing the attractors to change their position and strength throughout the heart cycle.

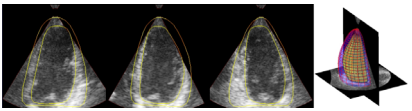

Tuesday Poster

P2F069-04

A Four-dimensional Model-based Method for Assessing Cardiac Dyssynchrony in Mice

Yinbo Li, Patrick Helm, Christopher Garson, Brent French, John Hossack; *University of Virginia, Biomedical Engineering, USA.*

Background, Motivation and Objective

Comprehensive four-dimensional (4D, or 3D + time) analysis is necessary to assess cardiac contractile function - especially in the asymmetric left ventricle (LV) after myocardial infarction (MI). We propose using a 4D mathematical cardiac model fitted to the acquired 2D + time image data sets to provide for improved, noise-robust, analysis of cardiac dysfunction and dyssynchrony encompassing the entire 3D LV in mice after surgically induced MI.

Statement of Contribution/Methods

B-mode image sequences were acquired at 30 MHz high frequency (VisualSonics) from C57Bl/6 mouse LV's, each with 5-6 short-axis slices and 3 long-axis slices at 1-mm intervals. The endocardial and epicardial contours were manually traced at end-diastole, and were automatically detected by a speckle-tracking guided segmentation for the subsequent approximately 100 cardiac phases. We used a 4D mathematical model and reconstructed the contraction-relaxation motion of the 3D LV over the complete cardiac cycle by surface fitting with a shape constraint to normalize irregularities caused by noise. 3D regional wall thickness was calculated and thereafter 3D radial strain was derived as the change in 3D wall thickness. 3D contractile dysfunction and dyssynchrony were analyzed by the regional strain deficit and time to peak strain (T_peak), respectively.

Results

The RMS error between the contour points segmented from actual images and the model-fitted contour points of the 3D LV surface over the cardiac cycle was 0.23 mm (~4.5% of epicardial diameter) for the epicardial surface, and 0.20 mm (6.4% of endocardial diameter) for the endocardial surface. The 3D function analysis revealed >50% reduction in peak radial displacement, an 8-15 ms delay near the infarct zone, and a 6-10 ms standard deviation of T_peak in post-MI mouse hearts.

Discussion and Conclusions

This is the first report of a 4D model-based method for analyzing cardiac dysfunction and dyssynchrony in the 3D murine LV, which yields a more comprehensive and noise-robust assessment than conventional 2D methods.

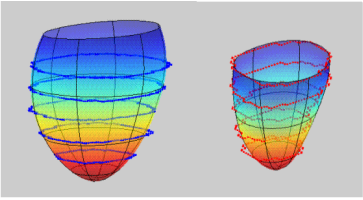

Model-fitted epicardial (left) and endocardial (right) surfaces; blue and red dots are contour points segmented from images.

P2F070-05

Improving Ejection Fraction Estimation for 2D Ultrasound Using a Computer-generated Cardiac Model

Mahdieh Khoshniat[1], Thomas Szabo[1], Peder Pedersen[2]; *[1]Boston University, Department of Biomedical Engineering, USA, [2]Worcester Polytechnic Institute, Department of Electrical and Computer Engineering, USA.*

Tuesday Poster

Background, Motivation and Objective

Present methods of estimating left ventricular (LV) volume and ejection fraction (EF) from 2D cardiac ultrasound (US) vary in their accuracy as shown in the result table. Our objective is to match a computer-generated 4D model of the beating heart to real clinical US data in order to estimate LV volumes more accurately.

Statement of Contribution/Methods

We have adapted a cardiac torso computer-generated model that closely resembles the anatomical structures and simulates cardiac and respiratory motions of a normal human subject. William Segar's dynamic Non-uniform Rational B-spline (NURBS)-based cardiac torso (NCAT) phantom was based on CT and MRI clinical data. Due to the fact that in the current version of the NCAT software, the valves have not been modeled yet, we used activity phantoms and assign different activity parameters for the left atrium and LV, so that they can be distinguished. In order to mimic standard US cardiac views, NCAT 2D slices were selected and then manipulated by contrast enhancement, resolution improvement, and negative imaging.

Results

Three methods of LV volume and EF estimation were compared to the numerical calculation from the NCAT simulation: 2D ellipsoid and stacked-disk estimators and 3D volume measurement using a region-growing snake algorithm to detect the LV boundaries for each slice of the 3D NCAT dataset followed by Simpson's formula. The following table summarizes the results of the LV volume and EF calculation for different methods. This table shows that our region growing-snake segmentation technique closely matches the NCAT calculation of the EF with slight differences in the actual values of LV volume at end-diastole (ED) and end-systole (ES).

Discussion and Conclusions

These results indicate that the 4D simulation model is a more accurate estimator of LV volume and EF than earlier 2D methods. 4D US data is being obtained to independently verify the model. Scan planes from the model are being matched to actual 2D US cardiac image loops through scaling and feature correspondence. Challenges include absence of certain clinical landmarks such as valves in the model and wall dropouts in the images. The adapted NCAT phantoms can be used for US imaging demonstrations and the simulation of cardiac disease.

Normal Heart	NCAT	Region-Growing-Snake 3D volume estimation	Ellipsoid Estimation (2D)	Stacked-disk Estimation (2D)
EF	60.42%	60.29%	65.22%	50%
ED volume	108.82 ml	106.21 ml	95.49 ml	159.53 ml
ES volume	43.07 ml	42.18 ml	33.21 ml	79.77 ml

P2F071-06

Tangential oscillations for motion estimation in echocardiography

Herve Liebgott, Adrian Basarab, Stefan Marincas, Olivier Bernard, Denis Friboulet; *CREATIS-LRMN, France.*

Background, Motivation and Objective

Motion estimation in echocardiography is an important field of research that encounters limitations to estimate with high precision motion perpendicular to the beam axis. This paper investigates the feasibility of applying transverse oscillations (TO) techniques (developed for blood flow and elastography) in the field of echocardiography.

Statement of Contribution/Methods

TO techniques are beamforming methods that aim at producing images with oscillations in both spatial directions of the ultrasound RF images. They are based on dynamic focusing along the beam axis together with dynamic apodization functions featuring two peaks. It has been shown that TO images can lead to better motion estimation, especially in the lateral direction, thanks to the use of a specific 2D motion estimator.

This kind of beamforming has never been used in a sectorial configuration, which is the geometry commonly used in echocardiography. We propose to adapt the TO methods for cardiac imaging.

Results

We have evaluated our method on a numerical phantom of 5x5mm containing 100 scatterrers located at 50mm depth. Image acquisition is simulated using Field II. Apodization functions have two peaks of width at half maximum 2.5mm with a distance of 5mm between them. A translation is applied to the tissue and the corresponding new image is simulated. The displacement is estimated between the 2 resulting images. This is done 100 times for different translation magnitudes and directions. The obtention of TO is validated on our data that have TO of 6.6 degrees/oscillation. The motion is estimated using a previously developped estimator working directly on the polar RF data. The results are compared with a block matching (BM) approach. The results are given in Fig 1. They show that TO increase transverse motion estimation accuracy. For the lateral motion, in terms of standard deviation, the TO approach (Meanstd=0.029mm) is better than BM (Meanstd=0.13mm). For the lateral motion mean error, TO (MeanError=0.012mm) also performs better than BM (MeanError=0.022mm).

Discussion and Conclusions

This paper shows the feasibility of TO images for motion estimation in a sectorial geometry. Application of this method to in vivo cardiac motion implies evaluating accuracy on more realistic motions (i.e. deformation) and optimizing the beamformer parameters. These aspects represent the next future of this work.

Fig1: True and estimated displacements. Estimation are done using specific and BM estimators. Estimations are presented as mean +/- standard deviation.

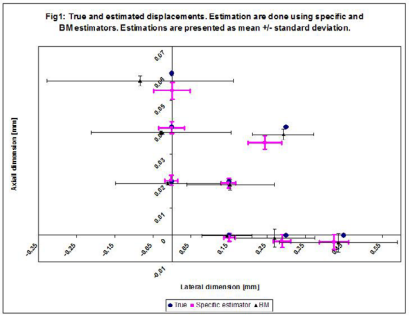

Tuesday Poster

P2G. Medical Imaging Transducers

2nd and 3rd Floor Foyers

Tuesday, November 4, 2008, 3:00 pm - 4:30 pm

Chair: **K Shung;**
University of Sothern California, CA, USA.

P2G072-01

Evaluation of Inline Transmitter/Receiver System for Intravascular Ultrasound Imaging Using $Pb(Zn_{1/3}Nb_{2/3})O_3$–$PbTiO_3$ Single Crystal and Polyvinylidene Fluoride

Masayuki Tanabe[1], Kan Okubo[1], Norio Tagawa[1], Tadashi Moriya[2]; *[1]Tokyo Metropolitan University, Department of Information and Communications Systems Engineering, Hino, Tokyo, Japan, [2]Professor Emeritus of Tokyo Metropolitan University, Japan.*

Background, Motivation and Objective

Recently, a fine intravascular ultrasound image has been required to diagnose detailed tissue properties. In our past studies, we proposed a novel inline transmitter/receiver system for intravascular ultrasound imaging to obtain the images with high resolution and high signal-to-noise ratio. This system uses a single crystal PZN-PT as a transmitter and two PVDF films as receivers, as shown in Fig.1(a). The beam axis of a transmitter should coincide with that of receivers. The preliminary experimental investigations demonstrated the feasibility of the proposed system. That is, the system is suitable for tissue harmonic imaging using pulse compression, because it can remove only transmitted signals by canceling system using two PVDF films. However, we obtained no unequivocal conclusion about the best suited thickness of the PVDF layer. This study aimed at investigating the characteristics of PVDF and optimizing the thickness of it as a matching layer.

Statement of Contribution/Methods

This study evaluates our inline transmitter/receiver system using the PZFlex software package: it is a finite element time domain piezoelectric simulator. To verify the preliminary experiments, we model the system using that simulator under the same condition. The thickness, width, and length of PZN-PT are 0.4 mm, 2 mm and 2 mm, respectively. We examined PVDF films with various thickness including 28 μm, 52 μm and 110 μm ones used in preliminary experiments.

Results

We used a linear FM-chirp signal with a central frequency of 4.5 MHz, a bandwidth of 2 MHz, and a duration of 5 μsec as a transmitted pulse. The acoustic pressure was measured near the transmitter on the beam axis. The result is shown in Fig.1(b).

Discussion and Conclusions

The results clarified that transmission performance strongly depend on the thickness of PVDF films. Additionally, the thickness has the optimum value not only as a receiver but also as a matching layer. Based on the results, we will produce a prototype of an IVUS probe in near future.

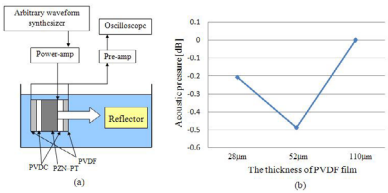

Fig. 1 (a) Outline of proposed inline transmitter/receiver system and (b) the acoustic pressure.

Tuesday Poster

P2G073-02

Novel biomedical imaging that combines intravascular ultrasound (IVUS) and optical coherence tomography (OCT)

Hao-Chung Yang[1], Changhong Hu[1], Qifa Zhou[1], Dawei Wu[1], Jonathan Cannata[1], Jianping Su[2], Jie-Chen Yin[2], Zhongping Chen[2], K. Kirk Shung[1]; *[1]University of Southern California, Biomedic Engineering, Los Angeles, CA, USA, [2]University of California, Irvine, Biomedical Engineering, Irvine, CA, USA.*

Background, Motivation and Objective

Intravascular ultrasound (IVUS) is a medical imaging methodology that has been used to show the anatomy of the wall of blood vessels in living animals and humans. It provides the cross-sectional image of blood vessels. Optical coherence tomography (OCT) is a non-invasive imaging modality that uses coherent gating to obtain high-resolution surface images of tissue microstructure. In vivo images of living animals have been demonstrated by using a MEMS motor-based scanning endoscopic probe. Generally, OCT can have excellent surface resolution. However, IVUS has larger penetration depth. The motivation of this paper is developing a novel system combining high frequency IVUS transducer with 3-D scanning OCT probe to obtain the high-resolution cross-sectional intravascular images.

Statement of Contribution/Methods

A single element 45 MHz ultrasound transducer has been fabricated. The transducer incorporated a single conductive matching layer and a highly attenuating conductive backing. The pulse echo measurement result shows -6 dB bandwidth of 55%, which is in good agreement with KLM modeling.

A 3-D endoscopic microscope was developed based on a rotational micro-electromechanical system (MEMS) probe. Four thousand A-lines were taken for one frame. The MEMS motor was driven at a rotating speed of 300 rpm to be synchronized with the B-scan. The overall image display rate was 1 frame/sec. The 3-D helix scan mode was realized by combining a MEMS motor rotational scan and linear stage transversal movement. An OCT system with a broadband fast swept laser was used to coordinate the high spin speed of MEMS motor inside the endoscope.

Results

A novel biomedical imaging system combining IVUS and OCT has been developed. The in vitro images of rabbit trachea and blood vessel from a 40 MHz ultrasound transducer and an OCT device have been acquired. These results demonstrate that the complementary nature of these two modalities which may yield beneficial results that could not be obtained otherwise.

Tuesday Poster

P2G074-03

A 100-MHz 32-array transducer using lithographically-made electrodes and vapor-deposited polyurea film

Toshiki Takayasu[1], Marie Nakazawa[2], Kentaro Nakamura[3], Sadayuki Ueha[3]; *[1]Tokyo Institute of Technology, Precision and Intelligence Laboratory, Yokohama, Kanagawa, Japan, [2]Hitachi Ltd, Japan, [3]Tokyo Institute of Technology, Japan.*

Background, Motivation and Objective

High frequency dense array transducers are required for higher resolution in medical ultrasonic diagnosis. However, conventional fabrication methods for array transducer based on the machining of piezoelectric ceramics and PVDF films are encountering the limitation in miniaturization. We have proposed to utilize polyurea film as ultrasonic transducers, and investigated the fundamental characteristics in transmitting/receiving high frequency ultrasonic waves up to 100 MHz. The polyurea film of 0.1 μm to 5 μm is prepared through vapor deposition with high controllability in thickness. Miniature array electrodes can be fabricated using lithographic technique since the polyurea has chemical resistance. Taking advantage of the features of polyurea film, a 32-element linear array working at 100 MHz is prototyped in this study.

Statement of Contribution/Methods

Two types of different configurations are tested in prototyping array transducers using polyurea film. In the first configuration, the bottom electrode deposited on a polyimide substrate is etched into 32 elements before the deposition of the polyurea layer and top electrode. In the second configuration, the top electrode made on the surface of the polyurea film is etched into 32 sections. The width of each element is 10 μm, and the spacing between the elements is 20 μm.

Results

We observed the resonances at around 30, 65 and 100 MHz for each element of 32 through the electrical admittance measurements. The effective electromechanical coupling coefficient for the resonance of 100 MHz was 0.132. We carried out beam steering experiments being based on phased array method for receiving ultrasonic pulses launched from the angle of 0.4°, 2.3° and 2.7°. The angles were successfully recognized with the beam width of around 7°. Pulse/echo operation was also tested.

Discussion and Conclusions

Through the beam steering experiments and the pulse/echo tests, the feasibility of polyurea-based array transducers for high frequency operation has been successfully confirmed. The polyurea layer survived the chemical etching process of the array electrodes. This means that the polyurea is one of the most promising materials for making high frequency dense array transducer with the use of lithographic techniques.

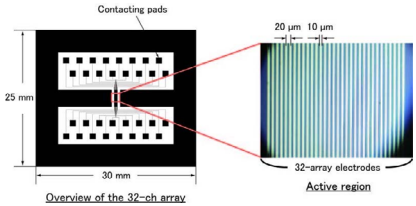

P2G075-04

Fundamental and Third Harmonic Operation of a Medical Phased Array Transducer

Martijn Frijlink, Lasse Løvstakken, Hans Torp; *Norwegian University of Science and Technology (NTNU), Department of Circulation and Medical Imaging, Trondheim, Norway.*

Tuesday Poster

Background, Motivation and Objective

Some applications in medical ultrasound incorporate third harmonic signals. One example is the detection of nonlinear scattering at the third harmonic from ultrasound contrast agents. Another application is "third harmonic transmit phasing" for tissue harmonic enhancement or suppression, where the transmit signal is a combination of a fundamental and third harmonic components. These applications demand dedicated transducers that are sensitive at several frequency ranges. Therefore, the well known phenomenon of higher harmonic thickness resonances of a transducer with a single piezo layer might be used beneficially. In this study we investigated if the third harmonic resonance mode could be used to add third harmonic sensitivity to a conventional cardiac transducer. This was done by means of experiments and simulations.

Statement of Contribution/Methods

An experimental PZT-based phased array probe (f_c = 3 MHz, 64 elements, elevation focus at 60 mm) was used to investigate the performance at the third harmonic resonance mode. Impedance analyzer measurements of electrically untuned elements indicated that the third harmonic thickness resonance was located at 10 MHz. Serial tuning inductors were then replaced to tune around 10 MHz. A water tank set-up allowed for hydrophone and pulse-echo (PE) measurements of the transfer function (TF) and transmit pulses of the 10-MHz-tuned elements at 3 and 10 MHz. A 1D KLM-model of the experimental transducer was used to simulate the thickness resonances. 2D finite element modeling (FEM) of the same transducer element was used to take into account lateral vibration modes too.

Results

The one-way TF measured at 60 mm from a 10-MHz-tuned element clearly showed two sensitivity peaks at the fundamental and third harmonic frequency. The fundamental sensitivity was reduced by 6 dB, while the sensitivity around 10 MHz was increased by >23 dB compared to a conventionally tuned element. For Gaussian enveloped (80% fractional bandwidth) excitation pulses centered at 3 and 10 MHz, the relative bandwidth of the measured transmit pulses were 60% and 22% for the 3 and 10 MHz pulse respectively. The measured two-way TF from PE experiments with a flat steel reflector at 30 mm indicated the receive potential at both the fundamental and third harmonic for the re-tuned element. The simulated TFs, as calculated with the 1D and 2D simulation tools, both confirmed the expected second sensitivity peak at the third harmonic. However, for frequencies above 6 MHz, the 2D FEM result approached the measured TF better, due to the interfering effect of lateral vibrations.

Discussion and Conclusions

It was shown that a conventional phased array cardiac transducer could be electrically tuned to obtain both high sensitivity at the fundamental and the third harmonic frequency. This study might help transducer development for applications that include third harmonic signals.

P2G076-05

Fabrication of MEMS Diaphragm Transducer Array Based on Epitaxial PZT Thin Film for 2-D Hydrophone Application

Nagaya Okada[1], Kazuki Higuchi[1], Yoshiyuki Asakura[1], Kazuto Kobayashi[1], Mikinori Ito[2], Masashi Takabe[2], Mikito Otonari[2], Ikuo Kanja[2], Daisuke Akai[2], Kazuaki Sawada[2], Makoto Ishida[2]; *[1]HONDA ELECTRONICS CO., LTD., Japan, [2]Toyohashi University of Technology, Japan.*

Background, Motivation and Objective

The increasing interest in 3-D imaging and high frequency applications leads to investigate new solutions for transducer arrays. Achieving an adequate signal-to-noise ratio with piezoelectric elements of this size is quite challenging, because their reduced sectional area of element leads to a poor sensitivity. We propose a MEMS diaphragm transducer array based on a Pt/PZT/Pt/γ-Al_2O_3/Si structure for 2-D hydrophone application. The Epitaxial PZT / Epitaxial γ- Al_2O_3 films on Si substrates could improve sensitivities of elements.

Statement of Contribution/Methods

The pMUT array containing 8 x 8 two dimensional elements was fabricated. Figure (a) is the schematic structure of the sensing element in the ultrasonic hydrophone array. The epitaxial growth of γ- Al_2O_3 (001) film on Si (001) substrate by CVD. Pt and $SuRuO_3$ bottom electrodes layer was grown by rf sputtering. A PZT film with 1 μm in thickness (with Zr : Ti ratio = 52 : 48) was prepared by using conventional sol-gel method. A dry etching of the top Pt, PZT and the bottom Pt films was carried out. To make a protection of etching damage and a reinforcement of diaphragm structure, a polyimide was coated. Si under the transducer area was removed by using XeF_2 gas etching to form a membrane structure. A data acquisition system is composed of the developed hydrophone array, peripheral electronic circuits and digital system.

Results

The 1μm-thick epitaxial PZT films were successfully deposited on Si substrate using γ- Al_2O_3 buffer layer. Figure (b) shows a photograph of the fabricated transducer array element. A center frequency of a transmitted spectrum was 8 MHz.

Discussion and Conclusions

The diaphragm structured pMUT has been demonstrated by the combining silicon micromachining and the epitaxial PZT film deposition technique. FEM simulations suggest that the frequency response is corresponding to a mechanical resonance of the radial vibration at the diaphragm structure. In this method, the center frequency of the transducer is determined by element size tuning having little influence of an overetching. In addition, fabrication of the ultrasonic hydrophone on silicon allows the integration of signal processing circuits and thus the sensitivity can be improved.

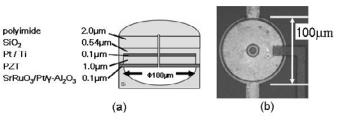

P2G077-06

Symmetric ReflectorPlates Doubling Transducer Efficiency

Minoru Toda; *Measurement Specialties Inc, USA.*

Background, Motivation and Objective

Ultrasonic transducers commonly utilize wave radiation from the front surface only and the back energy is often wasted. Some high efficiency transducers use the reflected backward wave constructively added to the front wave, but the propagation path lengths of the two waves are different and the bandwidth becomes narrower.

Statement of Contribution/Methods

This paper proposes a new structure using Symmetric Reflector Plates (SRP) mounted at front and back of a transducer with a 45 deg. angle so that acoustic waves from both sides are reflected, forming a main beam parallel to the transducer plane (Fig. 1). Since propagation path lengths of the two beams are identical both are constructively added at all frequencies.

Results

Results Detailed SRP directivities have been calculated showing a much sharper far field pattern. Experiments using PVDF air ultrasonic transducer (20 x 14cm2, 50kHz) have shown doubled acoustic pressure in the far field and the predicted directivity sharpness. When the transducer position was shifted from the center line of symmetry, the beam pattern due to phase difference between the two beams was calculated and the observed beam patterns agreed with the calculated results. The performance of thickness mode transducer (MHz region) with front and back matching layers having equal radiation has been calculated assuming SRP, and a broader bandwidth with higher efficiency has been shown.

Discussion and Conclusions

SRP fully utilize front and back waves, improving efficiency by ~100%. They have proven to be advantageous for a super high directivity loudspeaker (parametric array-ultrasound modulated by audio signal, demodulated during non-linear propagation). SRP have been proposed for wideband, high efficiency medical imaging transducers.

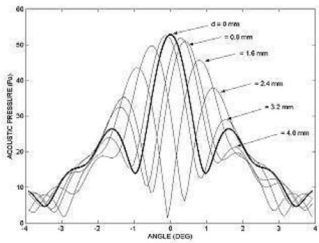

Fig.2 Directivity for displacement d normal to the center of symmetry line

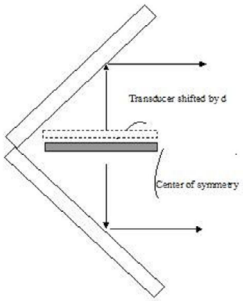

Fig.1 SRP added transducer

Tuesday Poster

P2G078-07

Frequency-adjusted Fresnel lens design for a broadband transducer with varying thickness

Sheng-Yung Chen, Jian-Hung Liu, Pai-Chi Li; *National Taiwan University, Taipei, Taiwan.*

Background, Motivation and Objective

Fresnel lens design has been used for annular arrays. In this case, the surface area of each concentric ring is the same. In other words, the aperture is uniformly sampled at x2, where x is the distance from the transducer center. By doing so, the phase shift between adjacent transducer elements remains constant when focusing at depth. Recently, a 40 MHz transducer has been proposed with increased bandwidth by varying the thickness of the piezoelectric material from the transducer center to the edge. In other words, the center frequency is effectively changing across the aperture. Although the equal area design can maintain uniform spectral weighting for such a transducer, this also results in non-uniform phase shift between adjacent transducer elements. To maintain uniform phase shift, the surface area of each transducer element needs to be adjusted based on its center frequency. It is the hypothesis of this study that the frequency adjusted Fresnel lens design can provide larger depth of field (DOF) than conventional Fresnel lens design.

Statement of Contribution/Methods

A finite-element analysis software (PZFlex, Weidlinger Associates, Los Altos, CA) was used. The axial symmetry of the transducer was used so that a simple two-dimensional model can be used to represent the three-dimensional transducer geometry. The model consisted of six transducer elements, electrodes, two matching layers, a backing layer, and the water interface. Properties of the 36°-rotated, Y-cut LiNbO3 were used in the model. The mean thickness of the piezoelectric material was set at 91.75 µm, corresponding to an operating frequency at 40 MHz. The thicknesses of the center and outermost subelements were 66.75 µm and 116.75 µm, respectively, with corresponding resonance frequencies ranging from 31.5 MHz to 55 MHz. At edges of the model, absorbing boundary conditions were used and infinite backing layer was effectively achieved. A single cycle of a 40 MHz sine wave was used to excite the transducer. Transducer bandwidth, lateral resolution and DOF were used as indicators of imaging quality.

Results

With conventional Fresnel sampling (i.e., six uniform area transducer elements), the transducer had a 78.4% fractional bandwidth, 105.8 µm lateral resolution (-6 dB beam width), and 1.48 mm DOF. With the proposed frequency adjusted Fresnel sampling (i.e., product of the surface area and the center frequency is a constant for all six elements), the transducer bandwidth was approximately the same (76.8%) but the DOF increased to 1.70 mm (15% improvement). The tradeoff is that the lateral beam width also increased to 113.2µm (7% degradation).

Discussion and Conclusions

PZFlex models were developed and simulations were performed to investigate the new frequency-adjusted Fresnel lens design. It was found that the broad bandwidth of the non-uniform thickness transducer was maintained, and the DOF was effectively improved.

P2H. Nonlinear Propagation

2nd and 3rd Floor Foyers

Tuesday, November 4, 2008, 3:00 pm - 4:30 pm

Chair: **Valery Proklov;**
IRE RAS, Russia.

P2H079-01

Acoustic radiation force on objects and power measurements of focusing source (HIFU)

Zu Wen Qian[1], **Zhemin Zhu[2],** Shigong Ye[1], Wenhua Jiang[1], Houqing Zhu[3], Jinshen Yu[1], Yi Yuan[1], Yaqin Yang[1]; *[1]Laboratory of Medical Acoustics, Institute of Acoustics, Chinese Academy of Sciences, and Beijing YU, Beijing, China, [2]Laboratory of Medical Acoustics, Institute of Acoustics, Chinese Academy of Sciences, China, [3]Institute of Acoustics, Chinese Academy of Sciences, China.*

Background, Motivation and Objective

Recent years, the focusing sound source (HIFU) has been used as a tool in ultrasound surgery[4], knowing its acoustic power output has actually become a more and more important task. Most works to estimate the acoustic power output of the focusing sound sources are still based on the measurements of the radiation forces. In order to deal with such kinds of problems, especially focusing sound sources, it is crucial to establish a relationship between the radiation forces and the their corresponding acoustic power output.

Statement of Contribution/Methods

In order to find the range where the radiation force measurements are independent of the target's position, an investigation will be given by the authors.Based on the analytic expression of the acoustic field for focusing sound source given by T. Hasegava et al.. (J.Acoust. Soc. Am. 79(4) (1986) 927-931), the radiation force on an absorbing target was investigated and numerical calculation of integrals was carried out by using the symbolic computation program.

Results

The calculations show that for a spherical focusing source and a plane circular absorbing target with its size of large enough to completely cover the beam of the focusing sound source, there is a range of target¡¯s position where the radiation force is independent of target¡¯s position. By use of the digital force gauge and the HIFU setup (FEP-BY02) the radiation forces were measured on four targets (one square and three circular, including two rubber targets and a brush absorbing target). The experimental results also demonstrate that there is a range of the target¡¯s position where the radiation force is independent of target¡¯s position even though at high electric drive power.

Discussion and Conclusions

For a spherical focusing source (krc>>1) and a plane circular absorbing target with size large enough to completely cover the beam of the source, there is a range of target¡¯s position of which the radiation force is independent. This range obeys equation b/zd>tanB, where b,zd and B are the target's radius, the distance of the target from the focus and the angle of elevation (the observer views the borderline of the target from the focus). However, in order to sufficiently guarantee the ¡°independence-upon- target¡¯s position¡± in the acoustic power measurements of a focusing source, the target¡¯s position (R-zd)/R from 0.7 to 0.8 seems to be proper.

Tuesday Poster

P2H080-02

Stress Mapping Using Nonlinear Ultrasound

Dan Xiang[1], Guangfan Zhang[1], Fei Yan[1], John Welter[2]; *[1]IAI, USA, [2]WP AFB, USA.*

Background, Motivation and Objective

Ultrasound has been used to measure stress through the thickness or on the surface of a specimen, because the speed of sound in a solid is altered in the presence of mechanical stress (as often referred to as acoustoelasticity). Conventional ultrasonic stress measurement methods that detect the time-of-flight (TOF) of sound pulses suffer from low sensitivity and thus have limited applications in the field. A time-resolved acoustic microscopy technique has been suggested by Eva Drescher-Krasicka, which utilizes the interference among stress-induced acoustic waves to map internal and surface stress in a solid sample. In that method, the amplitude measurement of two quasi-shear waves was used to replace the conventional TOF detection, which greatly increases the sensitivity of ultrasonic stress measurements.

Statement of Contribution/Methods

In this paper, we present the investigation of utilizing the nonlinearity of stress-induced quasi-shear waves to further enhance the sensitivity of stress measurements. This approach is based on the nonlinear effect of stress-induced material anisotropy on acoustic shear waves. A diametrally compressed aluminum disk (3 mm thick and 40 mm in diameter) was used as the sample. A spherical focus transducer in conjunction with an acoustic microscope operating at the pulse mode was used to scan the compressed Al disk. The detected time-waveforms of the quasi-shear waves were recorded and processed to reconstruct the stress distribution in the compressed disk sample.

Results

We have compared stress mapping based on features extracted in time, frequency, and wavelet domains. Time domain features include the TOF and amplitude. Frequency domain features include the fundamental frequency and harmonics. In the wavelet domain, we extract features using different scales. Significant improvements for contrast or sensitivity in stress mapping have been achieved through the wavelet analysis, in comparison with the results in the time and the frequency domains.

Discussion and Conclusions

The use of wavelet to extract the nonlinear features outperforms the time-domain and frequency-domain features for ultrasonic stress mapping, in the sense of stress detection sensitivity and image contrast. This is due to the fact that acoustoelasticity is a nonlinear effect and the wavelet transform is capable of providing both the time and frequency information simultaneously. Therefore, small variations in the time instant and interval in recorded time-waveforms can be extracted and detected when a particular spectral component occurs. Thus the extracted nonlinear information enhances the sensitivity in ultrasonic stress mapping.

P2H081-03

Using SFAI Method for Spherical Resonator Characteristics Determination

Rudolf Bálek, **Ilona Ali Bláhová,** Milan Cervenka, Jaroslav Plocek; *Faculty of Electrical Engineering, Czech Technical University in Prague, Department of Physics, Prague, Czech Republic.*

Background, Motivation and Objective

The methods for measurements focused to dynamics of single-bubble cavitation (SBC) and single-bubble sonoluminiscence (SBSL) have been prepared. The frequency spectrum of a single-bubble cavitation is analysed with respect to the diameter of the bubble, the intensity of acoustic generating field, and other conditions necessary for creation and sustainment of the bubble. For these experiments very specific conditions are demanded. A cell for these experiments has to have certain characteristics. The Swept Frequency Acoustical Interferometry (SFAI) method has been used for characteristics determination of used cell.

Statement of Contribution/Methods

For the measurements the spherical glass cell filled with distillate degassed water has been used. Its diameter is 65 mm. Piezoelectric circular transducers with working frequency of 200 kHz and 20 mm in diameter have been used. They have been stick in a parallel way on the glass cell on its equator. The measuring card National Instruments PCI 6251 has been used for transducer excitation and for data recording. Signal processing has been made in system Matlab.

Results

At the beginning a lot of cells have been compared and the best one has been chosen for later experiments. In the experimental arrangement used cell creates an acoustical resonator. A transmission function, sound speed and attenuation, liquid density and eigenfrequencies of this resonator have been determined on the base of measurement made by SFAI method. The mathematical model of this resonator has been calculated and obtained eigenfrequencies have been compared to experimental results. A frequency mode with a high quality factor convenient for SBC and SBSL measurements has been determined.

Discussion and Conclusions

The optimal conditions for further experiments with SBC and SBSL have been investigated. The working frequency for SBC and SBSL measurements has been assessed. Measurements with other liquids suitable for SBC and SBSL are prepared.

P2H082-04

Nonlinear Planar Forward and Backward Projection

Gregory Clement; *Harvard Medical School, BWH, Radiology, Boston, MA, USA.*

Background, Motivation and Objective

Planar projection methods, such as the angular spectrum approach, have been shown to rapidly relate fields between two planes in space/time, with only a single measurement plane needed to characterize an entire field. Variants of the method have been used for medical transducer characterization, as well as for HIFU treatment planning. Although nonlinear versions have been described, they have not been widely implemented due to the need to transform between real space and frequency space at each iteration in the algorithm. Presently, two potential advantages of such an approach are considered: (i) That by operating in the temporal frequency domain, backward planer projection is invariant with respect to the spatial dimension, even in the presence of anomalous dispersion. (ii) In the case of a weakly nonlinear field, large steps may give the approach a significant time advantage over time-domain modeling.

Statement of Contribution/Methods

For comparison with previously-published results, the model used a wavevector-frequency representation of the Westervelt equation, which was rewritten as an ODE with the axis of propagation, z the independent variable. A 30-cm-diameter 2.65 MHz planar radiator was modeled over a 160 mm range in front of the source. The simulation was repeated for a range of step sizes (0.2 mm to 2 mm) and a range of starting acoustic pressures (0.05 MPa to 6.4 MPa) to investigate the rate of error as a function of dz and pressure p. Planes in the post focal region at 160 mm from the source were then used as starting pressures and projected backward toward the source for comparison with the forward case. Spatial and temporal sampling was kept within the Nyquist limit, which tracked the first 6 harmonics of the fundamental.

Results

Error was found to increase proportionally with both step size and initial pressure. However relatively large step sizes (~1 mm) were found to yield reasonable results, particularly at lower pressure levels, suggesting the approach can be competitive with – or exceed the efficiency of time-domain modeling of the same physical situation. When a step size of dz = 0.2 mm was used to project the field, processing times of 5-10 minutes were observed in the algorithm implemented using Matlab (XP 64-bit OS, 2 duel-core 3GHz processors, 8GB RAM). Furthermore, successful back-projection of the data demonstrated the invariance of the independent variable z in the ODE.

Discussion and Conclusions

The current study was conducted using the dispersion relation dictated by the Westervelt equation. The use of the equation allowed straightforward comparison with previously-reported methods. However, a particular advantage of the approach may be its ability to easily handle cases of anomalous dispersion, which have simple form in the frequency domain. Furthermore, in the case of weakly nonlinear fields, the approach may be performed with significant computational efficiency.[Funding by US NIH Grant U41RR019703]

P2H083-05

Computation of Nonlinear Circular Symmetric Fields using X Waves with Operator Splitting

Paul Fox; *University of Southampton, ISVR, United Kingdom.*

Background, Motivation and Objective

The paper is motivated by the continued interest in the development of efficient numerical methods for the computation of nonlinear ultrasound fields. A number of methods currently exist, but each with its advantages and disadvantages and consequently there remains scope and interest in the proposition of alternative methods. The objective here is to present a new computational method, based on combining X wave field analysis with the operator splitting tecnique applied here in the context of the nonlinear Westervelt equation.

Statement of Contribution/Methods

The contribution is a new method for computing nonlinear circular symmetric ultrasound fields. It adopts an alternative approach, by using limited diffraction (X wave) field analysis for linear systems [1] with an operator splitting approach [2] to obtain an estimate of the nonlinear field. This is achieved by sequentially computing a linear element followed by a nonlinear distortion of the the linear field as it propagates over a series of virtual planes within the field. A similar technique was adopted earlier in [3], but in the context of generating virtual rectangular grid planes within Field II and leading to an inherent degree of ambiguity for to the appropriate propagation distance to be respresented in the nonlinear distortion phase of the pulse. The use of X wave basis functions removes this ambiguity due to their nondiffracting propagation entirely perpendicular to the transducer surface. An unambiguous computation method is subsequently obtained by making use of nondiffracting beam functions in the linear element of the computation phase.

Tuesday Poster

Results

The figure demonstrates pulsed propagation in water from a simple piston transducer diameter 10mm and center frequency 2MHz emitting at pressure magnitude 2MPa. The upper and lower plots show the surface (z=0mm) and propagated (z=33mm) centreline pressures. Note the typical nonlinear sawtooth shape in the propagated pulse, along with its larger positive than negative peak pressure magnitudes (+4.4MPa vs -2.8MPa).

Discussion and Conclusions

An new nonlinear computation method is illustrated, with the full paper giving an outline of its extension to noncircular-symmetric fields. Refs. [1] Fox, Cheng, Lu. JASA 113(5), 2412-2423, May 2003. [2] Tavakkoli, Cathingol, Souchon. JASA 104, 2061-2072, 1998. [3] Jensen, Fox, Taylor, Schlaikjer. IEEE Ultr.Symp. 2002. 1690-1693.

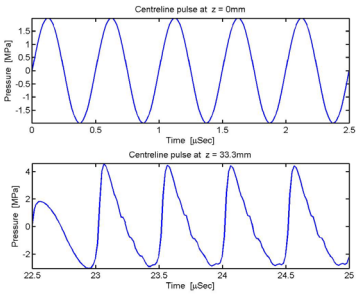

P2H084-06

Excitations of Nonlinear Vibration in Plates by High-intensive Ultrasonic Pulses

Zhao-jiang Chen, Kai Zheng, Shu-yi Zhang, Tao Zhang, Feng-mei Zhou; *Lab of Modern Acoustics, Institute of Acoustics, Nanjing University, Nanjing 210093, China.*

Background, Motivation and Objective

The nonlinear vibration phenomena of metal plates excited by intensive ultrasonic pulses have been studied by several groups, by which the subharmonics and anomalous (quasi-) subharmonics have been observed. However, the experimental conditions and theoretical calculations for the nonlinear phenomena have not been studied completely.

Statement of Contribution/Methods

In this paper, the experimental and theoretical studies on the excitations of the subharmonics in metal plates by the intensive ultrasonic pulses injected via a magnitude transform horn are presented. A series of experiments is performed to study the various nonlinear vibration behavior of rectangular stainless steel plates. Meanwhile, an improved nonlinear vibro-impact model is put forward to explore the generation mechanism of the complicated nonlinear vibration in the plates. Considering the plate is continuously impacted by the horn tip, the horn is simplified as an active oscillator with constant frequency and amplitude and the plate is simplified as a damped oscillator. A nonlinear contact model is used in this paper, which ensures that the contact forces evolve continuously upon the contact, which is more consistent with the practical circumstance and also has more clear physical sense.

Results

The experimental results show that the excitations of the different order subharmonics change remarkably with different materials, sizes and fix (boundary) conditions of the plates, as well as the preload forces between the horn and the plates. According to the model described above, the theoretical calculation results are in agreement with the subharmonic phenomena observed in the experiments (see Fig.1), and the harmonic, subharmonic and chaotic vibrations, etc., can also be calculated.

Discussion and Conclusions

The theoretical and experimental results indicate that there exist complex nonlinear vibration behavior in the thin plates when the plates impacted by the horn. The results are very useful for ultrasonic applications, such as ultrasonic drilling/coring (USDC) and/or ultrasonic infrared thermography (UIR), in which the existence of subharmonics can greatly enhance the efficiency of ultrasonic processes.

This work is supported by National Natural Science Foundation of China, No: 10574073.

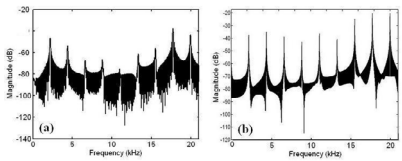

Fig.1. (a) Experimental and (b) theoretical 9-order subharmonics in a stainless steel plate (200×100×2.5mm³) with the excitation frequency 20 kHz.

Tuesday Poster

P2I. Ultrasonic Wave Propagation II

2nd and 3rd Floor Foyers

Tuesday, November 4, 2008, 3:00 pm - 4:30 pm

Chair: **Ji Wang;**
Ningbo University, Ningbo, China.

P2I085-01

Development of General Solution of Cumulative Second Harmonic by Lamb Wave Propagation

Mingxi Deng; *Logistics Engineering University, Department of Physics, Chongqing, China.*

Tuesday Poster

Background, Motivation and Objective

Considering the advantages of Lamb wave inspection for plate-like structures and the high sensitivity of nonlinear ultrasonic measurements to material properties, the nonlinear effect of lamb wave propagation gradually attracts more and more attention. It is expected that the convenient and effective numerical analyses are required for possible applications of nonlinear Lamb waves.

Statement of Contribution/Methods

Usually interest is focused on the second-harmonic generation with a cumulative growth effect. Here we will develop a general solution, straightforward and convenient for numerical analyses of the cumulative second harmonic by Lamb wave propagation in a solid plate. The present analyses focus on the cases where the phase velocity of the fundamental Lamb wave is exactly or approximately equal to that of the dominant Double Frequency Lamb Wave (DFLW) component.

Results

The formation process of the second harmonic with a cumulative growth effect and the corresponding general solution convenient for numerical computations will be presented.

Discussion and Conclusions

Based on the general solution obtained, both the theoretical analyses and the numerical results show that the cumulative second-harmonic fields are associated with the position of excitation source for the fundamental Lamb wave, and also with the difference between the phase velocity of the fundamental Lamb wave and that of the dominant DFLW component. This presentation provides a straightforward manner to understand the physical process of cumulative second-harmonic generation by Lamb wave propagation.

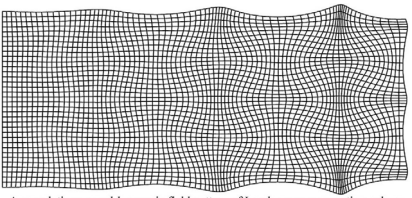

A cumulative second-harmonic field pattern of Lamb wave propagation, where frequency=2.10MHz, aluminum sheet thickness=2mm. The phase velocity of the fundamental Lamb wave is 5.945 MHz.mm, and the phase velocity of the domain DFLW is 5.750 MHz.mm. The position of line source is located on the surface of the sheet.

P2I086-02

Ultrasonic wave propagation in layered piezoelectric semiconductor plates

Bernard Collet; *Institut Jean Le Rond d'Alembert, CNRS-UMR-7190,case162, Tour 65, Université Pierre et Marie Curie, (Paris 6), Paris, Paris Cedex 05, France.*

Background, Motivation and Objective

The piezoelectric materials are either dielectric or semiconductors. A ultrasonic wave propagating in a piezoelectric crystal or piezoelectric ceramic is usualy accompagnied by an electric field. When the crystal is also semiconducting, the electric field produces currents and space charges resulting in dispersion and acoustic loss. The interaction between a travellling ultrasonic wave and mobile charges in piezoelectric semiconductors is currently called acoustolectric effect. It was shown experimentally and proved theoretically that an ultrasonic wave travelling in a piezoelectric semiconductor can be amplified by application of an initial dc electric field. The acoustoelectric amplification of ultrasonic waves have led to the development of acoustic devices.

Statement of Contribution/Methods

Piezoelectric devices, dielectrics or semiconductors, often have structural design of multi-layered plates or plates (multi-layered plates)coated on substrates.

In this paper we purpose a theoretical framework which describes harmonic anti-plane waves propagation and their amplification by dc electric field in infinite bilayered and sandwich piezoelectric semiconductor plates specialized to widely crystals of cubic (or hexagonal) symmetry.

Results

The analytical and numerical investigations permit to obtain the dispersion linear spectra, as well as field the spatial distributions in the composite structures, which are discussed.

Tuesday Poster

P2I087-03

Influence of the external electric field on propagation of Lamb waves in thin piezoelectric sheets

Sergey Burkov, Olga Zolotova, **Boris Sorokin;** *Siberian Federal University, Solid State Physics, Krasnoyarsk, Krasnoyarsk region, Russian Federation.*

Background, Motivation and Objective

Propagation conditions of acoustic waves in piezoelectric sheets always represented an essential interest for producing of perspective devices of acoustoelectronics, in particular dispersion filters. Special practical interest has a possibility of controlling of acoustic wave properties by the modification of electrical boundary conditions using an application of external electrostatic field to piezoelectric sheet.

Statement of Contribution/Methods

Influence of homogeneous electric field E on Lamb wave propagation conditions in piezoelectric crystalline sheet has been considered on the basis of the theory of bulk acoustic waves propagation in piezoelectric crystals subjected to the action of a bias electric field. Boundary conditions used should satisfy to such equations: components of stress tensor $\sigma_{3j}=0$ on boundaries of sheet (thickness h) at $x_3=h$ and $x_3=0$; normal component of an electric displacement vector at $x_3=h$ and $x_3 = 0$; wave electrical potential $\Phi=\Phi^{vac}$ at $x_3=h$ and $x_3=0$. We should modify the determinant of boundary conditions to take into account effects of geometrical and physical non-linearity of deformed media. As an example physical non-linearity is associated with with

effective elastic, piezoelectric and dielectric constants of a crystal which are now the linear proportional functions of E

$C^*_{ABKL}=C^E_{ABKL}+(C^E_{ABKLQR}d_{JQR}-e_{JABKL})M_JE$

$e^*_{NAB}=e_{NAB}+(e_{NABKL}d_{JKL}+H_{NJAB})M_JE$

$\varepsilon^*_{NM}=\varepsilon_{NM}+(H_{NMAB}d_{PAB}+\varepsilon_{NMP})M_PE$

Quantities C_{ABKLQR}, e_{JABKL}, ε_{MNP}, H_{ABKL} are nonlinear elastic, piezoelectric, dielectric and electrostriction material constants respectively; k_j and M_j – components of wave and unit electric field vectors respectively.

Results

The analysis of the changing of structure of acoustic wave as a consequence of a crystal symmetry and material constants modification has carried out. Detailed computational calculations of Lamb wave propagation peculiarities on examples of $Bi_{12}GeO_{20}$ and $La_3Ga_5SiO_{14}$ crystals under the E various variants application have obtained.

Discussion and Conclusions

Thus if linear and non-linear electromechanical constants of a crystal are known it is possible to carry out the analyses of dispersive character of ultrasonic Lamb modes in a piezoelectric sheet under the application of electric field. The data can be useful to making of field controlling devices and searching other practically important effects.

P2I088-04

Method of Extracting Unloaded Q Applied Across Different Resonator Technologies

Rich Ruby[1], Reed Parker[2], Dave Feld[2]; [1]*Avago Technologies, Wireless Semiconductor Division, menlo park, CA, USA,* [2]*Avago Technologies, USA.*

Background, Motivation and Objective

When comparing different resonator technologies, it is essential that fundamental properties such as the unloaded Q be accurately portrayed. Many papers on resonator technologies have been published along with their respective Q values. Important Figure-of-Merit (FOM) numbers for resonators include operating frequency, coupling coefficient (kt2), Q, and the products -- kt2*Q and f*Q. Three of the five Figure's of Merit depend on an accurate evaluation of unloaded Q.

Tuesday Poster

We have seen many cases where the calculated Q is incorrect due to either the method of calculating Q or to the incorrect application of a particular Q equation. It is essential to have a single equation that can be applied to measured data that will give a fair estimate of Q across technologies.

Statement of Contribution/Methods

We have derived (from Bode[1]) an equation for Q that allows one to extract Q vs. frequency of any resonator -- as long as Q is relatively high. The derivation begins with Bode's description of a general function, Φ, of a passive network where $\Phi = A + I*B$ must be analytic. Bode derives the following

$$A = A_o - (\omega/Q)\, dB/d\omega \; ; \; B = B_o - (\omega/Q)\, dA/d\omega$$

where Φ is a perturbation of the function Φ_o representing a lossless network. With the appropriate choice of Φ one can derive an approximation equation for Q that depends only on the measured group delay, the measured magnitude of S11 at each frequency .

In the case of high impedance resonators (such as MEMs type devices), one needs to transform the the source impedance appropriately. In short, adjust the source impedance such that the Q circle is now centered on the Smith Chart--properties that are easily set up and read off a Network Analyzer.

Results

We obtained S1P data files from the community at large, representing SAW, FBAR, AlN Contour Mode (or Rayleigh-Lamb mode resonators) and MEMS whispering mode resonators. The following algorithm was applied. First, a careful fit was done to each resonator using a mBVD model as the generic resonator topology. We used ADS[tm] Optimizer to achieve the best fit between data and model, creating a S1P for the model. We then calculate the total energy stored in the 3 reactance terms divided by the power dissipated in the 3 loss terms to determine (by "Brute Force") the unloaded Q over frequency. We then apply Bode's equation to both sets of S1P files, the measured S1P file and the model's S1P and compare against the "Brute Force" Q calculation. We see excellent correlation between the three methods across the four resonator technologies studied.

Discussion and Conclusions

We derive an approximation formula for Q and apply this to one-port terminal measurements of a resonator and compare to a "brute Force" mBVD model fit and achieved excellent agreement for Q vs. frequency for a variety of resonator technologies.

[1]H.W. Bode “Network Analysis and Feedback Amplifier Design” , Norstrand, N.Y. 1945

P2I089-05

Love Wave Propagating in Functionally Graded Magneto-electro-elastic Material Structure

Jianke Du, Wuchao Chen, Ji Wang; *Ningbo University, China.*

Background, Motivation and Objective

A new-style material called functionally graded material (FGM) was proposed to solve problems in the thermal-protection systems of a space-plane in 1980s. From then on, FGM has attracted interest of investigators from many kinds of disciplines. Today, FGM can be used not only in thermal-protection systems but also in electronic and many other fields. Recently, the magneto-electric effect in composite structures consisting of a piezoelectric phase and a piezomagnetic phase has been drawing attentions. The composites made of piezoelectric/piezomagnetic materials exhibit magneto-electric effect that is not present in single-phase piezoelectric or piezomagnetic materials. Consequently, the coupling nature of piezoelectric phase and piezomagnetic phase has led to wide applications in adaptive material systems, and they are extensively used as sensors, actuators and acoustic devices. The results obtained for the FGM layered structures lead us to consider that the FGM may be applicable to surface acoustic wave (SAW) devices made from the functionally graded magneto-electro-elastic material (FGMM). It is well known that techniques for fabricating FGMMs have been developed, such as for BaTiO3 and CoFe2O4, so it is necessary to analyze the Love waves propagating in FGMM structure for application of the SAW devices.

Statement of Contribution/Methods

In this study, an exact approach is used to investigate Love waves in functionally graded magneto-electro-elastic material layer bonded to a semi-infinite homogeneous substrate. The piezoelectricity is polarized in z-axis direction(i.e. antiplane direction) and the material properties change gradually with the thickness of the layer. We here assume that all material coefficients of the graded magneto-electro-elastic layer have the same exponential function distribution along the thickness direction.

Results

The analytical solution of dispersion relations are obtained for electrically open and short boundary conditions. The effects of the gradient variation about material constants on the phase velocity, group velocity, coupling magneto-electromechanical factor are discussed in detail. The displacement, electric potential, magnetic potential and stress distributions along thickness of the graded layer are calculated and figured.

Discussion and Conclusions

Numerical examples show that the phase velocity, displacement, magnetic potential, and the electric potential of the first mode augment with the increase of the gradient factor β, and the coupling magneto-electromechanical factor decreases with the increase of the gradient factor. The results also indicate that appropriate gradient distributing of the material properties make Love waves to propagate along the surface of layer, which is in favor of acquiring a better performance of the SAW devices.

P2I090-06

Sound radiation from a finite FGM cylindrical covered with a compliant layer

Buqing Xu[1], **Shaohua Li[2];** *[1]Beijing Jiaotong University, School of Mechanical, Electronic and Control Engineering, China, [2]Shijiazhuang Railway Institute, China.*

Background, Motivation and Objective

Functionally graded material (FGM) was first produced in Japan in the mid-1980s. FGM is a multi-phase material comprised of different material components. An FGM plate or shell can be designed with material properties that vary gradually in the thickness direction, such that the plate or shell is non-homogeneous in that direction only. The gradual variation in material composition rather than sharp interfaces, as in the case of multilayered systems (i.e., laminated composites), significantly enhances the thermal and mechanical features of FGM. Furthermore, FGM can be designed to meet particular requirements, such as enhanced stiffness, toughness and resistance to corrosion, wear and high temperature, by using materials or material systems with various properties. Consequently, in the last two decades, FGM have been used in numerous demanding engineering applications including military armor, thermal barrier coating for turbine blades and internal combustion engines and machine tools.

At the same time, most of the research in this area involves the development of graded coatings and interfacial regions for the purpose of reducing residual and thermal stresses and increasing the bonding strength. However, investigations of sound radiation of FGM are limited.

Statement of Contribution/Methods

In this work, the characteristics of vibration and sound radiation from a finite FGM cylindrical shell with the outer shell coated with compliant layer and immersed in water are systematically studied. The shell's motion function is expressed by the FGM cylindrical shell motion, whereas the layer motion is described by means of the three-dimensional Navier's equations. Since there are no exact solutions allowing simple coupling to the supporting shell and to the outer acoustic medium, displacement solutions of Navier's equations are expressed using asymptotic expansions in the layer thickness. In this analysis, provided that the thickness layer divided by the dilatation wavelength in the compliant layer (e/ ε0) remains small compared to unity, one can develop the layer displacement field in powers of ε truncated at order S. The general formulation truncated at order S is presented as well as the numerical application of the method truncated at order 2. Numerical results are shown that exhibit the influence of the coating layer on the vibroacoustic behavior of the FGM shell.

Results

The solution of Navier's equations is feasible for the sound radiation from the baffled finite FGM cylindrical covered with a compliant layer.

Discussion and Conclusions

The main features of the radiated sound field by a finite FGM cylindrical shell covered with a compliant layer are discussed in the light of numerical calculation.

P2J. Ultrasonic Motor Innovations

2nd and 3rd Floor Foyers

Tuesday, November 4, 2008, 3:00 pm - 4:30 pm

Chair: **Oliver Kripfgans;**
University of Michigan, MI, USA.

P2J091-01

Resonant Frequency Tracking Control of Ultrasonic Motors Using the Maximal Power Point Tracking Method

Markus Flueckiger, José M. Fernandez, Yves Perriard; *Ecole Polytechnique Fédérale de Lausanne - EPFL, Switzerland.*

Background, Motivation and Objective

The properties of ultrasonic piezoelectric motors depend on applied load and temperature. The output behavior is characterized by the nonlinearity of the power transmission at the friction interface between stator and rotor. Because of these inherently nonlinear characteristics, a resonant frequency tracking control is imperative when direct speed or position sensing is not applicable. A variety of adaptive control methods have been presented, but they have often either poor control performance or they are too complex for industrial applications. We suggest a maximal power point tracking (MPPT) approach well known from contactless energy transmission systems.

Statement of Contribution/Methods

A resonant converter drives the ultrasonic motor. The electric resonant frequency of the drive circuit must match mechanical resonance of the piezoelectric actuator. For given load and ambient conditions, the maximum transmissible power corresponds to the optimal working frequency. The instantaneous power is composed of the reactive power and the active power p which is proportional to the power transmitted to the actuator. It is measured indirectly by multiplication of phase current and line voltage.

Instead of applying a constant frequency f0 to the power device, a variation Δf is superposed on the constant value. This variation generates a variation of power Δp. If the signals Δf and Δp are in phase, the system is on the positive slope of the power curve. Hence the frequency value f0 must be increased. On the negative slope, they are out of phase and f0 must be decreased. As the power curve presents a global maximum at the optimal frequency, the system is stable.

Results

The MPPT controller was compared to a phase-locked loop controller for ultrasonic motors known from literature, by the means of PSpice simulations for the analog case, and an implementation on microcontroller for the discrete case. In both cases, the resonant frequency can be tracked over a far wider working range compared to the phase locking range. Also, the MPPT control circuit is very easy to tune and no sophisticated loop gain design is needed. The analog version of the MPPT controller was built and tested on linear and rotary ultrasonic motors.

Discussion and Conclusions

A new adaptive controller for ultrasonic motors was developed. No motor model is needed and the only parameter to be determined is the impedance of the motor for initial resonance matching. Results showed that performance of the MPPT controller is comparable to state of the art phase-locked control loops, but it is able to track the optimal frequency over a much wider range without any stability concerns. Offsets of the electronics are automatically compensated. However, the variable frequency component applied for indirect measurement purposes may influence the motor behavior. Further research on this subject is necessary to find an optimized configuration.

P2J092-02

A Study on the Metal Tube Type Ultrasonic Motor (MTTUSM)

Jwo Ming Jou, De Chuan Hong; *Cheng Shiu University, Department of Mechanical Engineering, Kaoshiung County, Taiwan.*

Background, Motivation and Objective

Tuesday Poster

The main motivation of this study hopes to understand the characteristic of the metal tube type ultrasonic motor through simple components, different driving or operation ways, its characteristic includes the revolution speed, load ability, phase angle and the relation of operation time and temperature rise. And hopes it can be applied to drive the small-scale optics lens or precision fixed position system.

Statement of Contribution/Methods

The metal tube type ultrasonic motor (MTTUSM) is by metal tube type piezoelectric stator, screw and nut make up. Which the piezoelectric stator includes two piezoelectric ceramic slices and one right angle form metal tube. Moreover, the screw is set up within the metal tube type piezoelectric stator, but the nut is pasted on metal tube type piezoelectric stator. While operating, so long as two piezoelectric ceramic slices on the metal tube type piezoelectric stator exerts the driving voltage, phase angle and resonance frequency, can let the screw produce revolution motion. And the main contribution of this study is to make use of revolution motion of this screw to push the optics lens or precision fixed position component to move.

Results

According to the experimental results, the maximum revolution speed of the metal tube type ultrasonic motor (MTTUSM) is 2,075 rpm under 140V driving voltage, 62kHz driving frequency and 60 degrees phase angle conditions. The maximum rising temperature of the metal tube type ultrasonic motor (MTTUSM) is 55.8 degrees of C under 140V driving voltage, 62kHz driving frequency and 60 seconds operation time conditions. The maximum revolution speed of the metal tube type ultrasonic motor (MTTUSM) is 1,160rpm under different driving frequency and impedance conditions.°

Discussion and Conclusions

We find several facts in this study:

(1) Under the same driving conditions, the maximum revolution speed of MTTUSM happens in 60 degrees phase angle, and the minimum revolution speed happens in 150 degrees phase angle;

(2) Under the same driving conditions, the rising temperature of MTTUSM is in direct proportion to operating time;

(3) Under the same driving voltage condition, the maximum revolution speed of MTTUSM takes place in the minimum impedance;

(4) When it is applied to push the optics lens, it can cooperate with the proper elastic supporting to avoid tilt.

Tuesday Poster

P2J093-03

Control of Multiple Ultrasonic Motors with Robust Parameter Design

Zhijun Sun, **Huafeng Li,** Weiqing H; *Nanjing University of Aeronautics & Astronautics, China.*

Background, Motivation and Objective

Ultrasonic motors (USMs) have been used in many practical applications such as in Canon optical zoom mechanism; vibration alarm and drive of calendar mechanism in Seiko watch. In the near future, several USMs will be used and simultaneous controlled in one device. However, most of paper about control of USMs has concerned only one USM. Although some control methods have been proposed in these papers, they may not be effective to multiple USMs control in one device. In order to research the simultaneous control of multiple USMs, a typical multiple joint robot driven by USMs is selected as an experimental set-up. The task of the three-joint robot is to draw figures or write words on a flat plane in its workspace. The aims of the control are to ensure accurate tracking of the nib of the robot and smooth motion of the robot.

Statement of Contribution/Methods

In order to obtain good performance of the robot, a new position-velocity PID feedback control strategy especially for USMs was proposed by the authors. However, there are many controller gains needed to be tuned, it is crucial to find a good method which can easily obtain a robust set of control gains suitable for arbitrary figures drawn by the robot. Robust parameter design has been adapted, in which the derivation of the tracks of joints is chosen as noise factor and The S/N ratio is mainly depended on IAE (the integral of the absolute value of the error) of the joint.

Results

The index of average position error of joints has been reduced significantly, as shown in the Fig.1and Fig.2

Discussion and Conclusions

Briefly, robust parameter design is suitable in the experiments and can obtain an optimal and robust set of PID controller gains.

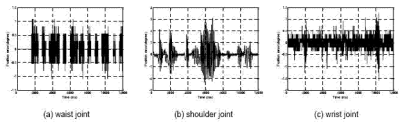

(a) waist joint (b) shoulder joint (c) wrist joint

Fig.1.Position error of each joint with manual tuned controller gains

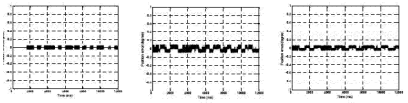

(a) waist joint (b) shoulder joint (c) wrist joint

Fig.2 position errors of each joint with controller gains using robust parameter design

P2J094-04

Design and Optimization of a Novel Annular Sector Curvilinear Ultrasonic Motor

Shiyang Li, Ming Yang; *Shanghai Jiaotong University, Department of Instrument Science and Engineering, Shanghai, China.*

Background, Motivation and Objective

Compared with linear and rotary ultrasonic motors, the curvilinear ultrasonic motor has been of significant research interests due to their special behaviors. Smithmaitrie proposed theoretically an arc curvilinear ultrasonic motor. However, damping materials and two phases travelling wave are needed in this motor.

In this paper, a novel annular sector curvilinear ultrasonic motor with simple structure was presented. Its operating mode is a composite in-plane bi-mode, which consists of the first circumferential and the second bending vibration mode. Therefore, this motor can be driven by only one single frequency. To design this motor, several design parameters needs to be simultaneously determined. So, this novel annular sector curvilinear ultrasonic motor was optimally designed. In addition, the frequency and motion characteristics of the motor are also discussed.

Statement of Contribution/Methods

The stator of the annular sector curvilinear ultrasonic motor is comprised of an annular sector brass plate with four groups of piezoelectric ceramic plates. Basic operating principle of the designed motor depends on the coupling of the first circumferential and the second bending vibration mode. There are four driving feet for generating thrust force at the two sides of the annular sector brass plate. Four groups of piezoelectric plates were bonded to the upper surface of the annular sector brass plate. When the working frequency is close to these two resonant frequencies, the superposition of the first circumferential and the second bending vibrations can produce elliptical motions on its four driving feet. To effectively excite the vibration mode, structure dimensions of the annular sector motor was optimally designed. The design problem is formulated and design variables are selected by sensitivity analysis. A mathematical model of the stator is established using finite element method and genetic algorithm. Finally, the optimization dimensions of the annular sector stator are determined. The prototype motor is fabricated. The frequency and motion characteristics of the motor are analyzed and tested.

Results

The dimensions of the stator with outer radius 81.4mm, inner radius 70.4mm, sector angle 30 degree and thickness 2mm are finally determined. Herein, the minimum frequency difference between these two resonant frequencies is only 0.003 kHz. According to the optimization results, the prototype motor is fabricated. The frequency and motion characteristics of the motor are also analyzed and tested. When a sine-wave working frequency 41.7 kHz with voltage 160V was applied, the motor reaches the velocity of 180 mm/s.

Discussion and Conclusions

A novel annular sector curvilinear ultrasonic motor with composite in-plane bi-mode was proposed and designed optimally. The test results show that the motor can work well driven by only one single frequency.

P2J095-05

Research on longitudinal and bending hybrid spherical ultrasonic motor with single-vibrator

Xuetao Zhao, Xiuting Wei; *Shandong University of Thchnology, School of Machincal Eenineering, Zibo, Shandong, China.*

Background, Motivation and Objective

Presently, most of multi-degree of freedom ultrasonic motor (MDF-USM) adopt multi-vibrator configuration which combine several single-degree of freedom motion realized by corresponding vibrators into specific multi-degree of freedom motion. However, due to the variance of vibrators in manufacturing and assembling, there exists difference in vibration and friction properties among vibrators, thus cause the poor mechanical output. This paper presents a MDF-USM with cross shaped single-stator, and driving point trajectories can be modified in three-dimensional way by controlling the input exciting.

Statement of Contribution/Methods

The structure of proposed ultrasonic motor was shown as Fig. 1. The cross shaped vibrator was amounted on the basement via fixed plates, and the spherical shape rotator was pressed on the driving foot through ball bearing pretightening mechanism. Three type of orthogonal elliptical trajectories was generated at driving foot by superimposed different combination of longitudinal and bending modal. The rotator can rotate around three orthogonal axis to realize controllable multi-degree of freedom motion.

The degeneration of longitudinal and bending resonant frequency was carried out by adjusting vibrator structure parameters, and the final degenerated resonant frequency is 36.46kHz.

Under 100V voltage exciting, the relation between driving point amplitude and frequency was attained by performing harmonic analysis using FEM software ANSYS, and the results showed that vibration amplitude was large enough to generate driving force in the frequency band of 36.2kHz?6.7kHz.

Tuesday Poster

Results

A prototype was fabricated and its mechanical output was: maximum torque 0.97 N•m and maximum rotary speed 11r/min when rotating around X or Y axis; maximum torque 0.27 N•m and maximum rotary speed 66r/min when rotating around Z axis.

Discussion and Conclusions

The results showed that proposed single-vibrator type multi-degree of freedom ultrasonic motor overcomes the shortcomings of traditional multi-vibrator type and showed merits such as high efficiency, large torque, compact structure and simple driving.

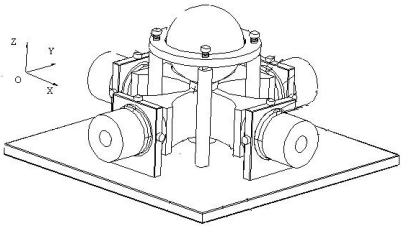

P2J096-06

A novel ultrasonic motor driver with independently controllable voltage and frequency

Huafeng Li, Hongzhan Wang; *Precision Driving Lab., China.*

Background, Motivation and Objective

Traditional method of driving traveling-wave ultrasonic motor (TRUM) uses series inductance to step up the voltage to certain high value. But such driver has a very big shortcoming that the voltage of the motor is uncontrolled. This means the driving voltage of motor will be changed following the frequency modulation. In order to solve this problem, a new driver is designed in this paper. The voltage of the motor is independent to the working frequency, and causes the working status of the motor controllable.

Statement of Contribution/Methods

The driver is mainly composed of two parts: the first part enhance 15V DC voltage to a high voltage which value may be adjusted according to the status of the motor by a push-pull DC/DC converter; the second is a half bridge DC/AC inverter composed by two bridge arms, its DC input is the output of the first part, and the output are two phase high voltage square wave with 90 degree difference. In order to reduce the current loss of the switching tube, each phase of the motor parallels an inductance; its value matches the motor¡¯s equivalent capacitance, carries on the idle work compensation.

Control function of the system is realized by a piece of programmable chip (PSoC) CY8C29466. The push-pull converter is controlled by an internal 16 bits PWM1 generator, and the other internal PWM generators (PWM2, PWM3) are used for half bridge inverters. The system function is: gathering the output voltage of the push-pull converter which is also the working voltage of the motor through the AD module of in the chip, after comparing with a given value, stabling the output of the converter through adjusting the duty ratio of PWM1. Gathering the voltage of the monitor electrode which can represent the speed of motor through another AD module of PSOC, after compared with the given value, then changing the speed of motor through adjusting the output frequency of PWM2 and PWM3, which is also the driving frequency of the motor.

Results

An ultrasonic motor with 45mm diameter is used in this study. The range of voltage of the driver can be set to 300-600V(Vpp) and keeps invariable, the working frequency is about 45kHz, and they are independently controllable.The motor works well.

Discussion and Conclusions

The new driver realizes the voltage amplitude and the driving frequency independently controllable, and provides a good method for the status's adjustment of motor.

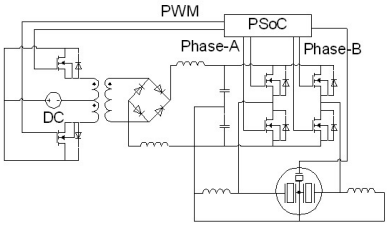

Tuesday Poster

P2J097-07

Experimental Study on Non-contact Linear Motors Driven by Surface Acoustic Waves

Huan-huan Gu, Li-ping Cheng, Shu-yi Zhang, Feng-mei Zhou, Xiu-ji Shui; *Lab of Modern Acoustics, Institute of Acoustics, Nanjing University, Nanjing 210093, China.*

Background, Motivation and Objective

Ultrasonic motors driven by surface acoustic waves (SAWs) have been studied by several groups, in which the rotors (or sliders) are driven by friction forces in contact. However, the direct contact between the rotors (or sliders) and stators restricts the velocity and the working life of the motors, and it needs high driving power. Then non-contact ultrasonic motors were developed, in which a fluid layer is loaded between the rotor (or slider) and stator, and the rotor (or slider) is driven by acoustic streaming.

Statement of Contribution/Methods

In this paper, a kind of non-contact linear motors driven by SAWs are presented, in which the stators are SAW delay lines fabricated by 128ºY-cut X-propagation LiNbO3 substrates with the frequency range of (10-50) MHz and the sliders are circular aluminum pieces floating in thin aqueous solution layers on the surfaces of the substrates. As the SAWs are excited in the stators, SAW streaming will be induced to drive the sliders to move linearly.

Results

The experiments on the velocities of the motors with the driving voltages, dynamic viscosities and the depths of the aqueous solution layers are given. The slider velocity is proportional to the driving voltage shown in Fig.1 and decreases exponentially with increasing dynamic viscosity of the aqueous solution. However, the relations between

the velocities and the depths of the aqueous solutions are more complicated. Meanwhile, the experimental results show that the driving voltage decreases greatly, even more than 10 times, compared with the contact SAW motors in the same frequency range.The further investigations are in progress.

Discussion and Conclusions

Generally, the non-contact linear SAW motors have the advantages of low driving voltage, high velocity, low loss and long working life, etc., which will have great potential to be applied to biochemistry, bioengineering and high technology fields and so on.

This work is supported by National Natural Science Foundation of China, No. 10774073.

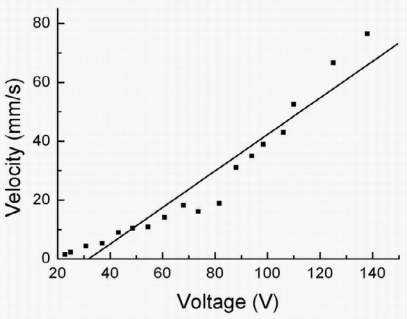

Fig.1. Velocity of slider vs driving voltage

Tuesday Poster

P2J098-08

A wear evaluation of friction materials used for rotary ultrasonic motors

Wei Zheng, Chunsheng Zhao; *Nanjing University of Aeronautics and Astronautics, China.*

Background, Motivation and Objective

The wear estimation of the friction materials used for rotary type wave traveling ultrasonic motors is strongly required to predict life of ultrasonic motors from a design point of view. However, the wear evaluation of friction is not constant. The wear loss is proportional to the pre-load and sliding distance between stator and rotor of ultrasonic motors according to the wear theory. The pre-load is not constant by the influence of the ultrasonic vibration on the frictional properties of ultrasonic driving.

Statement of Contribution/Methods

In this paper, ultrasonic vibration of stator surface points at the contact region of stator and rotor in ultrasonic motor is resolved into horizontal and vertical vibration. The horizontal vibration produces friction driving force and vertical vibration affects horizontal driving effect. The role of vertical ultrasonic vibration of stator surface point in ultrasonic motors is equivalent to the role of ultrasonic vibration being perpendicular to sliding direction in common sliding test. The effects of two direction vibration on ultrasonic motors are analyzed. The ultrasonic vibration on ultrasonic motors is different from common ultrasonic vibration. The pre-load with the ultrasonic vibration is less than the normal pro-load because of the effect of ultrasonic vibration. The sliding distance between stator and rotor of ultrasonic motors is proportional to the stator/rotor speed and ultrasonic motors' running time. The rotor speed can measured when ultrasonic motors work. The stator surface speed can be calculated by analysis of the traveling wave motion of surface. The running time is the ultrasonic motors life.

Results

The experiment about ultrasonic motors' life was carried. The setup is designed and manufactured by Precision Driving Lab in NUAA. The ultrasonic motor that was tested was also manufactured by Precision Driving Lab in NUAA was tested. The test was carried out 600 hours and the wear volume of ultrasonic motor was measured.

Discussion and Conclusions

The wear volume of ultrasonic motor that is 0.034g after the ultrasonic motor has work 600 hours. It is 5 percent difference between experiments and prediction.

P2J099-09

Predictive Control of Piezoelectric Actuators with Friction Drive Mechanism

Seiji Hashimoto; *Gunma University, Dept. of Electronic Eng., Kiryu, Gunma, Japan.*

Background, Motivation and Objective

In the manufacturing industry especially in the semiconductor, the requirement for high-speed, fast-response and high-precision performances is critical. The technology node, which is defined by the DRAM half pitch size reaches 65 nanometers in 2007 and will be expected to 45 nanometers in 2010. In this situation, the positioning accuracy of the precision stage is one tenth of less of the node, and it has already reached sub-nanometer range.

In this paper, the main objective is the construction of the ultra-precision stage control system driven by the developed non-resonant piezoelectric linear actuator named SPIDER.

Statement of Contribution/Methods

The developed linear actuator has the strong non-linearity due to the friction drive mechanism. Therefore, the control object is at first compensated by the friction control based on the bang-bang control. Next, the plant considering the friction is identified by the system identification strategy. Then, the model predictive control is applied to the identified plant. Here, the identified plant with the frictional compensation still has the uncertainty originate from the change of the mass as well as the frictional condition such as the wearing and change of the temperature. Therefore, considering the uncertainty, the adaptive mechanism is introduced to the model predictive control.

Results

The effectiveness of the application of the model predictive control to the ultra-precision stage as well as the proposed control approach is verified through the simulation and experiments. From the results, the stick-slip phenomenon due to the Stribech and static friction was compensated. Moreover, it can be confirmed that the MPC system is quickly track to the reference due to the multi-step ahead prediction and the receding horizon strategy. As a result, a positioning time was shortened by 18.5 % comparing the conventional PID control system.

Discussion and Conclusions

The robustness of the designed MPC-based control system is evaluated. In the experiments, the weighting mass is loaded to the stage□fs moving part. For the PID system, the control performance is degraded due to the weighting mass. On the contrary, the MPC system with adaptive mechanism can still attain the tracking performance. The extension ratio of the positioning time was 135 % and 107 % for the PID system and the MPC system, respectively.

In the paper, the model predictive control has been applied to the ultra-precision stage with frictional drive mechanism. Nonlinear friction compensation is firstly performed to the stage. Next, the identification and design of the MPC considering the frictional effect are investigated. The adaptation of the model predictive control is also discussed. The experiments with the linear actuator-driven stage prove the validity of the proposed design and control approach.

Tuesday Poster

P2K. Acoustic Wave Sensors

2nd and 3rd Floor Foyers

Tuesday, November 4, 2008, 3:00 pm - 4:30 pm

Chair: **Jacqueline Hines;**
Applied Sensor Research and Development Corporation, USA.

P2K100-01

Development of a new Love wave liquid sensor operating at 2GHz with an integrated micro-flow channel

Philippe Kirsch, **Badreddine Assouar,** Patrick Alnot; *Nancy University - CNRS, France.*

Background, Motivation and Objective

SAW devices based on waveguide modes with shear-horizontal polarization (Love modes) are very promising for sensor applications, especially in liquid media. They can be used for the determination of liquid density and viscosity as well as chemical sensors. A Love wave sensor is based on layer-substrate combination with the layer having a lower shear wave velocity than substrate to trap the acoustic energy near the sensitive surface. In this work we have developed a sensor based on SiO2/36°YX-LiTaO3. Our objective is to improve the sensitivity of liquid sensor based on Love wave propagation. Up to now, several systems have been reported based on Love modes operating at low frequencies, up to hundreds of MHz*. To reach maximum sensitivity, the operating frequency of the sensor should be higher.

Tuesday Poster

Statement of Contribution/Methods

We present here the realization of the 2GHz operating frequency sensor, using electron beam lithography to realize the submicronic interdigital transducers (IDTs). The IDTs have a special design allowing the interfacing of submicronic fingers (width of 500nm) of IDTs with contacting pads for frequency measurements. The SiO2 guiding layer plays also a role of passivation and protection of IDTs against chemicals species in liquid. We have used an integrated micro flow channel derived from the commonly found flow cell. The micro flow channel having a width of 300µm is realized in a silicone polymer (PDMS) stamp using a micromold. The whole sensing unit is installed inside an aluminium base which acts at the same time as mechanic protector, electric interface and hydraulic interface.

Results

The frequency characterisation of realized sensor before the interaction with liquid has exhibited an interaction between the electromagnetic wave emitted by the contacting pads and the propagating acoustic wave. The signal processing was done to extract only the acoustic signal from the frequency response, and then to measure the sensitivity of the sensor in liquid media. Used our developed sensor operating at 2 GHz, we have carried out an alternate cycle of nitrogen and water circulating in the PDMS micro flow channel. We have measured an absolute sensitivity of -19001 Hz•mm2/ng due to the interaction of sensor with water. This sensitivity is higher than the other devices operating at lower frequencies.

Discussion and Conclusions

The mechanism detection, including gravimetric, viscous and permittivity effects at high frequency will be discussed.

References

[*]. Kondoh et al
IEEE Ultrasonics sympoium, (1996), p : 389

P2K101-02

Carbon dioxide gas sensor using SAW device based on multiwall carbon nanotubes films

Changbao Wen[1], Changchun Zhu[2], Qinghong Liu[2]; *[1]Chang'an University, China, [2]Xi'an Jiaotong University, China.*

Background, Motivation and Objective

As one of the most important green house gases and pollutants, the monitor and measure of carbon dioxide (CO2) gas has received considerable attention and widely researched.SAW sensor has high sensitive, small size and low price compared with other chemical and electrochemical techniques. For SAW sensor, the performances of SAW device itself and the properties of sensitive film determine how well the sensor performs as gas detector.

Statement of Contribution/Methods

In this paper, CO2 gas sensor using SAW device based on MWNTs was proposed. This surface acoustic wave (SAW) gas sensor with dual track and Multistrip couplers (MSC) was fabricated on 128¡ãY-X LiNbO3 piezoelectric substrate, and sensitive film of MWNTs were deposited onto the measurement track.

Results

An experiment of a SAW gas sensor coated with MWNTs films sensitive to CO2 gas is presented. Fig. 1 shows the SEM graph of mixed acid treated sample.Fig. 2 shows the internal architecture of SAW gas sensor.Experiment results confirm that the sensor has good reproducibility and response properties for different concentration CO2 gas.

Discussion and Conclusions

The dual track architecture and MSC were applied to the SAW CO2 gas sensor, which reduces the insertion loss and suppresses the BAW. The Experiment results confirm that the gas sensor has good reproducibility and response properties for different concentration CO2 gas. The sensor has excellence linearity, and its sensitivity is approximately 6.8 KHz/ppm. Moreover, the sensor can measure and monitor the CO2 gas concentration of 0.154 ppb by means of the resolution of 1Hz obtained by network analyzer, which ensures that this sensor has high sensitive, and promise for the applications in environment protected and commercial field.

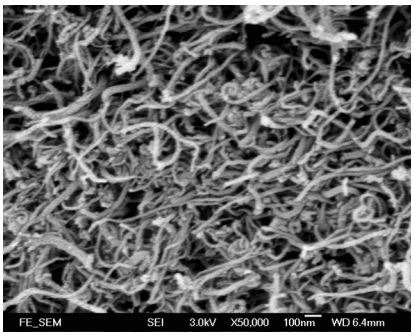

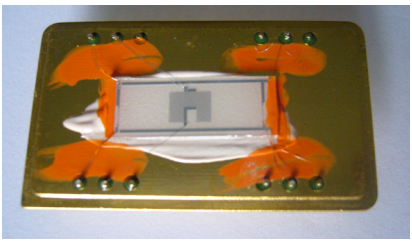

P2K102-03

SAW Gas Sensors with Carbon Nanotubes Films

Michele Penza[1], Riccardo Rossi[1], Marco Alvisi[1], Patrizia Aversa[1], Gennaro Cassano[1], Domenico Suriano[1], Massimiliano Benetti[2], Domenico Cannatà[2], Fabio Di Pietrantonio[2], **Enrico Verona[2];** *[1]ENEA, Physical Technologies and New Materials, Brindisi, Italy, [2]CNR, Institute of Acoustics "O.M. Corbino", Rome, Italy.*

Background, Motivation and Objective

Surface Acoustic Waves (SAW) are electro-acoustic highly-sensitive tools for miniaturized chemical sensors [1] in both gaseous and/or liquid environments and biosensing applications. The SAWs have a high acoustic energy-density on the top-surface of a piezoelectric substrate, thus they are very sensitive to the surface perturbations of the propagation medium; hence the SAWs are suitable probes for high-performance gas sensor applications. Since the mass sensitivity increases with the SAW resonating frequency, the use of higher frequency in SAW devices should enhance the mass sensitivity.

Statement of Contribution/Methods

Electro-acoustic Rayleigh 433 and 915 MHz two-port resonator microdevices based on SAW quartz substrate are described. A coating of nanocomposite based on carbon nanotubes films has been prepared by Langmuir-Blodgett technique onto SAW device in order to promote improved gas adsorption of the targeted organic vapors, at room temperature [2]. The results obtained demonstrate high gas sensitivity up to sub-ppm level of detection of organic solvents. The S21 curves in magnitude and phase of SAW devices are measured by a Network Analyzer and reported.

Results

In this study, nanocomposite layers (5-30 nm thick) with filler of carbon nanotubes at 10 and 50 wt.% in an organic host-matrix of cadmium arachidate have been deposited by Langmuir-Blodgett technique onto SAW quartz two-port resonators operating as differential frequency oscillators at 433 and 915 MHz, for organic vapour sensing of alcohols, acetone, m-xylene, at room temperature.

Discussion and Conclusions

The nanocomposite layers based on carbon nanotubes are widely perceived as very promising nanomaterials to develop high-performance SAW chemical nanosensors. In fact, it has been demonstrated that the carbon nanotubes, at single-walled and multi-walled format, are very attractive for detecting vapour and gas molecules in nanoscale molecular sensors [3] with high sensitivity and fast response to implement chemical nanosensor arrays of SAW devices.

[1] D. S. Ballantine, R. M. White, S. J. Martin, A. J. Ricco, E. T. Zellers, G. C. Frye, and H. Wohltjen, "Acoustic Wave Sensors," 1997 Academic Press: San Diego, USA.

[2] M. Penza, M. A. Tagliente, P. Aversa, M. Re, and G. Cassano, "Effect of purification of single-walled carbon nanotube bundles on alcohol sensitivity of nanocomposite Langmuir-Blodgett films for SAW sensing applications," Nanotechnology, vol. 18, 185502, 2007.

[3] M. Penza, G. Cassano, R. Rossi, M. Alvisi, A. Rizzo, M. A. Signore, Th. Dikonimos, E. Serra, and R. Giorgi, "Enhancement of sensitivity in gas chemiresistors based on carbon nanotube surface functionalized with noble metal (Au, Pt) nanoclusters," Appl. Phys. Lett., vol. 90, 173123, 2007.

Tuesday Poster

P2K103-04

wireless polymer-coated love-wave based chemical sensor

Wen Wang, Shitang He; *Institute of Acoustics, Chinese Academy of Sciences, Beijing, China.*

Background, Motivation and Objective

Love wave devices are of great interest for gas sensing owing to high sensitivity and IDTs protection for liquid/gaseous environment. The first purpose of this paper is to establish a theoretical model on response mechanism of polymer-coated love-wave chemical sensor considering the viscoelastic effect. Another aim is to develop a novel wireless love-wave CO_2 sensor, which utilizes a reflective delay line on ST-90^{o}X quartz, a PMMA guiding layer and a Teflon AF 2400 sensitive film.

Statement of Contribution/Methods

The PMMA film with optimal thickness was deposited by spin-coating onto the ST-90^{o}X quartz with a 440MHz SH-wave reflective delay line pattern, on which a 200nm gold IDT and three shorted grating reflectors were deposited. ~2μm Teflon AF 2400 film was brushed onto the PMMA surface between the 1st and 2nd reflectors for CO_2 sensing. The sensor signal is determined by evaluating the phase shifts of the reflection peaks monitored by network analyzer.

Results

Fig.1 shows the calculated gas response vs. guiding layer thickness for the love wave device coated different type polymer sensitive films with 2μm thick towards to 80ppm CO_2, resulting in ~2.5μm optimal PMMA thickness. The repeatability (by subjecting to four consecutive on-off exposures of 200ppm CO_2, as shown in the inlet of Fig.2) and sensitivity (8.68^o/ppm, Fig.2) of the fabricated sensor were evaluated at 25^{o}C, 1atm and 5%RH.

Discussion and Conclusions

A theoretical analysis on response mechanism on polymer coated love-wave chemical sensor was performed. The gas sensor experimental results of the fabricated wireless love wave sensor show passive, excellent repeatability, high sensitivity and good response linearity.

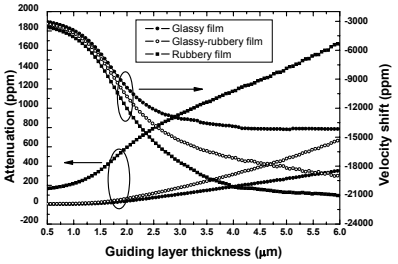

Fig.1 Gas response vs. guiding layer thickens

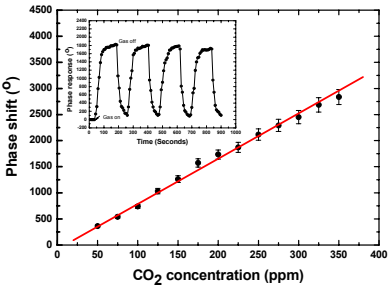

Fig.2 Repeatability (inlet) and sensitivity evaluation of the fabricated love-wave gas sensor

P2K104-05

Experimental Study on Love-wave Sensors with $SiO_2/LiTaO_3$ Structures

Feng-mei Zhou, Zhe Li, Tao Zhang, Wei Lin, Li Fan, Xun Gong, Shu-yi Zhang; *Lab of Modern Acoustics, Institute of Acoustics, Nanjing University, Nanjing 210093, China.*

Background, Motivation and Objective

It has been shown that love-wave devices are very promising for sensor applications, especially in liquid environments because of their shear horizontal propagation mode and high sensitivity. Several devices have been reported based on ST-cut quartz. But these devices are suitable for low dielectric liquids, and suffer from large attenuation in aqueous or saline environments because of the low dielectric constant of quartz. Recently, more attention has been concentrating on the devices based on 36°YX $LiTaO_3$ which exhibits a high dielectric constant. Various polymers such as polymethyl methacrylate (PMMA), polyimide, polystyrene etc. have been investigated as the guiding layers to trap the acoustic energy near the sensing surface.

Statement of Contribution/Methods

Here, we present a kind of Love wave sensors with SiO_2/36°YX $LiTaO_3$ structures for monitoring antibody-antigen immunoreactions in aqueous solutions in real time.

Results

In this study, a low loss is achieved and it is only 15 dB when the device is in direct contact with the solution at the operating frequency of 127 MHz. In the immunosensing measurements, goat anti human-immuno-globulin G (HigG) is immobilized on the device surface as a receptor layer for detecting HigG in buffer solution. The frequency shift of 10 KHz can be obtained in 30 min and 13.7 KHz can be obtained in 60 min at a HigG concentration of 100 μg/ml in buffer solution (static cell) as shown in Fig.1.

Discussion and Conclusions

It is demonstrated that this sensor system should be applicable for biosensing and chemical sensing applications in liquid environments. Further studies for improving the sensitivity are in progress.

This work is supported by National Natural Science Foundation of China, No. 10774074.

Tuesday Poster

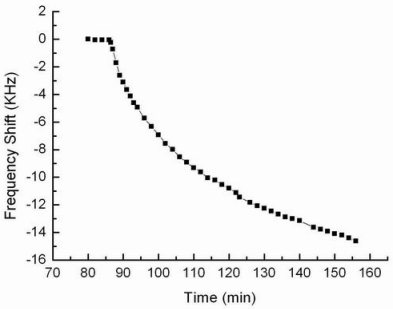

Fig. 1 Frequency response of Love wave sensor to 100 μg/ml HigG in buffer solution

P2K105-06

Simulation of Wireless Passive SAW Sensors Based on FEM/BEM Model

Dongxiang Zhou, Wei Luo, Yi Wang, Jianling Wang, Qiuyun Fu; *Department of Electronic Science and Technology, Huazhong University of Science and Technology, Wuhan, Hubei, China..*

Tuesday Poster

Background, Motivation and Objective

The Wireless passive surface acoustic wave (SAW) impedance-loaded sensors are introduced for remote monitoring and controlling recently for they have many outstanding properties. Coupling-of-modes (COM) model is the classical simulation model in devices optimizing design process for its flexibility and relative accuracy. However, it¡¯s no more rigorous for these impedance-loaded sensors since they usually work in the RF band. We present a new simulation method for the impedance-loaded SAW sensors based on a numerical combined finite element method and boundary element method (FEM/BEM) model.

Statement of Contribution/Methods

The key point of the task is the simulation of the SAW transponder which consists of one transmitting/receiving interdigital transducer (IDT) and one or more programmable reflectors. One reflector is connected to the outside conventional sensors and the others are used as reference. A numerical combined FEM/BEM model is used frequently to simulate SAW IDT recently for its high accuracy. In this paper, we try to make the simulation results more accurate by using FEM/BEM model to determine some key parameters used in the COM model of impedance-loaded SAW sensors. We use a finite element method to account for the mass loading effect of electrodes and use a Green¡¯s function to model the piezoelectric substrate.

Results

After solving the system of equations, the harmonic admittance curve and the dispersion curves of the grating can be described and the COM parameters can be calculated. The dispersion curves calculated by another method FEMSDA proposed by Kenya Hashimoto are also given for comparison. After calculating the admittance matrix of the transponder using FEM/BEM model, the response of the entire SAW chip with one programmable reflector is simulated in Fig.1.

Discussion and Conclusions

Comparison between the two kinds of dispersion curves shows there are only a little differences between them. We explain the reason from the point of physical principle. Comparison between simulations and measurements on real SAW devices shows good agreement and proofs the effectiveness of the developed simulation tool.

Due to the fact that the FEM/BEM model does not make any a priori assumptions concerning crystal cuts and/or wave types employed in the simulated device, it is widely applicable.

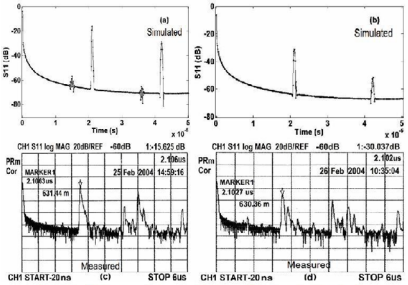

Fig.1 Simulated (a, b) and measured (c, d) results in time domain (when the programmable reflector is open (a, c) and shorted (b, d))

P2K106-07

Detection of dangerous gases in disturbing gases using ball SAW gas chromatograph

Masanori Sakuma[1], Toshihiro Tsuji[1], Kentaro Kobari[1], Shingo Akao[2], Kazuhiro Noguchi[1], Noritaka Nakaso[3], Kazushi Yamanaka[1]; *[1]Tohoku University, JST,CREST, Japan, [2]Toppan Printing Co. Ltd,Tohoku University, JST,CREST, Japan, [3]Toppan Printing Co. Ltd, Japan.*

Background, Motivation and Objective

In environment and security, it is needed to detect a wide variety of dangerous gases hidden in disturbing gases. The gas chromatography (GC) can separate and detect many gases, but compact and high performance system has not been established. In this situation, we have developed the ball SAW sensor and realized precise measurement of delay time and amplitude. By combining a micro electromechanical systems (MEMS) separation column and a ball SAW sensor, we proposed high-performance micro GC. In this study, we applied it to detection of a nerve gas simulant among disturbing gases.

Statement of Contribution/Methods

We used a 3.3mm across langasite (LGS) ball SAW sensor with poly-isobthylene (PIB) sensitive film. A mixture of dimethylmetylphosphonate (DMMP), buthanol and decane was used as the sample, where DMMP was used as simulant of a nerve gas saline. The MEMS column and the ball SAW sensor were installed nto a table-top GC oven. Injected and gasified sample was separated into each constituent by the MEMS column, and then detected by the ball SAW sensor. A thermal conductivity detector (TCD) was used for an additional detector, and was compared to the ball SAW sensor.

Results

DMMP was separated from disturbing gases, and we obtained the delay time and amplitude responses for each constituent with a good signal to noise ratio (S/N) as shown in Figure 1.

Discussion and Conclusions

It was found that peak height of ball SAW sensor responses increased with increasing molecular weight in contrast to that of the TCD. Consequently, dangerous gasses with larger molecular weight are expected to be advantageous targets for ball SAW GC. Thus, examination of mixture of larger number of gases is feasible.

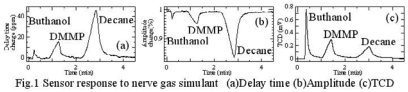

Fig.1 Sensor response to nerve gas simulant (a)Delay time (b)Amplitude (c)TCD

P2K107-08

Development of a Calibration Procedure for Torque and Temperature Sensors Based on SAW Resonators

Victor Kalinin, Raymond Lohr, Arthur Leigh; *Transense Technologies plc, United Kingdom.*

Background, Motivation and Objective

Contactless sensors employing SAW resonators positioned on either rotating shafts or disks have proven to provide a high accuracy of measurements of temperature compensated torque. They have demonstrated a potential for high volume applications, e.g. in automotive industry for measuring torque in a vehicle's powertrain. However, SAW

Tuesday Poster

sensors require an individual calibration over the entire automotive temperature range and this process noticeably increases their cost. The aims of this paper are to consider possible ways of reducing complexity of the calibration and develop a procedure viable for high-volume applications.

Statement of Contribution/Methods

A spread of calibration characteristics of the 433 MHz SAW torque and temperature sensors is investigated at various stages of manufacturing. It is established that a high accuracy of torque measurement (better than 1% FS) can only be achieved if every sensor is calibrated at nine to six temperature points from –40° to +125°C. This process takes up to 20 hours and requires a lot of energy. The first way of reducing time and energy spending is to use a fast temperature ramp instead of slow steady-state measurements. Investigation of dynamic temperature characteristics has shown that they differ from the static characteristics in an unpredictable way by up to 20…30 kHz which introduces unacceptably large torque measurement errors up to 5% FS and temperature errors up to 15°C peak-to-peak.

The second approach is to reduce the number of temperature calibration points to a minimum. The proposed procedure requires first finding a set of generic calibration parameters for a particular type of the SAW torque sensor by averaging a sufficiently large number of individual sensor characteristics. After that each individual sensor is calibrated either just at one point (room temperature) or at two points (room temperature and nominal operating engine temperature). The information obtained is used to adjust the generic calibration parameters for each individual sensor.

Results

Statistical analysis has shown that one-point calibration gives large torque measurement errors at the nominal operating temperature of 90°C up to ±4.5% FS. However, two-point calibration gives acceptable torque measurement errors, less than 1% FS within a wide range of temperatures from 0° to 110°C.

Discussion and Conclusions

The latter approach can be regarded as a basis for development of a calibration procedure for high-volume applications.

Tuesday Poster

P2K108-09

Assessment of Fatigue Damage in Solid Plates Using Ultrasonic Lamb Wave Spectra

Junfeng Pei, **Mingxi Deng;** *Department of Physics, Logistics Engineering University, Chongqing, China.*

Background, Motivation and Objective

Lamb waves have shown great potential for structural health monitoring. Changes in the properties of a solid plate (including elastic constants, mass density and thickness, etc), induced by fatigue damage, will influence the features of lamb wave propagation such as dispersion, amplitude and attenuation. In the case of early stages of fatigue damage in solid plates, the relative change in the properties of solid plates will be insignificant. Thus, it has difficulty in the effective assessment of fatigue damage in solid plates by conventional ultrasonic lamb wave techniques (i.e. low-order Lamb mode approach).

Statement of Contribution/Methods

Based on some numerical simulations on Lamb wave propagation, it is found that higher modes of Lamb wave propagation show more sensitivity than lower modes of Lamb wave propagation for the same relative changes in the properties of solid plates. In general, for a given Lamb wave mode, the tendency of change in the features of Lamb wave propagation (with the relative changes in the properties of solid plates) is not monotonic. Thus, Lamb wave spectra (amplitude spectra versus frequency and phase velocity) may have a potential for comprehensively understanding the influences of the relative changes in the properties of solid plates on the features of Lamb waves. The possible influences of fatigue damage in solid plates on the features of Lamb wave propagation were analyzed, and the feasibility of using ultrasonic lamb wave spectra to assess fatigue damage in solid plates was discussed.

Results

For a given aluminum (2024-T3) sheet, the amplitude-frequency curves of before and after cyclic loading (the number of cyclic loading was in the early stage of fatigue life) were measured with the established experimental set-up for ultrasonic Lamb wave spectra. Based on the data measured, the ultrasonic lamb wave spectra diagrams were established. Changes in the ultrasonic lamb wave spectra diagrams were comparatively studied for the two cases before and after cyclic loading. Clear difference between the two spectra diagrams, consistent with numerical simulations, could be found.

Discussion and Conclusions

Based on the experimental results and theoretical considerations, it is concluded that ultrasonic lamb wave spectra may be used to effectively assess the early stages of fatigue damage in solid plates.

P2K109-10

A Novel Ultrasonic Sensing Based Human Face Recognition

Zhenwei Miao, Wei Ji, Yong Xu, Jun Yang; *Institute of Acoustics, Chinese Academy of Sciences, China.*

Background, Motivation and Objective

Human face recognition has been an active research area in the last two decades with advantages of being non-intrusive and well accepted by users. In current face recognition systems, variations of illumination, pose and facial expression etc. tend to deteriorate performance. Many efforts have been made to improve the recognition rate, but the face recognition in an uncontrolled environment is still a challenging problem.

In 1995, Dror et al. has proposed an active ultrasound sensing technology to recognize human face by using a sonar neural network. The face recognition rate was 81% when recognizing six different faces in his experiment. Recently, McKerrow et al. studied the mapping relationship of human facial feature and its ultrasonic echoes emitting and receiving in front of that face. The classification result was good with a small database (10 faces) without analyzing the disturbance of echoes reflecting off other parts beside the faces.

The aim of our work is to develop a robust ultrasonic sensing-based face recognition system free of the lighting conditions, and then design and set up a large and accurate database to verify the system performance.

Statement of Contribution/Methods

This paper presents a novel ultrasonic sensing based face recognition system, which can complement traditional vision-based recognition due to its unobtrusiveness, low-cost and robust to environmental conditions. For different configurations of Transmitter-Receiver (TR) pairs, ultrasonic chirp signal is chosen as the transmitted signal and demodulated with the echo for face recognition.

Effective feature extraction algorithms are proposed for improving classification rate of human faces. A large database was collected in a carefully designed experiment, which was adopted to verify the recognition performance. This database covered 110 individuals consisting of 55 females and 55 males with different ages and occupations. Videos and pictures of the subject were also obtained while the ultrasonic echoes were recording for the further analysis of information.

Results

By optimizing and improving the classifier and the feature extract methods, the present ultrasonic face recognition system can achieve an average correct rate of over 90% when classifying 110 different faces using one TR pair. Moreover, the maximum classification rate can reach 99% in the case of ultrasonic transmitters angled with multi-directions toward the human face in the experiment.

Discussion and Conclusions

Based on the ultrasonic sensing technique, the developed human face recognition system could achieve a high recognition rate by using effective feature extraction algorithms and proper configurations of TR pairs. The experimental results show that the proposed ultrasonic face recognition has potential usage in the automatic face recognition.

P2K110-11

Rayleigh Wave Propagating in Layered Magneto-electro-elastic Material Structure

Jianke Du, Xiaoyu Cheng, Ji Wang; *Ningbo University, China.*

Background, Motivation and Objective

It is well known that numerous investigations have been undertaken for the characteristic analysis of Rayleigh waves in piezoelectric media. The magneto-electric effect in composite structures consisting of a piezoelectric phase and a piezomagnetic phase exhibit magneto-electric effect that is not present in single-phase piezoelectric or piezomagnetic materials. The coupling nature of piezoelectric phase and piezomagnetic phase has led to wide applications in adaptive material systems, and they are extensively used as sensors, actuators, acoustic devices, and transducers. The development of micro-acoustic sensors in biosensing and chemical sensing fields provide the need for further investigations of the Rayleigh wave propagation in layered magneto-electro-elastic structure, where an

elastic substrate is covered with a thin magneto-electro-elastic layer. A number of acoustic wave modes have been utilized for various sensor applications.

Statement of Contribution/Methods

In this paper, an analytical approach is taken to investigate Rayleigh wave propagating in layered magneto-electro-elastic structure where a thin layer bonded to a semi-infinite elastic substrate. The governing equations of the Rayleigh waves can be obtained on the basis of the linearly magneto-electro-elastic theory. The displacements, electric potential, magnetic potential, stresses, electric displacement, and magnetic induction are continuous across the interface of the thin layer and the substrate together with the traction free and the magneto-electrically open and short conditions on the surface of the structure.

Results

The analytical solution of dispersion relations are obtained for mechanical and magneto-electrical boundary conditions for the composite material thin layer of BaTiO3 and CoFe2O4. The phase velocity is calculated and figured. The distributions of the displacements, electrical potential and magnetic potential are also investigated and figured. The effect of the piezoelectric, piezomagnetic coefficients and the magneto-electric coefficient on the properties of the Rayleigh waves is discussed in detail.

Discussion and Conclusions

It can be seen from the results that the piezoelectric and piezomagnetic coefficients have significant effect on the phase velocity, on the distributions of displacements, electric potential and magnetic potential of Rayleigh waves. The phase velocity augments with increase of the piezoelectric coefficient, and decreases with increase of the piezomagnetic coefficient. The magneto-electric coefficient has also effect on the phase velocity of Rayleigh waves. The results can be helpful for the design of the piezoelectric/piezomagnetic sensors or resonators.

Tuesday Poster

P2K111-12

New measurement method to characterize piezoelectric SAW substrates at very high temperature

Pascal Nicolay, **Omar Elmazria,** Frederic Sarry, Thierry Aubert, Laurent Bouvot; *Nancy University - CNRS, Laboratoire de Physique des Milieux ionisés et Applications (LPMIA) UMR 7040, Vandoeuvre les Nancy, France.*

Background, Motivation and Objective

SAW devices are a very promising solution for high temperature sensing. Among the materials of interest for such application, let's highlight Langasite (LGS) and GaPO4 but also several promising structures such as AlN/Sapphire or GaN/Sapphire. Experiments have been carried out in order to study their behavior at high temperature. Temperatures as high as 750°C have been reached [1]. The measurement method commonly employed consists in settling a complete temperature-proof SAW device (with all its circuitry) in an oven. This is a very difficult task because each part of the system (structure, coaxial cables, 50-ohm coplanar transmission line, wire bonds, metal InterDigital Transducers (IDT) and substrate) must be able to sustain high temperature. One of the main limitations comes from the maximal temperature before failure of the special coaxial feed-lines, which is hardly higher than 1000°C. This temperature therefore becomes the critical threshold to overtake. In this paper, we propose a radically new measurement method to study the characteristics of SAW sensors above 1000 °C.

Statement of Contribution/Methods

The new method consists in hanging a small piece of self-warming piezoelectric SAW device in a vacuum chamber. The device is made of the piezoelectric material to be tested equipped with its IDT plus a heating resistance, both in Platinum. The whole system is suspended from a PCB by mean of classical gold bonding wires. It is therefore thermally isolated from the rest of the experimental set-up. This allows using standard low-cost circuitry, to connect the SAW device to the measurement apparatus (standard coaxial feed-lines and SMA connectors). The warming being localised on the piezoelectric substrate, it also becomes possible to reach very high temperature, quickly and at low energy cost. This allows easy making of temperature cycles to test the aging of materials.

Results

In a first step, TCF values for Quartz ST and LiNbO3 Y-128° were measured in the range [20-500 °C], then compared to calculated ones. Because the obtained results were in good agreement, it was possible to validate the above-proposed test method. In a second step, one LGS Y-X SAW Delay-Line with Pt/Ta IDT was characterized using this test method, in the range [20-1000 °C]. The obtained 'center frequency vs. temperature' curve starts shifting from the calculated one above 250°C. This could be due to the relative inaccuracy of the available sets of temperature coefficients for the LGS elastics constants. A complete discussion on this topic is given in the paper.

Discussion and Conclusions

To summarize, we designed and successfully tested a new simple solution to characterize piezoelectric substrates in a temperature range beyond 1000°C. That method is a powerful new tool for the study and the development of innovative various types of high temperature SAW sensors.

References

[1] J.A. Thiele et al., IEEE Trans. UFFC, Vol. 52, N°4, April 2005

P2K112-13

A single transformer-based electrical impedance matching technique with load capacitance cancellation for ultrasound transducers

Sai Chun Tang, Gregory Clement; *Harvard Medical School / Brigham and Women's Hospital, Radiology, Boston, MA, USA.*

Background, Motivation and Objective

Electrical impedance matching is almost universally used for power transfer optimization in ultrasound transducer driving systems. Traditionally, a transformer-based impedance matching can only match the transducer impedance magnitude to the desired value, an additional reactive component connected in parallel to the secondary side is required to compensate the load capacitance. This configuration represents an additional cost, and an increase in size and weight to the ultrasound system. In this paper, a cost-effective impedance matching means for ultrasound transducers is presented.

Statement of Contribution/Methods

The proposed method uses a single transformer with adjustable magnetizing inductance and appropriate turns-ratio to match both the magnitude and phase of a transducer load to the desired values. In this study, a 10mm×15mm 1.5MHz piezoelectric planar transducer with impedance magnitude and phase of 284 Ohm and -60° was matched to 50 Ohm and 0° using the proposed method and a traditional LC matching circuit for comparison. Small signal and operating power condition tests for both methods were performed.

Results

In the small signal tests, experimental results show that both methods can match the transducer to the required impedance with an error of less than 5% in magnitude and 2° in phase. In the operation power condition tests, with input power from 1W to 15W, the gain variation of the transformer-based matching circuit was found to be 4.9 times less than that using the LC circuit (Fig. 1). The phase shift of the transformer gain was less than 2°, while the LC circuit shift was between -80° and -72° (Fig. 2).

Discussion and Conclusions

The study demonstrates a stable matching circuit with negligible phase shift that can be accomplished by a single transformer without additional components.

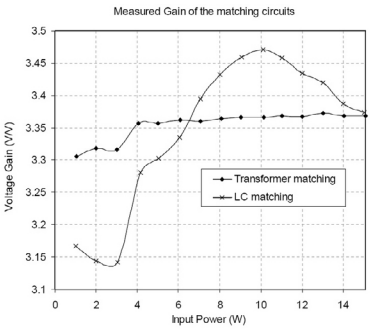

Fig. 1 Measured voltage gain of the transformer and the LC matching circuits versus input power.

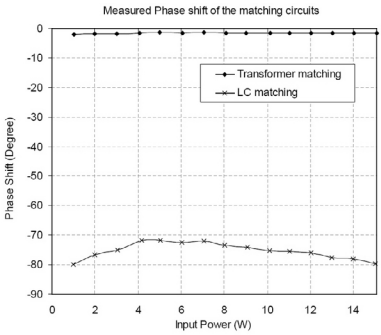

Fig. 2 Measured phase shift of the transformer and the LC matching circuits versus input power.

P2L. Acoustical Imaging and Signal Processing

2nd and 3rd Floor Foyers

Tuesday, November 4, 2008, 3:00 pm - 4:30 pm

Chair: **Erdal Oruklu;**
Illinois Institute of Technology, IL, USA.

P2L113-01

A Reconfigurable System for Subband Decomposition Algorithms in Ultrasonic Detection Applications

Erdal Oruklu, Joshua Weber, Jafar Saniie; *Illinois Institute of Technology, Electrical and Computer Engineering, Chicago, IL, USA.*

Tuesday Poster

Background, Motivation and Objective

Ultrasonic target (flaw) detection system has applications in many industries ranging from manufacturing to maintenance of materials. To achieve target detection, high scattering noise (clutter) echoes must be suppressed by signal processing methods. In addition, real-time requirements place tight constraints on computation time and increase the communication bandwidth needs for the capture, processing, analysis, and presentation of data. Due to these challenges, it is not feasible to implement a real-time, portable ultrasonic imaging device using conventional signal processing systems.

Statement of Contribution/Methods

In this paper, we present an FPGA based real-time reconfigurable architecture and the accompanying application software to perform frequency-diverse target detection using subband decomposition. The subband decomposition contains many parameters (such as number of subband filters, filter bandwidths and frequency range) that strongly impact its performance with different data sets. Through the configurable implementation the changes in parameters can be realized during run-time application. This allows the configuration of the FPGA for multiple subband decomposition methods including FFT, DCT, WHT and DWT transforms without any redundant hardware logic for different experimentation setups. The ultrasonic detection system was realized using Xilinx Virtex-4 FPGA and the software C code running on an embedded 32-bit RISC CPU with accelerator IP-cores for each transform method.

Results

The flaw detection algorithm performs robustly and an average of 10dB flaw echo visibility improvement is achieved based on experimental data sets. The reconfigurable hardware architecture meets real-time operation timing requirements and the ultrasonic system is capable of using transducers with up to 20MHz center frequency for real-time imaging applications.

Discussion and Conclusions

In this study, a reconfigurable hardware implementation of subband signal decomposition with application to real-time ultrasonic imaging system is presented. The selection of the subband decomposition transforms has a large impact on its overall detection performance. With this in mind, a modular architecture has been designed. The hardware implementation improves the execution time of the software implementation by almost 1000 times. Furthermore, the modular architecture presented in this paper is a valuable research tool and it can be used to fully explore the performance of the flaw detection algorithm through parameter changes. It also provides a hardware framework for experimenting with new subband decomposition algorithms.

P2L114-02

A New Lossy Compression Algorithm for Ultra-Sound Signals

Miguel Freitas[1], Henrique dos Santos[1], Marcelo Jimenez[1], Claudio Camerini[2], Jean Pierre von der Weid[1]; *[1]Pontifical Catholic University of Rio de Janeiro, Inspection Technology Research Centre, Rio de Janeiro, RJ, Brazil, [2]Petrobras, CENPES, Brazil.*

Background, Motivation and Objective

Many types of equipment that use ultra-sound signals for NDT use embedded data acquisition systems that must stay off-line acquiring data for a long time, need an efficient compression algorithm to save the acquired data. Lossy compression algorithms benefit from the fact that they are able to achieve much higher compression ratios than their lossless counterparts. Ultra-sound applications may allow the use of lossy compression algorithms, as long as some characteristics of interest of the original signal are preserved. The objective of this work is to present a new Constant Bit Rate (CBR) compression algorithm in order to achieve full A-scan recording in devices that are both space and resource limited. Field programmable gate arrays (FPGAs) have become a popular way to implement filtering and compression due to its great logic density and versatility [1], and the present algorithm is simple enough to be implemented even on lower-end FPGAs

Statement of Contribution/Methods

The new method consists in giving priority to store the largest variations over the smaller ones found in the original wave. This has a side effect of cleaning the signal from low amplitude noise.

Results

The most important features of the ultra-sound signal are preserved in compression rates 1:10 or 1:20, specially the echoes' peak positions, as seen in the figure. The algorithm can be easily implemented on lower-end FPGAs using a simple pipelined architecture. The two-phase design operates in real-time speed. Depending on the relative amplitude of the signals, even higher compression ratios can be achieved while keeping the signal usability for later analysis

Discussion and Conclusions

Preserving the signal's peak position and at the same time achieving high compression ratios is the top feature of this algorithm. Comparison with existing compression techniques targeted for FPGA implementation [1] is provided, showing that the proposed algorithm can achieve better signal representation for the same compression rate.

[1] A Full Featured Ultrasound NDE System in a Standard FPGA, C. Fritsch, J. Camacho, A. Ibañez, J. Brizuela, R. Giacchetta, R. González - ECNDT 2006

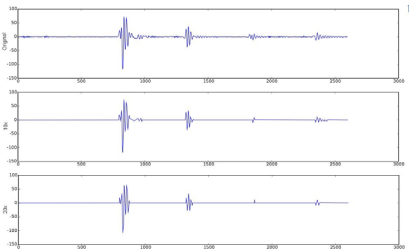

P2L115-03

Resolution Improvement of Shallow Underground Imaging Using Super-Magnetstriction Vibrator and Pulse Compression Method

Tsuneyoshi Sugimoto, Hiraku Kawasaki; *Toin University of Yokohama, Electronics and Information Engineering, Yokohama, Japan.*

Background, Motivation and Objective

To detect buried relics and ruins at shallow depths, a ground-penetrating radar(GPR) has been widely used. However, electromagnetic signals are strongly attenuated by the presence of water and electrolytes. Therefore, underground imaging using shear waves has been proposed. In our past research, a hammer method was used to make shear waves, but the axial resolution(about 0.5m) was difficult to improve.

Statement of Contribution/Methods

In this report, we newly introduce a shear sound source using super-magnetstriction vibrator and pulse compression method for improving axial resolution. A super-magnetstriction vibrator can change the frequency and the waveform easily at low frequencies(0 to 3kHz). Utilize this feature, pulse compression method is applied. We employ chirp signals applied by a window function for smooth movement of the vibrator.

Results

From the simulation results, when Δf(the difference between start and stop frequency) is more than 700Hz, axial resolution become under 0.2m. To confirm this result, exploration experiments are carried out. The buried object is hollow plastic container (0.13Wx0.12Dx0.05H) and buried at 0.5m depth. A down chirp wave (800-300Hz, duration 100ms) is used. Compared with underground images of hammer method and pulse compression method, we confirmed that the image by the pulse compression is much higher resolution than that of by the hammer method and axial resolution is about 0.2m which is almost same as the result of the simulation results.

Discussion and Conclusions

We confirmed that the validity of the pulse compression method for resolution improvement of underground image.We will improve the lateral resolution using dynamic focusing technique.

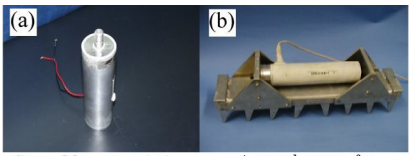

Super-Magnetostriction Vibrator

A sound source for shear waves

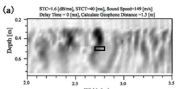

Using pulse compression method (800-300Hz down chirp, duration 100ms)

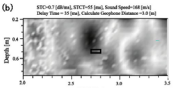

Using hammer method Boundary rectangle is a buried object.

Tuesday Poster

P2L116-04

Non-contact Observation of Cultured Cells by Acoustic Impedance Microscope

Aiko Nakano[1], Naohiro Hozumi[1], Masayuki Nagao[2], Sachiko Yoshida[2], Kazuto Kobayashi[3], Seiji Yamamoto[4], Yoshifumi Saijo[5]; *[1]Aichi Institute of Technology, Japan, [2]Toyohashi University of Technology, Japan, [3]Honda Electronics Co. Ltd., Japan, [4]Hamamatsu University School of Medicine, Japan, [5]Tohoku University, Japan.*

Background, Motivation and Objective

We are proposing an acoustic microscope for imaging cross sectional acoustic impedance of biological tissues. A focused acoustic beam is transmitted to the object placed on the "rear surface" of a plastic substrate. By scanning the focal point on the surface, a 2-D reflection intensity profile is obtained. A reference material is observed under the same condition. The reflection is interpreted into characteristic acoustic impedance. This presentation deals with a new system with a high resolution for observing cultured cells.

Statement of Contribution/Methods

A pulse voltage was applied to a ceramic transducer with a sapphire rod. The frequency range of the acoustic wave was 100 - 400 MHz. Fig. 1 shows the alignment for observation. A plastic film of 50 μm in thickness was pasted to the bottom of a dish with a small hole. Rat-derived glial (astrocyte) cells were cultured on the film. The same type of dish was filled with pure water and observed as the reference. The reflection was converted into local acoustic impedance at the focal spot.

Results

Figure 2 shows the acoustic impedance image. The distance between adjacent pixels was 2 μm, however, the diameter of the focal spot would be as large as 3 - 4 micrometers. The image reveals the morphological features of astrocyte. The acoustic impedance of the cells, calibrated by assuming vertical incidence, was 1.50 - 1.65 MNs/m3.

Discussion and Conclusions

Their exact value for acoustic impedance might be lower, because the angle of focusing was large. Its compensation by considering oblique incidence, as well as quantitative comparison with glioma cells, will be demonstrated in the session. This method is believed to be useful for observing cultured cells without direct contact.

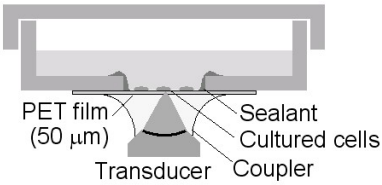

Fig. 1 Alignment for observation.

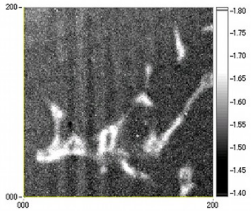

Fig. 2 Acoustic impedance images of glial cells indicated in MNs/m^3. 400 x 400 micrometers.

P2L117-05

A virtual instrument based in a digital signal processed ultrasound for measure void fraction in an upward air-water two-phase flow

Milton Nishida, João Paulo Massignan, **Rafael Daciuk,** Flavio Neves Jr, Lucia Arruda; *UTFPR, CPGEI, Curitiba, PR, Brazil.*

Background, Motivation and Objective

Two-phase flows are very common in the petroleum, chemical and nuclear industries, often involving harsh media, access difficulties and aggressive surroundings. Mainly in the oil industry there is a need to characterize and measure the dispersed phase holdup in two-phase flows using noninvasive techniques, as in testing centrifugal submerse pumps in several flow conditions. Measuring void fraction up to 13% is difficult and the methods studied in bibliography are limited to bubbly flows with lower void fractions. To solve this limitation a virtual instrument (VI) based on artificial neural networks (ANN) and parameters provided by ultrasound digital signal processing is proposed.

Statement of Contribution/Methods

The data was acquired in a laboratory test rig with air-water vertical upward flows in a 54-mm inner diameter acrylic pipe. A processing/acquisition system was built with pulse repetition rate of 8450 pulses per second and sample rate of 20 Msps at 12 bits resolution. Previous studies used only some characteristics of ultrasound signal in time dominium without processing, like maximum amplitude. This approach works well in bubbly flows but is limited to flows with 0% to 13% range void fraction. Hence the use of normalized broadband ultrasound attenuation (nBUA) and normalization against the value of the first negative peak with other signal characteristics into an ANN is proposed to solve this limitation problem. Broadband ultrasound attenuation (BUA) is a clinically-accepted measurement for osteoporosis diagnosis. Osteoporosis and increase of air in water cases are similar, thus nBUA works as well in a two-phase flow as in osteoporosis diagnosis. The first negative peak is less influenced by the two-phase flow. After the normalization, it is observed that the signal is stretched in the y-axis direction as the void fraction increases. Also the difference between maximum and minimum signal value has a linear behavior. These parameters together with others, like maximum signal amplitude or energy, are used to train an ANN to classify the void fraction.

Results

The raw data is processed to calculate the nBUA and then normalized against the first negative peak. The nBUA has a linear behavior compared to the void fraction up to 13%. Also the normalization has a linear behavior compared to the void fraction up to 16%. Both parameters and other characteristics of the ultrasonic wave were used to train the ANN. This approach improves the ANN performance in flows up to 8% and increases the range up to 13%.

Discussion and Conclusions

Two new parameters of the ultrasonic wave were proposed. These parameters have linear behavior compared to the void fraction up to 13%. The ANN trained with these new parameters increased the range for void fraction classification.

The ANN together with ultrasound processing is a practical virtual instrument that will be embedded in the hardware developed to classify the void fraction in submerse centrifugal pumps testing.

P2M. NDE Methods

2nd and 3rd Floor Foyers

Tuesday, November 4, 2008, 3:00 pm - 4:30 pm

Chair: **Kentaro Nakamura;**
Tokyo Institute of Technology, Japan.

P2M118-01

Study on feasibility of pressure pipe NDT based on ultrasonic guided wave

Li hua Shen, Yue min Wang, Feng rui Sun; *Naval Universtiy of Engineering, Wuhan, Hubei, China.*

Background, Motivation and Objective

For the efficient long-range non-destructive health examination of pipes, ultrasonic guided wave NDT has been widely used. The objective of the research presented is to investigate the feasibility of detecting flaws in pressure pipe using ultrasonic guided wave NDT technology based on magnetostrictive effect.

Statement of Contribution/Methods

A given pressure steel pipe is inspected respectively using magnetostrictive ultrasonic guided wave NDT system when it bears different pressure supplied by an air compressor. One artificial flaw is manufactured to simulate corrosion pit in the pipe. For this pipe, the guided wave dispersive curves of phase and group velocity are calculated in order to select the best exciting frequencies. Then the longitudinal mode guided waves of different frequencies, which are selected with the guidance of calculated curves, are excited in the given pipe. The ultrasonic guided wave reflects with the defect and pipe ends. Similar to ultrasonic guided wave¡¯s generation, the reflected guided wave signals are detected by magnetostrictive guided wave transducer.

Results

The echo signals, detected when the pipe bears different pressure, are investigated in detail. When the exciting frequency is at 20kHz, the dispersive phenomena of received signal waveforms is faintest. This result agrees with the calculated dispersive curves very well. Because there is only one longitudinal mode L(0, 1) existed and the slope of this curve tends toward zero at 20kHz in the dispersive curves. Compared with the signals received in the pipe at atmospheric pressure, the amplitudes of the guided wave signal attenuate rapidly at high pressure. And the reflected signals of simulated corrosion pit and pipe end can be distinguished obviously. One received signal waveform, when the air pressure inside pipe is 2.0Mpa, is shown in Fig. a.

Discussion and Conclusions

It is concluded that propagation of ultrasonic guided wave in pipe is affected by the pressure. And the attenuation of guided wave increases because of wave energy¡¯s leakage to the high-pressure air. The success of detecting the signal reflected from simulated corrosion pit demonstrates that it is feasible to inspect the defect in the pressure pipe using ultrasonic guided wave NDT technology.

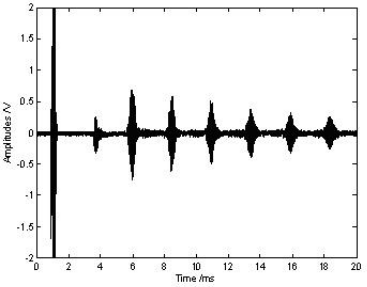

Tuesday Poster

P2M119-02

Laser-generated Surface acoustic waves for detection of surface-breaking defects based on two-wave mixing interferometers

Gang Yan[1], Jian Lu[2], Zhonghua Shen[3], Xiaowu Ni[3]; *[1]Nanjing University of Posts and Telecommunications, College of Mathematics and Physics, Nanjing, Jiangsu, China, [2]Nanjing University of Science and Technology, Department of Applied Physics, China, [3]Nanjing University of Science and Technology, China.*

Background, Motivation and Objective

In many ultrasonic methods, Surface acoustic waves (SAW) are particurly suitable for characterization of defects at the free surface of a specimen. SAW can be adopted to detect surface-breaking defects and are therefore of interest in nondestructive evaluation.The scanning laser line source (SLLS) technique is a novel laser-based inspection method for the ultrasonic detection of small surface-breaking defects. It has provided enhanced signal-to-noise performance compared to the traditional pitch-catch or pulse-echo ultrasonic methods.In recent years, a number of adaptive interferometers have been used for the remote detection of laser-generated ultrasonic waves. One type of adaptive interferometer uses two-wave mixing in a photorefractive material to form a real-time hologram, or adaptive beamsplitter. In this paper, we describe such an interferometric receiver based on two-wave mixing in photorefractive (PR) polymers. The PR polymers have a number of very promising technical features for this application.

Statement of Contribution/Methods

The interaction of surface acoustic waves (SAW) with the surface-breaking defects has been experimentally studied. The SAW were excited by employing a pulsed Nd:YAG laser on aluminum plate with artificial surface-breaking defects, and were detected by a laser interferometer based on two-wave mixing in photorefractive polymers. In this paper, the laser line source was accurately shifted by the motorized precision translation stages. When the laser line source was scanning over the defect, the amplitude and frequency changes of the ultrasound were monitored.

Results

In the far region of the defects, we attained the characteristics of reflected surface wave and transmitted wave generated by SAW interacted with the surface-breaking defects. The position of the defects could be confirmed by the arrival times of the direct surface acoustic wave and the reflected surface wave. However, in the near region of the defects, some kinds of surface wave modes overlapped and ultrasound mode conversion took place caused by the defects scattering. The amplitude and frequency characteristic of the surface wave signals varied obviously.

Discussion and Conclusions

The results will offer a detection method for the non-destructive evaluation of the small surface-breaking defects on metal by laser generated SAW and give convincing experimental evidence for the interaction mechanism between the SAW and the surface-breaking defects.

P2M120-03

Ultrasonic and optical characterization of forming colloidal films

Timo Karppinen[1], Heikki Pajari[2], Jonne Haapalainen[1], Ivan Kassamakov[3], Edward Hæggström[1]; *[1]University of Helsinki, Department of Physics, Helsinki, Finland, [2]Oy Keskuslaboratorio - Centrallaboratorium Ab, Espoo, Finland, [3]Helsinki Institute of Physics, Helsinki, Finland.*

Background, Motivation and Objective

In order to enhance the printing properties it is usual to coat paper with a colloidal suspension of mineral pigments, binders and water. This coating color is applied onto the paper web after that the surplus water is removed with intense heating. During water removal the coating color consolidates from a flowing suspension to a solid layer. The mechanisms for the consolidation of colloidal suspensions are not adequately characterized due to the lack of viable experimental techniques.

Statement of Contribution/Methods

We contributed to this question by combining ultrasonic and optical measurements. An ultrasonic pulse probed the coating that receded on the fused silica delay line. This provided longitudinal (L*) and shear (G*) moduli during water evaporation. Simultaneously, light reflection and scattering methods revealed the main formation stages: the moment of interparticle contact (FCC) and the moment of air entering the coating film pores (SCC). The samples were typical coating colors used in the paper industry.

Results

We saw the consolidation and film formation proceeding as follows (cf. Fig. below): 1)During the first stage of film formation the sample behaved like a colloidal suspension and the L* was 3±1 GPa, which is close to the bulk modulus for water, the main component in the sample. As evaporation proceeded the L* increased slightly but the G* remained close to zero. 2)After interparticle contacts were formed at FCC both of the moduli started to increase rapidly. 3)Between FCC and SCC the L* went through a maximum but the G* kept growing. The maximum was most probably due to capillary forces compressing the consolidating film and it is reached at SCC, as air starts to penetrate into the coating film. 4)After SCC the L* reached a minimum but the G* increased continuously. 5)Finally light scattering reached constant value indicating air filled pore space. After short delay the L* and G* reached constant levels and the final strength of the coating film was developed.

Discussion and Conclusions

To conclude we stress that our approach to monitor colloidal film formation using optical and ultrasonic means together is novel and our results compare well with the literature. The results clarify the effect of FCC and SCC on the film mechanical properties. In addition, the temporal L* estimated the capillary pressure in the suspension during drying.

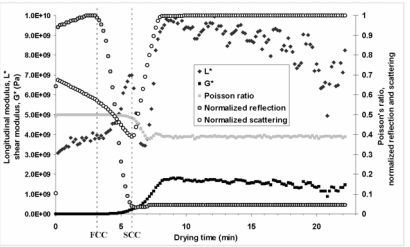

Tuesday Poster

P2M121-04

A Simple Maxwell Based Model in Order to Represent the Frequency-dependent Viscosity Measured by Ultrasound

Ediguer Franco[1], Julio Adamowski[1], Ricardo Higuti[2], **Flávio Buiochi[1]**; *[1]School of Engineering, University of São Paulo, Mecatronics and Mechanical Systems, São Paulo, SP, Brazil, [2]Universidade Estadual Paulista, Ilha Solteira, SP, Brazil.*

Background, Motivation and Objective

A previous work showed that viscosity values measured at high frequency by ultrasound agreed with the values measured at low frequency by the rotational viscometer when special conditions are met, such as relatively low frequency and viscosity. However, these conditions strongly reduce the useful range of the measurement cell. In order to obtain a better measurement range and sensitivity, high frequency must be used, but it causes a frequency-dependent decrease on the obtained viscosity values. This work introduces a new simple model in order to represent this frequency-dependent behavior.

Statement of Contribution/Methods

The model is based on the Maxwell model for viscoelastic materials, but it uses a variable parameter. This parameter has a physical meaning because it represents the linear behavior of the apparent elasticity measured along with the viscosity by ultrasound. Automotive oils SAE 90 and SAE 250 at 22.5±0.5°C with viscosities at low frequency of 0.6 and 6.7 Pa.s, respectively, were tested in the range of 1-5 MHz. The used cell measures the viscosity using longitudinal to shear wave mode conversion, and it is composed of an ultrasonic transducer, a water buffer, an aluminum prism bonded to a PMMA buffer rod and a sample chamber. The model was used in order to fit the obtained data using an algorithm of non-linear regression. By including the viscosity at low frequency as an unknown fitting parameter, it is possible to extrapolate its value.

Results

Relative deviations between the values measured by the viscometer and extrapolated using the model for the SAE 90 and SAE 250 oils were 5.0% and 15.7%, respectively, as shown in the Figure.

Discussion and Conclusions

The model showed to be successful for representing the viscosity in the measured range of frequencies and the extrapolation led to reasonable values of the viscosity at low frequency. However, scattered ultrasonic results led to

different extrapolated values, that is, the results depend on the tolerance parameter used to evaluate the convergence of the fitting algorithm.

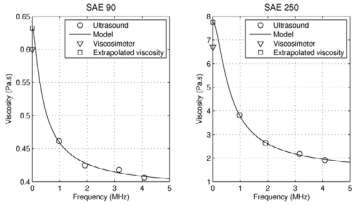

P2M122-05

Towards a simple acoustic method to evaluate the nonlinear parameter B/A of fluids

François Vander Meulen, Lionel Haumesser; *Université François Rabelais de Tours, INSERM U930/CNRS FRE 2448, Blois, France.*

Background, Motivation and Objective

The nonlinearity parameter is known to be an indicator of great interest in the medical field and for non destructive evaluation in industrial applications. Medical and industrial constraints often lead to reflection mode configurations.

The aim of this work is to present an easy-to-build and robust setup for measuring the nonlinearity parameter B/A in fluids using ultrasound in pulse - echo mode. The proposed method is based on voltage and current signal measurements, and requires one single element broadband acoustic transducer which is immersed in the fluid to be characterized.

Tuesday Poster

Statement of Contribution/Methods

The maximum incident voltage (100 V peak) corresponds in our experiments to a pressure of 0.2 MPa emitted in water at the fundamental frequency (f = 3 MHz). This amplitude was chosen high enough to generate a measurable amount of second harmonic, and low enough to remain in the quadratic nonlinear regime. The fundamental frequency is chosen to favor the double frequency component detection by the same transducer. Using the reciprocity principle, the calibration of the transducer at both frequencies is deduced from electrical measurements at f and at 2f.

In order to obtain a reliable evaluation of the nonlinear parameter, attenuation and diffraction effects are taken into account. The diffraction fields of an axisymmetric transducer at the fundamental frequency and at the second harmonic frequency are expressed as superpositions of gaussian beams.

Results

Expressions of these fields, in the pulse-echo configuration, have been derived.

Attention was paid to the nonlinearity originated from the apparatus (generator, and transducer). Calculations have been performed to check that in our configuration, this spurious nonlinearity is much less than the nonlinearity generated in the fluid to be characterized.

An aluminum plate was used as a reflector. A discussion on the influence of the reflector is reported and shows that it has to be heavier than the fluid to be characterized, else destructive interference of the nonlinear field occurs.

Discussion and Conclusions

The method has been validated in water with a good agreement with the litterature. Experiment in denaturated alcohol are also reported.

P2M123-06

The reflection and transmission of Lamb waves across a rectangular crack as a function of the crack geometry

Yongrae Roh[1], Byungsoo Kim[2], Zhi Tian[2], Susong Lee[2], Wonseok Lee[2]; *[1]Kyungpook National University, School of Mechanical Engineering, Daegu, Daegu, Korea, Republic of, [2]Kyungpook National University, Korea, Republic of.*

Background, Motivation and Objective

Lamb wave technique is a useful method to detect damages in a plate. This paper is on the use of the Lamb wave technique to detect a crack in a plate and to analyze the effects of crack dimensions on the scattering of the Lamb wave. Properties of the Lamb waves scattered by a crack in the path of the wave propagation are greatly influenced by the geometry of the crack, thus clear analysis of the dimensional effects of the crack allows higher accuracy and reliability of the nondestructive evaluation of structural damage with Lamb waves.

Statement of Contribution/Methods

When a Lamb wave encounters a crack during the propagation on a plate, it suffers reflection and transmission across the damage while undergoing mode conversion. The purpose of the present work is to derive the reflection and transmission coefficients of S0 and A0 mode Lamb waves incident on a rectangular crack in an elastic plate. The repeated and sequential scattering phenomenon at the crack was analyzed by introducing three independent processes according to the boundary shape of the crack and the direction of the wave propagation. Several local wave form matrices were composed to represent the scattering characteristics of each process, and the reflection and transmission coefficients of a multimode Lamb wave across the crack were calculated per each scattering cycle. By the superposition rule, the transmitted and reflected waves from all the cycles were summed to determine the overall steady state transmission and reflection coefficients at the crack boundary.

Results

The analysis scheme was applied to the determination of transmission and reflection coefficients for S0 and A0 mode wave incidences on a crack in an aluminum plate, and the results were used to analyze the effects of the dimension of the crack. The amplitudes of propagating Lamb wave modes in steady state responses turned out to vary in relation to the depth and width of the crack. The overall fluctuation in the amplitude of the scattered waves for A0 incidence was more prominent than that for S0 incidence.

Discussion and Conclusions

The analysis scheme and calculation results allowed quantitative examination of the characteristics of the waves scattered by a defect in a structure, thus is applicable to assess the health of a structure for ultrasonic nondestructive testing purpose. The same scheme can be expanded to analyze the effects of multiple cracks of different geometries on the reflection and transmission of Lamb waves.

Tuesday Poster

P2M124-07

Tomographic vortex airflow imaging from single view acoustic travel time data

Haiyue Li, Akira Yamada; *Tokyo University of Agriculture & Technology, Japan.*

Background, Motivation and Objective

A surveillance system for a gust of wind like a tornado is desired such as in railroads or airports. It is not realistic to use an anemometer for the purpose because ordinary anemometers are of fixed observation in situ and large numbers must be needed. On the contrary, acoustic tomography reconstructs airflow velocity profile by the calculation on the basis of measurement data of acoustic travel times in the channels between transmitters and receivers. It is based on the remotely-measured data around the medium, hence, placement of sensors in inaccessible atmospheric medium can be avoided. However, the method has a problem that it is difficult to install a number of sensors around the wide area of outdoor monitoring site.

Statement of Contribution/Methods

In this paper, we propose a method of acoustic tomography of two-dimensional vortex air flow profile, which can be reconstructed by arraying small number of transmitters and receivers in parallel. In particular, Fourier central slice theorem are applied to reconstruct the vortex flow vector fields from the single view set of travel time data under the assumption that wind field consists of single rotation symmetry vortex. Examinations were made to verify the feasibility of the present technique. To this end, an indoor imitation experiment system was fabricated as shown in Fig.1, where 10 pairs of ultrasonic transmitter/receiver (with center frequency 40kHz) were arrayed on a pair of opposite sides as they hold the square measurement territory of 36cm x 36cm between the opposite sides.

Results

Vortex wind fan source (with diameter 190 mm, moving speed 50 mm/s and maximum vortex airflow speed 5.4 m/s) was passed to examine the real time detectability of the present system assuming the passage of tornado. Vortex wind velocity field images were continuously reconstructed for every 1.2 s. As a result, it was demonstrated that precisions of the estimated vortex parameters (maximum airflow speed, size and moving speed of the vortex) were satisfactory which justifies the feasibility of the present method.

Discussion and Conclusions

A tomographic imaging technique of the vortex airflow profile by using a single parallel view observation data was demonstrated. From the indoor imitation experiment, results were obtained to open the way to the outdoor real time vortex wind monitoring applications.

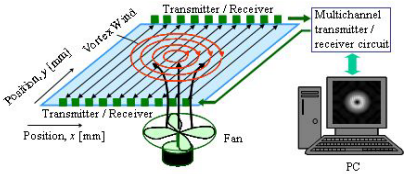

Fig.1 Air flow tomography system.

P2M125-08

Clamp-on Ultrasonic Flowmeters

Dharshanie Mahadeva, Roger C Baker, Jim Woodhouse; *University of Cambridge, United Kingdom.*

Background, Motivation and Objective

Flowmeters are widely used in industry. Operational technologies are various. This paper is concerned with ultrasonic transit time clamp-on flowmeters using upstream and downstream pulses to deduce flow velocity. In the clamp-on meter the transducers are clamped to the existing pipe. The uncertainty is relatively high (about ±5%). We have studied factors contributing to this, particularly the distance between the transducers. This paper will discuss experimental work, a ray tracing method and finite element models.

Statement of Contribution/Methods

There is limited published work due to commercial confidentiality. In order to understand the behaviour and uncertainty of the clamp-on flowmeter, we have tested it on a flow rig (Figure 1:Cambridge University Test Rig) which has been modified for the purpose.

A 2D ray tracing method has been developed and applied to the operation of the clamp-on flowmeter. It is being extended to 3D.

Results

This paper will present experimental work on the role of separation distance, acoustic coupling and temperature variation. It will also present 2D numerical results from the ray model. The simplest out-of-plane 3D results will also be discussed as illustrated in figure 2(end-on view of possible 3 D ray paths in pipes of different thickness).

Discussion and Conclusions

The ray model has been validated against Wave 2000, and its prediction compared to the experimental results. This model has good potential as a design tool for clamp-on ultrasonic flowmeters.

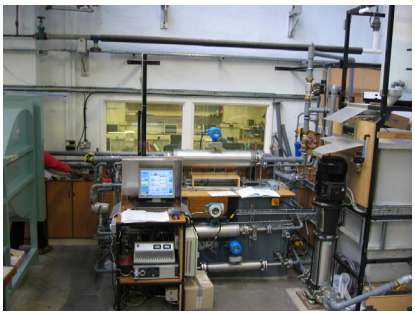

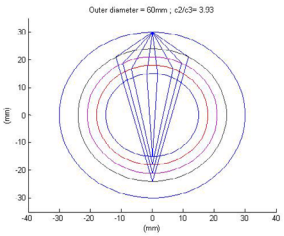

Tuesday Poster

P2N. Thin Film & Device Fabrication

2nd and 3rd Floor Foyers

Tuesday, November 4, 2008, 3:00 pm - 4:30 pm

Chair: **Bob Potter;**
Vectron International, USA.

P2N126-01

Development of 6GHz resonator by using AlN diamond structure

Satoshi Fujii, Takatoshi Umeda, Shuichi Kawano, Masashi Fujioka, Mitsuhiro Yoda; *Seiko-Epson, Advanced Technology Development Center, Suwa-gun, Nagano, Japan.*

Tuesday Poster

Background, Motivation and Objective

Diamond SAW resonators with a SiO_2/IDT/ZnO/diamond structure operate at high frequency and offer outstanding temperature stability. However, diamond SAW resonators operating at over 3GHz and having a SiO_2/IDT/ZnO/diamond structure should be have a thinner IDT than 2 to 3GHz resonators, as this structure has a large SAW reflection coefficient. The IDT of a 5GHz diamond SAW resonator realized by using this structure is 210Å thick. This thickness increases the series resistance and reduces the power durability of the SAW device. This paper reports the development of a AlN/diamond based resonator that has a smaller reflection coefficient than that of a ZnO/diamond based resonator.

Statement of Contribution/Methods

A 6.4GHz diamond SAW resonator with a SiO_2/IDT/AlN/diamond structure was fabricated. The diamond film was grown on a Si wafer by using Chemical Vapor Deposition. After diamond film growth, the surface was mechanically polished with a diamond polisher. The AlN thin film was deposited on the diamond/Si substrate to a thickness of 0.78μm by ECR sputtering. The aluminum thin film was deposited to a thickness 0.065um by DC magnetron sputtering. The film was patterned via a photolithographic process into the electrode of a pair of IDTs and a pair of reflectors beside the IDTs whose line width was 0.4μm. A 0.8μm SiO_2 film was deposited on the IDT/AlN/diamond by RF magnetron sputtering to achieve a zero temperature coefficient of frequency.

Results

The quality of the AlN film layer was characterized by X-ray diffraction analysis. The AlN film layer was highly oriented, with a c-axis on the diamond film. The full width of half maximum of the X-ray diffraction rocking curve was 2.5°. Fig. 1 shows the frequency characteristic, S21, of the diamond SAW resonator. A low insertion loss, 6.6 dB with a Q-value of 450, was obtained at 6.3GHz. A low, 6.8 ppm/°C temperature coefficient of frequency was obtained.

Discussion and Conclusions

The SiO_2/IDT/AlN/diamond structure enables a thicker Al-IDT layer and realizes lower series resistance and, hence, a low insertion loss for SAW over 3GHz compared to that of a SiO_2/IDT/ZnO/diamond structure. A 6.4GHz resonator with a low insertion loss at 6.6dB, a Q value of 450, and low TCF has been successfully obtained.

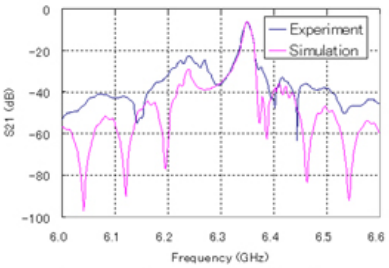

Fig.1 Frequency characteristics of the AlN diamond resonator

P2N127-02

Development of 4GHz Bulk Acoustic Wave Resonators by Sputtered Pb(Mn,Nb)O3-Pb(Zr,Ti)O3 Thin Films

Tomoaki Matsushima[1], **Norihiro Yamauchi[1],** Takeo Shirai[1], Takaaki Yoshihara[1], Yoshiki Hayasaki[1], Isaku Kanno[2], Kiyotaka Wasa[2]; *[1]Matsushita Electric Works, Ltd., New Product & Technologies Development Department, Kadoma, Osaka, Japan, [2]Kyoto University, Department of Micro-engineering, Kyoto, Kyoto, Japan.*

Background, Motivation and Objective

Recently piezoelectric thin film have been paid much attention for applications of RF-MEMS devices such as RF resonators and RF switches. The Pb(Zr,Ti)O3 (PZT) thin films show high dielectric constant and high electro-mechanical coupling constant. Although many researchers have developed the RF filters by PZT thin films, they have not obtained excellent RF properties by their films. We have developed 4GHz BAW(Bulk Acoustic Wave) resonators by sputtered Pb(Mn,Nb)O3-Pb(Zr,Ti)O3 (PMN-PZT) thin films for the first time.

Statement of Contribution/Methods

The 0.06Pb(Mn0.33Nb0.67)O3-0.94Pb(Zr0.52Ti0.48)O3 (PMN-PZT) thin films were deposited on single crystal MgO substrates by RF magnetron sputtering. A bottom electrode was SrRuO3/Pt. The substrate temperature was 500-650C. The thin films were quenched after the deposition.

Results

The film thickness was 200-400nm. The surface roughness RMS of the thin films was 1.5-3.5nm. Figure 1 shows the X ray diffraction pattern of our 0.06PMN-PZT thin film. As shown in fig. 1, the thin film shows highly (001) orientation. The crystal structure of in-plane for this film was also evaluated by the 4-circle X-ray diffractometer. It shows high quality tetragonal structure. We have fabricated the thin film BAW(Bulk Acoustic Wave) resonator using the MEMS technology. The schematic draw of our BAW resonator is shown in fig. 2. The MgO substrate was etched by H3PO4 solution.

Discussion and Conclusions

The RF properties of the resonator were evaluated by VNA (Vector Network Analyzer). It shows high electro-mechanical coupling constant kt and high Q-value at 4.17 GHz. The kt and Q-value are 0.69 and 157, respectively. The value of kt is highest, to our knowledge. In addition, the kt2 x Q of 74.6 is the highest value comparing with those of previously reported PZT-BAW resonators.

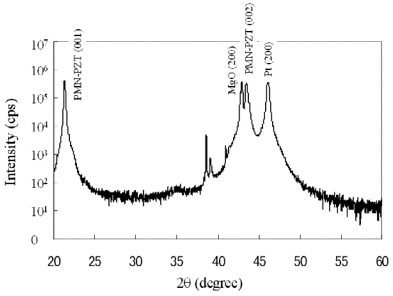

Fig. 1 X-ray diffraction pattern of PMN-PZT thin film.

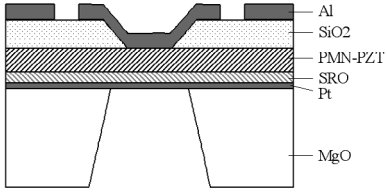

Fig. 2 Cross sectional view of the BAW resonator.

Tuesday Poster

P2N128-03

Surface Acoustic Wave Devices on AlN/Single-crystal Diamond for High Frequency and High Performances Operation

M. Benetti[1], D. Cannatà[1], **F. Di Pietrantonio[1],** E. Verona[1], S. Almaviva[2], G. Prestopino[2], C. Verona[2], G. Verona-Rinati[2], *[1]Italian National Research Council, "O.M. Corbino" Institute of Acoustics, Rome, Italy, [2]University of Rome Tor Vergata, Department of Mechanical Engineering, Rome, Italy.*

Background, Motivation and Objective

Surface acoustic wave (SAW) devices based on diamond substrates are very attractive because of the high acoustic wave velocity of this materials (~11,000 m/s, for the Rayleigh wave) that allows higher frequency operation at a given interdigital transducer (IDT) line-width resolution technology. Even though examples of SAW devices on AlN/Diamond structures have been reported in literature [1], all of them use poly-crystal diamond film. Use of single-crystal diamond would be greatly preferable because of its much higher homogeneity. This would lead to develop SAW devices operating at high frequencies with improved performances with respect to insertion loss, aging and resistance in harsh environments.

Statement of Contribution/Methods

In this paper we present recent results on fabrication of SAW and PSAW devices on AlN/Single-crystal Diamond. The AlN thin film was deposited by reactive magnetron sputtering technique, optimized to achieve an high degree of orientation value of the c-axis perpendicular to the plate surface and a low stress, while the single-crystal diamond was homoepitaxially grown by microwave plasma CVD on High Pressure High Temperature (HPHT) diamond substrate.

SAW propagation on the structure has been theoretically investigated together with the electromechanical coupling for the first 12 Rayleigh-type modes. The theoretical calculations show how high SAW velocities are achievable with good coupling efficiencies.

Tuesday Poster

Results

Experiments performed on AlN/Single-crystal Diamond test delay-lines have shown a good agreement between experimental results and theoretical predictions. Some 1-port resonators have been implemented on the multi-layered structure, one of which has a wavelength of 7.22 µm, a central frequency of 1.56 GHz for the 3rd Rayleigh-type mode and a Q-factor of about 2·104, as shown in figure.

Discussion and Conclusions

In conclusion the use of single-crystal diamond in conjunction with highly oriented, low stressed AlN piezoelectric films, lead to SAW resonators for high frequency operation with improved performances respect to SAW devices based on poly-crystal diamond substrates.

[1] M. Benetti, D. Cannatà, F. Di Pietrantonio, and E. Verona, "Growth of AlN piezoelectric film on diamond for high-frequency surface acoustic wave devices", IEEE Trans. Ultrason. Ferroelectr. Freq. Contr., vol. 52, pp. 1806-1811, 2005.

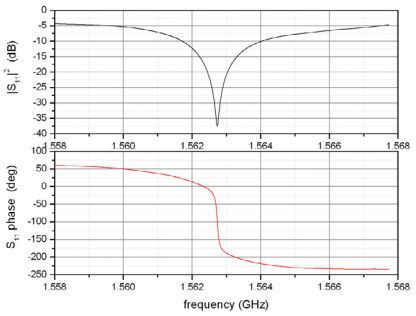

P2N129-04

Single Phase Transducer Consisting of AlGaN/GaN Film

Koji Hohkawa[1], Satoshi Oshiyama[1], Keishin Koh[1], Kazumi Nishimura[2], Naoteru Shigekawa[2]; *[1]Kanagawa Institute of Technology, Japan, [2]NTT Photonics Laboratory, Japan.*

Background, Motivation and Objective

Semiconductors devices with AlGaN/GaN film have found application in high–performance, front end integrated circuits operating in the range from GHz to submillimeter frequency. In addition, their piezoelectric properties have been researched extensively for developing high performance filters for high frequency ranges and semiconductor-coupled surface acoustic wave (SAW) devices 1). In this paper, we propose a novel transducer consisting of AlGaN/GaN film, in which a vertical electrical field was applied between a two-dimensional electron gas (2DEG) on AlGaN/GaN interface and its carriers density could be modulated by DC bias voltage between top and bottom electrode on AlGaN/GaN film.

Statement of Contribution/Methods

The AlGaN/GaN film is prepared on a (0001) sapphire substrate by metal organic chemical vapor deposition, and the aluminum mole fraction of AlGaN layer was nominally 0.255. The GaN layer thickness is about 2μm. The AlGaN layer thicknesses are 300nm and 100nm respectively. The top electrodes of single phase transducer is formed by electron beam lithography technology on the surface of the AlGaN film and the electrodes shape having electrodes finger width of 100 - 300nm is aligned parted with space length of 400 - 1200 nm. The two kinds of materials of a 100-nm-thick Al film and a 100-nm-thick Al-Ti film are used as electrode.

Results

We used DC source, microwave probes and network analyzer to estimate the frequency characteristics of test devices. When DC bias voltage (4V - 20V) is applied on top and bottom electrode on AlGaN/GaN film, we confirmed a generation and detection of SAW on single phase transducer. The pass band center frequency of SAW is about two times than that of double phase transducer for same electrode size.

Discussion and Conclusions

From experiment results, we found that effective electrode size of top electrode and configuration of bottom electrode in the transducer is very important parameters for obtaining good frequency characteristics. The structure of single phase transducer consisting of AlGaN/GaN film is easily integrated with AlGaN/GaN semiconductor devices and application possibility as a higher frequency variable filter etc are expected.

1) N. Shigekawa, K. Nishimura, T. Suemitsu, H. Yokoyama and K. Hohkawa; ″Interdigital Transducers with Control Gates on AlGaN/GaN Heterostructures″, Appl. Phys. Lett. 89, (2006). 033501.

P2O. SAW Simulation

2nd and 3rd Floor Foyers

Tuesday, November 4, 2008, 3:00 pm - 4:30 pm

Chair: **Ken-ya Hashimoto;**
Chiba University, Japan.

P2O130-01

3D Finite Element Modeling of Real Size SAW Devices and Experimental Validation

Sergei Zhgoon[1], Dmitriy Tsimbal[1], Alexander Shvetsov[1], Kushal Bhattacharjee[2]; *[1]MPEI, Russian Federation, [2]RF MD, USA.*

Background, Motivation and Objective

The size of the design problem becomes prohibitive when all the 3 dimensions are required to describe a real SAW device. That is why common techniques are mainly based on the description of only a half period of infinite periodic structures (electrode gratings), as, for example in the public domain package FEMSDA, that are subsequently introduced in COM equations based simulation [1]. However in many practical cases the description of all the elements of real SAW structures cannot be based only on periodic structures and on plane waves. It is very desirable to use one single design tool to predict response peculiarities related to diffraction and to waves and modes propagating in different directions and taking part in response formation and distortion.

Tuesday Poster

Statement of Contribution/Methods

We report on successful examples of using finite elements based software package for modeling SAW structures with dimensions above 100 wavelengths in the propagation direction including all the electrodes and spaces. The approach easily incorporates additional layers and elements with arbitrary 3D shapes that are common in SAW devices. Temperature behavior of the frequency response, SAW beam shape, bulk wave related data and other relevant information is stored in the solution and this helps determining the sources of response peculiarities. Personal workstation is used for modeling.

Results

One of the modeling examples describes a delay line on langasite (LGS) with two interdigital transducers of 51 electrodes each on a relatively thin substrate where Lamb wave propagation is clearly developed with multiple modes observed in a wide frequency range. The correct description requires dense meshing of the structure in all the 3 directions. The response obtained is compared to the response of an experimental test sample and it shows very good agreement with measured data.The modeling results for infinite periodic structures are also validated against the proven FEMSDA software and they show quite good agreement with measurements of resonator test samples.

Discussion and Conclusions

This work demonstrates the capabilities of finite elements based software running on contemporary personal computers to solve practical problems of SAW device design.

References:

1. K. Hashimoto and M. Yamaguchi. General-purpose Simulator for Leaky Surface Acoustic Wave Devices Based on Coupling-of-Modes Theory. Proc. of IEEE Ultrasonics Symp., 1996, p. 177-122.

P2O131-02

2D polynomial modeling of Acoustic Wave Resonators

Antoine Raherison[1], Jean-Etienne Lefebvre[2], Faniry Emilson Ratolojanahary[3], Lahoucine Elmaimouni[4], Tadeusz Gryba[2]; *[1]Universite de Valenciennes, IEMN-DOAE, Valenciennes cedex 9, France, [2]Universite de Valenciennes, IEMN-DOAE, France, [3]Universite de Fianarantsoa, LAPAUF, Madagascar, [4]Universite Ibn Zohr, Faculte polydisciplinaire d'Ouarzazate, Morocco.*

Background, Motivation and Objective

The demand for monolithic integration of acoustic wave resonators as core components in mobile communication systems call for efficient tools of simulation. 1D models allow only a partial description of resonator's performances. A full description requires to take into account the finite lateral dimensions of the resonator what can be done with 2D and 3D analytical models. However, they require a lot of memory space and computation time. Thus, semi-analytical models are highly desirable. We propose here a Legendre polynomial-based 2D semi-analytical approach able to take into account the finite lateral dimensions.

Statement of Contribution/Methods

Up to now, the Legendre polynomial method has only been applied to 1D modeling. An extended formulation is presented here for 2D modeling of laterally finite resonators. The equations of motion along with the Maxwell-Ampère and Maxwell-Faraday equations are solved by expanding each mechanical and electrical displacement component in a double series made up of products of Legendre polynomials. Through a unique formulation, the boundary conditions and the electrical source, either voltage or current, are incorporated into the field equations and are automatically accounted for. Thus, both the harmonic and modal analyses are studied through a unique formalism.

Results

Resonance and antiresonance frequencies, electric input impedance and field profiles, easily obtained, are presented for a PZT resonator. Both lateral and thickness resonances are highlighted. The results of our theory are compared against other calculations from the literature. The table hereafter illustrates the comparison for the resonance and antiresonance frequencies:

Discussion and Conclusions

A good agreement is obtained. It shows the polynomial method presented can be used to model 2D acoustic wave resonators. Although only fully metallized resonators are presented, partially metallized ones can be just as easily handled by the approach presented. Guidelines for this extension of the method are given.

1R.L. Jungerman et al., « Measurement of normal surface displacements for the characterization of rectangular acoustic array elements », J. Acoust. Soc. Am. Vol. 76, No 2. August 1984.

	Modes	Resonance frequencies	Antiresonance frequencies
Experimental	1	0. 91 MHz	1. 22 MHz
	2	2. 45 MHz	2. 51 MHz
Theoretical	1	0. 99 MHz	1.29 MHz
	2	2.47 MHz	2.49 MHz
Our results	1	0. 94 MHz	1. 26 MHz
	2	2. 43 MHz	2. 47 MHz

P2O132-03

COM Analysis for LSAW filters

Svetlana Malocha, Benjamin Abbott; *Triquint Semiconductor, USA.*

Background, Motivation and Objective

This paper presents an efficient COM-based analysis for LSAW ladder and coupled resonator filters.

As it was pointed out in earlier publications (for example, [1]), the "classic" version of COM analysis ignores the interaction between neighboring elements (transducers or gratings). The reason is that a device consisting of several transducers and gratings is modeled by cascading individual p-matrices of the elements, while the p-matrix for an individual element is calculated without regard to its neighbors. The result of this interaction can be especially pronounced in coupled resonator filters and must be taken into account.

Statement of Contribution/Methods

In the present work the abovementioned flaw is overcome by using a gap-centric cell instead of an electrode-centric cell typically used in COM analysis. This modification allows the entire device to be modeled by cascading p-matrices of individual elements thus keeping the simplicity and efficiency of COM formalism while including the interactions between the adjacent elements. The details of the implementation will be shown.

COM parameters are extracted from numerically calculated harmonic admittance for a range of normalized frequencies, a range of duty factors, and a range of metal thickness-to-period ratio. Method of parameter extraction essentially follows that in [2,3].

The accuracy of the model is further improved by taking into account the charge distribution associated with particular voltages applied to electrodes of adjacent transducers (and gratings).

Results

The analysis is successfully applied to the devices with arbitrary geometries, including varying periodicity and duty factors, arbitrary polarities and apodisation of both transducers and gratings.

Discussion and Conclusions

The good agreement between calculated and measured results will be shown for a number of LSAW devices (ladder filters and coupled resonator filters in 1 – 2 GHz range) built on LSAW cuts of Lithium Tantalate and Lithium Niobate.

[1] G. Kovacs, Ultrasonics Symposium, pp.707-710, 2003

[2] Th. Pasturaud, Ultrasonics Symposium, pp.80-84, 2004

[3] N. Naumenko, B.P.Abbott, Ultrasonics Symposium, pp.166-170, 2007

Tuesday Poster

P2O133-04

Precise Extraction of P-matrix as Frequency Dependent Function for Leaky Surface Acoustic Wave

Hao Wang[1], Weibiao Wang[2], Jiming Lin[3], Xianglong Shi[1], Haodong Wu[1], Yongan Shui[1]; *[1]Key Laboratory of Modern Acoustics, Institute of Acoustics, Nanjing University, Nanjing, Jiangsu, China, [2]Shoulder Electronics Limited, Wuxi, Jiangsu, China, [3]Guilin University of Electronic Technology, Information and Communication College, Guilin, Guangxi, China.*

Background, Motivation and Objective

In SAW device design, the extraction of COM parameters and simulation by P-matrix cascading has been extensively used to optimize the structure of device. Traditionally used COM parameters are taken as frequency independent. Since within the interested frequency range, the propagation attenuation of leaky surface acoustic wave on 42°$LiTaO_3$ is changing significantly, the parameters taken as constant will introduce a considerable error. Recently, researchers tried to extract COM parameters as frequency dependent function for 42°$LiTaO_3$ [1],[2]. They could get only four equations by the poles and zeros of harmonic admittance whereas there are five COM parameters to be determined, so it is impossible to obtain independent values of all the COM parameters. They had to introduce some approximation in its application to optimal design.

Statement of Contribution/Methods

In this paper, we propose a method to extract precise P-matrix as a function of frequency directly.

A cell within a periodical grating is in consideration, and if the grating has enough number of periods on both sides of the cell, its P-matrix could be taken as the typical representation of the components in device design. The Finite Element Method/Boundary Element Method (FEM/BEM) is used to obtain accurate electric charge distribution, stress distribution under all the electrodes and the fields (displacements and potential) of the forward and backward waves on both sides of the cell in consideration [3]. Using these wave fields, it is easy to obtain all the P-matrix element values at every frequency.

The key difference between the methods in [1],[2] and our method lies on that in their calculation only the propagation mode is used, and no reflection is regarded. Therefore, they were unable to get the mutual coupling parameter κ. In our method, the length of grating on both sides of the cell has finite number of periods, say, m. m is not infinite, so we have reflection in calculation, though it relates with the number m. However, we can cancel out the influence of number m and obtain an additional independent data.

Results

As an example, all elements of the P-matrix of one cell on 42°$LiTaO_3$ with relative aluminum electrode thickness of 8% and metallization ratio of 0.5 are presented as the functions of frequency. Using the obtained parameters, a DMS filter is simulated, and the result agrees well with the precise simulation and measurement.

Discussion and Conclusions

These parameters are also used to design a DMS SAW filter through a nonlinear optimization method, the result is improved significantly.

References:

[1]. Th. Pastureaud, 2004 IEEE Ultrasonics Symposium Proc. pp.80-84

[2]. B. V. Sveshnikov, et al, 2003 IEEE Ultrasonics Symposium Proc. pp.715-719

[3] W. Wang, et al, IEEE Transactions-UFFC, 2007,54(7),1445-1453

This project is supported by Natural Science Foundation of China No. 10774073.

P2O134-05

Simulation of STW Resonator using COMSOL Multiphysics

Wang Hualei, Shi Yu, Zhong Hui; *University of Electronic Science and Technology of China, State key Laboratory of Electronic Thin Films and Integrated Devices, China.*

Background, Motivation and Objective

The accurate simulation of STW resonator is still a challenge, even though some efforts have been done by some authors. It is difficult to predict the Q-factor of STW resonator by using the phenomenological models, such as the coupling-of-modes (COM) model and equivalent circuit models, because some loss mechanisms cannot be taken into these models like the loss due to bulk scattering in the non-periodic area and the attenuation in Al electrodes. To predict the feature of STW resonator accurately, we would like to show STW resonator as a typical example for simulating SAW devices using COMSOL Multiphysics, which is demonstrated for the first time.

Statement of Contribution/Methods

In this paper, the finite element combined boundary element (FEM/BEM) for finite length devices in COMSOL Multiphysics is used. We introduce two parameters including the propagation attenuation due to material itself in substrate and the loss in Al electrode In this method, the 3D approximation is made, assuming the fields are uniform along electrode, and all the acoustical and electrical interactions, as well as mass loading effects, are taken into account. STW devices with arbitrary electrode structure on substrates with AT quartz were modeled using this method, including the effects of bulk waves. The bulk wave scattering in the non-periodic area and the end effect of IDT (or reflector) are included naturally.

Results

A two-port STW resonator is simulated. The structure parameters of the resonator are: 401-electrode IDT, 500-electrode reflector, 50-electrode energy trapping Metal strip, 3¦Ìm electrical period and 600mm film. COMSOL Multiphysics shows the simulated deformed displacement along the horizontal direction of resonator, respectively for two electrode structure. The simulated Q-factor is 6500.

Discussion and Conclusions

The result of simulation shows that the STW resonator exists an optimum thickness of Al electrode, which depends only on the acoustic attenuation in Al. The optimum thickness also is a function of the center frequency of resonator. The Q-factor of resonator can be further increased by shifting the central frequency of reflectors down, so that resonance occurs in the center of the reflectors stopband.

P2P. Sensors and ID-Tags Based on SAW

2nd and 3rd Floor Foyers

Tuesday, November 4, 2008, 3:00 pm - 4:30 pm

Chair: **Victor Plessky;**
GVR Trade SA, Switzerland.

P2P135-01

High Frequency Lamb Wave Device composed of LiNbO3 Thin Film

Michio Kadota, Takashi Ogami, Kansho Yamamoto, Yasuhiro Negoro, Hikari Tochishita; *Murata Mfg. Co., Ltd., Japan.*

Background, Motivation and Objective

In order to realize a high frequency surface acoustic wave (SAW) device, there are several kinds of methods such as shortening the wavelength of the interdigital transducer (IDT) or using the substrate with high velocity. However, it is difficult to realize it by using their methods because of a limitation on the photolithographic process and no suitable substrates having both a high velocity and an optimum electro-mechanical coupling factor to realize a required bandwidth.

Tuesday Poster

Statement of Contribution/Methods

The following two kinds of waves on thin plate have modes with high velocity: (1) Lamb wave having mainly longitudinal and shear vertical (SV) components and (2) a shear horizontal (SH) wave type of thin plate wave having mainly the SH component. The IDTs composed on the thin plate can excite their waves as well as SAW, so it is convenient to design the devices using the plate wave. The Lamb wave using a quartz thin plate, a ZnO thin film/Pyrex/Si structure, and an AlN thin film/Si one has been reported. But, their frequency was not high (less than 600 MHz) and their coupling factor was too small to realize the required bandwidth. On the other hand, the Lamb wave using thin plates of LiNbO3 and LiTaO3 single crystals has been also reported. But their frequency was also too low (less than 100 MHz) because it is difficult to realize very thin plate to generate high frequency. It might be possible to realize the high frequency device if a very thin LiNbO3 or LiTaO3 film with a high quality could be deposited.

Results

Authors attempted to deposit a very thin LiNbO3 film with a high quality by a chemical vapor deposition (CVD) system and tried to realize a high frequency device using this film. As the result, authors have realized a 4.5GHz Lamb wave resonator with large impedance ratio of 52dB and a high velocity of 14,000 m/s composed of the very thin LiNbO3 film/air-gap/substrate structure. Where, the impedance ratio means 20xlog(anti-resonant impedance/resonant one).

Discussion and Conclusions

In order to realize a high frequency device, authors attempted to develop the Lamb wave using a very thin LiNbO3 film with a high quality. A high c-orientated thin LiNbO3 film was deposited by the CVD system. A resonator composed of the thin LiNbO3 film/air-gap/substrate was developed. As the result, a 4.5GHz Lamb wave resonator with large impedance ratio of 52dB and a high velocity of 14,000 m/s was realized for the first time.

P2P136-02

Feasibility of Ultra-Wideband SAW Tags

Sanna Harma[1], Victor Plessky[2]; [1]*Helsinki University of Technology, Department of Engineering Physics, Espoo, Finland,* [2]*GVR Trade SA, Bevaix, Switzerland.*

Background, Motivation and Objective

The currently emerging ultra-wideband (UWB) radio technology enables short-range communications with high speed and low power. The possibility of using wide frequency bands is especially attractive for SAW tags because the number of different codes that can be obtained is determined by the BT product, where B is the used frequency band and T is the coding time duration. As wider bands can be used, the delays can be shortened and the device size will be drastically reduced. Shorter delays also indicate a reduction of propagation losses.

Statement of Contribution/Methods

We propose a design of a UWB SAW tag, carry out numerical experiments on the device performance, and study signal processing in the system. We also estimate the potentially achievable reading distance. Experiments are currently being prepared.

Results

The proposed tag consists of a chirp transducer and an array of wide-band code reflectors. The tag can be read with a linear frequency modulated (LFM) interrogation signal. The chirp transducer allows for signal processing inside the tag: the interrogation signal is modified by the SAW tag and will be different from environmental echoes. The initial 1-μs delay normally required for the decay of environmental echoes can thus be significantly reduced. Fig. 1 shows the simulated tag response and the randomly generated environmental echoes (S/N = 0 dB) after being received by the reader.

In our example, the total power radiated by a reader is less than 40 μW, which is undeniably an attractive level, despite the fact that reading range is expected to be limited to 1 m or 2 m. The interrogation signal will be radiated in total for less than 0.1 ms per one reading. This puts the average power at the nanowatt level, assuming one reading per second sufficient for many applications.

Tuesday Poster

Discussion and Conclusions

UWB SAW tags are feasible and have many advantages over ordinary SAW RFID tags. They can have large information capacity while using short delays. Tag size and losses can be significantly reduced. Tags can be read with very low power. When a chirp transducer is used, tags are capable of signal processing, which makes them more resistant to environmental echoes. Moreover, standard optical lithography is perfectly mature for manufacturing such devices at low cost and in big volumes.

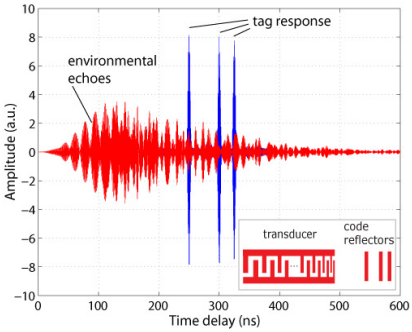

P2P137-03

Perfusion of Cell and Particle Suspensions into Microporous Structures Using Surface Acoustic Wave Fluid Actuation

Haiyan Li, James Friend, Leslie Yeo; *Micro/Nanophysics Research Laboratory, Department of Mechanical Engineering, Melbourne, VIC, Australia.*

Background, Motivation and Objective

When Surface acoustic wave (SAW) meets a liquid, it diffracts at the Rayleigh angle èR into the fluid and an acoustic streaming is generated. If the intensity of the acoustic radiation is sufficiently high, the SAW can transport a free droplet to move in the direction of the SAW without using any mechanically moving components [1]. This technology might be used in for perfusion cells and particles into microporous structures. The principle of tissue engineering is to repair damaged tissue/organs by culturing cells on biocompatible and biodegradable microporous scaffolds to generate new tissue. Seeding cells into a porous scaffold uniformly and efficiently without damaging the viability and function of the cells is vital to this process. The conventional cell seeding method called "static cell seeding" usually results in low efficient seeding due to the hydrophobicity of the polymer and the large capillary forces of the micro-porous structure in opposition to the fluid perfusion. In the present study, it has been proved that SAW actuation can be exploited as a method for quickly perfusing cells and particles into microporous structures.

Statement of Contribution/Methods

Polycaprolactone scaffolds were prepared using a conventional solvent casting-particulate leaching method. An aqueous suspension of 5-µm green fluorescent polystyrene (PS) microspheres (Duke Scientific Corporation, USA) with a concentration of 1.4x106 particles/ml was used to facilitate observation of the seeding process. A high-speed camera (Olympus i-speed, Tokyo, Japan) was used through a reflected fluorescent microscope system (Olympus BXFM, Tokyo, Japan) to monitor the dynamics of the seeding process. Primary mouse osteoblast-like (bone) cells were used for cell viability and proliferation assessment after SAW treatment by using flow cytometry (Becton Dickinson FACS) and a Beckman Coulter analyser (FC500-CXP).

Tuesday Poster

Results

Results show that there is a relationship between the velocity at which the particle suspension enters the scaffold and the particle seeding efficiency within the scaffold. The highest seeding efficiency was about 92% at an RF power of 570 mW. Above this power, the intense SAW radiation resulted in the atomization of the droplet containing the suspension even before it reached the scaffold. Seeding video captured by high speed camera showed that approximately 85% of the particles in the initial suspension were distributed within the scaffold in just 10 seconds, while the static method requires at least 30 minutes to complete this process. Cell viability remains above 80% after being treated by SAW under 500mW for 10s. In addition, the cells infused into the scaffold under this condition can still proliferate properly, which indicates that the SAW does not damage the cells during the seeding process.

Discussion and Conclusions

We present a promising low-cost and miniaturizable alternative for driving a particle suspension into a porous cell scaffold through SAW actuation.

P2P138-04

A surface acoustic wave sensor for detection of cell adhesion

Glen Guhr[1], **Raimund Brünig[1],** Martin Jäger[2], Rüdiger Poll[2], Hagen Schmidt[1], Manfred Weihnacht[3]; *[1]Leibniz Institute for Solid State and Materials Research Dresden, Germany, [2]Dresden University of Technology, Institute of Biomedical Engineering, Germany, [3]InnoXacs, Dippoldiswalde, Germany.*

Background, Motivation and Objective

Surface acoustic waves (SAW) are widely used as frequency filters, ID tags, gas sensors and recently also as biological sensors. SAW-devices are used to monitor DNA, enzyme and protein binding as well as antibody reactions, as it was already reported by several groups. In biosensor applications even cells can be used as sensing element. Being part of a living system, they have a natural sensitivity to the surrounding biological processes. While growing cells and detecting their behaviour at the same time, much information about biological processes can be collected. There is a great demand for advanced biosensors in a wide field of applications ranging from environmental monitoring, pharmaceutical drug screening to tissue engineering. For this reason the research in cell-based biosensors became a growing field in recent years.

Statement of Contribution/Methods

To date most investigations are done with optic fluorescence methods, impedance measurements or with quartz crystal microbalance (QCM). Among these methods, the QCM technique allows a direct measurement of mechanical properties of the cells. In this paper we present our results concerning the detection of the cell adhesion process with special designed SAW-sensors. In principal, such sensors are comparable with QCM. But working at higher frequencies also a higher sensitivity can be reached. Additionally, SAW devices can observed by inverted optical microscopy. We realized SAW-resonators and used a network analyzer to record changes of resonant frequency and bandwidth. The sensors are operating at 170 MHz. The culturing chamber was made of polycarbonate with sealings made of polydimethylsiloxane.

Results

The adhesion behaviour of murine fibroblast cell line L929 was investigated. Cells at an amount of 20.5*104 cells/ml were seeded. The cell adhesion and growing processes caused a decrease of resonant frequency of the SAW device in the first 4 hours. During this time the cells fell down and started to sediment on the sensor surface simultaneously expressing components of the extra cellular matrix. Afterwards the cell adhesion process follows by means of integrin binding. The cell segmentation began after the first 12 hours detected as further decrease of resonant frequency. After almost 30 hours a closed cell monolayer has been developed. At this time the cell settling is completed, no further changes of resonant frequency were observed.

Discussion and Conclusions

The suitability of SAW devices for the detection of cell adhesion processes was shown. Offering such perspective benefits as miniaturization, high sensitivity and cost effectiveness, SAW-devices have a great potential as assay for cell adhesion processes.

P2P139-05

The effect of parallelism of CMUT cells on phase noise for chem/bio sensor applications

Hyunjoo Lee, Kwankyu Park, Omer Oralkan, Mario Kupnik, Butrus (Pierre) Khuri-Yakub; *Stanford University, E. L. Ginzton Laboratory, Stanford, CA, USA.*

Background, Motivation and Objective

Micromechanical resonators (microresonators) based on MEMS technology find their way into a wide range of applications, such as reference oscillators and resonant chemical sensors. Our goal is to use a capacitive micromachined ultrasonic transducer (CMUT) as a microresonator in resonant chemical sensor application, where a large sensing area, low resonating mass, and good frequency stability are the key parameters to enhance mass sensitivity per unit area. Resonant chemical sensors based on flexural mode resonators, such as cantilevers and CMUTs, are thus attractive due to the low resonating mass. However, a CMUT resonates in air with a quality factor (Q) in the order of several 100s, which is much smaller compared to other microresonators, such as FBARs, BAWs, and SAWs (Q ~ 10,000). Despite this low Q, our CMUT-based oscillator exhibits excellent phase noise due to the parallelism hidden in the CMUT. A CMUT can inherently have 1000s of small microresonators (i.e. CMUT cells) operating all in parallel. In this study, we show that the CMUT-based microresonator is beneficial for phase noise due parallelism and investigate the relationship between phase noise and the number of CMUT cells resonating in parallel.

Statement of Contribution/Methods

We realized a low phase noise oscillator circuit (single-stage BJT Colpitts oscillator), in which a CMUT with 1000 cells, i.e. 1000 microresonators act in parallel as the frequency determining elements. In theory, when we assume that each microresonator produces uncorrelated noise, N number of microresonators connected in parallel generates a noise number $\sqrt{N}$ times smaller. For N number of quartz resonators connected in series, the phase noise reduces by a factor of 10 log N. For verification, we fabricated 18-MHz CMUT arrays with 1000 cells, and characterized the devices to measure the reduction in motional impedance. Then, we measured the phase noise and compared it to other microresonators with similar resonant frequencies.

Results

The phase noise of the 18-MHz oscillator employing a CMUT with 1000 cells connected in parallel is indeed comparable to oscillators employing other microresonators with high quality factors on the order of 10,000s. For example, the 15.4-MHz series resonant oscillator with a Q of 6,800 exhibits 109 dBc/Hz and -133 dBc/Hz, while our device with a Q of only 150 exhibits 83.7 dBc/Hz and -130 dBc/Hz at 1 kHz and far-from-carrier offset frequencies, respectively.

Discussion and Conclusions

Our measurements and comparisons to other microresonators show that the reduction in phase noise is related to the parallelism present in the CMUT. The reduction factor as a function of N depends on the amount of correlation between noise of each cell, which is influenced by the series/shunt configuration, crosstalk between neighboring cells, and various boundary effects.

P2P140-06

Errors of Phase and Group Delays in SAW RFID with Phase Modulation

Tao Han[1], Jiming Lin[2], Weibiao Wang[3], Hao Wang[4], Haodong Wu[4], **Yongan Shui[4];** *[1]Shanghai Jiaotong University, China, [2]Guilin University of Electronic Technology, China, [3]Shoulder Electronics Limited, China, [4]Key Laboratory of Modern Acoustics,Nanjing University, China.*

Background, Motivation and Objective

In a surface acoustic wave (SAW) RFID tag, many reflectors are arranged in a line with the interdigital transducer. In general the amplitudes and the group delay of the pulses are used for encoding. In case that the phase of carrier wave in reflective pulse could be utilized as well, the demodulation precision of the pulse time delay could be increased greatly, and thus, the code capacity of SAW RFID can be greatly increased in case of the same number of reflectors, or same area of the chip[1].

For a coding scheme in which the phase information is used, each bit is identified by the measured values of phase and group delays within certain ranges. When establishing the encoding scheme, in order to define the corresponding ranges of both group and phase delay, one has to know their errors. Otherwise, one has to extend the above ranges for the sake of the reliable identification. It means that the code capacity would be decreased.

Statement of Contribution/Methods

The errors originate from the design procedure, the fabrication, and the measurement. Because of the multi-reflection effects among reflectors, the bulk wave interferences and the diffraction, the phases of reflectors deviate from the specified data. In data processing, all the conditions deviate from the ideal ones also give rise to the error, for example, the replacement of Fourier transform by discrete Fourier transform. In addition, some additional errors are also introduced in the procedure of determination and calibration of the measuring temperature different from the designing temperature. The measuring errors in the process of demodulation come from the coherent demodulation components, phase noise of the local oscillator, the same frequency interference and the effective bits of A/D converter, etc. The fabrication errors include the error of metalized ratio, the electrode thickness error, etc.

Several tag prototypes with 10 reflectors in line on 128ºYX-Lithium Niobate are optimally designed based on the method described in [2]. The central frequency of 915 MHz and the bandwidth of ±20MHz are supposed. The temperature range in our investigation is -25-45ºC.

Results

The phase delay and group delay errors are presented in form of both statistical average error and maximum error within hundreds of data examples. The errors are illustrated for various cases.

References:

[1] C.S. Hartmann, Design of global SAW RFID tag devices, Proc. Second Int. Symp. on Acoustic Wave Devices for Future Mobile Communication Systems., Chiba, March, 2004, pp.15-19

[2] Han Tao, Wang Weibiao, Wu Haodong, Shui Yongan, Reflection and Scattering Characteristics of Reflectors in SAW Tags, IEEE Transactions on Ultrasonics, Ferroelectric and Frequency Control. 2008,55(6)

Tuesday Poster

Wednesday Oral Sessions

1H. Cardiac Imaging

Hall 3

Wednseday, November 5, 2008, 8:30 am - 10:00 am

Chair: **James Miller;**
Washington University in Saint Louis, USA.

1H-1

8:30 AM **Cardiac Monitoring Using Transducers Attached Directly to the Heart**

Lars Hoff[1], Andreas Espinoza[2], Halfdan Ihlen[2]; *[1]Vestfold University College, Horten, Norway, [2]Rikshospitalet University Hospital, Oslo, Norway.*

Background, Motivation and Objective

We have designed and tested a prototype ultrasound system to monitor cardiac function continuously during and after cardiac surgery. The system uses miniature transducers attached directly to the heart surface, and presents data as M-mode images and tissue velocity curves.

Statement of Contribution/Methods

Two 10 MHz transducers with 3 mm diameter are sutured to the heart wall during cardiac surgery. The transducers are excited simultaneously at pulse repetition rate 2500 s^{-1}. A passive diode network is used as transmit-receive switch and to separate the two receive channels. The received signals are amplified and digitized in a 14 bit AD converter connected to a PC. The transmitter timing and the ADC sample rate is controlled by a 40 MHz crystal oscillator, giving a sample rate exactly 4 times the transducer frequency.

The same pulses are used both for M-mode and velocity calculations. The received scanlines are grouped in blocks of typically 8 lines, giving 312 frames per second. This number can be varied, as a trade-off between time resolution and image quality. Quadrature demodulation is performed digitally by bandpass filtering the RF scanlines and extracting every 4th sample. M-mode images are calculated from the absolute value of the IQ-lines, while tissue velocity at every depth is calculated from the phase shift through one block of lines.

Results are presented real time on the computer, using software developed in LabVIEW. A graphical user interface was designed to make the system easy to operate for non-technical personnel. The sampled RF lines can also be stored for later analysis.

Results

The system has been tested on pigs. Two transducers were sutured to the heart, one close to the apex and one higher on the left ventricle. ECG and instantaneous blood pressure were recorded synchronously with the ultrasound pulses as time markers. It was verified that the system could continuously monitor heart contraction, giving M-mode images and tissue velocity curves of good quality. The LAD coronary artery was temporarily blocked to mimic a coronary occlusion, resulting in velocity pattern changes that correspond with known markers if ischemia.

Discussion and Conclusions

We have constructed a prototype ultrasound system to continuously monitor the heart function of patients during and after cardiac surgery. The preliminary results show that the system can measure local heart contraction in great detail, but an assessment of the medical value of the system requires a more thorough clinical evaluation of the data.

We have also shown how to construct a real-time experimental ultrasound system with good performance, using dedicated analog electronics and a PC with AD-board. We have demonstrated how this can calculate velocity and M-mode images real-time at high frame-rates. We believe this experimental system can be useful also in other ultrasound applications.

1H-2

8:45 AM **Adaptive Dynamic Grid Interpolation: A Robust, High-Performance Displacement Smoothing Filter for Myocardial Strain Imaging**

Shuhui Bu[1], Tsuyoshi Shiina[1], Makoto Yamakawa[2], Hotaka Takizawa[1]; *[1]University of Tsukuba, Japan, [2]Kyoto University, Japan.*

Background, Motivation and Objective

Accurately assessing local myocardial strain is important for diagnosing ischemic heart diseases because decreased myocardial motion often appears in the early stage. The abnormal contraction motion can be visualized by myocardial strain images, but the strain calculation is very sensitive to noise. In our previous research, we proposed a dynamic grid-interpolation method for overcoming the limitation of the trade-off between spatial resolution and accuracy in traditional moving-average filters. Here, we propose a novel adaptive dynamic grid-interpolation (ADGI) method with the ability to adjust smoothing adaptively for myocardial strain imaging.

Statement of Contribution/Methods

Before the ADGI processing, a myocardial mesh is created, and the displacement vectors in the region of interest are detected by a weighted phase-gradient method combined with an autocorrelation method. In the ADGI method, virtual springs are attached at each mesh's node in radial and circumference directions. Revising displacements are introduced, and a global error evaluation function is defined. Minimizing the function yields optimal revising displacements, and revised displacements are calculated by combining detected and revised displacements at each mesh node. The virtual springs' pseudo-elasticity parameters, which are decided by a displacement error function, control the revising effect. If the displacement noise in some region is high, the virtual spring's pseudo-elasticity parameter is made large; if the displacement noise is low, the pseudo-elasticity parameter is made small.

Results

The performance of this method was evaluated by numerically simulating the short-axis imaging of a 3-D myocardial model. The finite-element method is used to simulate the strain distribution in the myocardium. Young's modulus in a normal wall is taken as 75 kPa and 225 kPa in an infarcted wall, and Poisson's ratio is set to 0.48. Echo signals were generated by considering the parameters of typical ultrasonic scanner with a center frequency of 3.75 MHz. The signal-to-noise ratio is set to 10 to 30 dB. The optimized pseudo-elasticity parameters that control smoothing are set in the range of 20 to 2800 in the radial direction and 20 to 800 in the shear direction.

For example, in a model with the infarcted region located around 1 to 3 o'clock, the accuracy was improved from 66.3% to 37.6% without degrading spatial resolution compared to that generated by using median and moving averaging filters, even for a low SNR (20 dB). The contrast was improved from 28.5% to 48.2% in that model.

Discussion and Conclusions

Because the smoothing effect can be automatically adjusted based on the noise level, we can see from the results that, although the strain's dynamic range is small, the strain generated by the ADGI method is more accurate and robust, and the spatial resolution is retained. Therefore, the abnormal myocardial contraction region can be clearly identified.

Wednesday Oral

1H-3

9:00 AM **Ultrasonic Imaging of 3-Dimensional Propagation of Electric Excitation and Vibrations in Human Heart**

Hiroshi Kanai[1], Junya Ohkohchi[2], Hideyuki Hasegawa[2]; *[1]Tohoku University, Department of Electronic Engineering, Sendai, Miyagi, Japan, [2]Tohoku University, Graduate School of Biomedical Engineering, Sendai, Miyagi, Japan.*

Background, Motivation and Objective

If the heart wall vibration caused as the response to the electric excitation is visualized using transcutaneous ultrasound, regional physiological properties in action potential and mechanical properties of the viscoelasticity can be noninvasively revealed. We have already found that the pulsive vibration is excited on the myocardium 15 ms after the electrical stimulation to an isolated heart [Acoustical Science and Technology **24**, 17 (2003)]. Base on the fact, we have transcutaneously detected the propagation of minute vibration caused just around R-wave of the electrocardiogram (ECG). However, such visualization was limited to 2-dimentional (2D) plane obtained by scanning the ultrasonic beams. In this study, the propagation of the vibrations caused just around R-wave of ECG is visualized in 3-dimentional (3D) space.

Statement of Contribution/Methods

Since the propagation speed is several m/s along the heart wall, the necessary temporal resolution is at least 2 ms for the visualization. In our previous study, using a sparse sector scan in 2D plane [IEEE Trans. UFFC. **51**, 1931

(2005)], the vibration waves were measured almost simultaneously at about 10,000 points set in the heart wall at a high frame rate but the scanning direction was limited to 10-16. Thus, there is no space to detect the RF data in 3D space with high temporal resolution. In this study, therefore, the multiple 2D data are acquired during consecutive several cardiac cycles and the propagation properties in 3D space are reconstructed. The probe on the chest wall is rotated intermittingly by 15 degrees at each of the relaxation periods during the consecutive 13 cardiac cycles, and RF data are acquired in the 2D plane by sparse scan in 16 directions. Since the direction of the ultrasonic beam at the center of the 2D planes is common in the data acquisition, it is easy to synchronize the time of each cardiac cycle precisely using the detected vibrations, and then the propagation of the vibration of the myocardium can be reconstructed in 3D space.

Results

The method was noninvasively applied to healthy subjects. The consecutive spatial distributions of the spatially interpolated phase of the waves reveal wave propagation along the heart wall. Just after the Q-wave of the ECG, the propagation started at the center of the interventricular septum, where Purkinje fiber contacts with the myocardium, to the base side and apical side of the heart. Its propagation speed was slow (1 m/s), which shows the propagation of electrical excitation. After the R-wave of the ECG, other pulsive waves started to propagate from the base to the apex. Since its speed was several m/s for about 50 Hz but there was dispersion, this is the shear wave caused by the mitral-valve closure.

Discussion and Conclusions

The method noninvasively reveals the propagation of electrical conduction wave by measuring regional myocardial response to it in human heart, which will be a novel tissue characterization of the heart.

1H-4

9:30 AM **Mapping Cardiac Currents using Ultrasound Current Source Density Imaging**

Ragnar Olafsson[1], Russell S. Witte[2], Congxian Jia[1], Sheng-Wen Huang[1], Kang Kim[3], Matthew O'Donnell[4];
[1]University of Michigan, Biomedical Engineering, Ann Arbor, MI, USA, [2]University of Arizona, Department of Radiology, Tucson, AZ, USA, [3]University of Pittsburgh Medical Center, Cardiovascular Institute, Pittsburgh, PA, USA, [4]University of Washington, Bioengineering Department, Seattle, WA, USA.

Background, Motivation and Objective

Correcting cardiac arrhythmia with ablation requires detailed maps of the electrical cardiac activation wave. Mapping is conventionally guided by fluoroscopy and electroanatomical mapping in a slow procedure with poor spatial resolution. Ultrasound current source density imaging (UCSDI) is a new technique that can potentially improve on existing methods. UCSDI uses voltage recordings, modulated by ultrasound through the acousto-electric (AE) effect, to map electrical current distributions. The potential advantages of UCSDI are high spatial resolution dependent on the ultrasonic point spread function, rapid mapping with electronically steered beams, and automatic registration to B-mode ultrasound.

Statement of Contribution/Methods

We describe the first mapping of cardiac activation using UCSDI. An isolated rabbit heart was perfused with Krebs-Henseleit buffer containing an excitation-contraction decoupler to reduce motion. The heart was paced at 3 Hz from either apex or right atrium (green diamond). Both electrocardiograms (ECG) and AE modulated voltage were measured with four tungsten electrodes (1,2,3, and 4, red dots) inserted into the left ventricle. A 540 kHz transducer was scanned from apex to base in 20, 1 mm steps. At each step the transducer was triggered (500 triggers, trigger interval=625 microsec) in synchrony with the cardiac pacing signal. AE modulated voltage and pulse echo signals were collected simultaneously for each trigger.

Results

On the left is an UCSDI image (bipolar, hot/cold colorscale) superimposed on top of B-mode ultrasound (dynamic range 30 dB, grayscale). The interior of the heart is between the two dashed white lines. Middle, top row: M-mode UCSDI images that correspond to the lateral dotted line (z=100 mm) in the image on the left. Middle, bottom row: ECG signals measured simultaneously on the same pair of electrodes as the AE signals in the UCSDI images above. The maximum signal to noise ratio was 18 dB and the noise equivalent detection threshold was 0.1 mA/cm2.

Discussion and Conclusions

This is the first mapping of a cardiac activation wave using UCSDI. UCSDI coincides with the ECG and shows spatial patterns consistent with electrode layout. This study demonstrates that UCSDI is a potentially powerful technique for mapping current flow in the heart.

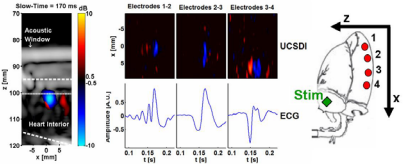

1H-5

9:45 AM **3D cardiac strain estimation using spatio-temporal elastic registration: in-vivo application**

An Elen[1], Andras Horvath[1], Javier Ganame[2], Brage Amundsen[3], Jens-Uwe Voigt[2], Piet Claus[2], Frederik Maes[1], **Jan D'hooge[2];** *[1]Catholic University of Leuven, ESAT, Belgium, [2]Catholic University of Leuven, Cardiovascular Diseases, Leuven, Belgium, [3]Norwegian University of Science and Technology, Circulation and Medical Imaging, Norway.*

Background, Motivation and Objective

Doppler- and speckle-tracking based deformation imaging of the heart has already proven its clinical value. Despite promising findings, both methodologies remain limited as they only assess 1 or 2 motion/deformation components of a truly 3D structure. Based on synthetic volumetric ultrasound (US) data of a kinematic heart model, we previously showed that spatio-temporal elastic registration should allow to measure myocardial motion and deformation in 3D. The aim of this study was to test the feasibility of this approach in-vivo.

Statement of Contribution/Methods

US volumetric data were recorded from 3 healthy volunteers using a Vivid7 (GE VingMed, Horten, Norway) equipped with a 2.5MHz transducer. Acquisition was gated over 6 cardiac cycles to achieve good spatial resolution at a temporal resolution of 27Hz. All volunteers were scanned twice. In addition, 3D data was collected from a patient with an apical aneurysm.

Voxel data were exported in Cartesian coordinates for off-line processing using the proposed methodology. To validate the quality of the estimated motion, the endocardial border was manually segmented at end-diastole (ED) and end-systole (ES) and interpolated with radial basis functions. The obtained ED-surface was propagated to ES using the motion estimates and compared to the ES-surface. Finally, to reconstruct the 3 normal myocardial strain components (εRR,εCC,εLL) a cardiac coordinate system was defined from an interpolating surface of the epicardial border at ED. Segmental 3D strain could then be calculated from the estimated motion field.

Results

The mean distance between the transformed and manually made ES endocardial surface was 1.58±1.16mm (at an intra-observer variability of manual contouring of 0.60±0.49mm). Average ES segmental strain was found to be respectively 31.11±11.24%, -11.18±2.77% and -5.64±2.70% for εRR,εLL,εCC. Example traces are shown in Figure1. Reproducibility of these traces between repeated acquisitions was good (data not shown).

Discussion and Conclusions

These preliminary findings show that 3D motion and strain estimation from currently available volumetric US data is feasible in the clinical setting using spatio-temporal registration. A more elaborate clinical evaluation is part of ongoing research.

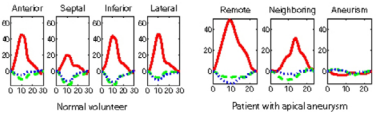

2H. Cavitation Therapy

Room 201 A/B/C

Wednseday, November 5, 2008, 8:30 am - 10:00 am

Chair: **Zhen Xu;**
University of Michigan, MI, USA.

2H-1

8:30 AM **Histotripsy for the treatment of BPH: evaluation in a chronic canine model**

Timothy Hall[1], Chris Hempel[1], Brian Fowlkes[2], Charles Cain[2], William Roberts[1]; [1]*University of Michigan Health System, Urology Surgery, USA,* [2]*University of Michigan, Biomedical Engineering, USA.*

Background, Motivation and Objective

Benign Prostatic Hyperplasia (BPH) is a condition of enlarged prostate growth leading to restriction of the urinary channel. The current gold-standard treatment is trans-urethral surgical resection using laser or electrocautery to core out a larger channel. In this study, non-invasive ultrasound therapy was evaluated as a method for prostate resection. Histotripsy uses brief, intense ultrasound pulses to induce cavitation at the focus of a transducer causing tissue disruption. Disrupted tissue is then easily irrigated from the urinary channel or passed with normal urinary voiding.

Statement of Contribution/Methods

Trans-abdominal histotripsy was performed on 24 anesthetized canines. Approximately a 4 cm^3 volume of prostate tissue was targeted for each subject spanning both the urethra and surrounding glandular tissue. A trans-rectal imaging probe was used for guidance. Therapeutic ultrasound exposure consisted of 15-20 MPa peak negative pressure 3 cycle 750 kHz pulses with a pulse repetition frequency (PRF) of 300 Hz applied with a dosing of 1000 to 10000 pulses/mm^3. Subjects were recovered with a urinary catheter in place for 1-3 days. Prostates were harvested on day 0, 7, 28, or 56 after treatment and analyzed grossly and histologically.

Results

The procedure was well tolerated by all subjects with no treatment related complications. An inflammatory response consistent with normal wound healing was noted. Re-urothelialization of the enlarged urinary channel was noted by 28 days (figure 1). At the 28 and 56 day time points, prostates treated with higher histotripsy doses had a similar appearance to standard surgical resection specimens (figure 1). The fibrous urethral wall was found to require a higher histotripsy dose for complete ablation than the glandular prostate tissue.

Discussion and Conclusions

Tailoring doses applied to various prostatic tissues (glandular and urethral) should allow optimization of histotripsy for non-invasive treatment of BPH. While in the canine, a trans-abdominal approach is used to access the prostate, in humans, a trans-rectal or perineal approach is favored. These are currently under evaluation.

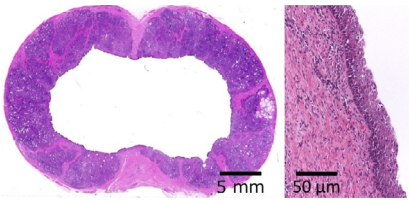

Wednesday Oral

2H-2

8:45 AM **The Role of Inertial Caviation in Acoustic Droplet Vaporization**

Mario L. Fabiilli, Kevin J. Haworth, Oliver D. Kripfgans, Paul L. Carson, J. Brian Fowlkes; *University of Michigan, Ann Arbor, MI, USA.*

Background, Motivation and Objective

The vaporization of perfluorocarbon (PFC) droplets using ultrasound, termed acoustic droplet vaporization (ADV), has been shown in vivo to occlude blood flow to targeted organs. It is hypothesized that inertial cavitation (IC) is one mechanism responsible for ADV. Previous work studied the influence of cavitation nuclei external to the droplets on the ADV threshold. We investigate the relationship between ADV and IC to determine when ADV, but not IC, occurs. This work focuses on the role of bulk fluid gas saturation, PFC boiling point, and type of bulk fluid.

Statement of Contribution/Methods

Emulsions were made with albumin, saline, and either C5F12 (PFP), C6F14 (PFH), or C8F18 (PFO) and sized using a Coulter Counter. Emulsions were diluted in the bulk fluid (water, 37°C), which was flowed at 2 cm/s through a 14.6 mm diameter dialysis tube. The gas content of the bulk fluid was measured. A 3.5 MHz single-element transducer (Panametrics, f/#=2, 12 ms PRP, 13 cycles) generated ADV while B-mode images were recorded using a 10 MHz linear array (GE L9). The mean echo power (MEP) in the B-mode images was calculated as a measure of ADV. Broadband noise in the range of 5-60 kHz was passively detected with a hydrophone as a measure of IC. The IC threshold was determined relative to degassed water, where no IC was assumed.

Results

Mean diameters of PFP, PFH, and PFO droplets were 2.1, 2.2, and 2.6 µm, respectively. For PFP droplets, the ADV thresholds in degassed (60 mmHg O_2) and gas saturated (170 mmHg O_2) water were 2.7±0.2 MPa and 2.8±0.1 MPa, respectively. No ADV was observed for PFH or PFO droplets, which unlike the PFP droplets, were not superheated. The IC thresholds for PFP droplets were 5.7±0.4 MPa (degassed water) and 6.0±0.3 MPa (gas saturated water). The IC threshold for PFH droplets was 6.4±0.2 MPa while no IC was detected for PFO droplets under 8 MPa. In whole blood the ADV and IC thresholds increased to 3.6±0.3 MPa and 7.1±0.1 MPa, respectively, for PFP droplets.

Discussion and Conclusions

The distinct ADV and IC thresholds indicate that ADV can occur independent of IC. The bulk fluid gas saturation level does not affect either threshold, suggesting that the IC nucleus is internal to the droplet. This is supported by the decrease in IC activity for PFH and PFO droplets. The thresholds increased in blood due to the increase in bulk fluid viscosity or scattering.

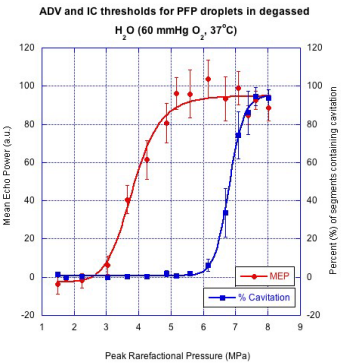

Wednesday Oral

2H-3

9:00 AM **Cavitation Detection with Subharmonic Emissions by Low-power Sustaining Ultrasound**

Shin Yoshizawa[1], Shin-ichiro Umemura[2], Yoichiro Matsumoto[3]; [1]*Tohoku University, Department of Electrical and Communication Engineering, Sendai, Japan,* [2]*Tohoku University, Graduate School of Biomedical Engineering, Sendai, Japan,* [3]*The University of Tokyo, Department of Mechanical Engineering, Tokyo, Japan.*

Background, Motivation and Objective

Control of acoustic cavitation by ultrasound pulse wave has been investigated recently. Cavitation detection is an important factor for the cavitation control. In this study, subharmonic detection which has been used to detect the acoustic cavitation in continuous sonication is applied to pulsed ultrasound sequence using low-power sustaining ultrasound.

Statement of Contribution/Methods

Figure 1 shows the ultrasound sequence with the sustaining ultrasound. The ultrasound was focused on a stainless steel wall in filtered and deionized water. The frequency of the ultrasound was 3.27 MHz, high-power pulsed ultrasound was 10 cycles, and its PRF was 100 Hz. The sustaining ultrasound is continuously irradiated and its power (I_{spta}) was 1.2 W/cm^2. The acoustic emission from the cavitation was detected with a hydrophone (HGL-0400, Onda).

Results

Figure 2 shows the spectrum of the emission measured with the hydrophone when the power of the high-power ultrasound was 12000 W/cm^2. A 50-µs Hamming window was applied to data just before the high-power pulsed ultrasound to avoid the reflected wave of the pulsed ultrasound. The subharmonic signal was clearly detected by this method.

Discussion and Conclusions

The power of the sustaining ultrasound is low enough to avoid cavitation inception by itself. However, when the microbubbles are generated and grow to the certain size by the high-power pulsed ultrasound, the sustaining ultrasound prevents the dissolution due to rectified diffusion. Finally, the bubbles can grow enough to emit subharmonic acoustic pressure. With this method, the cavitation generated by the pulsed ultrasound was successfully detected.

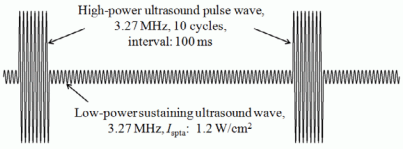

Figure 1: Waveform for the subharmonic detection by low-power sustaining ultrasound wave

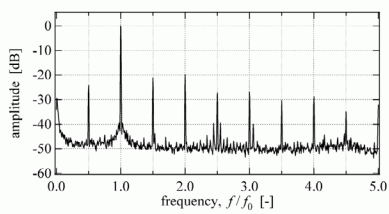

Figure 2: Spectrum of acoustic emission from the cavitating microbubbles by sustaining ultrasound wave

2H-4

9:15 AM **Non-invasive thrombolysis induced by histotripsy pulsed cavitation ultrasound therapy**

Adam Maxwell[1], Charles Cain[1], Hitinder Gurm[2], J. Brian Fowlkes[3], Zhen Xu[1]; [1]*University of Michigan, Department of Biomedical Engineering, Ann Arbor, Michigan, USA,* [2]*University of Michigan, Department of Internal Medicine, Ann Arbor, Michigan, USA,* [3]*University of Michigan, Department of Radiology, Ann Arbor, Michigan, USA.*

Background, Motivation and Objective

Blood clot formation is an essential response to injury but can be the cause of many cardiovascular diseases. Current treatments to remove blood clots (thrombolysis) include thrombolytic drugs and/or catheter-based techniques, both of which have significant drawbacks including risks of excessive bleeding and infection. Our goal is to develop a non-invasive thrombolysis method based on **Histotripsy**, a technique that mechanically fractionates soft tissue using controlled ultrasound cavitation. This paper investigates the feasibility and efficacy of this new approach to thrombolysis.

Statement of Contribution/Methods

Blood clots were formed *in-vitro* from whole porcine blood by adding $CaCl_2$ solution. Clots were placed in a 6 mm diameter LDPE tube and treated by histotripsy. The treatment targeting and monitoring were guided by ultrasound imaging. The histotripsy treatment consisted of 5 cycle ultrasound pulses delivered at a 1 kHz pulse repetition frequency and peak negative pressures of up to 14 MPa. Clots were treated until completely dissolved. Acoustic backscatter during treatment was collected for cavitation detection. Clots were also treated under flow rates up to 50 cm/sec in a circulatory model. To evaluate possible vascular damage, clots were treated in excised canine aorta and vena cava and histology of the vessels was examined for damage.

Results

Histotripsy can completely fractionate a clot weighing 300 mg (4 mm in diameter and 2 cm in length) in ~0.5 – 5 minutes (mean = 2.7 minutes, n = 32 clots). Histotripsy thrombolysis was initiated at peak negative pressures ≥ 8 MPa, and only after initiation of a cavitating bubble cloud was detected. The thrombolysis rate (clot weight/treatment time) increased with increasing pressure. Histotripsy fragmented the clot into debris no larger than 60 µm in diameter, with over 90% (by volume) of the debris having diameters < 8 µm. The treated vessels were intact upon initial histological evaluation. Histotripsy thrombolysis was effective both in high flow and static environments. The treatment targeting and progress can be clearly seen on an ultrasound image. Moreover, we observed that clot fragments are attracted to the vicinity of the bubble cloud, and can be trapped and further fragmented at the focus.

Discussion and Conclusions

Our results suggest that histotripsy is an effective and efficient non-invasive method for thrombolysis guided by real-time imaging. Most clot debris fragments generated are smaller than red blood cells. Large clot fragments can be trapped near the bubble cloud and further fractionated. This phenomenon is possibly due to a particular fluid flow pattern created by cavitation-induced microstreaming. We plan to use this property to create a Non-invasive Embolization Trap (NET) to prevent embolization caused by escaping clot fragments. These results suggest that histotripsy has the potential to emerge as a safe and effective non–invasive thrombolytic.

2H-5

9:30 AM **Mean Echo Power as a Measure of Flow Reduction for Bubble Occlusion Therapy**

Kevin Haworth[1], Mario Fabiilli[1], J. Brian Fowlkes[1], Man Zhang[1], Oliver Kripfgans[1], William Roberts[2], Paul Carson[1]; *[1]University of Michigan, Radiology, Ann Arbor, MI, USA, [2]University of Michigan, Urology, Ann Arbor, MI, USA.*

Wednesday Oral

Background, Motivation and Objective

In vivo blood flow reductions can be achieved using Acoustic Droplet Vaporization (ADV). Ultrasound was used to phase-transition perfluorocarbon (PFC) droplets into gas bubbles with diameters typically larger than capillaries. An in situ ultrasonic measurement of blood flow reductions is desirable. Since, in a simple model, initial flow reduction is proportional to the number of bubbles, and the mean echo power (MEP) in a B-mode image is related to the number of bubbles (off resonant scattering), it is hypothesized that the MEP can be used to estimate the relative flow reduction.

Statement of Contribution/Methods

A canine kidney was externalized and an ultrasonic flowmeter (Transonic TS420) was placed on the renal artery or one of its branches to measure volume flow. A focused 3.5 MHz single-element transducer (Panametrics, f/#2, 400 Hz PRF, 13 cycles, 7 MPa) was targeted on to the exposed artery. Lipid stabilized PFC droplets (5x10^9/ml) were injected IV and vaporized in the renal artery. B-mode images were recorded before, during, and after the vaporization using a linear array (10L, Logiq 9, GE). The MEP was computed for a region in the kidney cortex.

Results

Following ADV, the MEP generally returned to pre-vaporization levels as flow was being restored. For example, a 6 mL injection would require approximately 10 minutes for the MEP to return to half the pre-vaporization value. The time needed for the MEP to return to pre-vaporization levels was sufficient for the blood flow to stabilize, although not always returning to the pre-ADV rate. Flow restoration was typically faster than MEP restoration. In some cases, regions of increased echogenicity would persist. In addition, when achieving substantial occlusion (up to 85%) of the targeted artery, the kidney became significantly shadowed; precluding an MEP measurement for a region encompassing a significant portion of the kidney cortex.

Discussion and Conclusions

While changes in the MEP within the renal cortex were observed during ADV and followed general trends in blood flow changes, there were differences in the time course between MEP and flow measures. Focal regions of persistent MEP increases may be related to sustained decreases in flow but will require additional investigation. The acoustic shadowing present for ADV sufficient for substantial flow reduction may be require alternative methods for acoustic evaluation.

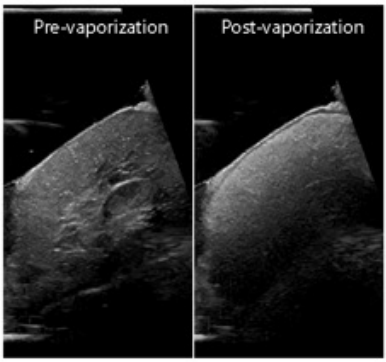

2H-6

9:45 AM **Cavitation assisted HIFU with phase-change nano droplet**

Ken-ichi Kawabata[1], Rei Asami[1], Takashi Azuma[1], Hideki Yoshikawa[1], Shin-ichiro Umemura[2]; *[1]Central Research Laboratory, Hitachi, Ltd., Japan, [2]Tohoku University, Japan.*

Background, Motivation and Objective

Although HIFU therapy is well established as a minimally invasive cancer treatment, there is a great demand for an improved throughput on total operation time. One of approaches for improving the throughput is coagulating broader area with each shoot of HIFU with the aide of microbubbles as sensitizers. We further propose the use of nano-sized precursor of microbubbles instead of microbubbles directly, for a controlled distribution of bubbles inside body[1]. The precursor is designed to convert into bubbles upon ultrasound pulses, thus microbubbles are generated only at the focus of the pulse. In this paper, preliminary *in vitro* and *in vivo* results on temperature rise and cavitation generation will be presented with the expose of relatively low frequency ultrasound (around 1 MHz) in the presence of the microbubble precursors.

Statement of Contribution/Methods

The nano sized microbubble precursor was prepared by high-pressure (20 MPa) homozinizing of the mixture of phospholipids liposome and volatile perfluorocarbons (phase-change nano droplet, PCND). Focused ultrasound transducer (frequency: 1.1 MHz, diameter: 40 mm, F number: 1.2) was used as the source for the activation of the precursor and HIFU exposure. The exposure time was set to 1 ms for the activation of PCND and 20 sec for HIFU therapy. Effect of the combination of PCND and ultrasound on temperature rise was investigated *in vitro* with gel phantoms containing albumin as an indicator of temperature rise. Cavitation generation was measured with a focused type hydrophone. *In vivo* effect of the ultrasound exposure was investigated with tumor-baring mice, injecting PCND intravenously.

Results

In phantom experiments, it was found that PCND can reduce the ultrasound intensity required for protein coagulation about an order of magnitude. Moreover, in the presence of PCND, phantom gel structures at the ultrasound focus were visibly broken after HIFU exposures, suggesting the generation of cavitation. The cavitation generation with PCND was further confirmed by the detection of subharmonics with hydrophone measurements. Ultrasound exposure to tumor tissues in the presence of PCND resulted in tissue erosions at the focus immediately after the exposure, while no clear damages were observed when ultrasound alone was used.

Discussion and Conclusions

Our results suggested that the combination of 1-MHz ultrasound and phase-change nano droplet can improve the throughput of HIFU therapy by increased temperature rise and cavitational effects. By generating microbubbles selectively in tumor tissues, the HIFU therapy would also be highly tumor selective. We further investigate the optimal blending of cavitational and thermal effects for cancer treatment.

Reference

[1] K. Kawabata, *et al*,; Jpn. J. Appl. Phys. **44** 4548 (2005)

Acknowledgement

Part of this work was supported by the New Energy and Industrial Technology Development Organization of Japan.

3H. Transducer Modeling and Design

Room 305 A/B/C

Wednseday, November 5, 2008, 8:30 am - 10:00 am

Chair: **Reinhard Lerch;**
Univ Erlangen, Germany.

3H-1

8:30 AM **Finite Element Modeling of Ultrasonic Transducer by Utilizing an Inverse Scheme for the Determination of its Material Parameters**

Felix Wolf, Tom Lahmer, Ludwig Bahr, Manfred Kaltenbacher, **Reinhard Lerch;** *University of Erlangen-Nuremberg, Department of Sensor Technology, Germany.*

Background, Motivation and Objective

The exact modeling of transducers asks for the precise knowledge of the material parameters of all parts involved in the transducer assembly. Meanwhile, a various number of approaches to characterize piezoceramics have been developed, often based on the conventional IEEE or CENELEC methods using mono-modal resonators to determine the piezoelectric material parameters. The main drawback of such methods is often the need of some well-defined geometries of the ceramic, as well as the isolated observation of the ceramic without considering the whole assembly.

Statement of Contribution/Methods

Our approach for modeling ultrasonic transducers is based on the finite element method. We propose an iterative scheme, recently introduced by our group in [T. Lahmer et al. IEEE Transactions on UFFC, 55(2):465-475] for the identification of the piezoelectric parameters based on measurements of the electrical impedance and/or mechanical displacement. We have extended our inverse scheme and allow now for the identification of a whole assembly.

Here, the practicability of the new method is tested in two different ways, analyzing an ultrasonic transducer setup, consisting of a piezoceramic disc and a matching layer with one quarter wavelength. In the first approach, the piezoceramic disc and the matching layer are investigated separately by performing impedance and mechanical displacement measurements. Applying the iterative scheme for each component individually delivers piezoelectric, mechanical and dielectric parameters for the piezoceramic disc as well as the mechanical parameters for the matching layer. In a second approach we investigate the electromechanical behavior of the whole assembly and directly apply the inverse scheme. As in the first approach, we use as starting values for our iterative method the manufacturer's data of the piezoceramic and the matching layer, respectively.

Results

To verify the results of the new method, simulations of the generated ultrasound field are performed with the material parameters obtained from both approaches and compared to measurements of the sound pressure level of the ultrasonic transducer. Regarding the measurements, two different methods are carried out: A conventional measurement using a hydrophone as well as Light Refractive Tomography, a non-reactive method based on interferometer measurements, which was developed by our group. Due to this precise measurements and the accurate identification of the material parameters in the second approach, the simulation shows a good agreement with the measured data (deviation is below 1 dB).

Discussion and Conclusions

The advantage of our method is that ultrasonic transducers can be characterized without suffering from inexact manufacturer data or time-consuming, expensive measurements. Our scheme needs no measurement data of the individual transducers components but allows a direct determination of the material parameters of the whole transducer.

3H-2

8:45 AM **A comparison of array element surface vibration calculated by FEM modelling and laser interferometer measurements**

Paul van Neer[1], Guillaume Matte[1], Jerome Borsboom[1], Philipp Gatta[2], Massimo Pappalardo[2], Nico de Jong[1]; *[1]ErasmusMC, Biomedical Engineering, Rotterdam, Netherlands, [2]Università Roma Tre, Dipartimento di Ingegneria Elettronica, Rome, Italy.*

Background, Motivation and Objective

For several years the standard in ultrasound imaging has been second harmonic imaging. Recently, a new imaging modality dubbed super harmonic imaging (SHI) was proposed. SHI uses the higher – third to fifth – harmonics produced by either nonlinear propagation or contrast agent response. This modality requires a transducer with a high bandwidth (>130%), which was achieved by choosing different frequencies for the odd (4MHz) and even (1MHz) elements. Next to the main issues of sensitivity and bandwidth, issues such as crosstalk and minimizing the contamination of the super harmonic signal by the third harmonic produced by the transmitting part of the interleaved design are important. The influence of geometry on these last design issues can not be determined using 1D models and requires a 3D finite element model (FEM) approach. In this paper we compare surface vibrations calculated by a FEM model with measured vibrations obtained using a laser interferometer system.

Statement of Contribution/Methods

An experimental array was built from CTS 3203HD material with an element size of 13 x 0.2 mm2, a resonance frequency of 1.7 MHz, no matching layer and a backing of 5.3 MRayl with an attenuation of 18 dB/cm at 1.7 MHz. The spatially and time dependant surface vibrations of the array elements were measured in air using a laser interferometer setup. The setup consisted of a laser mounted on a microscope. The element was mounted on an x-y table and the surface vibration was recorded with a step size of 27 µm. The laser spot diameter was 10 µm. The array elements were excited by either a continuous sinusoidal signal with amplitude 14.5 V or an impulse with amplitude -69 V. The array element (characterized by its dimensions, piezo parameters from the data sheet and measured bulk parameters of the backing, such as impedance and attenuation) was modeled using the ANSYS 11 FEM package and subjected to the same excitation.

Results

The fundamental resonance, third harmonic and fifth harmonic of the array elements were measured at 1.7, 6.4 and 9.8 MHz in an electrical impedance measurement. The FEM model predicts these resonances at 1.6, 6.1 and 9.1 MHz. A lateral mode was measured at 8.1 MHz, which was the same frequency as predicted by the FEM model. The maximum excursion measured during continuous wave excitation was between 14.5 and 32 nm with a mean maximum excursion of 27.6 nm, the FEM model predicts it between 16 and 36 nm with a mean maximum excursion of 27.3 nm. Both in the measurements and in the FEM model results the ripple in the y-displacement over the long axis of the element had a wavelength between 1.2 and 1.3 mm.

Discussion and Conclusions

Good agreement was achieved between the FEM predicted surface vibrations and the laser interferometer results. Next steps include the modelling of the matching layers, the electrical connection and the housing.

Wednesday Oral

3H-3

9:00 AM **Development of 1.5D Cylindrical HIFU Phased Array**

Gin-Shin Chen[1], Ruibin Liu[2], Hsu Chang[1], K. Kirk Shung[2]; *[1]National Health Research Institutes, Medical Engineering Research, Miaoli, Taiwan, [2]NIH Ultrasound Transducer Resources Center, University of Southern California, Biomedical Engineering, USA.*

Background, Motivation and Objective

High intensity focused ultrasound, HIFU has been used to non-invasively treat human tumors, such as uterine fibroids, prostate cancer, breast cancer, liver tumor, and brain tumor. However, the tumor in some organs can be moved by human breathing and heart beat, which may cause the ablation and damage of normal tissues during the sonication of HIFU. The purpose of this study was to develop a HIFU phased array for tracking the moving tumors which was designed to have a center frequency of 1.0 MHz and 512 elements that allowed symmetric control.

Statement of Contribution/Methods

PZT-4 1-3 composites were formed via the ″dice and fill″ technology and then shaped into a cylindrical structure.

Results

The results simulated by Field II demonstrated that the array in water had a dynamic focusing range from 145 mm to 175 mm in Depth and a steering range from -15 mm to 15 mm in azimuthal direction with respect to the center of the array. A prototype of the array was developed and shown as the below photo. The dimension of the array without the housing was 15 cm in azimuth as well as 12 cm in elevation and the radius of curvature was 15 cm. The impedance of each channel (a pair of elements) was measured and the average was 1500 Ohm. Intensities up to 12.6 W/cm2 were applied to one piece of cylindrical PZT4-composite consisting of 22 elements for 50 minutes, and the temperature of the composite was not observed to rise appreciably. A 256-channel amplifier was utilized to drive the array without impedance matching in water and a water line was observed at the natural focus of the array when the driving signal to each channel was zero-phase at 0.9MHz.

Discussion and Conclusions

The phase control and impedance matching circuits for each channel are being designed.

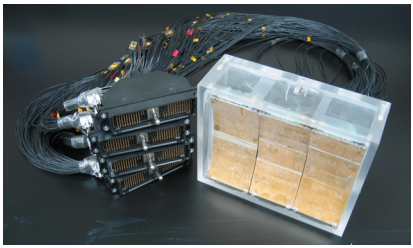

3H-4

9:15 AM **Piezoelectric membrane sensor and technique for breathing monitoring**

Yuu Ono[1], Dilshad Mohamed[1], Makiko Kobayashi[2], Cheng-Kuei Jen[2]; *[1]Carleton University, Canada, [2]National Research Council Canada, Canada.*

Background, Motivation and Objective

Monitoring of breathing conditions during sleeping is one of crucial information for appropriate diagnosis of sleep disorders. Polysomnography in a sleep laboratory is the standard technique for such diagnosis, but the test is expensive and not widely available. Currently a few home devices are commercially available which monitor breathing patterns by measuring temperature variations resulting from exhalation and inhalation. However, these devices are not able to provide quantitative information such as airflow rate which is necessary for the detailed diagnosis. Development of less costly sensors and technique capable of quantitative breathing monitoring for home sleep study is desirable.

Statement of Contribution/Methods

A piezoelectric membrane sensor, consisting of a stainless steel (SS) foil, a piezoelectric ceramic film and a top electrode, has been developed. Thick lead zirconate titanate composite film was fabricated onto the 40-µm thick SS foil using a sol-gel spray technique. The thickness of the film was 60 µm. The dimensions of the active transducer area were 4 mm by 20 mm. Due to the porosity in the film and thin substrate, the sensor has high flexibility. This sensor has worked as a unimorph-type bending sensor, which could be attached beneath the nose and/or above the mouth using a clip or tape for breath monitoring. Furthermore, a breathing simulator has been developed in order to investigate a technique for quantitative measurement of airflow variations during breathing. The simulator is composed of a reciprocal air pump surrounded by an electric heater, an air chamber where the sensor is installed, a spirometer to measure the airflow rate, and a data acquisition unit.

Results

Experiments were conducted by changing the airflow volume per breath from 100 to 500 ml with a step of 100 ml and the breathing cycle from 15 to 75 breaths per minute (bpm) with a step of 15 bpm using the simulator developed. The electric charge signals from the sensor caused by its bending motion due to the airflow pressure were amplified by a charge amplifier, digitized by an A/D converter, and recorded with the air temperature and airflow rate with a sampling rate of 100 Hz. Under the experimental conditions employed, the strength of the output signal increased with increasing the airflow rate (speed).

Discussion and Conclusions

A mathematical model for the sensor output with respect to the airflow speed has been developed for the presented measurement configuration using piezoelectric theory and Bernoulli's law. The model developed indicates that the sensor output signal is proportional to the square of the airflow speed, which agreed with the experimental results. The effect of air temperature variations on the sensor output has been also investigated and discussed. A calibration curve between the airflow speed and the output voltage was obtained experimentally. Thus, the sensor and technique developed could measure airflow variations quantitatively.

3H-5

9:30 AM **Design and Fabrication of a 40MHz Transducer with Enhanced Bandwidth**

Jian-Hung Liu, Sheng-Yung Chen, Pai-Chi Li; *National Taiwan University, Taipei, Taiwan.*

Background, Motivation and Objective

High-frequency ultrasound (>20 MHz) is now widely used in applications such as dermatology, ophthalmology, and small-animal preclinical studies. Several approaches have been proposed to improve performance of high frequency transducers. The purpose of this paper is to report a new type of high-frequency single-element annular transducer (SEAT) with increased bandwidth. Such a broadband transducer can be used to improve the axial resolution or to perform contrast and tissue harmonic imaging.

Statement of Contribution/Methods

Compare with the conventional single element uniform thickness (SEUT), the SEAT has an annular geometry with the thickness of the piezoelectric material increasing from the center to the outside. Schematics of the two types of ultrasonic transducers are shown in the following figure (left: SEUT, right: SEAT). The transducers were made with 36° rotated, Y cut lithium niobate (LiNbO3) with a longitudinal high sound velocity which is suitable for fabricating the non-uniform thickness of annular pattern. The SEAT consisted of six subelements, whose thickness ranged from 60 μm to 110 μm. Here each side of annular pattern is only electrically connected by a single electrode. The diameter of the SEAT was 6 mm.

Results

For comparisons, both SEAT and SEUT transducers were designed and fabricated. The mean center frequencies of the SEUT and SEAT are 41.3 MHz and 42.4 MHz, respectively. The -6 dB fractional bandwidths are 69% for the SEUT and 82% for the SEAT. The two-way insertion losses of the SEUT and SEAT are 16.4 dB and 19.5 dB, respectively. The measured -6 dB lateral beam widths are 92 μm for the SEUT and 108 μm for the SEAT. The depth of field of SEAT is increased by 33.5 % as compared with the SEUT.

Discussion and Conclusions

Fabrication methods for high frequency ultrasound transducers were successfully developed and implemented. The SEAT enhanced the overall bandwidth and with a tradeoff of slight degradation in sensitivity. This type of transducers can also be used for multiple band imaging.

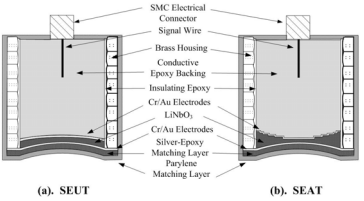

4H. Device Modelling

Hall 2A

Wednseday, November 5, 2008, 8:30 am - 10:00 am

Chair: **Clemens Ruppel;**
EPCOS AG, Germany.

4H-1

8:30 AM **Experimental and theoretical analyses of thermal sensitivity of periodically poled transducers for RF applications**

Emilie Courjon, Julien Garcia, Gwenn Ulliac, William Daniau, Sylvain Ballandras; *FEMTO-ST, Besançon, France.*

Background, Motivation and Objective

Periodically poled transducers (PPTs) built on Z-cut Lithium niobate thinned layers have been implemented and tested, showing their capability to operate at RF frequencies, with various wave polarisation and substrate conifgurations (self-supported plates or reported on silicon). They represent an alternative to standard surface acoustic wave (SAW) and bulk acoustic wave (BAW) devices, sharing advantages of frequency definition by planar photolithography with SAW and excitation using in-regard electrodes, separated by a strongly dielectric medium preventing misoperation due to electrode defects and allowing for supporting large excitation fields as for BAW. The temperature sensitivity of the PPTs modes however cannot be easily deduced, as their analysis requires finite element based tools which generally do not allow for such calculations.

Statement of Contribution/Methods

In this work, we experimentally and theoretically investigate the temperature sensitivity of PPTs.

In this purpose, test devices have been tested using a tip prober equiped with a thermally controlled chuck allowing for temperature excursions in the range usual temperature range. These test devices consist in long transducers with wavelength (i.e. mechanical periodicity for such devices) varying from 200 to 10 µm, yielding operation frequencies ranging from 17 to 650 MHz.

On the other hand, the theoretical prediction of frequency-temperature behaviour of PPTs has been achieved by developing this function in our finite element/boundary element (FEA/BEM) periodic code. The celebrated Campbell & Jones perturbation approach has been implemented, requiring for each temperature the thermal expansion of the mesh together with effective physical constant (elastic, piezoelectric, dielectric) calculation according to Pastureaud & al assumptions. Even if this approach is known to suffer from unperfect mathematical fundaments, it appears accurate enough to predict BAW and SAW temperature compensated cuts and then was implemented to predict PPTs thermal sensitivity. When considering PPT/Silicon, the Green's function used in the BEM part of the code also is computed for each temperature, yielding a reliable representation of the problem.

Results

Temperature sensitivities of both elliptically and longitudinally polarized waves of PPTs have been measured. For self supported LiNbO3 plates, we have measured -70 and -85 ppm/K respectively. Theoretical predictions are in a rather good agreement with these values, i.e. -75 and -90 ppm/K respectively. These figures dramatically reduces for PPTs reported on Silicon substrates, allowing for devices with reduced thermal sensitivities (near -40 ppm/K).

Discussion and Conclusions

We have a rather good agreement between experimental and theoretical predictions.

Any kind of structure thus can be now considered using our simulation tool, allowing for innovative solution to be tested before any practical implementation.

4H-2

8:45 AM **Simulation of Waveguiding in SAW Devices on Substrates with Anisotropic Slowness and Excitation**

Markus Mayer[1], Andreas Bergmann[1], Guenter Kovacs[2], Karl Wagner[1]; *[1]Epcos AG, SAW RD BT, Germany, [2]Epcos AG, SAW COM WT, Germany.*

Background, Motivation and Objective

The 2D P-matrix simulation method (Mayer et al., 2006) is extended to deal with SAW substrates exhibiting a strong anisotropy in slowness and excitation such as YZ-cut lithium niobate.

In these substrates the parabolic approximation of the slowness curve is in general not valid. Instead, the exact form of the slowness, obtained from solutions of the basic wave equations of the piezoelectric half space, needs to be employed. This has two major implications: Firstly, the imaginary branches cannot be simply determined as the complex roots of a parabolic equation.

The second implication is that the resulting transversal modes in general are not orthogonal as in the parabolic case. This is a consequence of the neglect of the vector nature of waveguide modes in the scalar potential approximation. Therefore employing these modes in the 2D P-matrix method energy conservation is not strictly fulfilled. We show that nevertheless reasonable results can be obtained with the approach.

Statement of Contribution/Methods

We determined the imaginary branches from analytical continuations of the exact slowness curve. The problem of non-orthonormal basis functions was dealt with by a projection technique including bounded as well as continuum modes. Besides the general anisotropy of the slowness also the anisotropy of the excitation is taken into acount. Thereto a convolution of the angle dependent excitation characteristic with the transversal charge distribution is determined.

Results

The method is verified at the example of very narrow resonators on YZ-cut lithium niobate, which exhibit strong diffraction effects. With respect to the parabolic approximation a significant improvement of simulation quality is observed.

Discussion and Conclusions

The method allows to account for effects of general anisotropies in SAW slowness and excitation. For the text structures investigated a good agreement of measurement and simulation was found.

Wednesday Oral

4H-3

9:00 AM **Quasi-2D COM model for diffraction calculation in slanted finger SAW devises**

Eduard Chilla[1], Alexander V. Osetrov[2], Bernd Steiner[1], Asger Jaffer[3], Richard Gruenwald[1]; *[1]Vectron International, Germany, [2]St. Petersburg State Electrotech. University, Russian Federation, [3]Vectron International, United Kingdom.*

Background, Motivation and Objective

The diffraction in surface acoustic wave (SAW) devices has been proved to significantly influence the SAW filter performance. Recently, Wagner et al. [1] have introduced a two-dimensional (2D) model for the simulation of waveguiding and diffraction. In contrast, Hirota and Nakamura [2] have developed a 2D coupling-of-modes (COM) model for grating waveguides.

[1] K. Wagner, M. Mayer, A. Bergman, and G. Riha: “A 2D P-matrix model for the simulation of waveguiding and diffraction in SAW components”, IEEE Ultrason. Symp. pp 380-388, 2006

[2] K. Hirota and K. Nakamura, “Analysis of SAW grating waveguides using 2-d conpling-of-modes equations”, IEEE Ultrason. Sympos. pp. 115-120, 2001

Statement of Contribution/Methods

In this paper, the authors describe a quasi-2D (Q2D) COM approach for SAW diffraction based on interaction between adjacent channels, where the diffraction depth, i.e. the number of channels talking to each other by means of angular spectrum of waves (ASoW), is calculated iteratively. Since the convergence is very fast, and requires a low number of iterations only, this diffraction simulation can be applied for daily design work. Furthermore, standard COM fitting procedures may be used. This increases the accuracy of the simulation significantly.

Results

After describing the Q2D theory, the authors apply the model for slanted finger interdigital transducer (SFIT) filter analysis. The forward (R-field) and backward (S-field) travelling acoustic modes are calculated and the impact of

refraction and diffraction on the bandwidth and stopband degradation is analysed. Finally, experimental data measured for various designs on different materials are compared with simulation with and without diffraction, respectively.

Discussion and Conclusions

The results demonstrate the simulation model's excellent prediction accuracy with regards to the paassband width, the filter skirts and stopband performance.

4H-4

9:15 AM **Two-Dimensional Grid Method for the Synthesis of SAW Filters**

Petr Ivanov[1], Vladimir Makarov[1], Jidong Dai[2]; *[1]Moscow Engineering-Physical institute, Moscow, Russian Federation, [2]RF Monolithics Inc., Dallas, Texas, USA.*

Background, Motivation and Objective

The advantages of different types of SAW filters are well known: transversal filters have the best roll-off, filters based on RSPUDT have medium insertion loss and small size, and LCR filters have low insertion loss. Structures and synthesis methods for different types of filters differ significantly. A uniform synthesis method for SAW filters that combine the advantages of different SAW filter structures is proposed in this paper. The method is based on two-dimensional coordinate grid representation of transducer structures and optimization algorithm used in the synthesis routine.

Statement of Contribution/Methods

This method includes the following features: Each transducer (or grating) can be represented as a composition of basic elements with widths equaled to a selected pitch. Usually a wave length is divisible by the pitch. Basic elements can be fingers connected to a transducer bus-bar or free space. A few neighboring fingers connected to a common bus-bar correspond to an electrode and a few free-space elements correspond to a gap. The second grid representation is a division of the transducer by layers along the filter aperture, that means that finger lengths can be changed in accordance with layer edges or each electrode can be apodized.

The optimization algorithm changes the transducer structure in series along SAW direction and aperture, simulates the filter response corresponding to the current structure and minimizes the error between the filter requirement and the parameters of the current structure developed. Restrictions for the synthesis routine are minimal and maximal electrode or gap widths. These restrictions depend on technological or physical limits. Besides, optimal or fixed matching circuits, parasitics, input and output impedances are accounted in the synthesis routine.

Results

The method has been applied for the synthesis of SAW filters on different substrates, not only for filters on substrates with the natural unidirectivity, but also for filters with leaky waves such as LCRF.

Discussion and Conclusions

Simulation and experimental results confirm effectiveness of this method for the improvement of filter parameters comparing with prototypes.

4H-5

9:30 AM **FEM/BEM Analysis of infinite periodic grating covered with an SiO2 overlay**

Pascal Ventura[1], Julien Gratier[2]; *[1]Ventura R&D Consulting, NICE, France, [2]Triquint Semiconductor Inc., Orlando, Florida, USA.*

Background, Motivation and Objective

In order to improve the temperature stability of RF SAW devices, it is worth adding a layer of SiO2 on the surface of the piezoelectric substrate.

This paper presents an original method which allows the computation of the Harmonic Admittance of an infinite periodic grating covered with an SiO2 overlay. The origins of this method can be found in previous paper [1].

Statement of Contribution/Methods

By comparison with S. Ballandras [2] work which have developed FEM models (using a FEM basis interpolation for charge distribution), this methods allows to take into account the very efficient Chebyshev-like charge distribution, together with a classical FEM basis interpolation for the stresses.

FEM is used to model mechanical behavior of complex shape electrodes and BEM using a periodic Green's function Kernel is used to take into account the semi-infinite piezoelectric substrate.

Results

Validations are presented by comparison with K. Hashimoto's publications.

Comparison between experimental data and simulation results are also presented.

Discussion and Conclusions

Comparison with both published data and experimental measurements are very satisfactory. Because of the very efficient interpolation of charge distributions an improved accuracy of the physical fields computations and of the harmonic admittance have been obtained.

[1] P. Ventura, J.M. Hodé, J. Desbois, M. Solal, "Combined FEM and Green's Function Analysis of Periodic SAW Structure, Application to the Calculation of Reflection and Scattering Parameters", IEEE Trans. Ultrason., Ferroelect., Freq. Contr., pp. 1259-1274, vol.48, no. 5, sept. 2001.

[2] S. Ballandras, V. Laude, T. Pastureaud, M. Wilm, W. Daniau, A. Reinhardt, W. Steichen, R. Lardat, "A FEA/BEM Approach to Simulate Complex Electrode Structures Devoted to Guided Elastic Wave Periodic Transducers", 2002 IEEE Ultrasonics Symposium, pp. 321-324.

4H-6

9:45 AM **Extraction of COM parameters on Pt/LGS for high temperature SAW sensor**

Thierry Aubert, Frederic Sarry, Omar Elmazria, Laurent Bouvot, Badreddine Assouar, Pascal Nicolay; *Nancy University-CNRS, Laboratoire de Physique des Milieux Ionisés et Applications UMR 7040, Vandoeuvre les Nancy, N/A, France.*

Background, Motivation and Objective

Many industrial processes take place in harsh environments, hardly compatible with conventional monitoring methods. It is now well established that surface acoustic wave are suitable for sensor applications such as pressure sensor, biosensor, temperature sensor and mass sensor. Industrial sectors such as power plants, nuclear sector or metallurgy are interested by sensors able to operate at high temperature up to 1000°C. The overall performance of these devices depends strongly on the type and cut of the piezoelectric substrate. It also depends on the kind of metallization used. Langasite (LGS) is a piezoelectric material that can operate up to its melting point at 1470°C, without phase transition or chemical decomposition as in quartz or LiNbO3 respectively. LGS substrate must be combined with metal suitable for high temperature use [600-1000°C] for the building of interdigital transducers (IDT). Platinum (Pt) is a good alternative to the commonly used Aluminum.

Statement of Contribution/Methods

In order to design, fabricate and evaluate a SAW delay line for high temperature applications incorporating LGS substrate and Pt IDT, we used software programs developed by K. Hashimoto. First of all, the physical constants of platinum (versus temperature) [1] were added in the FEM/SDA program to define a new electrode material. From the obtained responses, we extracted the Plessky's parameters at various temperatures and we injected them in the coupling of mode (COM) program to implement SAW filters operating at 292 MHz.

Results

In the same time, experimental test structures (Pt/LGS Y-X) were made to measure relevant parameters like velocity, attenuation, TCF, electromechanical coupling coefficient and propagation losses, at various temperatures. Simulation results were compared to experimental ones in order to adjust COM parameters at room temperature. Nevertheless divergences appear at high temperature. This should be mainly due to the incertitude on the temperature coefficients of elastic constants of LGS, previously used to extract COM parameters. In fact, several sets of material constants of LGS are available, but there are discrepancies between them. Constants published by Bungo et al. [2] seem to give the best results but divergence persist at high temperature over 250 °C.

Discussion and Conclusions

COM parameters of Pt/LGS structure were extracted using FEM/SDA program with experimental feedback, to allow the design of SAW devices at high temperature. Theoretical and experimental results are in good agreement up to 250°C, but discrepancies appear above this temperature. In the paper we point out the possible origins of that phenomenon. We propose theoretical explanations and experimental ways to solve the problem.

References

[1] S.M. Collard, R.B. Mc Lellan, Acta. metall. matter, vol. 40, n°4, pp 699-702, 1992.

[2] A. Bungo, C. Jian, K. Yamaguchi, Proc. IEEE Ultrason. Symp. pp 231-234, 1999.

5H. Material and Defect Characterization

Hall 2B

Wednseday, November 5, 2008, 8:30 am - 10:00 am

Chair: **Roman Maev;**
University of Windsor, Canada.

5H-1

8:30 AM **Laser ultrasonic detection of corrosion and adhesive disbond using Zero-Group Velocity (ZGV) Lamb modes**

Dominique Clorennec, **Claire Prada,** Marie Yoshida, Daniel Royer; *CNRS, Université Paris 7, ESPCI, Laboratoire Ondes et Acoustique, Paris, France.*

Background, Motivation and Objective

The use of adhesive bonding, particularly in automotive and aerospace industries, has been motivated by the need for stronger and lighter structures. Compared to other techniques like riveting or screwing, adhesive bonding is easier to process and provides continuous adhesion properties. However, manufacturing defects or degradation during service in the lap joint cause failure of the bond-line leading to corrosion of the structure. Then, one factor limiting the use of adhesive bonding is the lack of fast and reliable non-destructive testing methods. Conventional ultrasonic inspection requires a coupling medium for allowing the transmission of the ultrasound into the piece under test. The objective is to develop a local non-contact technique for investigating the integrity of a lap joint.

Statement of Contribution/Methods

The laser ultrasonic technique proposed for detecting small thickness variations and adhesive disbonds between two plates, exploits the resonance at the minimum frequency of the S1 Lamb mode dispersion curve. At this minimum frequency, the group velocity vanishes, whereas the phase velocity remains finite. As a result, the energy deposited by the laser pulse generates a local vibration. In our system this vibration is detected at the same point by an optical interferometer.

Results

A first experiment demonstrates the ability to image a 1.5 µm deep corroded area on the back side of a 490µm thick Duralumin plate. The thickness variations are deduced from the frequency variations of the S1 ZGV mode resonance. A Cscan image of the plate reveals this quasi-circular wash with a 0.1 µm accuracy. The spatial resolution is about 1 mm or twice the plate thickness, which is approximately half the wavelength of the S1 ZGV mode.

In a second experiment, the state of an adhesive joint between a 0.5-mm thick Duralumin plate bonded with a 0.2-mm thick epoxy layer to a 2-mm thick glass plate is investigated. A C-scan of the S1-mode resonance amplitude provides an image of an air bubble entrapped between the two plates. Since the ZGV resonance of the Duralumin plate is strongly attenuated when the plates are rigidly bonded, a 25-dB contrast is obtained.

Dispersion curves show that other ZGV modes can be supported by multilayered structures. The associated resonances have been observed in the case of thin adhesive layers (for example a 40-µm thick layer between a 0.5-mm Duralumin plate and a 1-mm glass plate).

Discussion and Conclusions

We have demonstrated that a laser ultrasonic system can be used to generate and to detect at the same point the resonance of the S1-ZGV Lamb mode in various plate-like structures. By scanning the sample relative to the laser beams, very small plate thinning and adhesive disbond have been imaged. This non contact method provides comparable results to a conventional immersion ultrasonic system. Further investigations are pursued in order to extend the method to the control of real bonded lap joints.

5H-2

8:45 AM **Homogenous TiO_2-SiO_2 Ultra-Low-Expansion Glass Evaluated by the Line-Focus-Beam Ultrasonic Material Characterization System**

Mototaka Arakawa[1], Jun-ichi Kushibiki[1], Tetsuji Ueda[2], Akira Fujinoki[2]; *[1]Tohoku University, Electrical Engineering, Sendai, Japan, [2]Shin-Etsu Quartz Products Co., Ltd., Research and Application Lab., Koriyama, Japan.*

Background, Motivation and Objective

Ultra-low-expansion glasses, having a coefficient of thermal expansion (CTE) within ±5 ppb/K at the desired temperature, are required as the basic substrate materials suitable for photomask blanks and reflective optics in extreme ultraviolet lithography (EUVL) systems. In this paper, we tried to fabricate a TiO_2-SiO_2 glass ingot, and homogenized the ingot. Then, we evaluated many specimens obtained from the ingot using the line-focus-beam ultrasonic material characterization (LFB-UMC) system.

Statement of Contribution/Methods

A TiO_2-SiO_2 porous soot was fabricated by the outside vapor deposition (OVD) method. The porous soot was dehydrated, and a glass ingot was obtained. A part of the ingot was heat-treated at 1660°C, and five specimens (Specimens A) were prepared with the specimen surfaces parallel to the soot-deposition direction. The rest of the ingot was homogenized by the zone-melting method. A specimen (Specimen B) with a size of 100 mm x 245 mm x 12 mm was prepared from the central part of the ingot.

Results

The LFB-UMC system evaluated the six specimens by measuring the velocity of leaky surface acoustic waves (LSAWs) propagated on the surfaces at 225 MHz. Line-scanning measurements along the soot-deposition direction for specimens A provided an averaged velocity of 3305.56 m/s with a maximum difference of 25.51 m/s among the five specimens. Two-dimensional LSAW velocity distributions were measured for specimen B (Fig. 1), having an averaged velocity of 3304.08 m/s with a maximum difference of 3.85 m/s. Striae were not observed for specimen B. The velocity distributions of specimen B were much less than those of specimens A because of the homogenization process.

Discussion and Conclusions

The velocity difference of specimen B corresponds to 17.0 ppb/K from the sensitivity of the LSAW velocity to the CTE {4.41 (ppb/K)/(m/s)}. However, the velocity distributions excluding the edge parts were within ±1.13 m/s corresponding to the CTE of ±5 ppb/K. We successfully obtained the homogeneous glass ingot, satisfying the CTE specification of the EUVL-grade glass. This experiment was in a preliminary glass production. It will be possible to fabricate more homogeneous and larger glass ingots with the required zero-CTE temperatures by feeding the evaluation results back to the production conditions.

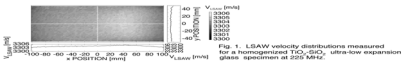

Fig. 1. LSAW velocity distributions measured for a homogenized TiO_2-SiO_2 ultra-low expansion glass specimen at 225 MHz.

5H-3

9:00 AM **Ultrasonic Imaging of Thin Layers within Multi-Layered Structures**

Fredrik Hägglund, Jesper Martinsson, Johan E. Carlson; *Lulea University of Technology, Dept. of Computer Science and Electrical Engineering, Lulea, Sweden.*

Background, Motivation and Objective

In the area of process control, non-destructive testing (NDT) using ultrasound is valuable due to the noninvasive properties. In process control, imaging of surface profiles is used to locate defects or problematic areas in order to quickly steer the process on track again. When dealing with multi-layered materials consisting of thin layers the measured ultrasonic signal is the sum of reverberant and overlapping echoes. Material properties of the individual layers, such as thicknesses, are therefore difficult to extract. Another problem in on-line process control is that if extensive analysis of the material is necessary for a complete control, unmanageable amounts of data are rapidly generated. Some means of data reduction is therefore also desired, without losing valuable information.

Statement of Contribution/Methods

This paper presents a method for imaging of thin layers within multi-layered structures. Due to the application in process control a parametric model is used, and all subsequent analysis is performed on the model parameters rather than on the signal waveforms, resulting in a necessary data reduction. The parameters in the model are directly connected to physical properties, such as the reflection coefficients, time-of-flights, and attenuation

coefficients. Assuming the speed of sound is known, the estimated model parameters are then used to obtain surface plots of the thickness and density of the embedded middle layer.

Results

We first briefly present the parametric model of the wave propagation in a multi-layered material. Experimental results are then shown of how the model parameters can be used in imaging of properties of a thin layer within the material structure. The results show that layers thinner than 30 μm can be imaged using a 20 MHz immersion transducer. The material in the middle layer has a speed of sound of approximately 5000 m/s indicating that the method can produce images of embedded layers with thicknesses several times smaller than the wavelength. The results are verified by comparing the images to microscopy photographs.

Discussion and Conclusions

The results show that the proposed method is able to image properties of layers within a material with thicknesses of fractions of the ultrasonic wavelength. The parametric modeling approach also results in a significant data reduction, enabling on-line process control. Since the entire signal waveform can be reconstructed from the model parameters, additional functionality can later be added to the process control.

5H-4

9:15 AM **Time reversal refocusing for a pulse signal through a randomly thinly layered heterogeneity**

Yinbin Liu; *Institute of Acoustics, Chinese Academy of Sciences, China.*

Background, Motivation and Objective

An acoustic or seismic signal propagating through a strong heterogeneity will be scattered into a long duration vibration and coda wave. Physically speaking, multiple scattering wave than primary wave carries more medium information because of the multiple communications within heterogeneity. Time reversal mirror, which is the refocusing for the multiple scattering after time reversal, presents an inspiration for identifying and monitoring strong small-scale heterogeneity.

Statement of Contribution/Methods

Propagator matrix approach which is an exactly analytical solution is employed to simulate time reversal refocusing for the multiple scattering in 1D heterogeneity. The fluctuation of the medium is of the order of hundreds of per cent (black for density and pink for velocity) and the medium is blocked into about 1600 layers.

Results

A 50-Hz zero-phase Ricker wavelet (yellow) is sent in the disordered layered media (the dominant wavelength of incident pulse signal is much bigger than the correlation length of medium but much less than the total thickness of medium) generating a scattered transmission signal, its primary arrives at about 1 second and its vibration duration is for several hundreds of seconds because of the multiple scattering (only 3 second signal is shown in the Figure, blue), then the whole signal is time reversed (green) and sent back into the same medium again. The new transmission signal (orange) is temporal compression or refocusing as if whole multiple scattered medium behaved as a coherent focusing source. The changes of heterogeneity of medium after the scattered transmission will cause the changes of the refocusing signal. In this work the influences of intrinsic absorption and heterogeneity strength of the medium as well as the length of time reversal window on the refocusing signal will be discussed and analyzed.

Discussion and Conclusions

The results indicate the potential use of time reversal refocusing approach in seismic reservoir characterization and monitoring.

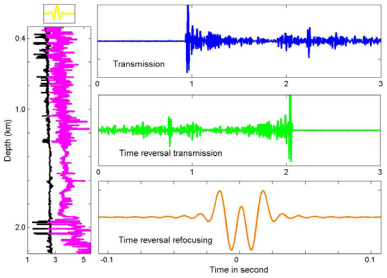

5H-5

9:30 AM **Defect detection in helical and central wires of steel strands using advanced ultrasonic guided wave technique with new type magnetostrictive transducers**

Zenghua Liu, Yinong Zhang, Su Liu; *Beijing University of Technology, China.*

Background, Motivation and Objective

Health conditions of high strength low relaxation steel strands influence directly the durability and security of whole prestressed structures. Under the effect of tensile forces, the defects in steel strands will tend to extend and finally bring these strands broken. It can lead to sudden structure collapse and service interruption. Even worse, these failures may cause serious human casualties.

Statement of Contribution/Methods

In this paper, we developed a comprehensive defect detection method for multi-wire steel stands using advanced ultrasonic guided wave technique with help of new type magnetostrictive transducers. According to its propagation characteristics, the lowest longitudinal mode, L(0,1) at 160kHz, is suitable and chosen for defect detection of steel strands. For its excitation and reception, a special magnetostrictive transducer is developed. Furthermore, impedance matching of this transducer is implemented for its improvement of working efficiency.

Artificial notches in helical and central wires of steel strands which nominal diameter is 17.80mm are detected using L(0,1) mode excited and received by a pair of magnetostrictive transducers. For analyzing the sensitivity to the notches with variable depth in different wires, the experimental relation curves between the amplitudes of notch echoes and the notch depths are obtained shown in Fig.1.

Results

Experimental results show that ultrasonic guided waves can be used for the inspection of whole steel strands. Furthermore, from the amplitudes of defect echoes in steel strands, it is found that L(0,1) modes excited and received by the magnetostrictive transducers is much more sensitive to the defects in helical wires than ones in central wires though the sizes of these defects in different wires are almost same.

Discussion and Conclusions

Therefore, it is of prime importance to develop ultrasonic guided wave inspection technique with non-contact new type magnetostrictive transducers for in-service whole steel strands to increase their safety and reliability.

5H-6

9:45 AM **Measurement of lubricant film thickness using normal incidence ultrasound**

Jingpin Jiao, **Qiang Zhang,** Bin Wu, Cunfu He; *Beijing University of Technology, College of Mechanical Engineering and Applied Electronic Technology, China.*

Background, Motivation and Objective

The durability of machine elements such as gears, bearings and seals relies on the integrity of the lubricant film separating the contact surfaces. Lubricant faults are one of the most frequent causes of failure of rotary machine. The traditional methods for measurement lubricant-film thickness, such as resistance and capacitance etc, are limited by measurement range and condition required. In this paper, an ultrasonic lubricant film thickness measurement technique is developed.

Statement of Contribution/Methods

On the basis of the continuity of stress and strain at each boundary in the multi-layered system, numerical continuum models is constructed and can be used to predict the reflection coefficient spectrum of wave (shown in Fig.1.). Based on frequency range and thickness of film the measured, the methods for measurement of lubricant-film thickness can describe as resonant model and spring model. The thickness of a thicker film can be characterized by its resonant frequencies in reflection coefficient; the thickness of a thinner film can be represented by its interface stiffness, which also can be calculated from reflection coefficient.

Results

To demonstrate the validity of two methods for measurement of lubricant film thickness, normal incidence ultrasound experiments have been conducted in graphite-water-graphite multi-layer using a 2.5MHz center frequency transducer. The typical results are shown in Fig.2 and Fig.3.

Discussion and Conclusions

It is indicated that using the current measurement system the spring model has a good precision when thickness of film is below 5 μm, and the measurement rang of resonant model is several hundred μm.Further experiments need to be conducted in actual mechanical seal using wide frequency transducer.

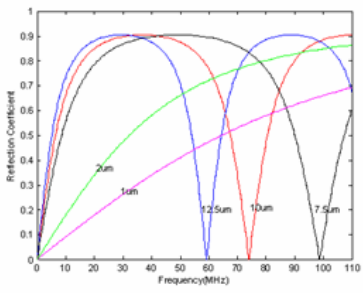

Fig.1 Continuum model prediction of the reflection coefficient spectrum from a layer

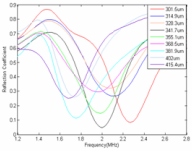

Fig.2 Measured reflection coefficient spectra for a range of fluid film thickness using a 2.5MHz center frequency transducer

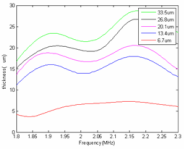

Fig.3 Measured reflection coefficient spectra for a range of fluid film thickness using 2.5MHz center frequency transducer

Wednesday Oral

6H. Optical & RF Ultrasonic Effects

Hall 2C

Wednseday, November 5, 2008, 8:30 am - 10:00 am

Chair: **Robert Aigner;**
TriQuint Semiconductor, USA.

6H-1

8:30 AM **Passband Flattening of Acousto-Optic Tunable Filter**

I Chang; *Accord Optics, Sunnyvale, CA, USA.*

Background, Motivation and Objective

With its advantages of high spectral resolution and low drive power due to extended interaction length, the collinear beam(CB)AOTF has shown to be most promising for use as a tunable filter or dynamic wavelength-selective switch in WDM optical networks. In a paper presented at the last year's Ultrasonic Symposium [1], we demonstrated that by using proper improved designs the CBAOTF could satisfy most of the specified performance requirement for a 100GHz channel spacing WDM system. Because of tolerance of misalignment and precision fabrication control,a flattop bandpass response is desired than the mere sidelobe suppression. More importantely, the realization of a nearly flattop AOTF response is also necessary to avoid severe degradation of the overall bandpass response of the multiple stage AOTFs,a standard configuration for suppressing the coherent crosstalk.The purpose of this paper is to develop advanced designs for realizing AOTFs with a nearly flattop bandpass response. For the specific purpose of improving the bandpass response near thepeak wavelength the proposed design for the passband flattening is directed to a high resolution CBAOTF for WDM optical network application.

Statement of Contribution/Methods

As a necessary tool we have described the momentum matching condition based on a set of modified Dixon equationstaking into account the anisotropic angular characteristics of the interacting optical and acoustic waves.The bandpassresponse of the AOTF satisfying the momentum matching condition are then derived by solving the coupled modeequations in the chosen specific finite AO interaction geometry. More accurate bandpass response at the high efficiency regime can be obtained by numerically solving the coupled equation

Results

Two approaches for flattening the AOTF bandpass response are proposed. The first approach is to employ amplitude apodization with a decaying multi-cycle sine type profile. Compared to the uniform interaction region significant reduction of the top-to bottom width ratio can be obtained with a two cycle apodized filter. An alternate approach is theuse of phased array transducers. The simplest design is to use the planar first order 180 degree phased array in the AOTF.The ease of fabricating the phased array transducer provides the advantage of this approach. Techniques for practical inplementing the bandpass flattening and the calculated results of the corresponding bandpass flattening of the AOTFswill be presented at the conference.

Discussion and Conclusions

In addition to the difficulty of precision control of the interaction profile,the improved bandpass flattening of the two-cycle apodized AOTF must also be traded with the disadvantage of the broadening of the half-power bandwidth or increasing crystal length. The simpler approach using phased array tranducers thus provides a better design for flattening the AOTF bandpass.

[1] I.C.Chang 2007 IEEE Ultrasonic Symposium Proceedings, p.821-824

6H-2

8:45 AM **Sound Pressure Measurement Utilizing Light Refractive Tomography**

Ludwig Bahr, Reinhard Lerch; *University of Erlangen, Department of Sensor Technology, Erlangen, Bavaria, Germany.*

Background, Motivation and Objective

In underwater ultrasound measurements hydrophones are the most commonly used sensors. A hydrophone outputs an electrical voltage proportional to the spatial integral of the acoustic pressure across its active element. Application for high frequency measurements is limited by the size of the active element. If the size is not significantly smaller than the wavelength, the integrative effect will corrupt the measured pressure signal. Since a hydrophone has to be submerged into the fluid where the wave propagates, the device itself perturbs the measured sound field. Furthermore, one cannot measure inside of some media, e. g. polyacrylamid phantoms, which may be of interest for application in medical ultrasonics.

Statement of Contribution/Methods

We propose an optical measurement technique, which reconstructs the sound pressure from interferometric measurements using computed tomography. In accordance with the term light diffraction tomography, we want to call the method light refractive tomography, because it is based on the sound pressure-induced refractive index change along the laser beam. We utilize 3 tomographic reconstruction algorithms applicable to axis-symmetric beam profiles, namely, the filtered back-projection, the Hankel-Fourier method, and the onion peeling method, the latter based on Nestor and Olsens algorithm. From the quality of the reconstruction of data generated by sound field simulation, the performance of the tomographic algorithms can be investigated. In addition, we can determine the spatial sampling, necessary to reconstruct all details of the sound field.

Results

Measurement results obtained by light refractive tomography were compared to measurements with a PVDF hydrophone in water. In the farfield of the transducer differences were less than 5% in case the sound pressure was reconstructed with the Hankel-Fourier method or the filtered back projection using a Hann-filtered Ram-Lak-kernel function. Differences found in the nearfield were attributed to diffraction effects of the hydrophone, because errors of the tomographic algorithms could not be held responsible for the deviations up to 20 %. We also will present sound pressure measurements conducted inside a Plexiglas cube, as well as sound transmission from inside the cube into water.

Discussion and Conclusions

Light refractive tomography is a promising new measuring technique to detect sound pressure. One can measure inside of liquid and solid media, as long as they are transparent to laser light. The spatial resolution could be increased up to the focus size of the laser beam, which lies in the low micrometer range.

6H-3

9:00 AM **A New Fiber-Optic Switch-Multiplexer Based on 2D High Efficiency Multi-frequency Acousto-optic Deflection**

Valery Proklov[1], Sergey Antonov[1], Alexander Vainer[1], Yuri Rezvov[2]; *[1]IRE RAS, Moscow, Moscow, Russian Federation, [2]NIRChTU, Novomoskovsk, Tula region, Russian Federation.*

Background, Motivation and Objective

Nowadays the fast industrial growth of fiber-optic communication systems needs for improvement in optical switching devices. Recently developed optical switches are usually based on the electro-optics or micro-electro-mechanics. At the same time it is well known that with this concern the acousto-optics (AO) at appropriate conditions can offer several functional advantages, like the enhanced number of output channels, the faster time response, the absence of mechanically moving parts, the decrease of driving voltage, the increase of optical damage threshold, etc.

Statement of Contribution/Methods

This work is devoted to the research and development of the new acousto-optic switch-multiplexer for fiber-optic multichannel telemetric and telecommunication systems with significant improvements of the most important parameters. The main idea is based on the use of the specified high efficiency multi-frequency Bragg diffraction without inherent intermodulation optical losses [1], combined with a 2D geometry of the AO switching.

Results

The presentation takes deal with getting a directive choice of an appropriate geometry and design of the 2D system with use of two high efficiency orthogonal AO deflectors each of both is no sensitive to input light polarizations. The experimental prototype of single-mode fiber-optic switch-multiplexer for wavelength 1.55 μm based on TeO2 was created and investigated, and the set of following parameters was measured in a good accordance with relevant calculations: the number of channels is 20, the switching time is 5 μs, the cross-talk ≤-38dB, insertion losses per each channel are ≈4dB, the driving power for one of two AO deflectors is ≈1.5 W.

Discussion and Conclusions

Finally, the comparative analysis of main existing alternatives in the field of fiber-optic switching has shown that the proposed AO switching design can provide a benefit to obtain the remarkably enhanced number of channels, moderate operating speed, satisfactory level of cross-talk, etc. To optimize main AO switch parameters we need to find a compromised decision in between of required the response time (from parts of μs up to several μs) and number of channels (from a few tens up to few hundreds). The mentioned parameters obviously depend on the ratio of the distance between neighbor fiber channels to the fiber core diameter.

Supported by the RFBR, Projects #08-02-12054-ophi and #07-02-00414-a.

[1] V.V.Proklov, S.N. Antonov, Yu.G. Rezvov and A.V. Vainer //Proc. 2006 IEEE Intern. Ultrasonics symposium. Oct. 3-6, Vancouver, Canada, pp. 248-251.

6H-4

9:15 AM **Characterization of functionally graded coating by laser ultrasonics**

Yongdong Pan[1], Xuehang Song[2], Zheng Zhong[2], Bertrand Audoin[3]; *[1]Tongji University, Institute of Acoustics, Shanghai, China, [2]Tongji University, School of Aerospace Engineering and Applied Mechanics, Shanghai, China, [3]Université Bordeaux 1, Laboratoire de Mécanique Physique, France.*

Background, Motivation and Objective

Functionally graded materials (FGMs) have spatial variations in composition and structure resulting in corresponding changes in material properties. FGMs show great potential, the nondestructive characterization of FGMs is still very limited and has to be developped. Laser ultrasonics is a technique through which the ultrasound is excited and detected by laser, it delivers a high spatial and temporal resolution in a noncontact mean (a large k and omega technique). This research is to address the challenging issue of determining the compositional profile of FGMs with the advantage of this technique.

Statement of Contribution/Methods

A model is proposed to predict the dispersion and waveform of surface acoustic wave (SAW) generated by laser in a functionally graded coating (FGC). After the laser line source is assumed as an ideal transient force, and the FGC is considered as an inhomogeneous plate along its thickness direction, the waveform of SAW and its dispersion are numerically solved by the Peano expansion method. A numerical inverse scheme is further developed to characterize the depth profile of the FGC, and numerical simulation is provided to show the feasibility of the numerical method. Laser ultrasonic experiment is carried out, and SAW is observed in the displacement field. To recover the profile, the corresponding dispersion is obtained by the two-dimensional fast Fourier transformation.

Results

Fig.1(a) shows elastic property for a 1mm thick coating with the power law profile, n=0 stands for a homogeneous coating, and n>0 for a graded coating. The straight line with 0% variation is for the comparison with no coating. Fig. 1(b) displays the corresponding SAW dispersion of coatings with profiles in Fig.1(a). There is a clear downward shift to the homogeneous material without any coating for frequency greater than 1 MHz as the power law exponent n increases. This is partly caused by the decrease of the mean stiffness of the coating. The large shift in higher frequency between the homogeneous coating (n=0) and no coating is due to the penetration depth of SAW in the order of its wave length.

Discussion and Conclusions

The dependence of the SAW dispersion on the profile shows the promise of coating characterization. Experiment is carried out on a FGC sample, and the corresponding profile will be obtained to show the feasibility of characterizing FGC in a noncontact way by laser ultrasonics.

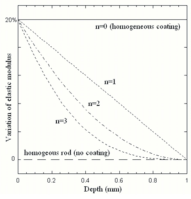

Fig. 1(a). Elastic modulus profiles with n power law spatial distributions.

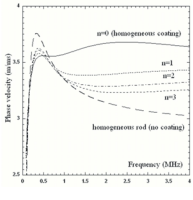

Fig. 1(b). SAW dispersion curves of 1mm thickness coating with profiles in Fig. 1(a).

Wednesday Oral

6H-5

9:30 AM **Towards thin film complete characterization using picosecond ultrasonics**

Pierre-Adrien Mante, Arnaud Devos, Jean-François Robillard; *IEMN-CNRS, France.*

Background, Motivation and Objective

Mechanical characterization of thin films is a main issue in the microelectronic industry. The knowledge of these properties is necessary in many fields such as copper line interconnection and bulk acoustic wave resonators. A few techniques are reliable at this scale. Nano indentation or conventional laser-ultrasonic techniques can't be effective in film thinner than 500 nm. Picosecond ultrasonics can also be used for thin film characterization. It is an efficient method to excite and detect vibrations within a thin film. A strong optical pulse warms a material surface, which leads to the creation of an acoustic wave propagating at the sound velocity. The waves propagation is longitudinal and it modifies the optical properties of the material. These modifications can be detected by a second time-shifted optical pulse.

Statement of Contribution/Methods

In this technique we use a metallic very thin film as a transducer and only longitudinal waves can be generated. Due to that the full mechanical properties of thin layer cannot be measured. Here we show that thanks to a nanostructuration of the transducer, in-plane propagating waves are added using the same experimental setup. In the case of an isotropic medium, we have now access to all the acoustic properties.

Results

We realized and studied 2D lattices of metallic nanocubes using e-beam lithography deposited onto the thin film to be charaterized. In a first experiment we will present results obtained on a 600nm-thick silica film.

Discussion and Conclusions

Experiments were performed both on the lattices and out of the array of nanocubes. We respectively obtained the Rayleigh's velocity and the longitudinal velocity of silica. Then we can deduce Poisson's ratio and Young's modulus of silica: E=72GPa and nu=0.16, which is in very good agreement with literature. This first result demonstrates that we are able to extract longitudinal sound velocity, Rayleigh's velocity, Young's modulus and Poisson's ratio in submicronic layers. Further results obtained on other materials isotropic and anisotropic will be also presented.

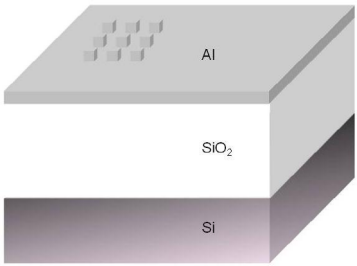

Wednesday Oral

6H-6

9:45 AM **Simultaneous observation of induced longitudinal and shear acoustic phonons by Brillouin Scattering**

Yasuhiro Yoshida[1], Mami Matsukawa[1], Takahiko Yanagitani[2]; *[1]Doshisha University, Faculty of Engineering, Kyotanabe, Japan, [2]Nagoya Institute of Technology, Department of Applied Physics, Nagoya, , Japan.*

Background, Motivation and Objective

Brillouin scattering measurement is a nondestructive method for measuring acoustic wave velocity at minute part of the material. This technique also enables us to measure longitudinal and shear wave velocities simultaneously. However, the measurement accuracy of the velocities is lower than those of other method such as pulse-echo measurement. This is mainly due to the weak Brillouin light scattering from the thermal phonons. In this study, we propose the use of induced longitudinal and shear waves for solving this problem.

Statement of Contribution/Methods

A c-axis tilted ZnO thin film transducer was deposited on side of the silica glass bar with the size of 3x10x35 mm3. Thus, excited continuous longitudinal and shear waves were propagated in the silica glass sample. Brillouin spectrum from silica glass sample were measured using RIΘA scattering geometry [1]

Results

Figure 1 shows the Brillouin spectrum of longitudinal mode phonons observed without and with longitudinal and shear waves excitation. A pair of peaks observed at 3.6 GHz corresponds to the scattering from longitudinal mode phonons. This frequency is near the thickness extensional third overtone mode resonant of the film transducer. Strongly amplified Stokes peak is observed due to the excited longitudinal wave propagating in one direction. Also for shear mode phonons, amplified Stokes peak at 3 GHz (thickness shear fifth overtone mode resonant frequency) is observed as shown in Fig. 2.

Discussion and Conclusions

This technique is useful for the sample which is easy to deteriorate because this technique realizes larger scattering even the use of lower laser power. Ref. [1]: J. K. Krüger et al., J. Phys. D: Appl. Phys 31 (1998) 1913.

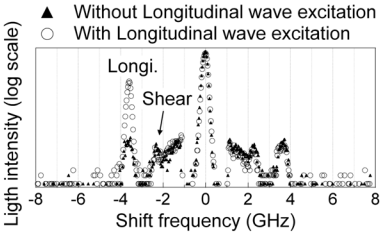

Fig. 1 Brillouin spectra of longitudinal phonons in silica glass sample.

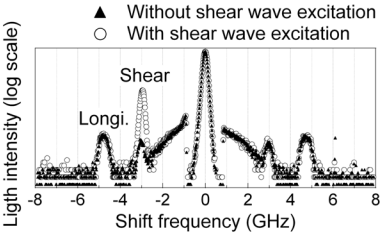

Fig. 2 Brillouin spectra of shear phonons in silica glass sample.

Wednesday Oral

1I. Cardiovascular Imaging

Hall 3

Wednseday, November 5, 2008, 10:30 am - 12:00 pm

Chair: **Chris de Korte;**
Radboud University Nijmegen Medical Centre, The Netherlands.

1I-1

10:30 AM **Rapid 3D Transesophageal Echocardiography using a fast-rotating multiplane transducer**

Kyriakos Nathanail[1], Marijn van Stralen[1], Christian Prins[2], Franc van den Adel[2], Paddy J. French[3], Nico de Jong[1], Anton F.W. van der Steen[1], Johan Bosch[1]; *[1]Thoraxcenter, Erasmus MC, Rotterdam, Netherlands, [2]Oldelft Ultrasound B.V., Netherlands, [3]TU Delft, Netherlands.*

Background, Motivation and Objective

3D TEE with acquisition gating for ECG and respiration is slow, cumbersome for the patient and prone to motion artifacts. We assess the technical and clinical possibilities of rapid 3D TEE.

Statement of Contribution/Methods

We realized a rapid 3D TEE solution based on a standard multiplane TEE probe (5MHz, 64 elements), extended with a fast-rotating transducer array (FRTEE). The fast left-right rotation (5Hz) allows acquisition of sufficient image data from the entire rotation range for the full heart cycle within one breathhold (10 seconds). No ECG- or respiration-gating is applied. In normal mode, the probe has uncompromised optimal 2D quality. The adapted probe's handle contains the motor for fast rotation and PCB for motor control and angle data export. A magnetic sensor in the tip accurately measures the transducer's rotation angle for each transmit beam. Due to continuously changing rotation speed and asynchronous acquisition, beams are distributed irregularly over space and cardiac phase. 10 seconds of image data with ECG and angle values are recorded using a Vingmed Vivid 5 system and post-processed with specially developed 4D reconstruction software based on normalized convolution interpolation. Sequences of 16 to 64 3D volumes per cardiac cycle are produced with an axial resolution of 0.3mm (from 2000-8000 beams/volume).

Results

High quality 3D images of phantoms were acquired, accurately depicting the imaged objects. Sequences of reconstructed 3D volumes of a cyclic moving (4D) balloon phantom show only minimal temporal artifacts. Preliminary results on 5 open chest pigs and 3 humans showed the overall anatomy as well as valvular details with good diagnostic accuracy and high temporal and spatial resolution. A bicuspid aortic valve was diagnosed from the 3D reconstructions (Fig. 1d) and confirmed by a separate 2D exam, proving the 3D diagnostic capabilities.

Discussion and Conclusions

Fast-rotating TEE can provide diagnostic quality 4D cardiac images with single-breathhold acquisition. Images of 3D and 4D phantoms are accurately reconstructed. Preliminary in-vivo results in pigs and humans are quite promising. 3D image quality should generally be better than current slow, gated TEE acquisition and competitive to a matrix TEE probe, while maintaining state of the art 2D image quality.

Figure 1. Left to right: 3 orthogonal slices, 3D view from aorta; visualisation: TomTec GmbH

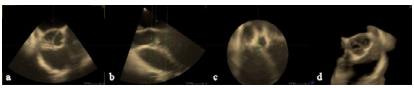

Wednesday Oral

1I-2

10:45 AM **Improvement of 3D Ultrasound Computer Tomography Images by Signal Pre-Processing**

Nicole Ruiter, Michael Zapf, Gregor Schwarzenberg, Hartmut Gemmeke; *Forschungszentrum Karlsruhe, Institute of Data Processing and Electronics, Germany.*

Background, Motivation and Objective

One drawback of synthetic aperture focusing technique (SAFT) imaging is the higher sensitivity to phase aberration errors due to longer and more different travel paths of the ultrasound waves.

Our USCT system has a cylindrical aperture of 18 cm x 15 cm with 1920 unfocussed transducers. The phase errors due to spatial deviations and temperature variations in the coupling water add up to 0.3 µs at known sound speed and average temperature. For a center frequency of 2.5 MHz this corresponds to the wavelength λ and thus limits the applicability of coherent imaging, which demands errors smaller than λ/2.

Incoherent imaging, i.e. forming the envelope of signals before summation, results in a lower resolution of FWHM 0.8 mm and additive accumulation of noise, instead of 0.2 mm for ideal coherent imaging. The aim of this work is to take the phase aberration in the pre-processing of the A-scans into account so that coherent imaging can be applied.

Statement of Contribution/Methods

The proposed pre-processing method detects the integral and time position of the signals using [1] and convolutes this comb-like structure with a truncated sinc function of a 0.6 µs main lobe representing the phase aberration and corresponding to a FWHM of 0.5 mm in the center of the volume).

To exclude speed of sound variations in the objects, ten nylon threads (0.2 mm) immersed in water are imaged. The contrast (SDNR) and resolution (FWHM) are evaluated.

Results

3 methods are compared:

(1) original data, denoised with [1] (coherent imaging), (2) envelope of data in (1) (incoherent imaging), (3) convolution with sinc function

The SDNR (FWHM) of (1) is 4.4 (N/A), of (2) 5.1 (1 mm) and of (3) 6.9 (0.6 mm).

Discussion and Conclusions

Coherent imaging yields no distinct image points per nylon thread. Incoherent imaging decreases the available resolution by a factor 4 against the theoretical limit of 0.2 mm. The sinc function approach images the threads clearly; only halving the resolution and increasing the SNDR by nearly 60%.

This new method is comparable to demodulation of the signal or reduction of emitted center frequency, but enables additionally signal de-noising, an optimal pulse shape and usage of full bandwidth with given transducers.

[1] Schwarzenberg, G.F.; et al: Model based pulse detection for 3D USCT. Proc. IEEE UFFC, 2007

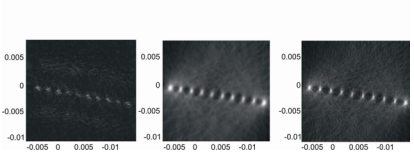

Wednesday Oral

1I-3

11:00 AM **Functional Imaging of the Heart**

Jan D'hooge, Piet Claus, Jens-Uwe Voigt, Frank Rademakers; *Catholic University of Leuven, Dept. of Cardiovascular diseases, Leuven, Belgium.*

Background, Motivation and Objective

The function of the heart is to eject blood into the aorta/pulmonary artery during systole (i.e. systolic function) and to refill with blood during diastole (i.e. diastolic function). The heart is able to do so by active contraction and relaxation of the heart muscle (i.e. the myocardium) resulting in changes in wall and cavity dimensions. This in turn results in cavity pressure changes accelerating the blood in or out of the ventricular cavity.

Ultrasound (US) imaging has been the modality of choice for the non-invasive assessment of cardiac function. Traditionally, M- or B-mode derived volume-changes are measured to assess systolic function while blood flow patterns measured using Doppler techniques are used as an index for diastolic function.

Technological developments in ultrasound imaging have resulted in new methodologies for the quantification of cardiac function.

Statement of Contribution/Methods

US approaches for the quantification of cardiac function can be categorized into methods that assess properties of the myocardium and methods that asses characteristics of the blood flow.

In the former approaches, myocardial motion and deformation imaging has taken an important role. Although the original methods were based on Doppler imaging, later developments allowed to measure motion and deformation within the image plane (2D) and recently also in 3D (using volumetric US). These methods have enabled assessing ventricular twist/untwist characteristics – the latter being an interesting parameter for diastolic function. The above measurements in combination with mechanical models of the heart allow estimating the force regionally developed by the cardiac muscle.

Besides of these mechanistic approaches, acoustic properties of the myocardium have also been studied to functionally characterize the heart. Integrated backscatter and its cyclic variation have shown to be of interest in a large number of studies.

3D US systems have allowed a better characterization of ventricular volume changes which has led to the introduction of several new functional parameters.

Color Doppler M-mode imaging of blood flow can be used to estimate intra-ventricular pressure gradients which in turn have been correlated to cardiac function. More recently, speckle tracking approaches have also been applied to characterize (2D) blood flow patterns within the ventricle. It might be an important new approach.

Results

In this review lecture, the above described techniques will be presented from a technical point of view together with the experimental validation and/or clinical findings already available. Pros and contras of the approaches will be discussed.

Discussion and Conclusions

Developments in cardiac US have driven new methodologies to more accurately quantify cardiac function. They provide us with tools to better understand cardiac (patho)-physiology and, as such, better diagnose and treat the individual patient.

Wednesday Oral

1I-4

11:30 AM **Non-Invasive Ultrasonic Measurement of the Relative Volume Change of the Arterial Wall – First in vivo Trial**

Hannes Mogensen[1], Åsa Rydén Ahlgren[2], Tomas Jansson[1], Kjell Lindström[1], Hans W Persson[1], **Magnus Cinthio[1];** *[1]Lund Institute of Technology, Lund University, Dept. of Electrical Measurements, Lund, Sweden, [2]Clinical Physiology and Nuclear Medicine Unit, Malmö University Hospital, Dept. of Clinical Sciences, Malmö, Sweden.*

Background, Motivation and Objective

Studies have shown that there is a correlation between arterial stiffness and the risk of cardiovascular diseases. When quantifying arterial stiffness, the change in arterial diameter has been investigated more extensively than the longitudinal and radial compression of the intima-media (IM) region (the inner-most layer of the arterial wall). In this study, measurement data of the change in arterial diameter has been combined with data of the IM compression to calculate the corresponding change in volume of the arterial wall during the cardiac cycle.

Statement of Contribution/Methods

The relative volume change of the arterial wall was measured using B-mode ultrasound. The longitudinal strain was measured by placing two regions-of-interests (ROIs), 4–12 mm apart, at distinct echoes of the intima. The longitudinal movement of the ROIs was then calculated using 2D cross correlation. The radial IM strain of the far wall and the change in diameter were calculated using a combined slope detection and threshold determination algorithm. When measuring the arterial diameter, the algorithm was adjusted for the different shapes of the leading and trailing edge of the pulse. By assuming the vessel walls to be the axisymmetric, the change in volume was estimated by combining the measured parameters. The R-wave of the ECG defined the point of zero strain.

The images were obtained 2-3 cm proximal to the bifurcation of the common carotid artery of five healthy normotensive humans, aged 28–53 years (two male and three female subjects).

Results

The figure shows the longitudinal and radial IM strain, respectively, along with the relative change in diameter and the resulting relative change of the volume of the arterial wall during the cardiac cycle. The maximum volume change was 4.6 % (SD 1.6), range 2.4 – 6.9 %, and the minimum change was -5.1 % (SD 3.0), range -1.6 – -9.3 %.

Discussion and Conclusions

This is the first recorded instance of non-invasive ultrasonic measurements of the volume change of the IM during the cardiac cycle *in vivo*. The results presented in this study is at least one order of magnitude larger than the results from previously published *in vitro* measurements. The method provides a new way of quantifying and examining the elastic properties of the arterial wall. However, further studies are needed to investigate the underlying mechanisms and its implications.

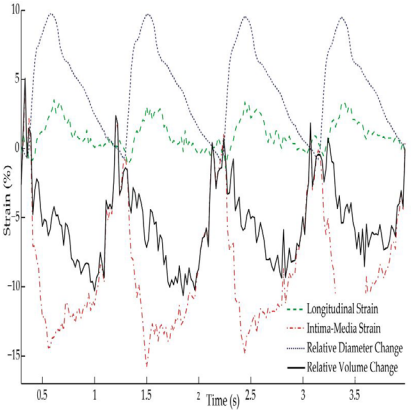

Wednesday Oral

1I-5

11:45 AM **Pulse Wave Imaging of Human Abdominal Aortas In Vivo**

Jianwen Luo, Wei-Ning Lee, Shougang Wang, Elisa Konofagou; *Columbia University, Department of Biomedical Engineering, New York, NY, USA.*

Background, Motivation and Objective

The abdominal aortic aneurysm (AAA) is a common but often silent vascular disease, with a prevalence rate of 1.3%-8.9% in men and 1.0%-2.2% in women. The current clinical criterion for treating AAA's is an increased diameter above a critical value but does not correlate well with aortic rupture, the main cause of death from AAA disease. AAA disease leads to changes in the aortic wall mechanical properties. The pulse-wave velocity (PWV) may indicate such a change. Because of limitations in temporal and spatial resolution, the widely used foot-to-foot method measures the global, instead of regional, PWV. However, mechanical properties are nonuniform along the arterial tree and pathological changes are typically regional. Pulse-Wave Imaging (PWI) was developed by our group to map the pulse-wave propagation along the abdominal aorta in vivo (Fujikura et al, Ultrason Imaging, 2007, 137-154; Luo et al, IEEE Ultrasonics Symp Proc, 2007, 985-988). In this study, the feasibility of PWI is shown in human abdominal aortas in vivo.

Statement of Contribution/Methods

A previously developed composite imaging system for high frame-rate and full-view cardiovascular ultrasound imaging (Wang et al, IEEE Ultrasonics Symp Proc, 2007, 880-883) was used. A Sonix RP system (Ultrasonix Medical Corp., Burnaby, BC, Canada) was employed with a phased array at 3.3 MHz, a field of view of 11-cm x 15-cm and a line density of 128 lines. Radio-frequency (RF) signals of the normal and AAA abdominal aortas were digitized at a sampling frequency of 20 MHz and a sampling resolution of 16 bits. 2-D full long-axis view RF frames were reconstructed from 5-7 narrow RF sector frames at the high frame rate of 481 Hz. The radial velocities of the aortic wall were estimated using 1-D cross-correlation (window size = 3.5 mm, 75 % overlap) and cine-loops during the entire cardiac cycle were generated.

Results

The sequences of PWI images can visually depict the propagation of the pulse wave along the aortic wall. In the normal aorta, the propagation of the pulse wave was relatively uniform, while in the aneurysmal aorta, the propagation of the pulse wave was highly nonuniform with increased PWV. The correlation coefficient of the linear fitting on the pulse-wave propagation in the healthy aorta ($r>0.95$) was significantly higher in the aneurysmal aorta ($r<0.80$). The estimated regional PWV's (4-6 m/s) were consistent with the previously reported values (Nichols and O'Rourke, McDonald's blood flow in arteries, 2005).

Discussion and Conclusions

The PWI technique was successfully implemented in both healthy and aneurysmal human aortas. The nonuniform pulse wave propagation indicated the inhomogeneities of the aortic wall properties in the aneurysmal case. The PWI technique may thus constitute an early detection tool of vascular degeneration as well as serve as a suitable predictor of AAA rupture. The potential of the PWI technique to provide quantitative information on the mechanical properties of the wall will also be discussed.

2I. Therapeutic Monitoring and Guidance

Room 201 A/B/C

Wednseday, November 5, 2008, 10:30 am - 12:00 pm

Chair: **Emad Ebbini;**
University of Minnesota, USA.

2I-1

10:30 AM **A Backscatter-based Method for the Guidance of High Intensity Focused Ultrasound Treatment**

Xinliang Zheng, Shahram Vaezy; *University of Washington, Bioengineering, Seattle, WA, USA.*

Background, Motivation and Objective

As a non-invasive treatment method, the use of High Intensity Focused Ultrasound (HIFU) has been investigated in various medical applications, including the treatment of tumor, internal bleeding, atrial fibrillation, and drug delivery to brain. In order to avoid unnecessary damage to normal tissue, there is a strong need to have a guidance method to determine the focus of HIFU at pre-ablative intensities. Magnetic Resonance Imaging (MRI) can evaluate temperature change during HIFU application as guidance, but it is expensive and has low temporal resolution. Meanwhile, ultrasound-based methods for temperature measurement have low sensitivity of the sound speed change in the temperature range used in HIFU application, making the guidance difficult.

Statement of Contribution/Methods

We investigated a method for the targeting of HIFU focus based on the change in backscattered radio frequency (RF) signals. Pre-ablative intensities of HIFU were applied on *ex vivo* chicken tissue and RF data were collected during the exposure. The intensity was then increased to induce tissue damage with the appearance of hyperecho in B-mode ultrasound images. We compared focus locations estimated from our RF-processing method and from the locations of hyperecho in B-mode images.

Results

The results showed that, the RF amplitude of the focal region increased immediately after the application of HIFU even at pre-ablative intensities. The region was clearly visualized in two-dimensional images of the increasing rate of RF amplitude. *In situ* focal intensity as low as 50 W/cm^2 could be used to detect the location of HIFU focus. The axial and lateral differences between RF-based and hyperecho-based focus locations were 0.25 ± 1.85 mm (mean ± standard deviation) and 0.39 ± 1.10 mm for 34 exposures, respectively, and no statistically significant difference was found between the focus coordinates (axial: p=0.50 and lateral: p=0.07).

Discussion and Conclusions

We demonstrated the feasibility of using our proposed RF-based method for the localization of HIFU focus at pre-ablative intensity levels. Using the increasing rate of RF amplitude as the signature of focus location, our method can detect HIFU focus before any significant damage is induced in tissue, without the appearance of hyperecho in B-mode images.

2I-2

10:45 AM **Real -time Monitoring of Mechanical and Thermal Tissue Response to Pulsed HIFU Beams**

Dalong Liu, **Emad Ebbini;** *University of Minnesota, Biomedical Engineering, Minneapolis, MN, USA.*

Background, Motivation and Objective

Pulsed HIFU beams produce thermal and mechanical responses in target tissues. The intensity, pulse-repetition frequency (PRF), duty cycle and total duration can be designed to produce largely thermal, largely mechanical, or mixtures the two leading to variability in lesion sizes, shapes, and damage profiles. Real-time monitoring of the thermal and mechanical responses during the application of pulsed HIFU may provide the necessary feedback control of lesion formation leading to reduced variability and increased predictability of the lesion parameters.

Statement of Contribution/Methods

We have developed a real-time system for monitoring tissue displacements in response to pulsed HIFU beams at high PRFs. The imaging component of the system comprises a customized FPGA-based signal processing unit for real-time filtering of M-mode pulse-echo data followed by real-time speckle tracking for tissue displacements before, during, and after exposure to pulsed HIFU. The latter can be used in evaluating temperature and/or viscoelastic response to the applied HIFU beam. To coordinate the application of HIFU and triggering of tracking sequence, a sophiscated beam sequencing control unit is also designed. The high acquisition rate of the M-mode system, together with the real-time displacement tracking are necessary for simultaneous estimation and separation of the thermal and viscoelastic tissue responses. In addition, the system provides a real-time link to MATLAB-based nonlinear spectral estimation routines for cavitation detection.

Results

In vitro experiments were performed on tissue samples from freshly excised bovine hearts. A highly focused 4-MHz HIFU transducer and a wideband 6 - 18 MHz imaging transducer were used in the experiments. The transducers were positioned so that their beams intersected at 90o in their respective focal spots. A variety of HIFU exposure levels were generated. M-mode RF data was acquired before, during, and after pulsed HIFU exposure. Spatio-temporal displacement maps along the axis of the imaging transducer were displayed in real-time to provide immediate feedback of the thermal and viscoelastic response to the application of pulsed HIFU. The displacement data was processed in MATLAB to separate thermal strain components from mechanical strains resulting from the radiation force effects.

Discussion and Conclusions

Noninvasiv temperature estimates were compared with temperature measurements obtained using thermocouples. The results show that the use of high frame rate HIFU-synchronized M-mode imaging was necessary to separate the mechanical and thermal tissue responses to pulsed HIFU. Failure to capture the mechanical strains near the HIFU focus results in poor and unreliable noninvasive temperature estimation. In addition, changes in thermal and mechanical tissue properties (due to lesion formation) can be reliably estimated simultaneously thus providing a powerful means of damage assessment.

2I-3

11:00 AM **Quantitative Image Feedback for Pulsed Cavitational Ultrasound Therapy- Histotripsy**

Tzu-Yin Wang, Zhen Xu, Frank Winterroth, Edward Rothman, J Brian Fowlkes, Charles Cain; *University of Michigan, USA.*

Background, Motivation and Objective

Histotripsy is a well-controlled ultrasonic tissue ablation technology that mechanically and progressively fractionates soft tissue using cavitation. Significant ultrasound backscatter reduction occurs as the tissue in the treated volume is increasingly fractionated. This paper studies the quantitative correlation between the degree of histotripsy-induced tissue fractionation and the backscatter reduction.

Statement of Contribution/Methods

A total of 55 lesions were produced in vitro using histotripsy in porcine kidneys. Histotripsy treatment consisted of high intensity (19 MPa peak negative pressure), short duration (15 cycles), 1 MHz ultrasound pulses delivered at 100 Hz pulse repetition frequency. Different degrees of tissue fractionation were generated by varying the number of pulses from 100 to 2000 pulses per treatment location (i.e., 3.75 to 75 pulses/mm3). RF imaging data of the treated tissue were recorded using a 10 MHz linear array imaging probe with a diagnostic ultrasound system. Ultrasound backscatter amplitude of the treated tissue was defined as the median of the pixel intensities within a 4×6 mm2 region-of-interest (ROI) in the treated area. Backscatter reduction of the treated tissue was calculated by the difference between the post-treatment and pre-treatment backscatter amplitude in ROI. The degree of tissue fractionation was assessed by the percentage of intact cell nuclei within the treated area via histological evaluation. The degree of tissue fractionation was then correlated to the backscatter reduction from the corresponding lesion.

Results

All pulse numbers resulted in significant backscatter reduction in the treated tissue ($p<0.001$; Student's t-test). As the number of pulses increased from 100 to 2000 pulses per treatment location, the backscatter amplitude reduced linearly from 0 dB to -16 dB ($R2=0.87$). Correspondingly, the percentage of intact nuclei in the treated area decreased exponentially from 100% to 0% ($R2=0.96$). Regression analysis showed a strong correlation between the degree of tissue fractionation and the level of backscatter reduction ($R2=0.93$).

Discussion and Conclusions

The strong correlation between tissue fractionation and backscatter reduction suggests that the backscatter reduction can provide quantitative image-based feedback for tissue fractionation. As tissue fractionation should be related to the cell death, backscatter reduction may be a potential real-time feedback parameter for histotripsy, allowing the prediction of local clinical outcomes, i.e. when a tissue volume has been sufficiently treated.

2I-4

11:15 AM **Use of passive arrays for characterization and mapping of cavitation activity during HIFU exposure**

Miklos Gyongy, Manish Arora, J Alison Noble, Constantin C Coussios; *University of Oxford, Department of Engineering, Oxford, Oxfordshire, United Kingdom.*

Background, Motivation and Objective

During tissue exposure to High Intensity Focussed Ultrasound (HIFU), cavitation has been shown to enhance the rate of heat deposition, whilst its associated acoustic emissions could provide an effective means of treatment monitoring. However, cavitation activity occurring pre-focally or growing unstable is known to impede safe and effective treatment delivery.

Statement of Contribution/Methods

A combined computational and experimental approach is used to develop a passive array-based technique for mapping and characterizing cavitation activity in real-time. Novel algorithms based on acoustic inversion and cross-correlation have been applied to pre-beamformed RF data acquired using a 5-10 MHz imaging array in order to create maps of cavitation activity. Simulations of array recordings in the presence of arbitrary narrowband and broadband source distributions have also been developed, to enable comparison with cavitation maps generated experimentally.

Results

Figure 1 shows a simulation of A-lines obtained using a high-frequency linear array consisting of 64 beamforming elements over a subaperture of 19mm, for a 5-10 MHz broadband noise source used to emulate an inertial cavitation event occuring at 60 mm from the array. Conventional scanners only provide dynamic receive beamformed (DRB) RF data, so that source amplitude can be estimated by generating an analytic signal or by taking the pixel variance over several frames. Our novel "multidimensional correlation" algorithm achieves localization of the broadband source with a much higher spatial resolution than either DRB algorithms. Cavitation maps were also generated by applying this novel algorithm to RF data obtained experimentally during continuous-wave insonation of a tissue mimicking material with 1.1 MHz HIFU. The onset and extent of cavitation activity shown by those maps were validated by using two single-element, focused, 15 MHz passive detectors to monitor cavitation activity at two different locations along the HIFU axis.

Discussion and Conclusions

The cavitation maps generated using our passive imaging algorithms provide a novel method of monitoring HIFU treatment. Future work will aim to decrease the frame rate to enable real-time cavitation mapping without loss of spatial resolution, so that the unstable nature of cavitation activity can be tracked while ensuring treatment is well localized.

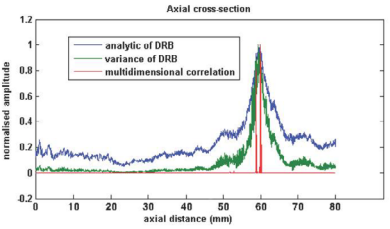

2I-5

11:30 AM **Reaching the optimal focusing and steering capabilities of transcranial HIFU arrays based on time reversal of acoustically induced cavitation bubble signature.**

Jerome Gateau[1], Laurent Marsac[2], Mathieu Pernot[1], Jean-Francois Aubry[1], Mickael Tanter[1], Mathias Fink[1]; *[1]Laboratoire ondes et Acoustique, INSERM, CNRS UMR 7587, ESPCI, PARIS, France, [2]Supersonic Imagine, Aix-en-Provence, France.*

Background, Motivation and Objective

Brain treatment with High Intensity Focused Ultrasound (HIFU) can be achieved through the skull by multichannel arrays using time-reversal focusing. Such a method requires a reference signal either sent by a real source embedded in brain tissues or computed from a virtual source, using CT based simulations. This non-invasive computational method allows precise focusing, but discretization and modeling errors can result in a reduction of the accessible acoustic pressure at focus in comparison with real experimental time-reversal using an implanted hydrophone. The goal of this study is to demonstrate the feasibility of reaching the optimal focusing based on the initial corrections obtained from CT-scan simulations. The optimal acoustic pressure at focus is recovered by inducing a cavitation bubble through the skull bone and using its ultrasonic emission for time-reversal transcranial focusing. The potential of this technique for improving both transcranial focusing and electronic beamsteering performances is investigated.

Statement of Contribution/Methods

Ex vivo experiments are performed on a half skull immersed in a degassed water tank maintained at 37 C. The ultrasound array is composed of 136 high-power individual transducers (central frequency 1MHz) mounted on a spherical surface with a semi random distribution. The simulation uses a 3D finite differences code and a model of the half skull based on CT data. Cavitation events occur in an agar gel, phantom for in vivo bubble formation. The pressure field at 1MHz is scanned at low amplitude levels with a hydrophone mounted on a 3D gantry.

Results

Ex vivo CT guided simulations allowed us to reach, at the geometrical focus of the array, 83% of the optimal pressure (hydrophone based time reversal). Cavitation bubbles were then created transcranially at this location with computed emission pulses. The 1MHz component of a single bubble acoustic emission was selected, time reversed and reemitted, restoring a mean pressure ratio of 96% (+/- 2%). The new focal peak, i.e the location of the cavitation event, was localized in the -2dB focal area of the initial pulse corresponding to a 0.5 mm uncertainty. When performing electronic steering from a reference signal optimally focusing at the geometrical focal point, 90% of the optimal pressure is still reached up to 8 mm away to the initial position in the focal plane. With six reference signals from cavitation bubble spots equally distributed on a 6 mm radius circle, this area was extended to 12 mm. Such cavitation bubbles were generated using electronic steering.

Discussion and Conclusions

A new non-invasive method to correct skull aberrations has been validated. From CT images based simulations, the focusing was restored through the skull by inducing a cavitation bubble at the targeted location, and the corrected zone was extended by electronic beam steering and discreet bubbles generation This method should greatly benefit transcranial brain therapy.

2I-6

11:45 AM **Energy-based Adaptive focusing of waves: Application to ultrasonic imaging and Brain therapy**

Eric Herbert, **Mathieu Pernot,** Gabriel Montaldo, Mickaël Tanter, Mathias Fink; *UMR 7587 CNRS, ESPCI, INSERM, Laboratoire Ondes et Acoustique, Paris, France.*

Background, Motivation and Objective

We propose a general concept of adaptive focusing through complex media based on the estimation or measurement of the wave energy density at the desired focal spot. As it does not require the knowledge of phase information, this technique has many promising applications in acoustics and optics for light focusing through diffusive media. The goal of this study is to demonstrate the potential of this technique for correcting ultrasonic aberrations. We present here two applications of this technique to the problem of aberration corrections in ultrasonic imaging and in High Intensity Focused Ultrasound (HIFU) treatments.

Statement of Contribution/Methods

The estimation of the wave energy density was based on the maximization of the ultrasound radiation force generated by multi-element phased arrays. A spatial coded excitation method was developed by using ad-hoc virtual transducers that include all the elements for each emission. The radiation force was maximized by

optimizing tissue displacements at a target zone. Tissue velocities were measured using classical RF-signals cross-correlation of consecutive ultrasound pulse-echo sequences that follow immediately the radiation force excitation generated by the phased array.

A first experiment was performed using a 64-element linear phased array working at 4.3 MHz central frequency. A thin aberrator made of PDMS was placed between the linear probe and a polyvinylalcool phantom. The focusing was optimized at depth of 40mm. After optimization the phantom was removed and the pressure field was scanned using a needle hydrophone. A second experiment was performed using a 64-element large phased array working at 1MHz developed for transcranial HIFU brain therapy experiment. The pressure field was optimized and measured through an ex vivo human half skull at depth of 140mm.

Results

In both experiments the phase aberrations correction was achieved with a good accuracy. The phase correction was obtained on the linear array with a standard deviation of 0.2 radians for aberrations on the order of π. The focus was completely restored and the pressure increases at the focus reached up to 10dB. The second experiment through the skull bone demonstrated that the acoustic intensity at the focus could be also restored through very large aberrations ($>2\pi$). After optimization through the skull, the pressure at the focus was increased by a factor 10.

Discussion and Conclusions

Optimal adaptive focusing was performed using a limited number (200) of short ultrasonic radiation force pushes. It allowed the array to perform a real autofocus based on tissue velocities estimation. This technique has many potential applications in ultrasound imaging and therapy. For practical implementation of this technique under MR guidance for therapeutic applications, the focal energy can be deduced from the local estimation of tissue displacements using dedicated MR sequences and provides an elegant MR-guided adaptive focusing approach.

3I. Polymers for Transducers

Room 305 A/B/C

Wednseday, November 5, 2008, 10:30 am - 12:00 pm

Chair: **K Shung;**
University of Sothern California, CA, USA.

3I-1

10:30 AM **Customizable Field Aiborne Ultrasonic Transducers based on Electromechanical Film**

Joao Ealo[1], Fernando Seco[2], Carlos Prieto[2], Antonio Jiménez[2], Javier Roa[2], Aikaterini Koutsou[2], Jorge Guevara[2]; [1]*School of Mechanical Engineering - Universidad del Valle, Cali, Colombia,* [2]*Instituto de Automática Industrial - CSIC, Arganda del Rey, Madrid, Spain.*

Background, Motivation and Objective

Recent research in reference to the use of the electromechanical film (EMFi) for airborne applications, such as bat research, phased arrays, ranging, etc., is mainly focused on its remarkable electromechanical properties, i.e., good charge storage capability, relatively high piezoelectric constant d33 up to 800 pC/N, good adaptation to the air and broadband response that covers from audible frequencies to its resonance frequency around 300 kHz. Besides, some incipient results have been reported regarding the possibility of increasing its sensitivity by stacking two or more sheets of film. However, short attention has been paid to its mechanical flexibility, which makes it possible to wrap it around developable surfaces, i.e. geometries which conform to a surface generated by extrusion (cylindrical surfaces), polyhedra or surfaces of revolution whose generatrix consists of straight lines

Statement of Contribution/Methods

In this work, it is shown that the behaviour of a sheet of cellular ferroelectret, which resembles a thin elastic film, opens up the possibility of designing ultrasonic transducers with customized emitting pattern by sticking the film on complex substrates.

Results

After interferometric measurements of the surface velocity of a fabricated conical transducer prototype, it was found that, neither the piston-like vibration mode of the film nor its frequency response, are influenced as the radius of curvature diminishes from 14mm to 1mm; showing similar values to those obtained with a flat substrate. Also, cylindrical prototypes of different radius (5, 7.5, 10 and 15 mm) were built in order to corroborate these results. The radiating acoustic pattern of the prototypes was measured with a calibrated microphone located at 30 cm far, showing a good agreement with theory. Figure 1 shows an EMFi-based ultrasonic transducer prototype fabricated on a substrate that approximates a sphere, designed to generate a 3D omnidirectional radiation pattern. The film pieces were stuck using a XYZ conductive tape.

Discussion and Conclusions

Obtained results indicate that the EMFi film can be purely bent, out of plane, to large deformations without changing its electromechanical performance. This characteristic makes electromechanical film suitable to easily combine developable surfaces in order to fabricate airborne ultrasonic transducers with an arbitrary customizable field.

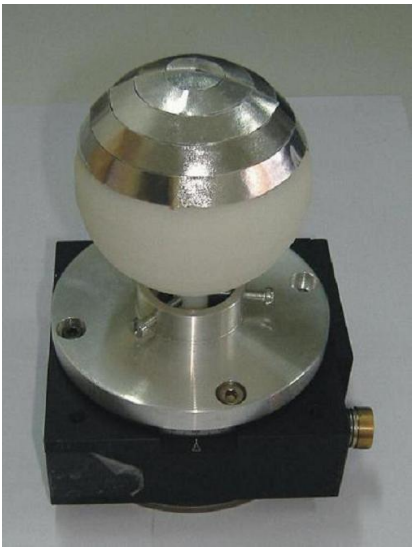

3I-2

10:45 AM **Low-acoustic attenuation and high-mechanical strength silicone rubber lens doped with ZnO nano-powder for medical array probe**

Yohachi (John) Yamashita[1], Yasuharu Hosono[2], Noriko Yamamoto[2], Kazuhiro Itsumi[2], Yasuhisa Makita[3], Takashi Takeuchi[3], Koichi Shibamoto[3], Minoru Aoki[3], Hiroyuki Shikata[3]; *[1]Toshiba Research Consulting Corp., Kawasaki, Kanagawa, Japan, [2]Corporate R&D Center, Toshiba Corp, Kawasaki, Kanagawa, Japan, [3]Toshiba Medical Systems Corp., Otawara, Tochigi, Japan.*

Wednesday Oral

Background, Motivation and Objective

Silicone (Q) rubber has been the predominant externally focused acoustic lens material applied for the medical array probe application since 1970, because it is safe, has a suitable sound velocity (c) (c~ 1000 m/s), and a reasonably low acoustic attenuation of 0.3 dB/mm/MHz. However, the acoustic impedance (Z) of pure Q rubber is approximately 0.97 MRayls, which is considerably different from the Z of human tissue (Z = 1.5 MRayls). Therefore, in order to bring the Z of the Q rubber close to that of human tissue, SiO2 powder has been doped into the Q rubber. Since SiO2 has a low density, 2.2 g/cm3, dopants content of 50 wt% (35 vol%) in Q rubber is necessary for obtaining Q rubber with the Z of higher than 1.4 MRayls. As a result, the SiO2-doped-Q rubber shows large attenuation > 0.9 dB/mm/MHz and low mechanical strength. The authors have reported the acoustic properties of room-temperature vulcanization (RTV) and high-temperature vulcanization (HTV) Q rubbers doped with 8 to 2000 nm Pt and Yb2O3 powder. However, these Q rubbers have also low mechanical strengths.

Statement of Contribution/Methods

Zinc oxide (ZnO) nanopowder doped HTV Q rubber was manufactured and the properties have been investigated, to develop an acoustic lens material with a low attenuation and a high mechanical strength.

Results

The ZnO-doped-Q HTV rubber showed a density of 1.62 g/cm3, with c = 849 m/s, characteristic acoustic impedance (Z) = 1.38 MRayls, attenuation = 0.67 dB/mm/MHz, and a figure of merit (FOM) (attenuation x c) of 569 at 5 MHz at 37oC. The material has also a high tear strength of 45 N/mm which is about double that of conventional SiO2-doped-Q lens materials. The ZnO-doped-HTV Q rubber provides increased sensitivity because it has the low attenuation and it realizes a thinner acoustic lens than is conventional HTV Q rubber does. The performance of 8 MHz linear array probes using the ZnO-doped-Q rubber lens showed an increase of 4 dB in sensitivity compared to that of conventional Q rubber lens..

Discussion and Conclusions

The low attenuation and excellent mechanical strength of the ZnO-doped-Q rubber mean that it is superior to the conventional Q rubber lens in terms of its ability to endure high performance during long operation in diagnosis for

the medical array probe application. In the presentation, real diagnostic images of the medical probe with the new lens and previous lens will be shown.

3I-3

11:00 AM **Optoacoustic sensor using self-assembled arrays of polystyrene microspheres**

Xinqing Guo, Takashi Buma; *University of Delaware, USA.*

Background, Motivation and Objective

Optical techniques are a promising technology for high frequency ultrasound imaging arrays. High sensitivity and broad bandwidth have been demonstrated with etalon sensors. Fine spatial resolution requires extremely thin etalons, which are typically fabricated by spin coating or evaporating polymers.

Statement of Contribution/Methods

We are exploring a different etalon structure based on self-assembly of dielectric microspheres. Highly ordered microsphere arrays have been demonstrated for diffraction gratings and photonic crystals. Monolayers formed by sub-micron diameter microspheres produce thin film optical interference in addition to diffraction. Polystyrene microspheres are readily available in sub-micron diameters, making monolayer arrays potentially attractive for realizing extremely thin etalons. A dilute aqueous suspension of 0.35 um diameter polystyrene microspheres are placed on a glass microscope slide. Slow evaporation of water produces polycrystalline layers of microspheres. A 50 nm thick gold layer is then deposited over these layers to enhance the optical reflectivity. This structure is attached to the side of a water tank containing a 25 MHz spherically focused f/2 transducer. The probe laser is a temperature controlled Fabry-Perot AlGaAs diode laser with a wavelength of 780 nm. The signal is averaged 4 times by a 200 MHz 8-bit digital oscilloscope.

Results

The microsphere structures produce strong optical diffraction at large angles of incidence, confirming self-assembly into ordered arrays. The weak dependence of diffraction upon the azimuthal angle of incidence suggests polycrystalline domains. The reflected optical interference at smaller angles of incidence confirms the formation of monolayers, bilayers, and even trilayers of microspheres. The recorded optical signal from the ultrasound transducer is shown below. The etalon and pulse echo data both have peak frequencies of 22 MHz. The corresponding -6 dB bandwidths are 14 MHz and 11 MHz, respectively. The signal-to-noise ratio of the optical signal is 26 dB over a 50 MHz bandwidth.

Discussion and Conclusions

Further theoretical and experimental investigations are under way to improve the performance and fabrication of these devices. Nevertheless, these encouraging results suggest the potential of optoacoustic detection by self-assembled arrays of polystyrene microspheres.

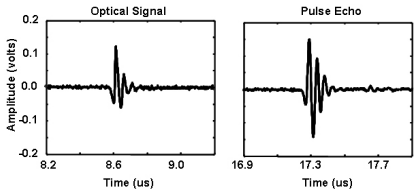

3I-4

11:15 AM **A Fabrication Procedure for Airborne Ultrasonic Phased Arrays Based on Cellular Electromechanical Film**

Joao Ealo[1], Jorge Camacho[2], Carlos Fritsch[2], Fernando Seco[2], Javier Roa[2]; *[1]School of Mechanical Engineering - Universidad del Valle, Cali, Colombia, [2]Instituto de Automática Industrial - CSIC, Arganda del Rey, Madrid, Spain.*

Background, Motivation and Objective

Array technology is widely used in ultrasonic applications, given its capability for electronically focusing and deflecting an ultrasound beam at different depths and angles without mechanical motion of the transducer. However, current manufacturing technology for air ultrasonic arrays, mainly based on either piezoelectric ceramic or capacitive elements, is expensive and impractical for many applications.

Recently, new array transducers based on cellular polymers have been introduced, which take advantage of the remarkable transducer properties of these materials. The reported fabrication process comprises structuring the upper and lower electrodes on both sides of the cellular film by sputtering and etching, and charging the active area of the aperture using a corona discharge, among other poling methods. This leads to an elaborated manufacturing process, requiring expensive and specialized instrumentation.

Statement of Contribution/Methods

In this work, we describe a new, fast and reliable fabrication process of airborne ultrasonic arrays which works with already polarized polymer films (specifically, commercially available Emfit film, metallized on one side only) and attains almost zero inter-element crosstalk, wide bandwidth, and does not sacrifice the material sensitivity.

In our fabrication process, the sheet of Emfit film is cut to a single rectangular piece with the size of the intended array full aperture. The metallized side of this piece is used as a common upper electrode, and the individual element lower electrodes are created with copper pads of a printed circuit board, stuck to the non-metallised side of the Emfit film with a through thickness conductive adhesive tape.

Results

In order to evaluate the new fabrication process, a linear array prototype of 32 elements, with a pitch of 3.4 mm, was built, and evaluated using a 32 channel phased array system. The acoustic field was measured with a calibrated microphone at different deflection angles and focus depths. A very low crosstalk among elements (less than -20 dB) was checked by interferometry. Likewise, a quite homogeneous acoustical response of the array elements, with a maximum deviation of 3 dB, was obtained. The ultrasonic beam parameters, namely lateral resolution, side lobes level, grating lobes and focus depth, agreed to a high accuracy with theory.

Discussion and Conclusions

Due to a combination of the conductive properties of the adhesive only in the axial direction and the low deformation of the Emfit material in the lateral direction, a very high electrical and mechanical isolation is achieved between electrodes, resulting in a very low crosstalk. Thus, the reported fabrication method permits a very precise control on the shape of the lower electrodes of the array in an easy way. The process can be employed also for array structures built on any developable surface if flexible printed circuit boards are used.

3I-5

11:30 AM **Piezoelectric polymer foams: Recent developments in polyolefine, polyester and cycloolefine ferroelectrets**

Michael Wegener; *Fraunhofer Institute for Applied Polymer Research, Functional Polymer Systems, Potsdam-Golm, Potsdam, Germany.*

Background, Motivation and Objective

Electrets offer different working mechanism for piezoelectric properties. In ferroelectric polymers such as polyvinylidene fluoride, the orientation of molecular dipoles is the origin of their piezoelectricity. Beside ferroelectrics, space-charge electrets were developed as piezoelectric systems. Especially in the last ten years a breakthrough is achieved, based on the progress in electret development and foam preparation. Now, foamed, piezoelectric active space-charge electrets are discussed as an own class of piezoelectric materials and named ferroelectrets [1, 2].

Statement of Contribution/Methods

Ferroelectrets are based on electret foams with cellular structures. Internal voids are essential for the working mechanism because the voids have to be charged at their roof and bottom with charges of opposite polarity in order to form large, macroscopic dipoles. In addition, the soft structure allows a large void – and thus dipole - deformation by a mechanical or an electrical stimulus resulting in piezoelectric activity with large piezoelectric coefficients. Here, an overview of ferroelectrets materials, processing possibilities and resulting piezoelectric properties is given.

Results

Ferroelectrets are prepared from non-polar as well as slightly polar polymers such as polypropylene (PP), polyethylene terephthalate (PET) and polyethylene naphthalate (PEN) as well as cycloolefine polymers. The cellular structure is achieved either by (i) extrusion of polymer films or (ii) by voiding of polymer films in supercritical carbon dioxide. In both cases the cellular structures and thus the piezoelectric and elastic properties are adjusted by stretching, inflation and electric charging processes.

Discussion and Conclusions

Based on the developed processing techniques as well as optimized parameters for electrical charging, ferroelectrets with piezoelectric coefficients up to 790 pC/N are fabricated. The elastic modulus in thickness direction of e.g. PET films can be adjusted from 0.3 up to 206 MPa. The modulus of PP as well as PEN films is adjustable within one order of magnitude between 1.3 and 14 MPa. Based on these as well as on geometry values the transducer-resonance frequencies are found between 120 kHz and 2 MHz. The determined acoustic impedances of 17 to 286x10³ kg/m²s are relatively low. Therefore the ferroelectrets discussed here are ideal transducer for air-borne ultrasonic applications [1, 3, 4]. For optimized ferroelectrets this is proofed with determined high values of a recently established Figure of Merit describing the air-borne ultrasonic transduction [3].

[1] M. Wegener and S. Bauer, ChemPhysChem 6, 1014-1025 (2005).
[2] M. Wegener, in S. Wilson and C. Bowen (eds.), Mat. Sci. Eng.: R: Rep. 56, 78-83 (2007).
[3] V. Bovtun, J. Döring, J. Bartusch, U. Beck, A. Erhard, Y. Yakymenko, Appl. Phys. A 88, 737-743 (2007).
[4] J.L. Ealo, F. Seco, and A.R. Jimenez, IEEE Trans. Ultrason. Ferroelectr. Freq. Contr. 55 (4), 919-925 (2008).

3I-6

11:45 AM **Ultralow Noise, High-frequency Ultrasound Detection Using Polymer Microring Photonic Resonators**

L. Jay Guo[1], Sheng-Wen Huang[2], Sung-Liang Chen[1], Tao Ling[1], Adam Maxwell[2], Shai Ashkenazi[2]; *[1]The University of Michigan, Department of Electrical Engineering and Computer Science, Ann Arbor, MI, USA, [2]The University of Michigan, Department of Biomedical Engineering, Ann Arbor, MI, USA.*

Background, Motivation and Objective

With the goal of achieving high resolution imaging using high-frequency ultrasound, we have developed a new, optically-based ultrasound sensor using microring photonic resonators. Optical detection of ultrasound can overcome the limitations imposed by traditional piezoelectric technology by offering superior sensitivity, and simpler signal connectivity, because multiple optical elements can be addressed by using a single optical fiber, replacing the complex and bulky multi-coax cables and interconnects used in electrical transducers.

Statement of Contribution/Methods

The device consists of a 100μm-diameter polystyrene ring waveguide coupled to an input/output bus waveguide, and is fabricated by nanoimprinting. Acoustic pressure causes change in the waveguide cross-section dimension and stress in the polystyrene material, resulting in a variation in the effective refractive index and a shift in resonant wavelength. The ultrasonic waveform can then be recovered from this modulation of optical output. By adjusting the Q factor of the devices during the fabrication process, the dynamic range and sensitivity of each microring can be tuned appropriately.

Results

The –3-dB detection bandwidth was measured to be ~90 MHz (Fig. 1a) using a broadband optoacoustic generation from a thin chromium film excited by a nanosecond laser. With a resonance Q-factor of 6,000, the polymer microring resonators are highly sensitive to ultrasound and have a noise-equivalent pressure of 0.3 kPa over 1–100 MHz—an ultralow NEP as compared with other types of transducers of similar size. At a low laser fluence of 0.35 mJ/cm^2, a 49 μm black bead was detected photoacoustically with no signal averaging using a synthetic 2D microring array. The reconstructed 3D image is shown in Fig. 1b with 15-dB dynamic range.

Discussion and Conclusions

Low-noise wideband ultrasound detection was demonstrated. To form a dense 2D array, addressing multiple microrings with smaller diameters using the same bus is required. We experimentally confirmed the feasibility of using a single waveguide to address four ring elements by means of wavelength division multiplexing. Rings with a diameter of ~20 μm can be realized by designing rings to operate in the visible wavelength range. These results demonstrate the potential of microring resonators for sensitive, high-frequency, 2D ultrasound detection arrays.

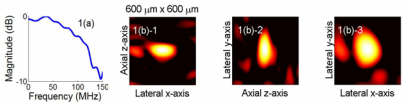

Wednesday Oral

4I. BAW Materials & Devices

Hall 2A

Wednseday, November 5, 2008, 10:30 am - 12:00 pm

Chair: **Gernot Fattinger;**
TriQuint Semiconductor, USA.

4I-1

10:30 AM **Thermally stable oscillator at 2.5 GHz using compensated BAW resonator and its integrated temperature sensor**

David Petit[1], Etienne César[2], Pierre Bar[1], Sylvain Joblot[1], Guy Parat[3], Jacques Verdier[4], Jean-François Carpentier[1]; *[1]STMicroelectronics, Crolles, France, [2]STMicroelectronics, Grenoble, France, [3]CEA, Grenoble, France, [4]INL, Lyon, France.*

Background, Motivation and Objective

High precision and miniaturized 2.5GHz frequency source based on Bulk Acoustic Wave is presented in order to address several application frequencies (provided by dividers) and so to contribute to better integration and lower consumption for handheld products. Basically bulky Quartz crystal is used to provide the time reference due to their excellent stability temperature. According to the Lesson's formula, it's possible to obtain the optimal phase noise for replacing a resonator with a low frequency (10 to 50 MHz) and a high quality factor (10000 to 30000) by a resonator with a high frequency (0.4 to 5 GHz) and a medium quality factor (400 to 2000). Our technology allows realizing sufficient compensated temperature resonator with a quality factor around 1000.

Statement of Contribution/Methods

The BAW resonator with a temperature sensor is assembled on the differential Colpitts oscillator in according to reach the good specifications. This oscillator is realized in bipolar technology. Co-design between the resonant element and the oscillator circuit is requested to reach the severe specifications. For instance, a trade-off has to be done between thermal deviation, quality factor and area of BAW resonator to achieve a low phase noise, low consumption and stable oscillator. The resonator uses an aluminium nitride piezoelectric layer. The presence of silicon dioxide layer having a positive Temperature Coefficient compared to other layers is used to reduce the resonator's TCF. The acoustic isolation consists of alternately low and high acoustic impedance materials having thicknesses which are optimized to reach a quality factor around 1000. For stability purpose, a thermistor is required to cancel the frequency drift versus temperature of the oscillator. To ensure this function, the sensor exhibits an excellent reproducible shape (linear) versus the temperature and it is integrated very close to the BAW resonator. It is based on Molybdenum material which is used to realize the electrodes of the resonator.

Results

The resonators measured with TCF down to 1 ppm/°C are reported in the paper. The reproducible shape of the thermal sensor is demonstrated at wafer scale.

Discussion and Conclusions

We established that higher thermal stability oscillator can be achieved for time reference applications with the used of an integrated reproducible thermal sensor which permits few calibration points.

4I-2

10:45 AM **A UMTS-900 FBAR Duplexer**

Kun Wang, Doug Clark, Stretch Camnitz; *Avago Technologies, San Jose, California, USA.*

Background, Motivation and Objective

The interest in UMTS-900 (Band 8) is rapidly increasing due to its significant benefits; low loss propagation which results in 60% reduction of base stations sites and excellent urban indoor coverage. In a UMTS-900 handset, a duplexer is used to isolate the receive (Rx) and transmit (Tx) signals. The percentage bandwidth for UMTS-900 is 4 % and the separation between Tx and Rx bands is only 10MHz which means that the filter in duplexer needs to

transit from low loss in the pass-band to high attenuation in the rejection band within a few MHz. Due to its wider bandwidth and narrow guard-band, the design and implementation of such duplexer is very challenging.

Statement of Contribution/Methods

In this paper, we will present the design, fabrication, and performance of a Band-8 duplexer using bulk acoustic wave resonator (FBAR) technology. Aluminum nitride (AlN) based FBAR resonators are used to synthesize the filter using a ladder structure. FBAR resonators have very high Q and low temperature coefficient. However, the electromechanical coefficient (kt^2) of AlN is relatively low (about 7%), too low for a 4 % percentage bandwidth filter. We have used external inductors to compensate the inadequate kt^2. High Q is a key factor to achieve sharp transition from pass-band to stop-band. Mutual inductors are used to help sharp transition from pass-band to stop-band. Filters are hermetically packed within a MicroCap. All components are integrated in a 3x3mm PCB footprint.

Results

Figure 1 shows the measured performance of a typical duplexer. We are able to achieve pass-band insertion loss below 2dB. The transition from pass-band to stop-band is within 5 MHz. In-band attenuations are better than 50dB. Tx-to-Rx isolation is better than 50dB.

Discussion and Conclusions

With help of finite element simulation tool, we are able to introduce useful mutual inductors and minimize harmful parasitic effects. The tool also helps us to place zeros at right positions, which is a key to achieve deep in-band attenuation. In addition, external inductors boost kt^2 of resonators to achieve adequate bandwidth. Detailed design considerations and approach will be discussed in the talk.

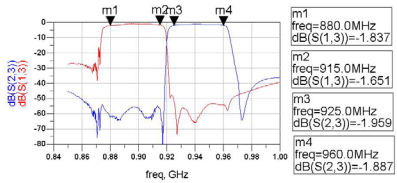

Fig. 1 Measured transmission function of a typical duplexer.

Wednesday Oral

4I-3

11:00 AM **Advanced Determination of Piezoelectric Properties of AlN Thin Films on Silicon Substrates**

Jose-Luis Sanchez-Rojas[1], Jorge Hernando[1], Abdallah Ababneh[2], Ulrich Schmid[2], Jimena Olivares[3], Marta Clement[3], Enrique Iborra[3]; *[1]Univ. Castilla-La Mancha, Spain, [2]Universität des Saarlandes, Germany, [3]Univ. Politecnica de Madrid, Spain.*

Background, Motivation and Objective

Piezoelectric thin films are currently used in the fabrication of filter elements based on bulk acoustic wave resonators for wireless communications. To design the resonators, accurate material properties, such as piezoelectric constants d33 and d31, are essential. d33 is commonly assessed by double-beam vibrometry, AFM or acoustic test devices. However, all these techniques require specific approximations that may lead to inaccurate values of the coefficients. We propose here a method to derive accurate values of d33 and d31 by combining scanning laser interferometry (SLI) measurements and finite element modelling (FEM) calculations.

Statement of Contribution/Methods

We have determined the piezoelectric coefficients of aluminium nitride (AlN) thin films deposited on silicon substrates. AlN piezoelectric capacitors consisting of a metal/AlN/metal stack were sputtered on silicon wafers. The electric field induced out-of-plane deformations in the top surface containing the top electrode were measured with a SLI system and compared with FEM analysis, which included the deformation induced in the silicon substrate. By fitting the model to the measurements, accurate values of d33 were obtained. Besides, the features at the edges of the top electrode, predicted by FEM model and clearly detected in the experiment, allowed to derive the d31 coefficient as well. The results were also compared with the longitudinal and transversal electromechanical coupling factors derived from surface and bulk acoustic wave devices, respectively.

Results

The FEM results demonstrated that the deformation of the silicon substrate at the metal/silicon interface is significant (see figure) and it is not detectable at the bottom of the wafer. Therefore, to assess the actual thickness of the AlN layer, the deformation of the silicon surface should be known. As a result, conventional measurement of either the surface of the films or both the surface and the back of the wafer cannot provide accurate values of d33.

Discussion and Conclusions

Accurate values of piezoelectric coefficients of AlN films are obtained by combining SLI and FEM analysis. The method demonstrates that the conventional measurements that disregard the deformation of the AlN/substrate interface do not provide exact values of d33 and d31. The method proposed is very convenient to determine the piezoelectric constants of thin films.

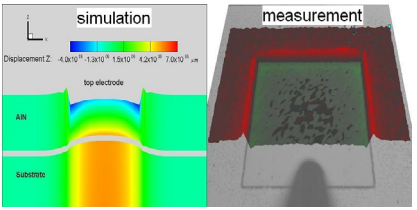

4I-4

11:15 AM **Growth of AlN on SiO_2 for high-Q composite Thin Film Bulk Acoustic Wave Resonators**

Alvaro Artieda, Paul Muralt; *Ecole Polytechnique Federale de Lausanne, Switzerland.*

Background, Motivation and Objective

Due to its outstanding acoustic properties and excellent chemical compatibilities with semiconductor front end materials, aluminum nitride is the most favorite one for thin film bulk acoustic wave BAW filters (TFBAR's) [1]. Current applications are mainly in RF filters for mobile communication. A further application would be in oscillators, where a large bandwidth (defined by the coupling constant k^2) is less important than resonance frequency definition and stability. One possibility to tune for this application is to use AlN/SiO_2 composites. We recently published on the increase of Q factor and reduction of thermal drift with symmetric $SiO_2/AlN/SiO_2$ sandwich structures [2]. In this contribution we focus on growth issues and film properties related to deposition of AlN on amorphous SiO_2.

Statement of Contribution/Methods

The growth of AlN films was studied as a function of substrate roughness. The variation of roughness was obtained through variation of growth conditions of a suitable sputtered film deposited on amorphous SiO_2. The samples roughness was measured with an atomic force microscope, AlN was deposited by pulsed reactive DC sputtering, and its structural properties assessed by means of X-ray diffraction including θ-2θ scans and rocking curve width of the (002) peak. The internal stress was evaluated with a stress analyzer. The piezoelectric constant of AlN films were measured with double beam interferometry at samples with a Pt electrode below the oxide film. Finally, for device assessment, membrane type TFBAR structures were fabricated.

Results

The properties of the AlN thin films turned out to be very sensitive to substrate roughness. An increase of its rms value from 0.1 nm to 0.7 nm resulted in an increase of the mechanical film stress in AlN from -700 MPa to -200 MPa. At the same time, the rocking curve width of AlN(002) increased from 1.3° to 1.8°, showing a clear correlation with substrate roughness. The best value of the piezoelectric constant $d_{33,f}$ was obtained as 4.0 pm/V. This value is in agreement with device simulations of the resonant behavior fitted to experimental results of symmetric $SiO_2/AlN/SiO_2$ TFBAR's.

Discussion and Conclusions

Piezoelectric layers of AlN grown on amorphous SiO_2 layers have been developed. This work has potential for the development of new composite TFBAR's.

[1] P. Muralt et al., Is there a better material for thin film BAW applications than AlN?, Proc. IEEE Ultrasonics Symposium, Rotterdam, pp. 50-53, 2005.

Wednesday Oral

[2] A. Artieda and P. Muralt, High-Q AlN/SiO_2 symmetric composite thin film bulk acoustic wave resonators, IEEE Trans.UFFC, in press (2008).

4I-5

11:30 AM **Shear mode BAW resonator based on c-axis oriented AlN thin film**

Evgeny Milyutin, Paul Muralt; *Ecole Polytechnique Federale de Lausanne, Switzerland.*

Background, Motivation and Objective

Thin film bulk acoustic wave resonators (TFBAR's) also showed potential as gravimetric sensors. In contrast to RF filters working with longitudinal modes, bio-medical applications usually require detection in a liquid, thus must employ shear modes. The principle has recently been successfully demonstrated with TFBAR devices employing tilted c-axis growth of ZnO [1, 2]. In this work, we show that it is also possible to use non-tilted AlN thin films when interdigitated (ID) electrodes (IDE) are used. A true shear BAW thickness mode can be excited. Parasitic Lamb waves are avoided by the use of acoustic reflectors.

Statement of Contribution/Methods

Performance and design of shear modes in AlN(001) films excited by ID electrodes were simulated by finite element modeling using the boundary element method (FEM-BEM). Devices have been fabricated with 1.5 microns thick (001)-textured AlN thin films on top of a Bragg reflector composed of 5 double layers of SiO2/AlN. The Al electrode system was defined by photolithography along with a lift-off process.

Results

The performances of resonators were assessed in air and silicon oil. Typically resonance frequency of the devices was between 1.8-1.9GHz. By using different electrode periodicities, the BAW nature of the resonance was confirmed through the absence of a shift. A quality factor of about 1000 was achieved when operated in air. Under immersion, the Q-factor decreased to 260. Experimental results are in a good agreement with simulations, when we consider acoustic emission through the Bragg grating as the only loss factor.

Discussion and Conclusions

The achieved results and the simplicity of fabrication of proposed device show their potential as gravimetric sensors for immersed applications. The achieve Q-factor is higher than reported in literature for tilted c-axis resonators [3]. Further optimization of design and materials is going on. The integration of an immobilization layer is in development.

1. Link, M., M. Schreiter, J. Weber, R. Gabl, D. Pitzer, R. Primig, W. Wersing, M.B. Assouar, and O. Elmazria, C-axis inclined ZnO films for shear-wave transducers deposited by reactive sputtering using an additional blind. J.Vac.Sci.Techn. A, 2006. 24: p. 218-222.

2. Weber, J., W.M. Albers, J. Tuppurainen, M. Link, R. Gabl, W. Wersing, and M. Schreiter, Shear mode FBAR as highly sensitive liquid biosensors. Sensors and Actuators A, 2006. 128: p. 84-88.

3. G. Wingqvist, J. Bjurstrom, L. Liljeholm, V. Yantchev, I. Katardjiev, Shear mode AlN thin film electro-acoustic resonant sensor operation in viscous media, Sensors and Actuators B 123 (2007), 466-473

4I-6

11:45 AM **A film bulk acoustic resonator fabricated with composite support diaphragm**

Liang Tang, Zhenhong Hao, Donghai Qiao, Chenghao Wang; *Institute of Acoustics,Chinese Academy of Sciences, MEMS laboratory, Beijing, China.*

Background, Motivation and Objective

Film bulk acoustic resonator (FBAR) has widely been investigated to use in RF filters and oscillators for its high quality factor, good power handling abilities and compatibility with integrated circuit processing. As for the diaphragm-structure FBAR, Si3N4 or SiO2 is usually used as the supporting material. In our previous work, we found that the residual stress of single Si3N4 or SiO2 membrane often caused wrinkling in the released support diaphragm, which degraded Q factor dramatically. In this work, we aim to fabricate a high-Q film bulk acoustic resonator with a flat support diaphragm.

Statement of Contribution/Methods

Based on the opposite stress characteristics of Si3N4 and SiO2, we proposed a diaphragm-structure FBAR with Si3N4/SiO2/ Si3N4 composite support diaphragm. After the silicon substrate of FBAR was etched away from the backside, the diaphragm was flat. Moreover, because the total residual stress of the composite support diaphragm

was small, none of the devices in a wafer was broken. Therefore, it is a suitable method to fabricate a FBAR device.

Results

We fabricated the FBAR device as follows: LPCVD Si3N4, PECVD LTO and another LPCVD Si3N4 were deposited to form the composite support diaphragm. Ti and Au were sputtered to form the bottom electrode. Then ZnO piezoelectric film was deposited using DC magnetic sputtering method. Another thinner Si3N4/SiO2/ Si3N4 composite film was deposited as an insulated layer. After that, Ti and Au were sputtered to form the top electrode. In the end, the silicon substrate was etched away from the backside. Fig.1 showed the SEM images from both the top and backside of the FBAR, and the support diaphragm was flat.

Discussion and Conclusions

S11 measurement showed three resonances in the frequency range from 0.4GHz to 2.6GHz. 1st, 2nd and 3rd harmonic resonances appeared at 0.662GHz, 1.491GHz and 2.371GHz respectively. keff2 and Q factor of the three resonances were 2.91%, 1.64%, 0.60% and 267, 202, 500 respectively. The reason why the Q factor of 3rd harmonic resonance was highest would be revealed in detail.

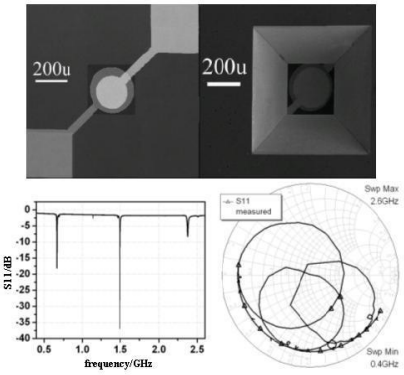

Fig.1 SEM images of the fabricated FBAR device(top) and measured S11 results(bottom)

Wednesday Oral

5I. Wave Propagation

Hall 2B

Wednseday, November 5, 2008, 10:30 am - 12:00 pm

Chair: **Massimo Pappalardo;**
University di Roma TRE, Italy.

5I-1

10:30 AM **Invariants of the Time Reversal Operator and Ultrasonic Applications**

Claire Prada, Mathias Fink; *CNRS, Université Paris 7, ESPCI, Laboratoire Ondes et Acoustique, Paris, France.*

Background, Motivation and Objective

It is well known that acoustic time reversal mirrors own outstanding focussing properties in complex media. Used in the pulse echo mode, the time reversal process can be iterated to achieve selective focusing on the most reflective point among a set of scatterers or to enhance and extract the echo from a defect in a noisy structure.

Statement of Contribution/Methods

The iterative time reversal process can be described by the Time Reversal Operator. This process has an ensemble of invariants that can be determined from the measurement of the array inter-element impulse responses and the singular value decomposition of corresponding array response matrix. The determination and analysis of these invariants is the object of the D.O.R.T. method (French acronym for Decomposition of the Time Reversal Operator).

It can be used to separate the echoes of several scatterers in an inhomogeneous medium. It also enables the separation of the radiation modes of a solid scatterer, like, for example, the various Lamb waves circumnavigating a hollow cylinder, leading to its characterization. Furthermore, when an estimate of the medium's Green function is available, high resolution and low noise images can be achieved using the back-propagation of the dominant invariants.

Results

This presentation will provide an overview of the different results obtained with the DORT method in the context of non detructive evaluation. Different improvements of the method will be shown, like the acquisition of the array response matrix using the Hadamard basis or focussed transmissions, or the coding of the inter-element impulse responses on 1-bit with little loss of information.

Several examples of invariants of the time reversal operator and applications to the detection and characterization of solid scatterers will be presented.

Discussion and Conclusions

The DORT method is a powerfull tool that can be used as a complement to conventional beamforming imaging technique. Furthermore, it allows detection and focusing through aberrating media where conventional beamforming fails.

5I-2

11:00 AM **Optimal Ultrasonic Array Focusing in Attenuative Solids**

Abhijit Ganguli[1], Robert Gao[1], **Kenneth Liang[2],** Jacques Jundt[2]; [1]*University of Massachusetts, Amherst, USA,* [2]*Schlumberger-Doll Research, Cambridge, MA, USA.*

Background, Motivation and Objective

This work addresses the focusing of ultrasonic waves in propagation media with high attenuation, such as rock formation, concrete structures, etc. In the absence of attenuation, it is well known from diffraction theory that the focal spot size narrows monotonically with increasing frequency. The presence of attenuation changes this behavior due to two factors: (1) ultrasonic waves are attenuated exponentially with frequency, (2) when the focusing is provided by a linear array, the contributions from array elements with longer path length to the focal point are attenuated exponentially more, thus rendering them less effective. It is intuitively expected that there exists an optimal frequency of operation where the focal point amplitude maximizes. This paper presents results

from a combined modeling and experimental study predicting the existence of the optimal frequency and measuring the focal spot size in a laboratory mock-up sample with high attenuation.

Statement of Contribution/Methods

In last year's presentation [Ref. 1], we predicted with an analytic solution and verified by Finite Element Modeling the existence of an optimal frequency for focusing ultrasonic wave in an attenuative medium. We have since constructed a cement block (60 x 40 x 40 cm) to simulate a lossy propagation medium with a Q = 14. We collected through-transmission synthetic-aperture waveforms with a pair of 250 kHz transducers (a single scanned transmitter and a single scanned receiver on opposite faces of the cement block). The transducers were directly coupled to the surface of the cement. The waveform data were post-processed to implement focusing at different locations on the receiver face. Two different techniques were used to effect focusing: the traditional time-delay method based on arrival times estimated from the transmission waveforms, and the time-reversal imaging method. The latter method does not require any arrival time estimation. The one-way transmission waveform was recorded, time-reversed and then back-propagated along the same path. Focusing is, in theory, automatic. The resulting synthetic focal-plane profiles were compared to modeling predictions.

[Ref. 1] A Ganguli, etal, "Investigation of Efficient Ultrasonic Array Focusing in Attenuative Solids," Proceedings 2007 IEEE Ultrasonics Symposium, New York, October 2007

Results

The acoustic properties of the block was found to be non-uniform. The compressional velocity had a mean value of 3812 m/s with a standard deviation of 9 m/s. The total attenuation over a propagation distance of 60 cm varied by as much as 20 dB depending on location. The mean attenuation was estimated to be about 110 dB/m at 250 kHz. Despite these heterogeneities, we obtained -3 dB spot sizes on the order of 5 cm at 190 kHz using either time-delay focusing or time-reversal focusing, which compares well with the modeled prediction of 4.5 cm assuming a uniform medium.

5I-3

11:15 AM **Guided Waves in Cylindrical Multi-layered Medium**

Hanyin Cui, Bixing Zhang; *Institute of Acoustics, Chinese Academy of Sciences, National Laboratory of Acoustics, Beijing, China.*

Background, Motivation and Objective

Propagation of guided waves in cylindrical multi-layered elastic solid medium is an interesting research topic. One important application is ultrasonic non-destructive evaluation (NDE) for inspection of the rockbolts which are installed to reinforce ground in mining and civil engineering structures. Although some studies have been reported on this topic, most of them focus on the dispersion characteristics without considering the excitation mechanisms. If one guided mode with good dispersion characteristics has less excitation intensity than other modes, it will be difficult to receive. Therefore, the excitation intensity is an important physical quantity for guided waves, yet little attention has been paid on it.

Statement of Contribution/Methods

In this paper, guided waves propagated in a cylindrical multi-layered elastic solid medium are studied. Not only are the dispersion characteristics analyzed further, but also the excitation mechanisms of all guided modes are investigated as keystone. The dispersion equation of the guided waves is generally a plural function for a real axial propagation velocity. We transform it into a real dispersion function, and employ the bisection technique to find all the real roots, in order to give all the dispersion curves of the guided waves robustly.

Results

All the guided modes propagated in two-, three-, four-, and five-layered models are studied. Each one of the guided wave dispersion curves begins at its cutoff frequency where phase velocity is equal to the shear velocity of the outside layer. And it finally meets its high-frequency phase velocity asymptote which is either equal to the smallest shear velocity (named as Vsmin) among all the layers for the normal waves, or less than Vsmin for the Stoneley waves.

The excitation intensities of the guided waves excited by symmetric point source, axial and radial force sources are investigated. They are highly relied on excitation frequency and radial position. Thus dominant modes are different with different excitation frequencies. Moreover, intensity of each mode reaches its maximum around the frequency where the group velocity reaches its minimum and finally tends to zero at high frequency. The displacement distributions of the normal waves along the radial direction are complicated. However, intensities of the Stoneley waves, which are interfacial waves propagated in cylindrical interfaces, decay with radial distance far from the interface into the outside layer, and finally approach zero at infinity. Moreover, the lowest branch of

flexural guided waves excited by radial force source holds the promise for NDE of rock bolts. It can be excited out with the largest intensity in the lower frequency range.

Discussion and Conclusions

Excitation intensity and dispersion curve have been investigated together to determine whether one guided wave is suitable for NDE. Moreover, primary testing results have been obtained by modeling experiments undertaken in laboratory.

5I-4

11:30 AM Plunging of metal pins using a 20 kHz ultrasonic vibration system

Jiromaru Tsujino[1], Tetsugi Ueoka[1], Toshiya Sakurai[1], Yuuki Haraguchi[1], Eiichi Sugimoto[2]; *[1]Kanagawa University, Faculty of Engineering, Yokohama, Japan, [2]Asahi EMS Co., Ltd, Tokyo, Japan.*

Background, Motivation and Objective

Plunging methods inserting metal pin or shaft to narrow holes by static force are widely used in various industries. It requires rather large static inserting force, as examples about 1,200 N for 2.5-mm-diameter steel pin and up to 50,000 N for 10-mm-to 20-mm-diameter center shafts of electric motor. When inserting pin or shaft, the material with holes happen to broken by plunging pin and also the motor shaft become inevitably eccentric. Using ultrasonic vibration, static force and eccentricity can be decreased due to decreasing frictional force. Plunging of metal pin or shaft using longitudinal vibration is studied.

Statement of Contribution/Methods

A 20 kHz large capacity longitudinal vibration system with eight transducers integrated by a R-L vibrator, 3 kW SIT power amplifier and hydraulic pressure source of 60,000 N maximum force are used. Vibration amplitude is measured using ring-type magnetic vibration detectors. Maximum vibration velocity at loaded condition is about 20 μm (peak-to-zero value).

As plunging specimens, hard steel pins (2.498 ± 0.002 mm diameter, 7.8 mm length; SUJ 2)and 28.4-mm-diameter steel gears with three holes (inner diameter; 2.462 ± 0.015; SMF5040) are used.

Results

At low speed plunging, the average plunging forces (require push in the pin) without vibration are 1285 N and the forces decrease 30% by ultrasonic vibration. The average required forces push out the inserted pin (holding force) are 767.5 N and the force with vibration increase 26%. And at higher speed, the plunging forces without vibration are 1330.5 N and the forces with vibration decrease 22%. The holding forces with vibration are 1690 N and the force with vibration decrease 22%.

The plunging and holding forces at high speed are larger than these at low speed. At low speed, the holding force without vibration decreases 40% but the force with vibration increases 7.6%. At high speed, the holding forces increase 30% compared with the plunging forces by vibration.

Discussion and Conclusions

The plunging force decreases by vibration due to decreased friction, furthermore the holding force increases due to partial welding of the surfaces. The holding force may be increased using complex vibration which induces effective vibration parallel to contact surfaces. Electric motor shafts of 10 to 20 mm diameter were successfully plunged using vibration with smaller force and eccentricity.

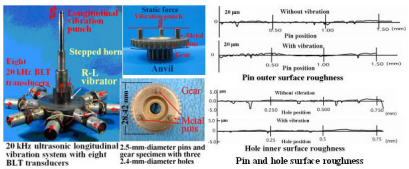

5I-5

11:45 AM **Development of temperature stable acoustic line based on piezoelectric plate and nanocomposite polymeric film**

Iren Kuznetsova[1], Boris Zaitsev[1], Anastasia Kuznetsova[1], Alexander Shikhabudinov[1], Vladimir Kolesov[2]; [1]*Institute of Radio Engineering and Electronics of RAS, Saratov Branch, Saratov, Russian Federation,* [2]*Institute of Radio Engineering and Electronics of RAS, Moscow, Russian Federation.*

Background, Motivation and Objective

As is well known one of the modern lines of investigation in acoustics is the search of such wave types and crystallographic orientations of wave-guides for which the value of electromechanical coupling coefficient is maximal and value of temperature coefficient of delay (TCD) is minimal. At present there exist the papers showing that fundamental shear-horizontal (SH_0) acoustic waves in thin (in comparison with wavelength) piezoelectric plates possess significantly more electromechanical coupling coefficient than surface acoustic waves. However, although the values of TCD of such waves are less than for SAW but this is not enough for development of temperature stable devices. It is known that velocity of SH_0 wave in lithium niobate plate always decreases when the temperature increases. From other hand it has been found that the velocity of SH_0 wave in plate always increases when dielectric permittivity of contacting media decreases. Recently, it has been also found that there exist such nanocomposite polymeric materials, which dielectric permittivity decreases with temperature increase. So, by using the structure containing nanocomposite polymeric film with certain value of dielectric permittivity one can significantly decrease TCD of SH_0 wave.

Statement of Contribution/Methods

We measured the temperature dependencies of dielectric permittivity of nanocomposite polymeric films with various contents of Fe and CdS nanoparticles. Then we theoretically studied the influence of temperature on velocity of SH_0 wave in structure "YX lithium niobate plate - nanocomposite polymeric film". The analysis was carried out by the example of aforementioned polymeric film. For analysis of wave propagation we used the motion equation, Laplace's equation, and constitutive equations for piezoelectric medium and polymeric film and appropriate mechanical and electrical boundary conditions. The influence of temperature was considered by using appropriate temperature coefficients of material constants and the temperature coefficient of expansion.

Results

As a result the TCD was calculated for SH_0 wave propagating in lithium niobate plate contacted with nanocomposite polymeric film containing different concentration of Fe and CdS nanoparticles. It has been found there exists such concentration of Fe and CdS nanoparticles when the TCD of SH_0 wave in considered structure is equal 15 ppm/C and 10 ppm/C, respectively, instead 70 ppm/C without nanocomposite film.

Discussion and Conclusions

In whole the obtained results open the real prospective of use of SH_0 wave in thin piezoelectric plates for development of temperature stable acoustic devices for signal processing and high sensitive sensors.

This work is supported by RFBR #06-08-01011, RNP.2.1.1.8014 and Rosnauka Contract 2007-3-1.3-07-15-036. Dr. I.Kuznetsova thanks Russian Science Support Foundation for help.

6I. Ultrasonic MEMS

Hall 2C

Wednseday, November 5, 2008, 10:30 am - 12:00 pm

Chair: **Amit Lal;**
Cornell University, USA.

6I-1

10:30 AM **Piezoelectric MEMS for Audio Signal Transduction, Microfluidic Management, Resonant Mass Sensing, and Movable Surface Micromachined Structures**

Eun Kim; *University of Southern California, Electrical Engineering - Electrophysics, Los Angeles, CA, USA.*

Background, Motivation and Objective

This paper describes (1) piezoelectric microphone and microspeaker, (2) micromachined self-focusing acoustic transducers for liquid droplet-ejection, mixing, pumping and transporting, (3) resonant mass sensors based on film bulk-acoustic resonators (FBAR), and (4) piezoelectrically actuated mirror array and tunable capacitor.

First presented will be micromachined microphones and microspeakers that consume very low power, and are small, rugged and highly sensitive. The microphones and microspeakers are built on micromachined diaphragms with a piezoelectric ZnO, and have large dynamic range, no need to have a polarization voltage, and no major performance/reliability problem due to water condensation. The fabrication processes for the transducers are relatively simple and very robust. We have incorporated various types of diaphragms that are cantilever-like, bimorph-type, containing partially-etched holes, corrugated, dome-shaped, etc.

Another line of presentation will be on microfluidic mixers, pumps, transporters and ejectors based on the self-focusing acoustic-wave transducer (SFAT). All the transducers are powered by a piezoelectric film or substrate, and are inherently fast, consume low power, and require no heat. The SFATs do not require any nozzle or acoustic lens, and their fabrications are very simple. Moreover, the SFAT ejector (unlike a nozzle-based ejector) can eject liquid droplets at any oblique angle, and does not have to be moved to ink a spot with different liquids. We have integrated a 2-D ejector array with microchannels, chambers and other microfluidic components on a single silicon chip for a small, portable, affordable DNA synthesis system.

Also described will be FBAR-based highly sensitive, resonant mass sensors that can operate in vapor and liquid. In vapor, the sensor based on an FBAR with Q of about 500 at 1 GHz can detect a mass change of 10-9g/cm2 on its surface. The following FBAR-based sensors will briefly be described: mercuric ion sensor, DNA hybridization sensor, explosive-vapor-trace detector, and a 1.5mm long, 250μm wide and 15μm thick polymer probe with an FBAR mass sensor at its tip.

Finally presented will be a piezoelectrically actuated array of cantilevers/bridges (whose facets can accurately be controlled by electrical voltage) for tunable capacitors, RF switches and projection displays. Through the implementation of a simply-supported bridge driven by two 100-μm-long ZnO-actuated cantilevers, a compact surface-micromachined tunable capacitor has been fabricated on a single chip without any warping, and shown to be capable of a 1,400% continuous tuning from 0.13 pF to 1.82 pF. Also shown will be a cantilever array with a pixel size of 100x100 μm2 that was developed for a projection display. A piezoelectric ZnO film was used to produce 0.116°/V vertical deflection of the cantilever.

6I-2

11:00 AM **Concentration and mixing of particles in microdrops driven by focused surface acoustic waves**

James Friend, Leslie Yeo, Ming Tan, Richard Shilton; *Monash University, MicroNanophysics Research Laboratory, Clayton, VIC, Australia.*

Background, Motivation and Objective

In the past decade, microfluidic research has grown exponentially due to the vast potential of its exploitation in a wide range of chemical, biological and biomedical applications. The concentration and indeed mixing of particle suspensions are important procedures in microfluidic processes. Relying on diffusion for mixing leads to unreasonably long mixing times, and enhancing or avoiding it by promoting chaotic mixing typically relies on complex geometries.

We report the use of focused SAW generated on 128-YX Lithium Niobate for greatly enhancing the concentration and mixing of microliter droplet particle suspensions at microscale dimensions, and in the presentation will explain why.

Statement of Contribution/Methods

Concentric circular (b) and elliptical (c,d) single-phase unidirectional transducers (SPUDTs) were used to focus the SAW. A comparison of the effects of focusing is provided by using a (a) straight EWC-SPUDT, two focusing elliptical EWC-SPUDTs, with eccentricities of (b) 0.831 (E1) and (c) 0.616 (E2), and a (d) circular EWC-SPUDT. A thin layer of amorphous Teflon prevented droplet spreading during induced rotation.

Results

Due to the increased wave intensity and asymmetry of the wave, we found both circular and elliptical SPUDTs concentrate particles in under one second (e), which is one order of magnitude faster than the straight SPUDT and several orders of magnitude faster than conventional microscale devices. The concentric circular SPUDT was found to be most effective at a given input power since it generated the largest azimuthal velocity gradient within the fluid to drive particle shear migration. On the other hand, the concentric elliptical SPUDT generated the highest micromixing intensity (f, Deff is effective diffusivity, D0 is inherent diffusivity) due to the more narrowly focused SAW radiation that substantially enhances acoustic streaming in the fluid.

Discussion and Conclusions

Rapid concentration of suspensions of particles and mixing of fluids in microdrops was demonstrated by producing acoustic streaming in drops via focused SAWs using straight, concentric circular, and elliptical SPUDTs. During the presentation, we will explain These focusing SAWs provide a very rapid and effective mechanism for particle concentration and micromixing several orders of magnitude faster than current microfluidic technology.

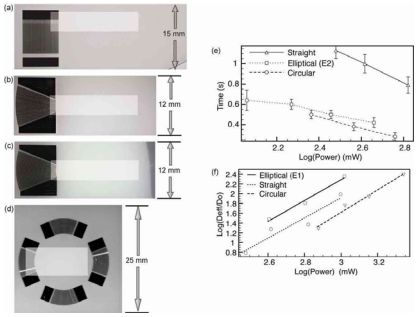

Wednesday Oral

6I-3

11:15 AM **Theoretical study of acoustic streaming induced cooling effect in the microscale**

Hongming Sun, **Hang Guo;** *Pen-Tung Sah MEMS Research Center, Xiamen University, Xiamen, Fujian, China.*

Background, Motivation and Objective

During the past 20 years, microelectronics, optoelectronics and MEMS technology have gained significant progress, with more functionalities integrated on a greatly reduced size chip. However, cooling for microdevces has not achieved the same progress. Most of microdevices, such as IC chips, LEDs and lab-on-a-chip, are still using the conventional scale cooling systems which are very bulk and high-power consumed. Thus, great efforts are being made to develop micro cooling devices. Heat transfer due to forced convection caused by acoustic streaming in the conventional scale has been shown to have a good cooling effect. Due to the size of the microdevices that is greatly reduced by using MEMS technology, heat transfer due to forced convection induced by acoustic streaming in the microscale is quite different from that in the conventional scale device. It is necessary to make theoretical studies on the acoustic streaming induced cooling effect in the microscale.

Statement of Contribution/Methods

In this paper, we study the acoustic streaming induced cooling effect in a proposed microdevice. The device is composed of a microchannel and a microcavity. It is fabricated on silicon substrate by using bulk micromachining technology and then bonded to a glass plate. Water is assumed to fill into the microdevice.One PZT piezoelectric ceramic plate is attached to bottom of the glass plate. Once the device is excited into vibration by applying an AC voltage on the PZT plate, an acoustic field will be generated in the microchannel and microcavity. This acoustic field can be coupled to the fluid inside the microchannel and induces acoustic streaming in it. Starting from the Navier-Stokes equations, we first set up an analytical model for acoustic streaming in the microchannel that is actuated by ultrasonic vibration and then investigate the influence of channel height and vibration frequency on driving force, velocity of streaming and the cooling effect. After that, we use computational fluid dynamics (CFD) package in ANSYS to study the two-dimensional model of proposed microdevice. The cooling effect is studied by comparing the average temperature of the heated region of the microdevice with and without the acoustic streaming in the microchannel.

Results

When the device vibrates with the amplitude of 0.1¦Ìm and frequency of 200KHz, the maximum velocity of fluid motion can reach up to 0.036m/s in the microchannel with the channel height of 0.1mm. And the acoustic streaming in microchannel can reduce the temperature of the wall of microdevice by about 1~10% for a channel height ranging from 0.1 mm to 1mm. If the channel height, vibration amplitude and frequency increase, the cooling effect may further enhanced.

Discussion and Conclusions

The results show that acoustic streaming induced cooling effect in the microscale is feasible and has potential for developing acoustic MEMS devices for micro cooling applications.

6I-4

11:30 AM **Electric power generation using a vibration of a polyurea piezoelectric thin film**

Daisuke Koyama, Kentaro Nakamura; *Tokyo Institute of Technology, Precision and Intelligence Laboratory, Yokohama, Japan.*

Background, Motivation and Objective

An electric energy harvesting using a polyurea piezoelectric thin film is discussed. In this energy harvesting system, the vibration energy of the device is converted to the electric energy through the piezoelectric effect of the polyurea film. The electric energy harvesting methods using the piezoelectric elements have been reported by several groups, and in most of these reports, the piezoelectric zirconate titanate (PZT) was employed as the piezoelectric material. However, the large stress with the large deformation cannot be applied to these devices since the PZT has the low fracture stress compared with the polymer piezoelectric. We propose the energy harvesting device at the low resonance frequency of tens to hundreds Hz and the large deformation using a flexible polyurea thin film, which is formed through the vapor deposition polymerization with 4,4'-diphenylmethane diisocyanete (MDI) and 4,4'-diamino diphesyl ether (ODA) and has the larger piezoelectric g constant than that of the PZT.

Statement of Contribution/Methods

The experiments were carried out with the electric power generation device having the polyurea thin film with the thickness of 3 μm attached to the beryllium copper cantilever with the length of 18 mm and the thickness of 0.1 mm. The vibration in the vertical direction, which induces the bending vibration of the cantilever, was applied to the device and the output voltage was measured by connecting the load resistances.

Results

The resonance frequency of the cantilever was 195 Hz, which corresponds to the theoretical value, and the electric power generation using the polyurea film at the low frequency was realized. The output voltage was proportion to the vibration velocity, and the output voltage of 69mVpp could be obtained with the vibration velocity of 25 mm/s and the load resistance of 390 kΩ at the resonance frequency of 195 Hz. The power output was measured with changing the load resistance value from 10 kΩ to 10 MΩ, and it was found the value of the load resistance has the optimum value of 910 kΩ (Fig.1).

Discussion and Conclusions

The conversion efficiency from the strain energy to the electric energy was also investigated.

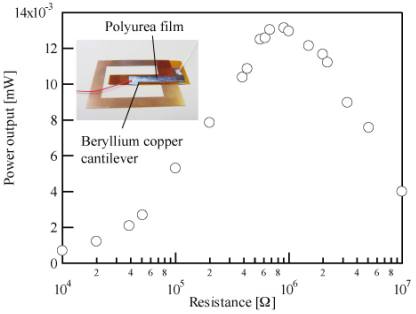

6I-5

11:45 AM **Experimental investigations on the collapse of cavity cluster in high power ultrasound fields**

Lixin Bai, Weilin Xu, Yichi Zhang, Yanfu Li, Defa Huang; *Sichuan University, China.*

Background, Motivation and Objective

Applications of high power ultrasound span many industrial sectors, from healthcare, through sonochemistry, to ultrasonic cleaning. These applications depend on the dynamics of cavity cluster. This study was conducted to investigate the collapse of cavity cluster in high power ultrasound fields.

Statement of Contribution/Methods

The cloud cavitation was produced by a 20 kHz ultrasonic horn used for sonochemistry. The dynamics of cavity cluster below the ultrasonic horn was recorded with high-speed photography in a framing rate of 100,000 fps. PIV (particle image velocimetry) techniques were also used to get a velocity field of acoustic streaming.

Results

The movement of cavitation bubbles was strongly influenced by the acoustic streaming. They moved from the perisphere downward towards the axis and convergent at a point about 2.5mm below the horn (where small bubbles incorporated into big bubbles) and then move downward along the axial direction. However, transient shift of bubbles divergent from acoustic streaming upwards towards the center of the cavity cluster was found. The growth and collapse of incipient cavitation bubbles in the cavity cluster in two acoustic cycles were recorded with high-speed photography and the variation of the diameter of bubbles in the same cavity cluster with time was investigated.

Discussion and Conclusions

The transient shift of bubbles divergent from acoustic streaming towards the center of the cavity cluster may be the combined action of primary Bjerknes force of ultrasonic field and microjet induced by the shock wave shooting towards the center of cavity cluster. The first collapse of incipient bubbles is influenced by the maximum diameter of cavitation bubbles with good regularity, while the subsequent rebound and collapse make the cluster very complicated. Asynchrony of collapse of bubbles in the same cluster was found, which may be an evidence of propagation of shock wave in the cavity cluster.

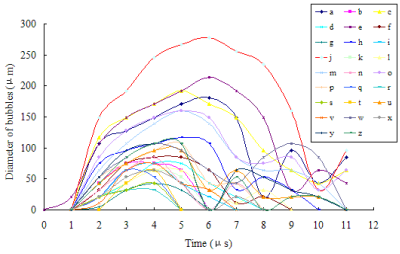

Variation of the diameter of cavitation bubbles with time in two acoustic cycles

1J. Cardiovascular Elastography

Hall 3

Wednseday, November 5, 2008, 1:30 pm - 3:00 pm

Chair: **Jan D'hooge;**
Catholic University of Leuven, Belgium.

1J-1

1:30 PM **Non-Invasive quantitative imaging of arterial wall elasticity using Supersonic Shear Imaging**

Mathieu Couade[1], **Mathieu Pernot[2],** Mickaël Tanter[2], Claire Prada[2], Emmanuel Messas[3], Mathias Fink[2]; *[1]SuperSonic Imagine, Aix-en-Provence, France, [2]UMR 7587 CNRS, ESPCI, INSERM, Laboratoire Ondes et Acoustique, Paris, , France, [3]Hôpital Européen Georges Pompidou, INSERM 633, Paris, France.*

Background, Motivation and Objective

Arterial elasticity is an important predictor of cardiovascular mortality. It is well known that arterial stiffness increases with age and in some diseases associated with cardiovascular risk, including hypertension and diabetes. We propose to apply the concept of Supersonic Shear Imaging (SSI) for non-invasive and quantitative assessment of the elastic modulus of the arterial wall. The goal of this study is to demonstrate the potential of this technique for quantifying precisely the elasticity of the arterial wall.

Statement of Contribution/Methods

A shear wave was generated on the artery wall using the acoustic radiation force induced by a conventional linear ultrasonic probe (8MHz). The shear wave propagation along the wall was imaged in real-time using an ultrafast scanner (10 000 frames/s). The velocities within the wall were obtained from conventional speckle tracking techniques and the shear wave phase velocity was derived at each frequency in the range of 100-1500Hz from a single broadband radiation force excitation. These results were compared to 3D finite differences simulations of the elastic wave propagation.

Experiments were performed in 3 arterial phantoms composed of different elastic materials (polyvinylalcool, natural rubber and agar-agar) with typical elastic modulus found in human arteries. Finally, an in-vivo study on the carotid artery of 10 sheep was conducted to show the feasibility and the reproducibility of the technique.

Results

The feasibility of imaging the shear wave propagation and measuring the elastic modulus of the arterial wall is demonstrated in phantoms with good accuracy (< 6 %) over a large bandwidth (100-1000Hz). The figure shows tissue velocities in color superimposed onto the grayscale B-mode images 0.3 ms, 1.2 ms and 2.4 ms after the shear wave generation. The experimental dispersions curves are in good agreement with the curves simulated for each phantom. Moreover, it is shown on the animal experiments that the assessment of the artery wall elasticity is feasible in vivo and can be performed up to 10 times per second.

Discussion and Conclusions

The reproducibility and the accuracy of the estimation are discussed, as well as the measurement dependence on the geometry and the elasticity of the surrounding tissues. This novel approach offers an efficient and reliable technique for imaging quantitatively the elasticity of the arterial wall.

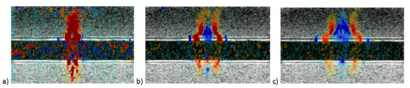

Wednesday Oral

1J-2

1:45 PM **BiPlane Cardiac Strain Imaging: A Study on Valvular Aortic Stenosis**

Richard G.P. Lopata[1], Maartje M. Nillesen[1], Inge H. Gerrits[1], Livia Kapusta[2], Johan M. Thijssen[1], Chris L. de Korte[1]; *[1]Radboud University Nijmegen Medical Centre, Clinical Physics Laboratory, Department of Pediatrics, Nijmegen, Netherlands, [2]Radboud University Nijmegen Medical Centre, Children's Heart Centre, Netherlands.*

Background, Motivation and Objective

Cardiac strain imaging is a non-invasive technique for mapping the functional properties of myocardial tissue and monitoring cardiac diseases. In previous work, the possibilities of 3D strain imaging using BiPlane and full 3D ultrasound imaging were investigated and reported. In this study, an animal model was used to examine the effects of an induced valvular aortic stenosis. BiPlane strain imaging was used to assess strain development and differences between the animals.

Statement of Contribution/Methods

Four healthy beagles underwent surgery at the age of eight weeks. One of the three cusps of the aortic valve was plicated, resulting in a stenotic valve and pressure overload of the left ventricle. An ultrasound exam was performed each month for a period of seven months. RF data of the beagles' heart were acquired with a Philips SONOS 7500 live 3D ultrasound system, equipped with an X4 matrix array transducer. BiPlane data were acquired using ECG-triggering at a frame rate of 100Hz for at least one heart cycle. Histological data of the heart muscle were obtained after animal termination. A 2D RF-based coarse-to-fine strain algorithm using re-correlation techniques was used to estimate frame-to-frame translations and deformations of the infero-lateral wall of the left ventricle in three orthogonal directions. A novel tracking method was developed to track each individual strain pixel within segmented regions of the wall for accumulation of displacements and strain. Measured displacements were used as an external force for mesh deformation. An internal regularization force was incorporated, based on the behavior of neighboring pixels. The forces were weighed using the difference between theoretical and measured cross-correlation values. The tracking method was tested using a thick wall tube phantom, which was heavily translated and dilated using a pressure colon. Next, the algorithm was applied on the animal data. After strain rate accumulation, mean strain curves in all three directions were generated.

Results

In the phantom, local strains were reconstructed correctly from frame-to-frame strain rate measurements despite large translations and vibrations. In the animals, tracked cardiac strain curves showed significantly less trend in strain values and higher peak strains compared to no or manual segmentation. The beagles developed a mean pressure gradient over the valve of respectively 20, 100, 120 and 200 mmHg. The corresponding mean maximum radial strains were 65, 45, 35 and 28% indicating a negative relation between pressure and strain. Histological findings confirmed a successful creation of a valvular aortic stenosis and revealed a positive relation between pressure gradient and the total amount of collagen.

Discussion and Conclusions

A realistic model of valvular aortic stenosis revealed a decrease in strain, correlating with increasing pressure gradient and collagen formation. The tracking algorithm enabled local strain rate accumulation.

1J-3

2:00 PM **Characterization of Wave Origins in Electromechanical Wave Imaging**

Jean Provost[1], Viatcheslav Gurev[2], Jianwen Luo[1], Natalia Trayanova[2], **Elisa Konofagou[1];** *[1]Columbia University, USA, [2]Johns Hopkins University, USA.*

Background, Motivation and Objective

Over the past four years, our group has shown that transient cardiac phenomena such as the contraction wave induced through electrical conduction at the beginning of systole [1] can be mapped and analyzed during propagation in murine, canine and human studies using ultra-high frame rates and high precision algorithms [2]. At the same time, recent achievements in 3D computational modeling techniques allowed the prediction of spatio-temporal electromechanics with high precision. The objective of this work is to utilize such established models to discriminate electrically induced transients (EIT) from mechanically induced transients (MIT) in Electromechanical Wave Imaging in vivo.

Statement of Contribution/Methods

The non-linear 3D finite element mesh that was employed incorporates ventricular passive mechanics, active tension, membrane kinetics, and the Purkinje network. Transient wave propagation during isovolumic contraction was reproduced, allowing thus the identification of their origins.

For in vivo validation, ultrasound RF frames of the murine left ventricle were acquired in long-axis views at the very high frame-rate (8 kHz) using a retrospective ECG-gating technique previously described [1]. A Vevo 770 system (VisualSonics Inc, Toronto, ON, Canada) was used with a single-element mechanical sector probe at 30 MHz. Axial displacement and strain were obtained through the use of 1D cross-correlation (window size: um, window overlap: 95%).

Results

Using the finite-element model, experimental axial velocities in the ventricular wall were reproduced and revealed timings of key cardiac events in vivo. The temporal profiles of the displacement in the septal and posterior walls of the murine heart showed excellent agreement between experiments and simulations. Through comparison of these variations, a clear identification of the following events in vivo was achieved: the onset of contraction following the electrical activation at the beginning of the systole, the atrial kick, and the pulmonary and aortic valves opening and closing . In addition, simulated electromechanical waves were shown traveling at velocities of similar amplitude to those imaged in vivo, i.e., 0.3-1 m/s.

Discussion and Conclusions

In simulations, MIT indicate the timing of the valves opening and closing, while the EIT can assess the electrical properties of the myocardium. In experiments, the same spatio-temporal events were identified in vivo and electromechanical waves were successfully separated from other mechanically- or hemodynamically-induced waves. Upon validation, these models can be adjusted to the human ventricular geometry and used to corroborate normal and abnormal conduction patterns. Examples from distinct pacing origins will also be shown.

Reference

[1] Pernot et al. Ultrasound in Medicine and Biology, 33(7): 1075-85, 2007.

[2] Konofagou et al., IEEE-EMBS Symp. Proc., 6648-6651, 2006.

1J-4

2:15 PM Fundamental Performance Assessment of 2-D Myocardial Elastography in a Phased Array Configuration

Jianwen Luo, Wei-Ning Lee, Elisa Konofagou; *Columbia University, Department of Biomedical Engineering, New York, NY, USA.*

Background, Motivation and Objective

Two-dimensional (2-D) myocardial elastography (ME) is a radio-frequency (RF)-based speckle tracking technique that can estimate and image the 2-D transmural motion and deformation components (Konofagou et al, UMB 2002: 475). Based on a 3-D finite-element (FE) normal canine left-ventricular model, a theoretical framework was previously developed by our group to evaluate the estimation quality of 2-D ME using a linear array (Lee et al, UFFC 2007, 2233). However, a phased array transducer is typically used in echocardiography. The fundamental performance of 2-D ME using a phased array remains to be assessed.

Statement of Contribution/Methods

Field II (Jensen and Svendsen, UFFC 1992: 262) was used to generate the RF signals of a normal and a left-circumflex ischemic FE model of the heart in a phased array configuration (3.5 MHz, 60% bandwidth) and under 3-D motion condition. The algorithm of 2-D ME was adapted for use with such a configuration. Axial and lateral displacements were estimated using 1-D cross-correlation and recorrelation methods in a 2-D search (2-mm window, 75% overlap), with the depth dependence of the lateral beam spacing being taken into account. The 2-D Lagrangian strain tensor was calculated in a polar coordinate system, consistent with the phased array. The least-square estimator with a fixed kernel length (4 mm) was used to calculate the displacement gradient in the axial direction. In the lateral direction, the kernel was fixed at 7.5 mm whereas the length in samples was adaptively selected to compensate the depth dependence of beam spacing. Radial, circumferential and principal strains were then calculated from axial and lateral strains (Zervantonakis et al, PMB 2007: 4063). The performance of 2-D ME was assessed using the mean absolute error (MAE). The effects of sonographic signal-to-noise ratio (SNRs), number of scatterers and attenuation were studied.

Results

All ME results were in excellent agreement with the FE solutions (i.e., MAE < 0.03 mm and 0.6% for incremental displacements and strains, MAE < 0.2 mm and 4% for end-systolic cumulative displacements and strains, respectively). Principal strains were estimated as angle- and centroid-independent measures in the phased array configuration and were found to closely approximate the radial and circumferential strains. The MAE's and correlation coefficients remained unaffected when the SNRs was higher than 30 dB, and rapidly deteriorated when the SNRs dropped below 20 dB. The number of scatterers (50,000 - 2,000,000) and attenuation (0 - 1 dB/MHz/cm) were found not to significantly affect the performance of 2-D ME.

Discussion and Conclusions

The proposed framework can be used to assess the quality, explore the theoretical limitation and investigate the effects of various parameters in 2-D ME under more realistic conditions. The algorithms optimized in the phased array simulation can be directly implemented in a clinical setting. In vivo validation of the performance in 2D will also be shown.

1J-5

2:30 PM **2D Speckle Tracking vs DTI-derived Elasticity Imaging on an Isolated Rabbit Heart**

Congxian Jia[1], Ragnar Olafsson[1], Kang Kim[2], Theodore J Kolias[3], Jonathan M Rubin[4], Hua Xie[5], Matthew O'Donnell[6]; *[1]University of Michigan, Biomedical Engineering, Ann Arbor, MI, USA, [2]University of Pittsburgh, Cardiovascular Institute, Pittsburgh, PA, USA, [3]University of Michigan, Internal Medicine, Ann Arbor, MI, USA, [4]University of Michigan, Radiology, Ann Arbor, MI, USA, [5]Philips Research North America, , Briarcliff Manor, NY, USA, [6]University of Washington, Bioengineering and Mechanical Engineering, Seattle, WA, USA.*

Background, Motivation and Objective

Ultrasound strain imaging has been proposed to quantitatively assess myocardial contractility. Cross-correlation based 2D speckle tracking (ST) and auto-correlation based Doppler tissue imaging (DTI) are competitive techniques for this application. Unlike ST, DTI is limited by angle dependency and suffers from low signal-to-noise ratio because a high pulse repetition frequency (PRF) is used to reduce decorrelation due to lateral or elevational motion. However, these methods have not been quantitatively compared on a well-controlled animal model. To address this, we tested both methods using a Langendorff preparation.

Statement of Contribution/Methods

An isolated rabbit heart was retroperfused through the aorta with oxygenated Krebs-Henseleit buffer and paced through the apex at 3Hz. Two coplanar linear probes (Sonix RP) were used to acquire radio frequency (RF) data (41 frames/cycle). The central beam of each probe was used to acquire RF data at a PRF appropriate for DTI (640Hz) with three kinds of transmit pulses P1, P4 and P12 (1, 4 and 12 cycles, respectively). The acquisition of RF data, left ventricular pressure and electrocardiograms were synchronized to the pacing signal. All data were acquired before and after left anterior descending artery (LAD) ligation. 2D ST estimated strain with a resolution of 1.2mm axially and 2.5mm laterally. M-mode color Doppler imaging estimated strain along the central beam (axial) with resolution about 0.2, 1.0 and 2.9mm.

Results

ST derived axial normal strain (ST in Fig. a) detected wall thinning during systole due to LAD ligation at point A in Evans Blue unstained area (Fig. d). DTI methods can also detect this abnormal motion but with accuracy dependency on transmit pulse length (P1, P4, P12 in Fig. a). 2D ST derived principal axes showed the directional change (Fig. b and c) due to LAD ligation, which matched the area unstained by Evans Blue (Fig. d).

Discussion and Conclusions

Unlike ST, DTI derived elasticity imaging detects abnormal motion only when the beam direction aligns well with the contraction direction. Its accuracy also depends on the transmit pulse length. Directional change of principal deformation axis derived using 2D ST method does not depend on the coordinate system and can detect the dysfunctional area.

This work was supported in part by HL-082640, HL-67647, HL-68658, EB-003451and CA-109440.

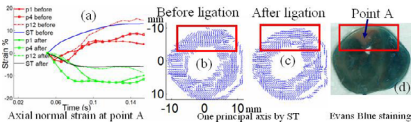

1J-6

2:45 PM **In Vivo Validation of Myocardial Elastography at Variable Levels of Ischemia**

Wei-Ning Lee, Jean Provost, Shougang Wang, Kana Fujikura, Jie Wang, Elisa E. Konofagou; *Columbia University, New York, NY, USA.*

Background, Motivation and Objective

Myocardial elastography (ME), depicting the full myocardial deformation field, has been assessed its good performance in a theoretical framework (Lee et al, TUFFC 2007: 2233), a phantom study (Gamarnik et al, IEEE IUS 2007: 741), and a clinical setting against MRI tagging in normal and pathological cases (Lee et al, IEEE IUS 2007: 749). In this paper, ME was validated on canine hearts in vivo against direct sonomicrometry measurements (SM), globally and transmurally, at variable levels of myocardial ischemia and infarction.

Statement of Contribution/Methods

Myocardial elastography, radio-frequency (RF)-based, comprised transmural: 1) 2D (lateral and axial) displacements using 1D cross-correlation in a 2D search and recorrelation (3.5 mm window size; 80% overlap); 2) 2D strain estimation using a least-squared strain estimator; 3) polar (radial and circumferential) strains based on coordinate transformation. An Ultrasonix RP system with a 3.3 MHz phased array (beam density of 128 lines) was used to acquire RF frames in a 2D short-axis view at the frame rate of 211 fps using an automatic composite technique (Wang et al, IEEE IUS 2007: 880).

A non-survival canine ischemic model (n=5) was performed by inducing an occlusion of the left anterior descending (LAD) coronary artery, from 0% to 100% at a 20% increment. Two separate sets of four piezoelectric crystals (3 in the sub-epicardium; 1 in the sub-endocardium) (Sonometrics Corp.) in a tetrahedral configuration were placed in the ischemic (i.e., anterior) and normal (i.e., posterior) regions. Polar strains were calculated from the coordinates of the crystals. A Millar catheter and an additional 4 crystals (at the apex, base, free wall and septum) were used to obtain real-time left ventricular Pressure-Volume curves to verify the onset and progression of ischemia throughout all experiments.

Results

At 0% occlusion, the total systolic radial thickening (SM: 18%; ME: 20%) and circumferential shortening (SM: -8%; ME: -11%) were found in excellent agreement between SM and ME in the anterior wall region, which becomes ischemic in the case of an LAD-occlusion. After 7 minutes of sustained 100% LAD-occlusion, opposite strains, i.e., radial thinning (SM: -8.5%; ME: -17%) and circumferential stretching (SM: 1%; ME: 5%), were observed. Although discrepancies were noted, mainly due to the distinct spatial resolutions in SM and ME, the ischemic region was verified with pathology. Augmented polar strains by 5% in the posterior wall compensated for the reduced systolic function in the anterior wall. Similar agreement was determined at the intermediate levels of ischemia.

Discussion and Conclusions

These findings demonstrate that ME, in good agreement with SM, could detect, localize and identify the level of ischemia. The correlation between strain estimates and distinct occlusion levels will be further quantified. Corroboration with an established finite-element canine left ventricular model will also be discussed.

2J. Beam Forming Algorithms and Strategies

Room 201 A/B/C

Wednseday, November 5, 2008, 1:30 pm - 3:00 pm

Chair: **Kai Thomenius;**
GE Global Research, USA.

2J-1

1:30 PM **Optimal Apodization for Ultrasound Imaging**

Mariko Yamamoto[1], Shin-ichiro Umemura[2]; *[1]Hitachi , Ltd., Central Research Laboratory, Kokubunji-City, Tokyo, Japan, [2]Hitachi, Ltd.,, Central Research Laboratory, Japan.*

Background, Motivation and Objective

An apodization design is a critical factor for high-quality imaging. In general, under a restriction of an aperture size and the maximum power of a transducer element, a trade-off exists between total acoustic power and strength of focusing. Until now, some typical apodizations such as rectangular-type apodization preferring total acoustic power or Gaussian and Hanning-type apodization preferring strength of focusing are known. But for optimal apodization, more flexibility and quantitative consideration of the trade-off is desired. In this study, we propose an optimal method with extended prolate spheroidal wave functions.

Statement of Contribution/Methods

Prolate spheroidal wave functions are eigen functions of finite Fourier transform and are well-used in an evaluation of a trade-off of signal localizations on time-frequency. We extend finite Fourier transform to consider ultrasonic features, e.g., 2 or 3-dimensional near field with pulse gain and coarse grained transducer element. With these transforms, we can get an optimal apodization which achieve the maximum possible strength of focusing and total power for a given aperture size and maximum power of a transducer element.

Results

Figure1 (a) shows the trade-off between total acoustic power and strength of focusing. Figure1 (b) shows corresponding apodizations. For arbitrarily-specified balance ratio, we can get an optimal apodization. Figure2 shows an example of extension to 2-dimensional space. As a dashed line on the graph, uniform and long focal zone is formed with resulting apodization and delay time. We also demonstrated both extension with pulse gain and coarse grained transducer element.

Discussion and Conclusions

As observed above, our method provides more flexiblity and quantitative consideration to an apodization design.

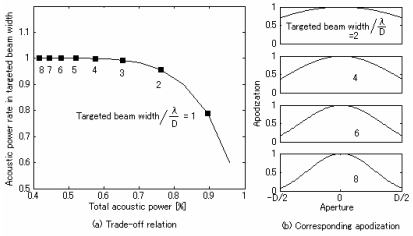

Fig.1 Trade-off between total acoustic power and strength of focusing.

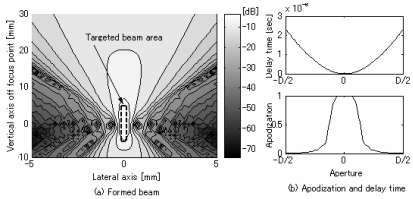

Fig.2 Example of 2D beam design

Wednesday Oral

2J-2

1:45 PM **Synthetic Aperture Sequential Beamforming**

Jacob Kortbek[1], Jørgen Arendt Jensen[2]; [1]*BK Medical, Denmark,* [2]*Technical University of Denmark, Denmark.*

Background, Motivation and Objective

In synthetic aperture (SA) imaging a transmitted spherical wave insonifies the region of interest and SA focusing is applied to construct an intermediate image. This process is repeated for multiple emissions where multiple intermediate images are focused and stored and finally added to yield a high-resolution image. With 200 image lines, the number of samples to beamform is 200 times larger compared to a conventional scanner. This SA imaging technique makes implementation very challenging. The objective is to design a SA imaging method with a complexity comparable to conventional imaging, but with performance comparable to prior art SA.

Statement of Contribution/Methods

Synthetic Aperture Sequential Beamforming (SASB) uses two sequential beamformers and is applied to array imaging. A focused transmission is generated from a sub-aperture and an intermediate image line is generated in a 1st stage beamformer (BF) with fixed receive focus in the transmit focus and stored in a line buffer. Multiple lines from a sliding sub-aperture are stored in the buffer. A line sample contains information from the arc of a circle with center in the focus point. An image point is thus represented in multiple lines. The line buffer is coupled to the input channels of a 2nd stage dynamic BF where multiple high resolution image lines are created. Each sample in the 2nd stage BF is focused by summing a weighted set of samples from lines in the buffer. This technique implements SA focusing yielding a range independent and improved lateral resolution, and improved signal to noise ratio. The additional system complexity relative to a conventional commercial system is restricted to a BF with a single delay profile and a line buffer memory.

Results

Field II has been used to simulate an acquisition with a 192-element, 7MHz linear array with a 64 element sliding sub-aperture. The fixed focus point is at 20 mm. SASB performance is compared to dynamic receive focusing (DRF) with transmit focus at 50 mm. Axial resolution for both SASB and DRF is 0.33 mm. SASB lateral resolution is range independent. At -6 dB it is between 0.5 mm and 0.7 mm at depths from 5 mm to 95 mm. For DRF it is between 0.2 mm and 2 mm. SASB lateral -40 dB resolution at 85 mm is 1.6 mm and 9.2 mm with DRF. Data has been acquired with a commercial scanner and processed off line. The improvement in lateral resolution is confirmed. The difference in system complexity between SASB and DRF is the presence of the single profile 1st stage BF for pre-processing. The 2nd stage BF is the same as applied in DRF but has 150 input channels instead of 64. An advantage is that the second beamformer does not need to have analog-to-digital converters.

Discussion and Conclusions

A novel synthetic aperture method has been investigated yielding a considerable improvement in lateral resolution with a factor of 4. Only a modest additional system complexity is required relative to a conventional commercial imaging system and the method is thus an obvious candidate for commercial implementation.

2J-3

2:00 PM **Focusing and steering ultrasound without creating detrimental grating lobes**

Armen Sarvazyan[1], Laurent Fillinger[1], Leonid R. Gavrilov[2]; [1]*Artann Laboratories, Trenton, NJ, USA,* [2]*N.N. Andreyev Acoustics Institute, Moscow, Russian Federation.*

Background, Motivation and Objective

Medical applications of ultrasound need methods and devices able to generate steerable focused fields, either to image or to treat given sites of the body. Phased arrays composed of hundreds of elements are conventionally used for that purpose but their ability to steer the focus is limited by the appearance of grating lobes unacceptable in certain applications. The hypothesis that the Time Reversal Acoustics (TRA) focusing system with drastically reduced number of elements will be able to produce and steer a complex focused ultrasonic field without creating detrimental grating lobes has been explored.

Statement of Contribution/Methods

The TRA system used in this study included a water-filled reverberator with a varying number (1-8) of piezotransducers attached to its outside walls. Experimental data obtained by the TRA system were compared with the simulation data for the phased array with 256 elements distributed regularly in a square pattern. The frequency of radiating elements in both the cases was 600 kHz and the aperture was equal to 6 cm.

Results

Experiments showed the ability to generate and steer four foci with 5 mm spacing at a distance of 5 cm from the radiating surface of the TRA focusing system using 8 or even a single radiating elements. With the steering of 4 foci, no grating lobes were observed at the shifts of foci up to, at least, 50 mm. Simulation of the 256 elements regular phased array showed that the intensities in the grating lobes became significant for steering more than 10 mm away from the axis of the array and exceeded the maximum intensities in the main set of foci at the distance over 20 mm (see Figure 1; Intensity field distributions for steering of 4 foci at a distance of 20 mm with the use of regular 256 element phased array and TRA 8 element system).

Discussion and Conclusions

The results demonstrate the superior ability of the TRA focusing system over the multi-element regular phased array to create complex focused patterns and to steer them without creating detrimental grating lobes. Moreover, the width of the focal spots is much narrower in the TRA focusing system despite drastically smaller number of radiating elements. These features of the TRA focusing systems could be important in numerous medical applications of focused ultrasound.

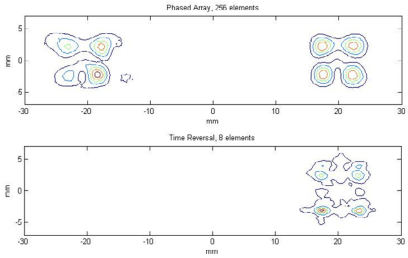

2J-4

2:15 PM **Rocking Convex Array used for 3D Synthetic Aperture Focusing**

Henrik Andresen[1], Svetoslav Nikolov Ivanov[1], Daniel Buckton[2], Jørgen Arendt Jensen[1]; [1]*Center for Fast Ultrasound Imaging, Elektro-DTU, Kgs. Lyngby, Denmark,* [2]*GE Medical Systems Kretztechnik, Zipf, Austria.*

Background, Motivation and Objective

Volumetric imaging can be performed using 1D arrays in combination with mechanical motion. Outside the elevation focus of the array, the resolution and contrast quickly degrade compared to the azimuth plane, because of the fixed transducer focus. The purpose of this paper is to use synthetic aperture focusing (SAF) for enhancing the elevation focusing for a convex rocking array, to obtain a more isotropic point spread function.

Statement of Contribution/Methods

This paper presents further development of the SAF method, which can be used with curved array combined with a rocking motion. The method uses a virtual source (VS) for defocused multi-element transmit, and another VS in the elevation focus point. This allows a direct time-of-flight (ToF) to be calculated for a given 3D point.

The method is evaluated using simulations from Field II and by measurements using the RASMUS experimental scanner with a 4.5 MHz convex array (GE Kretztechnik, Zipf, Austria). The array has an elevation focus at 40 mm of depth, and the angular rocking velocity is 55°/s. The scan sequence uses an $f_{\_prf}$ of 4900 Hz allowing 15 cm of penetration. For 80 emission per image, the motion in the elevation direction will be 2.82 λ per image at the transducer surface. The full width at half max (FWHM) and main-lobe to side-lobe ratio (MLSL) is used as quantitative measurements.

Results

The elevation FWHM for simulated scatterers placed at depths of 80, 100 and 120 mm was improved by up to a factor of 1.31, 1.84 and 2.33, and the MLSL ratio was improved by an average of 33.37 dB for the three scatterers using SAF. The lateral FWHM was 0.28% larger on average using SAF. The azimuth to elevation resolution ratio is 0.56 at 60 mm of depth and 0.72 at 120 mm of depth. For conventional imaging, the ratio between lateral and elevation resolution is 0.31 at 120 mm of depth.

Discussion and Conclusions

The method has shown the ability to improve the elevation focus and contrast below the physical elevation focus of a convex rocking array. The ability to create isotropic resolution increases with depth, as the effective aperture size increases. The best azimuth to elevation resolution ratio found is appr. 1:1.4. No loss in the lateral resolution or contrast is introduced because of the processing.

2J-5

2:30 PM **Effects of Data Density of Echo Fourier Domain on Quality of High Frame Rate Imaging**

Jian-yu Lu; *The University of Toledo, Bioengineering, Toledo, Ohio, USA.*

Background, Motivation and Objective

The high frame rate imaging method [1] that was developed based on the theory of limited-diffraction beams can be implemented with the fast Fourier transform (FFT) to reconstruct images of a quality that is equivalent to the continuous dynamic focusing in both transmission and reception of the conventional delay-and-sum method. The use of FFT reduces the amount of computations dramatically for the high frame rate imaging method as compared to that of the conventional beamformaing.

Statement of Contribution/Methods

In this paper, the effects of the number of data points of the echo Fourier domain on the quality of the high frame rate imaging are studied. In the study, the Fourier transform of echo data is performed across the aperture of an array transducer using FFT. To increase the accuracy of the interpolation that is necessary to reconstruct images with the high frame rate imaging method, zero padding is used to increase the number of data points in the echo Fourier domain.

Results

To find an optimum trade off between the data density and image quality, an experiment was performed. In the experiment, a home-made high frame rate imaging system [1] and a 2.5-MHz, 19.2 mm aperture, and 128-element broadband phased array transducer were used to obtain RF echo data. A commercial ATS539 tissue mimicking phantom was used as a test object. Images reconstructed have a +/-45 degree field of view and 120-mm depth. The images were obtained with 11 transmissions at an image frame rate of 486 frames/second. Images were reconstructed with 16-, 4-, 2-, and 1-fold increases in data densities, respectively. Results show that with 2 or more fold increase in the data density, the quality of images reconstructed with the bilinear interpolation is virtually the same as that obtained at higher data densities. It is also found that without data densifying (1-fold), images reconstructed have a lower resolution after about 9-cm in depth, in addition to having some random artifacts due to the inaccuracy in the interpolation process

Discussion and Conclusions

It is found in this study that a 2-fold densifying of data in the echo Fourier domain along the transducer aperture is satisfactory for image reconstructions using the high frame rate imaging method. This is significant since the increase of the number of points in the echo Fourier domain will not only increase the computation, but also the memory usage, which would increase the complexity of hardware used to implement the high frame rate imaging method. In the future 3D high frame rate imaging, having a smaller number of data points will be more significant since the Fourier transform will be over a 2D aperture and thus any data density increase will be squared.

[1] Jian-yu Lu, Jiqi Cheng, and Jing Wang, "High frame rate imaging system for limited diffraction array beam imaging with square-wave aperture weightings," IEEE Transactions on Ultrasonics, Ferroelectrics, and Frequency Control, vol. 53, no. 10, pp. 1796-1812, Oct. 2006.

2J-6

2:45 PM **The effect of cross-correlation method on the dual apodization with cross-correlation algorithm**

Chi Hyung Seo, Jesse T. Yen; *University of Southern California, USA.*

Background, Motivation and Objective

Sidelobes or clutter in ultrasound imaging are undesirable side effects since they degrade image quality by lowering contrast-to-noise ratio and the detectability of small targets. We previously presented a target-dependent clutter suppression method using pairs of apodization functions known as dual apodization with cross-correlation, or DAX. By using certain pairs of apodization functions, we can pass mainlobe signals and attenuate clutter signals using normalized cross-correlation coefficients of RF signals. A target-dependent weighting matrix is created that

will be multiplied to the standard beamformed image. In this work, we investigate the effect of different cross-correlation methods and cross-correlation segment size on contrast-to-noise ratio (CNR) using the DAX algorithm.

Statement of Contribution/Methods

For our experimental setup, individual element RF signals were collected for off-line processing from an ATS spherical lesion phantom containing a 3 mm anechoic cyst using an Ultrasonix Sonix RP ultrasound system having 40 MHz sampling frequency. In this experiment, a 128-element, 300 μm pitch, L14-5/38 linear array was used. A 1-cycle transmit pulse of 5 MHz and an f-number = 1.5 was used. In receive, element data was collected and receive beamforming was done off-line using Matlab. Dynamic receive focusing was used with focal updates every 0.1 mm. After creating beamformed RF data with two different apodization functions, the two sets of data are cross-correlated. We performed 1-D axial and 1-D lateral cross-correlation with segment sizes varying from 0.3 mm to 1.8 mm. We also performed 2-D cross-correlation with sizes varying from 0.3 mm × 0.3 mm to 1.8 mm × 1.8 mm. To further test the limits of the DAX algorithm, we have also performed a Field II simulation with the same system parameters as our experimental setup using a cylindrical 1.5 mm diameter anechoic cyst located at 30 mm depth embedded in a 3-D phantom of scatterers.

Results

When using 1-D axial cross-correlation, an axial segment size of 0.85 mm gave us the highest CNR of 125 % improvement. Using 1-D lateral cross-correlation showed a 91 % improvement in CNR with segment size of 1.05 mm. 2-D cross-correlation showed over a 150 % improvement with segment size of 0.6 mm axially by 0.45 mm laterally. A simulation using a cylindrical 1.5 mm diameter anechoic cyst located at 30 mm depth embedded in a 3-D phantom of scatterers gave us a CNR improvement of 40 % with 1-D axial cross-correlation.

Discussion and Conclusions

We have presented work which investigates the effect of cross-correlation method and cross-correlation segment size on DAX performance in terms of CNR using experimental data collected from a tissue mimicking phantom. These results show that axial 2-D cross-correlation gave the largest improvement in CNR compared to 1-D axial and 1-D lateral cross-correlation, but is more computationally intensive. Future work will involve evaluating DAX performance using in vivo data.

3J. Microbubbles: Theory and Characterization

Room 305 A/B/C

Wednseday, November 5, 2008, 1:30 pm - 3:00 pm

Chair: **Ayache Bouakaz;**
INSERM, Université Tours, France.

3J-1

1:30 PM **Oscillation of single microbubbles at room versus body temperature**

Hendrik Vos, **Marcia Emmer,** Nico De Jong; *Erasmus MC Rotterdam, Biomedical Engineering, Netherlands.*

Background, Motivation and Objective

The dynamic behavior of Ultrasound Contrast Agents (UCAs) is normally studied at room temperature (~21 oC). However, in a clinical setting the UCA bubble environment is the body temperature (~37 oC). Such temperature induces phase changes of the phospholipid materials that coat common types of UCA bubbles [1] and might result in significantly different oscillation behavior when compared to room temperature. Indeed, a population-based study showed strong temperature influence on the scattering of SonoVue (Bracco Int.) [2], but no study has yet addressed the influence on individual microbubbles.

Statement of Contribution/Methods

We studied the difference in oscillation of both Definity (Bristol-Myers Squibb) and SonoVue bubbles at room versus body temperature, using the ultrahigh speed Brandaris 128 camera, capturing the radial motion at ~13 million frames per second [3]. Bubbles were insonified with 1.7 MHz pulses and the acoustic pressure varied between 10 kPa – 80 kPa.

Results

Both agents showed highest radial excursion when having a diameter of 4 um, which was considered the resonant diameter for 1.7 MHz. With reference to Fig. 1, the radial excursion of resonant SonoVue was a factor of 2 higher at 37 oC compared to 21 oC, for acoustic pressure of 40 kPa (N=8 for both, $p<0.001$). Such difference in radial excursion was not observed for Definity (N=11 and 5, resp.). The radial excursion of the bubbles showed an onset level of acoustic pressure below which the excursion is insignificant and above which the excursion is linear with pressure [4]. SonoVue bubbles with diameters between 3.5 um and 4.5 um showed an average onset level of 24 kPa at 21 oC and 10 kPa at 37 oC (N=8 for both, $p<0.001$), while Definity showed 15 kPa and 7 kPa levels respectively (N=5 and 13, $p<0.02$).

Discussion and Conclusions

These results show significant influence of the temperature on the oscillation of phospholipid-coated microbubbles.

References

[1] M. A. Borden et al., Langmuir, vol. 22, pp. 4291 - 4297, 2006.
[2] C. Guiot et al., Ultrasonics, vol. 44, pp. e127 - e130, 2006.
[3] C. T. Chin et al., Rev Sci Instr, vol. 74, pp. 5026 - 5034, 2003.
[4] M. Emmer et al., Ultrasound Med Biol, vol. 33, pp. 941-949, 2007.

Fig. 1. Relative radial excursion of resonant SonoVue (N=8) and Definity (N=5 and 13) bubbles when insonified with 1.7 MHz pulses at 10 kPa – 80 kPa, at 21 oC and 37 oC temperature. Standard errors are shown by the vertical bars.

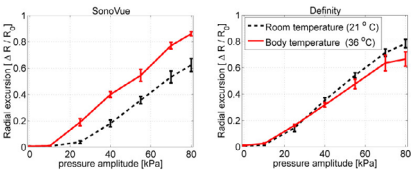

Wednesday Oral

3J-2

1:45 PM **Nonlinear Shell Dynamics near the Resonance Frequency of Ultrasound Contrast Agents**

Marlies Overvelde[1], Valeria Garbin[1], Benjamin Dollet[1], Nico de Jong[2], Detlef Lohse[1], Michel Versluis[1]; *[1]University of Twente, Physics of Fluids, Enschede, Netherlands, [2]Erasmus MC, Experimental Echocardiography, Thoraxcentre, Rotterdam, Netherlands.*

Background, Motivation and Objective

The key feature of ultrasound contrast agents (UCA) in distinguishing blood pool and tissue echoes is the so-called Contrast to Tissue Ratio (CTR). Current pulse-echo techniques rely on improved CTR through the nonlinear response of the microbubbles. A detailed understanding of the origin of nonlinear UCA dynamics is required to further improve these imaging techniques. The non-linear response of microbubbles is well described by the Rayleigh-Plesset equation. Here we investigate experimentally and numerically the contribution of a phospholipid shell to the nonlinear response of bubbles.

Statement of Contribution/Methods

Experimentally, resonance curves were recorded for BR14 microbubbles (Bracco, Geneva) in free space at a distance 200 µm away from a neighboring wall by a set of optical tweezers coupled to the Brandaris camera. The applied frequency was scanned from 1.5 to 3 MHz and the bubble dynamics was recorded at a framerate of 15 Mfps for increasing applied pressures from 10 to 50 kPa. Numerical simulations were performed by solving different Rayleigh Plesset type equations for uncoated and coated gas bubbles including the Marmottant model (JASA 2005), which accounts for buckling and rupture of the shell.

Results

It was found both in experiments and in simulations that by increasing the driving pressure the resonance curve becomes asymmetric resulting in a decrease of the frequency for which a maximum response is observed, by up to 50%, see Fig. 1A. Simulations of the maximum response frequency for a 3 µm radius bubble for increasing acoustic pressure for the various models are depicted in Fig. 1B. The maximum response frequency for both the uncoated and the purely elastically coated bubbles is only marginally changed for increasing pressure. The circles represent experimental data for a bubble of the same radius and it is seen that they follow the trend of the simulations with the Marmottant model.

Discussion and Conclusions

The experimental observed decrease in the maximum response frequency is well predicted by the Marmottant model. We conclude that at low acoustic pressures this nonlinear behavior of UCA microbubbles can be ascribed to the shell properties. These nonlinearity's can be exploited for existing pulsing schemes such as power modulation and they can be used to develop new schemes at low acoustic driving pressures.

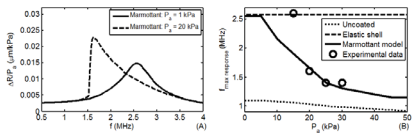

3J-3

2:00 PM **A 3D FEA Model for transient analysis of microbubble behavior**

Abhay Vijay Patil[1], Paul Reynolds[2], John A. Hossack[1]; *[1]University of Virginia, Biomedical Engineering, Charlottesville, Virginia, USA, [2]Weidlinger Associates, Inc., Mountain View, California, USA.*

Background, Motivation and Objective

Microbubbles provide the basis for perfusion measurement, early detection of molecular signatures of disease and as a vehicle for drug, or gene, delivery. Although, the response of a single microbubble to ultrasound has been characterized by radially symmetric 1D models and high speed camera-based experiments, a plethora of mechanisms, such as bubble-bubble interaction, bubble-cell interaction, and adherent bubble response are poorly understood. With few exceptions, 1D model are valid at low acoustic pressure, but are incapable of predicting phenomena such as mode oscillations or onset of bubble shell rupture. Also, 2nd order mode oscillations are a precursor to bubble shell rupture and subsequent cavitation [1]. In addition, parameters, such as shell stress and shell strain may be potential indicators of bubble shell fracture. In this work, we propose a full 3D FEA model that

Wednesday Oral

can track time variations in asymmetric 3D radial and translational bubble motion, and shell parameters such as regional variation in shell stress and strain.

Statement of Contribution/Methods

3D FEA Simulations were conducted using PZ-FLEX (Mountain View, CA). A model cell of water (20 x 20 x 20 microns) was generated that encompassed a bubble of desired size (Ro =1micron, lipid shell =1 nm, stiffness 0 and 0.5 N/m, and C4F10 core). 1.6 million elements were used to mesh the model and a time step of 4 nanoseconds was selected to provide a convergent solution. A single cycle Gaussian modulated pressure sine wave (f = 2.4 MHz P= 360 KPa) stimulated the bubble.

Results

Figure illustrates the R-T curves from this simulations (stiffness =0 N/m) superimposed over the results published in [2]. The excursions in 3D were coincident suggesting a symmetric motion. An average peak shell strain of +-50 % was observed during the rarefaction and compression of the bubble, respectively. For the bubble with stiffness of 0.5 N/m, the peak expansion and rarefaction reduced to 1.4, and -0.8 times the resting radius, respectively. The average peak expansion and contraction strains were +40 and -20 %, respectively. An asymmetric model was able to reproduce the principle waveform features in a corresponding previously observed 4 cycle result in [3].

Discussion and Conclusions

[1] Postema et al., Ultrasonics Socnochemistry, 24:438-44, 2007

[2] Morgan et al., IEEE UFFC 47(6):1496-1509, 2000

[3] Chomas et al., IEEE UFFC 49 (7): 883-92, 2002

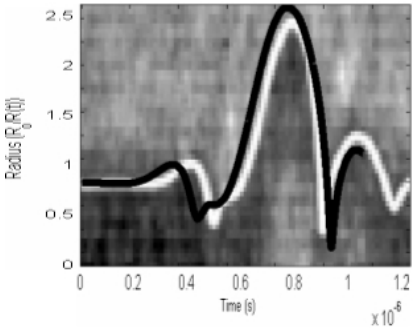

3J-4

2:30 PM **Spectral and Temporal Signal Modifications Occuring Between Stable and Transient Inertial Cavitation**

Mathieu Santin[1], Alexander Haak[2], Lori Bridal[1], William D. O'Brien[2]; [1]*Laboratoire d'Imagerie Paramétrique, UMR CNRS 7623, Paris, France,* [2]*University of Illinois at Urbana Champaign, Bioacoustics Research Laboratory, Urbana , IL, USA.*

Background, Motivation and Objective

Inertial Cavitation (IC) can be either stable (repeated during bubble oscillation) or transient (leading to bubble destruction). Certain cavitation-related bioeffects may be produced in stable IC, for example therapeutic heating. Other effects, however, such as acoustic delivery using a drug-laden microbubble require break-up of the bubble or transient IC. Our goal is to explore signal modifications occuring when bubble response changes from stable to transient IC.

Statement of Contribution/Methods

We have previously shown that post-excitation signals detected with a passive cavitation detector (PCD) are a marker of the microbubble rupture (transient IC). Dilute solutions of *Optison* and *Definity* were studied using a PCD with a 2.8-MHz transmitter and 13.0-MHz receiver. The dilution was such that each received signal should, on average, arise from a single microbubble.

Several hundred microbubble responses were acquired at each of three rarefactional pressures (1.6 ± 0.2, 2.0 ± 0.2 and 2.4 ± 0.2 MPa).

Each microbubble response was grouped with signals presenting post-excitation emissions (transient IC) or those with no evidence of post-excitation emission (stable IC).

For each incident pressure, we compared discrimination of the two groups using average signal to noise ratio (SNR) of peak-to-peak voltage and power of broadband noise (12-17.6 MHz), fundamental, 2nd, 3rd, and 4th harmonics.

We also modeled the acoustic response and shell rupture with the model of Marmottant et al.

Results

Throughout the studied pressure range, best separation between transient and stable IC groups was obtained with peak-voltage (4.7 ± 1.8 dB) and broadband noise (4.3 ± 1.9 dB) for *Optison*. For *Definity*, peak-to-peak voltage (5.3 ± 1.2 dB) and broadband noise (5.8 ± 2 dB) also provide separation between the two groups. Harmonics (2nd to 4th increased more strongly between the transient and stable IC groups (on the order of 6 dB) for *Definity* than for *Optison*. Response at the fundamental frequency is overlapped for the transient and stable IC groups. Model responses for *Definity* showed post-excitation signals when parameters allowed shell rupture, like $R_{break}=2R_0$.

Discussion and Conclusions

The level of the broadband noise with respect to the background was elevated both for transient and stable IC groups of *Optison* (SNR 20 to 30 dB) and *Definity* (SNR 14 to 35 dB).

The transition from stable to transient IC activity appears to lead to an additional increase of approximately 5 dB in peak-to-peak voltage and 4 to 6 dB for broadband noise.

Extrapolating results to estimate the attenuated response from a population of microbubbles with X-% stable and X-% transient events could help explore detection of bubble destruction in *vivo*.

3J-5

2:30 PM **Statistical Corrections for the Precise Estimation of Cyanoacrylate Microbubble Concentration in Targeted Imaging**

Monica Siepmann[1], Moritz Palmowski[2], Fabian Kiessling[2], Georg Schmitz[1]; [1]*Ruhr-Universitaet Bochum, Bochum, Germany,* [2]*German Cancer Research Center, Department of Medical Physics in Radiology, Heidelberg, Germany.*

Background, Motivation and Objective

Cyanoacrylate microbubbles (CMB) have shown promising results for ultrasound molecular imaging in small animal experiments. They can be linked to binding sequences specific for endothelial targets. The precise quantification of their concentration allows monitoring the expression of the targeted molecules. However, for high concentrations quantification approaches fail to precisely estimate the concentration of aggregated microbubbles (MB). Thus, we theoretically derived and experimentally validated a new method for determining even high MB concentrations using a statistical model of MB destruction distribution.

Statement of Contribution/Methods

CMB destruction produces distinct signals in Doppler ultrasound by loss of correlation. For high MB concentrations this is observed as a color flash not allowing for MB quantification. Thus Sensitive Particle Acoustic Quantification (SPAQ) was proposed by Reinhardt et al. [1]: By destroying all MBs in an image and then moving the transducer in sub-millimeter increments in elevation direction the destruction volume is reduced. Individual destruction events become visible and are quantified by measuring color pixel density. To calculate MB concentration from color pixel density, in [1] only an approximation was derived. We now developed a statistical model of SPAQ allowing the precise count of MBs even if the individual destruction events are not distinguishable. For this, only the average area of a single destruction event has to be known. The resulting correction was applied to SPAQ images of 5 gelatine phantoms with concentrations of experimental CMBs (DKFZ Heidelberg) ranging from 3*10^6 - 3*10^7 CMBs / ml. A Vevo 770 system (Visualsonics) with a 40 MHz scanhead (RMV 704) using the 3D Power Doppler mode was employed to obtain the images. At least 100 frames from different regions of each phantom were analyzed to obtain the acoustic counts. The average color pixel area of one MB destruction in the Doppler images was measured by imaging a phantom with a concentration low enough to display one event in every 5th image. The exact concentrations were determined optically by analysis of 25 100um z-sequence microscopy images of gelatine slices taken from each phantom.

[1] Reinhardt et al., Invest Rad 40:2-7

Results

The corrected acoustic quantification shows the expected linear dependence on the phantom concentration. Not all MBs are destroyed within a single SPAQ acquisition reducing the acoustic count to 37% of the optical counts. The filling factor of colored pixels in the ROI ranged from 30% to 98% for the highest concentration.

Discussion and Conclusions

We demonstrated that precise counts can be achieved even for filling factors up to 98%. Concentrations of up to 3*10^7 MBs / ml were quantified correctly. Without our correction concentrations would be underestimated by 75%, with the approximate correction of [1] by 50%. Thus, the correction will improve quantification in small animal molecular imaging considerably.

3J-6

2:45 PM **Nano-interrogation of a lipid shelled microbubble**

Vassilis Sboros[1], Emmanuil Glynos[2], Nikos Pelekasis[3], Vasileios Koutsos[2]; *[1]University of Edinburgh, Medical Physics, United Kingdom, [2]University of Edinburgh, Institute of Materials and Processes, School of Engineering and Electronics, United Kingdom, [3]University of Thessaly, Mechanical Engineering, Greece.*

Background, Motivation and Objective

Most microbubble (MB) theoretical models that assume fixed viscoelastic properties for shells have not been proven to successfully describe MB behaviour. Moreover, the acoustic pressure range that a model applies is not clarified. Experimental data are not available in this area and therefore research often resource to fitting shell parameters to acoustic or optical data.

Data on shell properties first were collected using the Atomic Force Microscope (AFM) for static experiments and relatively hard shelled MBs (BiSphere®). The force resolution of sub-nanonewtons is adequate to study the mechanical properties of soft lipids.

Statement of Contribution/Methods

MBs of the experimental agent BR14 (Bracco Research SA, Geneva, Switzerland) were chemically attached to Petri dishes using Poly-L-lysine as required for AFM experiments. The MFP-1D AFM (Asylum Research, Santa Barbara, CA, USA) was used with tipless cantilevers (CSC-20, MikroMash, Spain) with very low spring constants ranging from 0.01-0.07 N/m to achieve the stiffness measurement of soft shells. In addition, the 'fishing mode' was employed in order to avoid possible MB destruction upon contact. This ensured minimal initial contact in order to locate the MB accurately and avoid large forces.

Results

Optimal and reproducible stiffness measurements of 22 MBs with sizes between 1-10 μm were obtained. Initial work showed that forces above 10nN caused MB damage. It was possible to accurately control the maximum force applied to the MBs to lower than 5nN. The stiffness (effective spring constant) of the MBs averaged at 0.06 N/m, which is 50 times lower than the hard shelled BiSphere®. No dependence on size was observed. Using linear elasticity theory, and assuming a fixed shell thickness and no contribution from the gas, the Young's modulus of the lipid layer that constitutes the shell ranged between 0.5 and 4.0 GPa. Also, more than half of the bubbles provided reversible instabilities that were as low as 1 nN.

Discussion and Conclusions

It has been proposed that lipid MBs, when exposed to an ultrasound field, follow a strain-softening behaviour. The measurements here may be used as the boundary condition in the static regime for such a theoretical model. Moreover, the instability force measurement may be due to shell disruption and can be compared with forces applied during an ultrasound exposure providing information on the expected range of acoustic pressure that theoretical models are valid.

4J. Multilayer SAW Propagation

Hall 2A

Wednseday, November 5, 2008, 1:30 pm - 3:00 pm

Chair: **Mauricio Pereira da Cunha;**
University of Maine, ME, USA.

4J-1

1:30 PM **Piezoelectric Boundary Acoustic Waves: Their Underlying Physics and Applications**

Ken-ya Hashimoto[1], Yiliu Wang[1], Tatsuya Omori[1], Masatsune Yamaguchi[1], Michio Kadota[2], Hajime Kando[2], Teruhisa Shibahara[2]; *[1]Chiba University, Dept. EEE, Chiba, Chiba, Japan, [2]Murata MFG, Co. Ltd., Yasu, Shiga, Japan.*

Background, Motivation and Objective

For SAW devices, bulky and expensive packaging has been one of the vital problems for their further miniaturization and price cuts. Piezoelectric boundary acoustic waves (PBAWs) have long been expected to be one of the possible solutions to break down this problem. Very recently, Kando, et al. proposed the SiO2 overlay/heavy grating electrode/rotated Y-cut LiNbO3 (rot. YX-LN) substrate structure for developing PBAW devices. The remarkable advantage of this device is that the cavity over the chip surface can completely be got rid of. This makes the packaging most simple and enables the packaged device size to be minimized, whilst the device fabrication process is almost identical with that for traditional SAW devices.

Statement of Contribution/Methods

This paper reviews physical properties of PBAWs and their application to miniature and high performance RF filters/duplexers.

Results

First, basic properties of PBAWs are discussed. It is shown that PBAWs are supported in various structures provided that highly piezoelectric material(s) are employed as structural member(s). For example, the Si/SiO2/IDT/rot. YX-LN structure supports PBAWs with a large electromechanical coupling factor and moderate temperature coefficient of velocity. In the structure, the PBAW energy is confined around the relatively thick SiO2 layer, where the wave velocity is relatively small.

On the other hand, PBAWs are trapped near the electrode region in the SiO2/heavy grating electrode/rot. YX-LN structure. This means that PBAW properties in the structure are independent of the SiO2 layer thickness. This is a significant advantage for mass production. One may mind the fact with the structure, however, that the PBAW velocity should be smaller than the shear-wave velocity in SiO2, otherwise the PBAW becomes leaky.

Rot. YX-LN possesses piezoelectric coupling with Rayleigh-type waves as well as SH-type waves. Responses associated with the former have to be suppressed completely for filter applications. It is discussed how these two waves are dependent on the substrate rotation angle, electrode thickness, and metallization ratio.

The PBAW devices employing SiO2/Au electrodes/0-15°YX-LN are now being mass-produced. Because of the removed cavity from the chip surface, the packaged device size can be reduced dramatically. For example, a DMS filter based on PBAWs is developed for GSM900 Rx in a size of 0.8x0.6x0.25 mm3. The minimum insertion loss achieved in the passband (925-960 MHz) is 2.7dB (max), which is comparable to that of conventional SAW filters in a relatively large device size. The SiO2 layer is effective in achieving the improved temperature coefficient of frequency of -30 to -40 ppm/°C.

Discussion and Conclusions

The PBAW devices for various standards such as GSM1800 and GSM1900 have already been developed and are being mass-produced.

4J-2

2:00 PM **A Full-Wave Analysis of Surface Acoustic Waves Propagating on a SiO^2 Overlay/Metal Grating/Rotated YX-$LiNbO^3$ Substrate Structure**

Yiliu Wang, Ken-ya Hashimoto, Tatsuya Omori, Masatsune Yamaguchi; *Chiba University, Graduate School of Engineering, Chiba, Chiba, Japan.*

Background, Motivation and Objective

The authors have recently reported a full wave analysis of piezoelectric boundary acoustic waves (PBAWs) propagating in a SiO2 overlay/Cu grating/rotated YX-LN substrate structure [1]. In the analysis, the finite element method is used for the grating region, while the spectral domain analysis is applied to an isotropic overlay region as well as a piezoelectric substrate region. The paper discusses in detail how the excitation and propagation characteristics of the shear-horizontal (SH) and Rayleigh-type PBAWs are dependent upon the Cu grating thickness, substrate rotation angle and metallization ratio.

The structure consisting of a SiO2 overlay of finite thickness is also directly applicable to the development of high performance SAW filters [2]-[3]. To the best of authors' knowledge, however, it seems that detailed discussions have not yet been made on the propagation characteristics of the SH- and Rayleigh-type SAWs.

Statement of Contribution/Methods

This paper describes a full wave analysis of the SH- and Rayleigh-type SAW propagation in a finite SiO2 overlay/metal grating/rotated YX-LN substrate structure shown in Fig. 1.

Results

It is shown that the structure supports four types of propagation modes. Two modes concentrate their energy near the metal grating, and become the PBAWs when h2 gets infinite. Their electromechanical coupling is relatively strong even when h2 is large.

One of the other two modes concentrates its energy near the top surface of the SiO2 layer. With an increase in h2, its propagation characteristics approach to those for the non-piezoelectric Rayleigh-type SAW on a semi-infinite SiO2 layer, rapidly losing its piezoelectric coupling.

The remaining mode is the basis of a series of guided modes bounded in the SiO2 layer, in which the SiO2 layer behaves as a waveguide because of its low acoustic wave velocities.

Discussion and Conclusions

Detailed discussions are made on the dependence of the propagation characteristics of these four modes on the design parameters such as the layer and grating thickness. It is also discussed how the propagation characteristics are affected by the SiO2 flatness denoted by h3 in Fig. 1.

References

[1] Y.L.Wang, et al, Proc. IEEE Freq. Contr. Symp. (2008) [to be published]

[2] M.Kadota and T.Kimura, Proc. IEEE Ultrason. Symp. (2006) pp. 2305-2309.

[3] H.Nakamura, et al, Jpn. J. Appl. Phys., 47, 5B (2008) [to be published]. (330)

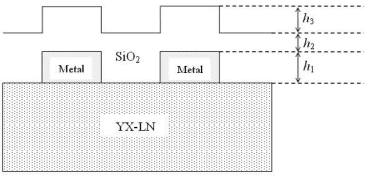

Fig. 1 Controlled shape SiO_2 overlay/metal grating/rotated YX-$LiNbO_3$ structure

Wednesday Oral

4J-3

2:15 PM **Temperature Compensation of Longitudinal Leaky SAW waves with Silicon Dioxide Overlay**

Mihir Patel[1], **Kushal Bhattacharjee[1],** Jason Reed[1], Sergei Zhgoon[2]; [1]*RF Micro Devices, Greensboro, North Carolina, USA,* [2]*Moscow Power Engineering Institute, Moscow, Russian Federation.*

Background, Motivation and Objective

Longitudinal Leaky Surface Acoustic Wave (LLSAW) is attracting considerable attention for its high velocity and reasonable coupling coefficient [1]. The intrinsic temperature coefficient of frequency (TCF) for these waves for different longitudinal cuts with metal gratings is in the range of -110 to -90 ppm/C. However, for filter applications the TCF of the LLSAW waves must be quite low in the range of -10 ppm/C. The introduction of a positive TCF overlay material (generally SiO2) alters the LLSAW wave characteristics. The modified LLSAW mode retains the same high velocity characteristics with an estimated improved TCF.

Statement of Contribution/Methods

A systematic study has been attempted by us to evaluate the effect of SiO2 on some interesting longitudinal cuts, such as, Y-Z' and 128 Y-Z' Lithium Niobate. Measurement data for the frequency-Temperature (f-T) behavior of different longitudinal cuts with metal gratings is first obtained. Based on these measurement data a three dimensional periodic Finite Element (FE) model using the Lagrangian Temperature Coefficients [2] is developed. The temperature coefficients of both the substrate and the metal gratings are incorporated in the FE model.

Results

A very good agreement between the FE model and measurement data for different longitudinal cuts is obtained. Based on these validations the effect of SiO2 on the f-T behavior of the modified LLSAW for different longitudinal cut angles is predicted using the FE model.

Discussion and Conclusions

The predicted results are then compared with the measurement data which shows a very good improvement in the f-T behavior of the modified LLSAW mode.

[1] T.Makkonen, Victor P. Plessky, Valeri I. Grigorievski, Laurent Kopp, Marc Solal, William Steichen and Martti M. Salomaa, "FEM/BEM Simulation and Experimental Study of LLSAW Resonator Characteristics on YZ-LiNbO3", Proceedings of the 2002 IEEE Ultrasonics Symposium, 2002, Pg. 317-320.

[2] Y-K.Yong and S. Kanna, "IDT Geometry and Crystal Cut Effects on the Frequency-Temperature Curves of A SAW Periodic Structure of Quartz", Proceedings of the 1998 IEEE Ultrasonics Symposium, 1998, pp. 223-228.

4J-4

2:30 PM **Study on SAW Characteristics of Amorphous-TeO2/36º Y-X LiTaO3 Substrates**

Xun Gong, Xiaoli Shang, De Zhang; *Key Laboratory of Modern Acoustics (Nanjing University), Ministry of Education, China.*

Background, Motivation and Objective

A layered structure is the basic approach on compensating for delay time changes of surface acoustic waves. Through experiments and calculations, improved temperature stability, sometimes even zero temperature coefficient of delay (TCD) have been observed in some layered structures such as SiO2/ZnO/diamond/Si, SiO2/LiNbO3, SiO2/LiTaO3, AlN/Si, AlN/Al2O3 etc. Both SiO2 and AlN are materials with negative TCD. However, the low deposition rate of SiO2 limits its application on low frequency devices where thick film is needed. On the other hand, highly C-axis oriented AlN film is not readily grown and zero TCD has not been reported yet.

Statement of Contribution/Methods

The amorphous TeO2/36ºrotated Y-X LiTaO3 structure was investigated in this study. 36º rotated Y-X LiTaO3 substrate is a transverse surface acoustic wave material. The wave mode used is called leaky surface acoustic wave. When a thin amorphous TeO2 film is deposited on the36º rotated Y-X LiTaO3 structure, the wave modes are changed. Sometimes, they are called interface waves. Generally, there are two kinds of interface waves, Love modes (transverse waves) and Rayleigh-like modes. The phase velocities of the interface modes change with the film thickness. For the amorphous TeO2/36º rotated Y-X LiTaO3 structure, the 1st love mode which is called Sezawa mode is used.

Results

This research investigated the temperature coefficient of delay (TCD) of the surface acoustic wave (SAW) on the amorphous TeO2 /36° Y-X LiTaO3 layered substrates has been investigated. Other characteristics important for SAW applications such as wave modes, and electromechanical coupling coefficient (K2) were also calculated. It is found that they simultaneously have a very high K2 around 8%, a pure transverse surface wave mode, and a zero TCD. The TCD can reach zero when the thickness of amorphous TeO2 film is much less than that of conventional SiO2 film, which means SAW devices on such substrates can be fabricated easily.

Discussion and Conclusions

The stuctures are very appealing for a wide range of SAW applications.

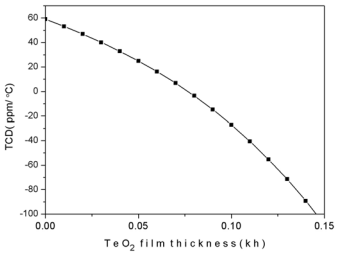

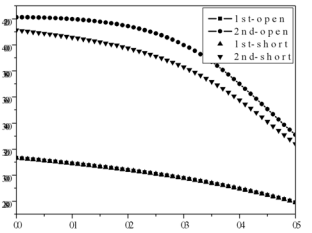

4J-5

2:45 PM **Optimal cut of lithium niobate with suppressed Rayleigh-type mode for application in resonator SAW filter**

Natalya Naumenko[1], Ben Abbott[2]; *[1]Moscow Steel and Alloys Institute, Moscow, Russian Federation, [2]TriQuint Semiconductors, Apopka, FL, USA.*

Background, Motivation and Objective

For applications in future communication systems, there is a strong demand for low-loss SAW filters with increased passband width. This requires using substrate materials with high electromechanical coupling, and rotated cuts of lithium niobate (LN) are the best choice for that purpose. In orientations with maximum piezoelectric coupling, the propagation loss can be suppressed, due to transformation of leaky waves into non-leaky SAW, if electrodes of resonator structure are sufficiently heavy. Another difficulty is to suppress parasitic Rayleigh-type mode, which can be a reason of degradation of filter performance. Shimizu [1] found experimentally that the Rayleigh-type mode can be minimized in 15°YX cut of LN, with gold electrodes of optimal thickness. Isobe [2] and Hashimoto [3] found optimal thickness of electrodes if Al or Cu is used as electrode material. However, experiments show that even with optimized metal thickness, the spurious mode deteriorates filter performance.

Statement of Contribution/Methods

To suppress this mode, we performed simultaneous optimization of orientation and electrode thickness, in rotated Y-cuts of LN. The resonant and anti-resonant frequencies, which refer to SH-type and parasitic Rayleigh-type modes, were extracted from calculated harmonic admittance, and the coupling of two modes was estimated, as function of cut angle and electrode thickness.

Results

In 15°YX cut of LN, the parasitic mode was found to show minimum coupling coefficient when electrode thickness is about 12 % of SAW wavelength for Al grating and about 9.5 % of wavelength for Cu grating. The parasitic mode occurs between resonant and anti-resonant frequencies of the main mode, and its coupling grows dramatically with small variation of electrode thickness around the optimal value, because of increasing interaction between two surface modes. Therefore, it is difficult to improve the resonator performance by optimization of electrode thickness if resonator utilizes 15°YX cut of LN. With increasing rotation angle of LN cut, the spurious resonance shifts to the middle of the interval between resonance and anti-resonance of SH-type mode, and its coupling nearly vanishes when the rotation angle of YX-cut is about 19° or 20°, dependent on material of electrodes. This result was confirmed experimentally.

Discussion and Conclusions

We report on the measured propagation velocities of two modes propagating in the optimal cut of LN, as functions of Al electrode thickness. The results of experiments are consistent with theoretical dependences, though the measured coupling of SH-type mode was lower than expected.

[1] H.Shimizu et al, Proc. 1990 IEEE Ultrason.Symp., pp.103-108.

[2] A.Isobe. et al, Proc. 1998 IEEE Ultrason.Symp., pp.111-114.

[3] K.Hashimoto et al, Proc. 2004 IEEE Ultrason.Symp., pp.1330-1334.

5J. Liquid and Gas Sensing

Hall 2B

Wednseday, November 5, 2008, 1:30 pm - 3:00 pm

Chair: **Mario Kupnik;**
Stanford University, USA.

5J-1

1:30 PM **Inductively coupled sensing using a quartz crystal microbalance**

David Greve, Wei Wu, Irving Oppenheim; *National Energy Technology Laboratory and Carnegie Mellon University, Electrical and Computer Engineering, Pittsburgh, PA, USA.*

Background, Motivation and Objective

Gas sensors often must operate in a hostile environment where direct connections to the sensor are difficult or impossible. Previous researchers have reported inductive coupling to a carbon nanotube resistive sensor [K. Ong et al., Sensors 2, 82-88 (2002)]. Here we explore inductive coupling for contact-less measurements using a gas-sensing quartz crystal.

Statement of Contribution/Methods

A 10 MHz quartz crystal with chromium/ gold contacts was coated with a gas-sensitive film of poly(ethyl methacrylate) approximately 0.6 micrometers in thickness. The terminals of the crystal were attached to a 10 turn coil 3 cm in diameter, which was placed near to an identical sensing coil. The crystal was exposed to a gas flow consisting of 0.4 to 1.5 % methanol vapor in a nitrogen carrier. Admittance measurements were performed using an HP 4192A impedance analyzer as the gas composition was varied in a step-wise fashion.

Results

In inductively coupled measurements, the measured admittance varies both as a consequence of the mass- induced shift in resonant frequency of the crystal and also variation in the stray and leakage mutual inductances. Analysis of the coupled equivalent circuit shows that the crystal series resonance is clearly observed at the terminals of the probe coil. We compared measurements of gas-induced changes to: admittance at a fixed frequency corresponding to the series resonance; phase at the same fixed frequency; and frequency corresponding to a constant phase. Gas composition changes were clearly resolved in these measurements. We will report on the effect of varying coil coupling and on the preferred measurement method. Finally, we will discuss the effect of separation between the two coils and practical limits on this separation.

Discussion and Conclusions

Inductive coupling is an attractive approach for accessing measurement data from a transducer located in a hostile environment. This paper extends this approach to the quartz crystal microbalance transducer.

This work was performed in support of ongoing research on carbon storage at the National Energy Technology Laboratory under RDS contract DE-AC26-04NT41817.

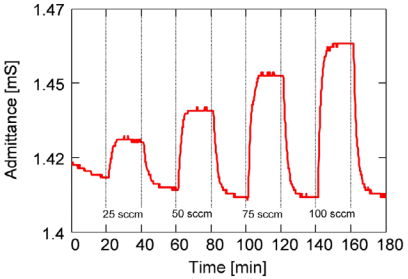

Wednesday Oral

5J-2

1:45 PM **Frequency response of a micromachined doubly-clamped vibrating beam for the measurement of liquid properties**

Christian Riesch[1], Erwin K. Reichel[2], Franz Keplinger[1], Bernhard Jakoby[2]; *[1]Vienna University of Technology, Institute of Sensor and Actuator Systems, Vienna, Austria, [2]Johannes Kepler University, Institute for Microelectronics and Microsensors, Linz, Austria.*

Background, Motivation and Objective

We have recently presented a micromachined doubly clamped vibrating beam (Riesch et al., IEEE Sensors Conf. 2007, Atlanta, Georgia, USA). The beam vibrations are excited by Lorentz forces. An optical readout allows determining the phase shift φ between the excitation current and the actual beam deflection. The interaction between the vibrating beam and the surrounding liquid leads to an additional mass loading m_a and damping γ of the beam, and allows for measurement of the liquid's viscosity η and mass density ρ. In a first attempt, a simple harmonic oscillator (SHO) model was fit to the frequency response φ(ω). However, the SHO model does not account for the frequency dependence of m_a and γ.

Statement of Contribution/Methods

We have adapted models (Sader et al., J. Appl. Phys, vol. 84, pp. 64-76, 1998; Weiss et al., Sens. Actuators A, vol. 143, pp. 293-301, 2008) for the doubly clamped beam, resulting in the phase response of the beam, $\varphi=\pi/2+\arctan(k-\omega^2 (m_e+m_a)/(\omega \gamma))$. k and m_e are the spring constant and the mass of the beam. m_a and γ describe the interaction with the liquid and are functions of frequency, beam geometries, and η and ρ.

Results

Using a variety of sample liquids we have carried out measurements. Exemplary results are shown as dots in the figure, solid lines depict the curve fit of the respective models. They indicate that the SHO model is incapable of describing the beam's frequency response properly. Consequently, the values of η and ρ determined by the beam sensor deviate from those obtained by conventional viscometers. The improved model however, accounting for the frequency dependence of mass loading and damping, represents the beam behavior well.

Discussion and Conclusions

The results demonstrate that the devised models are appropriate to describe the behavior of the immersed beam, and give a more accurate representation of its frequency response. Since the frequency dependences of m_a and γ gain influence as the damping increases, their consideration is crucial for the measurement of highly viscous liquids. Thus the described methods significantly expand the measurement range.

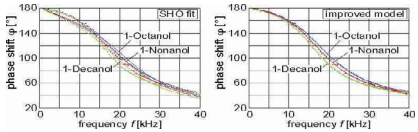

5J-3

2:00 PM **Ultrasonic sensor of liquid media utilising low grade transducers**

Alexander Kalashnikov, **Said Alzebda,** Ahmad Afaneh, Wei Chen, Richard Challis; *Nottingham University, United Kingdom.*

Background, Motivation and Objective

High frequency transducers for ultrasonic NDE sensors are designed to ensure a bandwidth of up to 50%. This has a large impact on their cost, however, much less expensive transducers with a bandwidth of a few percent are rarely considered for the monitoring of liquid media because of their long impulse response.

The objective of this development was to utilize narrowband ultrasonic transducers for ultrasonic sensors that are capable of monitoring the chemical changes that affect ultrasound velocity (e.g., [1,2]).

Statement of Contribution/Methods

The low bandwidth of the transducers considered ruled out their use in impulse mode. Instead, the oscillating mode of operation was adopted. In this mode, the ultrasonic transmitter faces the ultrasonic receiver; an amplifier closes

the signal loop and compensates for signal losses. The frequency of the obtained oscillator depends on the ultrasound velocity between the transducers; this frequency is considered as the sensor's output.

Results

The basic architecture of an oscillating ultrasonic sensor, as described above, was complemented by several additional features in the reported development. The design of the oscillating sensor allowed for the microprocessor control of the closed loop gain, phase shift and central frequency. These parameters were made controllable in order to facilitate experimentation with the sensor. This control enabled the selection of a particular harmonic out of the full range available, and tuning of the oscillator frequency to a preset value for the "normal" stationary state of the liquid medium under surveillance. In addition, the microcontroller was used to measure the output frequency of the sensor and communicate it to a PC. The sensor was found to be robust for monitoring such variables as temperature changes in a liquid already.

In addition to the frequency changes, the microcontroller measures losses in the signal loop as well by reducing the gain until the oscillations stop, and restoring it afterwards. This feature might be useful for non-homogeneous madia where both ultrasonic velocity and attenuation change over time.

Discussion and Conclusions

Reconsideration of auto-oscillating ultrasonic sensors seems worthwhile because modern advances in microelectronics have enabled comprehensive control over such oscillators at low cost. This control eliminates any erratic behaviour (e.g., sudden frequency jumps, difficulty to tune to a preset frequency) that limited the applications of these sensors in the past. The low cost of narrow band ultrasonic transducers will allow the application of this approach in cost conscious areas and the deployment of many sensors for online tomographic imaging.

1. A.N.Kalashnikov, K.L.Shafran, R.E.Challis, C.C.Perry, M.E.Unwin, A.K.Holmes and V.Ivchenko, Proc. 2004 IEEE Ultrason. Symp., pp. 549-552.

2. A.N.Kalashnikov, K.L.Shafran, V.I.Ivchenko, R.E.Challis, C.C. Perry, IEEE Trans. Instrum. Measurem., vol.56, iss.4, p.1329-1339, 2007.

5J-4

2:15 PM **Clamp-on Ultrasonic Transducers with Improved Dynamics for Flow Mesuring Applications**

Vakif Hamidullin[1], Roman Malakhanov[2], Kiril Degterev[1], Dmitriy Kryisin[2]; [1]*VZLJOT company, St. Petersburg, Russian Federation,* [2]*State University of Aerospace Instrumentation, Russian Federation.*

Wednesday Oral

Background, Motivation and Objective

Ultrasonic transducers contain a slab of piezoelectric material which is mechanically strained on application of external electric field and which generates an electric charge upon application of mechanical stress. Reflections of the ultrasonic waves within the transducer produce disturbances as some are reflected often enough to produce spurious signals in the transducer and yet not often enough to be internally absorbed.

This problem becomes some more complicated especially for relatively low sounding frequences, when the sizes of transducer parts and wavelengths are commensurable quantities. There is the other no less difficult problem as well. When the fluid has very low density, or is a gas, it carries very little signal energy compared to that in the pipe wall, and acoustic impedance mismatch may couple the signal poorly, resulting in passage of an extremely weak signal.

The objective of this work was to overcome the mentioned difficulties by improving transducer dynamic characteristics.

Statement of Contribution/Methods

Transducers with waveguides having stratified structures are proposed in order to improve their dynamic characteristics (bandwidth, waveform, signal-to-noise ratio). These transducers are capable to selectively generate and receive the Ao Lamb mode in the pipe wall through interrogating flow of liquid or gas. Simulation has been made using impulse response approach [1]. This approach is based on calculation of 3-D impulse acoustic field generated by a linear array of rectungular elements as a model of the proposing transducer.

Results

A quick-damping transient process of diffraction field has been obtained. In accordance with results of simulation the transducers with metal and plastic waveguides have been fabricated. The short pulses have been obtained for the Ao Lamb mode in the pipe wall at 275 kHz and lower in depending on the wall thickness. The signal-to-noise ratio was near 10. The tests with the flowcells for liquid and gas confirmed the efficiency of the proposed method.

Discussion and Conclusions

Analysis of conducted researches showed that a crystal which generates shear waves is preferably employed in the present transducer, although a crystal generating longitudinal waves could also be employed. Shear waves are better absorbed at the interface between laminas than are longitudinal waves and the energy transmitted into the controlled medium is better. All this enables to improve the transducer dynamics and accordingly the flow measurement resolution.

[1] V. K. Hamidullin, R. N. Malakhanov, A. A. Gnedov, G. R. Osokin, S. V. Nogaevskiy, "Waveguide Transducers With Limited Diffraction Beam For Ultrasonic Flow Measuring At High Temperature And Pressure" Proc. of 2007 IEEE International Ultrasonic Symposium, October 28-31, 2007, New York City, NY, USA, pp. 917-920.

5J-5

2:30 PM **2-Step Surface Modification Technology for Acoustic Chemical Sensor Arrays**

Yingchun Li, Ralf Lucklum, Peter Hauptmann; *Institute of Micro- and Sensor Systems (IMOS), Faculty of Electrical Engineering and Information Technology, Magdeburg, Saxony-Anhalt, Germany.*

Background, Motivation and Objective

Capacitive micromachined ultrasonic transducers (CMUTs) provide a new platform because of their important attribute of containing many resonant elements on one chip. One major challenge is a reproducible coating strategy to minimize or even preclude calibration. Here we concentrate on the determination of concentration of alcohols and other organic compounds in the percentage range, since those substances are more and more used as fuel.

Statement of Contribution/Methods

Calibration to ensure the comparability and repeatability between sensors from mass production is usually a bottleneck in sensor development since this process is time and money-consuming. We introduce a double-layer preparation technology which allows a localized deposition of different sensitive materials and overcomes the need of complicated calibration. Preparation of polystyrene nanoparticles (PSN) via dip-coating provides a bottom layer which defines the acoustic properties of the device. Calix[n]arene supermolecules are dispensed onto the PSN layer in the second step, which serves as the sensitive material. The fairly ordered arrangement of the PSN guarantees a sufficient uniformity of the sensitive film (see inset Fig. 1). Besides, large improvement in recognition capability is obtained due to the increased sensitive area. QCM is applied for the pre-test experiments for economical considerations and accessibility. The technology is optimized carefully in order to set up a simple method transferable to industry.

Results

We investigated the sensor response, including selectivity, sensitivity, reversibility, saturation effect and stability of the prepared sensors. Fig.1 shows the response of a sensor prepared in the above manner to different gases.

Discussion and Conclusions

The transfer function of acoustic microsensors depends very much on thickness and uniformity of the selective coating. Traditional methods like spin coating are not applicable to sensor arrays on one chip. The 2-step procedure is a convenient concept to apply microdispensing with minimized variation in the sensor sensitivity.

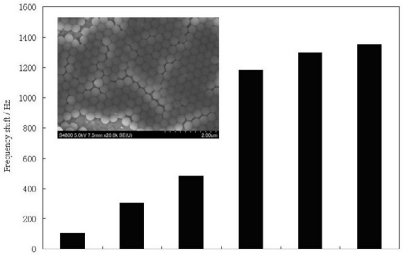

Fig. 1 Recognition ability of a 2-step coated QCM for different gases (gas concentration: 0.5%)

Wednesday Oral

5J-6

2:45 PM **A design of high-sensitivity micromachined capacitive ultrasonic mass resonators**

Li-Feng Ge; *Anhui University, School of Electronic Science and Technology, Hefei, Anhui, China.*

Background, Motivation and Objective

Piezoelectric ultrasonic mass sensors for chemical and biological detection have been in-deep investigated. An analytic comparison of the sensitivities (14cm2/g - 1014cm2/g) of bulk-wave, surface-wave, and plate-wave mass sensors was also reported [S. Wenzel and R. White, Appl. Phys. Lett. 54 (20):1976-1978, 1989]. Recently, capacitive mass sensors have obtained more attentions, such as, the development of the plate-wave and mass resonator sensors based on micromachined capacitive ultrasonic transducers. The micromachined capacitive ultrasonic mass resonator (mCUMR) is much promising due to its simple structure and high sensitivity, so that to establish an accurate analytical model is urgently needed.

Statement of Contribution/Methods

The TDK model previously developed for capacitive ultrasonic transducers can be applied here. The circular diaphragm on top of the vacuum-sealed air cavity is treated as a laminated plate made of stretched nitride film, gold electrode, and an additional polymer coating. The effect of the bias voltage is taken into account also. It is derived in this paper that the fundamental frequency of the diaphragm can be expressed in terms of the frequency parameter of the vibration of the diaphragm, area density of the diaphragm and bias voltage. The mass sensitivity of the resonator is further derived. Thus, the design of such a diaphragm-resonator can be computationally performed by our choice of physical dimensions and the material properties.

Results

A design based on the formulations derived above is given. Its resonance frequency (f0,0) is 10 MHz at the bias voltage of 30 V, and the frequency decreases lightly as the bias is increased, and will be 9.86 MHz at 300 V. For a given bias, both the resonance frequency and mass sensitivity decreases lightly as the mass adsorbed by the polymer coating is increased. The mass sensitivity is 1307 cm2/g for the first-order approximation. Since the mass sensitivity is intrinsically non-linear, so a calculated sensitivity curve is given. The mass resolution is also very high, that is a 1 Hz resonance frequency shift represents an added mass of 76pg/cm2.

Discussion and Conclusions

An analytical model for mCUMRs is developed, and the mCUMRs constitute an attractive choice for chemical and biological detection.

6J. Energy Harvesting & Magnetoelectrics

Hall 2C

Wednseday, November 5, 2008, 1:30 pm - 3:00 pm

Chair: **Mark Schafer;**
Sonic Tech, PA, USA.

6J-1

1:30 PM **A Magnetoelectric Transducer Consisting of Magnetostrictive and Piezoelectric Composite Array**

Ping Li, Yumei Wen; *Chongqing University, College of Optoelectronic Engineering, China.*

Background, Motivation and Objective

Composites made of piezoelectric materials and giant magnetostrictive rare-earth iron alloys have become an attractive topic in recent years due to their large magnetoelectric response. Piezoelectric/magnetostrictive composites have better magnetoelectric (ME) properties than single phase materials. Terfenol-D exhibits a large magnetostriction of more than 2000 ppm and the ME effect of laminate composites of Terfenol-D and PZT/PVDF is about 100-1000 times larger than that in the known ME materials (e.g. Cr2O3 and ferrite/piezoelectric ceramic composites). The maximum ME sensitivity of the three-phase laminate composites at resonant frequency can reach 2.7-8.70V/Oe. However, due to the contradiction between the high Q value and the wide bandwidth, it has proven difficult to further enhance the ME voltage coefficient since the voltage gain is directly proportional to the Q value. The new composite transducer array may have both a wider bandwidth and a higher efficiency than other prior sandwiched laminate composite transducers and can be used in many fields of magnetic detecting and magnetoelectric energy harvesting.

Statement of Contribution/Methods

This paper presents a new high-efficiency ME composite transducer consisting of magnetostrictive Terfenol-D arrays, piezoelectric PZT arrays and a substrate. Magnetostrictive resonant unidirectional transducer (MRUDT) array groups and a piezoelectric unidirectional transducer (PUDT) array group are created inside the transducer while propagating the unidirectionality required for low loss and converting the magnetic signal into resonant acoustoelectric wave with both the higher amplitude and the wider bandwidth. Because of the superimposed effect and the minor loop feedback (the partial resonance) in the MRUDT array, the contradiction between the higher quality (Q) value and the wider bandwidth can be settled and a higher ME voltage coefficients with a wider bandwidth can be obtained by using MRUDT arrays, PUDT array and a silicon substrate with a higher Q value.

Results

The composite array structure can enhance ME voltage coefficient and widen bandwidth due to superimposed effect, the minor loop feedback and the partial resonance. We design the scheme of the magnetoelectric transducer array with a wider bandwidth, a higher ME coefficient and a higher Q value. Experiments exhibits that the ME voltage coefficient of above 5V/Oe, the bandwidth of above 1% center frequency and the Q value of 1000 can be obtained.

Discussion and Conclusions

Experiments and measurement demonstrate that the composite transducer of PUDT, MRUDT and a substrate has a significantly widened bandwidth and an enhanced ME voltage coefficient relative to the prior sandwiched laminate composite configurations.

6J-2

1:45 PM **Magnetoelectric transducer of ferromagnetic alloy and piezoelectric ceramic for wireless power transmission**

Leixiang Bian, **Yumei Wen,** Ping Li; *Chongqing University, Chongqing, China.*

Background, Motivation and Objective

Many attentions have been paid to wireless energy transfer. The majority of the studies focus on inductive coupling . It is noted that magnetoelectric (ME) laminates have shown very large ME coupling at resonance .This feature enables ME composites to possess an ideal sensing and ME energy conversion ability around its resonance. The magnetostrictive property is found in a type of iron-nickel-based ferromagnetic alloy with constant elasticity. Although the piezomagnetic coefficient of d33m is evaluated to be only ~0.1ppm/Oe, the mechanical Q-factor of the alloy is greater than 9000. The piezoelectric Pb(Zr,Ti)O3 (PZT8) also features with high mechanical Q-factor ~1000. Thus, we propose a high Q-factor resonance-type ME transducer fabricated from ferromagnetic alloy and piezoelectric PZT8.

Statement of Contribution/Methods

The transducer is fabricated by bonding ferromagnetic alloy and piezoelectric PZT8 in layer. The dimensions of the piezoelectric PZT8 plate and the ferromagnetic plate are respectively 64×6.0×0.8 mm3 and 80×6.0×0.6mm3. The PZT8 plate is polarized along its thickness direction, while the ferromagnetic plate is magnetized in length direction. Because of the high mechanical Q-factors of constant elastic alloy and PZT8, the effective Q-factor of the laminate transducer is accordingly high. In this manner, the ME efficiency is high.

Results

The ME voltage and output power density as a function of load resistance at the resonance frequency of 29.65 kHz is shown in Fig.1. The data is taken under the driving of 0.3Oe root-mean-square (RMS) AC magnetic field superimposed with DC bias field of 30Oe. Fig.1 shows that the ME output power density at optimum load resistance achieves 0.5mW/cm3, from 0.3Oe RMS field.

Discussion and Conclusions

The ME transducer made from ferromagnetic alloy with constant elasticity and piezoelectric PZT8 has demonstrated strong ME coupling at resonance. The higher ME output density can be achieved by optimizing the dimensions of ferromagnetic alloy and piezoelectric PZT8. In addition, the output power is directly proportional to the square of exciting AC magnetic field. In this manner, output power density of 556mW/cm3 can be achieved by exciting of 10Oe RMS AC magnetic field. It is promising to replace the coils for wireless energy coupling by such type ME transducers.

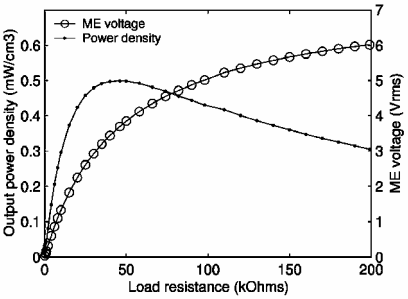

6J-3

2:00 PM **The Physical Acoustics of Energy Harvesting**

Stewart Sherrit; *Jet Propulsion Laboratory, California Institute of Technology, Advanced Technologies Group, Pasadena, CA, USA.*

Background, Motivation and Objective

Energy harvesting systems based on the transformation of acoustic vibrations into electrical energy are increasingly being used for niche applications due to the reduction in power consumption of modern day electronic systems. Typically these applications involve extracting energy at remote or isolated locations where local long term power is unavailable or inside sealed or rotating systems where cabling and electrical commutation are problematic. This paper will look at some of the limitations of these systems.

Statement of Contribution/Methods

A variety of modes of harvesting electrical power from acoustic vibrations or impacts generated by machines, humans or nature will be presented. These modes can be configured to extract energy from longitudinal, transverse, bending, hydrostatic or shear waves at frequencies ranging from less than a Hz to 10's of kHz. In order to aid in the design and optimization of these devices we have identified common elements of these systems.

Results

These common elements are: the input mechanical power spectrum, the effective matching of mechnical loads, the conversion of the input mechanical energy into electrical energy using piezoelectric or biased electrostrictive transducers and matching the electrical load. Recent results on an acoustic electric feed-through device demonstrated 1 kW power conversions at power densities of 70 W/cm^2 and 25 W/cm^3 using a pre-stressed stacked PZT ceramics operating at 16 kHz with an efficiency of 84%. In addition a variety of circuits have been designed and are currently available to optimize the electrical impedance matching. These results suggest the conversion and the electrical matching are not the limiting elements of these devices and we will show that the main impediment to increased power is the vibration source amplitude, frequency, inertia and the size limitations of the energy harvesting systems or in the case of human powered systems the requirement that the device remains unobtrusive.

Discussion and Conclusions

Although the power densities of these devices may be limited by the source and the matching of the mechanical loads there are plenty of applications that are feasible within the available power densities due to the wonders of CMOS.

6J-4

2:30 PM **Ultrasonic Thermoacoustic Energy Conversion**

Orest Symko, Myra Flitcroft; *University of Utah, Physics, Salt Lake City, UT, USA.*

Background, Motivation and Objective

When heat is applied to one end of a stack of plates inside an acoustic resonator, sound can be generated. This is the basis of a thermoacoustic engine called a prime mover. It consists of a resonator with a working gas, a cold heat exchanger next to the stack and a hot heat exchanger against the other end of the stack; heat is injected to the hot heat exchanger. The device is driven by a temperature gradient across the stack; above a critical gradient the onset for oscillations occurs. Being a resonant system the device size scales inversely with frequency. Certain applications have advantages in reducing device size and hence to operate in the ultrasonic range. The development of the technology dealing with this frequency range and device characteristics is presented here. By coupling a piezoelectric device to the thermoacoustic engine, conversion from heat to electricity is achieved. The unit makes a compact energy converter with essentially no parts. It can be used in energy conversion applications, especially waste heat to electricity conversion.

Statement of Contribution/Methods

In developing such small devices for the ultrasonic range it is important to scale down the critical dimensions from working audio frequency devices. With air as the working fluid the resonator (¼- wave resonator) length is 4.1mm for an operating frequency of 21 kHz. Heat, generated by a flame or other source, is applied to the hot heat exchanger. Above a threshold temperature difference between the hot and cold heat exchangers, acoustic oscillations are generated. Coupled to a piezoelectric device; it converts sound to electricity. Thermal interaction between the sound field and the element of the stack provides the correct phasing for sound production. This is achieved when the condition $\omega\tau \approx 1$ is met; ω is the angular frequency of the sound and τ is a thermal relaxation time given by $d2 / 2\alpha$ where d = an effective distance between stack elements and α = the thermal diffusivity.

Results

Scaling down in size thermoacoustic engines from the audio range led to miniature engines. The devices radiated sound when the injected heat created a temperature gradient above threshold. For devices 4.1mm long sound was radiated at 21kHz. Depending on the alignment of the cold and the hot parts, the temperature difference across the stack for onset of oscillations ranged from 85ºC to 180ºC.

Sound intensities outside the resonator varied with the Δ T across the stack; they reached levels of over 140dB. Generated acoustic energy is converted to electricity by means of a piezoelectric element.

Discussion and Conclusions

Since the acoustic devices are resonant systems, large power density can be achieved with ultrasonic devices for the 20kHz unit. At an acoustic intensity of 160dB, the power density would be ~2 Watts/cm3. To achieve high power levels, an array of such devices can be formed.

The results show the potential of a thermoacoustic-piezoelectric approach in the ultrasonic range for energy conversion from heat to electricity.

1K. Vector Velocity Imaging

Hall 3

Wednseday, November 5, 2008, 4:30 pm - 6:00 pm

Chair: **Hans Torp;**
Norwegian University of Science and Technology, Norway.

1K-1

4:30 PM **An Automatic Angle Tracking Method for Dual-Beam Vector Doppler Applications**

Piero Tortoli, Alessandro Dallai, Luca Bassi, Enrico Boni, Stefano Ricci; *Università di Firenze, Electronics & Telecommunications, Firenze, Italy.*

Background, Motivation and Objective

An original dual-beam vector Doppler method has been recently introduced (2006 Ultrasonics Symposium, p.979-988). Here, the flow direction is first identified by orienting one beam so that the Doppler spectrum backscattered from a selected sample volume (SV) results symmetrical around zero frequency, which represents a unique signature of the transverse beam-flow angle. Once the reference beam has been accurately oriented, the second beam can be used to directly estimate the velocity magnitude.

Although the technique has been thoroughly validated in vitro and in vivo, for its practical application it is desirable that the needed transverse angle be automatically tracked.

Statement of Contribution/Methods

Transverse angle tracking is achieved through the computation of two Doppler spectral parameters: the mean frequency, fd, and the spectral symmetry index (SSI), i.e. the % ratio of spectral power corresponding to positive and negative frequencies, respectively.

The tracking procedure has been implemented in a programmable ULtrasound Advanced Open Platform (ULA-OP), which can control a 192-element linear array transducer. Like in standard duplex mode, the operator suitably directs the reference M-line produced by a sub-aperture of the linear array, and places the Doppler SV within the vessel of interest. By starting the tracking procedure, the reference M-line direction is automatically corrected in order to decrement fd and increment the SSI, both being computed from 64 ensemble averaged Doppler spectra with 75% overlap. The steering correction is initially made in coarse steps (e.g.: 4°) which are progressively decreased down to 0.5° while the SSI increases. Once the SSI has overcome a suitable threshold, the steering angle is no more modified, and the flow direction is considered perpendicular to the current reference M-line. The ULA-OP system then selects another transducer sub-aperture and generates a second US beam, which intercepts the SV of interest with Doppler angle as far as possible from 90°. The velocity magnitude is directly estimated from echoes collected by this second beam.

Results

The novel ULA-OP system functionality has been successfully tested both in vitro and in vivo. In vitro experiments have been conducted in steady and pulsatile flow conditions, showing that, by setting the SSI threshold at 80%, the flow direction can be identified with errors $\leq \pm 1°$ whichever the initial Doppler angle is over a wide range. The angle tracking procedure has also been applied in vivo on the common carotid arteries of 8 volunteers, allowing the velocity to be measured with high repeatability.

Discussion and Conclusions

Finding the desired reference beam orientation may be uneasy, especially for medical doctors who are used to consider the 90° beam-flow angle as a "wrong" one. The novel angle tracking method makes the proposed dual-beam technique suitable for use in clinical applications.

1K-2

4:45 PM **In-vivo evaluation of three ultrasound vector velocity techniques with MR phase contrast angiography**

Kristoffer L. Hansen[1], Jesper Udesen[2], Niels Oddershede[3], Lasse Henze[2], Carsten Thomsen[1], Jørgen A. Jensen[2], Michael B. Nielsen[1]; *[1]University Hospital of Copenhagen, Department of Radiology, Denmark, [2]Technical University of Denmark, Denmark, [3]GN Resound, Denmark.*

Background, Motivation and Objective

Conventional Doppler ultrasound (US) only estimates the blood velocity along the US beam direction. In all modern scanners the velocity estimates are angle corrected by the operator assuming blood movement parallel to vessel walls. Unfortunately, the direction of the blood movement changes over time and space, thus no correct quantitative flow measurements can be done with conventional systems.

Three alternative angle independent vector velocity methods are evaluated in this paper: directional beamforming (DB), synthetic aperture flow imaging (STA) and transverse oscillation (TO) where quantitative blood flow measurements were compared to magnetic resonance phase contrast angiography (MRA).

Statement of Contribution/Methods

The performances of the three methods were investigated in-vivo by measuring the stroke volume in the right common carotid artery, two cm upstream of the bifurcation, of eleven healthy volunteers with MRA as reference. Thus, each volunteer was examined with all four methods at four different occasions.

The experimental ultrasound scanner RASMUS and a B-K Medical 5 MHz linear array transducer acquired the ultrasound (US) data. The right common carotid artery was scanned at 90° angles of insonation. From the data sets vector velocity sequences were constructed and stroke volume calculated.

MRA data were acquired using a 1.5 T whole body MR scanner (Magnetom Vision, Siemens AG), cervical coil and a conventional prospective ECG triggered phase contrast sequence (phase interval: 29 ms, pixel resolution: 0.52 x 0.39 mm2, FOV: 100 mm, slice thickness: 6 mm, VENC: +/-1 m/s). From the velocity maps of the right common carotid artery, stroke volume for every volunteer was likewise calculated.

Results

No significant differences were observed for any of the three comparisons using paired two-tailed t-test (DB vs. MRA: p=0.65; STA vs. MRA: p=0.24; TO vs. MRA: p=0.36). The correlations between the three vector velocity methods and MRA were: DB vs. MRA R=0.84 ($p<0.01$); STA vs. MRA R=0.95 ($p<0.01$); TO vs. MRA R=0.91 ($p<0.01$). Bland-Altman plots were additionally constructed and mean differences for the three comparisons were: DB vs. MRA = 0.17 ml (95% CI: -0.61 to 0.95); STA vs. MRA =-0.07 ml (95% CI: -0.54 ml to 0.41 ml); TO vs. MRA = 0.24 ml (95% CI: -0.32 to 0.81)

Discussion and Conclusions

According to the strong correlations and the low mean differences reliable estimates can be obtained with all the three methods. The three US vector velocity techniques yield quantitative insight in to flow dynamics and can potentially give the clinician a powerful tool in cardiovascular disease assessment.

Wednesday Oral

1K-3

5:00 PM **Double-Beam Diffraction-Grating Transducers for Improved Blood Flow Measurement**

David Vilkomerson; *DVX, Princeton, NJ, USA.*

Background, Motivation and Objective

Blood flow is crucial for keeping tissue alive. We reported several years ago (2004 IEEE International Ultrasonics Symposium) on using a diffraction-grating transducer (DGT) built into the wall of a prosthetic vascular graft to measure the graft's blood flow. A DGT produces beams at an angle to its surface, so that flat in the wall of a graft it produces beams with a component in the direction of flow, enabling Doppler measurements. As discussed in the earlier article, a double-beam DGT is particularly easily fabricated: transducer elements at ~ wavelength separation poled alternatingly "up" and "down" form a double-beam DGT when simple sheet electrodes connect the transducer elements' tops and bottoms. This symmetrical structure produces symmetrical beams of equal power and at equal angle to the transducer. These transducers have worked well in measuring blood flow, and that data (from blood flow in dogs) is being published elsewhere.

In these devices, one beam of the DGT's double beams was directed under a slab transducer receiver to produce CW Doppler signals for conventional processing. We investigated whether using both beams could improve blood flow measurement.

Statement of Contribution/Methods

Using both beams produces two simultaneous Doppler shifted frequencies. We have developed methods of using these Doppler frequencies to determine both velocity and angle to the vessel axis (two Doppler equations in two unknowns solved simultaneously). Directionality in this system can be obtained by "breaking its symmetry": making one portion of the transmitting DGT longer than the other produces more power in one Doppler power spectrum, so direction can be calculated.

In certain configurations, the Doppler frequency shift is independent of the driving frequency used (!); the Doppler shift becomes directly proportional to the ratio of velocity to the spacing of the transducer elements. Therefore simultaneous multiple drive frequencies, if separated by several times the Doppler shift bandwidth, will produce multiple Doppler power spectra that can be summed to reduce variance, therefore improving the accuracy of Doppler measurement.

Results

We have fabricated double-beam DGT transducers of PVDF-TrFE operating at 20 MHz (using the greater, i.e. f4, backscattering from blood cells at these frequencies to compensate for the lower sensitivity of this transducer material) with 80 micron element pitch, and measured flow in blood-mimicking fluid. The double-beam DGT's produced double Doppler shift frequencies that were independent of driving frequency, as predicted, and produced accurate blood velocity measurements.

Discussion and Conclusions

Using double-beam DGT transducers should lead to improved measurement of intravascular blood flow, e.g. in coronary arteries.

1K-4

5:15 PM **Fast Blood Vector Velocity Imaging using ultrasound: In vivo examples of complex blood flow in the vascular system.**

Kristoffer Lindskov Hansen[2], Jesper Udesen[1], Fredrik Gran[1], Michael Bachman Nielsen[2], Jørgen Arendt Jensen[1]; [1]*Technical University of Denmark, Denmark,* [2]*University Hospital of Denmark, Denmark.*

Background, Motivation and Objective

Conventional ultrasound methods for acquiring color flow images of the blood velocity is limited by a relatively low frame rate and are restricted to only give velocity estimates along the ultrasound beam direction. To circumvent these limitations, we have previously proposed a method, where the frame rate can be significantly increased and the full 2-D vector velocity of the blood can be estimated.

Statement of Contribution/Methods

The method used in this study takes advantage of three techniques: 1) The ultrasound is not focused during the transmit of the ultrasound signals and a full speckle image of the blood can be acquired for each pulse emission. 2) The transmitted pulse consists of a 13 bit Barker code, which is transmitted simultaneously from each transducer element. 3) The 2-D vector velocity of the blood is found using a 2-D SSD (sum of squared differences) estimator between segments in consecutive speckle images.

The method was tested with a 5 MHz linear array transducer connected to the experimental scanner RASMUS. The following vessels were scanned on five healthy volunteers: 1) The valves of Vena Saphena, 2) The valves of Vena Jugularis, 3) The bifurcation of the Carotid artery, 4) The bifurcation the Brachiocephalic artery, 5) The bifurcation of the Femoral artery. Each of the five scans yielded a vector velocity movie with duration of 3 seconds at a frame rate of 100 Hz and with a spatial resolution of approximately 1x1 mm^2.

Results

All five scans showed complex flow patterns. In the veins, large vortices were located around the valves. Backwards flow was present through the valves of vena jugularis contrary to the case of vena saphena where no backwards flow was observed. In the arteries, a large vortex was present in the bifurcation of the carotid artery as well as in the bifurcation the Brachiocephalic artery. For all five scans the maximum velocity in the scan plane was 0.4-1.2 m/s with the highest velocities in the arteries and the lowest in the veins. According to the literature these values are realistic for healthy subjects.

Discussion and Conclusions

It has been shown that vector velocity estimates of the blood can be obtained in vivo when complex flow patterns are present.

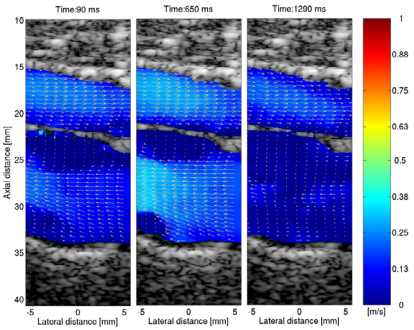

1K-5

5:30 PM **Estimation of Valvular Regurgitation Area by 3D HPRF Doppler**

Torbjørn Hergum[1], Thomas Renhult Skaug[1], Knut Matre[2], Hans Torp[1]; *[1]Norwegian University of Science and Technology, Department of circulation and medical imaging, Trondheim, Norway, [2]University of Bergen, Institute of Medicine, Bergen, Norway.*

Background, Motivation and Objective

Determining the severity of leakage through a heart valve is important, but difficult. Two of the parameters which are clinically interesting in this regard are the area and the geometry of the lesion. Current practice for non-invasive measurement of the severity of valvular regurgitation is qualitative, and based upon using color flow- and spectral Doppler techniques.

Wednesday Oral

Statement of Contribution/Methods

In search for quantitative measurements of regurgitant severity we used 3D high pulse repetition frequency (HPRF) color flow imaging to measure the Doppler signal from multiple beams distributed over the laminar vena contracta region near the orifice. A steep clutter filter was used to separate the jet flow Doppler signals from the Doppler signals of the slowly-moving blood of the ambiguous sample volumes.

The power from the closely spaced ultrasound beams are summed to yield the total Doppler power, which is known to be proportional to the amount of blood moving above the clutter-filter cutoff velocity. The cross sectional area of the jet was found by scaling the summed Doppler power from these beams using both a-priori knowledge of the lateral extent of the beams and a reference beam which is completely covered by the orifice.

Both in vitro trials and computer simulation have been used for validation. The in vitro measurements were made using a pulsatile flow phantom holding porcine valves with six different holes, ranging from mild to severe mitral regurgitation. The method can be applied to other high-velocity valvular jets.

Results

The mean value and standard deviation from the in vitro trials are plotted as red in the figure showing true area vs. estimated area. Two computer simulations are also included in the figure, the dashed and dotted lines are simulations respectively with- (blue) and without (black) stochastic variation.

Discussion and Conclusions

Small holes of sizes comparable to a single ultrasound beam are overestimated as expected from simulations, and the estimates of the larger holes fits well with the line of identity (green). According to the stochastic simulations the method should underestimate the area of large orifices, but this is not seen in the in vitro data. Regardless of this the in vitro data enables us to distinguish between the different regurgitation degrees.

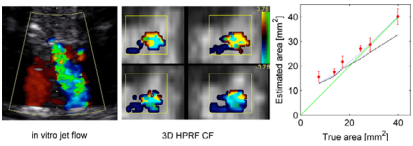

1K-6

5:45 PM **Vector Doppler Imaging with a Position Sensor for Measuring Complex Blood flow in Carotid Arteries**

Canxing Xu[1], Vijay Shamdasani[1], Daniel Leotta[2], Edward Stutzman[3], Kirk Beach[3], Yongmin Kim[1]; *[1]University of Washington, Department of Bioengineering, Seattle, WA, USA, [2]University of Washington, Applied Physics Laboratory, Seattle, WA, USA, [3]University of Washington, Department of Surgery, Seattle, WA, USA.*

Background, Motivation and Objective

Atherosclerosis in human arteries often occurs in regions of complex blood flow where there is low flow-induced shear stress. Also, the flow dynamics are considered to affect the progression and rupture of the plaque. Although ultrasound color Doppler imaging and spectral Doppler can be used to obtain the projection of flow velocities along the direction of ultrasound beams, evaluation of complex blood flow patterns, such as recirculation zones and turbulence, requires the flow vector information. Many methods have been proposed to measure 2D/3D velocity vectors by measuring velocity in two to three different directions simultaneously, but they all require a cumbersome arrangement of multiple ultrasound transducers, making their routine clinical use an uphill battle. More practical approaches were previously introduced in which flow vectors were computed off-line by combining multiple color Doppler images obtained from a single transducer with the ultrasound beams steered to multiple directions. Although this method is feasible on commercial ultrasound machines, the transducer must be kept steady to prevent misregistration between the color Doppler images.

Statement of Contribution/Methods

To register multiple color Doppler images from different angles more accurately, we attached a magnetic position sensor to a 7.5-MHz 1D linear array transducer. With the ultrasound beam steered to +20° and -20°, we acquired data sets from carotid arteries of 12 patients with atherosclerotic disease and 2 healthy volunteers. Each data set consists of 6 seconds of color Doppler data at 25 fps, including the transducer position and ECG signal for each image. The ECG signal was used to select images from the same cardiac phase while the position information was used to register the images. The 2D velocity vectors for the overlapped regions were calculated.

Results

Without using a position sensor, the motion between images acquired from different angles can be 2 to 5 mm even when experienced operators try to hold the transducer still. This motion resulted in misregistration error of 20 to 50 pixels. After correcting for this error by warping the color Doppler images based on the data from the position sensor, the error was reduced to less than 0.5 mm. The reconstructed velocity fields at the carotid artery bifurcation from patients with plaque and healthy subjects show complex patterns of blood flow, including flow reversal and turbulence. The results are consistent with the carotid artery bifurcation flow patterns that have been demonstrated by computational flow dynamics models, MRI, and previous vector Doppler systems.

Discussion and Conclusions

The results show that vector Doppler imaging with a position sensor can improve spatial correlation and hence increase the accuracy in measuring true blood velocity. At the same time, it is more clinically practical than most of the other vector Doppler systems.

2K. Adaptive Beam Forming

Room 201 A/B/C

Wednseday, November 5, 2008, 4:30 pm - 6:00 pm

Chair: **Sverre Holm;**
University of Oslo, Norway.

2K-1

4:30 PM **Sensitivity of Minimum Variance Beamforming to Tissue Aberrations**

Andreas Austeng[1], Tore Bjastad[2], Johan-Fredrik Synnevaag[1], Svein-Erik Masoy[2], Hans Torp[2], **Sverre Holm[1];**
[1]University of Oslo, Norway, [2]Norwegian University of Science and Technology, Trondheim, Norway.

Background, Motivation and Objective

In the last few years minimum variance (MV) (high resolution/Capon) beamforming has been applied to medical ultrasound with improved lateral resolution and improved contrast and edge definition as a result. The method computes a data dependent window, and the result may e.g. be an asymmetrical beam pattern that puts a zero on undesired interferers in the image. As the method's dependence on the data is key to the higher resolution, it is of great interest to find out whether it is robust enough to cope with realistic data that may have phase aberrations.

Statement of Contribution/Methods

We generated four data sets for a point target at 70 mm imaged with a 2.5 MHz 64 element phased array. The 1d aberrations were simulated as time-delays as if the aberrator was on the transducer surface. In all cases the correlation length was 2.46 mm and the delay was scaled to four values for these scenarios:

Weak (typical for imaging through thorax): 21 ns rms/90 ns peak

Intermediate (abdominal imaging): 35 ns rms/150 ns peak

Strong (abdominal imaging): 49 ns rms/210 ns peak

Very strong (breast imaging): 68 ns rms/290 ns peak

Images were formed with an unweighted delay-and-sum (DAS) beamformer and a MV beamformer.

Results

The main lobe of the MV beamformer was narrower or approximately equal to that of DAS with the -6 dB lateral beamwidth being 40%, 67%, 83%, and 106% of the DAS case for the four cases. The aberrations affected the sidelobe structure producing non-symmetric patterns, but with comparable values for the maximum sidelobe levels. For the weak aberrator, the MV beamformer performed better (1-5 dB) than the DAS beamformer.

The sidelobe structure of the point spread function (PSF) for the DAS beamformer has a butterfly shape. The MV beamformer spreads less in range, and for all scenarios we found a reduced range span for the butterfly shape. The range span for which the PSF is higher than -60 dB compared to the max value was decreased by approximately 40% for all scenarios. The only evident degradation observed for the MV beamformer was a slight reduction in sensitivity. In the case of very strong aberration, the main lobe value was decreased by 1.4 dB compared to the DAS beamformer. For the other scenarios, the decrease was 0.9, 0.6, and 0.4 dB.

Discussion and Conclusions

The minimum variance beamformer is controlled by a set of parameters that are central for balancing performance and robustness. We have used spatial smoothing which is important for dealing with multiple reflectors, diagonal loading which helps make the method robust, and time averaging over about a pulse length in estimating the covariance matrix. The latter ensures that the speckle resembles that of DAS.

The MV beamformer gives a substantial decrease in main lobe width without increase in sidelobe level in aberrating environments. Of great importance is that it does not degrade the beam even with very strong aberrators. Thus the method can handle realistic aberrations with a performance which is better than or equal to that of DAS.

2K-2

4:45 PM **Adaptive Imaging Using Principal-Component-Synthesized Aperture Data**

Meng-Lin Li; *National Tsing Hua University, Department of Electrical Engineering, Hsinchu, Taiwan.*

Background, Motivation and Objective

Sidelobe contribution from off-axis scatterers degrades image quality in ultrasound imaging. Focusing errors resulting from sound-velocity inhomogeneities in tissues, also known as phase aberrations, reduce coherence of the received signals and thus elevates the sidelobe level degrading the contrast resolution.

Statement of Contribution/Methods

In this study, we proposed a novel adaptive sidelobe-reduction technique using aperture data synthesized from mainlobe-dominant principal components. Principal component analysis of aperture data with proper delay being applied is performed here by singular value decomposition where the singular values are in order of large to small. These singular values describe how much energy of the aperture data is accounted for by the associated principal component. Because of the high coherence, the mainlobe-contributed energy in the aperture data concentrates on the principal components associated with the first few singular values whereas the one from sidelobe contribution spreads over all the principal components. In our method, the first few principal components are used to synthesize a new aperture data where undesired sidelobe contributions are partly reduced and then beamsum is performed on this new aperture data; thus reducing the effect of focusing errors and compensating the degraded image quality.

Results

Simulations and real array data are used to evaluate the efficacy of the proposed technique. Top panels in the figure are the original images; bottom panels are the one obtained with the proposed technique. All are displayed on a 60 dB dynamic range. From left to right are the cases with no distortion, 1x distortion, and 2x distortion, respectively. The proposed technique offers contrast enhancement from 0.4 (no distortion) dB to 5 dB (2x distortion) and improvement of contrast-to-noise ratio from 2.5 % (no distortion) to 24 % (2x distortion) in real ultrasound data.

Discussion and Conclusions

It is demonstrated that the proposed technique effectively reduces sidelobes contribution and thus restores the contrast resolution. The characteristics of the proposed technique including the effects of order selection of singular values and degree of aberrations, and comparison with the parallel adaptive receive compensation algorithm are also discussed.

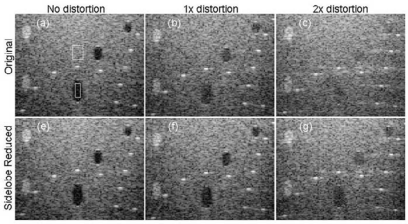

2K-3

5:00 PM **Investigation of Sound Speed Errors in Adaptive Beamforming**

Iben Kraglund Holfort[1], Fredrik Gran[2], Joergen Arendt Jensen[1]; *[1]Technical University of Denmark, Center for Fast Ultrasound Imaging, Kgs. Lyngby, Denmark, [2]GN ReSound A/S, Ballerup, Denmark.*

Background, Motivation and Objective

Recently, adaptive beamforming has been applied to ultrasound imaging with emphasis on the Minimum Variance (MV) beamformer. In contrast to the conventional delay-and-sum (DS) beamformer, the MV beamformer continuously updates the apodization weights. This provides a new set of data-dependent apodization weights for each beamformed response. Previous work has shown that the MV beamformer provides a significant increase of the resolution. However, the potential increase in resolution comes at the expense of a reduced robustness towards imprecise knowledge of e.g. the sound speed. As sound speed changes frequently occur in ultrasound imaging, the influence of sound speed errors on the MV beamformer is an investigation of significant relevance.

Statement of Contribution/Methods

This paper investigates the effect of sound speed errors on the subband MV beamformer. Each subband is processed independently by dividing the broadband data into frequency subband using the short-time Fourier transform. Using Field II, simulated ultrasound data is obtained for a 7 MHz, 128-element, linear array transducer with lambda/2-spacing. A single element is used as the transmitting aperture and all elements as the receiving aperture. The influence of sound speed errors are investigated by applying an error of the sound speed estimate to the ultrasound data. The correct sound speed was 1540 m/s, and the sound speed was changed from 0% to 20% of the true value.

Results

The performance of the MV beamformer response is compared to DS using Boxcar and Hanning apodization. The resolution is quantified by the Full Width at Half Maximum (FWHM). Using the correct sound speed, the three approaches, {DS Boxcar, DS Hanning, MV}, provide FWHM of {0.78, 1.25, 0.06} mm. For errors of 2%, 4%, 6%, 8% and 10% of the correct value, the FWHM are {0.81, 1.25, 0.34} mm, {0.89, 1.44, 0.46} mm, {0.90, 1.54, 0.57} mm, {0.92, 1.52, 0.50} mm and {1.01, 1.55, 0.38} mm, respectively. The lateral variation at a depth of 40 mm for sound speed errors of 0%, 2%, 8% and 10% are shown in the figure. It is seen that the MV response is degraded for increasing sound speed errors.

Discussion and Conclusions

For correct speed of sound estimates, MV provides a significant performance gain with respect to resolution and contrast. Even though the performance of MV is much degraded for incorrect sound speeds, it is not outperformed by the conventional DS beamformer.

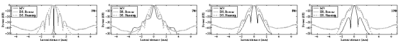

(a) 0% (b) 2% (c) 8% (d) 10%

2K-4

5:15 PM **Low-Complexity Data-Dependent Beamforming**

Johan-Fredrik Synnevåg, **Sverre Holm,** Andreas Austeng; *University of Oslo, Department of Informatics, Oslo, Norway.*

Wednesday Oral

Background, Motivation and Objective

The classical problem of choosing apodization functions for a beamformer involves a tradeoff between mainlobe width and sidelobe level, i.e a tradeoff between resolution and contrast. In recent years data-dependent beamformers, such as the minimum variance beamformer, have been an active topic of research in medical ultrasound imaging to overcome this limitation. Several authors have demonstrated significant improvement in image resolution, but the improvement comes at a considerable cost. Where the complexity of a conventional beamformer is linear with the number of elements (O(N)), the complexity of a minimum variance beamformer is up to O(N^3). In this paper we have applied a method suggested by Vignon and Burcher (IEEE UFFC 2008) which is data-adaptive, but selects the apodization function between a number of predefined windows, giving linear complexity.

Statement of Contribution/Methods

In the proposed method we select an apodization function for each depth along a scan line based on the optimality criterion of the minimum variance beamformer. But unlike the minimum variance beamformer, which has an infinite solution space, we limit the number of possible outcomes to a set of predefined windows.

The complexity of the method is then only k times O(N), where k is the number of predefined windows. We demonstrate significant improvement in image resolution with k as small as four.

Results

We have applied the proposed method to simulated phantoms of point targets and a cyst. We used four predefined windows: Rectangular, Hamming and two complex valued windows with assymetric beampatterns, designed for edge definition. Point target results are shown both for rectangular/Hamming, and for all four windows. The rectangular/Hamming results display the optimal combination of the two windows: Both the resolution of the rectangular window and the low sidelobe level of the Hamming window is retained. Using all four windows further improves the image. The mainlobe width is about half of that of the rectangular window, and the sidelobes are about 15 dB lower than for the Hamming window.

Applying the suggested method to the cyst phantom shows improved edge definition of the cyst. To retain similar speckle patterns as for the rectangular window, the decision must be based on an average of samples along the scan

line. However, the window is only applied to the current sample, such that no radial smoothing appears. It has previously been demonstrated that temporal averaging is required for the minimum variance beamformer as well.

Discussion and Conclusions

The suggested method gives significant improvement in image resolution at a low cost. The method is robust, can handle coherent targets and is easy to implement. The method can also be used as a classifier as the selected window gives information about the object being imaged. The key is to design a set of predefined windows which has desirable properties in different scenarios.

2K-5

5:30 PM **High Frame Rate Adaptive Imaging Using Coherence Factor Weighting and the MVDR Method**

Shun-Li Wang, Pai-Chi Li; *National Taiwan University, Taipei, Taiwan.*

Background, Motivation and Objective

Adaptive imaging has been extensively studied. Although some success has been demonstrated, these approaches generally are not suitable for high frame rate (HFR) imaging where broad transmit beams are required. In this study, we propose an effective adaptive imaging method suitable for HFR imaging based on coherence factor (CF) weighting and the minimum variance distortionless response (MVDR) method.

Statement of Contribution/Methods

The CF is a focusing quality index estimated from receive-channel data. It is the ratio between the energy of the coherent sum to the total incoherent energy. This method is an adaptive weighting technique in which the amplitude of each image pixel is weighted by the corresponding CF such that the unwanted sidelobes are reduced. Direct implementation of the CF weighting in HFR imaging does not provide satisfactory results because broad transmit beams required for HFR imaging affect accuracy of CF calculations. In this study, we solve this problem by applying the MVDR method to the delayed channel data. Specifically, the MVDR method is used for angle of arrival estimation. The beam sum data are then weighted by the estimated CF.

Results

A synthetic transmit aperture method is used for HFR imaging. Only 8 firings are required to form an image. Both simulations and clinical breast imaging data are used. In the simulations, an anechoic cyst phantom is imaged with a maximum $\pi/2$ near field phase screen. The correlation-based method proposed by Flax/O'Donnell is also implemented for performance benchmarking. The contrast and the contrast-to-noise ratio (CNR) improvements are 7.7 dB and 39.2% with the proposed method, respectively. Only 2.1 dB and 21.4% improvements are achieved using the correlation-based method. Clinical breast data are also acquired using a programmable array system. The following figures show images of a fibroadenoma lesion (left: original image, right: with the proposed method). With the proposed data, the contrast enhancement is 3.3 dB and the CNR enhancement is 13.4%.

Discussion and Conclusions

The proposed method combines CF weighting with the MVDR method. Simulations and clinical breast data are used to demonstrate the image quality improvement. Even for HFR imaging with only 8 firings per image, effective contrast enhancement and better lesion boundary can be achieved. Efficacy of the proposed method is clearly demonstrated.

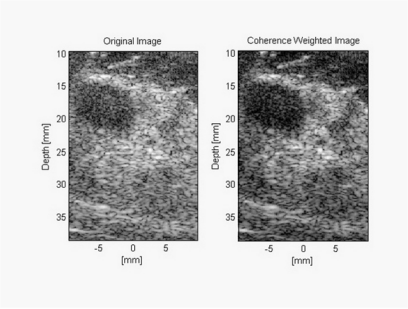

Wednesday Oral

2K-6

5:45 PM **Adaptive beamforming for photoacoustic imaging using linear array transducer**

Suhyun Park, Andrei Karpiouk, Salavat Aglyamov, **Stanislav Emelianov;** *The University of Texas at Austin, Biomedical Engineering, Austin, TX, USA.*

Background, Motivation and Objective

Photoacoustic signals, detected by a transducer array, need to be beamformed for subsequent use in a limited view angle tomography such as B-scan imaging. The backprojection method can be employed based on delay-and-sum (DAS) ultrasound beamforming. However, in the presence of the light scattering or phase aberration, the spatial resolution and contrast in the photoacoustic images is degraded. An adaptive weighting method such as coherence factor (CF) technique can improve the ultrasound and photoacoustic image quality significantly. In addition, photoacoustic images can be further improved by applying adaptive beamforming techniques developed for ultrasound imaging.

Statement of Contribution/Methods

In this study, an adaptive photoacoustic image reconstruction technique that combines an adaptive weighting factor (CF) and an adaptive apodization called minimum variance method (MV) is introduced. CF is known to improve the lateral resolution of photoacoustic images. In addition, MV adaptive beamforming method can further improve the image quality by suppressing signals from off-axis directions. Experiments were performed to analyze the spatial resolution and contrast using a phantom with point targets and a phantom with an inclusion inside, respectively. Ultrasound imaging system (Cortex by Winprobe Corporation, FL, USA), equipped with a 7 MHz center frequency, 14 mm wide, 128 element linear array transducer, was used for RF data acquisition. For photoacoustic imaging, the imaging system was interfaced with an OPO laser system (7 ns pulse duration, 10 Hz repetition rate, and 12.5 mJ/cm2 fluence at 720 nm wavelength).

Results

The lateral profiles of point sources show that the MV method with CF weighing lowers the sidelobe level more than 20 dB compared to DAS beamforming. Also, the width of the mainlobe was decreased approximately 50% from that of the simple DAS image. From the reconstructed photoacoustic images using the inclusion phantom, image contrast was calculated. The contrast of the beamformed images using DAS was about 16 dB. However, using CF weighting, the contrast was increased to 24 dB. The quality of photoacoustic image using CF weighting was improved noticeably due to the reduction of the sidelobe level. Furthermore, the contrast in photoacoustic images using both MV and CF was increased to approximately 26 dB. Although the improvement of the image quality was subtle compared to the CF weighted image, the beamforming artifacts are clearly reduced around the inclusion.

Discussion and Conclusions

In conclusion, DAS beamforming augmented with the MV adaptive method and CF weighting was investigated for photoacoustic imaging. CF weighing and MV adaptive method can significantly improve the photoacoustic image quality by enhancing the spatial resolution and contrast. Experimental and numerical photoacoustic imaging studies demonstrated the superior performance of MV adaptive method combined with CF weighting.

3K. Contrast Agent Imaging: Methods and Applications

Room 305 A/B/C

Wednseday, November 5, 2008, 4:30 pm - 6:00 pm

Chair: **Nico de Jong;**
Erasmus Medical Centre and University of Twente, The Netherlands.

3K-1

4:30 PM **Acoustic Characterisation of Individual Targeted Microbubbles with High-Frequency Ultrasound.**

Michael R. Sprague[1], David E. Goertz[1], Emmanuel Chérin[2], Raffi Karshafian[1], F. Stuart Foster[1]; *[1]University of Toronto, Department of Medical Biophysics, Canada, [2]Sunnybrook Health Sciences Centre, Toronto, Canada.*

Background, Motivation and Objective

Contrast agents targeted with antibodies or small peptides can resolve the signalling mechanisms of endothelial cells; improving our understanding of diseases with abnormal vascular growth. High-frequency ultrasound (20-50 MHz) has important applications in intravascular and small-animal imaging. Understanding the behaviour of bound microbubbles under high-frequency insonation will aid the quantification of signal receptors and improve non-linear detection methods, such as subharmonic imaging. An experimental study of the acoustic emission of individual targeted microbubbles under optical observation was undertaken, focusing on basic backscattering behaviour and subharmonic signal generation.

Statement of Contribution/Methods

A spherically focused, single-element transducer (f# 2.1) excited with a 30 MHz, 15% fractional bandwidth pulse was aligned with a 0.5 µm resolution optical microscope. A gelatin phantom with bound microbubbles (MicroMarkerTM) attached to a positioning system was insonified with pulses with peak-negative-pressures from 170 kPa to 3.0 MPa. The RF data for individual microbubbles with diameters between 1.3 and 6.5 µm were analysed. The fundamental and subharmonic signal components were measured relative to the noise floor, and microbubble disruption was measured optically and verified acoustically.

Results

The fundamental frequency backscattered signal increased linearly with pressure until the microbubbles approached their disruption threshold. Microbubble disruption was strongly correlated with diameter: microbubbles with a diameter less than 2 µm exhibited disruption thresholds of 400 ± 100 kPa, while microbubbles larger than 3 µm exhibited disruption thresholds of over 2 MPa. The absolute subharmonic component increased with pressure and microbubble size. However, it showed more variance than the fundamental component. The maximum subharmonic to fundamental frequency component ratio was inversely related to microbubble size; for microbubbles with a diameter less than 2 µm the ratio was -8 ± 4 dB, and for microbubbles larger than 3 µm, was -21 ± 5 dB.

Discussion and Conclusions

For a polydisperse population, the contribution of microbubbles smaller than 2 microns to the received signal may be transient if the disruption threshold is exceeded. Smaller microbubbles have a larger subharmonic to fundamental ratio and a larger absolute subharmonic signal relative to their volume and, may represent a more suitable target for subharmonic imaging.

3K-2

4:45 PM **In vitro measurement of ambient pressure changes using a realistic clinical setup**

Klaus Scheldrup Andersen, Jørgen Arendt Jensen; *Technical University of Denmark, Center for Fast Ultrasound Imaging, Lyngby, Denmark.*

Background, Motivation and Objective

Many attempts to find a non-invasive procedure to measure the local blood pressure have been made. In the last decade experiments have indicated that the amplitude of the subharmonic response from contrast agents is sensitive to the ambient pressure.

This paper presents results from a new experimental setup for measuring the subharmonic response of a contrast agent when subjected to ambient over pressure. The setup is very flexible offering completely arbitrary excitation and data acquisition, fast and accurate ambient pressure control, and precise timing. More importantly, it resembles a realistic clinical setup using a single array transducer for transmit and receive. The standard signal processing steps usually seen for these experiments are moreover accompanied by steps to reduce dependence on factors as bubble concentration and time.

Statement of Contribution/Methods

Up to now ambient pressure measurements have been carried out using two single element transducers. The measurement setup for this experiment consisted of a single B-K Medical (Herlev, Denmark) phased array transducer with 64 elements and a -6 dB bandwidth between 2 and 4 MHz. The transducer was sealed to an airtight phantom with inlets for injection of Sonovue (Bracco, Milano, Italy) and regulation of the ambient pressure, which was automatically adjusted from Matlab using a custom made pressure controller (Alicat Scientific, Tucson, AZ). Data was acquired using the experimental scanner RASMUS. 100 focused lines were acquired with a pulse repetition frequency of 50 Hz at 6 different ambient pressures in the interval 0 to 25 kPa. To ensure subharmonic generation, a 32 cycles cosine tapered pulse with a center frequency of 4 MHz and an acoustic pressure of 485 kPa was used for excitation. All 64 elements were used in receive and the RF data was filtered and beamformed before further processing. To compensate for variations in bubble response and to make the estimates more robust, each spectrum was normalized according to the fundamental before averaging and the energy of the respective components was chosen as measure over the peak amplitude.

Results

The measurements showed that the energy of the subharmonic component decreased by 10.3 dB when the over pressure was increased from 0 to 25 kPa. In the same interval, the fundamental changed by less than 1 dB. Fitting a line to the six measuring points shows a linear correlation of 0.78 for the subharmonic reduction yielding a pressure sensitivity of 0.41 dB/kPa.

Discussion and Conclusions

The experiment has for the first time shown it is possible to detect ambient pressure changes using a single array transducer setup as obligatory in a clinical situation. Moreover, suggestions for further signal processing was presented to increase the robustness of the estimates. The amount of subharmonic reduction obtained is in good correspondence with results by Shi et al (1999) and Adam et al (2005) who both used a receiver separated from the emitting single element transducer.

Wednesday Oral

3K-3

5:00 PM **Enhancement of static bubble signal in large vessels using composite dual frequency pulses**

Abhay Vijay Patil[1], Joshua J Rychak[2], Alexander L. Klibanov[3], John A. Hossack[1]; *[1]University of Virginia, Biomedical Engineering, Charlottesville, Virginia, USA, [2]Targeson LLC, Charlottesville, Virginia, USA, [3]University of Virginia, Cardiovascular Medicine, Charlottesville, Virginia, USA.*

Background, Motivation and Objective

Molecular ultrasound imaging and bubble-based site-specific drug delivery have potential for early detection of vascular pathology and improved therapeutic response. However, bubbles preferentially travel along the center of the vessels, reducing targeting efficacy. Microbubble targeting to vessel wall can be improved by radiation force [1]. It is helpful to not only monitor the bubbles while simultaneously pushing them, but also to discriminate signals from flowing and adherent bubbles. In this study, we demonstrate the application of composite dual frequency ultrasound pulses in large vessels for simultaneously applying radiation force, and selectively imaging adherent bubbles in near real-time regime.

Statement of Contribution/Methods

An Ultrasonix RP (Richmond, BC) programmable scanner was used to generate a composite dual frequency sequence. Imaging was performed at 10 MHz using pulse inversion (MI < 0.15). Radiation force was applied at frequencies from 1.6 to 6 MHz, 10 cycle pulse length (MI <= 0.15); slow time averaging was performed on successive RF frames to isolate signals from adherent bubbles [1]. A flow phantom with a 2 mm diameter channel was fabricated using 6% food-grade gelatin and 1% agar (Difco, Sparks, MD). Targestar-B (Targeson, Charlottesville, VA) lipid-coated microbubbles in saline (2.2 million or 22 million bubbles/ml) were administered in the phantom at a peak velocity ranging from 2.65 to 15.9 cm/s using a syringe pump (Harvard Instruments, Holliston, MA).

Results

In vitro experiments on a channel of a size similar to coronary arteries demonstrated that for a range of flows, radiation force was able to push the bubbles across the vessel, to the distal wall. The isolated mean adherent bubble signal reduced from 22 dB to 12 dB as the flow velocity increased from 2.65 to 15.9 cm/s. The adherent bubble signal was maximal when the center frequency of the radiation force pulse corresponded to the mean resonant frequency of the bubble population (~4 MHz). One order of magnitude increase in bubble concentration dose resulted in a 10 dB increase in adherent bubble signal.

Discussion and Conclusions

An application of a dual frequency composite sequence was verified in a large vessel, the imaging sequence successfully separated signals emanating from adhered bubbles from those scattered by free streaming bubbles.

[1] Zhao S. et al., Phy. in Med. & Bio., 52(2007), 2055-72

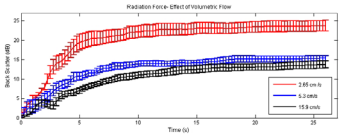

3K-4

5:15 PM **Ultrasound contrast agent microbubble displacement by primary radiation force including compression-only and threshold effects**

Peter Frinking, Emmanuel Gaud, Marcel Arditi; *Bracco Research S.A., Plan-les-Ouates, Geneva, Switzerland.*

Wednesday Oral

Background, Motivation and Objective

Spatial manipulation of ultrasound contrast agent microbubbles using primary radiation force has been suggested to improve bubble targeting efficiency in ultrasound molecular imaging applications. The displacement of the bubbles induced by radiation force strongly depends on bubble size and shell properties. However, compression-only and threshold effects, phenomena typically observed with phospholipid-shell microbubbles, have not been considered previously in this context. In this work, bubble displacement as a function of size was investigated experimentally at different transmit frequencies and acoustic pressure amplitudes. These results were used to validate a modified bubble-displacement model which includes compression-only and threshold effects.

Statement of Contribution/Methods

The experimental setup consisted of a 50 mL bubble-collecting tank which was connected to a vertically-positioned silicon tube (4-mm inner diameter) through a small opening made on the side of the tube. A diluted suspension of BR14 bubbles was fed through the tube at a flow rate of 5 mL/min. Radiation force was applied in continuous-wave mode at peak-negative pressure amplitudes of 40 and 80 kPa and at frequencies of 2.5, 4.0 and 5.8 MHz. For each experiment, the size distribution of the collected bubbles was measured after 20 minutes using a Coulter Multisizer III. For theoretical validation studies, the approach described by Vos et al.1 was used. It calculates the instantaneous bubble displacement and accounts for drag force and added mass. This approach was adapted by including the Marmottant model. Viscoelastic shell-parameters were estimated from a best-fit analysis between normalized simulated displacement curves as a function of bubble size and experimentally obtained size distributions.

Results

At an acoustic pressure amplitude of 40 kPa, distributions with median sizes of 4, 3.5 and 3.6 µm were measured for frequencies of 2.5, 4.0 and 5.8 MHz, respectively. At the higher pressure amplitude of 80 kPa, an increased number of smaller bubbles were collected. A good agreement between experimental and simulated results was

obtained in all conditions. Shell parameters obtained after best-fit analyses depended on median bubble size, with values between 0.8 and 1.4 N/m for shell elasticity and 16x10-9 and 27x10-9 kg/s for shell viscosity.

Discussion and Conclusions

Bubble displacement as a function of size using primary radiation force depends on both frequency and acoustic pressure amplitude. A good agreement between experimental and simulated results was obtained in all conditions. Moreover, the estimated shell parameters depend on median bubble size, with values significantly higher than values reported in the literature using conventional models. The experimental results obtained at different amplitudes suggest the presence of a threshold or activation phenomenon, particularly affecting smaller bubbles.

1Vos et al., IEEE Trans. UFFC 54(7), 2007.

3K-5

5:30 PM **Suppression of tissue-harmonics for pulse-inversion imaging using time-reversal**

Olivier Couture, Jean-François Aubry, Gabriel Montaldo, Mickael Tanter, Mathias Fink; *LOA, ESPCI, France.*

Background, Motivation and Objective

Pulse-inversion sequences are sensitive to the nonlinear echoes from microbubbles allowing an improvement in the blood-to-tissue contrast. However, at larger mechanical indexes, this contrast is reduced by harmonics produced during nonlinear propagation. A method for tissue harmonics cancellation using time-reversal is described and experimentally examined.

Statement of Contribution/Methods

The method is based on the transmission of dedicated signal waveforms on the probe elements, which are established during a calibration procedure. Nonlinear distorted pulses are acquired from the echo of a wire in water using a newly developed 128 channels featuring independent 12 bits analog transmitters and receivers. The linearity of the transmit electronic boards was ensured down to -30 dB. The distorted pulses backscattered by the wire are time-reversed, optimised (bandwidth profile correction) and used for pulse-inversion imaging with a 4.3 MHz linear array.

Results

In water, harmonics due to nonlinear propagation could be reduced by up to 20 dB. The time-reversed distorted pulses were also used to image microbubbles flowing in a tissue phantom. Compared to normal (straight) pulses, the time-reversed distorted pulses reduced the tissue signal in pulse-inversion by 11 dB (figure). The signal from microbubbles flowing in a wall-less vessel, also at the second harmonic, was unaffected by the correction.

Discussion and Conclusions

This technique can thus increase the blood-to-tissue contrast ratio while keeping the pressure and the number of pulses constant.

Fig: Pulse-inversion imaging of a wall-less vessel filled with a microbubbles solution using normal pulsing scheme (left) and using time-reversal (right). Bmode images are coded in a gray scale colormap ranging 40 dB.

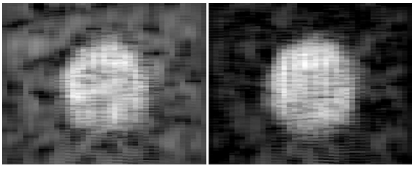

3K-6

5:45 PM **Nonlinear contrast imaging with Capacitive Micromachined Transducers**

Anthony Novell[1], Mathieu Legros[2], Nicolas Félix[2], Ayache Bouakaz[1]; *[1]INSERM UMR 930 - CNRS FRE 2448 and Université F. Rabelais, Tours, France, [2]Vermon SA, Tours, France.*

Background, Motivation and Objective

Aim: Advantages of Capacitive Micromachined Ultrasonic Transducers (CMUTs) such as wide frequency bandwidth could be used in nonlinear contrast imaging. However, the driving electrostatic force induces a nonlinear behavior of the CMUT generating thus undesirable harmonic components. Consequently, the use of CMUT for harmonic imaging, with or without contrast agents becomes challenging. To insure their exploitation for nonlinear imaging, two methods that compensate the nonlinear behavior are presented.

The 1st approach, called linear approach, consists in suppressing the unwanted harmonic components (nf0) by transmitting, in addition to the fundamental component, an inverted and delayed version of the frequency component at nf0. The second approach, called a nonlinear approach, takes advantage of the nonlinear behavior of the CMUT and is based on the nonlinear spectral interaction between the fundamental component and a second selected frequency component, generating thus two harmonic components at sum and difference frequencies. To cancel any harmonic component generated from the CMUT at nf0, the frequency of the 2nd transmitted component should be selected such as its sum or its difference with the fundamental frequency occurs at nf0.

Statement of Contribution/Methods

Methods: Compensation methods were evaluated on a 7 MHz center frequency 64-element CMUT array. Amplitude and phase of cancellation components were estimated using a needle hydrophone positioned at 3 mm from the source. Alternatively, a still wire (perfect reflector) was used and the reflected signal was measured using a single element 5-MHz transducer positioned perpendicularly. A fundamental excitation signal of 2.5 MHz Gaussian pulse at 40 kPa and 30% bandwidth was transmitted. Harmonic generation from a 1/2000 diluted solution of Sonovue® microbubbles was measured with and without compensation.

Results

Results: Using one element of the CMUT array, reductions in the 2nd harmonic amplitude of 17 dB and 15 dB were observed using linear and nonlinear methods respectively. Using the linear method, the optimal cancellation signal at 5MHz had 21% bandwidth and a phase of 15.3° while the cancellation signal at 7.5MHz for the nonlinear approach had a bandwidth of 18% and 10.8° phase. The nonlinear cancellation approach did not modify the fundamental signal amplitude while the linear method induced a 2 dB variation. This is attributed to an interaction between the fundamental component and the linear cancellation signal. With 10 elements interconnected in parallel, the reduction was 16.5 dB and 13.5 dB respectively. These finding were confirmed with measurements using Sonovue® microbubbles.

Discussion and Conclusions

Conclusion: The results demonstrate the need for compensation methods in nonlinear imaging and the opportunity to use CMUT with traditional harmonic imaging techniques.

5K. Acoustic Wave Sensors

Hall 2B

Wednseday, November 5, 2008, 4:30 pm - 6:00 pm

Chair: **Pierre Khuri-Yakub;**
Stanford University, CA, USA.

5K-1

4:30 PM **SAW Wireless, Passive Sensor Spread Spectrum Platforms**

Donald Malocha; *Univ. of Central Florida, SEECS, Orlando, Fl, USA.*

Background, Motivation and Objective

SAW technology has been identified as a possible solution for NASA's long term needs for ground, space-flight, and space-exploration sensor requirements. SAW has many unique advantageous over possible competing technologies, which include the following properties: passive, radiation hard, operable over wide temperature ranges, small, rugged, inexpensive, and identifiable. NASA has recently supported several approaches to achieve SAW passive wireless sensors; one approach being orthogonal frequency coding (OFC). There has been a tremendous effort in a plethora of sensors, which include physical, chemical and biological. However, a complete wireless, passive, coded SAW sensor platform and system has not been implemented for demanding space applications. The purpose of this paper is a focus on the platform and system constraints; not on any particular sensor. For remote sensing, the device and system platform is the essential element which enables the sensor information to be obtained.

Statement of Contribution/Methods

This paper's emphasis will be on multi-frequency coded, orthogonal frequency coded, and single frequency CDMA sensor tags. The parameters of interest are device insertion loss, system range, code diversity, center frequency and bandwidth. It will be shown that multi-frequency and OFC tags offer the possibility of much greater ranges and better code collision properties than the more conventional commercial SAW CDMA RFID tags. Reflectors can have less than 1 dB insertion loss, and when using unidirectional transducers, overall SAW device loss can be less than a few dB. Code collision interference can be minimized by using several techniques, which include both frequency and time diversity. Antenna size and gain are key parameters for small foot print and achievable range. By using spread spectrum techniques, processing gain can be encoded in the reflectors, the transducer, or both. The paper will present the fundamental engineering equations which define the system range, receiver dynamic range, minimum detectable signal and processing gain when used in a software-definable correlator receiver system. The theoretical system performance of both the multi-frequency and single frequency SAW RFID sensor will be discussed.

Results

Results will be shown for a prototype 250 MHz software defined SAW spread spectrum OFC radio system. The OFC SAW devices are used as temperature sensors, and the device and system operational parameters and performance will be presented. Results to date have shown sensor operation over approximately 3 meters using +10 dBm output power. These preliminary results will be compared to the theoretical predictions based on the current SAW sensor and system design.

Discussion and Conclusions

The current results verify the device platform approach and system operation at 250 MHz. Based on the analysis and measured results, predictions will be made for SAW wireless, passive OFC-type sensor range and operational parameters.

5K-2

4:45 PM **Wireless Multiple Access Passive Coded Sensor System**

Evan Dudzik, Ali Abedi, Donald Hummels, **Mauricio Pereira da Cunha;** *University of Maine, Electrical Engineering, Orono, ME, USA.*

Background, Motivation and Objective

Small wireless high-performance sensors are becoming highly desirable components for many modern technological applications, such as structural health monitoring, gas and oil exploration, environmental monitoring, agriculture and aerospace. Surface acoustic wave (SAW) sensors offer important capabilities, such as: passive wireless operation, small size, attachment to movable parts, low cost, and operation in harsh environments (high temperature, pressure, and hazardous chemicals). In this work, a new wireless differential-delay quasi-orthogonal coded SAW passive sensor and interrogation system is reported, which targets concurrent assessment capability of multiple sensors.

Statement of Contribution/Methods

A novel wireless sensor and identification system based on passive SAW devices is reported. Quasi-orthogonal pseudo-noise codes, which provide multiple access capability, were implemented using a differential delay line scheme on miniaturized passive sensor devices. These new devices permit the tracking of delay and/or operating frequency, providing flexibility for combining sensing and temperature compensation. A wireless sensor (center) and the corresponding transceiver interrogation unit (top left) have been designed, fabricated, and tested at the University of Maine. The system combines for the first time a differential-delay SAW device with quasi-orthogonal direct sequence spread spectrum (DSSS) coding.

Results

Search algorithms were developed to arrive at a set of 16 codes, 31 chips in length, suitable for sensor implementation (top right). Wireless interrogation with the matched coded sequence verified the predicted response at distances of at least several feet. The matched filter correlation processing allows the extraction of the sensor response (bottom) even when the arriving signal is below noise, due to the spread spectrum processing gain. As proof-of concept, the system was used for temperature sensing. The measured differential delay and operating frequency from 30 to 100°C are consistent with the expected temperature response of the YZ-LiNbO3 substrate used, around 90 ppm/°C.

Discussion and Conclusions

The new wireless SAW passive device system reported in this paper enables concurrent access to multiple sensors, opening new possibilities for physical, chemical or biological sensor applications.

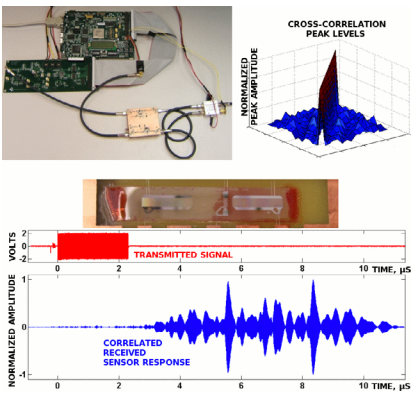

Wednesday Oral

5K-3

5:00 PM **A study of Love wave devices with SU8 guiding layer**

Ye Chen, Jie Zhao, Honglang Li, Shitang He; *Institute of Acoustics,Chinese Academy of Sciences, Beijing, China.*

Background, Motivation and Objective

Love waves are promising modes for a liquid sensor since Love waves do not have elastic coupling loss in liquids. Low propagation loss and high sensitivity can be reached simultaneously. In recent years, guiding layers usually consist of polymer layers (e.g. polymethylmethacrylate, PMMA, photoresist), rigid layers (e.g. SiO2). Polymer layers provide the advantage of higher sensitivity because of their lower shear wave velocity, but suffer from higher acoustic loss. Rigid layers have excellent elastic and thermal properties, but thick layers are required which results in lengthy deposition techniques.

Solidified SU8, as one kind of polymer, has low shear velocity (about 1/3 that of SiO2), while its rigidness is almost same with SiO2. SU8 can be spun on the substrate to a desired thickness. So SU8 is very appreciated for Love wave sensor.

Statement of Contribution/Methods

Firstly, the love wave dispersion equation is derived by solving elastic field equations with given boundary conditions. The mass sensitivity is calculated by perturbation theory. Then this method is applied in the analysis of love wave propagation in SU8/ST-90X cut QT structure. The relationship between mass sensitivity, phase velocity and relative guild layer thickness is given.

Results

Love wave sensors employing SU8 guiding layer are fabricated. The normalized layer thickness is 0~12.5%. The experimental results show that the SU8-based sensor can reach almost the same sensitivity with SiO2 while the normalized guild layer thickness, about 2.75% is less than that of SiO2. Its insertion loss is about -11dB when the split-finger interdigital transducers is used.

Discussion and Conclusions

A new guild layer, SU8, is presented to realize high mass sensitivity and loss propagation loss simultaneously. Corresponding theoretical analyze are derived by solving elastic field equations, which results are demonstrated by experimental results.

Wednesday Oral

5K-4

5:15 PM **Application of Lithium Niobate Etch Stop Technology to SAW Pressure Sensors**

Andrew Randles[1], Jan Kuypers[2], Masayoshi Esashi[1], Shuji Tanaka[1]; *[1]Tohoku University, Sendai, Miyagi, Japan, [2]University of California at Berkeley, USA.*

Background, Motivation and Objective

A passive wireless pressure sensor is useful for long-term pressure measurement in moving objects, such as car tires. To date, SAW-based pressure sensors have been developed by other researchers [1] and us [2]. For these pressure sensors, the sensing diaphragm thickness is determined by the thickness of the lithium niobate (LN) wafer used. The diaphragm wafer and a base wafer are bonded by a non-hermetic adhesive [1] or hermetic direct bonding [2] to form a reference pressure cavity. Because of the very fragile characteristics of LN, the minimum thickness of the diaphragm wafer is limited; e.g. 100 µm for wafer handling. As a result, a large diaphragm area is needed for the required sensitivity, making size and cost reduction of the sensor difficult.

Statement of Contribution/Methods

We have developed a novel thermal inversion etch stop technology to fabricate thin diaphragms in LN wafers [3]. Thermal inversion produces a layer with the opposite poling direction with respect to the bulk crystal. Because the etch rate of LN strongly depends on the polarization direction, the inversion layer acts as an etch stop to HF-based wet etching. The etched wafer with the diaphragms is bonded to another LN wafer using Au-Au bonding, resulting in reference pressure cavities. SAW transducers are then fabricated on top of the wafer with the diaphragms. As the external pressure changes, the shape of the diaphragm changes, causing a change in the time delay for the reflector on the other side of the diaphragm.

Results

We have demonstrated the fabrication of diaphragms and reference pressure cavities using 128° Y cut LN wafers. Diaphragms 1.5 mm × 1.3 mm and smaller with thickness of 10–40 µm were fabricated. A typical cross section of a sample is shown in the figure. It can be clearly confirmed that etch stop occurred at the boundary between the bulk crystal and the inverted layer.

Discussion and Conclusions

The core structure of the SAW passive pressure sensor was fabricated in 128° Y cut LN wafers using the thermal inversion etch stop and Au-Au bonding technology. The thickness of the sensing diaphragm was determined by the thermal inversion conditions. The thin diaphragms make it possible to realize smaller, more sensitive pressure sensors.

References

[1] Lee et al., Jpn. J. Appl. Phys. 45 (2006) 5974

[2] Hashimoto et al., IEEJ Trans. SM 128 (2008) 230

[3] Randles et al., Jpn. J. Appl. Phys. 46 (2007) L1099

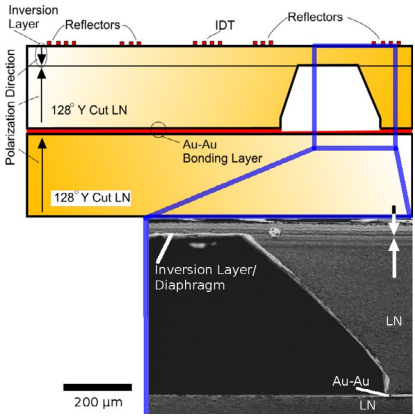

5K-5

5:30 PM **Development of Ball SAW Gas Chromatogram System for Analysis of Hydrocarbon and Alcohol**

Shingo Akao[1], Masanori Sakuma[1], Kentaro Kobari[1], Yutaro Yamamoto[1], Kazuhiro Noguchi[2], Toshihiro Tsuji[1], Noritaka Nakaso[2], Kazushi Yamanaka[1]; *[1]Tohoku University, Japan, [2]Toppan Printing Co. Ltd, Japan.*

Background, Motivation and Objective

For energy exploitation with natural gas and fuel cells, hydrocarbon and alcohol sensors are essential. The gas chromatograph (GC) is frequently used for the multiple-gas sensing but is not handy.□@We have developed the ball surface acoustic wave (SAW) sensor, where SAW with a specific width is naturally collimated and makes multiple roundtrips without diffusing by the diffraction. The collimated SAW has a longer propagation length and higher sensitivity for the velocity and attenuation change. Based on this excellent property, we propose a highly sensitive handy multiple-gas sensor.

Statement of Contribution/Methods

Fig. 1(a) shows dual channel ball SAW GC using two kinds of micro electromechanical systems (MEMS) columns and ball SAW sensors. We detect lower hydrocarbons, higher hydrocarbons and alcohols by using a open tube (OT) column coated with 5% phenyl 95% methylpolysilarylene and a packed column with styrenedivinylbenzene (SDB) micro beads.

Results

Fig. 1(b) shows separation of a higher hydrocarbon (tridecance) by a OT-MEMS column. The sensitivity of amplitude response of ball SAW sensor with a PIB film was 40 times higher than that of a commercial thermal conductivity detector (TCD). Separation of lower hydrocarbons (methane and ethane) was achieved by a micro packed column (silica capillary), and the signal was obtained with leaky loss of a ball SAW sensor without sensitive film.

Discussion and Conclusions

We succeeded in separation of lower- and higher-hydrocarbons with two kinds of columns. The micro packed column is being replaced by a packed MEMS column. It is therefore concluded that a high performance handy GC is feasible.

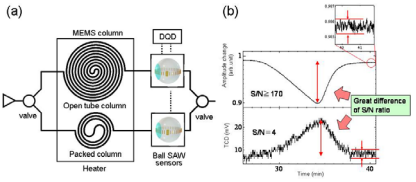

Fig. 1 Dual channel ball SAW GC (a) Concept (b) Excellent sensitivity of ball SAW sensor to tridecane.

5K-6

5:45 PM **Electrically Isolated Thickness Shear Mode Liquid Phase Sensor for High Pressure Environments**

Jeffrey Andle, Reichl Haskell, Maly Chap; *Vectron, Intl., SenGenuity Div., Hudson, NH, USA.*

Background, Motivation and Objective

There is a significant market opportunity for simple and reliable viscosity sensors capable of operating in a variety of harsh environments including extremes of temperature and pressure. As yet there is no viable sensor that offers the cost and reliability requirements of most high volume or high performance applications.

It is important that sensors be able to completely isolate various undesired interactions between the sensor and the environment from the desired response. For sensors intended to monitor a physical parameter or a mass loading response, the existence of an electrical or capacitive interaction with the environment leads to an interfering sensor response.

Prior methods of isolating a piezoelectric sensor's electronics from the environment employed the piezoelectric crystal as a membrane. These sensors are limited as to the operating pressures in which they can operate.

A method is desired that will allow a fully immersed sensor with the entire sensing surface electrically shielded and the electrical connections capable of complete isolation.

Statement of Contribution/Methods

The successful approach employs a symmetric composite resonator having the positive electrode(s) located between two "identical" piezoelectric plates and an essentially continuous ground plane surrounding the outer surfaces. The structure employed herein uses the monolithic crystal filter. Construction details are presented.

Results

Previous data on quartz and new data for langasite describe the fracture statistics of such standard membrane structures and allow the designer to estimate pressure limitations, motivating this project. In the interesting case of a viscometer, a figure of merit describing the product of the peak pressure and the peak measurable viscosity is obtained.

The proposed sensor is constructed and offers an insertion loss of ~6dB in air compared to ~3-6 dB for the simple MCF sensor. The excess losses are attributed to the "glass" bonding layer of the composite.

The sensor was immersed in a hydraulic press and measured with a network analyzer as the pressure was varied from ~30 PSI to ~10,000 PSI (~0.2 to 70 MPa). The sensor responds to real changes in density-viscosity product and is fully functional and reversible.

Insertion loss of the immersed composite sensor varied from 16 dB at low pressure to 22 dB at 10,000 PSI (70 MPa) compared to a range of 23 dB to 28.5 dB from ambient to 7,000 PSI for the fully immersed single-plate MCF. The single-plate MCF exhibited frequency decrease whereas the composite device increased in frequency, suggesting bond layer compression.

Discussion and Conclusions

A sensor geometry and prototype are presented that allow the complete electrical isolation of the sensor from its environment while offering the immersion mode of operation. Data is taken in a hydraulic press to the limits of the system with no deterioration in sensor performance. Further innovation in methods of bonding the plates and in packaging are needed.

6K. Medical Arrays

Hall 2C

Wednseday, November 5, 2008, 4:30 pm - 6:00 pm

Chair: **L. Scott Smith;**
GE Global Research, USA.

6K-1

4:30 PM **Comprehensive Design Considerations for 2D Matrix Arrays**

Xuan-ming Lu; *Siemens, USD, Issaquah, WA, USA.*

Background, Motivation and Objective

Solid state 2D transducers for real time 3D volume imaging are gradually becoming more prevalent in medical ultrasound. To design an optimal 2D matrix array, we need to understand some of fundamental differences from a 1D array. The 2D element is significantly smaller in size, therefore extremely high in impedance (>10 kΩ). A 2D array also has large number of elements (>1000), which is beyond current system and cable size limits. It is essential to have transmitter and receiver electronics (ASIC) very close to the elements (preferably directly underneath each element). To some extent, the element impedance can be modified by selecting the proper piezoelectric material (e.g. PZT or PMN-PT single crystal). The preamplifier characteristics (e.g., input impedance, noise) should be also designed around high element impedance to improve receiver SNR. For a typical 2D array, one approach is an ASIC layer (silicon) on the backside and signal ground layer on the front side of the diced elements. How these layers contribute to mechanical cross talk between elements needs to be evaluated.

Statement of Contribution/Methods

A 4MHz and 200x200um pitch 2D matrix was modeled with 1D simulation tools (equivalent KLM model) for both low and high preamp cases and compared transmit efficiency and receive SNR for PZT5H, high dielectric PZT and PMN-PT single crystal.

To understand mechanical cross talk of top (polyimide and copper for ground) and the bottom (silicon for ASIC) solid layers on diced elements, a FEM tool (PZFlex) was used. We modeled thin and thick top and bottom layers on a range of element pitches (0.5λ to 1.5λ) arrays.

Results

The high dielectric PZT is more sensitive in transmitting pressure than PZT5H and PMN-PT single crystal. Single crystal has advantages in receiver SNR if preamplifier impedance is much higher than the element and there is none or minimum parasitic capacitance. In case of a low input impedance preamp or more realistically some parasitic capacitance (e.g., 4pF) existing, the high dielectric PZT becomes better suited.

The cross talk level is related to layer thickness with some frequency dependency. Maintaining low aspect ratios (<0.4) by sub-dicing elements can reduce lateral modes, therefore improving directivity. However, these effects are degraded when the top layer becomes too thick. The element directivity may be improved by uneven dicing (i.e., wider major kerf and narrow minor kerf) for large pitch array. The top metal layer causes echo reverbs and spectrum ripples, which somehow were more severe in the small pitch array than in the larger pitch array.

Discussion and Conclusions

Based on our simulation case, the high dielectric PZT which reduce element impedance appears to be favorable for 2D matrix array performance than PZT5H and single crystal. Low impedance preamp seems a better choice when parasitic capacitances present and also it is less sensitive to parasitic capacitance variations than high input impedance preamp.

6K-2

4:45 PM **A 5-Plane CMUT Array for Operator-Independent Carotid Artery Screening: Initial Results**

Xuefeng Zhuang, Der-Song Lin, Jessica Faruque, Omer Oralkan, Sandy Napel, R. Brooke Jeffrey, Butrus T. Khuri-Yakub; *Stanford University, USA.*

Background, Motivation and Objective

CMUT arrays can be used for color Doppler detection of peak blood velocity (PBV), which is correlated with carotid stenosis. Taking advantage of the ease of array fabrication with the CMUT technology, we are developing an operator-independent color Doppler PBV detection method, using five parallel 1D CMUT arrays on the same silicon substrate.

Statement of Contribution/Methods

We propose to use 5 parallel 1D CMUT arrays on a single substrate with asymmetric lenses to obtain 5 parallel B-mode and color flow images of the carotid artery. Custom-built board-level electronics interfaces the 5-plane array with a commercial imaging system. In the elevation direction asymmetric acoustic lenses steer the acoustic beam at fixed angles for color Doppler measurements. We developed custom software that automatically computes the vessel trajectory, Doppler angles and angle-corrected peak velocities for the 5-plane transducer array.

Results

5-plane CMUT arrays are designed and fabricated using the SOI wafer bonding technique. Each 1D array consists of 132 elements (128 active + 2 dummy elements on both ends for improved array uniformity), each 200 μm by 4 mm in size. The target center frequency is 7.5 MHz. The array size and frequency are chosen to match with a commercial single-plane ultrasound probe, which we use for acquiring data to test our automatic screening software. In pulse-echo operation in immersion, a center frequency of 7.1 MHz, and a fractional bandwidth of 98% were measured for the fabricated arrays. The peak-to-peak output pressure at the transducer surface was 1.6 MPa when the CMUT was biased at 80 V, and excited with a 50-ns 100-V pulse. Studies of PDMS coating on CMUT surfaces showed minimum impact on the acoustic characteristics of the transducer. It is also shown that an offset lens design can be used to obtain the fixed elevational beamsteering. A hemi-cylindrical PDMS lens was used on a small CMUT as a proof of concept.

Discussion and Conclusions

The 5-plane CMUT array showed characteristics suitable for Doppler detection of PBV. Elevational beamsteering is shown to be feasible using a PDMS lens. Once the color Doppler data is obtained, the in-house software can determine the PBV automatically and accurately. Ongoing work includes: 1) implementation of interface electronics, 2) developing a method for reliable and repeatable formation of asymmetric acoustic lenses on the CMUT arrays.

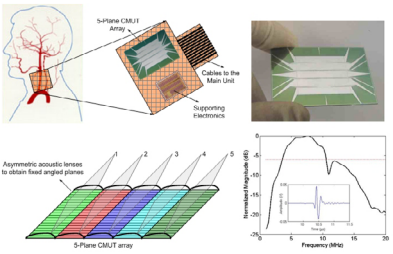

Wednesday Oral

6K-3

5:00 PM **A PZT-P[VDF-TrFE] dual-layer transducer for 3-D imaging**

Jesse Yen, Chi Hyung Seo, Samer Awad, Jong Jeong; *University of Southern California, USA.*

Background, Motivation and Objective

The difficulties associated with fabricating and connecting 2-D arrays with large numbers of elements have limited the development these arrays with more than 5,000 elements. However, 2-D arrays for rectilinear imaging of targets such as the breast, carotid artery, and musculoskeletal system require 128 x 128 = 16,384 to 256 x 256 = 65,536 elements.

To simplify transducer design and system requirements, we propose a PZT-P[VDF-TrFE] dual-layer transducer array design which uses perpendicular 1-D arrays for 3-D imaging of targets near the transducer. This transducer design reduces the fabrication complexity and the channel count.

Statement of Contribution/Methods

To demonstrate feasibility, we constructed a 4 cm × 4 cm prototype dual-layer array which consists of 256 elongated linear array elements with 145 micron pitch in each layer. The transmit layer is PZT-5H and the receive layer is P[VDF-TrFE] copolymer. The PZT elements were diced, but the copolymer elements were not diced. Overly high crosstalk is not expected in the copolymer layer since this material has low lateral coupling. The elements in the PZT layer are perpendicular to the elements in the copolymer layer. The PZT layer performs transmit beamforming in azimuth while the copolymer layer does receive beamforming in elevation. Since the copolymer has an acoustic impedance between tissue and PZT, it is able to serve as a rudimentary matching layer during transmission. To minimize reverberations in the acoustic stack, a 9.3 MRayl tungsten-epoxy backing was used.

Results

Pulse-echo measurements showed a -6 dB fractional bandwidth of 80% with a center frequency of 4.8 MHz. At 5 MHz, the nearest neighbor crosstalk of the PZT array was -30.4 ± 3.1 dB and -28.8 ± 3.7 dB for the PVDF array. After interfacing this dual-layer transducer with the Ultrasonix Sonix RP system and performing offline 3-D beamforming, we obtained volumes of axial nylon wire targets and an 8 mm diameter cylindrical anechoic cyst phantom. The theoretical lateral beamwidth was 0.51 mm compared to the measured beamwidth of 0.65 mm and 0.67 mm in azimuth and elevation respectively. A pair of nylon wire targets with 0.5 mm axial separation was distinguishable. Azimuth and elevation B-scans of the cyst show the short and long axes of the cyst respectively. Another long-axis view of the cyst is seen, parallel to the transducer face, in the C-scan.

Discussion and Conclusions

We have successfully prototyped a dual-layer transducer for 3-D imaging of targets near the transducer. Experimental results showed good agreement with simulation results. Future work will involve building cylindrical versions for this dual-layer design for 3-D transrectal imaging of the prostate.

6K-4

5:15 PM **Piezocomposite and CMUT Arrays Assessment Trough In Vitro Imaging Performances**

Mathieu Legros, Guillaume Férin, Cyril Meynier, Rémi Dufait; *Vermon S.A., Tours, France.*

Background, Motivation and Objective

Probes are well-known to be a capital element for ultrasound image quality. Many parameters can be tuned to optimise electro-acoustical and acoustical performances of Capacitive Micromachined Ultrasound (CMUT) or piezocomposite transducers. Nevertheless, the effects on image quality of these performances are not so well identified. To overcome such a limitation, we developed a quantitative method for image quality assessment. A set of algorithms was developed to assess in vitro images from CMUT or piezoelectric probes. The goal of this investigation is to link the electro-acoustical, acoustical performances and transducer parameters to the imaging performances.

Statement of Contribution/Methods

A CMUT linear array for vascular purpose was investigated and fully packaged with electronic preamplifier boards integrated. Then an equivalent probe with piezocomposite technology is realized. The design is done in regard to the geometric characteristics and to the acoustic response of the micromachined probe. Electro-acoustical measurements are then realized in the closest conditions for both probes.

Using an ultrasound imaging platform, B-mode images from a tissue mimicking phantom are acquired with a fixed set-up. Images assessment is then performed with our own computerized tool previously validated on simulated images. The algorithms take into account imaging parameters such as contrast, resolutions and signal to noise ratio.

Results

All image properties were analysed with respect to the probe performances, thus impact of electro-acoustical parameters on image quality can be identified for both transducers.

Piezocomposite probe demonstrates an axial resolution of 0,6 mm due to a wide bandwidth (6MHz centred, 90% at –6dB in pulse-echo) and a maximal image penetration of 70 mm thanks to high sensitivity. Lateral resolutions close to 1,5 mm and contrast to noise ratio are limited by the radiation field relative to piezoelectric transducers.

Despite a close electro-acoustical response, CMUT probe exhibits different image properties because of its principle of operation. Combination of broad frequency response and large radiation field leads to other imaging performances which will be discussed.

Discussion and Conclusions

Our study has provided additional and complementary informations about relations between image quality and electro-acoustical performances of transducers. Results of this work can subsequently be used to tune transducers parameters for ultrasound imaging improvement and to develop novel imaging modalities.

6K-5

5:30 PM **Recent results using a 256 × 256 2-D array transducer for 3-D Rectilinear Imaging**

Chi Hyung Seo, Jesse T. Yen; *University of Southern California, USA.*

Background, Motivation and Objective

In previous work, we presented initial experimental results using a 256 × 256 2-D array with row-column methods. The main benefits of this design are a reduced number of interconnects, a T/R switching scheme with a simple diode circuit, and an ability to perform transmit beamforming in azimuth and receive beamforming in elevation for volumetric imaging of targets near the transducer. In this paper, we present 3-D images of axial wires embedded in a clear gelatin phantom and of an 8 mm diameter cylindrical anechoic cyst phantom acquired from a new 256 × 256 2-D array transducer.

Statement of Contribution/Methods

To fabricate this 2-D array transducer, a 40 mm × 40 mm x 600 um wafer of PZT was diced in both directions and the kerfs were filled with Epotek 301. Next, any excess epoxy was lapped away and gold electrodes were sputtered on the top side. The PZT was then flipped over and lapped to the final desired thickness near 300 um. After resputtering the electrodes, they were scratch diced to create row and column electrodes. After interfacing this 2-D array transducer with an Ultrasonix Sonix RP system and performing off-line 3-D beamforming, we obtained volumes of axial nylon wire targets and an 8 mm diameter cylindrical anechoic cyst phantom.µ

Results

The final dimension of a transducer was 40 mm × 40 mm × 300 μm. The series resonant impedance was 120 Ohms at around 5 MHz. At 5 MHz, the average nearest neighbor crosstalk was -25 dB. We successfully acquired 3-D volumes of 70 x 70 x 70 mm gelatin phantoms containing 5 pairs of nylon wire targets with axial separation of 0.5, 1, 2, 3, and 4 mm and of an 8 mm diameter cylindrical anechoic cyst phantom. We display the azimuth and elevation B-scans as well as the C-scan. The cross-section of the wires and cyst are visible in the azimuth B-scan while the long axes can be seen in the elevation B-scan and C-scans. The pair of wires with 1 mm axial separation is discernible in the elevational B-scan while all the pairs of wires were distinguishable in the short-axis B-scan. Using a single wire from the axial wire target phantom, the measured lateral beamwidth was 0.69 mm and 0.72 mm at 33 mm dept in receive beamforming and transmit beamforming respectively compare to the theoretical beamwidth of 0.52 mm. The dimensions of the acquired volumes were 40 (azimuth) × 40 (elevation) × 45 (axial) mm.

Discussion and Conclusions

We have successfully acquired volumes of axial wire targets and anechoic cyst phantoms using a 5 MHz 256 x 256 2-D array. The array was made using 1-3 composite fabrication process on each side of the transducer. The future work includes obtaining 3-D images of in-vitro and excised tissue experiments.

Wednesday Poster Sessions

P3A. Tissue Characterization - Technologies

2nd and 3rd Floor Foyers

Wednseday, November 5, 2008, 3:00 pm - 4:30 pm

Chair: **James Miller;**
Washington University in Saint Louis, USA.

P3A023-01

Real-time cardiac 3D strain assessment in 3D echocardiography using a state estimation approach

Fredrik Orderud[1], Gabriel Kiss[2], Stian Langeland[3], Espen W. Remme[4], Hans G. Torp[2], Stein I. Rabben[3]; *[1]Norwegian Univ. Science and Technology (NTNU), Dep. Computer Science, Trondheim, Norway, [2]Norwegian Univ. Science and Technology (NTNU), Dep. Circulation and medical imaging, Trondheim, Norway, [3]GE Healthcare, GE Vingmed Ultrasound AS, Oslo, Norway, [4]Rikshospitalet University Hospital, Oslo, Norway.*

Background, Motivation and Objective

Current technology for analysis of myocardial strain is limited to 2D analysis. The advent of 3D ultrasound technology has enabled rapid acquisition of volumetric images of the heart, which can enable tracking of the full 3D myocardial deformation field. Several approaches for strain estimation in 3D ultrasound data have been proposed over the last years. Most approaches are, however, computationally intensive and require manual initialization.

Statement of Contribution/Methods

In this paper, we extend a framework for tracking of deformable subdivision surfaces in 3D echocardiography with speckle-tracking measurements. 3D tracking is performed using an extended Kalman filter to update the subdivision surface based on displacement vectors from 3D block-matching in the myocardium. The surface is initialized by using edge-detection to align the model to the endocardial boundary, making the whole process fully automatic.

Results

Tracking is demonstrated in a 3D echocardiography simulation of an infarcted ventricle. Figure 1,2,3 shows myocardial displacement vectors from end-diastole to end-systole of 0.159 +/- 0.941 mm, 0.232 +/- 0.992 mm and -0.278 +/- 1.27 mm (mean difference +/- 2STD) respectively for azimuth/X, elevation/Y and depth/Z. Figure 4 shows estimated and ground-truth end-systolic area strain.

Discussion and Conclusions

A new method for 3D cardiac strain estimation using a combination of edge-detection and 3D block matching in a Kalman filter framework has been presented. The proposed method fully automates the process of initialization and tracking, and is capable of operating in real-time due to its high computational efficiency. Credible tracking results were achieved, with the infarcted region correctly identified. Tracking in in-vivo data has also given promising results.

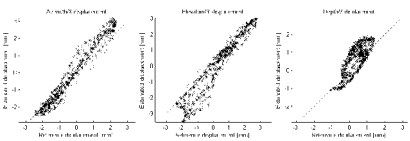

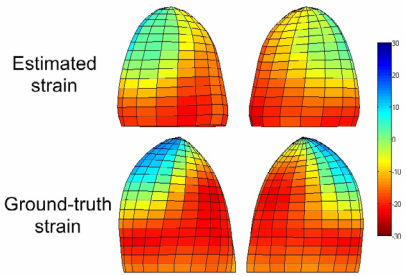

Wednesday Poster

P3A024-02

Parametric Imaging of Specular Reflections and Diffuse Scattering of Tissue from Multi-Directional Ultrasound Echo Signal Data

Michael Vogt, **Jörn Opretzka,** Helmut Ermert; *Ruhr-University Bochum, Dept. of Electrical Engineering and Information Technology, Bochum, Germany.*

Background, Motivation and Objective

In ultrasonic tissue characterization, quantitative parameters are extracted from echo signal data in order to classify different types of tissue. In this paper, an approach for the extraction of parameters for the differentiation and characterization of specular reflections and diffuse backscattering from multi-directional ultrasound echo signal data is presented and evaluated.

Statement of Contribution/Methods

Spatially resolved, tissue-describing parameters are calculated by analyzing the envelope of echo signals from different insonation angles. The echo signal amplitude is largely independent from the insonation angle for diffusely scattering point-like tissue structures. For specular reflections, which originate from spatially extended boundaries between tissue structures, the amplitude shows a maximum at the insonation angle perpendicularly to the boundary and decreases with increasing angular deviation. After scan-conversion of acquired echo signal frames, the echo signal amplitude at each pixel in the axial / lateral imaging plane is analyzed as a function of the insonation angle. Statistical first-order parameters (MN: mean, SD: std. deviation, MX: maximum, SK: skewness) are directly calculated from this data. Further parameters (PK: peak value, DR: decay rate, PP: peak position) are derived from fitted model functions. Calculated quotients SD/MN, MX/MN, PK/MN and DR/PK are amplitude-invariant measures to distinguish between specular reflections and diffuse backscattering. The centroid of the amplitude data and the parameters SK and PP are measures for the spatial orientation of specular reflectors in the imaging plane. This approach has been evaluated by means of phantom and in vivo measurements on skin with a 20 MHz high-frequency ultrasound system for limited-angle (up to +/-30°) echo-measurements with a single element transducer (15 mm focus length, 24° aperture angle).

Results

Results of measurements on a phantom (plastic tube surrounded by speckle) show that the proposed parameters SD/MN, MX/MN, PK/MN and normalized DR/PK enable to distinguish between specular reflections and diffuse scattering. From centroid, SK and PP parameter images, the surface orientation of the specular reflecting tube can clearly be extracted. In vivo parameter images show that specular reflections inside the skin, for example at scar tissue and at the border between the dermis and the subcutaneous fat, can be detected and differentiated from their surrounding based on the proposed parameters. Furthermore, spatial compound images with an axial and lateral resolution of 76 µm and 170 µm, respectively, are reconstructed.

Discussion and Conclusions

The proposed multi-directional parametric imaging approach has proven to deliver valuable information about the spatial composition and orientation of tissue formations.

Wednesday Poster

P3A025-03

50 MHz Ultrasound Characterization of Colitis on Rats, in vitro

Monica Soldan[1], Paulo Silva[2], Alberto Schanaider[2], Joao Machado[3]; *[1]Clementino Fraga Filho University Hospital - Federal University of Rio de Janeiro, Division of Gastroenterology, Endoscopy Unit, Rio de Janeiro, RJ, Brazil, [2]School of Medicine, Federal University of Rio de Janeiro, Department of Surgery-Center of Experimental Surgery, Rio de Janeiro, RJ, Brazil, [3]COPPE/Federal University of Rio de Janeiro, Biomedical Engineering Program, Rio de Janeiro, RJ, Brazil.*

Background, Motivation and Objective

There are important clinical applications for imaging methods, with sub-millimeter or microscopic resolution, on the visualization of superficial structures and structures accessible by endoscopic means. Ultrasound biomicroscopy (UBM) uses high frequencies and has compatible optical microscopic resolution. It is employed for medical and biological purposes including ophthalmic, dermatological and intravascular imaging in humans, mouse embryonic development and tumor biology. Literature reports on UBM characterization of intestinal wall are not found. This study objective is the high frequency ultrasound characterization of an induced colitis that mimics the inflammatory bowel disease in rats, an important animal model to study mucosa inflammation pathogenesis on this disease and used in pre-clinical studies of drug treatment.

Statement of Contribution/Methods

The present work contributes with measurements of acoustic parameters, at 50 MHz and important for image interpretation, of colitis. The measurement setup consisted of an UBM system using a focused 50 MHz PVDF transducer (f-number = 1.5, focal distance = 4.4 mm, -6 dB bandwidth of 31.2 MHz) and a temperature controlled micropositioned tissue cell. Colitis was induced on twenty Wistar rats, by 2,4,6-trinitrobenzene sulfonic acid (TNBS) mixed with ethanol at 30%. Colonic samples (n=38) obtained one week after induced colitis, confirmed by colonoscopy before necropsy, were placed on a flat sapphire plate with a 5x5 mm tissue fragment covered by a PVC membrane (9 µm in thickness) and immersed in saline at 37°C. The UBM scanner provided overview images of the sample microstructure, resulting in accurate targeting of homogeneous tissue regions for quantitative analysis. RF signals, collected over an 8x8 matrix with 50 µm separation, resulted from reflections at the membrane and sapphire face plus backscattering from tissue. They were amplified, digitized at 250 Ms/s, and used to calculate the speed of sound (c), the attenuation (α) and backscattering (μ) coefficients at 50 MHz, the exponential frequency dependence of the attenuation coefficient (γ) MHz and the integrated backscattering coefficient (IBC) as a function of tissue depth.

Results

Mean (±1 se) results are: 1624.90(±20.21) m/s for c; 5.12(±0.30) dB/mm for α; 3.26(±1.03)x10^-3 1/sr×mm for μ and 1.63 (±0.10) for γ. IBC, measured across the colon wall (n=4), ranges from 10^-3 to 10^-2 1/sr×mm, with the highest IBC values found in the submucosa layer.

Discussion and Conclusions

The result for speed of sound is similar to that of human sclera found in the literature. Results for attenuation and backscattering coefficients are in the same range of literature reports for human sclera and ciliary muscle, respectively. IBC plots allowed for ultrasound scattering quantification of the mucosa, submucosa and muscular layers for TNBS colitis.

P3A026-04

Ultrasound backscattering by three-dimensional distributions of aggregated red blood cells: A Monte Carlo study

Ratan Kumar Saha, Guy Cloutier; *University of Montreal Hospital Research Centre, Laboratory of Biorheology and Medical Ultrasonics, Montreal, Quebec, Canada.*

Background, Motivation and Objective

It is believed that in vivo and in situ evaluation of level of red blood cell (RBC) aggregation in human blood is possible by measuring ultrasound backscattering components. Till date a number of experimental investigating protocols were designed to achieve this end. Computer simulation studies were also made simultaneously to develop insights regarding the variations of ultrasound backscattering with different RBC distributions and to interpret experimental observations. However, earlier simulation studies were either dealt with lower dimensional systems or did not consider aggregating conditions for three dimensional cases. Therefore it would be interesting to carry out a Monte Carlo study to examine behaviors of frequency dependent ultrasound backscattering coefficients (BSCs) for simulated three dimensional configurations of non-overlapping RBCs at different aggregating conditions.

Statement of Contribution/Methods

The interaction energy profile per unit area between a pair of RBCs was mimicked by a Morse potential to incorporate aggregation in the model and hence total energy between them as a function of their separation was computed by integrating that potential over the interacting surface area. The total energy of the system at one configuration was determined by summing pair potentials under periodic boundary conditions and the Metropolis algorithm was then employed to generate other configurations. Consequently, ensemble averages of frequency dependent ultrasound backscattered intensities were evaluated from those distributions. The level of aggregation was controlled by fixing depth (D) and width (b) of the Morse potential.

Results

It was noticed that BSC increased as the aggregating potential was raised and the effect was more pronounced at higher hematocrits. For example, at D=3.65µJ/m/m and 1/b=160.5/µm, BSC for aggregated particles at H=40% enhanced by 5.0 dB with respect to that of non-aggregating RBCs for an incident wave frequency of 7.5 MHz, however, at H=20% the power increase reduced to 1.0 dB. The increment of BSC was more at lower frequency than that at higher frequency for fixed D. In addition, it was found that spectral slope (SS) was varied from 4.07 to 3.67 for H=40%.

Discussion and Conclusions

Our simulation results show that the model can consistently reproduce effects of RBC aggregation on BSC and SS which were observed experimentally. Further enhancement of BSC could also be made by increasing aggregation but that was avoided here because computational time grew non-linearly with aggregating potential. In conclusion this model might be used to generate three dimensional RBC clusters with known size distribution and consequently to evaluate performance of recently developed structure factor size estimator method in the regime of physiological hematocrit.

P3A027-05

Assessment of Red Blood Cell Aggregation Using Normalized Power Spectrum of High Frequency Ultrasound

Nobutaka Saitoh[1], Hideyuki Hasegawa[2], Hiroshi Kanai[1]; [1]*Graduate School of Engineering, Tohoku University, Japan,* [2]*Graduate School of Biomedical Engineering, Tohoku University, Japan.*

Background, Motivation and Objective

Red blood cell (RBC) aggregation plays an important role in blood rheology. RBC aggregation is formed by adhesion of RBCs because electrostatic repulsion between RBCs weakens as protein and saturated fatty acid in blood increase. Excessive RBC aggregation promotes various circulatory diseases in the clinical situation, such as atherosclerosis, thrombosis and so on. The purpose of this study is to establish a noninvasive and quantitative method for assessment of RBC aggregation.

Statement of Contribution/Methods

The spectrum of nonaggregating RBCs presents Rayleigh behavior, which means that the power of scattered wave is in proportion to the fourth power of frequency. By dividing the measured power spectrum by that of echo from a glass plate, the frequency response of transmitting and receiving transducer are removed from the measured power spectrum. The normalized power spectrum changes linearly with respect to logarithmic frequency and scatterer′s effective radius can be estimated from the intercept. In non-Rayleigh scattering, on the other hand, the spectral slope decreases. Therefore, it is possible to assess the RBC aggregation from the spectral slope and intercept value.

Results

Figure 1(a) shows the normalized power spectrum of the echoes from microspheres whose average radius is 2 μm. The center frequency of the ultrasonic transducer is 40 MHz. The spectral slope and intercept were determined to be 4.56 and -33.0, respectively. In this case, therefore, the scattered echo shows Rayleigh behavior, and effective radius was estimated to be 2.3 μm. Figure 1(b) shows the spectrum of echoes from the lumen of human vein. The slope and intercept were determined to be 4.49 and -35.6, respectively. Figure 1(c) shows the spectrum echoes from the lumen of the vein which was measured after stanching the blood flow for 30 s. the spectral slope dramatically decreased to be -0.01.

Discussion and Conclusions

The effective radius of nonaggregating RBC was estimated in vivo using the spectral intercept. Furthermore, the increase of scatterer′s radius due to avascularization led decrease of the spectral slope. These results show the possibility of the proposed method for the assessment of RBC aggregation.

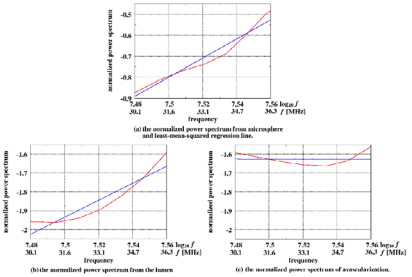

Wednesday Poster

P3A028-06

Strain Estimation with Center Frequency Correction and Reliable Displacement Selection.

Takao Suzuki, Takenori Fukumoto, Makoto Kato; *Panasonic Shikoku Electronics Co., Ltd., Yokohama, Japan.*

Background, Motivation and Objective

We have been developing the method which estimates the strain distribution in the arterial wall using ultrasound for the non-invasive diagnosis of atherosclerosis. In the previous method based on the phased tracking method, it was difficult to accurately estimate the strain distribution inside the wall because of the variation of the center frequency of the RF echo.

In this report, we propose the strain measurement method which corrects the center frequency change, selects reliable measurement points and estimates strain with only these selected displacements. We also check the validity of the new method through the experiment by using the artery-mimicking phantom.

Statement of Contribution/Methods

We prepared a homogeneous silicone cylindrical phantom (external and internal diameter is 6 mm and 10 mm, respectively) with carbon powder as scatters. The displacement and the strain were measured by the previous method and the proposed method using a linear probe with the center frequency of 7.5 MHz. With the proposed method, the strain distribution was estimated from the displacements on the reliable measurement points which were selected by magnitude and pulse width of the RF echo.

Results

The maximum displacement distribution along the radial direction of the phantom was shown in figure 1 ((a) previous method, (b) proposed method). In figure 1, the theoretical displacement is shown in a solid line. Using the proposed method, the displacement was almost corresponding to the theoretical displacement but the resolution along the radial direction was poor. The strain distribution of the phantom was shown in figure 2 ((a) theoretical, (b)previous method, (c) proposed method). In the proposed method, the accuracy of the strain estimation was clearly improved.

Discussion and Conclusions

We propose the new strain measurement method and confirmed the validity of the proposed method by means of the forementioned phantom experiment.

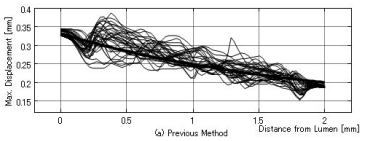

Figure 1 Maximum Displacement

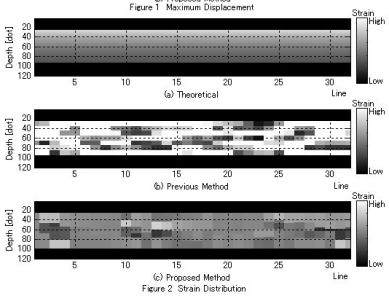

Figure 2 Strain Distribution

P3A029-07

Biomedical Application of Acoustic Microscopy - Diagnosis, Assessing Echogenecity and Biomechanics

Yoshifumi Saijo; *Tohoku University, Department of Biomedical Imaging, Sendai, Japan.*

Background, Motivation and Objective

SAM technology has been applied in medical and biological studies for 1) intra-operative pathological examinations since it does not require special staining techniques, 2) determining the origin of echo in clinical ultrasound imaging and 3) assessing the elastic properties of biological materials. In this short course, some examples of the application of scanning acoustic microscope (SAM) systems in medicine and biology are shown.

Statement of Contribution/Methods

The followings were the specifications of the acoustic microscope system. An electric impulse was generated by a high speed switching semiconductor and was used to excite a PVDF transducer with the central frequency of 100 MHz. The reflection from the tissue was received by the transducer and was introduced into a Windows-based PC via a high-speed A/D converter. The transducer was mounted on an X-Y stage with two linear servo-motors with the control by microcomputer board. Two-dimensional distributions of thickness, sound speed and attenuation were calculated and displayed by the system. Gastric cancer, myocardial infarction and atherosclerosis were involved in the series of studies.

Results

The gastric cancer tissues were classified into five groups according to their pathological findings. The values of the attenuation constant and the sound speed increased as the cellular differentiation proceeded and this increasing trend was regarded as the result of tightening of the intercellular attachment.

Four kinds of tissue elements; normal myocardium, degenerated myocardium, granulation and fibrosis, were observed in the myocardial infarction. The dB level of the interface between degenerated myocardium and fibrosis was calculated as 15.4 dB and that was identical to the dB value at the area of the scar in myocardial infarction in clinical echocardiography.

Based on the sound speed distribution of atherosclerosis, finite element meshes were generated and the finite element problem was solved for an intraluminal pressure load of 110 mmHg. The results indicated the peak stress distribution was observed in the shoulder lesion of fibrous cap.

Discussion and Conclusions

The SAM measurement of biological tissues is useful for classification of cancer tissues, determination of the origin of echo and application for assessing biomechanics in atherosclerosis.

P3B. Tissue Characterization - *In Vivo* Applications

2nd and 3rd Floor Foyers

Wednseday, November 5, 2008, 3:00 pm - 4:30 pm

Chair: **Stanislav Emelianov;**
University of Texas at Austin, TX, USA.

P3B030-01

Non-invasive staging of hepatic steatosis using Computer-Aided Ultrasound diagnosis

Johan Thijssen[1], Gert Weijers[1], Alexander Starke[2], Alois Haudum[2], Kathrin Herzog[2], Juergen Rehage[2], **Chris de Korte[3];** *[1]Radboud University Nijmegen Medical Centre, Pediatrics, Nijmegen, Gld, Netherlands, [2]University of Veterinary Medicine Hannover, Clinic for Cattle, Hannover, Germany, [3]Radboud University Nijmegen Medical Centre, Pediatrics, Nijmegen, Gld, Netherlands.*

Background, Motivation and Objective

Non-alcoholic fatty liver disease (NAFLD) is being considered a high risk factor in obesity. Assessment of liver fat content might be done by taking a biopsy, but this procedure has a high risk of complications. Last year we introduced the Computer-Aided UltraSound (CAUS) method to estimate the liver fat content non-invasively and showed its feasibility by using an animal model. A limited cohort of cows (n=12) was involved in that study. In the present, extensive study we further investigated the applicability by multiple regression and ROC analysis.

Statement of Contribution/Methods

Transcutaneous and intra-operative echographic B-mode images were obtained postpartum from dairy cows (n=151) using a convex array transducer (fc=4.2 MHz). During surgery, a biopsy was taken from the right lobe to assess the triglyceride (TG) and total fat contents in the liver and for a histopathological examination. First, the gray levels of images were calibrated to decibels relative to the background echo level in a tissue mimicking phantom. A control group of healthy cows (n=12) was used from which Automatic Gain Correction curves (AGC) for transcutaneous and intra-operative images were derived and that were applied to all images. Furthermore, abdominal wall attenuation was estimated and corrected for. Estimated echo characteristics were: mean echo level, residual attenuation coefficient and mean axial and lateral speckle size. Most of these parameters were significantly correlated to the TG. Multivariate analysis yielded a linear regression formula. This formula was used to predict the TG content for each animal. Finally ROC curves were estimated for different thresholds of TG content.

Results

Highest correlations with TG were obtained for the residual attenuation (r=0.80) and mean echo level (r=0.59). Multivariate linear regression revealed high correlation (r=0.83) of the estimated to the true TG content. Residual attenuation and axial and lateral speckle size were incorporated in the regression formula. ROC curve analysis show promising results for sensitivity (0.93), specificity (0.86), and the area under the curve (0.93) for distinguishing fatty livers from healthy livers.

Discussion and Conclusions

This study showed the feasibility of generic computer-aided ultrasound for non-invasively diagnosing, maybe even screening, of liver steatosis.

P3B031-02

A Compound Ultrasound Imaging Strategy in Carpel Tunnel Syndrome Diagnosis

Chih-Kuang Yeh[1], Ying-Jie Yue[1], Wen-Shiang Chen[2]; *[1]National Tsing Hua University, Department of Biomedical Engineering and Environmental Sciences, Hsinchu, Taiwan, [2]National Taiwan University Hospital, Department of Physical Medicine and Rehabilitation, Taipei, Taiwan.*

Background, Motivation and Objective

The diagnosis of carpal tunnel syndrome (CTS) is based on a combination of characteristic symptoms and electrophysiologic abnormalities. However, the electrodiagnostic examination remains an expensive and time-consuming procedure. Therefore, more investigators have reported on their experiences on CTS diagnosis with ultrasound image. CTS is generally attributed to external compression of the median nerve. Thus, distinguishing the median nerve shape from speckle-obscured ultrasound image provides a potential for the diagnosis of CTS. To lower the speckle interference, we propose a novel compound imaging strategy to reveal the significant signatures of median nerve.

Statement of Contribution/Methods

Figure (a) shows transverse section image of the carpal tunnel of a patient subject at the level of the pisiform bone. We observed that patient¡¦s fingers motion in ultrasound imaging deforms nerve shape and produces tissue movement. Figure (b) shows a typical image of an entire image sequence. Based on speckle decorrelation of image under different fingers motion conditions, speckle variations can be reduced by compounding technique. The primary assumption of compounding is that the ensemble average of a speckle image is the same as the incoherent average of the original object. In this study, the multi-level block matching and block sum pyramid integrated algorithms were adopted for speckle tracking and compounding between ultrasound images.

Results

The final compound image from original ten images is shown in Fig. (c). Figure (d) shows the SNR profiles along the horizontal axis. The results indicate that the efficacy of speckle reduction is clear and the positions of the two median nerve boundaries are unchanged. In particular, the internal punctuated echoes of medial nerve become more distinct.

Discussion and Conclusions

We also recruited and included 5 CTS patients and 5 controls cases to test. Ten unexperienced physicians delineated the median nerve boundaries by manual. The results show that average mean normalized true positive area overlaps between manual and reference contours are 82% and 92% in original and compound images, respectively.

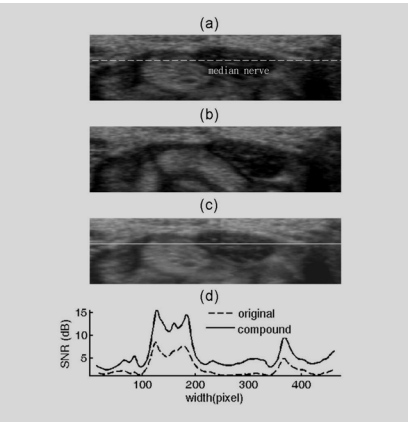

Wednesday Poster

P3B032-03

Quantitative assessment of burn degree using high frequency ultrasonic backscattered signals and parametric images

Yi-Hsun Lin, Chih-Chung Huang, Shyh-Hau Wang; *Chung Yuan Christian University, Biomedical Engineering, Chung Li, Tao Yuan, Taiwan.*

Background, Motivation and Objective

This study is to extensively assess the degree of burn tissues using both ultrasonic backscattered signals, collected from a 50 MHz high frequency ultrasound system, and parametric image.

Statement of Contribution/Methods

Animal experiments were carried out using the Wistar rats, which were anesthetized and a part of tissue in their back was burned with a piece of 100oC brass plate. Different degrees of burn tissues were achieved by contacting rats' skin directly with the heated brass plate for various durations, including 5, 10, 15, and 20 seconds. For each measurement, the collected signals covered an area of 6 (width) x 0.4 (depth) mm in the wound tissue, where each ultrasonic A-line signal was digitized at 500 MHz sampling frequency. The m parameter-based parametric image, calculated from each sub-window (3x3 pulse length) in the scanned image sequentially, was implemented to better address the spatial variation of burn tissues.

Results

The strengths and statistical parameter of backscattered signals associated with the region of interest (ROI) in the burn tissues showed that both decrease exponentially with the increase of burn degrees. The integrated backscatter of normal tissues decreases from -87 dB to -117 dB which corresponds to the tissue been burned for 20 seconds. Furthermore, those of m parameter, a statistical analysis of backscattered signals, tend to decrease from 0.6 to 0.2 indicating that envelops of backscattered signals vary toward pre-Rayleigh distribution.

Discussion and Conclusions

It demonstrated that the parametric image incorporated with other parameters is feasible to be applied to differentiate and assess the degrees and depth of burn tissues. Further works to correlate with results of tissue slice are necessary to allow ultrasonic measurements for diagnosing degree of the burn quantitatively.

P3B033-04

Accurate Ultrasonic Measurement of Myocardial Regional Strain Rate at High Temporal and Spatial Resolutions

Yasunori Honjo[1], Hideyuki Hasegawa[2], Hiroshi Kanai[1]; *[1]Graduate School of Engineering, Tohoku University, Japan, [2]Graduate School of Biomedical Engineering, Tohoku University, Japan.*

Background, Motivation and Objective

Methods for imaging of strain rate in the heart wall are useful techniques for the quantitative evaluation of regional myocardial function. However, a mechanism of the transitions between myocardial contraction and relaxation was unclear. Except for a method based on ECG triggering, a required temporal resolution was realized by scanning the heart wall sparsely at the expense of the lateral spatial resolution (H. Yoshiara et al., *Jpn. J. Appl. Phys.* Vol. 46, No. 7B, 2007, pp. 4889□E896). Therefore, the spatial resolution in measurement of the transition of myocardial contraction/relaxation in the lateral direction have been limited.

Statement of Contribution/Methods

In this study, the RF data was acquired in a typical cross-sectional image (interventricular septum (IVS) in the longitudinal-axis view of the left ventricle) based on parallel beam forming (PBF). A wide transmitted beam scanned 7 different directions sparsely and 16 receiving beams were created in each transmit. The angle between neighbor beams was 0.75 degree and the frame rate (FR) was 1014 Hz. During a cardiac cycle, the strain rate of the IVS was calculated and analysed.

Results

The figure shows strain rate images during a short period after R-wave of ECG obtained by (a) PBF (FR: 1014 Hz) and (b) previously proposed sparse scan (FR: 630 Hz). The strain rate obtained by spatial differentiation of the velocity distribution along the ultrasonic beam. Slight spatial transition of contraction/relaxation in the axial and lateral directions during a very short period less than 10 ms was visualized by PBF, as shown in Fig. (a). However, the transition in only the axial direction was visualized by sparse scan, as shown in Fig. (b).

Discussion and Conclusions

Measurement of myocardial strain rate at high temporal and spatial resolutions was achieved using PBF. *In vivo* experimental results show a possibility of this method for elucidation of the transition of myocardial contraction and relaxation in two dimensions. It is supposed that such transition corresponds to the propagation of myocardial excitation along the conduction system of the heart (from sinoatrial node to Purkinje fibers.)

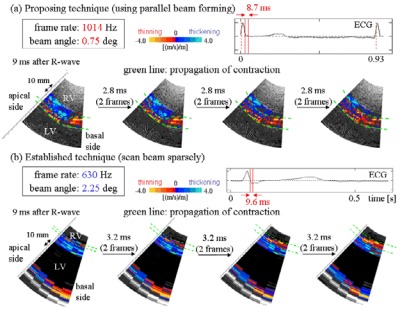

P3B034-05

Flow-Mediated Change in Viscoelasticity of Radial Artery Noninvasively Measured by 22-MHz Ultrasound

Kazuki Ikeshita[1], Hideyuki Hasegawa[2], Hiroshi Kanai[1]; [1]*Graduate School of Engineering, Tohoku University, Japan,* [2]*Graduate School of Biomecical Engineering, Tohoku University, Japan.*

Background, Motivation and Objective

It was reported that the endothelial dysfunction and the change in characteristics of smooth muscle are caused by early-stage atherosclerosis. Therefore, it is essential to develop a method for assessing the *regional* endothelial function and mechanical property of the arterial wall. There is an ultrasound-based conventional technique to measure the change in inner diameter of the brachial artery caused by flow-mediated dilation (FMD) after release of avascularization. For more sensitive assessment, we developed a method to measure the stress-strain relationship of the radial artery during FMD [Ikeshita, *et al, Proc. IEEE Intern'l Ultrason. Symp.* 2007]. In this study, the response of the arterial wall was further investigated by estimating its viscoelasticity using the measured stress-strain relationship.

Statement of Contribution/Methods

For this measurement, ultrasonic RF echo (transmit: 22 MHz) was acquired at a sampling frequency of 66.5 MHz for 2 seconds. The minute change in thickness (strain) of the radial artery was measured using the ultrasonic *phased tracking method* [Kanai, *et al,* IEEE. Trans. UFFC. 1996], together with the waveform of blood pressure (stress) which was continuously measured at the radial artery. We measured the stress-strain relationship and estimated viscoelastic parameters using the least-square method by minimizing the mean squared error between the measured and model waveforms of blood pressure (BP). The model waveform was obtained from the measured strain and viscoelastic constants of the Voigt model.

Results

Figure 1(a) shows the measured and estimated BP waveforms and the change in thickness during one cardiac cycle. The difference between the measured and model BP was 8%. As shown in Fig. 1(b), the stress-strain relationship obtained by the measured BP was in good agreement with that by the model BP. Figure 1(c) shows the transient changes in estimated constants, static elasticity and viscosity, during FMD.

Wednesday Poster

Discussion and Conclusions

The viscosity increased totally after recirculation, which corresponds to the increase of the area of loop after recirculation. These results show a potential of the proposed method for thorough analysis of the *transient change in viscoelasticity* due to FMD.

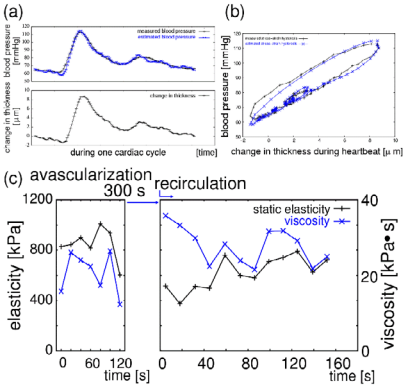

P3B035-06

Time-domain model of the ultrasonic wave propagation in an inhomogeneous anisotropic fluid/solid multilayer medium: application to cortical bone

Guillaume Haiat[1], Quentin Grimal[2], Talmant Maryline[3], Christophe Descelliers[4], Christian Soize[4], Salah Naili[5]; *[1]CNRS, B2OA, Paris, 75010, France, [2]Université Pierre et Marie Curie-Paris6, Laboratoire d'Imagerie Paramétrique, Paris, France, [3]CNRS, Laboratoire d'Imagerie Paramétrique, Paris, France, [4]Université Paris-Est, Laboratoire de Modélisation et Simulation Multi-Echelle, Marne la Vallée, France, [5]Université Paris-Est, Laboratoire de mécanique Physique, Créteil, France.*

Background, Motivation and Objective

The axial transmission technique is used clinically for cortical bone assessment. However, the ultrasonic propagation in this multiscale transverse isotropic medium remains unclear, because of the heterogeneous nature of cortical bone. At the macroscopic scale, the distribution of porosity induces a gradient of material properties oriented in the radial direction. The aim of this work is to evaluate the effect of a spatial gradient of material properties on the ultrasonic response of a transverse isotropic bone structure.

Statement of Contribution/Methods

A 2D finite element time-domain method is developed to simulate transient wave propagation in a three-layer medium constituted of an inhomogeneous transverse isotropic solid layer sandwiched between two acoustic fluid layers and excited by an acoustic linear source located in one fluid layer delivering broadband ultrasonic pulses (1 MHz center frequency). The model couples the acoustic propagation in both fluid media with the elastodynamic response of the solid. The conditions of continuity are used to model the fluid-structure interaction. A constant spatial gradient of material properties (stiffness coefficients and mass density) in the direction perpendicular to the layer is considered in the solid for two values of bone widths h corresponding to a relatively thick or thin bone (h=0.6 and 4 mm).

Results

Snapshots of wave propagation in the multiple layer domain shown in Fig. 1 illustrate the effect of a gradient of C11 (Fig 1(b)) compared to the homogeneous case (Fig 1(a)).

The first arriving signal (FAS) velocity depends on the material properties in the middle (respectively at the surface) of the solid layer when the thickness is lower (respectively higher) than the wavelength.

Discussion and Conclusions

For thin bone widths (0.6 mm), results are in agreement with the symmetric mode S0 of Lamb waves assuming a homogeneous material with spatially averaged material properties. For thick bone widths (4 mm), the results are in agreement with the propagation of a lateral wave. For thick bone width, our results allow the estimation of an equivalent penetration depth of the lateral wave in the case of a transverse isotropic inhomogeneous solid layer (0.6 and 0.95 mm for a gradient of C11 and mass density respectively).

This study was supported by the Agence Nationale de la Recherche (Contract BoneChar n° BLAN06-2_144779).

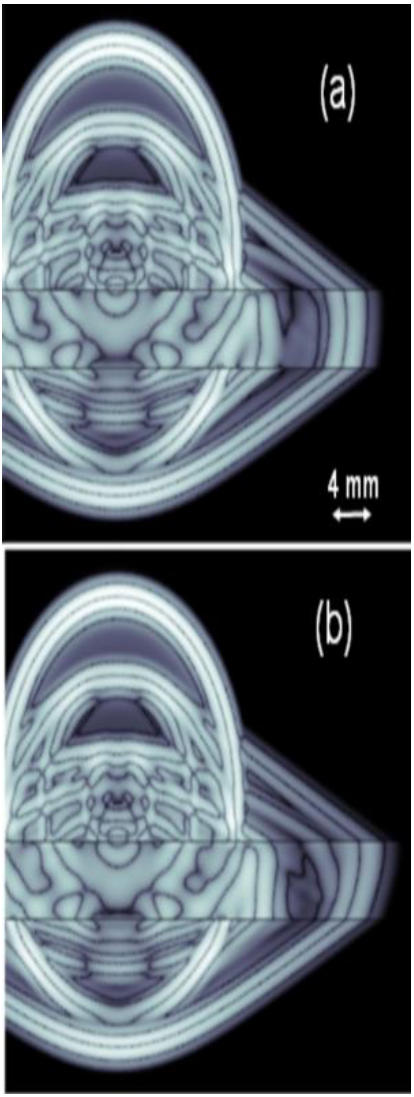

P3B036-07

Anisotropy of ultrasonic longitudinal wave in the cortical bone of bovine femur

Yuichiro Yaoi[1], Kazufumi Yamamoto[2], Takaaki Koizumi[1], Mami Matsukawa[1], Kaoru Yamazaki[2], Akira Nagano[2];
[1]Doshisha University, Kyotanabe, Kyoto, Japan, [2]Hamamatsu University School of Medicine, Hamamatsu, Shizuoka, Japan.

Background, Motivation and Objective

Quantitative ultrasound (QUS) is a good method to measure elastic properties of bone, which is expected to be an innovative technique to evaluate bone quality. We have investigated the distribution of ultrasonic longitudinal wave properties in the cortical part of bovine femur, considering the micro structure and hydroxyapatite (HAp) crystallites orientation [Yamato et. al. Calcified Tissue International, Vol.82, p.162, 2008]. In this study, the anisotropy of ultrasonic wave velocity and HAp crystallites orientation is experimentally investigated in detail, using cylindrical specimens obtained from bovine cortical bone.

Statement of Contribution/Methods

Three ring-shaped cortical bone samples were obtained from the mid-shaft of a 32-month-old bovine femur. Four cylindrical specimens (diameter 11mm) were taken from one ring sample as shown in the figure. The anisotropy of wave velocity in the axial-tangential plane was investigated by rotating the cylindrical specimens. Ultrasonic pulse measurements were performed using a polyvinylidene fluoride (PVDF) focus transmitter (Custom made, Toray) and a self-made flat PVDF receiver. A single sinusoidal signal with a center frequency of 1 MHz was applied to the transmitter. The longitudinal wave propagated through water, sample, and water. We placed the focal point of wave on the central axis of the cylindrical specimen. Ultrasonic wave always propagated perpendicular to the side surface of the specimen. HAp crystallites orientation in the specimen was also investigated using pole-figure analysis of X-ray diffraction (PANalytical. X-Pert Pro MRD).

Results

The figure shows the velocity data of a specimen obtained from the lateral part of a cortical ring. Velocity changed due to the rotation angle. Four specimens in the same ring showed similar tendency of velocity, which were higher in the axial direction. However, the direction of the fastest wave velocity observed was 5 to 10 degrees different from the axial direction. From the pole-figure of X-ray diffraction analysis, we also found the small tilt of the HAp crystallites orientation from the axial direction, which was in good agreement of the velocity data.

Discussion and Conclusions

This small tilt of 'Acoustic anisotropy', indicates the complicated elastic behavior. We could find the contribution of HAp crystallites on the elasticity in the cortical bone.

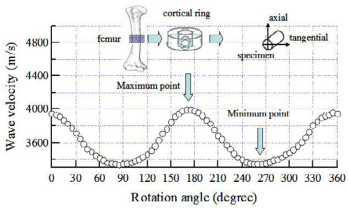

Wednesday Poster

P3C. Elastography

2nd and 3rd Floor Foyers

Wednseday, November 5, 2008, 3:00 pm - 4:30 pm

Chair: **Chris de Korte;**
Radboud University Nijmegen Medical Centre, The Netherlands.

P3C037-01

Comparison of Multiple Beam Sequences in Arterial ARFI Imaging

Russell Behler[1], Timothy Nichols[2], Elizabeth Merricks[2], Caterina Gallippi[1]; *[1]University of North Carolina at Chapel Hill, Department of Biomedical Engineering, USA, [2]University of North Carolina at Chapel Hill, Department of Pathology and Laboratory Medicine, USA.*

Background, Motivation and Objective

To maximize the potential of arterial ARFI imaging, it is important to understand the benefits and drawbacks of various radiation force excitation and displacement tracking methods. We hypothesize that different beam sequences will yield different information about plaque structure and composition.

Statement of Contribution/Methods

Imaging was performed with a Siemens SONOLINE Antares™ scanner and VF7-3 transducer (Siemens Medical Solutions USA, Inc. Ultrasound Division). We implemented 14 unique beam sequences with variable excitation F/# (1, 1.5, 2 and 3), number of excitations (1 or 2), tracking location (at or beside the region of excitation (ROE)), and tracking A-line acquisition method (single or 4:1 parallel receive). All 14 beam sequences were administered in each of 4 excised pig iliac arteries. The ex vivo imaging environment was highly controlled and so allowed for direct comparison of beam sequence performance. All 14 beam sequences were also administered in each of 3 in vivo pig iliac arteries. Both ex vivo and in vivo imaging results were validated by spatially matched immunohistochemistry.

Results

In an artery imaged ex vivo, a focal plaque on the far wall spanned ~8 mm laterally. Histology confirmed collagen deposition across the entire ~8mm range of the plaque, with heightened deposition in the center, and internal-elastic lamina degradation across ~8 mm below the plaque. A beam sequence consisting of a single 300 cycle (at 4.21 MHz) excitation impulse with F/1.5 single A-line tracking in the ROE yielded parametric peak displacement and recovery time images that delineated the plaque's geometry, including spatial changes in collagen and elastin composition. In contrast, a similar beam sequence that implemented 4:1 parallel receive tracking A-lines yielded parametric images that exhibited more spatial smoothing of compositional features. Finally, a SWEI beam sequence consisting of a 300 cycle (at 4.21 MHz) impulse and 4:1 parallel receive tracking A-lines yielded parametric images of average shear wave velocity that showed the highest degree of spatial smoothing but also provided information regarding induced shear wave velocities. Other ex vivo and in vivo experiments produced similar results.

Discussion and Conclusions

Different methods of radiation force excitation and tracking yielded different results in the same arteries under highly controlled experimental conditions. This supports the potential merit of combining beam sequences to fully describe the material characteristics of arterial plaques.

Wednesday Poster

P3C038-02

Acoustic Radiation Force Based Quantification of Tissue Shear Modulus within the Region of Excitation

Mark Palmeri, David Xuo, **Liang Zhai,** Kathryn Nightingale; *Duke University, Biomedical Engineering, Durham, North Carolina, USA.*

Background, Motivation and Objective

The speed of shear wave propagation in tissue is directly related to the tissue's shear modulus. Shear waves can be generated in tissue using focused, impulsive, acoustic radiation force excitations. Shear modulus reconstruction has typically been performed by monitoring shear wave propagation in regions that are spatially offset (off-axis) from the region of excitation (ROE), [e.g. SWEI, SSI, Lateral-TTP], but such methods require greater radiation forces than on-axis (within the ROE) methods [e.g. ARFI]. On-axis reconstruction methods have been discussed in the context of analytic excitation beam geometries [Sarvazyan 1998]; however, translation to linear array geometries has not, to date, been successful. The purpose of this study is to investigate an 'on-axis' method for quantifying shear moduli using conventional, diagnostic arrays.

Statement of Contribution/Methods

Previously validated 3D FEM models of soft tissue response to impulsive radiation force excitations, coupled with Field II simulations of ultrasonic displacement tracking, were utilized for this work. Simulations were performed for a given focal geometry (Siemens CH41 transducer) for a range of tissue stiffnesses (μ=1-15kPa). Linear, elastic, isotropic material properties were assumed, making the time-to-peak (TTP) displacement on the central axis of a radiation force excitation beam proportional to the shear wave speed in the tissue and the excitation beam geometry. Jitter smoothing algorithms were applied to the displacement estimates, and a series of curves relating TTP displacement, axial position, and stiffness were developed. These curves were then used to estimate the stiffness of calibrated simulation data, and experimental data in calibrated phantoms and soft tissues in vivo. The on-axis estimates were also compared with off-axis (Lateral-TTP) reconstructions in matched datasets.

Results

Simulation data indicate that the reconstructed shear moduli are independent of variations in tissue attenuation that impacts the spatial distribution of radiation force in the ROE. Phantom reconstructions yielded on-axis shear modulus estimates of 1.4 ± .12 kPa compared with 1.5 ± .04 kPa using the Lateral-TTP method. The axial ROI for each method is similar, but the lateral ROI is ~30x smaller for the on-axis method (0.2 mm vs 6 mm).

Discussion and Conclusions

Greater displacement magnitudes are present within the ROE compared with off-axis locations, producing greater displacement SNR and reducing the acoustic energy needed to generate accurate displacement estimates. This reduction of acoustic output leads to a decrease in associated transducer and tissue heating. Measuring TTP on-axis, instead of at multiple off-axis locations, also reduces data acquisition times, limiting motion artifacts in the data. The precision of the on-axis method is affected by jitter, but material shear moduli can be reconstructed with 0.1 kPa precision.

P3C039-03

A Combined ARFI Sequence For 2D Displacement Imaging and Shear Wave Velocity Mapping

Liang Zhai[1], Stephen Hsu[2], Kathy Nightingale[2]; [1]*Duke University, Biomedical Engineering, USA,* [2]*Duke University, USA.*

Background, Motivation and Objective

As pathological changes are normally accompanied with changes of mechanical properties, tissue elasticity is a potential diagnostic metric for a number of diseases. While elasticity imaging techniques have been successfully applied to delineate different tissues and malignancies based on their relative structural stiffness compared with surrounding tissues, a matched absolute tissue modulus map will provide complimentary and validating information in these relative stiffness images. In this study, a combined sequence of 2D ARFI imaging (relative stiffness) and shear wave velocity mapping (quantitative method) is proposed so that the on-axis displacements and subsequent lateral shear wave propagation can be monitored serially, without increasing the total number of excitation pulses.

Statement of Contribution/Methods

A modified Siemens AntaresTM scanner and a VF10-5 linear array were used for this study. Standard settings of ARFI excitation pulses were used. By utilizing 4:1 parallel receive, displacements were tracked simultaneously at 4 different lateral locations with a PRF of 9.5 kHz. In contrast to traditional parallel ARFI sequences, the 4 tracking beams monitored the pushing location only for the first 0.3 ms. Then the transmit aperture was subdivided to interrogate the wave behaviors at two separate lateral locations away from the region of excitation concurrently. Analytical models were developed to optimize tracking beam locations for monitoring shear wave propagation. The sequence was tested in a calibrated homogeneous tissue-mimicking phantom (E = 4.5 kPa).

Results

A novel ARFI sequence has been developed so that matched 2D ARFI images and maps of shear wave velocities can be generated without increasing the number of excitation pulses. The on-axis displacements estimates before 0.3 ms are used to generate the 2D displacement image while shear wave speeds are estimated from the two-location wave tracking. Analytical models indicated that the first beam should be positioned at least 1.4 times of the excitation beam width away from the excitation location laterally, and a trade-off exists between lateral resolution and the accuracy of measured shear wave velocities. Using 5 excitation pulses to create a 2D ARFI relative displacement image with an ROI of 20 x 10 mm, concurrently obtained shear wave propagation data provided a shear wave speed estimate around the focal depth of 1.22 +/- 0.02 m/s, which corresponded to a Young's modulus estimate of 4.45 +/- 0.16 kPa.

Discussion and Conclusions

By using the same number of excitation pulses for generating 2D ARFI displacement images, the new sequence will be able to provide both structural image of relative stiffness and a map of shear wave velocities. The matched images will cross-validate each other. The locations of tracking beams are dictated by the initial wave amplitude, material stiffness, tissue attenuation and limited by the transmitting aperture of the transducer.

P3C040-04

The Effect of Nonlinearity on Focused Impulsive Acoustic Radiation Force Excitations

Gianmarco Pinton, Gregg Trahey, Mark Palmeri, Kathy Nightingale; *Duke University, Biomedical Engineering, Durham, NC, USA.*

Background, Motivation and Objective

Focused, impulsive acoustic radiation force can be used to induce localized displacement in tissue. Linear models, such as Field II [1], can be used to predict the intensity for an acoustic radiation force excitation. However, the intensity levels used to generate appreciable radiation force may be large enough to require a nonlinear description of wave propagation. An ideal numerical solution also calculates the loss term resulting from nonlinear wave propagation. The purpose of this study is to calculate the spatially varying intensity and absorbed acoustical energy. These results will be used to calculate tissue heating and improve the mechanical simulations of tissue response to radiation force excitations.

Wednesday Poster

Statement of Contribution/Methods

A finite difference solution of the full-wave equation in a nonlinear arbitrarily attenuating medium with finite differences in the time domain is used to calculate the pressure and loss fields[2]. The pressure and absorption term are calculated at 400 MHz with a spatial resolution of 20 microns in all three spatial dimensions for a 4.2 MHz diagnostic ultrasound transducer focused at 2.4 cm, with and F-number of 1.5. The force calculated from the output of the nonlinear simulation is used as an input to an already established Finite Element Model of the tissue mechanical properties [3].

Results

Simulations show the differences in intensities and absorption for varying initial pressures. For example, for an initial pressure of 1.5 MPa and a pulse length of 2.4 us, the -10 dB beamwidth is 80% larger for the linear simulation when compared to the nonlinear simulation, which is consistent with experimental evidence of self-focusing in nonlinear propagation. The peak intensity along the axis is 23% larger for the nonlinear simulation and 30% narrower, indicating a more localized radiation force distribution than a linear simulation would predict.

Discussion and Conclusions

A nonlinear simulation that calculates the intensity and absorption in the acoustic field with fine spatial and temporal resolution has been established for a diagnostic imaging transducer. For large intensities the a nonlinear description of ultrasonic propagation predicts a higher peak intensity, and a narrower lateral and axial distribution.

The radiation force calculated from this more accurate simulation is closer to a point impulse than linear theory would predict.

[1]Jensen et al. "Calculation of pressure fields for arbitrarily shaped, apodized, and excited ultrasound transducers," IEEE UFFC, 39(2):262-267, 1992.

[2] Pinton et. al."A heterogeneous nonlinear attenuating full-wave model of ultrasound" IEEE UFFC, Accepted, 2008.

[3]Palmeri et al. "A finite-element method model of soft tissue response to impulsive acoustic radiation force," IEEE UFFC, 52(10):1699-1712, 2005.

P3C041-05

Improvement on the Elastic Visualization of Thermal Lesion Using Block Wavelet Shrinkage

Dachun Zhang, Mingxi Wan, Hongmei Zhang, Supin Wang; *Xi'an Jiaotong University, The Key Laboratory of Biomedical Information Engineering of Ministry of Education, China.*

Background, Motivation and Objective

Elastography is an effective modality to image the elastic parameters of the tissue lesion during thermal ablation. However, the elastographic noise arising from the ultrasound system noise, unapt signal processing parameters and decorrelation of the pre- and post-compression echo signals restricts the application of elastogram in clinic. Furthermore, the elastographic noise presents strongly spatial nonstationarity because of the strain-dependent decorrelation noise. Therefore, noise reduction in elastography is quite different from the usual signal-independent noise cases.

Statement of Contribution/Methods

In this paper, we propose a method called block wavelet shrinkage (BW-Shrink) to improve the strain visualization of microwave-induced lesion by denoising the estimated displacement. This method is based on that the normal tissue and the thermal lesion are separately distributed during the ablation. Within a small local region, unless it contains the lesion edge, the stiffness and the corresponding applied strain are near-uniform under the general elastographic conditions. Consequently, the elastographic noise in such region approximatively satisfies the independent and identical distributed (i.i.d), Gaussian condition for wavelet shrinkage. The implementation of the BW-Shrink is performed in 3 stages following the displacement estimation with correlation technique. First, the displacement in each scanning line is decomposed into 3 scales with wavelet. Second, the wavelet coefficients are divided into conjunctive blocks with size of several square millimeters, and shrinkage is operated in each block respectively. Finally, the denoised displacement in each scanning line is obtained with wavelet reconstruction.

Results

From the elastograms for the microwave-induced lesions of the porcine liver, it is shown that the signal-to-noise ratio (SNRe) and the contrast-to-noise ratio (CNRe) were significantly improved (more than 5-dB) while the lesion edge was well preserved with the proposed method. Also, the lesion sizes measured from the elastograms and the morphological samples had high correlation when the BW-shrink was used.

Discussion and Conclusions

The high efficiency of the BW-Shrink in noise reduction derives from its effective approach to the spatially unstable noise in elastography according to the elastic distribution of the underlying tissue. The BW-Shrink is proved to be valid to improve the strain visualization in thermal ablation.

P3C042-06

Robust Strain Estimation Using Adaptive Dynamic Grid-Interpolation Model

Makoto Yamakawa[1], Shuhui Bu[2], Tsuyoshi Shiina[2]; *[1]Kyoto University, Japan, [2]University of Tsukuba, Japan.*

Background, Motivation and Objective

An ultrasound scanner with tissue strain imaging technology is now being marketed, and its trial applications are being made in many fields. However, strain distribution cannot be correctly estimated in the present equipment in low-echo regions with a bad signal-to-noise ratio (SNR). In particular, an error sometimes occurs in a region of interest (ROI) if it is a low-echo region and has a bad SNR. Therefore, we propose a method for correcting local errors without degrading spatial resolution.

Statement of Contribution/Methods

We apply a dynamic grid-interpolation (DGI) model in order to correct local errors. This model consists of grid-like springs. The displacement distribution is restricted by these springs, so errors are corrected. However, in the DGI model, the spring constant is spatially uniform, so spatial resolution is sacrificed for robust estimation. Therefore, in this study, we propose an adaptive dynamic grid-interpolation (ADGI) model for robust estimation with high spatial resolution. In this adaptive model, spring constants change spatially according to the SNR of signals (correlation coefficient). That is, we set spring constants to correct strongly in the bad SNR region and to correct weakly in the good SNR region. Therefore, errors can be corrected in the bad SNR region, and spatial resolution can be kept high in the good SNR region.

Results

We evaluated the performance of this method by numerically simulating tissues which has a low-echo inclusion. Echo signals were generated by transmitting ultrasound pulse with center frequency of 7.5MHz. We changed the SNR of the inclusion and compared the results of the conventional method to those of the ADGI method. When the SNR of the inclusion degrades below 0dB (surrounding SNR is always 20dB), the conventional method generates errors. In contrast, the proposed method corrects the errors for all SNRs, as shown in the figure. Moreover, the difference (0.1 to 10 times) in the hardness of an inclusion is also identified with sufficient accuracy. Furthermore, the errors in vivo breast measurement data were also corrected, and no spatial resolution degradation was seen in the good SNR region.

Discussion and Conclusions

In conclusion, we can use the ADGI method to estimate strain distribution robustly and without degrading spatial resolution.

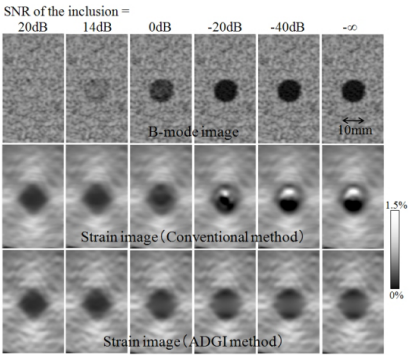

Wednesday Poster

P3C043-07

Reverberation Reduction in Vibro-acoustography using Channel Estimation Method

Yi Zheng[1], Aiping Yao[1], Jiangli Lin[1], Randy Kinnick[2], James Greenleaf[2], Mostafa Fatemi[2]; *[1]St. Cloud State University, Electrical and Computer Engineering, St. Cloud, MN, USA, [2]Mayo Clinic College of Medicine, Physiology and Biomedical Engineering, Rochester, MN, USA.*

Background, Motivation and Objective

Vibro-acoustography (VA) displays the vibroacoustic response of the object (tissue) induced by two intersecting ultrasound beams of different frequencies. VA image of a given object may vary depending on boundary conditions. Such variations are attributed to the reverberation of the sound emanating from the object in the acoustic environment of the experiment. This effect can be explained in terms of acoustic propagation through multiple paths before reaching the receiving hydrophone. The goal of this study is to reduce VA image variations caused by the acoustic multipath.

Statement of Contribution/Methods

A method based on channel estimation is developed to evaluate the effect of multipath and correct the received acoustic data from the object. This method uses a short ultrasound pulse followed by a long tone burst. A normalized version of the short pulse provides an estimate of the multipath channel between the focal point of ultrasound (vibration center) and the hydrophone. Because the channel is different for each point of the object, it is

estimated independently for every point of the object, i.e., every pixel of the VA image. The response to the long tone burst is corrected using the estimated channel. Then, the corrected signal is used to form the image.

VA images of a breast phantom with simulated lesions and a human prostate tissue were obtained with a prototype VA imaging system. A 3-MHz confocal transducer was used to produce two beams of ultrasound at 50 kHz difference frequency with the temporal form of a short pulse followed by a long tone burst. The acoustic response of the object was recorded by a hydrophone and sampled at 1 MHz. The ultrasound scanned the objects to produce 200×200-pixel VA images. The variability in the resulting VA images caused by reverberation was evaluated before and after correction for multipath.

Results

Channel estimation method is applied to correct VA images. The background and lesion variabilities are removed from VA images of the breast phantom and the prostate tissue. The simulated lesions and other object details that are overshadowed by reverberation in the initial image are restored in the corrected images.

Discussion and Conclusions

Channel estimation method is an effective technique to mitigate reverberation effect in vibroacoustography. [This research is supported by NIH grants EB2167, CA 127235, and CA 91956. (Disclosure of conflict of interest: Vibro-acoustography technique is patented by Mayo Clinic and some of the authors (MF and JFG)].

P3C044-08

Maximal accumulative respiration strain for the assessment of hepatic fibrosis: preliminary studies

Jinhua Shao[1], Xiangdong Hu[2], Ke Liu[1], Linxue Qian[2], Jinrui Wang[3], Jing Bai[1]; *[1]Department of Biomedical Engineering, Tsinghua University, China, [2]Department of Diagnostic Ultrasound, Youyi Hospital, China, [3]Department of Diagnostic Ultrasound, Peking University Third Hospital, China.*

Background, Motivation and Objective

Early detection of the progression of liver fibrosis is important for the treatment of chronic hepatitis. Unfortunately, commonly used medical imaging methods such as ultrasonography, computed tomography and magnetic resonance imaging are unable to provide fibrosis information. At present, liver biopsy is the gold standard for the evaluation of the liver fibrosis. However, it may cause problems such as hemorrhage and infection. Elastography can provide stiffness information of the tissue based on the detection of tissue strain. Nevertheless, this new imaging method is unavailable in most ultrasound machines in hospitals at present.

In this paper, ultrasound hepatic B-mode videos during normal respiration were acquired, and the maximal accumulative respiration strains (MARS) of a breath cycle were calculated from these sequences. The relationship of the MARS and the fibrosis stage was studied.

Statement of Contribution/Methods

The ultrasound B-mode video data of the liver were acquired from two groups of people (7 healthy volunteers and 7 patients with biopsy-proven grade 4 fibrosis). The videos were taken from the vertical plane of the patients close to ensisternum where the hepatic tissue movement was restricted almost in the imaging plane. All the B-mode videos were acquired under the same setup.

For each video, a complete respiration cycle was chosen. The inter-frame displacement was estimated based on a 2D cross-correlation method, and the average strain of the liver was calculated. After that, the MARS during the whole respiration cycle was calculated.

Results

A significant difference of the MARS parameter was found between these two groups. The mean MARS of the healthy group and the fibrosis group were 29.45 and 15.19 respectively. The results are shown in the figure 1.

Discussion and Conclusions

The results indicated that the MARS during a breath cycle was correlated to the hepatic fibrosis, and might be a potential parameter to assess fibrosis stage. Further studies should include more patients with different fibrosis stage.

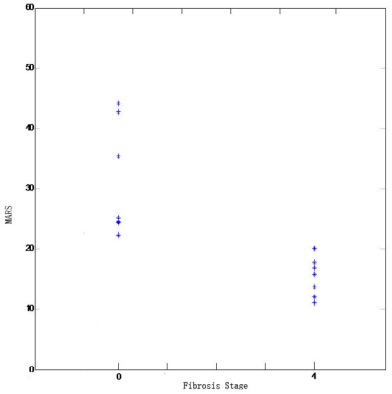

P3C045-09

Computer-aided Diagnosis of Diffuse Disease based on Ultrasound Elasticity Images

Masakazu Yamazaki, Tsuyoshi Shiina, Hotaka Takizawa; *University of Tsukuba, Tsukuba, Ibaraki, Japan.*

Background, Motivation and Objective

It is well known that as hepatic cirrhosis progresses, fibrosis area spreads and nodule increases, consequently, liver tissues become hard. However, it is not easy to diagnosis its early stage by conventional B-mode image because is not sensitive to the stage of fibrosis. On the other hand, practical equipment for tissue elasticity imaging has recently been developed. Results of clinical examination of breast confirmed that tissue elasticity imaging is useful for the detection of tumor. In the case of diffuse diseases like hepatic cirrhosis, change of tissue elasticity is widespread unlike tumor which produces locally hard area. However, it was revealed that texture of elasticity image changes as cirrhosis progresses. Therefore, we investigated to develop the CAD system based on elasticity image for diagnosing defused type diseases such as hepatic cirrhosis.

Statement of Contribution/Methods

Cirrhosis is categorized as 4 stages based on the extent of spreading fibrosis. We found that texture of elasticity image (strain) of cirrhotic liver reflected the stage of fibrosis and could be categorized into the four stages. In order to quantitatively evaluate the change of texture, two features were extracted from elasticity images. One is a shape of histogram about strain values. The value of strain is normalized with 32 levels to constitute its histogram. An index which represents the ratio of area of histogram between low and median strain was introduced. As the second feature, run length of strain image is used to detect the difference of size of nodules.

The CAD system for cirrhosis was constituted based on these two features. At learning process, the CAD extracts two features from texture of strain, and these features and the result of staging by doctors are inputted into discriminator. Distinction model is made by repeating these processes with elasticity image samples. The distinction model is used to diagnosis test image.

Results

The performance of the CAD system for discriminate normal liver or cirrhosis was evaluated using clinical data. We used 36 samples which consist of 18 normal liver and 18 cirrhosis. Leaving-one-out method was applied to constitute the distinction model for CAD. Results of diagsosis by the CAD implies that it is useful to diagnose normal liver and cirrhosis in serious stage with simple criterion based on two strain features (accuracy:72%, Specificity: 94%). However, the early stage (F1) was confused with normal liver because fibrosis tissues are scarce.

Wednesday Poster

Discussion and Conclusions

We have investigated to quantify the texture pattern of elasticity image and constitute the CAD system for diagnosis of hepatic cirrhosis. The results of clinical data analysis indicate that the CAD system based on elasticity images is promising as means for diagnosis of diffuse disease with simple criterion. For further investigation, it is necessary to improve the performance for diagnosing hepatic cirrhosis in early stage and staging of cirrhosis with the CAD system.

P3C046-10

An ultrasound imaging method for in vivo measurement of tracheal elasticity

Chao-Ling Wu, Chih-Yen Chen, Huihua Kenny Chiang; *National Yang-Ming University, Biomedical Engineering, Taipei, Taiwan.*

Background, Motivation and Objective

The airway mechanical properties in normal people are different to patient with airway diseases, like airway collapse and airway chronic diseases. With the advent of ultrasound imaging techniques in recent years, many in vivo techniques for measuring tissue mechanical properties have been presented. The objective of this paper is to determine the in vivo of trachea elasticity of normal persons by non-invasive ultrasound imaging method.

Statement of Contribution/Methods

The paper presents first in vivo measurement of tracheal elasticity of human subjects. Twelve normal subjects without any airway diseases were involved in this study (age from 23 to 40, 5 males and 7 females). A Threshold Positive Expiratory Pressure device (Threshold PEP, New Jersey, USA) was used to provide positive expiratory pressure therapy. All subjects were asked to breathe through a mouthpiece. Five different loads of PEP were applied at 0 cm H2O;5 cm H2O;10cmH2O;15cmH2O and 20cmH2O. A clinical ultrasound system (Terason 2000 Burlington, MA ,USA) with a 10MHz transducer for measuring the diameter of trachea anteroposterior and transverse from thyroid cartilage and suprosternal notch. Finally, the ultrasound image data was analyzed to calculate the elasticity, Young Modulus, by taking the ratio of stress over strain.

Results

Our result shows that the elasticity of normal subjects tracheal was in the range 50~150Pa(<200Pa), and the correlation coefficients were R2:0.86?.13, R2: 0.74?.31 for anteroposterior and transverse diameters respectively.

Discussion and Conclusions

In this study, we demonstrate the application of ultrasound imaging for measuring airway mechanical property, Young's Modulus. We also observed significant correlation in the stress to strain experiments. This paper provides a new approach to measure the elasticity of human tracheal in real time, patient-friendly way.

P3C047-11

Non-invasive in vivo strain imaging of carotid cross-sections: reproducibility of strain estimates obtained with and without beam-steering during subsequent heart cycles

Hendrik H.G. Hansen, Richard G.P. Lopata, Chris L. de Korte; *Radboud University Nijmegen Medical Centre, Nijmegen, Netherlands.*

Background, Motivation and Objective

Ultrasound strain imaging can be used to assess the vulnerability of atherosclerotic plaques, and with that probable risk for stroke and myocardial infarction. Intravascular elastography has shown to be suitable for distinguishing different plaque phenotypes. For superficial arteries, like the carotid, the technique might be converted to a non-invasive variant, thus enabling non-invasive plaque detection. In general, it is not possible to accurately estimate radial strains for an entire carotid cross-section. However, by combining mainly axial strain data obtained at multiple beam-steered angles it is possible, as previously shown in phantom experiments. For in vivo applications, this multi-angle approach combines ultrasound data recorded at subsequent heartbeats. However, in that case, the inter-heartbeat variability of the strain estimates should be small to avoid compounding errors.

Statement of Contribution/Methods

The reproducibility of axial strain estimation during subsequent heart cycles was investigated for cross-sections of 9 common carotids. Radio frequency data were acquired with a Philips SONOS 7500, equipped with an L11-3 transducer. All cross-sections were imaged without beam-steering. Five cross-sections were additionally imaged at 20° of beam-steering. The data were digitally sampled at 39MHz, and at a frame rate of 61 Hz. ECG signals were recorded simultaneously. Axial strains and displacements were estimated for a roughly defined region of interest

(ROI) using a 2D cross-correlation based iterative coarse-to-fine algorithm. After strain estimation, a more precise ROI was drawn in the frame corresponding to the first R-wave of each recording. The movements of the strain pixels of this ROI were tracked for the subsequent heartbeats using estimated displacements and strains as input. Displacement information of neighbouring pixels was incorporated to enhance the tracking. Because the ROI should return to the initial shape at each subsequent R-wave, linear detrending of the ROI was applied. The tracked strain values were accumulated in time, and normalized 2D cross-correlation values of similar frames in subsequent heart cycles were determined.

Results

The axial strains of carotid cross-sections have shown to be reproducibly estimated (cross-correlation values > 0.8) with and without beam-steering just before and right after the T wave of the ECG cycle. The strain level is between 0.5 and 6% at those moments, which corresponds to the optimal working range of the algorithm. Selective removal of frames with low cross-correlation values might enable reproducible strain estimation for the entire heart cycle. The shape of the accumulated strain curves is similar to that of the pressure pulse, which is as expected for healthy arteries.

Discussion and Conclusions

Combination of data acquired at different beam steered angles seems possible and provides evidence that non-invasive compound elastography might also be feasible in vivo.

P3C048-12

Quantitative elastography, solving the inverse elasticity problem using the Gauss-Newton method.

Mauro Sette[1], Juan F. Camino[2], Jan D'hooge[3], Hendrik Van Brussel[4], Jos Vander Sloten[1]; *[1]Katholieke Universiteit Leuven, Mechanical Engineering BMGO, Leuven, Belgium, [2]University of Campinas, School of Mechanical Engineering, Brazil, [3]Katholieke Universiteit Leuven, Cardiovascular Imaging and Dynamics Dept. of Cardiovascular Diseases, Belgium, [4]Katholieke Universiteit Leuven, Mechanical Engineering PMA, Belgium.*

Background, Motivation and Objective

Mechanical properties of soft tissues are used as means of identification of diseases. In a previous work [1] was presented an algorithm to estimate soft tissues Young's Modulus (YM) solving an inverse elasticity problem (IEP) based on ultrasound elastography (USe). This algorithm is faster than others proposed in literature. In this work the test of this algorithm on experimental data is presented.

Statement of Contribution/Methods

As described in [1] the IEP is posed as a least squares problem and solved using a constrained Gauss-Newton method. In practice, this problem is ill-posed. Moreover the measured USe is noisy. Thus regularization parameters are needed. For this IEP the regularization approach proposed is to penalize "aligned neighbors".

The IEP is posed as:

$\min(\|C*x-x\_b\|+r\|Ex,y - Ex+1\|+r\|Ex,y - Ey+1\|)$ s.t. $A*x=b$

C is the correspondence matrix, x and x_b are the numerical and experimental displacement field (DF), r is the regularization penalty, Ex,y is the YM in the element x,y, A is the stiffness matrix of the FEM and b is the force vector.

The USe was calculated on data acquired on a PVA phantom, the geometry consisted in a volume with a harder sphere in the middle (YM=1.49e4 Pa for the background and 5.25e4 Pa for the sphere) (Fig. 1, left side). Stopping criteria was $\|C*x-x\_b\|<10e-6$.

Results

The algorithm presented used a simultaneous updating of the optimization variables. This leads to an elapsed time for convergence 25% less than the sequential approach, commonly used to solve this problem. The value found for the YM of the inclusion was strongly dependent by the mesh size and the penalty. But with an accurate tuning of those variables value close to the real one (5.25e4 Pa) are obtained.

Discussion and Conclusions

The bigger is the mesh the better are the results (Fig.1) while for the rthe tradeoff value of 1+e-9 gives the best results. The time taken to solve the IEP is on average 25% less than the algorithms described in literature, this will lead to a more reliable application for real time systems.

Wednesday Poster

Caption Fig.1 The US image acquired on the phantom (left), (right) YM maps varying the penalty and the n° of meshes.

[1] M.M. Sette et al., Comparing Optimization Algorithms For The Young's Modulus Reconstruction In Ultrasound Elastography P4F3 p.445 2007 IEEE International Ultrasonics Symposium.

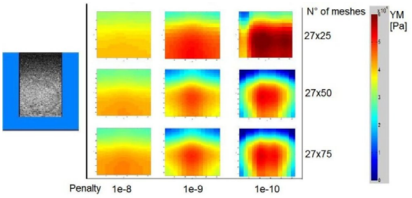

P3C049-13

Viscoelastic Characterization of Soft Tissues by Dynamic Micro-Elastography (Dme) in the Frequency Range of 300 Hz -1500 Hz

Cedric Schmitt, Anis Hadj Henni, Guy Cloutier; *Laboratory of Biorheology and Medical Ultrasonics, Montreal, Quebec, Canada.*

Background, Motivation and Objective

Some commercial apparatuses are well dedicated to measure the viscoelasticity of soft materials but they are limited to a frequency range of 0-400 Hz. In addition, mechanical parameters estimated by these devices are greatly affected by sample geometry and boundary conditions, which are difficult to control for biological organs. In this context, we propose dynamic micro-elastography (DME) to characterize, without any a priori on material properties, biological tissue viscoelasticity (dynamic storage G' and loss modulus G'') over a large frequency range of 300-1500 Hz. The resulting modulus spectra were fitted by different rheological behaviour laws to find which model better reproduced the observed dispersion curves.

Statement of Contribution/Methods

Plane shear waves at frequencies of 300-1500 Hz were generated inside the studied samples by vibrations of an in-contact rigid plate connected to a mini-shaker. A 35 MHz high frequency transducer, oriented parallel to the plate motion and translated along the wave propagation direction, acquired and reconstructed 2D RF sequences at a very high frame rate of 16 kHz with a Vevo 770 scanner (Visualsonics, Canada). From displacement fields calculated by cross-correlation estimator, wave velocity and attenuation were estimated by a spectral analysis of the complex shear wavelength. These two parameters served for the calculation of G' and G''. In this study, the DME method was first applied on homogeneous soft tissue mimicking phantoms (i.e. agar-gelatin, PVA-cryogel) to validate this approach, then characterizations were conducted on animal organs (i.e. liver).

Results

Our experimental setup was able to generate and accurately measure propagation of plane shear waves at the selected frequency range. Results for agar-gelatin and PVA phantoms demonstrated that Voigt's model didn't fully reproduce the relationship between G', G'' and frequency. More complex models, like Zener or Jeffreys laws, produced better fits both on G' and G''. In animal liver experiments, the tissue appeared rheologically softer and more dispersive than mimicking materials, i.e. G' = 1.95 kPa and 7.8 kPa at 300 Hz and 900 Hz, respectively.

Discussion and Conclusions

DME is proposed to measure viscoelasticity of soft tissues in a wide range of frequency (300-1500 Hz). As previously observed in the literature for lower frequencies, liver tissue is highly viscous. This mechanical characterization tool is also adequate to investigate soft tissue rheological behaviour evolution as a function of frequency. This information is very useful to predict, with theoretical models, the dynamic response of a tissue to a shear incident wave. To conclude, because wavelength of propagating shear waves are very small (< 3 mm at 1500 Hz) and motion tracking system very accurate, DME could also be applied to characterize millimetric organs.

P3D. Therapeutic Ultrasound Applications

2nd and 3rd Floor Foyers

Wednseday, November 5, 2008, 3:00 pm - 4:30 pm

Chair: **Greg Clement;**
Brigham & Women's Hospital, USA.

P3D050-01

Standing waves suppression in transcranial ultrasound therapy using random-signal-modulation excitation

Sai Chun Tang, Gregory Clement; *Harvard Medical School / Brigham and Women's Hospital, Radiology, Boston, MA, USA.*

Background, Motivation and Objective

Low frequency transcranial ultrasound (US) (<1MHz) has demonstrated the potential to serve as a therapeutic tool in the treatment of a range of disorders, including the enhancement of tissue plasminogen activator, in stroke treatment, the treatment of tumors, and the ability to locally open the blood brain barrier. Low frequency US, however, may increase the risks for adverse bioeffects related to the potential of producing standing waves in the brain. Presently, we examine an approach to suppress standing waves during continuous wave (CW) transcranial application.

Statement of Contribution/Methods

We hypothesize that a small randomization (20% bandwidth (BW)) in the frequency content of the signal is sufficient to significantly reduce or eliminate standing waves. The approach is studied in a plastic-walled chamber, representing idealized conditions, and in an ex vivio human skull. The randomized approach is compared to single frequency CW operation as well as to a chirped signal with a BW equal to that of the randomized signal.

Results

The measured 2D relative acoustic pressure field patterns in the chamber and the skull, respectively shown in Figs. 1 and 2, were generated by a focused US transducer (5-cm-diameter, 250kHz center frequency), and recorded with a hydrophone (PVDF, 1-mm-diameter). Figs. 1&2(a), 1&2(b), and 1& 2(c) respectively show the field patterns with the single frequency, the chirped and the randomized signals excitations.

Discussion and Conclusions

Both the chamber and skull experiments reveal near elimination of the standing wave with using the randomized signal, as compared to the single frequency and the chirped signals. The randomization process may play a critical role in providing a safer application of the US field in the brain and other areas where standing waves may be created.

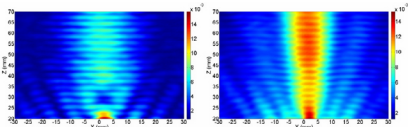
Fig. 1(a) Single frequency

Fig. 1(b) Chirped signal

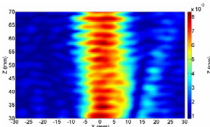
Fig. 2(a) Single frequency

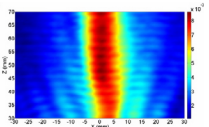
Fig. 2(b) Chirped signal

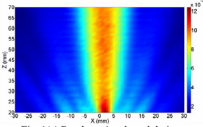
Fig. 1(c) Random-signal-modulation

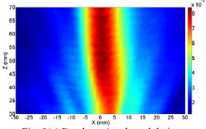
Fig. 2(c) Random-signal-modulation

Wednesday Poster

P3D051-02

Cavitation Enhanced Ultrasound Thrombolysis

Cheng Xu, Xiaojing Li, Mingxi Wan; *School of Life Science and Technology, Xi'an Jiaotong University, The Key Laboratory of Biomedical Information Engineering of Ministry of Education, Xi'an, Shaanxi, China.*

Background, Motivation and Objective

Application of ultrasound has been demonstrated as an effective way to realize thrombus dissolution, but external high intensity focused ultrasound (HIFU) thrombolysis without any agent has not yet been extensively explored. Cavitation is hypothesized to be an important mechanism of ultrasound thrombolysis, but the exact mechanism has not yet been elucidated. The purpose of this work was to study HIFU thrombolysis feasibility and the influence of ultrasound parameters on the thrombolysis efficiency when the spatial average intensity in focal region ISAL was larger than 400W/cm2 which was on the tumor ablation intensity level. The cavitation effect for the variety of thrombolysis efficiency was also investigated.

Statement of Contribution/Methods

In vitro porcine clots were separated into small pieces and inserted into small rubber tubes, then placed in the focal region of the 1.2 MHz HIFU field in a water tank. After HIFU thrombolysis, the debris of clots was microscopically observed, and the size thereof was measured by Coulter Counter. The thrombolysis efficiency was calculated as the ratio between the lysed clot weight and the initial clot weight which was measured with varying pulse length and duty cycle for 120s total duration in ISAL =4243W/cm2. The influences of ultrasound intensity and total application time on the efficiency were estimated under the selected optimal pulse parameters. At the same time, a passive cavitation detection method was used to investigate the role of both inertial and stable cavitation during thrombolysis. Normalized inertial cavitation dose (NICD) and normalized stable cavitation dose (NSCD) were introduced to correlate the quantified cavitation with thrombolysis efficiency.

Results

According to the results, the higher duty cycle, pulse length, higher intensity, and longer total application time resulted in the higher efficiency. Proper combination of duty cycle and pulse length was very important during HIFU thrombolysis. The high efficiency (90.83±3.72%) could be achieved at the optimal parameters (duty cycle of 1:10 and pulse length of 2ms). The debris diameters were mostly under 8um (>99.6%) which is subcapillary in size. The subharmonic and broadband noises were both present during insonification and changed over time. The NICD and NSCD generated by pulsed ultrasound exposure increased significantly with increasing duty cycle, pulse length, ultrasound intensity and total application time, which showed the same trends with thrombolysis efficiencies.

Discussion and Conclusions

Significant correlation between thrombolysis efficiency and cavitation dose indicated that the cavitation mechanism especially inertial cavitation should play an important role in the enhancement of thrombolysis. The observed marked effect on thrombus disruption by the applied high intensity focused ultrasound suggests promising clinical potentials.

P3D052-03

A Pre-treatment Planning Strategy for High-Intensity Focused Ultrasound (HIFU) Treatments: Optimized Source Placement

Phillip Jason White[1], Billy Andre[2], Nathan J. McDannold[1], Greg T. Clement[1]; *[1]Harvard Medical School, Brigham and Women's Hospital, Department of Radiology, Boston, MA, USA, [2]Boston University, Department of Biomedical Engineering, Boston, MA, USA.*

Background, Motivation and Objective

Most operational protocols for HIFU procedures do not incorporate a pre-treatment planning stage comparable to the rigorous pre-treatment planning that is mandated for other modalities of radiation therapy. Ongoing studies investigating pre-treatment strategies that would improve the efficiency and effectiveness of HIFU treatments are complex in nature. Most are based on the incorporation of predictive phase-aberration corrections of propagation-path-specific phase changes. We aim to show that the substantially simpler method of optimizing HIFU source placement in relation to layered tissue structures can have a significant effect on focal integrity, and that MRI scans and a wave-vector time-domain linear propagation model can be used to plan for optimized source orientation.

Statement of Contribution/Methods

Five ex vivo bovine tissue specimens with heterogeneous tissue structures were each mounted in rigid frames with acoustic windows for HIFU transmission. A spherically-focused HIFU source (f_c = 1.502 MHz, D_A = 10 cm, R_c = 10 cm) was positioned to transmit though each specimen at pre-selected orientations, and the transmitted

Wednesday Poster

ultrasound pressure fields were scanned for a series of orientations, followed by a series of T1-weighted MRI scans. Ultrasound transmission simulations were performed and compared with experimental results.

Results

Analyses performed on the acoustic field scans to quantify the level of focal distortion [Energy Distribution Index (EDI) = 1-(percent of energy localized within the focal zone)] demonstrated that over the 5 specimens, at least an average of 7.3% (range 5.6% to 12.3%, sd = 2.8%) improvement in EDI could be expected by source placement optimization (Fig. 1). The accurate simulation of ultrasound propagation through heterogeneous tissue layers using MRI data was also achieved (Fig. 1).

Discussion and Conclusions

The successful demonstration of HIFU focal optimization by source orientation is the first step towards the creation of a relatively simple pre-treatment planning procedure. The validation of a simulation algorithm that uses MRI data to predict focal aberration will be used in the development of an optimization scheme to plan for more efficient and effective HIFU treatments. (NIH 1U41RR019703-01A2)

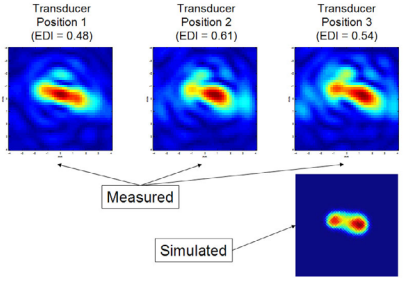

P3D053-04

A Nonlinear Method for High-Intensity Focused Ultrasound (HIFU) Aberration Reduction

Phillip Jason White, Pat von Pattenberg, Greg T. Clement; *Harvard Medical School, Brigham and Women's Hospital, Department of Radiology, Boston, MA, USA.*

Background, Motivation and Objective

A key limitation that prevents more widespread HIFU treatment is patient-specific variation in the presence of aberrating layers. We aim to reduce such variation by using a low-frequency (200 kHz - 400 kHz) transducer design that promotes the divergence of the low frequency beam while promoting the focusing of nonlinearly induced higher harmonic frequencies. In this manner, a low frequency (hence, less absorbed and less distorted) beam is passed through the near field and the high frequency components are then focused by means of the wavefront design. The approach could simplify treatment planning, reduce system complexity, increase the number of accessible targets, and decrease treatment variability.

Statement of Contribution/Methods

Large-amplitude focused acoustic pressure waves were propagated through bone phantoms and ex vivo human skull sections. Transmitted pressure fields were spatially scanned and reconstructed for analysis. Two source transducers, each driven at their fundamental thickness modes, were used for the experiments: one with a fundamental frequency of 0.272 MHz and the other at 0.544 MHz. Field reconstructions were performed at the fundamental frequencies for both scans; for the 0.272-MHz transducer, an additional field reconstruction was performed at its second harmonic, which by design, coincided with the fundamental frequency of the 0.544-MHz transducer. In addition, a simulation study was performed for a 6-element array (fc = 0.3 MHz) to examine the nonlinear field patterns of combined sources.

Results

A significantly less distorted second harmonic [Energy Distribution Index (EDI) = 1-(percent of energy localized within the focal zone) = 0.40] was observed, as compared to direct propagation of 0.544 MHz through the skull (EDI = 0.74) (Fig. 1). Similar results were obtained with phantom experiments (EDI = 0.44 and 0.75 respectively). The results from a 6-element array simulation indicate a sharp peak intensity of the 2nd harmonic (Fig. 1).

Discussion and Conclusions

Experimental and simulation studies indicated that harmonic focusing can be used to produce a less distorted transcranial HIFU field. Ongoing studies are examining the optimization of this method for transcranial applications and the extrapolation of this method for other anatomical sources of HIFU aberration. (NIH 1U41RR019703-01A2)

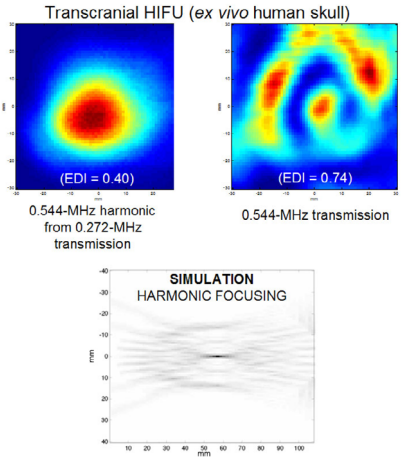

P3D054-05

Thermal Breakdown Caused by High-Amplitude and Long-Burst Pulse Transmission for Phase-Conversion Molecular Imaging

Takashi Azuma[1], Ken-ichi Kawabata[1], Shin-ichiro Umemura[2]; [1]*Hitachi Central Research Laboratory, Kokubunji, Tokyo, Japan,* [2]*Tohoku University, Japan.*

Background, Motivation and Objective

In phase-conversion ultrasonic molecular imaging (PCUMI) [1], tissue-selective nano-droplets are converted to contrast microbubbles by using higher power ultrasound with than that transmitted from a conventional imaging array. Developing wideband imaging arrays capable of PCUMI is useful since many developed imaging sequences will be available immediately after phase-conversion. Since the sensitivity of an array decreases as a result of the breakdown after the transmission of PCUMI, the limitations of duration and amplitude need to be overcome before an array for a PCUMI can be used. We carried out various experiments and numerical simulations to investigate the breakdown process. In our previous study, the conventional array using two PZT layers was broken after driving with 16 cycle pulses at 50 V caused by peeling of the adhesive between two PZT layers[2]. We measured breakdown conditions and breakdown process of an imaging array using single PZT layer.

Statement of Contribution/Methods

We measured the electric impedances and the waveforms of transmitting pulses of array elements in an imaging array using single PZT layer after high-amplitude and long burst transmission. These results were compared with the impedance and waveform calculated by PZFlex, a finite element code, by assuming several different ways of breakdown.

Results

Breakdowns of the array occurred after driving with 100 cycle pulses at 160 V. This single PZT layer array could transmit higher power than two PZT layer array before breakdown. Mechanical Q values were increased with duration length during this breakdown process. The experimental result was consistent with the simulation result assuming the peeling of the adhesive between PZT and the matching layer. These results indicated that suppressing increases in temperature is also essential for PCUMI using this improved array. Our simulation study has already showed that a new transducer structure that uses a heat conducting acoustic isolation layer (AIL) on a metal block that was designed to inhibit this type of breakdown while maintaining the wide bandwidth required for imaging. Experimental results of the thermal breakdown after PCUMI transmission from our proposed structure probe will also be discussed.

Discussion and Conclusions

The single PZT layer array is suitable for PCUMI because the peeling between PZT and matching layer occur at higher temperature than the peeling between two PZT layers. To prevent the peeling between matching layer and PZT, heat conductance around PZT should be improved. Our simulation indicates that the proposed structure improved heat conductance in a transducer array that uses AIL, and will be useful for PCUMI.

Part of this work was supported by the New Energy and Industrial Technology Development Organization, Japan.

[1] K. Kawabata, et al, IEEE Ultrason. Symp. (2006) 517-520.

[2] T. Azuma, et al, IEEE Ultrason. Symp. (2006) 836-839.

P3D055-06

Contrast Agent Kinetics in the Rabbit Brain During Exposure to Focused Ultrasound

David Goertz, Cameron Wright, Kullervo Hynynen; *Sunnybrook Health Sciences Centre, Toronto, Ontario, Canada.*

Background, Motivation and Objective

It has been established that ultrasound in combination with microbubbles is capable of producing transient blood-brain barrier disruption. A key factor that will influence the efficiency of BBB breakdown is the concentration of contrast agent within the focus, which will vary with time due to bolus dynamics, the breakdown of agent within the body, and its possible destruction and reperfusion within the beam. The objective of this study was to investigate the kinetics of contrast agent concentration within the brain when it is subjected to pulsed focused ultrasound.

Statement of Contribution/Methods

An ultrasound imaging array was mounted within the aperture of a 1.68 MHz focused therapy transducer. Experiments were performed in the brains of rabbits that had undergone skull window surgery, with the therapy beam focus localized within one hemisphere. Pulse lengths of 10 ms were employed at repetition rates of 0.1-2 Hz and acoustic powers of 0.1-1 watts. Contrast imaging was performed for up to 9 minutes following the bolus injection of Definity. Contrast signal power was then quantified in regions of interest within the acoustic focus of the therapy beam, as well as in the contra-lateral hemisphere.

Results

Following the injection of the contrast agent, signals peaked within 10 seconds and then underwent a period of slow decay. Individual therapy pulses resulted in microbubble depletion within the focus for powers >=0.25W, with full recovery of signal occurring within 1-3 seconds, depending on transmit power. As the pulse repetition rates increased, agent reperfusion between pulses was incomplete and the concentration within the beam was progressively diminished, to a degree dependent upon both power and repetition rates.

Discussion and Conclusions

These results demonstrate that microbubble concentration can be substantially influenced by destruction induced by therapeutic ultrasound pulses. The kinetics of this effect may therefore be a significant factor influencing the efficiency of BBB breakdown.

Wednesday Poster

P3D056-07

Characterization of sonicated breath films by Atomic Force Microscopy

Timur Saliev, Matt Mullan, Paul Campbell; *University of Dundee, Dundee, Scotland, United Kingdom.*

Background, Motivation and Objective

Ultrasound-induced drug delivery holds significant promise as a safe and controllable release modality for pharmacological therapeutics. For this purpose the principle of slow degradation of polymeric materials (under specific stimuli) has been exploited in different devices as to disengage drugs from compact reservoir. The novel concept has been devised to optimize functionality and add an on-demand release-selectivity to such bio-chips.

Statement of Contribution/Methods

Our acoustically activated drug delivery system contains a bubble embedded polymeric matrix, that responds to distinct acoustic cues. The micro-porous polymer films (Cellulose Acetate Butyrate) were developed as a model for such matrices and are easily fabricated by a spin coating procedure. Samples so formed can exhibit visually different appearances: either opaque or transparent. Each of such as-spun films was characterised by a stage-mounted JPK NanoWizard Atomic Force Microscope (AFM) operating in air-contact mode. Topographical data

showed that the surface of opaque (white) sites has a pocked character with pits exhibiting a uniform dense distribution.

Results

The average diameter of pits was 0.35 ìm and depth approx. 0.20 ìm. On the other hand, the AFM examination of transparent sites revealed the deficiency of pits population. Upon exposure to ultrasound radiation in different regimes (with a gradual increase of acoustic power and intensity), films were then subjected to AFM characterization. Surface measurement data illustrated dramatic changes of polymers microstructure, particularly within high-intensity mode which can be related to cavitation activity on the different topographies of each type of porous film.

Discussion and Conclusions

It was revealed a direct correlation between the degree of degradation of cellulose film and the augmentation of ultrasound intensity. These findings corroborate the hypothesis that such polymer-based matrix could play a role of controllable barrier in portable transdermal drug releasing devices.

P3E. Therapeutic Ultrasound Technologies

2nd and 3rd Floor Foyers

Wednseday, November 5, 2008, 3:00 pm - 4:30 pm

Chair: **Nobuki Kudo;**
Hokkaido University, Japan.

P3E057-01

Progress in CMUTs for HIFU ablation of lower abdominal cancer

Serena Wong[1], Ronald Watkins[2], Mario Kupnik[1], Kim Butts Pauly[2], Butrus T. Khuri-Yakub[1]; [1]*Stanford University, Electrical Engineering, Stanford, CA, USA,* [2]*Stanford University, Radiology, USA.*

Background, Motivation and Objective

Recently, high intensity focused ultrasound (HIFU) treatment guided by magnetic resonance imaging (MRI) is promising because it may reduce patient morbidity, lower costs, and increase accessibility of treatments. For example, resection of metastatic colorectal cancer increases 5-year survival from 8% to 30%, but only 20% of patients are suitable for resection. For the remaining 80%, a noninvasive treatment, like MRI-guided HIFU, would greatly improve their outcome. In previous work, we demonstrated that CMUTs have advantages including fabrication flexibility, improved bandwidth, and high power performance with minimal loss, compared to piezoelectric transducers. We also showed heating of a phantom by unfocused CMUTs under MR-temperature maps. In this paper, we report the first focused CMUT array operating for continuous wave therapy.

Statement of Contribution/Methods

An 8-element, equal-area concentric ring array with 3 cm diameter was designed to focus 35-55 mm into tissue and target 1.3 mm lesions in the focal plane for upper abdominal cancer ablation. Each element consists of close-packed circular cells, with 70 mm radius, 6 mm conductive membranes, and 0.4 mm gap heights, designed for operation at 2.5 MHz and 1.5 MPa peak to peak output pressure. After wire bonding the device to a printed circuit board, we investigated crosstalk by exciting the center element with a 2.5 MHz tone burst signal and measuring the cell displacement in neighboring elements to observe surface wave propagation. Then, we investigated the far field beam pattern of the center element using a hydrophone (HNV-400 Onda Corporation, Sunnyvale, CA) positioned 5.5 cm from the transducer's surface. Finally, we used a direct digital synthesizer with 4 outputs (DDS9m, Novatech, Dallas, TX), each with programmable phase and frequency, and a set of amplifiers (ZHL-1W, Minicircuits, Brooklyn, NY) to focus the 4 center elements. The time delay (phase) of each channel was calculated by taking the difference in distances from the center of each ring to the focal point. The array was focused to 35 mm and the beam pattern was measured.

Results

From crosstalk measurements, cells in neighboring elements showed a center displacement at least 10 dB down from the displacement of the excited element. We found surface waves traveling at 1000 m/s, which are related to dispersive guided modes. The measured far field beam pattern of the center element matched well with the expected beam profile, except that the dispersive guided mode caused the pressure to be increased in the edges of the beam profile; however, this effect was minimal. After focusing 4 elements with electronics, we obtained a beam width of 2 mm and a suppression of side lobes to –10 dB.

Discussion and Conclusions

Focusing 4 elements in the CMUT array showed minimal crosstalk and good agreement with models. In the future, we will expand the system and working elements to 8 rings; the focused heating will by measured under MRI to determine the heated spot size.

Wednesday Poster

P3E058-02

Development of a reliable ultrasound power source for metrological applications

Elyr Alves, Rodrigo Costa-Felix; *Inmetro, Laboratory of Ultrasound, Duque de Caxias, Rio de Janeiro, Brazil.*

Background, Motivation and Objective

In ultrasound biomedical applications, often undesirable lacks in traceability are a matter of concern. As consequence, reliability of biomedical devices is under check, and it has been reported in specialized literature. Particularly, ultrasound power measurements should only be undertaken if testing equipments, being radiation force balance (RFB) the most usual one, were properly calibrated. A metrological accepted way to provide traceability is through a stable continuous wave check source (SCWSC) as transfer device. At least one commercially available SCWSC exists. Nevertheless, some more specific metrological aspects regarding calibration of physiotherapy ultrasound equipment are not possible with that device. Features as the possibility of full remote control (measuring automation), intermittent and continuous output signals, and sets of different output frequencies and powers are not present in SCWSC.

This paper describes the development of a stable, reliable power source for metrological applications, initially designed to assure traceability of physiotherapy ultrasound RFB.

Statement of Contribution/Methods

The goal was to develop a metrologically reliable ultrasound power source that could reproduce main characteristics of usual ultrasound therapy equipment. Those were three output frequencies (1, 3 or 5 MHz), three output powers (10, 100 and 1000 mW), continuous and intermittent output signals with 5 duty cycles (10, 30, 50, 70 and 90%). Any combinations of those parameters can be chosen. Another possibility, not implemented yet, is a build-in feature of complete remote control, what is fundamental for measurement automation. User errors are minimized by that, and faster measurement protocol can be easily implemented.

Results

Beyond the self contained difference of the developed power source, which is a result by itself, the signal output quality was evaluated in a metrological base. Output signal frequency adjustment had a measured deviation of less than 1%, and signal to noise ratio was better than 48 dB. Power calibration disclosed repeatability of less than 5%, and deviation to nominal output value were less than 10%. All those characteristics were achieved due the construction of its electronic architecture, basically because of the implementation of a programmable digitally gain control to the power amplifiers. Although the development is of a prototype so far, the final cost of the source is estimated to figure about 4 times lesser than the sources available.

Discussion and Conclusions

Applicability of the source joined with its low cost profile can be used as a tool for traceability diffusion in ultrasound power. The developed source was compared with Brazilian national power source standard, and it was found good agreement regarding signal quality. Other features of the new power source let it be more useful as metrological equipment. Next step is to implement the remote control feature to the source.

P3E059-03

A harmonic cancellation technique for an ultrasound transducer excited by a switched-mode power converter

Sai Chun Tang, Gregory Clement; *Harvard Medical School / Brigham and Women's Hospital, Radiology, Boston, MA, USA.*

Background, Motivation and Objective

Switched-mode DC-to-AC power converters are commonly used for ultrasound piezoelectric transducer excitation because of their higher power density, high energy efficiency and low manufacturing cost compared to their linear counterparts. However, without additional filtering circuitry at the power converter output, the harmonics present in the output switching waveform produce undesired acoustic sidelobes in high intensity focused ultrasound (HIFU) applications, and also incur unnecessary power dissipation from the power converter and the transducer.

Statement of Contribution/Methods

This study examines the feasibility of using harmonic cancellation (HC) for therapeutic ultrasound transducers excited by a switched-mode power converter without an additional output filter. A switching waveform without the 3rd harmonic was created by cascading two switched-mode power inverter modules at which their output waveforms were pi/3 phase-shifted from each other. The waveform and harmonic contents of the acoustic pressure generated by a 1-MHz self-focused piezoelectric transducer with and without HC were evaluated.

Results

Measured results indicate that the acoustic 3rd harmonic-to-fundamental ratio at the focus was small (-48dB) with HC, compared to that without HC (-20dB). The measured acoustic levels of the 5th harmonic for both cases with and without HC were also small (-46dB) compared to the fundamental. Figs. 1 and 2 respectively show the relative acoustic pressure waveform, represented by hydrophone voltage, at 35mm from the transducer without and with HC.

Discussion and Conclusions

This study shows that it is viable to drive a piezoelectric ultrasound transducer using a switched-mode power converter without the requirement of an additional output filter in HIFU applications.

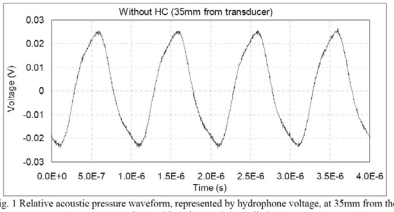

Fig. 1 Relative acoustic pressure waveform, represented by hydrophone voltage, at 35mm from the transducer without harmonic cancellation

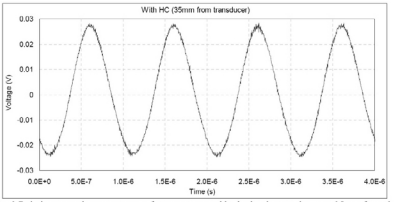

Fig. 2 Relative acoustic pressure waveform, represented by hydrophone voltage, at 35mm from the transducer with harmonic cancellation

P3E060-04

A Model-Based Displacement Outlier Removal Algorithm for Ultrasonic Temperature Estimation

Guoliang Ye, J. Alison Noble, Penny Probert Smith; *University of Oxford, Department of Engineering Science, Oxford, Oxfordshire, United Kingdom.*

Background, Motivation and Objective

In using ultrasound echo strain to estimate temperature for monitoring HIFU thermal therapy, block matching algorithms such as correlation analysis are used to estimate the displacement over two image frames. However the displacement will be estimated with outliers which will seriously bias echo strain estimation. This is due the HIFU exposures causing thermal acoustic lens and thermal expansion, leading to image distortion and artifact over image frames. This paper introduces a novel model-based algorithm to constrain the displacement estimation to reject the outliers.

Statement of Contribution/Methods

The displacement is initially estimated using correlation analysis and then the outliers on the displacement data will be removed by examining the difference between the data and a parameterized displacement model. Finally the removed outliers will be replaced by the expected values from the model or the interpolation from neighboring normal data. The ideal model in theory depends on the spatial distribution of the echo strain and hence the temperature distribution in medium, but in practice we found that a linear or second order polynomial is suitable since the displacement caused by temperature changes varies slowly in axial depth. The parameters of the model are automatically estimated by a weighted least squares method running iteratively to select the normal displacement data (non-outliers) to minimize the fitting error.

Results

To validate the model-based algorithm, data form a uniformly heated gel phantom and a bovine liver with HIFU exposures was used and the results were compared to a median filter which is an ordinary method to remove outliers. Since the median filter removes outliers by examining the difference between the data and the median values over its neighboring data, its length has to be long enough to cover enough normal data to produce a normal median value. The results of the above data showed that the length of the median filter up to 1.5 mm can remove most of the outliers except those closed to the end of the data. This is because there is no more normal data available outside the data though the length of the filter is increased. However, the results of the model-based algorithm successfully removed all the outliers. This is because its model is parametric and globally taking accounts of the whole displacement data.

Discussion and Conclusions

In conclusion, the model-based algorithm is the first method in this area to introduce a displacement model as prior information to remove outliers, which shows a great potential to improve the ultrasonic temperature estimation especially in low SNR ultrasound data due to HIFU exposures.

Wednesday Poster

P3E061-05

A Novel Ultrasonic-Imaging Based Temperature Estimation Approach by Instantaneous Frequency Detection

Hao-Li Liu[1], Sheng-Min Huang[1], Meng-Lin Li[2], Kuen-Cheng Ju[3]; *[1]Chang Gung University, Department of Electrical Engineering, Tao Yuan, Taiwan, [2]National Tsing-Hua University, Department of Electrical Engineering, Hsinchu, Taiwan, [3]I-Shou University, Department of Biomedical Engineering, Kaohsiung, Taiwan.*

Background, Motivation and Objective

Focused ultrasound thermal therapy relies on temperature monitoring for treatment guidance and assurance of targeting and dose control. In ultrasound-imaging based temperature estimation approach, a standard approach is to detect echo time shifts by using cross-correlation processing from the segmented radio-frequency (RF) data. In this study, we aim to propose a novel algorithm to perform temperature estimation by detecting the instantaneous frequency for better computational efficiency.

Statement of Contribution/Methods

A novel algorithm to perform fast temperature estimation from ultrasonic imaging was proposed. This new algorithm may serve as an alternative for implementing 2D temperature estimation into a clinical ultrasound imager. Focused ultrasound was used as the heating source, and the beamformed RF signals provided from a 2D ultrasound imager were used to verify the algorithm for temperature change estimation. Heating experiments of tissue-mimicking phantoms and ex-vivo porcine muscles were conducted.

Results

Our results show that the proposed new algorithm yields up to six times better computational efficiency while its contrast detection ability and precision rival those of cross-correlation-based algorithm. In the ex-vivo tissue experiments, we also presented the irreversibility of the echo time-shift effect in the necrotic region, which is different from that in the tissue-mimicking phantoms.

Discussion and Conclusions

In this study, we propose a new approach for temperature estimation by employing instantaneous frequency detection; it was implemented by using a simple zero-crossing algorithm. Some of the features of this approach are its superior computational efficiency and the possibility of higher spatial resolution for temperature mapping. Further, the experimental results have demonstrated that the proposed algorithm can provide similar temperature detection ability and precision as compared to the cross-correlation algorithm. Tissue irreversibility when approaching the necrotic temperature encounters difficulty in accurate temperature estimation, which has been proposed and discussed as an alternative possibility to detect tissue necrosis rather than temperature. This provides useful information as well as an alternative for the clinical applications of such an ultrasound-based temperature estimation technology.

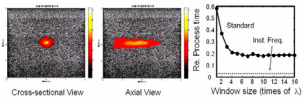

P3E062-06

Thermal imaging with ultrasound reflex transmission methods

Caleb H Farny, **Greg T Clement;** *Harvard Medical School, Radiology, Boston, MA, USA.*

Background, Motivation and Objective

Noninvasive thermal imaging is a tool that has a number of applications in medicine, most notably in thermal ablation monitoring. Ultrasound-based methods have been developed for monitoring temperature change, based on the relationship between sound speed and temperature in soft tissue, but current methods have not yet been reliably proven in in vivo settings. Recently, results were presented demonstrating the feasibility of applying an ultrasound phase-contrast method for determining the temperature change in water from a thermal plume in a through-transmission arrangement.

Statement of Contribution/Methods

Here we present results from reflex transmission measurements of steady-state heating from a HIFU transducer in a tissue phantom. A 1.68-MHz focused transducer interrogated the phantom and a near-acoustically transparent hydrophone was scanned throughout the sound field to obtain the reflection from the back surface of the phantom. The output from a 1.088-MHz HIFU transducer was interleaved with the diagnostic transducer transmission to induce a steady-state temperature change in the phantom. Two hydrophone scans were performed to obtain the reflex transmission signal before and during heating. The sound fields were numerically back-projected to the region of heating, integrated along the propagation axis, and tomographically reconstructed to obtain the phase change, from which the sound speed and temperature change was determined.

Results

Shown below, the heating induced in the phantom is clearly apparent from the decrease in phase change in the resulting image, revealing the oblong-shaped temperature field expected from the thermoviscous absorption of the HIFU sound field. Multiple temperature rises were tested, ranging from 10 – 18° C. The reconstructed temperature rise compared favorably with the expected temperature rise obtained with an embedded thermocouple.

Discussion and Conclusions

Due to the lengthy acquisition time, the temperature rise was necessarily steady-state, but the method is adaptable to dynamic heating measurements. Thermal lensing effects are visible in the images, but may be corrected for by applying a moving average filter. The result is a method which can visualize the temperature change over a spatial region sufficient for monitoring thermal ablation treatments. [Support from the NIH:U41 RR19703]

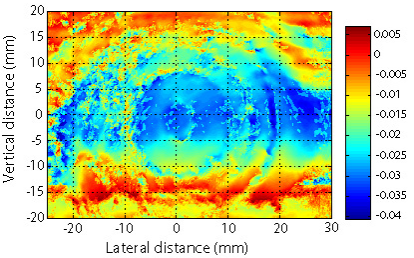

P3E063-07

Strong Spatially Localized Loss in High Intensity Ultrasound from Nonlinear Propagation

Gianmarco Pinton, Gregg Trahey; *Duke University, Biomedical Engineering, Durham, NC, USA.*

Wednesday Poster

Background, Motivation and Objective

Experimental and numerical investigations have determined that nonlinear propagation of ultrasound in tissue results in an enhancement of heat deposition[1]. As the wave propagates the nonlinear distortion creates higher frequencies components that are more strongly attenuated than an equivalent linearly propagated wave. The primary thrust of previous studies has been to characterize the effects of nonlinearity on heating. The goal of this paper is to numerically quantify the energy loss from nonlinear acoustic propagation for a diagnostic ultrasound transducer.

Statement of Contribution/Methods

A full-wave equation that describes nonlinear propagation in an arbitrarily attenuating medium is solved numerically with finite differences in the time domain[2]. Calibrated pressure measurements at the surface of a 2.22 MHz commercial diagnostic ultrasound transducer focused at 4.9 cm laterally are used as an input to the simulations. These simulations output both the acoustic pressure and the loss throughout the three dimensional field of view for varying pressures. A three dimensional simulation of the Khoklov-Zabolotskaya-Kuznetsov equation with arbitrary attenuation in the frequency domain is used to verify the predicted loss field and is shown to have good agreement with the full-wave simulation.

Results

For 3.2 MPa surface pressure the energy loss predicted by the nonlinear simulation is 5.3 times larger than the loss predicted by a linear simulation. Consistent with the self-focusing effects of nonlinear propagation the -6 dB beamwidth for the nonlinearly calculated loss in the lateral dimension at the focus 0.38 mm and 0.63 mm for the

linear loss. This corresponds to a difference of approximately 60%. The dropoff for the nonlinear loss is also much stronger resulting in an even greater self-focusing effect at -20 dB. This behaviour is also observed in the elevation plane where the self focusing is also 60% at -6 dB. At lower intensities, e.g. 1 MPa, the loss observed at the focus is only a factor of 1.4 larger than what is predicted by a linear simulation.

Discussion and Conclusions

For intensities at the upper range of commercial ultrasound transducers there is a significant difference in the lost energy at the focus that is not observed elsewhere in the acoustic fields. This loss has significant implications for heating and acoustic radiation force. These results suggest that small narrow region along the focus is quickly heated before thermal diffusion broadens the spatially localized loss.

[1] Bailey et. al. "Physical mechanisms of the therapeutic effect of ultrasound," Acoustical Phys., 49(4):437-464, 2003.

[2] Pinton et. al."A heterogeneous nonlinear attenuating full-wave model of ultrasound" IEEE UFFC, Accepted, 2008.

P3F. MUT Transducers

2nd and 3rd Floor Foyers

Wednseday, November 5, 2008, 3:00 pm - 4:30 pm

Chair: **Qifa Zhou;**
University of Southern California, CA, USA.

P3F064-01

Curvilinear Capacitive Micromachined Ultrasonic Transducer (CMUT) Array Fabricated Using a Reverse Process

Alessandro Caronti, Andrea Coppa, Alessandro Savoia, Cristina Longo, Barbara Mauti, Philipp Gatta, Giosuè Caliano, Massimo Pappalardo; *University Roma Tre, Aculab, Dept. of Electronics Engineering, Roma, Italy.*

Background, Motivation and Objective

Capacitive Micromachined Ultrasonic Transducers (CMUTs) have shown the potential for use in medical imaging. The development of curved probes, featuring a larger field of view at depth, enables a vast number of applications in the diagnostic imaging market. The motivation of this research is to cover a wider field of applications using the CMUT technology. This paper presents the manufacturing of a cylindrical curvilinear CMUT array developed using our patented reverse fabrication process, and concludes with experimental results demonstrating the ability of this process to make curved CMUTs.

Statement of Contribution/Methods

The curvilinear array consists of a flexible 192-elements CMUT array bonded to a curvilinear surface of backing material, and covered with a silicone rubber layer acoustically matched to the fluid medium. The flexible CMUT transducer is fabricated using the reverse process previously reported by the authors. In this process the silicon nitride CMUT membranes are surface micromachined over a silicon substrate, which is finally removed so as to leave the membranes lying over a flexible backing. The active device is 24 mm large and 6.5 micron thick after complete etching of the silicon substrate, the mechanical support being provided by the backing base. After the application of the frontal protective layer, the flexible transducer assembly looks like an array of micromembranes embedded in the backing and rubber layers.

Results

The functionality of the flexible curvilinear CMUT array was demonstrated by means of electrical impedance measurements and pulse-echo experiments. The transducer elements were wire-bonded to a flex printed circuit and electrically connected to a front-end electronics. The 24 mm wide flexible transducer assembly was curved with a radius of curvature of 10 mm preserving membrane and device integrity. The pulse-echo measurements showed a centre frequency of about 11 MHz with a fractional bandwidth as high as 100%. No deleterious effect or performance degradation resulting from curving of the CMUT were observed.

Discussion and Conclusions

The reverse fabrication process for CMUT arrays was successful to manufacture curvilinear arrays with the radii of curvature required in convex and endocavity probes. Further work is currently in progress to achieve the generation of ultrasound images by curved CMUTs.

P3F065-02

Dual-Electrode CMUT optimization for CMUTs with uniform and non-uniform membranes

Rasim Guldiken, Jaime Zahorian, Mujdat Balantekin, **Levent Degertekin;** *Georgia Institute of Technology, USA.*

Background, Motivation and Objective

Further improvements in the CMUT performance are needed to make it the transducer of choice for many imaging applications. Dual-electrode CMUT structure which has multiple electrodes in its dielectric membrane, has been developed to improve both the receive and transmit performance using larger design space for optimization. Previous experimental and simulation studies on dual-electrode CMUTs showed overall transduction gains exceeding 15dB with dual electrode structure when compared to a conventional CMUT [1]. Here, we extend our investigation to non-uniform membrane dual-electrode CMUT structures and consider the electrical crosstalk between electrodes in the membrane.

Statement of Contribution/Methods

In this paper, the electromechanical coupling coefficient (k2) is used as an optimization parameter for dual electrode CMUTs. Calculation of k2 is based on energy values which are directly obtained from the FEA without a need for post processing. The optimization study includes different mechanical membrane structures, such as non-uniform dielectric membranes. The active and crosstalk capacitances between the electrodes are simulated using FEA and the results are compared with experimental measurements. The effect of membrane and immersion medium properties on the internal cross talk is also discussed.

Results

The result indicate that k2 increases from 0.24 to 0.71 (for 90% of the collapse) when optimized dual electrode structure is employed in the design with a uniform nitride membrane. When the thickness of the membrane is allowed to be non-uniform over the center electrode, the optimized k2 increases to 0.85 along with increasing bandwidth and lower DC Bias. In addition, the transmit sensitivity is increased to 15.4kPa/V from 12.3kPa/V. Overall, dual-electrode CMUT with non-uniform membrane provides transduction gain of more than 20dB as compared to conventional CMUT with uniform membrane. The internal electrical cross-talk simulation results for uniform membrane dual-electrode CMUT detailed in [1] has cross talk ratio of -37.2dB, -34.7dB and -21.7dB for air, oil and water operation respectively. Depositing 5im parylene on the membrane improves the cross talk to -32dB for water operation. Experimental measurements match the simulations within 2dB.

Discussion and Conclusions

A fast, direct k2 calculation is used for optimization of dual electrode CMUTs. Significant transduction performance increase exceeding 20dB is obtained exploiting non-uniform membranes. An important concern for dual electrode operation – crosstalk between side and center electrodes- is investigated by simulation and experiments, and cross-talk reduction methods are proposed.

[1] R.O. Guldiken, J. Zahorian, M. Balantekin, and F. L. Degertekin, "Characterization of Dual-electrode CMUTs: Demonstration of Improved Receive Performance and Pulse Echo Operation with Dynamic Membrane Shaping" IEEE Trans. Ultra. Ferro. and Freq. Control, under review.

P3F066-03

The design and characterization of capacitive micromachined ultrasonic transducers (CMUTs) for generating high-intensity ultrasound for transmission of directional audio

Ira Wygant[1], Mark Wochner[2], **Mario Kupnik[1],** Jeffry Windsor[2], Wayne Wright[2], Mark Hamilton[2], Butrus Khuri-Yakub[1]; [1]*Stanford University, USA,* [2]*The University of Texas at Austin, USA.*

Background, Motivation and Objective

A directional source of audio sound created using a parametric array, sometimes called an acoustic spotlight, generates a sound beam that is much narrower than the sound beam generated by a conventional source. These directional sources, which are finding increasingly widespread use for localizing sound (e.g., in automobiles or on laptop computers), require the transmission of a modulated high-intensity ultrasonic carrier wave.

Capacitive transducers are well-suited for parametric array audio applications because they can efficiently generate high-intensity ultrasound with a relatively wide bandwidth. CMUTs with vacuum-sealed cavities are particularly advantageous because they lack squeeze-film damping, which increases bandwidth but reduces membrane displacement, and because their sealed cavities and permanently attached membranes make them relatively robust.

At last year's Ultrasonics Symposium, we described the design, fabrication, and initial testing of 8-cm diameter CMUTs for generating high-intensity 50-kHz ultrasound. In this paper, we examine these CMUTs as sources of directional sound.

Statement of Contribution/Methods

Previous work on audio frequency parametric arrays has focused on the acoustics of the parametric array and the signal processing required for generating distortion-free sound. In this work, we focus on the transducer requirements and how these requirements can be met with CMUT technology.

We used simulations based on the KZK equation to estimate the effective sound pressure levels at the face of the CMUTs and to verify measurements of sound as a function of distance. Finite element modeling and the parallel-plate capacitor model of the CMUT was used to predict resonance frequency and output pressures.

Results

Measurements made with an interferometer show that membranes at the edge of the device resonate at a higher frequency and have about one-half the displacement as those membranes in the center. These variations are a result of variations in cavity depth and account for wider than expected bandwidths and lower than expected average sound pressure levels. Accounting for the variation in cavity depth, we estimated sound pressure levels of 138 dB and 131 dB at the center of the wafer based on the measurements made at 3 m.

Using 48.5-kHz and 53.5-kHz primary frequencies, we used the CMUTs to transmit 5-kHz directional sound. We measured the sound pressure level at 5-kHz between 0.5 m and 4 m. The measured variation in sound pressure level as a function of distance agreed with simulation.

Discussion and Conclusions

Simulations show that measured 139-dB source pressure is adequate to transmit directional audio over several meters to tens of meters with a moderate source size. We are currently fabricating new CMUTs with thicker insulating oxide, an etch stop for uniform cavity depths, and piston-like membranes for improved performance.

P3F067-04

Co-optimization of CMUT and Receive Amplifiers to Suppress Effects of Neighbor Coupling Between CMUT Elements

Sigrid Berg, Trond Ytterdal, **Arne Rønnekleiv;** *Norwegian University of Science and Technology (NTNU), Dept. of Electronics and Telecommunication, Trondheim, Norway.*

Background, Motivation and Objective

Neighbor coupling between CMUT elements at the CMUT-water interface is a problem that many research groups have addressed. In a CMUT array made for medical imaging each element consists of several CMUTs, and when we steer the ultrasonic beam to an off axis direction, the various elements operate at different phase. This leads to local high-Q resonances which have a negative effect on the overall performance of the array by shorting the radiating part of the array impedance. Simulations show that these unwanted resonances occur in a frequency range below the center frequency, but well within the 100 % bandwidth of the device.

Statement of Contribution/Methods

It is important to co-optimize the CMUT and electronics design to reduce the effects of these unwanted resonances. We propose to utilize charge sampling amplifiers that have low input impedance to reduce the effects of the unwanted resonances.

Results

By providing a low impedance path, CMUT charge can be extracted even though unwanted modes have been excited. The low power amplifier based on field-effect transistors absorbs little energy and still manages to detect the signal without adding much noise. Insertion loss is hence irrelevant. The low load impedance means that the shorting due to unwanted resonances is strongly reduced, and hence their influence on the current from the CMUT is greatly reduced. The analysis further shows that the unwanted modes add noise to the front end, and hence increase the effective noise factor for the CMUT array in directions and frequency ranges where they are excited. The noise is very narrow banded, so the noise factor will still be acceptable looking at the entire bandwidth of the transducer. A critical parameter deciding the Q-factor of the resonances is the product of the frequency and the viscosity of the fluid outside the CMUT array. We will present a combination of MATLAB and Spice simulations showing how the CMUT array performance is influenced by the parameters of the receive amplifiers.

Discussion and Conclusions

The discussed charge sampling amplifier gives low distortion of the CMUT receiver response due to the unwanted resonances, and at the same time it gives a low noise factor. Suppression of noise is not as efficient as suppression of ripple, but integrated over a wide band, the total noise figure is not disturbing. The sampled output signal also provides good basis for making a circuit for electronic focusing on the chip. Hence the charge sampling amplifier is a good alternative as preamplifiers for CMUT array transducers.

P3F068-05

Accurate Modeling of Capacitive Micromachined Ultrasonic Transducers in Pulse-echo Operation

Mujdat Balantekin, **Levent Degertekin;** *Georgia Institute of Technology, George W. Woodruff School of Mechanical Engineering, Atlanta, GA, USA.*

Background, Motivation and Objective

Performance of a capacitive micromachined ultrasonic transducer (cMUT) is usually assessed by a small-signal equivalent circuit model [1]. Since we apply a large pulse during transmission, we cannot use the linear circuit model in pulse-echo operation scheme. Therefore, we need a large-signal model of cMUT to find the output pressure and consequently the received echo voltage. This simulation scheme will also help to estimate and optimize the performance of a cMUT prior to its fabrication and experimental characterization. [1] M. N. Senlik et al., in Proc. IEEE Ultrason. Symp., (2006) pp. 1951-1954.

Statement of Contribution/Methods

We present a large-signal model of a cMUT, based on previous studies of similar electrostatic MEMS actuators [2]. This model combined with the radiation impedance and a medium model is implemented in a circuit simulator. This enables us to obtain the membrane response to an applied pulse, and find the received echo voltage for a given transmit-receive circuitry. [2] F. Wen et al., J. Micromech. Microeng., vol. 14, pp. 452-461, (2004).

Results

As an example, we consider one element of the dual-annular-ring cMUT array designed for forward-looking intravascular ultrasound imaging [3]. An element of this specific array consists of 4 cells each has an area of 35×35 µm2. Our experiments in oil showed that it has a center frequency of 11 MHz and a 95% percent fractional bandwidth. Applying a 170V DC bias and 160V unipolar transmit pulse we obtained approximately 10 mV output voltage from the oil-air interface at 6 mm away from the array. We derived the model parameters from the physical dimensions and measured frequency response, and simulated the overall system. The echo signal from simulations for this specific case is shown in Fig. 1. [3] R. Guldiken et al., in Proc. IEEE Ultrason. Symp., (2007) pp. 1247-1250.

Discussion and Conclusions

Our first results demonstrate that the large-signal modeling of cMUTs can be helpful in estimating its performance. This in turn allows us to change the design parameters and optimize the variables of transmit-receive circuitry to achieve the highest signal-to-noise ratio without going through excessive fabrication and experimental characterization steps.

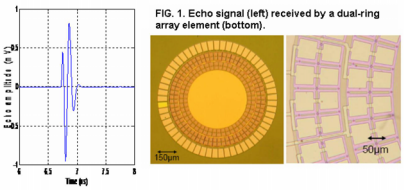

FIG. 1. Echo signal (left) received by a dual-ring array element (bottom).

Wednesday Poster

P3F069-06

Analytically Calculating Membrane Displacement and the Equivalent Circuit Model of a Circular CMUT Cell

Ira Wygant, **Mario Kupnik,** Butrus Khuri-Yakub; *Stanford University, USA.*

Background, Motivation and Objective

A small-signal equivalent circuit model and finite element analysis (FEA) often guide CMUT design. Typically, a combination of numerical and analytical methods (as described by Nikoozadeh et al. at the 2004 Ultrasonics Symposium) or FEA (as described by Lohfink and Eccardt in TUFFC 2005) is used to derive the equivalent circuit parameters. An analytical approach to CMUT design is desired because it provides design intuition and efficient numerical analysis.

Statement of Contribution/Methods

In this work, we derive the equivalent mass-spring-dashpot parameters, membrane displacement as a function of DC voltage, and the pull-in voltage of a CMUT with a circular membrane of uniform thickness.

The analysis assumes that the membrane deflection is small relative to the membrane deflection and that the shape of the membrane relative to its maximum deflection (sometimes referred to as the shape function) is constant with applied DC bias.

Results

The static deflection of a circular plate, clamped at the edge, is given by (1), where D is the flexural rigidity of the membrane material, p0 is a uniform pressure, a is the membrane radius, and r is radial position. From (1) we find that the average membrane displacement is 1/3 the peak displacement and the effective spring constant (average displacement per N of force) is equal to (2). Next, we assume that the mode-shape of the first resonance frequency is equal to the membrane shape given by (1), from which we can calculate the equivalent mass using the Galerkin method (3). Finally, we assume that the damping is given by (4), where Rmed is the plane-wave impedance of the medium. From these equations we can calculate the resonance frequency (5) and Q (6).

The capacitance as a function of membrane displacement is given by (7). Following the methodology described in Nemirovsky et al. (JMEMS 2005), we calculate membrane deflection as a function of DC voltage and the pull-in voltage. If we neglect the effect of atmospheric pressure, we find that the membrane always pulls in when the membrane displacement is 46% of the gap and that the pull-in voltage is given by (8). The calculated results are consistent with FEA.

Discussion and Conclusions

The presented equations allow for simple calculation of the CMUT's DC bias point from which the equivalent circuit model parameters are derived. The equations could also be used for a large-signal differential-equation-based model.

$$w = \frac{p_0}{64D}(a^2 - r^2)^2 \quad (1)$$

$$w_{avg} = \frac{\int_0^a 2\pi r w(r) dr}{\pi a^2} = \frac{p_0 a^4}{192D} = \frac{w_{max}}{3}$$

$$k = \frac{p_0 \pi a^2}{d_{avg}} = \frac{192D\pi}{a^2} \quad (2)$$

$$m = \rho h \int_0^a 2\pi r \frac{2d(r)^2}{d_{pc}} dr = \rho h \frac{9\pi}{5} a^2 \quad (3)$$

$$b = \pi a^2 R_{med} \quad (4)$$

$$\omega_0 = \sqrt{\frac{k}{m}} = 8\sqrt{\frac{5}{3}\frac{D}{h\rho}}\frac{1}{a^2} \quad (5)$$

$$Q = \frac{m\omega_0}{b} = \frac{9}{5}\frac{h\rho}{R_{med}}\omega_0 \quad (6)$$

$$C = \int_0^a \frac{2\pi r \varepsilon_0}{g_0 - w_{max}(1 - \frac{r^2}{a^2})^2} dr = \frac{a^2 \varepsilon_0 \pi \arctanh\left(\sqrt{\frac{w_{max}}{g_0}}\right)}{\sqrt{g_0 w_{max}}} \quad (7)$$

$$V_{c,l=0} = 5.31766\sqrt{\frac{Dg_0^3}{a^2 \varepsilon_0}} \quad (8)$$

Wednesday Poster

P3F070-07

New Technique for Fabrication of High Frequency Piezoelectric Micromachined Ultrasonic Transducers

Thomas Pedersen[1], Rasmus Lou-Moeller[2], Karsten Hansen[3], Tomasz Zawada[3], Erik V. Thomsen[1]; [1]*Technical University of Denmark, Department of Micro and Nanotechnology, Lyngby, Denmark,* [2]*InSensor A/S, Kvistgaard, Denmark,* [3]*Ferroperm Piezoceramics A/S, Kvistgaard, Denmark.*

Background, Motivation and Objective

High frequency ultrasound in the range of 30-120 MHz is used for medical imaging of eyes, skin, small animals or other areas where high resolution is needed. Fabrication of arrays of such transducer elements are however difficult with the traditional lapping and dicing processes. Thus, in this work we present a new technique for fabrication of arrays of piezoelectric elements for high frequency operation.

Statement of Contribution/Methods

The fabrication method is a result of integrating thick film lead zirconium titanate (PZT) deposition techniques with silicon micromachining techniques such that the transducer elements are fabricated on a silicon substrate. The method involves formation of trenches in the silicon substrate, these trenches are then used as moulds for PZT deposition.

Results

The process is illustrated in Fig. 1. KOH is used to etch trenches in the substrate and a 500 nm Pt bottom electrode is deposited, Fig. 1(a). The depth of the trenches will define the thickness of the PZT and hence the resonance frequency. The PZT paste is filled into the trenches with a metal blade, Fig. 1(b), and the organic vehicle is dried out, Fig. 1(c). This is repeated six times to fill up the trenches completely before sintering. Finally a top electrode is deposited by e-beam deposition, this is however not shown in the figure. A cross sectional SEM micrograph of a 13.7 µm thick transducer element is seen in Fig. 2. This illustrates the main benefit of the technique which is the high lateral and transversal dimension control of the elements as they are defined by standard silicon processing techniques.

Discussion and Conclusions

In conclusion a new technique for planar patterning of PZT thick films as transducer elements in ultrasonic transducers is presented. Using KOH etched trenches as moulds for PZT deposition is a simple and cheap method for obtaining very uniform transducer elements with a high operation frequency. This technique is also compatible with pre- or post-processing of other structures on the wafer due to the planar surface of the wafer after PZT deposition.

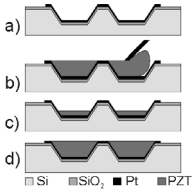

Figure 1: Schematic illustration of the fabrication process.

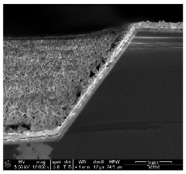

Figure 2: Cross sectional SEM micrograph of a fabricated element.

Wednesday Poster

P3G. Material Characterisation and Fabrication Technology

2nd and 3rd Floor Foyers

Wednseday, November 5, 2008, 3:00 pm - 4:30 pm

Chair: **Qifa Zhou;**
University of Southern California, CA, USA.

P3G071-01

An improved Sandwich Dipole Transducer for High Temperature Environment

Lin Zheng[1], **Weijun Lin[1],** Dong Wang[1], Jianguo Shen[2], Hailan Zhang[1], Xiuming Wang[1]; *[1]The State Key Laboratory of Acoustics, Institute of Acoustics, Chinese Academy of Sciences, Beijing, China, [2]The Laboratory of Acoustic Well Logging, Tianjin University, Tianjin, China.*

Background, Motivation and Objective

In oil fields sandwich dipole transducers are used in acoustic well logging to measure shear wave velocity and anisotropy of formation. The basic structure of the traditional sandwich dipole transducers consists of a metal plate or support slice adhering to two piezoelectric ceramic slices in each side. Due to the apparent difference between thermal expansion coefficients of two kinds of material, the traditional dipole transducer always encounters a technical difficulty that its adhesive layer becomes very weak in the high-temperature environment and piezoelectric ceramic slices might detach from the support slice.

Statement of Contribution/Methods

Aim at this difficulty, we present a novel scheme by cutting notches at the midline of the piezoelectric ceramic slices. As the piezoelectric ceramic slices are cut into small pieces, shear stress at the adhesive layer releases drastically and the piezoelectric ceramic slices would be stuck on the support slice tightly.

Results

Numerical simulations with a finite element method are conducted for evaluating the efficiency of the modified dipole transducer. The numerical results demonstrate that this structural improvement does not change vibration modes of the dipole transducer. Our finite element analysis also shows that there is a negative correlation between the notch width and the natural frequency, and this negative correlation will not be affected by the property of the medium where the transducer works. In our numerical simulations, natural frequency decreases approximately by 12Hz as the notch width increases in each 1mm and the natural frequency of the modified structure is roughly 20% lower than original one. As the transducer vibrates under certain electric stimulation, the average amplitude of displacement at its surface decreases less than 10%.

Discussion and Conclusions

In summary, since the notched sandwich dipole transducer releases the shear stress in the adhesive layer, it would improve stable conditions of the dipole transducer for the high-temperature environment. This improved design could be an alternative to the dipole transducers for acoustic well logging.

Wednesday Poster

P3G072-02

Design and Fabrication of a Novel PZT Films Based Piezoelectric Micromachined Ultrasonic Transducer

Junhong Li, Chenghao Wang; *Institute of Acoustics, Chinese Academy of Science, China.*

Background, Motivation and Objective

To 3D ultrasonic imaging of medicine, a 2D array transducer with lots of elements, high element density and small element size is needed. Achieving such an array is difficult when using conventional transducer fabrication techniques. Micromachined ultrasonic transducers (MUT) are interesting devices . The basic element consists of a micromachined membrane that is driven by either capacitive (cMUT) or piezoelectric actuation (pMUT).Compared with cMUT, pMUT has a lower impedance and easier fabrication processes, but its sensitivity is lower. In this work ,a novel pMUT was developed to enhance the sensitivity and limit the cross coupling between elements.

Statement of Contribution/Methods

A bridge type structure in flexure mode was adopted in this work for the design of pMUT element. Earlier pMUT element had diaphragms that were clamped on all four edges. In comparison, the bridge diaphragms are much more compliant and free from the clamped stress on two side edges in vibrating diaphragms. Moreover, a polyimide film was deposited on the open seams on the two side edges of diaphragms to avoid the acoustic leak. Therefore, pMUT with bridge type structure can obtain much greater deflection and higher sensitivity of transducers. The cross coupling between elements can also be limited. The supporting diaphragms includes a 1μm thick thermal oxide layer and a 4~6μm silicon layer. To fabricate silicon layer, wet etching with silicon etchant KOH was utilized with a boron etch stop. A 1~2μm thick PZT film was then deposited by sol gel techniques on (111)-textured Pt film as bottom electrodes sputtered on oxide. The raw materials included zirconium propoxide, titanium isopropoxide and lead acetate. Acetic acid and propyl alcohol were used as solvents. Wet films were annealed at 650 °C for 30 min. This process was repeated to get thicker films. The platinum top electrode was then sputtered. After the diaphragm was released by dry etch of the two side edges of diaphragms, a polyimide membrane with about 0.7μm thickness was then coated on the open seams.

Results

The elements with 50μm width were designed and fabricated. The PZT films deposited by sol gel techniques are crack free and exhibit preferred orientation in the direction of the (100) plane. The ferroelectric properties of the PZT films were measured, the results show better P-E hysteresis loops. The resonance frequencies for the pMUT elements in flexure-mode is about 3MHz.This paper presents the testing results.

Discussion and Conclusions

The effect of different thickness of PZT film and silicon layer on performance of elements are discussed .A bridge type structure can enhance the sensitivity and limit the cross coupling between elements.

P3G073-03

Effect of surface modification of titanium substrate by anodic oxidation on hydrothermally synthesized PZT poly-crystalline film

Takeyoshi Uchida[1], Tsuneo Kikuchi[1], Takurou Murakami[2], Norimichi Kawashima[2], Shinichi Takeuchi[2]; *[1]AIST, National Metrology Institute of Japan, Tsukuba, Ibaraki, Japan, [2]Toin University of Yokohama, Japan.*

Background, Motivation and Objective

We have been studied hydrophones using the PZT poly-crystalline film deposited by hydrothermal method. The PZT poly-crystalline film has piezoelectricity without polling process and it is easy to form the piezoelectric film on the titanium substrate with extremely small size by hydrothermal method. The hydrophone is used for performance evaluation of medical ultrasound equipment such as ultrasonic diagnostic equipment. Therefore, improvement of hydrophone′s performance is important for human safety. We reported the manufacturing and the receiving sensitivity of the miniature needle type hydrophone using hydrothermally synthesized PZT poly-crystalline film at 2005 IEEE International Ultrasonics Symposium in Rotterdam. However, the PZT poly-crystalline film of hydrophones have some problems concerning pinholes in the deposited PZT film, low receiving sensitivity compared to generally PVDF hydrophone and existence of peak or dip in frequency characteristics of receiving sensitivity etc. Consequently, we attempted the improvement of characteristics of the PZT poly-crystalline film on the titanium substrate by surface modification of titanium substrate using anodic oxidation. Anodic oxidation is that metal surface is oxidized by electrolysis in acid solution.

Statement of Contribution/Methods

At first, titanium substrate surface was pretreated using anodic oxidation for resolving the problems. Then, the PZT poly-crystalline film was formed on the titanium substrate in the KOH solution with Pb ion, Ti ion and Zr ion under high temperature about 160 degrees centigrade and high temperature about 0.6 MPa using hydrothermal method. Young′s modulus of the PZT poly-crystalline film on titanium substarte with and without the pretreatment was measured for investigation of characteristics of PZT poly-crystalline film.

Results

As the results, characteristics of PZT poly-crystalline film on the anodized titanium substrate were improved. Young′s modulus on the PZT film was increased by the pretreatment of titanium substrate. Young′s modulus of the PZT film on the titanium substrate with the pretreatment was about 47 GPa. Young′s modulus of the PZT film without the pretreatment was about 31 GPa.

Discussion and Conclusions

In this study, we attempted the improvement of characteristics of PZT poly-crystalline film on titanium substrate by surface modification of titanium substrate using anodic oxidation. Preliminary experiments showed that young's modulus of PZT poly-crystalline film was increased by the pretreatment of titanium substrate.

P3G074-04

Thick Film Based Piezoelectric Micromachined Ultrasonic Transducers

Tobias Hedegaard[1], Thomas Pedersen[1], Rasmus Lou-Moeller[2], Karsten Hansen[3], Tomasz Zawada[3], Erik V. Thomsen[1]; [1]*Technical University of Denmark, Department of Micro and Nanotechnology, Lyngby, Denmark,* [2]*InSensor A/S, Kvistgaard, Denmark,* [3]*Ferroperm Piezoceramics A/S, Kvistgaard, Denmark.*

Background, Motivation and Objective

This abstract reports on a design and fabrication outline for a cheap wafer scale fabrication of piezoelectric Micromachined Ultrasonic Transducers (pMUTs) using MEMS technology. The piezoelectric layer is a thick film PZT deposited at Ferroperm Piezoceramics. It is patterned using low cost screen printing and gives larger signals than thin film PZT. The design enables fabrication of arrays of pMUTs and can be altered to cover a wide range of operating frequencies.

Statement of Contribution/Methods

The design has been modelled by the Finite Element Method using COMSOL Multiphysics. The process integrates screen printed thick film PZT and MEMS technology and can be altered to meet specific resonance frequencies by varying the membrane width as shown in Fig 1.

Results

The process uses a Silicon On Insulator wafer in which cavities are etched from the backside with an Advanced Silicon Etch using photo resist as a masking layer. The etch stops at the buried oxide layer and the device layer of 20 µm silicon now serves as a membrane. A 500 nm SiO2 layer is thermally grown and a 50 nm Ti layer and a 500 nm Pt layer are deposited by e-beam evaporation as bottom electrode, and patterned by wet chemistry. A 30 µm PZT layer is deposited and patterned using a low cost screen printing technique. A 500 nm Al top electrode is deposited and patterned using a lift off process. Screen printing the PZT entails sloped edges. The top electrode can thus run from the PZT layer to bonding pads placed on the silicon substrate without short circuiting the device. Finally the PZT layer is polarized. A sketch of the device is shown in Fig 2.

Discussion and Conclusions

The fabrication process enables cheap fabrication of pMUT arrays and the design can meet a wide range of frequencies. The process integrates screen printed thick film PZT with MEMS technology.

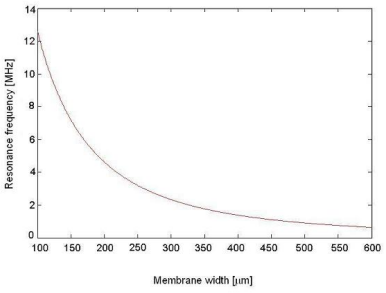

Fig. 1 Resonance frequency as function of membrane width

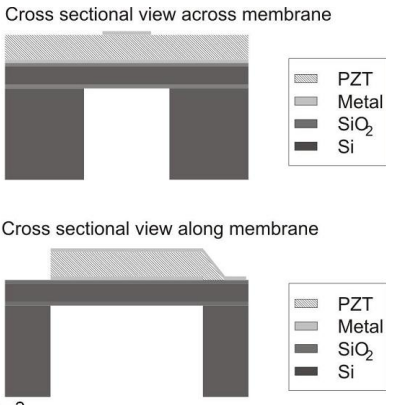

Fig. 2
Sketch of single element pMUT.

Wednesday Poster

P3G075-05

Characterization of PZT ferroelectric thin films prepared by a modified sol-gel method

Daqun Bao, Yi Zhang, **Hang Guo;** *Xiamen University, Pen-Tung Sah MEMS Research Center, Xiamen, Fujian, China.*

Background, Motivation and Objective

Lead zirconate titanate (PZT) is a typical ferroelectric material that is generally used in nonvolatile memory and dynamic random access memories (DRAM). With the rapid development of MEMS technologies during the past 20 years, many investigators are studying to develop PZT-based ferroelectric MEMS devices for new applications. This requires that PZT thin films can be prepared on the silicon substrate with an appropriate thickness and good performance.

Statement of Contribution/Methods

In this paper, we present a method of precursor-monomer to prepare PZT ferroelectric thin films by sol-gel processing. PZT thin film is synthesized in Pb:Zr:Ti=1.1:0.52:0.48 with 0.2-0.4M PZT precursor, containing 10% mole excess Pb in order to account for the loss of Pb during the later thermal treatment. The PZT films are coated by spinning the precursor solution on different substrates at 3500rpm for 30 seconds. A thermal process is adopted for crystallization of each layer of PZT thin film, which is to dry each layer of PZT thin film. The measured average thickness of an annealed PZT single layer is ~200 angstrom. The PZT thin films with desired thickness are achieved by repeating spin-coating and thermal treatment cycles. The thickness of films after 8 cycles is 2500 angstrom and samples are pre-fired to remove the residual organics and then annealed under a flowing oxygen atmosphere for final crystallization. To minimize the stability of pyrochlore phase and expedite direct perovskite phase formation, all samples are put into the temperature-preset furnace directly, and then followed by a natural cooling to room temperature. Then, we study the influence of annealing temperatures, different film thickness and different substrates, including titanium and platinum layers on silicon substrate, on the ferroelectric performance of PZT thin films by analyzing the polarization hysteresis of PZT thin films.

Results

Measurement results show that the PZT film with single-layer heating treatment at 400ºC and annealing treatment at 650ºC on the Ti electrode is relatively (110) preferentially oriented, resulting in maximum polarization (PM) of 13mC/cm2, remanent polarization (Pr) of 8.6mC/cm2 and coercive field (Ec) of 39.7kV/cm under an applied voltage of 3V. The PZT thin film with single-layer heating treatment at 400ºC and annealing treatment at 650ºC on the Pt/Ti electrode has larger maximum polarization of 30.5mC/cm2 and remanent polarization of 11.0mC/cm2, owing to the preferential orientation of PZT (100).

Discussion and Conclusions

By multiple coatings and thermal treatments in sol-gel processing, we get PZT thin films that have the desired thickness and are characterized to have good performance. The PZT thin films prepared by our modified sol-gel method can be used for developing PZT-based ferroelectric MEMS devices.

P3G076-06

Properties of PSN-PMnN -PZT ceramics synthesized by B-site precursor method and their applications on therapeutic transducers

Cheng-Che Tsai[1], Te-Kuang Chiang[1], Sheng-Yuan Chu[2]; *[1]Southern Taiwan University, Electronic Enginneering, Tainan, Taiwan, [2]National Cheng Kung University, Electrical Engineering, Tainan, Taiwan.*

Background, Motivation and Objective

Develop of power therapeutic transducers must have piezoelectric materials with good electrical properties, the lower aging rate (good life time) under cyclic electrical strength applied and fine-grain microstructure and the good temperature stability of the static capacitance and resonant resistance. Many ternary and quaternary solid-solutions have been synthesized by modifications or substitutions to meet above specific functions of transducers. However, these systems are prepared by conventional ceramic (MO) method or columbite method. A little work had been study B-site oxide precursor (BO) method which potentially made fine-grain piezoelectric ceramics possessing superior electrical properties and stable reproducibility for mass productions. In this paper, the temperature coefficient of static capacitance (TCC), temperature coefficient of resonant resistance (TCR), dielectric and piezoelectric properties of PSN-PMnN-PZT ceramics system by BO method are investigated to develop a well power therapeutic transducers.

Statement of Contribution/Methods

The BO method provides a new method to improve the temperature stability of static capacitance and resonant resistance, the bulk density and the fine-grain microstructure without doping dopants and sintering aids. In addition, we found that the input power degradation of therapeutic transducer fabricated would be lessened as compared to MO method under open-loop power circuit driving.

Concerning BO method, two stages of calcination were performed. In the first stage, B-site metal oxides were calcined to form (Sb1/2Nb1/2)0,02-(Mn1/3Nb2/3)x-(0.98-x) (ZryTi1-y)O2 precursors at 1400oC for 6 h; in the second stage, the PSN-PMN-PZT based solid solutions were synthesized by reacting the above precursors with a stoichiometric amount of PbO, CaCO3, and Li2CO3 at 750oC for 3 h.Then,the calcined powders followed by the same processing as a MO method to make samples.

Results

The suitable composition, obtained at x = 0.04, possessed electromechanical properties kp = 0.64, kt = 0.50, Qm =1450, and £`33T/£`0 = 1460, and tan£_ = 0.018%, sintered at 1050oC. In addition, the temperature coefficient of static capacitance and resonance resistance were 0.18 %/oC and 0.08 %/oC in the temperature range of 20-100oC we found that the degradation of input electrical power using B-oxide precursor method is less than that using conventional method at maximum operating temperature 60oC.

Discussion and Conclusions

This study has characterized and compared PSN-PMN-PZT based ceramics prepared by the conventional ceramic method and B-oxide precursor method. The SEM micrographic examination of the two type piezoelectric ceramics shows that the BO type ceramics has better and more regular grain structure, allowing us to predict better piezoelectric and mechanical properties. Therefore, the B-site metal oxides through high temperature sintering could be verified to improve the physical and electrical properties

P3G077-07

Investigations on the effects of ultrasonic vibrations in the wire drawing

Hai-qun QI, Jiang-bo Yuan, Tao Xie; *Harbin Institute of Technology, Harbin, Heilongjiang, China.*

Background, Motivation and Objective

It is a major problem of conventional wire drawing to introduce high force into the forming area and complicated technics. Some material was difficult to process in conventional machining The forces during wire drawing can be reduced and the difficult machining material become easy to process by superimposing ultrasonic oscillating. Compared with conventional wire drawing, the forming process limits can be extended by superimposing ultrasonic waves due to decreasing drawing force.

Statement of Contribution/Methods

In this paper, in order to study the function of ultrasonic in forming process and the influence of ultrasonic amplitude, speed of processing in drawing force. The transducer was designed and manufactured, and the experimental system was built, all experiments approaching actual production were carried out in a drawbench in the cable factory of harbin, it was showed in Fig.1.

Results

The drawing velocity was133.13mm/s, and superimpose voltage on piezoelectric ceramic was 200V. Compared withnot ultrasonic vibration, the drawing force decreases approximately 29% with ultrasonic vibration. The drawing force reduction as a function of the amplitude. And using higher voltage, drawing force is smaller. While increasing drawing velocity the drawing force increases, however the function of ultrasonic is weaker with increasing drawing velocity.The surface of drawing wire with and withnot superimposed ultrasonic vibrations are scaned by a electron microscope(FEIsirion200),it was shown in fig2. Compared with the obtained under no-ultrasonic vibration,the brass wire drawn under ultrasonic vibration conditions has a more smooth and flaw less surface.

Discussion and Conclusions

The influence of ultrasonic-performance or rather amplitude, drawing velocity concerning drawing force and surface quality of wire was investigated. Compared with conventional wire drawing, the drawing force can reduce with ultrasonic vibration, the reduction of the drawing force is mainly a function of the ultrasonic amplitude, increasing higher voltage, the drawing force is smaller. With increasing drawing velocities, the drawing force reductions are lower, because of decreasing oscillations per unit of length. And the brass wire drawn under ultrasonic vibration conditions has a more smooth and flaw less surface compared with those obtained under no-ultrasonic vibration.

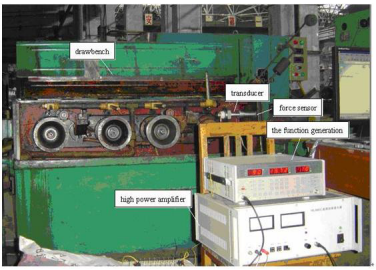

Fig.1 experiment systems

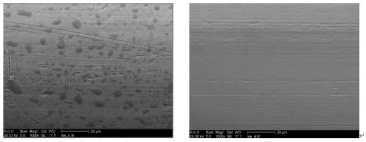

a) Non-ultrasonic drawing b) Ultrasonic drawing

Fig.2 surface of brass wires without and with ultrasonic

P3G078-08

Model-based Dynamic Characteristics Investigation of Ultrasonic Transducers for MEMS Packagingψ

Fujun Wang[1], Xingyu Zhao[1], Dawei Zhang[1], Yimin Wu[2], Yunchao Sun[1]; *[1]Tianjin University, School of Mechanical Engineering, Tianjin , China, [2]Hebei University of Technology, Department of Mechanical Engineering, Tianjin, China.*

Background, Motivation and Objective

In MEMS Packaging, there are two main electrical interconnection technologies: wire bonding and flip-chip bonding. Wire bonding constructs electrical connections using metal. With the trend in shrinking MEMS dimensions, the thermosonic flip-chip bonding has been highly advocated in the past few years, and it achieves connections using bumps of electrically conducting material. During thermosonic bonding process, heat, pressure and ultrasonic energy are applied simultaneously. The ultrasonic transducer converts electrical energy into acoustic energy and transmits energy to bonding interface. Or et al. studied the dynamic characteristics of ultrasonic transducer for wire bonding using FEA without considering piezoelectric effect. Tsujino brought forward novel ultrasonic transducers with higher frequency. Sherrit studied the modeling of horns for ultrasonic applications by electromechanical equivalent method. To provide faster, more repeatable and stronger MEMS bonding technology, the dynamic characteristics of transducers are studied in this paper using analytical and numerical method. The PLL frequency control of the transducer is also presented.

Statement of Contribution/Methods

The electromechanical equivalent circuitry of the ultrasonic transducers, composed of the piezoelectric converter and two-step concentrator, are established. The frequency equation of the transducer are gained, which lays foundation for dynamic analysis. Based on FEA, the vibration information of transducer driven by sinusoidal voltage can be obtained through harmonic response analysis. The transient response is figured out by transient analysis. The frequency control by using CPLD is adopted. The electrical resonance and mechanical vibration characteristics can be tested by impedance analyzer and laser Doppler vibrometer, respectively. The numerical simulation and bonding experiments are carried out to investigate the influence of the diameter of the bolt on bonding quality.

Results

The transducer works in the longitudinal direction at the frequency of 100 kHz. The total length of the ultrasonic transducer is one and a half wavelength. The tip amplitude of vibration displacement is 1.01 μm, which is suitable for finer bonding. By using CPLD, the voltage and current of the ultrasonic transducer are kept the same with each other. When the diameter of bolt is 4 mm, the best bonding results are obtained.

Discussion and Conclusions

The analytical method and FEA shows great potential in predicting the characteristics of ultrasonic transducers, and the results of analytical method and FEA basically match with the experimental results.

The rule of ultrasonic energy transmission in spatial domain, time domain and frequency domain was obtained, and the results provide instructions for the design of transducers and the optimization of bonding process.

The phase loop lock has been accomplished, and therefore the ultrasonic conversion efficiency is improved.

P3G079-09

A design of ultrasonic compaction tools for metal powder magnetic core of motors

Shinichi Kikuchi, Daisuke Koyama, Kentaro Nakmura; *Tokyo Institute of Technology, Japan.*

Background, Motivation and Objective

To fabricate efficient electromagnetic motors being based on the optimized design, a technique to produce three-dimensionally-shaped magnetic core is required. The metal powder compaction method is a promising candidate for making arbitrary shaped cores. However, it is difficult to increase the density and uniformity using conventional pressing machine. This means that the magnetic efficiency in low and the mechanical strength is not enough for the applications. To overcome this problem, we investigate the use of ultrasonic vibrations in the compacting process, expecting the effects of the vibration on the density and strength as well as the reduction in the friction between the die and the work. A design method for the vibrating die and punch is considered in the first past of the report, while the effects of the ultrasonic vibrations on the compaction rate are experimentally studied in the later part.

Statement of Contribution/Methods

An ultrasonic power combiner for eight Langevin transducers was designed through finite element modeling for the compaction die. A vibration system for the pressing punch was also developed using a vibration direction converter. The die was vibrated radially at 28 kHz, while the upper and lower compacting punches were excited by 40-kHz longitudinal vibrations.

Results

The die is made of SKH-9 steel, and operated in the fundamental radial mode at 28 kHz. It has a 10-mm-diameter compacting part in the center, and eight bolt-clamped Langevin PZT transducers. Using finite element analysis, the peripheral shape of the die was determined as shown in Fig. 1 to obtain a larger vibration amplitude at the inner surface of the center hole. A 40-kHz ultrasonic vibration punch consists of a longitudinal-longitudinal vibration direction converter and two BLT transducers. In the design, the punch head is separated from vibration system, and the condition for the efficient vibration transmission is considered.

Discussion and Conclusions

The performance of the vibration systems were evaluated through the electrical admittance measurements, the vibration distribution measurements and the high amplitude operation test. Using the developed vibration system and an oil pressing machine, the compaction ere carried out experiments for the metal powder called gSoft Magnetic Composite□h. It is iron powder covered with insulating and banding layer.

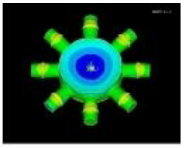

P3H. Material Properties III

2nd and 3rd Floor Foyers

Wednseday, November 5, 2008, 3:00 pm - 4:30 pm

Chair: **Yook-Kong Yong;**
Rutgers University, NJ, USA.

P3H080-01

Crystal Orientation and Stress in AC Reactively Sputtered AlN Films on Mo Electrodes for Electro-Acoustic Devices

Valery Felmetsger, Pavel Laptev; *Tegal Corporation, PVD Product Group, San Jose, CA, USA.*

Background, Motivation and Objective

Piezoelectric AlN films with strong (002) crystal orientation are widely used in resonator-based applications such as BAW and FBAR filters, oscillators and resonating sensors. Device performance is tied to the AlN sputter technology in terms of film uniformity, texture, and stress. Two major reactive sputter techniques are employed in mass production of electro-acoustic devices: pulsed dc magnetrons, and ac powered S-Gun magnetrons. The S-Gun, due to its dual ring target arrangement, is uniquely able to realize reactive sputtering processes free of parasitic arcing and disappearing anode effects. Crystal orientation of AlN films also depends on properties, especially surface roughness and texture, of the bottom electrode. This is why technological solutions ensuring formation of well-textured and low-stressed AlN and Mo electrode layers are of high interest to the piezoelectric resonator community.

Statement of Contribution/Methods

We describe ac (40 kHz) reactive sputtering processes by a dual cathode S-Gun magnetron and present effective technological solutions enabling independent control of AlN film properties, particularly stress, thickness uniformity, and texture. 100 – 3000 nm thick AlN films deposited on Mo electrodes are characterized by X-ray diffraction, scanning electron microscopy, atomic force microscopy, and residual stress measurements.

Results

Rocking curve measurements have shown that FWHM of AlN (002) diffraction peak has a direct correlation with FWHM of Mo (110) under-layer diffraction peak. AlN films having FWHM < 2° may be obtained only on well-textured Mo electrodes with FWHM below 3°. A dc sputtering process by the S-Gun, in combination with pre-deposition RF plasma etch and thin AlN seed layer deposition, enables formation of these well-textured Mo electrodes. Orientation of AlN films is improved with increasing film thickness, due to development of more thorough columnar structures in the thicker films. FWHM improved from 2.5° to 0.9° for 100 nm and 3000 nm thick films, respectively. Residual stress in AlN films deposited by the S-Gun is well controlled by varying Ar gas pressure in the magnetron. But, since deposition rate and film thickness uniformity depend on gas pressure too, we looked for independent stress control methods. We found that an effective way to reduce tensile stress is a two-step deposition with rf substrate bias, while diminishing compressive stress may be realized by suppression of the flux of charged particles to the substrate during deposition by means of redistribution of discharge currents between electrodes of the S-Gun.

Discussion and Conclusions

The S-Gun reactive sputter technology enables independent control of AlN film properties, simultaneously ensuring superior texture, with FHWM = 1.2° (film thickness 1200 nm), near-zero stress +/-30 MPa (or, if required, compressive stress up to -1 GPa), and thickness uniformity deviation less than 0.5% on 150 mm wafers in volume production.

P3H081-02

High Temperature Elastic Constants of Langatate from RUS Measurements up to 1100°C

Peter Davulis[1], Amit Shyam[2], Edgar Lara-Curzio[2], Mauricio Pereira da Cunha[1]; [1]*University of Maine, Electrical and Computer Engineering, Orono, ME, USA,* [2]*Oak Ridge National Laboratory, High Temperature Materials Laboratory, Oak Ridge, TN, USA.*

Background, Motivation and Objective

There is a demand for high performance sensors and frequency control devices capable of operating above 500°C for applications in the aerospace, automotive, energy, and petroleum industries. Acoustic wave (AW) technology has become an attractive possibility for such applications, in particular after the introduction of piezoelectric crystals capable of withstanding harsh environments, such as the langasite family of crystals (LGX). In order to identify crystal orientations and design high temperature AW devices, one needs to have knowledge of the elastic constants and their temperature coefficients in the temperature range of operation. In this work the temperature coefficients of the six independent langatate (LGT) elastic constants at temperatures from room temperature to 1100°C are extracted using resonant ultrasound spectroscopy (RUS).

Statement of Contribution/Methods

To the best of the authors′ knowledge there is no complete set of published elastic constants for LGT covering the room temperature to 1100°C range, which is reported in this work. Based on these coefficients, predictions can be made of acoustic behavior at high temperatures for the development of sensors and frequency control AW devices. The elastic constants were extracted at each measurement temperature by fitting the resonant peaks with those calculated by Lagrangian mechanics. In addition, this work will report on long-term stability of LGT at high temperature using the RUS technique.

Results

Six parallelepiped LGT samples were aligned, cut, ground, and polished at the University of Maine. Two types of 2.9x12.6x18.6 mm^3 parallelepiped samples were fabricated: one with these dimensions along the XYZ crystalline axes, and the other along the XZY axes. The two sample types increase the reliability of the constant fitting because they have different resonant peaks, thus providing more diversity in the measurement. Long-term stability of LGT was examined by holding a sample at 300°C, 550°C, and 800°C for a period of 168 hours. The results reported in this work indicate consistent resonant peak responses. The temperature coefficients of the elastic constants were independently extracted from each sample measured up to 1100°C. For the six independent elastic constants, C_{14} shows the higher percent variation, decreasing by 34% over the range from room temperature to 1100°C. On the other hand, C_{44} only decreased by 8% for the same temperature span.

Discussion and Conclusions

Multiple samples along two different orientations for improved data sampling were measured using the RUS technique from room temperature to 1100°C. The extracted LGT elastic constants presented in this paper represents a critical step towards the characterization of the LGT temperature behavior above a few hundred °C necessary for the design and fabrication of high temperature LGT AW devices.

Wednesday Poster

P3H082-03

Investigation of high-pressure transitions in castor oil using SH surface acoustic waves

Piotr Kielczynski[1], Marek Szalewski[1], Aleksander Rostocki[2], Jan Gladysz[2]; [1]*Polish Academy of Sciences, Institute of Fundamental Technological Research, Warsaw, Mazowsze, Poland,* [2]*Warsaw University of Technology, Faculty of Physics, Warsaw, Poland.*

Background, Motivation and Objective

Monitoring and studying the pressure effect on liquid viscosity are becoming increasingly important in the food, chemical, cosmetic, and pharmaceutical industry as well as in laboratory research.

High pressure technologies (pressures up to 1 GPa) have proved a great potential in modern bioengineering as a method of modification of biotechnological materials. The knowledge of rheological properties of treated substance is essential for understanding, design and control of the process technology. Measurement techniques for in-situ rheological investigations under high pressure allow insight into the phenomena governing the microstructural modifications.

Statement of Contribution/Methods

The conventional mechanical methods can not be operated to this aim due to their inherent limitations. Using these methods it is practically impossible to measure the viscosity of liquids in the range above 300 MPa.

This is why ultrasonic methods for the measurement of the viscosity of liquids under high pressure were introduced. Among them, the methods using SH surface acoustic waves are the most sensitive. To this end, the authors have applied a new ultrasonic method, i.e., the Bleustein-Gulyaev (B-G) wave method. In Ref.1, it was proven that this method is more sensitive than that which employs Love's waves. The sensor consists of the Bleustein-Gulyaev (B-G) wave waveguide made of PZT piezoceramics and sending-receiving transducer. The operating frequency was 2 MHz.

Results

The measurements of the viscosity of liquid (castor oil) were carried out in function of hydrostatic pressure up to 800 MPa. During the measurement we stated the phase transformation of castor oil. During the phase transition the drop of pressure and large increase of viscosity were observed. After the phase transition the viscosity has risen to the new value characteristic for the high-pressure phase of castor oil. The decomposition of the high- pressure phase during the decompression process has shown large hysteresis of the dependence of viscosity on pressure.

Discussion and Conclusions

To the authors' knowledge, the measurement of the viscosity of liquids under high pressure during the phase transition and during the decompression process is the novelty.

The usefulness of the surface B-G wave for measuring liquid viscosity at high pressures has been stated. The B-G wave method can be computerized. This enables continuous (on-line) monitoring of the rheological parameters of a liquid in-situ during the course of technological processes.

Small dimensions of the viscosity sensor and the absence of moving parts are substantial advantages of this method.

1. P. Kielczynski, R. Plowiec, J. Acoust. Soc. Am., 86, 818 (1989).

P3H083-04

Phase transitions in Ti-Ni alloys – acoustic studies

Andrei Abramovich[1], Elena Charnaya[2], Sergei Vasilkov[2], Sergei Belyaev[3], Aleksandr Volkov[3]; [1]*St. Petersburg University of Plant Polymers, Department of Physics, St. Petersburg, Russian Federation,* [2]*St. Petersburg State University, Department of Physics, St. Petersburg, Russian Federation,* [3]*St. Petersburg State University, Department of Mathematics and Mechanics, St. Petersburg, Russian Federation.*

Background, Motivation and Objective

The titan-nickel alloys belong to a large family of materials with martensite phase transitions. Such ferroelastic alloys are of great importance for applied science, techniques, and medicine. Acoustic methods are very appropriate for studying ferroelastics because of strong coupling of strains in the elastic waves with the order parameters which are responsible for the transition. They provide valuable information on the nature and kinetics of the phase transitions, order parameter symmetry, transition temperatures, hysteretical phenomena and so on. However, early studies of the martensite phase transitions were restricted to the temperature range above the transition due to scattering of the ultrasonic waves by ferroelastic domains in the ferroelastic state. Here we report results of acoustic studies of the martensite phase transitions in titan-nickel alloys of various concentrations within large temperature ranges.

Statement of Contribution/Methods

Polycrystalline samples of titan-nickel alloys with the Ni concentration around 50 at% were studied. The phase transition temperatures were from 260 to 400 K. The measurements were carried out before and after tempering the samples using both transverse and longitudinal acoustic waves within a temperature range of 220 to 470 K upon slow cooling and warming.

Results

Pronounced anomalies of ultrasound velocity and attenuation caused by the phase transitions were observed. They depended on wave polarization, deep minima being seen for the velocity of the transverse waves and diffused steps for the longitudinal ones. Large thermal hysteresises were found upon warming and cooling. Shifts of acoustic anomalies were obtained as a result of tempering. For some compositions, anomalies corresponded to two successive phase transitions were observed.

Discussion and Conclusions

The discussion of the acoustic properties is within the framework of the Landau theory for the ferroelastic phase transitions from a cubic to monoclinic structure, Pm3m to P21/m. An intermediate R structure can be also formed.

The transition is the proper ferroelastic one of the first order. The group-theory analysis shows that it is described by two order parameters (three-component and two-component). The particular forms of the order parameters explain the different behavior of transverse and longitudinal acoustic waves through the phase transitions. The obtained experimental results agree with these theoretical predictions.

P3H084-05

Step-by-step Electrospray Deposition of Organic Sensitive Film for Surface Acoustic Wave Sensor

Toshihiro Tsuji[1], Tetsuro Hotta[2], Yutaro Yamamoto[1], Kentaro Kobari[1], Shingo Akao[3], Noritaka Nakaso[4], Kazushi Yamanaka[1]; *[1]Tohoku University, JST, CREST, Japan, [2]Tohoku University, Japan, [3]Toppan Printing Co., Ltd., Tohoku University, JST, CREST, Japan, [4]Toppan Printing Co., Ltd., Japan.*

Background, Motivation and Objective

In elastic wave sensors, precise control of organic sensitive film thickness is important to optimize the performance. However, it is not easy in common methods such as spin- and drop- coatings. The electrospray deposition (ESD), generating submicron-sized droplets by a coulomb explosion, is not ideal for insulating substrates due to the charging effect. However, step-by-step deposition is feasible because the deposition is automatically stopped due to charging, and can be re-started after neutralization e.g. by an ionizer.

Statement of Contribution/Methods

Poly(isobutylene) (PIB, average molecular weight 400k) sensitive to non-polar molecules was dissolved to tetrahydrofran by 0.1wt%. The film was deposited on a ball SAW sensor (langasite, φ3.3mm, 150MHz) by the step-by-step ESD.

Results

After a deposition, sparse granular particles were formed with equivalent thickness of 1nm, as shown in Fig.1(a). The step-by-step increase of equivalent thicknesses was observed in successive depositions, as shown in Fig.1(b). Fig.2 shows the initial part of the delay time and amplitude changes of a ball SAW sensor at 50 turns as a function of the equivalent thickness, caused by exposure to gasses specified in the figure. The amplitude change clearly increased with increasing thickness without molecular weight dependence, in contrast to the complex behavior of the delay time change.

Discussion and Conclusions

It is noted that 1% amplitude change was obtained even at 1 nm equivalent thickness. It may be caused by the change of the viscosity of PIB. Comparison between Figs. 2(a) and (b) is useful for revealing the nature of interaction between PIB particles and gas molecules. Thus, unique role of step-by-step ESD was verified.

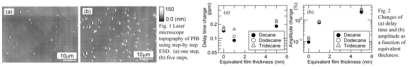

Wednesday Poster

P3I. Bulk Wave Effects & Devices

2nd and 3rd Floor Foyers

Wednseday, November 5, 2008, 3:00 pm - 4:30 pm

Chair: **John D. Larson;**
Avago Technologies, USA.

P3I085-01

Optimal Electrode Shape and Size of Plate Thickness-Shear Mode Piezoelectric Resonators

Zengtao Yang[1], Shaohua Guo[2], Jiashi Yang[3]; *[1]Central South University, Institute of Mechanics and Sensing Technology, School of Civil Engineering and Architecture, Changsha, Hunan, China, [2]Central South University, China, [3]University of Nebraska, USA.*

Background, Motivation and Objective

Electrodes are necessary parts of piezoelectric resonators. They are used for electrically exciting mechanical vibrations. The motional capacitance of a resonator is an important design consideration and is calculated from the charge (or current) and voltage on the electrodes. Electrode mass is known to be responsible for the localization or confinement (energy trapping) of thickness-shear modes in plate resonators. Due to the need of resonator miniaturization, there has been growing research effort on the optimal design of electrode configuration including electrodes of varying thickness for strong energy trapping, and the effect of electrode boundary curvature and the related electromechanical field concentration. Electrode shape and size also need to be optimized in design for which published results are relatively few. At present circular and rectangular electrodes are routinely used in resonator manufacturing. We study optimal electrode shape and size of plate thickness-shear resonators in the sense that Bechmann¡¯s number is satisfied in every direction. As a consequence there are no nodal points (lines) in the electroded region in the operation of the resonators.

Statement of Contribution/Methods

For singly rotated resonators an early expression obtained by Mindlin is employed in our calculations of optimal electrodes. For doubly rotated resonators the Stevens-Tiersten equation for plate thickness mode resonators is used to determine and calculate optimal electrodes.

Results

Results of optimal electrode size and shape for quartz and langasite resonators of various cuts are presented. In most cases the optimal electrodes are close to but are not exactly elliptic. In some cases the optimal electrodes are not close to an ellipse.

Discussion and Conclusions

Our results show that the optimal electrodes differ significantly from the usual rectangular or circular electrodes currently in use. This calls for immediate design optimization and improvement of resonator electrodes.

Wednesday Poster

P3I086-02

Reflection and refraction of bulk acoustic waves in piezoelectric crystals under the action of bias electric field and uniaxial pressure

Boris Sorokin[1], **Sergey Burkov[1],** Kirill Aleksandrov[2], Aleksey Karpovich[1]; *[1]Siberian Federal University, Solid State Physics, Krasnoyarsk, Krasnoyarsk region, Russian Federation, [2]L.V. Kirensky Institute of Physics, Siberian Branch of the Russian Academy of Sciences, Krasnoyarsk, Krasnoyarsk region, Russian Federation.*

Background, Motivation and Objective

There are many aspects of interest to processes of acoustic waves reflection/refraction on the boundary of two hard contacting mediums: ultrasonic wave propagation problems, acoustoelectronics devices, acoustic microscopy et cetera. Basic equations of such processes were obtained in 50th of 20 century.

Statement of Contribution/Methods

Now we have developed above mentioned approach involving the influence of a bias external fields. First the theory of reflection and refraction of bulk acoustic waves (BAW) on a boundary of two crystalline piezoelectric solids has obtained. We have taken into account early results concerning with BAW propagation in the infinite homogeneous piezoelectric single crystals subjected to the action of constant electric field E or uniaxial mechanical pressure P [1]. So it was necessary to take into consideration effects of geometrical and physical nonlinearities. First one is defined by statically finite samples deformation (non-orthogonal one in general case), second one is associated with the changing of material constants of crystals by external fields. Naturally corresponding boundary conditions have been considered.

Using formulas obtained and the known data on material “linear” and “nonlinear” constants such as dielectric, piezoelectric, elastic constants and nonlinear ones and electrostriction we have carried out the full computational analyses of reflection/refraction processes. Results in the form of cross-section of reflection/refraction coefficients surfaces have given in details the anisotropy of BAW propagation in these conditions for the lot of BAW propagation and E or P directions for such systems as vacuum-Bi12GeO20 crystal boundary, two piezoelectric crystals LiNbO3/Bi12GeO20 boundary and some other ones.

Results

It was shown that bias electric field or mechanical pressure leads to decreasing of the point symmetry of a crystal and ensures the transformation of some types of the reflected and refracted waves.

Discussion and Conclusions

Thus using given theory it is possible in details to analyze the character of reflection and refraction of acoustic waves on the hard boundary of piezoelectric solids under the application of bias fields. The data obtained can be useful to searching of practically important combinations of crystals for acoustoelectronics devices and sensors.

1. Zajtseva M. P, Kokorin Ju.I., Sandler J.M., Zrazhevsky V.İ, Sorokin B.P., Sysoyev A.M. Non-linear electromechanical properties of non-centrosymmetric crystals. Novosibirsk: Nauka. 1986. 177 pp.

P3I087-03

Wireless energy transmission through a thin metal wall by shear wave using two piezoelectric transducers

Hongping Hu, Yuantai Hu, Chuanyao Chen; *Huazhong University of Science and Technology, Department of Mechanics, Wuhan, Hubei, China.*

Background, Motivation and Objective

There has been recent interest in periodically charging and/or recharging batteries that power electronic devices operating in a sealed armor or other hazardous environments, such as spacecraft, nuclear reactor, and dangerous chemical container. This is because the use of feed-through wires in such systems often brings some disadvantages, such as leakage, thermal or electrical insulation problem and stress concentration. Thus it is necessary to develop the wireless energy-supply techniques. Wireless energy-supply techniques are with two aspects of implications: one is to scavenge energy directly from the operating environment of electronic devices, for example piezoelectric energy harvesters can scavenge energy from ambient vibrations and convert it into electric energy; the other aspect is to transmit power into sealed solid metallic structures without damaging the outer shells. This can be achieved using piezoelectric transducers and acoustic waves. There are also other possible applications of the technology like data transmission through a wall.

Statement of Contribution/Methods

We propose a system to wirelessly convey electric energy through a thin metal wall. Two piezoelectric transducers working with thickness-shear modes are used to realize energy transformation between electric and mechanical, and a rechargeable battery is employed to store the transmitted energy, both are integrated as a system through a modulating circuit. A synchronized switch harvesting on inductor (SSHI) in parallel with the transducer system is introduced to artificially extend the closed interval of the modulating circuit.

Results

The process of transmitting-energy is computed and the performance of the transducers is optimized in detail for the prescribed external electric source.

Discussion and Conclusions

Numerical results show that the SSHI can artificially extend the closed circuit interval of the rectifier, and there exists an optimal rectified voltage to make the charging-battery more efficiently. The obtained results are useful in the understanding and design of wireless energy-supply systems.

P3I088-04

Acoustic Resonance Spectroscopy of Nanoceramics

Natalia Polzikova[1], Georgy Mansfeld[1], Sergey Alekseev[1], Iosif Kotelyanskii[1], Sergeev Fedor[2]; *[1]Institute of Radioengeneering and Electronics RAS, Moscow, Russian Federation, [2]Moscow Institute of Physics and Technology, Moscow, Russian Federation.*

Background, Motivation and Objective

Application of ceramic as a material for acoustoelectronics can be promising because of isotropic nature of ceramics and it's relatively simple procedure of synthesis. Acoustic losses in ceramic mainly caused by waves scattering on pores and obey Raleigh scattering law f^4 which limit application of ceramic at frequencies $f > 1$ GHz. With modern technologies it is possible to produce practically nonporous nanoceramics of the same density as single crystals and thus eliminate Raleigh scattering. An yttrium aluminum garnet (YAG) crystals has extremely small acoustic losses so YAG nanoceramics are expected to be a perspective material for high-Q resonators.

Statement of Contribution/Methods

In present work frequency dependencies of acoustic losses in a dense YAG nanoceramics were studied. Acoustic losses were measured using resonance acoustic spectroscopy method in frequency range from 0.3 to 4 GHz. Samples of YAG ceramics were prepared by the method of YAG nanopowder sintering.

Results

Sound velocities found from measured resonance frequencies occur to be very close to values calculated by averaging YAG elastic constants. For the acoustic losses in the best available nanoceramics quadratic frequency dependence was experimentally obtained. It may correspond to two mechanisms: acoustic wave interaction with thermal acoustic phonons (the Akhiezer's theory) and to the acoustic waves scattering on rough surface. For the estimations of losses due to wave scattering on surface, the surface roughness measurements were made using scanning probe microscope.

Discussion and Conclusions

The obtained values of sound velocities and quadratic frequency dependence of acoustic losses prove that the influence of pores on sound propagation is negligible. The value of absorption coefficient exceeds the known experimental data for crystals. The estimations of losses due to energy scattering on surface roughness could not explain the difference. So model of sound attenuation in ceramic needs further development. The best Q-factor of our resonators based on ceramics equals to 20000 on the frequency 1GHz. Thus the first results obtained show that YAG nanoceramics is promising material for microwave acoustoelectronic devices.

This work was partially supported by RF President Grant for Scientific Schools 2929.2008.9

P3I089-05

The Analysis of Overtone Vibrations of Quartz Crystal Resonators with Lee Plate Theory

Ji Wang, Rongxing Wu, Jianke Du; *Ningbo University, Mechanics and Engineering Science, Ningbo, Zhejiang, China.*

Background, Motivation and Objective

The design and analysis of quartz crystal resonators in the fundamental thickness-shear mode have been extensively studied with many methods including the simple model based on infinite plates for the vibration frequency and Mindlin plate theory for couplings of the fundamental thickness-shear and spurious modes in finite plates. These methods are widely used in the design process for the optimal determination of crystal blanks and electrode configuration. The accurate results from these analyses in turn have prompted the inclusion of thermal and other bias fields in the consideration and the finite element implementation of the equations for more detailed analysis. In order to study the overtone vibrations of quartz crystal resonators, Lee plate theory is used in the form of the third-order equations to obtain the dispersion relation and frequency spectra in the vicinity of the third-order thickness-shear mode.

Statement of Contribution/Methods

Overtone vibrations of the thickness-shear mode can be analyzed for infinite plates to obtain the appropriate frequencies and effect of electrodes. In our earlier studies, a set of correction factors have been suggested for the Mindlin plate equations to be accurate at the cut-off frequencies at the third-order thickness-shear mode. Lee plate theory is based on the trigonometric expansion of displacements and has been improved lately. Its accuracy at

overtone frequencies has been validated and simple equations have been provided. By checking the accuracy at the cut-off frequencies, the third-order plate equations are chosen for the calculation.

Results

The dispersion relation for a plate vibrating in the third-order overtone of the thickness-shear vibration is compared with three-dimensional results for validation. In a manner similar to our analytical procedure for the fundamental mode, we calculated the frequency spectrum based on analytical solutions from coupled equations of the flexural and thickness-shear modes and their overtones with straight-crested waves. The effect of electrodes on frequency is also studied with the mass ratio.

Discussion and Conclusions

The solutions of coupled vibrations will provide information on the coupling and effect of the crystal blanks and electrodes. To study the circuit parameters of a quartz crystal resonator, equations that include the electrical potentials are needed for the optimization and improvement of resonator design. The coupling of modes and effect of electrodes for the third-order overtone vibrations at the thickness-shear vibrations will be used for the design of quartz crystal resonators vibrating at higher-order overtone modes. We can also calculate the electrical parameters with the consideration of material damping, which is essential for the calculation of electrical resistance, with our procedure on crystal plates with viscosity.

P3I090-06

A Theoretical Time-Course Model of Acoustic Tweezers: Pulse-Wave Mode

Shih-Tsung Kang, Hsiao-Chun Ting, Chih-Kuang Yeh; *National Tsing Hua University, Department of Biomedical Engineering and Environmental Sciences, Hsinchu, Taiwan.*

Background, Motivation and Objective

The optical tweezers has been a very important technique to manipulate macromolecules and cells. Due to the finite penetration ability of laser in tissue and only utilization in opaque particles, these limitations reduce the potential of optical tweezers in-vivo performance. In this paper, we propose a theoretical time-course model with pulse-wave mode for acoustic tweezers to predict the particle spatial track versus time and furthermore to locate the particles trapping regions.

Statement of Contribution/Methods

The trapping mechanism arises from momentum transfer between acoustic wave and object. Due to acoustic wave behavior with ray acoustic regime, the size of object must be six to eight times of the wavelength of acoustic beam. In the study, the theory is based on time-varying acoustic fields produced by 100-MHz focused transducer, and then the acoustic filed is used to calculate the force. By introducing quantity of velocity potential, instantaneous power of pulse wave can be evaluated and then the spatial radiation force distribution can be obtained. A particle sustains force at a certain time can be calculated by summing entire the radiation force on the particle. Given the particle mass, the acceleration of the particle can be obtained by means of Newton's laws of motion. By iteration method, the spatial track versus time of the particle can be predicted. The convergence of track represents the particle can be trapped by acoustic tweezers.

Results

The figure shows that a 50% Gaussian pulse was introduced to impinge on an object with a radius of 120 micron. Radiation force patterns at three different positions are shown in (a), (b), and (c) and the negative force was found from 60-170 micron away from the focus as shown in (d). The maximum force can achieve 10^-6 Newton if transmit pulse wave was 1 MPa. The (e), (f) and (g) represent the corresponding particles spatial tracks versus time after impinging of one pulse wave.

Discussion and Conclusions

We found that speed of sound in material and f-number of transducer are also essential factors to trap particles. Those results certainly show the feasibility of acoustic tweezers using pulse-wave mode.

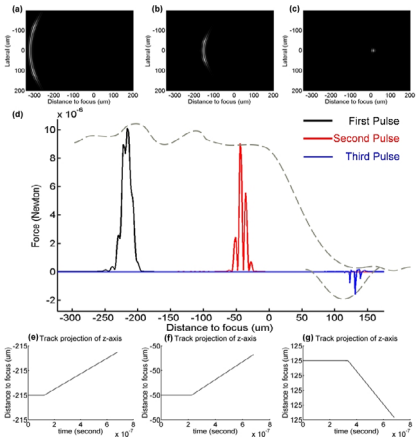

P3J. BAW & MEMS Materials & Devices

2nd and 3rd Floor Foyers

Wednseday, November 5, 2008, 3:00 pm - 4:30 pm

Chair: **Dave Feld;**
Avago Technologies, USA.

P3J091-01

Piezoelectrically Actuated Micromechanical BAW Resonators

Piia Rosenberg, Antti Jaakkola, James Dekker, Arto Nurmela, Tuomas Pensala, Tommi Riekkinen, Tomi Mattila, Ari Alastalo; *VTT Technical Research Centre of Finland, Finland.*

Background, Motivation and Objective

Traditionally, off-chip ceramic and SAW devices have been used as frequency references in modern handsets. However, small, low cost, mass produced silicon micromechanical resonators are considered an attractive alternative to these, and capacitively transduced MEMS resonators are already commercially available. However, for a good electromechanical coupling, voltages in excess of 10 V over sub-100 nm capacitive gaps are needed, which might be problematic in low cost IC circuits.

To overcome these problems, we have investigated MEMS resonators, which are actuated with a piezoelectric layer deposited on top of the beam. The resonance is evoked through Poisson ratio excitation. We report results about single crystal silicon beam resonators, which are transduced with an AlN thin film. We show that it is possible to achieve a good electromechanical coupling while maintaining low dissipations in the resonator.

Statement of Contribution/Methods

We designed 13 MHz beam resonators working in the first length extensional mode. We first modelled the electromechanical coupling and energy leakage through anchor loss with 3D FEM. On the basis of our simulation results, we designed new resonators, in which we tried to decrease the anchor loss. Then our fabrication process was optimised for the processing of resonators with narrow anchors.

Results

The FEM simulations showed that the anchor loss could best be decreased by narrowing the resonator anchors to under 6um and by orientating the resonator beam along the [110] crystal direction, where the lateral Poisson ratio is the smallest: 0.06. Our measurements support the simulation results. The measured quality factors depend strongly on the orientation of the beam and on the anchor width. Furthermore, the length of the piezoelectric layer on top of the beam, the beam width, and the length of the anchors affect the quality factor. The highest measured quality factors at 13 MHz were over 50 000.

Discussion and Conclusions

We have successfully simulated, designed, and processed piezoelectrically actuated MEMS resonators. In our designs we have aimed at decreasing the anchor loss as much as possible. Our measurements indicate that the resonator quality factor is not anchor loss limited anymore, but limited by other dissipation mechanisms, including loss in different material layers.

Wednesday Poster

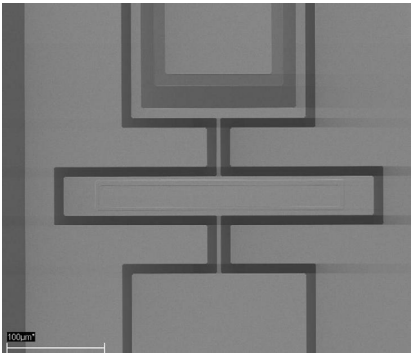

P3J092-02

Design of Experiments: a powerful tool for the numerical design of BAW filters

Alexandre Reinhardt[1], Sylvain Giraud[2], François de Crecy[1], Stéphane Bila[2], Enrique Iborra[3], Marc Aïd[1]; *[1]CEA-Leti Minatec, , Grenoble, France, [2]XLIM-CNRS, Limoges, France, [3]Universidad Politécnica de Madrid, Madrid, Spain.*

Background, Motivation and Objective

With the increasing complexity of filter and duplexer architectures, the acoustical design of BAW resonators needs to satisfy more and more constraints at the same time. This puts an increasing number of specifications on unitary resonators like resonance frequency, but also effective coupling factor, quality factor, sensitivity to temperature... The fabrication process also puts many constraints. For this reason, defining a material stack for BAW resonators becomes a very complex task and designers need to find optimum material combinations to satisfy all these constraints at the same time. This can be achieved by the knowledge of the physical behavior of a resonator and sometimes by the use of an optimization algorithm. However, resonator specifications evolve very often during a filter design, as they are function of the overall architecture and of all the other elements included in the filter or duplexer. This means that the material stack may have to be redesigned many times, what is very time consuming.

Statement of Contribution/Methods

In this paper, we show that Design of Experiments (DOE) methods can be applied to part of the design of BAW resonators. Resonator properties, like frequency and effective coupling coefficient can be modeled as simple polynomial functions of layer thicknesses. Therefore, in a given parameter range, 1D or even 2 or 3D simulation models can be replaced by much simpler polynomial metamodels which can be generated from only a few material stack simulations with a minimum lack of precision. Once these metamodels have been generated, optimization can be performed, even under multiple constraints. Moreover, if specifications have to change during the filter or duplexer design, the metamodel remains the same: only the optimization process needs to be renewed, so that updates are very quick and do not require a large amount of full stack simulations.

Results

We apply this optimization method to the case of a DCS filter, which shows very demanding specifications. As the bandwidth for such a filter is very large, the effective coupling factor needs to be as high as possible. To show the versatility of the proposed design method, we propose two types of metamodels: one based on the 1D simulation of a classical Mo/AlN/Mo piezoelectric stack, and the other on the simulation of a new Ir/AlN/Mo stack. Since Iridium has a very large acoustic impedance, it helps reaching higher effective coupling factors. Three sets of designs are obtained with only little efforts:

- one in which the two stacks are optimized independently,
- one in which as much layers as possible are kept of the same thickness while optimizing one of the stacks,
- and finally, one in which the same specifications are targeted for the two stacks.

Discussion and Conclusions

This example demonstrates that the use of design of experiment methods can shorten the time required by the numerical design of a BAW filter, compared to traditional approaches which directly use full 1D or 2D models.

P3J093-03

BAW Resonators with Iridium Electrodes for Digital Wireless Transmissions

Enrique Iborra[1], Marta Clement[1], Jimena Olivares[1], Sheila González-Castilla[1], Nick Rimmer[2], Amit Rastogi[2], Brice Ivira[3], Alexandre Reinhardt[3]; *[1]Universidad Politécnica de Madrid, Grupo de Microsistemas y Materiales Electrónicos, Madrid, Spain, [2]Aviza Tecnology Inc., Newport, United Kingdom, [3]CEA-Leti Minatec, Grenoble, France.*

Background, Motivation and Objective

Bulk acoustic wave (BAW) resonators based on aluminium nitride (AlN) and derived products, such as bandpass filters and duplexers, are being currently used in consumer products for mobile communication systems (DCS and W-DCMA). Since DCS filters exhibit a very large relative bandwidth, resonators with optimum piezoelectric coupling coefficients are required. Reaching the specifications for DCS filters with conventional molybdenum (Mo) electrodes is not straightforward. Iridium (Ir) electrodes, which provide higher acoustic impedances and promote the growth of AlN films of excellent piezoelectric activity, appear as solid candidates for the fabrication of BAW resonators. In this paper, we investigate the possibility of using resonators based on AlN films grown on Ir layers for the fabrication of viable filters for the 2 GHz range, addressing both the WCDMA and DCS standards.

Statement of Contribution/Methods

The performance of AlN-based solidly mounted resonators (SMR) with Ir and Mo electrodes was assessed. Ir/AlN/Ir and Mo/AlN/Mo metal stacks were grown on top of insulating Bragg mirrors composed of λ/4 silicon oxi-carbide and silicon nitride layers. AlN was sputtered after soft-etching the Ir and Mo electrodes with Ar+ ions. The structure and morphology of the different layers were analysed by x-ray diffraction (XRD) and atomic force microscopy (AFM). The frequency response of the SMRs was assessed by measuring the input scattering parameter S11 and fitting the experimental data to the BVD circuital model. The effective electromechanical coupling factor (k^2) and the quality factor (Q) of the resonators were derived from the experimental data. The influence of the geometry, k^2 and Q values of the resonators on the modelled response of filters was investigated.

Results

AlN films of excellent crystal quality and high piezoelectric activity, almost independent of the texture and roughness of the underlying substrate, were obtained on Ir electrodes. The SMRs exhibited k^2 ranging from 6% to 7% and almost independent of the FWHM of the RC around the AlN 00•2 reflection. The high acoustic impedance of Ir provided k^2 values higher than those obtained with Mo electrodes and almost independent of the Ir to AlN thickness ratio. Quality factors derived from the BVD circuital model ranging from 400 to 1000 were achieved.

Discussion and Conclusions

Well performing SMR devices based on AlN films grown on Ir electrodes were successfully fabricated. The frequency response of SMRs revealed the high piezoelectric activity of AlN grown on Ir with k^2 as high as 7%. These results suggest that Ir is a promising material to achieve the high values of the coupling factors necessary to achieve the large bandwidth of DCS filters. The fabrication technology of DCS filters with Ir electrodes is being currently developed.

This work was partially supported by the 6th European FP through the project MOBILIS.

Wednesday Poster

P3J094-04

Spurious Vibration Suppression by Film Thickness Control for FBAR

Shoichi Tanifuji, Yuji Aota, Hiroshi Oguma, Suguru Kameda, Tadashi Takagi, Kazuo Tsubouchi; *Tohoku University, Research Institute of Electrical Communication, Sendai, Miyagi Prefecture, Japan.*

Background, Motivation and Objective

The band pass filters based on the film bulk acoustic resonators (FBAR) have a great advantage of the good cut off characteristics at over 2GHz. We have fabricated 5GHz FBAR using aluminium nitride (AlN) film because AlN has higher acoustic velocity than other piezoelectric materials. We have successfully grown the *c*-axis oriented AlN film using the metal organic chemical vapor deposition (MOCVD) method on the SiO_2/Si substrate. However, there was the case that a large spurious existed between the resonant frequency and the anti-resonant frequency on the admittance characteristics of the prototype FBAR. When we consist the band pass filters, this spurious will become major problems, such as the spike response in the pass band. In this paper, we analyzed the incidence of spurious vibration mechanism using the three-dimensional (3-D) simulation, and discussed how to suppress this spurious.

Statement of Contribution/Methods

We used the CoventorWare, which is the 3-D finite element method (FEM) simulator from Coventor Inc., to analyze the admittance characteristics and the vibration mode from the 3-D models of FBAR structure. AlN and Ru were employed for the piezoelectric and the electrode film, respectively. This is because we normally used those materials in our MOCVD process to fabricate FBAR. The thickness of the film is a significant parameter to determine the resonant frequency. In this case, we adjusted the thickness of AlN and Ru to control the resonant frequency at 5GHz. Then we tried various models that had the different thickness of the films and shapes of the resonant area.

Results

As the simulation result, the strong spurious vibration was observed between the resonant frequency and the anti-resonant frequency as well as the actual measurement. We sampled the vibration mode at the spurious frequency. We investigated the animated vibration form of the 3-D models, and the displacement distribution in each of *x, y* and *z* axis. The spurious clearly vibrated in the longitudinal direction of the film on the edges of the electrode by the animation outputted from the simulator. Moreover, the large displacement was only observed in the direction of the thickness at the edges of electrode, though it was not observed in the other directions. It did not depend on the shapes of the models.

Discussion and Conclusions

We considered the spurious frequency could shift by adjustment of the film thicknesses. When the total film thickness of AlN and Ru became thick, the spurious frequency was shifted to the low-frequency side. In this case, to fix the resonant frequency at 5GHz, AlN was thickened and Ru was thinned. If the spurious frequency would match the resonant frequency, it could be completely eliminated. Also, we could not observe the spurious vibration mode at the resonant frequency. In conclusion, it is possible to remove the spurious from the frequency range by the optimal thickness design of FBAR.

P3J095-05

AlN Film using Low Temperature MOCVD Process for FBAR

Yuji Aota, Shoichi Tanifuji, Hiroshi Oguma, Suguru Kameda, Tadashi Takagi, Kazuo Tsubouchi; *Tohoku Univ., RIEC, Japan.*

Background, Motivation and Objective

We have investigated a 5 GHz band film bulk acoustic resonator (FBAR) for wireless local area network (WLAN) filters. We used an AlN as a piezoelectric material grown using a metal organic chemical vapor deposition (MOCVD) method. In our previous work, we reported that high oriented AlN(0002) film was achieved at the FBAR structure and realized the good FBAR resonance characteristics at 5 GHz using the Mo/AlN/Ru/Ta/SiO_2/Si(100) structure. However the cracks of AlN film were the significant problem. It was because of the thermal stress in the high temperature MOCVD process over 1000 °C.

In this paper, we propose that the MOCVD process using the N_2 gas instead of the H_2 gas to suppress the temperature of AlN deposition.

Statement of Contribution/Methods

AlN was deposited using the MOCVD method with source gasses of NH_3 and Tri-methyl Aluminum (TMA). At first, thermal annealing was carried out in order to clean the surface and to improve the orientation of the Ru/Ta bottom electrode. Next, AlN deposition was carried out in a quartz reactor. The TMA gas was carried to the reactor by the inactive carrier gas. In our previous work, the H_2 gas has been used to the thermal annealing and the TMA carry gas at AlN deposition. In this work, the N_2 gas was used in stead of the H_2 gas. The N_2 has possibilities to help the NH_3 molecules degradation at the low temperature in the MOCVD process. Therefore, the thermal stress in AlN film is expected to be decrease without degradation of AlN quality using the low temperature MOCVD process.

Results

The mean surface roughness (Ra) and the full width at half maximum (FWHM) of Ru/Ta after N_2 thermal annealing had same tendencies as the H_2 gas. The value of Ra was less than 5 Å under 1000 °C and increased rapidly over 1050 °C. Therefore the AlN deposition at low temperature was needed. The FWHM of Ru(0002) was improved gradually as the temperature becomes higher. From these results, the N_2 thermal annealing was effective to improve the Ru/Ta orientation and the surface flatness as well as the H_2 gas. Next, the FWHM of AlN(0002) was evaluated at low temperature MOCVD process. The FWHM of AlN(0002) using the N_2 gas was excellent value of under 2.5 ° at 800 °C in the MOCVD process. The best temperature condition using H_2 gas was 1050 °C. Consequently, the AlN cracks were decreased than that of using the H_2 gas because of the lower temperature MOCVD process.

Discussion and Conclusions

We used the N_2 gas to lower the temperature in the MOCVD process because of the N_2 effect on the NH_3 molecules degradation at the low temperature. As a result, we successfully achieved to obtain the high orient and the low cracks AlN film using low temperature MOCVD process.

P3J096-06

Lithium niobate surface structuration for phononic crystal fabrication

Sarah Benchabane[1], Laurent Robert[1], Gwenn Ulliac[2], Samuel Queste[1], Abdelkrim Khelif[1], Vincent Laude[1]; *[1]FEMTO-ST, MN2S, Besançon, France, [2]FEMTO-ST, DOPMD, Besançon, France.*

Background, Motivation and Objective

Surface structuration of lithium niobate (LN) can be of significant interest for tailoring surface acoustic wave propagation as in the case of phononic crystals, opening new prospects in the wireless telecommunication field. Yet, however well-known LN might be, it remains a non-conventional material from a microfabrication point of view. Most of the reported works are devoted to optical cuts (X- and Z-cuts), and if exception is made of deep structures realized through domain inversion and wet etching of Z-cut substrates, typical achievable depths are of the order of a couple of microns for low aspect ratios (below 0.5). Reactive Ion Etching (RIE) remains amongst the most interesting and accessible methods for LN etching. It is in itself a highly controllable and versatile dry process involving both physical and chemical effects to achieve directive and anisotropic material removal. It has already been demonstrated that LN can be dry etched using fluorin-based chemistries, although problems can be encountered when dealing with the fabrication of very deep or very high aspect ratios structures, due to redeposition phenomena impeding the material removal. A key element in the etching process lies then in the choice of the material constituting the etching mask.

Statement of Contribution/Methods

In this work, we report on RIE-based techniques for etching micron-sized holes which are several microns in depth on several cuts of LN and more particularly on Y- and Y-rotated substrates. Several etching masks and gas mixtures have been tested and compared to ensure high process selectivity and good sidewall verticality. Evaporated, sputtered or electroplated metals masks were used. The etching process is mainly based on a fluorin-based chemistry as sulfur-hexafluoride was chosen to be the etching gas. Effects of inductively-coupled plasma (ICP) or of the adjunction of argon in the etching plasma have also been investigated.

Results

The technique has been applied to the fabrication of phononic crystals for surface acoustic waves designed to operate at a frequency around 200 MHz. The phononic structure consists of periodical arrays of 9 µm diameter holes with a 10 µm period etched in Y-cut LN. Structures with smaller diameters have also been aimed at, in order to allow for the realization of devices in the GHz range. Maximum mask selectivity was found to be of the order of 20. Etching depths larger than 10 µm and aspect ratios well above 1.5 have been achieved. Sidewall verticality larger than 75° has also been obtained.

Discussion and Conclusions

Lithium niobate has been dry-etched using RIE-based techniques in view of structuring the material surface. The underlying idea is the realization of phononic crystal devices, though the process can also be of significant interest in the field of acousto-optics. Devices at an operating frequency of a few hundreds of MHz have been fabricated, but further developments related to the etching process itself need to be achieved to switch to the GHz range.

Wednesday Poster

P3J097-07

Picosecond Ultrasonics: the prefered tool for BAW characterization

Patrick Emery[1], Arnaud Devos[1], Pascal Ancey[2]; *[1]CNRS, IEMN, UMR CNRS 8250, Villeneuve d'Ascq, France, [2]STMicroelectronics, CROLLES, France.*

Background, Motivation and Objective

Since the 80's, RF-filtering has carried the developments of Bulk Acoustic Wave (BAW) resonators. At the same time, picosecond ultrasonics, a non-contact and non-destructive technique for mechanical characterization, sees the light of day in the metrological tools' arsenal for on product process control measurements. The operating principle of a BAW resonator is the excitation of the thickness mode of a piezoelectric layer sandwiched between two electrodes, and picosecond ultrasonics is well-suited to work in the natural geometry of the component. This technique uses a pulsed laser source to excite and detect longitudinal acoustic waves at very high frequencies (100 GHz to 1 THz). Thus, it enables the measurement of decisive parameters of materials in thin films for the modeling of BAW resonators (sound velocity, thickness, density, acoustic attenuation, temperature coefficients).

Results

On this poster we will present experimental results obtained on BAW materials (AlN, Mo, SiO2, W, SiN) for mechanical characterization. Then we will present results obtained on BAW stacks that enables an accurate modeling of resonant frequencies and coupling coefficient.

Discussion and Conclusions

These results will show that more than just a process control tool, picosecond ultrasonics can be a frequential characterization technique and replace RF-tests.

P3J098-08

Wireless Temperature Sensing using a Passive RFID Tag with Film Bulk Acoustic Resonator

Jon Hong Lin[1], **Yao Huang Kao[2];** *[1]National Chiao-Tung University, Communication Engineering, Hsinchu, Taiwan, [2]Chung Hua University, Communication Engineering, Hsinchu, Taiwan.*

Background, Motivation and Objective

Temperature sensing during a certain time is needed in scientific, medical and industrial applications. The network can be constructed with wired sensor nodes for power and data transmission. The cable and the maintenance costs dominate the system cost. In some dangerous environments, the temperature should be sensed wirelessly. This means that the energy needed for the temperature sensor has been provided by the reader. Passive RFID tags recover the inductive RF power for internal circuits¡¦ power consumptions. A passive RFID tag integrated a temperature sensor will fulfill the requirement.

Statement of Contribution/Methods

125 kHz is chosen as the frequency of the reader. It is heavily used below 135 kHz because it is not reserved as an ISM frequency range. This frequency range allows reaching large ranges with low cost tags. Miniaturized tag formats can be achieved by use of ferrite coils in tags. Low absorption rate or high penetration depth in nonmetallic materials and water are available due to lower frequencies. Block diagram is shown in Fig. 1.

Results

An Al/AlN/SiN/Au FBAR with membrane structure was applied in this RFID tag. The RF to DC converter recovers the inductive RF power to DC power. The voltage regulator stabilizes the DC power and supplies for the oscillator with FBAR. The oscillator is design as a power oscillator. In this structure, the RF power amplifier is not needed. The resonance frequency of FBAR will vary with environment temperature. Using a frequency counter, we can read the temperature easily as shown in fig.2.

Discussion and Conclusions

The use of acoustic wave device in sensing is increasing because as sensing devices they have higher sensitivity and reliability than other types of sensors. In this work, measurement result shows the sensitivity of 34.5ppm per degree C and very good linearity.

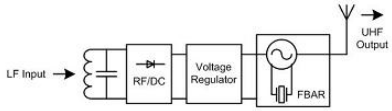

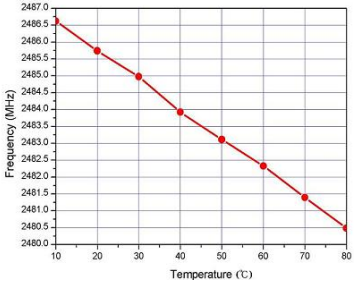

P3J099-09

Anchor limited Q in Flexural Mode Resonators

Joshua Lee, **Jize Yan,** Ashwin Seshia; *University of Cambridge, United Kingdom.*

Wednesday Poster

Background, Motivation and Objective

Silicon micromechanical resonators are seen as a promising alternative to quartz crystals as timing references for their excellent scaling properties and mechanical properties allowing for high quality factors (Q). In designing microresonators, the elimination of dissipation sources to achieve a high Q is desirable in a timing-element of a frequency reference – limited in part by the anchors of the resonator.

Statement of Contribution/Methods

Through a comparison of various flexural mode resonators, including elliptical ring mode, a double-ended tuning fork (DETF) excited in the tuning fork mode and in-phase mode, and a doubly clamped beam in a SOI MEMS process, we demonstrate how the effect of anchors on dissipation can be effectively minimized to enhance the Q of the resonator. This has been achieved through both FEA simulations as well as electrical transmission measurements of fabricated devices.

Results

Finite element simulations are utilised to estimate the fraction of elastic energy in the resonators lost through the anchors. As an example, the relative distribution of elastic energy stored in the resonator structure (ES) and anchors (EA) was calculated for an elliptical mode ring resonator suspended by a) straight beam spring anchors, and b) T shaped spring anchors, using ANSYS FEA. The FEA shows that, in relative units that have been normalized, ES = 15.7, while EA (beam spring) = 0.3 and EA (T spring) = 0.07, indicating that anchor effects will be relatively much more dominant in the former. Q values of fabricated devices modeled in FEA were extracted from electrical transmission measurements and summarized in Table 1.

Discussion and Conclusions

Table 1 shows the highest Q values measured among several doubly clamped beams. For the ring resonator, Q (beam-spring) > Q (T-spring), in agreement with the FEA results, and also » Q (clamped beam). For the tuning fork, Q (in-phase mode) » Q (clamped beam) since one end of the tuning fork beam is not clamped but only simply constrained. The Q of the in-phase mode is slightly lower than Q (tuning-fork mode) due to the mutual cancellation of stress waves meeting at the anchor of the tuning-fork. We thus show from both the cases of the DETF and the Ring that the anchors can be effectively de-coupled from the resonant structure, as indicated by a lower EA calculated from FEA, thereby enhancing the Q for flexural mode resonators.

Table 1. Measured *Q* values of fabricated SOI devices

	Beam Spring	T Spring
Elliptical Ring Mode	13600	76700
	In-phase	**Tuning-fork**
Clamped-Free DETF	58800	79200
	Beam A	**Beam B**
Doubly clamped beam	6040	6920

Wednesday Poster

P3K. Thin-Film & Propagation

2nd and 3rd Floor Foyers

Wednseday, November 5, 2008, 3:00 pm - 4:30 pm

Chair: **Don Malocha;**
University of Central Florida, FL, USA.

P3K100-01

Zero LSAW Propagation Loss in a SiO_2/Periodic Grating/$LiTaO_3$ Structure

Sergey Biryukov[1], Manfred Weihnacht[2]; [1]*IFW Dresden, Dresden, Germany,* [2]*INNOXACS, Dippoldiswalde, Germany.*

Background, Motivation and Objective

The known temperature compensation technique for leaky surface acoustic wave (LSAW) devices on rotated Y-cut lithium tantalate uses a silicon dioxide film covering a periodic electrode grating. As known from the recent papers [1] and [2], a large surface corrugation, which results from thick metal electrodes and conventional sputtering, increases propagation loss. This loss at resonance - (short circuit) and anti-resonance (open circuit) frequencies defines the Q-factors of resonator filters. It was mentioned there that the shape of surface corrugation can be get smoother by an advanced deposition method and, in turn, the propagation loss can be reduced, however attendant undesirable reduction of reflection coefficient demands some compromise. The purpose of the present work is to find a way for reduction of propagation loss without reduction of reflection coefficient.

Statement of Contribution/Methods

Our calculations show that the situation can be improved considerably by changing of crystal cut angle. Moreover, the simple conventional sputtering, which results in a corrugation thickness approximately equal to the electrode thickness and hence in a large reflection coefficient, is quite enough. The considered structure has been analysed by the known impedance method/natural boundary element method (IM/NBEM) [3]. The frequency dependent propagation loss is extracted from the calculated electrical admittance of electrode grating.

Results

As a function of frequency the propagation loss has a minimum (practically zero) at some frequency depending strongly from the electrode thickness and cut angle. By changing these parameters the minimum can be shifted to the fundamental frequencies of resonance or anti-resonance. If the silicon dioxide thickness/wavelength ratio is equal to 20% and the electrode thickness/wavelength ratio is changed from 0% to 7%, then the zero propagation loss at fundamental frequencies is achievable for cut angles in the range from 34 to 49 degrees and from 43 to 71 degrees for the cases of resonance and antiresonance, correspondently.

Discussion and Conclusions

It is shown that by rotation of the crystal cut angle in SiO2/periodic grating /LiTaO3 structure created by conventional sputtering the minimum propagation loss with keeping of a large reflection coefficient is achievable. The effect of silicon dioxide film thickness and metallization ratio on the crystal cut selection is also discussed. But these impacts on the minimum propagation loss angle are small compared with the influence of electrode thickness.

[1] R. Takayama, H. Nakanishi, Y. Iwasaki, T. Sakuragawa, and K. Fujii, 2004 IEEE Ultrasonics Symposium, pp. 959 - 962.

[2] G. Kovacs, W. Ruile, M. Jakob, U. Rösler, E. Maier, U. Knauer, and H. Zottl, 2004 IEEE Ultrasonics Symposium, pp. 974 - 977.

[3] S. V. Biryukov and M. Weihnacht, J. Appl. Phys., vol. 96, no. 6, pp. 3117-3126 (2004).

Wednesday Poster

P3K101-02

Propagation of the Anisimkin Jr.' Plate Modes in $LiNbO_3$ and Te Single Crystals

Yuri Gulyaev; *Institute of Radio Engineering and Electronics of RAS, Russian Federation.*

Background, Motivation and Objective

Finding new waves is an important event in solid-state acoustics. In 2003 Ivan Anisimkin has found quasi-longitudinal (QL) modes, propagating in crystal plates of definite thickness and orientation. Recently, properties of the modes have been studied in quartz plates. The mode existence in other crystals remains unknown. Present paper exams the question for other two trigonal crystals characterized by common ($v_{QL} > v_{QSH} > v_{QSV}$) and uncommon ($v_{QSH} \geq v_L > v_{QSV}$) BAW velocity combinations.

Statement of Contribution/Methods

First, dispersion curves v_n (h/λ) and surface displacements $u1^{surface}$, $u2^{surface}$, $u3^{surface}$ are numerically calculated for all modes existing in 128Y,X+90-LiNbO3 (Eugler angles – 0, 37.86, 90) and 210Y,X-Te (0, 120, 0) with plate thickness h/λ = 0 - 2.5 (h – thickness, λ - wavelength, n - mode number). Then, modes with dominant longitudinal displacement $u_1^{surface}$ at relevant h/λ are looking for and, if any, displacement profiles for the modes are calculated over the whole plate thickness. In what follows after the first two steps are velocities vn and plate thickness h/λ, supporting QL modes with $u_1 >> u_2$, u_3 and $u_3 \approx$ constant in both crystals. Finally, one and two faces of the plates are shorted and QL-property together with two coupling constants $K_n^2 = 2\Delta v_n/v_n$ are examined. Calculations are accomplished with step in h/λ-format equal 0.02.

Results

Anisimkin Jr.' modes may exist both in $LiNbO_3$ and Te plates with free and shorted faces, but the mode properties in the crystals are remarkably different from each other and from those found in quartz. In $LiNbO_3$, having $v_L > v_{QSH} > v_{QSV}$, two different QL modes may propagate simultaneously for small plate thickness h/λ = 0 - 0.06. Velocity of the 1st QL mode is close to the longitudinal bulk wave velocity. It is varied with h/λ and piezoelectrically stiffened (maximum $K_n^2 = 39\%$ at h/λ = 0.08). Velocity of the 2nd QL mode is close to the shear-horizontal bulk wave velocity, not varied with h/λ, and not stiffened ($K_n^2 = 0$).

On the contrary, Te crystal, having $v_{QSH} \geq v_L > v_{QSV}$, supports only one QL-mode, but it is very wide-ranging and low-dispersive: the mode exists for all h/λ = 0 - 2.5 and its velocity is almost permanent in the range. The coupling constant of the mode approaches 2% at h/λ = 0.13.

Discussion and Conclusions

Variety of the Anisimkin Jr.' modes in different materials makes them attractive for some applications. The existence of the modes in crystals other than trigonal is yet unknown.

P3K102-03

Piezoelectric and elastic properties of SNGS and STGS single crystals at elevated temperatures

Andrei Sotnikov[1], **Hagen Schmidt[2],** Konrad Suschke[2], Manfred Weihnacht[3], Margitta Hengst[4], Jens Götze[4]; *[1]A.F.Ioffe Physical-Technical Institute, St. Petersburg, Russian Federation, [2]IFW Dresden, Dresden, Sachsen, Germany, [3]InnoXacs, , Dippoldiswalde, Germany, [4]Freiberg University of Mining and Technology, Freiberg, Germany.*

Wednesday Poster

Background, Motivation and Objective

For many years single crystalline quartz (SiO_2) was the standard material for temperature-stable BAW and SAW applications. In the last years there is an increasing demand for devices which can operate at elevated temperature. Due to its phase transition at 573°C the application range of quartz is limited. To overcome this limitation among others new materials of the CGG group came into focus, which can operate at very high temperatures up to their melting point. Additionally they have the advantage of higher electromechanical coupling coefficients. These SNGS ($Sr_3NbGa_3Si_2O_{14}$) and STGS ($Sr_3TaGa_3Si_2O_{14}$) single crystals are isomorphic with $Ca_3Ga_2Ge_4O_{14}$ (CGG) and belong to the same trigonal crystal class 32 as quartz. Elastic and piezoelectric constants of SNGS and STGS crystals are presently known only in the low-temperature range. These material constants which are necessary for the design of microacoustic devices are still unknown for the high temperature region.

Statement of Contribution/Methods

In this communication, we report on the measurements of some piezoelectric and elastic constants of SNGS and STGS single crystals at temperatures up to 900°C. SNGS and STGS single crystals were grown by the Czochralski technique. Transparent boules of pale-yellow color of up to 60 mm in length and 15-18 mm in diameter were obtained. The elastic and piezoelectric constants as a function of temperature were derived from the velocity data

of bulk acoustic waves measured by an ultrasonic pulse-echo- method and by a resonance-antiresonance method. Y- and X-oriented bars and plates were used for the measurements. The components of the dielectric constant tensor were determined using X-, Y-, and Z – cut thin plates.

Results

Temperature dependences of dielectric and piezoelectric coefficients as well as of elastic constants for SNGS and STGS single crystals were measured in a wide temperature range from 25°C to 900°C. For instance, it was found that C_{11} and C_{66} elastic constants for both measured crystals decrease with the temperature increasing. Moreover, the piezoelectric coefficient e_{11} decreases by a factor of 1.3-1.5 with the temperature increasing but piezoelectric activity is still high enough even at the highest temperature.

Discussion and Conclusions

From our BAW measurements it turned out that SNGS and STGS single crystals are useful candidates for high temperature microacoustic devices for up to at least 900°C. Therefore in a next step IDT structures should be used to evaluate the SAW design parameters for these crystals.

P3K103-04

Leaky-SAW Properties on Reverse-Proton-Exchanged LiNbO₃

Shoji Kakio, Hidenori Shimizu, Yasuhiko Nakagawa; *University of Yamanashi, Kofu, Japan.*

Background, Motivation and Objective

Leaky surface acoustic waves (LSAWs) have an inherent attenuation because LSAWs lose energy by continuously radiating the bulk wave into the substrate. The authors reported that, in a certain range of rotation angles for rotated Y-X $LiNbO_3$ (LN), the attenuation can be reduced by forming a proton-exchanged (PE) layer with an elastically soft property on the substrate. However, the coupling factor was reduced. On the other hand, reverse proton exchange (RPE) has been proposed as a method of exchanging lithium ions and protons on the surface of a PE layer to fabricate buried optical waveguides. It can be expected that the RPE layer with a property similar to that of bulk LN prevents the degradation of the coupling factor and the buried PE layer reduces the attenuation. In this study, the LSAW properties on the rotated Y-X LN substrate with the RPE layer and the buried PE layer were investigated.

Statement of Contribution/Methods

The elastic constants of the PE layer are approximately 60% of those of bulk LN. For convenient calculation, a layered structure of air/bulk LN/softened LN was assumed and the elastic constants c'_{ij} of the softened LN were expressed by Ac_{ij}, where c_{ij} are bulk values and A is a parameter. The cut angle of both the substrate and the layer with the depth d was identically set to be the rotated Y-X. A simple delay-line sample with different depths of the RPE layer was fabricated on 41° Y-X LN by immersing a PE sample in an equimolar mixture of $LiNO_3$-$NaNO_3$-KNO_3 at 350°C. An initial PE layer with a depth of 1.9 µm was formed by immersing the LN substrate in a solution of benzoic acid at 240°C for 2 h and 40 min. Interdigital transducers with a period length λ of 20 µm were fabricated on the sample. The propagation loss PL was estimated by subtracting the insertion loss of a path length of 100 λ from that of 300 λ.

Results

When the softened LN substrate was assumed to have the same material constants as those of the bulk except the elastic constants and d was fixed to be 0.2 λ, the rotation angle from the Y-axis giving zero attenuation shifted from 64° toward 5° for a metallized surface, and the range of the rotation angles giving zero attenuation markedly expanded to -30°~95° for a free surface as A was decreased from 1.0 to 0.6. The measured PL on 41° Y-X LN for the metallized surface was decreased by carrying out the RPE process for 10 h from 0.036 dB/λ of a virgin sample to 0.015 dB/λ. The decrease of the PL for the free surface was also observed.

Discussion and Conclusions

The layered structure on the rotated Y-X LN substrate with the RPE layer and the buried PE layer reduced LSAW attenuation. We will experimentally apply the layered structure to a 5°~15° rotated Y-X LN substrate with a large coupling factor.

P3K104-05

Application of Compound Matrices to the Study of SAW and PSAW Propagation in Layered Structures

V.I. Fedosov[1], Y. V. Gulyaev[1], I. I. Chusov[1], M. Benetti[2], **D. Cannatà[2],** F. Di Pietrantonio[2], E. Verona[2]; [1]*Russian Academy of Sciences, Institute of Radioengineering and Electronics, Moscow, Russian Federation,* [2]*Italian National Research Council, "O.M. Corbino" Institute of Acoustics, Rome, Italy.*

Background, Motivation and Objective

Use of compound matrices in the matrix formalism has shown [1] to make possible surface acoustic mode velocity calculations in layered structures in case of thick film layers (5 wavelengths or more) and, moreover, to be a useful tool to derive the analytic expressions describing the acoustic mode propagation.

Statement of Contribution/Methods

The advantages, as well as the weak points related to the use of compound matrices in matrix formalism with respect to usual matrices are discussed, when applied to calculation of SAW and PSAW propagation in layered structures, exploiting thick films.

Results

In this paper we report a number of theorems referring to compound matrices and required for their implementation. A brief demonstration of the theorems is also reported, when not available in the literature. Results of the calculations performed exploiting the compound matrices and the conventional ones are discussed and compared for the specific case of SAW and PSAW propagation along a layered structure consisting of an AlN piezoelectric film deposited on a thick isotropic diamond layer, grown, in turn, on a single crystal, [1-11]- cut Si substrate, for the [110] propagation direction.

Discussion and Conclusions

The calculations, based on the conventional matrices, have been reported, for this structure, in [2]. Compound matrices have also been used to calculate the propagation of SAWs and PSAWs along the same layered structure, when the single crystal Si substrate is replaced by an isotropic poly-crystal silicon one. Calculation results obtained for the two different structures are discussed and compared.

[1] V.I. Fedosov, V.I. Anisimkin, I.M. Kotelyanskii, C. Caliendo, P. Verardi, E. Verona, Analysis of acoustic waves in multilayers using compound matrices, 1996 IEEE Ultrasonics Symp. Proc., pp. 207-212.

[2] M. Benetti, D. Cannatà, F. Di Pietrantonio, E. Verona, V.I. Fedosov, Y.V. Gulyaev, Theoretical Investigation of PSAW Generation and Propagation in AlN/Isotropic Diamond/Si Structure, 2006 IEEE Ultrasonics Symp. Proc., pp. 2318-2321.

Author Index

A

B

C

D

E

F

G

H

I

J

K

L

Author Index

M

Author Index

N

O

P

Q

R

Author Index

S

T

U

V

W

X

Y

Z

BICC Floor Plan

First Floor of BICC:

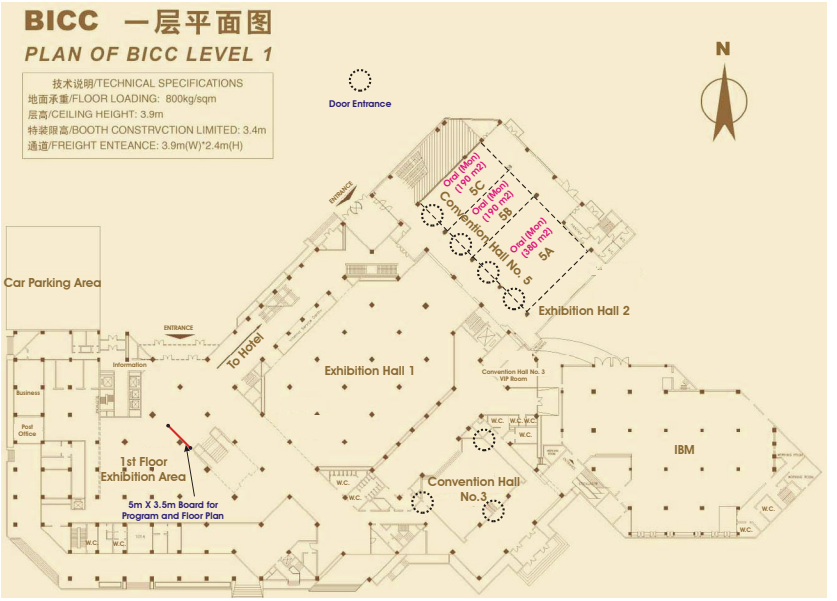

Second Floor of BICC:

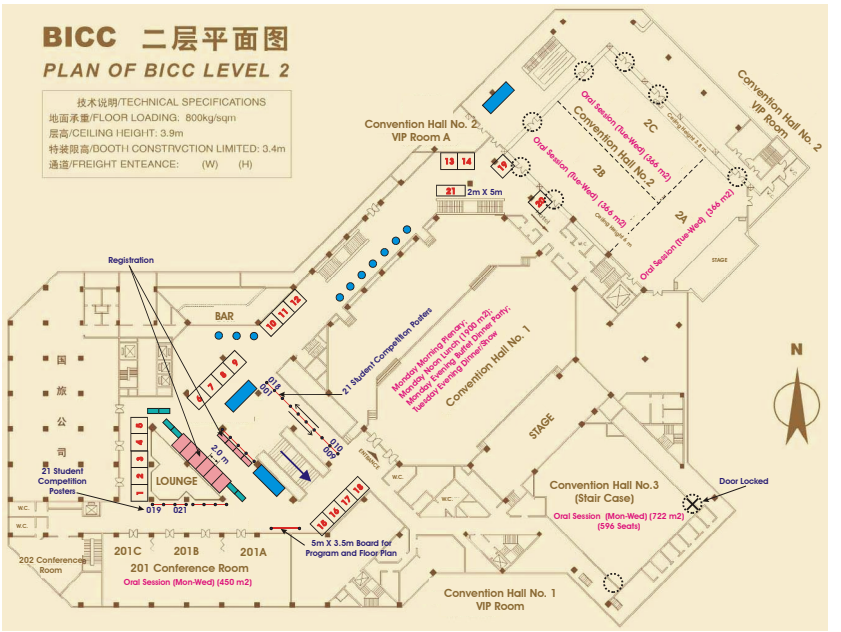

Third Floor of BICC:

Saturday – Sunday (November 1-2, 2008):

Condensed Program of 2008 IEEE International Ultrasonics Symposium

Beijing, China, November 2-5, 2008

Room Names:

Hall 1: Convention Hall No. 1 (2nd Floor)
Hall 2: Convention Hall No. 2 (2nd Floor)
Hall 3: Convention Hall No. 3 (1st&2nd Floors)
Hall 5: Convention Hall No. 5 (1st Floor)
Room 201: 201 Conference Room (2nd Floor)
Room 305: 305 Conference Room (3rd Floor)
Room 307: 307 Conference Room (3rd Floor)
Room 308: 308 Conference Room (3rd Floor)
Room 311: 311 Conference Room (3rd Floor)

Color Codes:

Group I: **RED:** Medical Ultrasound; Group II: **ORANGE:** Sensor, NDE; Group III: **GREEN:** Physical Acoust Group IV: **Violet:** Microacoustics; Group V: **BLACK:** Transducers; **(1I):** 1 Invited Talk; **(2I):** 2 Invited; **(3I):** 3 Invited

SATURDAY, Nov. 1	Condensed Program --- 2008 IEEE International Ultrasonics Symposium, Beijing, China, November 2-5, 2008
	Symposium Registration *(2nd Floor Foyer), 6:00 p.m. – 9:00 p.m.*

SUNDAY, Nov. 2	Short Courses *(with Refreshments on 3rd Floor Foyer from 10:00 a.m. - 10:20 a.m.; 3:00 p.m. - 3:20 p.m.; and 8:00 p.m. - 8:20 p.m.)*		
	Symposium Registration *(2nd Floor Foyer), 7:00 a.m. – 7:00 p.m.*		
	Short Courses *(8:00 a.m.-12:00 noon)*:	**Short Courses** *(1:00 p.m.-5:00 p.m.)*:	**Short Courses** *(6:00 p.m.-10:00 p.m.)*:
	Course 1A: Med. Ultrason. Transducers (311A/B)	**Course 1B:** Ultrason. Elastography (311A/B)	**Course 1C:** Ultrason. Contrast Agents (311A/B)
	Course 2A: Ultrason. Imag. Systems (307)	**Course 2B:** Acoust. Microscopy (307)	**Course 2C:** CUMTs (307)
	Course 3A: Photoacoustic Imag. & Sensing (308)	**Course 3B:** Therapeutic Ultrasound (308)	**Course 3C:** Time Reversal Acoustics (308)
	Course 4A: Tissue Motion & Blood Flow (311C)	**Course 4B:** SAW Modeling Techniques (311C)	**Course 4C:** Acoust. Near-Field Imag. (311C)

Condensed Program (Monday)

Monday (November 3, 2008):

MONDAY, Nov. 3	Hall 3	Rooms 201A/B/C	Hall 5A	Hall 5B	Hall 5C	Room 307
	Symposium Registration (2nd Floor Foyer), 7:00 a.m. – 6:00 p.m.			Exhibits (2nd Floor Foyer), 8:00 a.m. – 5:00 p.m.		
8:00 a.m. – 10:00 a.m.	Plenary Session (Convention Hall 1 - For All Attendees)					
10:00 a.m. – 10:30 a.m.	Refreshments (Locations: 2nd and 3rd Floor Foyers)					
10:30 a.m. – 12:00 noon	1A. Blood Flow Measurements (1I)	2A. Tissue Characterization	3A. Imaging Systems and Methods	4A. Transducer Materials Characterization	5A. Material Properties I (2I)	6A. Thin Film & Device Characterization
12:00 noon – 1:30 p.m.	Lunch (Convention Hall 1 - For All Attendees)					
1:30 p.m. – 3:00 p.m.	1B. High-Frequency and Small Animal Imaging (1I)	2B. Bone I	3B. Ultrasonic Motors - Technology Advances	4B. Single Crystals I (2I)	5B. NDE Signal Processing	6B. Advances in Materials & Propagation
3:00 p.m. – 4:30 p.m.	Posters and Refreshments (Locations: 2nd and 3rd Floor Foyers)					
	PS. Student Competition P1A. Photoacoustic Imag. P1B. Medical Beamforming	P1C. Medical Imaging P1D. Medical Signal Proc. P1E. Transducer Modeling	P1F. Piezo. & Ferro. Mat. P1G. Sonar Propa. & Det. P1H. Ultrason. Motor Appl	P1I. Phononic Crystals II P1J. NDE Signal Proc. P1K. NDE Applications	P1L. BAW Modeling P1M. Microwave Acoust. Devices for Wireless Front Ends	
4:30 p.m. – 6:00 p.m.	1C. Shear Wave and Shear Strain Imaging (1I)	2C. Bone 2	3C. Phononic Crystals I - Bandgap & Focusing	4C. Single Crystal II (1I)	5C. Bulk Acoustic Wave Sensors (1I)	6C. SAW Devices
6:30 p.m. – 10:00 p.m.	Buffet Dinner Party (Convention Hall 1 - For All Attendees)					

Condensed Program (Tuesday)

Tuesday (November 4, 2008):

TUESDAY, Nov. 4	Hall 3	Rooms 201A,B/C	Rooms 305A,B/C	Hall 2A	Hall 2B	Hall 2C
	Symposium Registration *(2nd Floor Foyer), 7:00 a.m. – 5:30 p.m.*			**Exhibits** *(2nd Floor Foyer), 8:00 a.m. – 5:00 p.m.*		
8:30 a.m. – 10:00 a.m.	**1D.** Elasticity Imaging: Applications	**2D.** Contrast Agents: Targeting & Therapeutics	**3D.** Medical Signal Processing I	**4D.** cMUTs	**5D.** Industrial Measurement	**6D.** Bulk Wave Resonators - I **(1I)**
10:00 a.m. – 10:30 a.m.			**Refreshments** *(Locations: 2nd and 3rd Floor Foyers)*			
10:30 a.m. – 12:00 noon	**1E.** Clinical Cancer Imaging **(3I)**	**2E.** Arrays and Therapeutic Devices	**3E.** Medical Signal Processing II	**4E.** cMUT Modeling	**5E.** Flow Measurements **(1I)**	**6E.** Ultrasonic Wave Propagation - I
12:00 noon – 1:30 p.m.	**Lunch** *(On Your Own)*					
1:30 p.m. – 3:00 p.m.	**1F.** 3-D Elasticity Imaging **(1I)**	**2F.** Ultrason. Mediated Delivery of Therap. Agents	**3F.** Photoacoustic Imaging	**4F.** SAW vs BAW **(1I)**	**5F.** Acoustic Imaging and Microscopy	**6F.** Ultrasonic Motors & Droplet Processing
3:00 p.m. – 4:30 p.m.	**Posters** *and* **Refreshments** *(Locations: 2nd and 3rd Floor Foyers)* **P2A.** Blood Flow **P2B.** Improv. Contrast Imag. **P2C.** Contrast Agents: M/C. **P2D.** Bioeffects **P2E.** High Freq. Tech. **P2F.** 3D / Cardiac Imag. **P2G.** Med. Imag. Transd. **P2H.** Nonlinear Propag. **P2I.** Ultrason. Wa. Prop. II **P2J.** Ultrason. Mot. Innov. **P2K.** Acoust Wave Sen. **P2L.** Acoust Imag. Sig. Proc. **P2M.** NDE Methods **P2N.** Thin Film & Device Fab. **P2O.** SAW Simulation **P2P.** Sen. & ID SAW Tags					
4:30 p.m. – 6:00 p.m.	**1G.** Visco-elasticity	**2G.** Therapeutic Ultrasound	**3G.** High Frequency Transducers	**4G.** Acoustic MEMS Devices **(1I)**	**5G.** NDE Phased Arrays	**6G.** Material Properties II - Crystals & Composites
6:30 p.m. - 10:00 p.m.	**Banquet Dinner and Shows** *(Convention Hall 1 - For All Attendees)*					

Condensed Program (Wednesday)

Wednesday (November 5, 2008):

WEDNESDAY, Nov. 5	Hall 3	Rooms 201 A/B/C	Rooms 305 A/B/C	Hall 2 A	Hall 2 B	Hall 2 C
	Symposium Registration *(2nd Floor Foyer), 7:00 a.m. – 1:00 p.m.* **Exhibits** *(2nd Floor Foyer), 8:00 a.m. – 12:00 noon*					
8:30 a.m. – 10:00 a.m.	**1H.** Cardiac Imaging **(1I)**	**2H.** Cavitation Therapy	**3H.** Transducer Modeling and Design	**4H.** Device Modeling	**5H.** Material and Defect Characterization	**6H.** Optical & RF Ultrasonic Effects
10:00 a.m. – 10:30 a.m.	**Refreshments** *(Locations: 2nd and 3rd Floor Foyers)*					
10:30 a.m. – 12:00 noon	**1I.** Cardiovascular Imaging **(1I)**	**2I.** Therapeutic Monitoring and Guidance	**3I.** Polymers for Transducers	**4I.** BAW Materials & Devices	**5I.** Wave Propagation **(1I)**	**6I.** Ultrasonic MEMS **(1I)**
12:00 noon – 1:30 p.m.	**Lunch** *(On Your Own)*					
1:30 p.m. – 3:00 p.m.	**1J.** Cardiovascular Elastography	**2J.** Beam Forming Algorithms and Strategies	**3J.** Microbubbles: Theory and Characterization	**4J.** Multilayer SAW Propagation **(1I)**	**5J.** Liquid and Gas Sensing	**6J.** Energy Harvesting & Magnetoelectrics **(2I)**
3:00 p.m. – 4:30 p.m.	**Posters** *and* **Refreshments** *(Locations: 2nd and 3rd Floor Foyers)*					
	P3A. Tiss. Charac. - Tech.	**P3D.** Therapeutic Ultrasound Applications		**P3G.** Material Characterisation and Fabrication Tech.		**P3J.** BAW & MEMS Mat. & Dev.
	P3B. Tiss. Charac. - In Vivo	**P3E.** Therapeutic Ultrasound Technologies		**P3H.** Material Properties III		**P3K.** Thin-Film & Propag.
	P3C. Elastography	**P3F.** MUT Transducers		**P3I.** Bulk Wave Effects & Devices		
4:30 p.m. – 6:00 p.m.	**1K.** Vector Velocity Imaging	**2K.** Adaptive Beam Forming	**3K.** Contrast Agent Imaging: Methods & Appl.		**5K.** Acoustic Wave Sensors	**6K.** Medical Arrays

	Hall 3	Rooms 201A/B/C	Rooms 305A/B/C	Hall 2A	Hall 2B	Hall 2C
Sizes of Rooms:	530 m2 *(1st & 2nd Floors)*	450 m2 *(2nd Floor)*	450 m2 *(3rd Floor)*	366 m2 *(2nd Floor)*	366 m2 *(2nd Floor)*	366 m2 *(2nd Floor)*

		Hall 5A	Hall 5B	Hall 5C	Room 307
Note: Roughly 1 square meter (m2) per person.	**Sizes of Rooms:**	About 380 m2 *(1st Floor)*	About 190 m2 *(1st Floor)*	About 190 m2 *(1st Floor)*	185 m2 *(3rd Floor)*

Notes

Notes

Abstract Book

2008 IEEE INTERNATIONAL ULTRASONICS SYMPOSIUM (IUS)

Beijing International Convention Center (BICC)
November 2-5, Beijing, China

Forbidden City

Temple of Heaven

Summer Palace

The Great Wall

UFFC

IEEE